University of Belgrade,
Technical Faculty in Bor

Chamber of Commerce
and Industry of Serbia

XVI International Mineral Processing & Recycling Conference

2025 IMPRC

INTERNATIONAL MINERAL PROCESSING & RECYCLING CONFERENCE

Proceedings

Editors:
Zoran ŠTIRBANOVIĆ
Milan TRUMIĆ

28-30 May 2025
Belgrade, Serbia

University of Belgrade,
Technical Faculty in Bor

Chamber of Commerce
and Industry of Serbia

XVI International Mineral Processing & Recycling Conference

2025 IMPRC
INTERNATIONAL MINERAL PROCESSING & RECYCLING CONFERENCE

Proceedings

Editors:
Zoran ŠTIRBANOVIĆ
Milan TRUMIĆ

28 – 30 May 2025, Belgrade, Serbia

XVI International Mineral Processing & Recycling Conference

PUBLISHER:
University of Belgrade, Technical Faculty in Bor

FOR THE PUBLISHER:
Dean: Prof. Dr Dejan Tanikić, University of Belgrade, Technical Faculty in Bor

EDITORS:
Prof. Dr Zoran Štirbanović, University of Belgrade, Technical Faculty in Bor
Prof. Dr Milan Trumić, University of Belgrade, Technical Faculty in Bor

TECHNICAL EDITORS:
Dr Vladimir Nikolić, University of Belgrade, Technical Faculty in Bor
MSc Dragana Marilović, University of Belgrade, Technical Faculty in Bor
MSc Katarina Balanović, University of Belgrade, Technical Faculty in Bor

PROCEEDINGS COVER DESIGN:
MSc Aleksandar Cvetković, University of Belgrade, Technical Faculty in Bor

PRINTED BY:
Grafika Galeb, Niš, Serbia
Printed: 200 copies

PUBLICATION YEAR:
2025

===========================
CIP - Каталогизација у публикацији
Народна библиотека Србије, Београд

622.7(082)
502.131.1:628.477.6(082)
628.477.6(082)

INTERNATIONAL Mineral Processing and Recycling Conference (16 ; 2025 ; Belgrade)
Proceedings / XVI International Mineral Processing and Recycling Conference, IMPRC, 28 – 30 May 2025, Belgrade, Serbia ; editors Zoran Štirbanović, Milan Trumić. - Bor : University of Belgrade, Technical Faculty, 2025 (Niš : Grafika Galeb). - XIX, 706 str. : ilustr. ; 25 cm

Na vrhu nasl. str.: Chamber of Commerce and Industry of Serbia. - Tiraž 200. -
Bibliografija uz svaki rad.

ISBN 978-86-6305-158-4

а) Руде -- Припрема -- Зборници б) Отпадне материје -- Одрживи развој –
Зборници в) Отпадне материје -- Рециклажа -- Зборници

COBISS.SR-ID 168462601 -ID 114566153
==========================

GENERAL SPONSOR

Conference is financially supported
by the Ministry of Science, Technological
Development and Innovation
of the Republic of Serbia

GOLD SPONSORS

ZiJin
SERBIA ZIJIN COPPER DOO BOR

ZiJin
SERBIA ZIJIN MINING

SILVER SPONSORS

EMJM PROMISE
Erasmus Mundus Joint Master
in Sustainable Mineral and
Metal Processing Engineering

minerals

metals
an Open Access Journal by MDPI

HBIS SERBIA

RUDNIK

EXHIBITORS

BSI BALTIC SCIENTIFIC INSTRUMENTS

GLOBAL MET TECH

KRUG
KRUG INTERNATIONAL LTD.

novos
partnership through science

FRIENDS OF THE CONFERENCE

PRO FORCE
SERBIA

SCIENTIFIC COMMITTEE

Prof. Dr Milan Trumić, University of Belgrade, Technical Faculty in Bor (Serbia) President
Prof. Dr Grozdanka Bogdanović, University of Belgrade, Technical Faculty in Bor (Serbia) Vice President
Prof. Dr Jovica Sokolović, University of Belgrade, Technical Faculty in Bor (Serbia) Vice President
Prof. Dr Zoran Štirbanović, University of Belgrade, Technical Faculty in Bor (Serbia) Vice President
Prof. Dr Corby Anderson, Colorado School of Mines (USA)
Prof. Dr Zhiyong Gao, Central South University (China)
Prof. Dr Pablo Brito-Parada, Imperial College London (United Kingdom)
Prof. Dr Junbeum Kim, University of Technology of Troyes (France)
Prof. Dr Srećko Stopić, RWTH Aachen University (Germany)
Prof. Dr Lijie Guo, Beijing General Research Institute of Mining and Metallurgy (China)
Prof. Dr Mauricio Torem, Pontifical Catholic University of Rio de Janeiro (Brazil)
Prof. Dr Georgios Anastassakis, National Technical University of Athens (Greece)
Prof. Dr Przemyslaw Kowalczuk, Norwegian University of Science and Technology (Norway)
Prof. Dr Kerstin Forsberg, KTH Royal Institute of Technology (Sweden)
Prof. Dr Alexandre Chagnes, Université de Lorraine (France)
Prof. Dr Erin Bobicki, University of Alberta (Canada)
Prof. Dr Kazutoshi Haga, Akita University (Japan)
Prof. Dr Quentin Campbell, North-West University (South Africa)
Dr Fardis Nakhaei, Missouri University of Science and Technology (USA)
Dr Aleksandar Janković, Kresnik Pty Ltd (Australia)
Prof. Dr Rraghupatruni Bhima Rao, Aryan Institute of Engineering and Technology (India)
Prof. Dr Magdalena Regel-Rosocka, Poznan University of Technology (Poland)
Prof. Dr Juan M. Menéndez Aguado, University of Oviedo (Spain)
Prof. Dr Efrén Garcia Ordiales, University of Oviedo (Spain)
Prof. Dr Alejandro Rodriguez Pascual, University of Cordoba (Spain)
Prof. Dr Antonis Peppas, National Technical University of Athens (Greece)
Prof. Dr Komnitsas Konstantinos, Technical University of Crete (Greece)
Prof. Dr Semra Kurama, Eskisehir Technical University (Turkey)
Prof. Dr Mehmet Polat, Izmir Institute of Technology (Turkey)
Prof. Dr Valery Morozov, National University of Science and Technology MISiS (Russian Federation)
Dr Kadriann Tamm, Tallinn University of Technology (Estonia)
Prof. Dr Maria Sinche Gonzalez, University of Oulu (Finland)
Prof. Dr Sônia Denise Rocha, Federal University of Minas Gerais (Brazil)
Prof. Dr Rodrigo Souza, Pontifical Catholic University of Rio de Janeiro (Brazil)
Prof. Dr Frederico Marques Penha, KTH Royal Institute of Technology (Sweden)
Prof. Dr Silvie Heviánková, VSB – Technical University of Ostrava (Czech Republic)
Dr Hector Muñiz Sierra, Institute of Chemical Process Fundamentals of the Czech Academy of Sciences (Czech Republic)
Dr Slavomir Hredzak, Institute of Geotechnics of the Slovak Academy of Science (Slovakia)
Dr Vladimir Joković, University of Queensland (Australia)
Prof. Dr Gabor Musci, University of Miskolc (Hungary)
Prof. Dr Francisc Popescu, University Politehnica Timisoara (Romania)

Prof. Dr Adian Cioabla, University Politehnica Timisoara (Romania)
Prof. Dr Irena Grigorova, University of Mining and Geology "St. Ivan Rilski" (Bulgaria)
Prof. Dr Jakob Lamut, University of Ljubljana (Slovenia)
Prof. Dr Filip Kokalj, University of Maribor (Slovenia)
Prof. Dr Aleksandra Anić Vučinić, University of Zagreb (Croatia)
Asst. Prof. Dr Branimir Farkaš, University of Zagreb (Croatia)
Prof. Dr Ilhan Bušatlić, University of Zenica (Bosnia & Herzegovina)
Prof. Dr Svjetlana Sredić, University of Banja Luka (Republic of Srpska, Bosnia & Herzegovina)
Prof. Dr Afrodita Zendelska, University "Goce Delchev " (North Macedonia)
Prof. Dr Aleksandar Jovović, University of Belgrade, Faculty of Mechanical Engineering (Serbia)
Prof. Dr Milena Kostović, University of Belgrade, Faculty of Mining and Geology (Serbia)
Prof. Dr Predrag Lazić, University of Belgrade, Faculty of Mining and Geology (Serbia)
Prof. Dr Željko Kamberović, University of Belgrade, Faculty of Technology and Metallurgy (Serbia)
Prof. Dr Vlada Veljković, University of Nis, Faculty of Technology (Serbia)
Prof. Dr Goran Vujić, University of Novi Sad, Faculty of Technical Sciences (Serbia)
Prof. Dr Srđan Rončević, University of Novi Sad, Faculty of Sciences (Serbia)
Prof. Dr Bogdana Vujić, University of Novi Sad, Technical Faculty "Mihajlo Pupin" (Serbia)
Prof. Dr Marina Stamenović, The Academy of Applied Technical Studies Belgrade (Serbia)
Prof. Dr Dimitrije Zakić, University of Belgrade, Faculty of Civil Engineering (Serbia)
Prof. Dr Vladimir Pavićević, University of Belgrade, Faculty of Technology and Metallurgy (Serbia)
Prof. Dr Nada Štrbac, University of Belgrade, Technical Faculty in Bor (Serbia)
Prof. Dr Milan Antonijević, University of Belgrade, Technical Faculty in Bor (Serbia)
Prof. Dr Zoran Stević, University of Belgrade, Technical Faculty in Bor (Serbia)
Prof. Dr Dejan Tanikić, University of Belgrade, Technical Faculty in Bor (Serbia)
Prof. Dr Ljubiša Andrić, University of Belgrade, Technical Faculty in Bor (Serbia)
Prof. Dr Snežana Šerbula, University of Belgrade, Technical Faculty in Bor (Serbia)
Prof. Dr Snežana Milić, University of Belgrade, Technical Faculty in Bor (Serbia)
Prof. Dr Mira Cocić, University of Belgrade, Technical Faculty in Bor (Serbia)
Prof. Dr Maja Trumić, University of Belgrade, Technical Faculty in Bor (Serbia)
Asst. Prof. Dr Vladan Milošević, University of Belgrade, Technical Faculty in Bor (Serbia)
Asst. Prof. Dr Vladimir Nikolić, University of Belgrade, Technical Faculty in Bor (Serbia)
Dr Mile Bugarin, Mining and Metallurgy Institute Bor (Serbia)
Dr Zoran Stevanović, Mining and Metallurgy Institute Bor (Serbia)
Dr Radmila Marković, Mining and Metallurgy Institute Bor (Serbia)
Dr Jelena Petrović, Mining and Metallurgy Institute Bor (Serbia)
Dr Ivana Smičklas, Vinča Institute of Nuclear Sciences (Serbia)
Dr Ivana Jelić, Vinča Institute of Nuclear Sciences (Serbia)
Dr Miroslav Sokić, Institute for Technology of Nuclear and Other Mineral Raw Materials (Serbia)
Dr Dragan Radulović, Institute for Technology of Nuclear and Other Mineral Raw Materials (Serbia)
Dr Sonja Milićević, Institute for Technology of Nuclear and Other Mineral Raw Materials (Serbia)
Dr Milinko Radosavljević, Mining Institute (Serbia)
Dr Svetlana Polavder, Mining Institute (Serbia)
Dr Miroslav Ignjatović, Chamber of Commerce and Industry of Serbia (Serbia)

ORGANIZING COMMITTEE

Prof. Dr Zoran Štirbanović, University of Belgrade, Technical Faculty in Bor, President
Prof. Dr Milan Trumić, University of Belgrade, Technical Faculty in Bor
Prof. Dr Grozdanka Bogdanović, University of Belgrade, Technical Faculty in Bor
Prof. Dr Jovica Sokolović, University of Belgrade, Technical Faculty in Bor
Prof. Dr Maja Trumić, University of Belgrade, Technical Faculty in Bor
Dr Vladimir Nikolić, University of Belgrade, Technical Faculty in Bor Secretary
Dr Miroslav Ignjatović, Chamber of Commerce and Industry of Serbia
MSc Dragana Marilović, University of Belgrade, Technical Faculty in Bor
MSc Katarina Balanović, University of Belgrade, Technical Faculty in Bor
MSc Ivana Ilić, University of Belgrade, Technical Faculty in Bor
MSc Tamara Gavrilović, University of Priština – Kosovska Mitrovica
MSc Oliver Marković, University of Belgrade, Technical Faculty in Bor
MSc Dragan Milenković, University of Belgrade, Technical Faculty in Bor
MSc Sandra Vasković, University of Belgrade, Technical Faculty in Bor
BSc Vera Ražnatović, Chamber of Commerce and Industry of Serbia
Dobrinka Trujić, University of Belgrade, Technical Faculty in Bor

LIST OF REVIEWERS

Prof. Dr Georgios Anastassakis, National Technical University of Athens (Greece)
Prof. Dr Pablo Brito-Parada, Imperial College London (United Kingdom)
Prof. Dr Milan Trumić, University of Belgrade, Technical Faculty in Bor (Serbia)
Prof. Dr Srećko Stopić, RWTH Aachen University (Germany)
Prof. Dr Grozdanka Bogdanović, University of Belgrade, Technical Faculty in Bor (Serbia)
Prof. Dr Ljubiša Andrić, University of Belgrade, Technical Faculty in Bor (Serbia)
Prof. Dr Jovica Sokolović, University of Belgrade, Technical Faculty in Bor (Serbia)
Prof. Dr Zoran Štirbanović, University of Belgrade, Technical Faculty in Bor (Serbia)
Prof. Dr Maja Trumić, University of Belgrade, Technical Faculty in Bor (Serbia)
Dr Radmila Marković, Mining and Metallurgy Institute Bor (Serbia)
Dr Jelena Petrović, Mining and Metallurgy Institute Bor (Serbia)
Dr Stefan Đorđijevski, Mining and Metallurgy Institute Bor (Serbia)
Dr Vesna Conić, Mining and Metallurgy Institute Bor (Serbia)
Dr Ivana Jelić, Vinča Institute of Nuclear Sciences (Serbia)
Prof. Dr Maja Nujkić, University of Belgrade, Technical Faculty in Bor (Serbia)
Prof. Dr Ivana Marković, University of Belgrade, Technical Faculty in Bor (Serbia)
Prof. Dr Marija Petrović-Mihajlović, University of Belgrade, Technical Faculty in Bor (Serbia)
Prof. Dr Žaklina Tasić, University of Belgrade, Technical Faculty in Bor (Serbia)
Prof. Dr Radoje Pantović, University of Belgrade, Technical Faculty in Bor (Serbia)
Prof. Dr Snežana Milić, University of Belgrade, Technical Faculty in Bor (Serbia)
Dr Ljiljana Avramović, Mining and Metallurgy Institute Bor (Serbia)
Prof. Dr Przemyslaw Kowalczuk, Norwegian University of Science and Technology (Norway)
Prof. Dr Alexandre Chagnes, Université de Lorraine (France)
Prof. Dr Aleksandar Nikoloski, Murdoch University (Australia)
Dr Dragana Medić, University of Belgrade, Technical Faculty in Bor (Serbia)
Prof. Dr Ljubiša Balanović, University of Belgrade, Technical Faculty in Bor (Serbia)
Prof. Dr Juan M. Menéndez Aguado, University of Oviedo (Spain)
Dr Hector Muñiz Sierra, Institute of Chemical Process Fundamentals of the Czech Academy of Sciences (Czech Republic)
Dr Vladimir Nikolić, University of Belgrade, Technical Faculty in Bor (Serbia)
Dr Dragana Božić, Mining and Metallurgy Institute Bor (Serbia)
Dr Marija Šljivić-Ivanović, Vinča Institute of Nuclear Sciences (Serbia)
Dr Dragan Radulović, Institute for Technology of Nuclear and Other Mineral Raw Materials (Serbia)
Prof. Dr Maria Sinche Gonzalez, University of Oulu (Finland)
Prof. Dr Kerstin Forsberg, KTH Royal Institute of Technology (Sweden)
Dr Srđan Stanković, University of Belgrade, Faculty of Biology (Serbia)
Prof. Dr Igor Miljanović, University of Belgrade, Faculty of Mining and Geology (Serbia)
Prof. Dr Milena Kostović, University of Belgrade, Faculty of Mining and Geology (Serbia)
Dr. Yu Yuexian, Xi'an University of Science and Technology (China)
Dr. Yunfeng Song, Central South University (China)
Prof. Bojan Marinkovic, Pontifical Catholic University of Rio de Janeiro (Brazil)

Prof. Dr Aleksadra Fedajev, University of Belgrade, Technical Faculty in Bor (Serbia)
Dr Ljiljana Tolić Stojadinović, Innovation Center of the Faculty of Technology and Metallurgy (Serbia)
Dr. Vasily Timofeevich Lebedev, Petersburg Nuclear Physics Insttitute (Russian Federation)
Prof. Maurício Leonardo Torem, Pontifical Catholic University of Rio de Janeiro (Brazil)
Prof. Dr Vesna Alivojvodić, The Academy of Applied Studies Polytechnic, Belgrade (Serbia)
Dr Saied Karimi, Hamedan University of Technology (Iran)
Dr Mathilde Perrin, University of Grenoble Alpes, CEA-Liten (France)
Dr Aleksandar Janković, Hatch (Australia)
Dr Vladan Milošević, University of Belgrade, Technical Faculty in Bor (Serbia)
Prof. Dr Milan Antonijević, University of Belgrade, Technical Faculty in Bor (Serbia)
Dr Sonja Milićević, Institute for Technology of Nuclear and Other Mineral Raw Materials (Serbia)
Prof. Dr Milan Gorgievski, University of Belgrade, Technical Faculty in Bor (Serbia)
Prof. Dr Dragan Manasijević, University of Belgrade, Technical Faculty in Bor (Serbia)
Prof. Dr Semra Kurama, Eskişehir Technical University (Turkey)
Dr Aleksandra Mitovski, Engineering Dobersek GmbH (Germany)
Prof. Dr Carmen Mihaela Neculita, Research Institute on Mines and Environment, University of Québec in Abitibi-Témiscamingue (Canada)
Dr Janine Rodrigues Figueiredo, Federal University of Ouro Preto, (Brazil)
Prof. Dr Ana Radojević, University of Belgrade, Technical Faculty in Bor (Serbia)
Dr Jelena Jordanović, University of Belgrade, Technical Faculty in Bor (Serbia)
Prof. Dr Komnitsas Konstantinos, Technical University of Crete (Greece)
Dr Jelena Avdalović, Institute of Chemistry, Technology and Metallurgy (Serbia)
Dr Milica Mladenović, Vinča Institute of Nuclear Sciences (Serbia)
Prof. Dr Xiaomin Ma, Taiyuan University of Technology (China)
Prof. Dr Snežana Urošević, University of Belgrade, Technical Faculty in Bor (Serbia)
Prof. Dr Milan Radovanović, University of Belgrade, Technical Faculty in Bor (Serbia)
Prof. Dr Ana Simonović, University of Belgrade, Technical Faculty in Bor (Serbia)
Prof. Dr Francesco Ferella, University of L'Aquila (Italy)
Prof. Dr Fatma Arslan, Istanbul Technical University (Turkey)
Prof. Dr Gülay Bulut, Istanbul Technical University (Turkey)
Dr Samah S. Abdallah, Central Metallurgical Research and Development Institute (Egypt)
Prof. Dr. Vesna Grekulović, University of Belgrade, Technical Faculty in Bor (Serbia)
Dr. Vandana Kumari Jha, KTH Royal Institute of Technology (Sweden)
Dr Vesna Krstić, Mining and Metallurgy Institute Bor (Serbia)
Dr Sanja Petrović, Mining and Metallurgy Institute Bor (Serbia)
Dr Goran Pačkovski, Mining and Metallurgy Institute Bor (Serbia)
Dr Ivana Jovanović, Mining and Metallurgy Institute Bor (Serbia)
Prof. Dr Tanja Kalinović, University of Belgrade, Technical Faculty in Bor (Serbia)
Dr Jelena Kalinović, University of Belgrade, Technical Faculty in Bor (Serbia)
Dr Predrag Stolić, University of Belgrade, Technical Faculty in Bor (Serbia)

TABLE OF CONTENTS

PLENARY LECTURES 1

Pablo R. Brito-Parada 3
A MINERAL'S JOURNEY – UNRAVELLING FLOTATION PHENOMENA THROUGH PARTICLE TRACKING

Srecko Stopic, Duško Kostić, Mitar Perušić, Richard Schneider, Bernd Friedrich 9
RECOVERY OF VALUABLE METALS FROM BAUXITE RESIDUE (BR) USING DECARBONIZING TECHNOLOGIES

Corby G. Anderson 19
HOW THE RARE EARTHS BECAME THE LANTHANIDES AGAIN

Junbeum Kim 21
EMERGING TECHNOLOGIES AND EMERGING WASTES: CHALLENGES AND OPPORTUNITIES

INVITED LECTURES 23

Aleksandar Nikoloski, Pritam Singh, Tina Chanda Phiri 25
AN OVERVIEW OF GLOBAL COPPER SMELTING SLAG PRODUCTION AND REPROCESSING APPROACHES

Maria Sinche-Gonzalez 37
EDUCATION IN MINERAL PROCESSING AND FILLING THE GAP OF TALENTED MINERAL PROCESSING ENGINEERS

Predrag Umičević, Ivica Karoglan, Gregor Radišić, Viktor Simončič 44
INNOVATIVE BIODEGRADABLE WASTE TREATMENT AS A POSSIBLE SOLUTION FOR RECULTIVATION OF TAILINGS AND SLAG LANDFILLS

Kerstin Forsberg 50
CRYSTALLIZATION CHALLENGES IN HYDROMETALLURGY

Belinda McFadzean, Avuyile Wali, Megan Becker, Stefan Geldenhuys 55
CRITICAL MINERALS: CHALLENGES AND OPPORTUNITIES IN PLATINUM GROUP MINERAL FLOTATION

Alexandre Chagnes, Pierric Hubert, Safi Jradi 62
INNOVATIVE STRATEGIES FOR METAL RECOVERY FROM LFP-NMC LITHIUM-ION BATTERY BLENDS

Michal Šyc, Jiří Hykš 66
FROM LINEAR TO CIRCULAR ECONOMY – STORY OF THE BOTTOM ASH

Przemyslaw B. Kowalczuk 70
CRITICAL RAW MATERIALS (CRM) RECOVERY FROM NORWEGIAN DEPOSITS: CHALLENGES AND OPPORTUNITIES

SESSION LECTURES 73

Massoud Aghamirian Vu Truong, Kristina Muntu, Jean-Gabriel Fraboulet, Sean Salour, Brian Kawenski Cook 75
INVESTIGATIONS INTO LITHIUM MINERALS PROCESSING

Héctor Muñiz Sierra, Michal Šyc, Ayse Asya Arslanturk 86
THE APPLICATION OF PHYSICAL CONCENTRATION TECHNOLOGIES IN THE RECYCLING OF NEW WASTE STREAMS

METALS YOUNG RESEARCHER AWARD 89

Diego Poblete, Claudio Leiva, Maria Sinche-Gonzales, Claudio Acuña 91
HOLLOW DROP BUBBLES A PROPOSED NEW TECHNOLOGY FOR OPTIMIZED METAL EXTRACTION VALIDATED IN THE LABORATORY

Wanjia Zhang, Zhitao Feng, Zhiyong Gao 98
PREDICTION OF COLLECTOR FLOTATION PERFORMANCE BASED ON MACHINE LEARNING AND QUANTUM CHEMISTRY: A CASE OF SULFIDE MINERALS

Helir Muñoz, Sophia Korili, Antonio Gil 106
SYNTHESIS OF MOF@ALUMINUM SALINE SLAG COMPOSITES FOR CO_2 CAPTURE AS A NEW STRATEGY OF VALORIZATION OF SECONDARY ALUMINUM WASTES

Jernej Imperl, Mitja Kolar, Vilma Ducman, Gorazd Žibret, Lea Žibret 113
SELECTIVE SEPERATION OF MAGNESIUM FROM SLOVENIAN DOLOMITES

Vladan Nedelkovski, Dragana Medić, Aleksandar Cvetković, Sonja Stanković, Žaklina Tasić, Milan Radovanović, Snežana Milić 119
ANODE NANOMATERIAL RECOVERED FROM SPENT BATTERIES FOR PEROXIDE-ASSISTED CRYSTAL VIOLET PHOTOCATALYTIC DEGRADATION

Dragana Marilović, Sonja Stanković, Grozdanka Bogdanović 125
EFFECT OF TEMPERATURE ON THE LEACHING COPPER FROM FLOTATION TAILINGS WITH IONIC LIQUID

PAPERS 131

Iyiola Olatunji Otunniyi, Oluwayimika Olasunkanmi Oluokun 133
CLEAN GOLD SOLUTION FROM PRINTED CIRCUIT BOARD PHYSICAL PROCESSING DUST BY SELECTIVE COMPLEXATION

Ugur Ulusoy Fırat Burat, Guler Bayar, Behrad Mojtahedi, Gulsah Guven 142
CHARACTERIZATION AND COMPARISON OF THE PARTICLE SHAPE OF MICRONIZED GRAPHITE GROUND IN DIFFERENT MILLS USING DIA

Aleksander Sokolov, Edvins Letko, Vitalijs Kuzmovs, Ulises Miranda Ordonez 148
ON-LINE XRF ANALYSIS OF ELEMENTS IN MINERALS ON A CONVEYOR BELT

Aleksandra Mitrovic, Jelena Vucicevic 154
LABORATORY-SCALE REACTORS EMPLOYING MOVING BED BIOFILM REACTOR (MBBR) TECHNOLOGY: A COMPREHENSIVE REVIEW

Vesna Marjanović, Emina Požega, Miomir Mikić, Milutin Stojadinović 160
INCREASING RECYCLING RATES IN THE FIELD OF CONSTRUCTION AND DEMOLITION WASTE MANAGEMENT BY IMPLEMENTING THE LEGAL ACT OF THE REPUBLIC OF SERBIA AND THE EUROPEAN UNION

Radmila Marković, Vesna Marjanović, Aleksandra Ivanović, Milutin Stojadinović 166
CHARACTERISTICS OF COPPER POWDER OBTAINED AT LOWER VALUES OF CATHODE CURRENT DENSITY

Messai Ali, Berrekbia Linda, Meramria Ikram, Juan M. Menéndez-Aguado, Begoña Fernández Pérez, Vladimir Nikolić, Milan Trumić, Boustila Amir 171
POTENTIAL OF USING ZINC PROCESSING TAILINGS (ZPT's) IN THE PRODUCTION OF BURNT CLAY BRICKS

Aleksandra Božić, Dominik Brkić, Marina Stamenović, Marija Miletić 179
DETERMINATION OF PCB CONCENTRATION IN SOIL

Stefan Milanović, Nikola Simić, Lazar Kričak, Milanka Negovanović, Miljan Gomilanović, Nikola Đokić 184
ENVIRONMENTAL IMPACT WITH THE GREENHOUSE GASES AND AIR POLLUTANT PREDICTION BY DRILLING AND BLASTING WORKS

Dragan Milošević, Jasmina Nešković, Pavle Stjepanović, Svetlana Polavder 190
LANDFILL FOR COMBUSTION PRODUCTS FROM THE KOSTOLAC THERMOELECTRON

Fatma Arslan, Gülay Bulut 196
EVALUATION OF MINERAL PROCESSING AND METALLURGICAL PLANTS WASTES

Abhishek Gupta, Tom Newman, Frank Hrach 202
BENEFICIATION OF MINERAL ORES USING TRIBO-ELECTROSTATIC SEPARATOR

Valentin Alexeyevich Chanturia, Valeriy Valentinovich Morozov, Galina Petrovna Dvoichenkova, Elena Leonidovna Chanturia 208
THE SELECTION OF APPLICATION MODES OF AGENTS MODIFYING DIAMOND SPECTRAL CHARACTERISTICS IN THE PROCESS OF X-RAY LUMINESCENCE SEPARATION

Valeriy Valentinovich Morozov, Galina Petrovna Dvoichenkova, Irina Vasilyevna Pestryak, Valentina Anatolyevna Chut-Dy 214
UP-TO-DATE METHODS AND TECHNOLOGIES FOR IMPROVING THE PERFORMANCE OF FOAM SEPARATION OF DIAMOND-BEARING KIMBERLITES

Plamen Georgiev, Marina Nicolova, Irena Spasova, Mihail Iliev, Ralitsa Ilieva 220
NON-FERROUS METALS BIOLEACHING FROM PYROMETALLURGY COPPER SLAG USING SPENT MEDIUM OF DIFFERENT FUNGAL SPECIES

Milica Zdravković, Vesna Grekulović, Edina Huseinović, Robert Vianello, Nada Štrbac, Melita Huremović, Milan Gorgievski 226
UV-VIS IDENTIFICATION OF COPPER COMPLEXES WITH INHIBITOR ORGANIC COMPONENTS IN THE ELECTROLYTE

Moloud Nazeri, Maria Sinche-Gonzalez, Emad Abkhoshk 232
DISSOLUTION KINETICS OF LOW-GRADE ZINC SILICATE ORE IN HYDROXIDE SOLUTION

Ivana Smičiklas, Mihajlo Jović, Jelena Amidžić, Snežana Dragović 238
EVALUATION OF WASTE MATERIALS FOR CADMIUM REMOVAL: COMPARATIVE STUDY OF SORPTION CAPACITY AND STABILITY

Tanja Kalinović, Ana Radojević, Jelena Kalinović, Jelena Jordanović, Snežana Šerbula 244
CASE STUDY ON METAL(LOID)S DISTRIBUTION IN LINDEN TREE PARTS, IN AREAS WITH HIGHT ENVIRONMENTAL POLLUTION

Branimir Farkaš, Ana Hrastov, Iva Štefičar 250
POSSIBILITY OF INSTALLATION OF SOLAR POWER PLANTS IN EXPLOITATION SITES

Marija Simić, Marija Kovačević, Katarina Stojanović, Branislava Savić Rosić, Dragana Vasić Anićijević, Tanja Brdarić, Danka Aćimović 256
ELECTROCHEMICAL OXIDATION OF BISPHENOL S WITH SnO_2-MWCNT ELECTRODES

Marija Simić, Marija Kovačević, Katarina Stojanović, Marija Ječmenica Dučić, Dragana Vasić Anićijević, Danka Aćimović, Tanja Brdarić 261
COMPARATIVE STUDY OF ELECTROCHEMICAL DEGRADATION OF RHODAMINE B USING GLASSY CARBON, STAINLESS STEEL, AND NICKEL ELECTRODES

Marija Kovačević, Marija Simić, Katarina Stojanović, Danka Aćimović, Sanja Živković, Tanja Brdarić, Dragana Vasić Anićijević 267
PHOTODEGRADATION OF CIPROFLOXACIN WITH COPER-MODIFIED TITANIUM(IV)-OXIDE

Francielle Câmara Nogueira, Carlos Alberto Pereira, Leandro Vinícius Alves Gurgel, Stephânia da Consolação Silva Nogueira, Iranildes Daniel Santos 273
PROCESS WATER REUSE IN IRON ORE FLOTATION: REDUCING AMINE CONSUMPTION

Jovica Sokolović, Ivana Đolović, Dejan Tanikić, Zoran Štirbanović, Ivana Ilić 279
THE EFFECT OF PARTICLE SIZE ON THE FLOTATION KINETICS OF RAW AND WASTE COAL

Zuzana Danková, Alexandra Bekényiová, Zuzana Kollová, Erika Fedorová, Pavel Bačo, Jaroslav Briančin 286
SLOVAK DOLOMITE AS A RAW MATERIAL SOURCE FOR METAL MAGNESIUM PRODUCTION

Fatma Arslan, Cüneyt Arslan 292
RECYCLING OF WASTE CELL PHONES

Fulya Mennik, Nazlım İlkyaz Dinç, Beril Tanç Kaya, Fırat Burat 298
THE RECYCLING OF PLASTICS AND METALS FROM END-OF-LIFE NMC-TYPE ELECTRIC VEHICLE LITHIUM-ION BATTERIES USING SELECTIVE FROTH FLOTATION

Paul Delaney 306
PERFORMANCE OF IRON ALUMINIUM AND COPPER IRON BIMETALLIC PARTICLES IN REMOVAL OF HEAVY METALS AND METALLOIDS

Samah S. Abdallah, Samah M. El-Sayed, Mohamed A. Abdel-Khalek 313
SELECTIVE BIO-FLOCCULATION OF HEMATITE MINERAL USING BACILLUS SUBTILIS FOR PHOSPHOROUS REMOVAL FROM IRON ORES

Patrycja S. Bednarek, Nima Razavi, Przemyslaw B. Kowalczuk 320
THE ROLE OF ADDITIVE MANUFACTURING IN MINERAL AND METAL EXTRACTION

Zeynep Üçerler Çamur, Tülay Türk, Murat Olgaç Kangal 327
INVESTIGATION OF SURFACE PROPERTIES OF PVC FOR SELECTIVE RECOVERY

Martin Straka 333
ELECTROCHEMISTRY OF INDIUM IN METHYL-TRIOCTYLAMMONIUM BIS(TRIFLUOROMETHYLSULFONYL)IMIDE IONIC LIQUID

Seyed Hamzeh Amiri, Maria Sinche-Gonzalez 340
GRADE IMPROVEMENT OF IRON ORE CONCENTRATE BY APPLYING PLANT AUDITS, STANDARDIZATION AND PROCESS OPTIMIZATION

Henrique Dias Gatti Turrer, Josue Mesquita De Souza Junior, Gillian Nikka Omaga, Juliette Laine, Marcello Rodrigues Cruz, Nubia Bottosso, Vinicius Seerig 347
ADVANCEMENTS IN MINERAL PROCESSING: COLLABORATIVE EFFORTS AND TECHNOLOGICAL INNOVATIONS AT ARCELORMITTAL

Zuzana Kollová, Pavel Bačo, Zuzana Danková, Zoltán Németh 353
THE POTENTIAL SOURCES OF CRITICAL RAW MATERIALS IN SLOVAKIA

Amalia Andreas, Titus Nghipulile, Godfrey Dzinomwa 359
SELF-FLOTATION OF GALENA IN A COMPLEX SULPHIDE ORE FROM A COPPER MINE IN NAMIBIA

Janine Rodrigues Figueiredo, Érica Linhares Reis, Arthur Silva de Oliveira 368
PROCESSING OF FINE LITHIUM MINERAL TAILINGS

Theodor Steller, Stefan Eisert, Bernd G. Lottermoser 375
EXPLORING ELECTROHYDRAULIC FRAGMENTATION FOR PROCESSING ELECTRIC ARC FURNACE SLAGS

Yergeshev Akim Ruslanovich, Tokpayev Rustam Rishatovich, Khavaza Tamina Narimanovna, Karmeyeva Marina, Nauryzbayev Mikhail Kasymovich, Ignatkina Vladislava Anatolyevna 381
REFRACTORY POLYMETALLIC ORES BY FLOTATION. DIRECTIONS FOR IMPROVING METALLURGICAL BALANCE

Valentine A. Chanturia, Igor Zh. Bunin, Maria Ryazantseva 389
THE USE OF DIELECTRIC BARRIER DISCHARGE TO REGULATE THE TECHNOLOGICAL PROPERTIES OF CHALCOPYRITE AND SPHALERITE

Luis Verdugo, Barbara Etschmann, Maryam Abdus-Salam, Andrew Hoadley, Jorge Menacho, Joel Brugger 395
MECHANOCHEMICAL LEACHING OF CHALCOPYRITE IN LOW MOISTURE CONDITIONS

Miomir Mikić, Milenko Jovanović, Radmilo Rajković, Daniel Kržanović, Sandra Milutinović 401
RECULTIVATION PROCEDURE OF FLOTATION TAILINGS AT THE LOCATION OF RTH IN BOR

Vandana Kumari Jha, Christophe Duwig, Samaneh Teimouri, Kerstin Forsberg 407
METAL RECOVERY FROM SPENT BATTERIES THROUGH ANTISOLVENT CRYSTALLIZATION IN A T-MIXER USING A COUPLED CFD-PBE APPROACH

Luka Ceyssens, Nina Miladinović, Giuseppe Granata, Tom Van Gerven 413
MECHANOCHEMICAL ACTIVATION OF ARGON OXYGEN DECARBURIZATION SLAGS FOR IMPROVED MINERAL CARBONATION

Miomir Mikić, Vesna Marjanović, Emina Požega, Radmilo Rajković 416
TREATMENT OF ACIDIC MINE WATERS BY THE NEUTRALIZATION PROCESS

Julio Valenzuela Elgueta, Silvia Ahualli Yapur, Angel Vicente Delgado Mora 422
INFLUENCE OF CATIONIC SURFACTANTS ON THE ELECTROKINETIC PROPERTIES AND STABILITY OF SILICA-KAOLINITE SUSPENSIONS UNDER COPPER HYDROMETALLURGY CONDITIONS

Dragana Medić, Maja Nujkić, Žaklina Tasić, Vladan Nedelkovski, Stefan Đorđievski, Slađana Alagić, Snežana Milić 429
CHARACTERIZATION OF ELECTRODE MATERIALS FROM SPENT BATTERIES IN THE PROCESS OF RECOVERING VALUABLE METALS

Stefan Đorđievski, Dragana Adamović, Miloš Đukić, Ana Petrović, Jelena Petrović, Zoran Štirbanović 435
IMPROVEMENT OF BOR RIVER WATER QUALITY THROUGH TREATMENT AND RECIRCULATION OF MINING AND METALLURGICAL WASTEWATER

Kristina Pavićević, Danica Jovašević, Maja Rajković, Ivana Jelić, Marija Janković, Marija Šljivić-Ivanović 441
BIOCHAR IN WASTEWATER REMEDIATION: A BRIEF REVIEW OF CHARACTERISTICS AND PREPARATION MATERIALS

Semra Kurama, Hüseyin Boğaç Poyraz, Zahide Bayer Öztürk 449
A PROPOSAL FOR ZERO WASTE IN THE IRON AND STEEL INDUSTRY: ZIRCONIA NOZZLE WASTE EVALUATION

Boris Borche Fidanchev, Afrodita Zendelska 457
NEW SAG-BALL MILL AND FLOTATION LINE FOR RECONSTRUCTING OF “ZLETOVO” FLOTATION PLANT-PROBISHTIP, NORTH MACEDONIA

Nela Vujović, Vesna Alivojvodić, Dragana Radovanović, Marija Štulović, Miroslav Sokić, Filip Kokalj 463
POTENTIAL OF RECYCLING AND REUSE MINING WASTE IN SERBIA: CHALLENGES AND PROSPECTS

Haldun Kurama 469
DISSOLVED AIR FLOTATION: IS IT REALLY A SUITABLE SOLUTION FOR INDUSTRIAL PURIFICATION PROCESSES?

Carmen M. Neculita, Flavia L. Braghiroli 476
VALORIZATION OF RESIDUAL MATERIALS IN THE PREVENTION AND TREATMENT OF CONTAMINATED MINE WATER AND AIR

Vladimir Topalović, Ana Vujošević, Anja Antanasković, Veljko Savić, Marija Djošić, Zorica Lopičić, Jelena Nikolić 483
CHEMICAL STABILITY AND FERTILIZER EFFICIENCY OF BIOGLASS AND BIOCHAR ON ROSE PLANTINGS

Vladimir Topalović, Veljko Savić, Marija Djošić, Danijela Smiljanić, Snežana Zildžović, Snežana Grujić, Jelena Nikolić 490
THE EFFECT OF FLUXING AGENT CATIONS IN FLY ASH-BASED GLASS ON CHEMICAL STABILITY

Aleksandar Cvetković, Marija Petrović Mihajlović, Žaklina Tasić, Milan Radovanović, Ana Simonović, Vladan Nedelkovski 497
INFLUENCE OF ORGANIC COMPOUND STRUCTURE ON BRASS CORROSION INHIBITION EFFICIENCY

Aleksandar Cvetković, Vladan Nedelkovski, Dragana Medić, Sonja Stanković, Žaklina Tasić, Milan Radovanović, Snežana Milić 503
WASTE TO RESOURCE TRANSFORMATION: INNOVATIVE APPROACHES TO RECYCLING CATHODE MATERIALS FROM LITHIUM-ION BATTERIES

Gašper Tavčar, Davide Mombelli, Carlo Mapelli, Gianluca Dall'Osto, Dragan Radulović, Ivica Ristović, Mateusz Ciszewski, Jasna Kastivnik, Ana Mladenovič, Alenka Mauko Pranjič 509
OPTIMIZING METAL RECOVERY FROM EAF DUST: A COMPREHENSIVE APPROACH BEYOND THE WAELZ KILN PROCESS

Amir Mohammad Bidmeshki, Mahmoud Abdollahy 515
SOLVENT EXTRACTION OF La, Ce, AND Nd ELEMENTS FROM THE NiMH BATTERIES LEACH SOLUTION

Igor Zh. Bunin 522
LOW-TEMPERATURE ATMOSPHERIC PLASMA IN THE COMPLEX PROCESSING OF HARD-BENEFICIATION MINERAL RAW MATERIALS

Xiaopeng Peng, Lijie Guo, Xingshan Jin 529
THE STUDY ON THE STRESS CHARACTERISTICS OF BACKFILL BARRICADE IN UNDERGROUND METAL MINES BASED ON SIMULATION EXPERIMENTS

Sonja Stanković, Vladan Nedelkovski, Milan Radovanović, Stefan Đorđievski, Dragana Medić, Snežana Milić 537
SUSTAINABLE PRODUCTION OF GRAPHENE OXIDE AND ZINC OXIDE NANOPARTICLES FROM SPENT Zn-C BATTERIES

Jasna Kastivnik, Gašper Tavčar, Dragan Radulović 543
ENHANCING EU ECONOMIC RESILIENCE: EXPLORING NEW SOURCES AND BENEFICIATION OF CRITICAL RAW MATERIALS NIOBIUM AND TANTALUM FROM CENTRAL AFRICA

Džafer Dautbegović, Mirsada Hasanbašić 549
THE IMPACT OF THE TRANSFER STATION ON THE ORGANIZATION OF MUNICIPAL WASTE COLLECTION

Genc Demi, Bukurosh Koci, Islam Nika 556
RECYCLING OF CHROMIUM TAILINGS IN BULQIZA PLANT

Mafeni Samuel Ramatsoma, Veruska Govender, Deshenthree Chetty, Olga Bazhko 562
KINETIC AMD PREDICTION FOR A MINE TAILINGS DUMP: A SOUTHERN AFRICAN MINE CASE STUDY

Dragan S. Radulović, Jovica Stojanović, Gašper Tavčar, Vladimir Jovanović, Dejan Todorović, Branislav Ivošević, Sonja Milićević 568
CHARACTERIZATION OF AN ORE SAMPLE FROM CONGO BASED ON TANTALUM AND NIOBIUM FOR POSSIBLE FURTHER TECHNOLOGICAL TESTS

Dragan S. Radulović, Jovica Stojanović, Grozdanka Bogdanović, Vladimir Jovanović, Dejan Todorović, Branislav Ivošević, Vladimir Simić 575
STUDY OF MINERALOGICAL AND PHYSICOCHEMICAL PROPERTIES OF SAMPLES OF FLOTATION TAILINGS "RUDNIK“ MINE

Sara Živojinović, Živko Đorović, Miloš Vuleta 581
OPTIMIZATION RECYCLING IN IRON AND STEEL METALLURGY: UTILIZATION OF BY-PRODUCTS FOR EFFICIENCY AND SUSTAINABILITY

Aleksandra Milosavljević, Marijana Pavlov - Kagadejev, Ana Kostov 587
IR CAMERA APPLICATION IN CONTROL OF THE CURRENT STATE OF AN INDUCTION FURNACE IN LABORATORY CONDITIONS

Kostović Milena, Bajić Sanja 592
WASTE FOUNDRY SAND REGENERATION

Ilhan Bušatlić, Nadira Bušatlić, Nevzet Merdić, Nedžad Haračić, Lejla Mujezinović 598
GEOPOLYMERS BASED ON FLY ASH WITH THE ADDITION OF GRANULATED BLAST FURNACED SLAG

Sadaf Samadi-Tavanaa, Saeid Karimi, Mehdi Pourabdoli, Zoran Štirbanović 605
RECYCLING OF PRINTED CIRCUIT BOARDS (PCBS) USING VARIOUS DEEP EUTECTIC SOLVENTS (DESS) AND INSIGHTS FROM DFT SIMULATIONS

Kristina Muntu, Jean-Gabriel Fraboulet, Sean Salour, Christine Bonnet, Enkhzul Bayarmagnai, Brian K. Cook, Massoud Aghamirian 613
VARIABILITY IN FLOTATION PERFORMANCE OF LEPIDOLITE SAMPLES FROM THE EMILI DEPOSIT, FRANCE

Titus Nghipulile, Theophile Mwaku, Godfrey Dzinomwa, Benjamin Mapani, Jaquiline Tatenda Kurasha 620
REPROCESSING OLD MINE TAILINGS TO RECOVER COPPER AND PRECIOUS METALS USING FROTH FLOTATION

Sonja Milićević, Jovica Stojanović, Ivana Jelić, Snežana Zildžović, Vladimir Jovanović, Dejan Todorović 626
ZEOLITE ACID (UN)STABILITY AS MAJOR DISANDVANTAGE FOR ITS HUMAN CONSUMPTION

Paweł Tomach, Jacek Feliks, Marta Łuczak, Grzegorz Fabijański 632
INVESTIGATION OF ULTRA-FINE GRINDING OF AGGLOMERATED BASALT DUST

Francesco Ferella, Svetlana B. Zueva, Ionela P. Birloaga, Valentina Innocenzi, Nicolò M. Ippolito, Francesco Vegliò 639
PRODUCTION OF HIGH-PURITY QUARTZ FOR OPTICAL APPLICATIONS

Roshanak Adavodi, Adriana Zuffranieri, Soroush Rahmati, Pietro Romano, Francesco Ferella, Francesco Veglio' 646
SELECTIVE EXTRACTION OF MOLYBDENUM, NICKEL, AND COBALT FROM SECONDARY RESOURCES USING BIFUNCTIONAL IONIC LIQUIDS

Predrag Stolić, Zoran Jovanović, Željko Mravik, Marko Jelić, Sonja Jovanović 652
SELECTED ASPECTS OF SENSOR APPLICATION IN THE DESIGN AND IMPLEMENTATION OF INTELLIGENT INSTRUMENTATION FOR RECYCLING SYSTEMS

Maja Trumić, Katarina Balanović, Tamara Gavrilović 659
PREDICTION OF RESULTS OF FLOATATION PROCESS USING ARTIFICIAL NEURAL NETWORKS

Tomasz Suponik, Paweł Friebe, Umut Kar, Dawid Franke, Pengbo Chu 665
FINANCIAL AND TECHNOLOGICAL POTENTIAL OF ECO-EFFICIENT RECYCLING OF WASTE ELECTRONIC EQUIPMENT

David Oluwasegun Afolayan, Adamu Hassan Abubakar, Samuel Olumide Ogunmodimu 674
GRAVITY CONCENTRATION OF FINE PARTICLES COMPLEX ORES-CONTAINING BARYTE USING LABORATORY-BUILT MINERAL JIG

Olajuyi Seun Isaiah, Afolayan David Oluwasegun, Ogunmodimu Samuel Olumide 681
PRELIMINARY INVESTIGATION ON NIGERIAN LITHIUM ORES FOR EFFICIENT LITHIUM OXIDE EXTRACTION

Anđelija Bogdanović, Hassene Affouri, Ivan Kojić, Ksenija Stojanović 690
ORIGIN, DEPOSITIONAL ENVIRONMENT AND MATURITY OF ORGANIC MATTER IN EOCENE COALS FROM TUNISIA

Andriela Dutra Norberto de Oliveira, Luis Gonzaga Santos Sobral, Armando Lucas Cherem da Cunha 696
THE INFLUENCE OF DIFFERENT FORMS OF MINERAL PROCESSING ON THE BIO-OXIDATION OF SULPHIDE MINERALS BEARING GOLD

Andriela Dutra Norberto de Oliveira, Luis Gonzaga Santos Sobral, Armando Lucas Cherem da Cunha 702
BIODESULPHURISING HIGH SULPHUR CONTENT TAILINGS FROM COAL MINING IN BRAZIL

ABSTRACTS 707

Maria Cristina Vila, Maria Lurdes Dinis, Laura Ferrando-Climent, Nirosham Gajendra, Deniz Avsar, Duygu Yilmaz, Erika Levei, Iulia Török 709
INNOVATIVE PRE-FEASIBILITY STUDIES TOWARDS THE SUSTAINABLE PRODUCTION OF RARE EARTH CONCENTRATES FOR SELF-SUPPLY IN EUROPE

Randal Tzeou Hah Fauline, Agnès Grandjean, Antoine Leydier, Emeric Brun, Florian Herbelet, Xavier Heres, Justine Taurines 711
MODELING AND SIMULATION OF SOLID PHASE EXTRACTION FOR LEACHED ORE PURIFICATION

Michelle Airah N. Pablo, Joshua P. Pocaan, Jacob Louies Rohi W. Paulo, Piolo N. Gervacio, Arnel B. Beltran, Carla Mae J. Pausta, Aileen H. Orbecido 712
LEACHING OF CALCIUM FROM PHOSPHOGYPSUM FOR CARBON SEQUESTRATION

Michael Angelo B. Promentilla 713
A PROBLEMATIQUES APPROACH FOR UNDERSTANDING CIRCULAR ECONOMY INTEGRATION BARRIERS IN THE MINING AND MINERAL PROCESSING SECTOR

Joshua Pocaan, Brian Gerald Bueno, Jaica Mae Pagaduan, Aileen Orbecido, Carlito Tabelin, Ana Santos, Anne Jungblut, Vannie Joy Resabal, Renan Ma. Tanhueco, Michael Angelo Promentilla, Arnel Beltran 714
DEVELOPMENT OF LIMESTONE-BASED PASSIVE TREATMENT SYSTEM FOR COPPER-RICH ACID MINE DRAINAGE

Mathilde **Perrin,** Emmanuel **Billy** 715
BLACKMASS FLOTATION OF END-OF-LIFE BATTERIES: HOW TO DO WITHOUT PRE-TREATMENT?

PLENARY LECTURES

XVI International Mineral Processing
and Recycling Conference
28-30 May 2025, Belgrade, Serbia

DOI: 10.5937/IMPRC25003B Original research article

A MINERAL’S JOURNEY – UNRAVELLING FLOTATION PHENOMENA THROUGH PARTICLE TRACKING

Pablo R. Brito-Parada[#], 0000-0001-6252-246X,
Department of Earth Science and Engineering, Imperial College London,
London, United Kingdom

ABSTRACT-Froth flotation is one of the most important separation techniques in mineral processing, yet studying the complexities of particle dynamics within flotation cells is very challenging. Positron Emission Particle Tracking (PEPT) offers a unique approach to investigate the complex behaviour of mineral particles within flotation cells, by tracing the trajectories and velocities of individual particles, thus providing unprecedented insights into their behavior within the pulp and froth phases. The insight into particle behaviour, both for valuable minerals and gangue, is particularly relevant when assessing the effect of changes in flotation cell design. This paper showcases the capability of PEPT to provide a deeper understanding of the fundamental mechanisms at play in froth flotation, and highlights some of the challenges and opportunities for future research.

Keywords: Positron Emission Particle Tracking, Froth Flotation, Flotation Cell Design, Flotation Optimisation.

INTRODUCTION

Positron Emission Particle Tracking (PEPT) is a non-invasive technique that allows the tracking of the position of a tracer particle within a container over time. Unlike methods relying on visual transparency, PEPT's ability to "see through" materials makes it ideal for studying opaque, high-solids fraction environments, like flotation cells.

PEPT makes use of positron emission tomography (PET) [1], a common medical imaging method, but employing particle tracers. In PEPT, a radioactive tracer particle emits positrons, which then annihilate with nearby electrons, producing a pair of back-to-back gamma rays. When a PET scanner simultaneously detects these γ-rays, the annihilation point is located along the line connecting the detectors. By gathering numerous such lines of response (LoRs), the moving tracer particle's position can be tracked over time through triangulation [1].

PEPT has been used in flotation research to study particle dynamics in different flotation equipment [2-4] and recent studies have used PEPT to assess the effect of different design modifications on flotation hydrodynamics [3,5].

This paper will focus on examples of flotation cell design modifications, specifically the effects of two impeller designs on flotation hydrodynamics.

[#] corresponding authorp.brito-parada@imperial.ac.uk

EXPERIMENTAL

Flotation cell, impeller design, and reagent system

Experiments were carried out in a 4-litre continuously overflowing bench-scale flotation cell designed to run flotation experiments so that they can achieve steady-state. This is achieved by recirculating the concentrate into the tank.

Two impeller designs were considered, both of 60 mm diameter, a standard Rushton turbine and a rotor system similar to the Outokumpu OK rotor. The effect of a stator was also considered. Fig 1 shows the dimensions and positions of the rotor and impeller designs within the bench-scale cell.

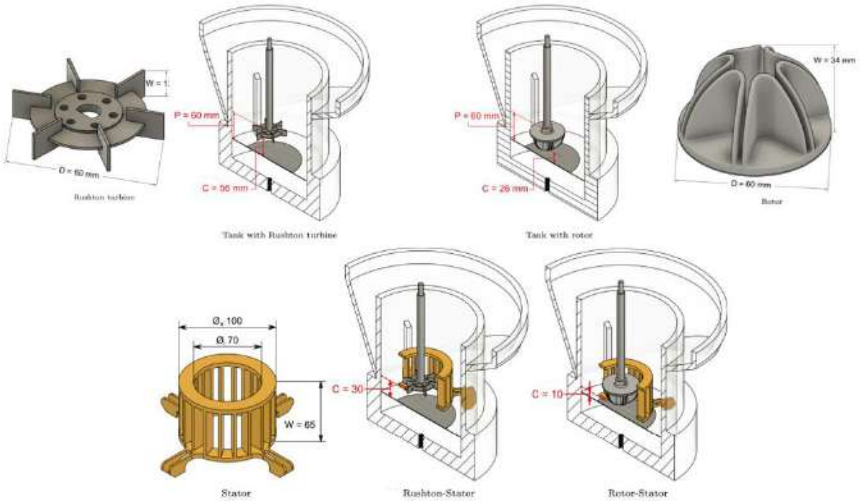

Figure 1 Dimensions and position in the flotation cell of the Rushton turbine and OK rotor system, as well as the stator used for the experiments

The slurry consisted of glass beads (75 µm-150 µm), which were used to prepare a pulp with 20% solid content by weight. The frother used was Dowfroth 250 (Nasaco) at 4 ppm and Tetradecyltrimethylammonium bromide, TTAB (Sigma Aldrich), was used as the collector at 4 g t^{-1}.

PEPT experiments

Tests were conducted at iThemba LABS, South Africa, using a Siemens HR++ PET camera. For the tests, superficial gas velocity was set as 0.98 cm s^{-1} (15 lpm air flow) and impeller speed at 1200 RPM, with a froth depth of 4 cm. Tracer particles consisted of 68Ga-labelled Purolite NRW100 resin beads, prepared by elution from a 68Ge/68Ga generator and subsequent mechanical agitation. The tracers were coated with epoxy resin to create hydrophilic tracers or with an additional silanized ballotini layer for hydrophobic tracers. Full details of the PEPT methodology can be found in Cole et al. [6]. Initial tracer activities ranged from 700 µCi to 1600 µCi, with coated diameters between 450 µm and 600 µm.

RESULTS AND DISCUSSION

Velocity data is analysed by decomposed it into its vectorial components, considering the peak of a Gaussian kernel estimation of the probability density function fitted to the data in each voxel. Figures 2-3 show the vertical velocities for the hydrophilic and hydrophobic tracers, respectively. In the figures, pathlines are also shown that represent the tracer average trajectories, which are calculated from the vertical and radial velocity components.

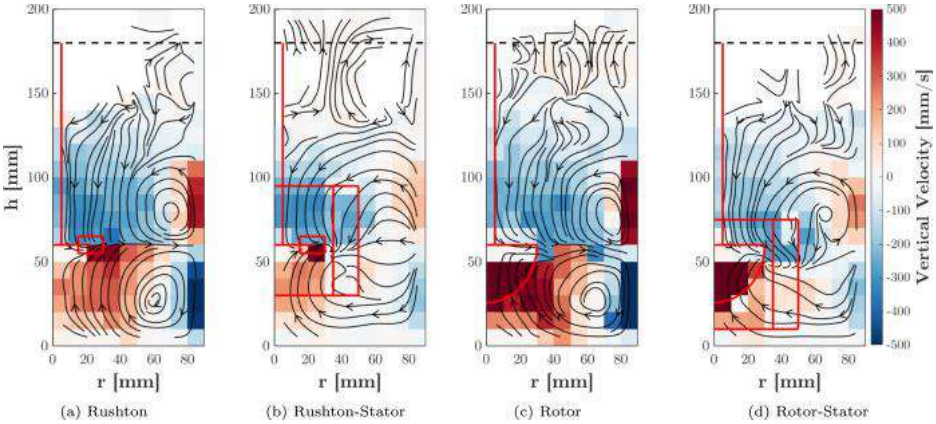

(a) Rushton (b) Rushton-Stator (c) Rotor (d) Rotor-Stator

Figure 2 Vertical velocity of the hydrophilic tracer extracted from PEPT data. Subfigures show the different impeller designs studied (with the impellers and stator designs shown in red lines). Particle trajectories are shown as black arrows.

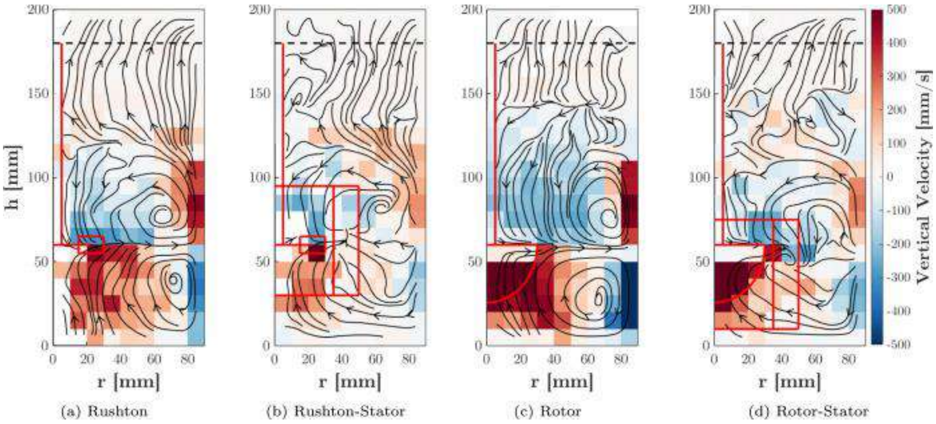

(a) Rushton (b) Rushton-Stator (c) Rotor (d) Rotor-Stator

Figure 3 Vertical velocity of the hydrophobic tracer extracted from PEPT data. Subfigures show the different impeller designs studied (with the impellers and stator designs shown in red lines). Particle trajectories are shown as black arrows.

The results show that the impellers, in the absence of a stator, produce a radial behaviour, with two mixing loops observed from the pathlines. When the stator is present, it modifies the hydrodynamics of the system, affecting these loops.

Interestingly, the average vertical velocities in the lower pulp region were similar for different tracers with each impeller, suggesting that fluid dynamics primarily govern particle motion in this zone, irrespective of surface properties. Conversely, vertical velocities in the upper pulp-froth interface and froth zone varied with tracer type, where hydrophobic particles ascended and hydrophilic particles exhibited downward flow. Comparing impellers, the rotor generated faster vertical flows in the pulp mixing zone, particularly in the lower loop. The presence of a stator reduced vertical velocities outside the impeller-stator region, especially near the cell walls.

To further analyse the difference between designs in a statistically robust way, and to avoid bias in the testing to the normality of the velocity distributions for each voxel, a non-parametric approach, the Jensen–Shannon distance, is calculated. This is a statistical metric that determines the similarity between two probability distributions and is calculated as the square root of the Jensen–Shannon divergence. Using this metric, Figure 4 shows distinct vertical velocity profiles between the rotor and rotor-stator configurations. While the stator generally reduces modal vertical speeds in the pulp zone (except a localized high-speed region between rotor and stator), the overall velocity distributions, particularly at the base, remain statistically similar according to the Jensen-Shannon distance. In the froth zone, the rotor-stator design appears to hinder hydrophilic particle entrainment, resulting in statistically different froth hydrodynamics compared to the rotor alone. Conversely, for hydrophobic tracers, the stator leads to significantly faster flows at the pulp-froth interface and within the froth, suggesting enhanced froth recovery.

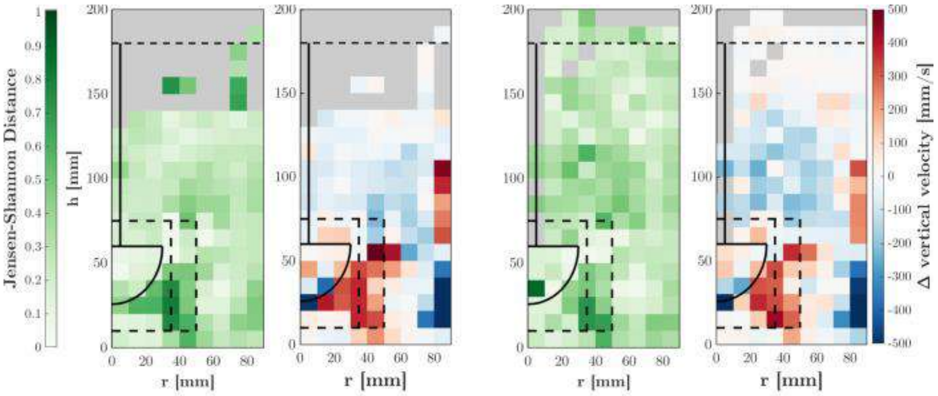

(a) Hydrophilic tracer

(b) Hydrophobic tracer

Figure 4 Comparison of vertical velocity between the rotor and the rotor–stator designs using a (a) hydrophilic and (b) hydrophobic tracer. The Jensen–Shannon distance between the velocity distributions are shown (green voxels) on the left of each subfigure, whereas on the right side, the modal vertical velocity difference between both designs is shown

Other valuable information that can be obtained from the PEPT date includes occupancy values, which show the zones where the tracers spent more time in the vessel, as well as radial velocity, which in particular has proven to provide insight into key phenomena near the pulp-froth interface. This additional analyses, as well as an overview of the latest developments in PEPT for froth flotation, along with the challenges and future work envisioned, will be presented as part of the plenary presentation.

CONCLUSION

PEPT is a powerful technique that can be used to further our understanding of flotation cell hydrodynamics. In particular, PEPT data can be exploited to assess the effect that changes in flotation cell design have on various key phenomena within the system. This paper has shown an example of the potential of PEPT to study impeller designs and stators in flotation cells under typical high solid-content three-phase conditions. By tracking hydrophobic and hydrophilic tracers, the influence of the designs on particle behaviour and motion is analysed, thus providing quantitative characterization of the hydrodynamic modifications.

This work showed that the stator reduces particle velocities outside the impeller-stator region, likely due to turbulence dissipation, and diminishes swirl motion not only at the impeller but also at the pulp-froth interface, leading to a more stable froth zone. Statistical analysis using the Jensen-Shannon distance confirmed that the stator significantly alters pulp zone hydrodynamics, creating velocity profiles distinct from those without a stator, and substantially impacts both the pulp-froth interface and the froth zone. These findings, consistent with reported improvements in air and metallurgical recovery for the same impeller designs with a stator, highlight the importance of considering impeller and stator design effects on the froth zone to optimize flotation performance.

ACKNOWLEDGEMENT

The work in this paper, and other research on PEPT to study froth flotation to be presented as a plenary talk at IMPRC 2025, is the result of collaborative research on this topic. The author acknowledges the valuable contributions of colleagues including K. Cole, D. Mesa, S. Neethling, J. Cilliers, M. van Heerden, and R. Perin.

REFERENCES

1. Parker, D.J., Broadbent, C.J., Fowles, P., Hawkesworth, M.R., McNeil, P. (1993) Positron emission particle tracking - a technique for studying flow within engineering equipment. Nucl. Instrum. Methods Phys. Res. A, 326 (3), 592-607.
2. Waters, K.E., Rowson, N., Fan, X., Parker, D., Cilliers, J.J. (2008) Positron emission particle tracking as a method to map the movement of particles in the pulp and froth phases. Min. Eng., 21 (12–14), 877-882.
3. Mesa, D., Cole, K., van Heerden, M.R., Brito-Parada, P.R. (2021) Hydrodynamic characterisation of flotation impeller designs using Positron Emission Particle Tracking (PEPT). Separation and Purification Technology 276, 119316.

4. Mesa, D., Hampel, D.M., Neethling, S.J., Kokalova Wheldon, T., Brito-Parada, P.R. (2024) Characterisation of the multiphase fluid dynamics of the CoarseAIR™ fluidised bed flotation cell using the Large Modular Array (LaMA) for positron emission particle tracking (PEPT). Minerals Engineering 211, 108700.
5. Cole, K., Mesa, D., van Heerden, M., Brito-Parada, P.R. (2023) Effect of Retrofit Design Modifications on the Macroturbulence of a Three-Phase Flotation Tank – Flow Characterization Using Positron Emission Particle Tracking (PEPT). Industrial & Engineering Chemistry Research 62 (19), 7580–7591.
6. Cole, K., Barker, D.J., Brito-Parada, P.R., Buffler, A., Hadler, K., Mackay, I., Mesa, D., Morrison, A.J., Neethling, S., Norori-McCormac, A., Shean, B., Cilliers, J. (2022) Standard method for performing positron emission particle tracking (PEPT) measurements of froth flotation at PEPT Cape Town. MethodsX 9, 101680.

XVI International Mineral Processing
and Recycling Conference
28-30 May 2025, Belgrade, Serbia

DOI: 10.5937/IMPRC25009S Original research article

RECOVERY OF VALUABLE METALS FROM BAUXITE RESIDUE (BR) USING DECARBONIZING TECHNOLOGIES

Srecko Stopic[1#], 0000-0002-1752-5378,
Duško Kostić[1,2], 0000-0002-4115-8571,
Mitar Perušić[2], 0000-0001-9335-1405,
Richard Schneider[1], 0009-0008-9321-0547,
Bernd Friedrich[1], 0000-0002-2934-2034,
[1]IME Process Metallurgy and Metal Recycling, RWTH Aachen University, 52056 Aachen, Germany
[2]Faculty of Technology Zvornik, University of East Sarajevo, Karakaj 34A, 75400 Zvornik, Republic of Srpska, Bosnia and Herzegovina

ABSTRACT – Bauxite residue, also known as red mud (RM) is waste produced during alumina production in Bayer process. It is posing a significant threat to the enivorment due to its high alklalinity, fine particle size and complex structure various compounds. This study presents a sustainable, approach to its utilization, with focus on the recovery of valuable metals such as titanium. Different decarbonizing technologies were used presented in this work: hydrogen reduction without smelting in rotary kiln, high pressure leaching in an autoclave, ultrasonic spray pirolysis and aluminothermic reduction. Firstly red mud was subjected to hydrogen reduction in order to selectively remove iron, which can be used and transfered in the steel industry. Separation of Iron and solid residue was done using magnetic property of iron and magnetite, Solid residue is further processed in acid leaching with high pressure of oxygen in an autoclave. Leaching process optimizes various process parameters to extract titanium in the form of titanium oxy sulfate as well as iron and aluminium. Additionally, aluminum and iron solutions were also obtained by this process. The remaining solid residue, primarily composed of calcium sulphate and silica, was evaluated for potential use as an adsorbent in wastewater treatment. This innovative process demonstrates an efficient method of bauxite residue utilization with near zero waste concept, offering a promising solution to both environmental and industrial challenges. The planned improvement of proposed research strategy can be reached using solvent extraction and remelting process.

Keywords: Hydrogen plasma reduction, Bauxite residue, Leaching, Zero-waste.

INTRODUCTION

Since its reactivity makes it difficult to get in pure form, Ti, one of the most plentiful metals in the Earth's crust, has only been manufactured on an industrial scale since the 1950s. Titanium was discovered in 1791. With a high melting point and exceptional resistance to corrosion, it is a light metal. An essential white pigment is its oxide. Titanium possesses excellent mechanical properties, unrivalled corrosion resistance, and biocompatibility. Still, it is restricted to some niche applications due to its high embodied

---

[#] corresponding author: sstopic@ime-aachen.de energy consumption and production cost [1]. “Decarbonisation” means switching from the use of fossil fuels such as coal, natural gas or oil to carbon-free and renewable energy sources as quickly as possible. Recovery of valuable metals from bauxite residue using decarbonizing technologies contains hydrogen reduction of bauxite residue, acidic leaching of solid residue, ultrasonic spray pyrolysis of water solution to produce titanium oxide and aluminothermic reduction.

Hydrogen reduction of bauxite residues was performed in tubular furnace without smelting process [2] and in electric arc furnace with formation of metallic Fe and slag [3] in static conditions. The separation of iron and formed solid residue was performed using magnetic separation, what takes time and bring different metal losses. Therefore, a H_2-reduction process of BR in rotary kiln in dynamic conditions is studied in this work.

In the case of the reduction of stable oxides such as titanium oxides, metallothermic reduction is required for the synthesis of metal alloys. Synthesis of as-cast Ti-Al-V Alloy from titanium-rich material was performed by aluminothermic reduction [4]. According to the thermochemical analysis, the method of synthesizing as-cast Ti-Al-V alloys through aluminothermic reduction is feasible. The synthesis reaction is a liquid–solid reaction. Process parameters such as slag-metal separation and the heat introduced into the system are adjusted by adding additives such as $KCLO_4$ and CaO. Extraction of Ti allied with the realization of low-oxygen Ti via deoxygenation [5].

Al-Ti alloys were electrodeposited from equimolar chloroaluminate molten salts containing up to 0.1 M of titanium ions, which were added to the electrolyte by potentiostatic dissolution of metallic Ti [6]. Titanium dissolution and titanium and aluminum deposition were investigated by linear sweep voltammetry and chronoamperometry at 200 and 300 ◦C.

Ultrasonic spray pyrolysis is a flexible technique used for producing metallic, oxidic and composite powders. Using titanium oxy sulphate the primary product of the USP method is predominantly titanium dioxide [7]. The obtained titanium-based powders between 700°C and 1300°C had spherical morphology with different particle sizes, from nanometer to submicron, depending on the influence of reaction parameters.

The preparation of the precursor titanium oxy sulfate was performed using high pressure leaching of titanium and aluminum residues from different metallurgical processes [8, 9]. The leaching experiments conducted on both Tionite S and slag after reduction in electric arc furnace using 5 M sulfuric acid under varying conditions of temperature, oxygen pressure, and reaction time offer valuable insights into the effectiveness of the leaching process for extracting iron (Fe), titanium (Ti), and aluminum (Al). The results highlight significant differences in the leaching behaviors of these two materials, which can be attributed to their distinct mineralogical properties and thermal histories.

MECHANISM OF DECARBONIZING PROCESSES

In this work the four decarbonizing processes are considered: 1) hydrogen reduction of red mud; 2) acidic dissolution of solid residue forming titanium oxy sulphate, 3) ultrasonic spray pyrolysis of titanium oxy sulphate in hydrogen and oxygen atmosphere producing TiO_2, and 4) Production of titanium-aluminum vanadium alloys during aluminothermic reduction

Hydrogen reduction of red mud

Reduction by hydrogen, even with small ratios of H_2/red mud lead to reduction of Fe_2O_3 to Fe and transformation of CoO and NiO to metallic forms. All these components can be easily recovered by magnetic separation. Reduction of hematite by hydrogen proceeds in two or three steps, under and above 570 °C, respectively, via magnetite (Fe_3O_4) and wustite (FeO) according to the following equations:

$3Fe_2O_3 + H_2 \rightarrow 2Fe_3O_4 + H_2O$ (1)

$Fe_3O_4 + H_2 \rightarrow 3\ FeO + H_2O$ (2)

$FeO + H_2 \rightarrow Fe + H_2O$ (3)

$NiO + H_2 \rightarrow Ni + H2O$ (4)

$CoO + H_2 \rightarrow Co + H_2O$ (5)

Unfortunately, the reduction of stable oxides such as aluminum oxide, titanium oxide, calcium oxide and silica is not possible with hydrogen. These oxides stay in oxidic form in solid residue, that is dissolved in the acidic leaching process.

Acidic leaching of solid residue

The obtained solid residue is dissolved with sulphuric acid.

$Fe_2O_{3(s)}+3\ H_2SO_{4(aq)} \rightarrow Fe_2(SO_4)_{3(aq)}+3\ H_2O$ (6)

$TiO_2+H_2SO_4 \rightarrow [TiO]SO_4+H_2O$ (7)

$Al_2O_3+3\ H_2SO_4 \rightarrow Al_2(SO_4)_3+H_2O$ (8)

$CaO+H_2SO_4 \rightarrow CaSO_{4(s)}+H_2O$ (9)

After dissolution with sulphuric acid under high pressure conditions, titanium will be transformed in titanium oxy sulphate and iron sulphate. Solid residue contains calcium sulphate and silica. After purification of solution from iron, titanium oxy sulphate will be used for the Ultrasonic spray pyrolysis in order to produce TiO_2.

Ultrasonic spray pyrolysis

The obtained titanium oxy sulphate is treated by ultrasonic spray pyrolysis in hydrogen, oxygen, and in neutral atmosphere.

$[TiO]SO_4 \rightarrow TiO_2 + SO_3$ (10)

$[TiO]SO_4 + H2 \rightarrow TiO + H_2SO_4$ (11)

$TiO[SO_4]+\frac{1}{2}\ O_2 \rightarrow [TiO\text{-}O]SO_4$ (12)

Generally, produced TiO_2 is used for the aluminothermic reduction.

Aluminothermic reduction of TiO_2

The relevant equations in accordance with stoichiometry for synthesizing Ti-6Al-4V alloy are as follows (the molar ratio of CaO/Al_2O_3 is 0.4¸ and the calculated adiabatic temperature amounts 1750 K.

$$3\ TiO_2 + 4\ Al \rightarrow 3\ Ti + 2\ Al_2O_3 \tag{13}$$

$$3\ V_2O_5 + 10\ Al \rightarrow 6\ V + 5\ Al_2O_3 \tag{14}$$

$$TiO_2 + 0.021\ V_2O_5 + 1.52\ Al \rightarrow 3\ Ti - 6Al - 4V + 0.70\ Al_2O_3 \tag{15}$$

$$\begin{gathered} TiO2 + 0.021\ V_2O_5 + 1.52\ Al + 0.28CaO \rightarrow 3Ti - 6Al - 4V + \\ 0.25\ CaO \cdot 2Al_2O_3 + 0.035CaO \cdot 6Al_2O_3 \end{gathered} \tag{16}$$

The chemical composition of TiAlV-Alloy can be adjusting during refining process, what is not research subject of this work.

EXPERIMENTAL

The bauxite residue from Alumina Ltd., Zvornik was filtrated, washed and dried at 105 °C for 24 h. The main components in red mud (%): 49.3 Fe_2O_3; 12.0 Al_2O_3, 10.5 SiO_2; 8.2 CaO; 4.6 TiO_2, 2.5 Na_2O, 0.9 P_2O_5, 0.6 MgO and 0.2 % Ga_2O_3. XRD-analysis of red mud after finding the following phases: hematite, perovskite, cancrinite, ilmenite, calcite, diaspore, gibbsite and hydrogarnet. Iron is present in hematite and ilmenite structure. Titanium is present in perovskite and ilmenite structures, while aluminum is present in the structure of cancrinite, diaspore, boehmite, gibbsite and hydrogarnet, as shown in Figure 1.

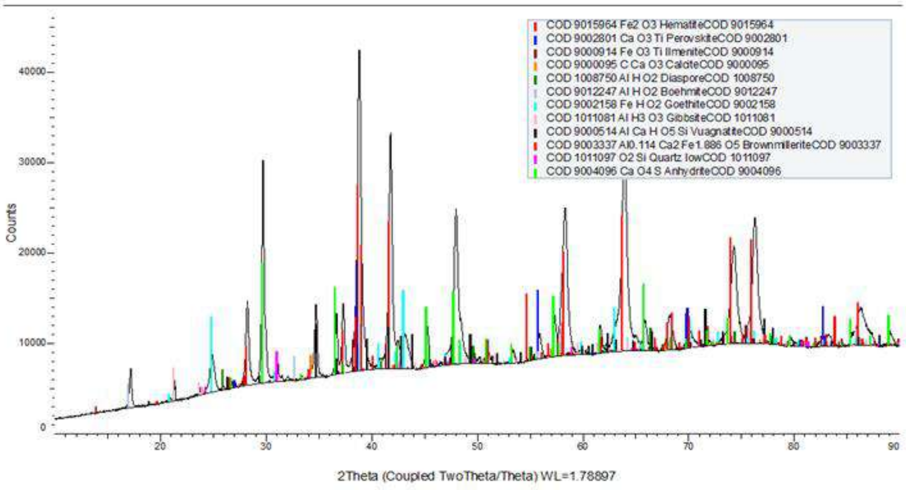

Figure 1 XRD Analysis of BR, Zvornik

The XRD-analysis in Figure 1 has confirmed the presence of hematite and other very stable oxides for hydrogen reduction. Particle size distribution analysis of BR found very fine particles with the following values ($x_{50,3}$= 4.70 µm and $x_{90,3}$= 5.98 µm). H_2-reduction of BR, Zvornik was performed using rotary kiln Carbolite, Germany, as shown in Figure 2. The used parameters for hydrogen reduction: Initial mass of sample: 200 g, temperature: 920°C, H_2 and N_2 atmosphere: flow rate: 1-2 L/min. Before the reduction, N_2- gas was used to evacuate O_2 from a cylindrical quartz tube situated in a rotary kiln, checking for leakage in system. Bubblers with demineralized water are used to check the continuous flow of gas in the system. Nitrogen is continuously supplied during heating. After successful BR reduction, the magnetic phase was separated from solid residues. H_2 reduction was performed below the iron melting point. Physical separation was employed to isolate magnetic from non-magnetic phases.

Figure 2 Rotary kiln for hydrogen reduction

This study investigates the extraction of valuable metals from reduced slag using sulfuric acid treatment. Key leaching parameters, including the solid-to-liquid ratio, pressure, and acid concentration, were maintained constant throughout the experiments. Variables such as temperature, reaction time, stirring speed, and particle size were optimized based on insights from prior experimental work. A 5 M sulfuric acid solution was prepared in a 1-liter flask and introduced into a Buchi autoclave (as shown in Figure 3), containing solid residue derived from the hydrogen reduction from the rotary kiln.

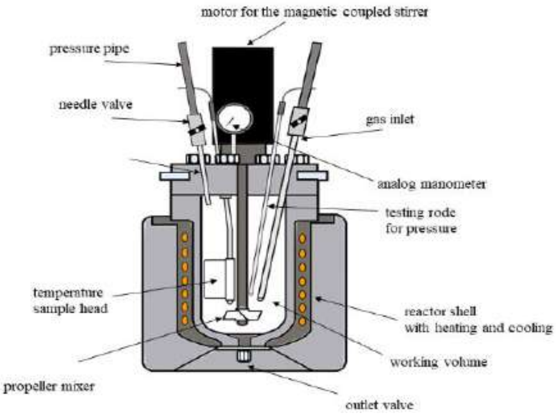

Figure 3 Illustration of the high pressure autoclave

The system was pressurized to 9 bars with oxygen, the temperature was set to the desired level, and the magnetic stirrer was operated at a speed of 500 rpm. The leaching process was conducted for up to 120 minutes. The leaching process was performed in a Buchi autoclave, Switzerland, a specialized system designed for acid leaching with a capacity of 1.53 L, a maximum pressure of 200 bars, and a maximum temperature of 270 °C, and 2000 rpm. The autoclave is equipped with a heat exchanger controlled by a thermostat, a mixer, pressure adjustment probes, and the capability for sample extraction during operation. The system is fully integrated with computer software, enabling precise control and real-time monitoring of operational parameters, with all data recorded for detailed post-experiment analysis. The pressure within the system was monitored using both a manometer and digital sensors, with the total pressure comprising oxygen (9-12 bars) and water vapour (12–15 bars). Cooling was achieved using a dedicated cooling system, and the heating rate was controlled at 10 °C/min. Prior to each run, the autoclave was manually sealed with screws and subjected to a pressure integrity test to ensure safe and reliable operation. After the leaching process was completed, the autoclave was cooled to room temperature, and the system pressure was carefully released. The leachate solution was then subjected to filtration and neutralization with distilled water. Filtration was conducted using a vacuum-assisted filtration system integrated into the setup, ensuring effective separation of solid and liquid phases.

In the USP method, the starting solution precursor is atomized to form an aerosol. These aerosol droplets are carried by a carrier gas (can be reducing gas), into a hot chamber where they undergo drying, contraction, precipitation, thermolysis, and sintering to form spherical particles. Very short residence times, typically a few seconds, are usually enough to ensure formation of spherical nanoparticles (Figure 4).

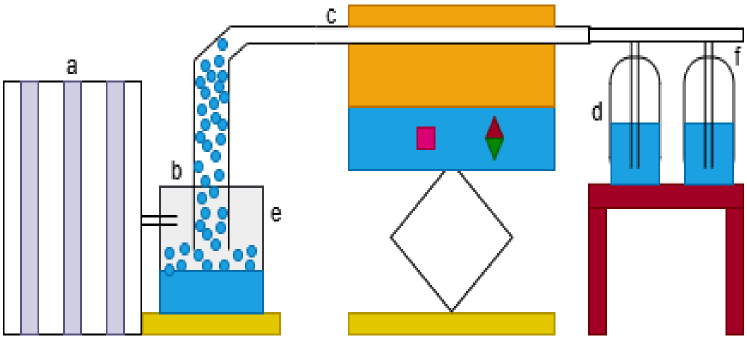

Figure 4 Scheme of USP equipment a) Gas flow regulation; (b) ultrasonic aerosol generator; (c) furnace with the wall-heated reactor; (d) collection bottles; (e) gas inlet, (f) gas outlet

Aluminothermic reduction is based on self-propagating high temperature reaction through reduction reaction of titanium oxide and vanadium oxide using aluminum powder. The reduction of titanium oxide with aluminum does not provide enough heat for self-propagation. The heat released from the reaction mixture must therefore be regulated by adding boosters such as $KClO_4$. Stoichiometrical values of Al to TiO_2 and V_2O_5 varied in order to prepare Ti60Al24V16. In order to improve the reaction behaviour and the separation of slag and metal, calcium oxide was added to the reaction vessel to adjust the melting point of the resulting slag system. The experimental setup is shown in Figure 5:

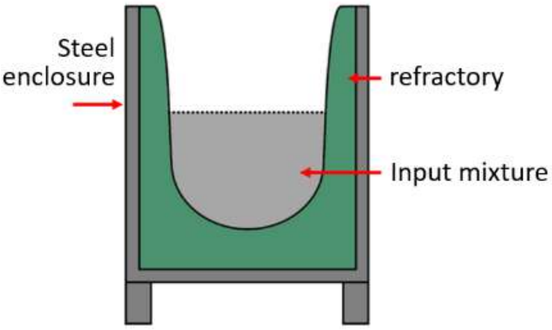

Figure 5 Aluminothermic reduction of $TiO_2$and V_2O_5 with aluminium powder

RESULTS AND DISCUSSION

Using ultrasonic spray pyrolysis method in hydrogen atmosphere we obtained ideal spherical titanium oxidic powders, as shown at Figure 6.

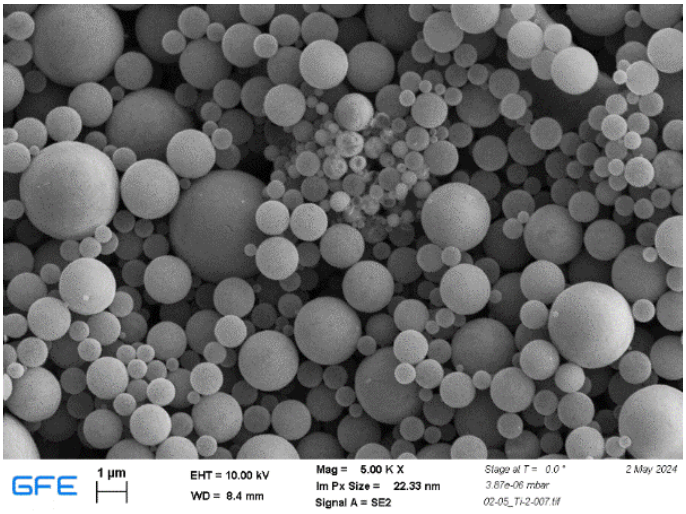

Figure 6 TiO_2-powder obtained at 1300°C using ultrasonic spray pyrolysis and hydrogen reduction

Typical EDS Analysis of obtained powder is shown at Figure 7.

In contrast to ideal spherical particles of TiO_2obtained by ultrasonic spray pyrolysis the particles of TiAlV-powder have irregular form as shown at Figure 8.

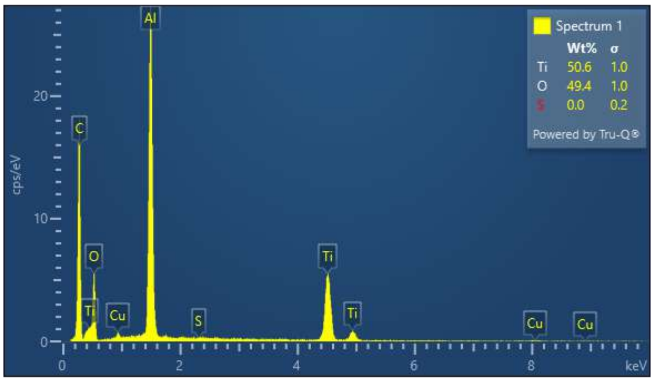

Figure 7 EDS analysis of Titanium oxide obtained at 1300°C using ultrasonic spray pyrolysis and hydrogen reduction

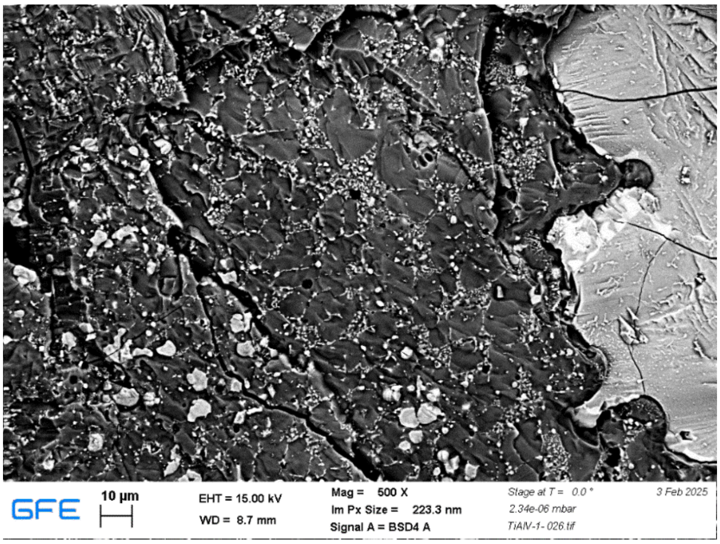

Figure 8 TiAlV-alloy obtained using aluminothermic reduction

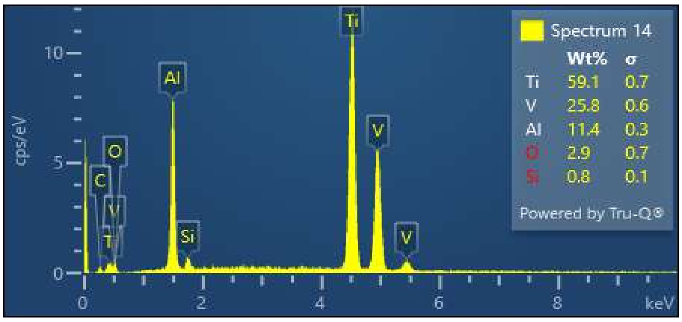

Figure 9 EDS analysis of the TiAlV-alloy obtained using aluminothermic reduction

The obtained chemical composition of TiAlV-alloys can be adjusted using refining process.

CONCLUSION

Recovery of valuable metals such as titanium from bauxite residue (red mud) was presented using different decarbonated technologies: hydrogen reduction, acidic leaching, ultrasonic spray pyrolysis and aluminothermic reduction, as shown at Figure 10.

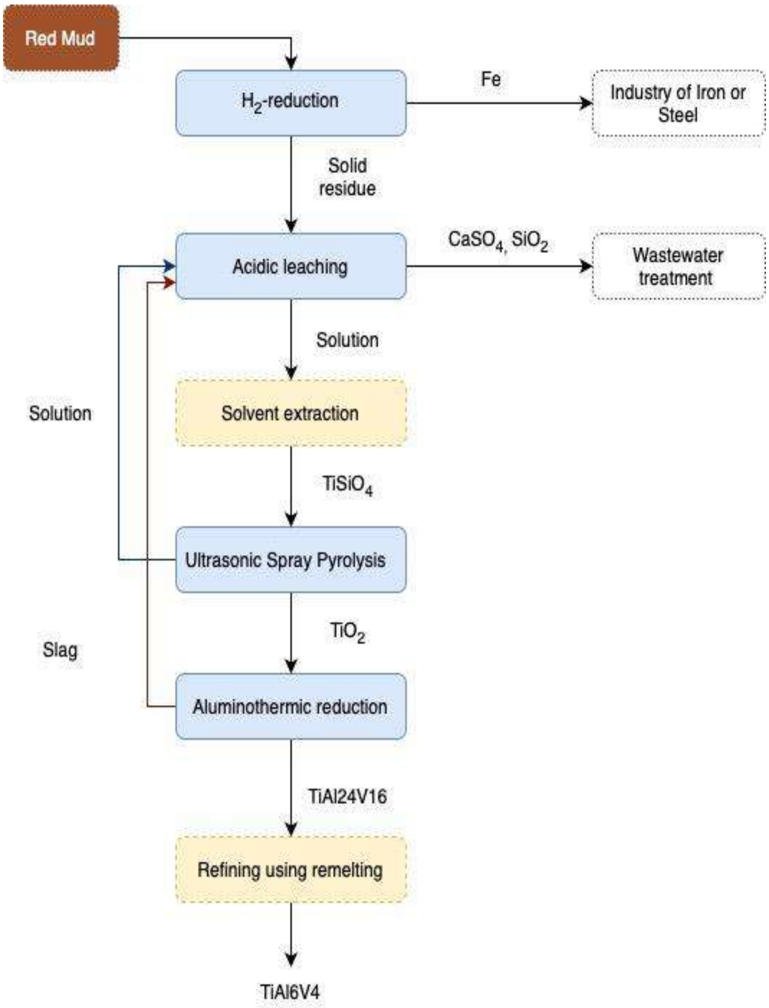

Figure 10 The proposed research strategy for treatment of red mud

The purification of solution from acidic leaching using solvent extraction and refining of TiAlV -alloy from aluminothermic reduction using of various remelting technologies (VIM, VAR) are the planned following steps as shown at Fig 10 (yellow color). Controlling of the oxygen content in the obtained metallic powders is main aim in future research in order to improve a quality of the obtained powder.

ACKNOWLEDGEMENT

This research was funded by European Commission, grant number 101135077 (EURO-TITAN).

REFERENCES

1. Williams, J.C, Rodney, R., Boyer, R.R. (2020) Opportunities and Issues in the Application of Titanium Alloys for Aerospace Components. Metals*,* 10, 705; doi:10.3390/met10060705
2. Stopić, S., Nikolić, N., Životić, D., Krstić, J., Rosić, M., Damjanović, V., Friedrich, B. (2024) Hydrogen Metallurgy for a treatment of bauxite residues-First results on the EURO-TITAN Project. Proceeding, Plenary Lecture, 1-11, XXV Yucorr Conference, Divcibare.
3. Jovičević-Klug, M., Souza Filho, R., Isnaldi Springer, H., Adam, C., Raabe, D. (2024) Green steel from red mud through climate-neutral hydrogen plasma reduction. Nature, 625, 704-717, 10.1038/s41586-023-06901-z
4. Cheng, C., Dou, Z. H., Zhang, T.A., Zhang, H. J., Yi, X., Su, J. M. (2017) Synthesis of As-cast Ti-Al-V Alloy from titanium-rich material by thermite reduction. JOM, 1-6. DOI: 10.1007/s11837-017-2467-7
5. Kumar Debajyoti, J., Xu, Y., Hayat, M., Zhang, W., Cao, P. (2021) Aiming at low-oxygen titanium powder: A review, Powder Technology, 394, 1195-1217.
6. Cvetković, V.S., Vukićević, N.M., Milićević-Neumann, K., Stopic, S., Friedrich, B., Jovićević, J.N. (2020) Electrochemical Deposition of Al-Ti Alloys from Equimolar $AlCl_3$ + NaCl Containing Electrochemically Dissolved Titanium. Metals, 10*,* 88.
7. Kostic, D., Stopic, S., Keutmann, M., Emil-Kaya, E., Volkov-Husovic, T., Perušic, M., Friedrich, B. (2024) Synthesis of Titanium-Based Powders from Titanium Oxy-Sulfate Using Ultrasonic Spray Pyrolysis. Materials, 17, 4779. https://doi.org/10.3390/ma17194779
8. Stopic, S., Kostic, D., Schneider, R., Sievers, M., Wegmann, F., Emil Kaya, E., Perušic, M., Friedrich, B. (2024) Recovery of Titanium from Red Mud Using Carbothermic Reduction and High Pressure Leaching of the Slag in an Autoclave. Minerals, 14, 1151. https://doi.org/10.3390/min14111151
9. Stopic, S., Kostic, D., Emil-Kaya, E., Uysal, E., Gürmen, S., Mitrašinovic, A., Perušic, M., Friedrich, B., (2024) High-Pressure and High-Temperature Dissolution of Titanium from Titanium and Aluminum Residues: A Comparative Study, Surfaces, 7, 1096–1108. https://doi.org/10.3390/surfaces7040072

XVI International Mineral Processing
and Recycling Conference
28-30 May 2025, Belgrade, Serbia

DOI: 10.5937/IMPRC25019A

Abstract

HOW THE RARE EARTHS BECAME THE LANTHANIDES AGAIN

Corby G. Anderson[#], 0000-0003-0193-2208,
Kroll Institute for Extractive Metallurgy, Mining Engineering Department,
Colorado School of Mines, Golden, Colorado USA

ABSTRACT – Rare Earths are vital for our modern life. Depending upon the definition they are comprised of 15 elements normally all found together in various mineral sources. They play a key role in many applications including magnets, batteries and catalysts. However, they are strictly known as the lanthanide series, and they are quite common in the earth's crust. The term Rare Earth originated from the initial inability to chemically identify them, Later, their concentration, extraction, separation and reduction proved formidable as each of the lanthanides has remarkably similar chemical properties. At the Kroll Institute for Extractive Metallurgy, we have carried out research and development in all aspects of Rare Earth mineral processing, extractive metallurgy and recycling. The included bibliography provides an example background of Rare Earths information and some of the recent Kroll Institute efforts.

In this presentation, the history, properties, concentration, extraction, separation and reduction concepts will be elucidated. By these developments, we will learn that the Rare Earths are now commonly found and produced members of the lanthanide series.

Keywords: Lanthanides, Rare Earths, Beneficiation, Separation, Reduction.

REFERENCES

1. N. K. Gupta and K. Chiranjib, "Introduction," in Extracitve Metallurgy of Rare Earths, Boca Raton, FL, CrC Press, 2016, p. 1.
2. S. Assis, L. Montenegro and A. Peres, "Utilisation of Hydroxamates in Minerals Froth Flotation," Minerals Engineering, vol. 9, no. 1, pp. 103-114, 1996.
3. D. Everly, "Surface Chemistry of Novel Collectors and their Application to Froth Flotation of Rare Earth Minerals," MSc Thesis, Golden, CO, 2018.
4. Sepro, "Falcon UF Gravity Concentrators," Sepro, 2018. [Online]. Available: http://seprosystems.com/products/gravity-concentrators/_falcon-uf-gravity-concentrators/. [Accessed 30 January 2018].
5. A. Norgren, "Gravity Separations," Thesis, Colorado School of Mines, Golden, CO, 2018.
6. USGS, "Rare Earths," USGS, 2017.
7. Namibia Rare Earths Inc., "How are Rare Earths Used?," 2017. [Online]. Available: http://www.namibiarareearths.com/rare-earths-industry.asp. [Accessed 11 January 2018].
8. USGS, "Risk and Reliance: The U.S. Economy and Mineral Resources," USGS, 12 April 2017. [Online]. Available: https://www.usgs.gov/news/risk-and-reliance-us-economy-and-mineral-resources. [Accessed 10 Januray 2018].

[#] corresponding author: cganders@mines.edu

9. D Everly, C Anderson, S Popova, V Bryantsev and B Moyer, Beneficiation of Bastnaesite Ore with New Flotation Collector Ligands, Aspects Min Miner Sci. 7(2). AMMS. 000657. 2021.
10. C D Anderson, P Taylor and C G Anderson Rare Earth Flotation Fundamentals: A Review, American Journal of Engineering Research, e-ISSN: 2320-0847 p-ISSN : 2320-0936 Volume-6, Issue-11, 12 pgs., 2017.
11. C D Anderson, Improved understanding of rare earth surface chemistry and its application to froth flotation, Kroll Institute for Extractive Metallurgy, Colorado School of Mines, PhD Thesis, 2015.
12. P. Keller, Surface Interactions And Locked Cycle Flotation Of Novel Collectors On Bastnäsite Ore, Kroll Institute for Extractive Metallurgy, Colorado School of Mines, PhD Thesis, 2020.
13. C.L. Owens, G.R. Nash, K. Hadler, R.S. Fitzpatrick, C.G. Anderson, and F. Wall Zeta Potentials of the Rare Earth Element Bearing Bastnäsite Series of Fluorocarbonate Minerals, Advances in Colloid and Interface Science, Volume 256, Pages 152-162, June 2018.
14. R. Chapleski Jr., A. Chowdhury, A. Wanhala, V. Bocharova, S. Roy, P Keller, D. Everly, S. Jansone-Popova, A. Kisliuk, R. Sacci, A. Stack, C G. Anderson, B. Doughty, B., V. Bryantsev, A Molecular-Scale Approach to Rare-Earth Beneficiation: Thinking Small to Avoid Large Losses ISCIENCE doi: https://doi.org/10.1016/j.isci.2020.101435, 2020.
15. Pradip and D. Fuerstenau, The role of inorganic and organic reagents in the flotation separation of rare-earth ores. International Journal of Mineral Processing, 32(1–2), 1-22, 1991.
16. Pradip and D. Fuerstenau, Design and development of novel flotation reagents for the beneficiation of Mountain Pass rare-earth ore. Minerals & Metallurgical Processing, 30(1), 1-9, 2013.
17. Pradip and D. Fuerstenau, The adsorption of hydroxamate collectors on semi-soluble minerals, part I: adsorption on barite, calcite and bastnaesite. Colloids Surf., 8, 103-119, 1983.
18. D. Schriner, and C. Anderson, Centrifugal Concentration of Rare Earth Minerals from Calcitic Gangue, Journal of Metallurgical Engineering, Volume 4, pgs 69-77, September, 2015.
19. D. Schriner, Advanced Beneficiation of Bastnaesite Ore Through Centrifugal Concentration And Froth Flotation, Kroll Institute for Extractive Metallurgy, Colorado School of Mines, MSc Thesis, 2015,
20. N. Williams, Bastnaesite Beneficiation by Froth Flotation and Gravity Separation, Kroll Institute for Extractive Metallurgy, Colorado School of Mines, MSc Thesis, 2018.
21. A. Norgren, and C. Anderson, Ultra-Fine Centrifugal Concentration of Bastnaesite Ore, Metals, Volume 11, 12 pgs, 2021.
22. A. Norgren, A. and C. Anderson, Recovery of Rare Earth Oxides from Flotation Concentrates of Bastnaesite Ore by Ultra-Fine Centrifugal Concentration, Metals, Volume 11, 15 pgs, 2021.

**XVI International Mineral Processing
and Recycling Conference
28-30 May 2025, Belgrade, Serbia**

DOI: 10.5937/IMPRC25021K Abstract

EMERGING TECHNOLOGIES AND EMERGING WASTES: CHALLENGES AND OPPORTUNITIES

Junbeum Kim[#], 0000-0003-0665-7989,
CREIDD Research Centre on Environmental Studies & Sustainability,
UR InSyTE (Interdisciplinary research on Society-Technology-Environment Interactions), University of Technology of Troyes, 12 rue Marie Curie B.P. 2060,
10010 Troyes, France

ABSTRACT – The exponential growth of emerging renewable energy technologies—including solar photovoltaic panels, wind turbines, lithium-ion batteries, and high-efficiency LED lighting systems—has been instrumental in driving the global shift toward carbon neutrality and sustainable energy systems, yet their widespread deployment is simultaneously generating unprecedented waste management challenges as these technologies begin to reach their end-of-life phases in increasingly large volumes, with European solar panel waste alone projected to escalate from a modest 50,000 tonnes in 2020 to a staggering 1.5 million tonnes by 2030, reflecting a thirty-fold increase within a single decade, while wind turbine waste is anticipated to climb to 4.7 million tonnes annually due to the enormous material requirements of approximately 400,000 tonnes per gigawatt of installed capacity, further complicated by the technical difficulties associated with recycling specialized components such as fiberglass-reinforced composite blades, which currently lack cost-effective recycling solutions, and photovoltaic panels containing hazardous materials like lead and cadmium that require careful handling to prevent environmental contamination, alongside the rapidly expanding stream of lithium-ion batteries from electric vehicles and renewable energy storage systems, which could surpass half a million tonnes of waste per year in Europe by 2030, creating pressing demands for innovative recycling infrastructure, circular economy business models, and robust regulatory interventions to improve material recovery rates, develop secondary markets for repurposed components, and prevent these green technologies from becoming the next major environmental liability, necessitating breakthroughs in advanced recycling techniques such as solvent-based separation for solar panel silicon recovery, thermal decomposition methods for breaking down composite materials in wind blades, and hydrometallurgical extraction processes for recovering high-purity cobalt, lithium, and nickel from spent batteries, complemented by comprehensive policy measures including harmonized EU-wide extended producer responsibility schemes, standardized material tracking systems, and financial incentives for recyclers to establish closed-loop material flows that transform these burgeoning waste streams into valuable secondary resources, thereby ensuring that the renewable energy revolution achieves its full sustainability potential without creating unintended consequences for future generations.

Keywords: Emerging technologies and wastes, solar photovoltaic, wind turbines, lithium-ion batteries, LED lamps.

[#] corresponding author: junbeum.kim@gmail.com

INVITED LECTURES

XVI International Mineral Processing
and Recycling Conference
28-30 May 2025, Belgrade, Serbia

DOI: 10.5937/IMPRC25025N

Original research article

AN OVERVIEW OF GLOBAL COPPER SMELTING SLAG PRODUCTION AND REPROCESSING APPROACHES

Aleksandar Nikoloski[#]**,** 0000-0002-5267-7262,
Pritam Singh, 0000-0002-3802-4900,
Tina Chanda Phiri, 0000-0001-6310-4147,
Murdoch University, Harry Butler Institute, 90 South Street, Murdoch WA, Australia

ABSTRACT – Copper and cobalt are essential metals for the transition to renewable energy and various aspects of modern life. Their extraction from primary sources, such as ores, requires metallurgical separation from unwanted host materials, generating a substantial amount of waste. One type of this waste is copper smelting slag, with 39 million tonnes produced and discarded globally each year. These large quantities of slag occupy significant land space, often near residential areas, and pose a potential hazard by releasing contaminants into the environment. However, they also contain residual amounts of valuable copper and cobalt. To address the challenge of mitigating the negative impacts of this waste and exploring the potential commercial opportunities of the contained critical minerals, this study reviews global smelting slag production over the past 25 years, as well as the composition and technical reprocessing options. It provides a summary of the chemical and mineralogical characteristics of copper slag from various research and an extensive overview of the processing strategies for metal recovery from copper slag, including flotation, pyrometallurgy, and hydrometallurgy. The study demonstrates that a significant amount of smelting slag has been produced with considerable variation and complexity, representing a major potential resource for cobalt and copper metals. The overview of production trends and reprocessing techniques shows that while some effective options exist or are emerging, further research is required to enhance the reprocessing of smelting slag waste to create economic value, improve energy efficiency in metal production, increase the supply of critical metals, and reduce environmental impacts.

Keywords: Copper and Cobalt, Mining, Smelting Slag, World resource, Waste utilization.

INTRODUCTION

Copper smelting slag is a waste material generated during the pyrometallurgical processing of copper concentrates. The slag is primarily composed of silica (SiO_2), ferrous oxide (FeO), ferric oxide (Fe_2O_3), and trace amounts of calcium oxide (CaO) and alumina (Al_2O_3), as well as metals such as copper (Cu), cobalt (Co), silver (Ag), nickel (Ni), zinc (Zn), lead (Pb), cadmium (Cd), and iron (Fe) in oxide, sulphide, and/or metallic forms [1]. Global production of smelting slag is estimated at 37.7 million tons per year [1]. A considerable amount of smelting slag containing hazardous elements is often dumped in a slag disposal pit, and most of it is not fully utilised [2-5]. These hazardous substances are toxic and can accumulate in organisms, causing serious health risks to all organisms [6,7]. With

---

[#] corresponding author: a.nikoloski@murdoch.edu.au fewer available sites for dumping smelting slag and stricter environmental regulations, the copper smelting industry has an enormous challenge in managing the slag waste. As a result, it is becoming increasingly important to reduce waste disposal by making better use of copper slag as a valuable resource of critical minerals.

Copper slag contains significant amounts of essential metals, averaging 1.83 wt.% Zn, 1.67 wt.% Ag, 1.36 wt.% Mg, 1.19 wt.% Cu, 0.94 wt.% Pb, and 0.48 wt.% Co [1]. This has sparked increased interest in recovering these valuable metals from copper slag using various techniques, including flotation, hydrometallurgy, pyrometallurgy, and a combination of pyrometallurgy and hydrometallurgy. The flotation process utilises various collectors, frothers, modifiers, and depressants to extract entrained metal compounds from copper slag [4,8-11]. The hydrometallurgy technique for leaching copper slag with various lixiviants has been widely exploited (8,12-16,65). The pyrometallurgical approach includes calcination, carbothermic reduction/smelting reduction, and reduction roasting, followed by magnetic separation. This technique has mostly been utilised to extract metals from copper slag via carbothermic reduction at temperatures ranging from 1400 to 1800°C [18,19]. An integration of pyrometallurgy and hydrometallurgy for processing copper smelter slag that involves roasting the smelting slag followed by water or acid leaching has also been suggested [15, 20-22]. However, no commercial application has been found for extraction of valuable metals from smelting slag using these techniques.

Copper slag is extremely heterogeneous and chemically diverse. Thus, characterisation of copper slag is critical in selecting the best technique for metal recovery, environmental impact assessment, and utilisation. Gorai et al. [2] conducted a comprehensive review of the characterisation of copper slag, as well as metal recovery and utilisation technologies. Piatak et al. [23] reviewed the properties of ferrous and non-ferrous slags, as well as their environmental impact and role as a valuable resource for reuse and recycling. Potysz et al. [5] examined existing knowledge of metallurgical slags, including their chemical and phase compositions, metal recovery, environmental risk, and fate. Phiri et al. [24] also undertook an in-depth review of the detailed chemical and mineralogical description of copper slag, as well as processing methodologies and usage of copper smelting slag.

In another study, Tian et al. [25] investigated all metallurgical techniques available for recycling and further cleaning copper slag. A recent study examined worldwide smelting copper slag generation as a potential source of cobalt and copper metals for a circular economy [1]. Metallurgical recycling and processing solutions for copper smelting slag are still at the development stage, despite intensive research over the last several decades. Therefore, a review of current knowledge is required to guide the further development of techniques capable of leveraging the resource potential of copper smelting slag for extraction of critical metals. The primary objective of this study is to present a comprehensive review of global copper smelting slag generation, as well as the various proposed approaches tested to date for extracting critical metals from copper smelting slag. Finally, the technical challenges and development bottlenecks of copper slag metallurgical processes, as well as potential measures to overcome these barriers, are summarised in order to provide useful and significant guidance for efficient copper slag processing and utilization.

WORLD OVERVIEW OF COPPER SMELTING SLAG

The global copper slag production is estimated at 966 million tons for the period between 2000 and 2024 from the 13 main producing countries (Figure 1). The average annual production is estimated at 38.6 million tons. Copper smelting slag is considered a potential world resource owing to the huge amounts being produced annually worldwide which contain substantial amounts of valuable metals [24].

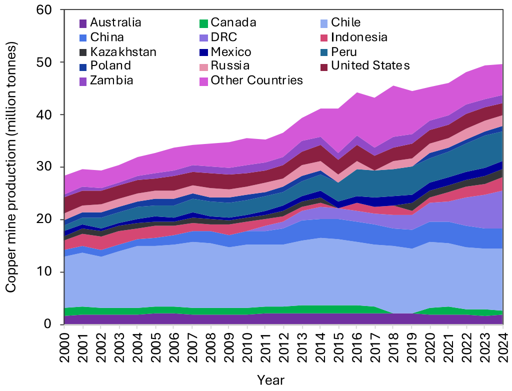

Figure 1 Global copper smelting slag production for the period 2000 to 2024. Approximately 966 million tons of copper slag waste has been produced in the last 25 years [26]

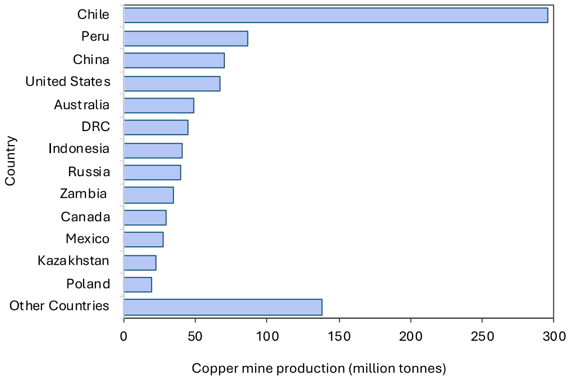

Figure 2 Total copper smelting slag generated in the 13 top producing countries for the period 2000 to 2024. Chile has the largest amount with 295 million tons of copper slag [26]

The total production figures of copper smelting slag by country show that Chile produced the highest amounts of copper slag in the last 25 years with 295 million tons, representing 31% of the total world production (Fig 2). Chile is followed by Peru, China, United States, and Australia as top five countries.

The production figures for the period between 2000 and 2024 serve as evidence that huge amounts of copper slag wastes are generated every year and the upward trend in these figures is expected to continue in the coming decade due to the increase in global population, economic growth and technological advancement.

Chemical composition of smelting slag

The bulk chemical composition of copper smelting slags is primarily determined by the metallurgical processes from which they are derived, which include the type of concentrate, fluxes and furnaces, and the cooling rates [2,5,23,27]. The principal oxides in slag are silica (SiO_2), ferrous oxide (FeO), ferric oxide (Fe_2O_3), limestone (CaO), and alumina (Al_2O_3). The average chemical composition of copper slag was calculated by considering studies conducted in each country at various copper smelting locations. The studies demonstrate substantial amounts of metals and metalloids, with an average of 3.05 wt.% Ca and 2.59 wt.% Al, 1.83 wt.% Zn, 1.67 wt.% Ag, 1.36 wt.% Mg, 1.19 wt.% Cu, 0.94 wt.% Pb, and 0.48 wt.% Co. Other metals and metalloids such as As, Ti, Ni, Mn, Sb, and Mo were also detected but in much lesser amounts (lower than 0.4wt.%). These results indicate that copper smelting slags are extremely heterogeneous in terms of chemical composition.

The grade of Co and Cu in the slag exceeds the average ore grade for most mines due to the depletion of high- grade deposits in recent years. These minor elements exist in the slag as entrained sulphides, oxides, and metallic elements. Older copper slags include more metals because older processes were less effective than modern ones [5,28].

Mineralogy of copper slag

Copper slag is primarily composed of fayalite and silicate glassy matrices, with crystalline oxides, sulphides, metallic elements, alloys, and intermetallic compounds as minor constituents [5,15,21,23,29-32]. The fayalite structure in copper slags is formed when pyrite is oxidized to iron oxide in the presence of silica and may contain minor amorphous silica phases [24,33]. In our recent study, the silicate phase was described as principally fayalite and kirschsteinite from the olivine group, while the copper phase was made up of copper matte and metallic copper [32]. Meanwhile, the magnetite phase was primarily found interbedded with the fayalite and kirschsteinite phases, forming a coherent structure with iron and other metallic components. Other research discovered certain common silicates with compositions equivalent to Melilite ($(Ca, Na)_2(Al, Mg, Fe^{2+})(Si, Al)_2O_7$) and willemite ($Zn_2SiO_4$) (6,28,34]. The other sulphide phases that have been found to be present within the copper slags are pyrite (FeS_2), galena (PbS), sphalerite ((Zn,Fe)S), pyrrhotite (Fe(1-X)S) and wurtzite ((Zn,Fe)S) whereas covellite (CuS), cubanite ($CuFe_2S_3$), digenite (Cu_9S_5), troilite (FeS), and pentlandite ($(Fe,Ni)_9S_8$) are rarely observed [23,28,35].

Shen and Forssberg [36] discovered that different copper slags involve different types of copper minerals, such as oxides, sulphides, or a combination of the two. This observation was consistent with Potysz et al. [5], who discovered that copper slags comprised several synthetic forms of naturally occurring mineral phases. Copper slags commonly contain sulphide minerals such as bornite (Cu_5FeS_4), chalcocite (Cu_2S), and chalcopyrite ($CuFeS_2$) [21,37,38,64]. The principal iron oxide minerals found in copper slag are fayalite (Fe_2SiO_4), spinels ($MgAl_2O_4$), hematite (Fe_2O_3), magnetite (Fe_3O_4) and wustite (FeO) [27,31,39,40]. Copper slags can contain trace amounts of oxides, including leucite ($K(AlSi_2O_6)$), hercynite ($FeAl_2O_4$) [5,41,42]. Pyroxene group minerals like diopside ($FeCaSi_2O_6$) and hedenbergite ($CaFeSi_2O_6$), as well as the olivine group minerals like kirschsteinite ($CaFe^{2+}SiO_4$) and forsterite (Mg_2SiO_4) are also found in copper slags [28,31,32,34,37,40,43]. Minerals that are occasionally discovered include chrysocolla $(CuAl)_2H_2Si_2O_5(OH)_4{\times}n(H_2O)$, leucite ($KAlSi_2O_6$), wollastonite ($CaSiO_3$), pyroxomangite ($MnSiO_3$), iscorite ($Fe^{2+}5Fe^{3+}2SiO_{10}$) and titanite ($CaTiSiO_5$) [28,34,43].

The cooling mechanisms for smelting slag, such as air-cooled or quenched (granulated) copper slag, have a significant impact on the diversity of phases. Granulated slags were discovered to contain a significant amount of calcium and chloride, as well as iron in the form of magnetite, fayalite, and ferrosilite. According to Ravindra et al. [31], fayalite is the most common mineral in copper slag samples, accounting for up to 57% in air-cooled slags and 15% in granulated copper slag samples. In another study, Potysz et al. [5] discovered that quenched slags had less phase diversity than slowly cooled slags. This could be because rapid cooling prevents crystallisation in quenched slags. Crystallisation of phases was discovered to occur closer to equilibrium during slow cooling, resulting in the formation of several phases [42]. These findings are consistent with previous observations that rapid cooling causes the formation of amorphous phases and metal oxide segregation, whereas slow cooling leads to the formation of vitreous and crystalline components [2,5,31,40,66]. This demonstrates that the cooling rate of the slag has a significant impact on phase composition.

DISCUSSION

To show the embedment of critical metals in copper slag, backscattered electron (BSE) imaging was used to examine the polished surface of the smelting slag sample [32]. Figure 3a depicts a BSE image containing multiple mineral phases interconnected within the copper slag. To get comprehensive BSE microstructure information, the highlighted areas X, Y, and Z in Figure 3a were deconvoluted and the results are presented in Figures 3b, 3c, and 3d, respectively. Tables 2 and 3 display the corresponding EDS chemical compositions of Figure 3b and Figure 3c, respectively.

The distribution of copper in the mapped areas (Figure 3) is not uniform, and a significant concentration of copper can only be observed in Area 2 (Figure 3c). Figures 3b and 3c, as well as Tables 2 and 3 show that copper is mostly distributed in silicate, copper matte, and metallic copper phases, with Cu contents of up to 5.08 wt.%, 73.52 wt.%, and 89.62 wt.%, respectively. In another study, Zhang et al. [44] revealed that although a slag had a considerably higher weight percentage of copper metal in iron phases than in fayalite and magnetite minerals, fayalite had a stronger ability to bind heavy metals. The study found that 89.7% As, 85.0% Pb, and 76.9% Cu were strongly bonded to the fayalite phase [44]. Previous research has shown that Cu tends to integrate into the fayalite structure by replacing Fe active sites [33,44,45]. Zhou et al. [46] examined the binary phase diagrams of Cu and Fe and noted that both Cu and Fe display miscible dissolution, which can be attributed to their similar chemical structures. In the study by Phiri et al.

[32], Cu was found in high concentrations in the copper phase, low concentrations in the silicate phase, and no copper was detected in the magnetite phase.

Cobalt was consistently found in various phases of copper slag, interspersed with other metals such as Cu, Fe, Ca, K, Al, Ti, and S. In the study by Phiri et al. [32], cobalt in copper smelting slag was mostly discovered embedded in the silicate and magnetite phases. According to the backscattered electron (BSE) images in Figure 3b and Table 1, the Co content was uniformly distributed in the magnetite, silicate, and copper matte phases, with up to 1.85 wt.%, 1.44 wt.%, and 0.38 wt.%, respectively. This finding is consistent with the research undertaken by Hu et al. [47], who found that Co predominantly occurs in the fayalite phase, specifically in the form of silicate and ferrite. The area labelled 2 in Figure 3b exhibited a perfect euhedral structure typical of iron oxide spinels. This area showed Co overlapping with other metallic elements including Fe, Si, Ca, Ti, Al, Mg and K as depicted in Table 1. Overall, the EDS results show that substantial amounts of cobalt and other valuable metals (such as Cu, Ti, Fe, Si, K, Mg, and Ca) were embedded in the complex silicate matrix and magnetite phase, making extraction challenging.

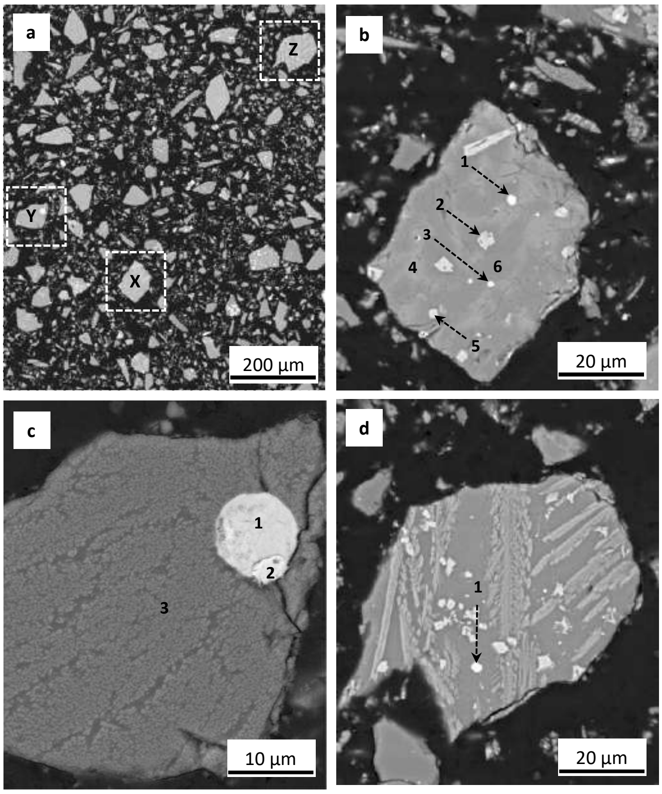

Figure 3 Backscattered electron micrograph of the polished surface in copper slag (a) and deconvoluted images of areas marked X (b), Y (c), and Z (d) [32]

Table 1 Elemental composition of the main phases in the copper slag in wt.% (Figure 3b) [32]

Mineral	Point	Co	Cu	S	Fe	Si	O	Ca	Al	Mg	Ti	K
Cu matte	1	0.38	57.56	20.8	11.01	2.34	4.76	0.6	0.64			0.46
Magnetit	2	1.85			51.33	3.94	24.87	1.43	2.49	0.34	1.14	1.08
Silicate	3	1.3	5.08	2.04	24.91	14.07	24.81	4.71	2.29	0.76	0.12	1.49
Silicate	4	1.25			31.11	16.29	28.37	2.51	3.9	0.39	0.14	3.52
Silicate	5	1.44			25.24	12.26	25.9	6	2.07	1.8	0.43	0.91
Silicate	6	1.32			20.9	19.44	31.46	7.98	3.43	2.41	0.16	1.18

Table 2 Elemental composition of the main phases in the copper slag in wt.% (Figure 3c) [32]

Mineral	Point	Co	Cu	S	Fe	Si	O	Ca	Al	Mg	Ti	K
Cu matte	1	0.11	73.52	18.36	2.5	0.08	0.67					
Cu metal	2	0.14	89.62	0.12	3.17	0.37	1.38	0.08				
Silicate	3	1.05	0.54		22.4	23.25	40.9	1.73	5.17	2.25	0.45	2.82

CRITICAL METAL PROCESSING STRATEGIES FOR SMELTING SLAG

Recovery of copper from smelting slag using flotation

The froth flotation technique has been found to be an essential operation in the recovery of copper from smelting slag [4,9-11,41,48]. The copper values in the smelting slag that are present either as independent metallic particles or in the form of sulphides, can be floated effectively. Flotation has been studied for the recovery of metals from copper slag employing various collectors, frothers, modifiers, and depressants. Froth flotation uses the differences in surface characteristics of minerals to separate valuable minerals from unwanted gangue minerals. The process produces an enriched concentrate, and the gangue or unwanted material reports to the tailings. Middlings are a third product composed of valuable and gangue minerals that have remained locked together. This material is typically reground to liberate the valuable mineral particles. Copper slag flotation resembles sulphide ore flotation [20,49,50]. The main parameters investigated for the flotation technique are particle size, collector dosage, and pH. The copper slag is fed into the flotation unit, where the sulphide minerals (Cu_2S, Cu_5FeS_4) are floated using collector and frother reagents to produce a concentrate.

Copper and cobalt recovery from smelting slag using hydrometallurgy

The hydrometallurgical route via leaching is the most common approach for recovering metals from low-grade materials like smelting slag. Because of its economic benefits and relatively minimal environmental impact, the hydrometallurgical technique offers a high potential for effective metal extraction. The hydrometallurgical technique to metal extraction from smelting slag has been examined using various parameters such as leaching system, extractant concentration, temperature, solid/liquid ratio, and leaching period. The emphasis has been on atmospheric leaching using lixiviants such acids, bases, and salts. Many of these lixiviants form aqueous solutions that can dissolve metals from ores, concentrates, and slag.

Sulphuric acid (H_2SO_4) is the most used lixiviant due to its low cost, assertiveness, and availability. It is thought to be an effective lixiviant for metal oxide leaching, as well as one of the strongest acids that is soluble in water at all concentrations. It can be used in diluted or concentrated form, or in combination with oxygen. Sulphuric acid has the potential for local (at plant) application because it is a common byproduct of copper smelters. Several investigations conducted using sulphuric acid as the leaching agent for copper slags have revealed remarkable metal extraction efficiency [12,13,15,16,20,51-55]. Yang et al. [16] used sulphuric acid to recover metal values from copper slag, which showed good metal extraction of 98%, 97%, and 89% for cobalt, zinc, and copper, respectively. The method also allowed for faster filtration and considerably decreased the negative impacts of silica and iron (III) oxides on target metal recycling. However, further research is required to reduce the excessive acid and lime consumption in this process.

Overall, acids have demonstrated a positive relationship between acid concentration and extraction efficiency for several leaching. Some studies observed that although there is high metal extraction efficiency, extraction from slags containing high silica involves a high consumption of sulphuric acid and yields silica gel [15,16,51,56,57]. This is because metals such as Co and Cu are dissolved in the spinel oxide, ferrite and silicates. The high consumption of sulphuric acid and lime, as well as poor settling and filtration characteristics caused by the formation of iron hydroxide precipitates and silica gel, limits the usefulness of the process [16,57]. To overcome these challenges, other studies have investigated combining acids with oxidants for recovery of metal values from copper slag [24].

Pyrometallurgical approaches for processing of copper slag

Pyrometallurgy involves chemical reactions of solids, gases or molten materials at elevated temperatures in a furnace. In carbothermic reduction, carbon is used as a reductant to transform the minerals in the slag into metallic phases at high temperatures. Yucel et al. [18] investigated the treatment of ancient Kure copper slag using a carbothermal reduction method in a DC arc furnace operating at high temperatures (1,430 °C and 1,480 °C), achieving maximum cobalt recovery of 95.7% and copper recovery of 90% in a closed system. Another method was developed by Hara and Jha [57] for reduction and sulphurisation of copper slag with activated charcoal, giving a highest copper recovery of 90% at 1323 K. Gas phase diffusion, with an activation energy of 118.059 kJ mol^{-1}, was the key rate limiting factor in the isothermal reduction process of carbon-bearing pellets from copper slag according to Zhang et al. [58]. However, the pyrometallurgical reduction process has been found to necessitate considerable energy consumption (with temperatures over 1,200 °C) [59-60]. This was stated to be due to the extremely high melting point of fayalite in copper slag [60]. Additionally, the reduction was rather challenging because of the substantial amount of fayalite in copper slag [61]. The process also has the potential to cause considerable environmental contamination because it ultimately results in the production of numerous different types of solid waste.

Pyro-hydrometallurgical approach for processing copper slag

The most common method for pyro-hydrometallurgical processing of copper smelting slag is roasting, followed by water or acid leaching. The pyro-hydrometallurgy involves the study of the effects of roasting time, acid/slag ratio, and roasting temperature, and the effect of thermal decomposition prior to leaching on metal dissolution were examined. The roasting of copper sulphide produces a calcine, which is then treated using the hydrometallurgical technique. Extensive studies have been done on the roasting of copper slag using roasting agents such as sulfuric acid (H_2SO_4) [15,20,21,52], pyrite (FeS_2) [62], ferric sulphate ($Fe_2(SO_4)_2$) [63], graphite [41] and ammonium sulphate ($(NH_4)_2SO_4$) [52] to yield metal sulphates. The recovery of Cu, Co and Zn from copper smelter and converter slags by roasting with sulphuric acid was conducted by Arslan and Arslan [20]. The study investigated the effects of roasting time, roasting temperature, and acid/slag ratio. Metal extractions of 88% of Cu, 87% of Co, 93% of Zn and 83% of Fe were achieved after two hours of roasting at 150°C and with a 3:1 acid/slag ratio. A recent study has shown that increasing the sulphation temperature could reduce the iron content in the leach liquor [21].

The carbothermal reduction of copper slag in a submerged type of DC arc furnace was investigated by Acma [64]. The study demonstrated that copper slag could be carbothermally smelted with partial reduction of iron oxide (FeO) to a metallic phase comprising copper and other metals at temperatures of 1400-1800°C. Thereafter, the material was leached with H_2SO_4 and the solution purified with H_2S to separate CuS. Fe was precipitated as goethite. A low temperature carbothermic reduction of copper slag with charcoal in the presence of borax followed by leaching with H_2SO_4 was investigated by Phiri et al. [22]. Thermochemical calculations, phase characterisation and experimental results demonstrated that using borax in carbothermic reduction could lower the temperature of fayalite reduction and expedite the transformation of copper slag microstructures to amorphous and metallic phases. The released metals were leached in H_2SO_4 yielding high Cu, Co, and Fe extractions of up to 83.80%, 84.75%, and 85.69% at 850 °C, respectively.

CONCLUSION

This study examined global smelting slag production over the past 25 years, uncovering significant quantities of the material. This slag represents a valuable potential resource for extracting cobalt and copper metals. The chemical and mineralogical analysis of smelting slag reveals its highly varied and diverse nature. Due to its high metal content, extensive research has focused on innovative methods for reprocessing these critical metals. Extracting copper and cobalt from copper slag could not only increase the supply of these essential metals, which are crucial for transitioning to green energy, but also address environmental issues related to slag disposal. The paper explores various processing techniques for recovering copper and cobalt from smelting slag. Froth flotation using xanthates is widely recognized as an effective technique for copper recovery from copper slags globally. A mixed collector system, including xanthates, enhances selectivity and adsorption on the slag surface, achieving better separation efficiency than any single collector. However, froth flotation is ineffective for copper oxide recovery. Therefore, sulfidation treatment of copper oxide-containing slags is essential for successful slag flotation. Although some collectors like hydroxamates have been used for copper oxide mineral flotation without sulfidation treatment, their large-scale efficacy for copper slags remains unproven. Cobalt recovery via flotation is impractical since cobalt is embedded in silicate and magnetite structures. Hydrometallurgical approaches, primarily through leaching, remain the most common method for extracting metals from smelting slag. However, the high consumption of sulfuric acid and lime, along with poor settling and filtration characteristics caused by iron hydroxide precipitates and silica gel formation, limit its application. Oxidants offer potential to overcome these challenges. Pyrometallurgical methods for recovering copper and cobalt at high temperatures are among the most effective techniques, though they demand considerable energy (exceeding 1,200 °C) and cause substantial environmental contamination. Research indicates that using basicity flux can reduce the temperature needed for fayalite disaggregation. A pyro-hydrometallurgical process involves roasting and reducing the smelting slag, followed by water or acid leaching of the resulting products to recover the metals. However, pilot-scale studies are necessary to assess the economic viability of this approach.

ACKNOWLEDGEMENT

The Schlumberger Foundation Faculty for the Future Fellowship, and Murdoch University provided financial support for this research, which the authors gratefully acknowledge.

REFERENCES

1. Phiri, T.C., Singh, P., Nikoloski, A.N., (2022) The potential for copper slag waste as a resource for a circular economy: A review – Part I, Minerals Engineering 180, 107474.
2. Gorai, B., Jana, R.K., Premchand., (2003) Characteristics and Utilisation of Copper Slag—A Review Resour. Conserv. Recycl. 39 (4), 299–313.
3. Alp, I., Deveci, H., Süngün, H., (2008). J. Haz. Mater. 159 (2), 390–395.
4. Roy S., Datta A., Rehani, S., 2015. Int. J. Miner. Process. 143, 43–49.
5. Potysz, A., Hullebusch, E.D.V., Kierczak, J., Grybos, M., Lens, P.N.L., Guibaud, G., 2015. Environmental Science and Technology, 45:22, 2424-2488.
6. Ettler, V., Piantone, P., and Touray, J. C., 2003. Mineralogical Magazine 67(6), 1269–1283.
7. Kambole, C., Paige-Green, P., Kupolati, W.K. Ndambuki, J.M., Adeboje, A., 2019. Comparison of technical and short-term environmental characteristics of weathered and fresh blast furnace slag aggregates for road base applications in South Africa.
8. Sanchez, R.M.I., Rivera, J., Frias, M., Esteban, J L., Olaya, M., 2004. ACI Special Publication 221-56, 925–940.
9. Sarrafi, A., Rahmati, B., Hassani, H.R., Shirazi, H.H., (2004) Miner. Eng. 3 (2004) 457–459.
10. Das, B., Mishra, B.K., Angadi, S., Pradhan, S.K,. Prakash, S., Mohanty, J.K., 2010. Waste Management & Research: 28: 561–567.
11. Fan, J., Li, H., Wei, L., Li, C., Sun, S., 2017. The Minerals, Metals & Materials Society.
12. Banza A N., Gock E., Kongolo K., 2002. Hydrometallurgy, 67(1): 63–69.
13. Altundoğan, H. S., Boyrazli, M., and Tümen, F. 2004. Minerals Eng. 17(3), 465–467.
14. Boyrazli, M., Altundoğan, H.S & Tümen, F., 2006. Canadian Metallurgical Quarterly, 45:2, 145-152.
15. Deng, T., Ling, Y., (2007) Waste Manage. Res. 25, 440–448.

16. Yang, Z., Rui-lin, M., Wang-dong, N., Hui, W., (2010) Hydrometallurgy 103, 25–29.
17. Nadirov, R. K., L. A. Mussapyrova., (2019) Journal of Chemical Technology and Metallurgy, 54, 3, 657-662.
18. Yucel, O., Addemir, O., Tekin, A., S. Nizamoglu., (1992) Mineral Processing and Extractive Metallurgy Review, 10:1, 99-107
19. Banda, W., N. Morgan, and J.J. Eksteen., 2002. Minerals Engineering15, 899-907.
20. Arslan, C., and Arslan, F., 2002. Hydrometallurgy, 67(1): 2804 J. Cent. South Univ. 24: 2799–2804 1–7.
21. Dimitrijevic, M.D., Urosevic, D.M., Jankovic, Z.D., and Milic, S.M., (2016). Physicochem. Probl. Miner. Process. 52(1), 409−421.
22. Phiri, T.C., Singh, P., Yotamu S. Hara, Y.S., Siame, J., Nikoloski, A.N., (2023). Mineral Processing and Extractive Metallurgy Review.
23. Piatak, N.M., Parsons, M.B., Seal, R.R., 2014. Appl. Geochem. 57, 236–266.
24. Phiri, T.C., Singh, P., Nikoloski, A.N., (2021) Minerals Engineering 172, 107150.
25. Tian, H., Guo, Z., Wang, D., Pan, J., Zhu, D., Yang, C., Xue, Y., Li , S., 2021. Conservation & Recycling 168, 105366.
26. U.S. Geological Survey. 2001-2025. Mineral commodity summaries: Reston, Virginia.
27. Lottermoser, B. G., 2010. Mine Wastes. Springer 3rd edition.
28. Lottermoser, B. G., 2002. Mineralogical Magazine 66(4), 475–490.
29. Kaksonen, A.H., Särkijärvi, S., Puhakka, J.A., Peuraniemi, E., Junnikkala, S., Tuovinen, O.H., 2016. Hydrometallurgy 159, 46–53.
30. Meshram, P., Bhagat, L., Prakash, U., Pandey, B.D., and Abhilash., 2017. Canadian Metallurgical Quarterly, 56:2, 168-178.
31. Ravindra, K., OBE, D., Brito J.D., Mangabhai, R., Lye, C.Q., 2017. Sustainable Construction Materials: Copper Slag. Elsevier. pp 28-86.
32. Phiri, T.C.; Singh, P.; Nikoloski, A.N., 2024. MineralogicalCharacterisation of Copper Slag and Phase Transformation after Carbocatalytic Reduction for Hydrometallurgical Extraction of Copper and Cobalt. Metals, 14, 1119. https://doi.org/10.3390/ met14101119.
33. Li, Y., Perederity, L., Papangelakis, V.G., 2008. Journal of Hazardous material. 152, 607-615.
34. Manasse, A., Mellini, M., 2002. J. Cult. Herit. 3, 187–198.
35. Ettler, V., Johan, Z., Krıbek, B., Sebek, O., and Michaljevic, M., 2009. Appl. Geochem. 24(1), 1–15.
36. Shen, H., and Forssberg, E., 2003. Waste Manage. 23(10), 933–949.
37. Vítková, M., Ettler, V., Johan, Z., Kribek, B., Sebek, O., Mihaljevic, M., 2010. Mineral. Mag. 74 (4), 581–600.
38. Sarfo, P., Das, A., Wyss, G., Young, C., 2017. Waste Manag., 70, 272-281.
39. Parsons, M. B., Bird, D. K., Einaudi, M. T., and Alpers Ch. N., 2001. California. Appl. Geochem. 16(14), 1567–1593.
40. Piatak, N. M., Seal, R. R., and Hammarstrom, J. M., 2004. Appl. Geochem. 19, 1039–1064.
41. Bulut, G., 2006. Waste Manage. Res. 24, 118–124.
42. Kierczak, J., Pietranik, A., 2011. Can.Mineral. 49 (5), 1281–1296.
43. Sāez, R., Nocete, F., Nieto, J.M., Capitān, M.A., Rovira, S., 2003. Mineral. 41, 627–638.
44. Zhang, S., Zhu, N., Shen, W., Wei, X., Li, F., Ma, W., Mao, F., Wu, P., 2022. Resources, Conservation & Recycling 178, 106098.
45. Zhao, Z., Wang, Z., Peng, N., Peng, B., Liang, Y., Qu, S., Dong, Z., Zeng, W., 2019. JOM 71 (8), 2891–2898.
46. Zhou, S., Wei, Y., Li, B., and Wang, H., 2018. Metallurgical and Materials Transactions B.

47. Hu, J.H, Wang, H, Zhao, L.M, Li, L, Liu H.L., 2011. Characterisation of copper slag from impoverishment. J Saf Environ 11(2):90–93. https://doi.org/10.3969/j.issn.1009-6094.2011.02.022.
48. Shamsi, M., Noparast, M., Shafaie, S.Z., Gharabaghi M., Aslani, S., 2015. Journal of Mining & Environment, Vol.6, No.2, 2015, 237-249.
49. Osborn, G.A., Garner, F.A., & Veasey, T.J., 1990. Paper presented at the Recycling of Metalliferous Materials Conference, Birmingham, UK.
50. Gulay, B., 2006. Waste Manage Res: 24: 118–124.
51. Anand, S., Rao, K. S., and Jena, P. K., 1983. Hydrometallurgy 10(3), 305–312.
52. Sukla, L.B., S.C. Panda, and P.K. Jena,1986. Recovery of cobalt, nickel and copper from converter slag through roasting with ammonium sulphate and sulphuric acid. Hydrometallurgy. 16(2): p. 153-165.
53. Basir, S. M. A., and Rabah, M. A. 1999. Hydrometallurgy 53(1), 31–44
54. Bese, A. V., 2007. Ultrasonics Sonochem. 14(6), 790–796.
55. Baghalha, M., Papangelakis, V. G., and Curlook, W. 2007. Hydrometallurgy 85(1), 42–52.
56. Potysz, A., Kierczak, J., Fuchs, Y., Grybos, M., Guibaud, G., Lens, P.N.L., van Hullebusch, E.D., 2016. J. Geochem. Explor. 160, 1–15.
57. Hara, Y., and A. Jha, 2016. Sustainability in the Mineral and Energy Sectors, 7, 105-124.
58. Zhang H, Wang G, Zhang S., 2019. Nonferrous Met. Sci. Eng; 10 (1):28–33.
59. Li S, Pan J, Zhu D., 2019. Powder Technol.; 347:159–169.
60. Zhang H., Hu C., Gao W. and M. Lu., 2020. Minerals, 10, 973.
61. Lan C., Zhang S., Liu R., Lyu Q., Yan G., & B. Wang, 2022. Ironmaking & Steelmaking, DOI:10.1080/03019233.2022.2091726.
62. Tümen, F. and N. Bailey, 1990. Hydrometallurgy: p. 317-328.
63. Altundoğan, H.S. and F. Tümen, 1997. Hydrometallurgy, 44(1–2): p. 261-267.
64. Acma E, Sesigur H, Addemir O, Tekin A., 1997. Trans Indian Inst Met; 50 (2-3):147-51.
65. Nadirov, R. K, Syzdykova, L. I., Zhussupova, A. K., and Usserbaev, M. T., 2013. Int. J. Mineral Processing, 124, 145–149.
66. Kuo, Y.-M., Wang, J.-W., Wang, C.-T., Tsai, C.-H., 2008. J. Hazard. Mater. 152, 994–1001

XVI International Mineral Processing
and Recycling Conference
28-30 May 2025, Belgrade, Serbia

DOI: 10.5937/IMPRC25037S Research article

EDUCATION IN MINERAL PROCESSING AND FILLING THE GAP OF TALENTED MINERAL PROCESSING ENGINEERS

Maria Sinche-Gonzalez[#], 0000-0002-7722-6839,
EMJM-PROMISE, University of Oulu, Oulu Mining School, Oulu, Finland

ABSTRACT – Mining countries such as Australia and the US have recognized the lack of mineral processing engineers as the demand for mineral resources increases for energy transition and climate change mitigation. However, this need is also due to the complexity of extraction, refining, quality control, environmental impact, supply chain and regulatory requirements associated with the increased demand of minerals and metals.

Within the European Union (EU), there is an acknowledged requirement for clean energy technologies that rely on critical minerals such as copper, lithium, cobalt, nickel, and rare earth elements. Also, the EU wants to be less dependent on the supply of critical raw materials (CRM). Therefore, the demand for mineral processing engineers and metallurgists in Europe is expected to increase substantially over the next decade. However, there is not a delineated road map emphasizing the more technical and skilled professionals' education for resolving the workforce and a talent crunch in mineral processing and mining engineering-related areas.

There are only a few attempts at filling the gap in education of talented mineral processing engineers. For example, the Erasmus+ program such as the Erasmus Mundus Joint Master in Sustainable Mineral and Metal Processing Engineering, EMJM PROMISE, is the first program focusing on mineral processing specialization.

Addressing the shortage of mineral processing engineers requires educational reforms, efforts to attract young professionals, and investment in modernizing the industry's image to emphasize sustainability and technological innovation and cooperation.

Keywords: Education, Mineral processing, Shortage of skills, Cooperation.

INTRODUCTION

Given the increasing demand of minerals and metals for the green transition, there is a growing need for domestic extraction, processing, recycling, and substitution of critical raw materials. However, a fundamental challenge lies in the shortage of skilled professionals across the entire raw materials sector.

Europe is facing an acute gap in skilled professionals, particularly in industrial operation, mostly due to limited public awareness of the importance of raw material [1]. This is exacerbated by declining enrollments in mining, metallurgy, mineral processing, and related engineering fields (Figure 1) alongside insufficient investment in education and training.

Unlike the U.S. and Australia, which have developed comprehensive educational roadmaps [2], Europe still lacks a cohesive, large-scale initiative to tackle the talent and workforce shortage in these critical sectors.

[#] corresponding author: maria.sinchegonzalez@oulu.fi

Figure 1 shows the number of students graduating from related mining engineering programs has declined since 2016 across Canada, the U.S., and Australia. The downtrend transcends are not a national phenomenon in those countries but reflects the global nature of the mining sector.

It could be very convenient to attribute the observed trend to the cyclical nature of the mining industry. However, the number of students joining and graduating from mining-related programs dropped significantly despite commodity prices holding steady or increasing.

Unfortunately, we cannot find data from the European Union on education in mining-related professions. However, the publication of Euractiv [3] recognizes that the mineral processing graduates in Europe are almost negligible.

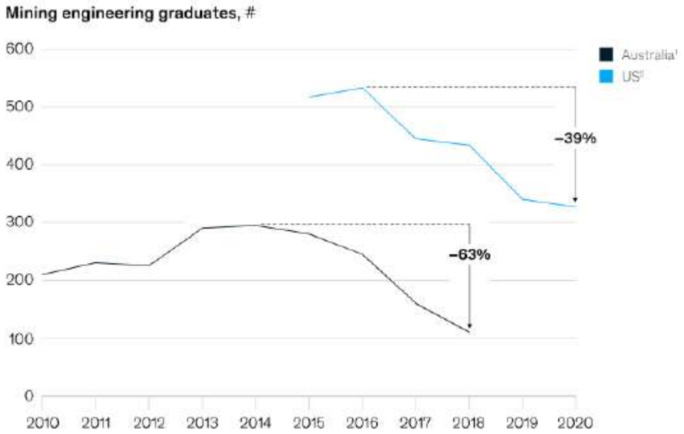

Figure 1 The number of students graduating from related Mining Engineering programs. Source [4].

METHODOLOGY

This paper considers an analysis of the need for mineral processing engineers making a review of the latest publications about education in the mineral processing in the EU.

The starting point was to reply to:

- What are the key areas that need mineral processing engineers?
- What are the reasons for the shortage of mineral processing engineers in Europe?
- How many mineral processing engineers will be needed?

An analysis of the competences of the new graduate's mineral processors and required by the industry, a survey of stakeholders collected the answers of 23 companies.

The existing mineral processing programs in the EU were identified and mapped.

Key areas of demand of mineral processing engineers

From electric vehicles to solar panels to future innovations, the global transition to clean energy is set to further heighten demand for critical minerals.

The global demand of minerals for energy transition will increase significantly in the coming decades. Figure 2 shows that between 2022 and 2050, demand for lithium will rise tenfold, nickel will double, and cobalt triple.

1. Lithium, vanadium, graphite, cobalt, and nickel processing: as the EU scales up battery production, engineers specialized in the processing and refining of these CRM will be critical.
2. Rare Earth Elements (REEs): the processing of rare earths, used in renewable energy technologies and electronics, will require specialists with niche skills in metallurgy and mineral processing.
3. Recycling and urban mining: metallurgists will also be needed in recycling facilities to recover metals from e-waste, batteries, and other discarded products.

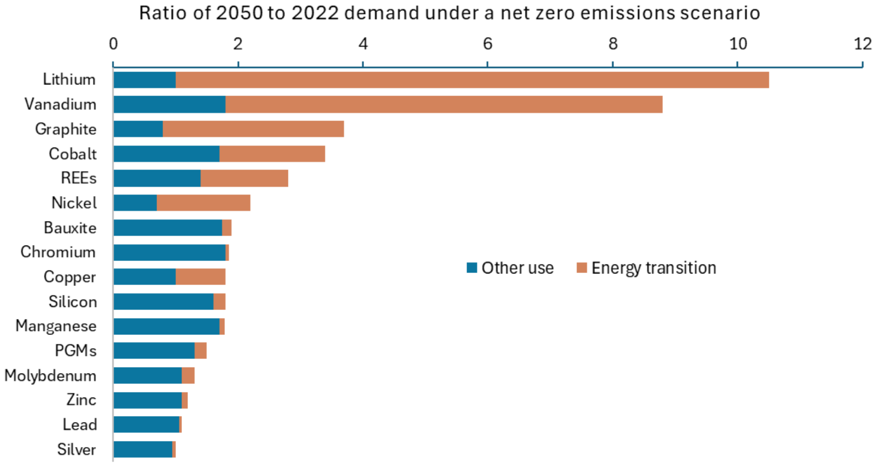

Figure 2 Increase in global demand for energy transition minerals.

*Source: International Energy Agency (IEA) in Surging Demand for Energy Transition Minerals, Projection under the IEA's net zero emissions transition scenario [5].

Reasons for the shortage of mineral processing engineers in Europe

There are various reasons for the shortage of engineers in the field of mineral processing, between them:

1. Limited investment in education and infrastructure
2. Aging workforce and retirements
3. Geopolitical and regulatory challenges
4. Declining enrolment in mining and processing programs
    a. Perceived environmental and social impact
    b. Competition with other sectors
    c. Boom and bust cycles in the mining industry
    d. Shift in industry focus
5. Digitalization and technological advancements
    a. Increased demand for critical raw materials

   b. Europe is aiming for increased self-sufficiency
   c. Reshoring of mineral processing activities
   d. Recycling and circular economy

6. Stakeholders’ different priorities, values, and expectations

How many mineral processing engineers will be needed?

Although exact figures are hard to determine, this industry necessitates expertise and know-how which is not available domestically and could require tens of thousands of professionals across mining, processing, and recycling sectors in coming years.

The demand for mineral processing engineers and metallurgists in Europe is poised to increase substantially over the next decade, driven by the magnitude of the shift towards green technologies, raw material independence, and recycling. It’s estimated that thousands of new jobs will be created over the next decade. For instance:

- The EU’s Raw Materials Action Plan could create upwards of 30000 direct jobs by 2030, many of which would be in fields like mineral processing and metallurgy.
- According to some projections, the battery materials supply chain alone could require more than 10000 metallurgists and mineral processing experts across Europe by 2030.

RESULTS AND DISCUSSION

Why is specialized expertise needed in mineral processing?

A key prerequisite to European competitiveness in Raw Materials is enhancing the competences of the mining and processing experts.

The survey carried out in 2021 collected the answers of 23 companies [6]. It shows the knowledge and skills expected from new graduates in mineral processing engineering in Figure 3.

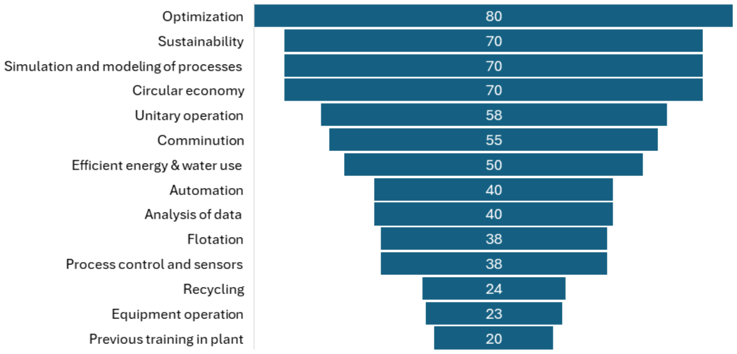

Figure 3 Stakeholder analysis of the needs of technical knowledge and skills [6].

An expert in mineral processing must have all the capabilities that support good decisions. These professionals must have knowledge and skills in chemistry, process mineralogy, breakage mechanism, theory and practice in sampling (TOS), comminution, flotation, separation processes, hydrometallurgy, pyrometallurgy, laboratory test, data analysis, as well as develop new abilities of 360° communication, teamwork, shape creative approaches to solving production problems, use digital tools such as modelling and simulation (use of both software and mathematics is complementary) and take responsibility for the completeness of projects. These skills are required to continually design and redesign more complex mineral processing operations, which also need to be run in even more resource-effective ways.

Education programs in the EU

An analysis of the education programs in Europe and results show that few education programs cover the area of mineral processing.

At the bachelor level, there are no mineral processing degrees (BSc) in Europe (some related exceptions). Therefore, there is not a distinctive degree in mineral processing. Some related programs are:

- Bachelor's degree in Mineral Resource Engineering, LUT
- Bachelor's degree of Science in Mineral Resources Engineering, MUL
- Bachelor's degree of Science in Mineral Resources and Raw Materials Engineering, Technical University Bergakademie Freiberg
- Bachelor of Science in Raw Materials Engineering, RWTH Aachen University

At the master level (Table 1), there are few specific programs in mineral processing or extractive metallurgy, other related programs have less than 30% of mineral processing courses in their curricula.

Table 1 Master in EU related to mineral processing (MinPro)

Programs related to MinPro	With some relation to MinPro
1. AGH University of Science and Technology (Poland), MSc in Extractive Metallurgy and Mineral Processing	2. Luleå University of Technology (Sweden), Master Program in Georesources Engineering /MSc Geoscience
3. University of Oulu (Finland), MSc in Mining Engineering, Mineral Processing and Geophysics – Specialization in Mineral Processing	4. Aalto University (Finland), MSc in Chemical Engineering – Major in Sustainable Metals Processing
5. University of Lorraine (France), MSc in Geosciences – Mineral Resources and Extractive Metallurgy	6. University of Bologna (Italy) MSc in Chemical Engineering – Specialization in Sustainable Chemical and Process Engineering
7. Delft University of Technology (Netherlands), MSc in Sustainable Energy Technology – Specialization in Raw Materials Processing	8. Instituto Superior Técnico, University of Lisbon (Portugal): MSc in Mining and Geological Engineering
9. Montanuniversität Leoben (Austria), MSc in Mining and Metallurgical Engineering	10. Technische Universität Bergakademie Freiberg (Germany), MSc in Geosciences – Specialization in Mineral Resources and Sustainable Process Engineering
11. RWTH Aachen University (Germany), MSc in Raw Materials Engineering	12. University of Porto (Portugal): MSc in Mining and Geo-Environmental Engineering
13. University of Exeter (UK), MSc Minerals Processing at Camborne School of Mines (no EU)	14. Master European Mining Course (EMC) 2023 leading into triple degree, by Aalto University, RWTH Aachen University and MU Leoben

Other programs

Although the EU commission is aware of the skills shortage, education is not its direct competence. It established the following programs to support the development of new high skills in engineering, material science, geology or earth observation.

1. The European Institute for Innovation and Technology (EIT) has been created to enhance Europe’s ability to innovate by integrating education and entrepreneurship with research and innovation at the EU level.
2. The Erasmus+ program includes the Erasmus Mundus Joint Master (EMJM) and Marie Sklodowska-Curie actions (MSCA) provides grants for a wide range of activities in education, training, youth, and sport.

EMJM PROMISE - Erasmus Mundus Joint Master in Sustainable Mineral and Metal Processing Engineering (EIT Labeled) provides a solid foundation in mineral processing and extractive metallurgy, preparing students for careers in both the technical and management aspects of the mining and minerals industry. Also, it emphasizes sustainability, green processing technologies, and environmental impact reduction, reflecting current trends in the field.

CONCLUSIONS

- The demand for mineral processing engineers and metallurgists in Europe is expected to increase substantially over the next decade, driven by the need for critical raw materials, the expansion of the green energy sector, and initiatives of the EU.
- Although exact figures are hard to determine, the industry could require tens of thousands of professionals across mining, processing, and recycling sectors.
- Addressing the shortage of mineral processing engineers requires educational reforms, efforts to attract young professionals, and investment in modernizing the industry's image to emphasize sustainability and technological innovation.
- The skill shortage needs to be addressed through communication and partnerships between civic society, public authorities, universities, research organizations, and industry. The Commission supports the development of new high skills in engineering, material science, geology or earth observation**.**

ACKNOWLEDGEMENT

The support of the funds of EMJM-PROMISE program to sponsor the participation in IMPRC 2025 is acknowledged.

REFERENCES

1. European Commission. Skills and education. https://single-market-economy.ec.europa.eu/sectors/raw-materials/areas-specific-interest/skills-and-education_en.
2. Drinkwater, D. (2017) *A Roadmap for Mineral Processing Education. Mineral Engineering Knowledge and Skills for Today’s Industry*. *IMPC Mineral Processing Commission*.

3. Stam, C. (2018) Europe’s mining sector faces skilled workers shortage. https://www.euractiv.com/section/circular-economy/news/raw-materials-industry-faces-skilled-workers-shortage-calls-for-linking-industry-with-education.
4. McKinsey & Company. (2023) *Metals & Mining and People & Organizational Performance Practices*. https://www.mckinsey.com/industries/metals-and-mining/our-insights/has-mining-lost-its-luster-why-talent-is-moving-elsewhere-and-how-to-bring-them-back.
5. Surging Demand for Energy Transition Minerals. (2024) https://www.voronoiapp.com/natural%20resources/Surging-Demand-for-Energy-Transition-Minerals-1174
6. Sinche-Gonzalez, M. (2024) Importance of the Erasmus Joint Mater in Sustainable Mineral and Metal Processing Engineering (EMJM-PROMISE) at the University of Oulu for the industry and the internationalization of education in the mining field in Finland. *Materi*a.

XVI International Mineral Processing
and Recycling Conference
28-30 May 2025, Belgrade, Serbia

DOI: 10.5937/IMPRC25044U Original research article

INNOVATIVE BIODEGRADABLE WASTE TREATMENT AS A POSSIBLE SOLUTION FOR RECULTIVATION OF TAILINGS AND SLAG LANDFILLS

Predrag Umičević[1#], 0009-0007-5295-6847,
Ivica Karoglan[2], 0009-0008-7458-9846,
Gregor Radišić[3], 0009-0007-0225-9445,
Viktor Simončič[3], 0009-0005-9162-5544,
[1]Composting d.o.o., Smederevo, Serbia
[2]Čistoća d.o.o., Split, Croatia
[3]Grevicon Consulting d.o.o., Sisak, Croatia

ABSTRACT – A low-cost technology has been developed that stabilizes and transforms biowaste into a soil improver with high biological activity, faster (in hours) than other commercial composting technologies (in weeks). When bio-waste of known origin is used, the produced material can be used unhindered even for the most demanding food production. When biowaste is an integral part of mixed municipal waste, even if quality material is obtained, its use is limited and practically impossible due to strict legal regulations. But it can be used to revitalize degraded areas. In many countries, there are significant large quantities of municipal biological waste and sewage sludge, with which it is not known what and where to dispose of. Different types of organic materials can be used for the revitalization (greening) of devastated lands. Quantities of these materials are usually limited and often very expensive, so successful revitalizations are rare. With a new low-cost technology, the total biowaste contained in municipal waste could be used for the revitalization of devastated areas. The paper explains the method of obtaining biologically highly active material and the reuse of this material in greening and erosion reduction at the waste disposal site in Split/Croatia is shown.

Keywords: Innovative Technology, Biowaste, Sewage Sludge, Degraded Areas.

INTRODUCTION

A low-cost technology has been developed that stabilizes and transforms biowaste into a soil improver with high biological activity, faster and with higher processing capacity than most other commercial plants for rapid decomposition of biomaterial.

When bio-waste of known origin is used, the produced material can be used unhindered for the most demanding food production. When biowaste is of unknow origin, as for example as an integral part of mixed municipal waste, even if quality material is obtained, its use is limited and practically impossible due to strict legal regulations. But because of some very specific characteristics, achieved through specific conditions of decomposition od organic waste, product obtained with the new technology, can be used for other purposes, as for example for mitigation of erosion and for revitalization of degraded areas such as unrehabilitated queries, mines, and ash and

---

[#] corresponding author: predrag.umicevic@gmail.com sludge dumps. Recent use has been confirmed as such by the Croatian Ministry of Environmental Protection and Green Transition. Problem of revitalization of degraded areas is usually related to the lack of appropriate cheap organic materials, because the needed number of materials like compost and other green materials (sawdust, straw) are usually limited and often very expensive to be used for revitalization [1]. New low-cost technology, enables to process different biowaste, in active cheap material, with such a property that could be used for mitigate the erosion and also for the revitalization of devastated areas. The example of utilizing otherwise unusable organic waste for the revitalization of certain spaces is a prime example of cooperation between the public and private sectors, based on the "win-win" principle, and an excellent example of circular waste management.

Innovative technology

A technology – a bio stabilizer - has been developed that allows the biological fraction to be adequately processed in a short time process, of the order of one day, compared to the example of a classic composting plant where the processes last at least two months. It is a mobile plant that generally does not require large spaces. The thermophilic conditions enables that the biological material is process, in hours, into product, with the quality of least as a "soil improver". The composter provides aerobic conditions during the entire process, due to which there are no unpleasant odours (NH_3, CH_4, H_2S...) from very beginning of the process. Process capacity, depends of local condition, and can be up to 10 and even more tons per day. Electricity consumption is around of 50-60 kW. The plant is, beside of the location in Smederevo (Serbia), where the plant is in operation for several years, currently in operation for processing of waste food and greenery from parks in Resort Valamar in Poreč (Croatia), and for different sorts of biowaste and municipal biowaste in the public company Čistoća Split (Croatia). Processing of sludge from wastewater treatment was approved on the waste water treatment plant (WWTP) in Mostar. In the next figure the outlook of the plant, on the disposal site of household waste in Mostar, is given.

Figure 1 Plant on the disposal site in Mostar (Bosnia and Hercegovina)

BIOWASTE TREATMENT

Municipal bio waste

In the next figure the outlook of the different biological input material, processed on the Landfill Karepovac (Split, Croatia) is given. Following biowaste is processed: on the source collected household biological waste, biowaste from restaurant, greenery from parks and seaweed.

Figure 2 Outlook of biowaste is processed in Split: on the source collected household biological waste, biowaste from restaurant and greenery from parks

In the next figure the outlook of the final products after only of few hours of processing in bio stabilizer are given. The final product, it is odourless. Besides that, the product material is dry and easy manipulative and easy for transport.

Figure 3 Outlook of the final products after only of few hours of processing in bio stabilizer

Sludge treatment (example of Mostar)

On WWTP the treatment of sludge, after the second stage water treatment, thickened on about 20 % dry matter, was tested. In the next figure outlook of, two years aged sludge on local landfill before treatment is shown.

Figure 4 Outlook of, after second stage waste water treatment sludge, two years aged, with 20 % dry matter, before treatment

Due to excessive humidity, with only 20% dry matter, the treatment of sludge was done with the addition of different types of auxiliaries: stabilized from mixed municipal waste, greenery and grass, leaves and/or sawdust.

In the next figure outlook of one of eight hours processed sludge is shown.

Figure 5 Outlook of treated sludge (600kg) with the addition of sawdust (200kg) after screening on 5 and 10 mm sieves

Sludge remains odourless, with even up to 90 % dry matter, and easy manipulative and easy for transport.

REUSE OF BIOSTABIIZED PRODUCTS FOR SOIL EROSIN CONTROL AND REVITALIZATION OF DEGRADABLE AREAS

Characteristics of bio stabilized material

Because of the specific operational conditions in bio stabilizer, the two parameters used in the practice for evaluation of the activity of organic material (and organic waste), Total Organic Carbon (TOC) and Dissolved Organic Carbon (DOC) remain relatively high. In commercial compost DOC is about 500 mg/kg DM (DM – Dry Matter) and after treatment in bio stabilizer on the level of several grams per kilogram. A high concentration of DOC in the material from the stabilizer may indicate that the compost is not completely stabilized. This can be a problem with controlled agricultural production, but not when it is necessary to speed up the return of nutrients and other values of the devastated soil. On the contrary, this increased value of DOC is most likely an advantage. The DOC in the material from the stabilizer, which is processed in a few hours, probably consists of slightly different, highly soluble organic molecules, compared to those in the classic composting process, which lasts for weeks.

Recultivation and soil erosion mitigation

Croatia, as well many other countries, records a significant increase in the number of fires in open spaces. After a fire, as a rule, the soil is depleted of nutrients and subject to erosion, so that burnt surfaces not only lose their primary function as a habitat for plants, but the surface part of the soil is physically lost by washing away [2]. Fire significantly affects soil properties because organic matter located on, or near, the soil surface is rapidly combusted. The changes in organic matter, in turn, affect several chemical, physical, and microbiological properties of the underlying soil [3]. The high contain of total and dissolved organic carbon led to idea, to test in the bio stabilizer produced material for soil erosion control at a landfill Karepovac in Split where erosion, after only few years after the landfill rehabilitation poses a great danger. Exceptionally intensive erosion is visible especially on the side embankments. In the next figure is shown that on the crown of the landfill, where it has not yet come to visible traces of erosion, to deep "holes and channels" due to the removal of the final layer of material.

Figure 6 Erosion on the landfill before bio stabilized material is used

The biostabilities material was spread over the surface, where are already visible holes on the side parts, were filled by mixing bio stabilized material with inert material.

In the next figure the results of used material are shown. The results were surprisingly good. In a very short time the first traces of greenery appeared.

Figure 7 Results after a short time of using the material

The addition of not stabilized compost with a high DOC (dissolved organic carbon) content can be an effective approach to speed up the restoration of devastated land after a fire or for stoppage of erosion like on the pictures above, because not stabilized compost, with a higher content of (most likely!) readily available organic matter, can provide a rich food source in the deeper soil layer, than conventional compost, for microorganisms and encourage a faster development of soil biological activity.

CONCLUSION

New opportunity has opened with the invention of a low-cost technology for biowaste that has no ecological or financial usage beside landfilling. When biowaste is an integral part of mixed municipal waste, even if quality material is obtained, its use is limited. In many countries, there are significant large quantities of municipal biological waste and sewage sludge, with which it is not known what and where to dispose of. At the same time, there are many degraded areas that need recultivation. Material used for recultivation od degraded areas is a win-win situation because the material is used and the degraded areas are being recultivated at the same time.

REFERENCES

1. Municipal Waste Report 2023 (Izvješće o komunalnom otpadu 2023. Godine),https://isgo-portal.mingor.hr/sites/default/files/izvjesca/2024-10/Izvje%C5%A1%C4%87e%20o%20komunalnom%20otpadu%20za%202023%20-%20rev1.pdf.
2. Faculty of Agriculture in Zagreb, head: Prof. Dr. Sc. Ivica Kisić (Agronomski fakultet u Zagrebu, voditelj prof. dr. sc. Ivica Kisić), (2018), Utjecaj otvorenih požara na kvalitetu tla i voda, https://www.agr.unizg.hr/upload/nastava/dan_doktorata/dan-dr2021_14_delac.pdf;
3. DeBano, Leonard F. 1991. The effect of fire on soil properties. In: Harvey, Alan E.; Neuenschwander, Leon F., compilers. Proceedings-management and productivity of western-montane forest soils; 1990 April 10-12; Boise, ID. Gen. Tech. Rep. INT-280. Ogden, UT: U.S. Department of Agriculture, Forest Service, Intermountain Research Station. p. 151-156.

XVI International Mineral Processing
and Recycling Conference
28-30 May 2025, Belgrade, Serbia

DOI: 10.5937/IMPRC25050F

Original research article

CRYSTALLIZATION CHALLENGES IN HYDROMETALLURGY

Kerstin Forsberg[#], 0000-0002-3239-5188,
KTH Royal Institute of Technology, Stockholm, Sweden

ABSTRACT – Crystallization and precipitation processes are of key relevance in extractive metallurgy. In battery recycling eutectic freeze crystallization has recently emerged as an energy saving alternative to evaporative crystallization. Crystallization of Ni, Co, and Mn sulphate salts of high purity can be obtained by this technology. Antisolvent crystallization can also provide interesting advantaged within extractive metallurgy. In particular the crystallization of rare earth salts has shown promising results. This work will highlight challenges and opportunities connected to these 2 unit operations.

Keywords: Battery Recycling, Eutectic Freeze Crystallization, Antisolvent Crystallization, Metal Recovery.

INTRODUCTION

The shift toward achieving climate neutrality relies heavily on specific energy-critical metals, which play a vital role in the generation and storage of renewable energy, as well as in electrified transportation. To facilitate this industrial transformation, it is crucial to develop sustainable methods for recycling materials and recovering resources. This presentation will discuss the challenges and opportunities associated with hydrometallurgical processing, focusing on material recovery and in particular new crystallization approaches.

According to the latest IPCC report, actions to limit global warming to 1.5°C, as agreed upon in the COP21 Paris climate accords, must include electrifying our industries and societies, as well as promoting a circular economy. These measures require a reliable and sustainable supply of essential technology metals, with recycling efforts being a key component. This session will explore two innovative technologies, antisolvent crystallization (ASC) and eutectic freeze crystallization (EFC), which have the potential to reduce the environmental impacts of hydrometallurgical processes for recovering critical raw materials.

LITHIUM-ION BATTERY PRODUCTION AND RECYCLING

Lithium-ion batteries (LiBs) are set to dominate the e-mobility and energy storage sectors over the next decade.[1] By 2019, the global market had approximately 218 GWh (over 1.2 million tons) of LiB energy storage capacity, with projections indicating an increase to 2,500 GWh (over 12.7 million tons) by 2030. This growth will generate a

---

[#] corresponding author: kerstino@kth.se

significant amount of waste, both from the manufacturing process and from decommissioned batteries.[2] Currently, the most common cathode material used in LiBs is $LiNi_{1/3}Mn_{1/3}Co_{1/3}O_2$, known as NMC111, but it is expected that materials with higher nickel content, such as NMC811, will take over in the future.[3,4]

Recycling LiBs helps mitigate raw material shortages and addresses concerns related to environmental impact and human health. For every ton of end-of-life LiBs, at least 22.2 tons of high-grade ore are needed to produce an equivalent market value. Despite the European Union's efforts to enforce battery collection and recycling targets, recycling rates remain low, reflecting the challenges in the system.

Various techniques have been developed to recycle LiBs. Among these, hydrometallurgy is considered more environmentally friendly than pyrometallurgy due to its lower energy consumption and higher recovery efficiency, particularly for lithium. Hydrometallurgical processes also offer greater metal selectivity and are better suited for handling complex and dilute waste streams, allowing for the recovery of valuable by-products and new battery materials.[5]

In conventional LiB recycling, the so-called "black mass" is typically first treated with sulfuric acid. After separation and purification, metals such as nickel, cobalt, and manganese are recovered as sulphates via evaporative crystallization, while lithium is recovered as lithium carbonate or lithium hydroxide.[6] These sulphates can then be used to synthesize NMC cathode materials through re-dissolution and co-precipitation of hydroxide precursors. One major challenge in this method is the large amounts of sodium sulphate produced as a by-product.

ANTISOLVENT CRYSTALLIZATION

Recently, anti-solvent crystallization has appeared as an energy effective alternative which also can provide a better control of the resulting salt purity.[7] ASC is commonly applied in the pharmaceutical industry where crystals of high quality are essential. Recently, we have demonstrated the use of ASC for crystallization of battery precursor salts and also for selective recovery of rare earth sulphates at ambient temperature and pressure.[7-10] ASC opens for exact control of the supersaturation through the dosage and mixing of anti-solvent to achieve the targeted purity of the final product. However, ASC is rarely applied in industrial scale for metal salt recovery even though it is a promising option for recovery of high-quality salts of critical metals needed e.g., for battery and permanent magnet production. We have developed an approach where ASC is applied to crystallize metal carboxylates, which can be directly calcined into new cathode material as an alternative to re-dissolution of metal sulphate salts and precipitation of mixed metal hydroxide precursors. By this approach no sodium sulphate waste is generated.

EUTECTIC FREEZE CRYSTALLIZATION

The world is currently facing a shortage of freshwater along with limited energy resources. Water treatment processes such as reverse osmosis, nanofiltration and ion exchange produce aqueous waste streams with a high salt content. The disposal of such brines is a growing concern globally. Eutectic freeze crystallization is a technology that can be used to sustainably recover pure water as well as dissolved salts from concentrated brines, emanating from e.g. desalination, pulp and paper, mining, metallurgy, textile, and petrochemical industries, with no chemical consumption and low energy demand.[11-20] EFC is expected to lead to more energy-efficient and environmentally sustainable processes where water can be recycled and waste minimized. This knowledge is of central importance for solving challenges within hydrometallurgy. Successful implementation of this technology will lead to increased resource recovery and waste minimization, thereby directly linking to the UN development goals to promote sustainable industrialization and access to clean water. In order to achieve this, the technology needs to be improved through a better understanding of how controlled growth can be achieved and how incorporation of impurities can be avoided.

One of the beauties with EFC is that the energy needed to separate water as ice is only one-seventh of that required to separate it as vapor. In addition, no addition of chemicals is required, and corrosion is minimal at low temperature. Furthermore, the process can be designed to recover the water and salts in a purer form than by e.g. evaporation. If successful, this technology can be applied to solve several industrial challenges connected to production of pure water and salts and disposal of wastewater streams.

The working principle of EFC is based on cooling a concentrated saline aqueous solution down to the eutectic point where salt crystals and ice crystals are formed simultaneously. The two types of crystals can in principle easily be separated from each other due to density differences in relation to the aqueous phase. The ice is expected to be relatively pure. Under certain conditions however, ice agglomeration can occur whereby salt crystals can be trapped into and pollute the ice product.[21] Due to the low temperatures, EFC normally produces highly hydrated salts. One of the highlights of EFC is the fact that the hydrated salts will transform into lower hydrates as the temperature is increased. In a continuous process, this can occur in a separate slurry-dewatering chamber, where the supernatant is re-circulated to the EFC crystallizer. This dissolution and re-crystallization will occur under a relatively low supersaturation, which favors impurity rejection. Downstream processing, such as washing and filtration, also has a large impact on the purity of the product crystals and depends heavily on crystal size and morphology. In addition, clever heat integration is key to achieving an energy- and cost-effective process.

There are many processes where EFC could replace conventional technologies to minimize energy consumption and to recover resources (pure water and salts).[14-18] EFC has been shown to be competitive compared to membrane distillation as a chemical-free process although scaling can occur in both processes.[12] In comparison with cooling crystallization, the potential yield is higher – theoretically 100% for a binary system. EFC is also strongly preferred to evaporative crystallization, as it requires much less energy.[1] This is evident since the heat of fusion of ice (6 kJ/mol) is lower than the heat of evaporation of water (41 kJ/mol). Recent pilot plant tests have proven that chloride-based EFC systems can be comparable to evaporation in economic terms.[14] EFC is a relatively novel technology that has until recently only been studied at lab and pilot scale at a proof-of-concept level. The first full scale plant for treatment of mining wastewater has recently been constructed in South Africa.

Eutectic freeze crystallization has recently been applied to recover Ni and Co sulphate hydrates in recycling of NMC batteries.[20]

CONCLUSION

Eutectic freeze crystallization is a potentially energy saving technology compared to evaporative crystallization. In hydrometallurgy EFC has shown promise in crystallization of metal sulphate hydrated salts. Antisolvent crystallization can produce crystals that are highly soluble in water solutions. In hydrometallurgy the technology show promise in crystallization of rare earth salts. Eutectic freeze crystallization and antisolvent crystallization present complementary capabilities in resource recovery and purification within hydrometallurgical processes. The techniques offer energy-efficient, environmentally friendly alternatives to conventional separation methods. Their integration into hydrometallurgical workflows can enhance process sustainability while enabling the recovery of valuable components from complex aqueous systems.

ACKNOWLEDGEMENT

The authors are grateful to the Swedish Energy Agency, Sweden for funding this research work within the program Batterifonden (P2024-02811).

REFERENCES

1. Utveckla myndighetssamverkan för Sveriges delar av en hållbar europeisk värdekedja för batterier, 2022, Statens energimyndighet, ISBN: 978-91-7993-089-9.
2. Melin, H.E.; Rajaeifar, M.A.; Ku, A.Y.; Kendall, A.; Harper, G.; Heidrich, O. Global implications of the EU battery regulation. *Science* 2021, *373*, 384–387.
3. Kim, T.; Song, W.; Son, D.-Y.; Ono, L.K.; Qi, Y. Lithium-ion batteries: Outlook on present, future, and hybridized technologies. *J. Mater. Chem. A* 2019, *7*, 2942–2964.
4. Malik, M., Chan, K.H., Azimi, G., 2022, Review on the synthesis of LiNixMnyCo1-x-yO2 (NMC) cathodes for lithium-ion batteries, Materials Today Energy, 28, 101066.
5. Neumann, J.; Petranikova, M.; Meeus, M.; Gamarra, J.D.; Younesi, R.; Winter, M.; Nowak, S. Recycling of Lithium-Ion Batteries—Current State of the Art, Circular Economy, and Next Generation Recycling. *Adv. Energy Mater.* 2022.
6. Ma Y., Svärd M., Xiao X., Gardner J., Olsson R., and Forsberg K. (2020). Precipitation and crystallization used in the production of metal salts for Li-ion battery materials. Metals, 10(8).
7. Seda Demirel, H. Svärd M., Uysal D., Murat Doğan Ö., Zühtü Uysal B., Forsberg K.* (2022). Antisolvent Crystallization of Battery Grade Nickel Sulphate Hydrate in the Processing of Lateritic Ores, *Separation and Purification Technology* (IF 7.3), Vol. 286, 120473.
8. Svärd, M., Sanku, M., Pawar, N. & Forsberg, K. (2025). Antisolvent crystallization of rare earth sulfate hydrates: Thermodynamics, kinetics and impact of iron. *Separation and Purification Technology*, 354.
9. C Ma, M Mohamoud, T Punt, J Li, M Svärd, K Forsberg. (2024) Crystallization of Cathode Active Material Precursors from Tartaric Acid Solution. *ChemSusChem*, e202401523.

10. Korkmaz K., Alemrajabi M., Rasmuson Åke C., Forsberg K. M.* (2020). Separation of Valuable Elements from NiMH Battery Leach Liquor via Antisolvent Precipitation. *Separation and Purification Technology* (IF 5.8), vol. 234.
11. Fernández-Torres M.J., D.G. Randall, R. Melamu, H. von Blottnitz A comparative life cycle assessment of eutectic freeze crystallisation and evaporative crystallisation for the treatment of saline wastewater. Desalination 306 (2012).
12. Naidu G., Zhong X., Vigneswaran S. Comparison of membrane distillation and freeze crystallizer as alternatives for reverse osmosis concentrate treatment. Desalination 427 (2018).
13. From crazy to conquest: a chilling waste solution, University of Cape Town, published on-line 2018-03-10, accessed 2018-04-02.
14. Ahmad A. Huiting H., Harmsen D., Petrutiu D., Toussaint V. (2017) Treatment of spent cation exchange regenerant with eutectic freeze crystallization. Feasibility study for Demin Water Plant Botlek (Techn report, proj nr 400533). Accessed 2018-03-31, TKI Water Technologie website.
15. Randall D.G., Nathoo J., Lewis A.E. A case study for treating a reverse osmosis brine using Eutectic Freeze Crystallization—Approaching a zero waste process. Desalination 266 (2011).
16. Randall D. G. Zinn C. Lewis E. Treatment of textile wastewaters using Eutectic Freeze Crystallization. Water Sci and Techn 70 (2014).
17. Becheleni E.M.A., Rodriguez Pascual M., Lewis A.E., Rocha S.D.F. Influence of Phenol on the Crystallization Kinetics and Quality of Ice and Sodium Sulfate Decahydrate during Eutectic Freeze Crystallization. Ind Eng Chem Res 56 (2017).
18. Lewis A.E., Nathoo J., Thomsen K., Kramer H.J., Witkamp G.J., Reddy S.T., Randall D.G. Design of a Eutectic Freeze Crystallization process for multicomponent waste water stream. Chem Eng Res and Des 88 (2010).
19. Hasan M., Rotich N., John M., Louhi-Kultanen M. Salt recovery from wastewater by air-cooled eutectic freeze crystallization. Chem Eng J 326 (2017).
20. Ma Y., Akbarkermani M., Svärd M., Xiao X., Sahadevan S.A., Gardner J., Olsson R.T., Forsberg K. (2024). Phase diagrams of $CoSO_4$-H_2O and $CoSO_4$-H_2SO_4-H_2O systems for $CoSO_4{\cdot}nH_2O$ (n=6,7) recovery by cooling and eutectic freeze crystallization. Hydrometallurgy, 106332.
21. Peters E. M., Chivavava J., Rodriguez-Pascual M., and Lewis A. E. Effect of a Phosphonate Antiscalant during Eutectic Freeze Crystallization of a Sodium Sulfate Aqueous Stream. Ind Eng. Chem. Res. 55 (2016).

XVI International Mineral Processing
and Recycling Conference
28-30 May 2025, Belgrade, Serbia

DOI: 10.5937/IMPRC25055M

Original research article

CRITICAL MINERALS: CHALLENGES AND OPPORTUNITIES IN PLATINUM GROUP MINERAL FLOTATION

Belinda McFadzean[#], 0000-0002-5905-2273,
Avuyile Wali, 0000-0002-0047-0892,
Megan Becker, 0000-0002-7025-137X,
Stefan Geldenhuys, 0000-0001-9408-5989,
Centre for Minerals Research, Cape Town, South Africa

ABSTRACT – Platinum group minerals (PGMs) are critical for the green energy transition, playing key roles as catalysts in fuel cells and catalytic converters. Their limited global supply as well as geopolitical challenges further elevate their strategic importance. Southern Africa continues to dominate the global supply of PGMs, but mining operations face increasing challenges as ore bodies become deeper and more mineralogically complex. These complexities include a higher prevalence of slower-floating PGM species, such as platinum arsenides, and problematic gangue minerals like talc and serpentine. This paper addresses these challenges by ranking the major PGM species in order of floatability and provides critical insights for optimizing flotation processes. Additionally, the importance of effective gangue management in mineralogically complex ores is illustrated through the decoupling of gangue recovered by entrainment or true flotation and, further, by mineral species. The findings offer broader implications for addressing mineralogical barriers to flotation, providing solutions applicable not only to PGM ores but also to other complex ore systems. These advancements aim to enhance the efficiency and sustainability of mineral processing in the face of evolving global resource challenges.

Keywords: Critical Minerals, Platinum Group Minerals.

INTRODUCTION

Platinum group minerals (PGMs), from which platinum group elements (PGEs) are sourced, have been classified as critical minerals in Australia, the United States, Japan, India and the Eurozone [1]. South Africa and Russia continue to dominate the PGM global supply, but mining operations are facing increasing technical challenges due to deeper and more mineralogically complex ore bodies. The specific challenges facing PGM ore bodies are: (1) the simultaneous flotation recovery of multiple PGM species, with increasingly higher prevalence of slower-floating species; (2) the introduction of greater mineralogical complexity in the form of high concentrations of phyllosilicate alteration minerals; (3) mass pull reduction targets due to environmental and economic constraints, including transport and downstream smelter operations; (4) impurities in the concentrate that incur smelter penalties, (5) high frequency of considerable ore variability.

[#] corresponding author: Belinda.mcfadzean@uct.ac.za

PGM ore bodies are made up of varying concentrations of PGMs, including sulfides, arsenides, tellurides and alloys [2]. Sperrylite ($PtAs_2$) is currently considered the least floatable of the PGMs [3]. Given that the highest concentration of sperrylite occurs in the Platreef, South Africa's largest PGM ore body, it presents a research topic of significant interest.

The gangue mineralogy of PGM ores is equally challenging, often containing high concentrations of soft, phyllosilicate alteration minerals that grind to ultrafine sizes. Their anisotropic surface charge leads to electrostatic interactions with both valuable and gangue minerals. This paper explores these challenges and potential remediation strategies.

EXPERIMENTAL

PGM species floatability

A combination of techniques was used in this study, including mineral synthesis, microflotation tests, open circuit potential and Raman spectroscopy. For detailed descriptions of each of these techniques, the reader is referred to Wali et al (2024) and Wali (2024) [4,5].

Effect of alteration minerals

Mineralogical analysis was performed on feed and concentrate samples generated in a hybrid, mechanical flotation cell using QEMSCAN (Quantitative evaluation of minerals by scanning electron microscopy). Entrainment was decoupled from true flotation by generating an entrainment factor at very high depressant dosages where all naturally floating gangue is depressed. This entrainment factor is then applied to standard depressant dosage conditions [6].

Mass pull reduction and penalty element impurities

Data is taken from a large metallurgical sampling campaign conducted on a PGM UG2 operation [7].

RESULTS AND DISCUSSION

PGM species floatability

Error! Reference source not found. shows the microflotation recovery at pH9 and pH3 of the arsenides, $PtAs_2$ (sperrylite) and Pd_2As (palladoarsenide), the tellurides, $PtTe_2$ (moncheite) and $PdTe_2$ (merenskyite), and PtS (cooperite). The natural hydrophobicity of the minerals, where no collector is added, shows that at both pH9 and pH3 sperrylite is very hydrophilic (recoveries of 7 and 8%, respectively), while the other minerals all have some degree of natural hydrophobicity. PtS is particularly hydrophobic, with a collectorless recovery of 95%. Collector addition (green bars) induces additional hydrophobicity, as would be expected. However, sperrylite remains the least floatable of the minerals, particularly at pH9, the natural pH at which PGM concentrators operate (22%). Some degree of hydrophobicity can be induced by collector addition at pH3, however, it is still poorly floatable (61%). Some minerals, such as PtS at pH9 and Pd_2As at pH3, show very little increase in hydrophobicity when collector is added compared to their natural hydrophobicity. However, unlike sperrylite, their recoveries remain good since they were already high in the absence of any collector.

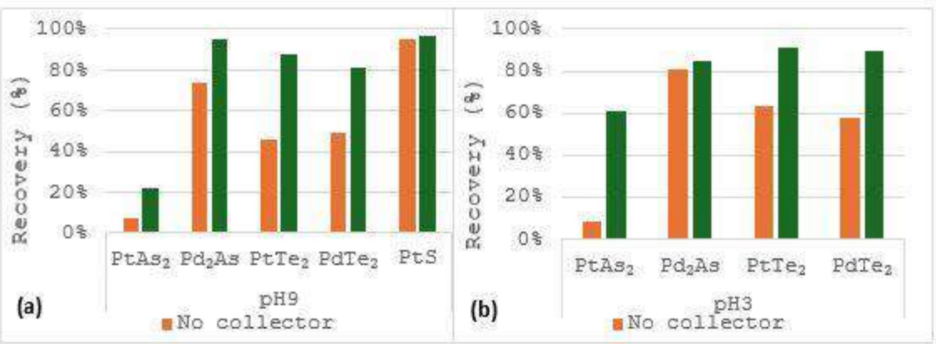

Figure 1 Microflotation recovery at pH9 (a) and pH3 (b) of the arsenides, PtAs2 (sperrylite) and Pd2As (palladoarsenide), the tellurides, PtTe2 (moncheite) and PdTe2 (merenskyite), and PtS (cooperite). Note data only available for PtS at pH9. Collector concentration was 1.7E-06 mol/g

In attempting to explain the poor floatability of sperrylite it is instructive to compare the change in mineral electrode potential (Eh) with the change in pH. A greater slope indicates greater reactivity to electron transfer reactions while a lower slope may indicate passivation or hydroxide layer formation [8]. **Figure 1** shows the microflotation recovery as a function of the slope of the Eh versus pH curve for each mineral. This shows that the Eh/pH dependence is low for sperrylite, which corresponds to lower recoveries. It is also clear that, generally, the dependence is lower at high pH, which would correspond to greater hydroxide surface coatings.

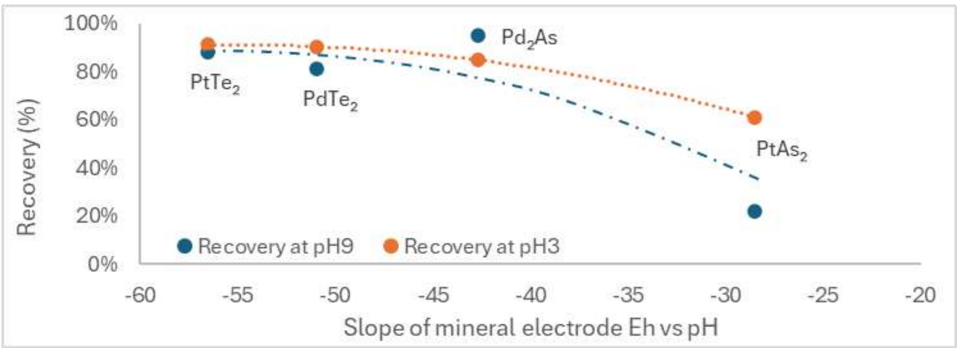

Figure 1 Microflotation recovery of the PGE-tellurides and -arsenides in the presence of collector at pH9 and 3, versus the dependence of the potential of each mineral electrode on pH

Not only has the sperrylite surface been shown to be relatively inert to electron transfer reactions, it has also been shown to have high affinity for water and hydroxide interaction [4]. Research is underway to provide alternative collectors or conditions conducive to the flotation recovery of this valuable mineral.

Effect of alteration minerals

All PGM ores contain alteration minerals in varying concentrations, with large variability even within ore types. Quantitative mineralogy was performed on 11 different PGM ores with alteration mineral content (talc, serpentine, chlorite, amphibole) varying between 4.5% and 32%. Some of these alteration minerals, such as talc and serpentine, are known to be problematic, while in others, such as amphibole and chlorite this has not directly been proven. Talc is a naturally floatable mineral that is an alteration product of pyroxene. As such, it is found highly disseminated through the pyroxene mineral which forms the bulk of most PGM ore bodies. A feed (a) and concentrate (b) from a PGM concentrator is shown in **Error! Reference source not found.** where the finely disseminated talc (in bright green) is clearly visible on the pyroxene particles (dark green) in the concentrate. This results in the true flotation recovery of the bulk pyroxene into the concentrate, which would not be otherwise floatable. This increases the mass pull, with all the associated consequences that this entails.

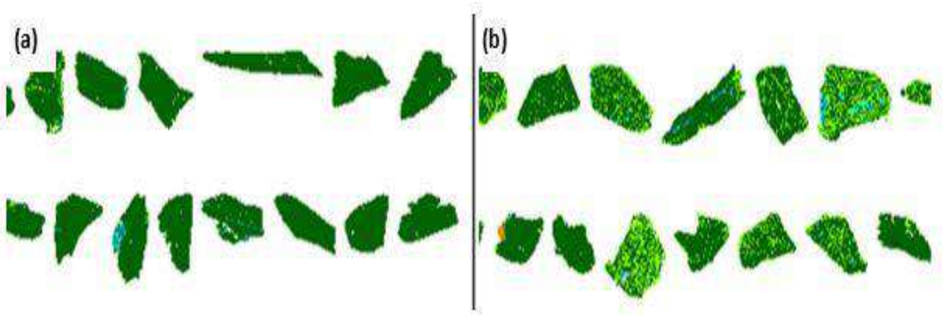

Figure 2 False colour images of particles from a primary rougher stream. Feed (a) and concentrate (b), 38-150 µm size fraction. Pyroxene in dark green, talc in light green

Serpentine, unlike talc, is not a floatable mineral but can cause substantial challenges in the flotation process. The softness of serpentine and the inherent structural charge imbalance result in very fine “slimes” particles that coats PGMs and increases slurry viscosity, both of which are detrimental to PGM recovery.

The detrimental effects of alteration minerals on platinum and palladium (2E) recovery are clearly shown in **Error! Reference source not found.**, where linear regression was applied on a number of common parameters affecting PGM recovery in batch flotation tests of the 11 ores referred to above. The only parameter found to be statistically significant at the 95% confidence level was the alteration mineral concentration, which had a pronounced detrimental effect indicated by its high normalized coefficient of -72.

Dispersants, such as sodium silicate, have been shown to be effective in slimes cleaning and rheology modification [9]. However, the dosages that are required are high and research is required to find dispersants that can deliver similar benefits at lower dosages.

Table 1 Linear regression on the given input parameters affecting 2E recovery of PGM in batch flotation tests. Min-max scaling was applied to normalise the coefficients

	Y-input (2E Recovery)	
	Coefficients	P-value
2E head grade (g/t)	20.25	0.17
Mass pull (%)	29.03	0.092
Alteration minerals (%)	-72.26	0.038
Depressant (g/t)	-101.17	0.098
Passing 75um (%)	19.50	0.067
Solids concentration (%)	-82.34	0.093
R^2	0.81	

Mass pull reduction and penalty element impurities

The commitment to reduce carbon emissions requires that mass pull is reduced, while maintaining recovery. Associated with that, concentrators that treat UG2 ore have the added challenge of incurring penalties for Cr_2O_3 concentrations above about 1.5%, which cause the build-up of highly refractory chromite spinel that affects furnace operation and capacity. Much of the gangue recovery to the concentrate is due to naturally floating talc as shown in the previous section. However, chromite is hydrophilic and is recovered by entrainment. There is, therefore, a need to decouple these two mechanisms of recovery to be able to better manage each one. In the laboratory study performed, **Error! Reference source not found.** shows that about half of the concentrate grade to a rougher concentrate came from true flotation, while the other half came from entrainment. Knowledge of the recovery mechanism allowed for better gangue management.

Table 2 Contribution to rougher concentrate grade from true flotation and entrainment for silicate minerals and chromite in a UG2 ore

	Concentrate grade from true flotation (%)		Concentrate grade from entrainment (%)	
	Silicates	Chromite	Silicates	Chromite
Unsized	43.6	5.3	26.6	24.5
+38	73.6	5.5	14.3	6.6
10-38	56.1	0.0	24.5	19.4
-10	27.6	9.2	31.6	31.6

Error! Reference source not found. shows the importance of circuit configuration on gangue management where data from a recleaner bank shows that residence time is more than 200 minutes. This is a surprisingly common occurrence where cleaner and recleaner banks are oversized for their application. By removing, repurposing or recycling streams from the last half of the recleaner bank gangue recovery by true flotation and entrainment can be reduced by about half and the grade of the concentrate upgraded substantially. Flotation models can be extremely successful in simulating these reconfigured circuits [7].

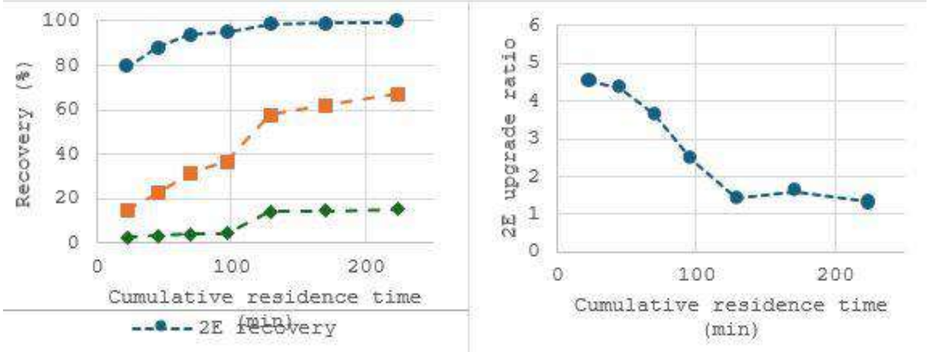

Figure 4 (a) 2E (Pt+Pd) recovery, gangue recovery by true flotation and entrainment as a function of recleaner bank residence time, (b) 2E (Pt+Pd) Upgrade ratio as a function of recleaner bank residence

CONCLUSIONS

This paper highlights that platinum group minerals, as critical minerals, share challenges with other ore types, including refractory behaviour, mass pull constraints and problematic floating and entrained gangue mineralogy. Alteration minerals were shown to be particularly problematic and PGM ores of all types show a strong negative dependence on recovery with increasing alteration mineral concentration. All aspects presented in this paper are topics of ongoing research to promote the sustainable use of this valuable resource.

REFERENCES

1. Creamer, M. (2022) Mining Weekly, https://www.miningweekly.com/article/platinum-group-metals-gaining-ground-in-australia-where-pgms-have-critical-mineral-status-2022-10-31
2. Corin, K.C., McFadzean, B.J., Shackleton, N.J., O'Connor, C.T. (2021) Challenges related to the processing of fines in the recovery of platinum group minerals (PGMs), Minerals, 11, 533. https://doi.org/10.3390/min11050533
3. Shackleton, N.J. (2007) Surface characterization and flotation behaviour of the platinum and palladium arsenide, telluride and sulphide mineral species. PhD thesis, University of Cape Town, South Africa.
4. Wali, A., Filippov, L., Fekry, A.M., O'Connor, C.T., McFadzean, B. (2024) An investigation into the effect of Eh and pH on the adsorption of a xanthate collector on sperrylite ($PtAs_2$): A surface and solution characterization study, Minerals Engineering, 217, https://doi.org/10.1016/j.mineng.2024.108949

5. Wali, A. (2024) An investigation into the floatability of platinum group arsenides and tellurides under varying collector and solution chemistries, PhD thesis, University of Cape Town, South Africa.
6. Wiese, J.G. (2009) Investigating depressant behaviour in the flotation of selected Merensky ores, MSc dissertation, University of Cape Town, South Africa.
7. McFadzean, B., Becker, M., Geldenhuys, S., Sweet, J. (2024) A methodology for gangue management in the flotation of a PGM-bearing ore through laboratory tests, mineralogical analysis and circuit modelling, Minerals Engineering, 208, https://doi.org/10.1016/j.mineng.2024.108604
8. Goktepe, F. (2002) Effect of pH on pulp potential and sulphide mineral flotation, Turkish Journal of Engineering and Environmental Science, 26, 309-318.
9. Molifie, A., Becker, M., Geldenhuys, S., McFadzean, B. (2023) Minerals Engineering, 195, https://doi.org/10.1016/j.mineng.2023.108024
10. Dagenais, K., Chamberlin, M. & Constantin, C. (2013) Modeling Energy Band Gap as a Function of Optical Electronegativity for Binary Oxides. Journal of Young Investigators. 25(3):1–6.
11. Hooge, F.N. (1960) Relation between Electronegativity and Energy Bandgap. Zeitschrift fur Physikalische Chemie. 24(3–4):275–282. DOI: 10.1524/zpch.1960.24.3_4.275.
12. Hu, Y, Gao, Z., Sun, W., Liu, X. (2012) Anisotropic surface energies and adsorption behaviors of scheelite crystal, Colloids and Surfaces A, 415, dx.doi.org/10.1016/j.colsurfa.2012.09.038

DOI: 10.5937/IMPRC25062C

Extended abstract

INNOVATIVE STRATEGIES FOR METAL RECOVERY FROM LFP-NMC LITHIUM-ION BATTERY BLENDS

Alexandre Chagnes[1#], 0000-0002-4345-6812,
Pierric Hubert[1], 0009-0004-9376-9907,
Safi Jradi[2], 0000-0003-1712-8986,
[1]Université de Lorraine-GeoRessources, Vandoeuvre-lès-Nancy, France
[2]Université Technologique de Troyes-L2N, France

Central to the energy shift and electric transport, lithium-ion batteries form the cornerstone [1-3]. The imminent future anticipates a surge in global gigafactories and recycling facilities dedicated to manufacturing and repurposing batteries, predominantly for electric vehicles. However, as the focus remains on electric vehicle batteries, the burgeoning market for smaller counterparts in electric bicycles propels the need for an evolving recycling industry. Distinguishing these batteries lies in their compositions. Electric vehicle batteries typically adhere to established NMC ($LiNi_xMn_yCo_zO_2$) or LFP ($LiFePO_4$) technologies. Conversely, electric bicycle and scooter batteries present a blend of NMC and LFP technologies, demanding adaptable processes to extract metals effectively from varying feed compositions.

The challenge lies in designing flexible chemical processes distinct from those tailored for electric vehicle batteries. Addressing this, the discussion spotlights the imperative to develop a versatile methodology capable of extracting metals despite shifting compositions. Additionally, the hydrometallurgical processes must efficiently recover cobalt, nickel, manganese, and lithium, even amid fluctuating and substantial iron concentrations, traditionally a hurdle in hydrometallurgy.

Hydrometallurgical processes treat black mass, which is a concentrate containing the valuable metals. The production of black mass from spent lithium-ion batteries involves several key steps [4, 5]. Initially, used batteries are collected and fully discharged to prevent any risk of short circuits or fires during subsequent processing. Following this, the discharged batteries undergo mechanical shredding into smaller fragments, breaking down the battery components, including the casing, electrodes, and separators. The resulting mixture then undergoes various separation techniques to isolate valuable materials. Physical separation methods, such as sieving, magnetic separation, and air classification, are employed to segregate materials based on their physical properties like size, magnetism, and density. Additionally, froth flotation exploits differences in surface

---

[#] corresponding author: alexandre.chagnes@univ-lorraine.fr

properties of materials; for instance, graphite from the anode is naturally hydrophobic, allowing it to be separated from hydrophilic cathode materials through flotation.

Figure 1 shows two typical hydrometallurgical flowsheets for processing NMC and LFP blackmasses [6, 7].

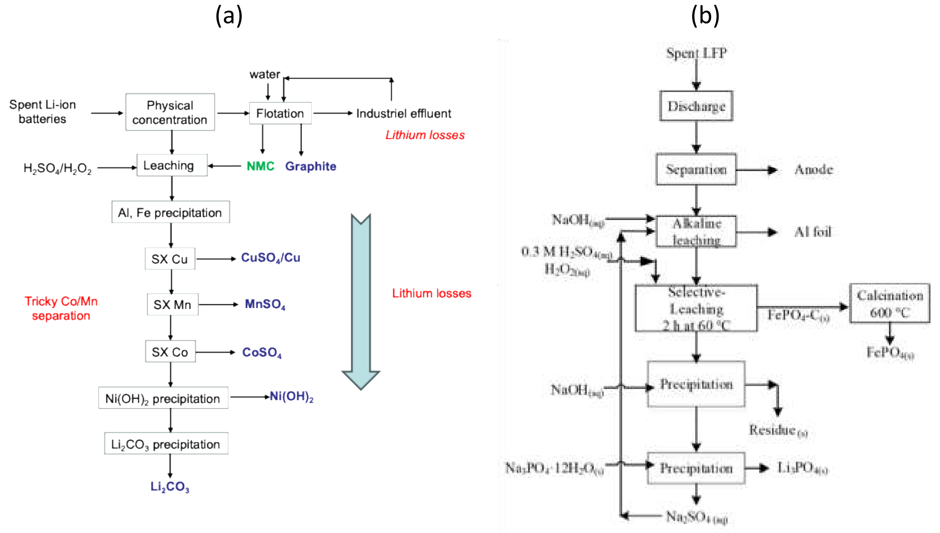

Figure 1 Typical flowsheets for processing (a) NMC black mass, and (b) LFP black mass [6, 7]

After leaching the NMC black mass with sulfuric acid in the presence of hydrogen peroxide, traces of aluminum and iron impurities are removed by precipitation around pH 3. Then, traces of copper can be precipitated as well or extracted by solvent extraction at low pH by using Acorga or LIX reagents depending on the copper concentration. Manganese is then extracted by using D2EHPA (di-(2-ethylhexyl) phosphoric acid) at pH 1.5. Cobalt is then extracted by solvent extraction at pH 4.2 and nickel can be precipitated as hydroxide whereas lithium is converted into lithium carbonate with sodium carbonate. This process works but the cobalt-manganese separation is challenging, and lithium loss occurs throughout the process.

The recycling of lithium iron phosphate (LFP) batteries is crucial for sustainable energy practices, given their widespread use in electric vehicles and energy storage systems. A prominent method for processing LFP black mass—the powdered residue containing valuable metals after initial battery dismantling—involves hydrometallurgical techniques.

Initially, the black mass undergoes treatment under alkaline conditions, leading to the dissolution of aluminum as aluminate ions ($Al(OH)_4^-$). Subsequently, lithium is selectively leached from the mixture, leaving behind iron phosphate. The extracted lithium is then precipitated as lithium phosphate by neutralizing the solution with sodium hydroxide, effectively removing remaining impurities.

While various hydrometallurgical flowsheets have been proposed in the literature, their economic viability remains uncertain, primarily due to the relatively low cost of LFP battery technologies. Consequently, direct regeneration of LFP materials is emerging as a potentially more efficient and cost-effective approach for recycling, as it aims to restore the active materials to their original state with minimal processing.

Conversely, mixtures of NMC and LFP appears are relevant stream for hydrometallurgical processes due to the presence of cobalt, nickel and manganese which increases its value. Figure 2a show a typical flowsheet to process blackmasses containing a blend of NMC and LFP.

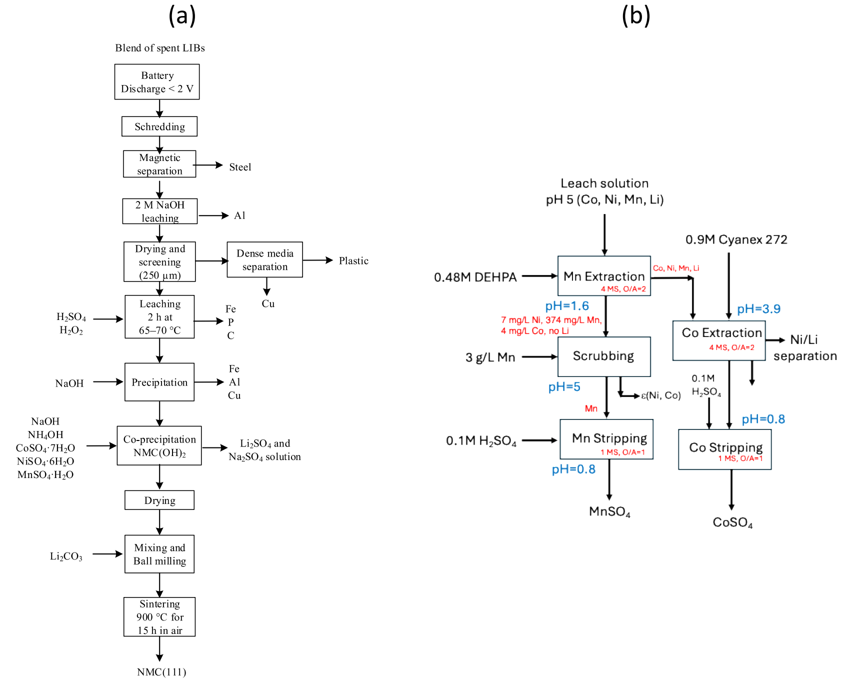

Figure 2 Hydrometallurgical flowsheet for processing NMC-LFP black mass from (a) literature and (b) from the present work [7, 8]

This talk presents experimental results aimed at understanding the physicochemical phenomena involved in acid-deficient leaching and optimizing key parameters to maximize leaching efficiency and selectivity. The study focuses on factors such as the solid-to-liquid ratio, sulfuric acid and hydrogen peroxide concentrations, and leaching time. Additionally, the optimization of experimental conditions for liquid-liquid extraction was carried out to efficiently extract and separate cobalt, manganese, nickel, and lithium. The collected data were then used to design the flowsheet shown in Figure 2a.

In this Figure, a blend of Nickel Manganese Cobalt (NMC) and Lithium Iron Phosphate (LFP) materials is leached using sulfuric acid and hydrogen peroxide. This process dissolves nickel, cobalt, manganese, and lithium, while iron and phosphate remain in the solid phase along with graphite. However, trace amounts of iron, aluminum, and copper may persist in the aqueous solution. These impurities are precipitated using sodium hydroxide. Subsequently, nickel, cobalt, and manganese are co-precipitated, separating them from lithium, to produce $NMC(OH)_2$, a precursor for cathode material production. The stoichiometry of this precursor is adjusted before precipitation by adding appropriate amounts of nickel, cobalt, and manganese sulfate. Co-precipitation is typically performed using a mixture of sodium hydroxide and ammonium hydroxide. The remaining lithium in the solution can then be precipitated as lithium carbonate using sodium carbonate.

In this presentation, we will outline the steps leading to the design of an alternative flowsheet for processing LFP-NMC black masses, as depicted in Figure 2b. This flowsheet leverages the physicochemical properties of transition metals in the presence of phosphates to develop a robust leaching process. In particular, two approaches will be presented investigated: acid-excess leaching and acid-deficient leaching with residue recirculation. A design of experiments (DoE) framework was applied to assess the impact of key parameters, including sulfuric acid and hydrogen peroxide concentrations, as well as solid-to-liquid (S/L) ratios, on the dissolution yields of target metals (Ni, Mn, Co, and Li). Acid-excess leaching achieved nearly complete dissolution of target metals but required additional purification steps to remove impurities. Acid-deficient leaching with a 60% recirculation of leaching residue improved dissolution yields by up to 12.5%, reduced reagent consumption, and minimized operational complexity. The study also evaluated separation strategies for manganese and cobalt through solvent extraction. Results indicate that while acid-excess leaching offers higher yields, acid-deficient leaching with residue recirculation is more cost-effective and environmentally friendly.

AKNOWLEDGMENT

The authors want to acknowledge Mrs. Laure Clerget from Artemise Company (FRANCE) for funding this work within the framework of the Neolithics project.

REFERENCES

1. Chagnes, A., Pospiech, B (2013). J. Chem. Technol. Biotechnol. 88, 1191-1199.
2. Mennik, F., Dinc, N.I, Burat, F (2023) Results Eng. 2023, 17, 100868.
3. Shen, K., Yuan, C., Hauschild, M. (2023) CIRP Ann. 72, 13-16.
4. Vanderbruggen, A., Hayagan, N., Bachmann, K., Ferreira, A., Werner, D., Horn, D., Peuker, U., Serna-Guerrero, R., Rudolph, M. (2022) ACS EST Eng. 2, 2130-2141.
5. Werner, D., Peuker, U.A., Mutze, T. (2020) Metals, 10, 316.
6. Chagnes, A., Swiatowska, J. (2015) Lithium Process Chemistry: Resources, Extractions, Batteries and Recycling, 1st Edition, Elsevier, Amsterdam.
7. Larouche, F., Tedjar, F., Amouzegar, K., Houlachi, G., Bouchard, P., Demopoulos, G.P., Zaghi, K. (2020) Materials, 13, 801.
8. Hubert, P., Noclain, A., Jradi, S., Chagnes, A. (2025) Metals, 15, 74.

XVI International Mineral Processing
and Recycling Conference
28-30 May 2025, Belgrade, Serbia

DOI: 10.5937/IMPRC25066S Extended abstract

FROM LINEAR TO CIRCULAR ECONOMY – STORY OF THE BOTTOM ASH

Michal Šyc[1#], 0000-0002-3323-9638,
Jiří Hykš[2], 0009-0002-9441-9365,
[1]Institute of Chemical Process Fundamentals of the Czech Academy of Sciences, Prague, Czech Republic
[2]Danish Waste Solutions, Horsholm, Denmark

ABSTRACT – Incineration of municipal solid waste (MSW) with energy recovery is a key component of integrated waste management in the Czech Republic. In 2021, approximately 6 million tonnes of MSW were generated, with around 0.75 million tonnes processed annually in four operating waste-to-energy (WtE) plants. These facilities produce about 0.2 million tonnes of incineration bottom ash (IBA), which contains up to 13 wt.% ferrous and 3 wt.% non-ferrous metals. However, recovery of valuable metals remains limited due to the lack of advanced separation technologies. A detailed case study from the Prague WtE plant confirmed that most recoverable metals are found in particles >2 mm, accessible without intensive comminution. A full-scale metal recovery facility is planned, with expected commissioning in 2026/2027, and the potential to recover up to 2,500 tonnes of metals annually, saving approximately 15,000 tonnes CO_2-eq emissions. In 2021, a new legal framework enabled IBA utilization in road construction, under strict environmental and technical criteria. A pilot project using 1,000 tonnes of IBA demonstrated compliance and feasibility. These developments support broader IBA valorization, aligning with circular economy principles and national climate goals.

Keywords: Incineration Bottom Ash, Metal Recovery, Waste-to-Energy.

INTRODUCTION

Incineration of municipal solid waste (MSW) with energy recovery, commonly referred to as waste-to-energy (WtE), is a key technology for the management of residual waste streams, particularly in urban regions. In 2021, the Czech Republic generated nearly 6 million tonnes of MSW. In alignment with European Union (EU) objectives, which cap the share of incinerated MSW at 25%, a national WtE processing capacity of approximately 1.5 million tonnes per annum is required.

At present, the Czech Republic operates four WtE facilities with a combined processing capacity of approximately 0.75 million tonnes annually. These facilities produce an estimated 0.2 million tonnes of incineration bottom ash (IBA) per year. Based on previous analyses, IBA generated in the country contains up to 13 wt.% of ferrous metals and approximately 3.0 wt.% of non-ferrous metals (dry matter basis), indicating a significant resource potential.

[#] corresponding author: syc@icpf.cas.cz

Despite this, only around 11,000 tonnes of ferrous metals and 500 tonnes of non-ferrous metals are currently recovered annually, largely due to the absence of advanced non-ferrous recovery technologies. The remaining mineral fraction is mostly landfilled or used as landfill cover. This underutilization represents a missed opportunity from both environmental and economic perspectives.

The legislative landscape changed significantly with the introduction of Decree No. 273/2021 Coll., effective from July 2021, which provides a comprehensive legal framework for the utilization of IBA in road construction. This regulation sets strict technical and environmental criteria, including thresholds for leachability and pollutant content, aimed at ensuring environmentally sound use of IBA as a secondary construction material.

RESULTS AND DISCUSSION

A detailed characterization study was conducted on IBA produced at the Prague WtE plant, which primarily processes mixed MSW from Prague and its surrounding areas. In 2021, compositional analyses confirmed that the IBA contained approximately 13 wt.% of iron scrap and 3.0 wt.% of non-ferrous metals, calculated on a dry matter basis. Pilot-scale metal recovery trials demonstrated that the majority of recoverable metals are concentrated in particles larger than 2 mm. These particles are largely liberated and do not require additional mechanical comminution for effective separation. This finding significantly enhances the economic feasibility of full-scale recovery processes. Based on these results, a full-scale metal recovery facility is under consideration at the Prague WtE site, with planned commissioning in 2026/2027. The facility is expected to recover up to 1,500 tonnes of non-ferrous metals and an additional 1,000 tonnes of ferrous metals annually. These recovery activities are estimated to result in greenhouse gas (GHG) emission savings of approximately 15,000 tonnes CO_2-equivalent per year, aligning with the City of Prague’s climate goals.

Mineral matrix after the metal recovery should be used in construction industry. To support it, a demonstration parking slot utilizing IBA as a subbase layer—designed in full compliance with the new legal framework— was constructed. According to Decree No. 273/2021, IBA must be classified as non-hazardous waste and comply with stringent leachability and pollutant content limits (Table 1 and Table 2). Leaching behavior is evaluated using the EN 12457-4 standard, with tests required for every 5,000 tonnes of IBA designated for use. These limits have been intentionally set to prevent the direct use of untreated IBA, encouraging pre-treatment and aging processes.

The introduction of the new legal framework for IBA utilization in the Czech Republic is a significant step toward circular economy implementation in the waste management sector. It not only promotes the safe reuse of mineral fractions in road construction but also incentivizes investment in advanced metal recovery technologies.

The Prague WtE case study demonstrates that substantial amounts of valuable metals can be recovered from IBA without intensive mechanical processing. The planned full-scale facility is poised to unlock this potential, delivering both environmental and economic benefits, including significant GHG reductions.

Table 1. Limit values in leachate according to EN 12457-4

	Limit values (mg/l)
pH	9-11
Chlorides	700
Fluorides	6
Sulfates	1 000
As	0.03
Ba	3
Cd	0.005
Cr_{tot}	0.2
Cu	1
Hg	0.0008
Mn	0.3
Na	400
Ni	0.03
Mo	0.5
Pb	0.05
Sb	0.07
Se	0.1
V	0.3
Zn	0.6

Moreover, the limits are also set for the content of pollutants in IBA (see Table 2) that have to be verified at least four times a year.

Table 2 Limit values for pollutants content in IBA

	Limit value
As (mg/kg)	45
Cd (mg/kg)	20
Cr (mg/kg)	200
Cu (mg/kg)	7 000
Hg (mg/kg)	1
Ni (mg/kg)	500
Pb (mg/kg)	1 000
Zn (mg/kg)	10 000
TOC (mg/kg)	30 000
PAU (mg/kg)	1*
PCDD/F (ng I-TEQ/kg)	10

*sum of benzo[a]pyren, benzo(b)fluoraten, benzo(k)fluoranten, indeno(1,2,3-cd)pyren

The pilot parking slot using 1,000 tonnes of bottom ash (see Figure 1) served as a demonstration of the technical and environmental viability of IBA utilization, fostering confidence among municipalities and infrastructure developers. Over the coming years, these developments are expected to lead to the full exploitation of the IBA resource potential and the integration of modern IBA treatment strategies that are fully aligned with circular economy and climate neutrality principles.

Figure 1 Construction of demonstration unit with bottom ash

ACKNOWLEDGEMENT

This work has been partially funded with state support from the Technology Agency of the Czech Republic and Ministry of the Environment of the Czech Republic within the Programme Environment for Life (Project SS02030008).

DOI: 10.5937/IMPRC25070K

Abstract

CRITICAL RAW MATERIALS (CRM) RECOVERY FROM NORWEGIAN DEPOSITS: CHALLENGES AND OPPORTUNITIES

Przemyslaw B. Kowalczuk[#]**,** 0000-0002-1432-030X,
Norwegian University of Science and Technology, Department of Geosciences,
S.P. Andersens veg 15, 7031 Trondheim, Norway

ABSTRACT – The secure supply of critical raw materials (CRM) and critical industrial minerals is essential for modern industries, including renewable energy, electronics, and high-tech manufacturing. Norway hosts a wide range of CRM deposits, such as antimony, beryllium, bismuth, cobalt, copper, indium, nickel, niobium, platinum group elements (PGE), rare earth elements (REE), scandium, tantalum, tungsten, vanadium, and zirconium, along with critical industrial minerals including barite, magnesium in olivine and dolomite, phosphate, silicon in quartz, graphite, and feldspar (Fig. 1). This presentation focuses on the ore characterization and mineral processing challenges associated with Norwegian CRM and industrial mineral deposits. It highlights the need for advanced mineralogical analysis techniques, tailored beneficiation strategies, and emerging processing technologies required to unlock the potential of these resources. By improving mineral liberation, optimizing separation methods, and integrating advanced processing solutions, Norwegian mineral resources can be better utilized to meet industrial demands.

Keywords: Critical Raw Materials, Industrial Minerals, Mineral Processing, Sensor-Based Sorting, Metallurgy.

Figure 1 Significant deposits of critical metals and industrial minerals in Norway [1]

[#] corresponding author: pshem.kowalczuk@ntnu.no

REFERENCES

1. Norwegian Ministry of Trade, Industry and Fisheries (2023) Norway mineral strategy, Norway mineral strategy - regjeringen.no, (access date: 10.03.2025)

SESSION LECTURES

XVI International Mineral Processing
and Recycling Conference
28-30 May 2025, Belgrade, Serbia

DOI: 10.5937/IMPRC25075A

Original research article

INVESTIGATIONS INTO LITHIUM MINERALS PROCESSING

Massoud Aghamirian[1,#], 0009-0002-9002-9095,
Vu Truong[1], 0009-0000-0349-3291,
Kristina Muntu[1], 0009-0008-0884-057X,
Jean-Gabriel Fraboulet[2], 0009-0000-4133-3272,
Sean Salour[2], 0009-0003-8494-389X,
Brian Kawenski Cook[1,3], 0000-0001-9128-6996,
[1]SGS Canada Inc., Lakefield, ON, Canada
[2]Imerys S.A., Paris, France
[3]Robert M Buchan Dept. of Mining, Queen's University, Kingston, ON, Canada

ABSTRACT – Spodumene is the primary lithium mineral, however, other minerals like lepidolite, petalite, zinnwaldite, and Li-clays are gaining importance. Different processing approaches are needed to address different challenges. Dense Media Separation (DMS) can concentrate spodumene and petalite, but recoveries are often limited by grain size. Froth flotation is widely used to concentrate spodumene and is the main lepidolite beneficiation method, where spodumene is floated with anionic fatty acids and lepidolite with cationic amine collectors. Zinnwaldite, a high-iron lepidolite mineral, can utilize magnetic separation and to some extent, flotation, whereas and Li-clays (e.g., hectorite and illite) are primarily concentrated through size classification.

Keywords: Spodumene, Petalite, Lepidolite, Zinnwaldite, Flotation.

INTRODUCTION

The growing demand for lithium-ion batteries (Li-Bs) in electric vehicles (EVs) and other transportation applications is driving the global lithium market. In response, the mining industry has experienced substantial growth in the development of new lithium projects worldwide. Historically, hard-rock minerals and brine deposits have been exploited for lithium production, but clay deposits, and secondary sources such as spent lithium-ion batteries are gaining attention [1,2].

Commercial lithium minerals commonly found in pegmatite deposits, include spodumene ($LiAl(SiO_3)_2$), lepidolite ($KLiAl_2Si_3O_{10}(OH,F)_3$), petalite ($LiAlSi_4O_{10}$), and amblygonite ($(Li,Na)AlPO_4(F,OH)$) [3]. Zinnwaldite, an iron-rich mica containing 0.8-1.9% Li, in gaining interest but may pose processing challenges due to its lower lithium content [4,5]. Lithium-rich clays such as hectorite and illite (1.35-3.6% Li), have strong potential due to their extensive deposits, although commercial processing is under development [6].

[#] corresponding author: massoud.aghamirian@sgs.com

At present, spodumene is responsible for over half of the global lithium supply. Typical concentration methods to produce battery-grade concentrates (>6.0% Li_2O and <1.0% Fe_2O_3) include Dense Media Separation (DMS) and froth flotation. DMS is best suited for coarse spodumene particles (1–20 mm), while finer fractions (<1 mm) require complex flotation circuits using fatty acid-based collectors under slightly alkaline conditions (pH 7.5–8.5). By-products from spodumene flotation circuits, such as feldspar, quartz, tantalite, microlite, and beryl, can also be targeted to enhance economic feasibility [7-9].

Lepidolite flotation typically employs cationic collectors under acidic conditions but faces selectivity challenges due similarities with other mica-type minerals like muscovite. Petalite processing uses the same techniques as spodumene (DMS and flotation), however, flotation is more challenging due to lower reactivity. Zinnwaldite beneficiation involves magnetic separation to exploit the high iron content, and sometimes low-pH amine flotation similar to lepidolite. Lithium clays have a limited amenability to flotation and are processed primarily through classification to remove coarser gangue minerals for downstream leaching given their fine-grained nature.

This manuscript summarizes recent advances in spodumene and lepidolite flotation, highlighting key findings from research at SGS Lakefield to support the expanding lithium mining industry.

SPODUMENE BENEFICIATION

History of Spodumene Processing

During the 20th century, particularly during WWII and the Cold War, the strategic importance of lithium compounds accelerated advancements in spodumene mining and processing, notably in King’s Mountain, North Carolina and the Black Hills of South Dakota [10,11]. Early manual sorting of spodumene was replaced by Dense Media Separation (DMS), a cost-effective method exploiting density differences between spodumene (~3.1 g/cm^3) and silicate gangue minerals (~2.65 g/cm^3) which is best suited for coarse grained spodumene (1-20 mm). For finer grained spodumene (<1 mm) froth flotation was the most effective beneficiation method, which relied on fatty acid-based collectors to selectively separate spodumene from gangue minerals like quartz and feldspar. In the case of historic operations at King’s Mountain, the superior performance of flotation led to the removal of DMS from all North Carolina operations after 1973. Although they are currently being redeveloped, operations in North Carolina ceased in the early 1990’s which coincided with the emergence of operations at Greenbushes in Australia which remains one of the largest lithium producers [7,9,12].

Modern beneficiation flowsheets producing battery-grade concentrates will integrate ore sorting and magnetic to remove problematic iron-bearing minerals, while using DMS and flotation (often in series) to produce concentrates. Spodumene flotation can also produce by-products such as feldspar, quartz, tantalum minerals (tantalite, microlite), and beryl, enhancing economic feasibility [8,9,13]. A common hybrid spodumene flowsheet incorporating DMS and flotation is presented in Figure 1.

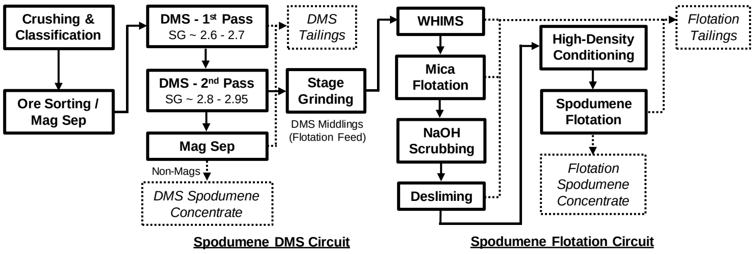

Figure 1 Example of a potential spodumene flowsheet with DMS and flotation circuits

Flowsheet Development

The preferential flowsheet for each spodumene deposit will vary slightly depending on their characteristics including, but not limited to feed grade, spodumene grain size, and mineralogy. The following sections outlines how the optimal flowsheet is designed.

Heavy Liquid Separation Testing (HLS)

Heavy Liquid Separation (HLS) is used as an initial evaluation of the amenability of a sample to DMS. This is typically conducted on coarse crushed spodumene samples with a top size of 6.35 mm (¼”), but sometimes up to 20 mm, and barren of finer particles (<0.5-1.0 mm) that are not amenable to DMS. The material is submerged in a liquid with a specific gravity (SG) controlled to set intervals typically between SG 2.60 and 3.00 to determine the optimal SG values for separating spodumene from low-density gangue minerals. The high SG sink products, or spodumene concentrate, will then be subjected to high-intensity magnetic separation to remove iron-bearing impurities. The sinks products from each interval and the final float products are assayed to determine the mass balance and construct grade-recovery and impurity charts. Figure 2 presents a typical grade-recovery and impurity charts produced from the HLS testing and used to identifying the ideal conditions for a spodumene DMS operation. These results reveal Li_2O enrichment exceeding 6.5% at SG 3.00, and production of a 6.0% Li_2O concentrate around SG 2.90. Significant impurity reduction is also observed, particularly in Fe_2O_3, Na_2O, and K_2O, emphasizing the effectiveness of combined HLS and magnetic separation in spodumene beneficiation and flowsheet design.

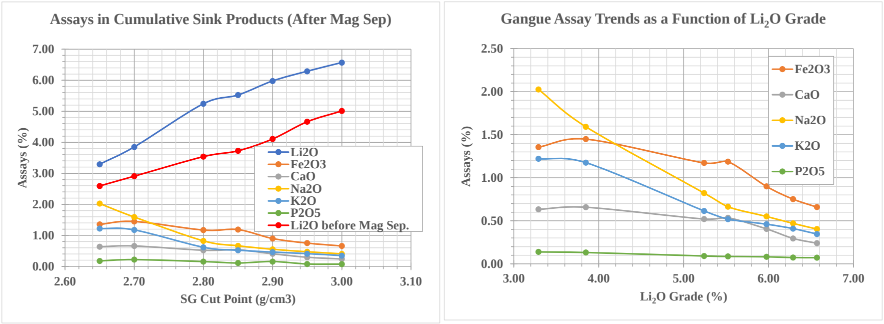

Figure 2 An example of typical HLS test results

Dense Media Separation

Dense Media Separation (DMS) is the continuous gravity separation process used to produce spodumene concentrate. Industrial operations such as Pilbara Minerals' Pilgangoora, Talison Lithium's Greenbushes (Australia), and Sigma Lithium's Grota do Cirilo (Brazil) validate DMS effectiveness, consistently producing concentrates at 5.5-6.0% Li_2O.

As noted, a finer bypass fraction (<0.5-1.0 mm) is screened out upfront of DMS to improve efficiency, as selectivity is difficult with finer particle sizes. The DMS process generally involves two passes at different SG cut-points. The first will reject barren silicate gangue (SG 2.65-2.70) and the second (SG 2.85-2.95) produces high-grade concentrate (>6.0% Li_2O), which is subjected to magnetic separation to reduce the iron content to <1.0% Fe_2O_3. The first pass floats are considered tailings, while the second pass floats still contain significant lithium and can be combined with the bypass fraction as feed for flotation. Optimizing DMS involves selecting the appropriate SG cut-points initially based on the HLS results, managing near-density material, and classifying the feed into separate fractions, which can require smaller-diameter cyclones at smaller size fractions.

An example of pilot plant results (Table 1) demonstrate the two-stage DMS approach with two size fractions. Coarse (–9.50 + 3.35 mm) and fine (–3.35 + 0.60 mm) feed fractions were passed through DMS at 1st and 2nd pass SG cut-points of 2.65 and 2.88 g/cm³, respectively, followed by magnetic separation on the DMS concentrate. The combined non-magnetic concentrate recovered 69.8% of the lithium at a grade of 6.21% Li_2O and 0.61% Fe_2O_3, while only representing 11.8% of the mass. The tailings only contained lithium losses of 1.8% with 37.1% of the total mass, confirming strong spodumene liberation and the effectiveness of DMS with this sample.

Table 1 An example of DMS pilot plant results

Fractions	DMS Stage	Target Density (g/cm^3)	Feed Rate (kg/h)	DMS Concentrate, NonMag				Mag Conc. (from DMS Li Conc.)	DMS Tailing	
				Weight %	Grade (%)		Dist.(%)	Dist. (%)	Weight %	Dist.(%)
					Li_2O	Fe_2O_3	Li_2O	Li_2O		Li2O
-9.50+3.35mm	1st Pass	2.65	99	9.00	6.08	0.61	52.20	4.10	25.80	1.20
	2nd Pass	2.88	89							
-3.35+0.60mm	1st Pass	2.65	99	2.80	6.62	0.60	17.60	1.00	11.30	0.60
	2nd Pass	2.88	72							
Combined				11.80	6.21	0.61	69.80	5.10	37.10	1.80

Spodumene Flotation with Fatty Acid Collectors

Spodumene flotation circuits involve multiple stages, including wet high-intensity magnetic separation (WHIMS), mica pre-flotation, desliming, alkaline scrubbing (NaOH), high-density conditioning, and flotation using fatty acid collectors. At an industrial scale, direct flotation with fatty acids is preferred over reverse silicate gangue flotation due to its robustness (Banks et al., 1953; Bale, 1989).

Owing to the complexity, flotation represents the most challenging yet critical stage in spodumene beneficiation. The upstream processes are vital for successful spodumene concentration with fatty acids. Spodumene is typically well liberated at coarse sizes (up to 500 µm), but K_{80} values are typically closer to 200 µm due to physical particle size limitations of conventional flotation equipment. While liberation is critical, it is also important to minimize slimes production (<15–20 µm) as these are removed to ensure froth quality and selectivity with amine and fatty acid collectors. Iron bearing silicates are commonly removed by WHIMS as these minerals are readily floatable under the same mechanism as spodumene. Lithium losses during WHIMS can be significant due to particle association, entrainment, or the presence of iron within the spodumene crystal. Micas will also float with fatty acids, and are removed through pre-flotation at alkaline pH (~10.5) with amine collectors with moderate to low lithium losses (1.5-7.0%). If they are of high quality, micas can also be targeted as a by-product. Spodumene is then activated through alkaline scrubbing (NaOH) by exposing Al^{3+} adsorption sites to enhance fatty acid adsorption.

High-density conditioning has long been identified as one of the most significant stages for producing successful spodumene flotation with fatty acids [11,14,15]. Conditioning is performed at high pulp density (~60% solids) to ensure proper dispersion of the insoluble fatty acid collectors in the pulp. Collector dosages range from 500 to 1000 g/t and flotation is performed at a pulp pH around 7.5-8.5 [7,9]. The ideal flotation pH of 8-8.5 has been determined from first principle studies and aligns well with current and historic commercial operations [16]. While fatty acids remain effective, newer research into modified fatty acid collectors, cationic/anionic collector blends, and activators like Ca^{2+} or Mg^{2+} show promise but require further validation with real ore systems [17,18]. At present, tight operation of upstream stages, high-density conditioning, precise pH control, and optimized collector dosage can yield consistent recoveries and grades ≥5.5% Li_2O in commercial applications.

Controlled tests demonstrated optimal spodumene flotation performance is achieved at a pH around 8.4, achieving high lithium recovery (96%) and good concentrate grades (5.2% Li_2O). As pH is increased, lithium recovery decreases with improved selectivity. The results presented in Figure 3 highlight the importance of the pH modifier, as soda ash is observed to have a greater negative impact on recovery at high pH (~10) than NaOH.

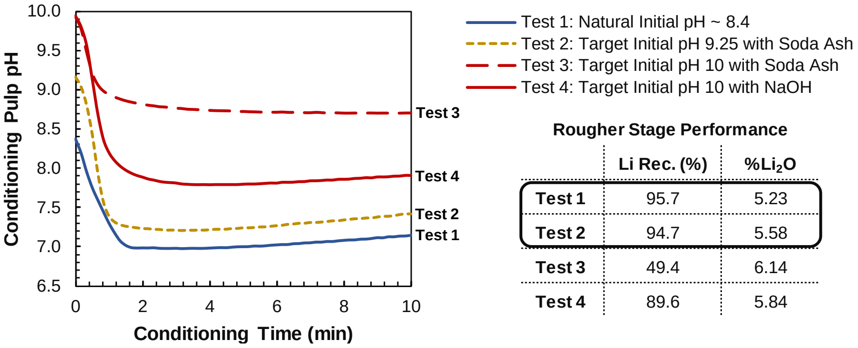

Rougher Stage Performance

	Li Rec. (%)	%Li_2O
Test 1	95.7	5.23
Test 2	94.7	5.58
Test 3	49.4	6.14
Test 4	89.6	5.84

Figure 3 Pulp pH profiles during high-density conditioning and corresponding rougher performance

Spodumene flotation kinetics are relatively fast compared to other flotation systems. When conducted at ~35% solids and pH ~8.5 with a 2kg charge, the maximum lithium recovery is achieved in nearly 1.5 minutes with little additional recovery provided by increasing to 2.5 minutes (Figure 4). Cleaning stages (usually two) use minimal additional collector (~5% of the rougher dosage) and maintain conditions similar to rougher flotation, which is why the quality of the initial rougher conditioning is so critical. Lithium and mass losses during cleaning typically remain low (1-5%) unless poor conditioning results in high carry-over of gangue minerals. Strong overall flotation circuit recoveries are typically between 70 and 85%.

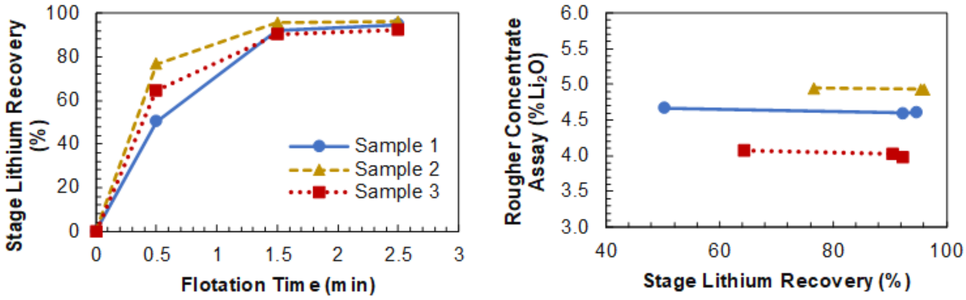

Figure 4 Rougher flotation kinetics and grade vs. recovery curves for three pegmatite feed samples

Hybrid DMS and Flotation Flowsheets

A common approach for deposits containing coarse and fine-grained spodumene is combining DMS and flotation, which can help to maximize spodumene recovery. Table 2 provides an example of combined DMS and flotation results, showing significant lithium enrichment to produce a final concentrate (17.8% mass pull at 5.89% Li_2O) with about 86.0% lithium recovery. Effective gangue rejection is confirmed by low lithium content in the tailings (0.13% Li_2O) with high mass rejection (71.7%). Intermediate losses occur during magnetic separation and mica flotation, but these are vital to reject impurities that negatively impact concentrate purity. Overall, these results validate the appeal of combined DMS-flotation flowsheets for spodumene beneficiation to maximize production.

Table 2 Combined DMS and Flotation Mass Balance

Final Products		Assays (%)									Distributions (%)							
	%	Li	Li_2O	SiO_2	Al_2O_3	Fe_2O_3	CaO	Na_2O	K_2O	P_2O_5	Li	SiO_2	Al_2O_3	Fe_2O_3	CaO	Na_2O	K_2O	P_2O_5
DMS Concentrate	11.9	2.78	5.98	66.6	24.3	0.75	0.14	0.78	0.72	0.21	58.6	10.8	17.9	16.4	6.1	2.2	3.3	8.3
Flot Concentrate	5.9	2.66	5.72	64.0	24.1	0.72	1.10	1.03	0.58	0.92	27.4	5.1	8.8	7.8	24.1	1.4	1.3	17.8
DMS Conc. & Flot Conc	17.8	2.74	5.89	65.7	24.2	0.74	0.45	0.87	0.68	0.45	86.0	15.9	26.7	24.1	29.8	3.7	4.6	26.1
DMS and Flot Tail	71.7	0.06	0.13	77.1	13.2	0.27	0.17	5.19	2.77	0.23	7.9	75.1	58.8	35.4	46.3	88.3	76.1	53.3
Flot Mica Conc	4.4	0.26	0.55	55.7	28.8	1.11	0.29	1.99	7.24	0.27	2.1	3.3	7.8	9.0	4.8	2.1	12.1	3.9
Mag Conc	0.8	0.61	1.31	55.3	18.0	8.62	2.13	2.28	3.19	2.81	0.9	0.6	0.9	13.2	6.6	0.4	1.0	7.6
Total Slimes	5.4	0.32	0.69	69.4	17.2	1.84	0.63	4.33	2.96	0.51	3.1	5.1	5.7	18.3	12.5	5.5	6.1	9.1
Feed, Calc	100	0.56	1.21	73.5	16.1	0.54	0.27	4.21	2.61	0.30	100	100	100	100	100	100	100	100

LEPIDOLITE BENEFICIATION

Similar to spodumene, concentration of lepidolite is essential for downstream lithium extraction. While flotation is the primary method for concentrating lepidolite, flotation efficiency can be enhanced by cleaning the feed through upstream processes like magnetic or gravity separation – which have the potential to recover valuable by-products such as tantalum (Ta), niobium (Nb), and rubidium (Rb), frequently present in lepidolite-bearing pegmatites. Gravity separation effectively concentrates high-density Ta-Nb minerals (tantalite, columbite), while magnetic separation primarily removes iron-bearing impurities but can also recover tantalite and columbite due their paramagnetic properties. Electrostatic separation has shown moderate success recovering lepidolite at coarser sizes, but is limited by liberation [19,20].

Lepidolite flotation is typically achieved with cationic amine collectors (e.g., dodecylamine) under acidic conditions (optimal pH ~2-3). Acidic flotation allows for selective rejection of silicate gangue minerals like quartz and feldspar by exploiting differences in the iso-electric point (iep), although selectivity remains challenging due to similar surface properties. Recent research highlights improved flotation results using ether monoamine (EDA) or novel Gemini collectors due to enhanced collector adsorption. Additionally, innovative neutral-pH approaches using mixed collectors (SDS-NaOL-DA) have shown promising preliminary results, which would address issues related to acid consumption and corrosion, though further validation with complex ore systems are still needed [20,21].

In addition to lithium, the lepidolite structure frequently incorporates economically significant elements (Rb, Cs, Ta, Ga), which can further increase its value and supports integrated extraction processes. Future beneficiation improvements require ongoing research into selective collector formulations, advanced pre-concentration methods, and deeper understanding of flotation chemistry to maximize lithium and by-product recovery efficiency.

Optimizing Lepidolite Flotation

SGS Lakefield has developed and piloted optimized flowsheets for lepidolite beneficiation, which typically incorporate staged collector addition and do not require high-density conditioning – a major difference from spodumene. A case study of lepidolite flotation is provided, where an ore containing 15-25% lithium-bearing lepidolite/muscovite with quartz and feldspar as the main gangue minerals was processed with desliming, lepidolite flotation, and feldspar flotation as a by-product. In this instance, feldspar recovery from the flotation tailings – which is not included in this manuscript – was a successful by-product opportunity.

Desliming prior to flotation was determined to be essential due to the negative impact of <20 µm particles on flotation with the amine collectors. Screening (Figure 5) provided better lithium recovery with lower lithium losses (7.2% loss) than desliming via hydrocyclone (9.6%), although the latter is more practical at scale. In addition to the slimes, flotation pH also a significant effect on selectivity. Tests at pH 2.5, 3.5, and 4.5 confirmed that pH 2.5 offered optimal selectivity and final concentrate performance

(Figure 5). At higher pH, the gangue recovery increased and leading to an undesirable reduction in concentrate grade despite higher rougher-stage lithium recovery. Pulp density and conditioning time (Figure 6) can also significantly influence lepidolite flotation performance. It was determined that the optimal pulp density was around 25% solids, which produced the highest grade and recovery >4.6% Li_2O and 79%, respectively. Higher densities led to froth mobility/stability issues to high froth loading from the increase in fine mica content. In addition, it was identified that longer conditioning times (≥3 minutes) improved scavenger and cleaner flotation performance. Resulting in lower lithium losses and maintaining high recovery, while shorter conditioning times accrued significantly higher losses, which was attributed to weaker collector attachment.

Due to the strong correlation between lithium and rubidium ($R^2 = 0.9381$), Rb assays via XRF were used a proxy for Li concentration for quicker evaluations, reducing the time delay for ICP analysis. Hydrometallurgical recovery of Rb is also a viable approach to produce a by-product. While lepidolite processing is less developed than spodumene, consistent lab and pilot-scale results at SGS confirm its viability as a lithium source, warranting further development as the global lithium demand increases.

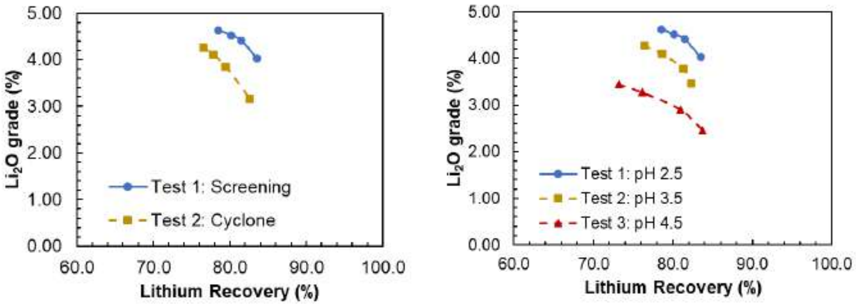

Figure 5 The effect desliming method (left) and the impact of pH (right) on lepidolite flotation

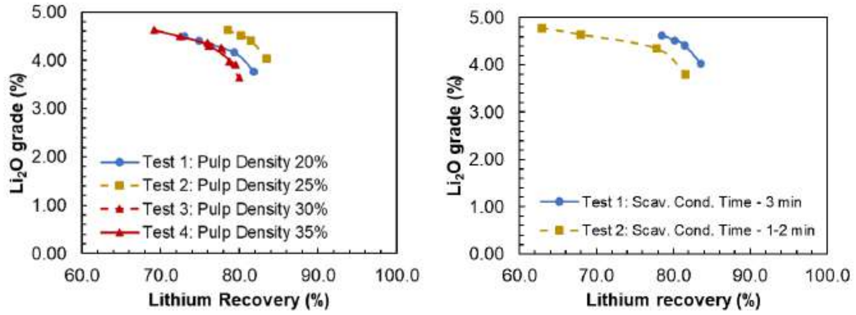

Figure 6 Impact of rougher stage pulp density (left) and conditioning (right) on lepidolite flotation

PETALITE PROCESSING

Petalite ($LiAlSi_4O_{10}$) is another important lithium resource for the battery market due to its relatively high lithium content (~3–4.5% Li_2O) and low iron content. Although petalite is less common than spodumene in modern lithium chemical production, it remains valuable for the glass/ceramics industry and there is growing interest in using it as a source to produce lithium carbonate. Major petalite-bearing deposits exist in Zimbabwe, Canada, Brazil, and Australia where the two main beneficiation methods are DMS and froth flotation.

Dense Media Separation of Petalite

In contrast to spodumene, the SG of petalite (~2.4 g/cm^3) is lower than the primary silicate gangue minerals (~2.6 g/cm^3) and petalite is typically concentrated to the floats fraction. Although the SG contrast is low, DMS has been successfully applied at operations like the Bikita Mine and the Arcadia project in Zimbabwe, where high-grade petalite concentrates (>4.0% Li_2O, <0.05% Fe_2O_3) were produced. At Arcadia, up to 80% of petalite coarser than 1.7 mm was shown to be recoverable with DMS, but finer particles (<0.5 mm) require alternative processing due to reduced separation efficiency and increased gangue entrainment [22].

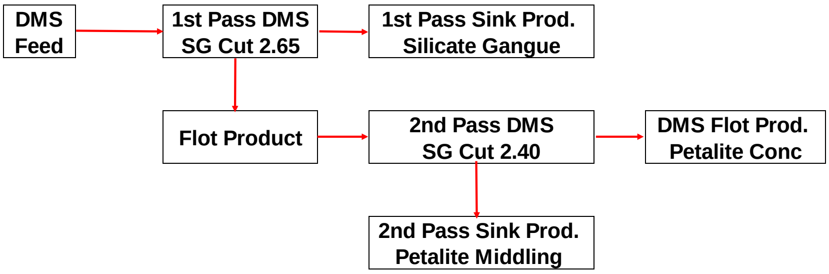

Figure 7 Typical Petalite DMS Pro cessing Flowsheet

A typical two-stage DMS flowsheet (Figure 7) can be applied to recover petalite. This includes an initial DMS stage (SG ~2.60-2.65) to reject high-SG gangue minerals, followed by a second DMS pass at ~2.40 SG to concentrate petalite in the float product. The sink product from the second pass forms the middlings, which can be recirculated or further processed with flotation. In some instances, significant amounts of petalite are present in spodumene deposits where it can be concentrated from what would typically be the DMS tailings. In the case presented in

Table **3**, the original spodumene tailings (SG<2.65) was revealed to be petalite-rich and was reprocessed through DMS at an SG of 2.40 to produce a petalite concentrate grading 3.95% Li_2O containing 12.3% of the overall lithium distribution. The significant lithium content in the DMS middlings (26.5%) was attributed to limited petalite liberation, while the lithium content in the DMS sinks (61.2%) was predominantly spodumene. Although petalite is not the primary mineral in this case, the results highlight the effectiveness of concentrating petalite through density-based separation.

Despite the flotation challenges – owing to similar surface properties as quartz and feldspar – flotation can be effective when DMS alone is insufficient. In some instances, petalite flotation with amine collectors complements DMS by recovering fine and interlocked petalite particles that become better liberated after grinding. For example, Anzaplan [23] discussed how combining DMS and flotation at the Arcadia project in Zimbabwe increased the overall lithium recovery from ~31% to >77%. However, flotation performance can often be limited by non-selective amine adsorption onto other silicates and surface contamination. Floating at a lower pH (<3) has been shown to improve selectivity but increases acid consumption, while reverse flotation using modified amine collectors (e.g., L0-503) has shown promising selectivity at neutral pH [21].

Table 3 Example of Petalite Recovery by DMS from a Spodumene-Bearing Sample

Product	SG	Weight	Assays (%)							Distribution (%)					
	Cut	%	Li	Li_2O	SiO_2	Al_2O_3	Fe_2O_3	Na_2O	K_2O	Li	SiO_2	Al_2O_3	Fe_2O_3	Na_2O	K_2O
Petalite Concentrate	-2.40	2.5	1.84	3.95	75.5	17.1	0.21	0.90	0.49	12.3	2.49	2.82	1.5	0.49	0.44
DMS Middling	-2.65+2.4	24.2	0.41	0.87	76.8	14.0	0.65	3.73	1.88	26.5	24.8	22.6	45.4	19.9	16.2
DMS Sink	+2.65	73.3	0.31	0.66	74.4	15.2	0.25	4.92	3.19	61.2	72.7	74.6	53.1	79.6	83.4
Head (calc.)		100	0.37	0.80	74.99	14.97	0.35	4.53	2.81	100	100	100	100	100	100

ZINNWALDITE PROCESSING

Zinnwaldite, a less common lithium mica, is amenable to high-intensity magnetic separation and flotation due to its high iron content. Coarse zinnwaldite (~500 µm) is effectively upgraded using dry high-intensity magnetic separation (DHIMS), achieving lithium recoveries >80%, while flotation is used for finer fractions at neutral pH using sequential addition of cationic and anionic collectors [24]. Pilot operations at Cinovec and British Lithium demonstrated flotation recoveries >95% and concentrate grades of up to ~8% Li_2O equivalent, confirming zinnwaldite's potential as a lithium source [25-28].

CLAY-BASED LITHIUM MINERAL PROCESSING

Lithium-bearing clays such as hectorite and illite require physical classification methods rather than conventional beneficiation methods like flotation due to their fine, laminated structure. Projects like Sonora and Thacker Pass use hydrocycloning and scrubbing to concentrate lithium into fine fractions (<20–75 µm), with up to 90% lithium recovery [29-31]. Reverse flotation helps remove carbonate gangue (e.g., calcite), reducing reagent consumption during leaching. Despite technical challenges—such as handling ultrafines and equipment wear—pilot studies confirm the viability of producing lithium-enriched clay concentrates.

CONCLUSIONS

To meet rising lithium demand, the current scope of lithium mineral processing must expand beyond spodumene to include alternative minerals like lepidolite, petalite, zinnwaldite, and lithium clays. Spodumene flotation is industrially established and benefits from high-density conditioning and desliming to produce >6.0% Li_2O concentrates. Lepidolite flotation, typically at pH ~2.5, is still under development but can yield concentrates >4.5% Li_2O. Petalite is effectively recovered through DMS and flotation, though selectivity remains a challenge and zinnwaldite processing combines magnetic separation and neutral-pH flotation. Clay beneficiation is unique as it largely relies on classification and carbonate removal. Continued research into these processes will be essential to improve flotation, adapt flowsheets to ore variability, and advance the processing of emerging lithium sources.

REFERENCES

1. Meshram, P., Pandey, B., & Mankhand, T. (2014). Hydrometallurgy, 150, 192-208. https://doi.org/10.1016/j.hydromet.2014.10.012.
2. Bowell, R. J., et al. (2020). Sustainable processing of lithium minerals. Min. Eng., 146.
3. Swain, B. (2017). Separation and Purification Technology, 172, 388-403.
4. Rentsch, L, … & Hock, M. (2018). Li Ext. from Zinnwaldite. Chem. Eng. & Tech, 41(5), 917-982.
5. Vikstrom, H., Davidsson, S., & Hook, M. (2013). Applied Energy, 110(10), 252-266.
6. Castor, S.B., & Henry, C.D. (2020). Minerals, 10(1), 68. https://doi.org/10.3390/min10010068
7. Redeker, I. H. (1979). Conc. of Spod. from N.C.. Mining Engineering. April 1979, 395-398.
8. Burt, R. O. & Flemming, J. (1986). Spodumene Processing at TANCO; 499-514
9. Bale, M. D., & May, A. V. (1989). Minerals Engineering, Vol. 2 (No. 3), 299-320.
10. Falconer, S. A. (1944). Flotation of Nonsulphide Minerals of Strategic Importance. 166(1754), 16.
11. McDaniel, W. (1980). Flot. of Spod. and Iron Minerals. (Conf. Rep. No. 80–6). NCSU Archives.
12. Banks, M. K., McDaniel, W. T., & Sales, P. N. (1953). Transactions AIME, 6.
13. Weir, L. J., & Moskovits, E. E. (1963). Flotation of Lithium and Berylium Pegmatites. 206, 143–153.
14. Browning, J. S., & McVay, T.L. (1961). Benef. Spod. from Gaston County, N.C. (No. 5729). U.S.B.M.
15. Cook, B.K., Aghamirian, M., & Gibson, C.G. (2023).
16. Moon, K.S., & Fuerstenau, D.W. (2003).
17. Xie, R., … & Li, Y. (2021). Min. Eng.,
18. Cook, B.K. & Gibson, C.G. (2023). Minerals.
19. Choi, J., … & Kim, H. (2012). Elect. Enrich. of Lepidolite via Flot. Mat. Trans., 53(12), 2191–2194.
20. Filippov, L. O., et al. (2022). Selective flotation of lithium micas. Min. Eng., 185.
21. Wei, C., et al. (2021). New collectors for lepidolite flotation. Sep. & Pur. Tech., 275, 119-150.
22. Filippov, L. O., et al. (2019). Spodumene and petalite flotation fundamentals. Min. Eng., 141.
23. Anzaplan. (2019). Arcadia Lithium Project: Locked-Cycle Flotation Testwork Report.
24. Xue, Z., … & Du, X. (2024). Flot. of Low-Grade Zinnwaldite. Int. J. Min. Sc. & Tech, 34(6), 881–891.
25. Kratochvíl, M., et al. (2016). Magnetic Sep. of Lithium Mica. 16th Int. SGEM Conference, Bulgaria.
26. British Lithium Ltd. (2022). Lithium Extraction from Cornwall Mica Deposits. Technical Report.
27. Grammatikopoulos, T., et al. (2022). Min. Char. and Proc. of Zinnwaldite Ore. Min. Eng., 182.
28. European Metals Holdings (2023). Cinovec Project – Flotation Testwork Results, 25 May 2023.
29. Bacanora Lithium. (2018). Sonora Lithium Project Feasibility Study. Ausenco Technical Report.
30. Lithium Americas. (2022). Thacker Pass Proj. Mine Plan of Operations. Lithium Americas Corp.
31. Arthur, J., et al. (2025). Evaluation of Gravity Sep. for Li Clay Beneficiation. Min. Eng., 203, 15–22.

XVI International Mineral Processing
and Recycling Conference
28-30 May 2025, Belgrade, Serbia

DOI: 10.5937/IMPRC25086M

Extended abstract

THE APPLICATION OF PHYSICAL CONCENTRATION TECHNOLOGIES IN THE RECYCLING OF NEW WASTE STREAMS

Héctor Muñiz Sierra[1#], 0000-0003-4584-4162,
Michal Šyc[1], 0000-0002-3323-9638,
Ayse Asya Arslanturk[2], 0009-0007-7065-6960,
[1]Institute of Chemical Process Fundamentals of the Czech Academy of Sciences, Prague, Czech Republic
[2]Istanbul Technical University, Istanbul, Turkey

ABSTRACT – Excluding major mineral waste, the total waste volume remains stable, but new waste streams, such as electronic waste and municipal solid waste incineration ashes, have emerged due to industrial and technological changes. The physical concentration technologies are demonstrated as a key factor for recovering valuable elements such as copper. This study demonstrates that a well-designed physical concentration circuit can recover over 65 %wt. of copper from the above-mentioned residues. Copper concentrations reached over 65 g/kg in incineration ash and 490 g/kg in electronic waste treatment residues, highlighting the effectiveness of these technologies.

Keywords: New waste streams, Material recovery, WEEE, fine-IBA.

Although the total amount of waste generated in the European Union has remained relatively stable in recent years - excluding major mineral wastes - technological advances and changes in consumption patterns have led to of new and more complex waste streams. In particular, waste electrical and electronic equipment (WEEE) and municipal solid waste incineration bottom ash (MSW-IBA) have become increasingly important due to their growing volumes and the valuable materials they contain. These waste streams are not only challenging from a treatment perspective, but also represent an opportunity for material recovery strategies aligned with circular economy goals. WEEE accounted for 4.9 million tonnes in Europe in 2021 [1], yet only a small proportion of its valuable metal content is currently recovered. MSW incineration, meanwhile, represents approximately 27% of municipal waste treatment [2], generating large amounts of MSW-IBA, particularly its fine fraction, which is often landfilled despite containing significant quantities of copper and other non-ferrous metals [3].

This work presents the results obtained in our facilities regarding the performance of physical separation technologies for recovering copper from two contrasting waste streams: MSW-IBA fine fraction and a WEEE plastic-rich residue. These materials differ

---

[#] corresponding author: muniz@icpf.cas.cz

in origin and composition but pose similar challenges for metal recovery due to their heterogeneity and particle size. Copper content, measured via acid digestion and ICP-OES, was 2.2–2.6 g/kg for MSW-IBA and 28.5 g/kg for the WEEE plastic-rich residue.

The MSW-IBA was divided into two size fractions: <500 µm and 500–2000 µm. Coarser material after two steps of wet shaking table treatment underwent magnetic separation and selective milling to liberate copper particles, while finer material was processed with wet shaking tables and magnetic separation. Intermediate-density fractions were recirculated to improve recovery. The process produced three copper-enriched outputs totaling 67.7 g/kg Cu and over 65% recovery. The design of the shaking table process and its operating parameters were informed by previous optimization studies [4].

For the WEEE residue, a three-stage treatment was applied: sink-float separation, LARCODEMS dense media separation, and a final wet shaking table step. This sequence yielded copper-rich fractions of up to 491.7 g/kg and 65.7% total recovery. One intermediate stream (123 g/kg Cu) may be reprocessed to further improve efficiency.

Figures 1 and 2 illustrate the treatment flowsheets. The integration of multiple physical steps and recirculation loops demonstrates the flexibility of physical separation systems. While not as selective as chemical extraction, these methods offer advantages in energy use and environmental impact, particularly as pre-concentration stages [5].

The study confirms that physical separation techniques are a viable route for recovering copper from complex waste. With appropriate design, they contribute significantly to circular economy strategies and reduce dependence on primary resources.

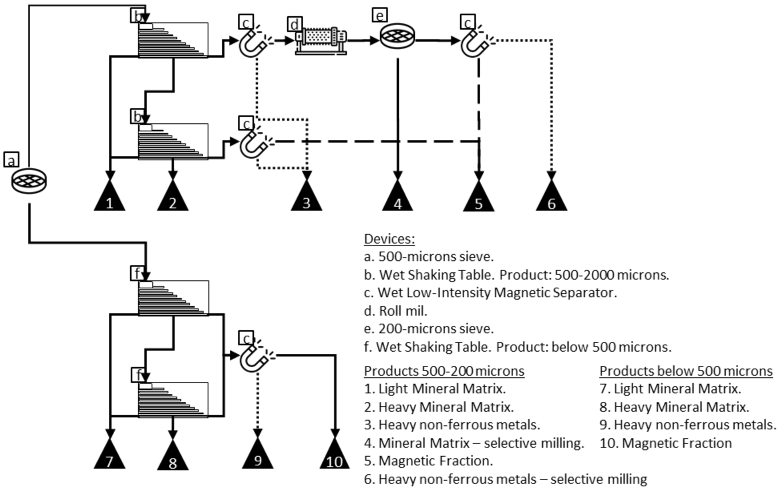

Figure 1 Flow Schema of copper recovery from MSW-IBA fine fraction

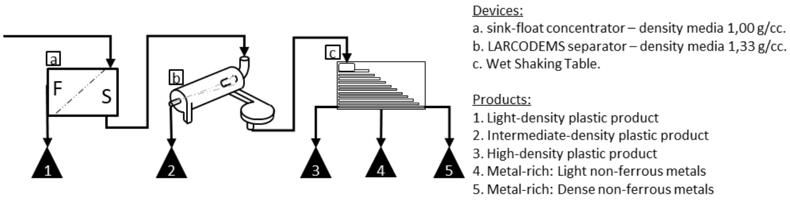

Figure 2 Flow Schema of copper recovery from WEEE plastic-rich residue.

ACKNOWLEDGEMENT

This work was supported by the MŠMT (Ministry of Education, Youth and Sports) and Co-funded by EU under grant number CZ.02.01.01/00/23_020/0008508 (Lifecycle of New Energy Sources (LiNES).

REFERENCES

1. Forti, V., Baldé, C.P., Kuehr, R., Bel, G. (2020) The Global E-waste Monitor 2020, UNU/UNITAR.
2. Eurostat (2024) Municipal waste statistics – Statistics Explained, https://ec.europa.eu/eurostat/statistics.explained/index.php?title=Municipal_waste_statistics.
3. Šyc, M., Simon, F.G., Hykš, J., et al. (2020) Metal recovery from incineration bottom ash: State-of-the-art and recent developments. J. Hazard. Waste, 393, 122433.
4. Muñiz Sierra, H., Šyc, M., Korotenko, E. (2024) Wet shaking table operating parameters optimization for maximizing metal recovery from incineration bottom ash fine fraction, Waste Management, 174, 539–548.
5. Wills, B.A., Finch, J.A. (2019) Wills' Mineral Processing Technology, 7th Ed., Butterworth-Heinemann.

METALS YOUNG RESEARCHER AWARD

XVI International Mineral Processing
and Recycling Conference
28-30 May 2025, Belgrade, Serbia

DOI: 10.5937/IMPRC25091P Original research article

HOLLOW DROP BUBBLES A PROPOSED NEW TECHNOLOGY FOR OPTIMIZED METAL EXTRACTION VALIDATED IN THE LABORATORY

Diego Poblete[1#], 0000-0002-7469-0943,
Claudio Leiva[1], 0000-0003-1568-1462,
Maria Sinche-Gonzales[1], 0000-0002-7722-6839,
Claudio Acuña[2], 0000-0003-2167-703X,
[1]Oulu Mining School, University of Oulu, 90570, Oulu, Finland
[2]Department of Chemical and Environmental Engineering, Universidad Técnica
Federico Santa María, 2390123, Valparaíso, Chile

ABSTRACT – A new technology for solvent extraction has been developed. This innovation, Hollow Drop, merges flotation with solvent extraction by using air bubbles coated with an insoluble extractant material. While the concept of coated bubbles is not new, our work focuses on advancing this idea by generating a swarm of coated bubbles to scale up the process.

Experimental tests were conducted using dissolved copper solutions, SX extractants, Iodine solutions, and Kerosene, achieving copper recoveries of 70% with aqueous-to-organic (A/O) ratios of 17. These results demonstrate that the coated bubble process can operate continuously and holds promise for industrial-scale implementation.

Keywords: Solvent Extraction, Hollow Drops, Coated Bubbles, Reactive Oily-Bubble.

INTRODUCTION

Taggart first introduced the concept of organic-coated hollow droplets [1]. He proposed that oil-coated hollow droplets could serve as effective collectors of hydrophobic particles, a theory later supported by Misra and Anazia(Misra & Anazia, 1987), through their study on the flotation of ultrafine carbon. Their research showed that the binding time of an oil-free hollow droplet to carbon, initially 88 ms, was significantly reduced by the encapsulated droplet in oil to 5 ms. These findings highlight that coated hollow oil droplets accelerate mass transfer at the interface and enhance the recovery of the target metal."

In the flotation of sulfide minerals, Liu [3] adapted this concept to reduce the unwanted recovery of gangue particles and the organic collector's consumption. In this experiment, an organic collector, which is used in flotation, is dissolved in Kerosene, which is mixed with air and passed through a porous glass to produce a reactive oily bubble [4,5].

[#] corresponding author: diego.poblete@oulu.fi

The reactive hollow droplet concept can also be applied to conventional solvent extraction. In this approach, the organic coating of the reactive hollow droplet extracts the metal ions of interest. Chen et al. first introduced this idea. [6] It is known as 'Air-Assisted Solvent Extraction' (AASX). The most common non-conventional SX technologies can be summarized as (i) air-assisted solvent extraction (AASX), (ii) technology based on gas compression where solvent extraction is through dissolved nitrogen in a pre-dispersed solvent (DNPDSE) or columnar flotation technology (CEF) and (iii) technology based on the gas without compression (GWC).

Air-assisted solvent extraction (AASX) uses bubbles coated in organics, which are bubbled through a continuous aqueous phase to enhance the mass transfer process. The difference in density between the coating agent and the aqueous phase allows for the fast separation of phases. [6–8]. The coating agent on the bubble is thermodynamically stable based on the spreading coefficient between the surface tension of the different layers. [9–11]. Dissolved nitrogen in a pre-dispersed solvent technology uses compressed air to generate an organic blend of extractant, which is then introduced into the aqueous phase. [12–14] This approach's objective is similar to that of coated bubble technology, where increasing the bubbles' surface area and buoyancy leads to improved performance compared to traditional methods.

Rahmati's research used the last gas technology without gas compression (Rahmati et al., 2019, 2020, 2024). They proposed creating a foam layer of organic material and air in a separate column. A Venturi tube system passes this foam layer, which is mixed with a high-speed aqueous solution. The resulting mixture then moves through a separating column, where the charged organics are removed at the top.

In this experiment, two solvent extraction processes were carried out. One used a copper solution of 5gr/lots of copper and Kerosene-containing extractant Oximes (90% LIX and 10% Cytoximes). The second experiment used an Iodine solution at 1,5gr/lt of Iodine, and Kerosene was used as an extractant.

EXPERIMENTAL

Device

The equipment developed to carry out the solvent extraction process using a swarm of coated bubbles consists of 4 special zones, listed from bottom to top:

- **Discharged organic zone (Zone I):** Here, a porous air injector generates bubbles, either micro-bubbles or macro-bubbles, which promote foam creation at the top of the discharged organic zone.
- **Coated bubble generator zone (Zone II):** In this zone, a porous filter has been placed, which traps the organic phase in its pores using a difference in hydrophobicity and drags it through an upward air stream.
- **Extraction mixer zone (Zone III):** The solvent extraction via bubbles occurs. These bubbles ascend through the aqueous phase, which contains the metal ions of interest to be extracted.

- **Settler zone (Zone IV):** Due to the bubbles' gaseous core, they rise in the aqueous phase, reaching the Settler zone where the bubbles break, letting go of their organic coat.

Materials

The solutions were used in the solvent extraction column using coated bubbles. The samples were obtained at various times following the logic of chemical kinetics, and then they were analyzed using spectrophotometric techniques. The summary of reagents is in Table 1

Table 1 Reagents used in the experiments

	Copper extraction	Iodine extraction
Reagents	Analysis grade copper sulfate, 99% purity	KI and KIO_3 at 98% purity
PH Modifier	Sulfuric acid at 99% purity	Sulfuric acid at 99% purity
Organic solvent	Kerosene	Kerosene
Extractant	90% LIX and 10% Cytoximes	

Methods

The timings between each kinetic reaction sample were defined first for the methodology. The timings are as follows: 1, 2, 3, 5, 8, 13, 21, and 34(minutes). Samples were taken from the aqueous solution to determine the amount of extraction over time. The test conditions for the experiments are in Table 2.

Table 2 Conditions for experiments

	Copper extraction	Iodine extraction
Air Flows(slpm)	0.87 1.1 1.74	0.87 1.1 1.74
PH	2,1	2,23
Aqueous flow(ml/min)	300	300
O/A	17.89	20

The Spectronic 20D spectrophotometer, configured with a wavelength of 640nm, was used for the spectrophotometry tests for copper solutions. This equipment has a transmittance accuracy of 0.1% and a precision of 98%, for the iodine redox volumetric method was used.

RESULTS AND DISCUSSION

Different extraction percentages were obtained from the analyses, reaching up to 97% in 34 minutes for the maximum condition of Jg of 2 and 90% for the minimum condition of Jg; the extraction percentages are found in the following graph.

Although a higher extraction was obtained at higher Jg, high turbulence was generated due to the chum turbulent state, producing an organic entrainment of 5% in the analysis samples. In comparison, at a lower Jg, the bubbly flow condition was better attained with a drag of less than 1%. The results for copper and Iodine are shown in Graphs 1 and 2.

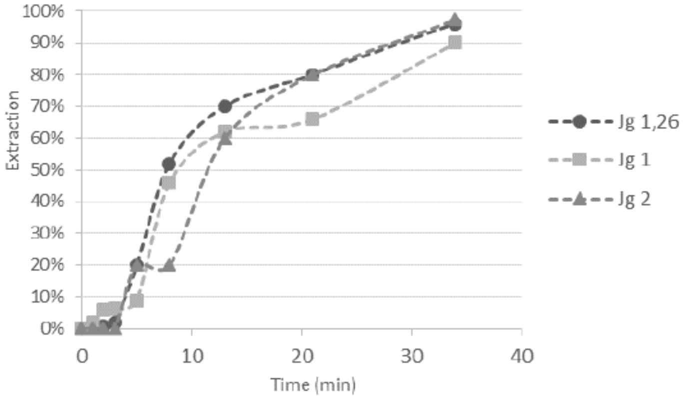

Figure 1 Copper extraction experiments

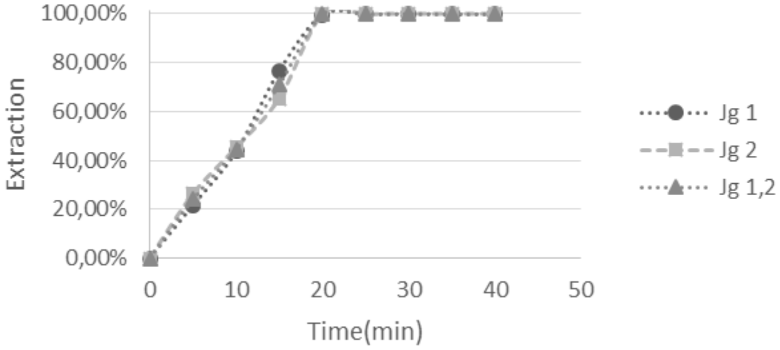

Figure 2 Iodine extraction experiments

Figures 1 and 2 show the extraction percentage in time of each experience. Copper extraction occurs more slowly than iodine extraction. This can be explained because in copper extraction, the rate is dependent on the extractant molecule. In contrast, in iodine extraction, the rate is controlled by the Iodine affinity in kerosene. In both cases, an almost 100% extraction was achieved using coated bubbles, Iodine is a polar compound that is only sparingly soluble in water. Its solubility in water is reported to be 0.34 g/kg at 25 °C and 0.549 g/kg at 40 °C. However, Iodine dissolves well in organic solvents like benzene, carbon disulfide, ethyl acetate, and ethyl alcohol. The resulting solutions typically exhibit red, violet, or brown colors.

To estimate the rate constant for extraction reaction, a first-order reversible equation according to equation 1 was used for copper, and a first-order non-reversible equation according to equation 2 was used for Iodine. Results for Iodine are in graph 3 and for copper in graph 4.

$$Ln\left(\frac{C_S - C_{s,eq}}{C_S^0 - C_{s,eq}}\right) = -(k) * t \tag{1}$$

$$Ln(C_s) = -(k) * t + Ln(C_0) \tag{2}$$

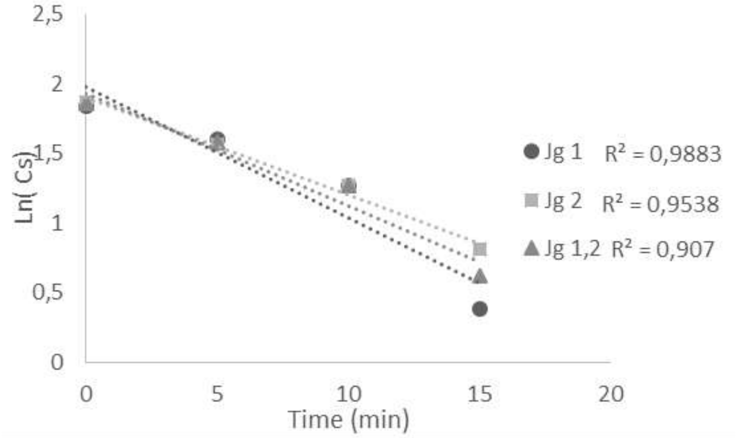

Figure 3 Iodine rate constant

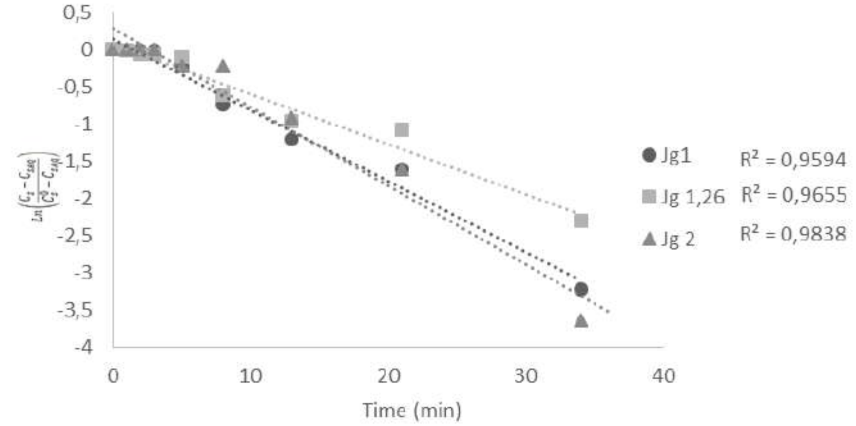

Figure 4 Copper rate constant

CONCLUSION

By designing and constructing a columnar flotation device, we successfully implemented a continuous process that generates a stable coated bubble swarm. This process was employed to achieve air-assisted solvent extraction of copper using a mixture of Kerosene and extractant at a 25% v/v concentration. T and extraction of Iodine from a solution using Kerosene as extractant.

Detailed extraction calculations demonstrated that our system could consistently produce a stable coated bubble swarm, resulting in up to 97% copper extraction efficiency. This was achieved at superficial gas velocities of 2 cm/sec, with an aqueous-to-organic phase volume ratio of 18, indicating that the system performs effectively under these conditions.

Despite these promising results, it is essential to note that our technology is still in the exploration phase. More extensive scale-up tests are required to refine the process and identify the ideal parameters, particularly for the aqueous ratio, gas superficial velocity, and feed flow rates. We constructed a functional system for generating a coated bubble swarm that is simple, efficient, and does not require moving parts or complex equipment, representing a notable advancement in the field.

ACKNOWLEDGEMENT

The authors wish to acknowledge the material support provided by Seven-C Project SpA and the financial support provided by Universidad Católica del Norte.

REFERENCES

1. Taggart AF. Handbook of ore dressing. J. Wiley & sons, Incorporated; 1927.
2. Misra M, Anazia I. Ultrafine coal flotation by gas phase transport of atomized reagents. Mining, Metallurgy & Exploration 1987; 4:233–6. https://doi.org/https://doi.org/10.1007/BF03402698.
3. Liu J, Mak T, Zhou Z, Xu Z. Fundamental study of reactive oily-bubble flotation. Miner Eng 2002;15:667–76. https://doi.org/10.1016/S0892-6875(02)00158-9.
4. Zhou F, Wang L, Xu Z, Liu Q, Chi R. Reactive oily bubble technology for flotation of apatite, dolomite and quartz. Int J Miner Process 2015;134:74–81. https://doi.org/10.1016/j.minpro.2014.11.009.
5. Zhenghe Xu, Jianjun Liu, Zhiang Zhou. Selective Reactive Oily Bubble Carriers in Flotation Processes and Methods of Generation and Uses Thereof 2005;1:1–27.
6. Chen F, Finch JA, Distin PA, Gomez CO. Air Assisted Solvent Extraction. Canadian Metallurgical Quarterly 2003;42:277–80. https://doi.org/10.1179/cmq.2003.42.3.277.
7. Tarkan HM, Finch JA. Air-assisted solvent extraction: Towards a novel extraction process. Miner Eng 2005;18:83–8. https://doi.org/10.1016/j.mineng.2004.05.015.
8. Courtney A. Young, Gerald H. Luttrell. Separation Technologies for Minerals Coal, and Earth Resources. vol. 1. 2012.
9. Tadmor R, Pepper KG. Interfacial tension and spreading coefficient for thin films. Langmuir 2008;24:3185–90. https://doi.org/10.1021/la702790b.
10. Pepper KG, Bahrim C, Tadmor R. Interfacial Tension and Spreading Coefficient of Thin Films: Review and Future Directions. J Adhes Sci Technol 2011;25:1379–91. https://doi.org/10.1163/016942411X555962.

11. Harkins WD, Feldman A. Films. The spreading of liquids and the spreading coefficient. vol. 44. 1922.
12. Tavakoli Mohammadi MR, Koleini SMJ, Abdollahy M. New dissolved nitrogen predispersed solvent extraction method, 1: Performance. Ind Eng Chem Res 2013;52:3842–51. https://doi.org/10.1021/ie300111r.
13. Reza M, Mohammadi T, Mohammad S, Koleini J, Abdollahy M. Features and Capabilities of New DNPDSE Method. Journal of Tethys 2014;2:357–74.
14. Mohammadi MRT, Koleini SMJ, Abdollahy M. New dissolved nitrogen predispersed solvent extraction method, 2: Selectivity. Ind Eng Chem Res 2013;52:3852–7. https://doi.org/10.1021/ie300114u.

XVI International Mineral Processing
and Recycling Conference
28-30 May 2025, Belgrade, Serbia

DOI: 10.5937/IMPRC25098Z

Original research article

PREDICTION OF COLLECTOR FLOTATION PERFORMANCE BASED ON MACHINE LEARNING AND QUANTUM CHEMISTRY: A CASE OF SULFIDE MINERALS

Wanjia Zhang[1], 0000-0003-3126-2145,
Zhitao Feng[2], 0000-0001-7892-1799,
Zhiyong Gao[1#], 0000-0003-0219-1077,
[1]School of Minerals Processing and Bioengineering, Central South University, Changsha, P. R. China
[2]Department of Chemistry, University of California, Davis, United States

ABSTRACT – Flotation, as a pivotal separation technology in the 21st century, facilitates the large-scale utilization of mineral resources. The development of high-performance surfactants, particularly collectors, is crucial for enhancing flotation efficiency. This study introduces a novel machine learning (ML) model designed to evaluate and predict the recoveries of sulfide minerals (chalcopyrite, galena, pyrite, and sphalerite) under various flotation conditions, including pulp pH, flotation time, and collector concentration. Quantum chemistry (QC) computations were employed to characterize the features of 116 collectors (e.g., electrostatic properties, atomic charges, molecular orbitals) and the sulfide minerals (e.g., surface charges, band gap, adsorption energies). These features, along with flotation conditions from the literature, served as input, while experimental recoveries of the four minerals were the output. The model was refined using 10 randomly selected collectors, achieving a mean absolute error (MAE) of 10.0%. The optimized ML model demonstrated high accuracy, successfully predicting the flotation performance of 23 new collectors with an MAE of 5.2%. This QC-ML approach offers a powerful tool for the high-throughput screening and rational design of flotation reagents, significantly advancing the field of mineral processing.

Keywords: Flotation, Sulfide minerals, Machine learning, Quantum chemistry, Performance prediction.

INTRODUCTION

Flotation, a key mineral processing technology using surfactants, has revolutionized resource utilization over the past century [1, 2]. With high-grade minerals depleting, efficient separation of low-grade, finely embedded minerals is critical, necessitating advanced flotation surfactants with strong bonding and high selectivity. Historically, collector development relied on trial-and-error methods, which are inefficient and costly [3, 4]. A theoretical framework for rational collector design remains a significant challenge.

Early efforts focused on linking chemical properties to flotation performance. Criteria like group electronegativity, coordination atoms, and frontier molecular orbitals (FMO) were proposed for collector prediction [5, 6]. For example, Wang et al. [5] used group

---

[#] corresponding author: zhiyong.gao@csu.edu.cn

electronegativity to predict sulfur-containing collectors' performance, while Liu et al. [6] studied thionocarbamate collectors for copper sulfides, linking FMO energy to electron affinity. Despite progress, high-precision quantum calculations are costly and challenging for high-throughput applications.

Quantitative structure-activity relationship (QSAR) models, using topological indices, have emerged as a data-driven alternative for predicting collector performance. For instance, Hu et al. [7] predicted quaternary ammonium salt performance, while Yang et al. [8] studied xanthate selectivity using genetic function approximation (GFA). However, QSAR models are limited to similar collector structures and simple mathematical forms, reducing their applicability.

The future of collector design lies in integrating theory and experiment. Machine learning (ML) [9, 10], a rapidly advancing field, has shown promise in areas like materials science and drug design. Recently, ML has been applied to flotation, with studies predicting performance based on process parameters or physicochemical properties [11-13]. However, a universal model explicitly considering collector structure is still lacking. With growing experimental data, ML offers untapped potential for collector design [14].

This work presents a novel ML workflow to predict flotation performance for diverse sulfide mineral collectors (chalcopyrite, galena, pyrite, sphalerite). The workflow includes data curation, theory-guided descriptor selection, and ML model training, demonstrating robust predictive ability and paving the way for high-throughput virtual screening of new collectors.

FEATURE ENGINEERING

Collector descriptors

This work employed 139 collectors, with flotation recoveries sourced from literature (86 collectors) or lab tests (53 collectors) (**Fig. 1**). Among these, 106 collectors were used for training, 10 for validation, and 23 for testing the ML model's predictive ability. Sulfide minerals exhibit intrinsically heterogeneous natural floatability. Thus, the relative recovery (*Rr*; i.e. collector-induced recovery) was used to replace recovery (*R*) to minimize discrepancies among flotation data, enhancing the accuracy and transferability of the model.

To build the ML model, collector structures were translated into machine-readable data via quantum chemistry (QC) calculations. Density functional theory (DFT) optimized 139 structures using Gaussian16 at the MN15/def2-TZVP level [15], with wavefunctions analyzed by Multiwfn [16]. Key descriptors included electrostatic potential (e.g., extrema, surface area), general interaction properties functions (GIPF), and molecular polarity indices, which relate to hydrophobicity and mineral interactions. Hirshfeld charges and dipole/quadrupole moments were used to model coordination with metal ions. Topological descriptors and molecular orbital properties were also included to assess reactivity and electron transfer.

Minerals descriptors

Our ML model predicts flotation performance for four sulfide minerals. Mineral surfaces were described using QC calculations with CP2K 8.2 [17]. Supercell dimensions were defined for chalcopyrite, galena, pyrite, and sphalerite. The PBE functional with D3 dispersion correction and DZVP-MOLOPT-SR-GTH basis set were used, with a 400 Ry energy cutoff. Hirshfeld charges for surface and bulk atoms were calculated, and adsorption energies of H_3O^+, OH^-, H_2O, CH_4, and benzene were included to represent mineral surface interactions. Zeta potential, Fermi energy, HOMO-LUMO gap, and metal ion properties were also considered.

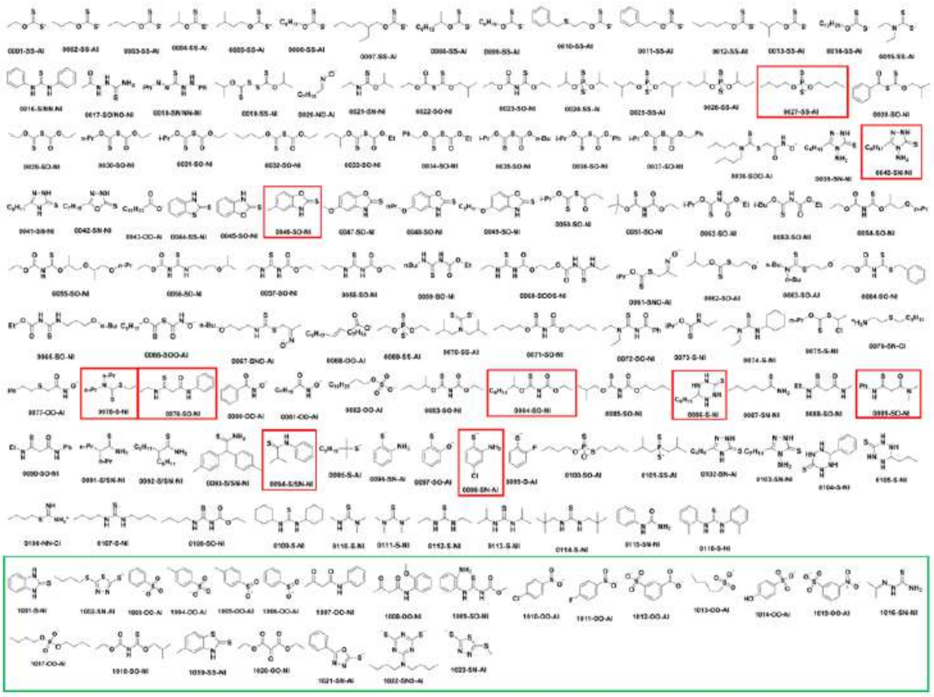

Figure 1 Structures and IDs of the collector molecules of training set (106, not framed), validation set (10, framed with red line), and test set (23, framed with green line).

Flotation descriptors

In our ML model, the flotation condition information is also converted into an array of numbers. Most parameters of flotation experiment are intrinsically quantitative, such as pulp pH, collector concentration, flotation time, so their values are recorded directly. The information about frother was simplified this to a true/false Boolean input denoting whether it is added or not.

ML MODEL CONSTRUCTION

Dataset splitting and visualization

The final dataset includes 7688 flotation tests (106 collectors for training, 10 for validation). Validation set collectors (10 molecules, 245 data points) were randomly selected to avoid overlap with the training set, ensuring model transferability.

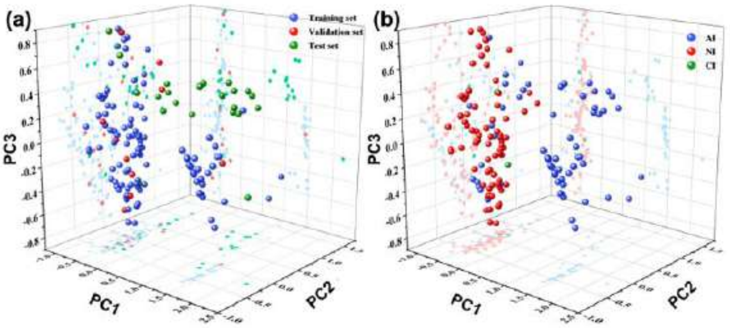

Figure 2 Color-coded PCA plot of the collector molecule in the dataset: (a) Data set classification (Training, validation and test sets); (b) Electrical property classification (Anionic (AI), cationic (CI) and non-ionic (NI) collectors); (c) Coordination mode classification; (d) Molecular skeleton classification.

Principal component analysis (PCA) with scikit-learn [18] was used to visualize the sets division. PCA reduces dimensionality to maximize separation between molecules. Each collector is mapped in a 3D chemical space defined by three principal components (**Fig. 2a**). The validation set spans the training set's chemical space, while the test set extends into unknown regions, challenging the model. PCA classifies collectors into neutral (blue) and ionic (red/green) categories (**Fig. 2b**).

Model optimization

Sections 2.1, 2.2, and 2.3 describe converting flotation experiments into 69-descriptor input vectors. The dataset (7688×69 matrix) trains the ML model to predict recovery from input vectors. For new collectors, QC calculations generate input vectors, and the model predicts recovery. The dataset is split into training, validation, and test sets. The model iteratively adjusts parameters to minimize error, and the best-performing model is selected based on validation set performance. We chose Extreme Gradient Boosting (XGBoost) [19], implemented in the XGBoost package [19], for its accuracy and efficiency in gradient-boosted decision trees.

$$Loss = \sum_{i=0}^{n}\left(R_{r,exp} - R_{r,pred}\right)^2 + \gamma T + \frac{1}{2}\lambda\sum_{j=1}^{T}\omega_j^2 \qquad (4)$$

The objective function comprises both squared loss of the recovery and the regularization terms. The performance of the XGBoost model is evaluated using the mean absolute error (MAE) value.

$$MAE = \frac{1}{N}\sum_{i=0}^{N}\left\|R_{r,exp} - R_{r,pred}\right\| \qquad (5)$$

Model hyperparameters (e.g., max depth, iteration number, eta, regularization) were optimized via grid search in scikit-learn to minimize MAE. Combining dataset development, QC calculations, descriptor generation, and model training, we established a workflow for flotation performance prediction (**Fig. 3**). This workflow can be extended to broader mineral types, diverse collector structures, and complex flotation conditions in the future.

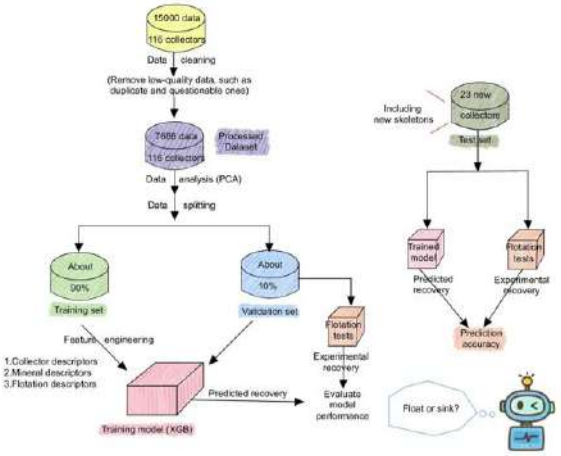

Figure 3 Overall workflow of the model training and evaluation.

Model performance on validation set

Figs. 4a-d show the XGBoost model's predictions versus experimental data on the validation set, which includes ionic/non-ionic mono-, bi-, and tridentate collectors (**Fig. 1**). The model achieves a mean absolute error (MAE) of 10%, with most predictions within ±10% error. Exceptions include 0027-SS-AI and 0079-SI-NI, which slightly exceed the range but remain qualitatively correct.

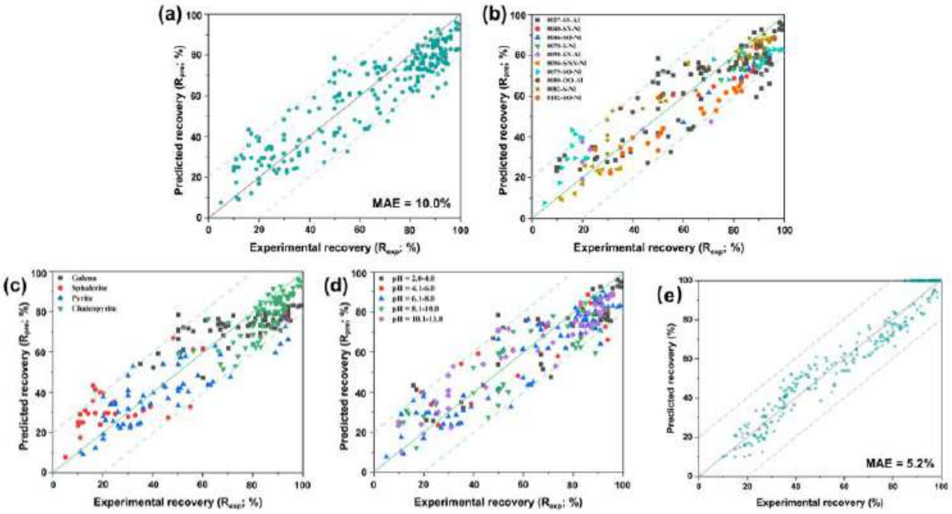

Figure 4 Model prediction performance over the collectors in the validation and test set: (a) Overall prediction of validation set; (b) Predictions of validation set color-coded by collector employed (c) Prediction of validation set color-coded by mineral type; (d) Prediction of validation set color-coded by pulp pH. (e) Prediction performance of test set. Dashed grey lines depict the ±10% limit.

Fig. 4c shows model performance across sulfide minerals. Chalcopyrite predictions are more accurate due to its narrower Rr range, while sphalerite and pyrite show larger errors, likely due to limited training data and complex flotation mechanisms. **Fig. 4d** confirms model robustness across pH 2~12, though errors increase under strongly acidic conditions (pH 2~4), possibly due to insufficient data. Future work will optimize the model, especially for sphalerite and pyrite.

Model performance on test set

Fig. 4e shows the XGBoost model's predictions for 23 test set collectors (1001-1023, **Fig. 1**), verified by flotation experiments. The test set MAE (5.2%) is lower than the validation set (10.0%), likely due to reduced systematic errors from using the same lab equipment and procedures. **Fig. 5** highlights four collectors with new frameworks. 1001-S-NI (**Figs. 5a-b**), a heterocycle-containing collector, separates sphalerite and galena from chalcopyrite. Its high selectivity stems from unique coordination interactions, influenced by heteroatoms and substituents. The model accurately predicted its performance (< 10% error), even for new NN-type heterocycles, demonstrating its potential for designing new sulfide collectors.

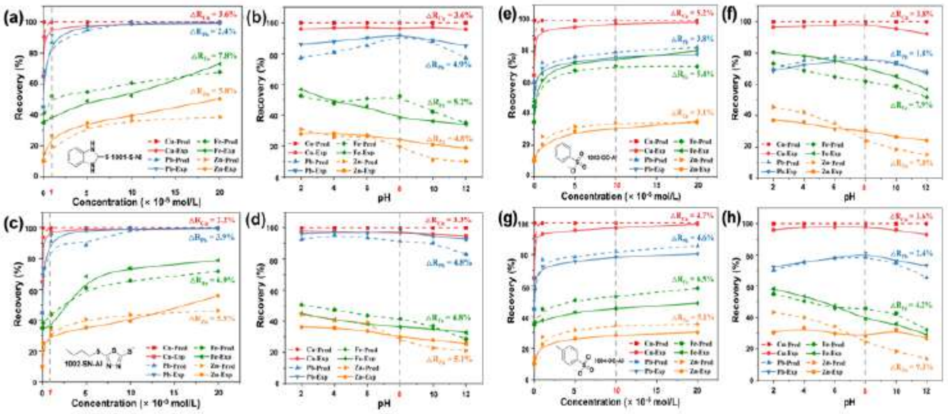

Figure 5 Experimental and predicted recoveries for four representative collectors. Solid and dashed lines are experimental and predicted flotation curves, respectively. Gray dashed vertical lines indicate the optimal and green reagent scheme (i.e., pulp pH and collector concentration). $\Delta \mathrm{R} = \frac{|R_{exp} - R_{cal}|}{100} \times 100\%$.

Predicting 1002-SN-AI (**Figs. 5c-d**) is challenging due to its unprecedented 1,3,4-thiadiazole skeleton. The ML model shows non-ionic collectors (e.g., 1001-S-NI) are more selective than ionic ones (e.g., 1002-SN-AI). Aromatic sulfonates and sulfinates, new sulfide collectors, effectively separate galena from pyrite. The "methyl effect" enhances selectivity, as predicted by the model (**Figs. 5e-h**). Outliers at extreme pH or high concentrations likely stem from insufficient data or altered flotation mechanisms. Future work will expand the database and include gas-phase properties (e.g., bubble size, frother concentration). While the current model focuses on sulfide minerals, the workflow can be adapted for other minerals, aiming for a more universal and robust model.

CONCLUSIONS

We have designed a practical method incorporating QC calculations and machine learning that can generate prediction models for the flotation performance of sulfide minerals. Descriptors for both collectors and minerals are generated by QC computations. Subsequently, an XGBoost model is trained on a sulfide flotation dataset and validated with a MAE of 10.0% for a wide range of collector scaffolds. The model was then tested on 23 novel collectors and has demonstrated excellent prediction performance (MAE = 5.2%). While the developed model demonstrates high precision in predicting the laboratory-scale flotation performance of single collectors for sulfide minerals, its predictive stability for complex industrial systems (e.g., polymetallic ores or mixed collector systems) requires further validation.

REFERENCES

1. Bulatovic, S.M. (2007) Handbook of Flotation Reagents: Chemistry. Theory and Practice: Flotation of Sulphides Ores, ed. S.M. Bulatovic., Amsterdam: Elsevier.
2. Chen, J. (2021) The interaction of flotation reagents with metal ions in mineral surfaces: A perspective from coordination chemistry. Minerals Engineering, 171: 107067.
3. Liu, G., Yang X., and Zhong H. (2017) Molecular design of flotation collectors: A recent progress. Advances In Colloid And Interface Science, 246: 181-195.
4. Liu, G., et al. (2018) New advances in the understanding and development of flotation collectors: A Chinese experience. Minerals Engineering, 118: 78-86.
5. Wang, D. (2016), Flotation reagents: applied surface chemistry on minerals flotation and energy resources beneficiation. Beijing: Springer.
6. Liu, G., et al. (2008) Investigation of the effect of N-substituents on performance of thionocarbamates as selective collectors for copper sulfides by ab initio calculations. Minerals Engineering, 21(12-14): 1050-1054.
7. Hu, Y., Chen P., and Sun W. (2012) Study on quantitative structure–activity relationship of quaternary ammonium salt collectors for bauxite reverse flotation. Minerals Engineering, 26: 24-33.
8. Yang, F., Sun W., and Hu Y. (2012) QSAR analysis of selectivity in flotation of chalcopyrite from pyrite for xanthate derivatives: Xanthogen formates and thionocarbamates. Minerals Engineering, 39: 140-148.
9. Janiesch, C., Zschech P., and Heinrich K. (2021) Machine learning and deep learning. Electronic Markets, 31(3): 685-695.
10. Jordan, M.I. and Mitchell T.M. (2015) Machine learning: Trends, perspectives, and prospects. Science, 349(6245): 255-260.
11. Cook, R., et al. (2020) Prediction of flotation efficiency of metal sulfides using an original hybrid machine learning model. Engineering Reports, 2(6): 1-15.
12. Gomez-Flores, A., et al. (2022) Prediction of grade and recovery in flotation from physicochemical and operational aspects using machine learning models. Minerals Engineering, 183: 107627.

13. Pu, Y., et al. (2020) FlotationNet: A hierarchical deep learning network for froth flotation recovery prediction. Powder Technology, 375: 317-326.
14. He, J., et al. (2022) A high throughput screening model of solidophilic flotation reagents for chalcopyrite based on quantum chemistry calculations and machine learning. Minerals Engineering, 177: 107375.
15. Frisch, M.J. (2009) Gaussian 16, Revision D.01. Gaussian, Inc.: Wallingford CT.
16. Lu, T. and Chen F. (2012) Multiwfn: a multifunctional wavefunction analyzer. Journal of Computational Chemistry, 33(5): 580-592.
17. Kuhne, T.D., et al. (2020) CP2K: An electronic structure and molecular dynamics software package - Quickstep: Efficient and accurate electronic structure calculations. Journal of Chemical Physics, 152(19): 194103.
18. Pedregosa, F., et al. (2011) Scikit-learn: Machine Learning in Python. The Journal of Machine Learning Research. 12: 2825–2830.
19. Chen, T. and Guestrin C. (2016) XGBoost, in Proceedings of the 22nd ACM SIGKDD International Conference on Knowledge Discovery and Data Mining, 785-794.

XVI International Mineral Processing
and Recycling Conference
28-30 May 2025, Belgrade, Serbia

DOI: 10.5937/IMPRC25106M

Original research article

SYNTHESIS OF MOF@ALUMINUM SALINE SLAG COMPOSITES FOR CO_2 CAPTURE AS A NEW STRATEGY OF VALORIZATION OF SECONDARY ALUMINUM WASTES

Helir Muñoz[#], 0000-0002-0481-5261,
Sophia Korili, 0000-0001-9086-4934,
Antonio Gil, 0000-0001-9323-5981,
INAMAT^2, Universidad Pública de Navarra, Campus de Arrosadía, 31006, Pamplona, Spain

ABSTRACT – Metal-organic framework (MOF) materials combined with aluminum saline slag wastes represent a relatively novel research direction. This innovative approach not only leverages industrial waste for the development of advanced materials but also promotes a circular economy and reduces the ecological footprint of aluminum production. Furthermore, it addresses the inherent stability challenges of pure MOFs. Notably, this study is the first to propose that this industrial by-product can serve as a novel, cost-effective, and environmentally friendly modulator, enabling the selective transition between the MIL-96(Al) and MIL-110(Al) phases. For the first time, novel composites of MOFs and the saline slag waste resulting from the initial aluminum extraction in an acidic medium (RW1*), have been developed. These composites, designated as MOF@RW1*-n (n = 25, 50, 75), were synthesized via the in-situ preparation of the MOF on RW1* using a hydrothermal treatment method and were subsequently evaluated as CO_2 adsorbents. The optimized content of RW1* in the composite significantly affect its role as a modulator in the formation of specific crystalline structures, whether MIL-96(Al) or MIL-110(Al), leading to hybrid materials with excellent textural properties and thermal stability.

Keywords: Aluminum industrial waste, MOFs, CO_2 adsorption.

INTRODUCTION

Scientific evidence indicates that the rapid increase in greenhouse gas emissions is already causing extreme weather events, rising sea levels, and more frequent wildfires, all of which contribute to the intensification of climate change [1]. The growing CO_2 emissions represent a major global environmental challenge, with sectors such as transportation, industry, and energy generation playing a significant role in this issue [1]. While technologies such as carbon capture, utilization, and storage (CCUS) have been implemented, more efficient solutions are required to meet the targets of the Paris Agreement [2]. In this context, metal–organic frameworks (MOFs) have emerged as promising materials for CO_2 capture and mitigation due to their structural versatility and high adsorption capacity, primarily through physical mechanisms such as van der Waals forces and electrostatic interactions [3]. Among them, aluminum-based MOFs (Al-MOFs),

---

[#] corresponding author: helirjoseph.munoz@unavarra.es such as MIL-96 and MIL-110, stand out for their thermal stability, low cost, and efficiency in CO_2 capture [3]. However, their synthesis is complex and requires strictly controlled conditions. Both materials crystallize from similar precursor reactants, but their formation depends on precisely tuned conditions such as pH, temperature, and reaction time. MIL-96 typically forms at pH between 1 to 3 after 24 h incubation at 210 °C, whereas MIL-110 requires more stringent conditions, often including pH values below 0.3 or 3.5 – 4.0, along with extended reaction times of up to 72 h [3].

Interestingly, this study is the first to propose that aluminum saline slags, an industrial byproduct from the secondary aluminum processes, can serve as a novel, cost-effective, and environmentally friendly modulator in the MOF synthesis of MIL-96 and MIL-110. Saline slags pose significant environmental and economic challenges due to its composition, which includes aluminum oxides, fluxing salts (NaCl and KCl), and hazardous compounds such as aluminum nitride (AlN), which can release toxic gases upon contact with water [4].

Annually, 4 to 5 million tons of saline slags are generated worldwide, and its disposal remains a critical issue [5]. Research has demonstrated that aluminum extraction from saline slags using acidic solutions enables the synthesis of various functional materials, including perovskites [6], hexaaluminates [7], and pillared clays [8]. However, current approaches primarily focus on the aluminum fraction, overlooking the residual waste left after extraction (RW1*).

This study explores the incorporation of this waste after aluminum acid extraction (RW1*) in MOF synthesis, promoting a circular economy approach. The impact of RW1* on the formation of crystalline structures was evaluated by analyzing the textural, structural, and chemical properties of the resulting materials, as well as their performance in CO_2 adsorption up to several temperatures and 80 kPa. In addition, MIL-96 was synthesized as a reference material to compare adsorption capacity and assess the effects of the waste on the final material properties.

EXPERIMENTAL

Aluminum extraction and production of saline slag residual (RW1)

Saline slag wastes (W) from *Iberica de Aleaciones Ligeras S.L. (IDALSA)* was processed for aluminum extraction using an acid-mediated method. The slag was treated with 2.0 M HCl under reflux at 100 °C for 2 h with a 1:15 g/mL waste-to-solution ratio [6]. The extracted aluminum was used for the synthesis of other functional materials [4,6]. The remaining solid residue was separated by centrifugation, dried at 60 °C, and labeled RW1.

Washing of saline slag (RW1)

RW1 was washed with deionized water at 80 °C (1:15 g/mL ratio) to remove chloride salts. The slurry was centrifuged, repeatedly washed, and dried at 80 °C for 12 h, resulting in RW1*. X-ray fluorescence (XRF) analysis confirmed a significant reduction in chlorine content, from 16.5% (RW1) to 0.32% (RW1*), demonstrating successful dichlorination.

Synthesis of MOF and MOF@RW1*-n composites

MIL-96(Al) and MOF@RW1*-n (n = 25, 50, 75) composites were synthesized by mixing aluminum nitrate nonahydrate ($Al(NO_3)_3·9H_2O$, 12.21 mmol) and trimesic acid (H_3BTC, 3.92 mmol) in deionized water, stirring for 40 min, and heating at 220 °C for 48 h in a sealed Teflon-lined autoclave [9]. After cooling, the crystalline product was filtered, washed, dried, and activated by immersion in methanol for 5 days, followed by vacuum drying at 100 °C. The final product, MIL-96(Al), was stored for further applications.

MOF@RW1*-n composites were synthesized via an *in-situ* method, following the same procedure but incorporating different RW1* amounts (~25, 50, and 75 wt.%). The resulting materials were designated as: MOF@RW1*-25, MOF@RW1*-50, and MOF@RW1*-75.

RESULTS AND DISCUSSION

The X-ray diffraction (XRD) patterns (**Figure 1a**) reveal that the proportion of RW1* slags used in the synthesis significantly affects the predominant crystalline phase. When lower RW1* proportions (25% and 50%) are used, the MOF@RW1*-25 and MOF@RW1*-50 composites primarily exhibit the MIL-96(Al) phase, matching the XRD pattern of MIL-96(Al) synthesized with commercial aluminum. However, at a higher RW1* proportion (75%), MOF@RW1*-75 preferentially forms the metastable MIL-110(Al) phase. This phase is highly dependent on strict synthesis conditions and extremely low pH (0 – 0.3) [10], emphasizing the role of RW1* as a modulator of crystalline structure formation. The XRD pattern of MIL-110(Al) shows characteristic peaks at 2θ = 4.8° and 8.3° (**Figure 1a**) [3], confirming the formation of this metastable structure in MOF@RW1*-75. These peaks are strong and narrow, indicating good crystallinity. The MIL-110(Al) structure (**Figure 1b**) consists of octameric aluminum clusters linked by trimesate (btc) ligands, where hexacoordinated aluminum cations form dimers stabilized by octahedral aluminum units. This arrangement generates uniform hexagonal channels (1.7 nm in diameter) (**Figure 1c**), which are crucial for adsorption applications. In contrast, MIL-96(Al) features a three-dimensional (3D) network formed by the connection of two-dimensional (2D) aluminum cluster networks through trinuclear clusters. These clusters consist of aluminum octahedra with μ_3-oxo bridges, while the 2D networks are composed of infinite chains of interconnected $AlO_4(OH)_2$ and $AlO_2(OH)_3(H_2O)$ units (**Figure 1d**) [10].

The thermogravimetric analysis (TGA) revealed that RW1* exhibits high thermal stability, with minimal mass loss, mainly around 600 °C due to water desorption. In contrast, MIL-96(Al) and MOF@RW1*-n composites showed three mass loss stages: (I) below 200 °C (adsorbed water release), (II) between 200–420 °C (crystalline water loss and hydroxide decomposition), and (III) between 420–740 °C (MOF structural collapse and BTC combustion). Composites with higher RW1* content (MOF@RW1*-50 and MOF@RW1*-75) demonstrated greater thermal stability, highlighting the role of RW1* in enhancing both crystallization and thermal resistance.

The SEM analysis shows that RW1* (**Figure 2a**) exhibits a heterogeneous and amorphous morphology with irregular particle sizes and shapes, typical of a residual material composed of metallic and non-metallic compounds such as oxides and silicates. This composition prevents the formation of well-defined crystalline structures. In the

MOF@RW1*-n composites, morphology evolves depending on RW1* concentration. At low concentrations, the crystals exhibit well-defined hexagonal prismatic structures similar to MIL-96 (**Figure 2b**), suggesting controlled crystal growth. As the RW1* concentration increases, the morphology becomes more heterogeneous, transitioning from hexagonal prisms to elongated hexagonal rods. At the highest RW1* concentration, the particles adopt a needle-like structure associated with MIL-110, as observed in MOF@RW1*-75 (**Figure 2c**), which forms under strongly acidic conditions. This gradual morphological shift indicates that RW1* acts as a modulator of crystal growth, likely due to ion competition affecting nucleation. At low RW1* concentrations, MIL-96—a thermodynamically stable phase—predominates, while higher concentrations favor MIL-110, a kinetically stable phase. These findings demonstrate that RW1* not only alters morphology but also influences the stability and composition of the resulting crystalline phases.

(a)

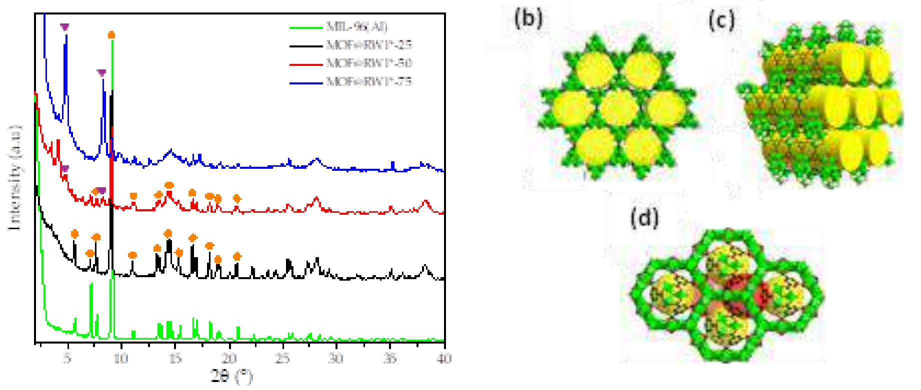

Figure 1 XRD patterns for MIL 96(Al) and synthesized MOF@RW1*-n composites (a). Peaks labeled with ▼,●, represent MIL-110(Al) and MIL-96(Al), respectively. On the right, representations of MOF structures: MIL-110 (b), the 3D structure of MIL-110 showing the arrangements of the hexagonal channels (c) and MIL-96 (d) [10]

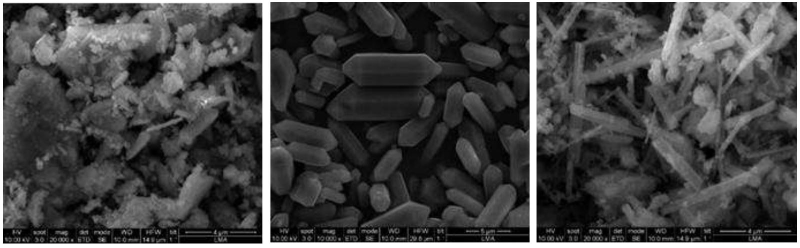
(a) (b) (c)

Figure 2 SEM images for RW1* (a), MIL-96(Al) (b), and MOF@RW1*-75 (c)

The textural properties of aluminum saline slags (RW1 and RW1*), MOF@RW1*-n composites, and MIL-96(Al) were analyzed using nitrogen adsorption-desorption isotherms at -196 °C. Aluminum saline slags (RW1 and RW1*) exhibited notably low BET and micropore surface areas, with values ranging from 31 to 33 m^2/g and 3 to 4 m^2/g, respectively, along with reduced pore volumes (0.051–0.118 cm^3/g). However, the formation of MOFs using these slags led to a marked improvement in textural properties. The synthesis method employed resulted in high BET surface areas for the prepared MOFs. As the RW1* content increased, the BET surface area of MOF@RW1*-n composites rose significantly, ranging from 86 to 483 m^2/g. Similarly, the micropore area increased from 22 to 336 m^2/g, and the total pore volume grew from 0.236 to 0.472 cm^3/g. These findings suggest that the predominant formation of the MIL-110 phase contributes to improved textural properties, likely due to enhanced pore accessibility and a more open structure (**Figures 1b, c**).

When comparing the textural properties of MOF@RW1*-75 with MIL-96(Al), a decrease in BET surface area (483 vs. 689 m^2/g) and micropore area (336 vs. 649 m^2/g) is observed. This reduction may be attributed to the incorporation of RW1*, which decreases the proportion of micropores in the structure. However, MOF@RW1*-75 exhibits a significantly larger total pore volume (0.472 vs. 0.264 cm^3/g), suggesting a possible reorganization of the porous structure towards larger mesopores, partially compensating for the loss of micropores.

The N_2 adsorption-desorption isotherms indicate that RW1* has a moderate adsorption capacity, corresponding to an incipient mesoporous structure with limited surface area. In contrast, the formation of MOF@RW1*-n composites results in a shift towards a hybrid type I/IV isotherm, reflecting the coexistence of micropores from the MOF framework and mesopores from interparticle voids. Notably, MOF@RW1*-50 and MOF@RW1*-75 exhibit a significant increase in N_2 adsorption at low relative pressures, confirming enhanced microporosity. The pore size distribution reveals mesopores ranging from 2 to 30 nm, supporting the hierarchical structure formed by integrating RW1* into the MOF matrix. Meanwhile, MIL-96(Al) displays a classic type I isotherm, indicating its purely microporous nature, with a higher adsorption capacity compared to the composites due to its greater specific surface area.

The XPS analysis of MOF@RW1*-50, MOF@RW1*-75, and MIL-96(Al) confirmed the presence of Al 2p, C 1s, and O 1s peaks, along with an additional Si 2p signal in the MOF@RW1*-50 and MOF@RW1*-75 composites, indicating the incorporation of silicon from RW1*. The C 1s spectrum revealed functional groups (-COOH and C-O) involved in the coordination of the organic ligand with Al^{3+}, promoting the formation of MIL-96 and MIL-110 structures. The O 1s spectrum confirmed the presence of O-Al-O bonds, characteristic of MOF frameworks, while the Al 2p peak at 73.9 eV validated the stable coordination of Al^{3+} with the ligand. These findings confirm the successful incorporation of RW1* and the formation of stable three-dimensional MOF networks.

The EDX analysis of MOF@RW1*-75 and MOF@RW1*-50 confirmed the presence of aluminum (Al), oxygen (O), silicon (Si), and carbon (C), consistent with previous XPS findings. This composition verifies the successful incorporation of RW1* into the MOF structure. Elemental mapping revealed a uniform distribution of Al and O, suggesting homogeneous integration of RW1* and MOF precursors during synthesis. These results confirm the effective functionalization of the materials, ensuring their structural and functional stability.

A static volumetric method is used to evaluate the CO_2 adsorption capacity at several temperatures [2,11]. Firstly, if the adsorption capacity of MIL-96(Al) is compared with that of other commercial MOFs (MIL-56(Al), Cu-BTC, Fe-BTC, ZIF-8 and UiO-66), a value of 1.66 $mmol_{CO2}/g$ is obtained compared to values between 1.03 (MIL-56(Al)) and 0.37 (ZIF-8) $mmol_{CO2}/g$, all these values determined at 50 °C. In the case of MOF@waste composites, the capacities vary between 2.40 10^{-3} $mmol_{CO2}/m^2$ (MIL-96(Al)) and 1.95 10^{-3} $mmol_{CO2}/m^2$ (MOF@RW1*-75), respectively.

CONCLUSION

In this study, MOF@RW1*-n composites were synthesized for the first time using a simple and cost-effective in-situ hydrothermal method. These materials were obtained from saline slags (RW1*), a byproduct of aluminum extraction in an acidic medium. X-ray diffraction (XRD) analysis revealed that MOF@RW1*-75 preferentially formed the metastable MIL-110(Al) phase. Furthermore, N_2 adsorption-desorption experiments at low pressure demonstrated that MOF@RW1*-75 exhibited superior properties compared to MOF@RW1*-25, MOF@RW1*-50, and RW1*, including a higher specific surface area, microporous surface area, and total pore volume. Scanning electron microscopy (SEM) analysis confirmed that MOF@RW1*-75 displayed an elongated, needle-like hexagonal morphology, characteristic of the MIL-110(Al) structure. X-ray photoelectron spectroscopy (XPS) results verified the successful coordination of the ligand to the Al^{3+} center, leading to the formation of stable three-dimensional MOF networks. Additionally, composites with a higher RW1* content exhibited enhanced thermal stability, likely due to the intrinsic thermal resistance provided by RW1*. These findings suggest that aluminum saline slags can serve as a precursor for synthesizing MOF composites, such as those with MIL-96(Al) and MIL-110(Al) phases, which could be effectively applied as greenhouse gas adsorbents, particularly for CO_2 capture at moderate temperatures between 200 and 400 °C.

ACKNOWLEDGEMENT

The authors are grateful for financial support from the Spanish Ministry of Science and Innovation (MCIN/AEI/10.13039/501100011033) and the Government of Navarra (Department of Rural Development and Environment, Waste Fund 2023) through projects PID2023-146935OB-C21 and 0011-4387-2023-000001. HJM thanks the Universidad Pública de Navarra for a doctoral grant.

REFERENCES

1. Li, P.F., Xu, Y., B. Q. (2024) Chen, Sustain. Energy Technol. Assessments 67, 103836.
2. Torrez-Herrera, J.J., Korili, S.A., Gil, A., (2023) Powder Technol. 429, 118962.
3. Haouas, M., Volkringer, C., Loiseau, T., Férey, G., Taulelle, F. (2012) Chem. Mater. 24, 2462–2471.
4. Muñoz, H.J., Korili, S.A., Gil, A. (2025) Catal. Today 447.
5. Muñoz, H.J., Korili, S.A., Gil, A. (2024) Catal. Rev. 00, 1–53.
6. Muñoz, H.J., Galeano, L.A., Vicente, M.A., Korili, S.A., Gil, A. (2024) Chem. Eng. J. 499.
7. Torrez-Herrera, J.J., Korili, S.A., Gil, A. (2022) Chem. Eng. J. 433, 133191.

8. Cardona, Y., Korili, S.A., Gil, A. (2021) Chem. Eng. J. 425 130708.
9. Abid, H.R., Rada, Z.H., Shang, J., Wang, S. (2016) Polyhedron 120, 103–111.
10. Li, J., Hurlock, M.J., Goncharov, V.G., Li, X., Guo, X., Zhang, Q. (2021) Inorg. Chem. 60, 4623–4632.
11. Gil, A., Arrieta, E., Vicente, M.A., Korili, S.A. (2018) Chem. Eng. J. 334, 1341–1350.

XVI International Mineral Processing
and Recycling Conference
28-30 May 2025, Belgrade, Serbia

DOI: 10.5937/IMPRC25113I Original research article

SELECTIVE SEPERATION OF MAGNESIUM FROM SLOVENIAN DOLOMITES

Jernej Imperl[1#], 0009-0002-5472-5990,
Mitja Kolar[1], 0000-0001-5095-6172,
Vilma Ducman[2], 0000-0002-6430-3305,
Gorazd Žibret[3], 0000-0002-9957-1895,
Lea Žibret[2], 0000-0002-0132-0896,
[1]Faculty of Chemistry and Chemical Technology, University of Ljubljana, Ljubljana, Slovenia
[2]Slovenian National Building and Civil Engineering Institute, Ljubljana, Slovenia
[3]Geological Survey of Slovenia, Ljubljana, Slovenia

ABSTRACT – Although magnesium is one of the most abundant elements on Earth by weight, the demand for magnesium is constantly increasing due to its widespread use in a diverse range of industries such as metal alloys, electronics, batteries, agricultural and pharmaceutical compounds. For this reason, magnesium is categorised as a critical raw material by the European Union. Dolomite $CaMg(CO_3)_2$ is one of the most important mineral sources of magnesium, which in its pure form contains 13.18 % magnesium by weight. Various pyrometallurgical and hydrometallurgical processes have been developed and are used to extract magnesium from dolomite and other magnesium ores. In this study, samples of dolomite of different geological ages were collected in Slovenia and their elemental composition was analysed by microwave-assisted acid digestion and ICP-OES. Magnesium was then extracted by selective leaching and selective precipitation. Leaching was carried out with inorganic and organic acids. The separation of magnesium and calcium in a solution prepared by dissolving dolomite with acid was carried out by precipitation with hydroxide and oxalate. High extraction yields of magnesium and a significant separation between the two metals were achieved with both methods.

Keywords: Magnesium, Dolomite, Extraction, Selective Leaching, Selective Precipitation.

INTRODUCTION

Magnesium (Mg) is an alkaline earth metal and one of the most abundant elements by weight in Earth's crust and oceans. The most important mineral sources are magnesite ($MgCO_3$), dolomite ($CaMg(CO_3)_2$), and talc ($Mg_3Si_4O_{10}(OH)_2$). The other important source is seawater, which contains the soluble magnesium cation Mg^{2+}. Mg has many desirable properties and is therefore used in various industries (e.g., alloys, electronics, energy storage, agriculture, construction, pharmaceuticals). Mg is extracted from all its source materials and produced in large quantities [1,2]. With the ever-increasing demand and its current and other potential uses, the EU has categorised Mg as a critical raw material.

[#] corresponding author: jernej.imperl@fkkt.uni-lj.si

Mg production is largely centred on two processes: molten salt electrolysis of $MgCl_2$ salt extracted from seawater [3] and thermal reduction of carbonate minerals magnesite and dolomite [4]. Both processes are energy intensive, as they require high temperatures, and produce toxic emissions [1]. As an alternative, hydrometallurgical processes are used to extract Mg from its sources. These processes are being used more and more frequently, and new approaches are being developed. Mg is extracted and dissolved from its ores using various chemical solutions. The Mg-rich leachate is then either evaporated to obtain Mg salts or electrolysed to recover Mg metal [1,5].

Dolomite is a common mineral that is widely distributed in its rock form. Its molecular formula is $CaMg(CO_3)_2$, which corresponds to the molar ratio of Mg to Ca of 1:1. For this reason, pure dolomite contains 13.18 % Mg by weight. Dolomite is formed by dolomitisation, a process in which calcite or limestone ($CaCO_3$) undergoes cation exchange with Mg ions under certain conditions [6].

The territory of Slovenia is mostly covered by sediments, especially two sedimentary rocks – limestone and dolomite. Dolomites cover about 10 % of the surface and were formed by the process of dolomitisation in all geological periods (from the Permian to the Cretaceous) [7].

EXPERIMENTAL

Dolomite samples

Dolomite samples were collected throughout Slovenia where there are known dolomite deposits. The samples were collected from active and disused quarries and other natural areas. Five of the samples that were identified as pure dolomite rock and that correspond to all geological periods in which dolomite was formed on the territory of present-day Slovenia were included in this study (Table 1). The samples were collected in bulk and then ground into fine powder, which was stored in transparent plastic containers for further analysis.

Table 1 List of dolomite samples, their geological period and their appearance (colour) in powder form. Samples are arranged from oldest to youngest.

dolomite sample	geological period	appearance (colour)
D1	Permian	dull white
D2	Early and Middle Triassic	pure white
D3	Late Triassic	dull white
D4	Late Jurassic	light grey
D5	Cretaceous	light grey

Elemental analysis

Dolomite samples were prepared by microwave-assisted acid digestion in a microwave system (Ethos UP, Milestone, Italy). The samples were weighed into PTFE vessels with an approx. mass of 250 mg. Then 8 mL conc. hydrochloric acid (HCl, 37 %, pro analysi, KEFO, Slovenia) and 2 mL tetrafluoroboric acid (HBF_4) solution were added. HBF_4 was prepared in-house by dissolving boric acid (H_3BO_3, pro analysi, Honeywell, USA) in concentrated hydrofluoric acid (HF, 48 %, pro analysi, Merck, Germany). Acid digestion was carried out using a three-stage temperature programme: the samples were heated to 220 °C (over a period of 30 min), the set temperature was maintained for 15 min, and then the samples were allowed to cool to near room temperature before opening. The digested solutions were quantitatively transferred to 50 mL graduated polypropylene centrifuge tubes (Sarstedt, Germany) and diluted to the 50 mL mark with ultrapure water. The blank sample was prepared using the same procedure. The samples were digested in triplicate.

Selective leaching

Selective leaching of magnesium was carried out using solutions of sulfuric(VI) acid (H_2SO_4, 95-97 %, pro analysi, Honeywell, USA), tartaric acid (DL, $C_4H_6O_6$, ≥99 %, Merck, Germany), and oxalic acid ($C_2H_2O_4$ x $2H_2O$, pro analysi, Merck, Germany). The dolomite samples were weighed into centrifuge tubes with an exact mass of 1 g (±0.5 %). Then 10 mL H_2SO_4 solution or 20 mL organic acid solution was added. The centrifuge tubes were placed in a stand and shaken on an orbital shaker (Orbit 1900, Labnet, USA) for 30 min at 240 rpm. For the first 15 min the tubes were upright and open, then the tubes were closed and placed horizontally until the end of shaking. The resulting mixture was filtered through a filter paper (white mark, IDL, Germany) into a new centrifuge tube. The centrifuge tube was washed twice with 5 mL ultrapure water and the filter paper was washed once with 5 mL ultrapure water. The filtrate was acidified by adding 1 mL of conc. nitric(V) acid (HNO_3, 65 %, pro analysi, KEFO, Slovenia) and diluted to the 50 mL mark with ultrapure water. The samples were prepared in triplicate.

Selective precipitation

Hydroxide and oxalate solutions were prepared from sodium hydroxide (NaOH, pro analysi, Avantor, USA) and ammonium oxalate monohydrate ($(NH_4)_2C_2O_4$ x H_2O, pro analysi, Carlo Erba, Italy), respectively. They were used to selectively precipitate magnesium and calcium ions. First, dolomite samples with an exact mass of 1 g (±0.5 %) were weighed into centrifuge tubes. The samples were dissolved by adding 10 mL HNO_3 solution. The centrifuge tubes were shaken open for 15 minutes at 240 rpm in a vertical position. Then a further 15 minutes at 240 rpm in the horizontal position and closed. Then 10 mL NaOH solution or 20 mL $(NH_4)_2C_2O_4$ x H_2O solution was added, and shaken for 15 minutes at 240 rpm in horizontal position and closed. The suspension was centrifuged at 4000 rpm for 5 minutes (Centric 350, Domel, Slovenia). The supernatant was decanted into a new centrifuge tube and the suspension was washed twice with 5 mL ultrapure water, centrifuged and the supernatant collected. The collected supernatant was acidified by adding 1 mL of concentrated HNO_3 and diluted to the 50 mL mark with ultrapure water. The samples were prepared in triplicate.

ICP-OES measurements

The concentrations of the elements in the sample solutions were measured using inductively coupled plasma optical emission spectroscopy (ICP-OES, Agilent 5100 SVDV, Agilent Technologies, USA). The sample solutions were appropriately diluted with

1 % HNO_3 solution. Calibration standards were prepared in 9 concentrations ranging from 0.1-1000 µg/L, by mixing and diluting two certified multi-element standard solutions Periodic table mix 1 for ICP (33 elements, 10 mg/L, Merck, Germany), and VAR-CAL-1 (4 elements, 100 mg/L, Inorganic Ventures, USA) with 1 % HNO_3 solution. The elements measured were Li, Be, Na, Mg, Al, Si, P, K, Ca, Ti, V, Cr, Mn, Fe, Co, Ni, Cu, Zn, Ga, As, Se, Rb, Sr, Mo, Ag, Cd, In, Sn, Sb, Te, Ba, Tl, Pb, and Bi.

Preparation of solutions

In the case of H_2SO_4, tartaric acid, oxalic acid, and HNO_3, the solutions of the reagents were prepared so that the volume of solution added to 1 g of dolomite sample contained 105 % of the molar equivalent required for the total reaction between the reagent and the combined amount of magnesium and calcium in 1 g of ideal dolomite. For NaOH and $(NH_4)_2C_2O_4$, the solutions were prepared so that each addition contained 105% of the molar equivalent of only Mg and Ca (i.e., half the total amount). This resulted in the preparation of the following solutions: H_2SO_4 1.144 M, tartaric acid 0.570 M, oxalate acid 0.570 M, HNO_3 2.294 M, NaOH 1.140 M, and $(NH_4)_2C_2O_4$ 0.285 M.

All solutions of reagents or dilutions of concentrated acids were prepared with ultrapure water (resistivity >18.2 MΩ cm, Synergy Water Purification System, Merck Millipore, Germany).

RESULTS AND DISCUSSION

The results of the elemental analysis (Table 2) confirm that the identification of the samples as dolomite was correct. Samples D1 to D4 are almost pure dolomite, with the mass percentage *w* of magnesium and calcium being very close to the ideal values and the molar ratios of the metals being almost the same. The exception is the youngest dolomite D6, whose composition and molar ratio (m. r.) of only 0.8 Mg to 1 Ca shows incomplete dolomitisation. All samples contain less than 1% of impurities consisting of other common mineral elements such as Si, Al, Fe, Na, K, and Zn. The lowest amount of impurities, less than 0.1%, is present in D2, which is consistent with its appearance – sample D2 is pure white.

Table 2 Mass percentages *w* of Mg, Ca, and impurities in dolomite samples.

	w_{Mg} [%]	w_{Ca} [%]	m. r. (Mg:Ca)	*total* and main elemental impurities (ppm)
$CaMg(CO_3)_2$	13.18	21.74	1:1	/
D1	13.001 ± 0.023	22.203 ± 0.040	0.966:1	*(6020)* – Si (4000), Fe (733), Al (700), K (215), Na (191)
D2	12.75 ± 0.055	21.94 ± 0.13	0.959:1	*(970)* – Zn (354), Fe (142), Mn (121), Si (110), Al (83)
D3	12.82 ± 0.17	22.30 ± 0.21	0.948:1	*(3120)* – Si (1100), Al (653), Fe (579), K (427), Na (131)
D4	12.998 ± 0.085	22.29 ± 0.14	0.962:1	*(3060)* – Si (1860), Al (314), K (238), Na (221), Fe (203)
D5	11.690 ± 0.086	24.05 ± 0.10	0.802:1	*(1310)* – Si (709), Na (175), Sr (117), Al (93), Fe (48)

The aim of the selective leaching experiments was the selective solubilisation of magnesium ions, while calcium ions remained in solid form. This was done with three reagents H_2SO_4, tartaric acid and oxalic acid, whose Mg and Ca salts sulphate(VI), tartrate and oxalate show large differences in their solubility. In all cases, the Mg salt is the more soluble of the two [8].

The results are given as extraction efficiency η and molar ratio (m. r.) of the two metals in solution (Table 3). Of the three, H_2SO_4 extracted the largest amount of Mg – 70-75 % of the total mass percentage, and about 5 % of Ca for all dolomite samples. The Mg:Ca molar ratio improved to the lowest ratio of 10.6:1 and the highest ratio of 19.2:1. While both organic acids extracted less Mg, they outperformed H_2SO_4 in extraction selectivity. In both cases, the molar ratio increased strongly in favour of Mg.

Table 3 Extraction efficiencies η of Mg and Ca from dolomite samples with solutions of H_2SO_4, tartaric acid, and oxalic acid.

sample	**H_2SO_4**			**tartaric acid**			**oxalic acid**		
	η_{Mg} [%]	η_{Ca} [%]	m.r. (Mg:Ca)	η_{Mg} [%]	η_{Ca} [%]	m.r. (Mg:Ca)	η_{Mg} [%]	η_{Ca} [%]	m.r. (Mg:Ca)
D1	75.77	4.96	14.8:1	23.44	0.26	86.1:1	29.81	0.06	448:1
D2	76.61	3.82	19.2:1	45.57	0.17	259:1	26.80	0.14	184:1
D3	75.20	5.33	13.4:1	18.93	0.24	74.8:1	20.76	0.38	51.3:1
D4	74.87	5.24	13.7:1	14.99	0.32	45.7:1	21.00	0.15	137:1
D5	70.26	5.29	10.6:1	11.93	0.43	22.3:1	18.95	0.05	288:1

Dissolution of the dolomite samples with HNO_3 solution, in preparation for selective precipitation, was complete for all samples. The solutions contained >95 % of the mass percentages of magnesium and calcium in the dolomite samples as determined by elemental analysis. All solutions were clear, some were pale yellow, and all contained very small amounts of grey or brown coloured solid residues.

Selective precipitation, like selective leaching, was based on differences in the solubility of Mg and Ca salts of hydroxide and oxalate. While both Mg and Ca hydroxide are insoluble, the solubility product of the former is six orders of magnitude greater than the K_{sp} of the latter. The opposite is true for Mg and Ca oxalate. [8]

Table 4 Percentage η of precipitated Mg and Ca with hydroxide and percentage η of Mg and Ca remaining in solution after precipitation with oxalate.

sample	**NaOH**			**ammonium oxalate**		
	precipitate			*solute*		
	η_{Mg} [%]	η_{Ca} [%]	m.r. (Mg:Ca)	η_{Mg} [%]	η_{Ca} [%]	m.r. (Mg:Ca)
D1	72.70	5.11	13.7:1	94.46	5.43	16.8:1
D2	75.56	2.01	36.0:1	96.03	5.91	15.6:1
D3	73.80	5.34	13.1:1	93.14	5.83	15.1:1
D4	71.42	6.91	9.9:1	94.79	5.46	16.7:1
D5	80.72	0.17	391:1	95.89	10.15	7.6:1

The results for precipitation with hydroxide are given as a percentage η of the precipitated metals and with oxalate as a percentage η of the remaining metal ions in the solution. 70-80 % of Mg precipitated when hydroxide solution was added to the solution of dissolved dolomite. Small amounts of Ca also precipitated together with Mg, resulting in an improvement of the Mg:Ca molar ratio in the precipitate. For sample D6, the molar ratio changed significantly to 391:1 for Mg, while for all other samples it improved to around the order of 10 to 1. During precipitation with oxalate, most of the Ca precipitated (approx. 95 %) and approx. 5 % of Mg. The solution remained rich in Mg – the Mg:Ca molar ration was increased to about 15 to 1.

CONCLUSION

This study explored hydrometallurgical methods for Mg extraction from Slovenian dolomite, focusing on selective leaching and precipitation. Elemental analysis confirmed the composition of dolomite, and leaching with various acids and precipitation with hydroxide and oxalate demonstrated successful Mg enrichment. These results suggest that hydrometallurgical approaches offer viable pathways for Mg recovery from dolomite, with potential for optimisation to enhance efficiency and selectivity.

ACKNOWLEDGEMENT

Authors would like to acknowledge the financial support of the Slovenian Research and Innovation Agency (ARIS) for the Research Funding Programme under grant number PS-0153, and the Research Project under grant number J1-50032.

REFERENCES

1. González, Y., Navarra, A., Jeldres, R.I., Toro, N. (2021) Hydrometallurgical processing of magnesium minerals – A review, Hydrometallurgy, 201, 105573.
2. Pavčnik, T., Imperl, J., Kolar, M., Dominko, R., Bitenc, J. (2024) Evaluating the synthesis of $Mg[Al(hfip)_4]_2$ electrolyte for Mg rechargeable batteries: purity, electrochemical performance and costs, J. Mater. Chem. A, 12, 3386-3397.
3. Lee, T.-H., Okabe, T.H., Lee, J.-Y., Kim, Y.M., Kang, J. (2020) Molten Salt Electrolysis of Magnesium Oxide Using a Liquid-Metal Cathode for the production of Magnesium Metal, Metall. Matter. Trans. B, 51B, 2993-3006.
4. Fu, D., Wang, Y., Zhang, T., Feng, N. (2022) Review on the Silicothermic Process for Primary Magnesium Production, Metall. Matter. Trans. B, 54B, 1-23.
5. Erlund, R., Koivisto, E., Fagerholm, M., Zevenhoven, R. (2016) Extraction of magnesium from four Finnish magnesium silicate rocks for CO_2 mineralisation – part 2: Aqueous solution extraction, Hydrometallurgy, 166, 229-236.
6. Chen, C., Zhong, H., Wang, X., Ning, M., Wang, X., Ge, Y., Wang, H., Tang, R., Hou, M. (2023) Thermodynamic and Kinetic Studies of Dolomite Formation: A Review, Minerals, 13, 1479.
7. Hrvatin, M., Tičar, J., Zorn, M. (2020) Rocks and Tectonic Structure of Slovenia. In: The Geography of Slovenia (D. Perko, R. Ciglič, M. Zorn), Springer, Cham, 23-34.
8. Smith, R.M., Martell, A.E. (1976), Critical Stability Constants, Plenum Press, New York.

XVI International Mineral Processing
and Recycling Conference
28-30 May 2025, Belgrade, Serbia

DOI: 10.5937/IMPRC25119N

Original research article

ANODE NANOMATERIAL RECOVERED FROM SPENT BATTERIES FOR PEROXIDE-ASSISTED CRYSTAL VIOLET PHOTOCATALYTIC DEGRADATION

Vladan Nedelkovski#, 0000-0001-7724-1118,
Dragana Medić, 0000-0001-9980-5949,
Aleksandar Cvetković, 0009-0003-5184-6874,
Sonja Stanković, 0000-0003-0745-5422,
Žaklina Tasić, 0000-0001-6544-1980,
Milan Radovanović, 0000-0002-5175-6022,
Snežana Milić, 0000-0002-5000-9156,
University of Belgrade, Technical Faculty in Bor, Bor, Serbia

ABSTRACT – This study explores the photocatalytic degradation of Crystal Violet (CV) using anode nanomaterials recovered from spent nickel-metal hydride (NiMH) batteries, activated by hydrogen peroxide (H_2O_2). The research focuses on the potential application of recycled perovskite-based materials, such as Lanthanum Cobalt Oxide ($LaCoO_3$), Nickel Oxide (NiO), and Cerium Dioxide (CeO_2), for the efficient removal of organic dyes from textile industry wastewater. Structural characterization via X-ray diffraction (XRD) confirmed the presence of crystalline phases with high crystallinity, essential for photocatalytic activity. Photocatalytic experiments were conducted under UV-A light (λ = 395 nm) at pH 5.5, demonstrating a degradation efficiency of 99.52% within 60 minutes. The reaction followed pseudo-first-order kinetics, with a significant increase in efficiency over time. These findings highlight the potential of using recycled battery materials as sustainable and effective photocatalysts for wastewater treatment, offering a promising solution to mitigate environmental contamination caused by synthetic dyes and other persistent organic pollutants.

Keywords: Anode Material, Perovskites, Crystal Violet, Photocatalysis.

INTRODUCTION

Textile industry wastewater is a significant source of environmental contamination due to its high concentration of organic pollutants, particularly synthetic dyes. These dyes are known for their chemical stability and resistance to biodegradation, making their removal from water bodies a major challenge. The uncontrolled discharge of such pollutants into aquatic ecosystems leads to severe consequences, including reduced water quality, disruption of aquatic life, and long-term ecological imbalances [1].

In 2020, it was estimated that approximately 200,000 tons of organic dyes were released into textile industry wastewater, posing a substantial environmental threat. The accumulation of these persistent contaminants not only affects aquatic organisms but

---

corresponding author: vnedelkovski@tfbor.bg.ac.rs

also compromises human health through the contamination of drinking water sources. The widespread presence of dye pollutants in industrial effluents highlights the urgent need for effective and sustainable wastewater treatment methods to mitigate their adverse effects on ecosystems and environmental quality [2].

Traditional methods for dye removal from wastewater are often inefficient or economically unsustainable, driving the search for alternative approaches based on advanced oxidation processes (AOPs) [3]. Hydroxyl radicals generated during AOP exhibit strong oxidative properties, enabling them to degrade complex organic molecules into smaller, environmentally benign compounds such as water and carbon dioxide [4].

Photocatalytic degradation is one of the most promising solutions for breaking down organic pollutants, utilizing photocatalysts that, in the presence of light, generate reactive oxygen species capable of decomposing complex molecules into smaller, environmentally friendly products [5]. Special attention in recent years, has been given to the use of recycled materials, such as perovskite materials similar to the cathode materials that can be obtained from waste batteries [6, 7]. These materials can serve as a very efficient catalyst for dye degradation when activated by hydrogen peroxide.

This paper presents the efficiency of photocatalytic degradation of crystal violet using anode material from spent nickel-metal hydride (NiMH) batteries in combination with hydrogen peroxide. The aim is to examine the degradation kinetics, reaction mechanisms, and the potential application of this method in wastewater treatment.

EXPERIMENTAL

Sample Preparation

The examined sample originated from a discarded battery of an unidentified manufacturer. To ensure safe handling and prevent short circuits, the battery was first disassembled after fully discharging its six individual cells. The discharge process was carried out using a laboratory-made apparatus equipped with a 5.5 Ω resistive wire, enabling controlled discharging of the battery samples.

A hacksaw was used to remove the cell terminals, followed by a longitudinal cut to systematically separate the plastic casing, metal casing, anode, cathode, and separator. The anodic material was subjected to thermal treatment at 580°C for 10 minutes, facilitating its detachment from the current collector. Anodic material was finely ground using an agate mortar and pestle. To maintain sample integrity and prevent cross-contamination, meticulous cleaning of the equipment was performed between uses.

RESULTS AND DISCUSSION

X-ray Diffraction Analysis

XRD analysis was conducted via Rigaku MiniFlex 600 (Japan) to characterize the structural properties of the anode material derived from waste batteries and assess its suitability as a photocatalyst for the degradation of Crystal Violet. The diffraction patterns provide insights into the crystalline phases present, potential impurities, and any structural modifications resulting from material processing. The XRD pattern of anode material is shown in Figure 1.

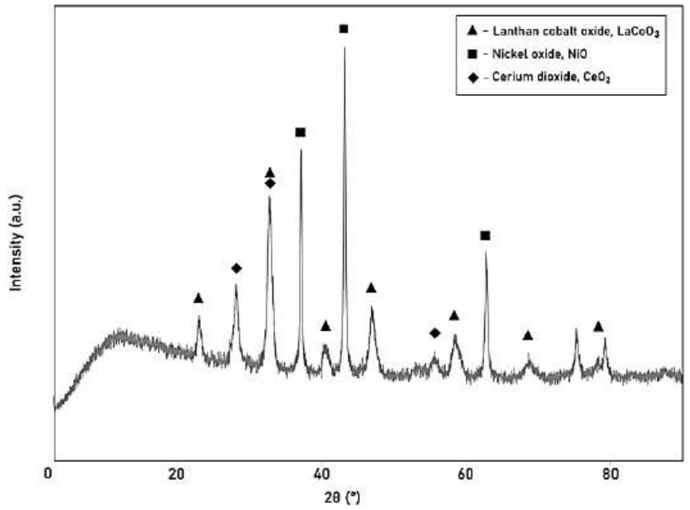

Figure 1 XRD analysis of anode material

The X-ray diffraction (XRD) pattern shown in Figure 1., reveals the crystalline phases present in the analyzed sample, confirming the presence of multiple components. The identified peaks correspond to Lanthanum Cobalt Oxide ($LaCoO_3$), Nickel Oxide (NiO), and Cerium Dioxide (CeO_2), as indicated by the reference diffraction patterns. The presence of $LaCoO_3$ suggests that the anode material retains its perovskite structure, which is crucial for its potential photocatalytic applications [6].

XRD pattern of analyzed material presented a high-intensity peak at 32.7^{o}, which might be associated with planes (110) and/or (104), corresponding to hexagonal crystal symmetry with an R3c space group, assuming angles a=b=90° and y = 120°, further allowing for calculation of crystal lattice constants [8].

The size of crystallites was assessed using the Scherrer equation: $D = 0.9\lambda / \beta \cos\theta$, where D denotes the crystallite size, λ represents the X-ray wavelength (1.5418 Å), θ corresponds to the Bragg diffraction angle, and β signifies the full width at half maximum (FWHM) of the diffraction peak. To evaluate the crystallite size of the sample, the peak broadening of the (024) reflection of the $LaCoO_3$ phase at $2\theta = 46.9°$ was analyzed [8].

Crystal lattice constants for the $LaCoO_3$ phase are determined as $a=b\approx5.47$ Å (hexagonal system) and $c\approx13.39$Å, while crystallite size calculated from the (024) peak is approximately 8.84 nm. The volume cell is determined to be $V\approx346.8$ $Å^3$.

Based on characteristic peaks and confirmed planes (111) and (002), crystal lattice constants for NiO in the cubic system are determined as $a=b=c\approx4.18$ Å, while the crystallite size calculated from the (002) peak is approximately 34.8 nm. The unit cell volume is determined to be $V\approx73.1Å^3$.

Crystal lattice constants for CeO_2 in the cubic system are determined as $a=b=c\approx$ 5.45 Å, while the crystallite size calculated from the (111) peak is approximately 11.0 nm. The unit cell volume is determined to be $V\approx161.9$ $Å^3$.

The strong and sharp diffraction peaks could indicate a high degree of crystallinity, suggesting that the material possesses well-ordered structural characteristics [9]. The presence of NiO and CeO_2 as additional phases might contribute to enhanced catalytic properties [10]. These structural insights are essential for understanding the material's reactivity and effectiveness in the photocatalytic degradation of CV when activated with hydrogen peroxide.

Photocatalytic Degradation and Kinetics

Degradation experiments were carried out using a previously prepared 20 ppm crystal violet solution to investigate photocatalytic properties, and accessed via CGOLDENWALL 721 UV-VIS spectrophotometer (China). The experiments were performed with exposure to UV-A light (λ = 395 nm), with the addition of peroxide in order to modify the pH. The collected data were analyzed using a pseudo-first-order model, expressed as [11]:

$$\ln\left(\frac{C_0}{C_t}\right) = kt \qquad (1)$$

Here, C_0 and C_t denote the concentrations of the model compound at the initial time (zero) and at time t, respectively, while k represents the rate constant of the reaction. Figure 2(a) illustrates the degradation efficiency of the CV with the addition of H_2O_2. The relationship between $\ln(C_0/C_t)$ and the irradiation time t is presented in Figure 2(b), showing a linear trend. The rate constants for the reaction were determined by calculating the slopes of the $\ln(C_0/C_t)$ versus time plots.

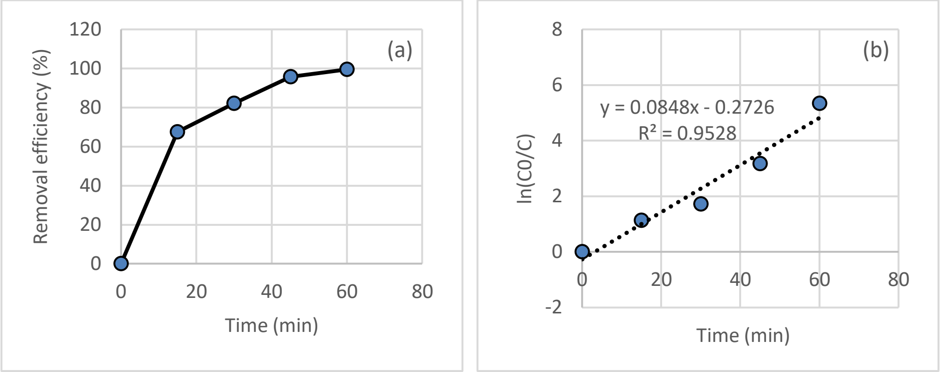

Figure 2 (a) Photocatalytic degradation efficiency of crystal violet, (b) Kinetic curve

The photocatalytic process shows a significant increase in efficiency over time. At 15 minutes, the degradation efficiency is 67.57%, reaching 99.52% at 60 minutes, indicating near-complete degradation of CV. CV degradation follows pseudo-first-order kinetics, which is typical for photocatalytic reactions.

In conclusion, the combination of this anode material and H_2O_2 demonstrates high efficiency in degrading CV, following pseudo-first-order kinetics. Most of the dye is degraded within the first 45 minutes, and near-complete removal is achieved within 60 minutes. This suggests that the anodic material is a promising candidate for the effective removal of CV from wastewater.

CONCLUSION

This study has shown that the combination of recycled anode material and H_2O_2 is highly effective in breaking down complex organic molecules, such as CV, into environmentally benign compounds. The use of recycled materials, such as perovskite-based anode nanomaterials, offers a sustainable and cost-effective approach to wastewater treatment. By repurposing waste from spent batteries, this method not only addresses the issue of environmental contamination caused by synthetic dyes but also contributes to the circular economy by reducing electronic waste. The findings suggest that these materials have significant potential for large-scale applications in industrial wastewater treatment, particularly in the textile industry, where dye pollution is a major concern.

In conclusion, this study highlights the feasibility of using recycled anode nanomaterials as efficient photocatalysts for the degradation of organic dyes. The combination of these materials with H_2O_2 under UV light provides a promising solution for the removal of persistent pollutants from wastewater, offering both environmental and economic benefits. Further research could explore the optimization of reaction conditions and the application of this method to other types of organic pollutants, paving the way for broader implementation in environmental remediation technologies.

ACKNOWLEDGEMENT

The research presented in this paper was done with the financial support of the Ministry of Education, Science and Technological Development of the Republic of Serbia, within the funding of the scientific research work at the University of Belgrade, Technical Faculty in Bor, according to the contract number 451-03-137/2025-03/200131.

REFERENCES

1. Ebrahimi, R., Yetilmezsoy, K., Maleki, A., Puttaiah, S.H., Rezaee, R., Hossienzadeh, K., Daraei, H., Safari, M., Shahmoradi, B., Ghanbari, R., Jafari, A. (2019) Effects of doping zinc oxide nanoparticles with transition metals (Ag, Cu, Mn) on photocatalytic degradation of Direct Blue 15 dye under UV and visible light irradiation. Journal of Environmental Health Science and Engineering, 17(1), 479–492.
2. Druzian, D.M., Oviedo, L.R., Wouters, R.D., Loureiro, S.N., Ruiz, Y.P.M., Galembeck, A., Pavoski, G., Espinosa, D.C.R., Dos Santos, C., Dos Santos, J.H.Z., Silva, W.L.D. (2023) A bimetallic nanocatalyst from carbonaceous waste for crystal violet degradation. Materials Chemistry and Physics, 297, 127455.
3. Mirzaei, A., Chen, Z., Haghighat, F., & Yerushalmi, L. (2017). Removal of pharmaceuticals from water by homo/heterogonous Fenton-type processes – A review. Chemosphere, 174, 665–688.

4. Salehi, K., Daraei, H., Teymouri, P., Shahmoradi, B., Maleki, A. (2015) Cu-doped ZnO nanoparticle for removal of reactive black 5: application of artificial neural networks and multiple linear regression for modeling and optimization. Desalination and Water Treatment, 57(46), 22074–22080.
5. Khan, S., Noor, T., Iqbal, N., Yaqoob, L. (2024) Photocatalytic dye degradation from textile wastewater: A review. ACS Omega, 9(20), 21751–21767.
6. Latsiou, A., Konstantinou, I., Bairamis, F., Lykos, C. (2022) Synthesis and characterization of $LaCo_xNi_{1-x}O_3$ perovskites as heterogeneous catalysts for phenolics degradation by persulfate activation. Journal of Chemical Technology & Biotechnology, 97(12), 3467–3480.
7. Christensen, B.H., Deganello, F., La Parola, V., Boffa, V., Jørgensen, M.K., Østergaard, M.B. (2023) Thermocatalytic performance of $LaCo_{1-x}NixO_{3-\delta}$ perovskites in the degradation of Rhodamine B. Catalysts, 13(2), 325.
8. Islam, M., Jeong, M.-G., Jung, H.-G., Ghani, F. (2015) Micro emulsion synthesis of LaCoO3 nanoparticles and their electrochemical catalytic activity. Journal of Electrochemical Science and Technology, 6(4), 121–130.
9. Shaban, Y., Alharbi, N.A. (2022) Sunlight-mediated photocatalytic removal of phenanthrene from wastewater using carbon-doped zinc oxide (C-ZnO) nanoparticles. Environmental Science and Pollution Research, 29(31), 47818–47831.
10. Atzori, L., Cutrufello, M.G., Meloni, D., Cannas, C., Gazzoli, D., Monaci, R., Sini, M.F., Rombi, E. (2017) Highly active NiO-CeO2 catalysts for synthetic natural gas production by CO_2 methanation. Catalysis Today, 299, 183–192.
11. Sliem, M.A., Salim, A.Y., Mohamed, G.G. (2018) Photocatalytic degradation of anthracene in aqueous dispersion of metal oxides nanoparticles: Effect of different parameters. Journal of Photochemistry and Photobiology A: Chemistry, 371, 327–335.

XVI International Mineral Processing
and Recycling Conference
28-30 May 2025, Belgrade, Serbia

DOI:10.5937/IMPRC25125M Original research article

EFFECT OF TEMPERATURE ON THE LEACHING COPPER FROM FLOTATION TAILINGS WITH IONIC LIQUID

Dragana Marilović, 0000-0001-8301-750X,
Sonja Stanković, 0000-0003-0745-5422,
Grozdanka Bogdanović[#]**,** 0000-0002-1013-4075,
University of Belgrade – Technical faculty in Bor, Bor, Serbia

ABSTRACT – Flotation tailings of copper ore contain a high concentration of valuable metals such as copper, gold and silver. Minerals are mainly found in the form of oxides and less in the form of sulfides that have not been separated by flotation concentration. Recovering these valuable resources would reduce the environmental impact and increase the economic benefits. Compared to sulphide ores and minerals, the presence of oxidising agents is generally not required for the leaching of raw materials rich in oxides. This paper presents the results of the study the influence of temperature on the copper leaching degree from flotation tailings by ionic liquid solutions of different concentrations. Based on the results obtained, it was found that increasing the leaching temperature significantly affects the leaching efficiency. After 120 minutes of leaching at 70°C, a copper leaching degree of 99.7% was achieved at lower ionic liquid concentration than at ambient temperature.

Keywords: Leaching, Flotation Tailings, Ionic Liquid, Copper, High Temperature.

INTRODUCTION

Copper is produced mainly from sulfide ores and usually occurs together with iron in a variety of minerals. Flotation tailings is a raw material consisting mainly of oxides and less of sulfides. Considering the fact that natural resources of rich sulphide ores are becoming increasingly depleted, the processing of secondary raw materials is becoming more important [1]. These particular raw materials are known for their low copper content, quick oxidation, an extremely fine particle size and complex copper phase composition [2]. The complexity creates challenges in their extraction, turning them into a difficult resource to process. Due to its composition, flotation waste, when disposed of in nature, contributes to the formation of acid mine drainage (AMD), which can pose a risk to the environment. In recent years, handling complex copper oxide raw materials has become as a significant and challenging issue for researchers in mining and metallurgy. The studies of flotation tailing leaching indicate that these raw materials have many impurities including silicate, iron and calcium which influence the quality of the product [3-5]. The hydrometallurgical method is an eco-friendly option, which includes processes like sulfuric acid leaching and chloride leaching with oxidants or ammonia

---

[#] corresponding author: gbogdanovic@tfbor.bg.ac.rs leaching with oxidants. Leaching with acid leaching agents, the impurities, especially iron can easily be dissolved [6].

Sulphuric acid leaching has advantages such as a higher copper extraction rate, lower environmental impact and lower energy requirements.

Newer generation reagents, such as ionic liquids (ILs), are increasingly taking the leading position in the leaching of mineral raw materials. Their application has been reported for mineral leaching, solvent extraction and electrochemical processes, showing that these compounds can play an important role in the recovery and purification of high-value metals from raw materials [7, 8].

Ionic liquid 1-butyl-3-methylimidazolium hydrogen sulfate ([bmim]HSO_4) was used as a leaching agent due to its advantages such as water solubility, low cost, environmentally safe and easy availability. Previous research has reported that [bmim]HSO_4 acts as an acid in the aqueous solutions [9-11].

Hydrogen ions, released from ionic liquid, along with dissolved oxygen, are important for the oxidative leaching of sulfide minerals. Compared with traditional acid solutions, [bmim]HSO_4 and its aqueous solutions showed higher efficiency at higher temperatures, which was attributed to increased oxygen solubility and improved transport of dissolved oxygen, accelerating the oxidation reaction [12].

This paper was focused on copper leaching with different concentration of ionic liquid [bmim]HSO_4 from a low-grade flotation tailing at a high temperature.

EXPERIMENTAL AND METHODS

For the experiments flotation tailings samples with the chemical composition showed in Table 1 were used.

Table 1 Chemical composition of copper flotation

Element	Cu	Cu_{ox}	Fe	Zn	Pb	S	SiO_2	Fe_3O_4	MgO	CaO	As_{ppm}
%	0.13	0.09	4.22	0.01	0.01	4.70	60.02	0.03	0.48	3.50	13.24

Based on the obtained qualitative mineralogical analysis, the following mineral composition was determined: Pyrite, Covellite, Chalcopyrite, Limonite, Rutile, Silicates, Quartz and Carbonates.

The leaching experiments were performed with an ionic liquid, 1-butyl-3-methylimidazolium hydrogen sulfate solution ([bmim]HSO_4) without oxidising agent at ambient temperature and at 70 °C. A 600 cm^3 glass reactor with a magnetic stirrer was used for the experiments. Once the operating conditions were established, 10 g of tailings were added to 200 ml of a solution with a specific concentration. The stirring speed was set to 400 rpm. At predetermined time intervals (5, 10, 15, 30, 60, 90 and 120 minutes), samples of 1 ml were taken and filtered. The concentration of copper and iron in the diluted samples was determined using optical emission spectrometer with inductively coupled plasma (ICP-OES Optima 8300; Perkin Elmer) and a multiparameter photometer Hanna HI 83200. This paper was focused on copper leaching with different concentration of ionic liquid from a flotation tailings at a high temperature.

RESULTS AND DISCUSSION

Influence of [bmim]HSO$_4$ concentration on the copper leaching degree at ambient temperature

The effect of [bmim][HSO$_4$] concentration on the copper leaching degree is shown on Figure 1. The leaching experiments at ambient temperature were done using three ionic liquid concentration 0.001, 0.1 and 1 mol/dm^3.

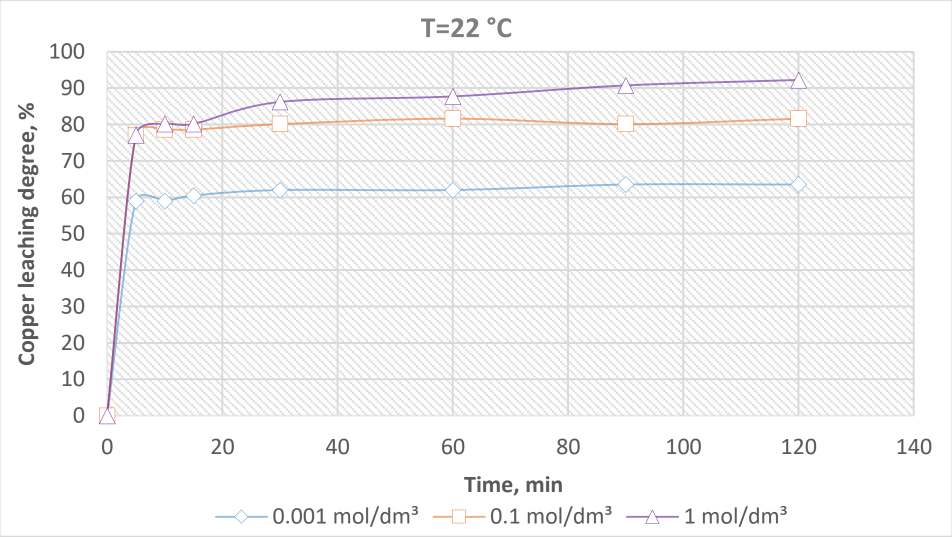

Figure 1 Effect of [bmim][HSO$_4$] concentration on copper leaching degree at ambient temperature, agitation speed 400 rpm, S:L ratio 1:20

The results show that the copper leaching rate is very rapid at ambient temperature in the initial leaching time for all concentrations of ionic liquids. The observed is probably due to the fact that the copper is predominantly in the oxide form. After the initial leaching of easily soluble copper oxide minerals, leaching of copper sulphide minerals begins, which can be observed during leaching with 0.1 mol/dm^3 and 1 mol/dm^3 [bmim][HSO$_4$]. With increasing duration of leaching, dissolution of copper minerals occurs at a lower rate for all concentrations of ILs studied.

The leaching of flotation tailings at ambient temperature using the lowest reagent concentration of 0.001 mol/dm^3 resulted in a copper leaching degree of 63.4% after 120 minutes of process time. Increasing the concentration of the ionic liquid to 0.1 mol/dm^3 increased the copper leaching degree up to 80%, while the highest concentration examined of 1 mol/dm^3 achieved a copper leaching degree of 90% in the same period. For all concentrations, no significant changes in copper leaching degree were observed after 90 minutes.

These results suggest that higher reagent concentrations are required to achieve higher copper recovery from flotation tailings at ambient temperature. Other authors [9] conducted experiments with a sample containing copper mainly in metallic form under conditions similar to those used in this work. The copper leaching degree they achieved without oxidants was less than 30%.

Influence of [bmim]HSO_4 concentration on the copper leaching degree at 70 °C

The effect of ionic liquid [bmim][HSO_4] concentration (0.001, 0.01 and 0.1 mol/dm^3) on the copper leaching degree at 70 °C is shown in Figure 2.

Figure 2 shows that the copper leaching degree increases with the increase in [bmim][HSO_4] concentration. The copper leaching rate from the tailings is highest during the leaching time of about 10 minutes due to the dissolution of the copper oxide minerals. The copper leaching degree ranges from 61% (0.001 mol/dm^3) to 79% (0.01 mol/dm^3 [bmim][HSO_4]). With a further increase in leaching time, leaching of the tailings occurs at a slower rate at [bmim][HSO_4] concentrations of 0.001 and 0.01 mol/dm^3. A greater influence of the ionic liquid at higher temperatures is observed in the leaching of tailings with 0.1 mol/dm^3 [bmim][HSO_4]).

At the lower reagent concentration (0.001 mol/dm^3) temperature does not significantly affect the leaching process and the copper leaching degree remained the same (63.49%). It can be because of the low ionic liquid concentration which shows that there may not be enough leaching agents to significantly affect the mineral dissolution kinetics even at high temperature.

When flotation tailings was leached with an ionic liquid solution concentration 0.01 mol/dm^3 a copper leaching degree of 78% was achieved. At the highest examined reagent concentration of 0.1 mol/dm^3, a copper leaching degree of 99.7% was achieved which indicates that copper sulphide minerals are also leaching. The final concentration of copper in pregnant leaching solution was 64.8 mg/dm^3. Comparing these results with those obtained at ambient temperature, it can be concluded that temperature has a significant impact on copper leaching. Higher recovery was achieved at a lower reagent concentration under high temperature conditions than at a higher concentration at ambient temperature.

Temperature significantly affects the process of copper leaching from primary and secondary raw materials, as an increase in temperature can improve the kinetics of mineral dissolution, increase the solubility of minerals and reduce the viscosity of the solution, which facilitates the diffusion of ions [13]. When studying the leaching of chalcopyrite by ionic liquids at higher temperatures, the authors found that the rate of chemical reaction almost doubles with every 10°C increase in temperature. It is assumed that this is due to the fact that sufficient activation energy is supplied to the molecules in this way to increase the kinetics of the reaction [14].

Research has shown that higher temperatures accelerate the leaching of copper from certain minerals. Earlier research concluded that the leaching of copper from minerals with sulfuric acid is most affected by temperature, then particle size, concentration of reagents, leaching time and at the end agitation speed [2].

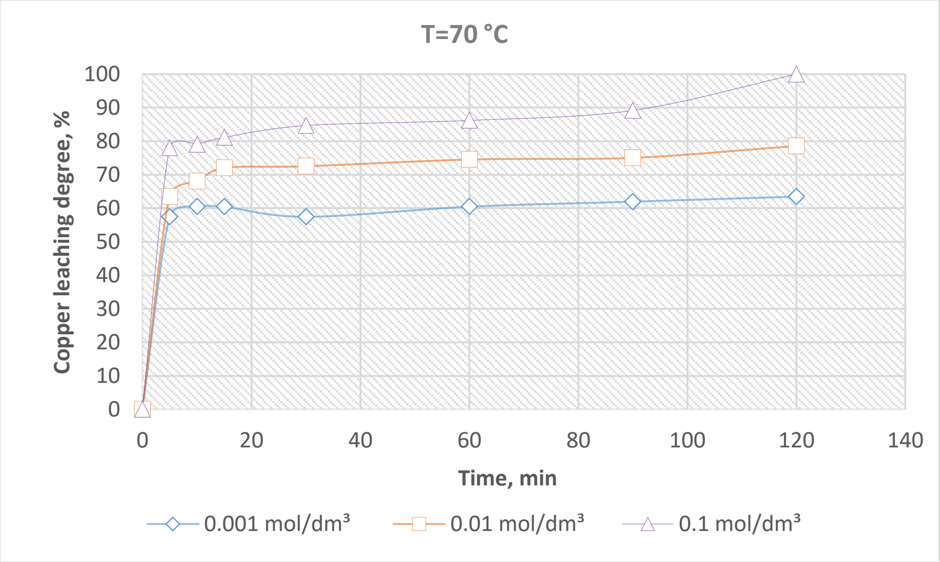

Figure 2 Effect of ionic liquid concentration on copper leaching degree at 70°C, agitation speed 400 rpm, S:L ratio 1:20

CONCLUSION

This paper shows the influence of temperature on the copper leaching degree from flotation tailings. Leaching experiments were done with ionic liquid different concentration at ambient temperature and high temperature without the presence of oxidizing agents. Based on the obtained results, it was found that the temperature has a significant influence on the leaching of copper from the flotation tailings.

The highest copper leaching degree of at room temperature was achieved at 1 mol/dm^3 [bmim][HSO_4] and was 92.2% after 120 minutes of leaching. When leaching at a temperature of 70°C, a lower concentration of leaching agent (0.1 mol/dm^3) is required to transfer the copper present almost quantitatively into the solution.

ACKNOWLEDGEMENT

The authors are grateful to the Ministry of Education, Technological development, and Innovations of the Republic of Serbia for financial support, within the funding of the scientific research at the University of Belgrade – Technical Faculty in Bor (No. 451-03-137/2025-03/ 200131).

REFERENCES

1. Yin, S.H., Wang L.M, Wu, A.X., Free M.L., Kabwe, E., (2018), Enhancement of copper recovery by acid leaching of high-mud copper oxides: A case study at Yangla Copper Mine, China. Journal of Cleaner Production, 202, 321−331.
2. Wang, G.R, Liu, Y.Y., Tong, L.L., Jin, Z.N., Chen, G.B., Yang, H.Y., (2019), Effect of temperature on leaching behavior of copper minerals with different occurrence states in complex copper oxide ores. Trans. Nonferrous Met. Soc. China, 29, 2192−2201.
3. Antonijević, M.M., Dimitrijević, M.D., Stevanović, Z.O., Serbula, S.M., Bogdanović, G.D., (2008), Investigation of the possibility of copper recovery from the flotation tailings by acid leaching. Journal of Hazardous Materials, 158, 23–34.
4. Santibáñez-Velásquez, L. E., Guzmán, A., Morel, M. J., (2022) Extraction of Iron and Other Metals from Copper Tailings through Leaching. Metals, 12, 1924.
5. Karppinen, A., Seisko, S., Lundstrom, M., Atmospheric leaching of Ni, Co, Cu, and Zn from sulfide tailings using various oxidants. (2024) Minerals Engineering, 207, 108576.
6. Ghasemi, S.M.S., Azizi, A., (2018) Alkaline leaching of lead and zinc by sodium hydroxide: kinetics modeling, Journal of material research and technology, 7(2), 118–125.
7. Łuczak, J., Joskowska, M., Hupka, J., (2008) Imidazolium ionic liquids in mineral processing, Physicochemical Problems of Mineral Processing, 42, 223-236.
8. Asrami, M. R., Tran, N. N., Prasad, N. K. D., (2021) Hessel V., Solvent extraction of metals: Role of ionic liquids and microfluidics. Separation and Purification Technology, 262, 118289.
9. Kilicarslan, A., Saridede, M. N., Stopic, S., Friedrich B., (2014) Use of ionic liquid in leaching process of brass wastes for copper and zinc recovery International Journal of Minerals, Metallurgy and Materials, 21, 2.
10. Whitehead, J.A., Zhang, J., Pereira, N., McCluskey, A., Lawrance, G.A., (2007) Application of 1-alkyl-3-methyl-imidazolium ionic liquids in the oxidative leaching of sulphidic copper, gold and silver ores. Hydrometallurgy, 88, 1-4, 109.
11. Whitehead, J.A., Zhang, J., McCluskey, A., Lawrance, G.A., (2009) Comparative leaching of a sulfidic gold ore in ionic liquid and aqueous acid with thiourea and halides using Fe(III) or HSO_5^- oxidant. Hydrometallurgy, 98, 3-4, 276.
12. Dong, T., Hua, Y., Zhang, Q., Zhou, D., (2009) Leaching of chalcopyrite with Brønsted acidic ionic liquid. Hydrometallurgy 99(1):33-38.
13. Chi, R., Tian, J., Zhu, G., Wu, Y., Li, S., Wang, C., Zhou, Z. A., (2006) Kinetics of Rare Earth Leaching from a Mangnese-Removed Weathered Rare-Earth Mud in Hydrochloric Acid Solutions, Separation Science and Technology, 41:06, 1099-1113.
14. Rodríguez, M., Ayala, L., Robles, P., Sepúlveda, R., Torres, D., Carrillo-Pedroza, F.R., Jeldres, R.I., Toro, N., (2020) Leaching Chalcopyrite with an Imidazolium-Based Ionic Liquid and Bromide. Metals, 10 (2), 183.

PAPERS

XVI International Mineral Processing
and Recycling Conference
28-30 May 2025, Belgrade, Serbia

DOI: 10.5937/IMPRC25133O Original research article

CLEAN GOLD SOLUTION FROM PRINTED CIRCUIT BOARD PHYSICAL PROCESSING DUST BY SELECTIVE COMPLEXATION

Iyiola Olatunji Otunniyi[#], 0000-0002-6445-5640,
Oluwayimika Olasunkanmi Oluokun, 0000-0002-7239-4876,
Chemical and Metallurgical Engineering, Vaal University of Technology,
Vanderbijlpark, South Africa

ABSTRACT – Two-step leaching process of PCB dust will produce a first leaching stream containing assorted metals that still requires more demanding multistage processing afterwards to recover base metals and precious metals. In this work, three-step selective complexations produce clean gold solution from printed circuit board dust. After optimizing for temperature and concentrations, first step under oxidative ammonia leaching, recovered no gold, 90 % Cu and 50 % Zn. Second step acid leaching recovered no gold, 89 % Fe, 48 % Zn, 94 % Ni. The recoveries generally increased with reducing dust particle sizes, except for zinc under oxidative ammonia, and it was noted that its various alloy forms in PCB can be responsible for this. At the third leaching step using acidified thiourea with 0.1 M H_2O_2 at 25 ^{O}C, gold recovery was 99 %. The leaching rate was shown to be chemically controlled, implying that reagent dosage control will compensate for feed assay shifts in an operation design. Copper, zinc and nickel will be easily recoverable from leach solutions of the first two steps in this leaching scheme. The third step produced a clean gold solution for easy processing downstream.

Keywords: Printed Circuit Board, Step Leaching, Selective Gold Recovery, Gold Thiourea Complexation, Rate Control Model.

INTRODUCTION

Printed circuit board contains assorted metals which work against recovery of values from this material stream using leaching methods because the leach solution can get very polluted, complicating downstream processing. Gold is a major process economics driver and getting it selectively into a leach solution is therefore a major processing objective. Cyanide, thiosulfate, and thiourea as lixiviants for gold recovery from ores, concentrates and secondary resources have been well reported [1-3]. With cyanide, iron, copper and nickel, all forms soluble complexes. Hence, cyanide will not have that selectivity advantage in this type of sample. Health and safety issues also exists with cyanide, though it is still very much in use. Gold recovery with thiourea is associated with faster reaction kinetics compared with using thiosulfate [4, 5]. However, gold dissolution in thiourea may be hampered by lixiviant consumption in the presence of base metals [6, 7] which forms stable complexes with the reagents. Actually, from free energies of formation of their various complexes presented in Table 1, selectively leaching gold directly from PCB dust, using thiourea, thiosulfate or cyanide, is not feasible

---

[#] corresponding author: iyiolao@vut.ac.za in the presence of many common base metals such as iron, nickel and copper. At the relatively high concentrations of these metals in PCB dust, gold leaching will be grossly compromised [8-10].

Table 1 Free energy of formation of gold and other metal complexes in different lixiviants

Lixiviants	Complex	Free energy of formation (kJ/mol)	Reference
Thiourea	$[Au(SC(NH_2)_2)_2]^+$	-39.37	[19, 20]
	$[Ag(SC(NH_2)_2)_3]^+$	-112.55	
	$[Fe(SC(NH_2)_2)_3]^{2+}$	-71.1	
	$[Cu(SC(NH_2)_2)_3]^{2+}$	-132.2	
Thiosulfate	$[Au(S_2O_3)_3]^{3-}$	-1046	[19, 21]
	$[Ag(S_2O_3)_2]^{3-}$	-190.37	
	$[Fe(S_2O_3)_2]^{3-}$	-519.30	
	$[Cu(S_2O_3)_2]^{3-}$	-183.26	
Cyanide	$[Au(CN)_2]^-$	-159.32	[22, 23]
	$[Ag(CN)_2]^-$	-85.69	
	$[Fe(CN)_6]^{3-}$	-182.42	
	$[Cu(CN)_2]^-$	-137	

A logical way around will be a leaching scheme, where base metals are selectively removed in some leaching steps ahead of gold. With this rationale, a two-step leaching was explored for gold leaching from PCB, using H_2SO_4 and H_2O_2 in the first step to remove the base metals, followed by a second step in which thiosulphate was recommended over thiourea [11]. While oxidative acid leaching used in the first step of that process will dissolve large quantity of iron in the dust into the same solution with copper, thiosulphate in the second step is known to be relatively slow. Thiourea will complex gold faster than cyanide or thiosulphate, and a process design able to produce separate economic stream for copper and gold will be a better approach for PCB leaching.

In this prospect, ammoniacal leaching can selectively complex copper and some base metals [12, 13]; the oxidation potential, pH and concentration of ammonia must be controlled to stabilise the formed amine complex [14]. Ammonia in principle can also complex Au, but under stricter conditions [15]. The kinetics is good only at high temperatures, and the low vapor pressure of ammonia solution will also necessitate autoclaving. With copper mostly as pure particles in PCB unlike other base metals that exists in other chemical forms [16-18], copper dissolution with ammonia is more predictable in this context. Metals such as iron, aluminum and manganese will not complex with ammonia but will leach in acid. Also, sulphuric acid will not compromise Au recovery unlike other mineral acids where it can be oxidized or form halide complex. With these backgrounds, in this work, ammonia, sulphuric acid and thiourea as ligands were investigated in three-step leching to explore their selectivity at each step for the different target metals in the dust. Concentration, temperature and agitation rate were varied in exploration for optimum conditions to maximize selective recoveries being sought. For gold, the recovery rate data was fitted for an indication of the rate controlling mechanism under the condition that gave best recoveries.

MATERIALS AND METHODS

PCB dust from airbags in comminution lines at a responsible waste PCB physical processing operation in Johannesburg South Africa was classified into three particle size distributions of –106+75 µm, –75+53 µm and -53 µm using corresponding sieve sizes on Endecotts EFL 2000 series sieve shaker. Each size fraction was assayed for Fe, Cu, Zn, Ni, and Au using aqua regia digestion and atomic absorption spectrometry (AAS). Ag content of the aqua regia digestion was also monitored; though this may not be absolute silver assay but indicative (Ogunniyi et al, 2009). Recoveries during all leaching steps were calculated relative to this feed assay values. Leaching tests were conducted in a Parr reactor 4848, connected to an external digital control console, and all reagents used were analytical grades. Particle size –106+75 µm was used for parameter optimization, while finer sizes were further studied at optimum parameter values to assess recoveries across the other sizes. All experiments were done and analyzed in triplicates.

Leaching Tests

Three-step leaching was investigated: first, oxidative ammonia treatment of the dust; second, acid washing of ammonia leach residue; and third, thiourea leaching of final residue. For the first step, using 1 g dust sample, preliminary tests were done to optimize concentration and temperature under varied ammonia concentration (0.5, 1, 2 and 3 M) and temperature (25, 40, 50, and 60°C) while keeping other parameters constant. Based on these preliminary tests, ammonia leaching stage was done using 75 ml 2 M NH_4OH, 25 ml 10 M H_2O_2 at 40°C for 2 hours reaction time. H_2O_2 is preferred in tests because oxidants that introduce metallic elements will confuse leaching assay. Acid washing parameter was selected after initial studies of two acid washing regimes A (100 rpm, 25°C and 1 hour) and B (400 rpm, 60°C, and 2 hours) with 100 ml 5 M H_2SO_4. Based on effective removal of Fe, Ni and Zn, regime B was used for further studies. Before thiourea leaching, residues (from acid washing) were oven dried at 70°C for 1 hour. The third leaching step used combinations of thiourea, sulphuric acid, and hydrogen peroxide in 3:1:1 volume ratio.

Thiourea is expected to complex gold as in Equation 1, while hydrogen peroxide drives the oxidation as in Equation 2.

$$Au + 2\,SC(NH_2)_2 \quad ===> [Au(SC(NH_2)_2)_2]^+ + e^- \qquad (1)$$

$$½O_2 + H_2O + 2e^- \quad ===> 2OH^- \qquad (2)$$

Thiourea concentration, temperature and sulphuric acid concentration are important on the recovery rate. Thiourea concentration was investigated between 0.1, 0.5 and 1 M $SC(NH_2)_2$. Sulphuric acid is significant to protonation of thiourea, which at high sulphuric acid concentration can obstruct gold thiourea complexation [24]. Therefore, concentration of sulphuric acid was investigated at 0.25 M and 0.5 M. Also, thiourea instability can be catalyzed at temperature above 45 °C to form cyanamide and sulphur [25]; hence, the impact of temperature on gold thiourea recovery was studied at 25°C and 40°C. To increase oxidation power of leach solution, hydrogen peroxide was used but at low concentration (0.1 M H_2O_2) to avoid thiourea degradation. As control investigations, direct leaching of the dust with thiourea and leaching of the ammonia leach residue directly without acid washing were investigated at same optimum condition used for the final leach residue (1 M $SC(NH_2)_2$, 0.5 M H_2SO_4, and 0.1 M H_2O_2 at 25°C). All thiourea leaching experiments were done in triplicates and carried out at constant agitation speed of 400 rpm.

Gold-thiourea complexation rate control mechanism

For insight into the gold thiourea complexation rate controlling mechanism, recovery over time was studied for 4hours by collecting about 2 ml leach solution at specific time intervals, diluted quantitatively and analysed using AAS. The recovery data was fitted to the first order leaching models according to shrinking core model (SCM) proposed by Levenspiel [26]. Models for diffusion control reactions and chemical control reactions were assessed.

RESULTS AND DISCUSSION

Feed Assays

Table 2, shows gold deports most to the finest dust, while copper follow opposite trends. This is understandable from many previous works [27]. Based on mass fraction of each size interval provided in Table 2, the dust assays average to 369.5 g/ton gold and 1.6 % copper. This dust is clearly a valuable gold concentrate.

Table 2 Elemental composition of PCB dust from aqua regia digestion and AAS analysis

µm	Fe (%)	Cu (%)	Zn (%)	Ni (%)	Ag (%)	Au (g/ton)
75-106	9.87	2.24	0.69	0.32	0.14	234
53-75	18.98	1.55	0.98	0.51	0.13	404
<53	25.43	1.40	1.56	0.89	0.13	635

Amine complexation and acid washing steps

The first step amine complexing worked well as projected. No gold was lost to that stage. With 2 M NH_4OH and 10 M H_2O_2, Cu and Zn were recovered from all the dust sizes (Fig. 1a). Copper recovery ranged from 89.9 % to 96.7 % in the coarsest to the finest fraction. Zinc recovery was relatively low compared with copper recovery and followed an opposite trend dropping from 50.44% to 30.23%, from the coarsest size fraction to the finest. Detailed composition studies of PCB has indicated that metallic contents of PCB are from different alloys, with notable exceptions such as copper and gold which are used in almost pure metal forms [27, 28]. Alloy forms in which zinc bearing particles exists in the dust would be responsible for low recovery obtained under this condition. Zinc solders are used notably in copper circuitry. Zn-Pb, Zn-Sn and Zn-Pb-Sn solders, for instance, will be less soluble in ammine system because tin and lead do not complex with ammonium ion. Zinc element will be in a different chemical environment in those alloys compared with zinc metal. However, lower recovery at finer size is unconventional. A detailed report on this behavior has been done [12], but further work could still be done. About selectivity, gold and iron were not detected in the first leach solution. This is as projected, and satisfactory for the process design.

Fig. 1b shows metal recoveries at different particle size distributions (PSDs) under acid washing with 5 M H_2SO_4 for 2 hours, 400 rpm and 60°C. Fe and Ni recovery increased with decreasing PSDs, with – 53 µm size giving maximum recoveries over 98 % for Fe and Ni. Residual zinc of the first stage leach was recovered in the acid washing process. This shows zinc exists in alloy forms not readily complexed by ammonia but can be leach by acid. Various alloys of zinc can be found in the PCB such as solder alloys [29], and leachability of these alloys will differs. Copper recovery from all PSDs was less than 5 % being residual from the first-stage ammonia leaching. Gold and silver were below detection limits, for assurance that precious metals were not compromised during the acid wash step. Iron, nickel and zinc recoveries at different PSDs can be explained by increased liberation at finer sizes.

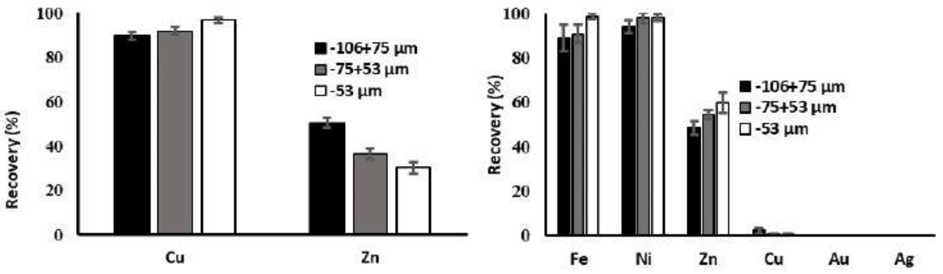

Figure 1a) Metal recovery (%) under oxidative ammonia first stage leaching of different PSDs of PCB dusts (condition: 75 ml 2 M NH_4OH, 25 ml 10 M H_2O_2; 40°C; 400 rpm; 2 hours) **Figure 1b)** Metal recovery (%) under H_2SO_4 washing of different PSDs of PCB dusts residue from ammonia leaching
(condition: 100 ml 5 M H_2SO_4; 60°C; 400 rpm; 2 hours)

Gold-thiourea complexation

Preliminary tests employing thiourea directly on PCB dust and on the residue after ammonia leaching without acid washing gave poor recoveries. Details of these tests could not be reported in this manuscript due to length limitation. After acid washing of ammonia leaching residue, good recoveries were obtained.

Concentration

From results presented in Fig. 2, gold recovery increased with increasing thiourea concentration and was optimum at 0.5 M. This result is similar in terms of gold recovery and thiourea concentration reported by [8], though impact of base metals in the PCB-thiourea leaching was not addressed in that report. The recovery of Au increased from 14 % to 76 % when thiourea concentration increased from 0.1 to 0.5 M; this dropped to 48 % when thiourea concentration increased to 1 M. The drop in gold recovery at high thiourea concentration may be as a result of disproportion of thiourea and sulphuric acid, such that formamidine disulphide is formed, which further decomposes to form cyanamide and elemental sulphur that passivates gold surface [6, 30, 31].

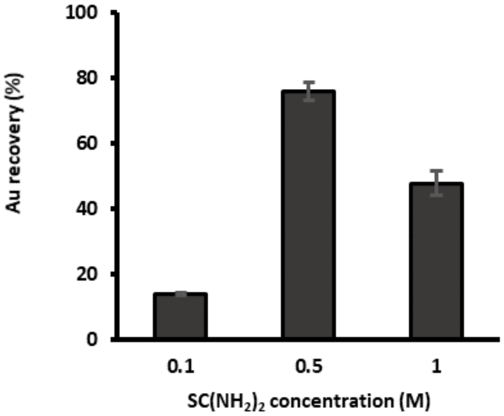

Figure 2 Effect of thiourea concentration on Au recovery with 0.1 M H_2O_2, 0.5 M H_2SO_4 and 25°C over 2 hours from 75 – 106 µm PCB dust acid-washed residue

Temperature

Results of the studies shows that at 25°C, 76 % Au was recovered while at 40°C gold recovery reduced to 56 % under the same reagent condition of 0.5 M $SC(NH_2)_2$, 0.1 M H_2O_2 and 0.5 M H_2SO_4 for 2 hours. It was observed that increasing temperature impeded Au thiourea complexation. This may be due to decomposition of thiourea at higher temperature [7]. Decomposition of thiourea normally occurs above 45°C [25]. Therefore, further investigations were conducted at 25°C.

Sulphuric acid concentration

The effect of sulphuric acid concentration on gold recovery was studied at 0.25 and 0.5 M under the same reagent condition of 0.5 M $SC(NH_2)_2$, 0.1 M H_2O_2 for 2 hours. At 0.25 M, 57 % Au was recovered compared to the initial recovery of 76 % Au at 0.5 M. Exploring lower sulphuric acid concentration reduced Au recovery. 0.5 M was selected as better acid conditioning to facilitate Au dissolution and was maintained in further study.

Gold Leaching Kinetics

Fig. 3a shows variation of Au recovery over leaching time. Within the first three minutes, gold recovery was below detection limit in the leach solution. By 7 minutes, the recovery gave 1.75 % Au recovery. This picked up reaching 45 % within 45 minutes and slowed down thereafter, reaching a recovery of 98.92 % Au in 4 hours. This is almost total recovery of gold after this sufficiently long time. Hence, 4 hours reaction time was considered appropriate to maximize gold recovery from acid-washed PCB dust fraction under this leaching condition. These optimized experimental parameters were tested at other dust PSDs (See Section 3.4). In Fig. 3b the gold dissolution rate was fitted to different equations of the shrinking core leaching models for an indication of the rate controlling mechanism. At a correlation co-efficient of 0.99 (with model equation $[1-(1-X)^{1/3}$ = kt]), the gold dissolution from PCB under this condition is effectively chemical controlled. From the slope of the straight line fit of the plot, the reaction rate constant (K_c) gave 0.0032 (Fig. 3b). This inference of thiourea leaching being chemically controlled is logical as prior leaching steps with ammonia and sulphuric acid were expected to have exposed particle surfaces, and transport barriers eliminated due to agitation at 400 rpm. This is a good indication of easy scale up of this process in an operation design as variation in feed dust assays can be compensated by reagent dosage.

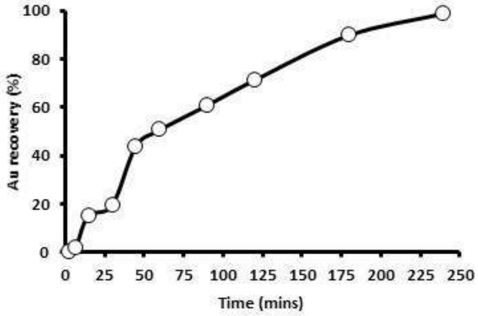

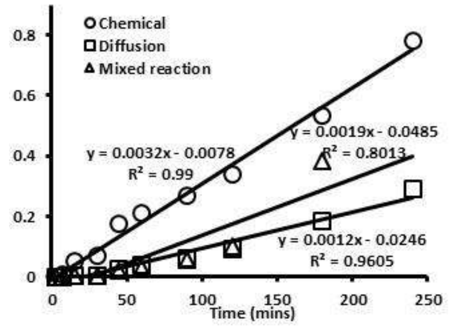

Figure 3a Au recovery rate form final PCB dust residue in acidified thiourea and hydrogen peroxide (0.5 M $SC(NH_2)_2$, 0.1 M H_2O_2, 0.5 M H_2SO_4, 25°C and 400 rpm). Figure **3b** Fitting of gold dissolution from acid washed PCB dust under 0.5 M $SC(NH_2)_2$, 0.5 H_2SO_4 and 0.1 M H_2O_2 at 25°C to chemical control $[1-(1-X)^{1/3}]$, diffusion control $[1-\frac{2}{3}X-(1-X)^{\frac{2}{3}}]$, and mixed control $[\frac{1}{3}\ln(1-X)+(1-X)^{-\frac{1}{3}}-1]$ leaching models versus time

CONCLUSION

A three-step leaching scheme of printed circuit board dust from air bags in comminution operation attained selective leaching of gold into a relatively clean stream with 99 % recovery, using acidified thiourea, under optimum condition of 0.5 M thiourea, 0.5 M sulphuric acid, and 0.1 M hydrogen peroxide. Copper was recovered up to 90 % in first leaching step and nickel up to 94 % in second step. Zinc recovery split into the first two steps due to various zinc alloy forms in the dust, but cumulatively also close to 90 %. Kinetic model fitting shows gold leaching was chemically controlled, implying that reagent dosage control will compensate for feed assay shifts in an operation design. This scheme produced a relatively clean gold stream, with two other streams valuable for easier downstream processing to recover copper, nickel and zinc.

ACKNOWLEDGEMENT

Research funds and resources of Chemical and Metallurgical Engineering Department, VUT was used for this research work, and duly acknowledged hereby.

REFERENCES

1. Akcil, C. Erust, C. S. Gahan, M. Ozgun, M. Sahin, and A. Tuncuk, "Precious metal recovery from waste printed circuit boards using cyanide and non-cyanide lixiviants–a review," Waste Management, vol. 45, pp. 258-271, 2015.
2. A. Tuncuk, V. Stazi, A. Akcil, E. Y. Yazici, and H. Deveci, "Aqueous metal recovery techniques from e-scrap: hydrometallurgy in recycling," Minerals Engineering, vol. 25, no. 1, pp. 28-37, 2012.
3. C. Chu, P. Breuer, and M. Jeffrey, "The impact of thiosulfate oxidation products on the oxidation of gold in ammonia thiosulfate solutions," Minerals Engineering, vol. 16, no. 3, pp. 265-271, 2003.
4. C. J. Oh, S. O. Lee, H. S. Yang, T. J. Ha, and M. J. Kim, "Selective leaching of valuable metals from waste printed circuit boards," Journal of the Air & Waste Management Association, vol. 53, no. 7, pp. 897-902, 2003.
5. J. Ficeriová, P. Baláž, and E. Gock, "Leaching of gold, silver and accompanying metals from circuit boards (PCBs) waste," Acta Montanistica Slovaca, vol. 16, no. 2, p. 128, 2011.
6. P. Lacoste-Bouchet, G. Deschênes, and E. Ghali, "Thiourea leaching of a copper-gold ore using statistical design," Hydrometallurgy, vol. 47, no. 2-3, pp. 189-203, 1998.
7. G. J. Sparrow and J. T. Woodcock, "Cyanide and other lixiviant leaching systems for gold with some practical applications," Mineral Processing and Extractive Metullargy Review, vol. 14, no. 3-4, pp. 193-247, 1995.
8. M. Gurung, B. B. Adhikari, H. Kawakita, K. Ohto, K. Inoue, and S. Alam, "Recovery of gold and silver from spent mobile phones by means of acidothiourea leaching followed by adsorption using biosorbent prepared from persimmon tannin," Hydrometallurgy, vol. 133, pp. 84-93, 2013.
9. P. Farinha, M. Correia, and J. Carvalho, "Leaching of gold from a Portuguese concentrate with thiourea," Minerals engineering, vol. 5, no. 8, pp. 953-959, 1992.
10. S. Ubaldini, P. Fornari, R. Massidda, and C. Abbruzzese, "An innovative thiourea gold leaching process," Hydrometallurgy, vol. 48, no. 1, pp. 113-124, 1998.
11. S. Camelino, J. Rao, R. L. Padilla, and R. J. P. M. S. Lucci, "Initial studies about gold leaching from printed circuit boards (PCB's) of waste cell phones," vol. 9, pp. 105-112, 2015.
12. O. O. Oluokun and I. O. Otunniyi, "Kinetic analysis of Cu and Zn dissolution from printed circuit board physical processing dust under oxidative ammonia leaching," Hydrometallurgy, p. 105320, 2020.
13. X. Meng and K. N. Han, "The principles and applications of ammonia leaching of metals—a review," Mineral Processing and Extractive Metullargy Review, vol. 16, no. 1, pp. 23-61, 1996.
14. B. Ghosh, M. Ghosh, P. Parhi, P. Mukherjee, and B. Mishra, "Waste printed circuit boards recycling: an extensive assessment of current status," Journal of Cleaner Production, vol. 94, pp. 5-19, 2015.
15. X. Meng and K. N. Han, "The dissolution behavior of gold in ammoniacal solutions," in Hydrometallurgy: Fundamentals, Technology and Innovations, Proc. 4th Milton E. Wadsworth Intl. Symp, 1993, pp. 205-221.
16. J. Cui and E. Forssberg, "Mechanical recycling of waste electric and electronic equipment: a review," Journal of hazardous materials, vol. 99, no. 3, pp. 243-263, 2003.
17. T. Hino, R. Agawa, Y. Moriya, M. Nishida, Y. Tsugita, and T. Araki, "Techniques to separate metal from waste printed circuit boards from discarded personal computers," Journal of material cycles and waste management, vol. 11, no. 1, pp. 42-54, 2009.
18. O. O. Oluokun and I. O. Otunniyi, "Chemical conditioning for wet magnetic separation of printed circuit board dust using octyl phenol ethoxylate," Separation and Purification Technology, vol. 240, p. 116586, 2020.

19. H. J. Brent and V. Atluri, "Dissolution chemistry of gold and silver in different lixiviants " Mineral Procesing and Extractive Metallurgy Review, vol. 4 pp. 95-134, 1988.
20. W. D. Donald et al., "The NBS tables of chemical thermodynamic properties, selected values for inorganic and C1 and C2 organic substances in SI units," Physics and Chemical Reference Data, vol. 11, no. 2, pp. 1-407, 1982.
21. R. Lemire, U. Berner, C. Musikas, D. Palmer, P. Taylor, and O. Tochiyama, "Chemical thermodynamics of iron, part 1," Chemical thermodynamics, vol. 13, 2013.
22. X. Wang and K. E. Forssberg, "The chemistry of cyanide-metal complexes in relation to hydrometallurgical processes of precious metals," Mineral Procesing and Extractive Metallurgy Review, vol. 6, no. 1-4, pp. 81-125, 1990.
23. J. H. Kyle and G. Hefter, "A critical review of the thermodynamics of hydrogen cyanide and copper (I)–cyanide complexes in aqueous solution," Hydrometallurgy, vol. 154, pp. 78-87, 2015.
24. B. K. Biswas, K. Inoue, K. Ohto, H. Harada, H. Kawakita, and A. Hoshino, "E-waste management through silver recovery from scrap of plasma TV monitors," presented at the Proc. of International Conference on Environmental Aspects of Bangladesh (ICEAB10), Japan, 2010.
25. G. Deschenes and E. Ghali, "Leaching of gold from a chalcopyrite concentrate by thiourea," Hydrometallurgy, vol. 20, no. 2, pp. 179-202, 1988.
26. O. Levenspiel, "Chemical reaction engineering," Industrial & engineering chemistry research, vol. 38, no. 11, pp. 4140-4143, 1979.
27. I. Ogunniyi, M. Vermaak, and D. Groot, "Chemical composition and liberation characterization of printed circuit board comminution fines for beneficiation investigations," Waste management, vol. 29, no. 7, pp. 2140-2146, 2009.
28. A. Priya and S. Hait, "Comprehensive characterization of printed circuit boards of various end-of-life electrical and electronic equipment for beneficiation investigation," Waste Management, vol. 75, pp. 103-123, 2018.
29. D. Groot and J. Van der Linde, "The processing of eWaste. Part 1: The preparation and characterization of a metallic alloy derived from the smelting of printed circuit boards," Journal of the Southern African Institute of Mining and Metallurgy, vol. 109, no. 12, pp. 697-700, 2009.
30. P. C. Gupta, "Analytical chemistry of thiocarbamides," Fresenius' Zeitschrift für analytische Chemie, vol. 196, no. 6, pp. 412-431, 1963.
31. T. Kai, T. Hagiwara, H. Haseba, and T. Takahashi, "Reduction of thiourea consumption in gold extraction by acid thiourea solutions," Industrial & engineering chemistry research, vol. 36, no. 7, pp. 2757-2759, 1997.

XVI International Mineral Processing
and Recycling Conference
28-30 May 2025, Belgrade, Serbia

DOI: 10.5937/IMPRC25142U
Original research article

CHARACTERIZATION AND COMPARISON OF THE PARTICLE SHAPE OF MICRONIZED GRAPHITE GROUND IN DIFFERENT MILLS USING DIA

Ugur Ulusoy[1#], 0000-0002-2634-7964,
Fırat Burat[2], 0000-0001-7051-0063,
Guler Bayar[3], 0000-0002-9060-4443,
Behrad Mojtahedi[4], 0009-0002-6324-4689,
Gulsah Guven[2], 0009-0004-0468-1592,
[1]Dept. of Chemical Eng., Sivas Cumhuriyet University, Sivas, Türkiye
[2]Mineral Processing Eng. Dept., Istanbul Technical University, İstanbul, Türkiye
[3]Dept. of Nanotechnology Eng., Sivas Cumhuriyet University, Sivas, Türkiye
[4]Materials Science and Eng., Sharif University of Technology, Tehran, Iran

ABSTRACT – Although particle shape plays a paramount role as much as particle size in the micronization and flotation stages used in the production of graphite material as LIB anode material, the relationship between graphite grinding and particle shape is almost non-existent. Therefore, this study aims to compare the particle shape of graphite particles at various grinding times with "tumbling" and "non-tumbling" mills, such as the most used laboratory ball mill and vibrating disc mill, by using DIA. According to both DIA and XRD, SEM, and stereo microscope results, VDM produced rounder particles in a shorter time than BM.

Keywords: Graphite, Particle Shape, Dynamic Image Analysis, Vibratory Disc Mill, Ball Mill.

INTRODUCTION

Since natural graphite is a key raw material central to the global net zero emissions target, it is on the critical materials lists of the United States, the European Union, and China. Because, the unique layered lattice structure of natural graphite allows easy electron transport between its layers, making it an indispensable material for the anode material of LIBs. Moreover, it provides better charging efficiency, energy density, and cell capacity with lower production cost [1], considering its special properties such as resistance to high temperatures, conductivity and thermal conductivity, lubricity, chemical stability, flexibility, and thermal shock resistance [2]. In addition, the weight of graphite in an EV battery can range from 44 to 66 kg, depending on the type of EV and battery type [3]. Besides, it has been reported that the global mine production of natural graphite in 2023 was 1.6 Mt [4].

The downstream processing of graphite, which includes micronizing, spheroidizing, and purification, is significantly influenced by the shape of the particles. Although natural

---

[#] corresponding author: uulusoy@cumhuriyet.edu.tr graphite can generally be purified by various separation methods such as gravity separation, flotation, hydrometallurgical, and pyrometallurgical methods after appropriate grinding to ensure sufficient liberation, it is well known that graphite can be successfully enriched by the flotation method due to its natural floatability. This requires a highly costly, energy-intensive, and labor-intensive grinding process to prepare the feed material at a size where flotation is efficient [5]. Thus, it is now well known that particle shape is an important parameter as particle size in flotation [6]. Moreover, the proper particle size, shape, and structural quality of graphite are necessary for lithium-ion intercalation chemistry [7]. Thus, better battery durability, efficiency, and reliability can be achieved by using the complementary effect of particle size and shape factors in battery production. As another example, anodes with improved safety performance, longer cycle life, lower first-cycle irreversible capacitance loss, and higher speed capacity and energy density may be produced by optimizing the morphology of graphite particles [8]. Furthermore, by grinding small flakes of natural graphite into a spherical shape, better performance consequently appeared with an increase in tap density of the anode, volumetric energy capacity, velocity capacity, reversible capacity, Coulombic efficiency, and packing efficiency, but with a loss in irreversibility capacity shape [9]. Since a different grinding type could also provide different breakage mechanisms, which directly influence particle characteristics such as size distribution, particle morphology, and crystallinity [10], particles of the desired shape can be produced using proper mill [6]. However, it has always been neglected in scientific studies, and mineral grinding studies have focused only on the effect of particle size due to the lack of a universal standard for measuring particle shape. However, thanks to the developing technology today, dynamic image analysis (DIA), which is widely used, can analyze the shape of many particles [11] quickly and effectively. Although comparison of the particle shapes of the products of quartz ground by different mills has been the subject of many studies before [12], the characterization of the particle shapes of the products obtained by grinding the graphite ore, which is the main LIB anode material, in different mills, has not yet been made using an accurate and reliable shape analysis method such as DIA. Furthermore, ball mill (BM) and vibrating disc mill (VDM) have never been applied before to study the particle shape of graphite particles. To fill this gap, this study focused on the measurements and comparison of shapes of graphite particles ground in the most widely used lab-scale BM and VDM by using DIA.

EXPERIMENTAL

Materials

Graphite ore samples from the Kutahya-Oysu in Turkey were used in this work [13]. The samples are sufficiently pure for shape analysis by DIA, as evidenced by the more than 72% C content of the samples produced after crushing, grinding, and sieving of these ore samples, as established by SEM-EDX analysis. By interpreting the XRD spectrum and the EDS spectrum SEM (Figure 1), it was understood that the major peak belongs to graphite, and other peaks consist of calcite, quartz, hematite, clay, and multiple silicate minerals are present as gangue minerals in the ore.

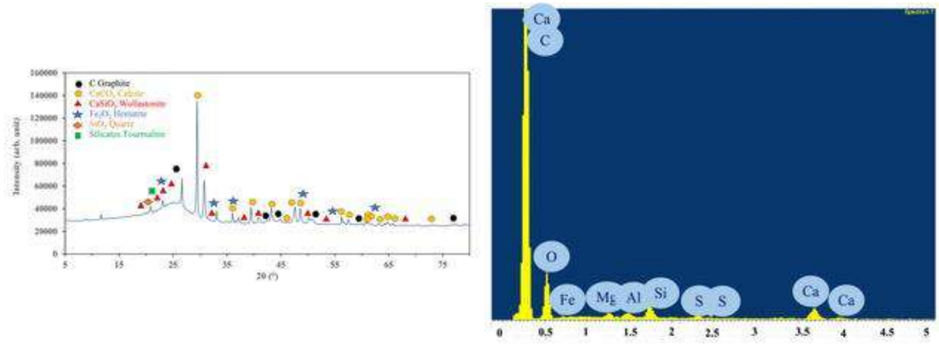

Figure 1 (a) mineralogical analysis by XRD (b) elemental distribution by SEM

Sample Preparation and Grinding

Two different mills applying different grinding forces on the particles, a BM as a tumbling mill and a VDM as a non-tumbling mill, were used in this study to reveal the change of graphite particle shape with grinding time using these mills and to compare it with the results of our previous study conducted with quartz material under the same conditions [12]. The ore sample was first reduced to 10 cm in a jaw crusher in a controlled manner and then sieved with 0.600—0.850 mm sieves to prepare the feed material for grinding tests. Then, 5475 g of mill feed material was ground at different times with steel balls of 30- and 26-mm diameter and 263.2 g weight in a laboratory-type BM (H=18 cm x ϕ=19.7 cm). 75% of the critical speed (77 rpm) required for first-order breakage, which is known to provide the best BM grinding [14], was used (J_B =0.2, fc = 0.04, and U=0.5). A laboratory-type VDM (Ünal Mühendislik, Turkey) was used as a non-thumbling mill for different grinding times, which is known as a high-speed and multi-amplitude vibration device (H=4.5 cm x ϕ=18.5 cm along with various steel rings (ϕ=14, 9.5, and 7.5 cm). The grinding times chosen to study the change of particle shape during grinding are 60, 120, 300, 600, 1200, and 2400 secs for BM and 20, 30, 40, and 50 secs for 10 VDM since it can produce very fine particles in a very short time compared to BM. Finally, both mill products were prepared into two size fractions (sf): 0.150—0.250 mm and 0.053—0.150 mm) by dry sieving through 250, 150, and 53 µm laboratory standard sieves along with a sieve shaker (Fritsch Analysette 3, Germany) under 10 min, 40 amplitude, and continuous frequency conditions, considering that the best working size range of DIA was 0.053—0.250 mm.

Dynamic Image Analysis

The sphericity of the particle shape of ground mineral particles can be best described by using DIA in terms of Bounding Rectangle Aspect Ratio (BRAR), which is expressed as the ratio of the bounding rectangle length to the bounding rectangle width [15]. Representative samples of each mill product were ground down to a few g with the help of a rotary spinner (Quantachrome® Instruments), washed with distilled water, placed in a glass beaker filled with 25 ml of water, and kept in an ultrasonic bath for 5 min, and a few drops of coarse particles at the bottom of the well-dispersed suspensions were fed into the DIA (Micromeritics® Instrument Corp., Norcross, USA).

Other Supporting Analysis (Stereo Microscopy, SEM, and XRD)

A binocular stereo microscope (Citoval 2, Carl Zeiss Jena, Aus Jena), SEM (MIRA3, TESCAN, Czech Republic), and XRD (Rigaku, MiniFlex 600) were used to visually inspect the particle shapes in the samples obtained at the beginning and end of grinding after the same graphite sample was ground in two different mills.

RESULTS AND DISCUSSION

As seen in Figure 2, the $\text{BRAR}_{\text{av.}}$ values of BM products were determined to be higher than those of VDM products for both sf, which was attributed to the dominance of abrasion forces in VDM and impact forces in BM [13]. It was also concluded that the particle shape of both mill products as a function of grinding time followed the same trend: $\text{BRAR}_{\text{av.}}$ values decreased with grinding time.

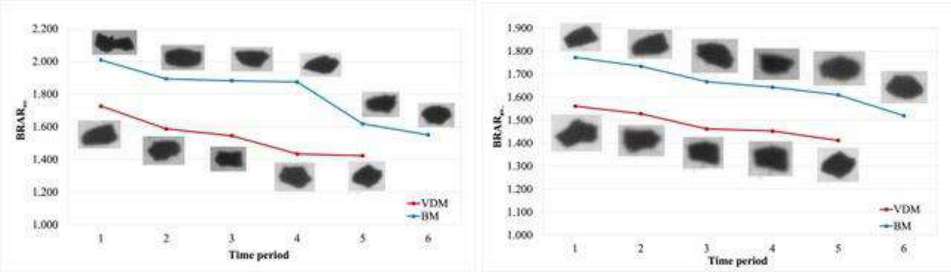

Figure 2 Evolution of AR values of particles by VDM and BM with respect to grinding time: (a) 0.150-0.250 mm sf, (b) 0.053-0.150 mm sf.

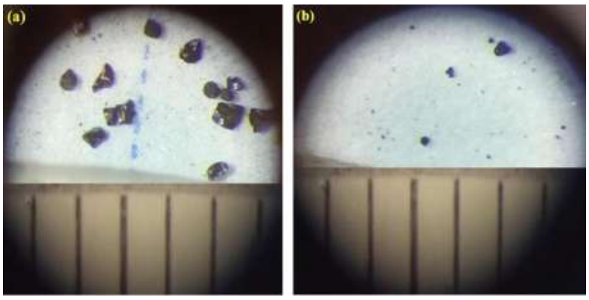

Figure 3 Comparison of Stereo microscopical images of particles: (a) 10-sec VDM product (b) 50-sec VDM product

Moreover, particles from the VDM product appear to have a higher sphericity than particles from the BM product. This finding is consistent with a previous study using quartz under the same milling conditions [12]. It has been observed that long-term grinding causes the particles to become rounded [13]. The stereo microscopic images

(Figure 3) and the SEM example (Figure 4) also support that the ground graphite particles become increasingly rounder during milling. In addition, although the positions of the graphite peaks in a single combined diffractogram (Figure 5) remained the same, the decrease in their intensities was also attributed to the rounding of the particle shape [12,13].

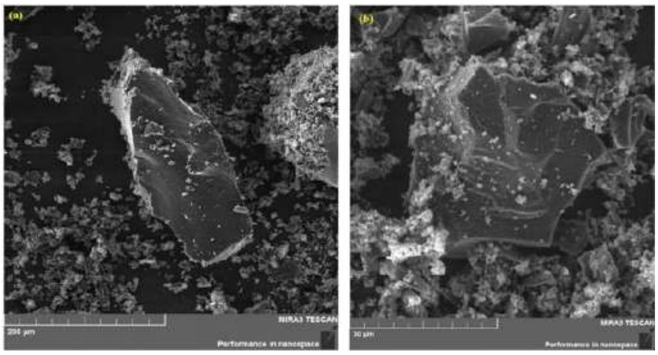

Figure 4 Comparison of SEM microphotographs of particles: (a) 10-sec VDM product (x250) (b) 50-sec VDM product (x500)

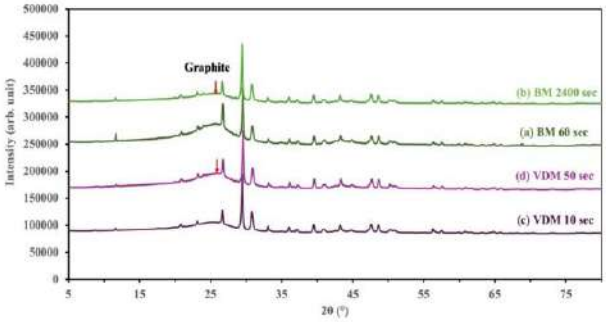

Figure 5 Comparison of XRD patterns of mill products

CONCLUSION

It was found that the grinding time changed not only the size but also the shape of graphite particles milled by BM and VDM, i.e., as the grinding progressed, the particle size decreased, and the particle shape became more rounded than the initial irregular and angular shape. Therefore, with this study, it will be possible to develop time-dependent shape models of the average AR values of milled graphite particles in BM and VDM, which will not only help to increase the efficiency of the milling process and the subsequent flotation process but will also help to predict how long the milling should be done to obtain the roundest particles as a sustainable LIB anode material.

ACKNOWLEDGEMENT

The authors thank Karabacak Mining Inc., İ. Danacı, H.İ. Çetintaş, and Dr. E.O. Şahin for providing graphite samples and their contributions in performing XRD and SEM analyses of the samples and interpreting the XRD diffractograms, respectively.

REFERENCES

1. Endo, M., Kim, C., Nishimura, K., Fujino, T., Miyashita, K. (2000) Recent development of carbon materials for Li ion batteries. Carbon, 38, 183-197.
2. Jr. Robinson, G.R., Hammarstrom, J.M., Olson, D.W. (2017) Graphite. chap. J of Schulz, K.J. Jr. DeYoung, J.H., Seal, R.R. II Bradley, D.C. (E. Editors), Critical mineral resources of the United States—Economic and environmental geology and prospects for future supply: U.S. Geological Survey Professional Paper 1802, J1-J24.
3. Transport & Environment, From dirty oil to clean batteries, (2021) https://www.transportenvironment.org/assets/files/2021_02_Battery_raw_materials_report_final.pdf, (accessed on 26 May 2024).
4. U.S. Geological Survey (2024) Mineral Commodity Summaries, January, https://doi.org/10.3133/mcs2024, accessed on 26 May 2024).
5. Jara, A.D., Betemariam, A., Woldetinsae, G., Kim, J.Y. (2019) Purification, application and current market trend of natural graphite: A review, Int. J. Min. Sci. Technol., 29, 671-689.
6. Ulusoy, U. (2023) A review of particle shape effects on material properties for various engineering applications: from macro to nanoscale. Minerals 13 (1) 91.
7. Buchmann, I. (2015) Lithium Ion Batteries: Fundamentals and Safety, Encyclopedia of Inorganic and Bioinorganic Chemistry; John Wiley & Sons, Ltd.: Hoboken, NJ, USA, 1-12.
8. Van Zyl, W. (2021) Analysis of Graphite for Lithium Ion Batteries, Thermo Fisher Scientific. https://www.thermofisher.com/blog/materials/analysis-of-graphite-for-lithium-ion-batteries, (accessed on 26 May 2024).
9. Zaghib, K., Song, X., Guerfi, A., Kostecki, R., Kinoshita, K. (2003) Effect of particle morphology on lithium intercalation rates in natural graphite. J. Power Sources, 124, 505-512.
10. Ulusoy, U., Çayirli, S., Bayar, G., Gokcen, H.S. (2023) Comparison of Particle Shape, Surface Area, and Color Properties of the Calcite Particles Ground by Stirred and Ball Mill. Minerals, 13 (1) 99.
11. Ulusoy, U. (2019) Quantifying of particle shape differences of differently milled barite using a novel technique: Dynamic image analysis. Materialia, 8C, December, 100434.
12. Ulusoy, U., Bayar, G. (2022) Prediction of average shape values of Quartz particles by vibrating disc and ball milling using dynamic image analysis based on established time-dependent shape models, Part. Sci. Technol., 40 (7) 870-886.
13. Ulusoy, U., Burat, F., Bayar, G., Behad Mojtahedi, B., Güven, G., (2024) Modeling the change of the sphericity feature of graphite particles ground in a ball and vibrating disc mill with grinding time, Journal of Energy Storage, 97PA, 112814.
14. Yekeler, M., Özkan, A., Austin, L.G. (2001) Kinetics of fine wet grinding in a laboratory ball mill. Powder Technol., 114, 224-228.
15. Particle Insight Manual, Micromeritics® Instrument Corp., Particulate Systems 4356 Communications Drive Norcross, GA 30093. USA, 2013.

XVI International Mineral Processing
and Recycling Conference
28-30 May 2025, Belgrade, Serbia

DOI: 10.5937/IMPRC25148S

Original research article

ON-LINE XRF ANALYSIS OF ELEMENTS IN MINERALS ON A CONVEYOR BELT

Aleksander Sokolov, 0000-0002-0930-1964,
Edvins Letko, 0000-0003-1748-4008,
Vitalijs Kuzmovs[#], 0009-0008-4891-5572,
Ulises Miranda Ordonez, 0000-0002-2144-4191,
Baltic Scientific Instruments, Riga, Latvia

ABSTRACT – Determination of the elemental composition of minerals and their derivatives at mining enterprises is important at all stages of materials processing. This paper is devoted to the results of development and application of an online XRF analysis method for monitoring mineral elements on a conveyor of mining enterprises. The paper gives an overview of mining applications in which we have successfully implemented the online analysis based on the CON-X industrial XRF analyzer in lump, ore, charge feed, cake and slag materials on conveyor belt. An evaluation of metrological characteristics achieved in these applications is presented.

Keywords: XRF Analysis of Minerals, Elemental Analysis, On-line Ore Analysis on Conveyor Belt.

INTRODUCTION

Determination of the elemental composition of minerals and products of their technological processing at mining and refining facilities is important at all stages of material processing (for example, mining and beneficiation). Many analyzing techniques have been developed that allow to accurately determine the chemical composition of prepared samples [1-3]. Such an analysis requires setting up special laboratories that have quite a complex and expensive analytical equipment, specially trained and highly qualified personnel. When analyzing materials on such an industrial scale, the main difficulties are related to delivering the representativeness of these materials' samples and the speed of analysis, the results of which often become known only after a few hours.

Operational analysis of materials on the conveyor of mining enterprises in most cases does not require sample preparation, which excludes the influence of a human factor and unpredictable accidents on the results of the analysis [4]. Such operational analysis can be based on various nuclear physics methods (e.g., radiometric, neutron activation, gamma activation, and X-ray fluorescence (XRF)) [4-7]. Of course, online analysis methods are usually less sensitive and precise than chemical ones. However, they provide analysis results in real time, which allows to quickly adjust technologies,

---

[#] corresponding author: office@bsi.lv

automate technological processes and eliminate significant human labor costs. Each of the nuclear physics methods has its advantages and disadvantages and solves a certain range of applications [4-7]. X-ray fluorescence analysis (XRF) is one of the most accurate and simplest analytical methods for studying a matter in order to obtain its elemental composition [5,7]. With the help of this method, various elements from aluminum (Al) to uranium (U) can be detected.

This paper is devoted to the results of development and application of an online XRF method for monitoring elements in minerals at conveyors of mining and processing enterprises. The paper also reviews those mining technological applications where we have successfully implemented the online method and presents an analysis of metrological characteristics achieved in these applications.

RESULTS AND DISCUSSION

The Chromite lump (Cr_2O_3 or $FeCr_2O_4$) content determination

Control of the chromium content in chromium-iron ore was provided to control the quality of the initial products on the conveyor of a mining company. The online XRF analyzer [8] was mounted above a conveyor belt on a standard suspension on four legs with shock absorbers to reduce the vibration of the analyzer (Fig. 1, a). The distance between the analyzer and the surface of ore pieces was 150 mm. The conveyor belt speed was 1 m/s, and the measurement time in this application was t=60 sec.

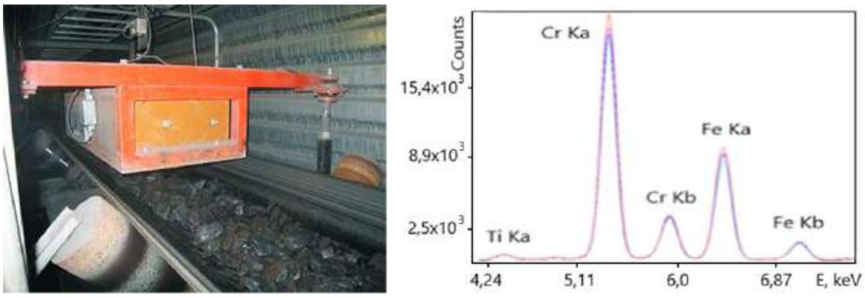

a) b)

Figure 1 a) Online XRF analyzer on a standard suspension on four legs above the conveyor belt; b) Spectrum of chromium-iron ore on the conveyor

The typical spectrum of chromium-iron ore flowing through the conveyor recorded online by the XRF analyzer, used to calculate the concentrations of elements in it and the calculation errors, is presented in Fig. 1, b. The spectrum clearly shows the peaks of chromium and iron, the concentrations of oxides of which in the ore range from 29 to 40% and 25 to 30%, respectively. The detection limits of chromium and iron in the ore were 0.07 and 0.08% abs. The accuracy of XRF analysis is confirmed by the data of chemical analysis of more than 300 ore samples, which were taken from the conveyor synchronously with the operation of the spectrometer. The standard deviation of the results of the two methods was 1.1% abs for Cr_2O_3 and 0.8% abs for Fe_2O_3.

Analysis of copper-zinc sulfide ore

Continuous monitoring of copper and zinc concentration in copper-zinc sulfide ore lumps is carried out by a company during conveyor transportation. The industrial online analyzer was installed above the conveyor at a height of 80 mm above the ore level on a simple suspension attached to a beam passing over the conveyor (Fig. 2, a).

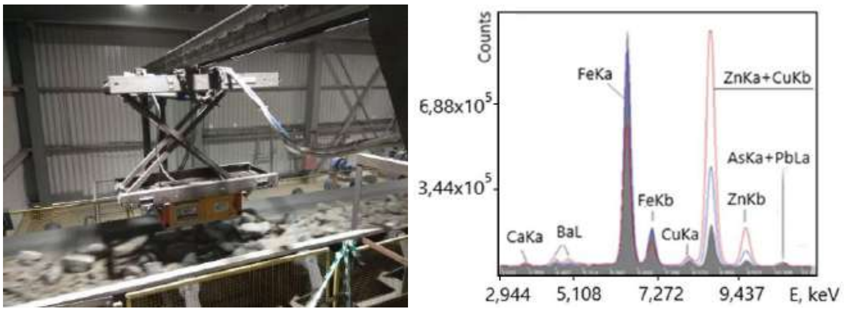

a) b)

Figure 2 a) Online XRF analyzer over the conveyor with lumps of copper-zinc sulfide ore; b) Spectrum of copper-zinc sulfide ore samples

The dimensions of ore lumps were 50-150 mm. Conveyor speed was 1 m/s, measurement time in a given application t=300 sec. A typical of copper-zinc sulfide ore spectrum recorded by the analyzer and used to calculate concentrations and measurement errors is shown in Fig. 2, b. The spectrum in Figure 2, b indicates that the XRF analyzer is capable of online measurement of Fe, Cu and Zn in copper-zinc sulfide ore. The spectra clearly show that the Cu-Kα peaks are very small, and this peak is completely covered by the Zn-Kα peak, since the zinc concentration is tens of times higher. The concentration ranges for copper in this ore were from 0.05 to 0.8%, its detection limit was 0.008%. The standard deviation of the results when compared with chemical analysis for copper was 9.45%. For zinc, the standard deviation of the results (3.6%) is significantly smaller, since the intensity of its peaks is much higher.

Analysis of chemical composition of the charge feed

For the production of cast iron from iron ore, agglomerate is used, the raw material for which is an iron-ore mixture (IORM) and limestone. The main task of managing the process of the agglomerate charge preparations to ensure the required chemical composition. The system for automatic continuous monitoring of the chemical composition of charge components (limestone and IORM) was developed on the basis of the XRF online method [4].

The iron-ore charge feed moves on a conveyor belt at a speed of 1 m/s (Fig. 3, a) and has the following granulometric composition: the content of 0-1 mm size class material in IORM is 68-83%, 1-3 mm – 12-23%, the remaining part of IORM consists of larger particles with a 3-8 mm size. The IORM level on the conveyor belt is very uneven.

To equalize the IORM level and ensure a constant distance between the analyzer detector and the IORM layer on the conveyor (40 mm), a floating suspension with a protective cover was developed. In case of heavy loads of the conveyor belt, the spectrometer is automatically lifted above the conveyor by command from the emergency level sensors. The expressiveness of the method for analyzing IORM directly in the process flow depends on the time of spectrum measurement and is 6 minutes.

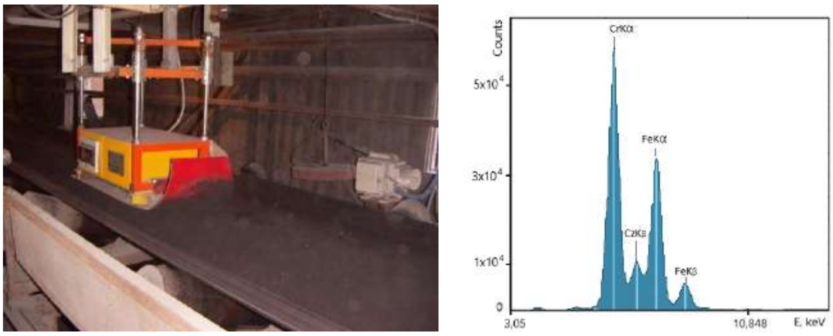

a) b)

Figure 3 a) Online XRF analyzer on an iron-ore mixture conveyor;
b) X-ray fluorescence spectrum of iron-ore mixture

The spectrum of X-ray fluorescence of IORM is shown in Fig. 3, b. The spectrum contains lines of iron, calcium, argon (in the composition of air), manganese, peaks of iron escape, total peaks of iron superposition, peaks of coherent and incoherent scattering of characteristic radiation of the tube (molybdenum line). The range of element concentrations in IORM during the industrial test period was 57.5-60.5; 3,58-4,96; 0.24-2.19% for Fe, CaO, MnO, respectively. The reproducibility of the results of CaO, MnO and Fe determination was 1.8; 12.0 and 0.2% rel., accordingly. For a sample with a CaO content of 2.56 and MnO content of 1.02%, the detection limits were 0.33 and 0.21%, respectively. The resulting detection limit for Fe was 0.16%. The error of the X-ray fluorescence determination of CaO, MnO and Fe in IORM directly in the process flow was: 6.4; 19.0 and 0.9% rel., accordingly. Experimental studies showed that the discrepancy between the results of iron determination in the samples and in the flow is characterized by a standard deviation of 1.6% rel.

Cobalt (Co) content determination in iron-cake

Concentration control of cobalt iron-cake is necessary for an enterprise to control the quality in the technological process. Such control was carried out directly on a belt filter with a cake moving at a speed of 0.3 m/s (Fig. 4, a). The distance from the lower plane of the analyzer to the surface of the cake was 50 mm, which was provided by the diameter of wheels supporting the analyzer on the surface of the cake. To prevent the wheels from falling into the cake, a dynamic suspension with a balancer has been developed, that kept the analyzer in a fixed position above the surface of cake.

The spectrum of the iron cake for the measurement time t=300 sec is shown in Fig. 4, b. The spectrum clearly shows the lines of all elements present in the cake. The task of determining the cobalt concentration is complicated by the fact that the intense Fe-Kβ line overlaps with the weak Co-Kα line. This creates difficulties in determining the Co concentration, but the analyzer performs the task due to the sufficiently high energy resolution of the detector. To measure the cobalt content in the required concentration range of 0.23 - 0.36%, the empirical coefficients method was used.

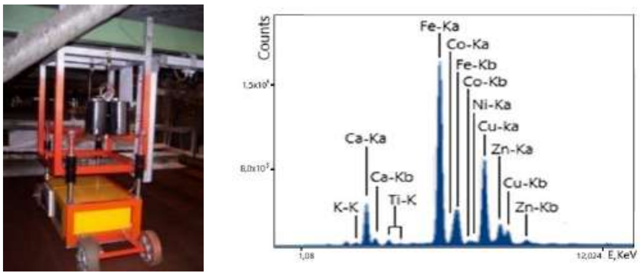

a) b)

Figure 4 a) Online XRF analyzer on the belt filter with iron-cake;
b) Spectrum of the iron-cake during the measurement t=300 sec

This method uses standard samples of different concentrations, close in composition to the real ore. To determine the cobalt concentration, we used a calculation option in which the cobalt peak area is normalized to the peak area (Fe- Kα), using the fundamental value of the Fe- Kα to Fe- Kβ ratio. The best results were obtained when the calibration curve was plotted directly from the ratio of Co/Fe intensities to the incoherent scattering intensity of the radiation. The average result received by the analyzer differs from the average result for the same samples in chemical laboratory: - for Co – 0.023% abs. (2.695% rel.); - for Fe – 0.642% abs. (6.766% rel.); - for Cu – 0.091% abs. (6.058% rel.).

Online analysis of Vanadium Slag

Vanadium content in this slag is to be measured before recycling of vanadium containing residues. Knowledge of the slag composition will help optimize the metal recovery. The online XRF analyzer is installed on the simplest suspension attached to the structure by a conveyor (Fig. 5, a).

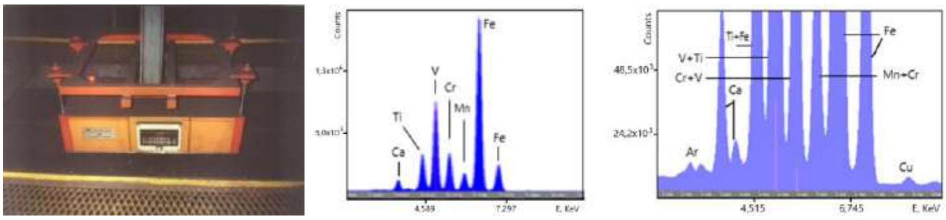

a) b) c)

Figure 5 a) Online XRF analyzer above the conveyor with Vanadium Slag; b) Spectrum of a vanadium slag; c) Zoom into low-intensity features of the vanadium slag spectruma

Distance between the slag and the analyzer is 50 mm (variable between 30 and 70 mm). Conveyor speed is 0.4 m/sec. Measurement time – 300 sec. An example of the XRF spectra of the vanadium slag samples is shown on Fig. 5, b (overview) and Fig. 5, c (zoom into low-intensity lines). The Ar line originates in the air between the analyzer and the sample. These data show that in five-minute measurements the online analyzer is able to quantify amount of Ca, Ti, V, Cr, Mn, and Fe in the vanadium slag samples. The standard deviation of the data measured over 180 sec is 0.09% with repeatability of measurements (n=33), which meets the Customer's requirements. The study indicates that V content can be determined in vanadium slag flow directly above a conveyor belt with an accuracy of not worse than 2% relative (respectively, 0.2% V absolute). The amount of some other elements (Ca, Ti, Cr, Mn, Fe) may also be determined on-line.

CONCLUSION

Despite the many fundamental problems and technological limitations in the online XRF method, which hinder its wider implementation, its use in the technological processes of mining enterprises continues to grow. As the results of this paper show, the online XRF method allows to solve rather non-standard problems of controlling the content of elements in ore materials (lump, ore, change feed, cake, slag) on conveyors of mining and processing enterprises.

REFERENCES

1. Whiten, B. (2007) Calculation of Mineral Composition from Chemical Assays. Mineral Processing and Extractive Metallurgy Review, 29 (2), 83-97.
2. Coomber, D. (1975) Radiochemical Methods in Analysis. Springer.
3. Gandhi, S.M., Sarkar, B.C. (2016) Essentials of Mineral Exploration and Evaluation. Elsevier.
4. Volkov, A.I., Alov, N.V. (2011) Automated systems for determining the chemical composition of bulk and lump materials on a conveyor (overview). Problems of Ferrous Metallurgy and Material Science, 2, 75-88 (Rus).
5. Beckhoff, B., Kanngießer, B., Langhoff, N., Wedell, R., Wolff, H. (2006) Handbook of Practical X-Ray Fluorescence Analysis. Springer.
6. Molnar, G. (2004) Handbook of Prompt Gamma Activation Analysis. Springer.
7. Edited by: Tsuji, K., Injuk, J., Van Grieken, R. John Wiley & Sons Ltd., (2004) X-Ray Spectrometry: Recent Technological Advances.
8. Baltic Scientific Instruments. On-line XRF conveyor analyzer CON-X. https://bsi.lv/en/products/ndt-analyzers/-line-xrf-conveyor-analyzer-con-x/ (Accessed on 13.01.2025).

XVI International Mineral Processing
and Recycling Conference
28-30 May 2025, Belgrade, Serbia

DOI: 10.5937/IMPRC25154M Review article

LABORATORY-SCALE REACTORS EMPLOYING MOVING BED BIOFILM REACTOR (MBBR) TECHNOLOGY: A COMPREHENSIVE REVIEW

Aleksandra Mitrovic[1,2#], 0000-0002-5183-6276,
Jelena Vucicevic[3], 0009-0008-5723-7363,
[1]Academy of Applied Studies Polytechnic, Belgrade, Republic of Serbia
[2]Faculty of Information Technology and Engineering, University “Union – Nikola Tesla”, Belgrade, Republic of Serbia
[3]Novos d.o.o., Belgrade, Republic of Serbia

ABSTRACT – Moving bed biofilm reactor (MBBR) technology has emerged as a highly efficient and robust process for biological wastewater treatment, offering advantages such as compact reactor footprint, enhanced biomass retention, and resistance to loading fluctuations. This review provides a comprehensive overview of the application of MBBR technology in laboratory-scale reactors, highlighting its underlying principles and comparing it to traditional suspended and attached growth systems. Emphasis is placed on design considerations, operational parameters, and performance evaluation in terms of pollutant removal efficiency and process stability. Moreover, the paper discusses the latest advancements and future perspectives concerning new carrier media materials, hybrid reactor configurations, and potential for full-scale implementation. The findings underscore the adaptability and effectiveness of MBBR technology in achieving superior treatment performance, making it an attractive option for researchers and practitioners seeking to address a wide array of wastewater challenges.

Keywords: MBBR, Biofilm, Wastewater, Treatment, Carriers.

INTRODUCTION

The growing global concern over water quality has prompted significant research and development of advanced wastewater treatment processes. Biological treatment systems are critical components of modern wastewater treatment plants, as they effectively remove organic pollutants, nutrients, and other contaminants through microbial metabolism. Traditional biological treatment processes can be broadly classified into suspended-growth systems, such as activated sludge processes, and attached-growth systems, such as trickling filters and rotating biological contactors. More recently, hybrid or combined systems have also gained attention [1-5]. Among these, moving bed biofilm reactor (MBBR) technology has garnered considerable interest owing to its compact design, high treatment efficiency, and robust performance under variable loading rates [6].

The MBBR process was originally developed in Norway during the late 1980s and early 1990s. Since then, numerous full-scale installations, as well as laboratory- and pilot-scale

---

[#] corresponding author: amitrovic@politehnika.edu.rs studies, have confirmed the technology's potential for removing organic matter, nitrogen, and other pollutants. The distinctive feature of MBBR is the presence of carrier elements in the reactor that facilitate biofilm growth, leading to improved biomass retention and treatment effectiveness [2,7]. This paper aims to provide a comprehensive review of laboratory-scale MBBR reactors, elucidating the key design and operational parameters, summarizing performance data from various studies, and discussing emerging trends and future perspectives related to the technology.

OVERVIEW OF MBBR TECHNOLOGY

MBBR technology is based on the principle of biofilm formation on specially designed carrier materials (often referred to as "media" or "carriers") that are continuously mixed throughout the reactor (Figure 1). The carriers, typically made of polyethylene or polypropylene, provide a protected surface area where microbial communities can attach and form biofilms. Aeration or mechanical mixing ensures that these carriers remain in constant motion, thereby enhancing contact between the wastewater and the biofilm. The result is a system combining the advantages of suspended growth (direct contact with contaminants) and attached growth (high biomass concentrations and resilience to shock loads) [8-11].

Figure 1 Example of an aerobic MBBR reactor with biomass growth clearly visible on the carrier surface [12]

MBBRs can operate with a significantly lower sludge age and higher organic loading rates than traditional activated sludge systems, leading to smaller reactor volumes. The biomass grows predominantly on the carrier surfaces, allowing for better retention and reduced washout. This feature also eliminates or reduces the need for a separate clarification step, a critical element in many conventional wastewater treatment processes. In addition, MBBR systems often exhibit greater stability when subjected to varying influent characteristics, pH fluctuations, and toxic shocks [9, 12-14].

In laboratory setups, MBBR technology is commonly deployed in cylindrical reactors made of glass or acrylic. The choice of carrier material is typically based on factors such as surface area-to-volume ratio, durability, and the ability to promote adequate biofilm growth. Aeration systems are designed to provide both oxygen supply and mixing to ensure the carriers remain well-suspended [15].

LABORATORY-SCALE MBBR REACTORS

Laboratory-scale MBBR reactors serve as an essential step before transitioning to pilot or full-scale implementations. They allow researchers to investigate fundamental aspects of MBBR performance under controlled conditions, including the influence of various operating parameters, carrier design, and wastewater compositions. Additionally, these smaller systems facilitate the rapid assessment of novel carrier materials, advanced process configurations, and new operational strategies [16].

The design of laboratory-scale MBBR systems typically involves a transparent vessel, which enables visual observation and documentation of biofilm growth on carrier surfaces. The carriers are placed inside the reactor at a defined fill fraction (ranging from 20% to 70% of the total reactor volume, depending on the intended loading). Continuous or intermittent aeration is provided through diffusers located at the bottom of the reactor to maintain dissolved oxygen concentrations sufficient for the microorganisms and to ensure the carriers stay in suspension. Depending on the nature of the study, the system can be operated under batch or continuous-flow conditions [17]. The feed composition may range from synthetic wastewater (with precise carbon, nitrogen, and phosphorus levels) to real municipal or industrial wastewater, depending on the specific research objectives.

One of the challenges in laboratory-scale MBBR experiments is accurately simulating real operating conditions, such as diurnal variations in influent characteristics or fluctuations in loading. Researchers often incorporate programmable logic controllers (PLCs) or automated control systems that can adjust influent flow rates or nutrient concentrations over time to address these issues. Another challenge lies in scaling up results. Because the hydrodynamics, oxygen transfer efficiency, and biofilm characteristics might differ in larger systems, careful attention should be paid to dimensionless parameters and similarity criteria during the design and interpretation of laboratory-scale experiments [18].

OPERATIONAL PARAMETERS IN MBBR SYSTEMS

Operational parameters play a significant role in determining the efficiency and stability of MBBR systems. One key parameters is the hydraulic retention time (HRT), which influences the contact time between the wastewater and the biofilm. In laboratory setups, HRTs can range from a few hours to more than a day, depending on the study's objectives and the desired removal efficiency [3].

Organic loading rate (OLR) is another critical parameter, reflecting the mass of biodegradable matter introduced per unit volume of reactor per day. Laboratory-scale studies typically explore a wide range of OLR values to understand how the system reacts to different pollutant loads. The balance between OLR and the available biomass (i.e., carrier fill fraction and microbial growth) is crucial to ensure that the system can handle the incoming load without risking overload or biomass washout.

Dissolved oxygen (DO) concentration is also essential, particularly for aerobic processes aimed at removing organic matter and nitrogenous compounds through nitrification. In well-aerated MBBR systems, DO levels are generally maintained above 2 mg/L, but this can vary based on the reactor's specific design and the target pollutants. Laboratory studies often employ oxygen probes and controllers to keep the DO within the desired range. Additionally, the mixing intensity, commonly measured by air flow rate in aerobic MBBR systems, determines the movement of carriers, the shear forces on the biofilm, and the overall oxygen transfer efficiency [19].

Temperature can significantly affect microbial activity and growth, especially for nitrifying bacteria, which have a narrower optimal temperature range. Laboratory reactors usually maintain a constant temperature using thermostatic baths or heating jackets to eliminate fluctuations that could confound experimental results. pH is another factor influencing microbial metabolism. Typically, MBBR systems are maintained at a near-neutral pH of around 7 to 8, although certain specialized processes (e.g., partial nitrification) might require different pH ranges [13].

PERFORMANCE OF MBBR IN LABORATORY REACTORS

In laboratory-scale investigations, MBBR systems have consistently demonstrated high removal efficiencies for chemical oxygen demand (COD) and biochemical oxygen demand (BOD). Removal rates above 85% are common, depending on the organic loading rate and carrier fill fraction. Successful nitrogen removal has also been reported in numerous studies, particularly when the MBBR system is combined with anoxic zones or operates in sequential aerobic–anoxic modes for nitrification-denitrification. Phosphorus removal, however, often requires additional treatment steps, such as chemical precipitation or the incorporation of enhanced biological phosphorus removal processes [2,3,16].

One of the most notable advantages of MBBR technology is its resilience to fluctuating load conditions. Laboratory experiments indicate that MBBR reactors can absorb sudden increases in organic or toxic loading with minimal impact on overall performance. This robustness is attributed to the stable biofilm communities established on the carriers, which can withstand short-term disturbances more effectively compared to conventional suspended-growth systems.

Researchers have also investigated the use of innovative carrier materials, including those made from biodegradable polymers or modified surfaces with immobilized nanoparticles to enhance biofilm formation or target specific pollutants such as heavy metals or recalcitrant organic compounds. These laboratory-based studies demonstrate the adaptability of MBBR technology to different wastewater streams, from municipal sewage to high-strength industrial effluents [20].

FUTURE PERSPECTIVES

Future developments in laboratory-scale MBBR research are expected to focus on hybrid configurations that combine MBBR with other advanced treatment processes, such as membrane filtration, electrochemical processes, or advanced oxidation. These integrated systems have the potential to expand the range of treatable pollutants and further improve the overall water quality. Additionally, the application of novel carrier media with tailored surface properties, higher surface area-to-volume ratios, and enhanced mechanical robustness remains a topic of ongoing investigation.

The increasing adoption of digital technologies and process modeling tools offers another promising direction. Advanced process simulations and real-time monitoring technologies can help researchers optimize operational parameters, reduce energy consumption, and predict system responses under dynamic conditions [21,22]. Machine learning techniques may also be employed to identify complex relationships between operating variables and treatment performance in laboratory MBBR reactors, ultimately leading to more robust and efficient full-scale processes.

CONCLUSION

Moving bed biofilm reactor technology has proven to be a reliable and efficient approach for wastewater treatment in laboratory-scale studies. Its capacity to maintain high biomass concentrations, tolerate fluctuating loads, and adapt to various wastewater characteristics has led to wide acceptance and continuous development. Laboratory-scale MBBR reactors provide valuable insight into the fundamental interactions between biofilms, carriers, and wastewater, informing the design and operation of larger systems. Key research directions include optimizing carrier materials, exploring hybrid configurations with other advanced processes, and employing modeling and real-time monitoring strategies to enhance system performance. As water quality regulations tighten and environmental challenges persist, MBBR technology will likely remain at the forefront of innovation in biological wastewater treatment.

REFERENCES

1. Ødegaard, H. (2006) Innovations in wastewater treatment: The moving bed biofilm process Water Science and Technology, 53 (9), 17–33.
2. Ling, Y., Totsuka, N., Ishii, K. (2020) Performance evaluation of a hybrid moving bed biofilm reactor (MBBR) for wastewater treatment and reuse. Journal of Water Process Engineering, (35), 101–189.
3. Zhang, Q., Chen, X., Zhang, Z., Luo, W., Wu, H., Zhang, L., Zhang, X., Zhao, T. (2020) Performance and microbial ecology of a novel moving bed biofilm reactor process inoculated with heterotrophic nitrification-aerobic denitrification bacteria for high ammonia nitrogen wastewater treatment. Bioresource Technology, (315), 123-813, ISSN 0960 - 8524, https://doi.org/10.1016/j.biortech.2020.123813.
4. Mishra, S., Singh, V., Cheng, L., Hussain A., Ormeci, B. (2022) Nitrogen removal from wastewater: A comprehensive review of biological nitrogen removal processes, critical operation parameters and bioreactor design, Journal of Environmental Chemical Engineering, 10, (3), 107-387, ISSN 2213-3437, https://doi.org/10.1016/j.jece.2022.107387.
5. Yang, Q., He, Q., Husham, I. (2012) Review on Moving Bed Biofilm Processes. Pakistan Journal of Nutrition, (11), 804-811. 10.3923/pjn.2012.804.811.
6. Madan, S., Madan, R., Hussain, A. (2022) Advancement in biological wastewater treatment using hybrid moving bed biofilm reactor (MBBR): a review. Appl. Water Sci, 12 (141) https://doi.org/10.1007/s13201-022-01662-y.
7. Gzar, A. H., et al (2021) J. Phys.: Conf. Ser. 1973 01202

8. Ivanovic, I., Leiknes, T.O. (2012) The biofilm membrane bioreactor (BF-MBR)—a review. Desalination and Water Treatment, 37 (1–3), 288–295. https://doi.org/10.1080/19443994.2012.661283.
9. Aslam, Z., Alam, P., Islam, R., Khan, H.A., Samaraweera, H., Hussain, A., Zargar, I.T. (2025) Recent developments in moving bed biofilm reactor (MBBR) for the treatment of phenolic wastewater-A review. Journal of the Taiwan Institute of Chemical Engineers, 166, Part (2), 105-517, ISSN 1876-1070, https://doi.org/10.1016/j.jtice.2024.105517.
10. Ren, Z., Zhou, Y., Lu, Z., Liu, X., Liu, G. (2023) Biofilm Reactor with Permeable Materials as Carriers Archives Better and More Stable Performance in Treatment of Slightly Polluted Water during Long-Term Operation. Water, 10.3390/w15132415, 15 (13) (2415).
11. Pratap, V., Kumar, R., Kumar, S., Yadav, R.B. (2024) Optimization of moving bed biofilm reactors for the treatment of municipal wastewater. Environmental Research, 10.1016/j.envres.2023.117560, 241, (117560).
12. Adrianus, van der H., Lubbe, van der J. (2012) Handbook of Biological Wastewater Treatment 2.
13. Ahmad, A., Priyadarshini, M., Yadav, S., Ghangrekar, M.M., Yadava, N.R. (2024) A Global Overview of Traditional Biological Treatment Technologies. Emerging Technologies in Biological and Hybrid Wastewater Treatment: Lessons from Developed to Enhancing Practices in Developing Countries, 10.1007/978-3-031-74515-7_2, 21-39.
14. Bruzzoniti, C.M., Rivoira, L., Mihail, S., Galea, B., Fibbi, D., Massimo, del B. (2024) Limits and Perspectives of Established Technologies for Urban Wastewater Depuration. Water Reuse and Unconventional Water Resources, 10.1007/978-3-031-67739-7_6, 125-141.
15. Ødegaard, H., (2014) Compact wastewater treatment with MBBR.
16. Gupta, B., Gupta, K.A., Ghosal, S.P., Lal, S., Saidulu, D., Srivastava, A., Upadhyay, M. (2022) Recent advances in application of moving bed biofilm reactor for wastewater treatment: Insights into critical operational parameters, modifications, field-scale performance, and sustainable aspects. Journal of Environmental Chemical Engineering, 10, (3) 107-742, ISSN 2213-3437, https://doi.org/10.1016/j.jece.2022.107742.
17. Biase, di A., Kowalski, S.M., anner Devlin, R.T., Oleszkiewicz, A.J. (2019) Moving bed biofilm reactor technology in municipal wastewater treatment: A review. Journal of Environmental Management, 247, 849-866, ISSN 0301-4797, https://doi.org/10.1016/j.jenvman.2019.06.053.
18. Saidulu, D., Majumder, A., Gupta, K.A. (2021) Systematic review of moving bed biofilm reactor, membrane bioreactor, and moving bed membrane bioreactor for wastewater treatment: Comparison of research trends, removal mechanisms, and performance. Journal of Environmental Chemical Engineering, 9, Issue (5) 106-112, ISSN 2213-3437, https://doi.org/10.1016/j.jece.2021.106112.
19. Bruzzoniti, M.C., Rivoira, L., Galea, S.M.B., Fibbi, D., Bubba, del M. (2024) Limits and Perspectives of Established Technologies for Urban Wastewater Depuration. In: Minella, M., Prevot, A.B., Maurino, V. (eds). Water Reuse and Unconventional Water Resources, Lecture Notes in Chemistry, 113. Springer, Cham. https://doi.org/10.1007/978-3-031-67739-7_6
20. Bal, Y., Pak, A.B., Bayrakdar, A., Sahinkaya, E. (2025) Optimization of moving bed membrane bioreactor process for improved water and nutrient recovery from domestic wastewater. Journal of Water Process Engineering, 10.1016/j.jwpe.2025.106934, 70, (106934).
21. Kong, Z., Li, L., Xue, Y., Yang, M., Li, Y.Y. (2019) Challenges and prospects for the anaerobic treatment of chemical - industrial organic wastewater: A review. Journal of Cleaner Production, 231, 913-927, ISSN 0959-6526, https://doi.org/10.1016/j.jclepro.2019.05.233.
22. Boltz, J.P., Morgenroth, E., Sen, D., Rittmann, B.E. (2017) Mathematical modelling of biofilm processes in MBBR systems: Current practices and future directions. Water Science and Technology, 75 (4), 649–663.

XVI International Mineral Processing
and Recycling Conference
28-30 May 2025, Belgrade, Serbia

DOI:10.5937/IMPRC25160M Research article

INCREASING RECYCLING RATES IN THE FIELD OF CONSTRUCTION AND DEMOLITION WASTE MANAGEMENT BY IMPLEMENTING THE LEGAL ACT OF THE REPUBLIC OF SERBIA AND THE EUROPEAN UNION

Vesna Marjanović#, 0000-0001-8005-5244,
Emina Požega, 0000-0001-6797-2435,
Miomir Mikić, 0000-0001-7659-769X,
Milutin Stojadinović, 0009-0005-7760-216X,
Mining and Metallurgy Institute Bor, Bor, Serbia

ABSTRACT The legal acts of the Republic of Serbia and the European Union (EU) aim to ensure a high quality of the environment, primarily in the member countries, but also more widely, for all citizens of Europe. The paper discusses the national legal acts and EU regulations that establish norms related to common procedures aimed at a greater degree of recycling of waste generated during the construction and demolition of buildings.

Keywords: Construction and demolition waste, Legal regulations, Recycling, Circular economy.

INTRODUCTION

Construction waste management has gained importance many times over with the entry into force of legal and by-laws in the Republic of Serbia, which define the management of construction waste. The implementation of regulations in practice is very important, as are concrete steps for efficient waste management, intending to reduce CO_2 emissions and preserve the environment. Waste owners should know the importance of recycling and reuse of construction waste to preserve the environment and reduce costs, as well as the practical application of circular economy. Disposal of construction waste is no longer a sustainable or profitable solution, and recycling and reuse bring not only significant environmental benefits but also practical savings in business. Construction and demolition waste is defined as waste generated during construction work on construction sites or preparatory work that precedes the construction of buildings, as well as waste resulting from the demolition and reconstruction of buildings, and includes non-hazardous and hazardous construction and demolition waste [1]. This waste can be non-hazardous waste (concrete, soil, brick, glass, stone, plastic, tiles and ceramics, copper, bronze, brass, iron, steel, insulation materials, plaster, wood, mixed waste, etc.) and hazardous waste (construction and insulating materials containing asbestos, sealants containing PCBs, glazes containing PCBs, construction and demolition waste containing mercury, other construction and demolition waste containing dangerous substances, etc.) [2].

---

corresponding author: vesna.marjanovic@irmbor.co.rs

The amount of waste generated from construction and demolition in the Republic of Serbia in 2020 amounted to 320,879 t according to The Report on the State of the Environment in the Republic of Serbia for 2020 [3], and 729,000 t according to the data of the Statistical Office of the Republic of Serbia [4], but the available statistics it does not give realistic potential amounts of waste generated.

Most of the waste, which is mixed construction and demolition waste, is deposited or, more often, disposed of together with municipal waste at municipal unsanitary landfills, while only metal waste is collected and recycled on a larger scale due to its economic value.

The basic stages in the recycling process are sorting, crushing, and sieving to obtain a finished product in the form of aggregates that can be used in construction, for landscaping, and as a substitute for gravel in concrete elements. The recycling of waste from construction and demolition is directed towards the recycling of non-hazardous materials.

To increase the degree of recycling, it is necessary to separately collect and store construction and demolition waste at the construction site and then transport it to the appropriate recycling facility. Any mixed collection increases the level of pollution and reduces recycling possibilities. If generated in reconstruction or demolition activities, mineral waste from construction and demolition is used for leveling or other types of surface leveling. Bituminous material is used to a certain extent for roads or is reused/used on-site for road maintenance. Construction and demolition waste that is of low quality and unsuitable for recycling is transported to a registered landfill. Excavated soil can be used for backfilling and leveling of terrain, for devastated sites, etc. The treatment of construction and demolition waste as a substitute for primary resources for construction activities is rather underdeveloped.

PLANNING FRAMEWORK OF THE REPUBLIC OF SERBIA AND NATIONAL REGULATIONS IN THE FIELD OF CONSTRUCTION AND DEMOLITION WASTE MANAGEMENT

The planning framework of the Republic of Serbia and national regulations in the field of waste management from construction and demolition are harmonized with the European Union legislation. The key programs, laws, and regulations that regulate this area are:

- **Waste Management Program in the Republic of Serbia 2022-2031.** [2], which was preceded by the Waste Management Strategy for the period 2010-2019. year [5] based on which the conditions were set for the establishment and development of an integrated waste management system at the national level. This Program stipulates that it is necessary to prevent the uncontrolled dumping of construction waste into the environment and to ensure its recycling. Some of the most important goals that this Program envisages are an increase in the reuse rate to 40% by 2029, i.e. pre-treatment of 70% of construction and demolition waste by 2034, as well as defining special goals for the recycling rate. Also, this Program envisages the development of supporting infrastructure to enable the implementation of regulations and improve the process of waste management from construction and demolition [2].

- **Circular Economy Development Program in the Republic of Serbia for the Period 2022-2024.** [6] includes the most important areas of importance for the circular economy: waste management; water management; renewable energy sources and energy efficiency; management of chemicals, etc. To fulfill the general goal, five specific goals have been set, with measures and activities that will be implemented in the period 2022-2024. year. Special goal 3, refers to the improvement of the waste management system through more efficient use of waste in the circular economy. This objective includes measures and activities that will contribute to the further development of the circular economy in the Republic of Serbia in the area of waste management. Implementation of the planned measures will contribute to the reduction of plastic waste generation, more efficient recycling of non-hazardous construction waste, as well as the improvement of recycling processes and ensuring the circularity of recycled material, which will be achieved by checking the presence and removing the most dangerous chemicals that can contaminate circular flows [6].
- **The Law on Planning and Construction** [7] determines the conditions and methods of spatial planning, arrangement, and purpose of construction land and the construction and use of buildings. The law stipulates that the responsible contractor is obliged to manage construction waste generated during construction on the construction site according to the regulations governing waste management and to use and/or store construction waste generated during construction on the construction site according to the regulations governing waste management. The law stipulates that the removal of a building, or part of it, can be carried out by a business company, other legal entity, or an entrepreneur, who is registered in the appropriate register for the construction of buildings, that is, for the performance of works. The responsible contractor manages the removal of the building. After the removal of the object, i.e. its part, the land must be arranged and the construction waste removed, by special regulations.
- **The Law on Waste Management** [1] defines the obligations of all subjects in waste management, including construction waste. The law sets basic guidelines for the collection, transportation, recycling, and disposal of waste, as well as responsibility for waste generation and proper management. This law defines, among other things, the general responsibilities and obligations of waste producers. The law stipulates that waste can be reused for the same or another purpose, for recycling, i.e. other reuse operations, to obtain raw materials for the production of the same or another product, as secondary raw materials, or to use the value of waste through its biodegradation or incineration of waste with the use of energy.
- **The Regulation on the Manner and Procedure of Construction and Demolition Waste Management** [8] describes in detail the specific procedures for the management of construction and demolition waste, including all waste gates, mandatory procedures for recycling and depositing, and the obligations of investors and contractors. According to this regulation, the waste producer is obliged to draw up a Construction and Demolition Waste Management Plan that contains information on the types of waste generated, procedures for waste reduction, and proposals for its recycling and final

disposal, to obtain approval for the Plan and organize its implementation. The Plan must be an integral part of the project documentation.

- **The Rulebook on Types of Waste for Which a Request Can Be Submitted, Allowed Procedures and Treatment Technologies for Types of Waste, and Other Special Elements for Determining the End of Waste Status** [9] prescribes the types of waste for which a request can be submitted for the conformity assessment procedure, allowed procedures and technologies treatment for waste types and other special elements for determining the end of waste status.

These include: iron and steel scrap, aluminum scrap, copper scrap, glass cullet, ground plastic, and recycled aggregate. Waste ceases to be waste if the technical requirements and other prescribed criteria are fulfilled.

- **The Rulebook on Categories, Examination, and Classification of Waste** [10] prescribes the Catalog of waste, that is, a summary list of non-hazardous and hazardous waste, according to which waste is classified into 20 groups depending on the place of origin and origin. Construction and demolition waste are marked with catalog number 17.
- **The Law on Communal Activities** [11] prescribes, among other things, the rights and duties of the municipal or city communal inspector, who, among other things, can prohibit by decision the disposal of waste construction material, soil, and other construction material outside the designated location.

OVERVIEW OF EUROPEAN UNION LEGISLATION IN THE FIELD OF CONSTRUCTION AND DEMOLITION WASTE MANAGEMENT

EU legislation takes several forms of legal instruments and each of them applies to different institutions and has a different legal force. All legal documents related to the EU can be divided into the following groups: laws, directives, decisions, recommendations, and opinions. For all members of the European Union, laws, directives, and decisions are binding, while recommendations and opinions have the function of guidelines for institutions and are legally non-binding texts.

As part of negotiations for EU accession, the Republic of Serbia, through Chapter 27, began the process of establishing a waste management system and adapting it to the goals and legal acquis of the EU [2]. Construction and demolition waste management in the EU is defined in the following documents:

- **A new Circular Economy Action Plan for a Cleaner and More Competitive Europe (COM/2020/98)** [12] sets ambitious measures to stimulate the transition to a circular economy, i.e. to develop an efficient and competitive economy that would ensure that by 2050, there will be no greenhouse gas emissions at the community level. Special attention is paid to the sectors of textiles, construction, electronics, batteries and vehicles, packaging, food waste, and plastics [12].
- **Directive 2018/851** [13] on the amendment of Directive 2008/98/EC [14] on waste is an amendment of the Framework Directive on waste in by previously prescribed waste management hierarchy.

The key requirements prescribed by this directive regarding the determination of specific objectives to be achieved at the EU level is the establishment of a construction waste classification system at least for wood, mineral fractions (concrete, brick, tiles and ceramics, stone), metal, glass, plastic, and plaster. Directive 2008/98/EC prescribed targets for the preparation for reuse and recycling of non-hazardous construction waste of a minimum of 70% of the mass of waste, which was to be reached by 2020.

- **Circular Economy Package**, among which the most significant is 2018/850 EU8 [15] on amendments to the Waste Directive (2008/98/EC) [14] and the EU Strategy "Construction 2020" (EU 2015, EU COM 2014, EU COM 2012) [16, 17] sets ambitious measures, which include the revision of legislative proposals on waste to have stimulated the transition to a circular economy in Europe. In the part related to construction and demolition waste, this directive, in addition to promoting measures to reduce waste and selective demolition, obliged member states to prepare up to 70% of construction waste by 2020 for reuse, recycling, or use for filling (non-hazardous waste). The activities proposed by the EU Action Plan for the Circular Economy will contribute to closing product life cycles through increased recycling and reuse, and environmental and economic benefits will be realized.
- **EU Construction and Demolition Waste Protocol and Guidelines (2016)** [18] provides EU guidelines in the field of construction and demolition waste management. The general goal of this Protocol is to increase confidence in the construction and demolition waste management process, as well as confidence in the quality of recycled materials from construction and demolition waste. The protocol plans to achieve these goals through: improved identification, separation at the point of origin and collection of waste; improved waste logistics; improved waste processing; quality control; appropriate policies, and framework conditions.
- **Guidelines for the waste audits before demolition and renovation works of buildings (2018.)** [19] provides guidelines on the best practices for estimating the costs of waste from construction and demolition, before the actual demolition or renovation of buildings and infrastructure.
- **Regulation (EU) No 305/2011 of The European Parliament and of the Council** [20] regulated building materials. All construction materials placed on the common market must be proven to meet the harmonized European standards for construction materials (CEN/EN).

CONCLUSION

National and European legislation sets ambitious goals for recycling and reuse of construction and demolition waste across Europe and in the Republic of Serbia after harmonization of domestic legislation with EU legislation and domestic resources. Laws and directives set binding environmental protection goals and the increasing application of circular economy. The legislation itself is flexible in terms of the way to achieve the set goals, as well as in terms of the organization and ownership of assets and the financing of the necessary activities, and in this way the society is open to innovation and technological progress. The positive sides of the EU legislation are also reflected in the provision of a solid basis for long-term planning at the technical, financial, and political levels.

ACKNOWLEDGEMENT

This work was financially supported by the Ministry of Science, Technological Development and Innovation of the Republic of Serbia, Contract No. 451-03-136/2025-03/200052.

REFERENCES

1. The Law on Waste Management, Official Gazette of the RS, No. 36/09, 88/10, 14/16, 95/18 – another law, and 35/23.
2. Waste Management Program in the Republic of Serbia 2022-2031., Official Gazette of the RS, No. 12/2022.
3. The Report on the State of the Environment in the Republic of Serbia for the year 2020., Environmental Protection Agency, 2021.
4. Statistical Office of the Republic of Serbia, 2021.
5. Waste Management Strategy for the period 2010-2019. Official Gazette of the RS, No. 29/10.
6. Circular Economy Development Program in the Republic of Serbia for the Period 2022-2024., Official Gazette of the RS, No. 137/22.
7. The Law on Planning and Construction, Official Gazette of the RS, No. 72/09, 81/09 - correction, 64/10 - US, 24/11, 121/12, 42/13 - US, 50/13 - US, 98/13 - US, 132/14, 145/14, 83/18, 31/19, 37/19 - another law, 9/20, and 52/21.
8. The Regulation on the Manner and Procedure of Construction and Demolition Waste Management, Official Gazette of the RS, No. 93/23, and 94/23 – correction.
9. The Rulebook on Types of Waste for Which a Request Can Be Submitted, Allowed Procedures and Treatment Technologies for Types of Waste, and Other Special Elements for Determining the End of Waste Status, Official Gazette of the RS, No. 19/24, and 47/24.
10. The Rulebook on Categories, Examination, and Classification of Waste, Official Gazette of the RS, No. 56/10, 93/19, and 39/21)
11. The Law on Communal Activities (Official Gazette of the RS, No. 88/11, 104/16, 95/18)
12. A new Circular Economy Action Plan For a cleaner and more competitive Europe COM/2020/98 final.
13. Directive (EU) 2018/851 of the European Parliament and of the Council of 30 May 2018 amending Directive 2008/98/EC on waste
14. Directive 2008/98/EC of the European Parliament and of the Council of 19 November 2008 on waste and repealing certain Directives
15. Directive (EU) 2018/850 of the European Parliament and of the Council of 30 May 2018 amending Directive 1999/31/EC on the landfill of waste
16. https://single-market-economy.ec.europa.eu/sectors/construction_en, (accessed, 29. 01. 2025)
17. European Commission (2020) Circular Economy - Principles for Building Design, https://ec.europa.eu/docsroom/documents/39984 (accessed, 29.01.2025).
18. https://single-market-economy.ec.europa.eu/news/eu-construction-and-demolition-waste-protocol-2018-09-18_en , (accessed, 25.01.2025).
19. https://www.europeandemolition.org/information/construction-and-circular-economy/guidelines-for-the-waste-audits-before-demolition-and-renovation-works-of-buildings (accessed, 31.01.2025).
20. Regulation (EU) No 305/2011 of the European Parliament and of the Council of 9 March 2011 laying down harmonised conditions for the marketing of construction products and repealing Council Directive 89/106/EEC Text with EEA relevance

XVI International Mineral Processing
and Recycling Conference
28-30 May 2025, Belgrade, Serbia

DOI: 10.5937/IMPRC25166M

Original research article

CHARACTERISTICS OF COPPER POWDER OBTAINED AT LOWER VALUES OF CATHODE CURRENT DENSITY

Radmila Marković[#], 0000-0001-9754-1150,
Vesna Marjanović, 0000-0001-8005-5244,
Aleksandra Ivanović, 0000-0002-0562-2824,
Milutin Stojadinović, 0009-0005-7760-216X,
Mining and Metallurgy Institute Bor, Bor, Serbia

ABSTRACT – This paper presents the influence of cathode current density on physical and chemical characteristics of electrolytic copper powder. The experiments were carried out on apparatus of semi-industrial size. During each experiment, powder was deposited on copper cathode bases of the comb shape. Deposited copper powder was shaking off from cathodes on each 20 min. The concentration of Cu^{2+} ion and H_2SO_4 in the electrolyte was kept in the next range: 5-8 g Cu/dm^3 and 130-160 gH_2SO_4/dm^3. The working electrolyte temperature was in the range 50±2 ºC. The electrolytic flow was 0.5 dm^3/min and the time duration of each experiment was 4 h. The influence of cathode current density on copper powder physical and chemical characteristics was investigated for the following values: 500, 750, and 1000 A/m^2 and obtained values are compared with the values obtained on current density of 2000 and 3000 A/m^2. Content of copper in copper powder is highest for next values of cathode current density: 500 and 750 A/m^2. The results of sieve analysis have pointed out a high content of particles finer than 45 µm, even 80%. Values for apparent density are in the range 0.5-0.8 g/cm^3, which is another evidence of very fine powders.

Keywords: Copper, Powder, Current, Density, Characteristics.

INTRODUCTION

Copper powders and copper alloys are more and more used in the various production branches [1,2]. In connection with this, the required technological characteristics of the copper powder are very important in the selection of methods for powder production. The best method is the one that produces copper powder with the required characteristics in the primary production phase [3,4]. The further treatment increases the powder price and decreases the productivity.

Electrolytical deposition is one of the basic methods for copper powder production [3]. The basic factors for determination of the electrolytic copper powder nature are: the copper ions concentration, electrolyte temperature, cathode current density, the material and shape of a cathode, electrolyte flow, and time interval of electrodeposition between the powder shaking off from the cathode [4, 5]. Also, high powder purity is

---

[#] corresponding author: radmila.markovic@irmbor.co.rs completely the result of the use of cathode copper with low content of impurities, as the starting material for an anode. The obtained dendritical powders present an irreplaceable component in electrographite compounds, although small, with almost poor fluidity, and present a limiting factor of application. Disadvantages of this method are high production price due to current consumption, and the use of high current density values in the industrial production process.

EXPERIMENTAL

Experimental procedure was carried out on an apparatus of semi-industrial size that consists of: electrochemical cell, collecting tank with electrical heating, feed vessel, electrolytical pump, current sources, and pipes system. The shape of the electrochemical cell is trapezoidal with a specially constructed conical bottom. The dimensions of the rectangular part of the cell are: 800x450x200 mm. The dimensions of the conical part are: 800x450 mm and the maximum height is 270 mm (Figure 1).

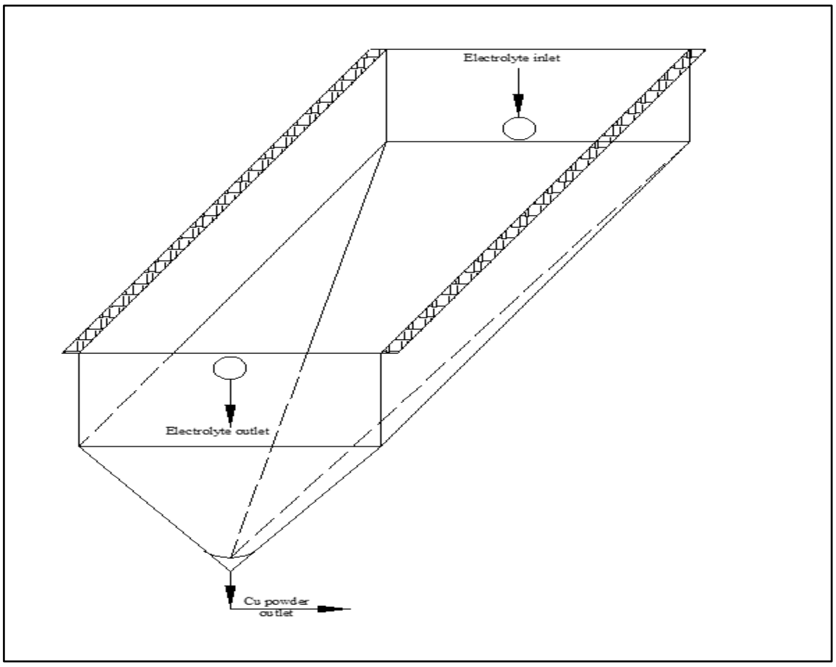

Figure 1 Electrochemical cell (schematic presentation)

Preparation of apparatus for process operation included the following operation: apparatus washing with demineralized water, preparation, and cleaning of current holders, cathode holders, current contacts, electrodes. Two cathodes and three anodes were put into the cell. Cathode copper of the following content (ppm): As < 3, Sb < 2, Bi < 1, Cr < 1, Fe < 5, Pb < 2, Ni < 1, Ag < 5, Te < 0.1, Sn < 2, Zn < 5, Se < 0.7 and Cu=99.95%, was used as the anode material. The anode size was 450x340 mm. The used cathode had a comb shape with four copper bars, ∅12 mm. Submersion depth of electrodes was 300 mm and the interaxial distance was 200 mm. The working volume of the electrolyte in a system was 220 dm^3. Copper(II)sulphate with five water molecules, sulphuric acid of technical quality and demineralized water were used for the electrolyte preparation. During the process, the values of cathode current, voltage on cell, pH, temperature of demineralized water for powder washing, and masses of wet and dry powder were maintained and measured. For each experiment, the used electrolyte had the following initial value: concentration of Cu^{2+} ion, (g/dm^3): 5-8; concentration of sulphuric acid, (g/dm^3): 130-160. The initial value of the concentration of the cupric ion, sulphurc acid, current intensity, and electrolyte volume were checked, and on each new start of the experiment were adjusted with suitable values. On each 20 min of an experiment, deposited copper powder was shaking off from the cathode. Electrolyte flow was adjusted to be 0.5 dm^3/min. The working temperature was 50 ± 2 ^oC. Cathode current density of 500, 750, and 1000 A/m^2 was used. Also, standard values of current density, 2000 and 3000 A/m^2 are used in two experiments for the aim of comparison with obtained results. The obtained powders were discharged as a pulp into a vessel aim to powder washing. The powder washing was done with demineralized water on a temperature of about 45 ^oC. The washed powder was stabilized with the potassium soap with a concentration of 1 g/dm^3. The stabilized powder was filtrated and then dried. Wet powder was dried in a cassette with blowing nitrogen. The maximum temperature in the dryer was 150 ^oC, and the drying time was 18-20 h.

RESULTS AND DISCUSSION

There were done:
- chemical characterization of copper powder,
- determination of percentage by mass of some powder fractions by sieve analysis,
- determination of the apparent density of powder.

The given results in Table 1 are the middle values from three experiments with equal technological parameters.

Table 1 Chemical characterization of the copper powder

Component	**Standard**[6]	**Cathode current density, A/m^2**				
		Sample 1.	**Sample 2.**	**Sample 3.**	**Sample 4.**	**Sample 5.**
		500	750	1000	2000	3000
Chemical content of Cu powder, %						
Cu	99 – 99.5	99.39	99.11	98.92	98.61	98.8
Weight Loss in H_2, %	0.1 – 0.75	0.01	0.015	0.012	0.015	0.01
Acid Insoluble, %	max 0.03	0.003	0.003	0.029	0.021	0.025

The content of copper is the highest for the lower values of cathode current density (500 and 750 A/m^2). Two experiments were carried out with standard values of current density, 2000 and 3000 A/m^2, samples 4 and 5, for the aim of comparison with obtained results. The values for purity of copper powder obtained using the cathode current density of 500 and 700 A/m^2 are in the standard range, as well as values for weight loss in H_2 and percentage of acid insoluble.

Figure 2 represents the results of cell voltage values during the copper powder production on the current cathode density, A/m^2: 500, 750, 1000, 2000, and 3000. The values increased with the current density increasing.

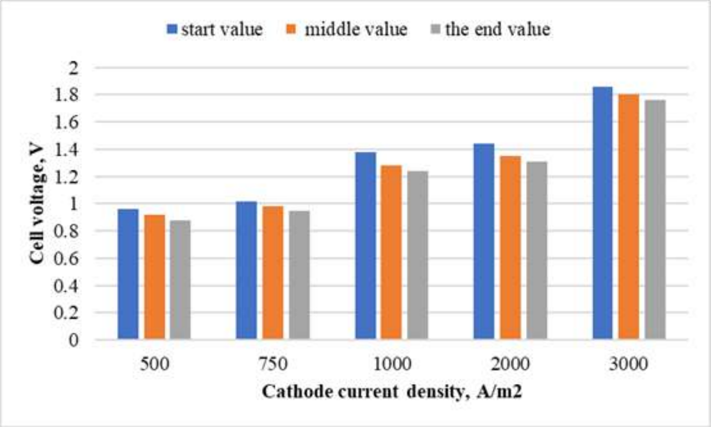

Figure 2 Cell voltage for different values of cathode current density

In Tables 2 and 3, are presented the results of sieve analysis and the values of apparent density.

Based on the presented results in Table 2, it can be seen that the percentage contribution of fine fractions is increased with increasing the current density. The results of sieve analysis show that by use of electrolyte with a concentration of copper ions in the range of 5-8 g/dm3, by the use of cathode current density in the range of 500 – 3000 A/m^2, finer fraction than 45 µm is the most present in each powder sample. Also, the mass percentage of the fraction smaller than 45 µm increases with current density increasing. Analysis of results presented in Table 3 shows that the values of apparent density increase with decreasing the values of cathode current density.

Table 2 Sieve analysis of copper powder obtained on different cathode current densities

Fraction	Unit	Cathode current density, A/m^2				
		500	750	1000	2000	3000
+ 150	%	0.2	0.12	0.16	0.4	0.44
- 150 + 75	%	2.08	1.92	2.84	1.52	2.16
- 75 + 63	%	5.7	6.56	5.1	2.6	2.21
- 63 + 45	%	13.46	16.72	11.6	7.4	4.08
- 45	%	68.18	75.7	80.32	88.1	91.1

Table 3 Apparent density of copper powder

Cathode current density, A/m^2	500	750	1000	2000	3000
Apparent density, g/cm^3	0.716	0.612	0.578	0.526	0.476

CONCLUSION

Based on the presented data, it could be said that by the use of lower values of cathode current density, 500 – 1000 A/m^2, with suitable content of copper ions in electrolyte and time of powder shaking from the cathode, the percentage of fraction smaller than 45 µm is in range of 68.18-80.32%.

The apparent density had higher values for lower current densities, but the order of magnitude is the same.

ACKNOWLEDGEMENT

This work was financially supported by the Ministry of Science, Technological Development and Innovation of the Republic of Serbia, Contract No. 451-03-136/2025-03/200052.

REFERENCES

1. Kundig, K. J., Cowie, J. G. (2006) Copper and Copper Alloys. Mechanical Engineers' Handbook: Materials and Mechanical Design (Myer Kutz), Volume 1, Third Edition, Wiley, New Jersey, 117-220.
2. Romano, T., Vedani, M. (2022) Chapter 6: Additive manufacturing of pure copper: Technologies and Applications. In: Copper-From the Mineral to the Final Application (Daniel Fernandez-Gonzalez), IntechOpen.
3. Abbar, A. H. (2008). Electrolytic preparation of copper powder with particle size less than 63µm. Al-Qadisiya Journal for Engineering Sciences, 1 (1), 32-45.
4. Orhan, G., Gezgin, G. G. (2012) Effect of electrolysis parameters on the morphologies of copper powder obtained at high current densities. Journal of the Serbian Chemical Society, 77 (5), 651-665.
5. Wojtaszek, K., Cebula, F., Partyka, B., Deszcz, P., Włoch, G., Socha, R. P., Wojnicki, M. (2023). Electrochemical Method of Copper Powder Synthesis on Rotating Electrode in the Presence of Surfactants. Arch. Metall. Mater. 68 (1), 375-386.
6. The Copper Development Association Inc.: https://www.copper.org/resources/properties/129_6/production.html, (accessed 12.02.2025)

XVI International Mineral Processing
and Recycling Conference
28-30 May 2025, Belgrade, Serbia

DOI: 10.5937/IMPRC25171A

Original research article

POTENTIAL OF USING ZINC PROCESSING TAILINGS (ZPT's) IN THE PRODUCTION OF BURNT CLAY BRICKS

Messai Ali[1#], 0000-0003-0165-5052,
Berrekbia Linda[1], 0009-0000-1669-1422,
Meramria Ikram[1], 0009-0000-1982-2774,
Juan M. Menéndez-Aguado[2], 0000-0002-6216-6984,
Begoña Fernández Pérez[2], 0000-0003-1239-4839,
Vladimir Nikolić[3], 0000-0003-1885-1156,
Milan Trumić[3], 0000-0002-4321-5218,
Boustila Amir[1], 0000-0002-1108-5105,
[1]National Higher School of Technology and Engineering, Department of Mining, Metallurgy and Materials Engineering, Annaba, Algeria
[2]University of Oviedo, Asturias Raw Materials Institute, Spain
[3]Univesity of Belgrade, Technical Faculty in Bor, Bor, Serbia

ABSTRACT – Zinc processing tailings (ZPTs) from the Kharzet Youcef processing complex (Setif- Algeria) are mainly stockpiled in tailings dumps without use, occupying a significant area with potentially influencing the environment and human health. Incorporating ZPTs in building materials manufacturing is an effective solution to meet the dual objectives of environmental protection and economic development. The study investigates the influence of integrating ZPTs to partially replace clays and firing temperature on the physic-mechanical properties of fired clay bricks (FCB). Microstructural, chemical, and mineralogical analyses of ZPT and clays were carried out by SEM-EDS, XRF and XRD, respectively. Seven mixtures were produced with various percentages of ZPTs added to clays (0%, 5%, 10%, 15%, 20%, 25% and 30%) and were fired to three different temperatures (950, 1000 and 1050 °C) at a ramp rate of 5 °C. Physic-mechanical tests were carried out on different brick specimens, and the results obtained showed the FCB incorporated with 30% of ZPTs produced the highest flexural strength of 6.24 MPa, compressive resistance of 29.78 MPa, bulk density of 1.37 g/cm^3 and water absorption of 15.1% at 900 °C. Therefore, recycling ZPTs for FCB manufacturing is a feasible alternative waste disposal solution for sustainable development while reducing negative environmental impacts.

Keywords: Zinc Processing, Fired Clay Bricks, Construction, Kharzet Youcef, Tailings Valorisation.

INTRODUCTION

Mineral resources, as non-renewable, are the basic blocks for global economic and social growth [1]. The exponential increase in mining activities has generated large amounts of waste and various types of waste. These wastes, mainly in tailings disposed of in dumps without proper management, inevitably affect the environment [2]. In this

---

[#] corresponding author: ali.messai@hotmail.com

context, zinc mining and processing tailings are a primary source of toxic heavy metals to the environment [1,3].

In this regard, recycling and utilisation of mining wastes and tailings as alternative raw materials is regarded as an environmentally friendly solution to mitigate its impacts on the environment on the one hand and to maximise the returns on investments by reusing all extracted materials on the other hand [4].

Furthermore, zinc wastes have a chemical composition similar to natural raw materials used in construction industries [5]. So they can be used as partial replacements in bricks [6-8], cement [9], concrete admixture [10], mortar [11], the production of ceramics [12-14], and cementitious paste [15].

In Algeria, Chaabet El Hamra deposit is the only zinc deposit currently exploited in the country; it's operated by the National Company of Non-Ferrous Mining Products (ENOF). Raw ore is extracted using the room and pillar method and directed to the mineral processing plant to increase quality. Froth flotation is the method used to produce a final high-grade concentrate while the rejects are deposited in a dump. This dump occupies an area of 07 ha, and it has been receiving Chaabet El Hamra treatment waste of ore since 1994.

Subsequently, the authors designed a research plan focused on characterising ZPTs generated from the Kharzet Youcef mineral processing factory and evaluating its suitability as a partial replacement of clays in fired brick manufacturing. Physical-mechanical testing and the microstructure of produced brick specimens were investigated.

STUDY AREA DESCRIPTION

Geographic location

The mineral processing plant of Kherzet Youcef ore (Chaabet El Hamra Mine) is located in Eastern Algeria, 5 km northwest of Ain Azel and approximately 50 km southeast of Setif municipality (Figure 1).

MATERIALS AND METHODS

Materials

The clays used in this study were obtained from El Amel brick factory in El Taref, Algeria. The sampling is done manually from the discharge of the rolling mill (<1 mm).

The ZPT samples were obtained from five distinctive dump locations at the zinc processing plant of Kharzet Youcef. Then, the subsamples of each zone were homogenised, and five samples were finally obtained. After that, the materials (Clays and ZPTs) were dried at 105 °C for 24 h. ZPTs are ground using a planetary ball mill type Welte WTR 950 W/R-V and then sieved to select particles with an average diameter of less than 0.074 mm.

Five samples of ZPTs collected from Kharzet Youcef dumps were thoroughly mixed and prepared by conning and quartering to prepare a single representative sample.

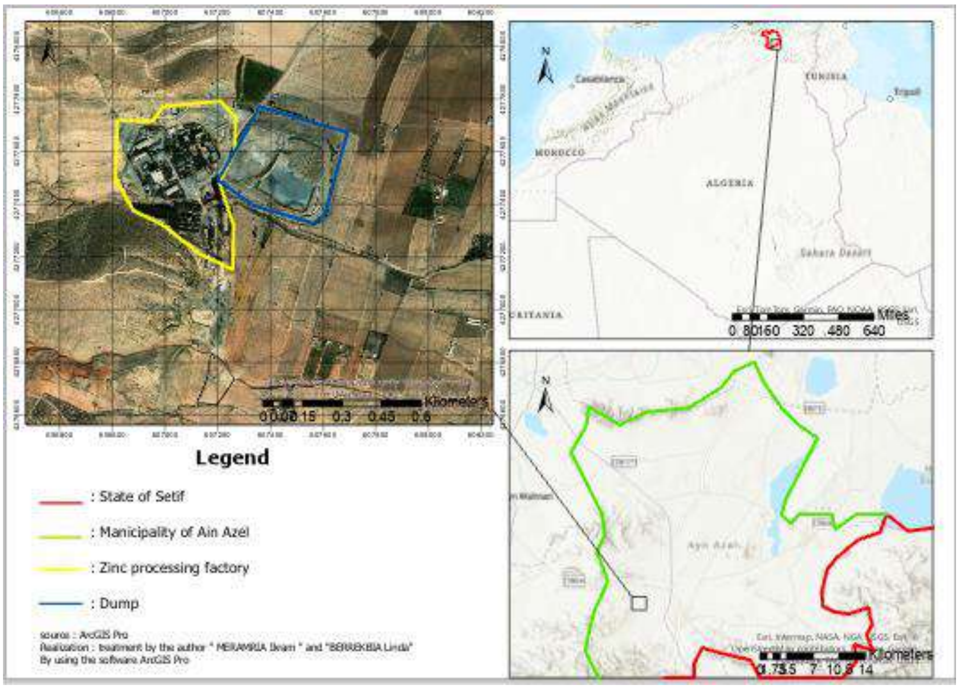

Figure 1 Geographic location of the study area

Molding and sintering of brick specimens

ZPTs were mixed with clays in varying portions to manufacture bricks (Table 1). The different mixtures were blended for 10 minutes in a blender, with 10% by mass of water, to get semi-dry homogenous mixes. Homogenised mixtures were manually pressed using a 40 × 40 × 160 mm mould to produce nine brick specimens for each combination.

Table 1 Mixtures specification

Formulations	**F0**	**F5**	**F10**	**F15**	**F20**	**F25**	**F30**
ZPT's (%)	0	5	10	15	20	25	30
ZPT's (g)	0	15	30	45	60	75	70
Clays (%)	100	95	90	85	80	75	70
Clays (g)	300	285	270	255	240	225	210

The obtained specimens were left in ambient air for 24 h, then dried in an oven at 105 °C for 24 h to decrease moisture content. The dried specimens were fired in a laboratory electrical furnace at a rate of 5 °C/min from room temperature to the desired firing temperature, where two different temperatures were targeted (900 °C and 1000 °C) and held for two hours at the desired firing temperature. After firing, natural convection inside the laboratory electrical furnace cooled bricks to room temperature.

Characterisation

The main chemical composition of the raw materials was determined by X-ray fluorescence spectroscopy (XRF PANalytical AXIOS minerals) and Inductively Coupled Plasma Optical Emission spectroscopy (Agilent Technologies 5900). The plasticity and liquidity limits of mixtures were determined according to ASTM D4318 and ASTM D4943—the sintered samples' bulk density and water absorption values. Linear shrinkage (%) was determined from the lengths of the brick specimens after drying and after sintering treatment by a calliper with a precision of ±0.01 mm according to ASTM C326-09. The compressive resistance and flexural strength were measured using a mechanical testing machine called the Bera Test.

RESULTS AND DISCUSSION

ZPTs and clay characterization

Chemical composition

Chemical analysis of the clays used in this study (Table 2) reveals a high content of SiO_2 (42.9) and Al_2O_3 (23.3), accompanied by significant levels of FeT (8.25) and CaO (8.9).

Table 2 Chemical composition of used clays

Elements	**SiO_2**	**Al_2O_3**	**Fe_T**	**CaO**	**K_2O**	**MgO**	**TiO_2**	**Na_2O**	**LOI**
Percentage (%)	42.9	23.3	8.25	8.9	2.8	4.1	2.7	1.1	5.95

The main components of ZPTs of composite samples are presented in Table 3. The sample is dominated by CaO (31.62%) and a high loss on ignition (LOI) of 35.46%, indicating a large amount of volatile or organic matter. SiO_2 and MgO are also in significant quantities, representing 9.45% and 10.74%, respectively.

Table 3 Chemical composition of Kharzet Youcef ZPT's

Elements	**SiO_2**	**Al_2O_3**	**Fe_2O_3**	**CaO**	**K_2O**	**MgO**	**MnO**	**Na_2O**	**P_2O_5**	**S**	**LOI**
Percentage (%)	9.45	2.2	5.05	31.62	0.38	10.74	0.08	0.54	0.05	3.18	35.46

In conclusion, the silica and alumina content in ZPTs can qualify them as a partial replacement for clays in brick manufacturing.

Physic-mechanical tests

The mass and volume of mixtures prepared for briquetting reveal interesting trends in density. The mass of the briquettes gradually increases with ZPT's added percentage, leading to higher material compactness. These results suggest that adding ZPTs to clays provides denser briquettes, enhancing strength.

The results of plasticity limits for mixtures illustrated in Figure 3 demonstrate the inverse correlation between adding ZPTs and plasticity. These results suggest that incorporating ZPTs affects clays' physical properties.

Figure 4 represents the results of the water absorption test in two cases: 900°C and 1000°C. At 900°C, a general increase in water absorption is evident, suggesting increased porosity of the briquettes. At 1000°C, variations in water absorption are less pronounced.

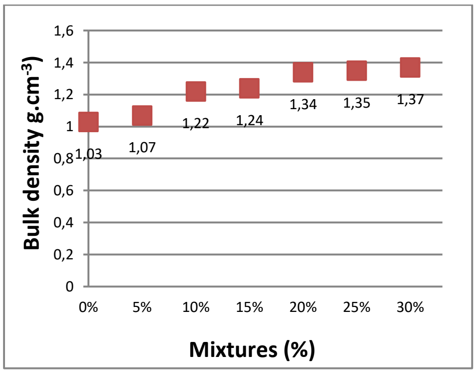

Figure 2 Variation of bulk density of different clay mixtures

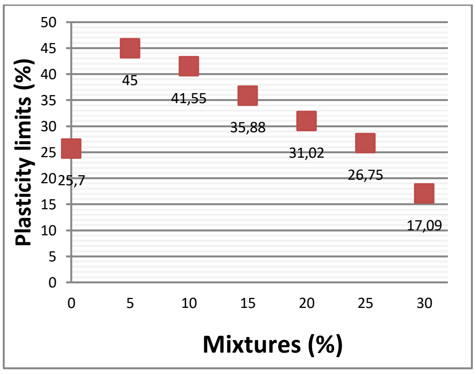

Figure 3 Results of plasticity limits

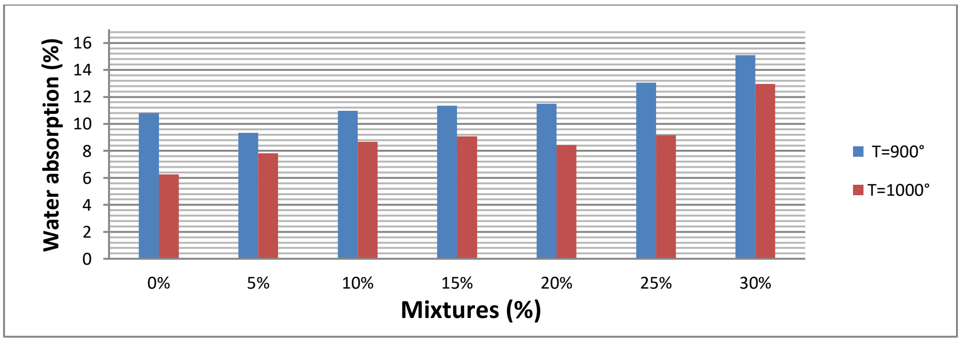

Figure 4 Water absorption as a function of mixtures fired at 900 °C and 1000 °C

Bulk density of bricks:

These results indicate that the firing temperature and the percentage of ZPTs significantly impact the compactness and density of the briquettes after firing, which can influence their mechanical properties and performance in practical applications.

The bulk density of the produced bricks for different proportions of ZPTs fired at various temperatures (900-1000 °C) was presented in Figure 5. The results reveal significant variations in the density depending on the added quantity of ZPTs and the firing temperature. As presented, the samples without ZPT's bulk density, fired at 900 °C and 1000 °C, were 1.18 and 1.40 g/cm^3, respectively. The addition of the ZPTs influences the bulk density of the bricks. At 900 °C, the density varies irregularly, with peaks at 5%

and 10% of added ZPTs. On the other hand, at 1000°C, density augmentation with the increase of ZPTs is observed, reaching maximum values at 15% and 20% added.

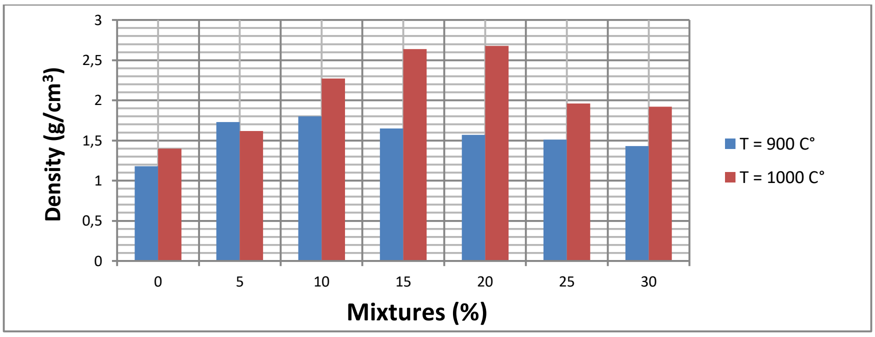

Figure 5 Density variation as a function of mixtures and firing temperature

Linear shrinkage:

Figure 6 shows a general reduction trend in linear shrinkage with increasing percentage of ZPTs, suggesting less contraction of the briquettes at higher added concentrations. This can be attributed to better adhesion and a more homogeneous structure of the materials at these concentrations, which reduces the internal tensions responsible for shrinkage. These results highlight the impact of the percentage of ZPTs on the physical properties of the briquettes, mainly their behaviour during drying, which may have implications on their final sizing and compatibility with the intended applications.

Figure 7 represents the shrinkage results obtained after the firing of bricks at 900 and 1000 °C. A significant variation in material shrinkage has been shown depending on the percentage of ZPTs and the firing temperature. At 900°C, linear shrinkage increases with the increase in the rate of ZPTs up to 15%, and then a decrease to 20% and 25% is added. In contrast, at 1000°C, linear shrinkage appears to vary irregularly, with maximum values observed at 10%, 20% and 30% of ZPTs.

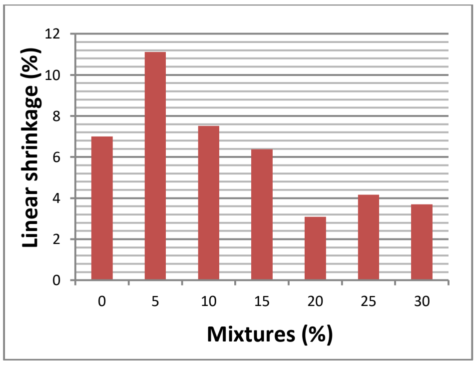

Figure 6 Linear shrinkage of bricks after drying

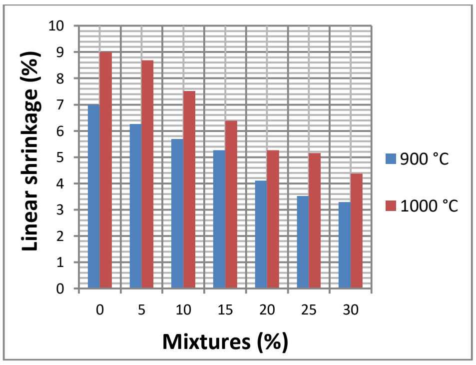

Figure 7 Linear shrinkage of bricks fired at 900 and 1000 °C

Mechanical resistance

The results of mechanical resistance tests of bricks manufactured with different mixtures of ZPTs and clays and subjected to different firing temperatures provide in-depth information on the mechanical performance of these materials. At the firing temperature of 900 °C, the flexural strength (R_F) shows an overall decrease with the increasing percentage of ZPTs, suggesting a reduction in the ability of the bricks to withstand flexural stresses.

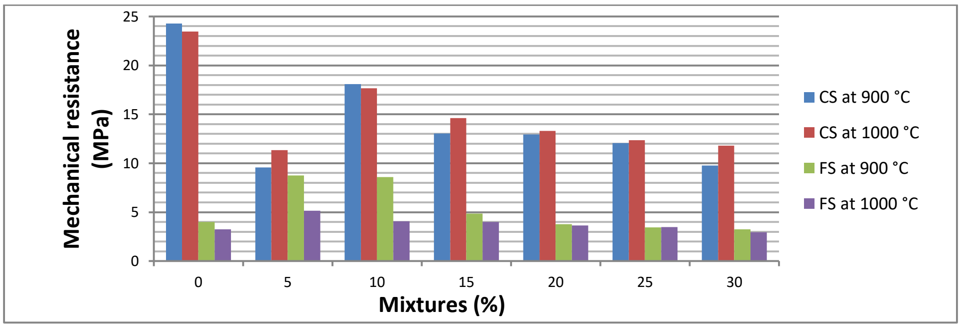

Figure 8 Mechanical resistance of fired clay bricks at 900-1000 °C with 0 to 30 wt% of ZPT's additions (CS: compressive strength; FS: flexural strength)

In contrast, the compressive strength (R_C) varies in a more complex manner, reaching maximum values at 0% and 30% ZPTs, which could indicate a better capacity of the briquettes to support axial loads at these concentrations. At a higher temperature of 1000°C, the downward trend in flexural strength is confirmed, while compressive strength shows more pronounced fluctuations, with peaks observed at 25% and 30% ZPTs. These results highlight the importance of considering both the percentage of ZPTs and the firing temperature in the design of the mixtures to obtain the desired mechanical properties because these parameters significantly influence the ability of the briquettes to resist the different forces and constraints to which they could be subjected in practical applications.

CONCLUSION

The advantage of this research is to reutilise the zinc processing tailings (ZPTs) as a partial replacement in manufacturing clay-fired bricks, an effective alternative treatment for waste resource recycling. It is possible to summarise the experimental findings that ZPTs can partially replace clays in fired clay bricks manufacturing with a percentage of 10% and a firing temperature equal to 900 °C.

ACKNOWLEDGEMENT

"The research presented in this paper was done with the financial support of the Ministry of Science, Technological Development and Innovation of the Republic of Serbia, within the funding of

the scientific research work at the University of Belgrade, Technical Faculty in Bor, according to the contract with registration number 451-03-137/2025-03/200131".

REFERENCES

1. Sun, R., Gao, Y., Yang, Y. (2022) Leaching of heavy metals from lead-zinc mine tailings and the subsequent migration and transformation characteristics in paddy soil. Chemosphere, 291, 132792.
2. Zhou, Y., Duan, X., Chen, T., Yan, B., Li, L. (2021) Mechanical properties and toxicity risks of lead-zinc sulfide tailing-based construction materials. Materials, 14 (11), 2940.
3. Nassiri, O., Rhoujjati, A., Moreno-Jimenez, E., Hachimi, M.L.E. (2023) Environmental and geochemical characteristics of heavy metals in soils around the former mining area of zeïda (high moulouya, Morocco). Water, Air, and Soil Pollution, 234 (2), 110.
4. Doğan-Sağlamtimur, N., Bilgil, A., Szechyńska-Hebda, M., Parzych, S., Hebda, M. (2021) Eco-friendly fired brick produced from industrial ash and natural clay: A study of waste reuse. Materials, 14 (4), 877.
5. Li, R., Yin, Z., Lin, H. (2023) Research status and prospects for the utilisation of lead–zinc tailings as building materials. Buildings, 13 (1), 150.
6. Yaras, A., Sutcu, M., Erdogmus, E., Gencel, O. (2021) Recycling and immobilisation of zinc extraction residue in clay-based brick manufacturing. Journal of Building Engineering, 41, 102421.
7. Long, Z., Sulian, Z., Huaju, M. (2022) Study on the Preparation and Performance of Lead-Zinc Mine Steam-free and Burn-free Brick. Multipurpose Utilization of Mineral Resources, 43 (3), 12-16.
8. Lin, H., Li, R., Li, S. (2024) Fabrication of Lead–Zinc Tailings Sintered Brick and Its Effect Factors Based on an Orthogonal Experiment. Materials, 17(10), 2352.
9. Zhao, T., Zhang, S., Yang, H., Ni, W., Li, J., Zhang, G., Teng, G. (2022) Influence on fine lead–zinc tailings solidified/stabilised by clinker-free slag-based binder. Journal of Environmental Chemical Engineering, 10 (6), 108692.
10. Saedi, A., Jamshidi-Zanjani, A., Darban, A.K., Mohseni, M., Nejati, H. (2022) Utilisation of lead–zinc mine tailings as cement substitutes in concrete construction: Effect of sulfide content. Journal of Building Engineering, 57, 104865.
11. Qu, G., Ge, R., Li, J., Zhang, Y. (2022) Lead-Zinc Tailings-Based Construction Mortars/Preparation, Performance and Stabilization Mechanism of Heavy Metals. Preparation, Performance and Stabilization Mechanism of Heavy Metals.
12. Li, C., Zhang, P., Li, D. (2022) Study on low-cost preparation of glass–ceramic from municipal solid waste incineration (MSWI) fly ash and lead–zinc tailings. Construction and Building Materials, 356, 129231.
13. Zhang, X., Li, L., Hassan, Q.U., Pan, D., Zhu, G. (2023) Preparation and characterisation of glass ceramics synthesised from lead slag and lead-zinc tailings. Ceramics International, 49 (10), 16164-16173.
14. Luo, Z., Guo, J., Liu, X., Mu, Y., Zhang, M., Zhang, M., Tian, C., Ou, J., Mi, J. (2023) Preparation of ceramsite from lead-zinc tailings and coal gangue: Physical properties and solidification of heavy metals. Construction and Building Materials, 368, 130426.
15. Zhang, F., Li, Y., Zhang, J., Gui, X., Zhu, X., Zhao, C. (2022) Effects of slag-based cementitious material on the mechanical behavior and heavy metal immobilisation of mine tailings based cemented paste backfill. Heliyon, 8 (9), e10695.

XVI International Mineral Processing
and Recycling Conference
28-30 May 2025, Belgrade, Serbia

DOI: 10.5937/IMPRC25179B

Original research article

DETERMINATION OF PCB CONCENTRATION IN SOIL

Aleksandra Božić[#]**,** 0000-0002-6790-0287,
Dominik Brkić, 0009-0004-2681-7710,
Marina Stamenović, 0009-0005-7278-6780,
Marija Miletić, 0009-0005-9537-5554,
Academy of Applied Studies Polytechnic, Belgrade, Serbia

ABSTRACT – The environment remains exposed to various pollutants that persist due to their decades-long accumulation. One such substance, no longer produced or legally used, yet still negatively impacting the environment due to past excessive use and accumulation, is polychlorinated biphenyls (PCBs). Their persistence in the environment makes them a significant concern. This study examines soil samples from three different locations to detect the presence of PCBs using gas chromatography. The concentration of PCBs in the analyzed samples was determined using this method, and the obtained values were compared with the legally prescribed maximum allowable concentrations. The results indicate that all measured concentrations are within the permissible limits.

Keywords: PCB, Soil, Chromatography, Environmental Pollution.

INTRODUCTION

Polychlorinated biphenyls (hereinafter: PCBs) are a group of synthetic organic chemicals composed of carbon, hydrogen, and chlorine atoms. They are a group of POPs (Persistent Organic Pollutants), toxic, man-made, hazardous organic chemicals that have dangerous effects on the environment and our health.

Although PCB production was banned or restricted in the late 1980s, their impact on the environment is still present due to their persistent nature. As a result, these compounds can easily enter the food chain, eventually reaching humans and posing serious health risks. PCBs persist in the environment for long periods and can travel over great distances through air, water and migratory species across international boundaries. They accumulate in fatty tissues and bio-magnify higher up in the food chain, where they can be harmful to top predators such as tuna, seals, polar bears and humans [1-3]. Unfortunately, in humans, the concentration of PCBs in fatty tissues is over a hundred times higher than in the food they consume.

There are no known natural sources of PCBs in nature. In the environment, these substances originate exclusively from anthropogenic sources. Sources of polychlorinated biphenyls in soil can result from the deposition of particles and gases from industrial

---

[#] corresponding author: abozic@politehnika.edu.rs activities. Additionally, PCBs can be present in the environment due to the combustion of municipal and industrial waste in incinerators.

Polychlorinated biphenyls have a strong tendency to be absorbed into the soil, where they have a high potential for persistence due to their chemical characteristics. The accumulation of these compounds in the soil can lead to contamination of crops and impact the food chain. Soil is essential for human life, and due to its proximity to people, exposure can occur through the consumption of contaminated food, as well as through ingestion, inhalation, or direct skin contact [4].

PCBs bind strongly to soil particles and are not easily transported deep into the ground by rainwater. Additionally, their degradation in soil is very slow, allowing them to persist for months or even years. The general rule for polychlorinated biphenyls is that the higher the number of chlorine atoms in their molecule, the more difficult and slower their decomposition. The distribution of polychlorinated biphenyls in soil is directly proportional to the organic carbon content in the soil [5-6].

In this study, concentration of PCBs in the three analyzed samples of contaminated soil was determined using method for analyzing and quantifying via GC-ECD (Gas Chromatography-Electron Capture Detector), and the obtained values were compared with the legally prescribed maximum allowable concentrations in soil.

EXPERIMENTAL

In this study, three (1, 2 and 3) samples taken from different locations in Belgrade were analyzed, where the presence of PCBs was considered more or less likely due to the proximity of the car mechanic and company for services motor oils.

The experiment conducted involved analyzing soil samples to determine the presence of polychlorinated biphenyls (PCB 28, 52, 101, 118, 138, 153 and 180). For this specific experiment, three soil samples were used, labeled as follows:

- **1** – Soil sample from a garden
- **2** – Soil sample from the yard of the company "MASS d.o.o." (Trade and services motor oils, spark plugs and cables, filters, brake pads and discs)
- **3** – Soil sample from a residential yard

MATERIALS AND METHODS

Chemicals and Reagents

Acetone (p.a. Fisher UK), *n*-hexane (p.a. Fisher UK), Anhydrous sodium sulfate (p.a. Sigma), Deionized water, Dimethyl Sulfoxide (p.a. Fisher UK), PCB-Mix 100 µg/ml (CPA chem).

Equipment and Instruments

Erlenmeyer flasks, Horizontal shaker (Grant-Bio), ultrasonic bath (Bandelin), 1000 ml separatory funnel, filtration setup, Kuderna-Danish concentrator, Gas chromatograph with an electron capture detector (GC-ECD, Shimatzu GC-2010Pro).

Sample preparation

Three soil samples were collected from different locations in Belgrade. Each sample (10 g) was weighed and placed in an Erlenmeyer flask. Then, 50 ml of acetone was added to the sample and extracted by shaking and sonication for 30 minutes to break up aggregates. After that, 50 ml of hexane was added, and the mixture was sonicated again for at least 1 hour. A horizontal shaker HS 501 digital was used to maximize solvent movement within the sample container (keeping it in a horizontal position). Once the solid particles settled, the supernatant was decanted. The solid phase was then washed with 50 ml of hexane and decanted again.

The extracts were collected in a 1000 ml separatory funnel, and acetone was removed by shaking twice with 400 ml of water. The extract was then dried over anhydrous sodium sulfate, filtered, and rinsed three times with 10 ml of hexane. Finally, the extract was concentrated by evaporation using a Kuderna-Danish concentrator until the final volume was reduced to 3 ml [7].

Chromatographic Conditions for GC-ECD Analysis

The experiment was conducted using a gas chromatograph (GC) equipped with an electron capture detector (ECD). The operating conditions were optimized to ensure effective separation and detection of polychlorinated biphenyls (PCBs).

GC Operating Conditions:

- Separation Column: Capillary column
- Oven Temperature Program:
  - 60°C, hold for 2 min
  - Increase by 30°C/min to 120°C
  - Increase by 5°C/min to 300°C
  - Hold at 300°C for 5 min
- Injector Temperature: 260°C
- Injection Mode: Splitless
  - Injection Volume: 1 µL
  - Splitless Time: 1.8 min
- Carrier Gas: Helium (0.8 mL/min to 1.0 mL/min)

These conditions were selected to optimize the separation of PCBs while ensuring high sensitivity and accuracy in the detection process.

Drying of solid soil samples

Moisture content of samples 1-3 was determined according to the standard SRPS EN 12880:2007 [8]. This European Standard specifies a method for the determination of dry residue and water content of sludges and sludge products. If PCB quantification is planned for the same sample, drying in a ventilated oven at 40°C must not be used. Complete drying of the sample is necessary when using the Soxhlet extraction method. It is also recommended for samples that need to be stored for an extended period [9].

RESULTS AND DISCUSSION

This section presents the results of moisture content and PCB determination. The obtained data are analyzed and discussed to evaluate their significance and accuracy. Table 1 shows the moisture content results for all samples, which are used to calculate the PCB concentration in the dry sample.

Table 1 Moisture content in samples

	Dry residue	Moisture content
Sample 1	86.94%	13.06%
Sample 2	99.34%	0.66%
Sample 3	99.30%	0.7%

The table 2 presents the results of soil analysis for the presence of different types of PCB in Sample 1, 2 and 3. Different retention times (the time a specific component remains in the system) correspond to different concentrations of polychlorinated biphenyls. Some PCB values were recorded as negative, indicating that these compounds were not present in the sample. To compare the results with regulations defining PCB limit values [10], the concentrations in ppm were converted to mg/kg.

Table 2 Soil analysis results for PCB presence in the samples

	Sample 1 (mg/kg)	Sample 2 (mg/kg)	Sample 3 (mg/kg)
PCB-28	0.0108	0.0063	/
PCB-52	0.0108	0.00441	0.0045
PCB-101	0.0135	/	0.017
PCB-118	/	/	0.009
PCB-153	/	/	/
PCB-138	/	/	0.018
PCB-180	/	/	/

As prescribed by the Regulation [10], the permitted PCB concentration in soil is 0.02 mg/kg. Observing the table, it can be seen that all PCB concentrations in soil are below 1 mg/kg, indicating that the values are not at levels that could endanger human health or the environment [10].

CONCLUSION

PCBs can be found in the environment, including water, air, and soil. They have a particular tendency to accumulate in human and animal tissue due to their lipophilic nature. This study examined soil samples suspected of containing polychlorinated biphenyls (PCBs). Gas chromatography was used to detect PCBs, as it provides high accuracy in determining their presence and concentration in the samples.

During sampling and experimentation, safety measures had to be followed to prevent risks to health and safety. Three samples were analyzed, each taken from a different location. Sample 2, collected from the premises of a metalworking company, showed a higher potential for PCB presence due to the possible use of various chemicals containing PCBs.

The analysis confirmed that none of the three tested samples contained PCB concentrations that could pose a risk to human health or the environment. According to the Regulation, the permitted PCB concentration in soil is lower than the maximum allowed concentration (0.02 mg/kg).

REFERENCES

1. A. Vijaya Bhaskar Reddy, M. Moniruzzaman, Tejraj M. Aminabhavi, (2019), Polychlorinated biphenyls (PCBs) in the environment: Recent updates on sampling, pretreatment, cleanup technologies and their analysis, Chemical Engineering Journal, Volume 358, , 1186-1207,
2. Othman N, Ismail Z, Selamat MI, Sheikh Abdul Kadir SH, Shibraumalisi NA, (2022), A Review of Polychlorinated Biphenyls (PCBs) Pollution in the Air: Where and How Much Are We Exposed to Int J Environ Res Public Health. 26;19(21):13923.
3. Jasna Đinović-Stojanović, Jelena Spasić, Aleksandar Popović, Danijela Vranić, Miroslav Nikčević, Aleksandar Hegediš, Dragica Nikolić, (2013), Distribucija organohlornih pesticida i polihlorovanih bifenila u dve vrste riba iz Dunava, Institut za higijenu i tehnologiju mesa br. 54.
4. Kumar B, Verma VK, Singh SK, Kumar S, Sharma CS, Akolkar AB, (2014), Polychlorinated Biphenyls in Residential Soils and their Health Risk and Hazard in an Industrial City in India. J Public Health Res. 1;3(2):252.
5. Safe, S. H. (1994), Polychlorinated Biphenyls (PCBs): Environmental Impact, Biochemical and Toxic Responses, and Implications for Risk Assessment. Critical Reviews in Toxicology, 24(2), 87–149.
6. Characterization of sludges - Determination of dry residue and water content, SRPS EN 12880:2007
7. 3550B from EPA's SW-846 - Ultrasonic Extraction – organic extraction and sample preparation
8. SRPS EN 12880:2007 - Characterization of sludges - Determination of dry residue and water content
9. Pravilnik o listi POPs materija, načinu i postupku za upravljanje POPs otpadom i graničnim vrednostima koncentracija POPs materija koje se odnose na odlaganje otpada koji sadrži ili je kontaminiran POPs materijama („Službeni glasnik RS“, br. 65/2011-21, 17/2017-64)
10. Uredba o graničnim vrednostima zagađujućih, štetnih i opasnih materija u zemljištu “Sl. glasnik RS”, br. 30/2018 i 64/2019. URL: https://www.paragraf.rs/propisi/uredba-granicnim-vrednostima-zagadjujucih-stetnih-opasnih-materija-zemljistu.html(preuzeto: 11.04.2025).

XVI International Mineral Processing
and Recycling Conference
28-30 May 2025, Belgrade, Serbia

DOI: 10.5937/IMPRC25184M Original research article

ENVIRONMENTAL IMPACT WITH THE GREENHOUSE GASES AND AIR POLLUTANT PREDICTION BY DRILLING AND BLASTING WORKS

Stefan Milanović[1,#], 0000-0003-4761-8716,
Nikola Simić[1], 0000-0002-7823-5868,
Lazar Kričak[1], 0000-0002-4253-7020,
Milanka Negovanović[1], 0000-0001-7882-4585,
Miljan Gomilanović[2], 0000-0002-1209-7423,
Nikola Đokić[3], 0009-0005-0871-9903,
[1]Faculty of Mining and Geology, University of Belgrade, Belgrade, Serbia
[2]Mining and Metallurgy Institute Bor, Bor, Serbia
[3]IGM Mladost, Leskovac, Serbia

ABSTRACT – During drilling and blasting in rocks, there is an emission of certain gases, such as CO_2, CO, NOx, etc. With the development of technology and the application of modern software available on the market today, it is possible to control the level of gas emissions, analyse their impact on the environment, and predict gas emissions produced by drilling and blasting. This paper will present the possibility of analysing and controlling gas emissions using the O-PitEco software, a product of the O-PitBlast company. Importing the parameters of drilling and blasting, as well as using the database of the software itself (technical characteristics of explosives, initiation systems, etc.), it is possible to control and analyse the results, as well as predict the environmental impact. The software offers overview data in the form of various diagrams, statistically processed data and the possibility of printing all the results in the form of an overview report. With the development of modern technologies, monitoring systems and the possibility of predicting certain segments in the mining field have significantly improved. In that case, there is the possibility of correcting certain parameters during the design of drilling and blasting works, to obtain the best possible effect of rock fragmentation with minimal emissions of harmful gases, which contributes to the reduced environmental impact.

Keywords: Greenhouse Gas (GHG), Modern Technologies, O-PitEco, Environmental Impact, Air Pollutants.

INTRODUCTION

In drilling operations, the main goal of equipment selection is to achieve maximum production output with minimum costs and environmental impact. During drilling, the main environmental problems are related to air pollutants (particulate matter PM_{10}, total suspended particulate matter TSP, carbon dioxide CO_2, carbon monoxide CO, nitrogen oxides NO_x, sulfur oxides SO_x and volatile organic compounds VOCs) [1].

During blasting, a considerable amount of gases is released, if the decomposition is

---

[#] corresponding author: stefan.milanovic@rgf.bg.ac.rs carried out during a normal explosion, then the produced gases are: nitrogen, carbon dioxide, water vapour and possibly smaller amounts of oxygen. In addition to the chemical composition of explosives, which influences the composition of gas products after blasting, also depends on blasting conditions, explosive cartridge plastic film, the physical characteristics of explosives, rock characteristics, stemming, etc. Harmful gases can also appear in the explosive decomposition products, such as carbon dioxide CO_2, carbon monoxide CO, nitrogen oxides; nitrogen monoxide NO and nitrogen dioxide N_2O, then sulfur gases; hydrogen sulphide H_2S and sulfur dioxide SO_2 [2].

Drilling and blasting operations must be well optimized to prevent negative impacts, where one of the negative impacts is the emission of harmful gases during drilling and blasting, i.e. environmental impact. Modern software for optimizing drilling and blasting parameters can be used for optimization to improve the effects of blasting and reduce the negative impact that occurs after blasting. Software that can be used for analysis, control and prediction of emissions of harmful gases during drilling and blasting is O-PitEco, a product of the company O-Pitblast [3]. O-PitEco is software designed to analyze, predict, and control emissions of GHG and air pollutants in mining operations. This software estimates the environmental impact of drill and blast activities and provides tools to minimise it [4].

GREENHOUSE GASES (GHG) AND AIR POLLUTANT

Greenhouse gases (GHGs) are gases in the atmosphere that raise the Earth's surface temperature, and what distinguishes them from other gases is that they absorb wavelengths of radiation emitted by the planet, resulting in the greenhouse effect [5]. GHG include seven gases: carbon dioxide (CO_2), methane (CH_4), nitrous oxide (N_2O), chlorofluorocarbons (CFCs), hydrofluorocarbons (HFCs), perfluorocarbons (PFCs), sulphur hexafluoride (SF_6) and nitrogen trifluoride (NF_3) [6]. Figure 1 shows the global emission of GHG gases by different economic sectors.

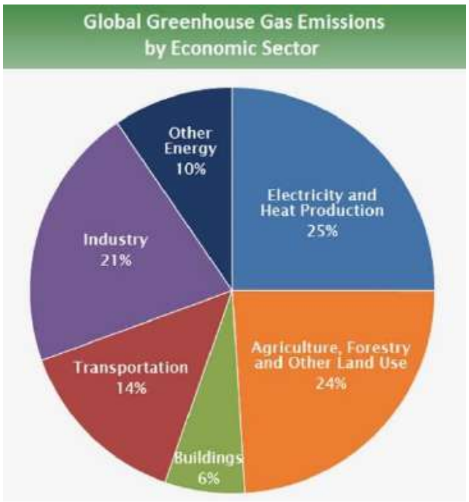

Figure 1 Global greenhouse gas emissions by economic sector [7]

Air pollutants are harmful to human health the environment and biodiversity. They can cause a range of adverse health outcomes for humans, including the risk of respiratory infections, heart disease and lung cancer. Air pollution also has an impact on biodiversity and the condition of the environment [8]. These pollutants are generally collected in two subgroups gaseous (SO_2, NO_x, HC, CO, CO_2) and dust (smoke, metallic smoke, fly ash, mist, aerosols) [9]. Some emissions of the main air pollutants are shown in Figure 2.

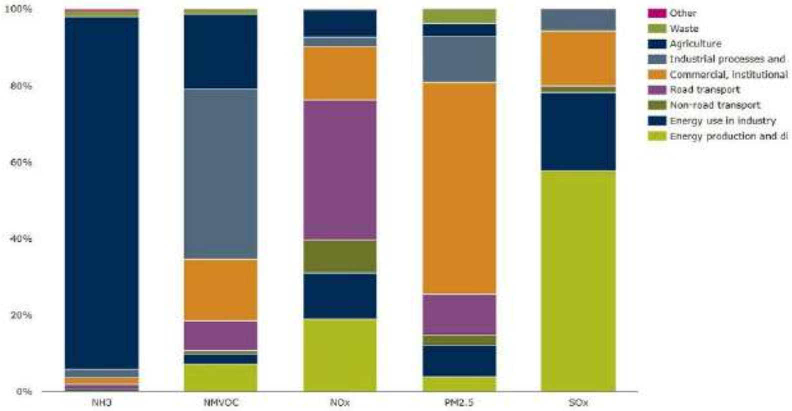

Figure 2 Emissions of the main air pollutants by sector group (NH_3: ammonia; NMVOCs: non-methane volatile organic compounds, such as benzene, ethanol, etc. NO_x: nitrogen oxides is a generic term for the mono-nitrogen oxides NO and NO_2; $PM_{2.5}$: fine particular matter consists of fine particles with a diameter of 2.5 micrometres or less; SO_x: sulphur oxides is a term that refers to many types of sulphur- and oxygen-containing components (SO, SO_2, SO_3, S_7O_2, S_6O_2, S_2O_7, etc.)) [10]

INPUT DATA FOR ANALYSIS

Rock properties

For the analysis, control and prediction of gas emissions during drilling and blasting for this paper, we use data from the quarry, where we have certain characteristics of the rock mass and projected drilling and blasting parameters. The characteristics of the working environment are shown in the following Table 1, where we have given the physical and mechanical properties of limestone.

Table 1 Rock mass properties

Rock mass	**Limestone**
Density (g/cm^3)	2.66
Compressive strength (MPa)	79
Velocity of P-wave (m/s)	3 500

Drilling and blasting parameters

Drilling and blasting parameters were done using O-Pitblast software, which is used to optimise drilling and blasting work. The design of the parameters was done in the software to obtain the best possible results in terms of fragmentation, with a minimum negative impact as possible during blasting. We exported the parameters designed in this way and presented the data in Table 2, to use them in the O-PitEco software and perform analysis and prediction of harmful gas emissions.

Table 2 Designed drilling and blasting parameters

Parameters	Value
Number of blastholes	114
Volume of production	22 572 m^3
Diameter of borehole	89 mm
Burden	3.3 m
Spacing	4 m
Subdrilling	0.5 m
Stemming	3 m
Bench height	15 m

Parameters in O-PitEco software

The development of specialised software in the area of drilling and blasting made it possible to optimize parameters while achieving the best possible blasting results and reducing the negative environmental impact. Digitisation is one of the biggest vectors of change in the industrial sector, particularly in the mining sector. Digital optimisation tools can dramatically increase the productivity and sustainability of drilling and blasting operations [10].

Imported parameters for analysis and evaluation are shown in the following Figure 3, where the software for the entered parameters has an additional database with a description of the amount of gas emissions during: production, transportation, charging and detonation.

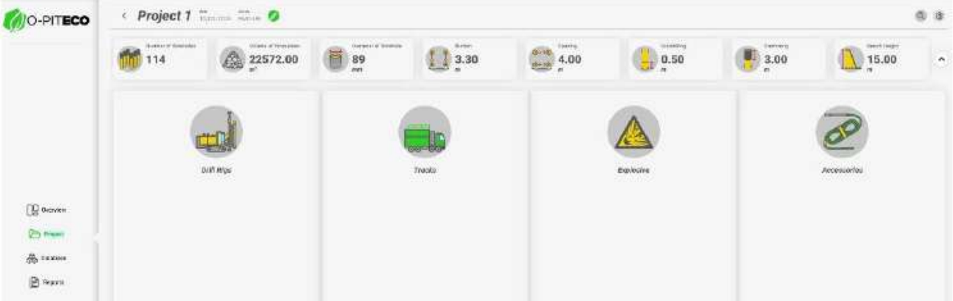

Figure 3 Drilling and blasting parameters imported in O-PitEco

RESULTS AND DISCUSSION

The software analysis used the drilling and blasting parameters shown in Table 1, while the database from the software itself was used for emission assessment or prediction. The database already has various characteristics, such as the technical characteristics of the explosives, where in this case emulsion cartridge explosives were used in combination with ANFO explosives with non-electric initiation systems. In this case of analysis, the emission of gases from the explosives and the assessment of which segment has the greatest impact on the environment will be shown. The following Figure 4 graphically shows the results based on the entered drilling and blasting parameters for the environmental impact (example for CO_2 emissions in kg).

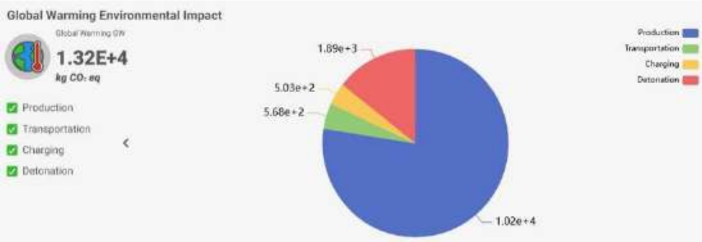

☑ Production
☑ Transportation
☑ Charging
☑ Detonation

Figure 4 Result of emission from O-PitEco for CO_2

After analyzing the entered drilling and blasting parameters, we have a diagram that shows the emission of harmful gases during blasting and the emissions for all segments as production, detonation, charging, and transportation of explosives. Where the amount of CO_2 total emissions is 13,200 kg, or by segments 1,890 kg during detonation, 503 kg for charging 568 kg for transportation, and 10,200 kg for production. Based on the analysis and the presented diagram for the emission of CO_2, we can see that of the mentioned processes, the most emissions occur during the production of explosives, followed by detonation and much less emissions during transportation and charging. For detonation calculated emission software for CO is 20.5 kg and for nitrogen oxides (NO_x) is 0.000182 kg, where this amount can be reduced by reducing drilling and blasting parameters.

CONCLUSION

Based on the application of the O-PitEco software, which is presented in this paper, it is possible to analyze and assess the impact, that is, the amount of gases during drilling and blasting. The application of such software can significantly contribute to the analysis and assessment of the impact on the environment in mining, but also to the prediction of emissions during the optimization of various drilling and blasting parameters. Changing various parameters in the optimization software, as well as by applying different types of explosives can be corrected in terms of emissions of harmful gases before blasting itself.

In addition to the presented emission assessment for CO_2, CO and NO_x, for explosives and how much each segment affects the amount of gas emissions, other analyses are possible. Impact assessment during drilling operations is one of the processes that can also be analyzed, as well as the impact during the application of mechanized vehicles for charging blastholes.

In terms of environmental protection, this kind of software can be very important, because recently the topic of emission of harmful gases and particles, which are dangerous to human health, in this case, gases as products of blasting or emission of GHG gases that affect global warming, is very current. The need for these and similar software tools will probably continue to grow and their development will certainly progress.

ACKNOWLEDGEMENT

The authors thank the Serbian Ministry of Education, Science, and Technological Development for their support and the funds provided under contract no. 451-03-136/2025-03/200126.

REFERENCES

1. Lashari A., Kecojević V. (2013) Assessment of Environmental Impact of Drilling Equipment, Journal of Powder Metallurgy & Mining, S1: 007.
2. Purtić N. (1991) Bušenje i miniranje, Rudarsko-Geološki fakultet, Beograd.
3. O-Pitblast - Rethinking the Drill & Blast Industry (2025), https://www.opitblast.com/ [Online] Available from: [Accessed 13/02/2025].
4. Green House Gas Emissions – O-PitEco (2025), https://www.o-pitblast.com/products/green-house-gas-emissions-o-piteco [Online] Available from: [Accessed 13/02/2025].
5. Climate Change 2021 – The Physical Science Basis Working Group I Contribution to the Sixth Assessment Report of the Intergovernmental Panel on Climate Change, pp. 2215-2256.
6. OECD - Air and GHG Emissions (2022), https://www.oecd.org/en/data/indicators/air-and-ghg-emissions.html [Online] Available from: [Accessed 18/02/2025].
7. EPA – Global Emission by Economic Sector (2010), https://19january2017snapshot.epa.gov/ghgemissions/global-greenhouse-gas-emissions-data_.html [Online] Available from: [Accessed 18/02/2025].
8. European Commission – Emissions of greenhouse gases and air pollutants (2025), https://ec.europa.eu/eurostat/web/environment/information-data/emissions-greenhouse-gases-air-pollutants [Online] Available from: [Accessed 18/02/2025].
9. Airqoon – Greenhouse Gases and Air Pollution, https://airqoon.com/resources/articles/greenhouse-gases-and-air-pollution/ [Online] Available from: [Accessed 18/02/2025].
10. EEA – Emission of the main air pollutants by sector group in the EEA-33, https://www.eea.europa.eu/en/analysis/maps-and-charts/share-of-eea-33-emissions-5 [Online] Available from: [Accessed 18/02/2025].
11. Kiala A., Saraiva B., Barbosa F., Leite F., Kouvonen T., Miranda V. (2023), A new approach to emission control in rock drilling and blasting, 12th World Conference of Explosive and Blasting, Dublin, Ireland, pp. 16-25, https://online.fliphtml5.com/kiig/ekgp/#p=1.

XVI International Mineral Processing
and Recycling Conference
28-30 May 2025, Belgrade, Serbia

DOI: 10.5937/IMPRC25190M

Research article

LANDFILL FOR COMBUSTION PRODUCTS FROM THE KOSTOLAC THERMOELECTRON

Dragan Milošević[#], 0000-0003-3714-1950,
Jasmina Nešković, 0000-0002-1798-1656,
Pavle Stjepanović, 0000-0003-2243-4232,
Svetlana Polavder, 0000-0002-5661-1578
Mining Institute Ltd. Belgrade, Serbia

ABSTRACT – The implementation of measures and activities aimed at preserving the environment is preceded by the categorization of products created by the application of technological processes. The emission of harmful substances within the limit prescribed values is defined by the valid legislation of the Republic of Serbia. The development of project documentation for the disposal of ash, slag and gypsum from the technological process of flue gas desulphurization (FGD) must be based on the application of modern technologies in order to preserve the surrounding ecosystem. The planning of the landfill space for the accommodation of combustion and desulfurization products requires the analysis of all input parameters of the technological process of electricity production. The use of ash, slag and gypsum as products of the production process of thermal power plants is not adequately accepted in the domestic industry. The role of new technologies should be directed towards the greatest possible utilization of stored products in order to produce new products, thus preserving mineral resources and protecting the conditions of the living environment.

Keywords: Ash, Slag, FGD Gypsum, Landfill.

INTRODUCTION

Combustion of coal in the process of electricity production results in the creation of various substances such as ash, slag, SOx, NOx, CO_2, waste water and synthetic gypsum. For this purpose, categorization is carried out, based on which the conditions of waste treatment and management are defined. Each of these materials falls into specific categories according to legislation, but also according to their nature, potential danger and possibilities for further use. Ash and slag generated in thermal power plants belong to specific types of industrial waste that are treated in accordance with their chemical composition and possible impact on the environment. Ash and slag from thermal power plants are characterized as hazardous waste if they contain heavy metals, such as cadmium, lead, arsenic or other toxic substances. Otherwise, it is classified as non-hazardous waste.

In the technological process of flue gas purification in power plants, limestone is used as a reagent, and the obtained gypsum is a unique synthetic product dominated by calcium sulfate. FGD gypsum has a wide range of possible applications: in the production

---

[#] corresponding author: dragan.milosevic@ribeograd.ac.rs of cement, it improves the properties of acidic soil, reduces erosion and promotes stabilization, in the production of artificial glass, in the application of drainage, then in the production of sawdust boards, as well as in road construction. The storage of ash, slag and gypsum requires landfill space, such that in the event of the need for their market application, a favorable possibility of taking them is provided. Ash, slag and gypsum from thermal power plants are industrial waste, which can be significantly recycled and used in various industries, provided they do not contain hazardous chemicals or heavy metals. Management of these materials must comply with environmental and waste legislation, paying attention to potential risks to health and the environment. Key guidelines for waste management include: conducting analyzes to determine the level of hazardous substances [2], recycling and reuse when possible and defining the technological procedure of material disposal / depositing.

LEGAL REGULATION FOR THE DISPOSAL OF ASH, SLAG AND GYPSUM WASTE

For the disposal of by-products from thermal power plants, the legislation of the Republic of Serbia includes both waste management and specific guidelines for hazardous and non-hazardous types of waste, which are based on the protection of the environment and the safety and health of people. In the Republic of Serbia and the EU, regulations are largely aligned with international standards, such as EU directives and the Convention on Transboundary Movement of Hazardous Waste. The Law on Waste Management is the basis for the treatment of ash, slag and gypsum from thermal power plants. Their classification is carried out according to the Rulebook on categories, testing and classification of waste. The basic guidelines for preserving natural resources and reducing pollution, including waste management, are regulated by the Law on Environmental Protection. As part of the negotiations for the Republic of Serbia's accession to the EU, the process of establishing a waste management system with the Waste Management Program in the Republic of Serbia has begun. The regulation on waste management in the European Union includes directives related to hazardous and non-hazardous waste, but also to the management of waste from industrial processes, such as thermal power plants. These are: Waste Directive, Landfill Directive, Industrial Emissions Directive, Mining Waste Management Directive. In order to preserve the environment and natural resources, as the conditions regarding the accommodation and storage of this type of by-products are defined, the conditions for the treatment and use of ash, slag and ODG gypsum in the industrial sphere should also be introduced through legislation. By reducing the need for landfill space, storage costs are also eliminated. Based on the above, it is necessary to develop and implement appropriate laws, standards and regulations that enable the safe and efficient use of these materials.

FORMATION OF LANDFILL SPACE

The construction of the landfill space is defined on the basis of: production capacity, construction parameters of the cassette, physical and mechanical characteristics of the substrate, specifications of the equipment provided for the disposal / depositing of material, analysis of the results of the landfill substrate, characteristics of the material, the orientation of the cassette, the position from which the material is taken, transport routes, accessibility of the location in the function of providing materials for market needs, etc. Design solutions for the selection of locations for the placement of ash, slag and FGD gypsum should be based on the conditions defined by legislation and in accordance with the principles of environmental protection. The selection of high-quality project solutions is the result of multiple analyzes and opinions, respectively project solutions from several technical and technological areas [5]. One of the conditions for defining the choice of accommodation location should be oriented in the direction of market research with the targeted formation of accessibility of cassettes to market conditions, figure 1. The modeling of the space is in accordance with the conditions that characterize surface mines and internal landfills with the basic goal of environmental protection.

Figure 1 Spatial location in the area of the thermal power plant for the accommodation of coal (1) and FGD gypsum (2)

After the end of the deposition, permanent closure and recultivation are carried out [3]. The closing of the cassettes includes preparatory works on filling and leveling in the projected slope for the formation of the upper covering layer prescribed by the Regulation on waste disposal. Technical reclamation includes a series of technical measures to give gypsum landfills and excavated areas such a form, which will ensure the ecologically favorable integration of these areas into the existing environment and create conditions for biological reclamation. Permanent stabilization, arrangement and matching with the landscape characteristics of the surrounding terrain precedes the establishment of ecological balance.

LANDFILL SPACE OF THE KOSTOLAC THERMAL ENERGY COMPLEX

The production of electricity in the Kostolac power plants is carried out in four blocks, namely: thermal power plant "Kostolac A1 and A2" and thermal power plant "Kostolac B1 and B2". In the beginning, the landfill "Middle Kostola Island" was formed for the purpose of storing ashes, with an area of about 70 ha, figure 2 and 3, and then it was expanded to about 240 ha. According to the planning documentation, the closure of the landfill is planned to be carried out gradually until 2017. But, due to the failure to provide a replacement accommodation space, the landfill still remains active.

After the reconstruction of the system of collection, transport and disposal of ash and slag from the blocks of the thermal power plant "Kostolac B", the location of the future landfill, the internal disposal site of the surface mine "Ćirikovac", was defined, figure 2 and 4. With the completion of the necessary infrastructure facilities, the landfill became active in 2010. As part of the repurposing of the open pit mine "Ćirikovac" and its internal disposal site, the entire area of the exploitation field was leveled with shaping of the slopes and depressions of the open pit mine.

The formation of this landfill originally meant the disposal of ash and slag only for the needs of the thermal power plant "Kostolac B", so that in the middle of 2016, the hydromix from the blocks of the thermal plant "Kostolac A" was also deposited in the storage area of the surface mine "Ćirikovac". The technological procedure of depositing is carried out through the distribution pipeline and the formed protrusions in stages, into the prepared storage area. It includes the planning of the foundation, the installation of a waterproof barrier, the superstructure of the barrier embankment and the evacuation organs of underground and process water. The transport pipeline from the thermal power plant "Kostolac B" to the landfill is about 5 km long, while the length of the transport from the thermal power plant "Kostolac A" to the landfill at the internal disposal site of the "Ćirikovac" surface mine is about 5.2 km. Currently, the "Drmno" surface mine provides coal production for the installed thermal energy capacities in Kostolac and Drmno. In addition to tailings disposal, ash, slag and FGD gypsum are also deposited on part of the internal disposal area, figure 2 (position 3) and 5. The basic guidelines for the formation of a landfill area for the accommodation of FGD gypsum at the internal landfill of the "Drmno" surface mine are based on the Spatial Plan of the Special Purpose Area of the Kostolac Coal Basin [1].

Figure 2 The position of landfill sites in the area of Kostolac (Source: Google earth) TE – The location of the thermal power plant in Kostolac ($TE_{(K)}$) and Drmno ($TE_{(D)}$); 1 – Ash and slag landfill "Middle Kostolac island"; 2 – Ash and slag landfill at open pit "Ćirikovac"; 3 – Ash, slag and gypsum landfills at the "Drmno" surface mine

Figure 3 Ash and slag landfill "Middle Kostolac island" (Source: RI archive)

Figure 4 Ash and slag landfill at open pit "Ćirikovac" (Source: Google earth)

Figure 5 Ash, slag and gypsum landfills at the "Drmno" surface mine (Source: RI archive)

The process of disposal of FGD gypsum is a linear transport process, which takes place with a system of conveyor belts from a closed warehouse to a landfill. Process management is performed remotely from the command center or locally during equipment service [4].

CONCLUSION

Design solutions for the construction of landfills for the storage of ash, slag and FGD gypsum must be coordinated with the "Spatial Plan of Special Purpose Areas". Environmental conditions of landfill sites can be characterized as complex due to the existence of populated areas. Expert analysis, opinions and adopted conceptual solutions must in any case be the basis of the principles of project development. Orientation is the objectives of the Project Assignment. All changes and deviations of the performed works in relation to the designed ones, it is necessary to complete them with applied solutions and performed works, documented and accompanied by monitoring, which includes technical observation of the landfill facility and monitoring of the impact of the landfill on the environment.

What needs special attention is the fact that these by-products are not used nearly enough in the construction industry of the Republic of Serbia, although they can become an important part of the national circular economy. Bearing in mind the produced quantities of these materials, as well as the possibility of their application, it is necessary to ensure participation in the highest possible percentage. In this way, the need for storage space would be reduced, the construction of which, with the provision and fulfillment of many conditions, requires significant material investments.

In order to simplify the use of by-products instead of storage, it is necessary for the relevant ministry with the help of the state to encourage on the one hand the producers and on the other the potential buyers of the by-products, through various legal incentives and possible subsidies, to follow the example of developed European countries, to use these materials in production and replacement to a certain extent of the raw material basis.

REFERENCES

1. Milošević D., Technical Mining Project of Transportation and Disposal of Gypsum from the Procedure of Flue Gas Desulpurification of Thermal Power Plant Kostolac B1 and B2 in the First Cassette at the Internal Landfill of the Drmno Surface Mine, Mining Institute Belgrade, 2015.
2. Praštalo Ž., Milošević D., Nešković J., Stjepanović P., Designing and planning of areas affected by surface dislocations at the open pits, Mining and Metallurgy Engineering, pp 19-24, Bor 2/2016.
3. Šubaranović T., Pavlović N., Technical solution for the reclamation of the Ugljevik East 1 surface mine and landfill, Mining and Geology Today International Symposium, pp. 251-260, 18 – 20. September 2017., Belgrade, ISBN 978-86-82673-13-2.
4. Kostović N., Technical Mining Project of Providing Space for the Expansion of the Landfill for the Disposal of Gypsum at the Drmno Open Mine for the Needs of the Kostolac Thermal Power Plant B1 and B2, Mining Institute Belgrade, 2021.
5. Nešković J., Hydration of newly synthesized belite cement with mineral additives, Technical Faculty in Bor, University of Belgrade, doctoral dissertation, 2024.

XVI International Mineral Processing
and Recycling Conference
28-30 May 2025, Belgrade, Serbia

DOI: 10.5937/IMPRC25196A Original research article

EVALUATION OF MINERAL PROCESSING AND METALLURGICAL PLANTS WASTES

Fatma Arslan, 0000-0001-7620-1165,
Gülay Bulut[#], 0000-0001-7016-8077,
Istanbul Technical University, Mining Faculty, Mineral Processing Engineering Department, Istanbul, Turkey

ABSTRACT – The mining process generates substantial waste containing various amounts of valuable metals. The conventional method for the disposal of waste is usually dumping. Mineral processing, pyrometallurgical, hydrometallurgical, and pyro-hydrometallurgical processes are applied to recover these metallic values. This study provides examples of studies conducted on evaluating wastes from some mineral processing and metallurgical plants in Turkey. Evaluation studies on mineral processing tailings such as iron, boron, and chromite, together with copper smelting and refining slags, are summarized. Related flow sheets developed as a result of experimental studies are also presented.

Keywords: Mining Plant Wastes, Mineral Processing Tailings, Metallurgical Slags.

INTRODUCTION

Mining waste includes the materials that are moved to gain access to minerals and the tailings, slags, and residues that result from the processing of the materials. During the production of metals from concentrates through the pyrometallurgical route, different types of products are accumulated and also contain considerable amounts of metallic values besides base metals.

The traditional method of waste disposal typically involves dumping. The increased dump of tailings not only occupies plenty of land, but also wastes resources and can potentially have an impact on the environment due to water pollution. Therefore, recovery of metals from the wastes and utilization of the wastes are important not only for saving metallic resources, but also for protecting the environment. Several processes used for the evaluation of such wastes are physical separation, flotation, and leaching. Thus, natural resources would be utilized more efficiently from the economic and environmental viewpoints.

EVALUATIONS OF WASTES

Some examples on the processing of mineral processing and metallurgical plant wastes from Turkey are presented in the following:

[#] corresponding author: gbulut@itu.edu.tr

Boron Tailings

As reported by Kistler & Helvacı [1] one of the few countries that have large resources of boron minerals is Turkey with five boron beneficiation plants. Various grades and fractions of concentrates of tincal, colemanite, kernite and ulexite are obtained from these plants [2]. Boron is beneficiated using scrubbing, washing, and classification following the size reduction step. Significant amounts of tailings and fines are generated as a result of the mining and processing steps, respectively. The fine fraction, classically less than 3mm is discharged to a tailing dam with associated process water, and this is a main cause of important storage problems and environmental pollution. Every year almost 600,000 tons of boron-containing fine clay tailings are produced in Boron Concentrator Plant in Turkey.

Processing techniques of boron minerals are generally related to the type of ore, the scale of the operation, and the type of the end product. Various dry (magnetic separation, pneumatic tabling, electrostatic separation, calcination) and wet (scrubbing and washing), jigging, tabling, flotation) concentration methods have been used alone or in combination [2].

All the boron minerals are floated using cationic and anionic collectors from tailings [3,4,5]. Some studies found that the scrubbing and flotation combination is an effective method to produce boron concentrate. For example, in a study, a colemanite tailings sample taken from a tailings pond was treated using scrubbing + screening followed by flotation to recover the lost boron. As a result of the experimental studies, a concentrate containing 44.5% B_2O_3 was produced with 68.4% B_2O_3 recovery [5].

Chromite Tailings

Turkey is an important producer in the world metallurgical-grade, high-chrome chromite market [6]. The chromite deposits are usually small in size, and chromite is generally concentrated by gravity methods such as shaking tables in mineral processing plants. The total amount of fine chromite gravity tailings in Turkey is around 3,000,000 tons with a quite high Cr_2O_3 content of about 9-20%. These fines are produced as a result of the inefficiency of conventional separation equipment at fine particle size due to finely grained feed and optimization problems [7].

According to a study using the Jones HIWMS (High intensity wet magnetic separation) followed by column flotation for minus 0.1 mm chromite tailings, a concentrate assaying 47.7% Cr_2O_3 could be obtained with a recovery of 66.4%. A tailings containing 5.84% Cr_2O_3 is discharged. Based on these studies, a flowsheet was developed, and a pilot plant was established to recover chromite from the tailings [8, 9]. The simple flowsheet of the pilot plant is given in Figure 1.

Iron Tailings

Iron ore tailings have become one of the most hazardous solid waste. In the Sivas-Divriği Iron Ore Concentrator, which is the biggest in Turkey, the total 600, 000 tons of tailings have been discarded annually. Huge amounts of tailings have already been deposited in ponds and stockpiles from previous production activities. Istanbul Technical University (ITU) researches on Divriği iron tailings [10-13]. included a detailed study on mineralogy, beneficiation, and feasibility. As a result of these researches, a general flowsheet was proposed which is given in Figure 2. According to this flowsheet, after grinding of tailings, flotation, sulphatizing roasting of coarse concentrate, and leaching of calcine with sulphuric acid, the recovery of Co, Ni, and Cu from solution with H_2S precipitation. Also iron was recovered from the coarse flotation tailing with magnetic separation. Applying this flowsheet makes it possible to produce CoS, NiS, and CuS precipitates along with iron concentrate from the iron tailings.

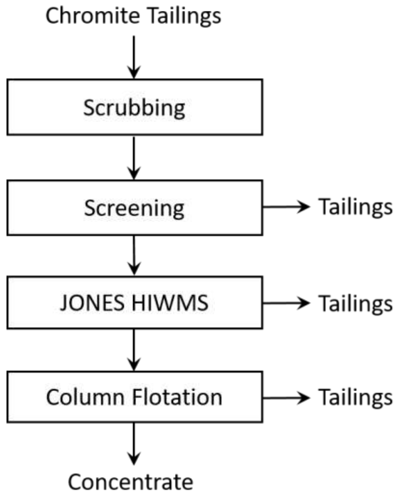

Figure 1 The pilot plant flowsheet of Üçköprü chromite tailings

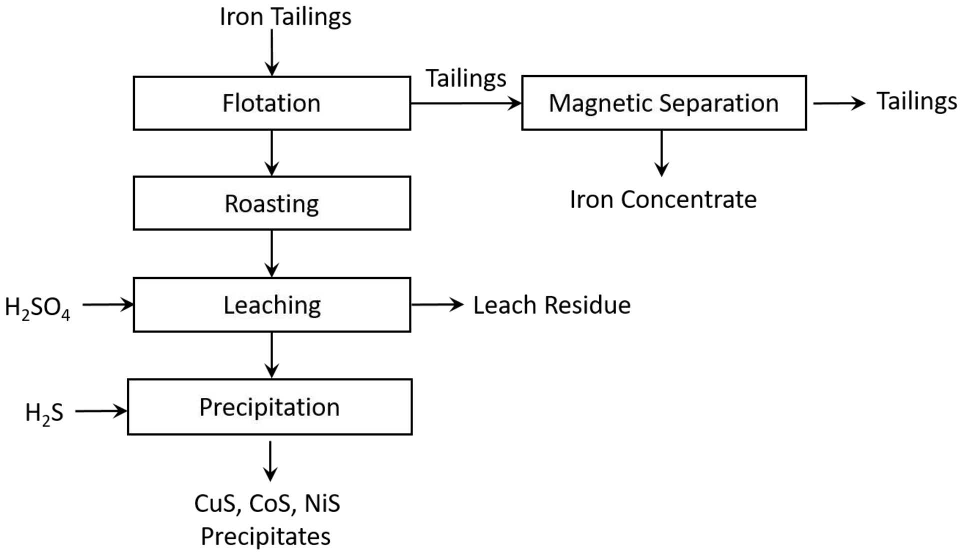

Figure 2 A proposal flowsheet for Divriği iron tailings

Copper Slags

During the production of metallic copper from copper concentrates and rafination of blister copper through a pyrometallurgical route, different products (slags, dusts, fumes, etc.) are accumulated and they contain considerable amounts of metallic values besides copper [14,15]. Mineral processing, pyro-, hydro-, and pyro-hydrometallurgical processes are applied to recover these values [14]. The flotation process plays an important role in the beneficiation of metal values from slags and is utilized in many copper smelting processes**.** In principle, copper slag flotation is the same as sulfide ore flotation [14, 16-18]. This means that only metallic Cu and sulfide minerals can be floated effectively. Because in some slags Cu occurs in the oxide form (Co is in homogenous distribution) and is disseminated in small amounts in the slag matrix, the application of flotation to copper slag processing could be limited, and the flotation method will not be effective for the recovery of Co, Ni and oxide Cu. Therefore, roasting and leaching processes need to be applied. Metals from leach liquors can be recovered by solvent extraction, precipitation, and electrolysis.

A study has been conducted on the recovery of copper, cobalt, and zinc from copper smelter and converter slags by roasting with sulfuric acid. Acid roasting of slags followed by hot water leaching was carried out to bring the metal values into solution. A total of 88% of copper, 87% of cobalt, 93% of zinc, and 83% of iron were extracted in 2 h of roasting at 150 °C and 3:1 acid/slag ratio [19]. The other study, 20 a combination process, such as flotation + roasting with pyrite + leaching (Figure 3).

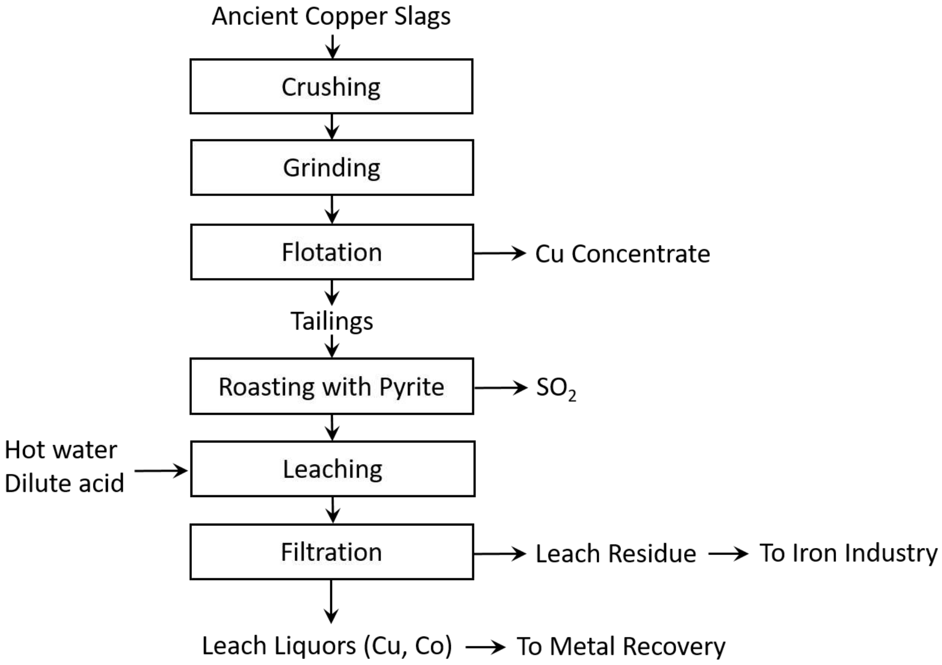

Figure 3 Proposed flowsheet for the evaluation of Küre ancient copper slag

CONCLUSION

In Turkey, 26 million tons of tailings are produced every year after mineral processing works. a lot of research has been done about the evaluation of tailings, there is no serious investment in this area because of still obtaining valuable metals from the potentially available reserves. In the future, evaluation of these tailings will be inevitable. All research about mineral tailings such as boron, chromite and iron, which are the subject of this paper, showed that tailings still contain valuable minerals that need to be explored. As a result, these tailings must be re-concentrated before using other purposes such as ceramics, cement, construction, and landfill.

REFERENCES

1. Kistler, R.B., Helvacı, C. (1994). Boron and borates, In: D.D. Carr (Ed.): Industrial Minerals and Rocks, 6th edition, Littleton, CO, Society for Mining, Metallurgy and Exploration Inc., pp. 171–186.
2. Özbayoğlu, G. (2006). Beneficiation of boron minerals. In: Önal, G., Acarkan, N., Çelik, M.S., Arslan, F., Ateşok, F., Güney, A., Sirkeci, A.A., Yüce, A.E., Perek, K.T.P. (eds.): Proceeding of the XXIII International Mineral Processing Congress, İstanbul- Turkey, 3-8 September, Promed Advertising Agency, Istanbul, Volume 2, pp. 1053-1062.
3. Bulut G**.,** Ören, E., Acarkan, N., Bakan S. (2004). A flotation study into the re-concentration of tincal tailings. In: Akar, A., İpekoğlu, Ü., Cöcen, İ., Polat, M. (Eds), Proceedings of the Xth International Mineral Processing Symposium, Üç Adım Matbaa-Reklam Ltd. Şti., 5-7 October Çeşme, İzmir, pp 253-263.
4. Gül, A.**,** Bulut, G., Tarkan H. M., Kaytaz, Y. (2001). Benefication of Colemanite Tailings. In: Barbosa, J.P., Dutra, A. B.J., Melamed, R., Trindade, R., B. E.(Eds.): Proceedings of VI Southern Hemisphare Meeting on Minerals Technology, CETEM, MTC, 27-31 May, Rio de Janeiro, Brasil, pp. 189-193.
5. Gül, A., Kaytaz, Y., Önal, G. (2006). Beneficiation of colemanite tailings by attrition and flotation. Minerals Engineering 19, 368–369.
6. Yiğit, Ö. (2011). Mineral Exploration: What, where and why in Turkey. Mining Sector, Mining & Earth Sciences Magazine, 1, 13-19.
7. Çiçek, T., Cöcen, İ. (2002). Applicability of Mozley multigravity separator (MGS) to fine chromite tailings of Turkish chromite concentrating plants, Minerals Engineering, 15, 91–93 (Technical note).
8. ITU Project, (2000). Evaluation of Etibank Üçköprü chromium old tailings, building of a research pilot plant with 5 ton/h capacity (Germany GBR, ETI Holding, ITU Foundation).
9. ITU Project, (2002). Optimizaton of Karagedik research pilot plant (Germany GBR, ETI Holding, ITU Foundation).
10. ITU Project, (1992). Beneficiation and feasibility study of Divriği iron ore concentration plant tailings in pilot scale, İTÜ, Mining Faculty, İstanbul.
11. ITU Project, (2004). Evaluation and feasibility study of Divriği iron ore concentration plant tailings, İTÜ, Mining Faculty, İstanbul.
12. Açma, E., Oktaybaş, C., Arslan, F., Addemir, O., Acarkan, N., and Önal, G. (1993). Recovery of copper, cobalt and nickel from Divrigi sulfide concentrates. In: Reddy R. G. & R. Weizenbach, N. (Eds): The Paul E. Queneau International Symposium Extractive Metallurgy of Copper, Nickel and Cobalt, Vol. I: Fundamental Aspects, Reno, NV, USA, The Minerals, Metals & Material Society, pp. 1269–1295.

13. Sirkeci; A. A., Gül; A., Bulut; G, Arslan; F., Önal; G., Yüce, A.E., (2006). Recovery of Co, Ni, and Cu from the tailings of Divriği iron ore concentrator, Mineral Processing and Extractive Metallurgy Review: An International Journal, 27, 131–141.
14. Arslan, F., K. Giray, K., ÖnaL, G., Gürkan, V., 2002. Development of a Flowsheet for Recovering Copper and Tin from Copper Refining Slags, The European Journal of Mineral Processing and Environmental Protection, Vol. 2, No. 2, 1303-0868, pp. 94-10.
15. Arslan, F., Giray, Ç., Öztürk, A., Orhan, G., Arslan, C., Kangal, O., (2006), Evaluation of copper refining fumace dusts, IMPC 2006, Proceedings of 23rd International Mineral Processing Congress, Istanbul Technical University, pp. 1505-1510.
16. Osborn, G. A., Garner F. A., and Veasey, T. J., (1986). Recovery of metal values from secondary copper slags, Proceedings of the 1*st* International Mineral Processing Symposium, Izmir, Turkey, 29 September-1 October, pp. 46-64.
17. Bulut, G., (2006). Recovery of copper and cobalt from ancient slag, Waste Management & Research, Vol. 24, pp.118-124.
18. Bruckard, W.J., Somerville, M., and Hao, F., (2004). The recovery of copper, by flotation, from calcium-ferrite-based slags made in continuous pilot plant smelting trials, Minerals Engineering, Vol. 17, pp. 495-504.
19. Arslan C., Arslan, F., (2002). Recovery of copper, cobalt, and zinc from copper smelter and converter slags, Hydrometallurgy, 67 1-7.
20. Bulut, G., Perek, K. T., Gül A., Arslan, F., Önal, G., (2007). Recovery of metal values from copper slags by flotation and roasting with pyrite, SMI, Mineral and Metallurgical Processing Journal (and Transactions), Vol.24. No.1, February, pp.13-18.

XVI International Mineral Processing
and Recycling Conference
28-30 May 2025, Belgrade, Serbia

DOI: 10.5937/IMPRC25202G

Original research article

BENEFICIATION OF MINERAL ORES USING TRIBO-ELECTROSTATIC SEPARATOR

Abhishek Gupta[#], 0009-0006-6153-9124,
Tom Newman, 0009-0008-9066-1350,
Frank Hrach, 0009-0006-0840-743X,
ST Equipment & Technology, Needham, MA, USA

ABSTRACT – ST Equipment & Technology (STET) has developed a tribo-electrostatic belt separator for mineral ore beneficiation, eliminating the need for water or chemical additives. This technology has been successfully scaled for diverse industrial applications, including the removal of unburnt carbon from fly ash, separation of silicates from calcite, magnesite from talc, and silicates from barite. STET's electrostatic separation technology offers an efficient and environmentally sustainable alternative to conventional minerals processing methods. The paper presents pilot-scale test results highlighting the technology's effectiveness in upgrading ultrafine iron ore, which is typically discarded as tailings, as well as a coarser air-classified iron ore sample.

Keywords: Electrostatic Separation, Tailings, Dry Beneficiation.

INTRODUCTION

Iron ore processing

Iron ore is one of the most important raw materials in the world and iron ore processing is one of the essential industrial processes. As the high-grade (>60% Fe content) iron ore deposits degrade, beneficiation of low-grade (<60% Fe content) deposits becomes essential to meet the quality requirements of the steel industry and maximizing ore utilization [1].

Wet magnetic separation is typically used in beneficiation of iron ores, utilizing the differences in magnetic properties of the ore components for separation of iron bearing minerals from gangue minerals. Wet low-intensity magnetic separators (LIMS) are widely used to process ores with strong magnetic susceptibility such as magnetite, whereas wet high-intensity magnetic separation (WHIMS) is used for ores with relatively weak magnetic susceptibilities such as hematite and goethite [2]. One of the challenges in magnetic separation is lower separation efficiency of fines particles, especially <20 micron because in this size range the liquid drag forces tend to be greater than the magnetic forces [3]. Flotation is another widely used process to beneficiate iron ores using either direct anionic flotation of iron oxides and reverse anionic or cationic flotation of quartz. However, the presence of fines poses a challenge, and de-sliming is conducted to remove fines (< 20 micron) to increase the effectiveness of flotation [4].

[#] corresponding author: agupta@steqtech.com

Both magnetic and flotation processes face challenges in processing fine iron ore, and typically these fines are rejected as wet tailings. Proper disposal of these tailings has become an environmental concern [5]. In addition, both processes demand large amounts of water and require wastewater processing.

STET tribo-electrostatic separator

A notable advancement in dry mineral separation is the STET tribo-electrostatic belt separator (Figure 1), which has extended the effective particle size range to finer particles. Tribo-electrostatic separation leverages electrical charge differences generated by surface contact, or triboelectric charging, between two materials. In this process, the material with a higher electron affinity acquires electrons, becoming negatively charged, while the material with lower electron affinity becomes positively charged. This differential charging enables efficient separation of mixed particles using an electric field.

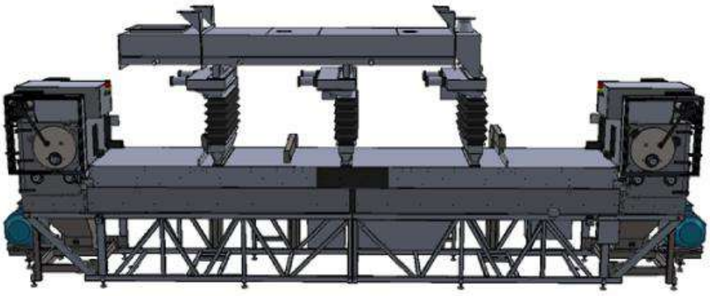

Figure 1 Model of STET separator

Material is fed into a thin gap (0.9–1.5 cm) between two parallel planar electrodes (Figure 2) charged up to +/- 10 kV, where particles acquire opposite charges through interparticle collisions. These charged particles are carried by a high-speed, continuous-loop, open-mesh belt toward opposite ends of the separator, guided by their attraction to electrodes of the opposite charge. The counter-current flow of particles and continual triboelectric charging enable multi-stage separation, achieving high purity and recovery.

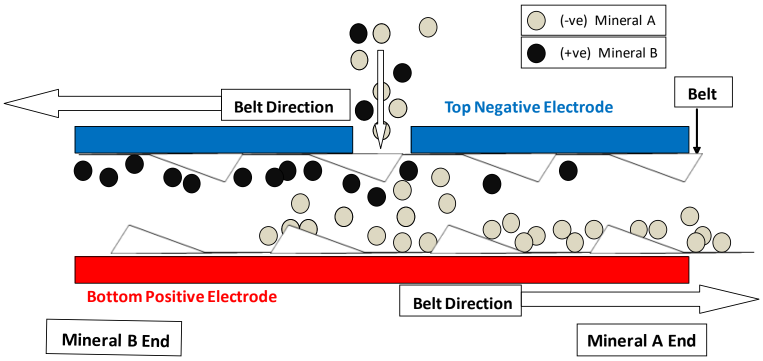

Figure 2 Schematic of separaton zone within the electrodes

Capable of processing up to 40 tons per hour, the compact STET separator measures 9.1 m long, 1.7 m wide, and 3.2 m high, with a power consumption of approximately 1 kWh per ton of material processed. This innovative technology has broadened the applicability of dry separation methods, offering a promising alternative for fine particle beneficiation. In this paper, STET tribo-electrostatic belt separation is presented as a possible beneficiation technology to upgrade iron ore.

EXPERIMENTAL

Materials

Two samples of iron ore were collected from iron ore processing plants in Brazil, and tested using a pilot-scale STET separator.

1. Ultrafine sample: This sample was the reject stream from a magnetic separation process, as the fines pose challenges in efficiency of magnetic separation.
2. Air-classified sample: This sample was collected from an air-classification step as fines.

The elemental composition was analyzed using a wavelength dispersive X-ray Fluorescence (WD-XRF) instrument and mineralogy was studied with the XRD (X-ray diffraction) technique. The loss on ignition (LOI) was determined by igniting a sample in a 1000 ºC furnace for 60 minutes and reporting the weight loss. Particle size distribution analysis (PSD) was conducted using a laser diffraction particle size analyzer - Malvern Mastersizer 3000 E.

The mineralogy of the samples is provided in Table 1. Hematite is the primary iron-bearing mineral in both samples, quartz and kaolinite being the primary gangue minerals. The elemental composition of the samples is shown in Table 2. Particle size distribution and moisture content of the samples is shown in Table 3. Samples were dried at 90 C prior to testing in the separator.

Table 1 Mineralogy of iron ore samples

Sample	Hematite	Goethite	Quartz	Kaolinite
Ultrafines	50.8%	17.9%	12.5%	18.5%
Air-classified	50.6%	3.4%	40.9%	3.5%

Table 2 Elemental composition (major elements) for iron ore samples

Sample	Al_2O_3	Fe_2O_3	Fe*	SiO_2	LOI
Ultrafines	7.7	66.0	46.2	20.8	4.3
Air-classified	2.2	59.7	41.8	*36.6*	1.0

*Calculated using stoichiometric relationship between Fe_2O_3 and Fe

Table 3 Particle size distribution for iron ore samples

Sample	Particle size distribution				Moisture content
	D_{10}	D_{50}	D_{90}	D_{98}	
Ultrafines	1 µm	4 µm	11 µm	16 µm	<0.2%
Air-classified	7 µm	32 µm	105 µm	215 µm	<0.2%

Method

Testing was conducted with the goals of enhancing concentration and minimizing the presence of gangue minerals, and to study effect of separator variables (Table 4) on product grade and mass yields. Pilot-scale testing is essential for evaluating separation performance at commercially viable feed rates and optimizing separator and feed variables for processing.

Table 4 Separator variables

Variables	Levels			Units
Belt speed	5	20		meter per second
Electrode gap	10	13		mm
Electrode voltage	6	10		kV
Feed port	1	2	3	
Top electrode polarity	Positive	Negative		

Tests were performed on the separators under batch conditions. Prior to each test, a small sub-sample of the feed material (referred to as "Feed") was collected. At the conclusion of each experiment, samples were collected, and the weights of the two product streams - designated as "Product E1" and "Product E2" were measured. In this setup, "Product E1" represents the gangue-rich product, while "Product E2" corresponds to the mineral-rich product. For each set of sub-samples (Feed, Product E1, Product E2), major elemental composition was analyzed using X-ray fluorescence (XRF).

RESULTS AND DISCUSSION

Air-classified iron ore

Optimization of separator variables was conducted, and three processing schemes were developed targeting a range of product grades. The feed grade was approx. 42% Fe content.

Scheme 1 involves a rougher stage followed by a cleaner stage, yielding a high-grade product with approximately 62% Fe content. The cleaner by-product is recycled and blended with the fresh feed. This scheme achieved an overall mass yield of 61% and a Fe recovery of 90%.

Scheme 2 involves only a rougher stage yielding a mid-grade product with approximately 57% Fe content. Additionally, a scavenger run was performed, with its product blended with the rougher stage output. This scheme achieved an overall mass yield of 67% and an Fe recovery of 91%.

Scheme 3 involves producing a high-grade product at the rougher stage and then a scavenger stage was used to increase overall recovery. The scavenger product was blended with the fresh feed. This scheme achieved an overall mass yield of 46% and a Fe recovery of 68%.

Table 5 summarizes the findings from air-classified iron ore testing, presenting the range of product grades achieved along with their corresponding mass yields and Fe recoveries.

Table 5 Summary of results from air-classified iron ore

Scheme	Product mass yield	Fe recovery	Product Fe content
1. High grade product (using rougher + cleaner)	60.9%	90.1%	61.8%
2. Mid grade product (using rougher + scavenger)	66.8%	90.8%	56.8%
3. High grade product (using rougher + scavenger)	46.1%	67.5%	61.1%

Air-classified iron ore

Similar optimization of separator variables was conducted, and processing schemes were developed targeting a range of product grades. The feed grade was approx. 46% Fe content.

Scheme 1 involves a rougher stage followed by a cleaner stage, yielding a high-grade product with approximately 59% Fe content. Additionally, a scavenger run was performed, with its product blended with the rougher stage output. The cleaner by-product is recycled and blended with the fresh feed. This scheme achieved an overall mass yield of 32% and a Fe recovery of 59%.

Scheme2 involves only a rougher stage, yielding a mid-grade product with approximately 55% Fe content. Additionally, a scavenger run was performed, with its product blended with the rougher stage output. This scheme achieved an overall mass yield of 55% and a Fe recovery of 66%.

Table 6 Summary of results from ultrafine iron ore

Scheme	Product mass yield	Fe recovery	Product Fe content
1. High grade product (using rougher + scavenger + cleaner)	31.9%	40.8%	59.2%
2. Mid grade product (using rougher + scavenger)	54.9%	65.9%	55.4%
3. Low grade product (using rougher + scavenger)	73.8%	82.3%	51.5%

By changing the belt speed and feed port of the separator, a low-grade product scheme was developed (Scheme 3) resulting in product grade of 51% Fe. Testing involved a rougher stage, and a scavenger run with its product blended with the rougher stage output. This scheme achieved an overall mass yield of 74% and a Fe recovery of 82%.

Table 6 summarizes the findings from air-classified iron ore testing, presenting the range of product grades achieved along with their corresponding mass yields and Fe recoveries.

CONCLUSION

The STET tribo-electrostatic belt separator provides an innovative, dry-processing alternative for mineral beneficiation, overcoming key challenges associated with conventional wet separation methods. Unlike traditional processes, this technology efficiently processes ultrafine particles while eliminating the need for excessive water consumption and mitigating environmental concerns related to wet tailings disposal.

This report presents pilot-scale results demonstrating the separator's effectiveness in upgrading iron ore. By adjusting separator variables, the system enabled the production of a range of product grades using difference processing schemes, while optimizing mass yield and Fe recovery.

These findings underscore the tribo-electrostatic separator's potential to enhance sustainable mineral processing by reducing waste, conserving critical resources, and promoting more efficient beneficiation practices.

REFERENCES

1. Levich B. (2021) Understanding the high-grade iron ore market. https://pearlgulliron.com.au/wp-content/uploads/2021/09/Understanding_the_high-grade_iron_ore_market_Fastmarkets.pdf (Feb 21, 2025).
2. Xiong, L. Lu, R.J. Homes. (2015). Chapter Title: Development in the physical separation of iron ore: magnetic separation. In: Iron ore - Mineralogy, Processing and Environmental Sustainibilty (L. Lu). Woodhead Publishing. 283-307.
3. Subrata Roy (2012). Recovery Improvement of Fine Magnetic Particles by Floc Magnetic Separation, Mineral Processing and Extractive Metallurgy Review: An International Journal, 33:3, 170-179.
4. L.O. Filippov, V.V. Severov, I.V. Filippova. (2014). An overview of the beneficiation of iron ores via reverse cationic flotation. International Journal of Mineral Processing, 127, 62–69.
5. F.L. Da Silva, F.G.S. Araujo, M.P. Teixeira, R.C. Gomes, F.L. von Kruger. (2014). Study of the recovery and recycling of tailings from the concentration of iron ore for the production of ceramic. Ceramics International, 40 (10), 16085-16089.

XVI International Mineral Processing
and Recycling Conference
28-30 May 2025, Belgrade, Serbia

DOI: 10.5937/IMPRC25208A Original research article

THE SELECTION OF APPLICATION MODES OF AGENTS MODIFYING DIAMOND SPECTRAL CHARACTERISTICS IN THE PROCESS OF X-RAY LUMINESCENCE SEPARATION

Valentin Alexeyevich Chanturia[1], 0000-0002-4410-8182,
Valeriy Valentinovich Morozov[2#], 0000-0003-4105-944X,
Galina Petrovna Dvoichenkova[1], 0000-0003-3637-7929,
Elena Leonidovna Chanturia[2], 0000-0002-5757-4799,
[1]Institute of Comprehensive Exploitation of Mineral Resources of Russian Academy of Sciences, Moscow, Russian Federation
[2]National University of Science and Technology "MISIS", Moscow, Russian Federation

ABSTRACT – The problem of choosing the optimal composition and conditions for processing diamond-kimberlite products with phosphor-containing reagents and modifiers has been solved. To solve the problem, the patterns of interaction of the organic collector with the surface of diamond crystals and kimberlite grains were determined and the necessary reagents – regulators were selected. The optimal phase composition and temperature conditions for the use of modifier reagents have been determined. The approbation of the selected processing modes has shown their effectiveness, providing increased diamond recovery during X-ray luminescent separation.

Keywords: Diamonds, Kimberlite, X-Ray Luminescence, Luminophores, Modifier.

INTRODUCTION

A promising way to solve the problem of recovery weakly and anomalously luminescent diamonds in X-ray luminescence separation is the use of state-of-the art technologies for optimizing the spectral characteristics of diamonds with luminophore-containing modifying agents [1]. The condition for the effectiveness of the applied technology is the maintenance of maximum differences in the level of luminophores fixation on diamonds and kimberlite minerals [2].

The purpose of this study was to increase the selectivity of fixing the modifier reagent on diamonds and kimberlite. To solve this problem, it is necessary to determine and maintain the optimal composition of the organic collector, to select the temperature conditions of modifying agent application and to use agent-regulators of interaction between the organic collector and the surface of diamond crystals and kimberlite grains [3].

[#] corresponding author: dchmggu@mail.ru

EXPERIMENTAL

Natural diamond crystals lost in the process of X-ray luminescence separation and kimberlite grains with a grain size of 1.5 to 3 mm, which correspond to the industrial range (Fig.1 a, b), were used for the research and testing.

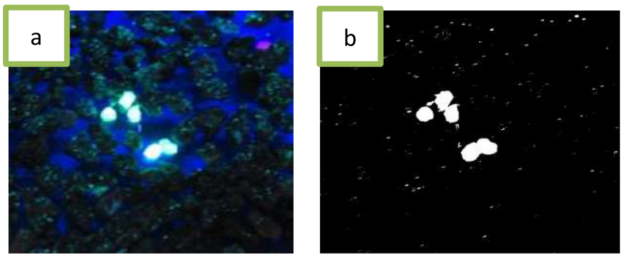

Figure 1 Natural weakly luminescent diamonds testing after treatment with agent in a) ultraviolet range; b) by visiometric analysis

In the preparation of the modifying agent, a hydrophobized inorganic luminophore was mixed with an organic collector. The obtained composition was dispersed in industrial water with additives of special dispersing agents. The obtained emulsion of the luminophore composition was fed into the installation for treatment of diamond-containing material (Fig. 2).

Figure 2 Installation for treatment of diamond-containing material with luminophore-containing composition (view from the side of material washing and unloading)

Excess emulsion after regeneration was returned to the emulsion preparation unit. The diamond-kimberlite product after removal of the emulsion was washed with industrial water (Fig. 2). After treatment and washing, the diamond-containing material was sent to a separator for diamond extraction using the amplitude-kinetic separation method. The luminophore-containing composition fixed on the diamond surface generates an optical signal in the range of 400-580 nm with the required spectral and kinetic characteristics, which ensures the extraction of weakly luminescent diamond crystals into the concentrate. To assess the luminophore fixation selectivity, we used the method of visiometric analysis of mineral surface coverage with luminophores using images obtained with a Renishaw InVia Raman confocal microscope with a 365 nm laser.

RESULTS AND DISCUSSION

Substantiation of methods for increasing the effectiveness of luminophore fixation on diamonds

Media temperature control is commonly used to regulate the fixation of organic apolar collectors on minerals [4]. Another technique to improve the stability of luminophore fixation on diamond surface is combining a high-viscosity collector and low molecular weight solvents. The mechanism of improving luminophore fixation is the increase in viscosity and the hysteresis component of the holding force after the low molecular weight solvent is transferred to the aqueous phase.

The studies of the effect of the modifying agent application temperature conditions included heating of the water-agent emulsion with maintaining the temperature of 35-40 °C in the medium of the diamond-containing material treatment and subsequent washing of the material at the temperature of 15-20 °C. Heating of the emulsion strengthens of the luminophore composition fixation on diamonds for all compositions of an organic collector and decreases the concentration of luminophore on the kimberlite mineral surface.

Table 1 Results of visiometric analysis of the effect of temperature conditions and collector composition on the effectiveness of luminophore fixation

No.	Organic collector composition	Temperature, °C					
		15	20	25	30	35	40
		Coverage of diamond surface with luminophore, %					
1	CCHGO (Cat cracking heavy gas oil)*	27.0	29.2	31.5	32.0	31.5	29.7
2	DTF	22.0	24.2	27.5	28.0	26.9	25.7
3	CCHGO (85%), DTF (15%)	27.4	31.4	33.0	32.1	31.2	28.7
4	CCHGO (90%), EMK (10%)	30.5	33.4	33.5	31.7	30.8	29.4
Kimberlite minerals surface coverage with luminophore, %							
1	CCHGO	3.0	3.8	4.3	4.0	2.1	1.5
2	DTF	4.6	5.3	5.0	4.6	2.8	2.3
3	CCHGO (85%), DTF (15%)	3.1	3.5	3.3	2.8	2.0	1.5
4	CCHGO (90%), EMK (10%)	2.7	2.9	3.0	2.9	2.5	2.1

*CCHGO is catalytic cracking heavy gas oil; DTF is diesel technical-grade fraction, EMK - ethyl methyl ketone

The selected temperature conditions with the emulsion heating and temperature decrease in washing process stage, as well as the use of compound collectors of the proposed composition provide stable fixation of luminophores on diamonds (the surface concentration more than 15%) while ensuring the selectivity of the separation (the surface concentration on the kimberlite mineral surface was less than 3%).

The basic process parameters of the diamond spectral and kinetic characteristics selective modification modes are the characteristics of a modifying agent: the ratio of luminophore/collector; the ratio of collector/aqueous phase, and the concentration of a dispersing agent. To determine the optimal composition of a modifying agent, the second-order factorial experiment method was used. The initial factorial experiment matrix (second-order orthogonal central composite design) was compiled according to the standard technique with the addition of zero and star points. The experimental array consisted of 15 experiments.

To reduce the optimization problem to a one-parameter one, the criterion "Selectivity of luminophore fixation on diamonds and kimberlite" (SLF_{DK}) was applied, calculated by the following equation:

$$SLF_{\mathrm{DK}} = (C_{\mathrm{LD}})/15 - (C_{\mathrm{LK}})/3 \qquad (1)$$

where C_{LD} - surface concentration of luminophores on diamond; C_{LK} - surface concentration of luminophores on kimberlite. The physical essence of the criterion is the uniform accounting of the deviations of the surface concentrations from the boundary values (3 and 15%).

The results of the mathematical processing of the experimental results in Excel environment using the second-order factorial experiment allowed determining the area of optimal ratios between the components of the MLA-3 modifying agent in the working emulsion: the ratio of water/collector of 80:1 - 100:1, the ratio of collector/ luminophore of 9:1.

The optimal concentration of sodium hexametaphosphate (HMF) at the selected values of the modifying agent emulsion parameters is 1.5 g/l.

Tests of X-ray luminescence separation with the use of modification with luminophore-containing agents

The effectiveness of the selected mode was tested using aqueous emulsion of modifying agents based on luminophores (FL-530), anthracene (MLA-1 and MLA-2), and E-515–115-G5 (MLA-3) [3] with the addition of sodium hexametaphosphate (as dispersing agent) to the aqueous phase with the selected ratios of the luminophores, a collector, and aqueous phase.

The testing results demonstrated high selectivity of the RLS of diamond-containing products in the tests of all modifying agents and treatment modes, confirmed by high recovery (ε) of diamonds (90 - 100%) with complete yield of kimberlite into the tailings (Table 2).

The visiometric method confirmed intensive fixation of the luminophore-containing compositions on both types of diamonds (the coverage degree of 15.5 - 17.0 %) when using a composition based on FL-515-125 luminophore (Fig. 3).

Table 2 Spectral and kinetic characteristics and recovery of diamonds and kimberlite in the testing separation process

Conditions	Mineral	kinetic parameters of the signal				ε, %
		Convolution	Tau, ms.	A_{SC}, mV	K_A	
No treatment	A1	0	50	56	0	0
	A2	0.01	0.8	422	35.6	0
	K	n.m.	n.m.	<50	n.m.	0
With treatment (average of six tests)	A1	0.13	2.33	305.67	8.10	90
	A2	0.17	2.33	902.50	6.03	100
	K	n.m.	n.m.	<50	n.m.	0.9

A1 - weakly luminescent diamonds, A2 - anomalously luminescent diamonds, K - kimberlite; n.m. - parameter is not measured due to A_{SC} value is beyond the measurement range

Figure 3 Fixation of luminophore-containing composition MLA-3 (E-515-115+CCHGO+DTF) on weakly luminescent (a), anomalously luminescent (b) diamonds, and a kimberlite grain (c)

The obtained results of the tests and the analysis of recovered diamonds fully correspond to the data of laboratory studies and show the feasibility of achieving the degree of diamonds coating with luminophores of more than 15% and their complete recovery in the process of X-ray luminescence separation.

CONCLUSION

The optimal phase composition and temperature conditions for the use of reagents modifiers of spectral and kinetic characteristics of diamonds have been determined. Testing of the selected modes has shown the possibility of increasing diamond extraction during X-ray luminescent separation.

REFERENCES

1. Chanturiya, V.A., Morozov, V.V., Dvoichenkova, G.P., Chanturiya, E.L. (2023) Selection of reagent compositions for modifying spectral characteristics of weakly and anomalously luminescent diamonds in the process of x-ray luminescence separation. Journal of Mining and Metallurgy, 59 A (1), 49-60.

2. Morozov, V.V., Chanturia, V.A., Dvoichenkova, G.P., Chanturia, E.L., Podkamenny, Y.A.. (2023) Selecting Organic Collectors for Luminophore-Bearing Modifying Agents to Extract Weakly Fluorescent Diamonds. Journal of Mining Science. 59, 292-301.
3. Chanturia, V.A., Morozov, V.V., Dvoichenkova, G.P., Podkamenny, Yu.S., Timofeev, A.S. (2023) Optimization of composition and conditions of application of means/agents for modifying spectral characteristics of diamonds in the process of X-ray luminescence separation. Gornye Nauki I Tekhnologii [Mining Sciences and Technologies], 8 (4), 313-326 (in Russian).
4. Morozov, V.V., Kovalenko, E.G., Dvoichenkova, G.P., Pestryak, I.V., Lezova, S.P. (2022) Selection of collector composition and temperature conditions for diamond foam separation. Journal of Mining and Metallurgy, 58 A (1), 21 – 28.

XVI International Mineral Processing
and Recycling Conference
28-30 May 2025, Belgrade, Serbia

DOI: 10.5937/IMPRC25214V Original research article

UP-TO-DATE METHODS AND TECHNOLOGIES FOR IMPROVING THE PERFORMANCE OF FOAM SEPARATION OF DIAMOND-BEARING KIMBERLITES

Valeriy Valentinovich Morozov[1#], 0000-0003-4105-944X,
Galina Petrovna Dvoichenkova[2], 0000-0003-3637-7929,
Irina Vasilyevna Pestryak[1], 0000-0002-1745-6579,
Valentina Anatolyevna Chut-Dy[2], 0009-0003-8081-5866,
[1]National University of Science and Technology “MISIS”, Moscow, Russian Federation
[2]Institute of Comprehensive Exploitation of Mineral Resources of Russian Academy of Sciences, Moscow, Russian Federation

ABSTRACT – The mechanism of stable hydrophobization of diamonds by asphaltene-resin cut fraction of fuel oils used as collectors for foam separation was considered. The use of special additives to collectors providing their active and strong fixation on a diamond surface was substantiated. It was proposed to use combined modes of ore and recycled water conditioning by acoustic, thermal, and reagent methods to restore the natural hydrophobicity of diamonds to increase their floatability. A technological mode of foam separation was developed, including thermal treatment of an initial diamond-containing product and maintenance of the required temperature in the conditioning with a collector, foam separation, and flotation. The developed reagents and modes were tested at a foam separation unit. The test results showed an increase in diamond recovery over a wide range of temperatures.

Keywords: Diamonds, Kimberlite, Foam separation, Conditioning, Reagents.

INTRODUCTION

One of the promising areas for increasing the output of fine diamond size classes is their recovery from kimberlites using the method of foam separation. The relevance of the foam separation and flotation process is due to the fact that it enables achieving extraction of -2 + 0.5 mm size class, in which more than 40% of the total quantity of diamonds contained in the ore is concentrated, which constitute up to 10% of the value of all the commercial products. At the same time, the recovery rate of small diamonds remains insufficiently high. Increasing the efficiency of a foam separation cycle can be achieved by optimizing the composition of collectors, using methods to restore the natural hydrophobicity of diamonds, selecting the temperature conditions of conditioning and flotation processes, and improving water recycling conditions [1,2]. The problem set is particularly relevant at low temperatures. For its solution the application

---

[#] corresponding author: dchmggu@mail.ru

of modified collectors with additives of diesel technological fraction (DTF) and aliphatic ketones was proposed. To restore natural floatability of diamonds it is advisable to use modifying agents of different composition. To achieve the required performance and stability of the foam separation production cycle, a reasonable choice of rational scheme and conditions of water recycling in the foam separation cycle, involving the maintenance of the optimal recycled water proportion and applying purification of water products from slurry, is required.

EXPERIMENTAL

A dynamic technique for evaluating the fixation of apolar collectors on minerals including the measurement of wetting angles (Θ) and wetting perimeter diameter (Dwet) was applied in the studies.

An extraction-spectrophotometric technique was used to measure the distribution of a collector (γc) between the products and phases of a flotation test. To investigate the fixation of the collector on diamonds, the method of optical microscopy on a Micromed-3-LUM microscope was used. The collector's viscosity was measured on an SV-10 vibrating viscometer.

The collecting properties of the studied collectors in relation to diamonds were tested using a Hallimond tube, a foamless flotation cell.

Ultrasonic treatment of pulp was performed using the IL100-6/1 unit. Thermal and reagent treatments were carried out in a thermostatic cell. The approbation of the modified collectors performance under the selected temperature conditions was carried out at the LFM-001S foam separation unit.

RESULTS AND DISCUSSION

The fuel oils used in diamond flotation are not optimal collectors by their composition, so it is advisable to modify their composition in order to improve the technological performance of the foam separation process. Based on the findings of historical studies, to increase the collecting ability of M-40 and F-5 fuel oils, it was proposed to change the asphaltene-resin cut fraction (ARCF) from the coarse-dispersed state into colloidal solution by adding light distillates [3] or by increasing the medium temperature [2, 4]. A promising approach to solving this problem is to modify the base collector by adding bisoluble organic compounds, for example, a number of ketones, which simultaneously ensure the autodispersing process [3].

In order to test the hypothesis of a decisive contribution of ARCF to improving diamond floatability, the studies of fixation of a collector of different composition on the diamond surface were carried out. M-40 fuel oil, diesel technical-grade fraction (DTF), and modified collectors based on M-40 fuel oil were selected as base collectors: M-40-20 (20% DTF)% , KSM-1 (20% DTF + 15% DEK); KSM-2 (20% DTF + 15% EMK); KSM-3 (20% DTF + 15% DMK) obtained by dilution of M-40 fuel oil with diesel technological fraction (DTF) and solvents of ketone group, diethyl ketone (DEK), ethyl methyl ketone (EMK), and dimethyl ketone (DMK). The additives to the base reagents were selected taking into account the historical research findings [3].

Our tests showed that the highest wetting angle (Θ) was measured for a DTF drop (Table 1, test 1). For the modified M-40 fuel oil, the wetting angle characterizing the adhesive ability of a collector, is 3.5 - 9.6 degrees less (tests 3-6).

Table 1 Parameters of collector fixation and foamless diamond flotation process

No.	Collector used	Θ, deg	η, mPa s (T °C)	D_{wet}, mm	$γ_c$, %	$ε_{diam}$, %
1	DTF	101.1	3.4-4.0 (25 °C)	2.5	34	48.3
2	M-40 fuel oil	84.5	59.1 -78.0 (80 °C)	4.4	45	68.4
3	M-40-20	91.5	18.6-22.3 (25 °C)	4.0	61	78.6
4	KSM-1	93.4	12.5-14 (25 °C)	3.9	82	92.2
5	KSM-2	97.9	10.5-12.5 (25 °C)	3.5	87	92.5
6	KSM-3	98.6	8.1-10.0 (25 °C)	2.9	80	88.7

The collector consisting of DTF, despite good wetting ability towards diamonds, does not demonstrate the best performance in terms of the parameters "Share of collector on diamonds" and "Diamond recovery $ε_{diam}$" (Table 1). However, for DTF, a significantly smaller diameter of the wetting perimeter of a droplet fixed on a diamond was established (Table 1). This result characterizes the tendency of low-viscosity DTF droplets to transition from the mineral-water interface to the air-water interface and decreasing the hydrophobicity of a diamond.

Comparison of the findings of these flotation tests and the data of physicochemical studies allows concluding that the best results are obtained when using collectors with a high wetting angle and a sufficiently high dynamic viscosity (η). It is these physicochemical characteristics of the collector that ensure its fast and stable fixation on diamonds.

To confirm the contribution of ARCF to an apolar collector fixation efficiency, the images of diamonds before and after the conditioning and flotation processes were obtained using combined optical microscopy (Fig. 1a, b). As a result of interaction with the collector, the floatated diamonds are covered with an almost continuous layer of the collector (Fig. 1b). After washing of medium molecular weight fuel oil fractions with carbon tetrachloride, the areas with color characteristics typical for ARCF were preserved on the diamond surface (Fig. 1c).

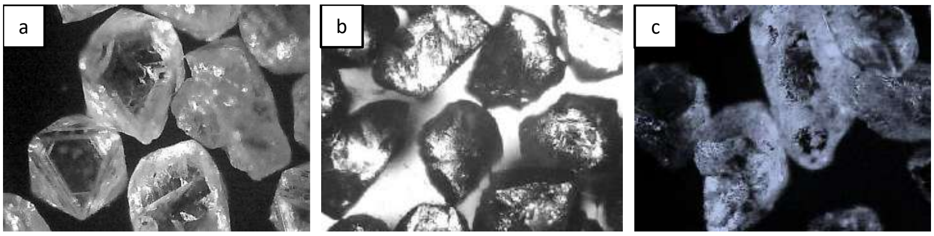

Figure 1 Images of diamond crystals at foam separation (a,b) with fixed asphaltene-resin cut fraction (c)

The ARCF fixation on diamonds is irreversible that increases the stability of the fixation of medium viscous fractions of fuel oil. The obtained research results confirmed increasing the stability of collector fixation on diamonds due to adhesion of ARCF as a crucial condition for effective flotation.

Increasing diamond recovery due to applying ultrasonic, thermal, and reagent treatment [4] was the basis for testing the effectiveness of the combined mode, involving the use of all three types of the treatment. The tests results showed that the combination of ultrasonic and thermal treatment with the addition of OEDP (oxy-ethylidene diphosphonic acid, a slurry dispersing agent) provides a noticeable increase in diamond recovery (Table 2).

Table 2 Effect of ultrasonic (UST) and thermal treatment of the initial feed and that of additives of oxy-ethylidene diphosphonic acid (OEDP) on foam separation outcomes

No.	Treatment conditions			ε, %	
	UST duration, sec.	Temperature, ℃	C_{OEDP}, mg/l	diamonds	kimberlite
1	-	24	-	82.5	0.86
2	30	24	-	87.5	0.65
3	-	24	100	85.0	0.55
4	-	85	-	87.5	0.68
5	30	85	-	90.0	0.59
6	30	24	100	90.0	0.39
7	30	85	100	92.5	0.60
8	60	24	100	90.0	0.40
9	60	85	200	90.0	0.33

The analysis of the results of testing the developed process modes at a foam separation unit showed that when using the combined mode the diamond recovery (tests 5-9, Table 1) was higher than in the basic test or at separate application of the treatment types (tests 1-4, Table 1). The yield of kimberlite into the concentrate remained at the same level (0.47 - 0.68 %) when using the combined modes.

The reasonable temperature range before deslurring process stage is 80-85 ℃, in conditioning with collector, 30-35 ℃, and in foam separation, 20-24 ℃. At such temperature conditions the effective dispergating of the collector and its fixation on diamonds is achieved. However, the application of thermal conditioning is an energy-consuming process. Therefore, we conducted studies on the selection of collectors for different temperature conditions.

The experimental study showed that at lower temperatures (10 and 14 ℃) the best results were obtained for the KSM collectors obtained by diluting M-40 fuel oil with diesel process oil cut fraction and aliphatic ketones: diethyl ketone (DEK), ethyl methyl ketone (EMK) and dimethyl ketone (DMK) (Table 3).

Based on the results of the study of temperature effect on foam separation performance, the recommendations were given to apply the systems for heating recycled water and collector to maintain the temperature of the medium in conditioning and foam separation process stages up to 24 ℃. If there is no possibility of increasing temperature in conditioning, foam separation, and flotation process stages, it is reasonable to use KSM-1 and KSM-2 compound collectors.

Table 3 Recovery of diamonds in flotation with compound collectors based on M-40 fuel oil at different temperatures

Collector	Diamond recovery into concentrate, %		
	10 ℃	14 ℃	24 ℃
M-40 fuel oil	54.4	68.7	74.4
M-40-20	72.3	78.6	88.5
KSM-1	86.3	92.2	88.4
KSM-2	85.2	92.5	85.9
KSM-3	81.5	88.7	87.0

Increasing the foam separation performance is promoted by application and improvement of closed water recycling system [5]. However, the accumulation of slurry at increasing the proportion of recycled water causes an increase in diamond losses, the cost of which exceeds the savings from reduced reagent consumption. The required result from increasing the proportion of recycled water is achieved by removing slurry from the recycled water. The recommended increase in the proportion of recycled water used from 70 to 85 % was tested for the foam separation cycle at the Processing Plant. The selected scheme included a single-stage clarification of the feed thickening overflow and two-stage clarification of the aqueous phase of the foam separation products. The results of the tests confirmed the feasibility of reducing the collector consumption by 8% while maintaining diamond recovery and concentrate quality at the same level (Table 4).

Table 4 Foam separation cycle performance when changing recycled water proportion

Recycled water proportion, %	Collector consumption, g/t		ε_{diam}, %	Kimberlite yield into concentrate, %
	F-5 fuel oil	butyl aeroflot		
70	1,100	25	87.9	0.65
75	1,050	23.5	87.9	0.64
80	1,035	23.1	87.8	0.64
85	1,020	22.8	87.8	0.63
90	970	21.5	85.8	0.62

CONCLUSION

The important role of the optimal combination of adhesion activity and strength of fixation of a collector on diamonds was shown. The important role of asphaltene-resin cut fractions in stable fixation of an apolar fuel oil-based collector on diamonds was demonstrated.

Based on the results of laboratory and industrial studies, the effectiveness of combined modes of ore and recycled water conditioning by acoustic, thermal, and reagent methods to increase the floatability of diamonds was shown.

A technological mode of foam separation was developed and tested, including thermal treatment of an initial diamond-containing product and maintenance of the required temperature in the operations of conditioning and foam separation. It was shown that under the conditions of low pulp temperatures the highest performance was demonstrated by collectors with additives of diesel process oil cut fraction and aliphatic ketones.

The regime of water recycling in the foam separation cycle involving the recycled water proportion up to 85% with clarification of the overflow of the initial feed -2 - +1 mm thickening and clarification of the foam separation concentrates and tailings was selected.

REFERENCES

1. Morozov, V.V., Kovalenko, E.G., Dvoichenkova, G.P., Pestryak, I.V., Lezova, S.P. (2022) Selection of collector composition and temperature conditions for diamond foam separation. Journal of Mining and Metallurgy, 58 A (1) 21–28.
2. Kovalenko, E.G., Babushkina, A.D., Chut-Dy, V.A. (2023) Application of multicomponent collectors and choice of temperature conditions in foam separation of diamond-bearing kimberlites. Gornyy Zhurnal [Mining Journal], 12, 72-76 (in Russian).
3. Morozov, V.V., Kovalenko, E.G., Dvoichenkova, G.P., Pestryak, I.V., Lezova, S.P. (2024) Current trends of improving the efficiency of foam separation of diamond-bearing kimberlites. Gornye Nauki i Tekhnologii [Mining Sciences and Technologies]. vol. 9, 2, 134-145 (in Russian).
4. Kovalenko, E.G. (2023) Application of compound oil-containing collectors in foam separation of diamonds. Vestnik Zabaikalskogo Gosudarstvennogo Universiteta [Bulletin of Transbaikal State University], 29 (1), 51-62 (in Russian).
5. Kovalenko, E.G. (2024) Improvement of the scheme and mode of closed-loop water recycling system in foam separation of diamond-bearing kimberlites. Vestnik Zabaikalskogo Gosudarstvennogo Universiteta [Bulletin of Transbaikal State University], 30 (2), 62-71 (in Russian).

XVI International Mineral Processing
and Recycling Conference
28-30 May 2025, Belgrade, Serbia

DOI: 10.5937/IMPRC25220G

Original research article

NON-FERROUS METALS BIOLEACHING FROM PYROMETALLURGY COPPER SLAG USING SPENT MEDIUM OF DIFFERENT FUNGAL SPECIES

Plamen Georgiev[#], 0009-0006-4655-9039,
Marina Nicolova, 0000-0002-4611-8755,
Irena Spasova, 0009-0009-6728-1701,
Mihail Iliev, 0000-0001-8441-8831,
Ralitsa Ilieva, 0000-0002-1618-6394,
University of Mining and Geology, Sofia, Bulgaria

ABSTRACT – This study aimed to compare the recovery of non-ferrous metals from a pyrometallurgy copper slag containing 1.93 % Zn, 0.36 % Cu, and 0.09 % Co by spent medium bioleaching of fungi *Aspergillus niger* and *Penicillium ochrochloron*. The fungal species were cultivated for a week; microbial biomass was separated, and the shake-flask technique carried out the leaching. Factors such as temperature, pulp density, the organic acids ratio and the amount of added acidity strongly affected the extraction of the non-ferrous metals from copper slag.

Keywords: Raw Materials, Copper Slag, Fungi, Bioleaching.

INTRODUCTION

Pyrometallurgical copper slags are used nowadays for road construction and preparing different types of cement. However, these wastes, especially old slags, contain significant quantities of valuable components (copper, cobalt, zinc and nickel in some cases) and, for that reason, are subject to further processing. Their flotation processing usually resulted in a final recovery not higher than 50 % [1]. The efficiency of chemical/ biological leaching of base metals is in the range of 85-95 % due to the combined action of several weathering processes such as acidolysis, oxidation, and complexolysis.

This study presents some results about the leaching of copper, zinc, and cobalt from old copper slags by the spent medium of fungi *A. ni*ger and *P. ochrochloron*.

EXPERIMENTAL

The copper slag sample was collected from the surface of the weathered zone of copper slag deposit Eliseyna, located in Northwestern Bulgaria. The sample was transported to the laboratory in a dust-free bucket and stored at a lower temperature for further use.

A representative sample of cooper slag was subjected to digestion with aqua regia, and the content of chemical elements in liquid obtained after that was analyzed by

---

[#] corresponding author: ps_georgiev@mgu.bg atomic absorption spectrometry and inductively coupled plasma. The mineralogical composition of copper slag was determined by X-ray Diffraction analysis EMPYREAN supplied with copper as anode material.

Table 1 Chemical content of copper slag used in this study

Index (in %)	Value
Al_2O_3	5.25
CaO	9.68
K_2O	1.16
MgO	3.07
MnO	1.10
Na_2O	1.70
P_2O_5	0.21
SiO_2	34.05
Fe	27.22
Cu	0.36
Co	0.09
Zn	1.93
S	0.91

Leaching experiments were carried out with grounded copper slags with dominant particle size – 75 µm to + 25 µm. The acid consumption of the slag was studied at 25 °C and 55 °C, respectively. It was determined by serial addition of sulfuric acid to pulp in a regime of agitation with an overhead mixer with a rate of 300 rpm. The acid addition stopped when the pulp's pH reached the targeted value (5.0, 4.0, 3.5, and 2.5) and remained constant for 6 hours.

The leaching abilities of fungal species *Aspergillus niger* and *Penicillium ochrochloron* to the mineral composition and non-ferrous metals in copper slag were compared. *Aspergillus niger* originated from the Microbial Culture Collection maintained at the Department of General and Industrial Microbiology, University of Sofia. *Penicillium ochrochloron CCM F-158* was obtained from the Czech Collection of Microorganisms to the Department of Experimental Biology at Masaryk University. The strains were maintained on Czapek Dox medium by sub-culturing at 25 °C and were preserved at 4 °C when needed. Each fungal species was cultivated in a medium consisting of sucrose (185 g/ L), KH_2PO_4 (3.0 g/ L), NH_4Cl (0.96 g/ L), $MgSO_4{\cdot}7H_2O$ (1.2 g/ L), and traces of $FeSO_4{\cdot}7H_2O$, $ZnSO_4{\cdot}7H_2O$, $CuSO_4{\cdot}7H_2O$. The medium was inoculated with 10^6 spores/ ml and incubated for 7 days at 25 °C under continuous shaking (150 rpm). The spent medium for further experiments was obtained by separating the fungal biomass with vacuum filtration. The extracellular organic acids in the spent medium were determined by Water's 510 HPLC, equipped with an E18 column, at a flow rate of 1 ml/ min, and six mM H_3PO_4 as a solvent, and the peaks` detection following the method described in Bosshard et al., [2]. The alkaline consumption (0.2 N NaOH) of the spent medium up to pH 8.5 was determined by the Metrohm 718 STAT Titrino titrator.

The leaching experiments were performed by the shake-flask technique using an Erlenmeyer flask of 500 ml volume containing 150 ml spent medium and copper slag at a pulp density of 5 %, 10%, or 15 %, respectively. The pulp was homogenized by an orbital shaker (150 rpm) at temperatures of 25° or 55 °C, respectively. The effect of sulfuric acid extra addition (5 g, 10g, and 25 g/ L) was studied also. The total duration of the leaching experiments was 72 hours. The solid residues from the Erlenmeyer flasks were separated by filtration and washed with tap water until the pH reached 7.0. The chemical and mineral content of solid residues obtained from each experiment were determined after drying out to constant weight.

All experiments were repeated in triplicate, and the results represent the mean value.

RESULTS AND DISCUSSION

Results of the chemical content revealed the presence of copper, zinc, and cobalt as raw materials in the higher amount in the copper slag (Table 1).

X-ray diffraction study showed that the main silicate mineral in the studied copper slag was fayalite (Fe_2O_4Si) (Figure 1). The higher content of protomangano-ferro-anthophyllite ($H_2Fe_{4.48}Mg_{1.08}Mn_{1.44}O_{24}Si_8$) revealed that the weathering process had carried out intensively near the surface of the copper slag deposit. The copper slag's chemical and mineralogical content determined the higher value of acid consumption, especially when the target pH was lower than 4.0 (Table 2). It was determined by the preferential leaching of iron oxides and the gradual increase of ferrous iron concentration in the pregnant solution. That process was combined with stepwise leaching of non-ferrous metals, as at pH 3.5, the copper, zinc, and cobalt leaching reached 38.5 %, 58.0 %, and 40.0 %, respectively. These results revealed that the non-ferrous metals` stock in pyrometallurgical copper slags could be unlocked and recovered using acidolysis as a leading process in their hydrometallurgical processing.

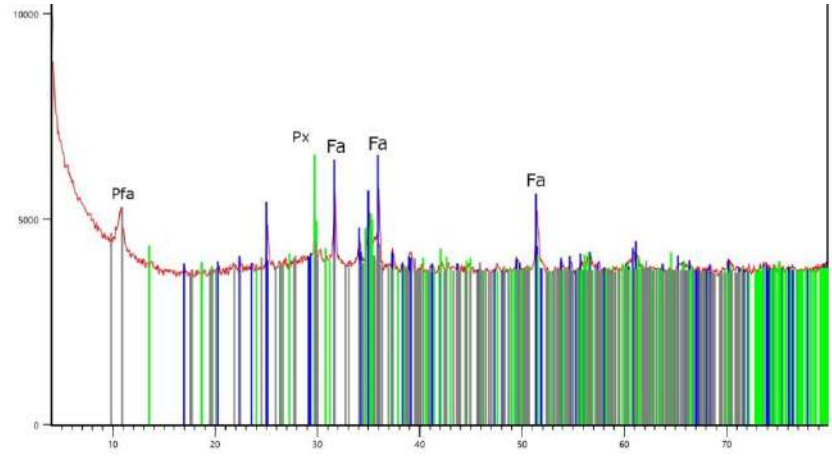

Figure 1 X-ray diffraction pattern of the copper slag sample showing the presence of Fa -Fayalite, Px-Clinopyroxene and Pfa-protomangano-ferro-anthophyllite (Minerals abbreviation according to [3])

There are twoapproaches to putting it into practice: slag leaching with strong inorganic or polycarboxylic acids (4). Sulfuric acid is an example of a strong inorganic acid that could be added to the slag's pulp or generated due to the activity of acidophilic chemolithotrophic bacteria growing on S° as a source of donors and energy. In that case, the main drawbacks are the considerable lowering of the pulp pH and substantial iron co-leaching, as its concentration could reach up to 30 g/ L. It turns the processing of laden leach solution into a challenging task [5]. Polycarboxylic acids contain more than one carboxylic group, which donates hydrogen ions in a wide pH range. Fungi produce a dozen such metabolites, and with higher concentrations are citric and oxalic acid (6). For example, oxalic acid is a diprotonic strong acid with lower pKa values of the carboxylic groups (1.25 and 4.14, respectively). In contrast, citric acid is a weak triprotonic acid with pKa values of 3.13, 4.76, and 6.39, respectively. The main advantage of citric acid is the excellent complexing properties of citrate anions towards already leached cations and complexes formation with a net negative charge, which enables their migration even at slightly acidic-alkaline pH. The peak concentration of citric acid in the spent medium of A. niger and P. ochrochloron was measured after seven days of cultivation. The spent medium of A. niger contained a higher amount of citric acid, had a higher value of citric: oxalic acid ratio (3:1), and the total amount of protons available for acidolysis reached almost 1.0 g H+/ L compared to the values measured in the spent medium of other fungal species (Table 3). It resulted in 22.5 %, 25.1 %, and 44.4 % of copper, zinc, and cobalt leaching, respectively, at an equilibrium pH of 4.39 on the third day of the leaching test (Table 4). Therefore, all further experiments were carried out with a spent medium of A. niger.

Table 2 Acid consumption of copper slag and its effect on the leaching of raw materials

pH	g H_2SO_4/ kg slag	Leached raw materials, mg/kg				
		Cu	Zn	Co	Fe	Si
4.9	12.0	220	3950	125	1190	18550
4.0	71.5	945	5350	255	49530	21880
3.5	292	1385	11190	360	138420	25990
2.5	505	2220	14450	490	210150	71280

Table 3 Characteristic of spent medium generated due to the growth of the tested fungal species

Index	*Aspergillus niger*	*Penicillium ochrochloron CCM F-158*
pH	2.58	3.24
Oxalic acid, g/L	8.1	10.9
Citric acid, g/ L	24.8	18.9
g H^+/ 1 L	0.94	0.65

The protomangano-ferro-anthophyllite was the mineral with the highest content and most reactive in the copper slag, and it consumed a substantial portion of protons in the spent medium instead of the non-ferrous metals` leaching; the experiments at a pulp density higher than 5 % revealed its negative effect on the recovery of non-ferrous metals (Table 5). For example, copper, zinc, and cobalt recovery at 15 % pulp density dropped by 16.7 %, 24.9 %, and 15.5 %, respectively. Therefore, all further experiments were carried out at 5 % pulp density.

Table 4 Effect of using the spent medium on the non-ferrous leaching from copper slag at 5 % pulp density and 25 °C

Index	*Aspergillus niger*	*Penicillium ochrochloron CCM F-158*
pH	4.39	5.27
$Cu_{leached}$, mg/ kg	810	715
$Zn_{leached}$, mg/ kg	4850	4490
$Co_{leached}$, mg/ kg	400	345
$Fe_{leached}$, mg/ kg	35500	23200

Table 5 Effect of pulp density on the non-ferrous leaching from copper slag with the spent medium of *Aspergillus niger* at 25 °C

Index	Pulp density, %		
	5	10	15
pH	4.39	5.07	5.34
$Cu_{leached}$, mg/ kg	810	725	680
$Zn_{leached}$, mg/ kg	4850	4370	3640
$Co_{leached}$, mg/ kg	400	385	335

Two crucial factors limited the non-ferrous leaching from copper slag - the temperature at which the processing was carried out and the available concentration of protons. The main advantage of indirect leaching compared to raw materials leaching in the presence of microbial cells is that both factors can be manipulated efficiently. For example, the gradual increase of the temperature from 25° to 55° C led to a higher rate of processes, which resulted in better leaching of non-ferrous metals - 26.6 %, 26.5 %, and 48.3 % for copper, zinc, and cobalt, respectively. The extra addition of sulfuric acid at the beginning of the test further improved the non-ferrous metals recovery, as in the case with 25 g H_2SO_4/ L and 55° C, it reached 78.9 %, 54.7 %, and 69.4 %, respectively, for the above-mentioned non-ferrous metals (Table 7).

Table 6 Effect of temperature on the non-ferrous leaching from copper slag with the spent medium of *A. niger*

Index	Temperature, °C		
	25	40	55
pH	4.39	4.77	5.16
$Cu_{leached}$, mg/ kg	810	875	960
$Zn_{leached}$, mg/ kg	4850	5040	5110
$Co_{leached}$, mg/ kg	400	420	435

Table 7 Effect of sulfuric acid addition to the spent medium of *A. niger* on the non-ferrous leaching from copper slag at 55 °C

Index	Added sulfuric acid, g/ L			
	0	5	10	25
pH	5.16	3.83	3.16	2.27
Cu $_{\text{leached}}$, mg/ kg	960	1770	2310	2840
Zn $_{\text{leached}}$, mg/ kg	5110	7970	9840	10560
Co $_{\text{leached}}$, mg/ kg	435	560	570	625

CONCLUSION

The higher content of citric acid in the spent medium of *A. niger*, compared to that of *P. ochrochloron,* determined it as a better leaching agent towards copper, zinc, and cobalt contained in pyrometallurgical copper slag. However, the concentration of hydrogen ions in the fungal spent medium was the main limiting factor on the leaching of non-ferrous metals due to the copper slag's mineral composition and a value of acid consumption higher than 200 g H_2SO_4/ kg slag.

ACKNOWLEDGEMENT

Co-financing of the project "Innovative copper slag processing for raw materials supply", Program: ERA-MIN3, by the Bulgarian Fund "Scientific Research", Ministry of Education and Science, Bulgaria (Grant number KP-06-D002/6) is thankfully acknowledged.

REFERENCES

1. Panda, S., Mishra, S., Rao, D.S., Pradhan, N., Mohapatra, U., Angadi, S., Mishra, B.K. (2015). Extraction of copper from copper slag: Mineralogical insights, physical beneficiation and bioleaching studies. Korean Journal of Chemical Engineering 32, 667-676.
2. Bosshard, P.P., Bachofen, R., Brandl, H. (1996). Metal leaching of fly ash from municipal waste incineration by *Aspergillus niger*. Environmental Science and Technology, 30, 3066-3070.
3. Kretz, R. (1983). Symbols of rock-forming minerals. American Mineralogist, 68, 277-279.
4. Srichandan, H., Mohapatra, R.K., Parhi, P.K., Mishra, S. (2019). Bioleaching approach for extraction of metal values from secondary solid wastes: A critical review. Hydrometallurgy 189, 105122.
5. Georgiev, P., Nicolova, M., Spasova, I., Groudev, S. (2023). Iron removal from laden leach solution by processes of solvent extraction and magnetite synthesis. Sustainable Extraction and Processing of Raw Materials, 4, 37-42.
6. Gadd, G.M. (1999). Fungal production of citric and oxalic acid: Importance in metal speciation, physiology and biogeochemical processes. Advances in Microbial Physiology, 41, 47-92.

XVI International Mineral Processing
and Recycling Conference
28-30 May 2025, Belgrade, Serbia

DOI: 10.5937/IMPRC25226Z Original research article

UV-VIS IDENTIFICATION OF COPPER COMPLEXES WITH INHIBITOR ORGANIC COMPONENTS IN THE ELECTROLYTE

Milica Zdravković[1,#], 0000-0001-9488-9151,
Vesna Grekulović[1], 0000-0001-6871-4016,
Edina Huseinović[2], 0009-0007-0222-383X,
Robert Vianello[3], 0000-0003-1779-4524,
Nada Štrbac[1], 0000-0003-4836-1350,
Melita Huremović[2], 0009-0001-5143-0356,
Milan Gorgievski[1], 0000-0002-9899-719X,
[1]University of Belgrade, Technical Faculty in Bor, Bor, Serbia
[2]University of Tuzla, Faculty of Natural Sciences and Mathematics, Tuzla, Bosnia and Herzegovina
[3]Laboratory for the Comp. Design and Synthesis of Functional Materials, Ruđer Bošković Institute, Zagreb, Croatia

ABSTRACT – The UV-VIS method is an effective, non-destructive method that enables a better understanding of the electrolyte during corrosion. The aim of the study presented in this paper is to determine the existence of an organometallic complex in a 0.5 M NaCl solution with the addition of *Rubus fruticosus L.* leaf extract (RFLE). The experiments were conducted in a 0.5 M NaCl solution with the addition of RFLE (5 g/L and 10 g/L) with and without the immersion of a copper coupon. The results show that after the copper coupon standing in the electrolyte, there is a change in the absorbance maximum in the solution with 5 g/L RFLE, while no change is observed in the solution with 10 g/L RFLE. Such a change indicates the existence of a copper-RFLE complex in the solution with lower inhibitor concentration. In the case of RFLE, forming a copper complex with caffeic acid, isoquercetin and astragalin is possible. The absence of the complex at a concentration of 10 g/L RFLE can be attributed to a change in the mechanism and the lack of copper ions in the solution due to adequate corrosion protection.

Keywords: UV-VIS, Organometallic Complex, Corrosion Inhibitor, *Rubus fruticosus L.*

INTRODUCTION

Corrosion of copper in saline environments, especially in 3.5% sodium chloride (NaCl) solutions, is challenging because it causes destruction of the metal that has major industrial applications, leading to significant economic losses and safety concerns [1]. One of the ways to reduce the metal corrosion rate is the application of corrosion inhibitors [2]. However, corrosion inhibitors, often synthetic and toxic, raise environmental issues that require the exploration of viable alternatives [3]. Plant

---

[#] corresponding author: mzdravkovic@tf.bor.ac.rs extracts are effective alternatives to conventional corrosion inhibitors [4].

Blackberry leaf extract (*Rubus fruticosus L.* leaf extract, RFLE) is a very effective copper corrosion inhibitor in 0.5 M NaCl. The maximum corrosion inhibition efficiency (99.1%) was determined, after standing for 10 days, at room temperature, in a solution of 0.5 M NaCl with the addition of 15 g/L RFLE [5]. Recent research notes important parameters to consider when discussing the application of environmental inhibitors. Solvents used to obtain the extract, sustainability, availability of the plant, toxicity of the extraction process, and costs of collecting and cleaning the plant were taken as important factors [6]. Since RFLE is obtained by extraction from water, a process similar to obtaining tea, it is a by-product of the production of blackberry fruit that is in excess compared to the needs of tea production, while preventing its burning on the plantation, this extract does not indicate the disadvantages mentioned earlier [7]. In addition to the investigation of RFLE as a copper corrosion inhibitor in a chloride environment at concentrations from 2 g/L to 15 g/L, it was determined that a complex is formed in the solution with the addition of 15 g/L RFLE. The physical adsorption occurs on the copper surface, which takes place according to the Langmuir adsorption isotherm. However, since it was determined by applying the electrochemical impedance method that two different adsorption mechanisms occur, it is necessary to additionally examine whether the formation of complexes occurs in the presence of 5 g/L and 10 g/L RFLE. Namely, the corrosion process is primarily controlled by diffusion (at concentrations lower than 15 g/L RFLE), after which it is controlled by charge transfer (at 15 g/L RFLE) [5, 8].

The UV-VIS method is an effective method for identifying metal complexes with corrosion inhibitor organic compounds [9, 10]. UV–Vis spectroscopy is a cost-effective, simple, versatile, non-destructive, and analytical technique. It is suitable for a large spectrum of organic compounds and some inorganic species. As a function of wavelength, UV–Vis spectrophotometers measure the absorption or transmission of light that passes through a medium [11]. The change in electrolyte absorbance in the presence of metal enables the identification of the organometallic complex, which allows the understanding of the corrosion inhibition process complexity due to the large number of species participating in the corrosion reactions [8-10].

EXPERIMENTAL

Materials and Sample Preparation

The oxygen-free phosphor copper sheet Cu-DHP (99.9% Cu, 0.0198% P, 0.0005% Pb) was used for making copper coupons. The copper sheet was cut to dimensions of 1 × 1 cm using an erozimate machine with a precision of 0.001 mm, to achieve the most precise cutting and reduce the copper crystal lattice damage. A 0.5 M NaCl solution was prepared using distilled water and the appropriate amount of NaCl salt p. a. purity manufactured by "Zorka Pharma", Serbia. The RFLE was added to obtain 0.5 M NaCl with the addition of 5 and 10 g/L. Aqueous blackberry leaf extract was prepared from dried blackberry leaves manufactured by "Adonis", Sokobanja, Serbia and distilled water. The solid: liquid ratio was 2 (kg): 15 (L). The leaves were poured with hot distilled water (95°C). The mixture was filtered after 12 h with cotton cloth and filter paper No1. Aqueous blackberry leaf extract was then evaporated on a rotary evaporator Buchi R-210

(BUCHI Labortechnik AG, Switzerland) at 72 mbar at 40°C. Evaporation was completed after obtaining a resin-like solvent-free extract. Working solutions were prepared before experiments. All experiments were performed at room temperature.

UV–VIS Spectroscopy

The UV–VIS method was used to interpret the possibility of the RFLE-copper complex formation in 0.5 mol/L NaCl. The experiments were performed in 0.5 M NaCl solution with the addition of 5 g/L and 10 g/L RFLE before and after the immersion of copper coupons for 24 h. The experiments were performed in the wavelength range of 200–400 nm using a UV–Vis spectrometer Lambda 25 (Perkin Elmer, USA).

RESULTS AND DISCUSSION

The UV-VIS results for the 0.5 M NaCl solution with the addition of 5 g/L RFLE before and after the immersion of the copper coupon are shown in figures 1a and 1b. Both UV-VIS spectra show absorption maxima at around 210 nm. No significant change in the absorption spectrum shape is observed when copper is added to the solution. However, a change in the absorbance maximum is observed, with a significant decrease in the maximum in the presence of copper. According to the literature, this change indicates the formation of a RFLE-copper complex [9, 10]. The corresponding absorption can be attributed to π–π* and n–π* electron transitions [9, 10, 12].

The π-π* transition is otherwise called the K band. It occurs in compounds with unsaturated centers (simple alkenes, aromatic compounds, carbonyl compounds). This transition requires less energy than the n-σ* transition. The n-π* transition is otherwise called the R band. In this case, the electron that does not belong to the shared electron pair of the hetero atom is excited into the π* antibonding orbital. In the case of aliphatic ketones, this transition occurs at about 280 nm and is the transition with the lowest energy [13].

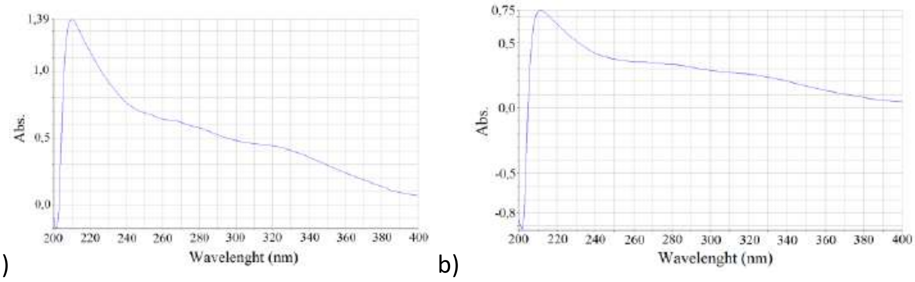

a) b)

Figure 1 UV–Vis spectra of the 0.5 M NaCl with 5 g/L RFLE (a) before and (b) after 24 h of copper coupon immersion

In an earlier investigation, the HPLC method determined the presence of three compounds in RFLE: caffeic acid, quercetin-3-O-glucoside and kaempferol-3-glucoside [8]. Each of these compounds can potentially form a complex with the copper ions present in the electrolyte. The results of research on metal chelation with flavonoids for the characterization of antioxidants indicate that flavonoids can form high-affinity complexes with transition metals, most often copper and iron [14, 15]. Copper (II) chloride is often used as a starting substance for the formation of organometallic complexes [14]. Based on the E-pH diagram and the pH value of the tested solutions of about 5.6, it is clear that during the corrosion process, the transfer of copper(II) ions into the solution occurs [16]. In this way, copper ions can form an organometallic complex with RFLE molecules.

Many studies point to the possibility of the copper complexes formation with all three organic compounds present in RFLE. Research confirms the formation of a caffeic acid complex with Cu(II) in NaCl solution [17]. Earlier studies showed that a complex is formed between copper ions and quercetin glucosides [18]. The stoichiometry of metals and flavonoids is 2:1 in the case of the complex formation with Fe (II), Ni (II), Co (II), and Zn (II), while with Cu (II) the mechanism is different. This happens due to simultaneous oxidation, because Cu (II) has a stronger oxidative activity and quercetin is more easily oxidized under acidic conditions [18, 19]. Organometallic complexes of kaempferol with Cu(II) ion were investigated in terms of antioxidant and prooxidative behavior. The results of this research indicate the formation of two types of complexes (1:1 and 1:2) [20].

UV-VIS results for the 0.5 M NaCl solution with the addition of 10 g/L RFLE before and after the immersion of the copper coupon are shown in figures 2a and 2b.

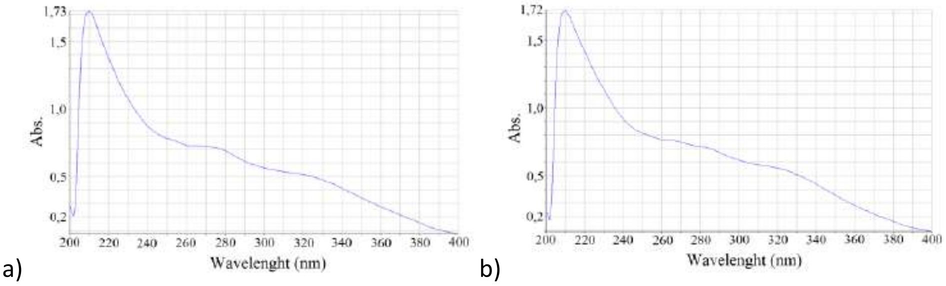

Figure 2 UV–Vis spectra of the 0.5 M NaCl with 10 g/L RFLE (a) before and (b) after 24 h of copper coupon immersion

In contrast to the previous change in absorbance, at a concentration of 10 g/L RFLE, no change in the UV-VIS spectrum occurs when the copper coupon is added. These results indicate that at a sufficiently high concentration of the inhibitor, there is a significant reduction in metal corrosion, so there are no copper ions present in the solution that would enable the formation of an organometallic complex. At higher concentrations than 10 g/L RFLE, the appearance of unstable complexes is expected, due to a change in the mechanism [5].

CONCLUSION

Using the UV-VIS method, UV-VIS spectra were obtained in 0.5 M NaCl solution with addition of 5 g/L and 10 g/L RFLE before and after immersion of the copper coupon. it was determined that in a solution with a lower concentration of corrosion inhibitor (5 g/L RFLE), the formation of organometallic complexes occurs. It is possible to create different complexes considering the complexity of the electrolyte composition. A caffeic acid, quercetin-3-O-glucoside and kaempferol-3-glucoside complexes with Cu(II) ions can be formed. The absence of an absorbance change at higher concentration can be attributed to the lack of copper ions in the solution, due to the adequate anti-corrosion effect of RFLE.

ACKNOWLEDGEMENT

The research presented in this paper was done with the financial support of the Ministry of Education, Science and Technological Development of the Republic of Serbia, within the funding of the scientific research work at the University of Belgrade, Technical Faculty in Bor, according to the contract with registration no. 451-03-137/2025-03/200131. The experiments were carried out within the ERASMUS KA107 mobility (1.4.-5.7.2022.) at the Faculty of Technology, University of Tuzla (Bosnia and Herzegovina).

REFERENCES

1. Gapsari, F., Hadisaputra, S., Sulaiman, A.M., Ebenso, E., Thakur, A., Kumar, A. (2024) Eco-friendly corrosion inhibition of copper in NaCl media using *Perseana americana* extract: Insights from quantum and electrochemical studies. Results in Surfaces and Interfaces, 17, 100327.
2. Dariva, C.G., Galio, A.F. (2014) Corrosion inhibitors–principles, mechanisms and applications. Developments in corrosion protection, 16, 365-378.
3. Njoku, C.N., Maduoma, T.U., Emori, W., Odey, R.E., Unimke, B.M., Yakubu, E., Anorondu, C.C., Udunwa, D.I., Njoku, O.C., Oyoh, K.B. (2024), Natural and synthetic drugs as eco-friendly and sustainable corrosion inhibitors for metals: a review. Pigment & Resin Technology, 53 (6), 1074-1087.
4. Dehghani, A., Ghahremani, P., Mostafatabar, A.H., Ramezanzadeh B. (2024) Plant extracts: Probable alternatives for traditional inhibitors for controlling alloys corrosion against acidic media—A review. Biomass Conversion and Biorefinery, 14, 7467–7486
5. Zdravković, M., Grekulović, V., Suljagić, J., Štrbac, N., Marković, I., Gorgievski, M., Marković, M. (2024) The *Rubus fruticosus* Leaf Extract as an Eco-Friendly Copper Corrosion Inhibitor. Protection of Metals and Physical Chemistry of Surfaces, 1-0.
6. Verma, C., Alfantazi, A., Quraishi, M.A., Rhee, K.Y. (2023) Are extracts really green substitutes for traditional toxic corrosion inhibitors? Challenges beyond origin and availability. Sustainable Chemistry and Pharmacy, 31, 100943.
7. Zdravković, M., Grekulović, V., Štrbac, N., Zdravković, B., Gorgievski, M., Marković, M., Marković, M. (2024) Raspberries and blackberries grown in Serbia from the perspective of the Green Agenda. ECOLOGICA, 31 (114), 137-143.
8. Zdravković, M., Grekulović, V., Suljagić, J., Stanković, D., Savić, S., Radovanović, M., Stamenković, U. (2023) Influence of blackberry leaf extract on the copper corrosion behaviour in 0.5 M NaCl. Bioelectrochemistry, 151.
9. Grudić, V., Bošković, I., Gezović, A. (2018) Inhibition of Copper Corrosion in NaCl Solution by Propolis Extract. Chemical and Biochemical Engineering Quarterly, 32 (3), 299.

10. Gadow, H.S., Motawea, M.M., Elabbasy, H.M. (2017) Investigation of myrrh extract as a new corrosion inhibitor for α-brass in 3.5% NaCl solution polluted by 16 ppm sulfide, RSC Advances, 47.
11. Khalid, K., Ishak, R., Chowdhury, Z. Z. (2024) Chapter 15 - UV–Vis spectroscopy in non-destructive testing. Non-Destructive Material Characterization Methods (A. Otsuki, S. Jose, M. Mohan, S. Thomas), Elsevier, 391-416.
12. Sherif, E.M., Park, Su-M. (2005) Inhibition of Copper Corrosion in 3.0% NaCl Solution by N-Phenyl-1,4-phenylenediamine. Journal of The Electrochemical Society, 152 (10), B428.
13. Kalsi, P. S. (2004) Spectroscopy of Organic Compounds. 6th edition, New age international publishers, New Delhi.
14. Mira, L., Tereza Fernandez, M., Santos, M., Roch, R., Helena, Florênci, M., Jennings, K.R. (2002) Interactions of Flavonoids with Iron and Copper Ions: A Mechanism for their Antioxidant Activity. Free Radical Research, 36 (11), 1199–1208.
15. Kejik, Z., Kaplanek, R., Masarik, M., Babula, P., Matkowski, A., Filipensky, P., Vesela, K., Gburek, J., Sykora, D., Martasek, P., Jakubek M. (2021) Iron Complexes of Flavonoids-Antioxidant Capacity and Beyond. International Journal of Molecular Sciences, 22 (2), 646.
16. Alfantazi, A.M., Ahmed, T.M., Tromans, D. (2009) Corrosion behavior of copper alloys in chloride media. Materials & Design, 30 (7), 2425-2430.
17. De Stefano, C., Foti, C., Giuffrè, O., Sammartano, S. Acid–base and UV behavior of 3-(3,4-dihydroxyphenyl)-propenoic acid (caffeic acid) and complexing ability towards different divalent metal cations in aqueous solution. Journal of Molecular Liquids, 195, 9-16.
18. Liu Y, Guo M. (2015) Studies on transition metal-quercetincomplexes using electrospray ionization tandem mass spec-trometry. Molecules 20, 8583-8594.
19. Lee, J., Kim, O.-H., Jung, B.-K., Cho, I.-S., Lee, Y.-J., Choi, H.-J., Kim, Y.-C., Oh, Y.-H., Jung, K., Cha, S.-H., Jang, K.-Il. (2019) Influence of Mineral Supplementation on the Results from Analysis of Flavonol Glycoside Content in Ginkgo biloba Dietary Supplements. Preventive nutrition and food science. 24.
20. Simunkova, M., Barbierikova, Z., Jomova, K., Hudecova, L., Lauro, P., Alwasel, S.H., Alhazza, I., Rhodes, C.J., Valko, M. (2021) Antioxidant vs. Prooxidant Properties of the Flavonoid, Kaempferol, in the Presence of Cu(II) Ions: A ROS-Scavenging Activity, Fenton Reaction and DNA Damage Study. International Journal of Molecular Sciences, 22 (4), 1619.

XVI International Mineral Processing
and Recycling Conference
28-30 May 2025, Belgrade, Serbia

DOI:10.5937/IMPRC25232N

Original research article

DISSOLUTION KINETICS OF LOW-GRADE ZINC SILICATE ORE IN HYDROXIDE SOLUTION

Moloud Nazeri[1#], 0009-0003-8845-2078,
Maria Sinche-Gonzalez[1], 0000-0002-7722-6839,
Emad Abkhoshk[2], 0009-0005-7913-3846,
[1]EMJM-PROMISE, University of Oulu, Oulu Mining School, P.O. Box 3000, Oulu, Finland
[2]Calcimin Company, Zanjan, Iran

ABSTRACT – A kinetic study of the leaching on a low-grade zinc silicate ore by concentrated sodiun hydroxide (NaOH) solution has been investigated. The effects of reaction time, temperature, NaOH concentration and particle size on the dissolution rate of zinc were examined. It was found that the dissolution rate of zinc is significantly influenced by temperature, particle size and concentration of NaOH solution. When an ore sample of -53+38 µm size was leached for 2 hrs at 85°C in the presence of 5 M sodium hydroxide solution, at liquid:solid ratio of 10:1 and agitation speed of 400 rpm, the zinc recovery was about 78%. The kinetic study indicate that the process is chemically controlled with an activation energy of 52.45 kJ/mol.

Keywords: Zinc Silicate Ore, Hemimorphite, Alkaline Leaching, Leaching Kinetics.

INTRODUCTION

The zinc smelting industry is mainly dependent on zinc sulfide ore [1]. However, the depletion of high-grade deposits has made it increasingly challenging to meet rising zinc demand, highlighting the need to utilize zinc oxide ores [2].

The hydrometallurgical processing of zinc oxide ores involves either acidic or alkaline leaching [3−5]. While acid leaching achieves a high zinc recovery, the presence of alkaline gangue and impurity metals leads to high sulfuric acid consumption and complicates purification [6,7]. Additionally, Si readily forms silica gels in acidic media, hindering solid-liquid separation [8].

The alkaline leaching process, including NaOH and ammonia leaching, offers several advantages such as the insolubility of impurities like Fe_2O_3, SiO_2, CaO, and MgO due to the high pH (6–7) of the solution. Additionally, solution purification is straightforward, and treating ores with high gangue content in an alkaline solution reduces reagent usage and avoids filtration challenges commonly encountered in acid leaching.

Ammonia leaching has been found to cause significant environmental pollution and ammonia loss due to its inherent volatility. Accordingly, the application of ammonia leaching technology must be improved [9,10].

[#] corresponding author: Moloud.Nazeri@student.oulu.fi

Compared to acid leaching of non-sulfide zinc, fewer studies have explored alkaline leaching with sodium hydroxide. This research aims to investigate zinc extraction using an alkaline solution and the kinetics of the leaching process. The study systematically examines the optimal conditions for zinc extraction from zinc silicate ore in a NaOH medium and the dissolution kinetics of the process.

EXPERIMENTAL

Materials

Zinc silicate ore from Bagherabad mine (11.65% Zn, 11.14% Fe, 24.7% CaO and 12.58% SiO_2) in central Iran, was used in this study. Mineralogical analysis of the sample was performed by X-ray diffraction (Fig 1), polished and thin sections microscopy. XRD analysis of the sample showed the presence of hemimorphite [$Zn_4Si2O_7(OH)_2{\cdot}H_2O$], sphalerite (ZnS), calcite [$CaCO_3$], dolomite [$Ca(Mg,Fe)(CO_3)_2$] and goethite [FeO(OH)] as the major mineral phases followed by smithsonite ($ZnCO_3$), cerussite [$PbCO_3$], kaolinite [$Al_2Si2O_5(OH)_4$], quartz (SiO_2) and jarosite [$KFe_3(SO_4)_2(OH)_6$] as minor phases.

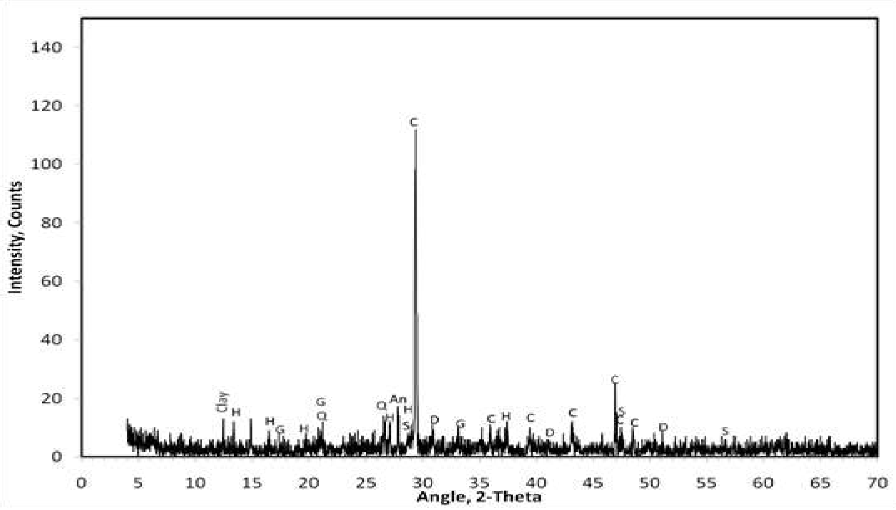

Figure 1 XRD pattern of the zinc silicate sample (H-Hemimorphite, G-Goethite, Q-Quarz, C-Calcite, S-Sphalerite, D-Dolomite, An-Anorthoclase)

Methods

Leaching experiments were conducted batch-wise with a total volume of 400 mL. A mechanical stirrer provided adequate dispersion of the mineral particles. Leaching solutions were prepared using NaOH crystals and distilled water. Unless otherwise stated, experiments were performed with 38–53 µm particles in 5 M NaOH at 85°C, stirred at 400 min^{-1}, and a solution volume of 200 mL. At selected time intervals, 2 mL of slurry was withdrawn, filtered, and analyzed for zinc content using atomic absorption spectroscopy (AAS).

RESULTS AND DISCUSSION

Effect of leaching time

The effect of leaching time on the dissolution of zinc silicate is shown in Fig 2. Zinc recovery increased with leaching time under the following conditions: 85°C, 5 mol/L NaOH concentration, 400 rpm agitation, liquid/solid mass ratio of 1:10, and particle size of -53+38 µm. After 60 minutes, 50% zinc recovery was achieved, rising to 78% after 120 minutes. A leaching time of 120 minutes was found to be optimal and was used for all subsequent experiments.

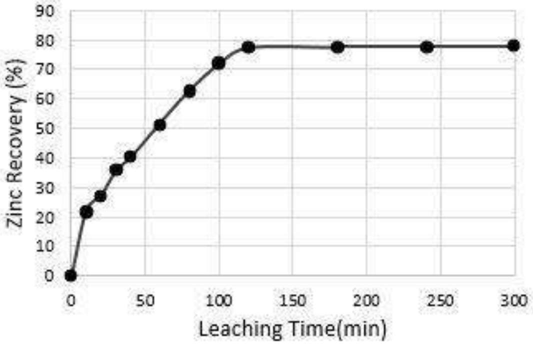

Figure 2 Effect of leaching time on zinc extraction.

Effect of sodium hydroxide concentration

The effect of NaOH concentration on zinc extraction is depicted in Fig 3. Other parameters were kept constant. Zinc extraction increased with NaOH concentration up to 6 M, with leached zinc rising from 41% to 80% after 120 minutes as the concentration increased from 3 M to 6 M. At concentrations of 7 and 8 M, the leaching rate decreased due to increased solution viscosity, which hindered the diffusion of reactants. A concentration of 5M is considered optimal, as increasing it to 6M resulted in only a 3% improvement in recovery.

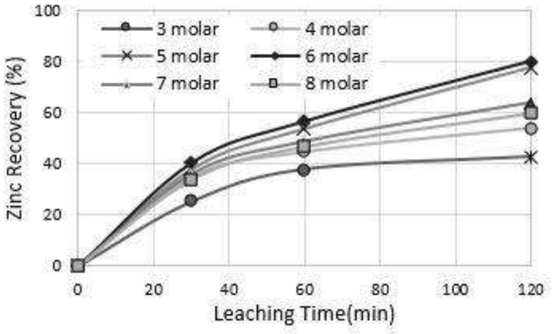

Figure 3 Effect of NaOH concentration on zinc extraction.

Effect of particle size

Fig 4 shows the effect of particle size on zinc extraction. The results indicate that reducing the particle size from -150+106 µm to -53+38 µm improved zinc extraction from 48% to 78%. This enhancement is due to the increased surface area of smaller particles, which provides more contact with the solution.

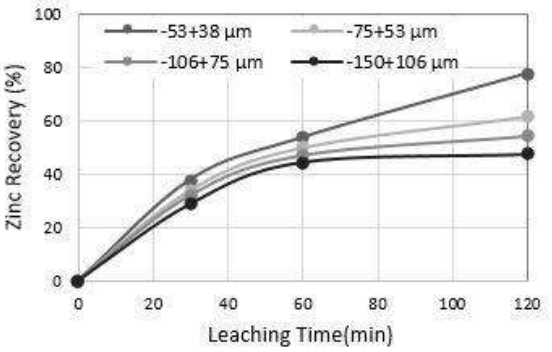

Figure 4 Effect of particle size on zinc extraction.

Effect of temperature

As seen from Fig 5, the temperature has strong influence on the zinc extraction. The zinc recovery increased as the temperature was increased. After 120 min, zinc extraction increased from 44% to 78% as temperature increased from 65 to 85 °C. It suggests that the process is chemically controlled, which has been confirmed in further kinetic analysis.

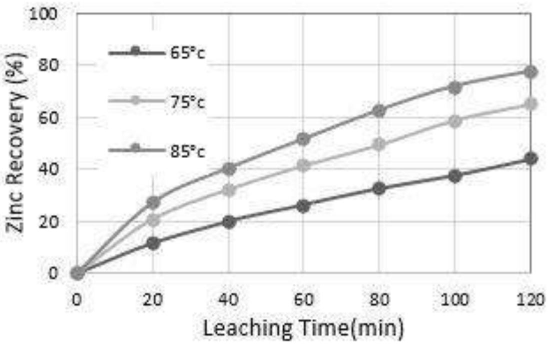

Figure 5 Effect of temperature on zinc extraction.

Leaching kinetics

Microscopic analysis of the residues revealed a progressive reduction in particle size during leaching, supporting the shrinking particle model. Data analysis showed that the

SPM model with chemical control good correlated with the results at all three temperatures (Fig 6). The R^2 values were acceptable, confirming that the process follows a chemical reaction model.

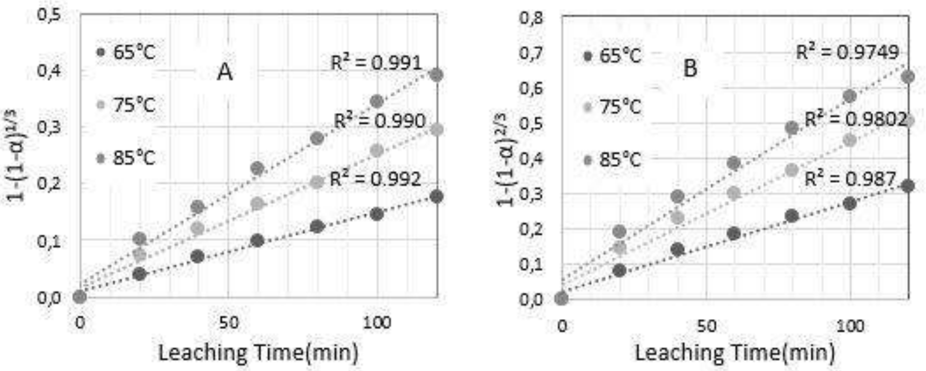

Figure 6 Plots of shrinking core model for chemical reaction control (A), and diffusion control (B), in various temperatures.

A chemically controlled process is highly temperature-dependent. Fig 7 presents the Arrhenius plot (ln k vs. 1/T), showing an activation energy of 52.45 kJ/mol. This high value confirms that zinc silicate leaching in NaOH is controlled by surface chemical reactions.

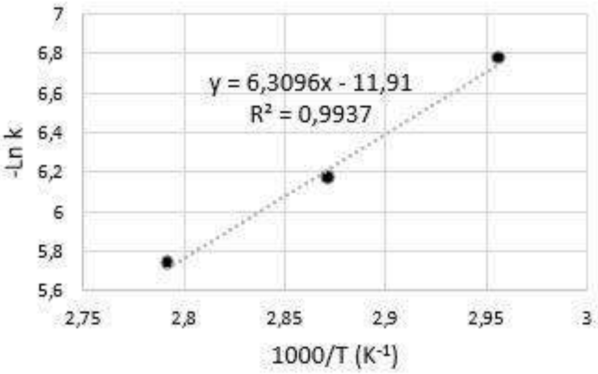

Figure 7 Arrhenius plot for leaching of zinc silicate ore

CONCLUSION

1) The dissolution kinetics of a low-grade zinc silicate ore in NaOH medium was studied. Mineralogical analysis of the sample showed the presence of hemimorphite [$Zn_4Si_2O_7(OH)_2 \cdot H_2O$] as major zinc phase.
2) When the ores of -53+38 µm size were leached for 2 h at 85°C in the presence of 5 M sodium hydroxide, liquid:solid ratio of 10:1 and agitation speed of 400 rpm, the leaching rate of zinc recovery was about 78%.

3) The dissolution kinetics of zinc silicate ore increases with increasing sodium hydroxide, temperature and with decreasing particle size.
4) The activation energy was found to be 52.45 kJ/mol which indicated a chemically controlled process is the controlling step.

ACKNOWLEDGEMENT

I gratefully acknowledge the financial support of the EMJM-PROMISE program for sponsoring my participation in IMPRC 2025.

REFERENCES

1. Yang, T.Z., Rao, S., Zhang, D.C., Wen, J.F., Liu, W.F., Chen, L., Zhang, X.W. (2016) Leaching of low-grade zinc oxide ores in nitrilotriacetic acid solutions. Hydrometallurgy, 161, 107−111.
2. Abkhoshk, E., Jorjani, E., Al-Harahsheh, M.S., Rashchi, F., Naazeri, M. (2014) Review of the hydrometallurgical processing of non-sulfide zinc ores. Hydrometallurgy, 149, 153−167.
3. Frenay, J. (1985) Leaching of oxidized zinc ores in various media. Hydrometallurgy, 15 (2), 243−253.
4. Yuan, T.C., Cao, Q.Y., Li, J. (2010) Effects of mechanical activation on physicochemical properties and alkaline leaching of hemimorphite. Hydrometallurgy, 104 (2), 136−141.
5. Yang, T.Z., Rao, S., Zhang, D.C., Wen, J.F., Liu, W.F., Chen, L., Zhang, X.W. (2016) Leaching of low-grade zinc oxide ores in nitrilotriacetic acid solutions. Hydrometallurgy, 161, 107–111.
6. Xu, H.S., Wei, C., Li, C.X., Fan, G., Deng, Z.G., Zhou, X.J., Qiu, S. (2012) Leaching of a complex sulfidic, silicate-containing zinc ore in sulfuric acid solution under oxygen pressure. Separation and Purification Technology, 85, 206–212.
7. Dou, A.C., Yang, T.Z., Yang, J.X., Wu, J.H., Wang, A. (2011) Leaching of low-grade zinc oxide ores in Ida_2−H_2O system. In: Proceedings of the School of Metallurgical Science and Engineering, Central South University, Changsha, China, 31 March 2010, 2 June 2011.
8. Chen, A.L., Zhao, Z.W., Jia, X.J., Long, S., Huo, G.S., Chen, X.Y. (2009) Alkaline leaching Zn and its concomitant metals from refractory hemimorphite zinc oxide ore. Hydrometallurgy, 97 (3–4), 228−232.
9. Chen, A.L., Zhao, Z.W., Jia, X.J., Long, S., Huo, G.S., Chen, X.Y. (2009) Alkaline leaching Zn and its concomitant metals from refractory hemimorphite zinc oxide ore. Hydrometallurgy, 97 (3–4), 228–232.
10. Santos, F.M.F., Pina, P.S., Porcaro, R., Oliveira, V.A., Silva, C.A., Leão, V.A. (2010) The kinetics of zinc silicate leaching in sodium hydroxide. Hydrometallurgy, 102 (1–4), 43–49.

XVI International Mineral Processing
and Recycling Conference
28-30 May 2025, Belgrade, Serbia

DOI: 10.5937/IMPRC25238S

Original research article

EVALUATION OF WASTE MATERIALS FOR CADMIUM REMOVAL: COMPARATIVE STUDY OF SORPTION CAPACITY AND STABILITY

Ivana Smičiklas#, 0000-0002-7384-7312,
Mihajlo Jović, 0000-0002-3293-5797,
Jelena Amidžić, 0000-0003-3973-9438,
Snežana Dragović, 0000-0003-0566-0182,
„VINČA" Institute of Nuclear Sciences - National Institute of the Republic of Serbia, University of Belgrade, Belgrade, Serbia

ABSTRACT – Cadmium (Cd) is a toxic metal requiring effective immobilization strategies. This study evaluated fly ash, rice husk ash, red mud, and treated bovine bones for Cd removal, comparing their performance to commercial products (ion exchange resin, activated carbon, calcium carbonate, and zeolite). Red mud and treated bones showed removal efficiency comparable to or better than commercial products across varying Cd concentrations. Sequential extraction revealed that treated bones ensured long-term Cd immobilization, with most Cd retained in the residual fraction. These findings emphasize the potential of using waste-derived materials as cost-effective alternatives for the remediation of Cd in water and soil.

Keywords: Cadmium, Separation, Immobilization, Waste materials, Sequential extraction.

INTRODUCTION

Cadmium (Cd) is one of the most mobile and bioavailable elements, which requires special attention due to the high risk of water and soil contamination, bioaccumulation, biomagnification in the food chain, and adverse health effects [1]. While geological weathering is a key natural source of Cd in soil and water, industrial emissions, mining, smelting, wastewater irrigation, agrochemicals, and improper waste disposal are primary anthropogenic inputs. The estimated ratio of anthropogenic to natural emissions of Cd is approximately 7:1 on a global scale [2].

The need for effective and affordable materials for separating Cd from aqueous media increased dramatically, particularly in low-income countries [3]. Furthermore, the remediation of Cd in contaminated soil has become a task of paramount importance [4]. Regardless of the soil properties, increasing levels of Cd contamination are characterized by the most notable increase of relative Cd amounts in the exchangeable fraction, which is easily accessible and mobile [5].

This study examined waste materials from food processing, metallurgy, and electric utilities as agents for Cd removal and immobilization. Their effectiveness was compared to commonly used water treatment and soil remediation products. Additionally, the

---

corresponding author: ivanat@vin.bg.ac.rs

distribution of Cd within the spent waste-derived sorbents was further investigated to assess the nature of the bonds between Cd and the materials studied.

EXPERIMENTAL

Waste and commercial materials

Several abundant waste materials with different chemical and mineralogical compositions were selected. Rice husk ash (RHA), sourced from “Agrino”, Greece, is a byproduct of the combustion of rice hulls and serves as a source of amorphous reactive silica [6]. Animal bones are a valuable biogenic calcium phosphate (apatite) resource. For this study, the bovine bones were prepared through chemical oxidation using hydrogen peroxide (BBH) and thermal treatment at 400°C (BBT) [7]. Red mud (RM) was sourced from the tailings pond of the "Alumina" factory in Zvornik, Bosnia and Herzegovina. This waste sludge generated from the Bayer process during bauxite ore processing comprises various components, mainly oxides of iron, aluminum, and silica [8]. Lastly, fly ash (FA), a common byproduct of coal combustion, was considered. The sample supplied from a thermal power plant in Kostolac, Serbia, is characterized by a high content of silica and lesser amounts of iron and aluminum oxides [9]. All materials were finely ground using a ceramic mortar.

The following products, commonly used for soil remediation and the treatment of water and wastewater, were examined for comparison: calcium carbonate ($CaCO_3$) from Merck; zeolite (“Zeokop”, Serbia) denoted as ZEOL; activated carbon (AquaSorb®HS) referred to as AC, and a mixed bed ion exchange resin (Resinex™ MX-11) referred to as IER, both sourced from Jacobi Group.

Determination of Cd removal efficiency and stability of resulting residues

Solutions with a range of Cd concentrations ($5 \cdot 10^{-6}$, 10^{-3} and 10^{-2} mol/L), and initial pH 5.5, were prepared from $Cd(NO_3)_2 \times 4H_2O$ (Merck, p.a.) and deionized water. The powdered materials and Cd solutions were mixed at a 1:20 (g/ml) soil-to-solution ratio using an overhead laboratory shaker (10 rpm). The experiments were conducted at room temperature (21±1°C) for 24 h to ensure equilibrium conditions. After centrifugation and filtration through 0.45 µm membrane filters, residual Cd concentrations were measured by an Inductively Coupled Plasma Mass Spectrometer (ICP-MS, model iCAP Q, Thermo Scientific). Final pH values were measured using the InoLab WTW pH meter.

The solid residues obtained after mixing the waste materials with 10^{-3} mol/L Cd solution were analyzed to determine the speciation of Cd in five operationally defined fractions: ion-exchangeable (F1), bound to carbonates/acid soluble (F2), bound to iron and manganese oxides/reducible (F3), bound to organic matter/oxidizable (F4), and residual (F5). For that purpose, a Tessier sequential extraction procedure [10] was applied and modified according to Marković et al. [5].

RESULTS AND DISCUSSION

Figure 1 displays the Cd removal efficiency of tested materials and the corresponding equilibrium pH values. Under equivalent experimental conditions, all materials completely removed Cd from 5·10^{-6} mol/L solution (Figure 1, a), resulting in residual Cd quantities below the detection limit (LOD; 0.05 µg/L). For comparison, the maximum permissible Cd concentration (MPC) in drinking water set by the World Health Organization (WHO) is 3 µg/L [11].

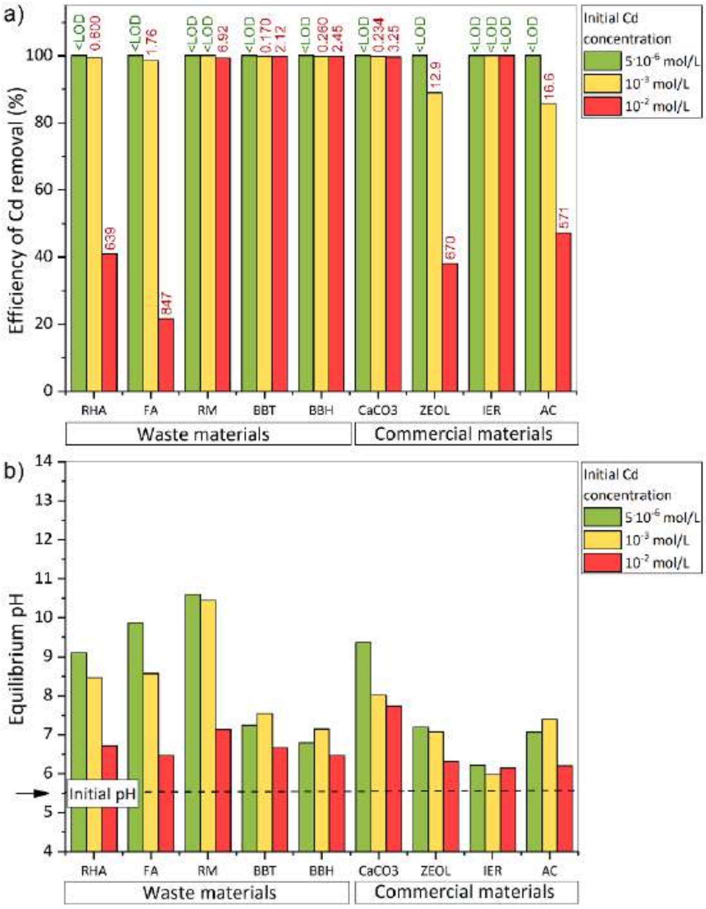

Figure 1 (a) Cadmium removal efficiency by waste and commercial materials (numbers above bars indicate the residual Cd concentration in mg/L; LOD = 0.05 µg/L) and (b) equilibrium pH values

As the initial concentration of Cd increased to 10^{-3} mol/L, the removal efficiencies of RHA (99.5%), FA (98.5%), ZEOL (89.0%), and AC (85.8%) declined compared to other materials that maintained efficiencies above 99.9%. Using a 10^{-2} mol/L concentration, RHA, FA, ZEOL, and AC capacities dropped significantly to 40.9%, 21.7%, 38.1%, and 47.2%, respectively. In contrast, RM removed 99.4%, $CaCO_3$ 99.7%, and bone-derived materials 99.8%, while the IER could still remove Cd completely. The results indicate that silicate-rich wastes RHA and FA are particularly affected by increases in Cd concentration, leading to a notable loss in their removal efficiencies.

These results are further analyzed by observing the equilibrium pH values (Figure 1, b). The hydrolysis of Cd ions starts at pH > 8, leading to an increase in the percentage of $Cd(OH)^+$ species, whereas $Cd(OH)_2$ precipitation occurs in the pH range of 10-12. RHA, FA, and RM are alkaline wastes that provided high equilibrium pH values but displayed a significant decrease in equilibrium pH with increased Cd concentration. Judging by the equilibrium pH values, sorption and ion exchange of $Cd(OH)^+$ may be the operating mechanism of RHA, FA, and RM for Cd concentrations of $5 \cdot 10^{-6}$ and 10^{-3} mol/L. A substantial pH decline associated with the highest initial concentration of 10^{-2} mol/L implies Cd ions sorption through inner-sphere complex formation with the surface (S-OH) groups following the reaction:

$$Cd^{2+} + S\text{-}OH \leftrightarrows S\text{-}OCd^{+} + H^{+} \quad (1)$$

In carbonate-rich environments, otavite ($CdCO_3$) precipitates at a pH of around 7.0 to 8.0, explaining the high efficacy of $CaCO_3$. Similarly to ZEOL, IER, and AC, the removal of Cd by bone-derived BBH and BBT occurred at near-neutral pH but with superior efficiency. Surface complexation, ion exchange with Ca ions in apatite lattice, and dissolution/precipitation are possible mechanisms of Cd removal by BBH and BBT.

To analyze the stability of sorbed Cd, residues with sorbed Cd amounts ranging from 2.307 mg/g to 2.341 mg/g were subjected to a sequential extraction protocol (Figure 2). The recovery of Cd across all five extraction fractions ranged from 95% to 118%.

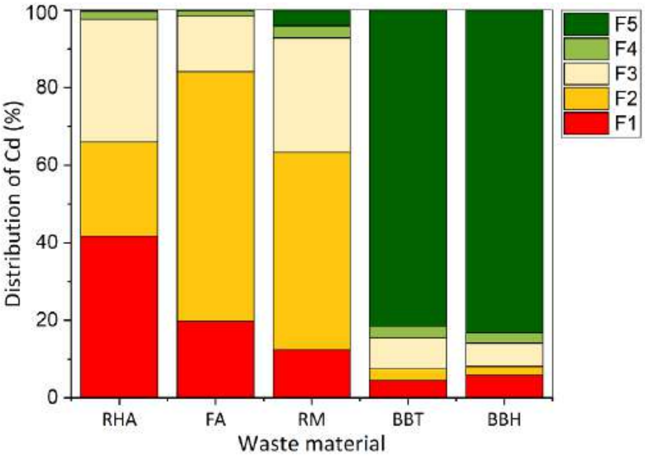

Figure 2 Distribution of Cd in various fractions of waste materials (F1- ion-exchangeable, F2 - bound to carbonates/acid soluble, F3 - bound to iron and manganese oxides/reducible, F4 - bound to organic matter/oxidizable, F5 – residual)

Considering the RHA, FA, and RM, Cd was found mainly in mobile fractions, with respectively 42%, 20%, and 12% in the ion-exchangeable (F1) phase and 24%, 64%, and

54% in the carbonate/acid soluble (F2) phase. Quite the contrary, BBT, and BBH hold most of the sorbed Cd (81% and 83%) in the residual (F5) fraction, which can be liberated only by the action of concentrated mineral acids, i.e., in conditions never encountered in the environment. A small portion was found in F1 (4-5%) and F2 (3-3%) fractions, which supports the dissolution of apatite and precipitation of poorly soluble Cd phosphate as the main mechanism of Cd removal. The presented results have implications for the stability of spent sorbents upon disposal, possible regeneration of sorbents, and their application in soil remediation.

Distribution of Cd in RHA, FA, and RM indicates the release of Cd in conditions of increased acidity and/or concentration of other cations. This suggests potential negative impacts on landfills for waste disposal while also indicating the relatively straightforward regeneration of sorbents and recovery of Cd. Sorbents derived from animal bones tightly bind Cd, establishing strong chemical bonds, which is a valuable performance in terms of spent sorbent stability and soil remediation.

The primary route for human exposure to cadmium (Cd) is through the consumption of vegetables [12]. This raises significant concerns, particularly in areas with cadmium-enriched farmland soil [4]. The forms of Cd that are considered mobile and potentially available for plant uptake include water-soluble, exchangeable, carbonate-bound, and those bound to iron and manganese oxides [4]. As a result, various techniques are employed to reduce Cd content in the labile fractions of contaminated soil, including chemical elution, electro-kinetic remediation, phytoremediation, stabilization and solidification, as well as combined remediation strategies [4]. Applying bone-derived materials to Cd-contaminated soil shows promise for *in situ* immobilization of Cd by enhancing the transfer of the pollutant from soluble and mobile fractions to a more stable residue fraction, effectively reducing their mobility and bioavailability.

CONCLUSION

Valuable minerals found in the waste materials studied can help mitigate Cd pollution. This approach addresses significant issues commonly faced in wastewater treatment, such as the high consumption of precipitating agents and the problems related to sludge formation. Depending on the level of Cd contamination, treatments using RHA, FA, and RM can be highly effective. However, the equilibrium pH of the treated water may exceed permissible discharge values, and monitoring is necessary for the potential leaching of trace impurities from the waste. Bone-derived materials have demonstrated superior efficiency in removing Cd under near-neutral conditions and have a high potential for long-term Cd immobilization, making them promising candidates for soil remediation. Further investigation is necessary to examine how wastewater composition and other factors impact the performance of studied materials.

ACKNOWLEDGEMENT

This work was supported by the Ministry of Science, Technological Development and Innovation of the Republic of Serbia (grant no 451-03-136/2025-03/200017).

REFERENCES

1. Kubier, A., Wilkin, R.T., Pichler, T. (2019) Cadmium in soils and groundwater: A review. Applied Geochemistry, 108, 104388.
2. Wright, D.A., Welbourn, P.M. (1994) Cadmium in the aquatic environment: A review of ecological, physiological, and toxicological effects on biota. Environmental Reviews, 2 (2), 187-214.
3. Hamid, N.H.A., Rushdan, A.I., Nordin, A.H., Husna, S.M.N., Faiz Norrrahim, M.N., Knight, V.F., Tahir, M.I.H.M., Li, G.X., Quan, T.L., Abdullah, A.M., et al. (2024) A state-of-art review on the sustainable technologies for cadmium removal from wastewater. Water Reuse, 14 (3), 312-341.
4. Tang, X., Li, Q., Wu, M., Lin, L., Scholz, M. (2016) Review of remediation practices regarding cadmium-enriched farmland soil with particular reference to China. Journal of Environmental Management, 181, 646-662.
5. Marković, J., Jović, M., Smičiklas, I., Šljivić-Ivanović, M., Onjia, A., Trivunac, K., Popović, A. (2019) Cadmium retention and distribution in contaminated soil: Effects and interactions of soil properties, contamination level, aging time and in situ immobilization agents. Ecotoxicology and Environmental Safety, 174, 305-314.
6. Vaskalis, I., Skoulou, V., Stavropoulos, G., Zabaniotou, A. (2019) Towards circular economy solutions for the management of rice processing residues to bioenergy via gasification. Sustainability, 11, 6433.
7. Dimović, S., Smičiklas, I., Plećaš, I., Antonović, D., Mitrić, M. (2009) Comparative study of differently treated animal bones for Co^{2+} removal. Journal of Hazardous Materials, 164 (1), 279-287.
8. Smičiklas, I., Jović, M., Janković, M., Smiljanić, S., Onjia, A. (2021) Environmental safety aspects of solid residues resulting from acid mine drainage neutralization with fresh and aged red mud. Water, Air, & Soil Pollution, 232 (12), 490.
9. Baščarević, Z., Komljenović, M., Petrašinović-Stojkanović, L., Jovanović, N., Rosić, A., Ršumović, M. (2006) Investigation of fly ash properties with purpose of its utilization as a secondary raw material for portland cement clinker production. Hemijska Industrija, 60 (9-10), 245-252.
10. Tessier, A., Campbell, P.G.C., Bisson, M. (1979) Sequential extraction procedure for the speciation of particulate trace metals. Analytical Chemistry, 51 (7), 844-851.
11. WHO (2011) Cadmium in drinking-water. Background document for development of WHO guidelines for drinking water quality. World Health Organization, Geneva, Switzerland.
12. Franz, E., Römkens, P., Van Raamsdonk, L., Van Der Fels-Klerx, I. (2008) A chain modeling approach to estimate the impact of soil cadmium pollution on human dietary exposure. Journal of Food Protection, 71 (12), 2504-2513.

XVI International Mineral Processing
and Recycling Conference
28-30 May 2025, Belgrade, Serbia

DOI:10.5937/IMPRC25244K Original research article

CASE STUDY ON METAL(LOID)S DISTRIBUTION IN LINDEN TREE PARTS, IN AREAS WITH HIGHT ENVIRONMENTAL POLLUTION

Tanja Kalinović[#], 0000-0003-0161-0065,
Ana Radojević, 0000-0003-3138-154X,
Jelena Kalinović, 0000-0003-0088-2683,
Jelena Jordanović, 0000-0002-8145-640X,
Snežana Šerbula, 0000-0001-7560-4130,
University of Belgrade – Technical faculty in Bor, Bor, Serbia

ABSTRACT – The investigation focuses on the distribution of Al, Fe, Cu, Zn, Pb, As, and Cd, in the roots, branches and leaves of linden tree, a very common plant species used in traditional medicine, sampled in the area affected by pollution from the mining-metallurgical facilities for copper production, and one unpolluted zone. Plant samples were collected and processed following the established scientific methods, while concentrations of metal(loid)s were determined using the ICP-AES. Distinct patterns in the metal(loid)s distribution in the linden parts were revealed, which varied depending on the environmental pollution levels, highlighting obvious differences between the polluted and unpolluted zones.

Keywords: Linden, Medicinal Plants, Environmental Pollution, Copper, Lead, Arsenic.

INTRODUCTION

Tilia sp. is highly adaptable to a wide range of environmental conditions, making it a vital species for urban greening due to its capacity to improve air quality. The flowers, leaves, and bark of *Tilia* sp. have edible values, with its flowers particularly appreciated for making herbal tea known to alleviate anxiety and promote better sleep [1]. The safety of the use of medicinal plants is an important public health concern in the polluted areas, due to the potential risk of their contamination with metal(loid)s [2]. Medicinal plants can readily absorb both organic and inorganic compounds from all environmental compartments (water, soil and air), which can ultimately be transferred to humans via teas, other drinks, cosmetics, etc. [3,4]. In the Review article about contamination of herbal medicinal products, by Opuni et al. [2], it was stated that metals were indicated as one of the predominant group of contaminants with 56.0%, in comparison with microbial, mycotoxins, pesticides, and residual solvents. Elements such as Cu, Zn, Mn, Fe, B, Mo and Cl, represent the essential micronutrients for all plants, required in small amounts, but their excessive contents can also adversely affect plant growth and metabolism. Aluminum is a common constituent of all plants, but its physiological function is not clear, although there is some evidence that low levels of Al can have a

---

[#] corresponding author: tkalinovic@tfbor.bg.ac.rs beneficial effects on the plant growth [5]. Arsenic, lead and cadmium are considered as non-essential and toxic for plants, significantly impacting a wide range of physiological responses [6-8]. This investigation aims to give insights about the distribution of metal(loid)s among parts of linden trees sampled in a polluted and unpolluted environment, which is in accordance with the pressing issue about contamination of medicinal plant species.

EXPERIMENTAL

Linden trees are a very common plant species in the study area that the local population has used in traditional medicine since the ancient times. Roots, branches and leaves of three to five healthy linden trees, were sampled from 10 sampling sites, located in 7 zones: UI (urban-industrial zone/sampling site), U (urban zone/sampling site), SU (suburban zone/sampling site), I1 and I2 sampling sites (industrial zone, I), T1 (Brestovac spa) and T2 (Bor lake) (tourist zone, T), R1 and R2 sampling sites (rural zone, R), B (background zone/sampling site, unpolluted area). Almost all sampling sites, except the site B, were under the influence of polluting substances emitted from the mining and metallurgical facilities, as well as from the flotation tailing ponds, and overburden dumps. The UI zone has been highly endangered for decades due to extreme air pollution with sulfur dioxide (SO_2) and metal(loid)s primarily emitted from the copper smelter [9]. The R zone was particularly emphasized due to its large area of agricultural land intended for food production, which was under the pollution from the copper smelter, flotation tailing ponds and acid mine drainage. Plant material was sampled in autumn, under the stable weather conditions. Leaves and branches (about 2 cm thick) were sampled at the high of 1.5 to 2 m, from the several sides of the canopy. One half of the composite leaf sample was remained unwashed, while the other half was washed in distilled water. Branches remained unwashed. Roots (up to 4 cm thick) were sampled at a depth of 10–20 cm, with several sides of the canopy. The composite samples of roots were repeatedly washed in distilled water with brushing. Plant samples were air dried at the room temperature and then milled. Microwave digestion of the plant material was performed according to the US EPA method [10]. The concentrations of Al, Fe, Cu, Zn, Pb, As, and Cd in the plant parts were determined at the Mining and Metallurgy Institute Bor, on the atomic emission coupled plasma–induced spectrometer, with radial and axial plasma observations, (ICP–AES). In order to compare the element concentrations in different linden parts, a paired Wilcoxon Signed Rank test was performed, since the statistical distribution of most variables determined by chemical analyses did not exhibit a normal distribution with the Shapiro–Wilk test. All significant differences were at $P<0.05$ level. The statistical significance of the difference between As and Cd in linden parts was not calculated because the contents of these elements were below the limits of determination in some samples.

RESULTS AND DISCUSSION

Linden roots contained higher Al concentrations than the branches and leaves, which can be presented by following order: branches<washed leaves<unwashed leaves<roots,

except at the sampling sites R1 and I1, where unwashed leaves had the highest Al contents (Figure 1a).

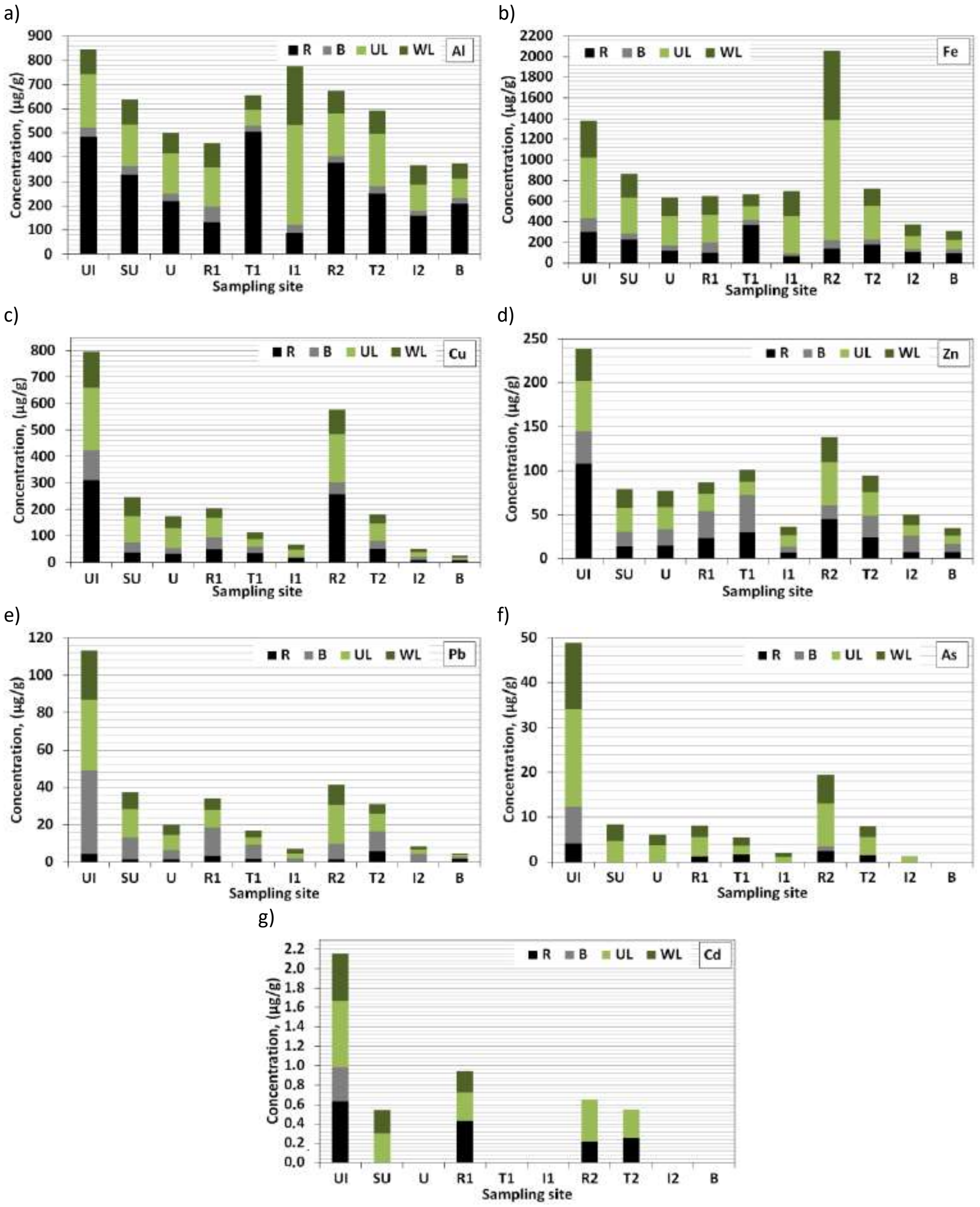

Figure 1 Distribution of a) Al, b) Fe, c) Cu, d) Zn, e) Pb, f) As, and g) Cd in the linden tree (R-roots; B-branches; UL-unwashed leaves; WL-washed leaves)

Such pattern could be influenced by the atmospheric particles rich in Al, deposited on the surfaces of leaves. From the obtained results it can be assumed that linden has naturally developed ability to retain the highest proportion of Al in its roots, which was in accordance with the distribution of Al within the linden tree from the B sampling site. Only difference between Al contents in the unwashed leaves and roots was not statistically significant (Table 1).

Table 1 Statistical significance of differences between concentrations of examined elements in linden parts (Wilcoxon Signed Rank test)

Linden parts	Al	Fe	Cu	Zn	Pb
UL-R	-*	-*	-*	-*	✓ **
UL-B	✓**	✓**	✓**	-*	-*
WL-R	✓**	-*	-*	-*	✓**
WL-B	✓**	✓**	✓**	-*	-*
R-B	✓**	✓**	✓**	-*	✓**
UL-WL	✓**	✓**	✓**	✓**	✓**

UL – unwashed leaves; WL –washed leaves; R-roots; B-branches; *- Not statistically significant difference; **Statistically significant difference at P<0.05 level.

The highest share of Fe was determined in the linden unwashed leaves, except at the T1 and B sampling sites, where roots contained the highest Fe levels (Figure 1b). At the B sampling site, roots contained slightly higher Fe content, compared to the leaves, which indicated that in the unpolluted environments, Fe is almost equally distributed between roots and leaves of linden, which is in accordance with the results by Ancuceanu et al. [11]. The lowest Fe concentrations were determined in the linden branches at all the sampling sites. Obtained results indicated that linden leaves have higher efficiency to trap atmospheric particles rich in Fe compared to branches. The differences were not statistically significant only between the Fe concentrations in the unwashed leaves and roots, as well as in the washed leaves and roots (Table 1).

Linden unwashed leaves contained higher Cu levels than the other parts, except at the sampling sites UI, T1, and R2, where roots were the plant parts with the highest Cu contents (Figure 1c). Such observation was in the accordance with the statement of Kabata-Pendias and Pendias [5], emphasizing that the roots of plants have a strong capability to hold Cu against the transport to aerial parts under the conditions of Cu excess, which was the case at the UI sampling site with the highest Cu soil content, about 5000 mg/kg [3]. At the B sampling site, where Cu concentrations in soil were the lowest [3], this metal was almost equally distributed in the roots, branches and leaves. The lowest Cu concentrations were predominantly determined in the linden branches, as in the case of Fe, suggesting that linden leaves have higher efficiency to trap atmospheric particles compared to branches. The differences were not statistically significant only between the Cu concentrations in unwashed leaves and roots, as well in the washed leaves and roots, as in the case for Fe (Table 1).

The highest share of Zn was found in the linden aboveground parts, unwashed leaves (at the sites SU, U, I1, R2, T2), and branches (at the sites R1, T1, I2, B), except at the UI sampling site, where linden roots had the highest Zn contents (Figure 1d). This is in agreement with the findings of Kabata-Pendias and Pendias [5] that roots predominantly contained much more Zn than above-ground plant parts, in Zn-rich soils, which was the case for the UI zone [3]. At the B sampling site, Zn was almost equally distributed among the linden parts. Differences between Zn concentrations in the analysed linden parts were not statistically significant, except for the Zn contents in the unwashed and washed leaves (Table 1).

The lowest contents of Pb were determined in the linden roots, except at the sampling sites T2 and B (Figure 1e). At the sampling site B, the Pb concentrations in the roots were the highest indicating the opposite pattern compared to the UI sampling site. At the rest of the sampling sites, the highest Pb concentrations were determined in the linden branches (sampling sites UI, RI, T1, T2, I2) and unwashed leaves (sampling sites SU, U, I1, R2). According to Kabata Pendias and Pendias [5], most of the Pb in soil is unavailable to plant roots, and the translocation of Pb from roots to aboveground plant parts is greatly limited, whereby only 3% of the Pb in the roots could be translocated to the aerial parts. However, there is evidence that airborne Pb, is also readily taken up by plants through foliage, which could be the case in this study. This was the indication of different ways of accumulation and translocation of this element in the linden tree, depending on the environmental pollution level. Differences were not statistically significant only for the pairs: unwashed leaves–branches, and washed leaves–branches (Table 1).

The linden unwashed, as well as washed leaves had the highest As contents at all the sampling sites where As concentrations were above the limit of determination. This suggests that linden leaves are more efficient in trapping the atmospheric particles rich in As, than linden branches (Figure 1f).

From the available data, it could be concluded that the highest Cd concentrations were detected in the unwashed leaves, and only at the sampling site R1 the highest Cd content was determined in the linden roots (Figure 1g). According to Kabata-Pendias and Pendias [5], when the amount of Cd is increased in the growth medium, the concentration of this metal in roots exceeds its content in the aboveground parts of plants by about 100 times, but this was not the case in this study for the UI sampling site. The possible reason for such behavior could be the certain quantity of Cd in the atmospheric particulates, which were absorbed by the linden leaves. Linden leaves are more efficient in trapping the atmospheric particles rich in Cd, than linden branches.

CONCLUSION

The obtained results showed that linden tree has naturally developed mechanisms to retain the highest proportion of Al in its roots. In the urban-industrial zone, the most polluted area, the highest share of Cu and Zn was observed in linden roots; the highest share of Fe, As and Cd was detected in linden unwashed leaves, and the highest share of Pb was observed in linden branches. In contrast to that, in the unpolluted zone (B), the highest contents of Fe and Pb were determined in the linden roots and of Cu in the unwashed leaves. The As and Cd concentrations in the linden parts from the B sampling site were under the limit of quantification. The linden leaves had higher efficiency to trap atmospheric particles compared to branches, according to the Fe, Cu, As and Cd distribution among linden parts, probably because larger surface area of leaves and smooth bark of the linden branches. It could be concluded that the share of studied metal(loid)s among linden parts was distinct among the unpolluted zone and in the zones under the influence of polluting substances from the mining and metallurgical facilities. Considering the obtained results, it is necessary to develop sustainable practices of raising public awareness about the risk of collecting and consuming the medicinal plants from the polluted areas. Ensuring the quality and safety of medicinal herbs is essential for their effective use, underscoring the necessity for continuous scientific research on the metal(loid)s uptake, distribution at the soil/water-plant interface, translocation from under-to-above plant parts and vice versa.

ACKNOWLEDGEMENT

The authors are grateful to the Ministry of Education, Technological development, and Innovations of the Republic of Serbia for financial support, within the funding of the scientific research at the University of Belgrade – Technical Faculty in Bor (No. 451-03-137/2025-03/ 200131).

REFERENCES

1. Zhou, Y., Ren, Q., Shen, Y., et al. (2025) Comprehensive review of *Tilia* L.: phytochemical profiles, edible value, therapeutic potentials, and ecological significance. Food & Medicine Homology, 2 (2), 9420035.
2. Opuni, K.F.M., Kretchy, J.P., Agyabeng, K., et al. (2023) Contamination of herbal medicinal products in low-and-middle-income countries: A systematic review. Heliyon, 9 (9), e19370.
3. Kalinovic, T.S., Serbula, S.M., Radojevic, A.A., et al. (2016) Elder, linden and pine biomonitoring ability of pollution emitted from the copper smelter and the tailings ponds. Geoderma, 262, 266-275.
4. Asiminicesei, D.-M., Vasilachi, I.C., Gavrilescu, M. (2020) Heavy metal contamination of medicinal plants and potential implications on human health. Revista de Chimie, 71, 16-36.
5. Kabata-Pendias, A., Pendias, H. (2001) Trace elements in soils and plants. 3rd ed. Boca Raton, Florida.
6. Ali, M., Nas, F. (2018) The effect of lead on plants in terms of growing and biochemical parameters: a Review. MOJ Ecology & Environmental Sciences, 3.
7. Meharg, A., Whitaker, J. (2002) Arsenic uptake and metabolism in arsenic resistant and non-resistant plant species. New Phytologist, 154, 29-43.
8. Moravčíková, D., Žiarovská, J. (2023) The effect of cadmium on plants in terms of the response of gene expression level and activity. Plants, 12, 1848.
9. Serbula, S.M., Milosavljevic, J.S., Radojevic A.A., et al. (2017) Extreme air pollution with contaminants originating from the mining-metallurgical processes. Science of the Total Environment, 586, 1066-1075.
10. U.S. EPA (U.S. Environmental Protection Agency), (1996) Acid Digestion of Sediments, Sludges, and Solids (3050B), Washington, DC.
11. Ancuceanu, R., Dinu, M., Hovaneţ, M.V., et al. (2015) A Survey of Plant Iron Content-A Semi-Systematic Review. Nutrients, 7 (12), 10320-51.

XVI International Mineral Processing
and Recycling Conference
28-30 May 2025, Belgrade, Serbia

DOI: 10.5937/IMPRC25250F

Original research article

POSSIBILITY OF INSTALLATION OF SOLAR POWER PLANTS IN EXPLOITATION SITES

Branimir Farkaš[1#], 0000-0002-2377-9446,
Ana Hrastov[2], 0009-0003-9087-4413,
Iva Štefičar[2], 0009-0003-9735-5675,
[1]Faculty of Mining, Geology and Petroleum Engineering, Zagreb, Croatia
[2]RUDAR PROJEKT d.o.o., Zagreb, Croatia

ABSTRACT – In response to increasing energy demands, driven by the constant need for energy commodities, a strategic shift towards adopting alternative renewable energy is today's reality. In pursuit of enhancing the efficacy of renewable energy production, with a primary focus on solar energy, the idea of using mineral exploitation fields as prospective domains for solar power plant deployment has emerged. These sites span from tens to hundreds of hectares and are presenting opportune terrains for the installation of large-scale solar infrastructure.

To underscore the potential for multifunctional spatial utilization and the augmentation of solar energy integration, this research undertakes a comprehensive analysis encompassing legislative frameworks and technological modalities governing the integration of solar power facilities within exploitation fields. Drawing upon this analysis, different variants and models for solar power plant installation are presented.

Keywords: Exploitation Fields, Renewable Energy, Solar Power Plants.

INTRODUCTION

Due to the increasing demand for energy products, we are rapidly turning to alternative renewable sources of energy production. To increase the possibility of producing energy from renewable sources compared to the current situation, and primarily the use of solar energy, exploitation fields of solid mineral raw materials were considered as potential areas for the installation of solar panels (SP) due to the large areas they occupy, from several tens to hundreds of hectares. In this way, exploitation fields can be used for multiple purposes, exploiting mineral resources and producing renewable electric energy using SPs.

Various authors have considered the possibility of using the space of abandoned open-pit mines, where the exploitation of mineral raw materials has ended, to produce electricity from renewable sources [1,2]. Heib (2022) analyses, in his paper, the advantages and disadvantages of installing solar systems in landfills created by the disposal of mine waste from coal exploitation [3]. Given that there is a great need for energy sources during the operation of machinery in open-pit mines, the authors Igogo et. al. (2021) and Whitbread-Abrutat et. al. (2011) in their papers deal with the

---

[#] corresponding author: branimir.farkas@rgn.unizg.hr integration of renewable energy sources (sun, wind, etc.) into the exploitation processes or conversion of the mining works area after the completion of exploitation works [4,5].

To point out the possibility of this way of managing space in the Republic of Croatia and increasing the use of solar energy, this paper has conducted an analysis that includes legislative frameworks and technical possibilities for the location of solar power plants (SPPs) within the area of exploitation fields. Based on the analysis, proposals for different Variants for the installation of SPPs and Electricity Utilization Models were given, as well as a proposal for optimal areas where it would be possible to install SPPs.

EXPERIMENTAL

For the possibility of multipurpose use of mining sites, i.e. for the simultaneous exploitation of mineral resources and the installation of SPPs, it is necessary to analyse numerous different data. This includes the spatial data of the Ministry of Economy [6] on exploitation fields and legal acts regulating the issue of exploitation of mineral resources, as well as those regulating the use of renewable energy sources and the installation of SPPs. Based on the analysis of the above, proposals for variant solutions for the installation of SPPs within the mining sites were given, as well as proposals for the need to amend the law.

Analysis of law provisions

Mining sites on which the exploitation of mineral resources is currently conducted or has been carried out are considered as a proposal for possible locations for the installation of SPPs, legal legislation in the field of mining, spatial planning, construction, environment, and energy have been analysed. Figure 1 shows the above-mentioned legal areas and highlights the most important laws, ordinances, and/or regulations, as well as some of the documents or procedures that need to be implemented to carry out the exploitation or installation of SPs.

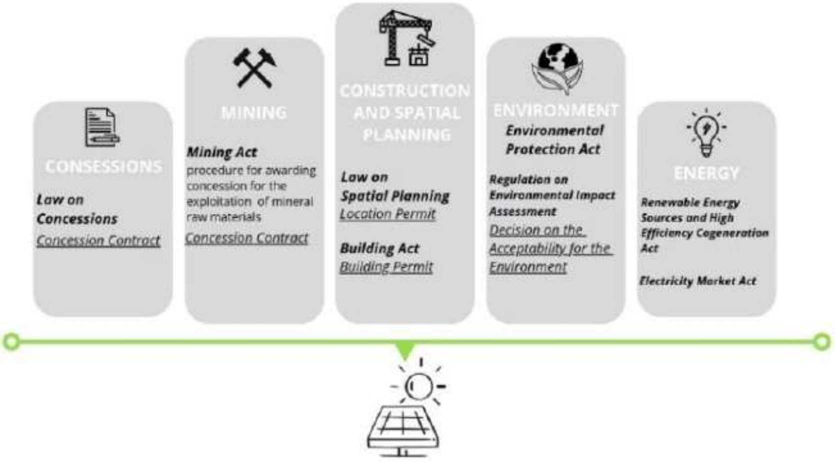

Figure 1 Law provisions for the possibility of installing SPP [7]

Analysis of technical possibilities of installing solar power plants at mining sites

According to the data of the Ministry of Economy and Sustainable Development [6], there are a total of about 800 exploitation fields in the Republic of Croatia, which includes active, inactive, and closed exploitation fields (Figure 2a). The mineral raw materials that are the most exploited are: technical-building stone, architectural-building stone (block and slab), construction sand and gravel, and clay (brick clay, bentonite, ceramic, and fire-resistant clay). Figure 2b shows the number of exploitation fields depending on the activity for the above-mentioned mineral raw materials.

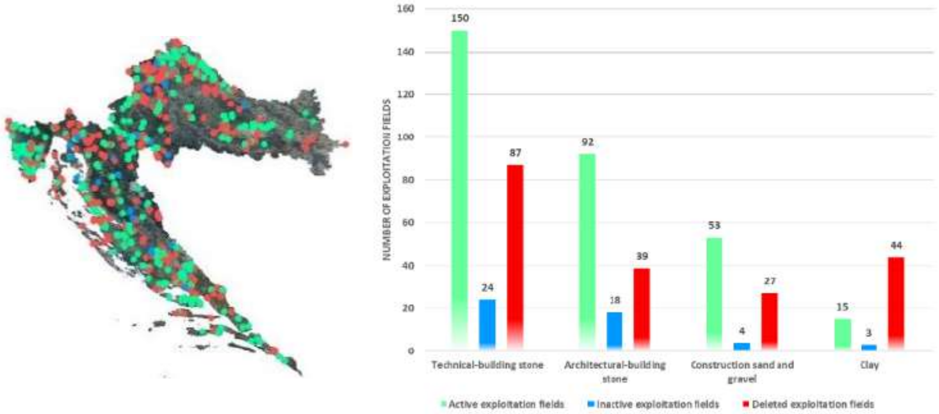

a) Exploitation fields in the Republic of Croatia

b) Distribution of exploitation fields by mineral raw materials and activity

Figure 2 View of exploitation fields and the most exploited mineral raw materials [6]

The technical possibilities of installing SPs within exploitation fields depend primarily on the type of mineral raw material that is exploited (concerning different exploitation technologies) and on the geometry of open-pit mines that occur due to exploitation [7].

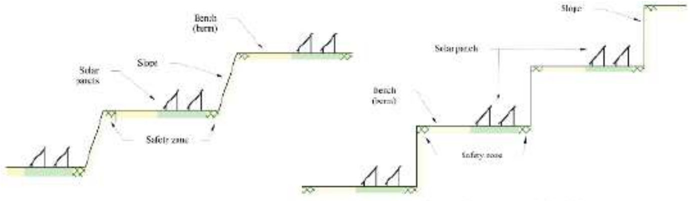

a) technical-building stone

b) architectural-building stone

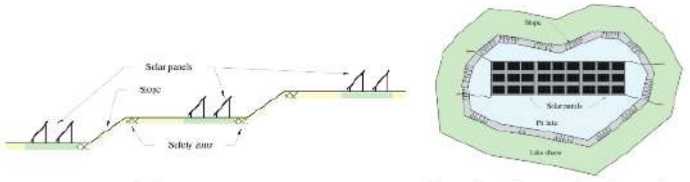

c) clay

d) construction sand and gravel

Figure 3 Possibility of placing SPs depending on the geometry of open-pit mines [7]

Surfaces that can be used for the placement of SPs are benches (berms) created by the exploitation of technical-building and architectural-building stone and clay (Figures 3a, 3b, 3c). The exploitation of these mineral raw materials is performed by drilling and blasting (technical-building stone), sawing blocks with a chain saw or diamond wire saw (architectural-building stone), or, in the case of clay exploitation mechanized – with excavators. In the exploitation of construction gravel and sand, dredgers are used, and consequently, water surfaces (lakes) are created that are suitable for the installation of floating SPs (Figure 3d).

RESULTS AND DISCUSSION

Based on the analyses [7], variant options for locating SPPs in open-pit mines have been proposed depending on the dynamics of mining operations (Variant 1, Variant 2, and Variant 3) and depending on electricity consumption (Model 1, Model 2, Model 3). The analysis of the legislative frameworks covering the exploitation of mineral raw materials in the Republic of Croatia and the production of energy from renewable sources has given suggestions for possible changes that would need to be implemented to enable the multipurpose use of the mining sites.

Proposal for necessary legal changes

The multipurpose use of mining sites requires the harmonization of several different areas of law, it is necessary to make some changes to them. To make this possible, it is needed to process or resolve issues that arise during the installation of SPPs in areas intended for the exploitation of mineral resources through legal legislation. For the harmonization of laws, i.e. their amendment, it is necessary to do the following [7]:

- harmonize spatial planning documentation,
- resolve property rights,
- designate the ministry responsible for issuing building permits,
- specify the allowed location of the SPP installation at mining sites,
- elaborate the installation of the SPP in a mining project,
- implementation of the environmental impact procedure,
- include the possibility of installing the SPP in the exploitation field in the concession obtaining procedure,
- tender conduction for secondary activity (establishment of the SPP at mining sites for which the concession fee is already paid).

Variant solutions for the placement of SPPs in exploitation fields

Variants of SPP installation depending on the dynamics of mining works

Depending on the dynamics of mining works performance, there are three possible variants of SP installation (Figure 7), whose positions within the boundaries of the exploitation field can be temporary or permanent.

Variants that occur depending on the dynamics of mining works are:

- Variant 1 – installation of SPs before awarding a concession for the exploitation of mineral raw materials (Figure 4a) – use of mobile solar panels,
- Variant 2 – installation of SPs during the mining works performance with a concession for the exploitation of mineral raw materials (Figure 4c) – use of fixed and mobile SPs,
- Variant 3 – installation of SPs after the completion of mining works (Figure 4b) – use of mobile SPs.

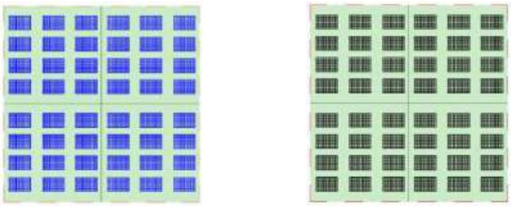

a) temporary positions b) permanent positions

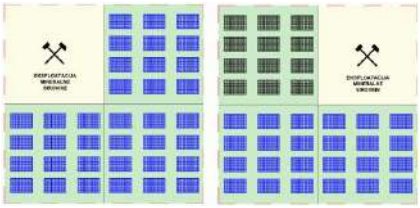

c) combination of temporary and permanent positions

Figure 4 Possibility of placing SPs depending on the dynamics of mining works [7]

Models of Electricity Usage

Each exploitation field on which mining works are carried out i.e. the exploitation of mineral raw materials in its technological process depends on some type of energy source (diesel fuel, electricity from the distribution network, or generators). All these forms of energy that are needed for a mining site to function can be efficiently replaced by electricity produced by SPPs located at mining sites.

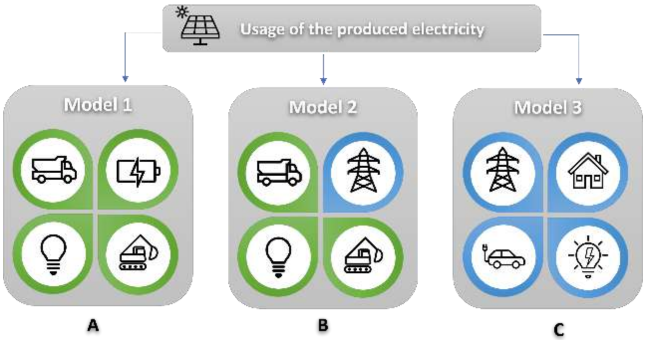

Figure 5 Models of electricity usage [7]

Depending on the needs within the exploitation field and the method of electricity delivery, SPPs can be divided into three models (Figure 5):

- Model 1 – the entire electricity produced is used for the needs of the exploitation field,
- Model 2 – the produced electricity is partly used for the needs of the exploitation field, and the surplus is handed over to the electricity grid,
- Model 3 – all electricity produced is handed over to the electricity grid for further distribution.

CONCLUSION

Multipurpose use of mining sites represents an integrated way of space planning that is not fully regulated by current legislation. By installing SPPs within the boundaries of exploitation fields, it would be possible for the authorized person/concessionaire to reduce its energy needs (electricity from the distribution system, diesel fuel, etc.) to a minimum or become completely energy-independent. Energy independence would enable a reduction in the price of mineral aggregates on the market, which would result in a decrease in the prices of construction of new buildings. In addition, the usage of electric mining machinery would completely nullify the harmful exhaust by-products of diesel fuel combustion in the engines of mining machinery and would significantly reduce the impact on the environment.

REFERENCES

1. Mert, Y. (2019) Contribution to Sustainable Development: Re-Development of Post-Mining Brownfields. J Clean Prod, 240.
2. Kim, H., Ku, J., Park, H.-D. (2021) Analysis of Photovoltaic Potential of Unused Space to Utilize Abandoned Stone Quarry. Tunnel and Underground Space, 31, 534–548, doi:https://doi.org/10.7474/TUS.2021.31.6.534.
3. Heib, M. (2022) Al ASSESSMENT OF ADVANTAGES AND LIMITATIONS OF INSTALLING PV ON ABANDONED DUMPS. Surface Mining.
4. Igogo, T., Awauah-Offei, K., Newman, A., Lowder, T., Engel-Cox, J. (2021) Integrating Renewable Energy into Mining Operations: Opportunities, Challenges, and Enabling Approaches. Appl Energy, 300.
5. Whitbread-Abrutat, P., Coppin, N. (2011) Exploring Alternative Energy Options for Mine Sites. In Proceedings of the Sixth International Conference on Mine Closure; Australian Centre for Geomechanics, pp. 559–568.
6. MINGO JISMS - WebGis Portal. Unified information system for mineral resources 2024. – (*In Croatian*: Jedinstveni informacijski sustav mineralnih sirovina).
7. Farkaš, B., Hrastov, A. (2023) Analysis of the Legislative Framework and Technical Possibilities of Placing Solar Power Plants on the Areas of Exploitation Fields of Solid Mineral Raw Materials – (*In Croatian*: Analiza Zakonodavnog Okvira i Tehničke Mogućnosti Smještaja Solarnih Elektrana Na Prostore Eksploatacijskih Polja Čvrste Mineralne Sirovine).

XVI International Mineral Processing
and Recycling Conference
28-30 May 2025, Belgrade, Serbia

DOI: 10.5937/IMPRC25256S

Original research article

ELECTROCHEMICAL OXIDATION OF BISPHENOL S WITH SnO_2-MWCNT ELECTRODES

Marija Simić[#], 0000-0001-9518-7709,
Marija Kovačević, 0000-0001-8858-6728,
Katarina Stojanović, 0009-0003-3467-9875,
Branislava Savić Rosić, 0000-0002-4632-7960,
Dragana Vasić Anićijević, 0000-0003-0566-3244,
Tanja Brdarić, 0000-0003-2547-7123,
Danka Aćimović, 0000-0001-7506-9684,
“Vinča” Institute of Nuclear Sciences-National Institute of the Republic of Serbia, Department of Physical Chemistry, Belgrade, Serbia

ABSTRACT – Bisphenol S (BPS) is a synthetic compound frequently used as an alternative to Bisphenol A (BPA) in the manufacture of various plastics and resins. Its widespread use has led to its detection in environmental samples, raising concerns about its potential endocrine-disrupting effects and toxicity. Recent research shows that BPS can leach from consumer products and accumulate in aquatic ecosystems, posing risks to both aquatic organisms and human health. Electrochemical oxidation of BPS has emerged as a promising approach for its degradation.

This study examines the electrochemical oxidation of Bisphenol S utilizing SnO_2-MWCNT (multi-walled carbon nanotubes) electrodes in a galvanostatic regime at different current densities (10, 15 and 20 mA cm^{-2}). The main objective of this study was to compare the removal efficiency and energy consumption during the degradation of BPS on various current densities. Experimental results indicated that an increase in current density corresponds to a rise in both removal efficiency and energy consumption. However, this observation highlights the necessity for careful optimization to balance efficiency and energy consumption in real-world applications.

Keywords: Bisphenol s, Electrochemical oxidation, SnO_2-MWCNT electrodes.

INTRODUCTION

Bisphenol S (BPS) was introduced as an alternative to bisphenol A (BPA) due to growing concerns over BPA’s potential health and environmental risks. It has since become widely utilized in the production of polycarbonate plastics and epoxy resins, which are commonly found in various consumer products, including food packaging, thermal paper, and electronic components. Bisphenol S (BPS) is structurally characterized by two hydroxyphenyl groups connected by a sulfonyl group, making it closely related to bisphenol A (BPA). Due to this structural similarity, concerns have been raised about its safety and the possibility of similar adverse effects. Notably, BPS exhibits

---

[#] corresponding author: marija.simic@vin.bg.ac.rs

greater resistance to heat and sunlight than BPA, making it a more durable alternative in industrial applications [1]. However, despite its widespread use, research on its safety remains limited. Preliminary studies suggest that BPS may pose equal or even greater risks than BPA in certain biological and environmental contexts. Several studies have reported its potential adverse effects on biological systems. These studies have highlighted concerns regarding its ability to disrupt the endocrine system, leading to hormonal imbalances that may affect various physiological functions. Additionally, BPS has been linked to cytotoxicity, indicating its potential to damage or impair cellular function. Some findings suggest that it may also exhibit mutagenic properties, raising concerns about its ability to induce genetic mutations that could contribute to long-term health risks. Furthermore, research has associated BPS exposure with an increased risk of obesity, potentially due to its impact on metabolic regulation. Notably, studies have also suggested that BPS may cause reproductive and developmental toxicity, posing risks to fertility, fetal development, and overall reproductive health. Despite these findings, further in-depth research is necessary to fully understand the extent of BPS toxicity and its implications for human and environmental health [2]. As the primary substitute for bisphenol A (BPA), bisphenol S (BPS) has become widely used in various industrial and consumer applications. Its production and utilization have significantly increased over the years, with the European Chemicals Agency (ECHA) reporting that the annual manufactured or imported volume of BPS in the European Economic Area ranged between 1,000 and 10,000 tons as of 2015. On a global scale, BPS has been detected extensively in aquatic environments, including surface water, riverine systems, and marine sediments, as well as in wastewater sludge. Its widespread presence in different environmental matrices highlights its persistence and potential for bioaccumulation [1]. The widespread presence of BPS raises concerns about its long-term effects on the environment and the potential risks it may pose to both wildlife and humans with continued exposure.

In addition to conventional methods for pollutant removal (coagulation, adsorption, membrane filtration, biological treatments, etc.), research is also focused on developing electrochemical advanced oxidation processes, which offer lower environmental risks and economic feasibility. Among these, electrochemical oxidation stands out as it utilizes electricity instead of additional chemicals to oxidize organic pollutants, often degrading them into carbon dioxide and water, depending on factors such as electrode material, applied current, and electrolysis duration [3, 4].

The aim of this study is to investigate the effect of current on the efficiency of bisphenol S removal from polluted wastewater, as well as its energy consumption, using electrochemical oxidation with a SnO_2-MWCNT electrode. A comprehensive comparison of BPS removal efficiency and energy consumption at various current densities is essential for optimizing the electrochemical oxidation process. By analyzing how different current densities influence both the effectiveness of BPS removal and the energy required, it is possible to identify the most efficient operating conditions, which can lead to more sustainable and cost-effective wastewater treatment methods.

MATERIALS AND METHODS

To evaluate the effect of current density on the degradation efficiency of bisphenol S, experiments were carried out in a two-electrode electrolytic cell. The setup included SnO_2-MWCNT electrodes as the working electrodes and stainless steel as the counter electrode. Electrolytic degradation was conducted at varying current densities of 10, 15, and 20 mA cm^{-2} under room temperature conditions. A Gamry Instruments Interface 1000 Potentiostat/Galvanostat (Gamry Instruments, USA) was used to regulate the electrochemical oxidation. It was performed on a 30 mg/L solution of bisphenol S in 0.01 M sodium sulfate at pH 4. Electrolyte samples were collected every hour over a 5-hour electrolysis period. To determine the concentration of BPS in the aliquots, liquid-liquid extractions were conducted using dichlor methane [4]. The extracts were then concentrated and analyzed by GC-MS [3].

The concentration of bisphenol S in the electrolyte was measured using a calibration curve, and the removal efficiency (%) was subsequently calculated using the following equation:

$$Efficiency\ removal = \frac{C_0 - C_t}{C_0} \qquad (1)$$

where c_o (mol dm^{-3}) is initial concentration BPS, c_t (mol dm^{-3}) represents the concentration of BPS in the aliquot taken at a specific time (t) of electrochemical degradation.

Overall, to analyze energy consumption at different current densities, the energy consumption per order (EE_0) in kWh/m^3 was calculated using Equation 2.

$$EE_0 = 1000\frac{\mathrm{Pt}}{Vlog\frac{C_0}{C_t}} = 1000\frac{\mathrm{UIt}}{Vlog\frac{C_0}{C_t}} \qquad (2)$$

where t is time of electrolysis (h), U (V) is applied potential in electrochemical system, and I (A) is applied current in electrochemical system [5].

RESULTS AND DISCUSSION

The electrolytic oxidation of 30 mg L^{-1} BPS was carried out at varying current densities of 10.0, 15.0, and 20.0 mA cm^{-2}. As shown in Figure 1, the removal efficiency of BPS increases as the current density rises, which aligns with findings from previous studies in the literature [6]. Notably, the most significant reduction in BPS concentration occurs during the first hour of electrolysis, with the removal efficiency showing a clear positive correlation with current density. During this period, the BPS concentration decreases by approximately 30% relative to the initial concentration at current densities of 15.0 and 20.0 mA cm^{-2}, indicating the enhanced effectiveness of the electrolytic oxidation process at higher current densities. This trend highlights the crucial role of current density in optimizing the efficiency of BPS removal from the electrolyte.

A significant difference in BPS removal is observed between current densities of 10 mA cm^{-2} and 20 mA cm^{-2}, resulting in efficiencies of 73.4% and 89.2%, respectively. However, the difference in efficiency removal between 20.0 mA cm^{-2} and 15.0 mA cm^{-2} is minimal, less than 4%, indicating that further increases in current density do not significantly affect the degradation efficiency.

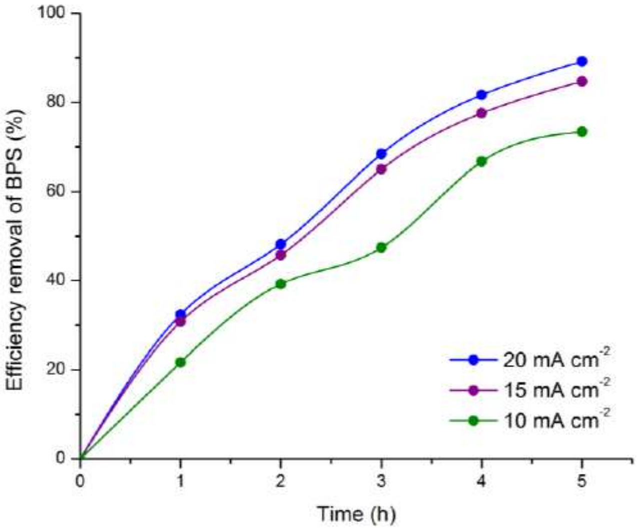

Figure 1 Efficiency removal of 30 mg L^{-1} 1 BPS at different current densities during anodic oxidation

The electric energy per order (EE_0), which is present an effective parameter for estimating energy consumption, is 9.4 kWh·m^{-3} on current density 10 mA cm^{-2}, 10.0 kWh·m^{-3} on 15.0 mA cm^{-2}, and 12.7 kWh·m^{-3} on 20.0 mA cm^{-2}. As it is depicted in Figure 2, calculated EE_0 indicates that an increase in current density leads to higher energy consumption, particularly at a current density of 20.0 mA cm^{-2}.

Based on these results and previous literature observations [7], it can be suggested that higher current densities likely accelerate parasitic reactions, such as O_2 generation, leading to increased energy consumption.

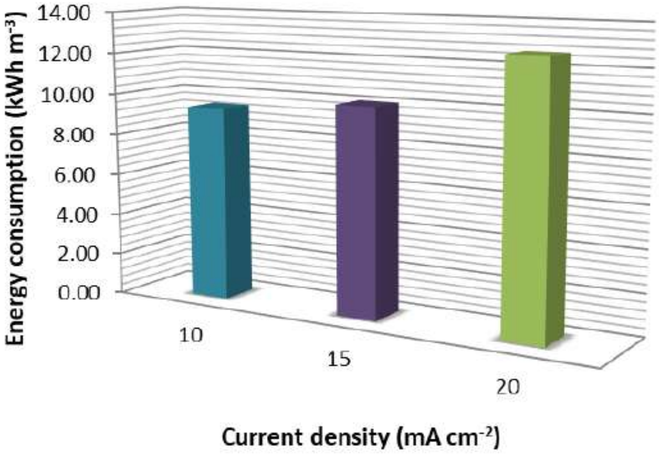

Figure 2 Energy consumption during anodic oxidation of BPS at different current densities

Considering that the efficiency removal of BPS at current densities of 15.0 and 20.0 mA cm^{-2} is similar, while energy consumption differs, electrochemical oxidation at a current density of 15.0 mA cm^{-2} should be selected for the most efficient operating conditions.

CONCLUSION

In conclusion, the electrolytic oxidation of BPS demonstrated that increasing current density improves the efficiency removal, with a notable reduction in BPS concentration occurring within the first hour of electrolysis. The degradation efficiency significantly differs between current densities of 10.0 and 20.0 mA cm^{-2}, with a minimal difference between 15.0 and 20.0 mA cm^{-2}. While higher current densities enhance BPS removal, they also result in increased energy consumption, particularly at 20.0 mA cm^{-2}. Therefore, a current density of 15.0 mA cm^{-2} is optimal, as it provides a more favorable balance between effective removal of bisphenol S and reduced energy consumption, making it the optimal choice for achieving efficient and cost-effective operating conditions in the process.

ACKNOWLEDGEMENT

This work was supported by the Ministry of Science, Technological Development, and Innovation of the Republic of Serbia [grant number 451-03-136/2025-03/200017].

REFERENCES

1. Oh, J., Choi, J.W., Ahn, Y.A., Kim, S. (2018) Pharmacokinetics of bisphenol S in humans after single oral administration. Environment International 112, 127–133.
2. Wu, L.H., Zhang, X.M., Wang, F., Gao, C.J., Chen, D., Palumbo, J.R., Guo, Y., Zeng, E.Y. (2018) Occurrence of bisphenol S in the environment and implications for human exposure: A short review. Science of the Total Environment 615, 87–98.
3. Simić, M.D, Brdarić, T.P., Savić Rosić, B.G., Švorc, Ľ., Relić, D.J., Aćimović, D.D. (2024) Degradation of bisphenol A via the electro–Fenton process using nanostructured carbon-metal oxide anodes: Intermediates and reaction mechanisms study. Journal of Environmental Chemical Engineering, 12 (5), 113369.
4. Simić, M.D., Savić, B.G., Ognjanović, M.R., Stanković, D.M., Relić, D.J., Aćimović, D.D., Brdarić, T.P. (2023) Degradation of bisphenol A on SnO_2-MWCNT electrode using electrochemical oxidation. Journal of Water Process Engineering 51, 103416.
5. Bolton, J.R., Bircher, K.G., Tumas, W., Tolman, C.A. (2001) Figures-of-merit for the technical development and application of advanced oxidation technologies for both electric- and solar-driven systems. Pure and Applied Chemistry 73 (4), 627–637.
6. Wu, W., Huang, Z., Hu, Z.-T., He, C., Lim, T. (2017) High performance duplex-structured SnO_2-Sb-CNT composite anode for bisphenol A removal. Separation and Purification Technology 179, 25–35.
7. Cai, J., Zhou, M., Pan, Y., Lu, X. (2020) Degradation of 2,4-dichlorophenoxyacetic acid by anodic oxidation and electro-Fenton using BDD anode: Influencing factors and mechanism. Separation and Purification Technology 230, 115867.

XVI International Mineral Processing
and Recycling Conference
28-30 May 2025, Belgrade, Serbia

DOI: 10.5937/IMPRC25261S

Original research article

COMPARATIVE STUDY OF ELECTROCHEMICAL DEGRADATION OF RHODAMINE B USING GLASSY CARBON, STAINLESS STEEL, AND NICKEL ELECTRODES

Marija Simić[#], 0000-0001-9518-7709,
Marija Kovačević, 0000-0001-8858-6728,
Katarina Stojanović, 0009-0003-3467-9875,
Marija Ječmenica Dučić, 0000-0002-6437-519X,
Dragana Vasić Anićijević, 0000-0003-0566-3244,
Danka Aćimović, 0000-0001-7506-9684,
Tanja Brdarić, 0000-0003-2547-7123,
“Vinča” Institute of Nuclear Sciences-National Institute of the Republic of Serbia, Department of Physical Chemistry, Belgrade, Serbia.

ABSTRACT – Rhodamine B is a synthetic dye commonly used in the textile and printing industries, recognized as a significant water pollutant. It enters aquatic environments primarily through untreated wastewater, posing serious threats to both environmental ecosystems and human health due to its toxic, carcinogenic, and non-biodegradable properties. The dye's persistence in water can result in harmful effects on ecosystems and contamination of vital water sources, underscoring the urgent need for effective removal methods. Electrochemical degradation has emerged as an eco-friendly technology to tackle this issue, breaking down Rhodamine B into less harmful byproducts and providing a sustainable approach for mitigating its environmental impacts. This study investigates the electrochemical degradation of Rhodamine B using glassy carbon (GC), stainless steel (SS), and nickel (Ni) electrodes in an undivided two-electrode system operating under a galvanostatic regime at a current density of $15\ \text{mA cm}^{-2}$. The primary goal was to compare the efficiency and kinetics of degradation across different electrode types. Experimental results demonstrated that GC electrodes, followed by SS, exhibited the highest degradation efficiency, with the process adhering to first-order kinetics. These findings highlight the advantages of GC electrodes in terms of speed and efficiency, offering valuable insights for optimizing treatment processes.

Keywords: Rhodamine B, Electrochemical degradation, Glassy carbon, Stainless steel, Nickel electrodes.

INTRODUCTION

Rhodamine B, also known as [9-(o-carboxyphenyl)-6-(diethylamino)-3H-xanthen-3-ylidene] diethylammonium chloride, is a synthetic dye extensively used in the food, textile, leather, and paper industries [1]. Numerous studies [2] have highlighted its toxic and potentially carcinogenic effects on both humans and animals, making it a significant environmental and public health concern. As a result, there has been a growing scientific focus on developing effective technologies for its degradation and removal [3]. Among the various processes, electrochemical degradation has gained significant attention as a

---

[#] corresponding author: marija.simic@vin.bg.ac.rs

highly effective method for the removal of organic pollutants, including Rhodamine B. This technique uses the electrochemical reaction occurring at the electrode surface, where pollutants undergo thought indirect or direct oxidation or reduction, resulting in the transformation of pollutants into safer, less toxic byproducts.

The process is highly adaptable and can be tailored to different contaminants, which makes it a versatile solution for wastewater treatment. One of the major advantages of electrochemical degradation is that it does not require the use of additional chemical reagents, which reduces the overall cost and environmental footprint of the treatment process. Furthermore, this method can be integrated into existing treatment systems, making it an appealing choice for large-scale applications. Another key benefit of electrochemical degradation is its high specificity, which allows for the selective breakdown of targeted pollutants while minimizing the formation of unwanted byproducts.

The degradation rate can be influenced by several factors, such as the applied voltage, electrode material, pH of the solution, and temperature, all of which can be optimized for maximum efficiency. The effectiveness of the electrochemical process is heavily dependent on the choice of electrode material, as different electrodes exhibit varying degrees of catalytic activity, stability, and conductivity. For example, boron-doped diamond (BDD) electrodes are known for their high stability and strong oxidative power, while carbon-based electrodes are often more cost-effective but may offer lower performance [4].

The electrochemical degradation of Rhodamine B is particularly promising because of its effectiveness in degrading organic compounds with high molecular stability. As research continues, efforts are also being made to scale up electrochemical degradation processes for industrial and municipal wastewater treatment, providing a more sustainable and cost-effective alternative to conventional methods. The primary goal of this study was to compare the electrochemical degradation of Rhodamine B using different electrode materials—specifically stainless steel (SS), nickel (Ni), and glassy carbon (GC) electrodes.

Each of these electrode materials offers distinct advantages and challenges that make them suitable for different electrochemical applications. SS electrodes, while cost-effective and widely available, may require surface modifications to enhance their catalytic efficiency and stability. Ni electrodes, known for their corrosion resistance and decent catalytic activity, provide an interesting option for degradation but may suffer from fouling over time. GC electrodes, on the other hand, are widely praised for their high surface area, conductivity, and customizability, making them an attractive choice for efficient pollutant degradation. By comparing these three materials, this study aimed to evaluate their efficiencies in degrading Rhodamine B, considering factors such as efficiency and kinetic rate. Additionally, the comparison provides insights into how electrode surface properties influence the electrochemical process, which is essential for optimizing treatment methods. The findings of this study may contribute to the identification of the most effective electrode material for electrochemical remediation of dye-contaminated wastewater, potentially aiding in the development of more cost-effective and sustainable wastewater treatment solutions.

EXPERIMENTAL

A 1x10^{-5} M solution of Rhodamine B in 0.05 M NaCl was prepared for the experiments. To assess the impact of electrolysis time on the degradation efficiency of Rhodamine B, experiments were conducted in a two-electrode electrolytic cell, with pairs of SS, Ni, and GC electrodes as the working and counter electrodes. Electrolytic degradation was performed at a constant current density of 15 mA cm^{-2} at room temperature using a Gamry Instruments Interface 1000 Potentiostat/Galvanostat (Gamry Instruments, USA). Aliquots of the electrolyte were collected at various time intervals, and absorbance at the peak wavelength of 554.5 nm was measured with a UV/Vis spectrophotometer (Lambda 35, Perkin Elmer, USA).

The concentration of Rhodamine B in the electrolyte was determined using a calibration curve. Removal efficiency was then calculated based on the following equation:

$$Removal\ efficiency\ (\%) = \frac{c_0 - c}{c_0}\ 100 \qquad (1)$$

Where c_0 is initial concentration Rhodamine B, c is concentration of Rhodamine B in taken aliquot in time, t of electrochemical degradation.

RESULTS AND DISCUSSION

Figure 1a presents the concentration profile of Rhodamine B during its electrochemical degradation on GC, SS, and Ni electrodes under constant current conditions (15 mA cm^{-2}). A decrease in Rhodamine B concentration over time was observed for all three electrodes, indicating improved degradation efficiency. SS and GC showed better performance compared to Ni. The degradation rate was rapid in the first 10 minutes, with Rhodamine B concentration decreasing by up to 50 % and 22 % for SS and GC, respectively, while the Ni electrode exhibited a significantly lower removal efficiency of only 12 % (see Figure 2).

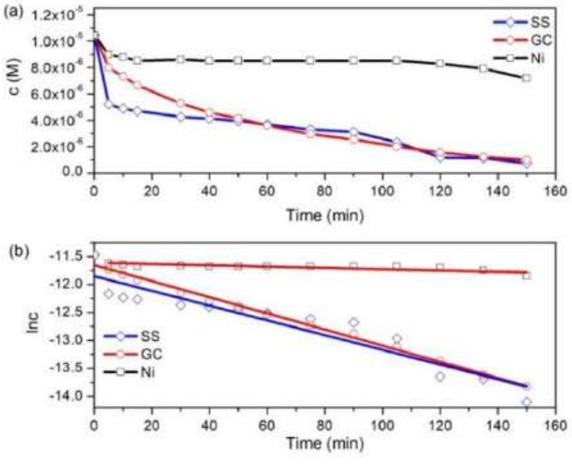

Figure 1 (a) Concentration profiles of Rhodamine B dye (1 x 10^{-5} M) at current density 15 mA cm^{-2} and (b) linear plot of lnc versus t

The concentration of Rhodamine B improved over time for SS and GC, indicating sustained degradation activity. After 150 min of electrolysis Rhodamine B removal efficiency on SS and GC is 92 and 90 %, respectively. In contrast, the Ni electrode displayed a noticeable decrease in concentration after 150 minutes, indicating a slower onset of degradation. The SS and GC electrodes showed a steeper increase in degradation efficiency throughout the experiment, indicating a more effective degradation process. On the other hand, the Ni electrode displayed a slower increase in removal efficiency (only 30 %), highlighting its weaker overall performance under identical conditions.

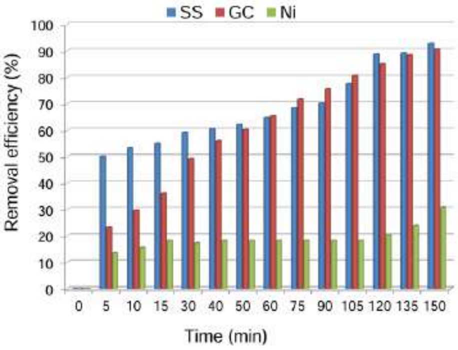

Figure 2 Degradation efficiency of Rhodamine B dye (1 x 10^{-5} M) at current density 15 mA cm^{-2}

A more detailed comparison between the SS and GC electrodes highlighted notable differences in their degradation behaviour. While the GC electrode exhibited a steady and uniform decrease in Rhodamine B concentration, the SS electrode followed a different trend. The most pronounced concentration of Rhodamine B decline for SS occurred within the first 30 minutes, followed by a slower degradation phase until approximately 90 minutes, after which a sudden and significant decrease in concentration was observed.

The observed differences in degradation efficiency can be attributed to the electrochemical properties of the electrodes and their surface interactions with the pollutant. It is well-known from the literature [5] that the GC electrode is stable, chemically inert, and highly electroconductive, which facilitates efficient electron transfer and hydroxyl radical (•OH) generation, ensuring continuous and uniform degradation of Rhodamine B. In contrast, the SS electrode exhibited an initial rapid degradation phase, likely due to its high catalytic activity in the early stages of electrolysis. However, as the reaction progressed, passivation effects became more prominent. The formation of an oxide or hydroxide layer on the SS electrode surface likely inhibits further electron transfer and reduces its catalytic efficiency, leading to a slower electro-degradation of Rhodamine B between 30 and 90 minutes. The final sharp decrease in Rhodamine B concentration observed after 90 minutes may be attributed to partial surface renewal or structural modifications that temporarily restored its activity.

Unlike SS and GC, the Ni electrode demonstrated the least efficient degradation performance. The delayed onset of degradation suggests that surface activation was required before electrochemical degradation could proceed effectively. This behavior may be attributed to the tendency of Ni to form oxide or hydroxide layers that limit electron transfer and reduce the formation of reactive oxidative species [6]. Furthermore, Ni electrodes are known to favor the oxygen evolution reaction (OER) rather than hydroxyl radical production, which could further reduce their efficiency in organic pollutant degradation.

These findings highlight the critical role of electrode material in determining the efficiency of electrochemical degradation. The superior performance of SS and GC electrodes suggests that they are more suitable for practical wastewater treatment applications, particularly in scenarios requiring rapid and sustained degradation of organic pollutants. However, the passivation effects observed for SS indicate the need for further optimization to maintain high degradation rates over extended electrolysis periods.

The rate of Rhodamine B degradation in an electrochemical reactor can be described by first-order kinetics:

$$\ln C = lnC_0 - kt \tag{2}$$

Where C_0 and C are the initial concentration of Rhodamine B and the concentration of Rhodamine B after reaction time t, respectively, and k is the reaction rate constant. The rate constant can be determined from the slope of the linear plot of −lnC versus t (see Figure 1b). The rate constants for the electrochemical degradation of Rhodamine B from wastewater using different electrodes are presented in Table 1. It can be observed that the rate constant is highest for the GC system, followed by SS and Ni.

Table 1 Kinetic rate constant

Electrode	R^2	k min^{-1}
SS	0.87	0.013
GC	0.99	0.014
Ni	0.96	0.001

CONCLUSION

This study compared the electrochemical degradation efficiency of Rhodamine B using SS, GC, and Ni electrodes under identical conditions. Results demonstrated that SS and GC electrodes exhibited significantly higher degradation efficiencies (92 % and 90 % after 150 minutes, respectively) compared to Ni (30 %). GC showed a steady and uniform degradation rate, attributed to its high conductivity and stability, while SS displayed rapid initial degradation followed by passivation effects that slowed the process. Ni electrodes were the least efficient due to slow surface activation and preference for oxygen evolution over hydroxyl radical production. Kinetic analysis revealed the highest reaction rate constant for GC (0.014 min^{-1}), followed by SS (0.013 min^{-1}) and Ni (0.001 min^{-1}). The study highlights the suitability of SS and GC for efficient electrochemical treatment of dye-contaminated wastewater, though SS may require surface modifications for sustained performance.

ACKNOWLEDGEMENT

This work was supported by the Ministry of Science, Technological Development, and Innovation of the Republic of Serbia [grant number 451-03-136/2025-03/200017].

REFERENCES

1. Tran Truc Phuong, N., Xoan Hoang, T., La Ngoc Tran, N., Gia Phuc, L.; Phung, V.D., Kieu Thi Ta, H., Ngoc Bach, T., Hoa Thi Tran, N., The Loan Trinh, K. (2021) Rapid and Sensitive Detection of Rhodamine B in Food Using the Plasmonic Silver Nanocube-Based Sensor as SERS Active Substrate. Spectrochim. Acta - Part A Mol. Biomol. Spectrosc., 263, 1–8.
2. Li, H., Li, N., Jiang, J., Chen, D., Xu, Q., Li, H., He, J., Lu, J. (2017) Molecularly Imprinted Magnetic Microparticles for the Simultaneous Detection and Extraction of Rhodamine B. Sensors Actuators B Chem., *246*, 286–292.
3. Ječmenica Dučić, M., Aćimović, D., Savić, B., Rakočević, L., Simić, M., Brdarić, T., Vasić Anićijević, D. (2022) Is It Possible to Restrain OER on Simple Carbon Electrodes to Efficiently Electrooxidize Organic Pollutants? Molecules, 2*7*.
4. Qiao, J., Xiong, Y. (2021)Electrochemical Oxidation Technology: A Review of Its Application in High-Efficiency Treatment of Wastewater Containing Persistent Organic Pollutants. J. Water Process Eng., 44, 102308.
5. Vieira, L. de S. (2022) A Review on the Use of Glassy Carbon in Advanced Technological Applications. Carbon N. Y., 186, 282–302.
6. Kartikaningsih, D., Huang, Y.-H., Shih, Y.-J. (2017) Electro-Oxidation and Characterization of Nickel Foam Electrode for Removing Boron. *Chemosphere 166*, 184–191.

XVI International Mineral Processing
and Recycling Conference
28-30 May 2025, Belgrade, Serbia

DOI: 10.5937/IMPRC25267K

Original research article

PHOTODEGRADATION OF CIPROFLOXACIN WITH COPER-MODIFIED TITANIUM(IV)-OXIDE

Marija Kovačević, 0000-0001-8858-6728,
Marija Simić[#], 0000-0001-9518-7709,
Katarina Stojanović, 0009-0003-3467-9875,
Danka Aćimović, 0000-0001-7506-9684,
Sanja Živković, 0000-0003-1499-1645,
Tanja Brdarić, 0000-0003-2547-7123,
Dragana Vasić Anićijević, 0000-0003-0566-3244,
University of Belgrade, Vinča Institute of Nuclear Sciences - National Institute of the Republic of Serbia, Belgrade, Serbia

ABSTRACT – In recent years, the issue of emerging pollutants, particularly antibiotics, in aquatic ecosystems has garnered significant attention due to their potential environmental and public health impacts. To address this, we synthesized TiO_2 modified with Cu at three different molar ratios (0.5%, 1%, and 2%) and applied these photocatalysts to degrade ciprofloxacin in an infusion solution. The photodegradation process was monitored over 240 minutes using UV-Vis spectroscopy. The results indicated that the degradation efficiency of all three photocatalysts was approximately 50%. However, determining the precise degradation efficiency solely through UV-Vis spectroscopy proved challenging. This is because some degradation by-products exhibited absorbance maxima similar to ciprofloxacin, leading to potential inaccuracies in measuring the true extent of degradation. Further analysis, such as high-performance liquid chromatography (HPLC) or mass spectrometry, would be required to more accurately quantify the degradation products and assess the overall efficiency of the photodegradation process. This study highlights the complexity of using UV-Vis spectroscopy alone for analyzing antibiotic degradation in aquatic environments.

Keywords: Photocatalysis, Ciprofloxacin, Rutile TiO_2, DFT Calculations, Metal Decoration.

INTRODUCTION

The environment faces increasing pollution from population growth, industrialization, and human activities, leading to the widespread detection of organic contaminants such as dyes, pesticides, and pharmaceuticals in water [1]. Antibiotics are particularly concerning due to their rising use in human and animal treatment, entering aquatic environments through wastewater from industries, households, farms, and hospitals, as well as agricultural runoff. Despite their low concentrations (micrograms to nanograms per liter), the increasing consumption of antibiotics raises concerns about bacterial resistance and health risks [2]. Annual antibiotic consumption has reached

---

[#] corresponding author: marija.simic@vin.bg.ac.rs

between 100,000 and 200,000 tons, with a 65% increase noted between 2000 and 2015, and it is projected to rise by over 200% by 2030 [3]. Commonly detected antibiotics in water include sulfamethoxazole, trimethoprim, and ciprofloxacin, with wastewater treatment plants often unable to fully remove these contaminants [2]. There are several factors that contribute to the presence of ciprofloxacin (CIP) in aquatic environments and nature. First, wastewater treatment plants are not fully capable of removing antibiotics. Additionally, ciprofloxacin (Figure 1), a synthetic fluoroquinolone derivative, is highly stable, making it more resistant to degradation. Lastly, ciprofloxacin is a widely used antibiotic for treating a variety of infectious diseases [4]. Its broad-spectrum activity targets both Gram-positive and Gram-negative bacteria by inhibiting bacterial DNA synthesis through interaction with DNA gyrase, an enzyme essential for bacterial chromosome replication [5].

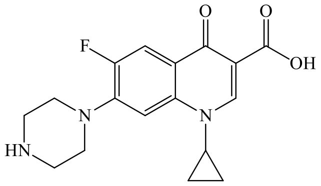

Figure 1 Structure of ciprofloxacin

There is a growing focus on developing effective methods for removing antibiotics from the environment, with UV-based photocatalysis emerging as a promising approach for degrading organic pollutants, including antibiotics [6]. This method offers key advantages such as low cost, energy efficiency, and the ability to operate at room temperature while using atmospheric oxygen for oxidation. Additionally, photocatalysts can be recovered and reused, making the process user-friendly and environmentally safe, as it requires no additional chemicals [2, 6]. However, current photocatalytic methods face limitations, particularly in industrial applications. These include limited visible light utilization (only 3–4% of sunlight is UV), rapid charge recombination, restricted migration of photogenerated electrons and holes, and potential toxicity of byproducts [2, 7]. Despite these challenges, advances in material science are promising. Studies have identified semiconductor materials like metal oxides (e.g., TiO_2, SnO_2) and metal sulfides (e.g., ZnS) as effective photocatalysts [2]. Among these, TiO_2 is noteworthy for its widespread use in degrading various organic substances, including dyes and pharmaceuticals [2, 8] . Its popularity is attributed to its excellent optical and electronic properties, stability, affordability, non-toxicity, and corrosion resistance [2, 7, 9]. However, TiO_2 has limitations, such as a large band gap and low UV light utilization [7]. Recent research aims to enhance TiO_2's performance under visible light through techniques like elemental doping, coupling with other semiconductors, and nanostructure synthesis. Doping can improve visible light absorption and photocatalytic performance by reducing the band gap and boosting charge separation [2, 7]. Furthermore, coating TiO_2 with a thin layer of noble metals (Au, Ag, Pt, and Pd) has shown improvements in photocatalytic efficiency, as these metals help trap photogenerated electrons, thereby extending the electron-hole pair lifetime and improving overall photocatalytic effectiveness [10, 11].

The aim of this study is to investigate the effect of a thin copper layer on the photocatalytic efficiency of titanium dioxide in the degradation of ciprofloxacin. Given that copper is more affordable than other noble metals, this approach presents a cost-effective alternative for enhancing TiO_2 photocatalysts. The research focuses on evaluating how copper deposition influences the rate, efficiency, and stability of TiO_2 in the photodegradation of ciprofloxacin under UV-light irradiation.

EXPERIMENTAL

Preparation of TiO_2

In this synthesis of TiO_2, 40 mL of titanium isopropoxide ($Ti(OCH(CH_3)_2)_4$) (Sigma-Aldrich, St. Louis, MO, USA, 97%) was dissolved in 6 mL of 2-propanol (Centrohem, Stara Pazova, Serbia, 99.5%) and stirred at room temperature for 10 minutes. Deionized water with a pH of 6 was then gradually added over 3 hours with vigorous stirring. The molar ratio of titanium isopropoxide, 2-propanol, and water was 5:3:10, respectively. The resulting precipitate was washed three times with ethanol (Reahem, Novi Sad, Serbia, 70%), centrifuged, and dried overnight in an oven at 100ºC. Calcination of the obtained titanium(IV) oxide was conducted at 700ºC for 5 hours, followed by cooling overnight [9].

Preparation of (Cu)TiO_2

The synthesis of titanium(IV) oxide modified with 0.5, 1, and 2% copper was performed by adding 0.5 g of titanium(IV) oxide to 50 mL of deionized water and dispersing it for 30 minutes at 90ºC in an ultrasonic bath. Then, 7.6 mg, 15.1 mg, and 30.25 mg of copper(II) nitrate trihydrate ($Cu(NO_3)_2{\cdot}3H_2O$, Merck, Darmstadt, Germany, 99.5%) were added for 0.5, 1, and 2% molar fractions of copper, respectively. Afterward, 12.5 mg of solid sodium hydroxide (Lach-ner, Neratovice, Czech Republic, 99.6%) was added, followed by 5 mL (γ = 0.5, 1, and 2 $g{\cdot}L^{-1}$) of sodium borohydride solution (BDH Chemicals Ltd., Poole, UK, 95%), and the mixture was stirred for 2 hours. The resulting precipitates were washed, centrifuged, and dried overnight at 100ºC in an oven [9].

Photodegradation of the ciprofloxacin infusion mixture

A vial of ciprofloxacin, a commercial injection solution (Marocen®, Hemofarm, Serbia), containing 100 mg of ciprofloxacin lactate in 10 mL, was diluted in deionized water using a 250 mL volumetric flask. Subsequently, 12.5 mL of this solution was further diluted to 250 mL in another volumetric flask. The resulting solution has a final molar concentration of $4.75{\cdot}10^{-5}$ $mol{\cdot}L^{-1}$, which corresponds to a mass concentration of 20 $mg{\cdot}L^{-1}$.

Photodegradation of ciprofloxacin

Photodegradation was performed using 20 mg of bare TiO_2 and (Cu)TiO_2 (0.5, 1, and 2%) suspended in 50 mL of ciprofloxacin solution. The reaction mixture was stirred for

30 minutes in the dark, along with a blank solution, to establish equilibrium before irradiation. Following this, the samples were exposed to UV light (Philips TUV 15W UVC Disinfection, Poland) for a duration of 4 hours. Aliquots were collected at various intervals: 0, 15, 30, 60, 120, 150, 180, 210, and 240 minutes for the mixture, with hourly samples taken from the blank. The progress of the photodegradation process was monitored using UV-Vis spectrometry (LLG Labware, Detroit, USA) [9].

RESULTS AND DISCUSSION

The UV-Vis spectra for ciprofloxacin degradation over 240 minutes of UV irradiation are shown in Figure 2. These spectra provide crucial insights into the photodegradation process of ciprofloxacin under UV light. The characteristic absorption maximum at 277 nm, which corresponds to the presence of ciprofloxacin, diminishes progressively over time, indicating that the compound is undergoing photodegradation. This reduction in absorbance suggests that the molecular structure of ciprofloxacin is being altered due to exposure to UV radiation, leading to its breakdown into various degradation products. The continuous monitoring of these spectra allows us to track the rate and extent of degradation, providing valuable information about the efficiency of the photocatalytic process.

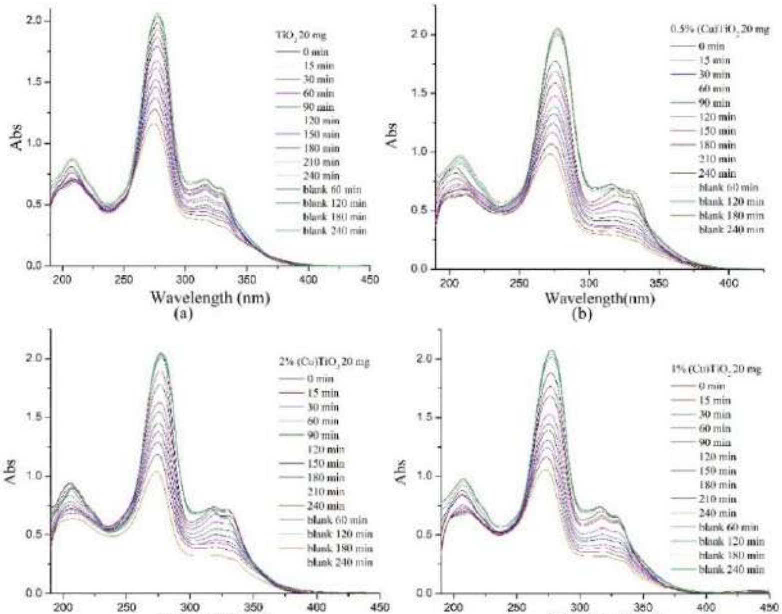

Figure 2 UV-Vis spectra of photodegradation of the ciprofloxacin solution with bare TiO2 (a), 0.5% (Cu)TiO2 (b), 1% (Cu)TiO2 (c) and 2% (Cu)TiO2 (d).

The efficiency of ciprofloxacin degradation was evaluated by measuring the decrease in absorbance at 277 nm, following pseudo-first-order kinetics described by the equation: $A=A_0\cdot e^{-kt}$, where k is the rate constant. The linearized form $\ln(A/A0)=-kt$ was used to calculate k from the graph's slope. The kinetic curves for ciprofloxacin degradation with 30 mg of photocatalysts are shown in Figure 3.

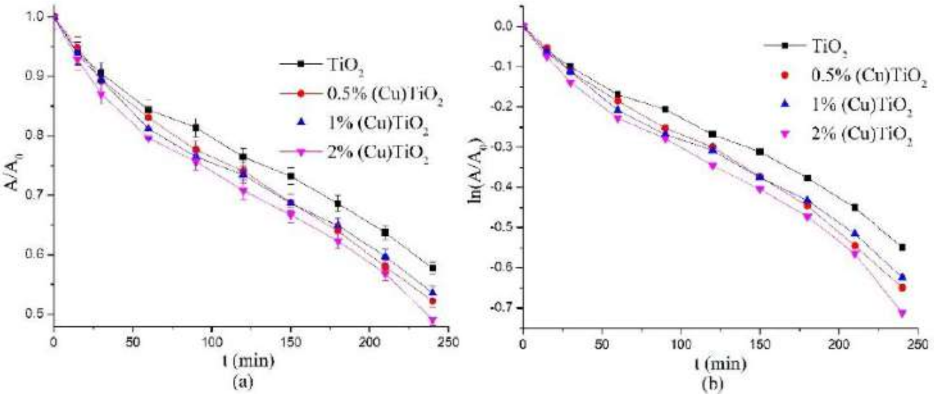

Figure 3 Degradation curves (a) and their linearized pseudo-first-order fits (b) of ciprofloxacin commercial solution for the infusion.

Table 1 presents the calculated pseudo-first-order rate constants, coefficient of determination, and percentage of degradation based on decreasing the absorbance values at 277 nm.

Table 1 Calculated pseudo-first-order rate constants of CIP degradation and percentage of degradation

Photocatalyst	k (min^{-1})	R^2	Degradation of CIP (%)
TiO_2	0.00208 ± 0.00008	0.98745	42.27
0.5% $(Cu)TiO_2$	0.00252 ± 0.00008	0.99102	47.81
1% $(Cu)TiO_2$	0.0024 ± 0.0001	0.98625	46.44
2% $(Cu)TiO_2$	0.0026 ± 0.0002	0.98112	50.91

The results indicate that the addition of 2% copper led to an increase in photocatalytic efficiency, achieving nearly 51% degradation over a 4-hour period. In comparison, the pure titanium(IV) oxide exhibited a lower degradation rate of 43%.

CONCLUSION

These findings highlight the potential of copper-modified titanium(IV) oxide as an effective photocatalyst for environmental applications, particularly in the degradation of organic pollutants. The enhanced performance observed with the copper addition suggests that the deposition of metal layers can improve the photocatalytic properties of TiO_2, making it a promising approach for developing more efficient catalysts. Further research could explore the underlying mechanisms of this enhancement and assess the long-term stability and applicability of the modified photocatalysts in real-world conditions.

ACKNOWLEDGEMENT

This research was funded by the Ministry of Science, Technological Development and Innovation of the Republic of Serbia (Contract number: 451-03-136/2025-03/ 200017).

REFERENCES

1. Jiang, T., Wang, B., Gao, B., Cheng, N., Feng, Q., Chen, M., Wang, S. (2023) Degradation of organic pollutants from water by biochar-assisted advanced oxidation processes: Mechanisms and applications. J Hazard Mater, 442, 130075.
2. Kutuzova, A., Dontsova, T., Kwapinski, W.: Application of TiO2-Based Photocatalysts to Antibiotics Degradation (2021) Cases of Sulfamethoxazole, Trimethoprim and Ciprofloxacin. Catalysts. 11.
3. Maghsodian, Z., Sanati, A.M., Mashifana, T., Sillanpää, M., Feng, S., Nhat, T., Ramavandi, B. (2022) Occurrence and Distribution of Antibiotics in the Water, Sediment, and Biota of Freshwater and Marine Environments: A Review. Antibiotics. 11.
4. Yaghoubi, F., Tavakoli, F., Dalil, D., Jamaloo, H.: Acute kidney injury following autoimmune hemolytic anemia due to simultaneous use of ciprofloxacin and hydrochlorothiazide (2023) A case report and review of the literature. Rheumatology & Autoimmunity, 3, 56–62.
5. Gezahegn, T., Tegegne, B., Zewge, F., Chandravanshi, B.S. (2019) Salting-out assisted liquid–liquid extraction for the determination of ciprofloxacin residues in water samples by high performance liquid chromatography–diode array detector. BMC Chem, 13, 28.
6. Akter, S., Islam, Md.S., Kabir, Md.H., Shaikh, Md.A.A., Gafur, Md.A. (2022) UV/TiO2 photodegradation of metronidazole, ciprofloxacin and sulfamethoxazole in aqueous solution: An optimization and kinetic study. Arabian Journal of Chemistry. 15, 103900.
7. Armaković, S.J., Savanović, M.M., Armaković, S.: Titanium Dioxide as the Most Used Photocatalyst for Water Purification: An Overview. Catalysts. 13, (2023).
8. Tatarchuk, T., Danyliuk, N., Shyichuk, A., Macyk, W., Naushad, Mu. (2021) Photocatalytic degradation of dyes using rutile TiO2 synthesized by reverse micelle and low temperature methods: real-time monitoring of the degradation kinetics. J Mol Liq. 342, 117407.
9. Kovačević, M., Živković, S., Ognjanović, M., Momčilović, M., Relić, D., Vasić Anićijević, D. (2023) In Silico Guided Design of Metal/Semiconductor Photocatalysts: A Case of Cu-Modified TiO2 for Ciprofloxacin Degradation. Materials, 16.
10. Chen, Y., Wang, Y., Li, W., Yang, Q., Hou, Q., Wei, L., Liu, L., Huang, F., Ju, M. (2017) Enhancement of photocatalytic performance with the use of noble-metal-decorated TiO2 nanocrystals as highly active catalysts for aerobic oxidation under visible-light irradiation. Appl Catal B, 210, 352–367.
11. Eskandarloo, H., Badiei, A., Behnajady, M.A., Mohammadi Ziarani, G. (2015) Photo and Chemical Reduction of Copper onto Anatase-Type TiO2 Nanoparticles with Enhanced Surface Hydroxyl Groups as Efficient Visible Light Photocatalysts. Photochem Photobiol, 91, 797–806.

XVI International Mineral Processing
and Recycling Conference
28-30 May 2025, Belgrade, Serbia

DOI: 10.5937/IMPRC25273C

Original research article

PROCESS WATER REUSE IN IRON ORE FLOTATION: REDUCING AMINE CONSUMPTION

Francielle Câmara Nogueira[1#], 0000-0001-5912-011X,
Carlos Alberto Pereira[1], 0000-0003-0510-0257,
Leandro Vinícius Alves Gurgel[1], 0000-0001-5249-8670,
Stephânia da Consolação Silva Nogueira[1], 0000-0002-5801-8241,
Iranildes Daniel Santos[2], 0000-0001-5493-1079,
[1]Federal University of Ouro Preto, Ouro Preto, Brazil
[2]Instituto Tecnlógico Vale – ITV Mining, Ouro Preto, Brazil

ABSTRACT – This study aimed to evaluate the reuse of process water through the immediate recirculation of water from reverse cationic flotation of iron ore in subsequent flotation cycles, focusing on reducing water and ether-amine consumption. Bench-scale flotation tests were conducted in rougher and cleaner stages using water from three different streams of an iron ore beneficiation plant located in Brazil. The recirculation of water containing ether-amines, originating from the concentrate and flotation stages, allowed for a gradual reduction of ether-amine dosage per cycle, totaling more than 15% savings over five cycles, without compromising mass and metallurgical recovery. The concentrates achieved iron grades above 67% and SiO2 levels below 2.6%, regardless of the water source used. Therefore, the results demonstrate technical feasibility at laboratory scale (technology readiness level 4) for saving water and ether-amines in the process, with potential for industrial-scale application.

Keywords: Process water reuse, Iron ore flotation, Water management, Ether-amine, Sustainable mining.

INTRODUCTION

Reverse cationic flotation is a technique widely used in the mineral industry to concentrate iron ores. In this process, fatty amines act as collectors, promoting the flotation of silica, while starch is used as a depressant for iron minerals, ensuring selectivity and making it possible to obtain concentrates with suitable commercial specifications [1]. Water recirculation is a common practice in mining companies, especially in processes that require large volumes of this resource, such as flotation [2, 3]. This strategy allows for the reuse of water from stages such as thickening and dewatering, reducing the consumption of fresh water and making it possible to recover residual amines present in the process water.

Different strategies for recovering and reusing amines have been studied. Oliveira *et al.* [4] found that more than 60% of the amine can be recovered by desorption from quartz. Alternatively, adsorbents such as angelim sawdust, sugarcane bagasse and

---

[#] corresponding author: francielle.nogueira@ufop.edu.br zeolites have shown high efficiency in the removal and recovery of amines [5-7]. In addition, studies indicate that the recirculation of water containing residual amines can reduce reagent consumption by up to 50% without compromising flotation efficiency [8-11]. Monte *et al.* [12] demonstrated that the reuse of water containing residual amine reduced the consumption of new amine by 46%, maintaining the quality of the concentrate at 68% Fe and 1.3% SiO_2.

The continuous recirculation of this water can lead to the accumulation of dissolved ions and organic compounds, which influence the interaction between the reagents and the minerals, compromising the selectivity of the flotation and the quality of the concentrate [13-14]. In addition, the interaction between amine and starch is sensitive to variations in pH, reagent concentration and conditioning time, making the behavior of the system even more complex [1,4,11]).

Despite the advances in reagent reuse, most studies have been conducted with distilled water, disregarding the effects of real process water. In this study, it was evaluated the feasibility of progressively reducing the ether-amine dosage in five sequential cycles of reverse flotation, on a laboratory scale and using process water collected at different points in a plant.

This study seeks to understand how the recirculation of process water can affect the quality of the concentrate, offering a more representative approach to industrial conditions.

MATERIALS AND METHODS

Bench scale flotation tests

Flotation tests were conducted at bench scale using a CDC-type flotation cell. The flotation circuit consisted of Rougher and Cleaner stages, with analyses carried out considering water recirculation over five cycles.

The process water used in these tests originated from a mining operation in the Quadrilátero Ferrífero (Iron Quadrangle) region, Brazil, and three different sources were evaluated, namely Tailings Overflow (OF/T), Concentrate Overflow (OF/C), and Scavenger Cell.

Recirculated water was obtained by combining the water recovered in the first cycle from the Rougher and Cleaner stages, forming a composite sample used to feed the subsequent cycles. The flotation process was carried out at 60% solids during conditioning. In the rougher stage, flotation was conducted at 50% solids for 2 minutes, while the Cleaner stage proceeded until froth exhaustion.

A gelatinized starch solution treated with sodium hydroxide (NaOH) was used as a depressant for hematite at a fixed dosage of 550 g/t, with a conditioning time of 6 minutes.

For quartz flotation, the ether-amine collector Flotigam 7100, a commercial reagent supplied by Clariant (Brazil), was employed. Sodium hydroxide (NaOH) and hydrochloric acid (HCl) solutions were used as pH regulators, maintaining the flotation at pH 10.3. The collector conditioning time was set at 1 minute. The starting ether-amine dosage was 180 g/t of silica, decreasing by 5% per cycle, totaling a 20% reduction by the fifth cycle (144 g/t).

RESULTS AND DISCUSSION

The ore sample used in the flotation tests was chemically analyzed by X-ray fluorescence (XRF) and its particle size distribution was determined by sieving. The initial sample contained 43% Fe and 37% SiO_2. Particle size analysis showed that 86% of the material was finer than 106 µm, with 46% passing through the 45 µm sieve.

Figures 1, 2, and 3 present the concentration of ether-amine in starting liquid phase, ending liquid phase, and solid phase (total ether-amine concentration adsorbed on solid phase) in each cycle, as well as new ether-amine and recirculated ether-amine in each cycle in recirculating water from the three process water flows containing residual ether-amine — Tailings Overflow (OF/T), Concentrate Overflow (OF/C), and Scavenger Cell. In Figures 1-3 it can be observed that recirculating water allowed for a gradual reduction in collector dosage per cycle, culminating in a total saving of 15% after five cycles.

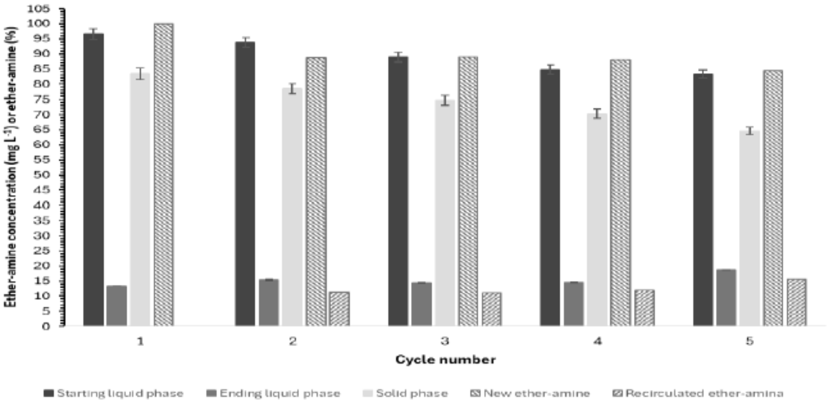

Figure 1 Ether-amine concentration and their amount in each flotation cycle using water from tailings overflow (OF/T)

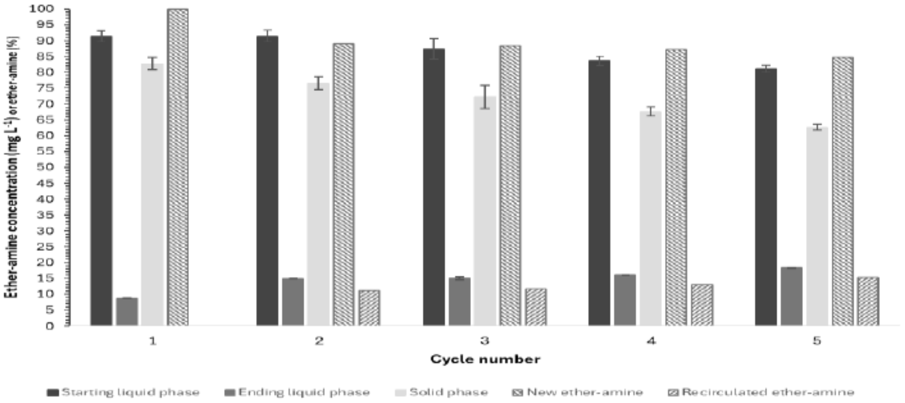

Figure 2 Ether-amine concentration and their amount in each flotation cycle using water from concentrate overflow (OF/C)

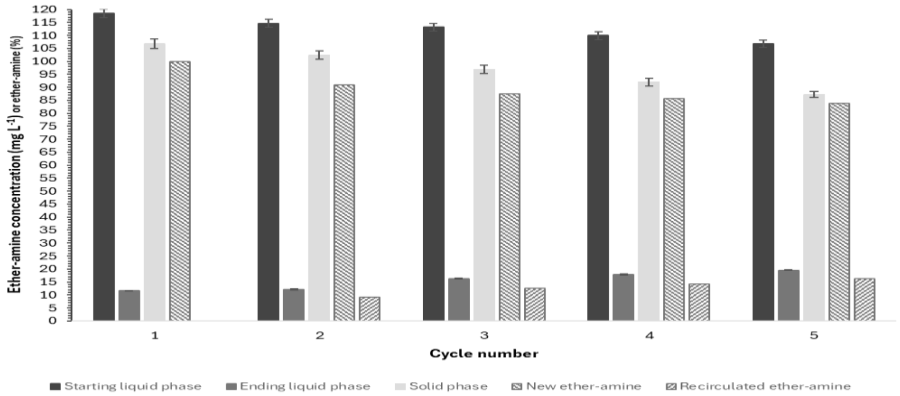

Figure 3 Ether-amine concentration and their amount in each flotation cycle using water from Scavenger cell

The results presented in Figures 4, 5, and 6 show the metallurgical and mass recovery (flotation yield), and quality concentrates (Fe and SiO$_2$ grades) using recirculating water from the three process water flows containing residual ether-amine.

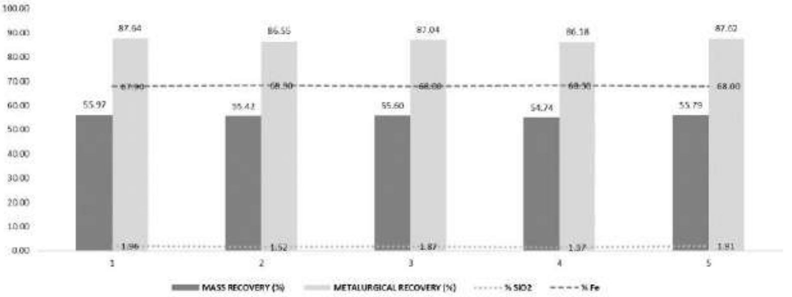

Figure 4 Mass and metallurgical recoveries, Fe and SiO$_2$ grades of the concentrates from each flotation cycle using water from tailings overflow (OF/T)

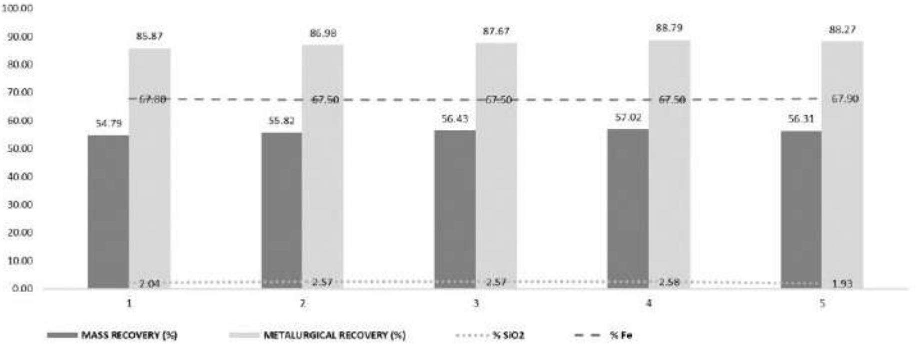

Figure 5 Mass and metallurgical recoveries, Fe and SiO$_2$ of the concentrates in each flotation cycle using water from concentrate overflow (OF/C)

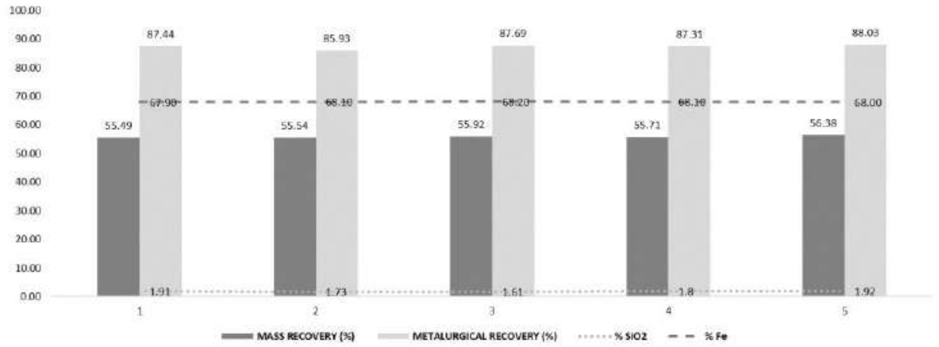

Figure 6 Mass and metallurgical recoveries, Fe and SiO_2 grades of the concentrates from each flotation cycle using water from Scavenger cell

As observed, the reduction of amine dosage did not compromise either the metallurgical recovery of the concentrate, which remained stable between 85% and 89%, or the iron grade of the concentrates (>67%) and mass recovery that ranged from 55.5%-56.3% for the different water flows. Tests using Concentrate Overflow (OF/C) water yielded the highest average mass recovery (56.3%), and metallurgical recovery (87.5%).

For the Rougher Tailings, the metallurgical recovery ranged from 6.24% (Scavenger Cell), 7.3% Tailings Overflow (OF/T), 7.4% Concentrate Overflow (OF/C). In the Cleaner Tailings, the metallurgical recovery ranged from 6.5% (Scavenger Cell), 5.76% (Tailings Overflow), 5.1% Concentrate Overflow (OF/C). The greatest iron loss in the cleaner tailings were observed in tests using water from the Scavenger Cell flow.

CONCLUSION

The recirculation of process water containing residual ether-amine allowed savings of more than 15% in the consumption of the new collector over five cycles, without compromising metallurgical recovery and iron content. Metallurgical recoveries remained between 85.0% and 89.0%, while the iron content of the concentrates remained above 67.0%. This reduction in reagent consumption represents an advance in process efficiency, reducing operational costs and environmental impacts associated with the disposal of chemical products. Finally, the industrial application of the technique requires additional studies to ensure its long-term stability and economic viability (TRL > 4).

ACKNOWLEDGEMENT

The authors are grateful to UFOP (Universidade Federal de Ouro Preto), EMBRAPII (Empresa Brasileira de Pesquisa e Inovação Industria,l and Vale S.A. for their support.

REFERENCES

1. França Neto, P.P., Mata, C.E.D., Silva, A.C., Silva, E.M.S., Silva, L.A. (2023) Influência da dosagem e do tempo de condicionamento de amina na flotação de minério de ferro utilizando a farinha de sorgo como depressor. Tecnologia em Metalurgia, Materiais e Mineração, 20, e2807.
2. Jing, G., Wang, J., Sun, W., Pooley, S., Liao, D., Shi, Z., Chen, Q., Gao, Z. (2023) Reuse of mine and ore washing wastewater in scheelite flotation process to save freshwater: Lab to industrial scale. Journal of Water Process Engineering, 53, 103674.
3. Liu, W., Moran, C.J., Vink, S. (2013) A review of the effect of water quality on flotation. Minerals Engineering, 53, 91–100. DOI: 10.1016/j.mineng.2013.07.011.
4. Oliveira, J.F. et al. (1996) Recuperação de amina adsorvida em quartzo ou contida na água flotada visando sua reutilização na flotação reversa de minério de ferro. *In: I Simpósio Brasileiro de Minério de Ferro*, Ouro Preto, Brasil, Anais [...].
5. Fernandes, H.D., Carvalho, C.F., Paula, C.C.P., Azevedo, L.S., Gonçalves, S.M.D. (2019) Reciclagem de éter-aminas, utilizadas na flotação de minério de ferro, por meio de adsorção. Engenharia Sanitária e Ambiental, 24(2).
6. Teodoro, A.L., Leão, V.A. (2004) Recuperação de aminas, utilizadas na flotação de minério de ferro, utilizando-se zeólitas naturais. Revista Escola de Minas, Brasil, 57(3), 197-201.
7. Barbato, D. et al. (2004) Adsorção de aminas em zeólitas para recuperação de reagentes na mineração. In: XX Congresso Brasileiro de Mineração, Belo Horizonte, Brasil, Anais [...].
8. Stapelfeldt, F., Lima, R.M.F. (2001) Recycling of process water containing amines in the reverse flotation of iron ores. IMWA Symposium, Belo Horizonte, Brasil.
9. Reis, O.B. dos. (2004) Estudo preliminar sobre reciclagem das aminas utilizadas em flotação de minério de ferro. Dissertação (Mestrado em Engenharia Ambiental), Universidade Federal de Ouro Preto, Ouro Preto, 63 f.
10. Araujo, D.M., Yoshida, M.I., Carvalho, C.F., Stapelfeldt, F. (2008) Reciclagem de aminas na flotação de minério de ferro. REM - Revista Escola de Minas, 61(4), 455-460. DOI: 10.1590/S0370-44672008000400008.
11. Batisteli, G.M.B., Peres, A.E.C. (2008) Residual amine in iron ore flotation. Minerals Engineering, 21(12–14), 873–876.
12. Monte, M.B.M., Santos, I.D., Veneu, D.M., Moura, C., Hertel, C. (2024) Reduction of Amine Consumption in Iron Ore Flotation through Direct Reuse of Process Water on Bench Scale. Disponível em: doi:10.21203/rs.3.rs-4013343/v1.
13. Tang, M., Wang, D., Wu,Y., Liu, D. (2022) Influences of process water chemistry on reverse flotation selectivity of iron oxides. Physicochemical Problems of Mineral Processing, 58(6), 151839.
14. Ribeiro, M.V., Medeiros, E.G., Rocha, S.D.F., Viana, P.R.M., Papini, R.M. (2008) Aspectos ambientais do uso de reagentes de flotação no processamento de minério de ferro. In: 60º Congresso Anual da ABM, Anais [...], Belo Horizonte, Brasil.

XVI International Mineral Processing
and Recycling Conference
28-30 May 2025, Belgrade, Serbia

DOI: 10.5937/IMPRC25279S Original research article

THE EFFECT OF PARTICLE SIZE ON THE FLOTATION KINETICS OF RAW AND WASTE COAL

Jovica Sokolović[#]**,** 0000-0002-2003-1141,
Ivana Đolović, 0000-0003-1169-0361,
Dejan Tanikić, 0000-0003-0702-5721,
Zoran Štirbanović, 0000-0001-7571-2844,
Ivana Ilić, 0009-0002-0905-2838,
University of Belgrade, Technical Faculty in Bor, Bor, Serbia

ABSTRACT – This paper investigates the effect of particle size on the flotation kinetics parameters of raw and waste fine coal from anthracite mine "Vrška Čuka, Serbia. Based on batch flotation test data of coal, non-linear fitting was conducted by using MatLab for modeling first order flotation kinetics. The cumulative combustible recovery against flotation time were correlated using the Classical model. The coefficient of determination (r^2) values of the proposed model were from 0.9904 to 0.9998 for raw coal and from 0.9555 to 0.9980 for waste coal. The maximum values of the flotation rate constant (k) for both coals were obtained for the particle size fractions (-0.1+0.053) mm. The relation between flotation kinetics constant (k) with particle size (d_{sr}) was estimated through equations presented in the paper (Eq. 3 and 4).

Keywords: Coal, Particle size, Flotation, Kinetics, Classical model.

INTRODUCTION

Coal flotation is a very complex physico-chemical process and difficult to control. Coal flotation plays an important role in coal processing and is a widely used method in coal processing technologies for the separation of fine coal below 0.5 mm and in some cases even below 1 mm [2].

The coal flotation theory and parameters affecting the coal flotation performance are explained in detail by Polat [1] and Laskowski [3]. Generally, coal flotation is affected by a number of parameters [1, 3]. The most critical parameter affecting the stability of bubble-particle aggregates is the particles size [4]. Particle size has an important role in coal flotation as well as flotation kinetics. The effect of particle size on coal flotation kinetics is complex, and it has been described by Sokolovic and Miskovic (2018) [5].

Many studies have been conducted to determine the effect of particle size on coal flotation kinetics [2, 6–18]. A number of kinetic models have been developed and tested for the coal flotation process. In general, the best-fit kinetic model varies for different

---

[#] corresponding author: jsokolovic@tfbor.bg.ac.rs coal types and flotation conditions. Based on available literature, it is found that the coal flotation follows the first-order kinetics model [2, 5–18].

The flotation rate constant is strongly dependent on coal particle size. In recent years, studies showed that the highest flotation rate can be obtained over an intermediate particle size range while it decreases sharply for fine and coarse particle sizes.

The relation between flotation rate constant and cumulative recovery with particle size was found to be nonlinear [12]. Studies showed that the first-order kinetic model with a rectangular distribution of floatability gave the best fit to the flotation experimental data for coal with particle size between 37 and 375 µm [5]. Furthermore, the nonintegral-order equation fit the test data of fine coal with average particle sizes between 188 and 100 µm.

Additionally, the physical and chemical properties of coal are usually altered by the oxidation processes. The oxidation processes result in the formation of oxygen functional groups, such as carboxyl, phenol and carbonyl functionalities on coal surface [19], which reduces the hydrophobicity of coal as well as coal flotation kinetics [20]. This paper investigates the effect of particle size on the flotation kinetics parameters of raw and waste coal from anthracite mine "Vrška Čuka", Serbia.

EXPERIMENTAL

Materials

Coal samples of about 250 kg were collected from the anthracite coal mine "Vrška Čuka" in Serbia. The first representative samples were collected from raw coal and the second from the coal waste ponds. Raw coal (RC) was sampled as feed from the “BSRI-1200” dense-medium separator, with a particle size range of 0–25 mm. Waste coal (WC) was sampled from the coal waste ponds, with a particle size range of 0–1 mm. The raw coal sample was screened at 1 mm for particle size analysis and flotation kinetics tests.

Methods

Particle size analysis

The raw and waste coal samples were sieved to determine the particle size distribution. Wet sieving on sieves: 0.5; 0.2; 0.1; 0.053 mm was applied for determining the particle size distribution of both coal samples.

Laboratory sieve shaker Retsch AS200 was used with amplitude 2 mm for 25 min. After drying, the ash content was determined according to the SRPS ISO 1171 standard from 2014 at 815 °C. The particle size distribution wise ash content is shown in Table 1.

The particle size analysis results of raw and waste coal show a similar mass distribution by size fractions. The lowest ash content in both tested coal samples was recorded in the size fraction (-0.5+0.2) mm and was 14.54% and 29.60%, respectively.

From Table 1, it can be seen that fine size fractions below 0.053 mm are 26.19% for raw coal and 22.77% for waste coal. Higher ash content (about 53%) in waste coal designates the presence of slime and clay in this fraction.

Table 1 Particle size distribution and ash contents of raw coal (RC) and waste coal (WC) samples

Particle size fraction d (mm)	**Raw coal (RC)**				**Waste coal (WC)**			
	Internal values		**Cumulative passing value**		**Internal values**		**Cumulative passing value**	
	Weight (%)	Ash (%)	Weight (%)	Ash (%)	Weight (%)	Ash (%)	Weight (%)	Ash (%)
+0.5	23.52	20.98	23.52	20.98	23.96	31.84	23.96	31.84
-0.5+0.2	21.04	14.54	44.56	17.94	28.31	29.60	52.27	30.63
-0.2+0.1	13.94	16.88	58.50	17.69	14.91	35.73	67.18	31.76
-0.1+0.053	15.31	17.22	73.81	17.59	10.05	42.20	77.23	33.12
-0.053+0	26.19	22.31	100.00	18.83	22.77	53.23	100.00	37.70

Flotation tests

A laboratory flotation machine Denver D-12 was used for flotation kinetics tests with the impeller speed of 1250 rpm. All coal flotation tests were conducted with feed slurries at 10% solids (by weight). The pH was adjusted to 7.5. Kerosene (1000 g/t), tannic acid (200 g/t), sodium silicate (200 g/t), and pine oil (45 g/t) were used as reagents in this study. In each flotation kinetics test, the pulp was first agitated in the flotation cell for 3 minutes. After 2 min of agitation kerosene was added, and the slurry was mixed for 0.5 min, when tannic acid, sodium silicate, and pine oil were added and the slurry was stirred for additional 0.5 min. Air was introduced after the conditioning stage, and flotation concentrates were collected at 30, 90, 150, and 360 s. After the final froth sample was collected, the machine was stopped. The froth flotation concentrates and the tailings were filtered, dried, weighed, and analyzed. Ash content analyses were conducted for all samples. Following flotation kinetics tests, all concentrates were dry sieved. Size-wise ash analysis for the five particle size fractions, 0.5; 0.2; 0.1, and 0.053 mm were conducted for froth concentrates and the tailings. Based on the obtained results, the combustible recovery (R) of non-ash materials for each fraction were calculated by:

$$R = Y\,(100 - Ac)\,/\,(100 - Af) \tag{1}$$

where Y is the percentage yield of the concentrate and A_c and A_f are the percentage ash contents in concentrates and feed materials, respectively [12].

Flotation kinetics

The yields for the individual particle size fractions were plotted as a function of flotation time. In this study, a classical first-order kinetics model, introduced by Zuniga (1935) [21], a given in Eq. 2, is used to obtain the parameters of k and R_∞ through fitting the flotation test data.

$$R = R\infty\,[1 - e(- k \cdot t)] \tag{2}$$

where R_∞ is the ultimate (maximum) recovery of non-ash materials (%) at time, t is the cumulative flotation time (min), and k is the flotation rate constant (min^{-1}).

MATLAB tool was used to fit the first-order kinetics model to the flotation test results to obtain R_∞ and k values [22]. If the coefficient of determination (R^2) was higher than 0.8, Eq. 2 can be applied.

RESULTS AND DISCUSSION

The curves of flotation kinetics of different particle size fractions of raw coal (RC) and waste coal (WC) are shown in Figure 1.

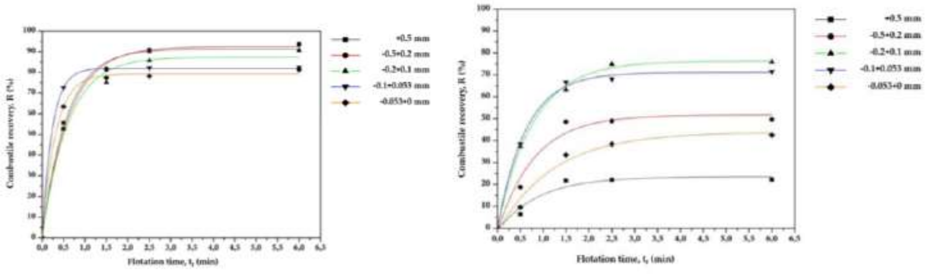

a) b)

Figure 1 Cumulative recovery of different particle size fractions of a) raw coal (RC) and b) waste coal (WC) against flotation time

Using MatLab tools, the values of the flotation rate constant and other flotation parameters were determined for the first-order classical flotation kinetics model. The obtained values are shown in Table 2.

Table 2 Kinetics parameters generated by the first-order classical model for various size fractions of raw coal (RC) and waste coal (WC) samples

	Raw coal (RC)			**Waste coal (WC)**		
Particle size fraction d (mm)	**k (min^{-1})**	**R_∞ (%)**	**r^2**	**k (min^{-1})**	**R_∞ (%)**	**r^2**
+0.5	1.6848	93.37	0.9996	1.0584	23.55	0.9555
-0.5+0.2	1.8084	93.74	0.9942	1.2056	51.76	0.9746
-0.2+0.1	1.5017	90.68	0.9904	1.2877	76.26	0.9980
-0.1+0.053	4.2624	82.28	0.9998	1.4557	71.70	0.9960
-0.053+0	2.9839	81.29	0.9980	0.7786	44.06	0.9789

(r^2 – the coefficient of determination)

Based on the results presented in Table 1, it can be concluded that the ultimate (maximum) recovery of non-ash materials from raw coal decreases as the particle size decreases. Furthermore, the highest ultimate (maximum) recovery for raw coal is observed in the +0.5 mm size fraction, while the lowest recovery for waste coal occurs in the same size fraction.

Figure 2 shows the dependence of the flotation rate constant (k) on particle size, i.e. the mean diameter of a narrow size fraction (d_{sr}).

Figure 2 shows the flotation rate constant variation with particle size. As it can be seen from Figure 2, flotation rate constant (k), for raw coal, first increases sharply and then decreases, indicating an optimum particle size (about 0.1 mm), while for waste coal, flotation rate constant values are lower and increases slightly with increasing d_{sr}. The maximum flotation rate constant (k) values for raw and waste coal are 4.2624 min^{-1} and 1.4557 min^{-1}, respectively, for the particle size fraction of (-0.1 + 0.053) mm.

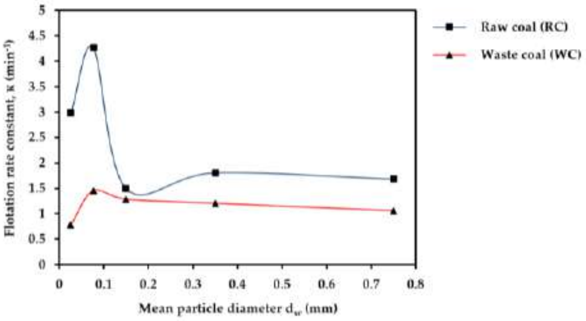

Figure 2 Dependence of the flotation rate constant on particle size of raw (RC) and waste (WC) coal

Using the MatLab tool, the values of the coefficients of determination were determined from 0.9904 to 0.9998 for raw coal and from 0.9555 to 0.9980 for waste coal. It can be concluded that the classical model well describes the first-order flotation kinetics. This model showed good applicability to experimental flotation data for both raw and waste coal. According to the results from Table 2 and Figure 2, the relation between flotation kinetics constant (k) with particle size (d_{sr}) was estimated through equations:

$$k_{rc} = (a + b \cdot d_{sr} + c \cdot d_{sr}^2)/(1 + d \cdot d_{sr} + e \cdot d_{sr}^2) \tag{3}$$

where: a = 2.728965; b = - 41.135466; c = 192.135603; d = - 18.675380; e = 102.500493

$$k_{wc} = a \cdot d_{sr} + b/d_{sr} + c/(d_{sr}^2) + d \tag{4}$$

where: a = - 0.1258396; b = 0.0451993; c = - 0.0014227; d = 1.1031061

The coefficient of determination (r^2) values for flotation kinetics constant for raw and waste coal were 0.9797 and 0.9911, respectively. Based on the observed trend, a proposed mathematical functions are a good fit for both coals.

CONCLUSION

The first-order classical model was applied as an effective tool for modeling the complex relation between the input and output variables in a coal flotation process. The r^2 values were obtained from 0.9904 to 0.9998 for raw coal and from 0.9555 to 0.9980, for waste coal, indicating a good relation.

The correlation between the flotation rate constant (k) and the mean particle diameter (d_{sr}) depends on the type of coal. The maximum values of the flotation rate constant (k) for raw and waste coal were obtained for the particle size fractions (-0.1+0.053) mm. The proposed mathematical models, given in Equations 3 and 4, provide a relationship between the flotation kinetics constant (k) and particle size (d_{sr}).

ACKNOWLEDGEMENT

The research presented in this paper was done with the financial support of the Ministry of Science, Technological Development and Innovation of the Republic of Serbia, within the funding of the scientific research work at the University of Belgrade, Technical Faculty in Bor, according to the contract with registration number 451-03-137/2025-03/ 200131.

REFERENCES

1. Polat, M., Polat, H., Chander, S. (2003) Physical and chemical interactions in coal flotation. International Journal of Mineral Processing, 72 (1), 199-213.
2. Brozek, M., Mlynarczykowska, A. (2013) An analysis of effect of particle size on batch flotation of coal. Physicochemical Problems of Mineral Processing, 49 (1), 341-356.
3. LaskowskI, J.S. (2001) Coal flotation and fine coal utilization, Elsevier, Amsterdam.
4. Polat, M., Arnold, B., Chander, S., Hogg, R., Zhou, R. (1993) Coal flotation kinetics-effect of particle size and specific gravity. In: Coal Science and Technology, 161-170.
5. Soković, J., Miskovic, S. (2018) The effect of particle size on coal flotation kinetics: A review. Physicochemical Problems of Mineral Processing, 54 (4), 1172-1190.
6. Panopoulos, G., King, R.P., Juckes, A. (1986) The effect of particle-size distribution on the flotation of two South African coals. Journal of the Southern African Institute of Mining and Metallurgy, 86 (5), 141-152.
7. Vanangamudi, M., Rao, T. C. (1986) Modelling of batch coal flotation operation. International journal of mineral processing, 16 (3-4), 231-243.
8. Vanangamudi, M., Kumar, S. S., Rao, T. C. (1989) Effect of fines content on the froth flotation of coal. Powder technology, 58 (2), 99-105.
9. Rao, T. C., Govindarajan, B., Vanangamudi, M. (1989) A kinetic model for batch coal flotation. Minerals Engineering, 2 (3), 403-414.
10. Mohns, C. A. (1998) Effect of particle size on coal flotation kinetics. Queen's University at Kingston.
11. Chaves, A. P., Ruiz, A. S. (2009) Considerations on the kinetics of froth flotation of ultrafine coal contained in tailings. International Journal of Coal Preparation and Utilization, 29 (6), 289-297.
12. Abkhoshk, E., Kor, M., Rezai, B. (2010) A study on the effect of particle size on coal flotation kinetics using fuzzy logic. Expert Systems with applications, 37 (7), 5201-5207.
13. Kor, M., Abkhoshk, E., Gharibie, K., Shafaei, S. Z. (2010) An investigation of the particle size effect on coal flotation kinetics using multivariable regression. 1 (1), 41-47.
14. Li, Y., Zhao, W., Gui, X., Zhang, X. (2013) Flotation kinetics and separation selectivity of coal size fractions. Physicochemical Problems of Mineral Processing, 49 (2), 387-395.
15. Xia, W., Xie, G., Liang, C., Yang, J. (2014) Flotation behavior of different size fractions of fresh and oxidized coals. Powder Technology, 267, 80-85.
16. Ni, C., Xie, G., Jin, M., Peng, Y., Xia, W. (2016) The difference in flotation kinetics of various size fractions of bituminous coal between rougher and cleaner flotation processes. Powder technology, 292, 210-216.
17. Bu, X., Xie, G., Chen, Y., Ni, C. (2017) The order of kinetic models in coal fines flotation. International Journal of Coal Preparation and Utilization, 37 (3), 113-123.
18. Liao, Y., Cao, Y., Liu, C., Zhao, Y., Zhu, G. (2017) Comparison of the effect of particle size on the flotation kinetics of a low-rank coal using air bubbles and oily bubbles. Journal of the Southern African Institute of Mining and Metallurgy, 117 (6), 561-566.
19. Sokolovic, J., Stanojlovic, R., Markovic, Z. (2012) Activation of oxidized surface of anthracite waste coal by attrition. Physicochemical Problems of Mineral Processing, 48(1), 5-18.

20. Soković, J., Stanojlović, R., Marković, Z. (2012) The effects of pretreatment on the flotation kinetics of waste coal. International Journal of Coal Preparation and Utilization, 32(3), 130-142.
21. Zuniga, H.G. (1935). Flotation recovery is an exponential function of its rate. Boln. Soc. Nac. Min., Santiago, Chile, 47, 83-86.
22. Brezani, I., Zelenak, F. (2010) MatLab Tool for Modeling First Order Flotation. http://www.mathworks.com/matlabcentral/fx_files/28703/2/content/html/Flotation_modeling.html.

XVI International Mineral Processing
and Recycling Conference
28-30 May 2025, Belgrade, Serbia

DOI: 10.5937/IMPRC25286D

Original research article

SLOVAK DOLOMITE AS A RAW MATERIAL SOURCE FOR METAL MAGNESIUM PRODUCTION

Zuzana Danková[1#], 0000-0002-5089-2479,
Alexandra Bekényiová[1], 0000-0002-7313-6801,
Zuzana Kollová[1], 0009-0009-4045-8706,
Erika Fedorová[1], 0000-0003-1709-2450,
Pavel Bačo[1], 0009-0000-5756-8076,
Jaroslav Briančin[2], 0000-0001-9195-507X,
[1]State Geological Institute of Dionýz Štúr, Bratislava, Slovak Republic
[2]Institute of Geotechnics, Slovak Academy of Sciences, Košice, Slovak Republic

ABSTRACT – In order to ensure within the EU, preferably, self-sufficiency, a stable supply of the essential mineral raw materials required for industry led to the establishment of the European Raw Materials Alliance (ERMA). One of the key objectives is access to sustainable raw materials, as well as support for exploration and mining of raw materials within the EU. Metallic magnesium has been included in the list of critical minerals for European Union countries since 2011. The most suitable raw material for the MgO production for method of silicothermic reduction is dolomite or magnesite, at which Slovak Republic has considerable resources of these carbonate raw materials. For technological research, six samples from different deposites were chosen. The samples were annealed at selected temperatures and characterized by differential thermal analyses. The results showed that for the silicothermic reduction of magnesium, it is necessary to individually verify the calcination conditions for each sample and determine the influence of the hydration activity/active sites in their structure to increase the reduction of magnesium.

Keywords: Dolomite, Calcination, Metal Magnesium.

INTRODUCTION

Magnesium is produced commercially either by electrolysing the magnesium chloride derived from raw materials, or by using a thermal reduction process, known as the Pidgeon process, using dolomite as the raw material [1]. At present, China is the largest producer and exporter of magnesium in the world, accounting for more than 85 % of the world's magnesium outputs [2, 3].

The magnesium metal has a special status between 26 elements and minerals defined as "critical raw materials for the EU" [4].

The dolomite in Slovakia occurs in several Middle and Upper Triassic formations thick up to several 100 metres, or forming intercalations, interbeds, lenses in beds irregularly alternating with surrounding limestones. They are present in numerous geological units,

---

[#] corresponding author: zuzana.dankova@geology.sk their cover sequences and tectonic nappes. The most significant are the Middle- and Upper-Triassic dolomites of the Hronic unit, bearing the important dolomite deposits in the Choč nappe of the Strážovská Highlands.

The reduced crystals of magnesium were prepared under experimental conditions by Kollová et al. [5].

In this paper the dolomite samples originated from different Slovak deposits were annealed with the aim to prepare suitable intermediate products for further silicothermic reduction in flowing argon to define a suitable thermal treatment of dolomite for preparing of magnesium metal according to the Pidgeon process.

EXPERIMENTAL

Raw samples

For experimental purposes, dolomite raw samples from the Slovak localities: Sedlice (SED-1, SED-2), Trebejov (TR-1), Stráňavy (ST-1, ST-2) and Kraľovany (KRA-1) were used. Bulk samples of dolomites were freely air-dried and subjected to preparatory work - crushing in three stages in jaw crushers and sorting on sieves of different sizes: + 8.0; 4.0 - 8.0; 2.0 - 4.0; 1.0-2.0; -1.0 mm; whereas all samples, or the grain fractions prepared from them were subsequently homogenized and quartered. From each raw sample after these works and from the grain size classes, individual homogeneous parts were prepared for further laboratory processing, including their grain size characteristics.

Experimental procedures

Annealing tests of dolomite fractions were carried out in an electric laboratory furnace ELOP-1200/15 at temperatures of 1000 °C and 1050 °C with a holding time of 0.5; 1; 2 and 2.5 hours. Optimized annealing tests of samples of fraction below 8.0 mm were carried out in an electric laboratory furnace KSL1600X-A2 at temperatures of 1150, 1200 and 1300 °C with a duration of 1.5 hours.

The crucibles were placed in a muffle furnace and then the furnace was heated up continuously from room temperature to selected temperature (the heating rate was 10 °C/min) with selected holding time. The products of calcination obtained at different temperatures were taken out and stored in a desiccator before DTA/TG analyses were carried out.

Methods of characterization

Qualitative mineralogical analysis of input samples was carried out by the X-ray diffraction (XRD) method on the BRUKER D2 Phaser device: CuKα radiation, monochromatic Ni filter, accelerating voltage of the X-ray radiation generator 30 kV, current intensity 10 mA, range of detected angles 5 – 70 ° 2theta, step 0.01 °, time 0.3 sec/step. Processing and evaluation of measured data were realized using DIFFRAC.EVA V3.1. software equipped with the PDF-2/2013 database.

NETZSCH STA 449 F3 Jupiter derivatograph (NETZSCH Gerätebau Gmbh., Selb, Germany) equipped with a Std SiC furnace and an Autovac MF Cs rotary pump was used for Differential thermal analyses/Thermogravimetric (DTA/TG) analyses. Measurements were made under the following conditions: heating range: 297 – 1273 K, heating rate 10 °C/min, reference material: powdered Al_2O_3, crucibles: ceramic Al_2O_3, furnace atmosphere: N_2 circulation: 20 ml/min.

The morphology of the prepared intermediate products was studied by scanning electron microscopy FE MIRA 3 (Tescan, Czech Republic) equipped by XRD energy-dispersive (EDX) analyzer of chemical composition (Oxford Instruments).

RESULTS AND DISCUSSION

For the samples KRA-1 and ST-1, the required thermal decomposition (above 98 %) was reached for all studied grain fractions at both temperatures (1000 and 1050 °C), as well as for the sample ST-2 except the fraction below 1.0 mm annealed at 1050 °C for 0.5 hour. For the samples SED-1 and SED-2 the decomposition occurs in the coarse-grained fraction (4-8 mm) at both temperatures with holding time of minimal 2 hours.

For sample TR-1, only annealing of fractions over 2 mm at the temperature of 1050 °C with a holding time of over 2 hours was effective [6].

After initial annealing tests, optimization of the process was carried out. Individual fractions of all samples were combined and annealed at temperatures at 1150, 1200 and 1300 °C for 1.5 hours in order to determine the appropriate temperature for the thermal decomposition of the investigated samples with respect to the theoretical loss by annealing. For samples SED-1, SED-2, TR-1 and KRA-1, the required thermal decomposition (above 98 %) occurred at temperatures of 1150 and 1200 °C. For samples ST-1 and ST-2, the required decomposition occurred only at a temperature of 1200 °C, Tab. 1.

Table 1 Parameters of calcined dolomites after annealing at selected temperatures

Temperature (°C)	Time (hrs)	Sample											
		SED-1		**SED-2**		**TR-1**		**ST-1**		**ST-2**		**KRA-1**	
		Annealing loss (%)	TD* (%)	Annealing loss (%)	TD (%)	Annealing loss (%)	TD (%)	Annealing loss (%)	TD (%)	Annealing loss (%)	TD (%)	Annealing loss (%)	TD (%)
1150	1.5	46.94	98.34	46.92	98.30	46.89	98.24	46.70	97.84	46.64	97.72	47.09	98.66
1200	1.5	47.11	98.70	47.22	98.93	47.01	98.49	46.98	98.43	47.02	98.51	47.01	98.49
1300	1.5	44.38	92.98	44.02	92.23	42.40	88.83	44.32	92.86	44.52	93.27	43.76	91.68

*TD - theoretical decomposition of dolomite to loss of annealing

In spite the shape of the DTA curves for each sample annealed at different temperatures was similar, Fig. 1, the most optimal annealing losses were achieved, except for the sample KRA-1, at a temperature of 1200 °C with a holding time of 1.5 hours. The annealing temperature of 1300 °C was already unsatisfactory for all samples. Low annealing loss values were determined for individual samples, probably due to reverse chemical reactions, but this was demonstrated on the DTA recording of the samples by only a weak hint of a peak at a temperature of around 400 °C for all the examined samples and another peak at a temperature above 600 °C for the ST-1 and KRA-1 samples (not shown here).

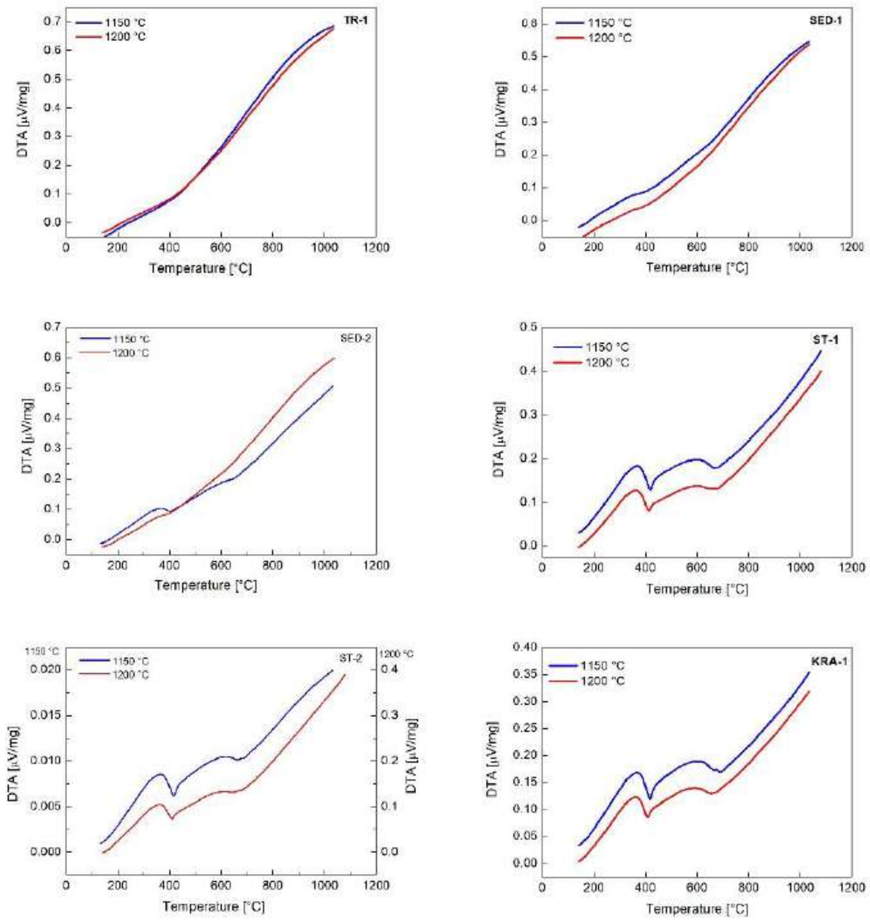

Figure 1 Comparison of DTA records of selected dolomite samples annealed at temperatures of 1150 °C and 1200 °C for 1.5 hours

Selected samples of dolomites (TR-1, SED-1, ST-1, KRA-1) annealed at temperature 1150 °C with holding time of 1.5 hours were subjected to repeated DTA/TG analysis after two months of "standing" in order to determine the degree of hydration of the samples, or stability of the prepared intermediates. The above analyzes resulted in the average weight loss for sample TR-1: 0.34 %, SED-1: 0.59 %, ST-1: 1.55 % and sample KRA-1: 1.54 %. In the dolomite sample, after repeated DTA/TG analysis after two months of "standing," the small agglomerated particles of dolomitic lime were observed on its surface, Fig. 2.

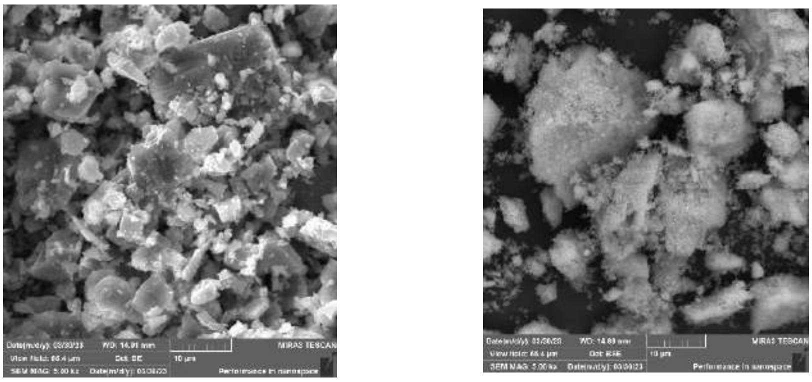

Figure 2 Morphology of the raw dolomite sample ST-1 (left) and sample after repeated DTA/TG analysis after two month of "standing" (right)

The results of DTA/TG analyzes correlate with previous results published by Danková et al. [6]. The recording of the sample TR-1 was almost identical even after two months of the sample "standing". For the sample SED-1, a small peak at a temperature of 400 °C was evident on the DTA curve, corresponding to the hydration of the sample. Higher weight losses were recorded for ST-1 and KRA-1 samples. The endothermic peaks in the temperature range of 350 - 450 °C (corresponding to the $Ca(OH)_2$ phase), present on the DTA records measured immediately after calcination, were more pronounced when measured after two months and slightly shifted to the right to higher temperatures. Individual weight losses correspond to the hydration activity of calcined dolomite and represent only its hygroscopicity, i.e. the ability to bind water molecules from the surrounding environment (air humidity) and do not fully represent its reducing activity [7]. In general, when the hydration activity is higher, the reducing activity is also higher. However, with the same hydration activity, the reduction activity may not be the same, due to the different structure of dolomite.

CONCLUSION

This study confirmed the hypothesis that for the silicothermic reduction of magnesium it is necessary to individually verify the calcination conditions for each sample and determine the influence of hydration activity/active sites in their structure to increase the reduction of Mg.

The DTA/TG analyzes of calcined samples ST-1 and KRA-1 correlated with analyzes of hydrated samples (after two months "standing"), so they appeared as the most suitable samples for the preparation of intermediate products for the production of metallic magnesium.

The results obtained from the laboratory technological processing of dolomites will enable to suggest the methods of magnesium intermediates preparation applicable for semi-operational to operational conditions of metal magnesium production. Given the current crisis situation caused by the lack of critical raw materials, the mentioned laboratory technological research is current and important also from the point of view of the use of high-quality domestic raw material resources, which can be interesting and beneficial especially for manufacturers operating in the Slovak Republic.

ACKNOWLEDGEMENT

This work was supported by the Slovak Research and Development Agency under the Contract no. APVV-21-0176. This material is also a contribution to the EuroGeoSurveys HORIZON-CSA Geological Service for Europe project.

REFERENCES

1. Mehrabi, B., Abdellatif, M. & Masoudi, F. (2012) Evaluation of Zefreh dolomite (central Iran) for production of magnesium via the Pidgeon process. Min. Proc. Ext. Met. Rev. 33, 316–326.
2. Wu L., Han, F. Liu, G. (2021) Comprehensive Utilization of Magnesium Slag by Pidgeon Process. SpringerBriefs in Materials, Springer, Singapore.
3. Zhang, K., Liu, Z., Xu, Z., Chang, Q., Fathy, D., Liu, R., Bai, E. (2024) Microbial and hydrothermal dolomite formation in Early Cretaceous lacustrine sediments in Yin'e Basin: Insights from petrology and geochemistry. Sedimentary Geology 471, 106739.
4. REPORT ON CRITICAL RAW MATERIALS FOR THE EU (2014) Report of the Ad hoc Working Group on defining critical raw materials, Ref. Ares (2015) 1819503 - 29/04/2015, 41 pgs, https://rmis.jrc.ec.europa.eu/uploads/crm-report-on-critical-raw-materials_en.pdf (2025-27-02).
5. Kollová, Z., Čechovská, K., Bačo, P., Németh, Z., Fedorová, E., Danková, Z. Bekényiová, A. (2023) Potenciál kritických nerastných surovín na území SR so zameraním na nerudné suroviny. (Potential of critical mineral resources in the territory of the Slovak Republic with a focus on non-ore raw materials). In: Zborník príspevkov, 62. Forum pro nerudy, Žlutice, Czech Republic, Proceedings, 2- 14 (in Slovak).
6. Danková, Z., Bekényiová, A., Čechovská, K., Fedorová, E., Kollová, Z., Bačo, P., Nováková, J., Zacher, T., Kandríková, V., Fabinyová, E., Briančin, J. (2023) Laboratory technological research of magnesium intermediates preparation from the dolomites raw materials suitable for magnesium metal production. Mineralia Slovaca, 55 (1), 71 - 84.
7. Che, Y., Zhang, C., Song, J., Shang, X., Chen, X., He, J. (2020) The silicothermic reduction of magnesium in flowing argon and numerical simulation of novel technology. Journal of Magnesium and Alloys, 8, 752 – 760.

XVI International Mineral Processing
and Recycling Conference
28-30 May 2025, Belgrade, Serbia

DOI: 10.5937/IMPRC25292A

Original research article

RECYCLING OF WASTE CELL PHONES

Fatma Arslan[1#], 0000-0001-7620-1165,
Cüneyt Arslan[2], 0000-0002-0034-7560,
[1]Istanbul Technical University, Mining Faculty, Mineral Processing Engineering Department, Istanbul, Turkey
[2]Istanbul Technical University, Chemical and Metallurgical Faculty, Metallurgical and Materials Engineering Department, Istanbul, Turkey

ABSTRACT - Recycling provides environmental benefits, such as energy savings, reduced volumes of waste, and reduced emissions associated with energy savings. Cell (mobile) phones are widely circulated in much of the world at the same time. Less than one percent of the millions of cell phones retired and discarded annually are recycled. Almost all the materials used to manufacture a cell phone can be recovered where metals, plastics, batteries, and packaging materials can be recycled and turned into new products. In this study, recycling technologies are summarized and, as a case study; the possibility of recovering valuable metals from waste cell phones by using acidic leaching was studied. The process steps include dismantling waste mobile phones, pre-processing to liberate the materials, and directing them to final treatment processes. In the leaching experiments, sulfuric, nitric, and hydrochloric acids are used. In the sulfuric acid leaching experiment, the effects of acid concentration, temperature, peroxide addition, and leaching periods on metal dissolution efficiencies are investigated. Leaching efficiencies of 97.9% Fe in 8 M H_2SO_4 solutions, 89% Pb, 100% Ni, 90.4% Co, and 4.1% Cu in 1M HNO_3 solutions, 100% Pb, and 100% Al in 4 M HCl solutions were found in one hour.

Keywords: Cell Phone, Recycling, Acidic Leaching.

INTRODUCTION

In today's society, it seems like everyone is glued to a cell phone. This results in about 100-120 million phones that are discarded every year [1]. With such high amounts, old cell phones have become the fastest growing form of electronic trash. This is causing a serious problem because electronic waste contains many hazardous materials. Within each mobile device, harmful chemicals and materials can contaminate soil and waterways, leading to long-term environmental effects that will eventually harm animal and human well-being [2]. More so because many people are to throw away their phones clogging landfills, polluting air and groundwater at an alarming rate. You can make a difference and stop the pollution by recycling your cell phone instead of carelessly discarding it. With innovative technologies, up to 80% of materials used in cell phones can be recycled and reused. Although cell phones consist of materials that differ from model to model and manufacturer to manufacturer, the guideline provides data characterizing the typical content of a mobile phone [3]. The substances identified

---

[#] corresponding author: arslanf@itu.edu.tr include primary constituents, minor constituents and micro or trace constituents. Typically, about 40% of the weight of a mobile phone (including handset, battery and accessories) is plastics, while 20% is glass and 10% copper. Cell phones contain numerous metals, including expensive ones. The most important ones are copper, nickel, silver, gold, platinum group metals, cobalt, lithium, lead, tin, zinc, rare earth metals (REM), gallium, indium, iron, chromium, niobium, tantalum, and titanium. Table 1 lists the cell phone components most important that the metals they contain [4].

Table 1 Metals found in the most important parts of cell phones [4]

Metals	**Cell phone parts**
Chromium	Shield plates
Cobalt	Batteries
Copper	Connectors, printed circuit boards (PCBs), resistors, coils, speakers
Gallium	Printed circuit boards
Gold	Connectors, printed circuit boards
Indium	LCD displays
Iron	Resistors, shield plates
Lead	Capacitors, resistors
Lithium	Batteries
Nickel	Connectors, capacitors, resistors, shield plates, batteries
Niobium	Printed circuit boards
Palladium	Printed circuit boards
REE	Permanent magnets, LCD displays, speakers
Silver	Printed circuit boards , capacitors, resistors
Tantalum	Printed circuit boards
Tin	Printed circuit boards, capacitors, LCD displays
Titanium	Capacitors
Zinc	Resistors

Recycling Processes

Waste cell phones are useful sources of metals, including copper, gold, silver, and palladium, among others. The material recovery and recycling chain consists of the following main steps: collection, segregation (sorting out cell phones from other electronic wastes, separation of components, separation of accessories, battery removal from handset, manual or mechanical disassembly of other parts, recycling of batteries, recycling of accessories, recycling of handsets, shredding or shredding and separation of materials, sampling and analysis for the determination of the individual material composition, smelting, i.e. upgrading of metal contents, metals refining, i.e. separation and purification of metals to marketable products [3]. A prerequisite step in the material recovery and recycling of end-of-life cell phones is the manual separation of batteries, in order to minimize contamination of other materials in subsequent material recovery and recycling stages as well as to maximize recovery of the substances contained in the batteries. Manual separation may also be used to separate certain accessories from mobile phone handsets and, in some cases, plastic parts may be separated for recycling. Mechanical separation, including shredding, crushing and size reduction, followed by various separation techniques, can also be used.

Two main techniques are applied to recycle the PCBs of waste cell phones (WCP); pyro-metallurgical and hydrometallurgical processes. During the pre-processing phase of the material, the battery and hardware parts are dismantled manually and only the PCBs are collected [5]. Then, it is shredded and ground to make it ready for chemical processing. Hydrometallurgical technologies are predictable and controllable methods for material extraction [6, 7].

Smelting and Refining

The environmentally sound recovery and recycling of waste cell phones (excluding batteries and accessories) can be achieved through manual or mechanical component separation, followed by processing in specialized smelters [8]. After mechanical separation, the circuit board and other remaining parts are most efficiently recycled in a smelter, where valuable metals such as copper, gold, silver, and palladium are recovered. Direct smelting also recovers most metals, except iron, magnesium, and aluminum, while plastics serve as both a heat source and a reducing agent.

Smelting electronics, including cell phones, requires specialized equipment, yet many smelters lack proper pollution control. However, with adequate controls, metals can be safely recovered and recycled. Metal recovery from separated batteries involves smelting, which may release metal fumes and particulates, posing risks to workers and communities [3].

Following smelting, electro-refining, dissolution, and precipitation processes further purify the metals. If the resulting slag contains significant metal content, it is either returned to the smelter or processed through selective leaching and precipitation. Only a limited number of smelters and refiners worldwide possess the necessary material handling capabilities and pollution control systems for efficient metal recovery from end-of-life cell phones [3].

Hydrometallurgical processes

Among hydrometallurgical processes that can be applied, leaching is the leading technique based on the principle of solid component solubility by through of contact with leaching agent. Different factors can influence the leaching process, such as pH, temperature, concentration and oxidation–reduction potential (ORP). Hydrometallurgical processes use cyanide and/or strong acids such as aqua regia, nitric acid, sulphuric acid, and hydrochloric acid, ionic liquids, and bacteria to selectively dissolve metals and separate them from other substances [9]. Addition to these acids, a wide variety of reagent systems (e.g. iodide, ammonia, cyanide, thiourea and thiosulfate) in the presence of a suitable oxidant (e.g. ozone, H_2O_2, O_2, Cu(II), Cl_2 etc.) have been tested for leaching of metals from PCBs. Hydrometallurgical processes normally require firstly removal of plastics, and grinding to a small particle size with a high surface area.

Thus, hydrometallurgical process for cell phones will take place at later stages of selective metal recovery, to extract specific desired metals.

Plastic recovery

Plastics from cell phones have not been widely recovered as plastics yet, because few facilities can efficiently sort plastics into clean streams of a single type [3]. In smelters with appropriate flue gas treatment, plastics may be utilized in the metal recovering process, where they serve as a source of heat and substitute for other hydrocarbon fuels and as a reducing agent. If cell phone cases could be designed to be easily removed, and free of contaminating substances like paints, labels and metals, as well as collected in a reasonably large volume, the engineered plastics of cell phones, usually an acrylonitrile butadiene styrene-polycarbonate (ABS-PC), could be recycled with a positive economic value. Manual disassembling of mobile phones prior to precious metal recovery can produce reasonably clean streams of such plastic.

Land disposal

Land disposal of mobile phones may place them in contact with co-disposed acids, and, over an extended period, the substances that are soluble in those acids may leach out. If a landfill is not bound by an impermeable barrier, substances may migrate into ground waters, and eventually into lakes, streams, or wells, and raise a potential exposure to humans and other species. The greater risk of land disposal will be from direct ingestion of contaminants, contaminated soil and water in landfills that are not controlled [3]. If cell phones appear to be in good condition and can be reused, they may be redirected to refurbishment. One other method of recycling cell phones is to take the working parts of broken phones and combine them with the working parts of other used cell phones to make one ready-to-use cell phone [10]. The rebuilt phone can then be sent back into circulation without ever needing newly manufactured parts or natural resources.

MATERIAL AND METHOD

As a case study, this experimental study aims to investigate the possibilities of recovering the valuable metals in the PCBs of the waste (end-of-life/used) cell phones (Figure 1). It includes preparation, characterization, chemical analysis, and hydrometallurgical studies. Figure 1 presents an experimental flow sheet showing all processing steps. After dismantling old cell phones, we subjected the PCBs to size reduction using a shredder, then took cut samples for sieve analysis. Chemical analysis of the sample related to the size ranges are done. According analysis results, all metal contents, except Cu, Au, and Fe, do not change much with particle size range changes where Cu content decreases and Au content increases with decreasing size range and Fe content fluctuates without depending on size range [11].

Before leaching experiments, we conducted dissolution tests to determine the sample's metal content. For this purpose, samples were ground below 1.0 mm and then dissolved in aqua regia. An average weight loss of 53.11% was accepted as the total metal content.

EXPERIMENTAL RESULTS

Before starting leaching experiments, the waste cell (mobile) phone sample (collected from friends and families and supplied by Exitcom Recycling Ltd. Co.-Turkey) is ground under 1 mm in size, and in the experiments, effects of acid concentration, hydrogen peroxide (H_2O_2) addition in sulfuric acid media, leaching time, and acid type on metal dissolution efficiencies were studied [11]. Fe, Ni, and Co dissolutions increased with increasing acid concentrations, while Pb, Zn, and Al are not affected by acid concentration changes. There were no significant changes in metal dissolution efficiencies in terms of H_2O_2 addition. Increasing leaching time had an increasing effect on metal leaching efficiencies. Results of different acid applications are summarized in Table 2.

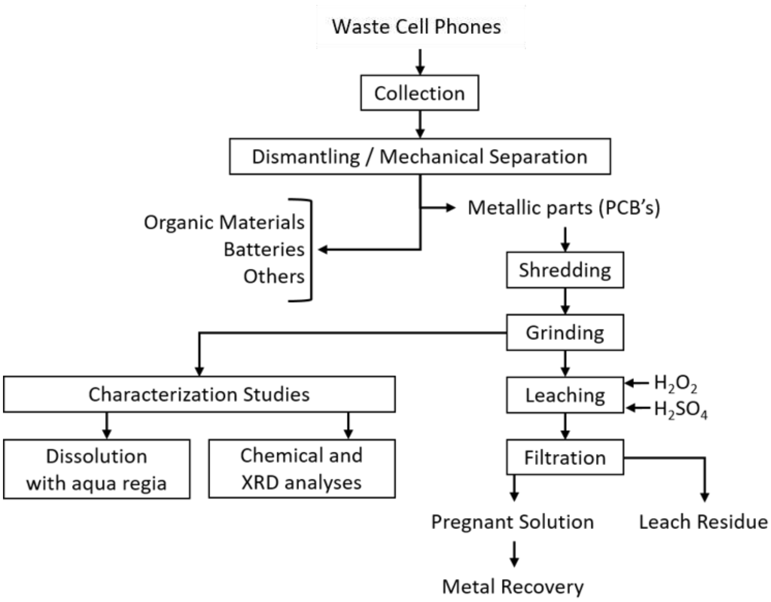

Figure 1 Experimental flow sheet for the recovery of metals from waste cell phones

Table 2 Effect of acid type on metal leaching efficiencies

Acid Type	Metal Leaching Efficiencies, %						
	Cu	Pb	Fe	Ni	Zn	Co	Al
1 mole/L H_2SO_4	0.09	0.54	31.45	3.30	7.69	36.09	61.09
8 mole/L H_2SO_4	0.16	3.32	97.90	7.75	9.59	61.78	24.02
8 mole/L H_2SO_4 + 20% of H_2O_2	0.15	4.06	88.65	15.09	9.30	62.25	36.69
1 mole/L HNO_3	4.13	87.98	21.84	100.00	25.66	90.40	37.20
4 mole/L HCl	0.74	100.00	48.84	17.69	18.80	77.57	100.00
8 mole/L HCl	0.85	100.00	49.25	17.61	19.97	71.36	100.00

In HNO_3 experiments, we observed higher leaching efficiencies for Co, Ni, and Pb; and in HCl experiments, higher efficiencies for Pb, Co, Al, and Fe while Cu leaching efficiency remained low in all cases, regardless of acid type. According to tables, 97.9% Fe leaching in 8 M H_2SO_4 solutions, 89% Pb, 100% Ni, 90.4% Co, and 4.1% Cu leaching in 1M HNO_3 solutions, 100% Pb, and 100% Al leaching in 4 M HCl solutions in one hour were found.

CONCLUSIONS

Less than one percent of the millions of cell phones retired and discarded annually are recycled. Almost all the materials used to manufacture a cell phone can be recovered where metals, plastics, batteries, and packaging materials can be recycled and turned into new products. Two main techniques are applied to recover metals from cell phones as pyrometallurgical and hydrometallurgical processes. As a case study, acidic leaching was applied. Experimental study yielded 97.9% Fe leaching in 8 M H_2SO_4 solutions, 89% Pb, 100% Ni, 90.4% Co, and 4.1% Cu leaching in 1M HNO_3 solutions, 100% Pb, and 100% Al leaching in 4 M HCl solutions within one hour. Therefore, for effective leaching of all metals, we recommend a sequential process using different acids. Precious metals can be dissolved by using cyanide, thiourea, and aqua regia. For metal recoveries from leach solutions, solvent extraction/ion exchange, precipitation, cementation, and electrowinning depending on metal types and compounds can be used.

REFERENCES

1. https://getrepowered.org/blog/importance-of-cell-phone-recycling/, 2025.
2. https://www.greentec.com/blog/e-waste-recycling-for-mobile-phones#the-e-waste-recycling-process-for-cell-phones-in-a-nutshell, 2025.
3. Project 2009. Guideline on Material Recovery and Recycling of End-of-Life Mobile Phones, Mobile phone partnership initiative (MPPI) - Project 3.1 Guideline on Material Recovery and Recycling of end-of-line Mobile Phones, Revised and Approved Text, UNEP & Basel Consumption, March 25, 2009.
4. Buchert M., Manharrrt A., Bleher D., Pingel D. (2012) Recycling critical raw materials from waste electronic equipment, Darmstadt: Öko-Institut, 80 p.
5. Okwu, P.I., Onyeje, I.N. (2014) Extraction of valuable substances from e-waste. American Journal of Engineering Research (AJER). 3, (1), 299-304.
6. Cui, J., Zhang, L. (2008) Metallurgical recovery of metals from electronic waste: a review. J. Hazard Mater. 158 (2-3), 228-256.
7. Abdelbasir, S.M., Hassan, S.S.M., Kamel, A.H., El-Nasr, R.S. (2018) Status of electronic waste recycling techniques: a review. Environ. Sci. Pollut. Res. 25 (17), 16533-16547.
8. Wang, H., Zhang, S., Li, B., Pan, D., Wu, Y., Zuo, T. (2017) Recovery of waste printed circuit boards through pyrometallurgical processing: a review. Resour. Conserv. Recycl. 126, 209-218.
9. https://www.wastecare.com/Articles/Cell_Phone_Recycling.htm, 2025.
10. Arslan, F., Perek, K. T., Arslan, C., Çuhadar, İ. E., Altun, A. (2022) Studies on Acidic Leaching of Waste Mobile Phones, International Journal of Mineral Processing and Extractive Metallurgy, 7(2): 36-42.
11. E. Salinas-Rodrigez et al. (2022) Leaching of Copper Contained in Waste Printed Circuit Boards, Using Thiosulfate-Oxygen System: A Kinetic Approach, Materials, 15, 2354.

XVI International Mineral Processing
and Recycling Conference
28-30 May 2025, Belgrade, Serbia

DOI: 10.5937/IMPRC25298M Original research article

THE RECYCLING OF PLASTICS AND METALS FROM END-OF-LIFE NMC-TYPE ELECTRIC VEHICLE LITHIUM-ION BATTERIES USING SELECTIVE FROTH FLOTATION

Fulya Mennik[1]**,** 0009-0004-9883-7833,
Nazlım İlkyaz Dinç[2]**,** 0000-0003-0720-667X,
Beril Tanç Kaya[3]**,** 0000-0002-1757-0566,
Fırat Burat[1#]**,** 0000-0001-7051-0063,
[1]Istanbul Technical University, Faculty of Mines, Mineral Processing Engineering Department, Istanbul, Türkiye
[2]Istanbul Technical University, Istanbul, Türkiye
[3]Istanbul Technical University, Faculty of Mines, Geological Engineering, Istanbul, Türkiye

ABSTRACT – The increase in end-of-life (EoL) Lithium-ion Batteries (LIBs) in recent times has become a major concern for the global community. Most of the research in the literature has focused on the recovery of cathode active metals from black mass. The separation of anode-cathode foils, plastics, and casing metals, which are essential parts of LIBs, remained limited. To reduce costs and maximize the recovery of valuable metals in the subsequent hydro or pyro metallurgical processes EoL LIBs need to be pre-treated accordingly. The main purpose of this study is to scrape off the black mass (or battery dust) adhering to the electrode foils as a result of gradual crushing and then to separate the plastic and copper from other metals by two-step selective flotation. The results showed that plastics with natural hydrophobicity could be removed with the help of a frother. After plastic flotation, the copper particles were floated in the presence of Aerophine 3418A, and a copper concentrate assaying 65.13% Cu was obtained with 96.4% Cu recovery at the end of the copper flotation circuit. In addition, the Al content in the material that could not float and remained in the cell was increased to approximately 77%.

Keywords: Lithium-ion Battery, Plastics, Copper, Aluminum, Recycling.

INTRODUCTION

Developments in energy storage technologies have caused significant transformations across various sectors and have become crucial for achieving a sustainable future. Moreover, the rising energy demand, the increasing use of renewable energy sources, and the extensive of electric vehicle (EV) technologies are contributing to the need for advanced energy storage systems. In particular, the high use rates of fossil fuels and the need to reduce environmental damage have led users to want to develop

---

[#] corresponding author: buratf@itu.edu.tr renewable and sustainable energy sources such as high-quality batteries, wind turbines, fuel cells, and solar panels [1].

Lithium-ion batteries can be identified by their compact size, lightweight design, high energy density, and voltage, expanded lifespan, absence of memory effect, efficient operation across a wide temperature range, and eco-friendly characteristics [2]. The incorrect disposal of discarded LIBs in the environment results in significant issues. The pollution of soil and water can be caused by the leakage of heavy metals and compounds from batteries. In addition to its environmental and economic benefits, the exploitation of the resource potential of scraps is significant for the conservation of natural resources and the sustainable development of metals and related industries [3, 4]. Besides, EoL LIBs contain many components (such as Li, Co, Cu, Al, Ni, Fe, Mn, and graphite) with high economic value [5]. LIBs consist of several fundamental components, each serving distinct functions. Each component is essential in influencing the energy storage capacity, safety, and lifespan of the battery. Alongside the cathode and anode, LIBs comprise additional components including the electrolyte, separator, current collectors, and casing. The structure of a standard battery module is illustrated in Figure 1 [1].

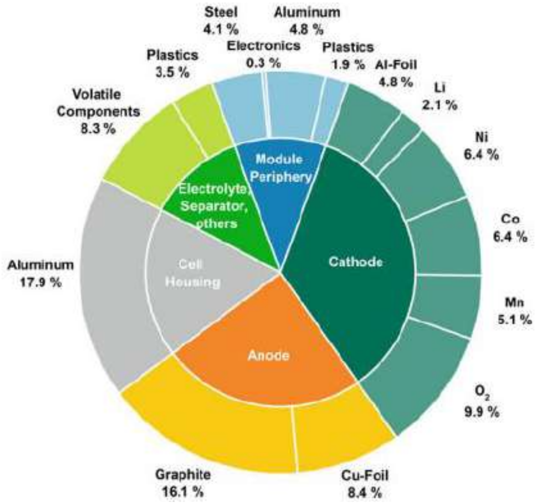

Figure 1 Components of LIBs [1]

Recycling LIBs enables the recovery of critical metals. The result of resource management reduces dependency on mining activities, protects natural resources, and supports sustainable production models. To recycle S-LIBs, different techniques are used, such as physical (dismantling, comminution, classification, gravity, magnetic, and electrostatic separation), physicochemical (flotation), hydrometallurgical (chemical precipitation, acidic leaching, electrochemical processes), and pyrometallurgical (roasting, thermal treatment). Nevertheless, the composition of LIBs is distinct from that of a natural ore due to their unique properties. Examining identical LIBs maintains the same physical properties, material amount, and type. On the other hand, different types of LIBs have different chemical structures, so the way they are recycled may be different depending on the type of battery [6, 7].

While flotation studies mostly focused on the separation of graphite from the black mass the selective recovery of coarse fractions including current collector metals (Cu and Al), case metals (Fe and Ni), plastics, and separators is very limited. Therefore, this study has aimed at the selective separation of plastics, Cu, Al, and case metals from NMC-type Lithium-ion batteries using different surface-active reagents. After separating the black mass from the metallic fraction through four stages of size reduction and sieving, in the first flotation stage, plastics with natural floatability were selectively removed with the help of a frother reagent (MIBC). In the second flotation stage, the effects of different collectors on copper flotation were investigated by collecting hydrophobic copper particles in float product and leaving the hydrophilic Al and case metals particles in the cell.

EXPERIMENTAL

In this study, approximately 60 kg of NMC-type EoL EV LIBs were supplied from Exitcom Co. located in Kocaeli, Türkiye. A multistage size reduction and classification system was applied and shown in Figure 2. The batteries were first fully discharged for 48 h with 5% NaCl solution, air dried, and then subjected to primary crushing using a dual shaft shredder in the recycling company to guarantee safety conditions. The crushed material was sent to the Mineral Processing Engineering Department Pilot Plant in Istanbul Technical University for subsequent comminution processes. The black mass 1 sample was separated using a 0.2 mm sieve and fed to a four-blade cutting mill (RAM200 model supplied from RANTEK Co.) for further scraping off the remaining black mass on collecting electrodes. The cutting mill was engineered to crush uniformly elastic, soft, medium-hard, fibrous, and heterogeneous materials. When the particles are reduced in size by shear forces, the material maintains its flat surface shape, which creates an advantage for the flotation process. The crushed material's size was adjusted by utilizing a replaceable sieve (6, 4, 2 mm, etc.,) located in the lower compartment of the mill. The black mass adhering to the surfaces of the current collectors was further removed using a 0.2 mm sieve and reserved for future studies. The coarse material (-2+0.2 mm), which constitutes about half of the feed, is mainly composed of copper foils, aluminum foils, battery casings, plastics, and separators. As seen in Figure 3, the d_{80} and the d_{50} sizes of the -2+0.3 mm fraction were determined as 1 mm and 0.65 mm, respectively. The coarse fraction accounts for about 32% of the feed, while the remaining amount belongs to the black mass.

Before flotation experiments, 50 g of the sample was weighed and added to 1000 mL of tap water, then mixed at 1500 rpm for 15 min to remove the remaining black mass. The dispersed black mass was removed through a 74 µm screen and the over-screen material was again fed to a 1.5 L self-aerated Denver-type flotation machine with an impeller speed of 1200 rpm. No pH adjuster was used to create a more environmentally friendly process. City tap water was used for all experiments and the natural pH of the pulp was around 8.3. After the reagents were sufficiently contacted with the particles, the air valve (3 L/min air flow rate) was opened and the floating particles were collected

(3 min flotation time). First-stage flotation experiment was carried out to separate the plastic fraction from metals. MIBC was preferred as the frother reagent in plastic flotation and no collector reagent was required. After the separation of plastics, the copper particles in the sink product were floated with the help of different collectors (KAX (Solvay Group), Aerophine-3418a, Aero-3739 (Syensqo), Aerofloat-242, and Aerofloat-211).

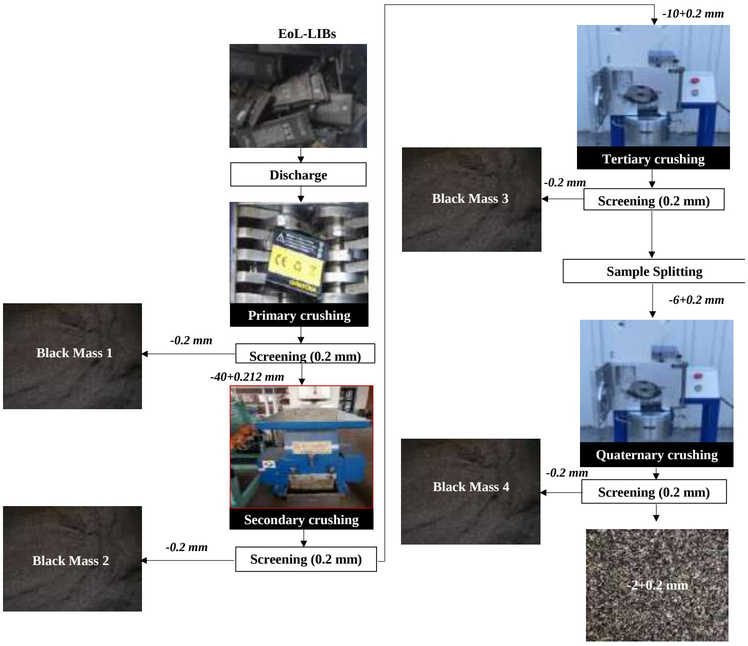

Figure 2 Flowchart of the multi-stage crushing process

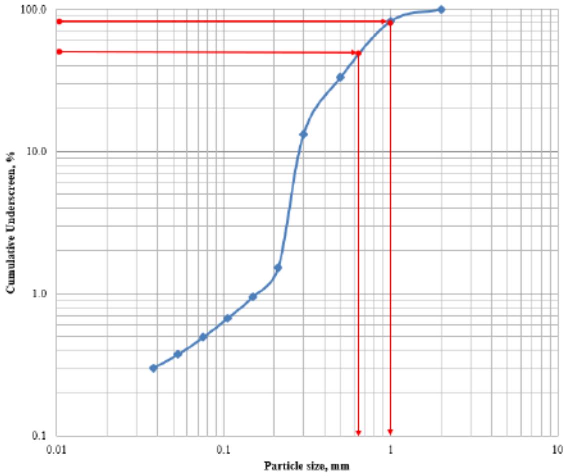

Figure 3 The particle size distribution of -2+0.2 mm fraction

The experimental data were interpreted based on the content and recovery of the products. The metal contents and distribution of metals were determined through chemical analysis. The XRF method was employed to determine the chemical properties of the LIBs sample in the geochemistry research laboratory at I.T.U. The analysis of the products was repeated at least two times and the weighted averages were calculated. The margin of error was around ±1.5%.

RESULTS AND DISCUSSION

The chemical modification of particle surfaces can regulate their hydrophobic or hydrophilic properties [8]. Plastics are known for their natural hydrophobic and their specific gravity is very low compared to metals. In froth flotation, a selective separation is made based on the hydrophobicity differences between the particles. Plastic flotation tests were carried out in 5 stages (no frother at the first stage and then 4x100 g/t MIBC). Without any frother, about 15% of the total plastics were floated and about 60% of the plastic particles were floated with the addition of 200 g/t of MIBC. The cumulative weight of the floated plastics systematically increased to 95% at 400 g/t. Although the surfaces of Al particles are more hydrophobic than Cu surfaces before the reagent addition, the wettability of Cu increases and exceeds that of Al with the addition of collectors, which were originally used in the flotation of natural copper ores [6]. The amount of collector concentration was fixed to 3x1000 g/t for the copper stage. Metal contents and recoveries of the flotation experiments are given in Table 1.

It is clear from Table 1 that approximately 16% of the material that was fed to the first flotation stage was removed as a plastic product. Approximately 5% by weight of the fine-sized Al particles, which have a greater floatability than Cu, were transferred into the floating product. This value is around 1.5% for Cu which has lower floatability over Al particles. A small portion of the cathode active materials still attached to the Al passed into the plastic product with this metal. With a cleaning flotation, the final plastic product can be obtained with lower metal contents. A copper concentrate assaying 65.13% Cu was successfully obtained with a 96.4% Cu recovery rate. Another commercial reagent which is mostly preferred in the flotation of natural copper ores, KAX, provided a successful flotation and a Cu concentrate assaying 62.47% Cu was produced with 95.8% Cu recovery. The image of floating copper particles is presented in Figure 4.

Although the other three collectors obtained concentrates with similar Cu contents, their recovery rates decreased due to the low amount of floating material. If the evaluation is made according to Al content, the best performance is again shown by the 3418A collector. A sink product with approximately 77% Al content was obtained with 71.6% Al recovery. The reason for the low Al recovery efficiency compared to Cu is the loss of small-sized Al particles mixed with the copper concentrate. To increase both Cu content and Al recovery, it can be suggested to reduce the floating ability of the Al particles using NaOH pre-treatment and feed to a cleaning circuit. Another solution can be to transform the particles into spherical shapes using a proper grinder and then to separate two metals using an electrostatic or Eddy current separator. After copper flotation, the sinking product with high Al content remaining in the cell cannot float and can be separated from the magnetic case metals accompanying this metal with the help of a magnetic separator. In this way, both the Al content is increased and a marketable product with high Fe and Ni content can be produced.

Table 1 Metal content and recoveries of flotation

Collector Type	Products	Amount %	Cu		Al		Co		Ni		Mn		LOI	
			C, %	R, %	C, %	R, %	C, %	R, %	C, %	R, %	C, %	R, %	C, %	R, %
KAX	Plastics	14.3	1.25	0.7	12.70	4.7	4.58	10.4	1.30	10.7	1.28	11.8	74.29	48.8
	Black Mass	8.5	1.24	0.4	6.30	1.4	20.18	27.3	5.66	27.6	5.14	28.1	50.96	19.9
	Copper	38.8	62.47	95.8	22.25	22.3	2.25	14.0	1.02	22.8	0.95	23.8	8.53	15.2
	Aluminium	38.5	2.02	3.1	71.84	71.6	7.84	48.3	1.75	38.9	1.46	36.3	9.03	16.0
	Total	100.0	25.28	100.0	38.63	100.0	6.25	100.0	1.73	100.0	1.55	100.0	21.69	100.0
3418A	Plastics	15.7	1.41	0.9	12.68	5.1	4.96	12.5	1.58	13.9	1.46	14.5	73.79	54.0
	Black Mass	10.0	1.33	0.5	6.28	1.6	19.96	32.0	5.51	30.7	5.41	34.2	51.81	24.1
	Copper	37.9	65.13	96.4	21.12	20.7	2.03	12.4	0.73	15.5	0.67	16.1	7.06	12.5
	Aluminium	36.5	1.52	2.2	76.98	72.6	7.33	43.1	1.95	39.9	1.52	35.2	5.55	9.4
	Total	100.0	25.58	100.0	38.70	100.0	6.21	100.0	1.78	100.0	1.58	100.0	21.43	100.0
AERO 3739	Plastics	15.5	1.52	0.9	12.47	4.9	5.03	12.7	1.56	14.1	1.40	14.5	74.03	55.3
	Black Mass	10.1	1.28	0.5	6.20	1.6	19.95	32.8	5.29	31.1	5.35	36.0	52.35	25.4
	Copper	5.9	63.27	15.0	21.97	3.2	1.83	1.8	0.74	2.5	0.63	2.5	8.69	2.5
	Aluminum	68.5	30.25	83.6	52.25	90.3	4.71	52.7	1.31	52.3	1.03	47.1	5.11	16.9
	Total	100.0	24.81	100.0	39.66	100.0	6.13	100.0	1.72	100.0	1.50	100.0	20.77	100.0
AERO 242	Plastics	15.1	1.65	1.0	12.84	4.9	4.70	11.5	1.47	13.4	1.36	13.9	74.00	53.6
	Black Mass	8.0	1.18	0.4	5.57	1.1	19.79	25.5	4.90	23.6	5.55	29.9	52.99	20.3
	Copper	21.4	65.85	56.6	15.93	8.5	1.56	5.4	0.94	12.2	0.78	11.3	12.33	12.7
	Aluminum	55.5	18.88	42.0	61.60	85.5	6.43	57.6	1.52	50.8	1.20	44.9	5.06	13.5
	Total	100.0	24.94	100.0	39.96	100.0	6.19	100.0	1.66	100.0	1.48	100.0	20.86	100.0
AERO 211	Plastics	15.7	1.58	1.0	12.32	4.9	4.83	12.1	1.48	13.2	1.44	14.5	74.12	53.8
	Black Mass	9.9	1.28	0.5	5.48	1.4	19.42	30.7	5.32	29.9	5.35	34.2	52.97	24.4
	Copper	28.6	69.22	80.1	16.21	11.8	1.82	8.3	0.68	11.0	0.60	11.1	8.82	11.7
	Aluminium	45.9	9.91	18.4	69.79	81.8	6.68	48.9	1.76	45.9	1.36	40.2	4.75	10.1
	Total	100.0	24.70	100.0	39.11	100.0	6.26	100.0	1.76	100.0	1.55	100.0	21.55	100.0

C: Content; R: Recovery

The LOI contents in Table 1 largely indicate a small amount of graphite that could not be removed as a result of the crushing and screening processes. Graphite is not used largely in the Al collector electrodes; however, graphite is mainly used as anode material on copper surfaces. This situation shows that some of the separator particles cannot float in the first flotation circuit (plastic) and the next copper circuit and remain in the sinking product.

Figure 4 The image of floating copper particles in the copper flotation stage

CONCLUSION

In the recycling process of EoL LIBs, chemical methods are preferred in obtaining battery powder, which has high economic value. In academic studies, the flotation method was used mainly to selectively separate anode and cathode active materials, but most of them are far from commercialization. The separation of other important economic values such as Cu and Al collector electrodes, case metals, and plastics remained in the background.

In this original study, the flotation method was used for the recovery of selective metal concentrates from EoL LIBs. As a result of the enrichment processes carried out in a rather large size compared to natural ores, plastics were separated with high content and recovery rates, while the copper particles in the remaining metallic fraction were concentrated with commercial copper reagents. The majority of plastic particles originate from separators.

A copper concentrate assaying 65.13% Cu was successfully obtained with a 96.4% Cu recovery rate using A3418. The drying process is required for the magnetic separation of case metals in sink product. The operational cost of drying will be low due to the coarse size and small amount of feed. A cleaning flotation stage can be added to produce a copper concentrate with much higher contents, or the Al and plastic particles can be recovered by electrostatic or Eddy current separation.

As a result of obtaining metallic concentrates with ore preparation and enrichment methods that reduce the complexity of the structure of LIBs, capacity can be increased in the refining process and toxic gas emissions can be prevented in the thermal process. Again, capacity can be increased and reagent savings can be achieved in the hydrometallurgical process. In conclusion, the findings in this study suggest an alternative process to efficiently recover metal foils, plastics, and case metals in LIBs.

ACKNOWLEDGEMENT

The present study is based on the results of the graduate thesis conducted at the Istanbul Technical University and supported by Istanbul Technical University, BAP (Scientific Research Project) Department with the project code MGA-2022-43640 and MYL-2023-44587. The authors sincerely thank the Mineral Processing Department for providing laboratory equipment and Exitcom Company for the supply of samples.

REFERENCES

1. Kaya, M. (2022) State-of-the-art lithium-ion battery recycling technologies, Circular Economy, 1 (2), 100015.
2. Mylarappa, M., Lakshmi, V. V., Mahesh, K. V., Nagaswarupa, H. P., Prashantha, S. C., Kumara, K. S., Raghavendra, N. (2017) Resource recovery and material characterization of metals from waste li-ion batteries by an eco-friendly leaching agent. Materials Today: Proceedings, 4 (11), 12215-12222.
3. Xu, J., Thomas, H.R., Francis, R.B., Lumb, K.R., Wanga, J., Liang, B. (2008) A review of processes and technologies for the recycling of lithium-ion secondary batteries, J. Power Sources 177, 512-527.
4. Zhang, T., He, Y., Wang, F., Li, H., Duan, C., Wu, C. (2014) Surface analysis of cobalt-enriched crushed products of spent lithium-ion batteries by X-ray photoelectron spectroscopy, Separ. Purif. Technol. 138 21-27.
5. Mennik, F., Burat, F. (2023) The effect of attrition scrubbing as a pre-treatment on the recovery of copper from end-of-life lithium-ion batteries in froth flotation. In: 28th International Mining Congress and Exhibition of Türkiye. Antalya, Türkiye, Proceedings, 1090-1101.
6. Mennik, F., İlkyaz, N. İ., Burat, F. (2023) Selective recovery of metals from spent mobile phone lithium-ion batteries through froth flotation followed by magnetic separation procedure, Results in Engineering, 17, 100868.
7. Çuhadar, İ. E., Mennik, F., Dinç, N.İ., Gül, A., Burat, F. (2023) Characterization and recycling of lithium nickel manganese cobalt oxide type spent mobile phone batteries based on mineral processing technology. Journal of Material Cycles and Waste Management, 25, 1746-1759.
8. Burat, F., Güney, A., Kangal, M.O. (2009) Selective separation of virgin and post-consumer polymers (PET and PVC) by flotation method. Waste Management, 29 (6), 1807-1813.

XVI International Mineral Processing
and Recycling Conference
28-30 May 2025, Belgrade, Serbia

DOI: 10.5937/IMPRC25306D Original research article

PERFORMANCE OF IRON ALUMINIUM AND COPPER IRON BIMETALLIC PARTICLES IN REMOVAL OF HEAVY METALS AND METALLOIDS

Paul Delaney[#], 0009-0003-8834-961X,
Western Australian School of Mines Curtin University of Technology, Perth

ABSTRACT – Acid Mine drainage (AMD) often leads to the mobilisation of elements that can be toxic and/or valuable. This study compared the performance of iron-aluminium and copper-iron bimetallic particles in removal of heavy metals, cadmium, arsenic and chromium. These particles were synthesised by a cementation process with four different elemental ratios. Sulphuric acid solutions containing heavy metals were synthesised and treated with the bimetallic particles over 24 hours, with timed samples tested with inductively coupled plasma spectroscopy. Copper-Iron bimetallic (~8.76% Cu) had the best performance with complete removal of chromium in five minutes, cadmium 1 hour and arsenic in ten minutes.

Keywords: Acid Mine Drainage, Bimetallics, Treatment.

INTRODUCTION

Since ancient times, mining sulphidic minerals has been crucial for accessing metals like copper, tin, and silver, vital for technological and economic advancement. The Iberian pyrite belt for example, mined by the Phoenicians and Romans, and later by the Spanish Empire, saw extensive extraction of these metals, with over 280 Mt of ore mined throughout history [1]. Disturbance of hitherto inaccessible sulphidic minerals though can cause economic and environmental harm due to their exposure to water and oxygen, resulting in Acid Mine Drainage (AMD) or Acid Rock Drainage (ARD). The reactions are complex and vary by location, affected by factors like climate, pH, mineral types, and bacterial activity [2]. Although the chemistry can vary from site to site, a proxy reaction such as shown in equation (1) can be used to represent the system, where a sulphide mineral in the presence of water and oxygen can produce acid [3].

$$4FeS_2 + 15O_2 + 14H_2O \rightarrow 4FE(OH)_3 + 8SO_4^{2-} + 16H^+ \tag{1}$$

In isolation, the acidity produced can be damaging to biological species, but it also allows the mobilisation of toxic heavy metal species, which can lead to widespread and persistent damage, particularly in an aquatic environment [4,5]. The Rio Tinto estuary that drains part of the Iberian pyrite belt for example is highly acidic (pH 2.5) and has 10^5 - 10^6 the levels of dissolved cadmium, zinc and copper when compared to uncontaminated water close by; with a sea water plume from its outlet observed to

---

[#] corresponding author: paul.delaney@postgrad.curtin.edu.au stretch for 300km into the Mediterranean Sea, and sediment core sampling of the Spanish continental showing increased contamination consistent with historical mining activities [1]. The widespread occurrence of AMD across the globe also frequently leads to economic losses. The USA, which is both a historic and current major mining jurisdiction [6], has listed liabilities in tens of billions of USD associated with its 23000km of AMD affected waterways [5,7].

Current methods of control of AMD can be grouped into active remediation, passive remediation, or prevention. Prevention, though ideal, is often impractical except for new sites and involves limiting access of oxygen, water, or bacteria to sulphide minerals [3]. Active remediation, commonly used in active mining sites, involves methods like adding lime to raise pH and precipitate metal species out which can be costly, and frequently produces a toxic sludge needing disposal [8,9]. Passive remediation is cheaper, but less flexible and generally only suitable for rehabilitation settings and includes methods like anoxic limestone drains and wetlands; these require less intervention but still need regular monitoring to remain effective [9]. The main theme with these processes though is that they treat AMD as a bulk waste product. Failing to separate components of AMD however will become less attractive over time. Many of the toxic constituents are becoming more valuable as various sectors of the economy increase their demand for materials such as cobalt, and if elements like this can be separated from the other components in an economic manner, it provides a route for revenue to offset treatment costs and making remediation of abandoned sites more appealing in countries such as Australia where state governments are responsible for defunct mines [10]. Secondly, much of the volume associated with AMD waste is associated with iron which is far less toxic than other constituents [11]. If the iron rich sludge can be decontaminated in an economical manner, it can reduce the disposal costs on a unit basis, which over time are predicted to increase above inflation due to tightening regulation [12].

The literature reviewed identified Bimetallic Particles (BMP) as a potential method for removing and/or valorising elements from an AMD stream. These particles, composed of solid element upon which an aqueous element is cemented upon in a core and shell configuration, have shown potential in related applications such as mercury removal, arsenic extraction, and chromium elimination [13,14,15]. The combination of the two metals within a BMP, create a synergistic pair that enhances adsorption capacity of the parent metals [15]. A combination of redox and precipitation reactions immobilises the target species onto the BMP, which can be separated through vacuum or magnetic filtration from the AMD solution [16]. Iron-based particles, particularly Fe-Al, have been noted as promising candidates which use cheap precursors [13,14,17]. Alternatively, Copper-based particles use a more expensive precursor but offers a simpler fabrication process [15]. Both types were examined in this study.

The three target species, arsenic, chromium, and cadmium, were chosen due to their presence in AMD samples from an Australian defunct mine site; with the levels far more than the specified guideline, with arsenic levels 2, cadmium 4, and chromium 5 orders of magnitude greater than the 99% protection level for aquatic life [11].

EXPERIMENTAL

Bimetallic Particle Synthesis

Precursor materials of lab reagent grade aluminium powder (99.9% with D50 38.91µm), iron powder (99.8% with D50 114.36µm), copper (II) sulphate pentahydrate and anhydrous ferric chloride (98.0%), along with hydrochloric (32%) and sulphuric acid (98%) were purchased. Iron was cemented onto aluminium particles after an initial acid wash as per the method by Aghaei [13] to produce Fe-Al BMPs. Copper was directly cemented onto iron particles as per the method outlined by Hu [14] to produce Cu-Fe BMPs. For each particle type, four particle species (labelled A-D) were synthesised by variation of the concentration of the initial cementation species. Pipette samples were taken of the both the initial loaded cementation solution and the spent cementation solution.

Particle Characterisation

Brunauer, Emmett and Teller (BET) analysis was undertaken by a Micrometrics Tristar II Plus with nitrogen used as the adsorbent. Sizing analysis was undertaken with a Mastersizer 2000 with a Hydro 2000S mixer.

Adsorption Testing

Single heavy metal solutions of 10ppm concentration were synthesised by dilution of 1000ppm ICP-OES standards of cadmium, arsenic and chromium within 50mL volumetric flasks using sulphuric acid solution as a dilutant (~pH2) to represent a simple AMD solution. A 1mL pipette was collected from the solution for ICP testing, and the remaining 49mL was transferred to a sealed 100mL Erlenmeyer flask. For each particle type, a 0.5g sample of the BMP was added, and for a period of 24 hours, these flasks were housed in an orbital shaker set at 250rpm within a temperature-controlled fume cupboard (25°C). 1mL pipette samples were taken at intervals of 5, 10, 20 minutes and 1, 6 and 24 hours. Each configuration of heavy element and particle type was tested twice, with the variation observed between the runs insignificant, with variation between concentrations observed in ICP no greater than 5% for any configuration. pH and electrode measurements were also taken but this not presented to preserve brevity of the paper.

RESULTS AND DISCUSSION

Pipette samples taken from the initial and spent solutions were analysed with Inductively Coupled Plasma Optical Emission spectroscopy using a Perkins Elmer Optima 8300. These were used along with the masses of solids to perform a mass balance and give the calculated percentage of cementation species for each particle type as presented in Table 1. For the Fe-Al BMPs, during particle synthesis there was some loss of mass due to the acid wash stage as some of the aluminium was dissolved. The increase in aluminium in solution was measured via ICP, and the cementation figures calculated take this loss into account.

Table 1 Bimetallic Particle Cementation Specie Percentage

	A	B	C	D
Fe-Al BMP	3.47	5.56	11.95	24.14
Cu-Fe BMP	0.13	0.88	1.85	8.76

The data obtained from particle characterisation is presented in table 2. Fe-Al BMPs all displayed adsorption isotherms consistent with Type IV a of the IUPAC classifications, whereas Cu-Fe BMPs all displayed isotherms consistent with a Type II.

Table 2 Particle Characterisation

		A	B	C	D
Fe-Al BMP	Particle Size (µm)	44.91	47.75	53.80	60.47
	Surface Area (m^2)	24.15	48.15	63.63	52.97
Cu-Fe BMP	Particle Size (µm)	124.77	146.94	166.67	173.52
	Surface Area (m^2)	6.05	2.96	8.91	8.80

The collection of pipette samples at regular intervals allowed the content of the target specie to be tracked for each run. From this the time taken for complete removal of the elemental species is presented in Table 3. All study species were removed from solution by the BMP types, except for the A particle type of Fe-Al. For this BMP type, no cadmium was observed to be removed from solution after 24 hours.

Table 3 Time for Complete Removal of Heavy Metal for Each BMP Particle Type

	Chromium	Cadmium	Arsenic
Fe-Al A	24 hrs	Not Observed	1hr
Fe-Al B	24 hrs	24 hrs	24 hrs
Fe-Al C	1 hr	6 Hrs	6 Hrs
Fe-Al D	24 hrs	24 hrs	1hr
Cu-Fe A	10 mins	6 Hrs	20mins
Cu-Fe B	5 mins	6 Hrs	10mins
Cu-Fe C	5 mins	1 Hr	1hr
Cu-Fe D	5 mins	1 Hr	10mins

The standard electrode potentials of chromium (2+), cadmium (2+) and arsenic (3+) are -0.9eV, -0.4eV and 0.24eV respectively and table 3 columns have been ordered in this manner. If the removal of the target species was purely because of redox reactions with the parent metals of the BMP, it would be expected that chromium removal would be most rapid, and arsenic removal the least rapid of the species removed. The data does not support this however, and in fact arsenic removal is quite rapid when compared to the cadmium. Furthermore, it would be expected that the aluminium, with a -1.68eV electrode potential for Al+3/Al, would have the strongest driving force to take the target species out of solution, and hence lead to the Fe-Al particles to have the best performance. However, the data obtained shown the Cu-Fe particles have the best performance, so redox reactions with the parent metals cannot be what is solely driving the removal from solution. This supports the hypothesis of various authors who attribute other mechanisms such as surface adsorption and intraparticle adsorption, and the contribution of these factors is believed to also contribute to the removal pathways in the systems under study in this paper [13,14,17]. One interesting observation that was noted was that chromium removal was slower than was seen in the literature example, but the system in the literature did not have any runs with such a low starting pH. The presence of sulphate ion is not thought to account for the difference, but it is possible the lower starting pH means that the contribution that formation of insoluble precipitates to the removal of the cadmium is delayed until the pH rises sufficiently. Another observation is that no iron was detected in any Fe-Al adsorption sample, but aluminium was detected. This suggests that the aluminium is successfully undertaking the role outlined by other authors in acting as an electron donor and preventing the formation of iron corrosion products [19]. The Cu-Fe adsorption test data did show increase in iron content as the target species was removed which is also consistent with the mechanism presented by Hu [14]. This model involves copper acting as an electron bridge where it donates electrons to the target specie which then forms an insoluble iron hydroxide specie but is also regenerates itself by accepting electrons from zero valent iron which leads to some of the iron going into solution. The differing mechanisms that the two BMP types will need to be considered in future work. Overall, the D type of Cu Fe BMP had the best performance of all BMPs, with the C type of the FE-Al having the best Fe-Al performance, but the increase in iron content that is observed with the Cu Fe BMP might be problematic. AMD is already a high iron content solution, and future work will need to ensure that this does not hinder the performance of these BMP types. Separate to this body of work, testing of adsorption of iron ions was conducted for these particles, and iron was shown to be removed from solution by Cu-Fe BMPS, but not Fe-Al BMPs. Adsorption was slow (between 6-24 hrs) but complete removal was observed. Hence although ions in this study were removed at fast rates, it is possible that complex mixture that is within AMD may slow these rates when the ions have other species competing with them, and further study is warranted to examine this. Although the highest copper content BMP was identified as the superior specie for this work, it is not believed that an even higher copper specie should be pursued. A limited run of Fe-Cu BMP particles that were ~11% copper was trialled for arsenic only, and it had performance like the C type BMP within table 3.

CONCLUSION

The study was able to show that a range of contaminants were able to be removed from solution representing an AMD solution which extended on work from other authors whose focus was wastewater. Cu-Fe BMPs had the superior performance, but they showed an increase in iron content of the final solution. Future work is required to understand the effect that the matrix composition has on removal, and whether the Cu-Fe BMPs continue to show superior performance over the Fe-Al BMPs as this study suggests. The effect of co located ions, in particular other target ions is also essential future work.

ACKNOWLEDGEMENT

Author gratefully acknowledges the support of Curtin University of Technology and a Research Training Program (RTP) Scholarship of the Commonwealth Government of Australia.

REFERENCES

1. Van Geen, A., Adkins, J. F., Boyle, E. A., Nelson, C. H. & Palanques, A. 1997. A 120 yr record of widespread contamination from mining of the Iberian pyrite belt. Geology (Boulder), 25, 291-294.
2. Akcil, A. & Koldas, S. 2006. Acid mine drainage (AMD): causes, treatment and case studies. Journal of cleaner production, 14, 1139-1145
3. Johnson, D. B. & Hallberg, K. B. 2005. Acid mine drainage remediation options: a review. Sci Total Environ, 338, 3-14
4. Park, I., Tabelin, C. B., Jeon, S., Li, X., Seno, K., Ito, M. & Hiroyoshi, N. 2019. A review of recent strategies for acid mine drainage prevention and mine tailings recycling. Chemosphere, 219, 588-606
5. Fashola, M. O., Ngole-Jeme, V. M. & Babalola, O. O. 2016. Heavy metal pollution from gold mines: Environmental effects and bacterial strategies for resistance. International journal of environmental research and public health, 13, 1-1.
6. Statista. 2022. Leading mining countries worldwide in 2020 [Online]. Available: https://www.statista.com/statistics/1114898/leading-mining-countries-worldwide-based-mineral-production-value/ [Accessed 2 March 2025 2025].
7. Naidu, g., Ryu, s., Thiruvenkatachari, r., Choi, y., Yeong, s. & Vigneshwaran, s. 2019. a critical review on remediation, reuse, and resource recovery from acid mine drainage. environmental pollution (1987), 247, 1110-1124.
8. Taylor, J., Pape, S. & Murphy, N. 2005. A summary of passive and active treatment technologies for acid and metalliferous drainage (AMD). 5th Australian Workshop on acid drainage. Australian Centre for Minerals Extension and Research (ACMER).
9. INAP. 2023. Global Acid Rock Drainage Guide [Online]. International Network for Acid Preventation. Available: http://gardguide.com/images/5/5f/TheGlobalAcidRockDrainageGuide.pdf [Accessed 2023].
10. DMP 2009. Acid Mine Drainage. In: PETROLEUM, D. O. M. A. (ed.). Perth.
11. DCCEEW 2023. The Australian and New Zealand Guidelines for Fresh and Marine Water Quality https://www.waterquality.gov.au/anz-guidelines [Accessed 4 July 2024]
12. Marsden Jacob Associates 2014. Estimate of the cost of hazardous waste in Australia. Melbourne: Commonwealth Government of Australia.
13. Aghaei, E., Tadesse, B., Tabelin, C. B. & Alorro, R. D. 2022. Mercury sequestration from synthetic and real gold processing wastewaters using Fe–Al bimetallic particles. Journal of cleaner production, 372, 133482
14. Hu, C.-Y., Lo, S.-L., Liou, Y.-H., Hsu, Y.-W., Shih, K. & Lin, C.-J. 2010. Hexavalent chromium removal from near natural water by copper–iron bimetallic particles. Water research (Oxford), 44, 3101-3108.
15. Liu, W.-J., Qian, T.-T. & Jiang, H. 2014. Bimetallic Fe nanoparticles: Recent advances in synthesis and application in catalytic elimination of environmental pollutants. Chemical engineering journal (Lausanne, Switzerland: 1996), 236, 448-463.
16. Allam, B. K., Musa, N., Debnath, A., Usman, U. L. & Banerjee, S. 2021. Recent developments and application of bimetallic based materials in water purification. Environmental challenges (Amsterdam, Netherlands), 5, 100405.

17. Meng, C., Mao, Q., Luo, L., Zhang, J., Wei, J., Yang, Y., Tan, M., Peng, Q., Tang, L. & Zhou, Y. 2018. Performance and mechanism of As(III) removal from water using Fe–Al bimetallic material. Separation and purification technology, 191, 314-321.
18. Fu, F., Cheng, Z., Dionysiou, D. D. & Tang, B. 2015. Fe/Al bimetallic particles for the fast and highly efficient removal of Cr(VI) over a wide pH range: Performance and mechanism. Journal of hazardous materials, 298, 261-269.
19. Chen, L.-H., Huang, C.-C. & Lien, H.-L. 2008. Bimetallic iron–aluminum particles for dechlorination of carbon tetrachloride. Chemosphere (Oxford), 73, 692-697.

**XVI International Mineral Processing
and Recycling Conference
28-30 May 2025, Belgrade, Serbia**

DOI: 10.5937/IMPRC25313A Original research article

SELECTIVE BIO-FLOCCULATION OF HEMATITE MINERAL USING *BACILLUS SUBTILIS* FOR PHOSPHOROUS REMOVAL FROM IRON ORES

Samah S. Abdallah[#]**,** 0000-0002-5824-7941,
Samah M. El-Sayed, 0000-0001-7862-7696,
Mohamed A. Abdel-Khalek, 0000-0002-0830-8232,
Central Metallurgical Research and Development Institute (CMRDI), Cairo, Egypt

ABSTRACT – *Bacillus subtilis* is used as a bio-surface modifier to flocculate hematite mineral (Fe_2O_3). The effect of bacterial interaction on the behavior of the hematite and apatite minerals as the main source of phosphorous in the iron ore was investigated using zeta-potential, and FTIR measurements. The effect of pH on the flocculation of the two minerals was investigated. The zeta-potential of hematite is strongly affected by *Bacillus subtilis* interaction while the maximum flocculation efficiency was achieved at pH 6. The hematite mineral could be separated from its mixture with apatite mineral in the presence of *Bacillus subtilis* at pH 6.

Keywords: *Bacillus Subtilis*, Phosphorous, Hematite, Apatite, Bio-Flocculation, Minerals.

INTRODUCTION

Iron ores became more complex in their mineralogical composition which carrying phosphorus more widespread. Phosphorus is harmful in the steel-making process which increases hardness and brittleness and decreases ductility. Phosphorus may occur as apatite [$Ca_5(PO_4)(F,Cl,OH)$], whereas wavellite [$Al_3(PO_4)_2(OH)_3.5(H_2O)$] is the second phosphate present in high phosphorus content iron deposits [1]. Phosphorus can be removed from iron ores by different processes depending on the mineralogy and cost. It is important to investigate fundamental studies to get the most effective separation process. The physical and biological processes are most likely techniques. They require low reagents, power requirement, facilities, equipment, and pollution [2-4]. Bio-leaching was used through acid-producing microorganisms, including filamentous fungi and iron-oxidizing bacteria [5]. Selective agglomeration was used in the presence of oleic acid as a collector [6, 7]. A fatty acid as collector and sodium silicate as a depressant was used in anionic flotation for apatite separation from iron oxides. Also, dodecyl amine was used for wavellite flotation [8]. Nowadays, biological processing routes are sought to solve the problems associated with lean grade ores and where the traditional methods fail to separate the minerals from complex ores. The Bio-beneficiation refers to selective removal of undesirable mineral constituents from an ore by utilizing microorganisms as surface modifiers, depressants, collectors, or dispersing agents to enhance the

---

[#] corresponding author: samahsaleh86@gmail.com separation of one mineral from another [8-13]. The behavior of bacterial cell on the mineral surface is the basis for a successful of the bio-beneficiation processes. The selective bacterial adhesion on mineral surface is important for selective surface modification which leads to the efficient flotation or flocculation processes [14-15].

Bio-beneficiation processes are relatively new and are under intense investigation in recent years [16]. Since the bacteria adhere to a mineral surface within a few minutes and alter the surface properties that are essential in mineral beneficiation techniques, the microorganisms have numerous applications in flotation and flocculation processes [17].

EXPERIMENTAL

Materials

Two samples of hematite and apatite minerals of high purity were supplied by the Egyptian Mineral Resources Authority (EMRA). *B. subtilis* strain was supplied by the mineral bio-processing Lab., CMRDI. All chemicals used in this work were of analytical grade.

Methods

Zeta potential measurements

A laser Zeta Meter [Malvern Instruments], Model Zeta Sizer NAno ZS' was employed for zeta potential measurements. A 0.05 g of solid sample is placed in 50 ml of 0.01 M KCl solution and interacted with known bacterial concentrations, conditioned for 10 min at desired pH at room temperature. Measurements were performed as a function of pH.

FTIR measurements

The solid mineral sample after interaction with bacterial cells was filtered, air dried, and mixed analytical grade KBr from Merck to prepare KBr pellet then subjected to FTIR for recording the spectrum. The FTIR spectrum was obtained with a Spectrum 2000 Perkin Elmer spectrometer was obtained between 4000 and 400 cm^{-1}.

Flocculation Experiments

A bench-scale flocculation experiment was carried out mixing the mineral with bacteria solution followed by decantation of the un-flocculated mineral. One gram of hematite or apatite minerals was conditioned in the bacteria solution of definite concentration for desired time at constant pH. The flocculation was carried out by decantation. Each flocculated and dispersed fractions were collected, dried, and weighted. For binary minerals mixture, each flocculated and dispersed fractions were collected, dried, weighted and chemically analyzed.

RESULTS AND DISCUSSION

Chemical Composition of Pure Minerals

The chemical analysis of apatite mineral which has a chemical formula [$Ca_{10}(PO_4CO_3)_6(OH,F,Cl)]_2$] confirmed its high purity, Table 1.

Table 1 Chemical composition of pure hematite and phosphate minerals.

Item	Weight %	
	Hematite	Apatite
Fe_2O_3	99.87	0.001
P_2O_5	0.001	34.58
CaO	0.005	56.97
MgO	0.007	0.005
SiO_2	0.018	0.003
Al_2O_3	0.015	0.016
K_2O	0.013	0.012
Na_2O	0.016	0.018
CO_2	0.054	4.498
F	0.001	3.897
Total	**100**	**100**

Mineral Bacteria Interaction

Zeta Potential Measurement

The presence of various ions alters the zeta potential of both bacteria and minerals. Hydrophobicity originated from the hydrogen bonding energy of cohesion of water molecules. Similarly altering the surface hydrophobicity can bring about a difference in adsorption. Thus by changing one or more of the properties of the interacting mineral surfaces, adsorption can be made more selective. Figure 1, shows that *Bacillus subtilis* is positively charged at less than pH 3.25 (its isoelectric point).

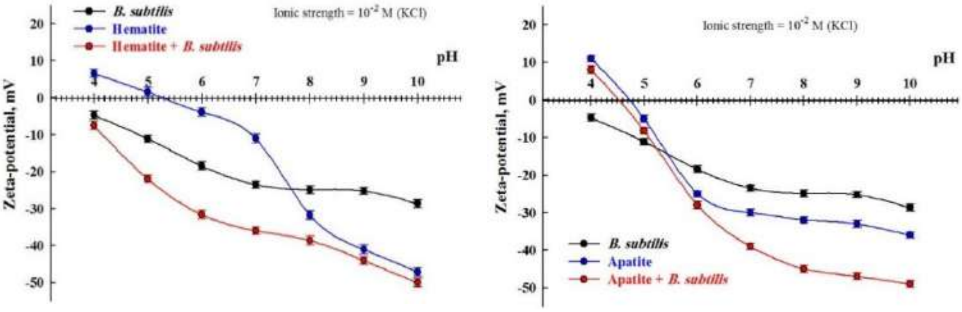

Figure 1 Effect of pH on zeta potential of treated hematite and treated phosphate with *B. subtilis.*

The hematite mineral has positive charge at pH less than 5.3 (its isoelectric point), while it turned negative charge at the pH range higher 5.3. It indicates that both H^+ and OH^- are potential determining ions. The results showed that the negativity of zeta potential increases sharply with increasing the pH. The hematite surface is strongly affected as a result of bacterial interaction. The results showed that the negativity of zeta potential increases sharply up to pH 7 then it is slightly increased. On the other hand, the apatite mineral has positive charge at pH less than 4.75 (its isoelectric point), while it turned negative charge at the pH range higher 4.75. The apatite mineral surface is slightly affected as a result of bacterial interaction up to pH 6. The isoelectric point (IEP) became 4.55 rather than 4.75 before treatment. Figure 1, showed that the negativity of zeta potential is significant increased at pH range higher than 6.

FTIR Investigation

The FTIR of bacteria, usually includes the O-H, C-C, CH_2, C-O, C-N and C=O bands for polysaccharides and lipids (protein). The main characteristic peaks for *Bacillus subtilis* are located at 1641 cm^{-1} which belongs to C=O of amide group and of O–C=O carboxylic groups. The broad band located in the range 2993 - 3592 cm^{-1} are attributed to stretch C–H, C–H_2 and C–H_3 of alkyl groups and stretching vibration of O–H and N–H, (Figure 2, which shows the typical FTIR spectrum of iron oxide. It exhibits various well-defined peaks at 459, 541, 991, 1485, 1637, 2843, 2919 and 3429 cm^{-1} [35]. The appearance of two well-defined peaks at 459, 541 and 991 cm^{-1} are due to the presence of iron–oxygen (Fe–O). The observed FTIR results confirmed the iron oxide without any significant impurity.

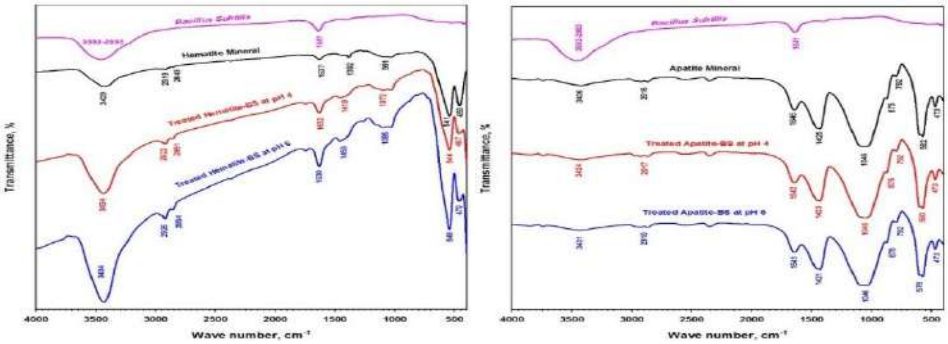

Figure 2 FTIR spectra of Hematite and Apatite before and after treatment with *B. subtilis* at different pHs

After interacting with *Bacillus subtilis* the band at 3429 cm^{-1} became more intense and shifted 3424 and 3434 cm^{-1} for treatment at pH 4 and 6 respectively. Also, the peaks at 2919, 2843 and 1637 became more intense and shifted to 2922-2926 cm^{-1}, 2851-2854 cm^{-1} and 1632-1631 cm^{-1}, for treatment at pH 4 and 6, respectively. The peaks at 1392 and 991 cm^{-1} were disappeared and new bands were appeared at 1419-1459 cm^{-1} and 1072-1085 cm^{-1}, respectively. In addition, more intense and little shift was noted for the peaks from 541 to 544-548 cm^{-1} and from 459 to 467-470 cm^{-1}. These results suggest the higher adsorption affinity of *B. subtilis* on to hematite surface. It agree with higher change in the surface charge which obtained by zeta-potential measurements.

Figure 2, shows the FTIR spectrum of the apatite mineral. Although, a little shift of some peaks but there is no significant change of the apatite mineral spectrum after interacting with *B.subtilis*, at different contact pH. These results suggest the lower adsorption affinity of *B. subtilis* to its surface. It agree with little change in the surface charge which obtained by zeta-potential measurements.

Flocculation of Pure Hematite and Apatite Minerals

Effect of pH

The pH is essential parameter which alters the zeta potential and hydrophobicity based on the hydrogen bonding and cohesion with water molecules. The effect of pH on the flocculation of hematite and apatite in the presence of 8×10^5 cells of *Bacillus subtilis* for 10 min is presented in Figure 3. The flocculation of hematite mineral was increased with increasing pH to reach its maximum value (99%) at pH 6 and then it decreased again. While the increasing of pH increases the apatite flocculation to 17% at pH 10. The maximum flocculation difference (95%) was achieved at pH 6. These results confirm the zeta potential measurements. The maximum change of hematite surface was achieved at pH 6 at which there is no significant change of the apatite surface.

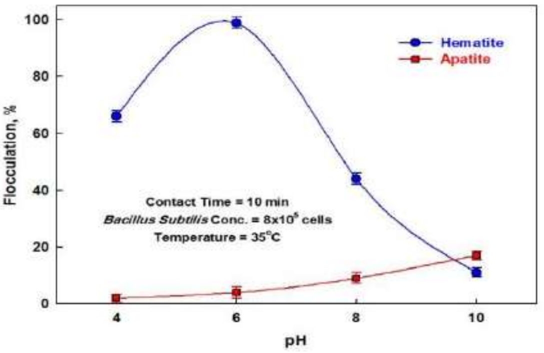

Figure 3 Effect of pH on the flocculation of pure hematite and apatite minerals

Binary mixture flocculation

The flocculation study of binary mixture aims to determine the effect interaction between the two minerals which may be occurred during their contact together rather than individual contact. One gram of synthetic binary mixture composed of 95% of hematite with 5% of apatite (≈ 1.729% P_2O_5) was employed. A concentrate of about 99.5% Fe_2O_3 with 95% recovery was obtained using *Bacillus subtilis* at pH 6. The apatite content was reduced from 5% (≈ 1.729% P_2O_5) to about 0.1% (≈ 0.0346% P_2O_5).

CONCLUSION

Bacillus subtilis was used to as a surface modifier to flocculate hematite mineral selectively from its mixture with apatite mineral. The hematite surface is strongly affected as a result of bacterial interaction while the apatite didn't affect. The FTIR proved the selective adhesion of *Bacillus subtilis* on the hematite mineral surface.

The maximum flocculation of hematite mineral was achieved at pH 6. A binary mixture of 95% hematite with 5% apatite produced a concentrate of 99% hematite with 95% recovery in the presence of *Bacillus subtilis* at pH 6.

REFERENCES

1. Ofoegbu, S.U. 2019. Technological Challenges of Phosphorus Removal in High-Phosphorus Ores: Sustainability Implications and Possibilities for Greener Ore Processing. Sustainability, 11, 6787.
2. Bao, Q.; Guo, L.; Guo, Z. 2021. A novel direct reduction-flash smelting separation process of treating high phosphorous iron ore fines, Powder Technology, 377, 149-162.
3. Wu, S.C.; Li, Z.Y.; Sun, T.C.; Kou, J.; Li, X.H. 2021. Effect of additives on iron recovery and dephosphorization by reduction roasting-magnetic separation of refractory high-phosphorus iron ore, Int. J. Miner. Metall. Mater. 1908-1916.
4. Buis, P.1995. Bioremediation techniques for the removal of phosphorus from iron ore. Michigan: Michigan Technological University USA. 129. (Dissertation - PhD for Mining Engineering).
5. XIA W.-t., REN Zheng-de, GAO Yi-feng, 2011. Removal of Phosphorus From High Phosphorus Iron Ores by Selective HCl Leaching Method, J. of Iron and Steel Res., Inter. 18,1-4.
6. Xu, C.Y.; Sun, T.C.; Kou, J.; Li, Y.L.; Mo, X.L.; Ligang, T.2012. Mechanism of phosphorus removal in beneficiation of high phosphorous oolitic hematite by direct reduction roasting with dephosphorization agent. Transactions of Nonferrous Metals Society of China. 22, 2806-2812.
7. Zhu, D.Q.; Chun, T.J.; Pan, J.; Lu, L.M.; He, Z. 2013. Upgrading and dephosphorization of Western Australian iron ore using reduction roasting by adding sodium carbonate, Int. J. Miner. Metall. Mater. 20, 505-513.
8. Nunes A.P.L., Pinto C.L.L., Valadão G.E.S., Viana P.R.de Magalhães., 2012. Floatability studies of wavellite and preliminary results on phosphorus removal from a Brazilian iron ore by froth flotation, Minerals Engineering, 39, 206-212.
9. Rao, K.H.; Vilinska, A.; Chernyshova, I.V. 2010. Minerals bioprocessing R & D needs in mineral bio-beneficiation, Hydrometallurgy 20, 465-470.
10. Hori, K.; Matsumoto, S. Bacterial adhesion: From mechanism to control. Biochemical Engineering Journal, 48, 2010, 424-434.
11. Kuyumcu, H.Z.; Vilinska, T.B.; Rao, K.H. 2009. Biocoagulation and its Application Potentials for Mineral Bioprocessing. The Open Mineral Processing Journal, 2, 1-11.
12. Geoghegan, M.; Andrews, J.; Biggs, C.; Eboigbodin, K.; Rolfe, S.; Scholes, J.; Ojeda, J.J. 2007. The Polymer Physics and Chemistry of Microbial Cell Attachment and Adhesion. Faraday Discussions, 139, 85-103.
13. Abdel-Khalek, N.A; El-Shall, H; Abdel-Khalek, M.A; El-Mahdy, A.M; El-Mofty, S.E. 2009. Carbonate separation from sedimentary phosphates through bioflotation, Minerals & Metallurgical Processing Journal, 26(2), 85.
14. Abdel Khalek, M.A.; Elmaidany, A.A. 2012. Application of *Bacillus subtilis* for reducing ash and sulfur in coal, Environmental Earth Sciences.
15. Elmahdy, A.M.; El-Mofty, S.E.; Abdel-Khalek, M.A.; Abdel-Khalek, N.A.; El-Midany, A.A. 2013. Bacterially induced phosphate–dolomite separation using amphoteric collector, Separation and Purification Technology, 102, 94-102.

16. Farghaly, M.G.; Abdel-Khalek, N.A.; Abdel-Khalek, M.A.; Selim, K.A.; Abdullah, S.S. 2021. Physicochemical study and application for pyrolusite separation from high manganese-iron ore in the presence of microorganisms, Physicochem. Probl. Miner. Process. 57(1), 273-283.
17. El-Sayed, S.; El-Shatoury, E.H.; Abdel-Khalek, N.A.; Abdel-Motelib, A.; Abdel-Khalek, M.A. 2021. Influence of *Bacillus cereus*-Gold Interaction on Bio-flotation of Gold in the Presence of Potassium Butyl Xanthate, Biointerface Research in Applied Chemistry 11(5), 13005-13018.

XVI International Mineral Processing
and Recycling Conference
28-30 May 2025, Belgrade, Serbia

DOI: 10.5937/IMPRC25320B Review article

THE ROLE OF ADDITIVE MANUFACTURING IN MINERAL AND METAL EXTRACTION

Patrycja S. Bednarek[1#], 0009-0003-6376-389X,
Nima Razavi[2], 0000-0002-2574-065X,
Przemyslaw B. Kowalczuk[1], 0000-0002-1432-030X,
[1]Norwegian University of Science and Technology, Department of Geosciences, Trondheim, Norway
[2]Norwegian University of Science and Technology, Department of Mechanical and Industrial Engineering, Trondheim, Norway

ABSTRACT – Mineral and metal production has been increasing annually, driven by the growing demands of advancing industries and green technologies. To meet this demand sustainably, mineral and metal extraction and processing must adopt environmentally conscious innovations. Among key innovations impacting these processes, Additive Manufacturing (AM, commonly known as 3D printing), alongside artificial intelligence and big data analytics, has significantly impacted these processes by enhancing productivity, increasing profit margins, and reducing operating costs. An AM technology offers numerous advantages, including enhanced customization and the capability to produce tailored components that meet specific requirements. Since its groundbreaking development in the 1980s, AM has contributed substantially across a wide range of industries. Numerous reviews document the integration of this manufacturing technology in industrial applications, for example, in wastewater treatment, to enhance separation efficiency for oil, heavy metals, and other pollutants. In recent years, AM has entered the domain of mineral and metal production; however, its scale remains largely unquantified. This paper presents the applications of AM in mineral and metal extraction and explores the advantages of implementing additive manufacturing in separation processes.

Keywords: Mineral and Metal Extraction, Additive Manufacturing, Applications.

INTRODUCTION

Extractive metallurgy is a broad field that encompasses various raw materials and numerous separation techniques. It is generally divided into two main branches: mineral processing and metallurgy [1].

The primary objective of extractive separation methods is to process materials to obtain a metal concentrate in its purest possible form [2]. Mineral processing involves separating valuable minerals from the gangue within the ore and concentrating them, while metallurgy extracts metals from their compounds and purifies them through chemical reactions [3]. The advantage of mineral processing lies in its reliance on physical concentration methods [2] and involves several different stages: 1) size reduction with 2) size separation (classification), 3) separation (beneficiation), and 4) dewatering [1]. In

---

[#] corresponding author: patrycja.s.bednarek@ntnu.no contrast, metallurgical processes, which occur either in aqueous solutions or at high temperatures, can be classified into: pyro-, hydro-, biohydro-, and electrometallurgy.

The demand for mineral and metal production has been rising annually, driven by the needs of advancing industries and green technologies [4]. To meet this demand sustainably, the extraction industry must integrate environmentally conscious innovations [5]. One such innovation contributing to industry sustainability is additive manufacturing (AM, also known as 3D printing). AM enhances sustainability in four key areas: 1) product and process redesign, 2) material input processing, 3) make-to-order component, and 4) product manufacturing [6]. These advantages translate into several environmental benefits, including eco-friendly design, reduced overproduction, minimized material waste, lower energy consumption, enhanced material recycling, decreased tooling requirements, and a more sustainable supply chain [7].

The initial approach to fabricating a 3D object through computer-aided design (CAD), known as rapid prototyping, emerged in the 1980s to manufacture models and prototype parts. The primary benefit of AM lies in its capability to construct nearly any conceivable shape, facilitated by its layer-by-layer production method [8]. The American Society for Testing and Materials has developed a set of standards that divides the range of AM processes into seven broad categories: vat photopolymerization (VP), powder bed fusion (PBF), material extrusion (ME), material jetting (MJ), binder jetting (BJ), sheet lamination (SL), and directed energy deposition (DED) [9].

Since its groundbreaking development, AM has contributed substantially across a wide range of industries. Numerous studies document its integration into industrial applications, including wastewater treatment [10], analytical chemistry [11], and medicine [12]. More recently, AM has begun to enter the domain of mineral and metal production; however, its adoption on a large scale remains unquantified. This paper presents the applications of AM in mineral and metal extraction and explores its potential advantages in separation processes.

APPLICATION OF AM IN MINERAL AND METAL EXTRACTION PROCESSES

Additively manufactured devices and components are utilized in two key stages of mineral processing: classification and upgrading. This includes a range of printed devices such as classifiers and gravity spiral separators, as well as critical components like classifier modules, dissolved air flotation (DAF) system elements, flotation impellers, and magnetic filters. In metallurgy, AM devices and components are primarily applied in hydrometallurgical processes, including solvent extraction and solid-phase extraction, where they serve as reaction vessels or adsorptive mesh structures. The following sections below present a more detailed discussion of AM application in extractive metallurgy.

Additively manufactured devices

Design modifications of hydrocyclones due to material costs and manufacturing time are usually limited to final design scaled metal model tests, where traditional manufacturing methods are commonly used. However, AM has the potential to enhance research in hydrocyclone designing and testing. Tina et al. [13] explored the use of fused deposition modeling (FDM- sub-category of ME AM) to fabricate hydrocyclones. Their study demonstrated that manufacturing time for a traditional hydrocyclone prototype can be reduced from 12–26 weeks to just 2 weeks, while costs can be reduced by 2.5 to 25 times. Moreover, AM combined with computational simulations enables even more precise experimental validation, as demonstrated elsewhere [14, 15]. A strategy based on integrating computational fluid dynamics (CFD) modeling with AM, was applied to address the limitations of hydrocyclone design. This approach facilitated the manufacturing and testing of hydrocyclones with varied crucial design parameters, such as vortex finder and spigot diameters or different arc inlet designs and cone angles. Xu et al. [15] observed that the proposed innovative arc inlet introduced a pre-classification effect, minimizing the misplacement of fine (<5 µm) and coarse (>10 µm) particles, a feature absent in traditional inlets. The simulation data were proved by the experimental comparison of the classification of ultrafine MnO_2 particles using the novel 3D-printed hydrocyclone and the conventional one. The results showed that the 3D-printed hydrocyclone significantly outperformed the conventional design, achieving a notable increase in fine particle removal efficiency from 72% to 93%. A similar approach, combining CFD methods with AM, was applied to another centrifugal classifier for gas-solid separation [16]. A series of cyclones with elliptical bodies were designed and manufactured by stereolithography (SLA- sub-category for VP AM), experimentally demonstrating 2% improvement in separation efficiency reaching 97% and 43% reduction in pressure drop.

AM has also been suggested as a viable method to design and manufacture new classification devices. Sun et al. [17] fabricated a conical centrifugal particle separator for valuable mineral separation directly on the lunar surface, serving as an alternative to conventional heavy auxiliary equipment or fluidic separation systems. The separation trials used a mineral mixture containing quartz, barite, and calcite, categorized into three particle size fractions: fine (<180 µm), medium (180–300 µm), and coarse (300–500 µm). During fine particle separation, the system achieved peak fine particle concentration, experimental recovery, and theoretical recovery values of 74%, 54%, and 46%, respectively. Another new design, the closed spiral classifier, inspired by spiral concentrators, was fabricated using FDM 3D printing [18]. The device achieved the separation efficiency comparable to hydrocyclones and was tested on silica particles. The mean size of the outer outlet sample was close to 75 µm, which is three times the mean size of the inner outlet sample.

A different approach was demonstrated by Munasinghe and Paul [19], members of the research team responsible for developing a large-scale industrial 3D printer to print Gravity Separation Spirals (GSS). While traditional mold-based manufacturing is often uneconomical for customizing specific spiral profiles, the full-scale 3D printer can easily accommodate such adjustments. The designed printer is an extrusion-based machine equipped with two robotic arms and a centrally positioned rotating column. If successful, the proposed strategy will open up the possibility of manufacturing fully customized separation devices directly at the processing plant location.

In hydrometallurgical applications, AM was utilized to produce oscillatory baffled reactors for Co(II) and Ni(II) separation [20]. The device was fabricated using SLA and showed a productivity of 117 g Co^{2+}/day, notably 3–4 higher than most other studies handling the cobalt extraction using Cyanex 272. Moreover, manufactured reactors provided satisfactory mechanical and chemical performance, low production cost, and optical access to the reactor's interior.

Additively manufactured components

AM can also serve as an alternative manufacturing method for iterative testing and wearable spare parts. A notable example was presented by Carpenter et al. [21], who manufactured classifier modules mounted on a spinning centrifuge generating 55 G-force. Each module consisted of AM inclined channels, with Accura Extreme plastic used as the feed material. Similarly, Zhou and Shen [22] proposed a specialized design for 3D-printed outlets that enable the collection of up to 10 different products with a narrow particle size distribution during air classification.

AM has also contributed to beneficiation processes such as flotation and magnetic separation. Kouhestani et al. [23] tested innovative pressure-release nozzles fabricated using AM technology from polylactic acid (PLA), designed to generate microbubbles in DAF systems. These nozzles were evaluated both in laboratory settings and in a full-scale plant. Laboratory tests revealed that the nozzle geometry with a perpendicular surface after the nozzle perforation enhanced the formation of smaller bubbles and the number of generated small bubbles is primarily influenced by the saturator pressure. Similarly, Gradov et al. [40] examined an auto-aspirated sparger for DAF systems designed by Outotec Oy and additively manufactured from stainless steel. The tested sparger generated bubbles ranging from 190 to 2500 µm in water, which were evenly dispersed. Yang et al. [24] proposed 3D-printed fractal impellers to enhance fluid turbulence and generate micro-vortices. These conditions not only improved the dispersion of mineral particles but also facilitated better adsorption of collectors onto mineral surfaces. In the field of magnetic separation, Wei et al. [25] introduced AM magnetic architectures for the removal of heavy metal ions. Net-shaped structures were fabricated using a direct ink writing (DIW), the ME-based method, with NiO, ZnO, and Fe_2O_3 powders. The removal process was enhanced by polymer-coated Fe_3O_4 nanoparticles, which effectively adsorbed metal ions such as Pb(II), Ni(II), Cu(II), and Co(II). The system demonstrated high adsorption capacity, fast kinetics, and efficient nanoparticle capture (>90%) by manufactured magnetic architecture and recovery under a low magnetic field.

In hydrometallurgy, AM has been utilized to fabricate devices for solid-phase extraction for analytical purposes, and for metal ions recovery from secondary resources. A photocurable resin and the digital light processing (DLP- VP-based method) were used to create a solid-phase extraction (SPE) column for extracting metal ions (Mn, Co, Ni, Cu, Zn, Cd, and Pb) from high-salt samples while also removing the sample matrix prior to inductively coupled plasma mass spectrometry (ICP-MS) analysis [26]. For lithium recovery, Yu et al. [27] successfully fabricated a monolithic adsorbent containing 75% lithium-ion sieve from lithium titanate (Li_2TiO_3), montmorillonite, and SiO_2 using a DIW technique. Virtanen et al. [28] explored using selective laser sintering (SLS, the PBF subcategory)-manufactured nylon-12 filters with incorporated phosphonic acid groups for recovering rare earth elements (REEs) from simulated mining waste solutions.

Additionally, SLS-manufactured nylon-12-based scavengers were tested for Au(III) recovery from the printed circuit board waste and a synthetic multimetal leach solution [29]. Figure 1 provides an overview of various additively manufactured devices and components in extractive metallurgy.

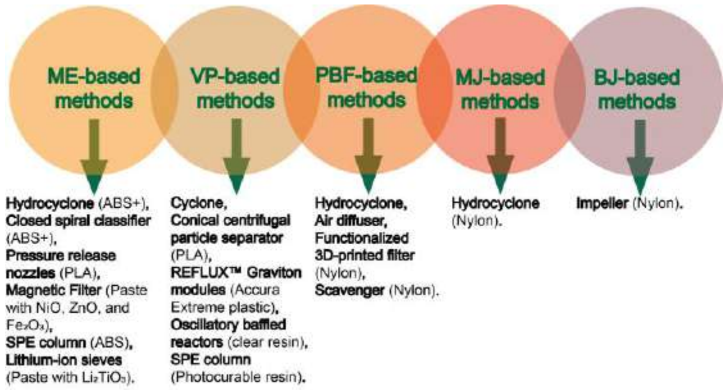

Figure 1 Additively manufactured devices and components utilized in extractive metallurgy, highlighting the applied methods and materials

CONCLUSIONS

AM applications in extractive metallurgy are expanding, offering benefits such as rapid prototyping, cost reduction, and customized designs across various processes, including classification, gravity concentration, flotation, magnetic separation, and hydrometallurgy. Integrating CFD simulations with AM enables design refinement before fabrication, directly contributing to cost savings. The geometric modifications of additively manufactured devices or components significantly impact separation efficiency and overall process performance. AM techniques such as ME, MJ, BJ, PBF, and VP have expanded the range of materials available for production, with polymers as first-choice material. The future potential of AM in mineral and metal extraction includes applications in space mining, multi-stage beneficiation, extraction from secondary resources, and enhanced fine particle separation.

REFERENCES

1. Drzymała, J., (2007) Mineral processing: foundations of theory and practice of minerallurgy. 1st ed, Oficyna Wydawnicza Politechniki Wroclawskiej, Wroclaw, Poland.
2. Fuerstenau, M.C. and K.N. Han, (2003) Principles of Mineral Processing, Society for Mining, Metallurgy, and Exploration, Inc.
3. Ghosh, A. and H.S. Ray, (1991) Principles of extractive metallurgy, New Age International.
4. Jowitt, S.M., G.M. Mudd, and J.F.H. Thompson, (2020) Future availability of non-renewable metal resources and the influence of environmental, social, and governance conflicts on metal production. Communications Earth & Environment, 1(1).
5. Zhou, L., (2023) Towards sustainability in mineral resources. Ore Geology Reviews, 160: p. 105600.

6. Ford, S. and M. Despeisse, (2016) Additive manufacturing and sustainability: an exploratory study of the advantages and challenges. Journal of Cleaner Production, 137: p. 1573-1587.
7. Javaid, M., et al., (2021) Role of additive manufacturing applications towards environmental sustainability. Advanced Industrial and Engineering Polymer Research, 4(4): p. 312-322.
8. Gardan, J., (2016) Additive manufacturing technologies: state of the art and trends. International Journal of Production Research, 54(10): p. 3118-3132.
9. Wu, Y., et al., (2022) A Critical Review of Additive Manufacturing Techniques and Associated Biomaterials Used in Bone Tissue Engineering. Polymers, 14(10): p. 2117.
10. Roy Barman, S., et al., (2023) 3D-Printed Materials for Wastewater Treatment. JACS Au, 3(11): p. 2930-2947.
11. Belka, M. and T. Bączek, (2021) Additive manufacturing and related technologies – The source of chemically active materials in separation science. TrAC Trends in Analytical Chemistry, 142: p. 116322.
12. Li, C., et al., (2020) Advances in Medical Applications of Additive Manufacturing. Engineering, 6(11): p. 1222-1231.
13. Tina, S., M. Bhamjee, and A. Nel, (2016) Design Life Cycle of a 3-D Printed Hydrocyclone.
14. Vega-Garcia, D., J.J. Cilliers, and P.R. Brito-Parada, (2020) CFD modelling of particle classification in mini-hydrocyclones. Separation and Purification Technology, 251: p. 117253.
15. Xu, Y., et al., (2023) Classification of Ultrafine Particles Using a Novel 3D-Printed Hydrocyclone with an Arc Inlet: Experiment and CFD Modeling. ACS Omega, 8(1): p. 998-1016.
16. Sun, Z., et al., (2024) Experimental and numerical investigation of the elliptical cyclone separator manufactured by 3D printing. Powder Technology, 441: p. 119746.
17. Mitchell, K., et al., (2023) 3D printing of conical centrifuge system for mineral particle separation. Separation and Purification Technology, 306: p. 122567.
18. Pukkella, A.K., R. Vysyaraju, and S. Subramanian, (2019) Enhanced gravity particle classifier: Experiments with 3D printed device and computational fluid dynamics simulations. AIChE Journal, 65(9): p. e16669.
19. Munasinghe, N. and G. Paul. *Path Planning for Robot Based Radial Advanced Manufacturing Using Print Space Sampling*. 2020. IEEE.
20. Adriaenssens, P., et al., (2025) Investigation of oscillatory baffled reactors for the hydrometallurgical separation of cobalt and nickel. Separation and Purification Technology, 355: p. 129465.
21. Carpenter, J.L., S.M. Iveson, and K.P. Galvin, (2019) Ultrafine desliming using a REFLUX™ classifier subjected to centrifugal G forces. Minerals Engineering, 134: p. 372-380.
22. Zhou, Y. and W. Shen, (2022) Numerical simulation of particle classification in new multi-product classifier. Chemical Engineering Research and Design, 177: p. 484-492.
23. Kouhestani, A., et al., (2020) Study of 3D-Printed Pressure Release Nozzle for Microbubble Formation in Full-Scale Dissolved Air Flotation (DAF). Chemical Engineering and Processing - Process Intensification, 155: p. 108070.
24. Yang, S., et al., (2024) Hydrodynamics intensification and interface control in the flotation conditioning process using fractal impellers. Separation and Purification Technology, 328: p. 125043.
25. Wei, X., et al., (2017) Low-Field Dynamic Magnetic Separation by Self-Fabricated Magnetic Meshes for Efficient Heavy Metal Removal. ACS Applied Materials & Interfaces, 9(42): p. 36772-36782.
26. Wu, C.-Y., J.-R. Chen, and C.-K. Su, (2021) 4D-Printed Temperature-Controlled Flow-Actuated Solid-Phase Extraction Devices. Analytical Chemistry, 93(33): p. 11497-11505.
27. Yu, J., et al., (2023) 3D-printed titanium-based ionic sieve monolithic adsorbent for selective lithium recovery from salt lakes. Desalination, 560: p. 116651.

28. Virtanen, E.J., et al., (2025) Recovery of rare earth elements from mining wastewater with aminomethylphosphonic acid functionalized 3D-printed filters*.* Separation and Purification Technology, 353: p. 128599.
29. Lahtinen, E., et al., (2017) Selective Recovery of Gold from Electronic Waste Using 3D-Printed Scavenger*.* ACS Omega, 2(10): p. 7299-7304.

XVI International Mineral Processing
and Recycling Conference
28-30 May 2025, Belgrade, Serbia

DOI: 10.5937/IMPRC25327U

Original research article

INVESTIGATION OF SURFACE PROPERTIES OF PVC FOR SELECTIVE RECOVERY

Zeynep Üçerler Çamur[#], 0000-0003-4000-683X,
Tülay Türk, 0000-0002-4219-8487,
Murat Olgaç Kangal, 0000-0003-4993-064X,
Istanbul Technical University, Faculty of Mines, Department of Mineral
Processing Engineering, Istanbul, Türkiye

ABSTRACT – The selective recovery of PVC as a sink product required an effective plasticizer to enhance its surface properties. In this study, the effects of Triton XL-100N and Gelatine were compared through surface tension, contact angle, and zeta potential measurements, along with microflotation tests using a Hallimond tube. Results showed that Triton XL-100N significantly reduced surface tension and contact angle, increasing PVC hydrophilicity. The isoelectric point shifted to pH 3 with Triton XL-100N and pH 6 with Gelatine. Microflotation tests confirmed that 0.1 M Triton XL-100N optimized PVC depression at pH 4, whereas Gelatine showed limited effectiveness. Therefore, Triton XL-100N was identified as the optimal plasticizer for selective PVC recovery.

Keywords: PVC, Selective Flotation, Surface Chemistry, Triton XL-100N, Gelatine.

INTRODUCTION

Recycling plays a crucial role in minimizing waste generated by human activities. However, the accumulation of polymer waste causes significant environmental challenges. Burning is not a viable recycling method for polymers, as it releases toxic gases. In particular, polyvinyl chloride (PVC) produces hazardous emissions such as hydrogen chloride (HCl) gas and chlorine-containing dioxins, which contribute to air pollution and reduce the lifespan of burning facilities. Additionally, PVC contamination complicates the recycling of other polymers. With a density range of 1.30-1.35 g/cm³, PVC cannot be effectively separated using conventional gravity-based methods. However, due to the natural hydrophobicity of polymers, therefore, froth flotation, a cost-effective and widely used technique in mineral processing, offers a promising alternative for PVC recycling due to its simplicity and efficiency [1]. For instance, collected polyethylene terephthalate (PET) bottles, commonly used for soft drinks, are often mixed with polyvinyl chloride (PVC) bottles, which are used for edible oils, detergents, and shampoos. Generally, different types of plastics cannot be recycled together due to their chemical incompatibility, variations in melting points, and differences in thermal stability [2]. The hydrophobicity of plastics follows the order: PS > ABS > PC > PET > PMMA > PVC

[#] corresponding author: ucerler@itu.edu.tr

> POM. Consequently, PET and PVC can be effectively separated from PP, PE, PS, or HDPE using flotation techniques [3]. However, the separation of PET and PVC can be influenced by various parameters, including the type and amount of frother [4], the plasticizer [5] used during column flotation, pH, as well as the treatment time and temperature with reagents such as NaOH or $KMnO_4$ [1, 2, 6, 7]. Typically, PVC is recovered as the sink product, while PET is obtained as the float product [8,9].

This study aims to determine the surface properties of PVC for its selective recovery by comparing two different plasticizers, Triton XL-100N and Gelatine. In this context, surface tension measurements, contact angle analysis on PVC particles, zeta potential measurements, and microflotation experiments were conducted to evaluate their flotation behavior under varying pH conditions and plasticizer concentrations. The objective is to assess the fundamental flotation characteristics of PVC in the presence of these plasticizers and to determine their effectiveness in facilitating selective PVC recovery.

MATERIALS AND METHODS

The representative sample virgin PVC polymers was obtained from Arçelik Company, and the d_{80} particle size of the sample was determined as 200 μm.

The surface properties of PVC were systematically analyzed to enable selective flotation during its recycling process. In this context, particular focus was placed on the plasticizers Triton XL-100N (BDH Chemicals, USA) and Gelatine (Merck KGaA, Germany). Surface tension measurements (Krüss Ring Tensiometer, Krüss GmbH, K6, Germany), contact angle (Goniometer, Rame-Hart Inc., United States) analyses, and zeta potential measurements (Zeta Meter +3.0, Malvern Panalytical, Germany) were conducted at varying concentrations of these chemicals on virgin PVC polymers. Additionally, microflotation experiments were performed under different concentration and pH conditions to assess the effects of both plasticizers on flotation efficiency. Surface tension measurements were conducted using the Du Noüy ring method with a Krüss tensiometer. During these measurements, concentrations from 0.1 to 1.0 M were examined for both plasticizers. For contact angle measurements, the sessile drop method was employed, and experiments were performed using a Rame-Hart goniometer. These measurements were carried out with a solution containing 1% plasticizer concentration, and the same concentration range (0.1–1.0 M) was investigated for both plasticizers. Zeta potential measurements were conducted using a Zetameter based on the principle of microelectrophoresis. These measurements were performed at different pH values of 2, 4, 6, 8, and 10, using both plasticizers at concentrations of 0.1, 0.2, 0.5, 0.7, and 1 M. Sulfuric acid (H_2SO_4) (95-98%) (Isolab Chemicals, Germany) and sodium hydroxide (NaOH) (Extra pure, Technical Grade, granules) (Tekkim, Türkiye) were used as pH regulators. By determining the surface properties, the selective flotation of PVC was investigated using a Hallimond tube as the microflotation cell. The primary objective of these investigations was to obtain PVC as a sinking product. Experiments were conducted with both plasticizers at concentrations from 0.1 to 1.0 M, under pH conditions of 2, 4, 6, 8, and 10.

RESULTS AND DISCUSSION

Surface tension measurements

In the surface tension measurements, Triton XL-100N and Gelatine were used as plasticizers, as specified. Figure 1 presents the measurements conducted with Triton XL-100N at concentrations from 0.1 to 1.0 M, while Figure 2 displayed the measurements performed with Gelatine at the same concentrations. The surface tension experiments revealed that the surface tension of PVC varied between 55 and 63.5 mN/m upon the addition of Gelatine. In contrast, the addition of Triton XL-100N resulted in a reduction of surface tension to the range of 35–38 mN/m. Yet, lower surface tension can enhance flotation efficiency, this condition may improve the flotation of PVC.

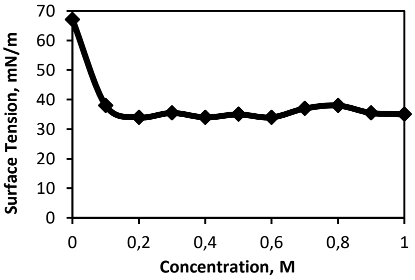

Figure 1 The Surface tension measurements of Triton XL-100N

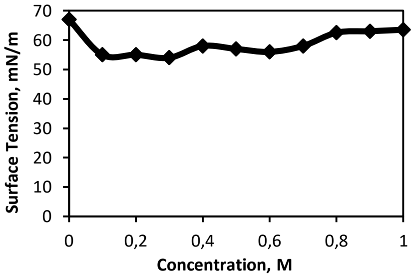

Figure 2 The Surface tension measurements of Gelatine

Contact angle measurements

Contact angle measurements were conducted at the same concentrations examined in the surface tension measurements and performed by Sessile Drop Method. The contact angle values of both plasticizers on PVC particles were determined and evaluated in terms of their impact on selective flotation of PVC. Contact angle measurements of Triton XL-100N and Gelatine were shown in Figure 3 and 4, respectively.

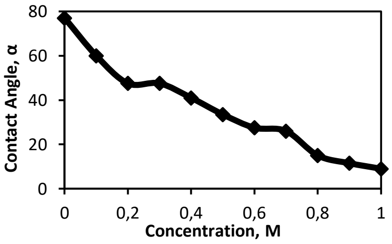

Figure 3 The contact angle measurements by Triton XL-100N

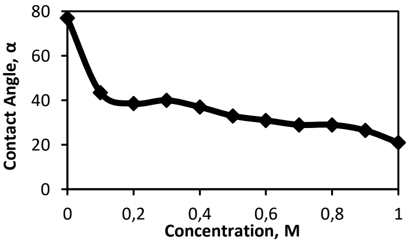

Figure 4 The contact angle measurements by Gelatine

As the concentration of both plasticizers increased, the contact angle measured on PVC particles decreased. However, Triton XL-100N reduced the contact angle significantly more than Gelatine, indicating that the naturally hydrophobic PVC particles underwent a greater degree of surface hydrophilization. The lowest measured contact angle was 10° at a 1.0 M concentration of Triton XL-100N, while the lowest contact angle measured with Gelatine at high concentration was 20°. Considering that the objective in flotation processes was to obtain PVC as a sink product, these results suggested that flotation experiments could be more successful at higher plasticizer concentrations.

Zeta Potential measurements

Zeta potential measurements were conducted using fine-sized PVC particles at pH values of 2, 4, 6, 8, and 10 with both plasticizers at concentrations of 0.1, 0.2, 0.5, 0.7, and 1.0 M. Additionally, measurements were performed using pure water as a reference. The results for Triton XL-100N were presented in Figure 5, while the measurements conducted with Gelatine were shown in Figure 6.

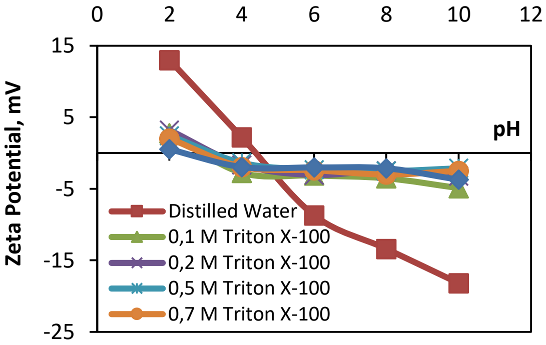

Figure 5 Zeta potential measurements of Triton XL-100 depending on different concentrations and pH values

As seen from the results, the iso-electric point (IEP) of PVC powders in distilled water was determined to be pH 4.2, which was consistent with similar measurements reported in the literature [5]. The iso-electric points in Triton XL-100N and Gelatine were found to be approximately pH 3 and pH 6, respectively. It was evident that the plasticizers could operate within different optimal pH ranges to effectively depress PVC.

Microflotation tests

Microflotation tests were conducted using a Hallimond tube to investigate the effect of Triton XL-100N and Gelatine on the recovery of PVC as a sink product at different concentrations and pH levels. In Figure 7, the effect of different concentrations of Triton XL-100N and in Figure 8, the effect of pH values followed by optimizing the concentration 0.1 M of Triton XL-100N were illustrated.

Microflotation tests showed that PVC was primarily recovered as a sink product at its natural pH when 0.1 M Triton XL-100N was used, with a flotation efficiency of approximately 40% as a float product. Thus, 0.1 M was selected as the optimum concentration for further pH-dependent tests. Flotation experiments at this concentration revealed the lowest flotation efficiency (~20%) at pH 4. Yenial *et al.* [7] demonstrated that Triton XL-100N facilitated PVC recovery as a sink product in batch flotation, while Marques and Tenorio [4] used calcium lignin sulfonate as a plasticizer at pH 4 for PET/PVC flotation in a column system. These findings confirmed that PVC could be recovered as a sink product at pH 4 with 0.1 M Triton XL-100N. To further investigate selective PVC recovery, additional tests were conducted using Gelatine, evaluating flotation efficiency as a function of concentration and pH (Figures 9 and 10).

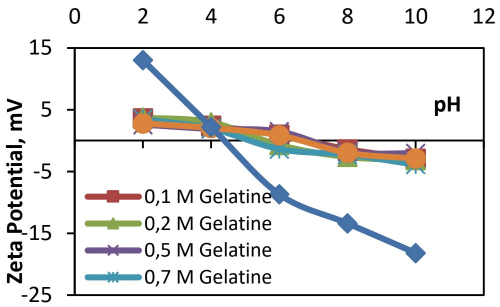

Figure 6 Zeta potential measurements of Gelatine depending on different concentrations and pH values

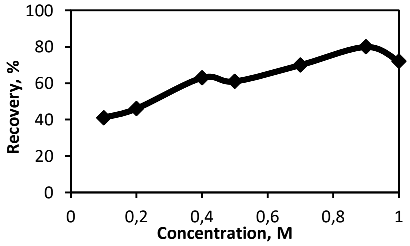

Figure 7 Microflotation tests conducted by different concentrations

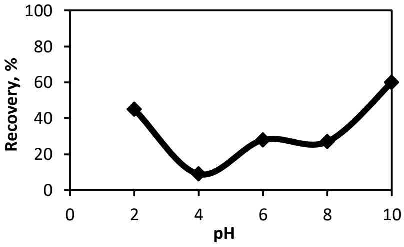

Figure 8 Microflotation tests performed on different pH values

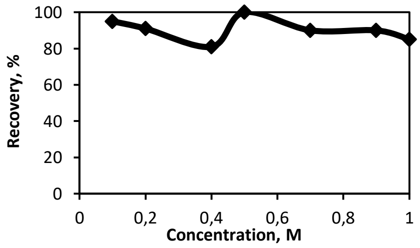

Figure 9 Microflotation tests conducted by different concentrations

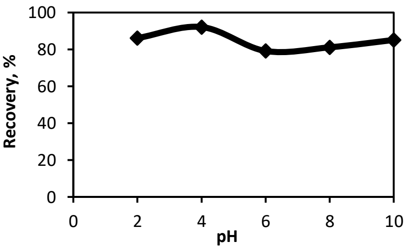

Figure 10 Microflotation tests performed on different pH values

The results indicated that Gelatine had minimal effectiveness in depressing PVC, as it consistently floated at all concentrations with high flotation efficiency. Even at 0.4 M, where the lowest efficiency was observed, the value remained relatively high (~80%). Thus, further tests were conducted at this concentration to examine the effect of pH. As shown in Figure 10, the lowest flotation efficiency was recorded at pH 6, yet it remained significant (~80%), confirming Gelatine's limited ability to facilitate to obtain PVC as sink product.

CONCLUSION

This study examined the selective recovery of PVC as a sink product using Triton XL-100N and Gelatine as plasticizers. Surface tension, contact angle, zeta potential, and microflotation tests were conducted. Triton XL-100N reduced surface tension more effectively, and increased PVC hydrophilicity. At 0.1 M, PVC remained a sink product at natural pH, with flotation efficiency dropping from 40% to 20% at pH 4. In contrast, Gelatine promoted PVC flotation, with the lowest efficiency (~80%) at 0.4 M and pH 6. Triton XL-100N was identified as the optimal plasticizer for selective PVC recovery.

REFERENCES

1. Burat, F., Güney, A., & Kangal, M. O. (2009). Selective separation of virgin and post-consumer polymers (PET and PVC) by flotation method. *Waste Management*, *29*(6), 1807-1813.
2. Wang, C., Wang, H., Liu, Y., & Huang, L. (2016). Optimization of surface treatment for flotation separation of polyvinyl chloride and polyethylene terephthalate waste plastics using response surface methodology. *Journal of Cleaner Production*, *139*, 866-872.
3. Shen, H., Pugh, R. J., & Forssberg, E. (2002). Floatability, selectivity and flotation separation of plastics by using a surfactant. *Colloids and Surfaces A: Physicochemical and Engineering Aspects*, *196*(1), 63-70.
4. Marques, G. A., & Tenório, J. A. S. (2000). Use of froth flotation to separate PVC/PET mixtures. *Waste Management*, *20*(4), 265-269.
5. Güney, A., Özdilek, C., Kangal, M. O., & Burat, F. (2015). Flotation characterization of PET and PVC in the presence of different plasticizers. *Separation and Purification Technology*, *151*, 47-56.
6. Drelich, J., Payne, T., Kim, J. H., Miller, J. D., Kobler, R., & Christiansen, S. (1998). Selective froth flotation of PVC from PVC/PET mixtures for the plastics recycling industry. *Polymer Engineering & Science*, *38*(9), 1378-1386.
7. Yenial, Ü., Burat, F., Yüce, A. E., Güney, A., & Kangal, M. O. (2013). Separation of PET and PVC by flotation technique without using alkaline treatment. *Mineral Processing and Extractive Metallurgy Review*, *34*(6), 412-421.
8. Buchan, R., & Yarar, B. (1995). Recovering plastics for recycling by mineral processing techniques. *JOM*, *47*, 52-55.
9. Fraunholcz, N. (2004). Separation of waste plastics by froth flotation-a review, part I. *Minerals Engineering*, *17*(2), 261-268.

XVI International Mineral Processing
and Recycling Conference
28-30 May 2025, Belgrade, Serbia

DOI: 10.5937/IMPRC25333S

Original research article

ELECTROCHEMISTRY OF INDIUM IN METHYL-TRIOCTYLAMMONIUM BIS(TRIFLUOROMETHYLSULFONYL)IMIDE IONIC LIQUID

Martin Straka#, 0000-0002-3041-1404
Nuclear Safety and Reliability Division, UJV Rez, Hlavni 130, Husinec-Rez,
CZ2568, Czech Republic

ABSTRACT – Electrochemical methods play important role in many schemes of metals recycling which is one of basic preconditions of circular economy. In this context, electrochemistry of indium (In) species was studied in an amide-type ionic liquid methyl-trioctylammonium bis(trifluoromethylsulfonyl)imide at 80°C. Cyclic voltammetry results show two-step reduction of In(III) to indium metal particles with In(I) as an intermediate product. Disproportionation of In(I) adds complexity to the process, but In metal deposition in form of nanoscale particles was achieved on both inert and reactive electrodes demonstrating the possibility of electrochemical recovery of In using ionic liquid as a carrier system.

Keywords: Indium, Ionic liquids, Critical raw materials, Recycling, Electrochemistry.

INTRODUCTION

Many green and digital technologies rely on scarce materials. Indium metal, which is of great importance for the production of solar cells, flat screen displays and several other electronic devices, is one of these materials. In this context, indium was added to EU´s list of critical raw materials and described both as economically important and in risk of supply chain breakdown, [1]. Therefore, the role of indium-containing waste recycling and new ways of mining residue treatment in minimizing risk of its shortage is highlighted as well as the basic precondition of its usage in circular economy.

In the last decades, ionic liquids (ILs) have been of increasing interest because of their physico-chemical characteristics including negligible vapor pressures, good electrical conductivity, wide electrochemical windows, high thermal stability, non-flammability or tunability by selection of different combinations of cations and anions, [2]. Importantly, usage of ionic liquids can fulfill the requirements of most of the widely known 12 principles of green chemistry as defined by Anastas and Warner [3].

Among other applications, ILs are considered to be good carrier systems for electrodeposition steps in metal recycling schemes in many areas of interest including recovery of important raw materials from waste, [4], or of nuclear fuel cycle and radioactive waste decontaminations [5]. Of course, using ionic liquids as carriers in electroseparation processes presents several challenges as well, such as high viscosity. Their complex physicochemical properties can also complicate system design and

---

corresponding author: martin.straka@ujv.cz

optimization. Additionally, the high cost and limited availability of certain ionic liquids may restrict their large-scale application and the level of IL degradation while used in industrial scale have to be assessed.

In this work, electrochemistry of indium in methyl-trioctylammonium bis(trifluoromethylsulfonyl)imide ionic liquid ([MOA][NTf2]) was studied to widen our knowledge of electrochemical behavior of indium in different types of ionic liquids and to define possibilities in usage of electrochemical separation methods within future rare metals recycling schemes and flowsheets.

[MOA][NTf2] belongs to a group of ILs with low hygroscopicity and therefore can be used without glovebox. Lack of necessity to use inert atmosphere is a big advantage for any hypothetical industrial process. Another advantage of [MOA][NTf2] is its relatively low viscosity compared to other widely studied ILs like imidazolium-based ionic liquids (0.60 Pa·s at 298.15 K according [6]). Thanks to its large cation, [MOA][NTf2] IL also has high extractability towards In(III) in common organic phase compared to other alkyl-methylimidazolium ILs as presented in [7] and combination of both liquid-liquid extraction and electrochemical separation can be therefore suitable for various indium recovery schemes.

Electrochemistry of indium and its electrodeposition were studied in several non-aqueous solvents including ionic liquids. Liu and Sun, [8], studied In(III) electrochemistry in chloroaluminate ionic liquids. Yang et al. studied electrodeposition of InSb alloys from 1-Ethyl-3-Methylimidazolium chloride/tetrafluoroborate ionic liquid system, [9]. Electrochemistry of In(III) and electrodeposition of indium from 1-Butyl-1-methylpyrrolidinium bis(trifluoromethylsulfonyl)amide was presented by El Abedin et al., [10]. Complex electrochemistry of In(III) in 1-butyl-1-ethyl-piperidinium bis(trifluoromethylsulfonyl)imide was studied and reported to be specific for In(III) introduction to the system in form of chloride in [11].

Cation-connected anomalous electrochemical behavior of indium during the deposition from 1-Butyl-1-Methylpyrrolidinium Dicyanamide was described by Liu, [12]. Matsumiya et al., [13], combined method of indium recovery using both liquid-liquid extraction and electrodepostion, one-step reduction process was studied within the electrochemical part of the study. Deferm et al., [14], studied electrochemistry of In(III) in trihexyl(tetradecyl)phosphonium chloride and suggested the mechanism of In(III) reduction to be two-step and involving In(I).

EXPERIMENTAL

Ionic liquid [MOA][NTf2] was of commercial origin (Sigma-Aldrich, purity above 99 %) and used without further purification. Sample of [MOA][NTf2] was tested for potential absorption of air-humidity. No increase in weight of 0.2 g sample was observed within 8 h of its exposition to air at room temperature.

In(III) was introduced to the IL in the form of Indium(III) triflamid (In(NTf2)3, Sigma-Aldrich, purity over 90 % with sulfur and nitrogen as most important impurities), i.e. substance with the same anion as for the [MOA][NTf2] carrier system.

Electrochemical experiments were carried out in the glass cell placed on a heater/stirrer equipped with temperature regulator. A three-electrode system was used for all measurements. Mo wire of 1 mm diameter was used as a working electrode. Prior to every measurement, its surface was washed with HCl and EtOh. Au and Pt working electrodes were used as counter and quasi-reference respectively. For alloying verification experiments, Au and Pt were also used as working electrodes in specific cases. The electrodes were connected to Metrohm Autolab PGSTAT204 potentiostat (Metrohm Autolab B.V., Utrecht, the Netherlands) controlled by PC with original software (Nova 2.1.4).

Samples after electrolytic experiments were inspected with a JEOL scanning electron microscope (SEM) JSM-6510LV equipped with an energy-dispersive spectrometer (EDS) by Oxford Instruments with a silicon-drifted detector. EDS measurements were carried out in high vacuum with an accelerating voltage of 10 kV. The EDS spectra were analyzed with INCA software by Oxford Instruments. For SEM/EDS measurements, samples were washed with EtOH, distilled water and were stuck to a conductive carbon adhesive tape.

RESULTS AND DISCUSSION

The electrochemical window of [MOA][NTf_2] was measured at 80°C with Mo working electrode and it was found to be almost 6.5 V with the main cathodic effect taking place at – 3 V vs. Pt and anodic one at +3.5 V vs. Pt (See Fig. 1a). Therefore, the electrochemical window of [MOA][NTf_2] is similar or even better compared to the majority of other ILs with $[NTf_2]^-$ anion, [15]. This value is 0.7 V wider than the electrochemical window of [MOA][NTf_2] on gold single-crystal working electrode reported by Ueda et al. in [16]

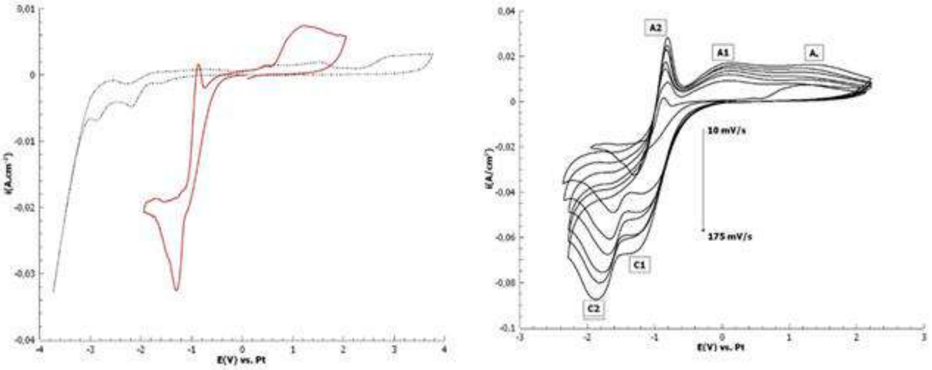

Figure 1 a) Cyclic voltammogram of pure [MOA][NTf_2] ionic liquid (black dashed line) and [MOA][NTf_2] containing 9.49 × 10^{-5} mol/g of $In(NTf_2)_3$ (red line) on Mo wire electrode, scan rate 10 mV/s, t=80°C, Pt quasi-reference, Au counter electrode b) Cyclic voltammograms of [MOA][NTf2] ionic liquid containing 9.49 × 10-5 mol/g of In(NTf2)3 at different scan rates (10 mV/s to 175 mV/s), Mo working electrode, Pt quasi-reference, Au counter electrode, t=80°C

On the cathodic side, several effects can be seen in the area from -3.0 V to -2.0 V vs. Pt. These peaks can be attributed to the irreversible reduction reactions of the organic cation. On the anodic side, there are also several minor electrochemical effects, which can be attributed to the adsorption of the organic cation on Mo substrate.

Indium was introduced to the [MOA][NTf2] ionic liquid in the form of In(NTf2)3, i.e. no other anion except those coming from possible impurities is present. Because of that, it can be assumed that In(III) occurs in the system mainly as $In_x(NTf_2)_y^{3x-y}$ complex.

Cyclic voltammogram of In(NTf2)$_3$/[MOA][NTf2] system is shown in Fig. 1a (80°C, scan rate 10 mV/s, In(III) concentration 9.49×10^{-5} mol/g, Au counter electrode, Pt quasi-reference electrode). It shows the reduction peak at -1.3 V vs. Pt, the anodic counter peak at -0.9 V vs. Pt and prior the main reduction peak, there is another cathodic effect mostly overlapped by the subsequent one. On the anodic side, another major anodic effect is also visible in more positive potentials (see Fig.1a).

Cyclic voltammograms were measured at various scan rates from 10 mV/s to 175 mV/s (see Fig.1b, scan rates were applied in random order). With an increasing scan rate, the smaller cathodic effect C1 is more apparent, and the new anodic effect labelled A1 probably connected with C1 appears prior Ax peak for scan rates of 50 mV/s and higher.

It can be also seen that peak potential for C2 shifts in negative direction with increasing scan rate which is characteristic of a quasi-reversible or irreversible system, [17]. Also, anodic peak A1 is not proportionate to C1 suggesting at least partially irreversible system. Because of these findings, In(III) redox process in [MOA][NTf2] is suggested to be based on following reactions, (1) – (3):

Reactions on the cathodic side:

$$In^{3+} + 2e^- = In^+ \tag{1}$$

$$In^{3+} + 3e^- = In^0 \tag{2}$$

$$In^+e^- = In^0 \tag{3}$$

On the anodic side, peaks A1 and A2 can be connected to reactions reversal to (1) – (3) in appropriate direction. One should also take into account that In(I) compounds are generally unstable, [18], commonly disproportioning according to the reaction (4).

$$3In^+ = 2In^0 + In^{3+} \tag{4}$$

It should be also noted that In(II) species can be theoretically involved in the mechanism as well and cannot be essentially excluded. However, no study proved its existence in ILs or any similar system so far. Therefore, In(II) was not considered when suggesting reaction mechanism.

It should be also noted that Traore et al., [11], presented cyclic voltammogram of In(III) in NTf2-based [BEPip][TNf2] IL containing only one cathodic peak and its anodic counterpeak corresponding with indium metal deposition/stripping process, i.e. without C1/A1 peaks. Nevertheless, paper [11] was mainly focused on systems containing chloride anions and CV in chloride-free system was measured only at very slow scan rate of 5 mV/s. Our results also show minimization of C1 and A1 peaks at low scan rates, therefore, these experimental results are not in direct contradiction.

Based on assumptions above, it can be suggested that In(III) is first reduced to In(I) (peak C1). In(I) starts to disproportionate and reduction reactions of In(I) and In(III) leading to indium metal deposit take place (peak C2). When the potential change direction is reversed, indium stripping leading to In(I) and resulting in peak A2 occurs.

Later, oxidation of In(I) to In(III) shows as peak A1 which is missing for low scan rates probably because In(I) disproportionation is faster compared to potential change in these cases and no electrochemical oxidation of In(I) takes place. During the whole scan, some processes can overlap each other, and CV therefore corresponds to the net total current due to parallel processes. This, altogether with In(I) disproportionation reaction, can explain cathodic and anodic peak disproportionality.

There is also peak labelled Ax at about +0.8 V vs. Pt. This peak cannot be interpreted within the In redox mechanism at this moment, however, the main impurity in commercial In(NTf2)3 is nitrogen. Peak Ax can be therefore attributed to oxidation of ammonia as described by Ji et al. in [19] for [C2mim][NTf2] and [C4mim][NTf2] ILs.

Several voltammograms were measured with Au and Pt working electrodes as well. As can be seen in Fig.3a, CVs were very complex in these cases which can be explained by alloying reactions of indium with Au and Pt, [20] and [21] respectively.

Potentiostatic electrolysis (C2 peak potential set for 3600 s) was done to verify indium deposition on Mo substrate. SEM/EDX analysis of the electrode surface shows compact layer of indium (see Fig. 3b). Detailed picture shows that the deposit is made of particles of mostly irregular shape and dominant dimension with maximum size of 500 nm. This is in general agreement with results by Traore et al., [11].

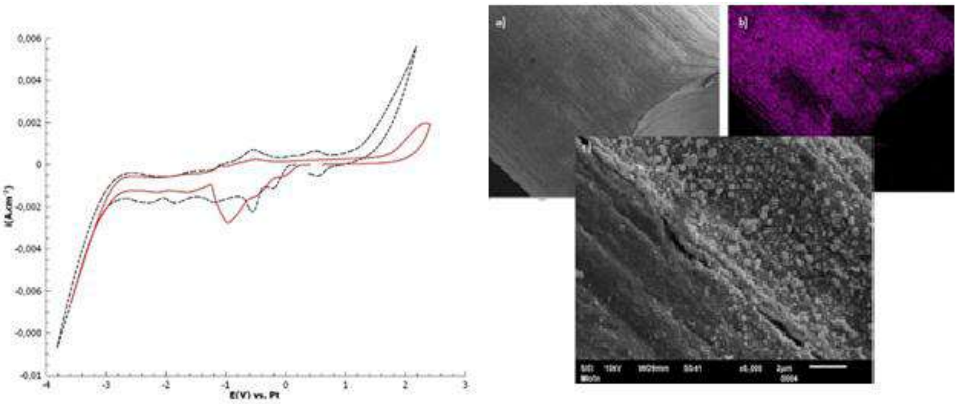

Figure 3 a) Cyclic voltammogram of [MOA][NTf2] ionic liquid containing 9.49 × 10-5 mol/g of In(NTf2)3, Au (black dashed line) and Pt (red line) working electrode, scan rate 50 mV/s, Pt quasi-reference, Au and Pt counter electrode respectively, t=80°C b1) SEM picture of In deposit layer on Mo wire electrode b2) SEM-EDX In map on Mo wire electrode, b3) detail of In deposit structure on Mo electrode, all pictures taken after potentiostatic electrolysis at C2 peak potential set for 3600 s

CONCLUSION

The electrochemical behavior of indium in methyl-trioctylammonium bis(trifluoromethylsulfonyl)imide ionic liquid at 80°C was studied for the first time. Indium was introduced to the IL in the form of In(NTf2)3, i.e. no additional anion was present in the system. Reduction mechanism was found to be generally two-step with

In(I) as the intermediate product. As In(I) is unstable, it was necessary to take it into account when defining overall reaction mechanism. Indium was deposited on Mo electrode, and it was shown by SEM/EDX analysis that it was in the form of particles with dominant dimension with maximum size of 500 nm. Alloying reactions of In with Pt and Au substrates during potentiostatic electrolysis were also found.

ACKNOWLEDGEMENT

Project TS01030229 "Ecological ways of concentrating critically important elements in natural rocks or wastes from their treatment and linking them to separation methods for the electrolytic recovery of these elements in their pure state" is co-financed from the state budget by the Technology agency of the Czech Republic under the Theta 2 Programme.

REFERENCES

1. G. A. Blengini et al., Study on the EU's list of Critical Raw Materials (2020) Final Report (2020).
2. C. Austen Angell, Y. Ansari, and Z. Zhao, Ionic Liquids: Past, present and future, Faraday Discuss, 154 (2011) 9.
3. P. T. Anastas and J. C. Warner, Green Chemistry: Theory and Practice, New York, Oxford University Press (1998).
4. A. J. Greer, J. Jacquemin, and C. Hardacre, Industrial Applications of Ionic Liquids, Molecules. 25 (2020) 5207.
5. M. Straka, Toward a greenish nuclear fuel cycle: Ionic liquids as solvents for spent nuclear fuel reprocessing and other decontamination processes for contaminated metal waste, Sustainable Green Chemistry, M. A. Benvenuto, Ed. Berlin/Boston: DeGruyter, (2017) 35–47.
6. B. Yoo, W. Afzal, and J. M. Prausnitz, Effect of water on the densities and viscosities of some ionic liquids containing a phosphonium cation, Zeitschrift fur Phys. Chemie, 227 (2013) 157.
7. A. Eguchi, K. Morita, and N. Hirayama, Ionic liquid chelate extraction behavior of trivalent Group 13 metals into 1-alkyl-3-methylimidazolium bis(trifluoromethanesulfonyl) imides using 8-quinolinol as chelating extractant, Anal. Sci., 35 (2019) 1003.
8. J. S. Liu and I. Sun, Electrochemical Study of the Properties of Indium in Room Temperature Chloroaluminate Molten Salts, J. Electrochem. Soc., 144 (1997) 140.
9. M.-H. Yang, M.-C. Yang, and I.-W. Sun, Electrodeposition of Indium Antimonide from the Water-Stable 1-Ethyl-3-methylimidazolium Chloride/Tetrafluoroborate Ionic Liquid, J. Electrochem. Soc., 150 (2003) C544.
10. S. Zein El Abedin, A. Y. Saad, H. K. Farag, N. Borisenko, Q. X. Liu, and F. Endres, Electrodeposition of selenium, indium and copper in an air- and water-stable ionic liquid at variable temperatures, Electrochim. Acta, 52 (2007) 2746.
11. Y. Traore, S. Legeai, S. Diliberto, G. Arrachart, S. Pellet-Rostaing, and M. Draye, "New insight into indium electrochemistry in a Tf2N-based room-temperature ionic liquid, Electrochim. Acta, 58 (2011) 532.
12. Y. C. Liu, Y. C. Chen, Y. T. Hsieh, and I. W. Sun, Anomalous Voltammetric Behavior Observed for Electrodeposition of Indium in the 1-Butyl-1-methylpyrrolidinium Dicyanamide Ionic Liquid. A Result of the Ionic Liquid Cation Adsorption, J. Phys. Chem. C, 121 (2017) 8907.
13. M. Matsumiya, M. Sumi, Y. Uchino, and I. Yanagi, Recovery of indium based on the combined methods of ionic liquid extraction and electrodeposition, Sep. Purif. Technol., 201 (2018) 25.
14. C. Deferm et al., Electrodeposition of indium from the ionic liquid trihexyl(tetradecyl)phosphonium chloride, Green Chem., 21 (2019) 1517.

15. M. Galiński, A. Lewandowski, and I. Stępniak, Ionic liquids as electrolytes, Electrochim. Acta, 51 (2006) 5567–5580.
16. H. Ueda, K. Nishiyama, and S. Yoshimoto, Electrochemical Behavior of Bis(trifluoromethylsulfonyl)imide-based ILs at Gold Single Crystal Electrodes, ECS Trans., 50 (2013) 175.
17. A. J. Bard and L. R. Faulkner, Elecrochemical Methods, New York: Wiley, 1980.
18. D. G. Tuck, The Lower Oxidation States of Indium, Chem. Soc. Rev., 22 (1993) 269.
19. X. Ji, D. S. Silvester, L. Aldous, C. Hardacre, and R. G. Compton, Mechanistic studies of the electro-oxidation pathway of ammonia in several room-temperature ionic liquids, J. Phys. Chem. C, 111 (2007) 9562.
20. H. Okamoto, Au-In (Gold-Indium), J. Phase Equilibria, 14 (1993) 532.
21. H. Okamoto, In-Pt (Indium-Platinum), J. Phase Equilibria Diffus., 26 (2005) 399.

XVI International Mineral Processing
and Recycling Conference
28-30 May 2025, Belgrade, Serbia

DOI: 10.5937/IMPRC25340H

Original research article

GRADE IMPROVEMENT OF IRON ORE CONCENTRATE BY APPLYING PLANT AUDITS, STANDARDIZATION AND PROCESS OPTIMIZATION

Seyed Hamzeh Amiri[#], 0000-0001-5137-2013,
Maria Sinche-Gonzalez, 0000-0002-7722-6839,
University of Oulu, Oulu Mining School, P.O. Box 3000, Oulu, Finland

ABSTRACT – One of the challenges at iron ore processing plants is achieving a concentrate by the desirable iron grade. It is crucial to implement optimizations for increasing the concentrate quality. In this research, the operation of a case study plant was investigated to find bottlenecks and improve the iron ore concentrate quality. For this purpose, the grinding and magnetic separation stages including ball mills, hydrocyclones and low intensity magnetic separators were investigated. The plant optimizations resulted in the Fe grade improvement of concentrate from 63.50% to 66.1% and reduction of concentrate particle size (P80) from 98 µm to 75 µm.

Keywords: Iron Ore, Optimization, Plant audit, Process Flowsheet.

INTRODUCTION

Iron ore is a vital resource for iron and steel production [1] and it can be processed by magnetic separation methods [2]. Among all iron ores, magnetite ores are naturally suitable for upgrading by low-intensity magnetic separators [3-6]. However, the quality of iron ore varies greatly, and it is typically necessary to control the process to produce an iron ore concentrate with higher Fe grade to meet the requirements of downstream processes. Optimization and improvement of Fe grade can be achieved through process audit [7-10] and it can be applied by a combination of sampling, laboratory analyses, practical measurements [11-12]. Also, the optimization can be formulated based on the process and operating constraints to increase productivity and reach certain product characteristics [13-17]. The modification of grinding and classification circuit could be considerable and improve the quality of the final product [18]. Therefore, the auditing process can be applied as a method for achieving higher throughput, a finer product, or reduced operating costs. The present paper provides insights into the audit method of a case study plant and its role in the improvement of plant operation, product and throughput.

MATERIALS AND METHODS

The process flowsheet and main equipment as well as the feed and product characteristics of the plant are presented in Figure 1. The plant includes two ball mill-

---

[#] corresponding author: s.hamzeh.amiri@gmail.com hydrocyclone circuits and five wet low intensity magnetic drum separators (LIMS) for processing the iron ore.

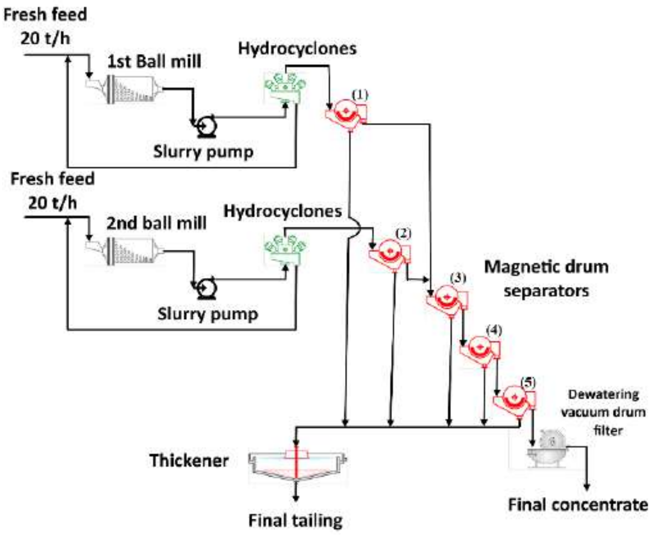

Figure 1 The simplified process flowsheet of iron ore beneficiation plant before optimization

In this flowsheet, the fresh feed (crushed iron ore) is fed simultaneously to two parallel ball mills. The water is added to the ball mills and the operation is done at the wet process. Five magnetic drum separators are in a series and the product of each drum separator is considered as the feed of the next drum separator. In each ball mill, the feed rate is 20 t/h. The magnetic intensity of LIMS was 0.10-0.12 Tesla. Table 1 represents the chemical characteristics of feed and product. Before audits, the Fe grade of concentrate was 63.5% and this amount is less than the typical Fe grade for iron ore concentrate feeding to the downstream pelletizing process. The XRD (X-ray diffraction) analyses showed that magnetite is the main iron-bearing mineral in feed. Quartz and calcite are the primary gangue minerals and the most sulfur-bearing mineral is pyrite. The particle size analysis of fresh feed and final product showed that the F_{80} of fresh feed and the P_{80} of product are 6.2 mm and 99 µm, respectively. The auditing consisted in observations of operating parameters of ball mills, hycrocylones, and drum separators as well as the chemical and physical measurements of the feed and product.

Table 1 The chemical analysis of feed and product

Composition	wt. (%)								
	Fe_{total}	FeO	S	P	MgO	CaO	Al_2O_3	SiO_2	TiO_2
Fresh feed	48.11	17.62	1.54	0.02	6.15	3.18	2.34	11.54	1.13
Product	63.50	22.05	0.23	<0.01	0.90	0.94	1.14	5.86	0.26

RESULTS AND DISCUSSIONS

Modification of equipment arrangement

At the process flowsheet, the tailings streams of all separators were forwarded to the dewatering thickener and the iron and water content measurements showed that it is possible to recycle the tailings of the final magnetic separation stage to the process because it mostly contains high volume of water and low solid content. In Figure 2, the grinding circuit of the first ball mill was changed from a close to open circuit. The hydrocyclones overflow of the first grinding stage is forwarded to the magnetic drum separators and the hydrocyclones underflow is considered as the feed of the second ball mill. In fact, the second ball mill acts as the regrinding mill. Due to this change, the proper balls' size and distribution for each ball mill was proposed and implemented.

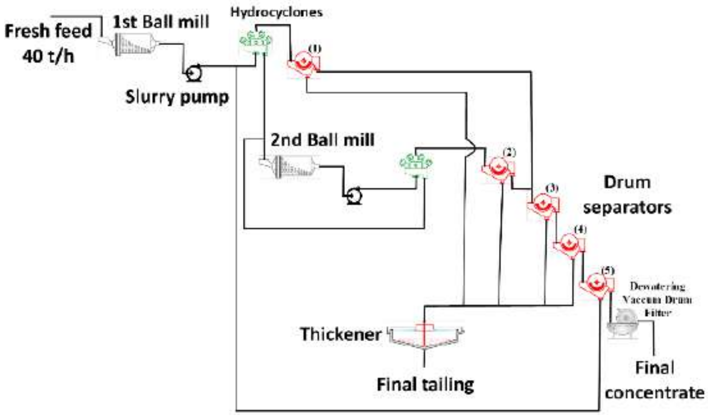

Figure 2 The process flowsheet of the case study plant after modifications

Liberation degree studies of iron minerals

The iron distribution in different size fractions of the concentrate was studied (Figure 3). The iron distribution at the coarse-sized fractions is lower than that of the other-sized fractions, which is the main reason for the failure to achieve the higher Fe grade at the final concentrate. The effects of the particle size reduction on the iron mineral liberation were investigated by grinding the feed samples to the d_{80} of 75, 53 and 45 µm and running Davis tube tests for magnetic separation. The results of Davis tube tests are presented in Table 2. It is clearly understood that the P_{80} of concentrate should be reduced to 75 µm for achieving the higher Fe grade.

Table 2 Davis tube tests on the case study iron ore

Sample	Particles Size	Fe grade (%)			Concentrate mass (%)	Fe recovery (%)
		Feed	Concentrate	Tailing		
Iron ore	d_{80}=75 µm	49.62	67.20	15.49	66	89.38
	d_{80}=53 µm	48.54	68.67	15.70	62	87.7
	d_{80}=45 µm	48.94	68.22	17.48	62	86.43

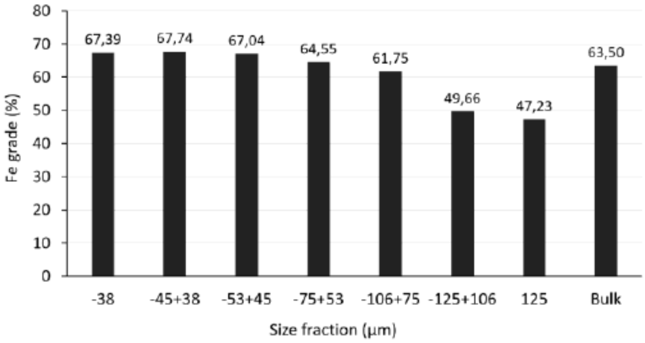

Figure 3 The iron distribution in different size fractions of iron ore concentrate

Grinding conditions of ball mills

The operating conditions of two ball mills are presented in Table 3, before and after modification in the process flowsheet.

Table 3 The operating conditions of ball mill circuits, before and after modifications

Operating conditions	First ball mill		Second ball mill	
	Before	After	Before	After
Ball filling ratio (%)	26	30	28	30
Ball charge size (mm)	60	70	60	40
Fresh feed rate (t/h)	20	40	20	-
Power draw (kW)	~510	~600	~460	~500
Solid content (%)	81	75	81	75

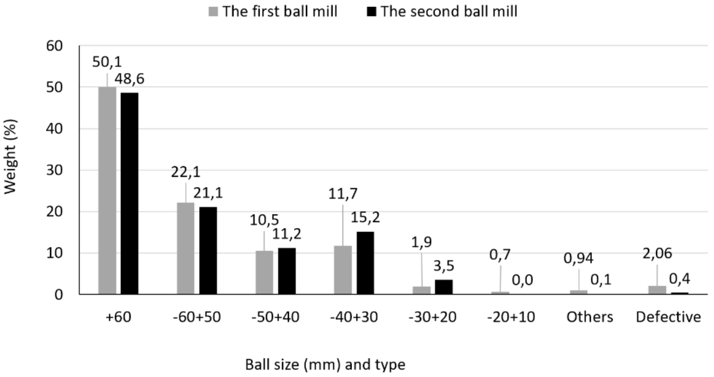

Figure 4 The balls size distribution inside ball mills by taking samples

The suitable solid content inside the ball mills was changed from more than 81% to 70%-75%. The ball samples were taken from the inlet, outlet and middle locations inside ball mills to modify the grinding operation in ball mills. The results of balls size distribution are illustrated in Figure 4. The balls inside both ball mills are bigger than 60 mm and, there is a low number of small balls. The optimum make-up ball size for each ball mill was found according to the new operating and feeding conditions. The ball size was determined by using the Bond equation [19] which is as the equation (1).

$$B = \left(\frac{F}{K}\right)^{\frac{1}{2}}\left(\frac{S*Wi}{Cs*\sqrt{D}}\right)^{\frac{1}{3}} \quad (1)$$

Where B is the ball diameter (mm), F is the F_{80} of feed (µm), K is the grinding correction coefficient, S is the density of bulk mass (g/cm^3), Wi is the specific energy consumption (kWh/t), Cs is the mill rotational speed (%) and D is the internal mill diameter (m). The calculated make-up ball size for the first and second ball mills were 70 and 40 mm, respectively. The balls' size distribution was corrected based on the Bond recommendation [19]. After modifications, the particles' size of the first ball mill output increases from 165 to 217 µm, which is due to the rise of feed rate from 20 to 40 t/h. In the second ball mill, the particles' size of the mill output decreased from 205 to 138 µm, due to the higher ball charge and the lower mill feed size.

Modifications of drum separators

The main problems related to drum separators were non-uniform feeding to the whole length of the drum separator, presence of blockages in the tailing orifice of some separators, and absence of washing water and cleaning scrapers on the discharge lip of the concentrate on each drum separator. It was observed that the concentrate product of the first drum separator is discharged at one point inside of the next drum separator tank and it causes an uneven feed distribution through the whole effective length of the drum separator. Consequently, it affects separation efficiency and the unsymmetrical wear of the drum surface lining as well. This problem was solved by adding a new pipeline in front of the drum separator to dispense the slurry feed to the whole length of the drum separator.

CONCLUSION

In this research, an iron ore beneficiation plant was audited to find optimizations for improving the iron ore concentrate quality. Before optimizations, the Fe grade of concentrate was 63.5% with P_{80} of 98 µm. The chemical analyses and mineralogical studies (XRD) showed that the main iron-bearing mineral is magnetite. The main reasons for the low Fe grade of iron ore concentrate were the insufficient liberation of iron minerals from gangues and inappropriate performance of magnetic separation stages. Davis tube tests on the ground feed samples with different particle sizes showed that the feed sample should be ground to d_{80} of 75 µm to achieve an iron ore concentrate with the minimum Fe grade of 66%. Two grinding circuits of ball mills were rearranged from operating in parallel to a series. The solid content inside ball mills was readjusted and reduced from 81% to 75% and the balls' size distribution in ball mills was optimized based on the mill feed size. The P_{80} of the final concentrate was reduced from 98 to 75 µm. The efficiency of separators was increased by optimizing the uniform feeding on the drum's surface. Also, the tailings streams of final drum separator were recycled to the process instead of removing from the circuit to have more dilution on the drum separators feed.

Conclusively, all these modifications led to an increase in the Fe grade of the final concentrate from 63.5% to 66.1%.

ACKNOWLEDGEMENT

The support of the funds of EMJM-PROMISE program to sponsor the participation in IMPRC 2025 is acknowledged.

REFERENCES

1. Holmes, R. J., Lu, Y., Lu, L., (2022) Introduction: Overview of the Global Iron Ore Industry. In: Iron Ore Mineralogy, Processing and Environmental Sustainability (Liming, B. T.), Woodhead Publishing, 1-42.
2. Wills, B. A., James, A. F. (2016) Chapter 13 - Magnetic and Electrical Separation. In: Wills' Mineral Processing Technology, Boston: Butterworth-Heinemann, 381–407.
3. Xiong, D., Lu, L., Holmes, R. J. (2015) Developments in the Physical Separation of Iron Ore: Magnetic Separation. In: Iron Ore Mineralogy, Processing and Environmental Sustainability (Liming, B. T.), Woodhead Publishing, 283–307.
4. Dworzanowski, M. (2010) Optimizing the Performance of Wet Drum Magnetic Separators. Journal of the Southern African Institute of Mining and Metallurgy, 110 (11), 643-653.
5. Luttrell, G. H., Kohmuench, J. N., Mankosa, M. J. (2004) Optimization of Magnetic Separator Circuit Configurations. Mining, Metallurgy & Exploration, 21 (3), 153–57.
6. Svoboda, J., Fujita, T. (2003) Recent Developments in Magnetic Methods of Material Separation. Minerals Engineering, 16 (9), 785–92.
7. Meloy, T. P., (1983) Optimizing for Grade or Profit in Mineral Processing Circuits - Circuit Analysis. International Journal of Mineral Processing, 11 (2), 89–99.
8. Krishna, S. J. G., Rudrappa, C., Ravi, B. P., Rudramuniyappa, M. V. (2015) Optimization of an Iron Ore Washing Plant. Procedia Earth and Planetary Science, 11, 111–14.
9. Flintoff, B.C., Mular, A.L. (1992) A Practical Guide to Process Controls in the Minerals Industry, 1st Edition, Dept. of Mining and Mineral Process Engineering, University of B.C., Vancouver.
10. Bhadani, K., Asbjörnsson, G., Hulthén, E., Evertsson, M. (2018) Application of Multi-Disciplinary Optimization Architectures in Mineral Processing Simulations. Minerals Engineering, 128, 27–35.
11. Yahyaei, M., Malcolm, P. (2019) Production Improvement Opportunities in Comminution Circuits. The Australasian Institute of Mining and Metallurgy.
12. Xu, Q., Zhang, K., Li, M., Chu, Y., Zhang, D. (2021) Multi-Objective Robust Optimization for Planning of Mineral Processing under Uncertainty. In: 33rd Chinese Control and Decision Conference (CCDC). IEEE, 4020–27.
13. Porkuian, O., Morkun, V., Morkun, N., Serdyuk, O. (2019) Predictive Control of the Iron Ore Beneficiation Process Based on the Hammerstein Hybrid Model. Acta Mechanica et Automatica, 13 (4), 262–70.
14. Bengtsson, M., Asbjörnsson, G., Hulthén, E., Evertsson, M. (2017) Towards Dynamical Profit Optimization of Comminution Circuits. Minerals Engineering, 103–104, 14–24.
15. Goodwin, G. C., Seron, M. M., Mayne, D. Q. (2008) Optimization Opportunities in Mining, Metal and Mineral Processing. Annual Reviews in Control, 32 (1), 17–32.
16. Delgadillo, J. A., Lopez-Valdivieso, A., Tello, A. (2008) Optimization of a Grinding and Classification Circuit of a Magnetite Ore Processing Plant through Computer Simulation. Mining, Metallurgy & Exploration, 25 (4), 223–28.

17. Ding, J., Wang, H., Liu, C., Chai, T. (2013) A Multiobjective Operational Optimization Approach for Iron Ore Beneficiation Process. In Proceedings of the 2013 International Conference on Advanced Mechatronic Systems, IEEE, 582–87.
18. Amiri, S. H., Zare, S. (2021) Influence of Grinding and Classification Circuit on the Performance of Iron Ore Beneficiation - A Plant Scale Study. Min. Proc. and Extr. Met. Review, 42(3), 143-52.
19. Bond, C. F. (1958) Grinding Ball Size Selection. Mining Eng., 10, 592–95.

XVI International Mineral Processing
and Recycling Conference
28-30 May 2025, Belgrade, Serbia

DOI: 10.5937/IMPRC25347D Research article

ADVANCEMENTS IN MINERAL PROCESSING: COLLABORATIVE EFFORTS AND TECHNOLOGICAL INNOVATIONS AT ARCELORMITTAL

Henrique Dias Gatti Turrer[#], 0009-0007-5619-2071,
Josue Mesquita De Souza Junior, 0009-0004-0965-012X,
Gillian Nikka Omaga, 0009-0004-1124-2408,
Juliette Laine, 0009-0000-5979-0746,
Marcello Rodrigues Cruz, 0009-0004-3887-5811,
Nubia Bottosso, 0009-0006-2894-0178,
Vinicius Seerig, 0009-0004-0450-5572,
ArcelorMittal, France

ABSTRACT – This article presents a comprehensive overview of recent advancements in mineral processing achieved by ArcelorMittal's Global R&D team. Through a multidisciplinary and innovative approach, the team has optimized beneficiation processes, reduced impurities, and improved product quality, contributing to operational efficiency and sustainability of the company. The studies highlighted in this article were developed in collaboration with universities and equipment suppliers, focusing on key areas such as mineral characterization, decarbonization, new beneficiation routes, comminution optimization, and chemical reaction modelling. ArcelorMittal aims to strengthen networking in Europe by seeking strategic partnerships with third-party companies, research centers, and universities. The exchange of knowledge and collaboration with new partners can further drive the development of advanced technologies and innovative solutions for the sector's challenges.

Keywords: Mineral Processing, Iron Ore, Collaboration, Research And Development.

INTRODUCTION

In 2024, ArcelorMittal demonstrated its significant global presence and operational strength with an EBITDA of $7.1 billion [1]. The company's mining sector also presented impressive performance, producing 42.4 million metric tonnes of iron ore [2]. The main seaborne iron ore mines are in Quebec, Canada, and Liberia, producing iron ore lump, concentrate, sinter feed, and pellets. The Mont-Wright mine in Canada, operational since 1974, is the largest open-pit iron ore mine in the country, with reserves for more than 30 years and a production capacity of around 26 million tonnes of iron ore concentrate annually [3]. In Liberia, operations are undergoing an expansion to increase production capacity to 15 million tonnes of iron ore concentrate, with commissioning expected in Q4 2024 [4]. The company also operates several other mines in Europe, Mexico, Brazil,

---

[#] corresponding author: henrique.turrer@arcelormittal.com

South Africa and India, often through joint ventures, primarily producing iron ore for internal consumption.

The Global Research and Development Group of ArcelorMittal counts with a mineral processing team located in Mazières-lès-Metz, France. The team consists of a few permanent engineers and technicians. Frequently, the team hosts people with temporary contracts, such as PhD’s students, apprentices and interns. Among the permanent staff, there are a few PhDs and MSc in mineral processing. Despite having an average engineer age of close to 36 years, the team collectively holds decades of experience in mineral processing across various plants. The team is highly diverse, comprising members from three nationalities across three continents – the Americas, Europe, and Asia – with women representing 48% of the team. The area is equipped with laboratory infrastructure capable of simulating mineral processing plant operations on bench scale, batch scale, and continuous pilot scale. The team’s activities are focused on five key pillars: safety, decarbonization, digitalization, knowledge, and operational support to plants. Additionally, the team collaborates with an external and internal network of partners to develop projects in areas outside its core expertise, such as, for example, mine planning, ironmaking, data science, etc. Some examples of past studies conducted by the company and published in the literature are summarized in the next paragraph.

The work by Barbosa et al [5] provided an overview of ArcelorMittal’s mining operations, addressing the various types of iron ore present in its global operations. Correa de Araujo and Reisinger [6] investigated the flotation of pyrrhotite from magnetite ores in a deposit in Kazakhstan. Barbosa et al [7] conducted a study on the development of alternative surfactants for flotation of phosphorus-bearing minerals, with a focus on the pelletizing plant at ArcelorMittal Lazaro Cardenas in Mexico. Xuan et al [8] developed an innovative solution for phosphorus removal from oolitic goethitic iron ores. Guimarães et al [9] explored the use of polyacrylate in the treatment of iron ores with high moisture content.

The objective of this paper is to present recent advancements in mineral processing, focusing on ArcelorMittal’s efforts to improve beneficiation methods and the technological innovations implemented across its mining operations.

DEVELOPMENT

In this chapter, several examples of recent studies produced and published by the Mineral Processing area of ArcelorMittal's Global R&D are presented. These articles exemplify the team's focus on various critical aspects of mineral processing, including mineral characterization, decarbonization of the steel production chain (production of high-grade iron concentrate), development of new treatment routes, optimization of comminution (for energy saving) and concentration (for iron recovery increase) processes, and modelling of chemical reactions in mineral processing. These works were developed in close collaboration with universities and equipment suppliers, highlighting the essential role of partnerships in driving innovation and achieving significant advancements in the field.

Material characterization is a crucial first step in mineral processing studies, providing essential data for subsequent beneficiation strategies. A key example of its importance in optimizing downstream processes is demonstrated in a study by Omaga et al. [10], who analyzed samples from two pits at Thabazimbi mine to support processing route development. The samples were crushed to -5mm and homogenized, and several techniques were used for characterization: optical microscopy for mineral identification, SEM-EDS for grain shape and chemistry analysis, AMICS for liberation studies, X-ray diffraction (XRD) for mineral composition, and DRIFTS for qualitative identification. Chemical composition was determined using ICP-AES. The analysis revealed that itabirite samples (BIF) had higher impurity content compared to waste dump samples (VDB), which was mainly hematite and quartz. The BIF samples contained iron-bearing silicates and carbonates, while the VDB sample had simpler mineralogy with minimal supergene alterations. Liberation analysis showed hematite and goethite were liberated in finer size fractions (50-80 µm for BIF and 160-250 µm for VDB), and gangue minerals like quartz and aegirine were liberated in coarser fractions. The findings suggest that gravity and magnetic separation could be effective for pre-concentration to reduce gangue material early on, with further investigation underway by a PhD candidate. XRD and FT-IR analyses confirmed the presence of quartz, kaolinite, and carbonates, with notable mineralogical differences between the sample types. SEM-EDS analysis indicated that gangue minerals, including aegirine, were concentrated in finer fractions, while modal analysis showed hematite and goethite were more abundant in these fractions. The study indicates that flotation could be an effective technique for recovering iron oxides from these ores.

A significant focus in the activities of the area is the optimization of concentration processes, as enhancing separation efficiency directly impacts overall plant performance. The following few examples focus on this objective.

Turrer et al. [11] conducted a study aimed at improving iron content in magnetite ore concentrates to support green steel production. The study evaluated magnetic separation performance in bench-scale and explored the potential use of HPGR for pre-concentration. Two samples were collected from an industrial plant: one before and one after the dry magnetic separation stage. The samples were crushed to 8 mm, and X-ray diffraction (XRD) analysis revealed that iron was primarily associated with magnetite and pyrrhotite, while gangue minerals included garnets, amphiboles, and pyroxenes. Magnetite liberation occurred below 425 µm, indicating benefits from finer grinding. Magnetic separation tests using an Outotec wet drum low-intensity magnetic separator (LIMS) at 30% solids and 1.5 l/min feed rate showed that lower drum speeds improved concentrate quality, achieving up to 66% Fe and 82% Fe recovery at a P_{80} of 105 µm. Magnet position had minimal impact on results. HPGR tests performed at the Weir lab in Venlo, Netherlands, produced two batches with P_{80} sizes of 1.5 mm and 3.5 mm. Dry magnetic separation of HPGR products showed similar performance between batches, with higher recovery at lower drum speeds.

A flotation process was investigated to upgrade magnetite concentrate from the Mont Reed deposit for DR pellet feed quality [12]. This research, part of a PhD project, aimed at developing a production route for the greenfield deposit, mainly containing magnetite, hematite, and minor iron silicates. Flotation tests on magnetic separation concentrate achieved an optimized Fe grade of 66.28% using ether amine as a collector and starch as a depressant. The optimized conditions (150 g/t collector, 400 g/t depressant, pH 10, 30 wt.% solids) produced a concentrate with 70.04% Fe, 1.68% SiO_2, 23.9% yield, and 52.0% Fe recovery. The results confirmed flotation as a suitable option for achieving DR quality, despite some Fe recovery loss.

Mesquita et al. [13] evaluated the Crago flotation process (largely used in phosphate industry) to recover iron from Mont-Wright fine tailings, achieving 65.63% Fe and 2.14% SiO_2 with 70.4% Fe recovery and 22.5% yield. The Crago process demonstrated superior selectivity and concentrate quality compared to conventional reverse cationic flotation.

Pilot-scale tests were conducted using a Reflux Classifier RC 100 model from FLSmidth [14], testing two different size fractions: coarse (-1000 +400 µm) and medium (-400 +100 µm). Three tests were performed for each fraction, with a feed rate of 120 kg/h and pulp density of 1,500 kg/m^3. The study aimed to assess the impact of bed density and fluidization water flow on the concentration process for a project in Western Africa. Results showed that both variables significantly influenced mass recovery and concentrate quality. For the coarse fraction, reducing bed density and fluidization water flow increased mass recovery but slightly raised SiO_2 content. However, excessive reductions led to process failure. For the fine fraction, fluidization water was more dominant in affecting mass recovery and concentrate quality. Lowering water flow and adjusting bed density improved mass recovery but also raised SiO_2 content, with the best results at lower water flow and reduced bed density. These findings emphasize the importance of optimizing both variables for better performance.

Comminution is a critical area of research due to its impact on liberation and downstream recovery. A study focused on optimizing grinding operations at Mont-Wright involved grinding tests on three ore blends using the Donda method to estimate energy consumption [15]. The tests were performed at three target particle sizes: 600 µm, 106 µm, and 75 µm. The ore blends had varying mineral compositions, including hematite, magnetite, quartz, and others. The estimated grinding energy to reach 600 µm was about 3.7 kWh/t, aligning with the average energy consumption at the Mont-Wright plant. Results suggested that this methodology could estimate ore grinding variability. Blend B3, a sample coming from a important region of the deposit, showed the highest energy consumption, particularly at the finest particle size (75 µm), with 30.5 kWh/t. This study contributed to the geometallurgical program development at Mont-Wright.

Recent research has incorporated chemical modeling to enhance process understanding, focusing on reagent-mineral interactions and beneficiation efficiency, supported by the University of Lorraine. Machine learning (ML) simulations were used to study water adsorption on kaolinite surfaces, overcoming the limitations of classical molecular dynamics (CMD) and ab initio molecular dynamics (AIMD). By combining traditional methods with ML models, more accurate simulations were achieved. Results showed stronger adsorption of water molecules on octahedral surfaces, with well-structured hydration layers potentially impeding flotation efficiency by blocking reagent adsorption and bubble adhesion (16). Similarly, the Machine Learning Force Field model (MLFF) was used to study water dynamics on iron oxide surfaces, revealing shorter residence times on ferrosilite, which improved reagent interaction and separation efficiency. The density profiles of water on hematite and magnetite indicated structured hydration layers that influence reagent adsorption and flotation efficiency, aiding in the design of effective reagents for optimizing flotation (17).

CONCLUSION

The studies highlight and summarize significant advancements made by ArcelorMittal's Mineral Processing team in collaboration with universities and equipment suppliers. Through innovation, the team optimized beneficiation processes, reduced impurities, and improved product quality, enhancing operational efficiency and sustainability. The team aims to strengthen networking in Europe by seeking partnerships with companies, research centers, and universities to foster knowledge exchange and develop advanced technologies to address sector challenges.

ACKNOWLEDGEMENT

We would like to express our gratitude to all internal and external collaborators who made these studies possible. Special thanks to the University of Lorraine, particularly to Professors Lev Filippovy, Michael Badawi and Yann Foucaud, for their invaluable contributions and support.

REFERENCES

1. ArcelorMittal (2025). Latest quarterly results. Accessed on March 7th 2025 at https://corporate.arcelormittal.com/investors/results
2. ArcelorMittal (2025). ArcelorMittal reports fourth quarter 2024 and full year 2024 results. Accessed on March 7th 2025 at https://corporate.arcelormittal.com/media/5rmh5v4y/4q24-earnings-release.pdf
3. ArcelorMittal Canada (2025). Nos Mines. Accessed on March 7th 2025 at https://mines-infrastructure-arcelormittal.com/nos-mines
4. ArcelorMittal Liberia (2025). Our Journey in Liberia. Accessed on March 7th 2025 at https://liberia.arcelormittal.com
5. Barbosa, M.G., Araujo, A.C., & Sylow, T. (2017). Overview of ArcelorMittal mining operations and research and development. In: Iron Ore Conference. Perth, Australia, 24–26 July 2017.
6. Araujo, A.C., Reisinger, M. (2012). Flotation of Pyrrhotite from Magnetite Ores – A Kazakh Case Study. In: 6th International Congress on the Science and Technology of Ironmaking – ICSTI, 42nd International Meeting on Ironmaking and 13th International Symposium on Iron Ore. October 14th to 18th, 2012, Rio de Janeiro, RJ, Brazil.
7. Barbosa, M.G., Araujo, A.C., & Kodukula, U.B. (2014). Studies on the Development of Alternative Surfactant in the Flotation of Phosphorous Bearing Minerals from Fine Iron Concentrate. In: 44th Ironmaking and Raw Materials Seminar, 15th Brazilian Symposium on Iron Ore and Brazilian Symposium on Agglomeration of Iron Ore. September 2014, Belo Horizonte, MG, Brazil.
8. Xuan, W., Souza, G.G., Ionkov, K., & Araujo, A.C. (2015). Dephosphorization of Oolitic Goethite Iron Ore by Roasting-Leaching Process. In: 45th Iron Ore Reduction and Raw Materials Seminar, 16th Brazilian Symposium on Iron Ore and 3rd Brazilian Symposium on Agglomeration of Iron Ore, ABM Week. 17th to 21st August 2015, Rio de Janeiro, RJ, Brazil.
9. Guimarães, F.A.V., Araujo, A.C., & Karkor, I. (2015). Utilization of Polyacrylate in Iron Ore Processing. In: 45th Iron Ore Reduction and Raw Materials Seminar, 16th Brazilian Symposium

on Iron Ore and 3rd Brazilian Symposium on Agglomeration of Iron Ore, ABM Week. 17th to 21st August 2015, Rio de Janeiro, RJ, Brazil.

10. Omaga, G.N., Filippov, L.O., Filippova, I., Turrer, H.D.G., Senez, L. (2023). Characterization of low-grade and complex iron ore stockpiles (Thabazimbi, South Africa) and identification of possible beneficiation strategies. In: Physical Separation '23. Cape Town, South Africa, Proceedings.
11. Turrer, H.D.G., Belissont, R., Kodukula, U.B., Spies, W., Lainé, J., & de Souza Junior, J.M. (2024). Concentrate Quality Improvement for a Magnetite Ore. In: Proceedings of the XXX International Mineral Processing Congress (IMPC), 2024.
12. Mesquita, J., Badawi, M., Belissont, R., Turrer, H., Foucaud, Y. (2024). Assessment of Flotation Process Efficiency in Producing DR Concentrate from a Low-Grade Iron Ore. Minerals Engineering, 216.
13. Mesquita, J., Foucaud, Y., Turrer, H., Badawi, M. (2025). Evaluation of the Crago flotation process to recover the iron contained in the fine tailings of Mont-Wright mine. Minerals Engineering, 2025.
14. Pinto, P., Rodrigues Cruz, M., Dias Gatti Turrer, H., Totti, E., Mesquita De Souza Junior, J., Seerig, V. (2024). Evaluation of the variation of fluidization water and bed density in the performance of the Reflux Classifier applied to Western African iron ore fines. In: Proceedings of the Physical Separations Conference. Cape Town, South Africa.
15. Bottosso, N., Mesquita, J., Araujo, A.C., & Guimaraes, F. (2023). Effect of Mineralogy on Grinding Energy of Mont-Wright Iron Ore. In: Proceedings of Comminution '23. Cape Town, South Africa.
16. Dell'Angelo, D., Lainé, J., Said, H., Foucaud, Y., & Badawi, M. (2024). Machine learning force field beyond the limits of classical and first-principles molecular dynamics simulations: The case of kaolinite hydration. Journal of Physical Chemistry C, 128(11), 11447–11455.
17. Dell’Angelo, D., Foucaud, Y., Mesquita, J., Lainé, J., Turrer, H., & Badawi, M. (2024). Enhanced Machine Learning Molecular Simulations for optimization of flotation selectivity: A perspective paper. Minerals Engineering, 218, 109016.

XVI International Mineral Processing
and Recycling Conference
28-30 May 2025, Belgrade, Serbia

DOI: 10.5937/IMPRC25353K Research article

THE POTENTIAL SOURCES OF CRITICAL RAW MATERIALS IN SLOVAKIA

Zuzana Kollová#, 0009-0009-4045-8706,
Pavel Bačo, 0009-0000-5756-8076,
Zuzana Danková, 0000-0002-5089-2479,
Zoltán Németh, 0000-0001-5343-6316,
State Geological Institute of Dionýz Štúr, Košice, Slovakia

ABSTRACT – Critical raw materials according to the fifth list of European Union from 2023, contain 34 raw materials [1]. This brief review will be focused on critical raw materials registered in Slovakia as reserved deposits or localities which show an economical potential. SGIDS has solved several projects aimed at verifying the potential of CRM in our territory. The solution resulted in the implementation of two technologically focused projects, to verify the source raw materials for the production of magnesium metal (dolomites, magnesites were tested) and silicon metal (vein quartz, quartzites were tested). The presence of a potential producer was one of the reasons for solving these projects. The suitability of the source raw materials was confirmed on several deposit objects of both types of source raw materials.

Keywords: Critical Raw Materials For EU Countries, Magnesium Metal, Potential Of Raw Materials.

INTRODUCTION

The situation regarding the availability of raw materials led to the development of the Regulation (EU) 2024/1252 of the European Parliament and of the Council establishing a framework for ensuring a secure and sustainable supply of critical raw materials. The new regulation sets out a series of comprehensive measures to ensure the European Union's access to secure, diversified, affordable and sustainable supplies of critical raw materials. This is essential for Europe's competitiveness, including in green and digital industries, as well as defence and aerospace, according to a European Commission report. The EU should have the capacity to extract 10%, process 40% and recycle 25% of its annual consumption of strategic raw materials within the EU by 2030, according to the agreed benchmarks.

The objectives of the regulation should also be achieved through specific Strategic projects and National Exploration Programmes, which should be developed by individual EU countries. Slovakia is currently completing National Exploration Programme based on knowledge of the metallogenetic development of the territory, focusing on potentially significant sources of selected CRM. Information on the availability of the CRM, which are essential for industrial production in the Slovak Republic, but also in the EU countries in general, has recently been processed in several geological synthesis works [2,3,4]. This

---

corresponding author: zuzana.kollova@geology.sk

paper presents the summary results of geological research made by the State Geological Institute of Dionýz Štúr in the field of CRM in recent years.

THE POTENTIAL OF CRM IN SLOVAKIA

Mineral resources that have registered economic reserves have the potential for extraction and processing in Slovakia [5] – Table 1, Figure 1. Raw materials such as tungsten (molybdenum) ores (Ochtiná I deposit - calculation of new reserves in 2016), barite (mined till 2019) and feldspar (mined sporadically) have registered economic reserves. Our anthracite reserves are maintained as economic, but use these reserves for the production of coke is not possible.

Table 1 The deposits and occurrences of the CRM in Slovakia, status as of 1.1.2024, complied and supplemented according Bačo et al. [2]

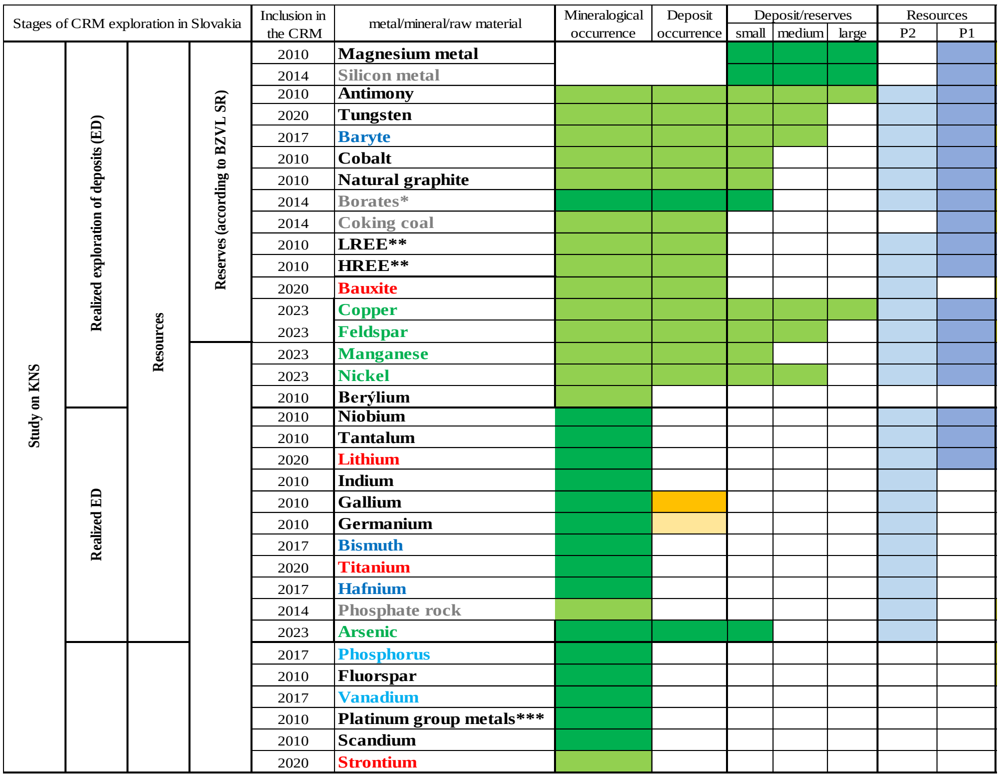

Stages of CRM exploration in Slovakia				Inclusion in the CRM	metal/mineral/raw material	Mineralogical occurrence	Deposit occurrence	Deposit/reserves			Resources	
								small	medium	large	P2	P1
Study on KNS	Realized exploration of deposits (ED)	Resources	Reserves (according to BZVL SR)	2010	**Magnesium metal**			■	■	■		🟦
				2014	**Silicon metal**			■	■	■		🟦
				2010	**Antimony**	🟩	🟩	🟩	🟩	🟩	▨	🟦
				2020	**Tungsten**	🟩	🟩	🟩	🟩		▨	🟦
				2017	**Baryte**	🟩	🟩	🟩	🟩		▨	🟦
				2010	**Cobalt**	🟩	🟩	🟩			▨	🟦
				2010	**Natural graphite**	🟩	🟩	🟩			▨	🟦
				2014	**Borates***	■	■	■			▨	🟦
				2014	**Coking coal**	🟩	🟩					🟦
				2010	**LREE****	🟩	🟩				▨	🟦
				2010	**HREE****	🟩	🟩				▨	🟦
				2020	**Bauxite**	🟩	🟩				▨	
				2023	**Copper**	🟩	🟩	🟩	🟩	🟩	▨	🟦
				2023	**Feldspar**	🟩	🟩	🟩	🟩		▨	🟦
				2023	**Manganese**	🟩	🟩	🟩			▨	🟦
				2023	**Nickel**	🟩	🟩	🟩	🟩		▨	🟦
				2010	**Berýlium**	🟩						
	Realized ED			2010	**Niobium**	■					▨	🟦
				2010	**Tantalum**	■					▨	🟦
				2020	**Lithium**	■					▨	🟦
				2010	**Indium**	■					▨	
				2010	**Gallium**	■	🟧				▨	
				2010	**Germanium**	■	🟨				▨	
				2017	**Bismuth**	■					▨	
				2020	**Titanium**	■					▨	
				2017	**Hafnium**	■					▨	
				2014	**Phosphate rock**	🟩					▨	
				2023	**Arsenic**	■	■	■			▨	
				2017	**Phosphorus**	■						
				2010	**Fluorspar**	■						
				2017	**Vanadium**	■						
				2010	**Platinum group metals*****	■						
				2010	**Scandium**	■						
				2020	**Strontium**	🟩						

Legend:

Inclusion in the CRM list : **Antimony - 2010**; **Silicon metal - 2014**; **Baryte - 2017**; **Bauxite - 2020; Manganese - 2023**

🟩 exploration of deposits for the specific raw material (e.g. Sb, W, ..)

■ exploration of deposits for source raw material (e.g. Dolomite-Mg), or as a by-product source (e.g. base metal deposits - In, Ge, Ga)

🟧 metal obtained during bauxite processing in Al processing plant of Žiar nad Hronom

🟨 metal refined from secondary raw materials - recycling of Ge-containing products - Žarnovica

BZVL SR - Register of Reserves of Reserved Deposits of the SR

Resources P1 and P2 - prognostic resources according Slovak legislative

Note:

REE - light REE (LREE): Ce, La, Nd, Pr, Sm + Sc

- heavy REE (HREE): Dy, Er, Eu, Gd, Ho, Lu, Tb, Tm, Yb, Y

PGM - Ir, Pd, Pt, Rh, Ru

However, source raw materials for the production of magnesium metal (Mg) and silicon metal (Si) – (Table 1) have the greatest potential in Slovakia. The source raw materials for Mg (magnesite and dolomite) are mined in large volume for the production of other materials. Their reserves (mainly dolomite, but also magnesite) are large enough to be used for the production of Mg without limiting their current use in the economy.

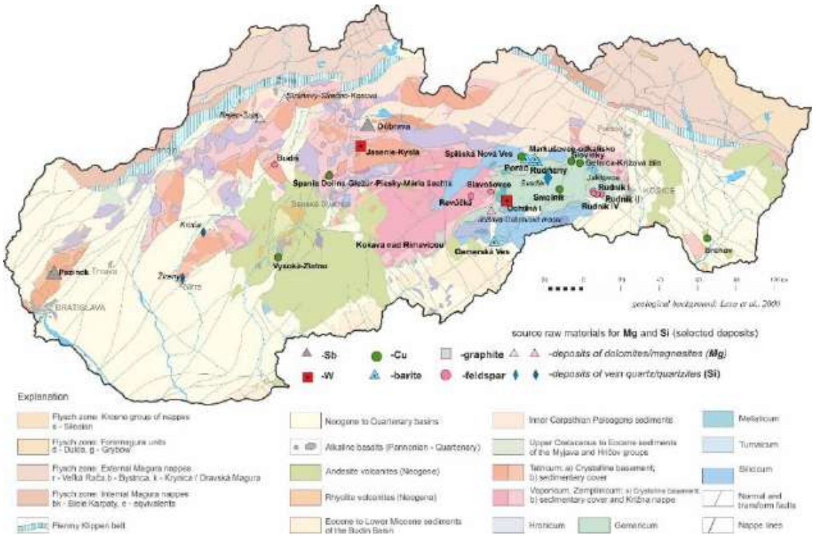

Figure 1 Deposits of CRM registered in Register of reserved deposits in Slovakia as of 1.1.2025.

Magnesium or silicon metal are from the CRM group, closest to real production in Slovakia. The reason is a real producer with a metallurgical operation for the production of ferroalloys (OFZ a.s., joint-stock company), which produced metallurgical silicon and had a real interest in participating in the production of magnesium. However, the real obstacle at the moment is the price of electricity, which is decisive in this case. We have sufficient reserves of source raw materials for the production of both Mg and Si.

Slovakia has relatively large reserves of antimony (Sb) and copper (Cu) ores. Antimony is a metal that was mined separately in several deposits in the past. The total remaining reserves in individual deposits are approximately 55,358 t Sb. Copper is another metal whose ores were mined in many deposits in the past and their mining and subsequent production of copper represented a significant part of its European production (18th and 19th centuries). In Slovakia, we record the remaining reserves of copper ores of approximately 316,429 t Cu. For now, they are registered as not economic, i.e., not economically exploitable. In the case of deposits of these ores, it would be appropriate to carry out economic feasibility studies (e.g., preliminary economic assessment). The potential miner himself will certainly prepare a feasibility study, which will be more time-consuming.

Until 2019, we covered the consumption of barite with our own mining. We register approximately 9 million tons of barite in deposits that are not mined yet. Manganese was mined in the 19th and 20th centuries, the residual non-balance reserves in three deposits are 24,779 kt of ore with a low Mn content (9-17%). For Slovakia, polymetallic nodules from the ocean floor may become an unconventional source of Mn. Slovakia participates in the research activities of Interoceanmetal (IOM) in the Pacific Ocean - in the Clarion-Clipperton tectonic zone.

For other CRM for which we register (As, graphite) or we registered (Ni, Co, tourmaline, bauxite, or others - Table 1) reserves, the potential will become clear during additional deposit exploration work, which, however, means a longer period of time (certainly over 5 – 10 years, exceptionally less).

The assessment of CRM potential resulted in the selection of two projects, where we solved technological research of source raw materials for the production of Mg and Si. We briefly present the results of our research in case of magnesium metal.

SOURCES OF RAW MATERIALS FOR Mg IN THE SLOVAKIA

The main sources of raw materials for the production of magnesium metal in the world are dolomites and magnesite, other sources are oceans, seawater and terrestrial salt lakes, which contain some salts rich in magnesium. The Slovak Republic has significant reserves of both dolomite and magnesite raw materials. We have 25 registered dolomite deposits with total reserves of 879,808 kt of raw materials and 10 magnesite deposits with reserves of 1,127,856 kt of raw materials. The dolomite in Slovakia occurs in several Middle and Upper Triassic formations up to several 100 meters, or forming intercalaction, interbeds and lenses in beds irregulary alternating with the surrounding limestones. They are present in numerous geological units, their cover sequences and tectonic nappes. The most significant are the Middle- and Upper- Triassic dolomites of Hronicum unit, bearing the important dolomite deposits in the Choč nappe of the Strážovská hornatina Highlands [6].

TECHNOLOGICAL RESEARCH OF SOURCE RAW MATERIALS

The geological-technological characteristics of dolomite deposits in Slovakia with suitable technological types for use in the production of Mg include specific conditions for the utilization of reserves for this purpose and also verification of homogeneity-technological stability in the entire volume of raw material in the deposit. [7].

The technological investigation, aiming to prepare the calcined products, appropriate for the silicothermic production was done applying dolomite samples. The prepared calcined products of dolomite samples from the several deposits: Trebejov, Dolný Lopašov, Trstín, Mníchova Lehota, Malé Kršteňany, Hubina and Rajec Šuja meet the required criteria. Concerning the required parameters, the CO_2 content varied within the range of 0.18% to 0.29%, content of further oxides (except CaO and MgO) was 0.81 to 2.23% and the ratio CaO:MgO was within the range 1.37:1 to 1.43:1 and thus met the required parameters [8]. The estimate of the sources of input raw materials (calcinated product) for the production of magnesium by the silicothermic method was made on the basis of the results achieved in the treatment of dolomites from specific deposits. Based on the laboratory-verified suitability of the prepared calcinated product and on the basis of experimental production of magnesium metal by the silicothermic method, an estimate of the sources of magnesium metal was made. With the estimated sources of dolomitic lime (164,023 kt) in the investigated deposits, according to the average recovery rate (77%) of the considered production method (Pidgeon method), approximately 31,270 kt of Mg metal can be potentially obtained [7]. From the final calcinated product of the sample from the Malé Kršteňany deposit, implemented into batch with ferrosilicon and calcium fluoride, the magnesium metal was produced with silicothermic method in laboratory condition. The detail study, applying the microprobe, has revealed the shrub shape of crystal intergrowths, the presence of lure magnesium metal in the central part and partly oxidic form of marginal, mainly apical parts (Fig. 2). The purity of the product was verified by microprobe up to 96% Mg.

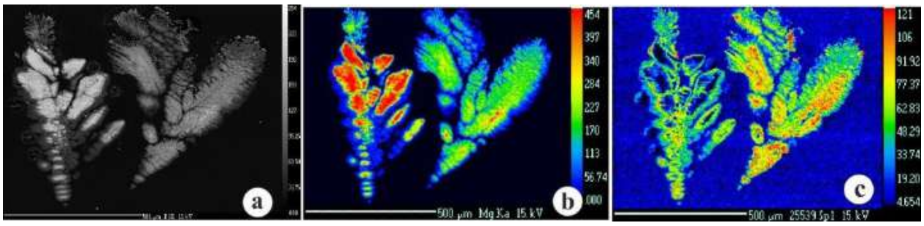

Figure 2 Habit of individual crystals of magnesium metal and their intergrowth (a - especially visible on BSE). Mg distribution map (b) and O distribution map (c). Photo: BSE images and distribution maps Konečný P.

This verified the suitability of the prepared intermediate product from a specific deposit in practice. Theoretically usable quantities of magnesium metal obtained from dolomite deposits indicate the possible multiple valorizations of this raw material [7]. The most significant potential source raw material for the production of Mg in Slovakia are dolomites. Currently known dolomite reserves in individual deposits are sufficient for this use. Dolomite is more suitable for the production of Mg, considering the possibilities of industrial applications of the source raw materials and the reserves and resources. The method of producing Mg from dolomite is more efficient with regard to economic (energy) and especially environmental aspects. The current price of 1 t of Mg is around 2,300 USD/t. According to some economic calculations, the profitable price should fluctuate around 2,500 to 3,000 USD per ton. The technological research of dolomite deposits in the vicinity of a potential producer of magnesium metal (OFZ a.s.) is underway. An important input in the Mg production process is ferrosilicon, which also represents the most financially and energetically demanding commodity. OFZ a.s. is direct producer of ferrosilicon, for the silicothermic process of Mg production it is necessary to provide calcinate, which does not represent high input financial costs.

CONCLUSION

The number of CRMs is constantly increasing, which means that their provision for the needs of the EU economy remains essential. An assessment of the potential of the Slovak Republic from the perspective of CRMs for the EU [1] pointed out the possibilities of using domestic raw materials. The potential of ore minerals in terms of possible rapid/immediate use is currently not realistic at present. The reason is mainly that – with the exception of one (precious metals – Banská Hodruša) – all deposits are closed. However, the potential is already quite interesting considering the reserves in registered ore deposits. The issue of critical minerals puts the deposits of Sb, Cu, W and Co metals, into the foreground, where we record reserves in our territory. Among the important raw materials of Slovakia, we can consider source raw materials for metal production, dolomites, magnesite (Mg) and quartz raw materials (Si). Such use represents a possible high valuation of these raw materials. For future final production, it is crucial to know its potential producer and to ensure the most comprehensive verification of the currently existing source raw material deposit in the given immediate environment in sufficient time in advance.

ACKNOWLEDGEMENT

This work was supported by the Slovak Research and Development Agency under the Contract no. APVV-21-0176. This material is also a contribution to the EuroGeoSurveys HORIZON-CSA Geological Service for Europe project.

REFERENCES

1. European Commission (2023) Study on the critical raw materials for the EU 2023 – Final report, Directorate-General for Internal Market, Industry, Entrepreneurship and SMEs, Grohol, M., Veeh, C., Publications Office of the European Union, 2023, https://data.europa.eu/doi/10.2873/725585
2. Bačo, P., Kollová (Bačová), Z., Németh, Z. (2018) Critical Raw Materials for the EU countries - potential in the Slovak republic, SGIDS, Bratislava, 39 p.
3. Gonda, S., Dzurenda, Š., Fajtová, D., Gluch, G., Miháľ, I., Mikušová, J., Pijaková, R., Pramuka, S., Radvanec, M., Stašík, Ľ. (2018) Surovinový potenciál Slovenskej republiky - analýza a prognózne prehodnotenie kritických nerastných surovín, (Raw material potential of the Slovak Republic – analysis and prognostic reassessment of critical raw materials) Final report. Manuscript. Bratislava, Archive SGIDŠ, 275 p. (In Slovak).
4. Kollová, Z., Bačo, P., Danková, Z., Čechovská, K., Fedorová, E., Bekényiová, A., Németh, Z., Kollárová, V., Mikušová, J., Gonda, S., Stašík, Ľ., Pijaková, R. (2023) Domáce zdroje surovín pre odvetvia obnoviteľnej energie a elektromobility, (Domestic sources of raw materials for the renewable energy and electromobility sectors) Final report. Manuscript. Bratislava, Archive SGIDŠ, 275 p. (In Slovak).
5. Šoltés, S., Kúšik, D., Mižák, J., Kubač, A. (2024) Nerastné suroviny SR 2023, ŠGÚDŠ, (Slovak Mineral Yearbook), ŠGÚDŠ, Bratislava, 220 p.
6. Zuberec, J., Tréger, M., Lexa, J., Baláž, P., (2005) Nerastné suroviny Slovenska, ŠGÚDŠ Bratislava, (Mineral resources of Slovakia), 350 p.
7. Bačo, P., Tuček, Ľ., Németh, Z., Kollová (Bačová), Z., Repčiak, M., Čechovská, K., Kovaničová, Ľ., Košuth, M., Marčeková, M. 2016: Potenciálne zdroje surovín na výrobu kovového horčíka, (Potential sources of source raw materials for Magnesium metal production) Final report, ŠGÚDŠ, archív Geofond, Bratislava, 117 p. (In Slovak)
8. Tomášek, K., Rabatín, R., Špeťuch, V., Šeševička, O., Urban, Ľ. & Siták, R., 1997: Spôsob využitia magnezitových surovín na výrobu horčíka. Úrad priemyselného vlastníctva SR, zverejnené 09.07.1997, C 22B 26/22; 5 p.

XVI International Mineral Processing
and Recycling Conference
28-30 May 2025, Belgrade, Serbia

DOI: 10.5937/IMPRC25359A
Original research article

SELF-FLOTATION OF GALENA IN A COMPLEX SULPHIDE ORE FROM A COPPER MINE IN NAMIBIA

Amalia Andreas, 0009-0003-1682-5357,
Titus Nghipulile[#], 0000-0003-4399-2620,
Godfrey Dzinomwa, 0000-0001-8763-699X,
Department of Civil, Mining and Process Engineering, Namibia University of Science and Technology, Namibia

ABSTRACT – The copper mine in Namibia, which processes a complex sulphide ore, faces a process challenge of high lead content in the copper concentrate. This study investigated the effectiveness of the self-flotation of galena in lowering the lead content in the copper concentrate by producing separate lead and copper concentrates. Differential flotation experiments were conducted with the first stage tailored for the self-flotation of galena (i.e., no lead collector was added). The effect of residence time during the self-flotation stage on Pb and Cu recoveries was investigated. The results showed an inverse relationship between lead recovery and residence time. Self-flotation of residence time of 20 seconds (lowest residence time tested) produced the best results. Incorporating a self-flotation stage made it possible to produce two quality concentrates of lead and copper. The concentrate had a copper recovery of only 2% and a lead recovery of 92%, while the copper concentrate had a copper recovery of 97% and a lead recovery of 5%. There is scope to optimise other operating parameters such as pH as well as the dosage conditioning time of the frother during self-flotation.

Keywords: Differential Flotation, Self-Flotation, Galena, Mine Sustainability.

INTRODUCTION

Copper is one of the critical metals needed for green transition and industrialisation, and it is thus expected that its demand will continue to increase [1]. Lead is needed for applications such as in construction (as an architectural metal), shielding in nuclear systems and batteries [2]. Copper in the ore body at the copper mine in Namibia exists in various minerals including chalcopyrite ($CuFeS_2$), bornite (Cu_5FeS_4), chalcocite (Cu_2S), Cuprite (Cu_2O), and malachite [3]. Galena and pyrite are also present in the ore body. Currently, the mine produces a copper concentrate as the product. In the past, a concentrate meeting the market specifications, in terms of permissible levels of impurities (i.e. 20 % Cu and above, less than 5 % Pb, and 10 % S and above), could be produced from the ore extracted from the ore zone with a grade of lead of less than 0.5% Pb. After the depletion of that ore, the mine shifted to a different zone with a lead grade ranging between 1 and 5% Pb [4]. This has resulted in copper concentrate having a lead content above the permissible concentration level of 5% Pb. Consequently, the mine

---

[#] corresponding author: tnghipulile@nust.na incurs high penalties when selling its concentrate to the smelters, which affects the mine's sustainability.

Several mines experienced the same challenge of high lead content in their concentrates. The main solution implemented was to apply differential flotation to produce the lead concentrate and the concentrate of the other sulphide mineral. One example is the Burgin Mine in North America, which had a high level of lead contamination in copper concentrate due to the presence of galena in the ore [5]. The mine incurred penalties when delivering its concentrate to the smelters**.** Differential flotation incorporating a stage of self-flotation of galena was applied at the mine to solve the problem. Self-flotation is a flotation process where the mineral naturally exhibits the ability to float without the need to add collectors. The same challenge of lead contamination in the zinc concentrate was experienced at Huize lead-zinc mine in China, and they also implemented differential flotation as a solution to the process challenge [6]. In Namibia, Rosh Pinah Zinc Corporation (RPZC) operates a lead-zinc mine where differential flotation is applied to produce lead and zinc concentrates [7]. Differential flotation to produce separate concentrates of the sulphide minerals has proven to be a viable processing option to reduce cross-contamination but also allow concentrators to sell two separate products to the smelters.

The study aimed to investigate the effectiveness of the self-flotation of galena to reduce the lead content in the copper concentrate by also producing lead concentrate. The effect of floating time on lead and copper recovery in the self-flotation stage was the key operating variable that was investigated.

MATERIALS AND METHODS

Sample preparation

Core drill samples of the Run-of-Mine (RoM) ore, weighing 87 kg, were used in the testwork. Some rocks were removed for mineralogical characterisation using optical microscopy to identify the mineral phases in the ore. The remainder of the sample was then crushed to 100% passing 2.5 mm using the laboratory gyratory crusher. The crushed sample was then homogenised using the 'coning and quartering' method before a rotary splitter was used to sub-divide the crushed sample into sub-samples used for chemical analysis, particle size analysis, milling and flotation.

Ore mineralogical characterisation

Mineralogical characterisation using optical microscopy of the uncrushed ore sample was done at the NUST Metallurgy laboratory to identify the mineral phases present in the ore and to deduce other mineralogical characteristics such as mineral association.

Thermo Scientific iCAP PRO Series Inductively Coupled Plasma Optical Emission Spectroscopy (ICP-OES) spectrometer and Thermo Scientific X-Ray Fluorescence (XRF) machine were used to determine the chemical composition of the ore. Three head samples were assayed. For XRF analysis, the Niton coin with a known composition was used as a reference material for validation purposes. The ICP OES used has a detection limit of 0.001% on copper, zinc, and lead, while for silver, the detection limit is 5g/t. For the rest of the elements, the detection limit is 0.002%. For ICP calibration, multi-standards were used to generate calibration curves. Quality control (QC) standards were used every time before the analysis to ensure that the results obtained were accurate. Solutions analysed on ICP were prepared using a four-acid digestion method. A solid sample of 0.5 g was placed in a 100 ml beaker. A mixture of 10 ml Nitric acid (HNO_3), 10 ml Perchloric acid ($HClO_4$), and 5 ml Hydrofluoric acid (HF) was added to the beaker with the sample before boiling the mixture until it dried up. When the mixture has dried up, it is then cooled before adding 10 ml of hydrochloric acid (HCl) and 10 ml of distilled water. The new mixture is boiled for 10 minutes. After 10 minutes, the solution is cooled and transferred into a 100 ml volumetric flask, which is filled with distilled water to the 100 ml mark. This solution was then taken for ICP analysis to quantify the elements in the sample.

To quantify the oxide and sulphide minerals for copper in the ore, acid leaching was done using sulphuric acid. This information was crucial to determine the flotation reagent suite. Samples of 0.5 g were leached for 60 minutes in a 100 mm beaker. After leaching was complete, the mixture was filtered, and then the pregnant leach solution (PLS) was assayed using the ICP to calculate the leaching efficiency of Cu.

Milling curve

Before the milling tests were conducted, the size distribution of the crushed ore was determined by wet screening two 1 kg samples on 2280, 250, 150, and 75 µm using the mechanical sieve shaker. The samples retained on each sieve, as well as the undersize of 75 µm, were dried in the oven at the temperature of 95˚C before they were weighed. The laboratory mill, whose specifications are listed in Table 1, was used to grind four 500 g samples for the residence times of 11, 21, 31 and 41 minutes respectively. The milling tests were conducted to generate the milling curve of the ore (i.e., cumulative percent passing 75 µm against grinding time) which was used to estimate the milling time yielding the target flotation feed size of 80% passing (P_{80}) 75 µm (this was benchmarked to the mine which supplied the sample). The milling time was established to be 32 minutes. This was used to mill the flotation feeds.

Table 1 Mill specification and milling conditions

Parameters	Unit	Value
Mill internal diameter	cm	26
Mill internal length	cm	42
Operating speed, N	rpm	67
Slurry density	% solids	29.3
Ore SG	-	2.85
Steel ball diameter	mm	38
Mass of steel balls	kg	33.3
Composition of steel balls	-	30% chromium

Flotation procedures

The Denver flotation machine, fitted with a 1.5 L cell, was used to conduct the flotation experiments shown in Figure 1. The schematic in Figure 1 shows the differential flotation of Pb concentrate in Stage 1 and Cu concentrate in Stages 2. No lead collector was added in Stage 1, as illustrated in Figure 1. Potassium amyl xanthate (PAX) as a collector for copper sulphide minerals was added in Stage 2 at the dosage level shown in Figure 1. Pine oil was added as the frother, and its dosage levels in the two stages are also shown in Figure 1. The pH was not adjusted. The natural pH ranged between 7.8 and 8.04. The operating parameter that was varied during the testwork was the flotation time in Stage 1. It was varied at 20, 30, 40, 50 and 60 seconds. The residence time of Stage 2 is the difference between the total flotation time of 7 minutes (constant in all tests) and the flotation time of Stage 1. The scalping of the concentrate was done every 10 seconds in all stages. The impeller speed and airflow rate were kept constant at 1000 rpm and 5 L/min respectively. Tap water was used to prepare the slurry for flotation, and deionized water was used to make up the solution of PAX. In all flotation tests, the concentrates and tailings were filtered using the filter press, dried in the oven set at a temperature of 95°C, and then weighed before subsampling for chemical analysis and assayed using ICP. All flotation tests were performed in duplicate to assess reproducibility.

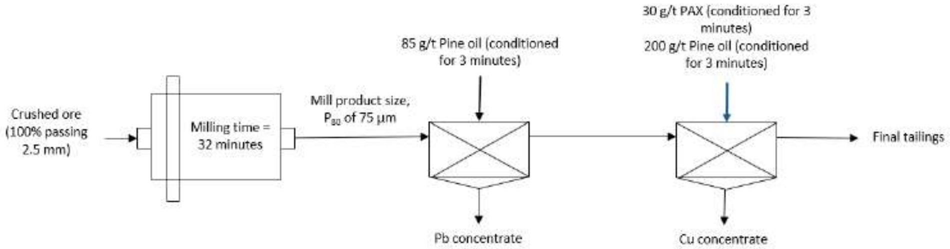

Figure 1 Scope of work for differential flotation of Pb and Cu concentrates

RESULTS AND DISCUSSION

Chemical and mineralogical composition of the ore

Table 2 shows the ICP assays for the three head samples. It can be observed that the ore had a copper-to-lead ratio of 1:1. Copper minerals (bornite and chalcopyrite) and galena (Pb mineral) were identified using optical microscopy in the ore, as shown in the micrograph in Figure 2. The co-existence of copper and lead sulphides presents a challenge during flotation due to their similar electrochemical behaviour [8]. Similar electrochemical behaviour is the main cause of cross-contamination in the sulphide concentrates [9] . Table 3 shows the leaching efficiencies (calculated from Cu assay in the PLS) for three head samples. The average leaching efficiency of copper was 4.5%. Since the leaching efficiency is for the copper associated with the oxide mineral(s), the result suggests that 95.5% of the copper in the ore is associated with the sulphides. Given the low concentration of oxide copper in the ore, no sulphidiser was added during the flotation testwork.

Table 2 ICP assays for the head samples

Head sample	(%)						(g/t)	(%)
	Pb	**Cu**	**Fe**	**Ca**	**Mg**	**As**	**Ag**	**Others**
1	1.10	1.25	1.05	19.19	5.33	0.64	13.12	72.54
2	1.01	1.08	0.96	18.97	5.57	0.65	9.62	71.76
3	1.09	1.12	1.03	19.14	5.51	0.65	10.30	71.46

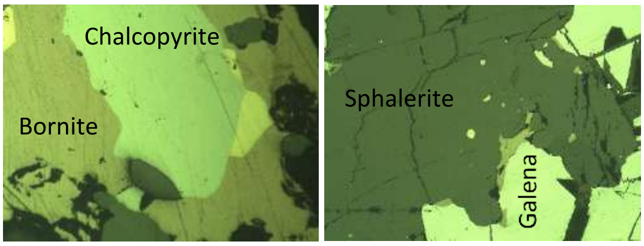

Figure 2 Micrographs from optical microscopy of the ore, magnification is x10 for both

Table 3 Leaching efficiency of copper in the ore

Sample	Leaching efficiency (%)
1	3.834
2	4.795
3	4.978
Average	**4.536**

Differential flotation incorporating self-flotation stage

Figure 3 shows the recoveries of copper, lead and iron for the flotation tests with different residence times during Stage 1 (self-flotation). Figure 4 shows the recoveries of copper, lead and iron during Stage 2. The residence time of Stage 2 is the difference between the total flotation time of 7 minutes and the flotation time of Stage 1. It can be observed in Figure 3 that the recovery of Pb in Stage 1 decreases with the residence time. This suggests that, for residence time greater than 20 seconds, the galena particles dissociate from the air bubbles in the froth and fall back into the pulp. On the other hand, the recoveries of copper and iron in Stage 1 are low, and they generally increase with the residence time. The lowest residence time of 20 seconds yielded the highest recoveries of 92% and 2% for Pb and Cu respectively. The results for Stage 2 in Figure 4 show the expected opposite trends for the recoveries of Pb and Cu. For example, the copper concentrate produced in the second stage after 20 seconds residence time in Stage 1 has the recoveries of 97% and 5% for copper and lead respectively. The chemical compositions of the lead and copper concentrates and tailings produced when the flotation time during self-flotation was 20 seconds are shown in Table 4. The grade of the concentrates can further be improved in the cleaning stages. The results from the study demonstrate that the self-flotation method can be applied to galena to produce two separate concentrates of copper and lead.

Table 4 Chemical composition of concentrates and tailings

Product	**Elemental composition (%, except Ag, which is given in ppm)**			
	Cu	**Pb**	**Fe**	**Ag**
Pb concentrate	0.218	8.158	1.118	9.424
Cu concentrate	2.607	0.131	1.947	24.879
Final tailings	0.129	0.045	0.134	0.500

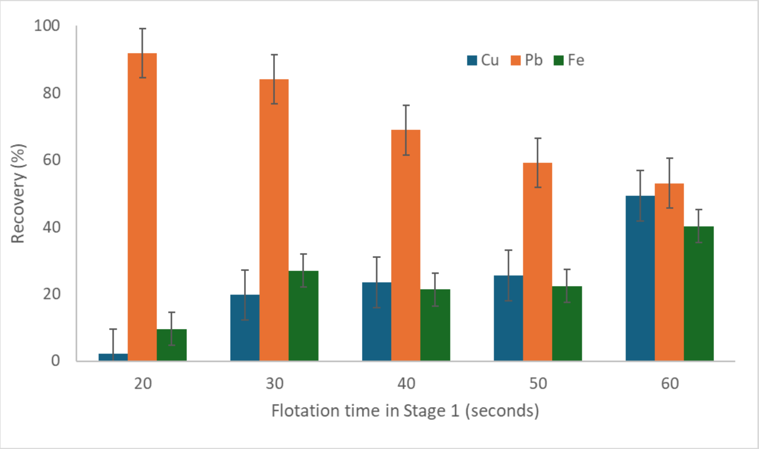

Figure 3 The effect of floating time vs. the recoveries of Cu, Fe and Pb in lead concentrate from self-flotation

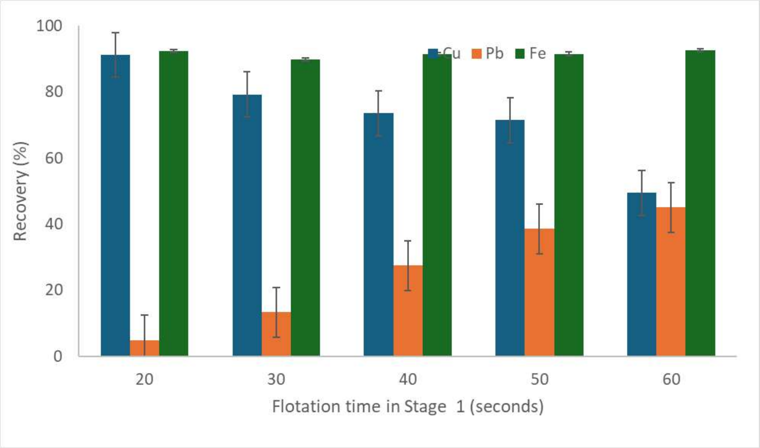

Figure 4 The effect of floating time vs. the recoveries of Cu, Fe and Pb in copper concentrate from self-flotation

Figures 5A and 5B show the grade-recovery curves of Cu, Pb and Fe for the lead and copper concentrates respectively. It is evident that for all three metals, there is a linear relationship between the concentrate grades and recoveries. From Figure 5A (Pb concentrate), the higher recoveries and grades of Pb are evident, while the recoveries and grades for Cu and Fe are comparable. The opposite trends can be observed in Figure 5B (Cu concentrate), where the recoveries and grades of Pb are lower compared to those of Cu and Fe. It can be concluded that Pb-bearing minerals can be selectively separated from the minerals of Cu and Fe. The separation of Fe mineral(s) from Cu mineral(s) can be optimized in Stage 2 (see Figure 1) and subsequent cleaning stage(s) to ensure the level of Fe in the copper concentrate is within the market specifications. The relationship between the mass pull and recoveries of Cu, Pb, and Fe are shown in Figure 6. It can be observed that the recovery of lead decreases as the mass pull of lead concentrate increases. However, the recoveries of copper and iron increase as the mass pull for lead concentrate increases. The trends are a result of the trends already shown in Figure 3, which demonstrate that the residence time is a key operating variable affecting the effectiveness of the selective self-flotation of galena.

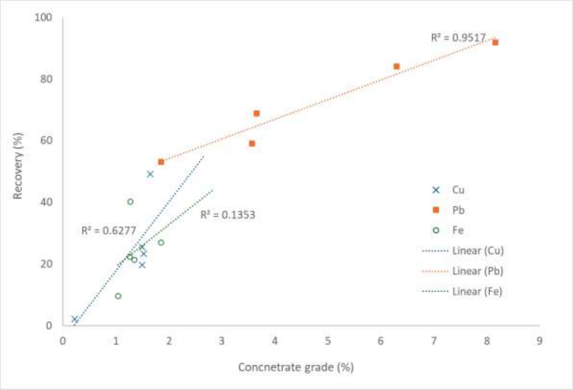

A: Lead concentrate

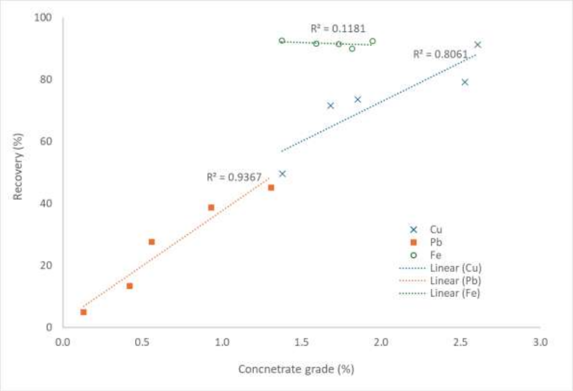

B: Copper concentrate

Figure 5 Grade-recovery curves of Cu, Pb and Fe in lead and copper concentrates

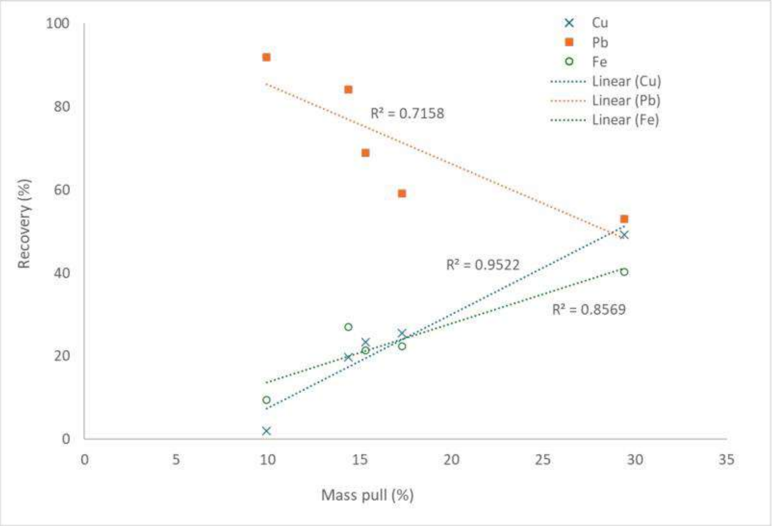

Figure 6 Relationship between recoveries of Cu, Pb and Fe and the mass pull during Stage 1 (lead concentrate)

CONCLUSION

A series of batch flotation experiments were conducted on the complex sulphide ore with the copper-to-lead ratio of 1:1. The main aim was to evaluate the effectiveness of the self-flotation of galena to allow the production of high-quality concentrates of lead and copper. Optical microscopy revealed that the ore has chalcopyrite, bornite, galena, and pyrite. Chalcopyrite is an abundant copper mineral. Self-flotation effectiveness as the beneficiation method for lead was investigated for different residence times in the range of 20 to 60 seconds. The results showed that there is an inverse relationship between lead recovery and residence time. Self-flotation of residence time of 20 seconds produced the lead concentrate (assaying 0.22% Cu, 8.16% Pb, 9.42 ppm Ag and 1.12% Fe) with recoveries of 2% copper and 92% lead. The copper concentrate (assaying 2.61% Cu, 0.13% Pb, 24.9 ppm Ag and 1.95% Fe) was produced with the recoveries of 91% and 5% for copper and lead respectively. The final tailings produced assayed 0.13% Cu, 0.045% Pb, 0.50 ppm Ag and 0.13% Fe. There is scope to optimise other operating parameters such as pH, as well as the dosage and conditioning time for the frother during the self-flotation stage.

The findings from the study demonstrated that the process challenge of high lead content in the copper concentrate can be addressed by retrofitting the self-flotation stage in the processing plant. The production of lead concentrate not only solves the process challenge at the mine but can also boost revenue generation from the sale of the by-product (lead concentrate), thus improving the sustainability of the mine.

ACKNOWLEDGEMENT

The authors are grateful to the plant manager and the rest of the management team at the mine for allowing the first author to conduct testwork and chemical analysis on site. We also acknowledge Mrs Jacqueline Kurasha and Prof Benjamin Mapani in the Department of Civil, Mining, and Process Engineering at Namibia University of Science and Technology for their assistance with microscopic analysis.

REFERENCES

1. Schroeder, W., Reller, A. (2013) Copper for sustainable development. Metals & Materials Society (TMS), vol. 65, no. 4.
2. Boldyrev, M. (2018) Lead: properties, history, and applications. WikiJournal of Science, pp. 12-13.
3. Lacaze, R., Venter, J. (2014) Kombat Mine: A historical overview of copper mining and challenges faced. Mineral Resources Review, vol. 47, no. 4.
4. Richard, A. (2024) Changes in Ore Body Composition at Kombat Mine: A Shift to Higher Lead Content. Journal of Mining Practices, vol. 42.
5. Corporation, K. U. C., (1978) Annual report 1978. Kennecott Utah Copper Corporation.
6. Song, S., Zhang, Z. (2016) Flotation separation of galena from sphalerite in the Huize lead-zinc ore. Minerals Engineering, vol. 94.
7. Diedericks, A. W., Fouche, P. A. P., Badenhorst, S. N. (2003) A systems approach in implementing Minerals Resource Management at a base metal mine (Rosh Pinah Zinc Corporation, Namibia). Journal of the South African Institute of Mining and Metallurgy, vol. 103, no. 1, pp. 11-18.
8. Somasundaran, A. (1990) The role of surface chemistry in the flotation of copper minerals. In Surface Chemistry of Froth Flotation.
9. Luo, Y., Zheng, Z. (2009) Electrochemical studies of sulfide minerals in flotation systems. Journal of Electro analytical Chemistry, vol. 632, no. 1-2.

XVI International Mineral Processing
and Recycling Conference
28-30 May 2025, Belgrade, Serbia

DOI: 10.5937/IMPRC25368R
Original research article

PROCESSING OF FINE LITHIUM MINERAL TAILINGS

Janine Rodrigues Figueiredo[#], 0000-0003-1396-7889,
Érica Linhares Reis, 0000-0003-3760-9904,
Arthur Silva de Oliveira, 0009-0008-8987-6573,
Federal University of Ouro Preto, Ouro Preto, Brazil

ABSTRACT – Spodumene is a primary lithium source found in pegmatite deposits, typically associated with tantalite, cassiterite, quartz, and albite. Common processing methods for spodumene include dense medium separation (DMS), magnetic separation, and flotation. DMS exploits differences in specific density among minerals; however, the similar densities of spodumene and gangue minerals pose significant challenges to this method. This research aims to assess the potential of using DMS, as a processing method, to recover lithium from fine tailings generated by a tantalite processing plant in Brazil. Heavy liquid separation (HLS) tests were conducted on fine particle size fractions (850/150 µm), yielding high-grade lithium concentrates with up to 4.40% Li_2O. These results highlight the potential for DMS in the processing of fine lithium-bearing minerals.

Keywords: Spodumene, Lithium Recovery, Dense Media Separation, Processing.

INTRODUCTION

Lithium mineral processing plants typically encompass several stages, including comminution, dense medium separation, flotation, magnetic separation, and gravity concentration. Dense medium separation (DMS) is commonly employed as a pre-concentration stage in processing coarse size fractions (+850 µm) of spodumene, to separate gangue minerals before grinding [1]. According to Tadesse *et al*. [2], following the particle size adjustment through grinding and size classification, a gravity separation stage can be implemented to recover coproducts of tantalite and cassiterite. The flotation stage is essential for processing fine particles and generating high-grade concentrates, ensuring the successful flotation and separation of spodumene from the tailings. Ultimately, a magnetic separation stage may be required to remove substantial quantities of iron oxide-containing gangue minerals, for the final lithium concentrate. While there has been considerable advancement in studies related to spodumene concentration via flotation [3], relatively few studies discuss the concentration of spodumene using DMS [1].

Pegmatite processing using DMS can be complex due to the small difference in specific gravity between valuable and gangue minerals found in pegmatites. The specific gravity of spodumene ranges from 3.1 and 3.2 g.cm^{-3}, making it slightly heavier than most gangue minerals, including quartz (2.65 g.cm^{-3}), albite (2.60 g.cm^{-3}), and muscovite (2.8

[#] corresponding author: janine.figueiredo@ufop.edu.br g.cm^{-3}). Consequently, spodumene can sink in a dense medium with a suitably matched specific gravity, while gangue minerals will float [2].

This paper aims to evaluate the feasibility of using DMS as a spodumene concentration method, for minerals derived from fine tailings (-850 µm) from a tantalite processing plant. The analysis consists of tailings characterization through chemical and mineral analysis. Then, heavy liquid separation (HLS) laboratory tests using Bromoform were executed in different particle size fractions to determine the distribution of Li_2O in the sink and float products.

EXPERIMENTAL

Case study

The case study focuses on lithium fine tailings from a tantalite mineral processing plant of the Volta Grande mine, located in Nazareno in Minas Gerais state, Brazil. Nazareno lies within the Pegmatitic Province of São João del Rei, which hosts numerous pegmatitic bodies mineralized, with elements Sn, Nb, Ta, and Li. Commonly found minerals include spodumene, cassiterite, tantalite, columbite, and microlite. The Li-enriched pegmatitic bodies are particularly concentrated in the Nazareno region and named the Volta Grande pegmatite swarm [4]. The main products of this operation are tantalite and cassiterite, with lithium being a byproduct derived from reprocessing pegmatite tailings. Currently, lithium concentrates are produced by flotation and magnetic separation techniques.

Sample Preparation

About 20 kg of tailing samples were collected from the tantalite processing plant from the Volta Grande mine. A head sample of 2 kg was split into representative subsamples for chemical and mineral analysis, and heavy liquid separation (HLS) tests. Then each subsample was screened into five size fractions: +850 µm, -850/ +500 µm, -500/ +297 µm, -297/ +149µm, and -149 µm.

Particle Size Analysis

Particle size distribution was carried out by wet sieving, performed on a series of Tyler sieves. The minimum mass of a representative sample, according to Pierre Gy's Theory, and the maximum mass to be retained on each screen were determined a total mass of 160 g. The wet sieving was done through the following process: first wet sieving (-37 µm/+2360µm); the oversized material of each screen was filtered using a porous filter paper, dried, and weighed.

Mineral Analysis

The qualitative mineral identifications of the samples were performed by X-ray diffraction (XRD) using the total powder method. The samples for mineralogical characterization were prepared in powder form, by pulverization and homogenization of each sample. An X-ray diffractometer equipped with a copper tube (λ = 1.5406 Å) was used; the analysis was performed considering a 2θ array scan in the range of 5 to 90º, with an operating voltage of 45 kV, current intensity of 40 mA and collection time equal to 15 minutes. The diffractograms were obtained using specific software (X-ray Data Collector) and their interpretation was performed with the aid of another software (HighScorePlus), using the ASTM standard diffractogram database.

Chemical Analysis

The chemical content was determined by Inductively Coupled Plasma Optical Emission Spectroscopy (ICP-OES). The samples were pulverized and dissolved in appropriate acids to convert target elements into a liquid solution. The solution was then filtered to remove solid residues and diluted with a suitable solvent to adjust element concentrations for ICP-OES detection. The sample prepared was introduced into the equipment via a nebulizer, generating a fine aerosol directed to the plasma torch. The data obtained were compared with reference standards for precise concentration determination.

Heavy Liquid Separation Tests

The heavy liquid separation (HLS) tests were performed with Bromoform (2.89 g/cm^3), under a laboratory fume hood. Due to chemical toxicity, personal protective equipment was used.

The tests were conducted in duplicate for the particle size fractions +850 µm, -850/ +500 µm, -500/ +297 µm, -297/ +149µm, and -149 µm. For each HLS test, approximately 20 g sample mass was added into 50 mL of Bromoform, using a separatory funnel to separate the heavier (sink) material from the light (float) material. Then, the material was stirred gently, every two minutes, to release the particles. After minerals separation, the sink material was removed by opening the funnel. The Bromoform was recovered by passing through the funnel opening, and therefore the float material was also recovered. The sink and float fractions were filtered using a glass funnel with filter paper, washed with ethyl alcohol to remove the Bromoform residues, and dried at room temperature. The sink and float products were weighed, and subsamples were taken for chemical and mineral analysis.

RESULTS AND DISCUSSION

Particle Size Analysis

Particle size analysis of the head sample allows an understanding of the distribution of grain sizes of tailings. Figure 1 shows that 80% of particles were smaller (P_{80}) than 869 µm, which is interesting for this study (evaluate the feasibility of processing lithium minerals below 850 µm); on the other hand, a coarser fraction is above 870 µm; and 50% of the particles are passing (P_{50}) in 360 µm.

Mineral Analysis

According to the XDR results shown in Figure 2, the main minerals to separate from the spodumene ($LiAl(SiO_3)$) are: quartz (SiO_2), albite ($NaAlSi_3O_8$), muscovite, ($KAl_3Si_3O_{10}(OH)_2$), and microcline ($K(AlSi_3O_8)$). The intensity of the diffraction peaks indicates that quartz is the predominant mineral, suggesting that the tailings from the Volta Grande mine still contain a significant amount of free silica. The presence of albite and microcline indicates the presence of feldspars minerals, commonly found in pegmatites and granites. Although, spodumene has less intense peaks is related to a low concentration in the tailings. Additionally, the detection of muscovite implies the presence of phyllosilicate minerals, which could potentially impact a dense media separation process.

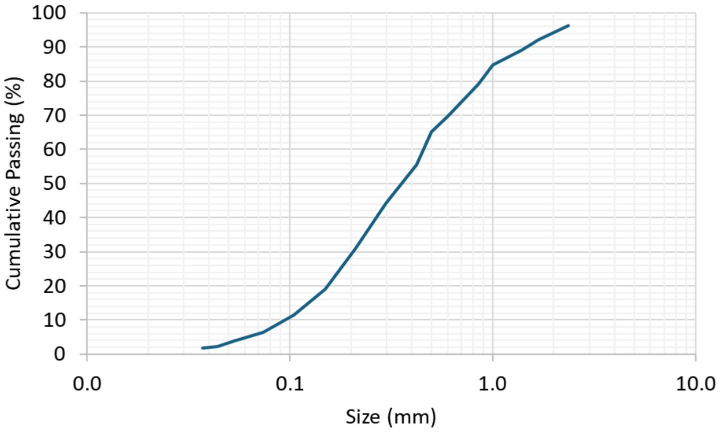

Figure 1 Particle size distribution of the tailing head sample from the Volta Grande mine

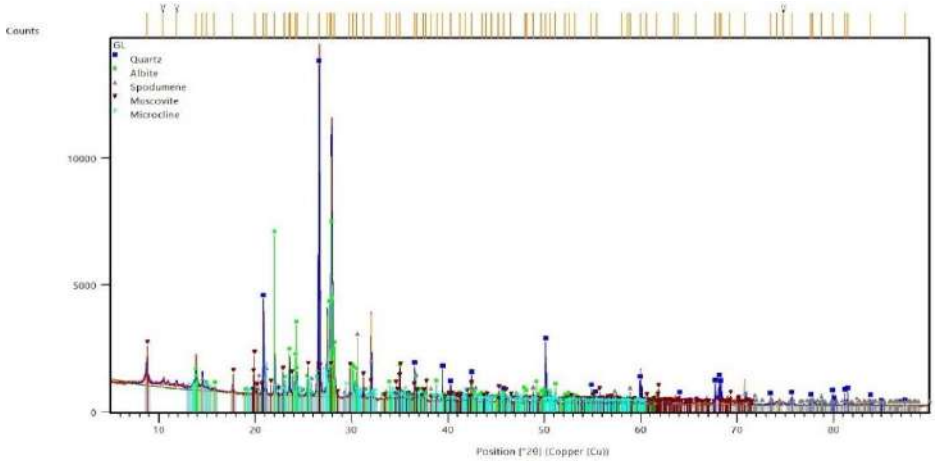

Figure 2 XRD mineral analysis of tailings head sample from the Volta Grande mine

Mineral Analysis

Chemical analysis confirmed the presence of the main minerals identified in the XRD analysis. The ICP-OES analysis detected the presence of SiO_2, Al_2O_3, Na_2O, and K_2O as the most abundant chemical components in the tailings head sample, as shown in Table 1.

Table 1 Chemical results (%) of the tailings head sample, as measured by ICP-OES

SiO_2	Al_2O_3	Fe_2O_3	Na_2O	K_2O	CaO	P_2O_5	MgO
71.74	14.58	1.13	5.20	2.12	1.10	0.19	0.47
MnO	**TiO_2**	**F**	**Ta_2O_5**	**Nb_2O_5**	**Sn**	**S**	**Li_2O**
0.18	0.08	0.19	1.60	0.28	1.23	0.02	1.05

The high silica content suggests that the tailings fraction consists of a substantial amount of non-lithium-bearing minerals. The grade of Fe_2O_3 indicates the presence of impurities in silicate minerals, which may influence the processing choice. A magnetic separation stage might be necessary if the material is intended for ceramics. According to Banks *et al*. [5], the spodumene concentrate should ideally contain less than 0.5% Fe_2O_3; however, regarding lithium extraction through chemical processing, Fe_2O_3 is not a significant concern.

The chemical components P_2O_5, F, and S may indicate the presence of phosphate minerals, fluorapatite, and sulfides, respectively. Fluorine may be associated with spodumene or the presence of residual fluorite.

The chemical analysis shows that valuable economic metals (Ti, Ta, Nb, Sn, and Li) are also present given that it is a tailing sample from tantalite and cassiterite concentration plants. The tailings have economic potential in lithium recovery, which may justify reprocessing. But, also, Ta_2O_5, Nb_2O_5, and Sn remain in the tailings, which may justify reprocessing to increase tantalum, niobium, and tin recovery.

Results from the granulochemical analysis of the head sample (Figure 3) identified higher grades of SiO_2 in all fractions (+850/ -149 µm), and slightly higher of Al_2O_3. Related to the lower-grade components, Na_2O has the highest content in all size fractions. Finally, Li_2O has a higher grade in the fraction +850 µm.

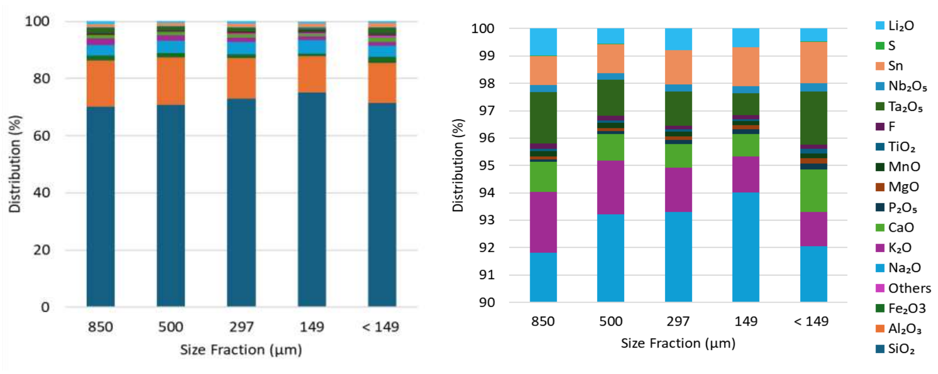

Figure 3 Granulochemical analysis of tailings head sample of the Volta Grand mine

HLS Tests

Spodumene was separated from gangue minerals in the HLS tests using Bromoform. The distribution of Li_2O in dense medium products of different size fractions was determined based on the chemical content of this element provided by ICP-OES. The HLS test results are shown in Table 2, which contains the Li_2O distribution (%) for float and sink products, in different size fractions.

Table 2 Results for the HLS tests of different particle size fractions in Bromoform

Size Fraction (µm)	Products (%)	Weight (%)	Li_2O (%)	Li_2O Distribution (%)
+850	< 2.89	67.13	0.12	5.10
	> 2.89	32.87	4.56	94.84
	Total	100.00	1.58	100.00
Size Fraction (µm)	**Products (%)**	**Weight (%)**	**Li_2O (%)**	**Li_2O Distribution (%)**
-850/+500	< 2.89	72.55	0.18	9.53
	> 2.89	27.45	4.52	90.52
	Total	100.00	1.37	100.00
Size Fraction (µm)	**Products (%)**	**Weight (%)**	**Li_2O (%)**	**Li_2O Distribution (%)**
-500/+297	< 2.89	76.89	0.07	5.13
	> 2.89	23.11	4.40	96.77
	Total	100.00	1.05	100.00
Size Fraction (µm)	**Products (%)**	**Weight (%)**	**Li_2O (%)**	**Li_2O Distribution (%)**
-297/+149	< 2.89	83.93	0.14	17.03
	> 2.89	16.07	3.56	83.00
	Total	100.00	0.69	100.00
Size Fraction (µm)	**Products (%)**	**Weight (%)**	**Li_2O (%)**	**Li_2O Distribution (%)**
-149	< 2.89	83.95	0.30	37.04
	> 2.89	16.05	2.67	63.06
	Total	100.00	0.68	100.00

A strong negative correlation exists between the Li_2O grade, the particle size fractions, the sink products, and the liberation of Li_2O minerals. Namely, lithium has a higher content in the coarser size fractions, as well as a greater distribution in the sink products as the granulometry increases, consequently its liberation.

Regarding the Li_2O distribution, over 90% of lithium is concentrated in the heavy fraction, demonstrating a high separation efficiency level, particularly for the size fractions: +850 µm; -850/ +500 µm; and -500/ +297 µm. In these size fractions, only about 5% of the lithium was found in the float fraction, indicating minimal loss in the tailings. Also, the sink fraction (> 2.89 g/cm³) concentrates most Li_2O, with grades above 4.40%. On the other hand, the float fraction (< 2.89 g/cm³) has low grades of Li_2O (between 0.07% and 0.18%).

In finer size fractions (-297/+149 and -149 µm), lithium content and distribution in the sink product decreases, possibly due to an increased feldspar content, as suggested by the granulochemical analysis. As noted by Banks *et al.* (1953), when spodumene content decreases, feldspar content increases. This is significant because feldspar may be an important byproduct of the process and can be further recovered.

CONCLUSION

This paper aims to evaluate the feasibility of processing fine lithium mineral tailings using the dense medium separation method. Although many studies have investigated the application of DMS for the pre-concentration of spodumene in coarser particle size fractions (+ 840 µm), this work is unique in studying DMS applied to fine lithium tailings particles (- 840 µm).

The results of the HLS tests suggest that Dense Medium Separation (DMS) has the potential to effectively separate spodumene from gangue minerals such as quartz, albite, microcline, and muscovite. Most of the Li_2O content was found in the sink fraction (greater than 2.89 g/cm^3), whereas the float fraction exhibited low lithium contents. By adjusting the medium density according to particle size, it may be possible to further enhance the separation efficiency. Therefore, the reprocessing of tailings from the Volta Grande mine using DMS has the potential to be further used to improve the recovery of valuable metals.

ACKNOWLEDGEMENT

This work was funded by FAPEMIG and the FINEP in Brazil. The first author thanks the National Council for Scientific and Technological Development (CNPq) for financial support. We also appreciate AMG Mining for providing tailings samples and ICP-OES analysis from the Volta Grande Mine.

REFERENCES

1. Gibson, C.E., Aghamirian, M., Grammatikopoulos, T., Smith, D.L., Bottomer, L. (2021) The recovery and concentration of spodumene using dense media separation. Minerals, 11 (649), 1-17.
2. Tadesse, B., Makuei, F., Albijanic, B., Dyer, L. (2019) The beneficiation of lithium minerals from hard rock ores: A review. Minerals Engineering, 131, 170-184,
3. Filippov, L., Farrokhpay, S., Lyo, L., Filippova, I. (2019) Spodumene flotation mechanism. Minerals, 9(6), 372-383.
4. Lagache, M., Quéméneur, J. (1997) The Volta Grande pegmatites, Minas Gerais, Brazil: an example of rare-element granitic pegmatites exceptionally enriched in lithium and rubidium. The Canadian Mineralogist, (35), 153-165.
5. Banks, M., McDaniel, W., Sales, P. (1953) A method to concentration of spodumene from North Carolina pegmatite ores. Mining Engineering, 181-186.

XVI International Mineral Processing
and Recycling Conference
28-30 May 2025, Belgrade, Serbia

DOI: 10.5937/IMPRC25375S

Original research article

EXPLORING ELECTROHYDRAULIC FRAGMENTATION FOR PROCESSING ELECTRIC ARC FURNACE SLAGS

Theodor Steller[1#], 0009-0007-0940-377X,
Stefan Eisert[2], 0009-0006-3563-6975,
Bernd G. Lottermoser[1], 0000-0002-8385-3898,
[1]Institute of Mineral Resources Engineering, RWTH Aachen University,
Aachen, Germany
[2]ImpulsTec GmbH, Radebeul, Germany

ABSTRACT – Electric arc furnace slags (EAFS) are steelmaking by-products rich in valuable metals such as Fe, Mn and Cr. As the steel industry moves towards decarbonization and increases the use of electric arc furnaces, the generation of EAFS is expected to rise, highlighting the need for efficient metal recovery to support waste reduction and circular economy goals. Conventional mechanical processing methods often cannot effectively separate metals from other slag components. This study conducted geochemical, mineralogical, and structural characterization of EAFS to assess the suitability of electrohydraulic fragmentation (EHF) for processing. Mineral Liberation Analysis (MLA) results showed that EAFS comprises finely intergrown magnetic, Fe-rich oxide phases and non-magnetic, Ca-rich oxide and silicate phases with mean grain sizes of <60 µm. EHF was applied to enhance the liberation of metal phases, followed by sieving and magnetic separation. EHF effectively liberated granular metal components in coarse grain fractions (>1 mm), while chemical analysis found no significant enrichment of Fe in magnetic fractions for smaller grain sizes. The findings indicate that combining EHF with sieving and magnetic separation may effectively enhance metal recovery from EAFS. This integrated approach offers a promising method for recycling slag waste and contributes to sustainable practices in the steel industry.

Keywords: Electrohydraulic Fragmentation, Electric Arc Furnace Slags, Metal Inclusions, Mineral Liberation Analysis, Magnetic Separation.

INTRODUCTION

Electric arc furnace slags (EAFS) are the most significant by-products generated during steelmaking in electric arc furnaces, which primarily recycle metal scrap to produce steel. In 2018, approximately 103 million tonnes of EAFS were produced globally [1]. This number is expected to rise in the future as the steel industry transforms towards low-carbon processes by increasing the use of electric arc furnace technology to meet international climate and environmental goals. Currently, EAFS are mainly reused in the construction industry, serving as aggregates in bituminous mixtures for road construction and as additives in cement and concrete [2,3]. While these applications provide a

---

[#] corresponding author: steller@mre.rwth-aachen.de sustainable outlet for EAFS, their potential may not be fully exploited, especially regarding the recovery of valuable resources. Conventional crushing and magnetic separation techniques often cannot fully separate metal and slag materials. As a result, while the chemical compositions of EAF slag can vary widely, they often contain high amounts of valuable metals, such as Fe (10-50 wt.% FeO) and Mn (3-8 wt.% MnO) as well as significant concentrations of Cr_2O_3 and V [4,5]. These metals are usually incorporated in oxides and silicates; however, elemental iron may also be present [6]. Consequently, exploring reprocessing techniques to recover these metals may offer economic benefits, reduce the demand for primary raw materials, improve recycling rates, and promote a circular economy, aligning with the EU's Circular Economy Action Plan on waste reduction and resource efficiency.

Here, one potential alternative processing method in electrohydraulic fragmentation (EHF) is explored, which utilizes high-voltage electrical discharges in a fluid medium to generate mechanical shockwaves that preferentially fragment materials along mechanical weak points, such as interfaces of materials with different acoustic properties, e.g., grain boundaries, allowing for high material selectivity [7]. This process can enhance the liberation of individual grains, establishing a basis for magnetic- or gravity-based separation methods. EHF has been successfully applied to selectively comminute various composite materials and recover valuable components from electronic waste, such as photovoltaic panels, as well as for the fragmentation of rocks [7,8]. To optimize the application of EHF for EAFS processing, comprehensive characterization of the slags regarding phase composition and distribution, grain sizes, and overall microstructural information is essential for adjusting EHF process parameters, such as energy input and pulse frequency, and therefore to enhance the efficiency and selectivity of the fragmentation process. By effectively liberating metal-rich phases from the slag matrix, the EHF process may improve metal recovery rates, offering a more sustainable and economically viable method for processing EAFS.

EXPERIMENTAL

Materials

Approximately 500 kg of EAFS representing the 0/32 mm fraction (charge ID: FG02) were collected from a German slag processing facility. The bulk material was thoroughly homogenized to obtain representative subsamples suitable for analytical procedures and EHF processing.

Mineral Liberation Analyses

Automated SEM analysis was performed using Mineral Liberation Analysis (MLA) on a polished, carbon coated, epoxy-embedded block (measurement area: 22.5 x 22.5 mm) of EAFS sample FG02/1 at ERZLABOR Advanced Solutions GmbH, Freiberg, Germany. The Grain X-ray Mapping (GXMAP) measurement mode was used, which combines X-ray mapping with grey-level analysis from backscattered electron (BSE) imaging to enhance slag phase discrimination for phases with similar BSE contrasts, allowing for phase distribution mapping. The analysis was conducted using appropriate measurement parameters as shown in Table 1.

Table 1 Summary of MLA measurement parameters

Voltage	Emission current	BSE image calibration	Working distance	MLA single image size	BSE single image size	BSE image resolution
25 kv	10 nA	Cu 249	12 mm	500 x 500 px	1.5 x 1.5 mm	3 µm/px

Electrohydraulic Fragmentation

The EAFS samples were subjected to EHF to enhance the liberation of metal inclusions and improve subsequent separation efficiency. The treatment was carried out using a laboratory-scale IMPULSTEC EHF lab unit at ImpulsTec GmbH, Radebeul, Germany. For the batch tests, high-voltage electrical discharges were generated in a water-filled vessel to comminute approximately 1.4 kg of EAFS sample type FG02. The samples were exposed to electrical pulses with high pulse energy. Following EHF treatment, the fragmented slag samples underwent mechanical screening, using integrated sieves, separating them into five size fractions: >1 mm, 0.8-1 mm, 0.5-0.8 mm, 0.25-0.5 mm, and <0.25 mm. Subsequently, the samples were dried, and each grain size fraction was subjected to magnetic separation using a ferrite (F1) hand magnet to separate strongly magnetic grains, followed by two neodymium hand magnets (N1, N2) to capture weakly magnetic grains.

Chemical Analysis

To gain approximate information about the chemical composition of the EHF fractions, chemical analyses were performed using an Olympus Vanta C-series portable XRF (pXRF) instrument equipped with a 50 kV Ar target X-ray tube. Analyses were conducted in “GeoChem” measurement mode with a measurement time of 60 s per sample. Each measurement was repeated three times to obtain a reliable dataset.

RESULTS AND DISCUSSION

MLA of EAFS sample FG02/1 identified Fe-rich oxides that, based on their modal composition, resemble magnetite, magnesiowustite and chromite – phases that often occur in these slags [4] – as well as Ca-rich oxides and silicates as the most prevalent phases. In addition, phases of mixed composition were observed, labeled as Fe-ox (an FeCaAlMgSiMnO-mix phase) and Ca-ox (a CaAlFeSiMgMnO-mix phase), as depicted in Figure 1. These mixed phases occur when the interaction volume of the electron beam exceeds the size of the individual grains. As a result, the beam overlaps multiple phases at grain boundaries, producing mixed EDX spectra that reflect compositions of both adjacent minerals. The high modal abundance of the mixed phases (ca. 30%) likely results from the overall small median grain sizes (P_{50}) of <60 µm for most phases (Figure 1a). The modal phase composition suggests that approximately 70% of the slag components are magnetic, with the metals of interest (Fe: 88%, Mn: 86%, Cr: 100%) largely present in these phases, assuming that Fe-ox is predominantly a Fe-oxide phase with magnetic behavior, while Ca-ox is non-magnetic (Figure 1b). Phase association analysis (Table 2) indicates that the magnetic phases are often intergrown with non-magnetic phases (M:NM = 0.59), whereas the non-magnetic phases are rarely associated with other non-magnetic phases (M:NM = 2.96).

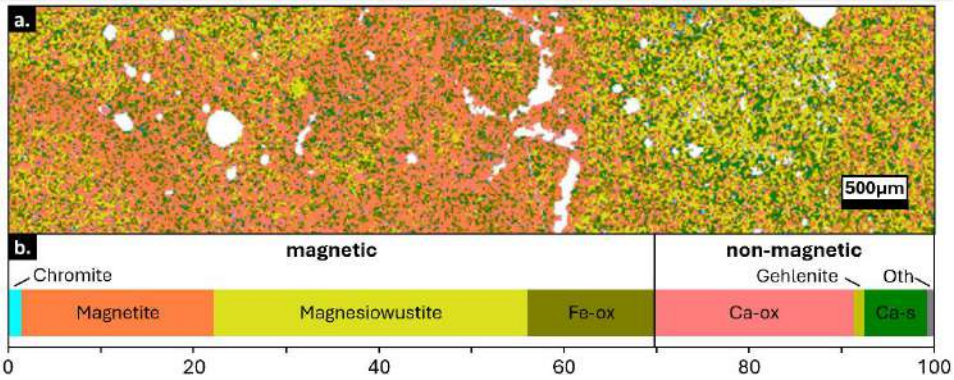

Figure 1 (a.) False-color MLA mineral map of sample FG02/1. **(b.)** Corresponding modal phase composition, categorized into magnetic and non-magnetic fractions. Fe-ox = FeCaAlMgSiMnO-mix, Ca-ox = CaAlFeSiMgMnO-mix, Ca-s = Ca-silicate, Oth = Others.

Table 2 Proportional magnetic and non-magnetic phase association in sample FG02/1 as shown by MLA analysis. M:NM represents the ratio of magnetic to non-magnetic phase associations

	Magnetic Association (M)	Non-Magnetic Association (NM)	M:NM
Magnetic phases	24.9 %	42.5%	0.59
Non-Magnetic phases	21.4%	7.2%	2.96

EHF tests demonstrate that, across all grain size fractions, most grains exhibit at least weakly magnetic behavior, with the total proportion of processed material summing up to 73.0%, which aligns closely with the 70% of magnetic phases estimated from MLA observations (Figure 2).

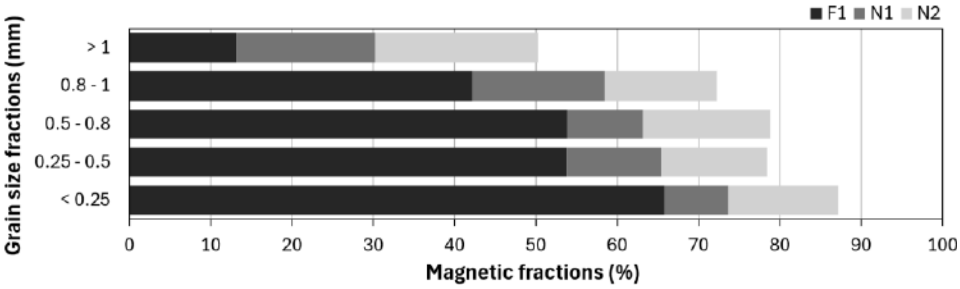

Figure 2 Grain size fractions and their magnetic proportions (F1: ferrite magnet, N1/N2: Nd magnets) within EAFS sample FG02 after EHF processing

The most significant increase in the proportion of magnetic material occurs between the >1 mm fraction and the 0.8-1 mm fraction, beyond which differences in magnetic content among finer fractions become less pronounced. The expected intergrowth of magnetic and non-magnetic phases in larger grains may reduce their overall magnetizability, hindering their recovery during magnetic separation and explaining the lower proportion of magnetic material in the >1 mm fraction. However, in fractions with smaller grain sizes, the opposite effect may occur, where non-magnetic grains may be drawn into magnetic fractions due to agglomeration effects, leading to a significant portion of Ca-oxides and silicates in the magnetic fractions. This is supported by the results from pXRF analysis that found that the Fe content for the magnetic fraction of >0.25 mm is 35.0 wt.%, while for the same grain size in the non-magnetic fraction the Fe content is 33.3 wt.%, only marginally lower. Thus, due to the high association of magnetic phases with non-magnetic phases and the small median grain sizes of the investigated phases, efficient separation may only be achieved at much smaller particle sizes than those investigated in this study.

While granular metal particles are not visible in smaller fractions, in the >1 mm fraction they can be clearly distinguished from the dark matrix material that rarely shows residual metal components attached to it (Figure 3a, b). This observation indicates that EHF effectively liberates metal components from other phases, consistent with expectations that fragmentation of the slags preferentially occurs at grain boundaries. It also suggests that metal inclusions may have a minimum size threshold for their formation and are not further fragmented during EHF treatment. Thus, while EHF successfully separates metal particles from the slag matrix, the larger metal inclusions remain intact, potentially facilitating their recovery. However, due to the total weight of only 16 g (equals ca. 1% of sample weight) for the hand-sorted metallic fraction (Figure 3a), extracting significant amounts of metal solely from this fraction may not be sufficient and therefore, additional recovery from finer fractions is necessary.

Figure 3 Grain fractions in EAFS sample FG02 after EHF processing. Liberated and hand-sorted grains from the >1 mm magnetic fraction showing the effectiveness of phase separation by EHF processing of metallic components **(a.)** from the slag-matrix **(b.)**. No visual differences between the magnetic **(c.)** and non-magnetic fraction **(d.)** for smaller grain sizes (< 250 µm) could be identified.

CONCLUSION

This study investigated the potential of EHF to enhance the liberation and recovery of valuable metals from EAFS. MLA of a representative EAFS sample revealed that Fe-rich oxides and Ca-rich oxides and silicates are the most prevalent phases, with significant fine-grained intergrowth between magnetic and non-magnetic phases. This microcrystalline intergrowth poses challenges for efficient separation using conventional methods. EHF processing tests showed that granular metal components could be effectively liberated from surrounding slag material, aligning with expectations that material is preferentially fragmented at grain boundaries. The occurrence of metal particles only in the coarse grain fractions (>1 mm) suggests that these are not further fragmented during EHF treatment. However, the effectiveness of magnetic separation and liberation for specific grain sizes and magnetic fractions requires further investigation. The median grain sizes of the liberated phases of <60 µm, the high rate of Fe-rich magnetic intergrown with Ca-rich non-magnetic phases and the similar Fe concentrations between magnetic and non-magnetic fractions suggest that efficient separation may only be achievable for much smaller particles sizes than investigated in this study. Thus, EHF parameters need to be adapted to enhance fragmentation and liberation at finer grain sizes. Additionally, future studies should focus on developing improved separation techniques to maximize metal recovery from EAFS, especially for small grain size fractions. This may include exploring more advanced magnetic separation methods, gravity concentration, or flotation. By addressing these challenges, the EHF process could offer a more sustainable and economically viable method for processing EAFS, contributing to waste reduction and resource efficiency in the steel industry.

ACKNOWLEDGEMENT

The research was funded by the Germany Ministry of Education, Science, Research and Technology (BMBF) under 033RK109A.

REFERENCES

1. Singh, S.K., Vashistha, P., Chandra, R., Rai, A.K. (2021) Study on leaching of electric arc furnace (EAF) slag for its sustainable applications as construction material. Process Safety and Environmental Protection, 148 (2021), 1315-1326.
2. Skaf, M., Manso, J.M., Aragón, Á., Fuente-Alonso, J.A., Ortega-Lopéz,V (2017) EAF slag in asphalt mixes: A brief review of its possible re-use. Resources, Conservation and Recycling, 120 (2017), 176-185.
3. Jiang, Y., Ling, T., Shi, C., Pan, S. (2018) Characteristics of steel slags and their use in cement and concrete—A review. Resources, Conservation and Recycling, 136 (2018), 187-197.
4. Menad, N., Kana, N., Seron, A., Kanari, N. (2021) New EAF Slag Characterization Methodology for Strategic Metal Recovery. Materials, 14, 1513.
5. Piatak, N., Ettler, V., Hoppe, D. (2021) Geochemistry and Mineralogy of Slags. In: Metallurgical Slags: Geochemistry and Resource Potential (N. Piatak), Royal Society of Chemistry, London, 59-124.
6. Gao, W., Zhou, W., Lyu, X., Liu, X., Su, H., Li, C., Wang, H. (2023) Comprehensive utilization of steel slag: A review. Powder Technology, 422 (2023), 118449.
7. Nevala, S., Hamuyuni, J., Junnila, T., Sirviö, T., Eisert, S., Wilson, B., Serna-Guerrero, R., Lundström, M. (2019) Electro-hydraulic fragmentation vs conventional crushing of photovoltaic panels – Impact on recycling. Waste Management, 87 (2019), 43-50.
8. Pijaudier-Cabot, G., La Borderie, C., Reess, T., Chen, W., Maurel, O., Rey-Berbeder, F., de Ferron, A. (2016) Electrohydraulic Fracturing of Rocks. No. 1, Wiley-ISTE, London.

XVI International Mineral Processing
and Recycling Conference
28-30 May 2025, Belgrade, Serbia

DOI: 10.5937/IMPRC25381A

Original research article

REFRACTORY POLYMETALLIC ORES BY FLOTATION. DIRECTIONS FOR IMPROVING METALLURGICAL BALANCE

Yergeshev Akim Ruslanovich[1,2#], 0000-0003-0581-4620,
Tokpayev Rustam Rishatovich[2], 0000-0002-0117-4454,
Khavaza Tamina Narimanovna[2], 0000-0002-1614-3060,
Karmeyeva Marina[2], 0000-0002-8577-8801,
Nauryzbayev Mikhail Kasymovich[2], 0000-0002-6781-6464,
Ignatkina Vladislava Anatolyevna[1], 0000-0003-2552-206X,
[1]National University of Science and Technology «MISiS», Moscow, Russia
NUST "MISiS"
[2]Center of physico-chemical methods of research and analysis of
al-Farabi Kazakh National University, Almaty, The Republic of Kazakhstan

ABSTRACT – The beneficiation complexity of the lead-zinc ore from the Shalkiya deposit is associated with the fine dissemination of galena and sphalerite, a high zinc module, and the presence of carbonaceous material. The flotation kinetics of carbonaceous material, galena, and sphalerite under different reagent regimes have been studied. Apolar and sulfhydryl collectors, as well as flotation depressants for carbonaceous material based on lignosulfonates, have been tested. The composition and surface properties of the carbonaceous material were analyzed using elemental composition analysis, X-ray photoelectron spectroscopy (XPS), infrared (IR) spectroscopy, and acid-base centers characterization. A rational collective-selective flotation scheme has been substantiated.

Keywords: Flotation, Galena, Sphalerite, Carbonaceous Material, Reagent Regime.

INTRODUCTION

The main useful minerals in the ores of the Shalkiya deposit are sphalerite, galena and pyrite, which have phenocrysts from dusty to 0.1 mm and are characterized by close intergrowth between themselves, as well as with minerals of waste rock, in particular quartz and carbonates. The very fine phenocrysts of lead and zinc minerals are complicated by the presence of carbonaceous matter, which is present both in the host rocks and in the useful minerals. In earlier studies on the development of ore enrichment technology of the Shalkiya deposit were proposed collective-selective and selective flotation schemes [1,2].

Glembotsky V.A. and Dmitrieva G.M. studied 28 galena samples with a lead content ranging from 86.07% to 62.16% [3], However, no clear correlation between conductivity

---

[#] corresponding author: akim9797@mail.ru

type and galena flotation activity was identified. The authors distinguished two groups of galena. The first group contains a minimal amount of impurities, allowing it to actively interact with ethyl xanthate and dithiophosphate. The second group is characterized by increased surface heterogeneity and a greater tendency to oxidation, which results in weak interaction with ethyl xanthate and resistance to flotation by dithiophosphates.

In recent decades, in addition to the known factors affecting the flotation properties of sulfides—such as the impurity composition of minerals, the degree of surface oxidation, and the presence of pyrite—the presence of carbonaceous material in ores has also been recognized as an influencing factor. This further affects the selection of the reagent regime and the flotation scheme [4-6].

Carbonaceous material, which belongs to naturally hydrophobic multiphase minerals [7], leads to significant mutual losses of galena and sphalerite between the commercial concentrates.

EXPERIMENTAL

Materials and Methods

Materials

The mineral composition of the sample, calculated on the basis of the data of microscopic studies, X-ray spectral and mass spectrometric analysis, is given in **Table 1.** Ore minerals are represented by galena, sphalerite, and pyrite. The host rocks are represented by quartz and carbonates (dolomite and calcite), the ore also contains small amounts of carbonaceous matter, feldspars, and muscovite.

Table 1 Mineral composition of the sample

Mineral Group	Content, wt. %	Mineral Group	Content, wt. %
Galena	1.57	Sulfides (FeS_2, $CuFeS_2$, $Cu_{12}As_4S_{13}$)	4.28
Sphalerite	6.94	Mica and clay minerals (muscovite, kaolinite, chlorite)	3.38
Smithsonite	0.02	Iron hydroxides	0.23
Quartz	38.13	Other barren minerals	0.17
Carbonates	43.97	Carbonaceous matter	1.30

According to MLA data, the main mineral concentrators of elements are:

- zinc: sphalerite and carbonates with a distribution of 87.44% and 8.04%, respectively;
- lead: galena and carbonates with a distribution of 86.99% and 10.64%, respectively.

Sulfide fractions were prepared from hand specimens by manual grinding in an agate mortar and dry classification. The -10 µm fraction was removed using a wet sedimentation method based on settling velocity.

Before flotation or adsorption, sulfide samples were soaked in 1% NaOH solution for 24 hours and then rinsed with distilled water in five specific volumes until reaching a neutral pH. The carbonaceous material was separated by flotation in a mechanical flotation machine without collectors or frothers, then dried and fractionated into narrow size classes.

Methods

Figure 1 shows the IR spectrum region of the carbonaceous material extracted from lead-zinc ore from the Shalkiya deposit.

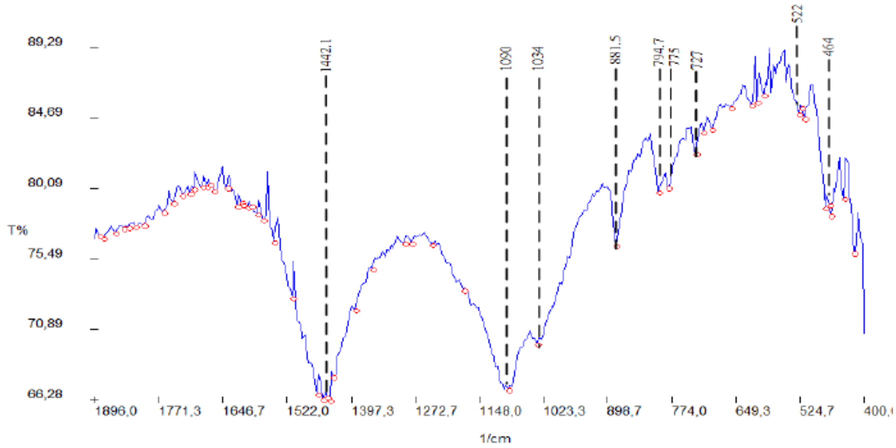

Figure 1 Transmission IR spectrum of carbonaceous material (±2 cm^{-1})

Characteristic Bands

A strong absorption band with a transmission minimum at 1452 and 1440 cm^{-1} corresponds to C-O stretching vibrations (νCO) at the carbonates. A strong band with minima at 1090 and 1034 cm^{-1} is associated with Si-O stretching vibrations. The bands at 881.5 cm^{-1}, the doublet at 794.7 and 775 cm^{-1}, and bands of varying intensity at 727, 522, and 464 cm^{-1} correspond to deformation and out-of-plane vibrations of X-O bonds, where X may represent Si, C, or other elements present in the carbonaceous sample. The IR spectra of the carbonaceous material from the ore, based on the main characteristic bands, are consistent with the IR spectrum presented in the study by Lee et al. (2023). [7] Table 2 presents the characteristics of sulfides and carbonaceous material. The chemical composition was determined using X-ray fluorescence spectrometry (XRF) (Shimadzu XRF-1800 spectrophotometer, Japan). The specific surface area of the fractions was measured using the low-temperature nitrogen adsorption method (BET) (Nova 2200E, Quantachrome Instruments, USA).

XPspectroscopy was used for a specific fracture -100 +44 µm of the samples in order to define the elemental composition of carbonaceous samples surface layer at 2 nm depth and to define oxygen and carbon state in coal and graphite. The research was done using X-ray photoelectronic spectrometer PHI5000VersaProbeII (ULVAC-PHI).

A narrow fraction (-71 +41 µm) of sulfides and carbonaceous material was studied. The reagent addition sequence in the mechanical flotation machine chamber followed the procedure described in Section 1.2.

Table 2 Chemical composition of galena, sphalerite, and carbonaceous material (CM)

<table>
<tr><td rowspan="2">Sample</td><td rowspan="2">Fraction, µm</td><td rowspan="2">Specific surface area, m²/g, ± 2.00</td><td colspan="11">Elemental composition, % ±0.02</td></tr>
<tr><td>Pb</td><td>Zn</td><td>S</td><td>Fe</td><td>Cu</td><td>Cd</td><td>Al</td><td>Si</td><td>C ±2.0</td><td>other</td><td>Total</td></tr>
<tr><td>PbS</td><td>-44 +10</td><td>0.52</td><td rowspan="2">83.86</td><td rowspan="2">1.17</td><td rowspan="2">12.65</td><td rowspan="2">0.69</td><td rowspan="2">0.13</td><td rowspan="2">-</td><td rowspan="2">0.04</td><td rowspan="2">0.19</td><td rowspan="2">-</td><td rowspan="2">1.26</td><td rowspan="2">100.00</td></tr>
<tr><td></td><td>-71 +41</td><td>abs</td></tr>
<tr><td rowspan="2">ZnS</td><td>-44 +10</td><td>0.86</td><td rowspan="2">1.50</td><td rowspan="2">63.10</td><td rowspan="2">31.07</td><td rowspan="2">1.20</td><td rowspan="2">0.10</td><td rowspan="2">0.40</td><td rowspan="2">0.03</td><td rowspan="2">0.90</td><td rowspan="2">-</td><td rowspan="2">1.70</td><td rowspan="2">100.00</td></tr>
<tr><td>-71 +41</td><td>abs</td></tr>
<tr><td colspan="14">Carbonaceous material</td></tr>
<tr><td colspan="2" rowspan="2">Fraction, µm</td><td rowspan="2">Specific surface area, m²/g, ± 2.00</td><td colspan="11">Elemental composition, %</td></tr>
<tr><td>C ±2.0</td><td colspan="2">H ±3.1</td><td colspan="2">N ±0.2</td><td colspan="2">O ±0.5</td><td>S 0.2</td><td>Ash content A, %, ± 0.5</td><td colspan="2">Total</td></tr>
<tr><td colspan="2">-71 +41</td><td>12.93</td><td>10.2</td><td colspan="2">-</td><td colspan="2">-</td><td colspan="2">4.7</td><td>0.7</td><td>84.4</td><td colspan="2">100.00</td></tr>
</table>

Concentrate fractions were collected at 0.1, 0.5, 1, 2, 3, and 5 minutes. The flotation rate constant (k, min^{-1}) for the fast-floating fraction (flotation duration of 1 minute) was determined graphically as the slope of the straight line in the coordinates $\ln(100/(100-\varepsilon)) = f(t)$.

For direct definition of Lewis-Bronsted active acid-base centers on surface Gammet indicators with different pK_a values were used [8-10]. Table 3 shows the characteristics of the Gammet indicators used to define types of acid-base centers on the surface of studied carbonaceous samples based on Gammet indicator adsorption.

Table 3 Gammet indicators' characteristics to define types of acid-base centers

Indicator	Formula	Molecular mass	λ, nm	pKa	Active center type
Bromocresol purple	$C_{21}H_{16}Br_2O_5S$	540.22	590	6.4	Bronsted acid
Bromthymol blue	$C_{27}H_{28}Br_2O_5S$	624.39	610	7.3	Bronsted base

Spectophotometer UV-VIS-NIR Cary 6000i by Agilent Technologies (USA) with wave range 175 to 1800 nm was used to control characteristic strip absorption intensity before and after interaction with the carbonaceous sample.

RESULTS AND DISCUSSION

Panoramic specters (Figure 3) prove impurities' content for the surface of carbonaceous material (CM) recovered from sulphidic ore.

Table 4 shows elemental composition of studied samples' surface.

Table 4 Sample surface elemental composition, ± standard edviation, %

Sample	C ±1.0	O ±1.0	Si ±0.5	Mg ±0.5	Al ±0.5	Ca ±0.5	Zn ±0.5	Fe ±0.3	S ±0.2	Pb ±0.1
CM	49.2	34.5	5.1	2.5	1.9	2.5	2.8	0.4	0.7	0.4

The flotation kinetics

The flotation of a narrow-size monomineral fraction of sulfides and CM under different preparation conditions for research are presented in Figure 4. Butyl xanthate

(KButX) was selected as the sulfhydryl collector, while fuel oil (FO) used as the non-polar reagent.

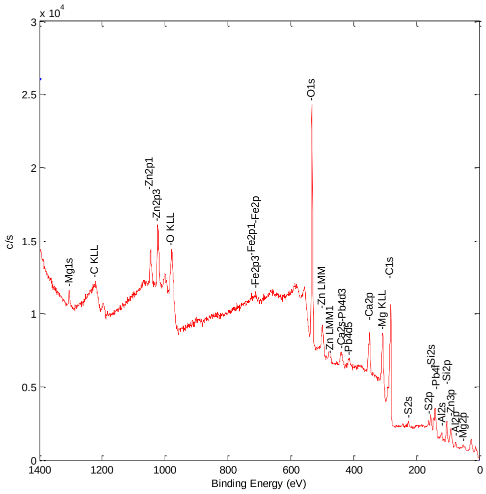

Figure 3 Panoramic XPS specters of carbonaceous material (CM) sample from polymetal sulphidic ore

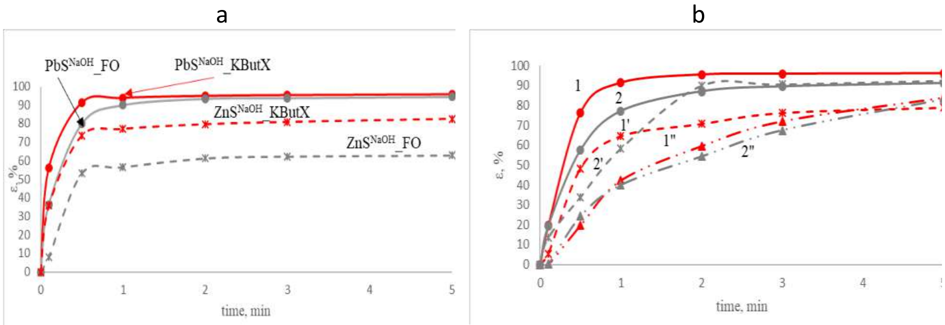

Figure 4 The flotation kinetics of PbS (1,2), ZnS (1’,2’) and CM (1”,2”) by KButX (1, 1’, 1”) and FO (2,2’,2”) under different preparation conditions of sulfides
[C_{init} (KButX) 10^{-4} M (18 mg/l), FO 50 mg/l, PO 10 mg/l
a - with pre-treatment NaOH; b - without pre-treatment]

Preliminary alkaline treatment of sulfides demonstrates increased floatability of PbS with KButX (εPbS = 91% in 0.5 min) in comparison with ZnS (εZnS = 61% in 2 min). The flotation activity of galena with FO in the concentrate is higher than that of sphalerite (εPbS = 90.1% in 1 min and εZnS = 77.1% in 1 min).

Aged sulfides (figure 4a) showed high flotation activity for galena with KButX (εPbS=96% in 0.5 min) and sphalerite (εZnS = 76.2% in 3 min), as well as with the apolar collector (εPbS = 89.5% in 2 min and εZnS = 84%). The carbonaceous material demonstrated lower floatability, with both collectors achieving similar recovery levels (εCM = 74% in 4 min). The flotoability of aged sulfides and CM in terms of recovery is comparable, suggesting that their separation may be obstructing.

The flotation kinetics of fast floating fraction was defined graphically with flotation duration of 1 min. the data are presented in Table 5.

Table 5 The flotation parameters of sulfides and CM with a flotation duration of 1 min

The reagent regimes	k, min^{-1}	ε_{max}, %	The reagent regimes	k, min^{-1}	ε_{max}, %
Without preprocessing					
PbS_KButX	2.46	91.4	CM_FO	0.56	40.0
ZnS_KButX	1.08	64.5	PbS_FO_LS	1.21	54.6
CM_KButX	0.61	42.4	ZnS_FO_LS	0.74	17.7
PbS_FO	1.71	88.3	CM_FO_LS	0.16	77.9
ZnS_FO	1.25	77.1			
With NaOH and rinsing					
PbS_{NaOH}_KButX	2.11	93.8	PbS_{NaOH}_FO	2.04	90.1
ZnS_{NaOH}_KButX	0.81	56.6	ZnS_{NaOH}_FO	1.12	77.1

The rate constant of galena decreases slightly, while that of sphalerite decreases significantly, when carbonaceous material depressors are used during the flotation of primary ores. When carbonaceous material depressors are used, the flotation rate constant decreases only during the first 2 minutes. However, with the increase in flotation time, the flotation kinetics rises, and the maximum recovery reaches at least 50% after 5 minutes of flotation

The results of the determination of acid-base centers in the investigated pH range during flotation and adsorption are presented in table 6.

Table 6 The results of dtermination of acid-base centers in the pH range of 6-8

Sample	PbS	ZnS	CM
Bronsted acid pKa=6.4, µmol/m^2	3.0	4.3	0.3
Bronsted base pKa=7.3, µmol/m^2	25.3	10.0	4.4

The active surface centers in the investigated pH range mainly correspond to Bronsted bases. They act as donors in donor-acceptor interactions. It can be assumed that surface reactions occur with nonionic collectors containing unsaturated bonds or that they promote xanthate formation through dixanthogen.

The following mechanism of interaction of lignosulphonates with surface of the separated minerals and CM is assumed based on experimental data. Carbonaceous material (CM) interacts strongly with lignosulphonates due to its complex surface structure such as silicates, carbonates and hydrophobic carbon films. At near neutral pH, surface metal hydroxide groups (e.g. Al-OH, Ca-OH) remain protonated and thus positively charged or amphoteric. This promotes electrostatic attraction with anionic sulphonate groups of lignosulphonates. In addition, hydrophobic interactions with carbon-rich domains contribute to adsorption. Despite this, CM recovery could not be reduced below 50%, indicating persistent flotation activity due to residual hydrophobic sites. Galena (PbS) retains strong flotation activity due to the highest Brønsted base site density (25.3 µmol/m²). At pH ~6.4-7.3 the surface is less oxidised and more reactive, but shows limited affinity for lignosulphonates. This is probably due to lower surface heterogeneity and a dominance of Pb^{2+} rather than hydroxylated species. As a result, galena remained effectively floatable. Sphalerite (ZnS), primarily in cleiophane form, has fewer surface base sites (10.0 µmol/m²) and a higher tendency toward surface hydroxylation or oxidation. At near-neutral pH, $Zn(OH)^+$-type sites can facilitate moderate lignosulphonate adsorption, resulting in reduced flotation rate but insufficient depression for selective separation. Thus, in the pH range 6.4-7.3, lignosulfonates are partially effective as depressants, but selective suppression of CM is not achieved.

Taking these factors into account, the established dependencies provide a solid basis for the selection of collective selective flotation technology for lead-zinc sulphide ores, where it is advisable to remove the carbonaceous material prior to collective flotation.

CONCLUSION

It has been experimentally shown, that the weathered low-iron modification of sphalerite (cleiophane) floats similarly to galena, including using of FO in reagent regimes. Alkaline treatments of the galena and sphalerite surfaces before flotation allows achieving the expected flotation results – galena floats faster and higher than sphalerite.

Flotation kinetics of galena, sphalerite, and carbonaceous material with butyl xanthate and fuel oil, both individually and in the presence of carbonaceous material depressors and lignosulfonates, demonstrated the inability to achieve selective depression of the carbonaceous material compared to galena and sphalerite, as recovery below 50% could not be achieved.

The obtained results on monomineral fractions of cleiophane, galena and carbonaceous material made it possible to determine the reason for the low process efficiency of direct selective flotation without the removal of carbonaceous material at the Shalkiya deposit. This is due to the low contrast in the flotation properties of cleiophane and galena.

Due to the multiphase nature of the carbonaceous material and the obtained flotation kinetics results, it is advisable to remove the carbonaceous material prior to collective flotation. The established dependencies serve as the basis for selecting a collective-selective flotation technology for lead–zinc sulfide ores, in which the finely disseminated sphalerite grains are present as cleiophane.

ACKNOWLEDGEMENT

This work was supported by the Science Committee of the Ministry of Science and Higher Education of the Republic of Kazakhstan (grant number AP19680419).

REFERENCES

1. Mityaeva, N.M., Iskakova, G.A. (1988) Material composition and technological properties of Shalkiya ores. In: Geology and Mineral Resources of Southern Kazakhstan, Almaty.
2. VNIITsvetmet (2003) Development of beneficiation technology for lead-zinc ores of the Shalkiya deposit with the production of lead and zinc concentrates and recommendations for implementation. Research report, No. 6-03-35, G.I. Ivanov (Ed.), Ust-Kamenogorsk.

3. Glembotsky, V.A., Dmitrieva, G.M. (1965) Influence of mineral genesis on their flotation properties. Nauka, Moscow.
4. Konieczny, A., Pawlos, W., Krzeminska, M., Kaleta, R., Kurzydlo, P. (2013). Evaluation of organic carbon separation from copper ore by pre-flotation. Physicochemical Problems of Mineral Processing, 49(1), 189-201.
5. Pan, Z., Xiong, J., Cui, Y., Wei, Q., Jia, W., Zhang, Z., Jiao F., Qin, W. (2022). Effect mechanism of carbonaceous materials on the flotation separation of lead–zinc ore. Separation and Purification Technology, 294, 121101.
6. Hua Z., Shi B., Dong Y., Fu Y., Zeng Y., Sun W., Liu R., Tang H. (2025). Evaluation of Mineralogical Characteristics and Flowsheet Improvements for Carbon-Bearing Lead-Zinc Ore. JOM, 77(2), 830-841.
7. Lee, S., Gibson, C., Borschneck, A., Ghahreman, A. (2023) Transformer oil vs. kerosene: Selective collectors for C-matter flotation from a double refractory gold ore. Minerals Engineering, 191, 107951.
8. Tanabe, K. (2012) Solid Acids and Bases: Their Catalytic Properties. Elsevier. https://books.google.ru/books?hl=ru&lr=&id=tFfBYuHg4vAC.
9. Ryazantseva, M.V., Bunin, I.Z. (2015) Modifying acid–base surface properties of calcite, fluorite and scheelite under electromagnetic pulse treatment. Journal of Mining Science, 51, 1016–1020.
10. Atchabarova, A. A., Abdimomyn, S. K., Abduakhytova, D. A., Zhigalenok, Y. R., Tokpayev, R. R., Kishibayev, K. K., & Djenizian, T. J. (2022). Role of carbon material surface functional groups on their interactions with aqueous solutions. Journal of Electroanalytical Chemistry, 922, 116707.

XVI International Mineral Processing and Recycling Conference
28-30 May 2025, Belgrade, Serbia

DOI: 10.5937/IMPRC25389C

Original research article

THE USE OF DIELECTRIC BARRIER DISCHARGE TO REGULATE THE TECHNOLOGICAL PROPERTIES OF CHALCOPYRITE AND SPHALERITE

Valentine A. Chanturia, 0000-0002-4410-8182,
Igor Zh. Bunin, 0000-0002-8618-5119,
Maria Ryazantseva[#], 0000-0003-3261-8625,
Melnikov' Institute of Comprehensive Exploitation of mineral resources Russian Academy of Sciences, Moscow, Russia

ABSTRACT – The modification of structural and chemical properties of natural chalcopyrite and sphalerite as a function of dielectric barrier discharge (DBD - treatment) parameters were investigated experimentally with the help of the adsorption of acid and base indicators, sorption and flotation tests. It was determined that DBD - treatment during of 5 - 30 second results to the increasing of the electron - accepting properties of chalcopyrite and sphalerite. Thus, single mineral flotation tests showed that DBD - treatment resulted to the improvement of the sorption activity of the sphalerite and chalcopyrite and floatability.

Keywords: Chacopyrite, Sphalerite, Dielectric Barrier Discharge, Floatability, Surface Properties.

INTRODUCTION

The problem of selective separation of bulk concentrates of sulfides minerals is very important. Ionizing radiations and high - energy impacts (accelerated electrons, neutrons, gamma rays, low - temperature plasma, high - voltage nanosecond pulses, etc.) are viewed as additional operations in mineral processing for directed changes in the mechanical, electrophysical, physicochemical and technological properties of non-ferrous, noble and rare metal minerals, calcium bearing minerals *etc.* [1]. The use of high - power nanosecond electromagnetic pulses (HPEMP - treatment) and low - temperature dielectric barrier discharge plasma (DBD - treatment) for treatment of minerals increases the efficiency of opening mineral intergrowths and causes the development of solid - phase chemical reactions on the surface of sulfide minerals with the formation of micro - and nanophases in the form of hydrophobic elemental sulfur and various hydrophilic oxygen - containing compounds, which helps to increase the selectivity of flotation separation of sulfides with similar physicochemical properties [1].

EXPERIMENTAL

In this study, two natural mineral samples of high purity were used: chalcopyrite ($CuFeS_2$) and sphalerite (ZnS) which came from the Dalnegorskoe ore field (Primorye,

---

[#] corresponding author: ryzanceva@mail.ru

Russia). The mineral samples contain small amount of other components. The XRF analysis was used to determine the chemical composition of samples (Table 1).

The DBD - treatment of mineral samples was carried out in air and the following parameters of the pulses initiating the discharge: leading edge pulse time — 250 - 300 ns, pulse duration — 8 µs, voltage on the electrodes in the barrier discharge cell— 20 kV, pulse repetition frequency — 16 kHz (10 kHz;5 kHz,8 kHz;2 kHz) the range of variation of the DBD sample treatment time 10 - 100 s; the length of the interelectrode gap was about 5 mm. The mineral samples were placed in the discharge and the working surfaces of the samples were located on the surface of the dielectric barrier.

The Hammett indicator adsorption method was used to differentiate and study the acid - base properties of the mineral surface [1]. The list of indicators, pKa values, working concentrations of indicator' solutions, and wavelengths corresponding to the absorption maximum are presented in Table 2.

Table 1 Chemical composition of the mineral samples

Element present (mass %)									
	Cu	**Fe**	**Zn**	**S**	**Pb**	**Ca**	**Mn**	**Mg**	**As**
$CuFeS_2$	28.54	27.54	1.91	29.17	3.19	0.70	0.04	0.01	0.006
ZnS	0.29	4.08	<50.00	29.30	6.61	0.19	0.129	0.02	0.153

Table 2 Indicators names and parameters

Indicator	pKa	λ max, nm	C_{ind}, mmol /l
dinitroaniline	-4.4	340	1.20
brilliant green	1.3	610	0.33
bromophenol blue	4.1	590	0.08
bromocresol purple	6.4	590	0.16
bromothymol blue	7.3	430	0.36
Indigo carmine	12.8	610	0.40

The optical density of the initial indicator solution D_0 and the indicator solution after adsorption - desorption equilibrium with the mineral sample D_1 were measured spectrophotometrically (Shimadzu UV - 1700). The change in the optical density of the indicator solution as a result of the interaction of the studied mineral with distilled water D_2 was also taken into account, which made it possible to exclude this factor during the analysis of the results. The concentration of surface active centers, equivalent to the amount of adsorbed amount of indicator q_{pKa}, and it was determined using the following formula [3]:

$$q_{pK\alpha} = \frac{C_{ind} V_{ind}}{D_0} \left[\frac{|D_0 - D_1|}{m} \pm \frac{|D_0 - D_2|}{m} \right] \tag{1}$$

where C_{ind} is the indicator concentration (mol/l), V_{ind} is the indicator volume (ml), m is the sample weight (g). The signs "+" and "-" correspond to the opposite and unidirectional changes of D_1 and D_2, respectively. According to [3], indicators with the lowest (negative) pKa values are selectively adsorbed on the active centres of the Lewis basic type, containing an unshared electron pair and capable of capturing a proton during hydrolytic dissociation of a water molecule. As the pKa of indicators increases, their selective adsorption occurs on Bronsted acidic centers (pKa = 0 - 7, surface OH groups with a tendency to split off a proton), Bronsted basic (pKa = 7 - 14, surface OH groups with a tendency to split off the entire hydroxide) and Lewis acidic centers (pKa ≥ 14, atoms with a free orbital, capable of capturing a hydroxyl with dissociative adsorption of water).

Sorption activity of chalcopyrite and sphalerite samples were studies with DRIFT spectroscopy IR Affinity (Shimadzu) equipped with diffuse reflection attachment DiffusIR (Pike Technologies).

Single mineral flotation test was carried out using 1.0 g mineral sample in a special 20-ml laboratory flotation cell. Butyl potassium xanthate (30 g/t) was used as a collector and MIBC as frother. All flotation tests were performed at pH 9.5 after adjustment using CaO solution. The accuracy of recovery results can be estimated around 2 %.

RESULTS AND DISCUSSION

The influence of DBD - treatment parameters on flotation properties chalcopyrite and sphalerite was studied carefully (Table 3). The obtained results showed that floatability increase for both minerals considerably as a function of the treatment duration for the size fraction of - 44 µm. While for the size fraction of -100 + 50 µm there is no significant changes in the flotation properties of minerals with variations of DBD - treatment parameters. It occurs due to rising of the specific surface area of the crushed sample with decreasing particle size; also, the specific surface area of the particles increases due to the increase in the number of microdefects (pores, microcracks, electrical breakdown channels) formed as a result of the action of the DBD - treatment. Therefore, the efficiency of DBD - treatment of minerals increases with decreasing mineral size and increasing number of particles involved in the process of exposure to such DBD - treatment factors as a strong electric field, ion wind, increased particle mobility in the interelectrode gap [1, 2], as well as the increasing action of chemically active plasma particles (O_3, singlet oxygen $O_2(a^1\Delta_g)$, H_2O_2 and OH) [3, 5], formed in interparticle microdischarges [4].

Table 3 Influence of DBD - treatment parameters of the chalcopyrite and sphalerite floatability (size fraction -44 µm)

	2.0 kHz	5.8 kHz	10.0 kHz	16.0 kHz
8µs	$CuFeS_2$ ↑ 8-14 % ZnS=const	$CuFeS_2$ ↑ 7-16 % ZnS↑ 6-10 %	$CuFeS_2$ ↑ 7-14 % ZnS↑ 2-15 %	$CuFeS_2$ ↑ 4-16 % ZnS↑ 10-17 %
4µs	$CuFeS_2$ ↑ 6-18 % ZnS= const	$CuFeS_2$ ↑ 4-18 % ZnS = const	$CuFeS_2$ ↑ 9-13 % ZnS↑ 4-11 %	$CuFeS_2$ ↑ 5-17 % ZnS↑ 5-10 %

As it, follows from the Table 3 there are DBD - treatment conditions those results to the rising of the floatability for the both minerals in 10 - 20 %. At the same time, obviously, there are the treatment conditions that leads to the growth of the chalcopyrite floatability only. It means that the DBD - treatment can be used in the process of the bulk or copper concentrate separation process depending on goals.

For the DBR - treatment mode that results to the highest simultaneous recovery of chalcopyrite and sphalerite into the froth flotation product, the effect of DBR - treatment on the acid-base properties of the surface were studied. The obtained results are presented in the Figure 1.

As can it be seen from the obtained results for sphalerite, as a consequence of DBD - treatment, the negative charge of the mineral surface drops because the number of active centers with pKa = 0.29 (electron duplet) reduce. More over the number of active centers p_{Ka} = 12.0 increases. The appearance of the active centers with p_{Ka} = 12.0 indicates an increase in the acceptor force of the mineral surface. A similar changes was identified for chalcopyrite surface (Figure 1). In other words, as a result of the DBR - treatment of chalcopyrite and sphalerite, firstly, the negative charge of the surface of the minerals decreases, and secondly, the acceptor capacity of the surface increases.

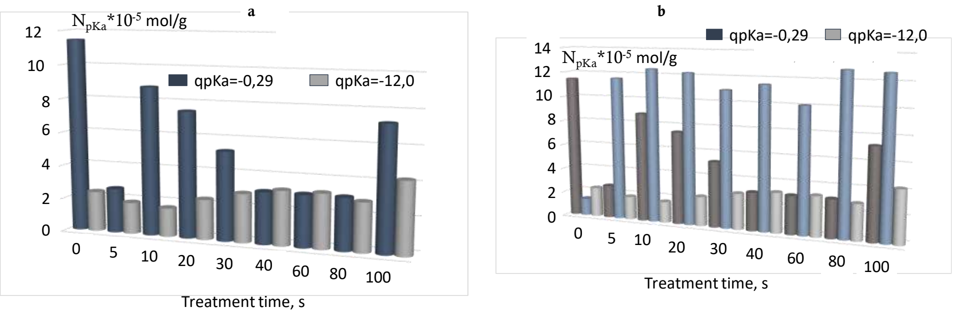

Figure 1 Influence of DBD - treatment parameters on the concentration of the surface active centers.

The alterations in the in the energy state of the mineral surface caused by DBR - treatment should have contributed to a change in its sorption activity in relation to reagents with electron-donor properties. Therefore, the influence of DBR - treatment on the sorption activity of chalcopyrite and sphalerite towards butyl xanthate was studied using DRIFT. Figure 2 shows the obtained results. The vibrations of 1043 cm^{-1}1201cm^{-1} 1267 cm^{-1} in Figure 2a belong to vibrations of the adsorbed collector hydrocarbon skeleton. The peak positions indicates that collector molecules is adsorbed in the form of dixanthogen. A similar picture is observed for sphalerite surface (Figure 2b).

The calculation of the of the integrated band intensities attributed to the vibrations of potassium butyl xanthate bands demonstrates that the after the DBD - treatment the integrated intestines of bands raised in 1.2 - 1.3 times as compared to untreated sample that means that the sorption of collector on the mineral surface increased.

The applicability DBD - treatment for intensification of the copper recovery from natural mineral objects was confirmed by using flotation of copper middlings. Table 4 presents the data obtained.

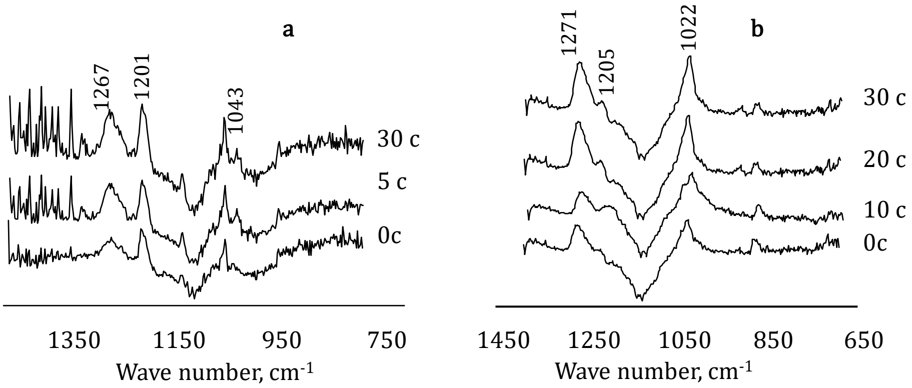

Figure 2 Influence of DBD - treatment parameters on the sorption activity of chalcopyrite and sphalerite.

Table 4 Influence of DBD - treatment on recovery of copper from middlings obtained from copper - zinc ore of the Alexandrinsky deposit

Treatment time	product	weight		Cu	$\varepsilon Cu_{concentrate.}$, %	$\varepsilon Cu_{tails.}$, %
0		g.	γ,%	β, %		
	concentrate	20,56	41,33	14,76	**48,80**	
	tails	29,19	59,21	11,08		51,20
10 s	total	49,75	100			100
	concentrate	30,46	60,97	14,20	**69,73**	
	tails	19,50	39,03	9,94		30,27
30 s	total	49,96	100			100
	concentrate	25,45	50,86	14,74	**58,89**	
	tails	24,59	49,14	10,71		41,11
	total	50,04	100			100

The table shows that preliminary DBD - treatment in a low-temperature plasma field allows to increase the recovery of copper in the froth product of the flotation. The recovery of copper in the froth product was about 48 % before the treatment. The DBD - treatment during the 10 s allows to improve the recovery of the copper to 69 %, i.e. by 20 %. The DBD - treatment during 30 s results the rising of the copper recovery to 58, 8%, i.e. by 10 % as compared to untreated sample.

CONCLUSION

It was defined that dielectric barrier discharge (DBD - treatment) can change the floatability of monomineral chalcopyrite and sphalerite (-44 µm). DBR - treatment can be used to improve the selectivity of chalcopyrite and sphalerite separation. It was identified that there are the DBD - treatment conditions where the flotation of chalcopyrite increases in 5 - 18 % while the floatability of sphalerite is invariable (duration of initiating discharge pulses $\tau_{imp.}$ = 4 and 8 µs, pulse repetition frequency $f_{imp.}$= 2 kHz). At the same time the another DBD - treatment parameters can be used for the recovery increasing for both minerals in 5 - 17% ($\tau_{imp.}$= 8 µs, $f_{imp.}$=16 kHz).

With application of Hamet' indicators adsorption method, it was defined that the changes in the flotation properties of chalcopyrite and sphalerite as a result of DBD - treatment results from the acid - base (donor-acceptor) properties of the minerals surface. Because of DBD - treatment, the negative charge of the minerals surface decreases, and the acceptor force of the surface increases. It results to the improvement of the sorption ability of the mineral surface towards butyl xanthate and as the consequence to the improvement of the floatability.

The results of the flotation of the middlings obtained from copper - zinc ore of the Alexandrinsky deposit showed that DBD - treatment allow to increase the recovery of copper in the concentrate by 10.1 - 20.9 %.

REFERENCES

1. Bunin, I.Zh., Ryazantseva, M.V., Samusev, A.L., Khabarova, I.A. (2017) Theory and practice of using combined physical, chemical and energy effects on geomaterials and water suspensions. Mining Journal, 11, 77 - 83.
2. Chanturiya, V.A., Bunin, I.Zh., Ryazantseva, M.V. (2019) XPS study of sulfide minerals surface oxidation under high - voltage nanosecond pulses. Miner. Eng., 143, 105939.
3. Nechiporenko, A.P. Burenina, T.A., Koltsov, S.I. (1985) Indicator method for studying the surface of solids. Journal of general chemistry, 55 (9), 1907 -1911.
4. Bunin, I.Zh., Chanturiya, V.A., Ryazantseva, M.V., Koporulina, E.V., Anashkina, N.E. (2020) Changes in the surface morphology, microhardness, and physicochemical properties of natural minerals under the influence of a dielectric barrier discharge. Bull. Russ. Acad. Sci. Phys., 84, 1161 - 1164.
5. Avtaeva, S.V. (2009) Barrier discharge. Research and application. Publishing house of KRSU, Bishkek.
6. Bobkova, E.S., Khodor, Ya.V., Kornilova, O.N., Rybkin, V.V. (2014) Chemical composition of plasma of dielectric barrier discharge of atmospheric pressure with liquid electrode High temperature thermal physics., 52 (4), P. 535 - 542.
7. Chanturia, V.A., Bunin, I.Zh., Kovalev, A.T. (2008) Energy concentration in electrical discharges between particles of semiconductor sulfide minerals under the influence of powerful nanosecond pulses. Bulletin of the Russian Academy of Sciences. Physical Series, 72(8), 1118 - 1121.

XVI International Mineral Processing
and Recycling Conference
28-30 May 2025, Belgrade, Serbia

DOI: 10.5937/IMPRC25395V
Original research article

MECHANOCHEMICAL LEACHING OF CHALCOPYRITE IN LOW MOISTURE CONDITIONS

Luis Verdugo[1#], 0009-0000-3398-6943,
Barbara Etschmann[1], 0000-0002-7807-2763,
Maryam Abdus-Salam[1], 0000-0003-2554-3311,
Andrew Hoadley[1], 0000-0001-9605-6858,
Jorge Menacho[2], 0009-0000-6776-242X,
Joel Brugger[1], 0000-0003-1510-5764,
[1]Monash University, Melbourne, Australia
[2]DRM Eng., Santiago, Chile

ABSTRACT - Copper concentrates represent 80% of the world's copper production. The main processing routes for copper extraction are pyrometallurgical via smelting or hydrometallurgical using moderate to high temperatures and/or high-pressure conditions, which affects the processing costs. An alternative presented in this work is the mechanochemical processing of concentrates, where the combined use of grinding and oxidizing reagents accelerates the leaching kinetics. Several mechanochemical tests were run in a laboratory mill using chalcopyrite in conjunction with various oxidants in low moisture conditions. The oxidants were ferric chloride ($FeCl_3$), ferric sulfate $Fe_2(SO_4)_3$, and ferric sulfate with silver added as a catalyst. The best results were for ferric chloride with 56% copper recovery after grinding for 15 min and ferric sulfate with added silver with 63% copper recovery after grinding for 25min.

Keywords: Mechanochemical Leaching, Mineral Processing, Grinding, Copper Extraction.

INTRODUCTION

Over the past decades, mechanochemical reactions have captured the attention of many researchers due to their versatility and simplicity in synthesizing new materials and processing raw materials [1]. This allows the synthesis and production of chemical compounds and materials that are difficult under normal conditions with respect to reaction time, reactivity, and consumption of reagents such as water, which is critical in the chemical and mining industry.

Copper concentrates represent approximately 80% of the world's copper production. Smelting, used to produce metallic copper and by-products such as industrial gases and sulfuric acid [2] generates significant amounts of pollution. For this reason, studies are focusing on the hydrometallurgical processing of copper concentrates. These processes typically use oxidants based on ferric ions which results in the formation of elemental sulfur and the release of (oxidized) copper into the

---

[#] Luis Verdugo: luis.verdugogallegos@monash.edu solution for further extraction. This process is illustrated in equation (1) [3]:

$$CuFeS_2 + 4Fe^{3+} \rightarrow Cu^{2+} + 5Fe^{2+} + 2S^0 \tag{1}$$

Equation (1) highlights that copper leaching is proportional to the concentration of ferric ion in the solution, though additional aspects need to be considered such as redox potential and temperature, both of which critically influence leaching kinetics. Redox potential, i.e. the electrochemical couple [Fe^{3+}]/[Fe^{2+}], given by the anodic reaction (2):

$$4Fe^{3+} + 4e^{-} \rightarrow 4Fe^{2+} \tag{2}$$

controls the oxidative potential of solution, which impacts the leaching kinetics [4].

Chalcopyrite is a mixed n-p semiconductor with a low electrical conductivity (29 S/cm) [5]; this results in inefficient electron transfer between chalcopyrite and ferric ions. Additionally, during leaching at atmospheric pressure and low to medium temperatures a passivating layer of elemental sulfur is formed. This coating is detrimental to the leaching process as it blocks ferric ions accessing the chalcopyrite and minimises the mass transfer of copper [6].

Grinding, while leaching, aids in removing the sulfur passivating layer on the surface of the chalcopyrite, allowing ferric ions to continue to interact with the mineral. This has been demonstrated by the ROL (rapid oxidative leach) process developed by FLSmith™, with the oxidative leaching of chalcopyrite and other copper sulfides using a stirred reactor with grinding media [3]. In this process, by reducing the passive layer and particle size during the mechano-oxidative process, it is possible to recover up to 95% copper in 6 h processing time.

In this study, the mechanochemical leaching of chalcopyrite at room temperature is tested by grinding in a low moisture media. This enables a high concentration of oxidant to be present on the surface of the mineral, increasing the oxidation potential, while simultaneously cleaning the passivating layer. Overall, this accelerates the leaching process.

EXPERIMENTAL PART

Materials and characterisation methods

Chalcopyrite from Wallaroo (courtesy of the South Australian Museum) with a particle size D_{50} = 45 µm was used in this study. This mineral is composed of 34.24% Cu, 30.05% Fe and 30.74% S (measured by portable-XRF).

Chemicals used in the experiments were: ferric chloride hexahydrate $FeCl_3 \cdot 6H_2O$ (Sigma Aldrich, reagent grade), ferric sulfate hydrate, $Fe_2(SO_4)_3 \cdot xH_2O$ (Sigma Aldrich, reagent grade), ferrous sulfate heptahydrate $FeSO_4 \cdot 7H_2O$, (Sigma Aldrich, reagent grade), silver nitrate $AgNO_3$ (Sigma Aldrich, reagent grade), cupric chloride dihydrate, $CuCl_2 \cdot 2H_2O$, (Sigma Aldrich, reagent grade), cupric sulfate pentahydrate, $CuSO_4 \cdot 5H_2O$ (CSA Scientific, Australia, reagent grade) and sulfuric acid (96%, Merck, analytical grade).

A ring mill 0.2 L (Rock labs, New Zealand) was used for the grinding tests (Figure 1). Tables 1-2 detail the grinding conditions and chemical mixtures that were used.

Table 1 Processing Conditions Used in Grinding Experiments

Processing Condition	Units	Value
Mill Volume	L	0.20
Grinding Material	--	WC/SiN_3
Grinding Speed	rpm	1000
Mill Power	kW	1.1
Moisture Content (Dry basis)	wt%	8 - 21

Table 2 Moisture Solutions Composition Used in Grinding Experiments

Experiment	Chalc., g	Ox., g	H_2SO_4, g	Moist. Sol., g	Added Liquid Composition, g/L				
					Cu^{2+}	Fe^{2+}	Fe^{3+}	H_2SO_4	Ag^+
$FeCl_3$	3	13	0.17	1.29	2	1	3	5	---
$Fe_2(SO_4)_3$	3	6.5	0.11	2.02	2	1	3	5	---
$Fe_2(SO_4)_3$ & Ag^+	3	6.5	0.11	2.02	2	1	3	5	10

Figure 1 Grinding Equipment Used During the Experiments

The feed materials and leaching products were characterized by: (i) a laser diffraction particle sizer, Malvern Panalytical, model Mastersizer 2000, UK, was used to measure the particle size distribution. (ii) Elemental analysis of leaching solutions was carried out using ICP-OES analyser, model: iCAPTM 7400 duo ICP–OES, Thermo Fisher, USA, using reference standards for different elements in a concentration between 0-100 mg/L respectively. (iii) The elemental composition of the feed material and leaching products were quantified using an Olympus portable X-ray fluorescence analyzer (model Vanta, USA). (iv) X-ray diffraction (XRD) was carried out using a Rigaku benchtop powder XRD, model Miniflex600, Japan, using 40 kV and 15 mA with a copper cathode as the radiation source.

Experimental procedure of mechanochemical trials

All the experiments were carried out at room temperature (15-20°C). For each grinding experiment, 3 g of chalcopyrite was used and variable compositions of oxidant (either $FeCl_3 \cdot 6H_2O$ (13 g) and $Fe_2(SO_4)_3 \cdot xH_2O$ (6.5 g)). The moisture content in the mill (between 8 wt% - 21 wt% water) was controlled using acidic solutions containing oxidizing reagents, with compositions specified in Table 2 for each experiment.

The materials were placed in the ring mill and were ground for 5, 15 and 25 min at 1000 rpm. After the experiment the solid was collected from the mill and washed with an acid solution containing 50 g/L H_2SO_4, for 15min and the slurry was filtered and solids were dried for 18h at 50°C in an oven (Qualtex, Thermstat, Australia). Then all samples were weighed using a scale (Mettler Toledo, model MS204S/02, Switzerland) and analysed. The washing solution products were collected, filtered using a 0.45µm pore size syringe filter (Pall corp., USA) and analysed with ICP-OES.

Leaching data processing methodology

The amount of copper extracted during each test was calculated based on the mass and grades of materials in the head, solutions, and residues collected at the specified time intervals. The leaching kinetics is defined by parameters such as the kinetic rate constant (k) and the ultimate recovery (RI). They were calculated using a first-order leaching kinetic model.

$$R = RI\,[1 - exp\,(-k\,(t)] \tag{4}$$

These parameters are obtained from the logarithmic-linear correlation given in equation (5).

$$\ln(\frac{\text{RI - R}}{\text{RI}}) = \text{-kt} \tag{5}$$

The slope of the linear regression gives the kinetic rate constant in equation (5).

RESULTS AND DISCUSSION

The amount of copper extracted was relatively similar for experiments using ferric chloride and ferric sulfate + silver (Figure 2a). However, in Figure 2b, kinetic analysis indicated a faster copper extraction for experiments using ferric chloride compared to ferric sulfate + silver. Experiments using only ferric sulfate had the slowest leaching kinetics with a low copper extraction of ~10% after 25 min grinding time. The standard deviation (σ_{Exp}) shown in the table inset is moderate, indicating a good reliability for these experiments based on ICP-OES analysis of solutions after leaching. Note that copper extraction and kinetics were based on ICP-OES analysis as pXRF results for solids had a high standard deviation.

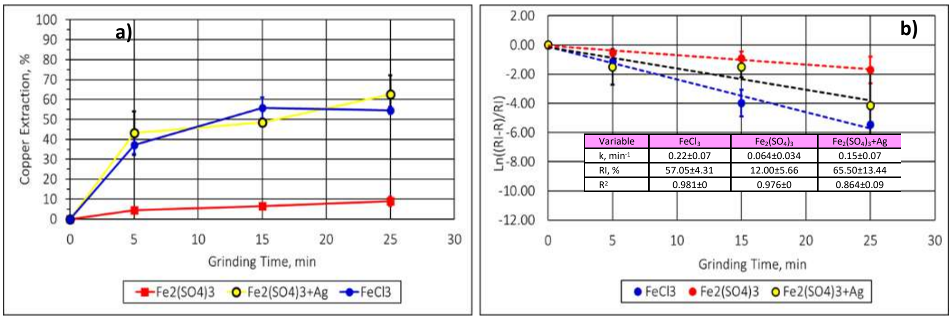

Variable	$FeCl_3$	$Fe_2(SO_4)_3$	$Fe_2(SO_4)_3$+Ag
k, min^{-1}	0.22±0.07	0.064±0.034	0.15±0.07
RI, %	57.05±4.31	12.00±5.66	65.50±13.44
R^2	0.981±0	0.976±0	0.864±0.09

Figure 2 Copper Ext. versus Time (a) and Kinetic Plot (b) for All Experiments Tested.

The effect of the oxidant type and grinding time on the chalcopyrite leaching is shown by the intensity of XRD chalcopyrite peaks found for feed and leaching products. This is shown in Figure 3 (a to c).

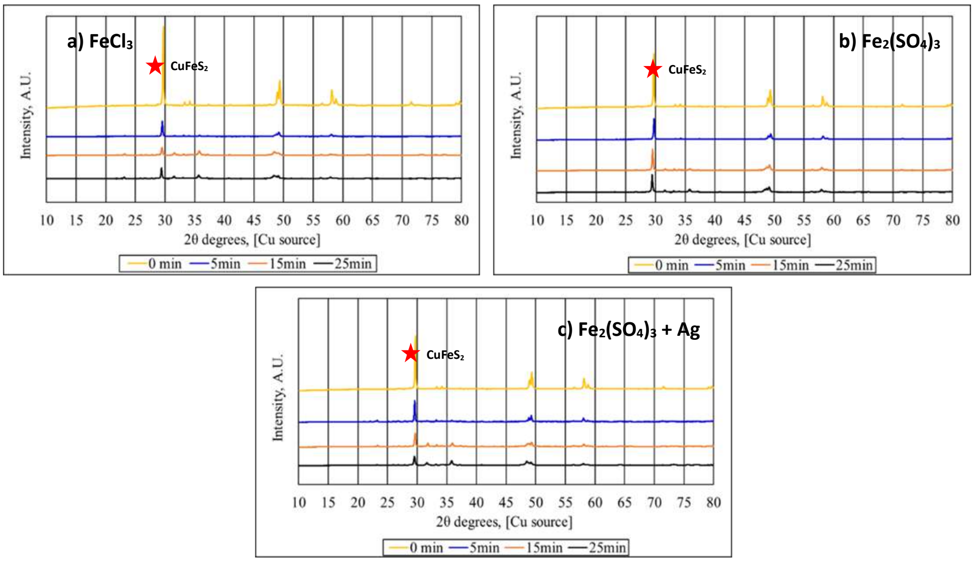

Figure 3 XRD Patterns versus Time for All Experiments Tested

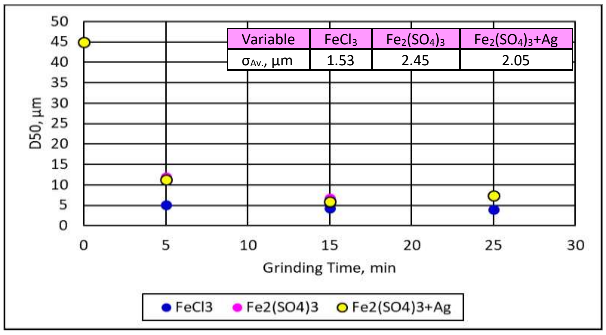

Figure 4 Particle Size D_{50} versus Grinding Time.

It is difficult to extract quantitative kinetics from XRD data due to the appearance of variable amounts of other phases (e.g. WC from the mill). However, the area of the dominant chalcopyrite peak at 2θ ~ 29° can be correlated with the reaction extent. These peak decreases rapidly for experiments using FeCl$_3$, and slowly for Fe$_2$(SO$_4$)$_3$. However, when silver is added into the solution, the copper extraction kinetics increases substantially, showing similar results to FeCl$_3$. This could be related with the generation of more soluble and conductive copper species such as CuS and geerite (Cu$_8$S$_5$) [7,8]. The effect of the mechanochemical reaction on the particle size (D_{50}) is analysed in Figure 4. Grinding has the largest first order impact, thus the three oxidants have a similar particle size after grinding for 25 mins. However, there is a noticeable difference in particle size between chloride and sulfate oxidants after grinding for only 5 mins; this can be explained by the highly oxidizing nature of ferric chloride, along with the added benefit that chloride complexes well with copper (I) ions, promoting more reaction and leading to smaller average chalcopyrite particles.

CONCLUSIONS

In this study, the mechanochemical processing of chalcopyrite in low moisture conditions and using common reagents were carried out using a ring mill. The main conclusions of this work are the following:

1. Experiments showed that a high copper extraction can be achieved in a relatively short grinding time (15-25 min), under low moisture conditions.
2. Grinding experiments using ferric chloride shows the fastest leaching kinetics, followed by ferric sulfate + silver and ferric sulfate without silver.
3. Silver used in a high concentration (10 g/L) in the moisture solution has a big impact on the leaching kinetics, improving the oxidation in sulfate media.
4. Grinding experiments using ferric sulfate showed the slowest leaching kinetics. This could be related to the low stability of Cu(I) ions in sulfate media.

ACKNOWLEDGEMENTS

We would like to thank Newcrest (now Newmont Corporation) for supporting this work through an ARC linkage grant (LP190101230). Part of this work was funded by ARC DP220100500.

REFERENCES

1. Baláž, P., & Baláž, P. (2008). Mechanochemistry in minerals engineering 413pp. Springer, Berlin.
2. International Copper Study Group (2024), World Copper Factbook, 68pp. Lisbon.
3. Karcz, A. P., Damø, A. J., Illerup, J. B., Rocks, S., Dam-Johansen, K., & Chaiko, D. (2017). Electron microscope investigations of activated chalcopyrite particles via the FLSmidth® ROL process. Journal of Materials Science, 52, 12044-12053.
4. Córdoba, E. M., Muñoz, J. A., Blázquez, M. L., González, F., & Ballester, A. (2008). Leaching of chalcopyrite with ferric ion. Part II: Effect of redox potential. Hydrometallurgy, 93(3-4), 88-96.
5. Mukherjee, S., Ramakrishnan, A., Chen, K. H., Chattopadhyay, K., Suwas, S., & Mallik, R. C. (2019, July). Tuning the thermoelectric properties of chalcopyrite by Co and Se double substitution. In AIP Conference Proceedings (Vol. 2115, No. 1). AIP Publishing.
6. Yang, Y., Harmer, S., & Chen, M. (2015). Synchrotron-based XPS and NEXAFS study of surface chemical species during electrochemical oxidation of chalcopyrite. Hydrometallurgy, 156, 89-98.
7. Price, D.W.; Warren, G.W. (1986). The influence of silver ion on the electrochemical responsef chalcopyrite and other mineral sulfide electrodes in sulfuric acid. Hydrometallurgy, 15, 303-324.
8. Córdoba, E., Muñoz, J., Blázquez, M., González, F., Ballester, A., 2008c. Leaching of chalcopyrite with ferric ion. Part III: effect of redox potential on the silver-catalyzed process. Hydrometallurgy 93 (3), 97–105.

XVI International Mineral Processing
and Recycling Conference
28-30 May 2025, Belgrade, Serbia

DOI: 10.5937/IMPRC25401M Research article

RECULTIVATION PROCEDURE OF FLOTATION TAILINGS AT THE LOCATION OF RTH IN BOR

Miomir Mikić[#], 0000-0001-7659-769X,
Milenko Jovanović, 0000-0002-6757-4143,
Radmilo Rajković, 0000-0001-5905-6613,
Daniel Kržanović, 0000-0003-3841-8667,
Sandra Milutinović, 0000-0003-0146-8636,
Mining and Metallurgy Institute Bor, Bor, Serbia

ABSTRACT – The RTH flotation tailings in Bor represents a critical environmental issue due to prolonged exploitation and inadequate closure of mineral processing facilities. This paper presents an integrated approach for the technical and biological reclamation of the RTH tailings, relying on field experience, comparative regional cases, and practical planning measures. A phased plan is proposed which includes surface profiling, application of cover soil, and long-term revegetation using native and tolerant plant species. The goal is to reduce environmental risks, stabilize the terrain, and create a functional green landscape.

Keywords: Flotation Tailings, RTH, Reclamation, Ecological Restoration, Bor, Soil Rehabilitation, Recultivation, Degraded areas, Phases, Species.

INTRODUCTION

Mining activity has considerably increased due to notable population growth and worldwide demand for mineral resources [1]. This increase coincides with a new awareness in which environmental concerns have become a growing challenge for all of the agents within the sector [2-3]. The social demand has increased for the sustainable development of all of the activities related to mining, particularly the adequate management of waste products during each phase of the mining process, including prospection and exploration, development, extraction, transport and treatment of product obtained, etc. [4]. The mining process generates a large quantity of residues that must be strategically treated and managed to combine economic efficiency with demands for environmental sustainability. Energy requirements, environmental and human health risks, demands on water resources, and the required technology must all be taken into account [5].

One of the greatest environmental problems caused by the mining and refinement of strategic elements, is the problem of waste management. This becomes a problem when mines and refineries that do not adhere to regulations regarding proper waste disposal.

[#] corresponding author: miomir.mikic@irmbor.co.rs

This can result in soil and water contamination by substances such as heavy metals and radioactive materials. This affects the ecosystem around the waste disposal site; and, if the contaminants get into the water table, it can affect areas beyond the site.

Improper waste disposal is often the largest of mine and refinery pollution Waste is generally categorized into two different types: tailings and waste rock stockpiles. Tailings have the most damage potential because they tend to be composed of smaller, finely milled particles, whereas waste rock stockpiles are made up of coarser particles, which are not absorbed into the water and the ground as easily. In addition to the small particles, tailings contain waste water and flotation chemicals. Tailings are typically placed in impoundment areas exposed to precipitation and water runoff, which can allow toxic substances to be washed out. Groundwater can be contaminated if the impoundment area is not leak-proof. Impoundment areas also run the risk of overflowing during periods of heavy rain, if the areas are not made large enough to contain great amounts of rain and runoff. The most serious risk, however, is that of a collapsed dam, which would allow the toxic tailings to flood the area. Although the exact composition of tailings is site-specific, they generally contain heavy metals, acids, fluorides, sulphides, and radioactive material.

This paper is analyzing location of RTH flotation tailing. In order to prevent impact on environmental there has been performed analysis to determine the optimal method of recultivation. This recultivation procedure has many goals such as: prevent air pollution and erosion of tailings material through torrents and its transport to the surrounding land. Special attention has paid to the possibility of afforestation and greening of degraded areas by deciduous and coniferous species. In this way, i.e. by applying biological reclamation, seedlings of birch, and juniper, are planned. The alternating combination of these plant species enables the binding of the substrate and gives a beautiful aesthetic appearance to the environment.

Two phases are adopted: technical and biological. Each of them has specific works that are presented in this paper.

LOCATION OF INTEREST

Flotation tailings facilities in the Bor region, especially the RTH, are legacy environmental burdens. Decades of flotation processes have left behind surfaces with limited ecological value and high erosion potential. This study proposes a solution based on tested practices and local environmental data.

The RTH tailings pond covers around 27 hectares and includes fine-grained waste with high acidity and metal content. Problems include dust pollution, acid mine drainage, slope instability, and lack of vegetation. Environmental monitoring confirms elevated levels of heavy metals such as Cu, Pb, and Zn.

The RTH flotation tailing (Figure 1) was built southeast of the boron flotation pit in the RTH open pit mining area. After mining was completed, the RTH open pit area was filled. Due to the need for additional storage space, the original Bor Valley flotation landfill was expanded to the northwest and southeast. The river valley leading to the metallurgical slag heap and the abandoned boron open pit in the northwest was blocked by Dam No. 1 (Figure 1). Downstream, the Bor River valley was blocked by Dam No. 2

(Figure 1). The east side of the flotation ore retention pit borders the eastern landfill of the boron open pit, and a cofferdam was built on the west side of the flotation tailings.

Figure 1 Spacial representation of the location of the flotation tailing RTH [6]

Based on the analysis of the flotation tailings, several conclusions were reached [7]:

1. In the side dams of Dam No. 1 (I) and Dam No. 2 (II) and the RTH flotation residues, a homogeneous technogenic material predominates. Morphologically, this material consists of fine sand. This matrix leads to poor water vapor conditions and is unfavorable for plant growth.
2. In some locations in the dam where sulfur-sulfide oxidation has not yet taken place, the pH value of the flotation residues is about 6. This flotation material reacts neutrally with high concentrations of active phosphorus and a complete lack of potassium.
3. Where sulfide sulfur oxidation occurs, the pH value of the matrix is about 3
4. The lack of clay particles containing organic matter in the flotation residue impairs self-renewal and plant growth. Clay and humus particles in the flotation residue activate the soil microflora, initiate soil-related humus formation processes and the formation of available plant nutrients. Therefore, humus-rich soil materials are added to the substrate.
5. The addition of organic matter to the substrate in the form of humus accelerates microbial processes and provides a constant influx of plant assimilates to promote the development of grass and shrub plant species, as envisioned by biorecultivation.

DEGRADED AREAS FOR RECULTIVATION

The new project addresses the elevation of the dam from elevation K+378 to elevation K+390. Based on the projected state of the flotation tailings, with an elevation up to K+390, the surface area of the flotation tailings RTH, which will be treated by recultivation, represents internal and external slopes, dam crest and tailing beach (K+385). Total degraded area projected for recultivation is 551.200 m^2.

TYPES OF RECULTIVATION AND CHOICE OF RECULTIVATION METHODS

Reclamation is a complex of mining-technical, engineering, reclamation, forestry and agricultural works, which are carried out in a certain time, aimed at bringing degraded terrain to a state suitable for reuse, in the previous or in a new way, compared to the state before the degradation. [8]

Reclamation measures must ensure the most necessary abiotic and biotic conditions of the habitat, its biotization, the creation and support of the formation of initial life communities on the meliorated habitat and corresponding communities at a higher level of cenotic structure and complexity. [8]

The aim of recultivation is to, through a series of activities foreseen by the recultivation project, in some form, "return" what was previously borrowed from nature through exploitation.

In the world and in Serbia, for the recultivation of degraded areas, the following is applied:

- autorecultivation,
- semi-recultivation,
- optimal recultivation.

Optimum results in terms of recultivation are achieved by applying complete recultivation - eurecultivation. Complete recultivation means the procedure when all the foreseen phases of recultivation are carried out: technical, agrotechnical and biological recultivation.

Due to the condition of the surfaces after the disposal of the flotation tailings and the specific pedological, microclimatic and climatic conditions, for the recultivation of the RTH flotation tailings, optimal recultivation with grassing is foreseen.

Reclamation works are consist of two phases:

1. Technical phase of reclamation,
2. Biological phase of recultivation.

TECHNICAL AND BIOLOGICAL RECULTIVATION

The technical phase include engineering interventions consist of reprofiling slopes, sealing the surface with clay layers, and installing drainage systems. Application of cover soil is planned using material from surrounding plots. Protective berms, erosion mats, and water redirection structures will be integrated.

The second – biological phase includes planting metal-tolerant grasses (Festuca rubra, Agrostis capillaris) and nitrogen-fixing trees (Robinia pseudoacacia). The objective is to create initial ground cover and enable soil development for future succession. Later afforestation will include birch, pine, and other native forest species. Monitoring of growth and coverage will be performed annually.

A biological method of recultivation will be applied for the greening of degraded areas at the site in question, namely:

1. Sowing a mixture of grasses 49 kg/ha: Red fennel (50%), English rye (35%), Yellow star (10%), White clover (5%),
2. Woody plants: Betula alba L. (birch) – a total of 47,974 seedlings, Acer campestre L. (juniper) – a total of 4787 seedlings.

On the outer slope of the flotation tailings pond, only grass is planned. It will be done using hydroseeding. The other areas will be grassed using agricultural machinery. After weeding, the next phase is afforestation.

The planting of trees, chub, on the internal slopes of the dam will be done according to a triangular scheme at a distance of 3 m between the seedlings. This means that about 1100 seedlings can be planted on one hectare. The planting of trees on the crown of the dam will be done in two rows, with a space of 4 m wide for the road, 6 m between these rows. Birch seedlings are planted at a distance of 3 m. The total number of seedlings per hectare is about 1100.

For the beach of the flotation tailings, afforestation was designed according to a mosaic layout. At the same time, birch and chub are planted according to a square pattern at a distance of 3 m between the seedlings. In this way, about 96% of the area will be forested, while the rest will be the space reserved for the road (4%) for the passage of machinery.

Works on the formation, i.e. the raising of green areas on the beach consists of the formation of individual mosaics that will consist of shrubby and woody plants. Woody plants (birch) will be used within one mosaic. Planting will be done two meters from the edge at a distance of 3 m between seedlings (square scheme). In this way, about 1100 seedlings will be planted per hectare. Seedlings aged 2+1 will be used for planting.

Bushy vegetation (clump) will be used for roundabouts. Planting will be done two meters from the edge at a distance of 3 m between seedlings (square scheme). In this way, about 1100 seedlings will be planted per hectare. Seedlings aged 2+1 will be used for planting.

CONCLUSION

The recultivation of RTH tailings is not only a technical task but an ecological necessity. By integrating engineering and ecological techniques, the proposed plan addresses environmental hazards and promotes gradual transformation into a stable and green space.

ACKNOWLEDGEMENT

The authors are grateful to the Ministry of Science, Technological development and Innovation of the Republic of Serbia for financial support according to the contract with the registration number 451-03-136/2025-03/ 200052.

REFERENCES

1. Reichl, C.; Schatz, M.; Zsak, G. World-Mining-Data. In Minerals Production; International Organizing Committee for the World Mining Congresses: Vienna, Austria, 2016; Volume 31.
2. Dold, B. Sustainability in metal mining: From exploration, over processing to mine waste management. Rev. Environ. Sci. Bio/Technol. 2008, 7, 275–285.
3. Gómez Ros, J.M.; García, G.; Peñas, J.M. Assessment of restauration success of former metal mining areas after 30 years in a highly polluted Mediterranean mining area: Cartagena-La Union. Ecol. Eng. 2013, 57, 393–402.
4. Bakken, G.M. Montana, Anaconda, and the Price of Pollution. Historian 2007, 69, 36–48. Available online: http://www.jstor.org/stable/24453910 (accessed on 14 April 2018).
5. Durucan, S.; Korre, A.; Muñoz-Melendez, G. Mining life cycle modelling: A cradle-to-gate approach to environmental management in the minerals industry. J. Clean. Prod. 2006, 14, 1057–1070.
6. Google earth
7. Supplementary mining project of the elevation of the RTH flotation tailings pond. Institute of Mining and Metallurgy Bor, 2022.
8. Mikić M., Milutinović S., Jovanović M., Urošević D. Recultivations of pyrite concentrate landfill, flotation trailer and neutralization sludge landfill at location Čukaru Peki, Serbia. Rudarstvo 2022, 170–179. https://ritnms.itnms.ac.rs/bitstream/id/2565/61.2.pdf.

XVI International Mineral Processing and Recycling Conference
28-30 May 2025, Belgrade, Serbia

DOI: 10.5937/IMPRC25407K Original research article

METAL RECOVERY FROM SPENT BATTERIES THROUGH ANTISOLVENT CRYSTALLIZATION IN A T-MIXER USING A COUPLED CFD-PBE APPROACH

Vandana Kumari Jha[#]**,** 0000-0003-4013-8218,
Christophe Duwig, 0000-0001-5886-415X,
Samaneh Teimouri, 0000-0003-2511-8040,
Kerstin Forsberg, 0000-0002-3239-5188,
KTH Royal Institute of Technology, Stockholm, Sweden

ABSTRACT – The growing demand for electric vehicles and energy storage systems has led to a rise in battery production, resulting in a growing volume of spent batteries. To address the environmental and economic challenges associated with battery waste, efficient and sustainable recycling processes are crucial. In this context, crystallization offers a promising approach for recovering valuable metals. This study presents a population balance model (PBM) coupled with computational fluid dynamics (CFD) to simulate recovery of nickel sulphate hexahydrate ($NiSO_4 \cdot 6H_2O$) crystals through the antisolvent crystallization technique. Growth and particle size distribution (PSD) of crystals are analyzed within a continuous 3D T-mixer system under laminar flow conditions for a single case of *Re* = 150. The impact of impinging flow on mixing, which affects local supersaturation and PSD, is clearly visible. Additionally, the crystal size at the distribution maximum correlates directly with supersaturation consumption. This approach provides a comprehensive framework for understanding and predicting the PSD in the crystallization process, helping to understand mixing, flow dynamics and supersaturation profiles. This study also evaluates the T-mixer's ability in promoting uniform crystal growth, targeting a narrow PSD. These findings contribute to the development of sustainable crystallization systems, supporting efficient metal recovery in battery recycling applications.

Keywords: Battery Recycling, Population Balance Model (PBM), Antisolvent Crystallization, Metal Recovery, Particle Size Distribution (PSD).

INTRODUCTION

The transition to sustainable energy solutions has become a key priority, as the world moves towards a greener future. Lithium-ion batteries (LIBs) have emerged as a favourable means to attain this goal, offering a promising solution. With their ability to store large amounts of energy in a lightweight and compact form, they have transformed industries ranging from consumer electronics to electric vehicles (EVs). However, LIBs pose significant recycling challenges due to scarcity and valuable constituent metals, such as Ni, Co, Mn [1]. Recycling of cathodes using advanced techniques is essential [2] as they are crucial in terms of cost and effectiveness. This not only supports circular economy [3] but also aligns with Sustainable Development Goals (SDGs) 9 and 12, which

---

[#] corresponding author: vkjha@kth.se

promote resource efficiency, industry innovation, and waste reduction through recycling [4,5].

Crystallization is a promising method for recovering valuable metals from spent batteries, with particle size distribution (PSD) playing a crucial role in product quality. In antisolvent crystallization, mixing influences nucleation and growth by affecting local supersaturation. High supersaturation can lead to impurity incorporation, while controlled antisolvent addition improves purity [6,7]. Overcoming mixing inefficiencies in traditional batch systems is essential for improving crystal quality and optimizing battery recycling processes [8].

In this study, the population balance model (PBM), coupled with the computational fluid dynamics (CFD), is applied to simulate the evolution of PSD in a continuous 3D T-mixer. The model investigates the influence of reactor hydrodynamics on $NiSO_4{\cdot}6H_2O$ crystallization via the antisolvent method, focusing on flow characteristics, supersaturation profiles, and PSD at *Re* = 150. By understanding the mixing features, influenced by impinging flow, this research aims to enhance crystallization processes for improved product quality, and reduced energy consumption, in battery recycling.

NUMERICAL MODELING

CFD model

CFD is used to s equations governing the balance of momentum, mass, and chemical species. Numerical study is conducted using the commercial CFD software COMSOL Multiphysics® 6.2. The velocity field is solved using the laminar flow interface under steady-state conditions. Simultaneously, the crystallization process is simulated through the chemistry interface, coupled with the transport of concentrated species.

PBM model

Population balance equation (PBE) describes the distribution of characteristic crystal length, represented by the particle diameter. The general form of PBE (Eq. (1)) is expressed as follows [9,10]:

$$\frac{\partial n}{\partial t}+\nabla\cdot(un)+\frac{\partial\big(G(S,L)n(L)\big)}{\partial L}=\nabla\cdot(D\nabla n)+B_{nuc}\delta(L-L_0)+B_{agg}-D_{agg}+B_{break}-D_{break} \qquad (1)$$

where *n* is the number density function (1/m^4), *u* is the flow velocity (m/s), *t* is the time (s), *G (S, L)* is the size independent particle growth rate (m/s) and is a function of supersaturation, *L* is the characteristic crystal size (m), *D* is the diffusion coefficient (m^2/s), B_{nuc} is the nucleation rate (1/(m^4-s), and B_{agg}, B_{break} and D_{agg}, D_{break} represent the birth and death terms (1/(m^4-s) due to agglomeration and breakage, respectively. To solve the discretized PBM in time and space, it needs to be coupled with CFD. For the system considered here, nucleation, agglomeration and breakage terms are neglected.

Supersaturation and crystal growth

Supersaturation is generated by the reduction in solubility caused due to the addition of ethanol in the $NiSO_4{\cdot}6H_2O$-water solution. The initial aqueous nickel sulphate solution is saturated and contains seeds of $NiSO_4{\cdot}6H_2O$. The size independent growth rate is applied during the crystallization process and is given by the power law kinetics expression as shown in Eq. (2).

$$G = k_g (S-1)^g \tag{2}$$

where S is the supersaturation, k_g is the growth rate constant (m/s), and g the growth rate exponent. The degree of supersaturation in the process is given by:

$$S = \frac{c}{c^*} \tag{3}$$

where c is the concentration of $NiSO_4{\cdot}6H_2O$ and c^* is the equilibrium concentration.

Geometry and meshing

The schematic of the 3D circular T-mixer system is shown in Figure 1(a), illustrating the boundary conditions and dimensions. The computational domain comprises of a T-mixer with two oppositely placed inlets, an outlet and a mixing channel length. One inlet serves for the $NiSO_4{\cdot}6H_2O$-water solution and the other for the ethanol. The study considers a *Re* of 150, which falls within the laminar flow regime. The mean channel velocity is 0.23 m/s and is assumed to be fully developed at the inlets. The system is maintained at a constant temperature of 25°C. A mesh-refinement study was performed, and a custom mesh setting was adopted, as shown in Figure 1(b).

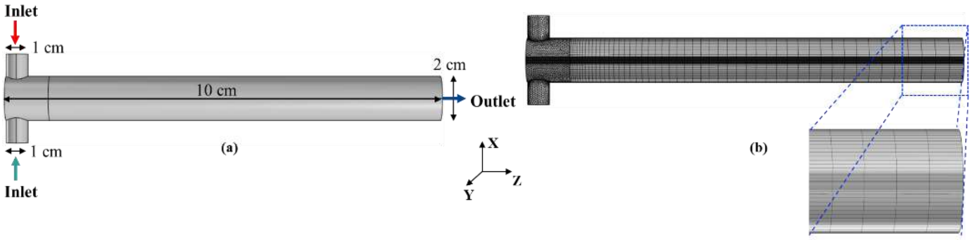

Figure 1 (a) Schematic of the 3D T-mixer geometry; **(b)** depiction of custom mesh

Governing equations and boundary conditions

To simplify the computational model, the following assumptions were made: (a) fully developed flow at the inlets; (b) fluids are incompressible, and density is computed dynamically based on water-ethanol composition; and (c) nucleation, aggregation, and breakage terms were neglected. The governing equations are:

Continuity equation: $$\nabla \cdot (\rho u) = 0 \tag{4}$$

Incompressible Navier-Stokes equations:

$$\frac{d(\rho u)}{dt} + (\nabla \cdot \rho u u) = -\nabla P + \nabla \cdot \left[\mu \left(\nabla u + (\nabla u)^T \right) \right] \tag{5}$$

where ρ is mixture-density, u is the velocity vector, P is the pressure and μ is the dynamic viscosity.

Transport of species: $$\frac{d(\rho c)}{dt} + \nabla \cdot (\rho u c) = \nabla \cdot (\rho D \nabla c) + R \tag{6}$$

where *c* is the concentration of the species, *D* is the diffusion coefficient (m^2/s) and *R* is the source term (mol/m3-s). Convective transport was modeled based on the velocity field, while diffusive transport was modeled according to Fick's law.

Boundary conditions: Fully developed flow is applied at the respective fluid inlets and no-slip boundary conditions at the walls. A Dirichlet boundary condition was defined at each inlet setting the ingoing number density for each interval to zero, except for interval 1 at inlet 1. Additional details are provided in Table 1.

Table 1 Summary of boundary conditions

Condition	Equation	Applied at
Constant velocity	$v = v_A$	Inlet 1
Constant velocity	$v = v_O$	Inlet 2
No-slip	$v = 0$	T-mixer walls
Pressure outlet	$P = P_{atm}$	Outlet
$NiSO_4.6H_2O$ concentration	$c_{NiSO4.6H2O} = c_{inlet,NiSO4.6H2O}$	Inlet 1
C_2H_5OH concentration	$c_{C2H5OH} = c_{inlet,C2H5OH}$	Inlet 2
Outflow	$\frac{\partial c}{\partial n} = 0$	Outlet

RESULTS AND DISCUSSION

Flow characteristics

The flow characteristics of the mixing channel at *Re* = 150 is illustrated in Figure 2(a)-(b), highlighting velocity contours at different cross-sections, and streamlines in both 3D and 2D views. The velocity distributions at multiple cross-sections along the main mixing channel, showing how flow evolves downstream, is displayed. The enlarged inset provides a detailed view of velocity variations at a specific cross-section, revealing regions of high and low flow intensity. The streamlines depicting fluid motion, with a zoomed-in view near the inlet showing strong mixing and recirculation zones, are also presented in a 2D view. High velocity regions are seen near the inlet and lower velocities further downstream. As the flow progresses, it becomes more homogeneous along the length of the channel. The geometry features a mixing channel significantly longer than the mixing zone, ensuring sufficient residence time. This visualization helps analyze mixing efficiency and hydrodynamic effects, crucial for crystallization process.

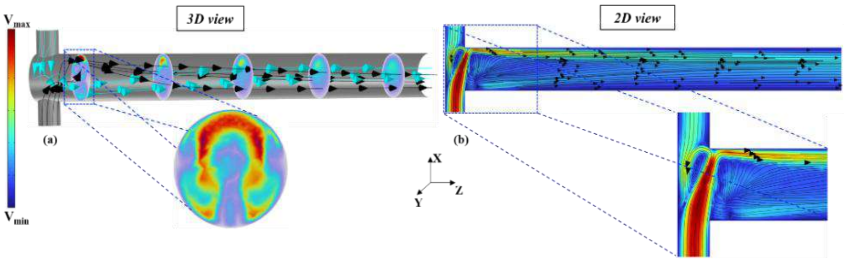

Figure 2 Contour and streamline plots shown at a center cut XZ-plane inside the T-mixer along with the insets, at Re = 150: (a) in 3D view; (b) 2D view

Supersaturation profiles

The supersaturation plot along the centerline of the T-mixer channel geometry is shown in Figure 3, illustrating how mixing influences the spatial variation of supersaturation. The supersaturation is more evenly distributed along the channel length, promoting uniform crystal growth and resulting in a narrower outlet size distribution. The left side corresponds to the inlet region, where the antisolvent and solution first interact, generating a high supersaturation zone. As the flow progresses downstream, supersaturation decreases due to mixing and diffusion, and crystal formation, indicating lower supersaturation levels. The smooth gradient suggests a gradual mixing process. Understanding this distribution is crucial for optimizing crystal growth and ensuring uniform particle size.

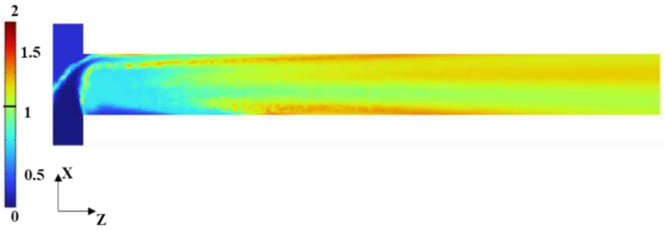

Figure 3 Supersaturation plot shown at a center cut XZ-plane inside the T-mixer

Particle size distribution

Particle size analysis was done at the XZ- and XY-planes, as shown by different cut planes (Figure 4(a)). The spatial evolution of crystal size along the length of the channel is shown in Figure 4(b). There is an increase in crystal size as the seeds flow from inlet to the outlet, suggesting crystal growth with the increase in residence time. Normalized number density at: outlet (Z = 0 cm), Z = 2.5 cm and Z = 5 cm is shown (Figure 4(c)). The distribution shows a shift in the particle size towards larger values as the particles approach the outlet, i.e., as the value of Z decreases. This trend confirms the progressive growth of crystals along the flow direction, and peak around 10-11 µm, indicating most crystals form within this range. Gradual broadening of peaks suggests a wider distribution, due to the effects of hydrodynamics and local supersaturation.

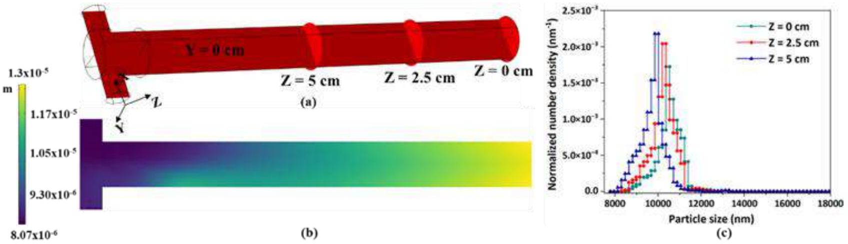

Figure 4 (a) Different cut planes shown inside the T-mixer; (b) contour plot showing the distribution of crystal size at XZ-plane where Y = 0; (b) normalized distribution at the outlet (Z = 0 cm), Z = 2.5 cm and Z = 5 cm

CONCLUSION

This study presents a comprehensive numerical approach integrating CFD with the PBM to simulate the antisolvent crystallization of nickel sulphate in a continuous 3D T-mixer geometry. The model accurately predicts the particle size distribution (PSD) under steady-state laminar flow conditions (*Re* = 150). The numerical results provide insights into the influence of flow dynamics and mixing intensity on crystal growth and PSD. The impact of impinging flow on local supersaturation levels is also highlighted, emphasizing its role in crystallization efficiency. Additionally, this study evaluates the T-mixer's ability to promote uniform crystal growth, targeting a narrow PSD, high-purity crystals, and improved recovery rates. These findings contribute to the development of sustainable crystallization systems, supporting efficient metal recovery in battery recycling applications.

ACKNOWLEDGEMENT

The simulations and data management were performed using the resources provided by the National Academic Infrastructure for Supercomputing in Sweden (NAISS) at the PDC Center for High Performance Computing, partially funded by the Swedish Research Council, Sweden through grant agreement no. 2022-06725. The authors are grateful to the Swedish Energy Agency, Sweden for funding this research work within the program Batterifonden.

REFERENCES

1. I. Energy Agency, Global EV Outlook 2022 (2022) Securing supplies for an electric future. www.iea.org/t&c/.
2. Fraser, J., Anderson, J., Lazuen, J., Lü, Y., Heathman, O., Brewster, N., Bedder, J., Masson, O. (2021) Study on future demand and supply security of nickel for electric vehicle batteries. Publications Office of the European Union.
3. Geissdoerfer, M., Savaget, P., Bocken, N.M.P., Hultink, E.J. (2017) The Circular Economy – A new sustainability paradigm?. J Clean Prod, 143, 757–768.
4. Department of Economic and Social Affairs. Goal 9. eng. year missing. url:sdgs.un.org/goals/goal9 (visited on 23/01/2025).
5. Department of Economic and Social Affairs. Goal 12. eng. year missing. url:sdgs.un.org/goals/goal12 (visited on 23/01/2025).
6. Moldoveanu, G.A., Demopoulos, G.P. Producing (2002) High-Grade Nickel Sulfate with Solvent Displacement Crystallization. J. Met., 49–53.
7. McGinty, J., Chong, M.W.S., Manson, A., Brown, C.J., Nordon, A., Sefcik, J. (2020) Effect of process conditions on particle size and shape in continuous antisolvent crystallisation of lovastatin. Crystals (Basel), 10, 1–17.
8. Madane, K., Ranade, V.V. (2022) Anti-solvent crystallization: Particle size distribution with different devices. Chemical Engineering Journal, 446, 137235.
9. Schwarzer, H.C., Peukert, W. (2004) Combined experimental/numerical study on the precipitation of nanoparticles. AIChE Journal, 50, 3234–3247.
10. Tang, H.Y., Rigopoulos, S., Papadakis, G. (2022) On the interaction of turbulence with nucleation and growth in reaction crystallisation, J Fluid Mech, 944.

XVI International Mineral Processing
and Recycling Conference
28-30 May 2025, Belgrade, Serbia

DOI: 10.5937/IMPRC25413C

Extended abstract

MECHANOCHEMICAL ACTIVATION OF ARGON OXYGEN DECARBURIZATION SLAGS FOR IMPROVED MINERAL CARBONATION

Luka Ceyssens[1], 0009-0000-6516-8726,
Nina Miladinović[1], 0009-0003-6181-9087,
Giuseppe Granata[1,2], 0000-0001-6593-6270,
Tom Van Gerven[1#], 0000-0003-2051-5696,
[1]Process Engineering for Sustainable Systems (ProcESS), Department of Chemical Engineering, KU Leuven, 3001 Leuven, Belgium
[2]Sustainable Material Processing and Recycling (SeMPeR), Department of Materials Engineering, Leuven, Belgium

INTRODUCTION

Mineral carbonation, a promising negative emission technology, involves the reaction of alkali-earth metal-containing materials with carbon dioxide in water, forming stable carbonates. The mineralogical composition and powder morphology of AOD slag make it an ideal candidate for mineral carbonation. Quantitative X-ray diffraction (qXRD) studies reveal that an inert outer shell of amorphous silica and calcium carbonate forms during carbonation, which hinders further reaction [1]. Planetary ball milling can enhance mineral carbonation by reducing particle size, removing inert reaction products, amorphizing the material to increase reactivity [2], and causing localized temperature increases at collision sites [3], which boost reaction rates. This study aims to investigate the effect of different milling modes in a Fritsch Pulverisette 7 Premium Line planetary ball mill on the carbonation uptake of AOD slags.

EXPERIMENTAL

The fresh AOD slag chemical composition was determined using wavelength dispersive X-ray fluorescence. The theoretical maximum carbonation uptake was estimated based on the calcium and magnesium content in the slag. For the mineral carbonation experiments, AOD slag was placed in a zirconium oxide grinding bowl within a stainless steel casing (Fritsch), along with zirconium oxide grinding beads and ultrapure water. Three different process modes were evaluated: concurrent milling and carbonation (with the grinding bowl pressurized to 5 bar with pure CO_2), sequential milling and carbonation (milling without CO_2 followed by carbonation in a pressurized reactor), and staged milling and carbonation (alternating 10-minute cycles of milling

---

[#] corresponding author: tom.vangerven@kuleuven.be and carbonation). Carbonation uptake was measured using pressure calcimetry and confirmed with thermogravimetric analysis. The mineralogical composition was analyzed using quantitative X-ray diffraction, particle size distribution was measured by laser diffraction, and particle morphology was examined using scanning electron microscopy.

RESULTS AND DISCUSSION

As shown in Fig. 1, concurrent wet milling and carbonation result in the fastest reaction rate due to the presence of mechanochemical effects during the carbonation process.

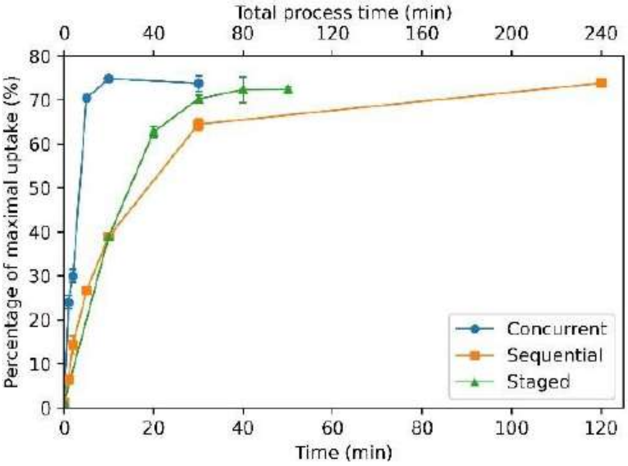

Figure 1 (a) Carbonation uptakes of various process modes at 500 rpm of milling

The other two process modes eventually achieve similar final uptakes, but at a slower rate because the mechanochemical effects are separated from the carbonation step. In all cases, a high carbonation uptake is achieved, exceeding 70% of the theoretical maximum uptake, which corresponds to an absolute uptake of 0.37 g CO_2 per g AOD slag. This value represents a plateau, as higher carbonation uptake levels were not observed. Fig. 2a shows that in the concurrent process mode, the mean particle diameter (D50) initially decreases and then sharply increases. In the staged mode, the milling step reduces particle size, followed by an increase during carbonation. This cycle repeats until milling can no longer reduce particle size, at which point carbonation effectively stops. This suggests that the carbonation plateau is partially due to particle agglomeration. Additionally, Fig. 2b indicates that the concentrations of certain Ca- and Mg-containing mineral phases remain relatively constant, suggesting they are not reactive under the tested conditions. Most mineral phases in AOD slags, such as bredigite, merwinite, and γ-C2S, are either mostly or completely consumed during carbonation. Excluding the Ca and Mg in these phases from the theoretical maximum uptake calculation raises the carbonation level to above 80%.

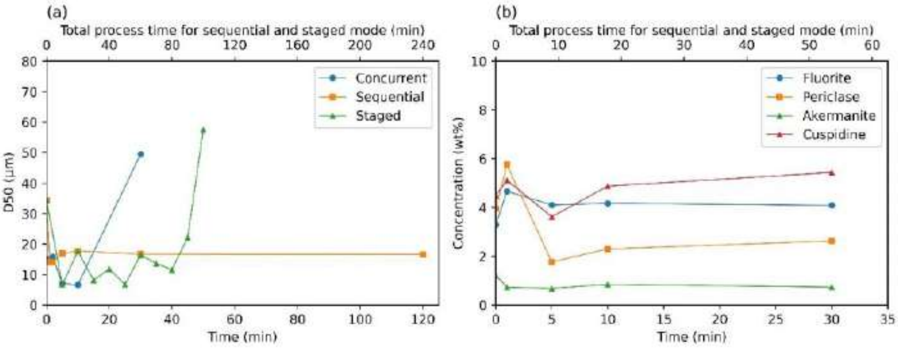

Figure 2 Evolution of (a) mean particle diameter for different process modes during carbonation and (b) concentration of non-reactive mineral phases

CONCLUSION

This study explores the direct aqueous mineral carbonation of AOD slags, enhanced through mechanochemical activation using a planetary ball mill. The process of planetary ball milling greatly boosts carbonation uptake, with the concurrent mode delivering the highest and quickest results. While sequential carbonation is more practical for industrial applications, staged carbonation, despite being slightly more effective, is more intricate and energy-demanding. Additionally, particle agglomeration and the presence of non-reactive crystalline phases were identified as factors contributing to incomplete carbonation conversion.

Keywords: Mechanochemistry, Mineral carbonation, Planetary ball mill.

ACKNOWLEDGEMENT

The Research Foundation—Flanders (FWO) is gratefully ac-knowledged for funding this research as part of the C-Farms(S004023N) and AgriCarb (G0A4821N) projects.

REFERENCES

1. de Schutter, A., Ceyssens, L., Granata, G., Van Gerven, T. (2024) “Improving the Carbonation of Steel Slags Through Concurrent Wet Milling,” J. Sustain. Metall., doi: 10.1007/s40831-024-00895-2.
2. Senna, M. (2001) “Recent development of materials design through a mechanochemical route,” International Journal of Inorganic Materials, vol. 3, no. 6, pp. 509–514, doi: 10.1016/S1466-6049(01)00060-5.
3. Maruthupandian, S., Chaliasou, A., Kanellopoulos, A. (2021) “Recycling mine tailings as precursors for cementitious binders – Methods, challenges and future outlook,” Construction and Building Materials, vol. 312, p. 125333, doi: 10.1016/j.conbuildmat.2021.125333.
4. van der Sloot, H.A., Heasman, L., Quevauviller, P. (1997) Harmonization of leaching/extraction tests, Elsevier, Amsterdam.

XVI International Mineral Processing
and Recycling Conference
28-30 May 2025, Belgrade, Serbia

DOI: 10.5937/IMPRC25416M
Research article

TREATMENT OF ACIDIC MINE WATERS BY THE NEUTRALIZATION PROCESS

Miomir Mikić#**,** 0000-0001-7659-769X,
Vesna Marjanović, 0000-0001-8005-5244,
Emina Požega, 0000-0001-6797-2435,
Radmilo Rajković, 0000-0001-5905-6613,
Mining and Metallurgy Institute Bor, Bor, Serbia

ABSTRACT – Mine water is one of the biggest challenges facing the global mining industry. This water is primarily produced by the oxidation of sulfide minerals when exposed to air, water, and microbial activity in active or abandoned mines containing polymetallic sulfide ores or coal mines. It is characterized by high acidity, with a pH value usually below 4, which usually indicates high concentrations of sulfates and dissolved metal ions. There are two different treatment strategies: removing toxic metals and reducing the acidity of mine water. Processes for neutralization of acid mine waters with lime are the most commonly used. This process has low operating costs. untreated acid mine water is used, and the regulation of the pH value with lime leads to the precipitation of insoluble metal hydroxides.

Keywords: Acid Mine Waters, Sulphide Minerals, Neutralization, Lime.

INTRODUCTION

Mine waters represent one of the global mining industry's most significant challenges. These waters are primarily formed by the oxidation of sulphide minerals when they are exposed to air, water, and microbiological activity in active or abandoned mines of polymetallic sulphide ores, coal mines [1-4]. It is characterized by high acidity, which confirms the pH value, which is usually below 4, which generally confirms the high concentration of sulfates and dissolved metal ions [5].

Discharge of mine water without prior treatment leads to contamination of nearby water sources, flora, and fauna. This has serious negative impacts on biodiversity and causes high levels of metal ions in soil to reach the top of the food chain, ultimately creating a risk to human health. Therefore, the treatment of water in question is one of the most important topics in the field of environmental protection. During the past decades, researchers have made every effort to purify these waters by reducing acidity and removing metal ions to reduce their negative impact on the environment and human health [6]. Available treatment methods have confirmed that lime neutralization is a frequently applied and inexpensive technique. However, the main disadvantage of the

---

corresponding author: miomir.mikic@irmbor.co.rs

mentioned method is the creation of a large amount of sludge, which does not favor the comprehensive utilization of useful metals and sulfates from treated waters [7]. Other conventional approaches such as ion exchange [8], chemical precipitation [9], adsorption [10], membrane separation techniques [11, 12], electrochemical processes (electrodialysis, electrocoagulation, electrokinetic) are also often used to treat mine waters [13], with most of these techniques mainly focusing on the neutralization of acidity, metal ions and sulfates in the treated waters rather than the valorization of useful and high-value components adequately.

FORMATION OF MINE WATERS

Mine waters are highly acidic, which confirms the pH value, which is usually below 4 and they are one of the main pollutants of the environment. Generally, they are formed by the oxidation of sulphide minerals due to exposure to air, water, and microbial activity [14, 15].

Pyrite is one of the most abundant and widespread sulphide minerals and is widely considered to be the dominant cause of acid mine waters (AMD) formation [16, 17]. Moreover, arsenopyrite, chalcopyrite, galena, pyrrhotite, and sphalerite also contribute to AMD formation [18]. A series of chemical reactions involved in the formation of AMD is shown in Figure 1 [19]. Pyrite exposed to water and air is first oxidized, releasing H^+, SO_4^{2-}, and Fe^{2+} ions on the surface, and the Fe^{2+} ions continue to be further oxidized to Fe^{3+} in water exposed to air. At low pH, Fe^{3+} ions will be hydrolyzed and precipitated to form $Fe(OH)_3$ precipitate, while some Fe^{3+} ions can continue to oxidize pyrite to produce sulfate and acid, leading to the formation of AMD [15, 20].

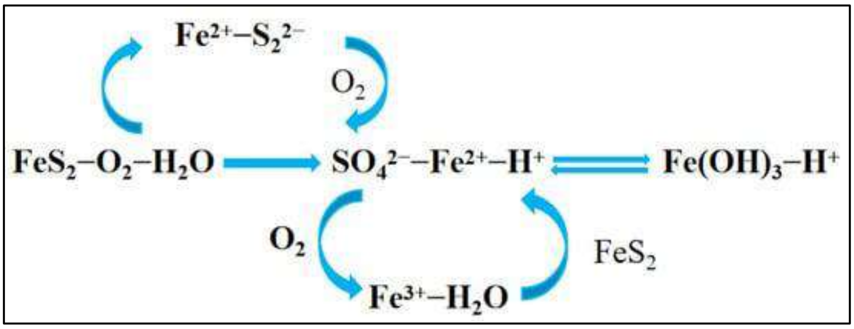

Figure 1 Chemical reactions are associated with the formation of AMD [19]

CHEMICAL COMPOSITION AMD

The chemical composition of mine waters is determined by the composition of ores and ore minerals. Deposits of different mineral raw materials are characterized by different chemical compositions of groundwater. In addition to the mineralogical composition, general structural-geological, modern climatic, and other factors, the formation of the chemical composition of groundwater of mineral deposits is influenced by various processes that take place in different geochemical environments. [21]

Geochemical processes take place in three natural geochemical environments: oxidizing, reducing, and metamorphic. The formation of the chemical composition of natural waters, and therefore of groundwater in ore deposits, takes place under the influence of basic geochemical processes: sulfuric-acidic, oxygenic, carbon dioxide, and hydrolytic.

Sulfuric acid processes are the leading processes for the decomposition of sulphide minerals. It is most active in the oxidation zone of sulfide-type copper deposits and polymetallic ores, enriched with Fe and Cu disulfides. Depending on the character of the reactions taking place, the sulfuric-acid process can have an oxidizing or reducing character. These processes significantly affect the migration ability of elements, their dispersion, and concentration. [22] Table 1 shows the chemical composition of the accumulated mine water. The pH value of acidic mine waters ranges from 2 to 4.

Table 1 An example of the chemical composition of accumulated mine water in an inactive open pit [25]

Element	**Zn**	**Cd**	**Cr**	**Cu**	**Ni**	**Fe**	**Pb**	**As**	**Hg**
mg/l	12.82	0.12	0.06	29.56	0.62	149.28	0.16	<0.020	<0.0005

BASIC PRINCIPLES OF THE NEUTRALIZATION PROCESS

The most commonly used method is neutralization with lime in neutralization reactors. High efficiency in removing dissolved heavy metals and low operating costs make this method the most commonly applied. Lime treatment consists of regulating the pH value of untreated water to a value at which metal pollutants are insoluble, which leads to the precipitation of metal hydroxides. After that, these sediments are separated to obtain purified wastewater that meets the regional criteria for discharge into the recipient.

Each metal in solution contributes to a certain acidity of acid mine waters, and in addition, each metal precipitates at a certain pH value, Table 1. Many metals have amphoteric properties, and their solubility decreases with an increase in pH up to a certain limit value, above which their solubility increases again, due to the formation of soluble complexes. Table 2 shows that most of the metal cations present in acid mine water can be settled if the pH of these waters is increased to a pH of around 9.5.

The solid/liquid separation forms sludge, which, depending on the applied process, can contain from 1 to 30% of solid matter. This sludge must be disposed of outside the system in an environmentally acceptable manner [23].

The advantages of the technology of treating acidic mine waters with lime are its effectiveness for the treatment of highly acidic waters, its simplicity, it has been checked and tested. The water after neutralization is of such quality that it can be directly discharged into the receiver. Changing the quality and quantity of acid mine waters can be easily adjusted by adjusting the basic parameters of the operation [24].

Disadvantages of the technology of treatment of acidic mine waters with lime are high maintenance costs, the resulting sludge is chemically unstable, complex, has a low density, and is gelatinous, which poses a problem during its disposal, and has no commercial value. The precipitation of metal ions such as Mn requires a high pH value, which can interfere with the precipitation of other metal hydroxides, e.g., Al.

Table 2 The theoretical value of pH at which the solubility of metal hydroxide is minimal [24]

Metal cations that precipitate as hydroxides	**Precipitation of hydroxide**	**pH value that corresponds to the minimum solubility of metal hydroxide/L**
Fe^{3+}	$Fe^{3+} + 3OH^- \rightarrow Fe(OH)_3 \downarrow$	~ 3,5
Sb^{2+}		~ 4,2
Al^{3+}	$Al^{3+} + 3OH^- \rightarrow Al(OH)_3 \downarrow$	~ 4,5
Pb^{2+}	$Pb^{2+} + 2OH^- \rightarrow Pb(OH)_2 \downarrow$	~ 6,5
Cu^{2+}	$Cu^{2+} + 2OH^- \rightarrow Cu(OH)_2 \downarrow$	~ 7,0
Fe^{2+}	$Fe^{2+} + 2OH^- \rightarrow Fe(OH)_2 \downarrow$	~ 8,0
Zn^{2+}	$Zn^{2+} + 2OH^- \rightarrow Zn(OH)_2 \downarrow$	~ 8,5
Ni^{2+}	$Ni^{2+} + 2OH^- \rightarrow Ni(OH)_2 \downarrow$	~ 9,3
Cd^{2+}		~ 10,0
Mn^{2+}		~ 10,6
Co^{2+}	$Co^{2+} + 2OH^- \rightarrow Co(OH)_2 \downarrow$	

The basis of the neutralization of acidic mine waters with lime is the insolubility of heavy metals in a basic medium. Metal ions Fe, Zn, Cu, Al, Pb, etc., are deposited up to a pH value of 9.5, while Mn and Cd require a higher pH value (pH=10.5-11).

Metal deposits that occur in all processes of lime processing represent waste, better known as waste sludge, which is hazardous waste and should be handled according to legal regulations. Given that the costs of sludge disposal can be significant, the volumetric amount of sludge must be minimal.

CONCLUSION

The main sources of acid mine waters are mines and process tailings, ore, and mining operations related to ore extraction. The main pathway for the release of acidity, metals, and metalloids into the environment is water. Acid mine waters represent a major environmental problem caused by mining. Acid mine water is unique among industrial pollutants because of its leaching capacity, which is enhanced by bacterial activity and is self-perpetuating. Processes for treating acidic mine waters with lime have advantages and disadvantages. They can be simple with older processing methods or complex with modern and efficient systems. Older methods are less efficient and do not have good control over the processing system. While modern processes require huge capital investments, they are significantly more efficient regarding lime use and waste treatment.

ACKNOWLEDGEMENT

The authors are grateful to the Ministry of Science, Technological development and Innovation of the Republic of Serbia for financial support according to the contract with the registration number 451-03-136/2025-03/ 200052.

REFERENCES

1. Levio-Raiman, M.; Briceño, G.; Schalchli, H.; Bornhardt, C.; Diez, C.M. Alternative treatment for metal ion removal from acid mine drainage using an organic biomixture as a low cost adsorbent. Environ. Technol. Innov. 2021, 24, 101853.
2. Rambabu, K.; Banat, F.; Quan, M.P.; Ho, S.H.; Ren, N.Q.; Show, P.L. Biological remediation of acid mine drainage: Review of past trends and current outlook. Environ. Sci. Technol. 2020, 2, 100024.
3. Wang, Z.L.; Xu, Y.X.; Zhang, Z.X.; Zhang, Y.B. Review: Acid Mine Drainage (AMD) in Abandoned Coal Mines of Shanxi, China. Water 2020, 13, 8.
4. Yang, B.J.; Luo, W.; Hong, M.X.; Wang, J.; Liu, X.D.; Gan, M.; Qiu, G.Z. Inhibition of hematite on acid mine drainage caused by chalcopyrite biodissolution. Chin. J. Chem. Eng. 2022, 44, 94–104.
5. Carneiro Brandao Pereira, T.; Batista Dos Santos, K.; Lautert-Dutra, W.; de Souza Teodoro, L.; de Almeida, V.O.; Weiler, J.; Homrich Schneider, I.A.; Reis Bogo, M. Acid mine drainage (AMD) treatment by neutralization: Evaluation of physical-chemical performance and ecotoxicological effects on zebrafish (Danio rerio) development. Chemosphere 2020, 253, 126665.
6. Fernández-Caliani, J.C.; Giráldez, M.I.; Barba-Brioso, C. Oral bioaccessibility and human health risk assessment of trace elements in agricultural soils impacted by acid mine drainage. Chemosphere 2019, 237, 124441.
7. Aguiar, A.O.; Andrade, L.H.; Ricci, B.C.; Pires, W.L.; Miranda, G.A.; Amaral, M. Gold acid mine drainage treatment by membrane separation processes: An evaluation of the main operational conditions. Sep. Purif. Technol. 2016, 170, 360–369.
8. Silva, D.; Weber, C.; Oliveira, C. Neutralization and uptake of pollutant cations from acid mine drainage (amd) using limestones and zeolites in a pilot-scale passive treatment system. Miner. Eng. 2021, 170, 107000.
9. Öztürk, Y.; Ekmekçi, Z. Removal of sulfate ions from process water by ion exchange resins. Miner. Eng. 2020, 159, 106613.
10. Geoffroy, N.; Demopoulos, G.P. The elimination of selenium (IV) from aqueous solution by precipitation with sodium sulfide. J. Hazard. Mater. 2011, 185, 148–154.
11. Zheng, Q.; Zhang, Y.; Zhang, Z.; Li, H.; Wu, A.; Shi, H. Experimental research on various slags as a potential adsorbent for the removal of sulfate from acid mine drainage. J. Environ. Manag. 2020, 270, 110880.
12. Foureaux, A.F.S.; Moreira, V.R.; Lebron, Y.A.R.; Santos, L.V.S.; Amaral, M.C.S. Direct contact membrane distillation as an alternative to the conventional methods for value-added compounds recovery from acidic effluents: A review. Sep. Purif. Technol. 2020, 236, 116251.
13. Chen, G.; Ye, Y.C.; Yao, N.; Hu, N.Y.; Zhang, J.; Huang, Y. A critical review of prevention, treatment, reuse, and resource recovery from acid mine drainage. J. Cleaner Prod. 2021, 329, 129666.
14. Acharya, B.S.; Kharel, G. Acid mine drainage from coal mining in the United States—An overview. J. Hydrol. 2020, 588, 125061.
15. Chen, Y.T.; Li, J.T.; Chen, L.X.; Hua, Z.S.; Huang, L.N.; Liu, J.; Xu, B.B.; Liao, B.; Shu, W.S. Biogeochemical processes governing natural pyrite oxidation and release of acid metalliferous drainage. Environ. Sci. Technol. 2014, 48, 5537–5545.
16. Ouyang, Y.; Liu, Y.; Zhu, R.; Ge, F.; Xu, T.; Luo, Z.; Liang, L. Pyrite oxidation inhibition by organosilane coatings for acid mine drainage control. Miner. Eng. 2015, 72, 57–64.
17. Park, I.; Tabelin, C.B.; Jeon, S.; Li, X.; Seno, K.; Ito, M.; Hiroyoshi, N. A review of recent strategies for acid mine drainage prevention and mine tailings recycling. Chemosphere 2019, 219, 588–606.

18. Chopard, A.; Benzaazoua, M.; Bouzahzah, H.; Plante, B.; Marion, P. A contribution to improve the calculation of the acid generating potential of mining wastes. Chemosphere 2017, 175, 97–107.
19. Buzzi, D.C.; Viegas, L.S.; Rodrigues, M.A.S.; Bernardes, A.M.; Tenório, J.A.S. Water recovery from acid mine drainage by electrodialysis. Miner. Eng. 2013, 40, 82–89.
20. Simate, G.S.; Ndlovu, S. Acid mine drainage: Challenges and opportunities. J. Environ. Chem. Eng. 2014, 2, 1785–1803.
21. Thomas, G.; Sheridan, C.; Holm, P.E. A critical review of phytoremediation for acid mine drainage-impacted environments. Sci. Total Environ. 2022, 811, 152230.
22. M. D. Dimitrijević. Kisele rudničke vode, Bakar 1. 2012, vol.37, str. 33-44.
23. B. Aubé, J. Zinck. Lime Treatment of Acid Mine Drainage in Canada. Presented and published at “Brazil-Canada Seminar on Mine Rehabilitation, Florianópolis, Brazil. 2003, December 1-3.
24. M. D. Dimitrijević, M. M. Nujkić, S. M. Milić. Obrada kiselih rudničkih voda krečom. Bakar 1, 2012, vol. 37, 45-56.
25. V. M. Marjanović, R.Marković, Calculation of Calcium Oxide Consumption in the Mine Wastewater Treatment from Inactive Open Pits of the Copper Mine, D. Božić, EcoTER'24, 18–21 June 2024, Hotel Sunce, Sokobanja, Serbia.

XVI International Mineral Processing
and Recycling Conference
28-30 May 2025, Belgrade, Serbia

DOI: 10.5937/IMPRC25422V

Original research article

INFLUENCE OF CATIONIC SURFACTANTS ON THE ELECTROKINETIC PROPERTIES AND STABILITY OF SILICA-KAOLINITE SUSPENSIONS UNDER COPPER HYDROMETALLURGY CONDITIONS

Julio Valenzuela Elgueta[1#], 0009-0005-2857-5505,
Silvia Ahualli Yapur[2], 0000-0002-7329-0817,
Angel Vicente Delgado Mora[2], 0000-0003-1843-5750,
[1]Universidad Católica del Norte, Antofagasta, Chile
[2]Universidad de Granada, Granada, España

ABSTRACT – Small particles, such as silica and clays, complicate hydrometallurgy by forming crud that floats or remains suspended. Adding surfactants may promote sedimentation, but requires evaluating their composition and dosage. This study uses dynamic electrophoretic mobility to assess CTAB adsorption on silica/kaolinite mixtures under low pH, high ionic strength, and particle concentrations above 3%. Electroacoustic analysis predicts surfactant effects on individual and mixed particles, aligning with sedimentation rates and size measurements. SEM images confirm aggregate formation with CTAB. Identifying optimal surfactant doses to flocculate and separate particles addresses operational issues caused by crud in hydrometallurgy processes.

Keywords: Clay, Copper mining, Electroacoustics, Surfactants, Stability.

INTRODUCTION

A major challenge in oxidized copper ore beneficiation is the formation of mineral complexes due to particle interactions in the solid matrix, carried by the leaching solution to solvent extraction. These interactions, driven by low pH and high ionic concentration, lead to aggregation and crud formation—a dispersed particle layer complicating separation processes [1, 2].

A solution involves using low-concentration cationic surfactants to modify particle stability. Surfactants adsorb onto particles, neutralizing electrokinetic charge, promoting flocculation, and destabilizing particles via hydrophobic attraction. They outperform inorganic ions by achieving these effects at lower concentrations, with longer chains enabling bridging flocculation. Polymers like polyethylene oxide and polyacrylamide-acrylate also effectively control slurry stability, evaluated through particle size and zeta potential measurements. Electroacoustic techniques provide simultaneous insights into particle size and electrokinetic properties.

Interfacial properties are crucial in processes like froth flotation, where mineral-solution interface charges determine efficiency. Electroacoustic methods and adsorption measurements effectively study these interactions. This study applies the Electrokinetic

---

[#] corresponding author: jvalenzuela01@ucn.cl

Sonic Amplitude (ESA) technique to assess CTAB adsorption on silica/kaolinite mixtures under hydrometallurgical conditions of low pH, high ionic strength, and high particle concentrations—key factors in crud formation.

By evaluating CTAB adsorption, the study offers strategies to control particle aggregation, mitigating crud formation and improving mineral extraction and separation efficiency.

EXPERIMENTAL

Materials

To replicate conditions in copper hydrometallurgy, the colloidal suspensions consist of silica and kaolinite particles dispersed in 80 mM copper sulfate solution at pH 2. Materials (Merck & Co., USA) included Ludox TMA silica, natural kaolinite, $CuSO_4{\cdot}5H_2O$, sulfuric acid (95–98% purity), and the cationic surfactant CTAB. Surface areas of kaolinite (15 m^2/g) and silica (63.2 m^2/g) were determined using N_2 adsorption at 77 K with BET analysis (Nova 2200e, Quantachrome Instruments). Solutions were prepared with Milli-Q deionized water. The colloidal suspensions studied were as follows:

1. Silica suspensions in 80 mM $CuSO_4$ at pH 2.
2. Kaolinite suspensions in 80 mM $CuSO_4$ at pH 2.
3. Mixtures of kaolinite/silica at the same volume fraction, 80 mM $CuSO_4$ at pH 2.

Methods

Particle size

The hydrodynamic radius of the particles was determined by dynamic light scattering by means of a Malvern Zetasizer NanoZS (Malvern Instruments, UK), yielding a number average diameter of 22 ±7 nm (silica) and 800 ±130 nm (kaolinite).

Microscopic observations

The structures formed by kaolinite and silica for the different experimental conditions were observed by scanning electron microscopy (Model SU5000, Hitachi, Japan).

Electrokinetic measurements

The electrokinetic characterization was carried out in two phases. As a first approximation, the DC electrophoretic mobility of dilute suspensions was measured in the Zetasizer NanoZS. Then, the dynamic mobility was measured using the AcoustoSizer IIc ESA apparatus (Colloidal Dynamics, USA). Since the ionic concentration of the suspensions is rather high, background correction of raw data was carried out in all cases, for the correct determination of u_d.

Stability tests

In order to evaluate the stability of the suspensions, a sedimentation test was carried out using a 6705 UV/VIS spectrophotometer (Jenwat, UK). The sedimentation was followed by recording the optical absorbance as a function of time. The wavelength was set at 470 nm.

RESULTS AND DISCUSSION

Electrophoretic mobility

The electrical surface properties of silica, kaolinite, and their mixtures were analyzed by observing the effect of CTAB concentration (up to 1 mM, near the critical micelle concentration) on the electrophoretic mobility (u_e) of particle suspensions under hydrometallurgical conditions (80 mM $CuSO_4$, pH 2).

Fig. 1 shows that silica's mobility remains largely unchanged as CTAB increases, contrasting with studies indicating strong CTAB affinity for silica at various pH levels [3]. The minimal mobility reduction, saturating at low CTAB concentrations, may result from the small particle size and high hydrophilicity limiting CTAB adsorption.

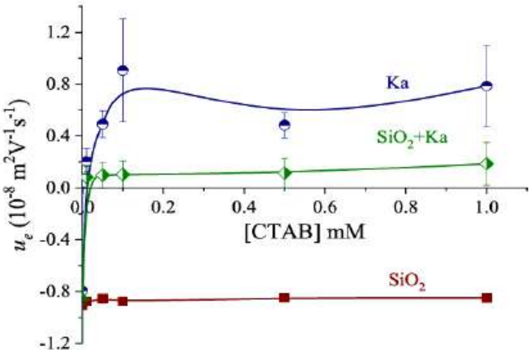

Figure 1 Electrophoretic mobility (u_e) as a function of CTAB concentration for suspensions of silica (SiO_2), kaolinite (Ka) and a 1:1 mixture (SiO_2 +Ka), in 80 mM $CuSO_4$ solutions at pH 2. Error bars correspond to ±SD (n =12)

Conversely, kaolinite exhibits significant mobility changes with CTAB addition, including a charge polarity reversal due to overcharging from effective surfactant adsorption. This aligns with reports [4, 5] that low pH enhances adsorption, suggesting low CTAB doses can neutralize kaolinite charge and promote aggregation in crud.

For silica-kaolinite mixtures, mobility values lie between those of individual particles, skewed toward kaolinite, likely due to its dominant light scattering contribution. It remains unclear if CTAB preferentially adsorbs on specific particles or alters their interactions, an aspect explored in subsequent sections.

Dynamic electrophoretic mobility of individual particles

Electroacoustic measurements of 2.5% silica suspensions in 80 mM $CuSO_4$ (pH 2) were analyzed using dynamic mobility theories to determine zeta potentials (Table 1). The results align with static electrophoretic data, confirming reliability. Mobility decreases monotonically with CTAB, likely due to low zeta potential from high ionic strength and particle aggregation, which increases size and lowers relaxation frequency.

Table 1 Zeta potential (ζ) of silica particles in 80 mM $CuSO_4$ and pH 2, as obtained from DC electrophoresis and from electroacoustic measurements

[CTAB], mM	ζ mV (DC electrophoretic)	ζ mV (ESA)
0.00	-18.4 ± 0.4	-20.0 ± 0.5
0.05	-10.9 ± 0.2	-14.0 ± 0.5
0.10	-11.2 ± 0.4	-13.5 ± 0.5
0.50	-10.8 ± 0.3	-12.0 ± 0.5
1.00	-10.9 ± 0.5	-11.5 ± 0.5

CTAB has minimal impact on silica's zeta potential (Table 2), causing only slight decreases in $|\zeta|$. In contrast, kaolinite shows a stronger response due to its silica and alumina layers. CTAB adsorption on negatively charged silica faces increases zeta potential and alters charge density. Fig. 3 shows kaolinite mobility rising without CTAB due to MWO relaxation, indicating highly charged surfaces. CTAB addition neutralizes the negative charge, with high concentrations reversing polarity. At 1 mM CTAB, aggregation dominates, reducing relaxation frequency and mobility.

Table 2 Zeta potential (ζ) of kaolinite particles in 80 mM $CuSO_4$ and pH 2, as obtained from DC electrophoresis and from electroacoustic measurements

[CTAB], mM	ζ mV (DC electrophoretic)	ζ mV (ESA)
0.00	-10.1 ± 0.2	-13.0 ± 0.2
0.05	+6.2 ± 0.5	+6.3 ± 0.3
0.10	+11.5 ± 0.5	11.3 ± 0.5
0.50	6.2± 0.3	+6.5± 0.5
1.00	+9.9 ± 0.2	+10.2 ± 0.4

Kaolinite's structure promotes CTAB adsorption on its silica faces, enhancing aggregation and altering size distribution, as shown by zeta potential (Table 2) and dynamic mobility data. In contrast, silica's high hydrophilicity and small size limit surfactant interaction. Overall, CTAB significantly affects kaolinite, proving effective for modifying clay particle behavior in suspension.

Dynamic mobility of Silica/Kaolinite mixtures

Adding CTAB (Fig. 2) shifts mobility toward kaolinite's behavior as CTAB concentration increases. At 0.1 mM CTAB, mobility resembles silica's, suggesting significant silica coating on alumina, driven by silica's higher negative charge and selective siloxane adsorption on kaolinite edges at low pH. These silica-kaolinite interactions, not captured in the model, explain deviations between predictions and observations.

Higher CTAB concentrations reduce charge differences between kaolinite faces and edges, halting silica-kaolinite interactions. Kaolinite dominates again, with mobility decreasing at high frequencies, indicating large aggregate formation.

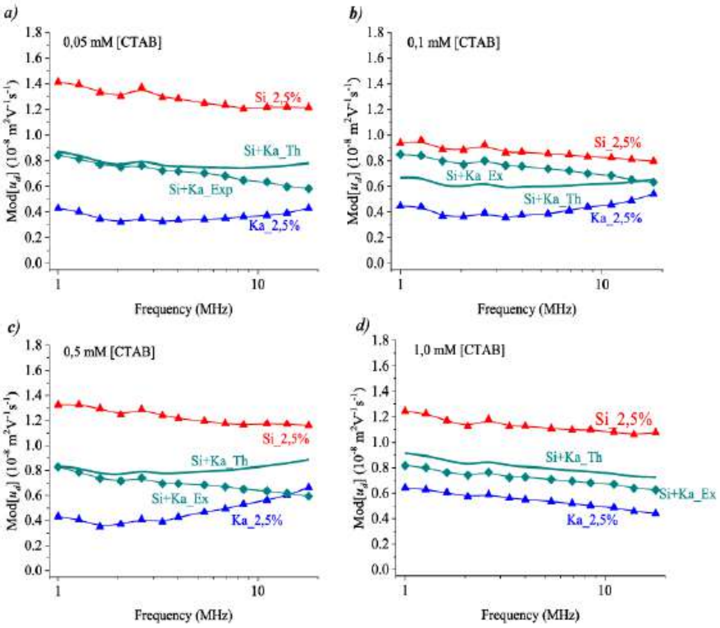

Figure 2 Frequency dependence of the modulus of the dynamic mobility of suspensions containing 2.5% silica (Si_2,5%), 2.5% kaolinite (Ka_2,5%), and their mixture (Si + Ka_Ex), including the theoretical predictions

Size distribution and stability test

In order to assess the effects of surfactant addition to the stability of suspensions of pure silica and kaolinite and their mixtures, changes in particle size distribution and sedimentation rate were measured as a function of the dose of surfactant, applied in hydrometallurgy conditions. The stability data corresponding to the mixed suspensions are plotted in Fig. 3a (size distribution) and 3b (time variation of absorbance).

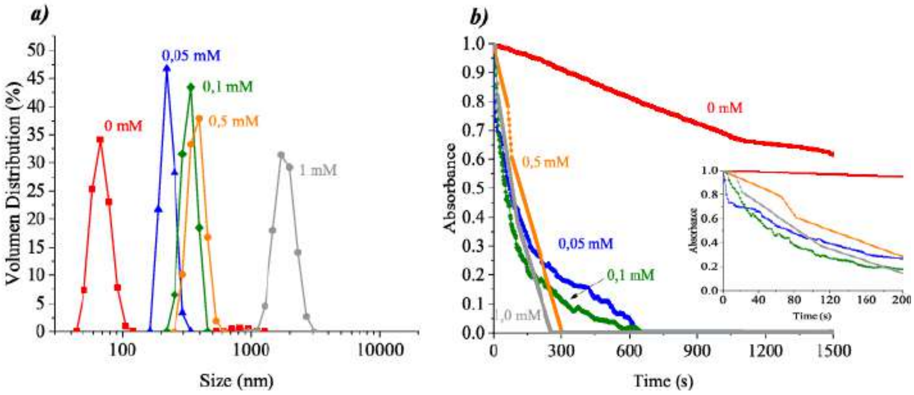

Figure 3 Same as Fig. 7, but for mixed suspensions containing 2.5% silica and 2.5% kaolinite

The sedimentation rate is also much faster in mixed systems, which undergo practically full sedimentation in less than five minutes, something not found in the individual components. It is suggested that in the presence of increasing CTAB concentrations the adsorption of silica on kaolinite is favored, as above mentioned, and this provokes the formation of structures at the experimental conditions (low pH and high ionic strength), which have been previously studied by several authors. The structure formation was ascribed to the generation of siloxane complexes, acting as a kind of binder between the larger particles, thus enhancing the flocculating effect of the surfactant.

Microscopic observations

In order to obtain an empirical proof of the hypothesized structures, a morphological analysis of the samples was performed by Scanning Electron Microscope observations. Fig. 9 shows the SEM images obtained for the various concentrations of surfactant used. The picture corresponding to 0 mM CTAB shows that silica nanoparticles have an apparent preference for adhering primarily to kaolinite edges, as described in our previous work [5].

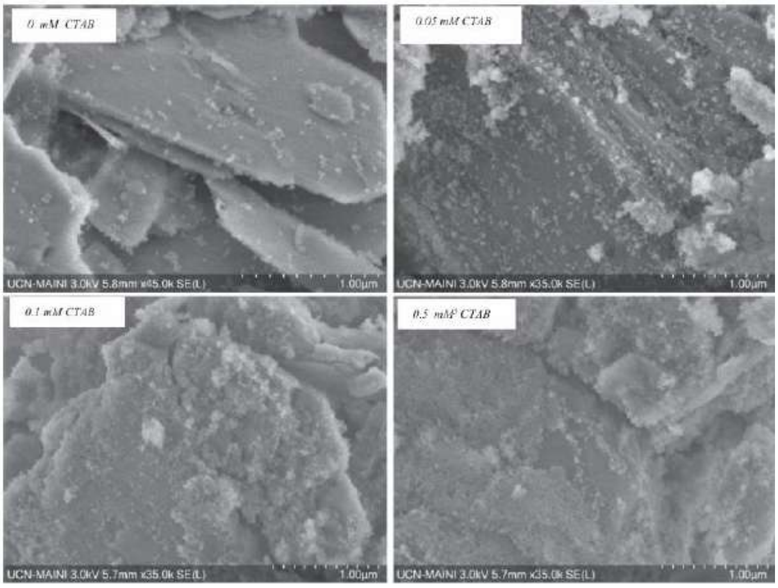

Figure 4 SEM images for the applied surfactant concentration range

By adding the CTAB surfactant, the silica and kaolinite form aggregates between themselves and also it is possible to observe silica aggregates to adhere onto the kaolinite surface in a heterogeneous form. It can be noted that, by increasing the surfactant concentration, the aggregation becomes massive, forming more complex structures. These results are consistent with what was observed in the evolution of the particle size distribution and with the behavior shown in the stability tests.

CONCLUSIONS

The dynamic mobility of kaolinite suspensions has been investigated in the same conditions, and in this case a change was produced in the polarity of the particle charge when CTAB concentration is increased. Even more, the mobility rise corresponding to a Maxwell-Wagner- O'Konski relaxation changes with the electrokinetic charge density, and at the highest CTAB concentration the inertial relaxation suggests an increment of particle size. This result is coherent with the average particle size determinations and, consequently, with the increase in sedimentation rate. Finally, the behavior of silica/kaolinite mixtures has been studied under surfactant addition. The differences at high frequency between model predictions (calculated as the weighted average of the two kinds of particles) and experimental results show that aggregation between kaolinite and silica particles is taking place. This conclusion is ascertained by size distribution spectra and sedimentation rate. Also, SEM images reveal the evolution of the aggregates forming increasingly complex structures as CTAB is added.

REFERENCES

1. Virnig, M.J., Olafson, S.M., Kordosky, G.A., Wolfe, G.A. (2003) Crud formation: Field Studies and Fundamental Studies In: Copper VI: Hydrometallurgy of Copper (BOOK 2) Modeling Impurity Control and Solvent Extraction. Canadian Institute of Mining, Metallurgy and Petroleum, Westmount.
2. Ritcey, G.M. (1980) Crud in solvent-extraction processing. Review of causes and treatment. Hydrometallurgy 5, 97–107.
3. Elias, D.S., Rabiu, A.M., Oluwaseun, O., Seima, B. (2016) Adsorption characteristics of surfactant on different petroleum reservoir materials. The Online Journal of Science and Technology 6, 6–16.
4. Kamal, S., Kamal, A., Shahzad, T., Rehman, S., Azeem, M., Bibi, I. (2017) Potential kaolinite as adsorbent to remove anionic surfactant from simulated wastewater. Desalin. Water Treat. 88, 85–92.
5. Figdore, P.E. (19829 Adsorption of surfactant on kaolinite, NaCl versus CaCl 2 Journal of colloid and science interface 87, 500–517.

XVI International Mineral Processing
and Recycling Conference
28-30 May 2025, Belgrade, Serbia

DOI: 10.5937/IMPRC25429M Original research article

CHARACTERIZATION OF ELECTRODE MATERIALS FROM SPENT BATTERIES IN THE PROCESS OF RECOVERING VALUABLE METALS

Dragana Medić[1#], 0000-0001-9980-5949,
Maja Nujkić[1], 0000-0002-6110-5135,
Žaklina Tasić[1], 0000-0001-6544-1980,
Vladan Nedelkovski[1], 0000-0001-7724-1118,
Stefan Đorđievski[2], 0000-0003-1737-8766,
Slađana Alagić[1], 0000-0002-2893-9285,
Snežana Milić[1], 0000-0002-5000-9156,
[1]University of Belgrade, Technical Faculty in Bor, Bor, Serbia
[2]Mining and Metallurgy Institute Bor, Bor, Serbia

ABSTRACT – The chemical and phase analysis of electrode materials from spent batteries is essential for identifying recyclable components and optimizing metal recovery processes. In this study, the electrode material from a spent cell of an unknown manufacturer was analyzed using inductively coupled plasma mass spectrometry (ICP-MS) and powder X-ray diffraction (XRD). XRD results revealed that the anode material consists of three crystalline phases: NiO, $LaCoO_3$, and CeO_2, while the cathode material contains $Ni(OH)_2$ and Ni. ICP-MS analysis confirmed the presence of lanthanides in the anode material. Given that lanthanide deposits are concentrated in only a few countries, their recovery from spent batteries presents an opportunity for nations without natural reserves to secure their supply through recycling. This study highlights the potential for sustainable resource management by recovering metals from electronic waste.

Keywords: Recycling, Spent batteries, Characterization, Lanthanide.

INTRODUCTION

The increasing demand for battery materials has led to growing concerns about the depletion of natural resources and the environmental impact of waste disposal. Spent batteries, including lithium-ion (LIBs) and nickel-metal hydride (NiMH) batteries, contain valuable metals such as lithium (Li), cobalt (Co), nickel (Ni), and lanthanides, making them an important secondary source of these critical raw materials [1,2].

Among these critical materials, lanthanides play a key role in battery electrodes and are classified by the European Union (EU) as critical raw materials (CRMs) due to their strategic and economic importance. However, the global supply of rare earth elements (REEs) is highly concentrated in a few countries, particularly China, raising concerns over supply security. To address this issue, the recovery of lanthanides and other valuable

---

[#] corresponding author: dmedic@tfbor.bg.ac.rs metals from spent batteries offers an opportunity to reduce dependence on primary sources and promote a circular economy. Hydrometallurgical, pyrometallurgical, and other methods were explored to enhance the efficiency of metal recovery [3].

Given the growing need for sustainable resource management, modern materials science is shifting from merely improving material properties to optimizing the reuse of secondary raw materials. The complexity of these multi-component materials requires detailed characterization to facilitate their reintegration into new applications. Understanding their chemical and structural composition is crucial for developing efficient recycling strategies and ensuring the quality of recovered materials [4].

To evaluate the quality and applicability of recycled materials, several analytical techniques are employed. Inductively coupled plasma mass spectroscopy (ICP-MS) is widely used to determine the concentrations of metals, while X-ray Diffraction (XRD) plays a critical role in determining the phase composition of the samples [5].

By integrating sustainable recycling strategies with advanced material characterization techniques, the recovery process can contribute to a more efficient and environmentally friendly battery supply chain. In this study, the recovered materials were analyzed using XRD to determine their phase composition and ICP-MS to assess their chemical composition, providing essential insights into their suitability for reuse.

EXPERIMENTAL

Sample Preparation

The analyzed sample was a spent battery from an unknown manufacturer. After opening the battery, six individual cells were extracted and fully discharged to prevent short circuits before disassembly. Using a hacksaw, the cell terminals were removed, followed by a longitudinal cut to separate the plastic casing, metal casing, anode, cathode, and separator (Figure 1). The anodic material was thermally treated at 580°C for 10 minutes to detach it from the current collector. Both anodic and cathodic materials were then ground into a fine powder using an agate mortar and pestle.

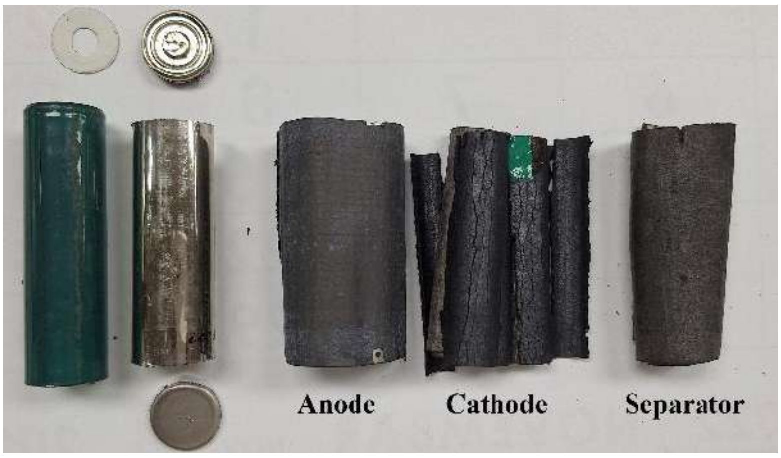

Figure 1 Basic components of a battery

Analytical Techniques

The metals from the recovered anode material were extracted using acid digestion. A 0.375 g sample was treated with 15 mL of aqua regia (a mixture of HCl and HNO_3), leaving behind a small portion of undissolved residue. The resulting solution was diluted to 100 mL with deionized water in a volumetric flask, then further diluted 25-fold in a 25 mL volumetric flask. Additional dilutions of 10-, 100-, and 10,000-fold were prepared to ensure that element concentrations fell within the linear range of the calibration curve before analysis using ICP-MS (PerkinElmer NexION 1000). Multi-element calibration standards (AccuStandard PE-MECAL2-ASL-1 and MES-21-1) were used for calibration and quality control of the measurements.

To accommodate the wide range of element concentrations, multiple dilutions were necessary, as their levels spanned several orders of magnitude. However, extensive dilution can introduce greater analytical errors, particularly for elements present in higher concentrations, potentially affecting measurement accuracy. The standard deviations between different dilutions ranged from 1.0% to 28.4%, indicating variable repeatability for different elements. Additionally, the obtained element concentrations do not represent the total elemental content of the sample, as an undissolved residue remained after digestion. Therefore, the determined values should be interpreted as the fractions extracted by aqua regia, rather than the total elemental concentrations.

The phase composition of the cathode and anode materials was characterized using powder X-ray diffraction (XRD). Measurements were carried out on a Rigaku MiniFlex 600 diffractometer equipped with a high-speed D/teX Ultra 250 detector and a copper anode X-ray tube. Data were collected over a 3–90° 2θ range with a step size of 0.02° and a scan speed of 10°/min. The instrument operated at 40 kV and 15 mA. Phase identification was performed using PDXL 2 software (Version 2.4.2.0), with diffractograms compared with reference patterns from the ICDD PDF-2 2015 database.

RESULTS AND DISCUSSION

Chemical Composition Analysis

The elemental composition of the anode material was analyzed to assess the presence of valuable metals and rare earth elements (REEs). The results (Table 1) indicate a high concentration of lanthanides, with lanthanum (14.6 %), neodymium (1.85 %), and cerium (1.32 %) as the most abundant. These elements, crucial for electrochemical performance, highlight the potential for REE recovery from spent batteries. Additionally, significant amounts of nickel (7.33 %) and manganese (3.07 %) were detected, confirming their role as key electrode components. The presence of cobalt (1.03 %) and copper (0.14 %) suggests recovery potential for secondary applications, while yttrium (0.20 %) and gadolinium (0.06 %) further emphasize the importance of recycling REEs.

Table 1 Elemental chemical composition (%) of the anode material

Element	Ce	Gd	La	Nd	Pr	Y	Co	Cu	Li	Mn	Ni
Content (%)	1.32	0.06	14.6	1.85	0.58	0.20	1.03	0.14	<0.01	3.07	7.33

A similar study was conducted by Bertuol *et al.* [6], who characterized five different NiMH batteries and concluded that the chemical composition of spent NiMH batteries can vary significantly depending on battery type, manufacturer, and intended application.

These findings reinforce the need for sustainable recycling strategies to minimize environmental impact and secure critical raw materials for future applications. Efficient recovery methods can support the circular economy by reducing dependence on primary sources and promoting the reuse of valuable metals.

Phase Composition Analysis

To determine the phase composition of the recovered materials, XRD analysis was conducted on both the anode and cathode samples. The resulting diffraction patterns provide insights into the phase composition of these materials, which are essential for evaluating their suitability for reuse and further processing. The diffractograms of anode and cathode materials are presented in Figures 2 and 3, respectively.

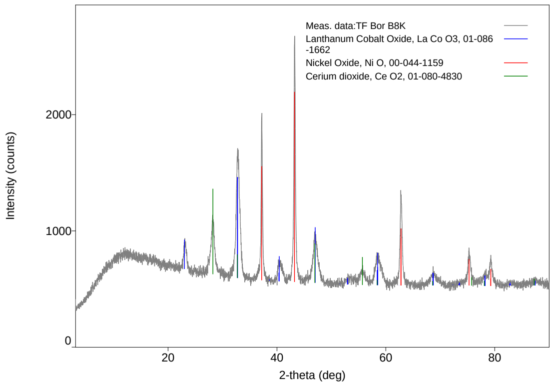

Figure 2 Diffractogram of the anode material

The diffractogram of the anode material (Figure 2) confirms the presence of three crystalline phases, identified as lanthanum cobalt oxide ($LaCoO_3$), nickel oxide (NiO), and cerium dioxide (CeO_2). These findings are in agreement with the results reported by Kanamori *et al.* [7], who also identified NiO, CeO_2, and $LaCoO_3$ as the main phases recovered from NiMH battery waste by chemical separation methods. Their study further demonstrated the applicability of these oxides as catalysts in methane dry reforming, emphasizing their potential for both metal recovery and functional reuse.

Other elements, such as Gd, Nd, Pr, Y, Cu, and Mn, may substitute for La, Co, Ce, and Ni within these crystalline structures. However, the exact distribution of these elements cannot be determined solely by XRD analysis, as phase identification relies on peak positions, which may overlap among different crystalline phases. Additionally, the XRD pattern exhibits well-defined peaks with no significant amorphous background, indicating a high degree of crystallinity in the analyzed sample.

The composition of the original NiMH anode typically consists of a metal alloy primarily composed of Ce, La, Pr, Nd, Ni, Co, Mn, and Al [8]. The detection of $LaCoO_3$ and NiO suggests that oxidation occurred during the annealing process, which was used to separate the anodic material from the current collector. Additionally, the formation of CeO_2 further confirms the oxidation of rare earth elements, emphasizing the impact of thermal treatment on the phase composition. These findings reinforce the need to optimize recycling processes to maximize the efficient recovery of critical raw materials.

The diffractogram of the cathode material (Figure 3) reveals two distinct crystalline phases, with the identified peaks corresponding to $\beta\text{-Ni(OH)}_2$, which is a more abundant phase, and metallic nickel (Ni), which is less abundant. The presence of $\beta\text{-Ni(OH)}_2$ indicates a nickel hydroxide phase, which is characteristic of secondary battery cathode materials. This observation is consistent with previous studies, including the work of Batsukh *et al.* [9], which identified $\beta\text{-Ni(OH)}_2$ as a major phase in the cathode materials of spent NiMH batteries. These findings provide essential insights into the structural properties of the recovered cathode material, which are crucial for determining its feasibility for further processing and reuse in battery recycling applications.

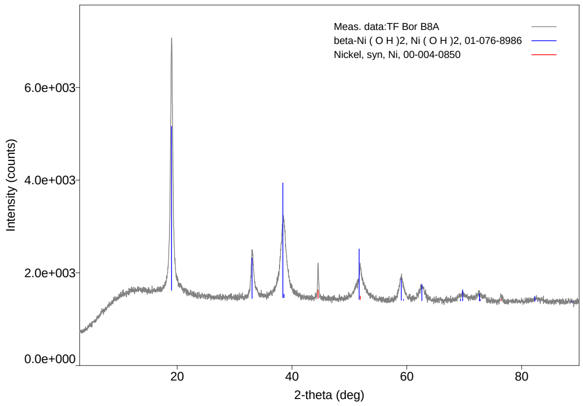

Figure 3 Diffractogram of cathode material

CONCLUSION

The characterization of electrode materials from spent NiMH batteries revealed significant amounts of valuable metals such as nickel, cobalt, and rare earth elements. Chemical and phase analyses identified stable oxide phases, including NiO, CeO_2, and $LaCoO_3$, indicating a high degree of stability and well-defined metal speciation within the electrode structure. These insights are essential for optimizing recycling processes, as they enable selective planning of extraction and separation methods. While some oxides, such as NiO, can be readily reduced and used as raw materials, rare earth oxides require more intensive approaches, including reduction, complexation, or thermal treatment.

In addition to metal recovery, the obtained materials also show potential for direct functional applications, including catalysis and photocatalysis, further increasing the value of these secondary raw materials. This approach contributes not only to the economic viability but also to the sustainability of recycling processes. Understanding the mineralogical and chemical forms of metals in battery waste is key to developing efficient and environmentally friendly technologies that enable the implementation of circular economy principles.

ACKNOWLEDGEMENT

The research presented in this paper was done with the financial support of the Ministry of Education, Science and Technological Development of the Republic of Serbia, within the funding of the scientific research work at the University of Belgrade, Technical Faculty in Bor, according to the contract number 451-03-137/2025-03/ 200131, and within the funding of the scientific research work at the Mining and Metallurgy Institute Bor, according to the contract number 451-03-136/2025-03/200052.

REFERENCES

1. Ahn, N.-K., Shim, H.-W., Kim, D.-W., Swain, B. (2020) Valorization of waste NiMH battery through recovery of critical rare earth metal: A simple recycling process for the circular economy. Waste Management, 104, 254–261.
2. Sarkar, M., Hossain, R., Sahajwalla, V. (2024) Sustainable recovery and resynthesis of electroactive materials from spent Li-ion batteries to ensure material sustainability. Resources, Conservation & Recycling, 200, 107292.
3. Ahn, N.-K., Swain, B., Shim, H.-W., Kim, D.-W. (2019) Recovery of rare earth oxide from waste NiMH batteries by simple wet chemical valorization process. Metals, 9, 1151.
4. Nogueira, C.A., Margarido, F. (2007) Chemical and physical characterization of electrode materials of spent sealed Ni–Cd batteries. Waste Management, 27, 1570–1579.
5. Lie, J., Lin, Y.-C., Liu, J.-C. (2021) Process intensification for valuable metals leaching from spent NiMH batteries. Chemical Engineering & Processing: Process Intensification, 167, 108507.
6. Bertuol, D.A., Bernardes, A.M., Tenório, J.A.S. (2006) Spent NiMH batteries: Characterization and metal recovery through mechanical processing. Journal of Power Sources, 160, 1465–1470.
7. Kanamori, T., Matsuda, M., Miyake, M. (2009) Recovery of rare metal compounds from nickel–metal hydride battery waste and their application to CH_4 dry reforming catalyst. Journal of Hazardous Materials, 169, 240–245.
8. Marins, A.A.L., Boasquevisque, L.M., Muri, E.J.B., Freitas, M.B.J.G. (2022) Environmentally friendly recycling of spent Ni–MH battery anodes and electrochemical characterization of nickel and rare earth oxides obtained by sol–gel synthesis. Materials Chemistry and Physics, 280, 125821.
9. Batsukh, I., Adiya, M., Lkhagvajav, S., Galsan, S., Gansukh, M., Batmunkh, M. (2024) Recovering nickel-based materials from spent NiMH batteries for electrochemical applications. ChemElectroChem, 11, e202400135.

XVI International Mineral Processing
and Recycling Conference
28-30 May 2025, Belgrade, Serbia

DOI: 10.5937/IMPRC25435D Original research article

IMPROVEMENT OF BOR RIVER WATER QUALITY THROUGH TREATMENT AND RECIRCULATION OF MINING AND METALLURGICAL WASTEWATER

Stefan Đorđievski[1#], 0000-0003-1737-8766,
Dragana Adamović[1], 0000-0003-3683-4122,
Miloš Đukić[1], 0000-0002-3307-4669,
Ana Petrović[1], 0000-0002-9815-6884,
Jelena Petrović[1], 0000-0002-3749-5110,
Zoran Štirbanović[2], 0000-0001-7571-2844,
[1]Mining and Metallurgy Institute Bor, Bor, Serbia
[2]University in Belgrade, Technical Faculty in Bor, Bor, Serbia

ABSTRACT – The Bor, Krivelj, and Bela Rivers, impacted by mining and metallurgy, have historically exhibited acidic conditions and high dissolved metal concentrations. This study evaluates the effects of wastewater treatment and smelter reconstruction in 2022 on water quality. The pH of the Bor River increased from 2.37 to neutral in mid-2022, leading to a sharp decrease in dissolved Cu and As concentrations. However, resuspension of contaminated sediment increased particulate form of Cu in water. The results showed significant water quality improvement due to environmental investments.

Keywords: Mining, Metallurgy, Wastewater, River, Monitoring.

INTRODUCTION

The Bor and Krivelj Rivers have been receiving wastewater from the mining and metallurgical facilities operating in the Municipality of Bor in Eastern Serbia. These two rivers merge to form the Bela River, a tributary of the Timok River, which ultimately flows into the transboundary Danube River, affecting Bulgaria and Romania as well.

The oldest recorded information about the quality of Bor River dates back to 1931, when its acidity downstream from the mine and near the village of Slatina was 171 and 105 mg$CaCO_3$/L, respectively [1]. The pH value measured close to these locations in 1935 were 4.5 and 5.7, respectively, indicating the acidic signature as well [2]. More recent measurements from 2011 and 2015 also indicated acidic pH values in the water of Bor River before merging with Krivelj River (4.8 and 4.2, respectively) [3,4]. Besides acidic pH value, high concentrations of sulfates, Cu, As, Mn, and other elements were measured in these rivers, indicating the influence of copper mining and smelting [3,4].

In 2022, the reconstruction of copper smelter in Bor included building wastewater treatment plant that would stop the release of acidic metallurgical wastewater into the

---

[#] corresponding author: stefan.djordjievski@irmbor.co.rs

Bor River [5]. Additional investments in environmental protection were made, aiming to achieve measurable improvements in the state of the environment [6].

Preliminary research has confirmed that the water quality of Bor, Krivelj, and Bela Rivers has improved [7,8], however, additional research is needed to understand the changes resulted from the innovations in treatment of wastewater from mining and metallurgy operations. This paper aims to give contribution in evaluating the effects of the new wastewater treatment plant and other recent investments in environmental protection on the quality of water in Bor, Krivelj, and Bela Rivers impacted by copper mining and smelting in Eastern Serbia.

EXPERIMENTAL

Water samples from the Bor, Krivelj, and Bela Rivers were collected monthly from January 2022 to February 2025. The sampling locations for the Bor River (44.029342, 22.208157) and Krivelj River (44.030524, 22.207850) were about 50 m upstream of their confluence, while the sampling location for the Bela River (44.030729, 22.210704) was about 200 m downstream of the confluence. The pH and electrical conductivity (EC) were measured in the field. Samples were filtered in the laboratory to remove particulate matter, and the filtrate was analyzed for dissolved sulfates, Cu, As, and Mn.

To investigate the partitioning of Cu, As, and Mn between particulate and dissolved forms, both filtered and unfiltered water samples from the Bor, Krivelj, and Bela Rivers were collected on December 18, 2023, and the pH was measured in the field. The concentrations of these elements in particulate form were calculated by subtracting their concentrations in the filtrate from those in the unfiltered samples.

Sulfates were determined in the filtrate by developing turbidity with barium chloride, which was measured using a WTW Turb 550 IR turbidimeter. The concentrations of Cu, As, and Mn were determined using an ICP-MS Perkin Elmer NexION 1000.

A sediment sample was collected from the Bor River riverbed at a location approximately 2 km upstream of its confluence with the Krivelj River (44.028667, 22.187167). The sample was dried at 40°C, sieved to pass a 2 mm sieve, and milled in a ring mill. The sample was digested using a microwave system (ETHOS UP) and analyzed with an ICP-MS Agilent 7700 according to the standard method EPA 6020A.

RESULTS AND DISCUSSION

The pH value of Bor River from January 2022 to April 2022 was very acidic, with values below 3, and minimum measured value 2.37 (Table 1 and Figure 1). In May and June 2022, the pH value slightly increased to 3.52 and 3.25, respectively. However, in July 2022, a drastic increase in pH value was observed, reaching the value of 7.24. From July 2022 until February 2025, which is the final month of the monitoring period, the pH value was constantly neutral, never going below 7.00, with the maximum value of 9.04.

The pH value of Krivelj River was acidic only in January and February 2022 (3.49 and 3.20, respectively), after which it increased and stayed neutral until the end of the monitoring period, with the maximum value of 8.28. The change of pH in Bela River followed the similar pattern of Bor River, reflecting the significant influence of its water.

EC in the Bor and Bela Rivers was relatively higher from January to April 2022, peaking at 8676 and 2870 µS/cm, respectively. In contrast, from May 2022 to February 2025, EC levels in the Bor, Krivelj, and Bela Rivers remained relatively stable, with moderate fluctuations around their median values of 1347, 1585, and 1350 µS/cm, respectively.

Sulfate concentrations in the Bor, Krivelj, and Bela Rivers varied throughout the study period, reaching maximum values of 2954, 1700, and 2500 mg/L, respectively.

Copper and arsenic concentrations in the Bor and Bela Rivers exhibited similar temporal trends, with high values recorded from January to June 2022, followed by a sharp decline and stable conditions. However, arsenic decreased more rapidly, reaching near-background levels by April 2022, whereas copper remained elevated until June. This difference in removal dynamics is closely linked to pH variations, as shown in Figure 1. Until April 2022, the pH in the Bor and Bela Rivers remained below 3, preventing significant metal precipitation. In May, the pH rose above 3, facilitating iron(III) hydroxide [$Fe(OH)_3$] particle formation. Since arsenic readily adsorbs onto $Fe(OH)_3$, its removal occurred rapidly. In contrast, copper does not sorb as efficiently onto $Fe(OH)_3$ and remained in solution until the pH reached near-neutral conditions in July 2022. From mid-2022 to February 2025, both metals remained at low, stable concentrations, indicating that pH stabilization played a crucial role in long-term water quality improvement.

Although the pH remained stable from July 2022 onward, Mn concentrations in all three rivers did not decrease as drastically as those of Cu and As. This is because Mn remains in dissolved form across a wide pH range, and the transition from acidic to neutral conditions did not significantly affect its concentration.

Table 1 Minimum, median, and maximum values of parameters measured monthly in water from Bor, Krivelj, and Bela Rivers from January 2022 to February 2025

Parameter	unit of measure	Statistical value	Measured concentrations in river water		
			Bor River	Krivelj River	Bela River
pH	-	minimum	2.37	3.20	2.25
		median	7.63	7.80	7.63
		maximum	9.04	8.28	8.92
Electrical Conductivity (EC)	µS/cm	minimum	453	505	528
		median	1347	1585	1350
		maximum	8676	2870	8902
Sulfate (SO_4^{2-})	mg/L	minimum	373	338	337
		median	699	1144	805
		maximum	2954	1700	2500
Copper (Cu)	µg/L	minimum	6.2	11.0	6.8
		median	41.2	88.3	46.6
		maximum	74328	25231	42483
Arsenic (As)	µg/L	minimum	<2.1	<2.1	<2.1
		median	2.8	<2.1	2.9
		maximum	7541	1069	4440
Manganese (Mn)	µg/L	minimum	370	358	445
		median	2764	4292	3310
		maximum	23826	9583	10634

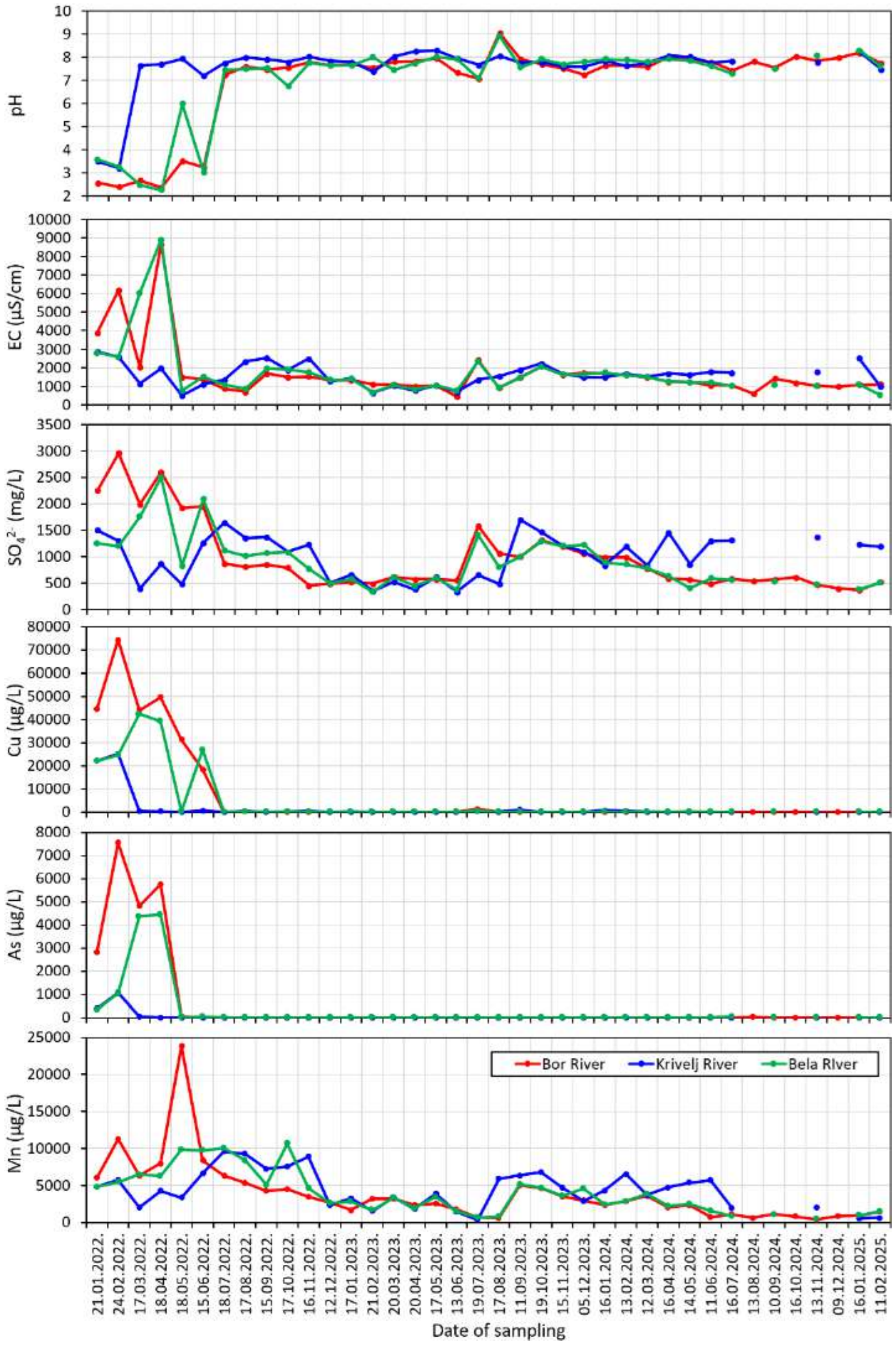

Figure 1 Diagrams showing the changes of pH and EC values, and the concentrations of SO_4^{2-}, Cu, As, and Mn in water of Bor, Krivelj, and Bela Rivers in the studied period

The concentrations of Cu, As, and Mn discussed here refer to their dissolved forms, as the measurements were conducted on filtered water samples. Although the dissolved concentrations of these elements significantly decreased from mid-2022 onward, the extent to which they persisted in particulate form remained unclear. To address this, concentrations of Cu, As, and Mn in particulate form were measured on December 18, 2023 (Table 2). At the time of sampling, the pH in the Bor, Krivelj, and Bela Rivers was approximately 8. The concentrations of copper in particulate form were 1444, 3725, and 1481 µg/L, respectively, indicating that approximately 98% of the total copper was present in particulate form. Although copper remained predominantly in particulate form after the pH stabilized at neutral values, its concentrations were about 50 times lower than the dissolved copper concentrations observed under acidic conditions. The concentration of arsenic in particulate form was negligible, similar to its dissolved form, while a significant portion of manganese remained in dissolved form.

The source of particulate copper remains unclear; however, one possible explanation is contamination from riverbed sediment. A sediment sample collected from the Bor River on April 16, 2024, approximately 2 km upstream from its confluence with the Krivelj River, contained 9770 mg/kg of copper. The resuspension of this sediment could contribute to elevated concentrations of particulate Cu in the water.

When the reconstruction of the smelter in Bor began in April 2022, metallurgical operations were discontinued, leading to the cessation of metallurgical wastewater generation. Since the newly built wastewater treatment facility within the metallurgical complex became operational in April 2023, the treated wastewater has been recirculated within the technological process. Stopping the direct discharge and implementing wastewater recirculation significantly improved the water quality of the Bor River by reducing free acid and dissolved metal and arsenic concentrations.

On the other hand, treated wastewater from the Čukaru Peki mine was discharged into the Bor River after treatment at the wastewater treatment facility. However, measurements confirmed that the pH of this treated wastewater remained consistently neutral or slightly alkaline, while parameters such as EC, SO_4^{2-}, Cu, As, and Mn were either lower or close to those in the Bor River before the discharge of this wastewater. This suggests that the treated wastewater from the Čukaru Peki mine did not negatively impact the water quality of Bor River.

Table 2 pH and the concentrations of particulate and dissolved forms of Cu, As, and Mn in water samples collected from Bor, Krivelj, and Bela Rivers on December 18, 2023

Parameter	Unit of measure	Form	Measured concentrations in river water		
			Bor River	Krivelj River	Bela River
pH	-	-	8.09	8.36	8.35
Copper (Cu)	µg/L	Particulate	1444	3725	1481
		Dissolved	28.7	69.6	27.3
Arsenic (As)	µg/L	Particulate	22.2	<2.1	8.6
		Dissolved	<2.1	<2.1	<2.1
Manganese (Mn)	µg/L	Particulate	2933	158	748
		Dissolved	407	5196	1685

CONCLUSION

This study confirms significant improvements in the water quality of the Bor, Krivelj, and Bela Rivers following the reconstruction of the Bor smelter and the implementation of a wastewater treatment and recirculation system. Prior to mid-2022, the Bor River exhibited extreme acidity and high dissolved metal concentrations, but a sharp pH increase in July 2022 led to sustained neutral conditions. As a result, arsenic levels rapidly declined after pH increased above 3, while copper remained in dissolved form until the pH reached neutrality. Manganese persisted in dissolved form due to its stability across a wide pH range. After mid-2022, copper was present in particulate form in river water, likely due to the resuspension of contaminated riverbed sediment. The release of treated wastewater from the Čukaru Peki mine did not negatively impact the water quality of Bor River. These findings highlight the effectiveness of recent environmental measures and emphasize the need for continued monitoring.

ACKNOWLEDGEMENT

This work was funded by the Ministry of Science, Technological Development, and Innovation of the Republic of Serbia under contracts no. 451-03-136/2025-03/200052 (Mining and Metallurgy Institute Bor) and 451-03-137/2025-03/200131 (Technical Faculty in Bor).

The data presented in this paper were obtained from test reports on surface water, wastewater, and sediment, which were issued by the Mining and Metallurgy Institute Bor for Serbia Zijin Mining d.o.o. Bor. The latter granted permission and provided support for their use in this study.

REFERENCES

1. Andrejić, B. (1983) Sulfuric fume from 1908 to 1935 – archive material. Book XXVIII, Štampa, radio i film, Bor, Serbia, p. 114.
2. Andrejić, B. (1983) Sulfuric fume from 1935 to 1941 – archive material. Book XXIX, Štampa, radio i film, Bor, Serbia, p. 161.
3. Ishiyama, D., et al. (2012) Geochemical Characteristics of Mine Drainage Water and River Water in the Bor Mining Area, Serbia: Results of Study in 2011. Akita University, 33 (1), 41–49.
4. Đorđievski, S., Ishiyama, D., Ogawa, Y., Stevanović, Z. (2018) Mobility and natural attenuation of metals and arsenic in acidic rivers from Bor copper mines (Serbia) to Danube River. Environ. Sci. Poll. Res. 25 25005–25019.
5. https://kolektiv.co.rs/sest-meseci-od-pocetka-rekonstrukcije-topionice-i-rafinacije-u-boru/ (Accessed: March 11, 2025).
6. https://kolektiv.co.rs/srbija-zidjin-koper-za-cetiri-godine-u-zastitu-zivotne-sredine-ulozila-2034-miliona-dolara/ (Accessed: March 11, 2025).
7. Đorđievski, S., Adamović, D. (2023) History of surface water pollution by mining and metallurgical activities in Bor, Serbia. In: The 54th International October Conference on Mining and Metallurgy, 18-21 October 2023, Bor Lake, Serbia, 501–504.
8. Marković, R., Marjanović, V.M., Stevanović, Z., Gardić, V., Petrović, J., Kovačević, R., Štirbanović, Z., Friedrich, B. (2024) Importance of changes in the copper production process through mining and metallurgical activities on the surface water quality in the Bor area, Serbia. Metals, 14 (1), 649.

XVI International Mineral Processing
and Recycling Conference
28-30 May 2025, Belgrade, Serbia

DOI: 10.5937/IMPRC25441P Review article

BIOCHAR IN WASTEWATER REMEDIATION: A BRIEF REVIEW OF CHARACTERISTICS AND PREPARATION MATERIALS

Kristina Pavićević[#], 0009-0003-3743-2894,
Danica Jovašević, 0009-0006-6722-4588,
Maja Rajković, 0009-0008-7701-7819,
Ivana Jelić, 0000-0003-1406-2416,
Marija Janković, 0000-0002-2255-7163,
Marija Šljivić-Ivanović, 0000-0001-5897-0083,
Vinča Institute of Nuclear Sciences, Belgrade, Serbia

ABSTRACT – The rapid growth of industry has significantly increased water pollution, especially from heavy metals which are not biodegradable and tend to accumulate in living organisms through the food chain. Consequently, the development of a sustainable low-cost wastewater treatment approach has attracted more attention from policymakers and scientists. Traditional methods, such as chemical precipitation, filtration, and activated carbon adsorption, often require high operational and capital costs. Recently, biochar has emerged as a promising sorbent due to its eco-friendliness, favorable surface and structural properties, and high adsorption capacity. Additionally, biochar can be produced from a variety of biomass feedstocks, which will be illustrated in this paper through specific examples. This process not only addresses the issue of heavy metal contamination in wastewater but also provides a viable alternative for managing bio-waste that would otherwise be discarded. While biochar's efficiency in removing contaminants has been well demonstrated at the lab scale, mainly focusing on the sorption of a single metal from spiked solutions, further in situ studies are necessary to evaluate performance with real effluents and assess the environmental impact before its large-scale application.

Keywords: Water pollution, Heavy metals, Biochar, Bio-waste management.

INTRODUCTION

Heavy metals (e.g., Cd, Cr, Cu, Ni, Pb, Hg, Zn) enter the environment primarily through large-scale industries such as leather, metallurgical, petroleum, batteries, textile, fertilizers, nuclear, and pesticides [1]. Once discharged, these metals pose risks to indigenous habitats and human health alike [2].

While certain metals, such as zinc, iron, and chromium, are essential in trace amounts for biological processes, others, such as lead, cadmium, and mercury, are highly toxic and have no biological need in the human body. Thus, the removal of these elements from contaminated water is both important and urgent [3]. Activated carbon typically adsorbs only a few milligrams of metal ions per gram, and regeneration issues further complicate its use. Due to these limitations, there is a growing interest in the scientific community

---

[#] corresponding author: kristina.pavicevic@vin.bg.ac.rs in using pyrolyzed biomass – biochar, as a sustainable alternative. Biochar offers even superior adsorption capacities which has consequently attracted growing interest evidenced by the increasing number of published articles over the past decade [4].

Biomass feedstock can include any organic waste materials as shown in Figure 1. Previously considered useless, these wastes are now converted into valuable resources through pyrolysis, finding applications across various fields [5].

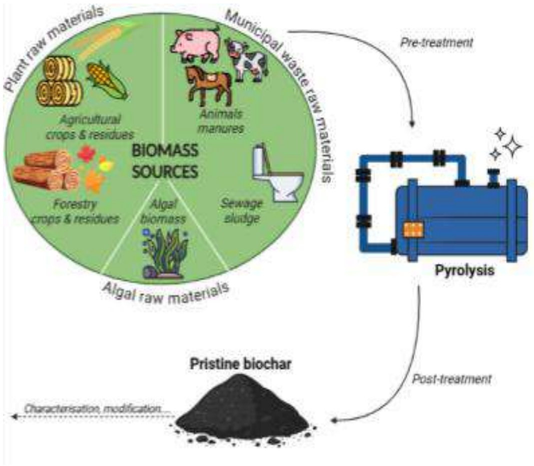

Figure 1 Production of biochar through pyrolisis from various biomass sources

Pyrolysis is the most common method for producing biochar, whereas material obtained through gasification and hydrothermal carbonization generally does not meet the typical definition of biochar [4].

Several factors, including the operating temperature, heating rate, and residence time, influence the resulting biochar's properties. During pyrolysis, the components of the feedstock, such as lignin, cellulose, hemicellulose, and fats, undergo thermal degradation in an oxygen-free environment.

This process enriches the carbon content of the material by removing non-carbon elements like oxygen and hydrogen. As a result, the removal of these elements in the form of gases and volatiles leads to a reduction in the O+N/C and H/C atomic ratios, while enhancing the aromaticity and carbon content, which in turn increases the biochar's stability.

When the pyrolysis temperature exceeds 500°C, the biochar becomes more hydrophobic, with an increase in surface area and micropore volume, making it more suitable for the removal of organic pollutants. In contrast, pyrolysis at temperatures below 500°C produces biochar with smaller pores, lower surface area, and a higher concentration of oxygen-containing functional groups, making it highly amenable for adsorbing inorganic pollutants [6].

However, to ensure the feasibility of biochar in wastewater treatment, the factors involved in its preparation that influence its characteristics and adsorption capacity must be understood [7].

This study aims to review the relevant literature to identify types of biomass that have demonstrated effectiveness in removing specific metals from water samples and to provide a broader perspective on other potential materials that could be further explored.

CORE CONCEPTS OF BIOCHAR

Characterizing biochar after preparation is crucial for understanding its chemical composition, morphology, and surface properties, which directly influence its performance in applications like adsorption. Commonly used analytical techniques, such as X-ray diffraction (*XRD*), Fourier transform infrared spectroscopy (*FTIR*), X-ray photoelectron spectroscopy (*XPS*), and Nuclear magnetic resonance (*NMR*), provide insights into the biochar’s chemical structure, functional groups, and surface characteristics. In addition, techniques like Brunauer-Emmett-Teller (*BET*) surface area analysis, extended X-ray absorption fine structure (*EXAFS*), scanning electron microscopy (*SEM*), and energy dispersive X-ray spectroscopy (*EDX*) provide information on surface area, porosity, and morphology, all of which are critical for adsorption performance. Together, these methods give a comprehensive view of biochar's properties, helping predict its adsorption capabilities and guide potential modifications to optimize its functionality [4].

Researchers worldwide are working on different methods of biochar preparation to enhance its efficiency. Pristine biochar refers to biochar produced directly from biomass through pyrolysis, without any significant modifications. Engineered or designer biochar, on the other hand, is biochar that has been intentionally modified or tailored to possess specific properties. These modifications aim to improve certain characteristics making biochar more suitable for specialized applications.

The adsorption capacity of biochar is closely linked to its physicochemical properties, such as surface area, pore size distribution, functional groups, and cation exchange capacity. These properties can vary depending on the preparation conditions, and various chemical or physical modification methods have been adopted to improve them. In addition to traditional modifications, researchers have also started creating biochar-based composite materials by incorporating synthetic materials to further enhance biochar's efficiency [8].

These composites not only improve the physicochemical properties of biochar but also combine their advantages with those of other materials. Biochar-based composites can be specifically designed for target pollutants by adding functional materials, magnetic substances, or nanoparticles, resulting in materials enriched with functional groups that address the limitations of pristine biochar in environmental remediation [9].

In the course of the adsorption processes, modified biochar works on both physical and chemical adsorption. However, the dominant adsorption mechanisms may differ depending on the type and properties of the adsorbed pollutant. While ion exchange and electrostatic interactions are found to be common mechanisms of metal removal which in turn depends on the nature of biomass, process conditions, and metal, it is found that modifications and mechanisms are strongly interrelated [3].

Figure 2 illustrates the different biochar modifications alongside the key adsorption mechanisms. While these two aspects are not directly related in the figure, it serves to visually summarize the modification methods and adsorption processes discussed, giving a clearer understanding of how biochar's properties can be tailored for various applications.

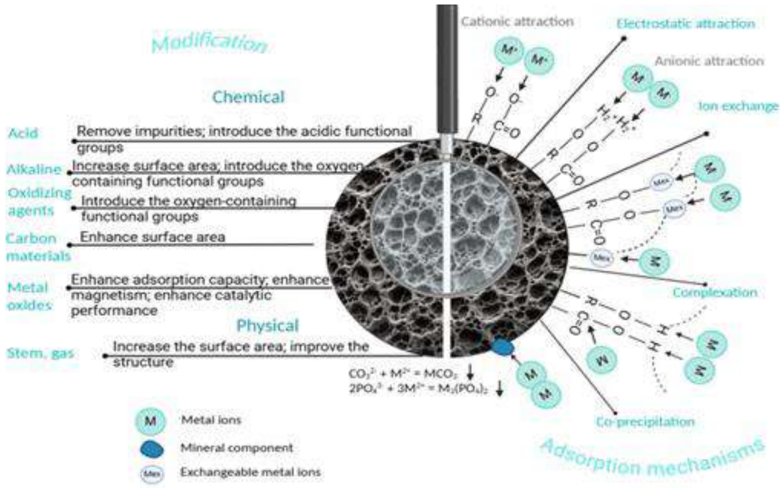

Figure 2 Biochar modifications and associated adsorption mechanisms

LITERATURE REVIEW

Direct comparison of adsorption capacities is challenging due to inconsistencies in the data found in the literature. The reported sorption capacities are measured under varying conditions such as different pH levels, temperatures, adsorbate concentration ranges, biochar doses, particle sizes, and surface areas. Additionally, biochars are applied to treat a variety of water sources, including groundwater, drinking water, synthetic industrial wastewater, and real-world wastewater, each with distinct types and concentrations of interfering ions. Another challenge in comparing biochar adsorbents is the variation in preparation conditions, such as temperature, time, and atmosphere. Studies that prepare biochar from the same feedstock using different methods and then test it with the same adsorbates are limited. Similarly, to evaluate reproducibility, it is essential to conduct studies using identical biochar preparations from the same feedstock and test them with the same adsorbates [2].

Since the properties of biochar are influenced by the type of feedstock, it is essential to select appropriate materials to achieve the desired characteristics in the produced biochar [1]. Figure 3 provides an overview of some notable materials that have been used in biochar production, offering perspectives on potential feedstocks for future improvements and innovations.

In natural waters, various heavy metals often coexist with other pollutants, leading to competition for sorption sites on the biochar surface between metals, other ions, and organic pollutants. Currently, only a few studies have explored the competitive sorption of metals by biochar, and there are no reports of biochar being used in field applications to remove heavy metals from contaminated wastewater [26]. Given this complexity, machine learning (*ML*) techniques offer a promising solution by helping to optimize biochar properties and predict its behavior in competitive sorption scenarios. By analyzing large datasets, ML algorithms can identify key factors influencing biochar's performance, allowing for more efficient and targeted use of biochar in environmental remediation [5].

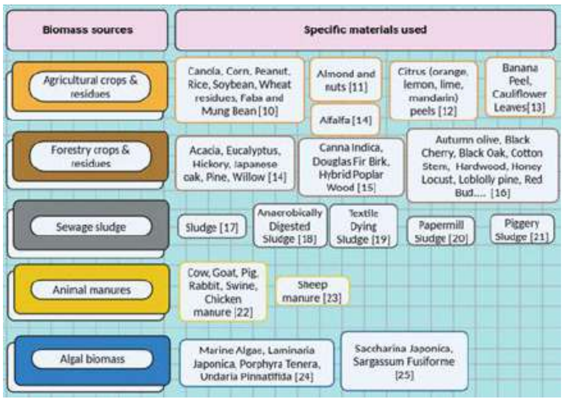

Figure 3 Overview of materials used in biochar production

TREATMENT OF USED BIOCHAR

Commonly used separation methods for segregating biochar from treated water are filtration, sedimentation, or centrifugation. However, managing adsorbents saturated with heavy metals presents a significant environmental challenge, as these materials can become hazardous waste. Therefore, implementing appropriate strategies for their safe handling, such as stabilization and disposal at specialized facilities, is highly needed. Until now, the disposal of end-of-life adsorbents and the subsequent recovery of contaminants has been a major practical challenge. The spent adsorbents are typically either regenerated for reuse as soil amendments, capacitors, and catalysts, or safely disposed of through incineration and landfilling. Although incineration can reduce waste volume, it requires substantial energy and generates harmful emissions. The resulting ash can be solidified afterward, but care must be taken to prevent the leaching of metals. A different approach would include utilizing biochar in the construction industry, where biochar containing immobilized metals could be used as a construction material providing an energy-efficient solution. Another viable option is desorption, where metals are extracted from the biochar using dilute acids like HCl or HNO_3. This process allows for further processing or reuse of the metals. Additionally, regenerating the adsorbent facilitates its repeated use, leading to cost savings. Selecting appropriate desorption agents is crucial to preserve the biosorbent's effectiveness and ensure environmental safety [27].

CONCLUSION

Due to the rising concern regarding health issues caused by heavy metals found in wastewater, biochar is being profoundly studied. Biochar has been identified as a great solution for purifying contaminated waters, offering several advantages that have been discussed in this paper. However, the biggest obstacle remains the process of scaling it up on the industry and market level. The papers published so far are entirely based on laboratory experiments, showing outstanding results and the potential for using biochar in the future. The real-world environment is much more complex, with pollutants often coexisting, which leads to uncertainty about its practical application. This paper provides a foundation for exploring the variety of materials that can be used for biochar production, highlighting the potential for a range of feedstocks in wastewater treatment. In order for biochar to be recognized as a standard practice in wastewater treatment, further research needs to be conducted under industrial circumstances, including studies that explore the competitive properties of pollutants during sorption.

ACKNOWLEDGMENTS

The research presented in this paper was completed with the financial support of the Ministry of Science, Technological Development and Innovation of the Republic of Serbia, with the funding of scientific research work at the University of Belgrade, Vinča Institute of Nuclear Sciences (Contract No. 451-03-136/2025-03/200017).

REFERENCES

1. Chen, W. H., Hoang, A. T., Nižetić, S., Pandey, A., Cheng, C. K., Luque, R., & Nguyen, X. P. (2022). Biomass-derived biochar: From production to application in removing heavy metal-contaminated water. Process Safety and Environmental Protection, 160, 704-733.
2. Mohan, D., Sarswat, A., Ok, Y. S., & Pittman Jr, C. U. (2014). Organic and inorganic contaminants removal from water with biochar, a renewable, low cost and sustainable adsorbent–a critical review. Bioresource Technology, 160, 191-202.
3. Gupta, S., Sireesha, S., Sreedhar, I., Patel, C. M., & Anitha, K. L. (2020). Latest trends in heavy metal removal from wastewater by biochar-based sorbents. Journal of Water Process Engineering, 38, 101561.
4. Wang, J., & Wang, S. (2019). Preparation, modification and environmental application of biochar: A review. Journal of Cleaner Production, 227, 1002-1022.
5. Olugbenga, O. S., Adeleye, P. G., Oladipupo, S. B., Adeleye, A. T., & John, K. I. (2024). Biomass-derived biochar in wastewater treatment - a circular economy approach. Waste Management Bulletin, 1(4), 1-14.
6. Enaime, G., Baçaoui, A., Yaacoubi, A., & Lübken, M. (2020). Biochar for wastewater treatment—conversion technologies and applications. Applied Sciences, 10 (10), 3492.
7. Kamarudin, N. S., Dahalan, F. A., Hasan, M., An, O. S., Parmin, N. A., Ibrahim, N., ... & Wikurendra, E. A. (2022). Biochar: A review of its history, characteristics, factors that influence its yield, methods of production, application in wastewater treatment, and recent development. Biointerface Res. Appl. Chem, 12(6), 7914-7926.
8. Gope, M., & Saha, R. (2021). Removal of heavy metals from industrial effluents by using biochar. In Intelligent environmental data monitoring for pollution management (pp. 25-48). Academic Press.

9. Liang, L., Xi, F., Tan, W., Meng, X., Hu, B., & Wang, X. (2021). Review of organic and inorganic pollutants removal by biochar and biochar-based composites. Biochar, 3, 255-281.
10. Yuan, J. H., & Xu, R. K. (2011). The amelioration effects of low-temperature biochar generated from nine crop residues on an acidic Ultisol. Soil use and management, 27(1), 110-115.
11. Ortiz, L. R., Torres, E., Zalazar, D., Zhang, H., Rodriguez, R., & Mazza, G. (2020). Influence of pyrolysis temperature and bio-waste composition on biochar characteristics. Renewable Energy, 155, 837-847.
12. Selvarajoo, A., Wong, Y. L., Khoo, K. S., Chen, W. H., & Show, P. L. (2022). Biochar production via pyrolysis of citrus peel fruit waste as a potential usage as solid biofuel. Chemosphere, 294, 133671.
13. Ahmad, Z., Gao, B., Mosa, A., Yu, H., Yin, X., Bashir, A., ... & Wang, S. (2018). Removal of Cu (II), Cd (II), and Pb (II) ions from aqueous solutions by biochars derived from potassium-rich biomass. Journal of Cleaner Production, 180, 437-449.
14. Hopkins, D., & Hawboldt, K. (2020). Biochar for the removal of metals from solution: A review of lignocellulosic and novel marine feedstocks. Journal of Environmental Chemical Engineering, 8(4), 103975.
15. Cui, E., Wu, Y., Zuo, Y., & Chen, H. (2016). Effect of different biochars on antibiotic resistance genes and bacterial community during chicken manure composting. Bioresource Technology, 203, 11-17.
16. Shaheen, S. M., Niazi, N. K., Hassan, N. E., Bibi, I., Wang, H., Tsang, D. C., ... & Rinklebe, J. (2019). Wood-based biochar for the removal of potentially toxic elements in water and wastewater: a critical review. International Materials Reviews, 64(4), 216-247.
17. Zhao, M., Dai, Y., Zhang, M., Feng, C., Qin, B., Zhang, W., ... & Qiu, R. (2020). Mechanisms of Pb and/or Zn adsorption by different biochars: Biochar characteristics, stability, and binding energies. Science of the Total Environment, 717, 136894.
18. Ni, B. J., Huang, Q. S., Wang, C., Ni, T. Y., Sun, J., & Wei, W. (2019). Competitive adsorption of heavy metals in aqueous solution onto biochar derived from anaerobically digested sludge. Chemosphere, 219, 351-357.
19. Wang, X., Li, C., Li, Z., Yu, G., & Wang, Y. (2019). Effect of pyrolysis temperature on characteristics, chemical speciation, and risk evaluation of heavy metals in biochar derived from textile dyeing sludge. Ecotoxicology and Environmental Safety, 168, 45-52.
20. Cho, D. W., Kwon, G., Yoon, K., Tsang, Y. F., Ok, Y. S., Kwon, E. E., & Song, H. (2017). Simultaneous production of syngas and magnetic biochar via pyrolysis of paper mill sludge using CO2 as reaction medium. Energy conversion and management, 145, 1-9.
21. Liu, J., Huang, Z., Chen, Z., Sun, J., Gao, Y., & Wu, E. (2020). Resource utilization of swine sludge to prepare modified biochar adsorbent for the efficient removal of Pb (II) from water. Journal of Cleaner Production, 257, 120322.
22. Yang, H., Lee, C. G., & Lee, J. (2023). Utilizing animal manure-derived biochar in catalytic advanced oxidation processes: A review. Journal of Water Process Engineering, 56, 104545.
23. López-Cano, I., Roig, A., Cayuela, M. L., Alburquerque, J. A., & Sánchez-Monedero, M. A. (2016). Biochar improves N cycling during composting of olive mill wastes and sheep manure. Waste Management, 49, 553-559.
24. Jung, K. W., Jeong, T. U., Kang, H. J., & Ahn, K. H. (2016). Characteristics of biochar derived from marine macroalgae and fabrication of granular biochar by entrapment in calcium-alginate beads for phosphate removal from aqueous solution. Bioresource Technology, 211, 108-116.

25. Son, E. B., Poo, K. M., Chang, J. S., & Chae, K. J. (2018). Heavy metal removal from aqueous solutions using engineered magnetic biochars derived from waste marine macro-algal biomass. Science of the Total Environment, 615, 161-168.
26. Godwin, P. M., Pan, Y., Xiao, H., & Afzal, M. T. (2019). Progress in preparation and application of modified biochar for improving heavy metal ion removal from wastewater. Journal of Bioresources and Bioproducts, 4(1), 31-42.
27. Baskar, A. V., Bolan, N., Hoang, S. A., Sooriyakumar, P., Kumar, M., Singh, L., ... & Siddique, K. H. (2022). Recovery, regeneration and sustainable management of spent adsorbents from wastewater treatment streams: A review. Science of the Total Environment, 822, 153555.

XVI International Mineral Processing
and Recycling Conference
28-30 May 2025, Belgrade, Serbia

DOI: 10.5937/IMPRC25449K Original research article

A PROPOSAL FOR ZERO WASTE IN THE IRON AND STEEL INDUSTRY: ZIRCONIA NOZZLE WASTE EVALUATION

Semra Kurama[1#], 0000-0002-7554-3419,
Hüseyin Boğaç Poyraz[1], 0000-0001-5351-6658,
Zahide Bayer Öztürk[2], 0000-0001-8069-0694,
[1]Eskişehir Technical University, Department of Materials Science and Engineering, Eskişehir, Türkiye
[2]Nevşehir Hacı Bektaş Veli University, Department of Metallurgy and Materials Engineering, Nevşehir, Türkiye

ABSTRACT – With the increase in environmental awareness, it is seen that there are two focusing methods in industrial production. Therefore, the usability of one sector's waste as a potential raw material for another sector can play an important role in terms of energy and cost.

In the study, zirconia nozzles, used in the iron and steel industry, are consumed quickly. It is aimed at finding a solution to the accumulation of waste formed by the end of service life of them.

In the first part of the study, it was investigated the integrating waste zirconia nozzles from the Bilecik Iron and Steel Company (Bilecik, Turkey) into the production of ceramic floor tiles. After processing and firing in an industrial kiln, the formulated recipes are subjected to comprehensive physical and mechanical evaluations [19]. In the second part of the study, to aim for zero waste, existing waste was evaluated in the production of refractory bricks, and the use of alternative resources to zirconia, an expensive raw material, was examined. It showed the potential of waste zirconium nozzles as a sustainable alternative in ceramic tile/refractory production. It demonstrates its feasibility in reducing waste generation, lowering production costs, and promoting environmentally sound practices without compromising.

Keywords: Ceramic Tile, Refractory, Zirconia Nozzle, Waste, Recycling.

INTRODUCTION

The iron and steel industry represents a strategically significant sector with substantial global production capacity [1]. However, its production processes inherently generate various waste materials, the complete elimination of which remains a considerable challenge. While waste management efforts predominantly focus on minimizing waste generation within a given sector, the cross-sectoral utilization of industrial by-products has gained prominence as a sustainable alternative. The ceramic industry not only produces waste during its own manufacturing processes but also presents a viable avenue for the valorization of waste materials originating from different industries. Numerous studies in literature have explored the incorporation of industrial waste into ceramic-based applications, including ceramic tiles, sanitaryware, and

---

[#] corresponding author: skurama@eskisehir.edu.tr refractory materials. Notably, integrating industrial by-products into ceramic tile formulations has emerged as an effective and environmentally sustainable strategy for waste reduction [2]. Several studies have investigated the utilization of diverse industrial residues in ceramic tile production, including granite waste [3], glass shards [4], various slags [5-7], boron-related residues [8], waste clay [9], and different types of ashes [6, 10]. These research efforts highlight the potential of industrial waste repurpose within the ceramic sector, contributing to both environmental sustainability and resource efficiency.

In response to growing ecological concerns, research within the refractory sector, a subset of the broader ceramic industry, has increasingly focused on minimizing the reliance on virgin raw materials and reducing production costs, thereby promoting more sustainable practices. Ghonaim et al. [11] conducted a study on the preparation of traditional refractory concrete, incorporating 50% alumina grog or bauxite as key components. Similarly, Khalil et al. [12] investigated the production of mullite-based refractories using a composition of 40% recycled alumina-silicate waste and 60% bauxite, which was subsequently sintered through pressing at 1600°C. Their findings indicated significant improvements in the physical properties of the resulting materials. Furthermore, Mazzanti et al. [13] analyzed the mechanical and thermal performance of refractories by incorporating ceramic waste derived from alumina silicate. Their study demonstrated that the inclusion of ceramic waste effectively enhanced the modulus of rupture (MOR), thermal shock resistance, phase composition, and microstructural characteristics from ambient temperature up to 1500°C. Notably, their results indicated that refractory compositions containing 20% ceramic waste exhibited comparable performance to those produced using untreated alumina-silicate materials, underscoring the potential of recycled ceramic waste in refractory applications.

The utilization of high-temperature-resistant materials is crucial in the iron and steel industry, particularly for applications requiring durability under extreme thermal and chemical conditions. In this regard, zirconia (ZrO_2) nozzles are extensively employed for regulating liquid metal flow due to their exceptional thermal resistance and chemical stability. These ceramic nozzles are widely used across various industrial sectors and can be manufactured through different advanced fabrication techniques, including additive manufacturing and direct ink writing [14]. The production process typically begins with high-purity zirconia powder, which is shaped into the desired nozzle form and subsequently subjected to high-temperature sintering to attain the necessary mechanical and thermal properties [15]. One of the most significant applications of zirconia nozzles is in the continuous casting of steel, where they serve as critical components in tundish refractory systems, ensuring controlled metal flow and operational efficiency [16, 17].

In the iron and steel industry, molten metal is transported using ladles and subjected to various metallurgical treatments at different processing stations, such as ladle furnaces and converters. Following these processes, the liquid metal is transferred to the continuous casting system, where it is shaped into semi-finished or finished products. During this stage, the molten metal passes through a tundish and is subsequently directed into open-bottomed copper molds. Precise control of metal flow from the tundish to the mold is critical for regulating casting speed, optimizing production planning, and ensuring product quality. To achieve this, flow control systems are installed beneath the tundish, consisting of a fixed zirconia nozzle and a replaceable zirconia nozzle. These nozzles are periodically replaced through a waste removal and disposal system to maintain production efficiency in accordance with operational parameters [18].

Despite their widespread application, limited research has focused on the reuse of zirconia nozzle waste generated in steel production facilities. However, some studies have investigated the potential of repurposing this waste as a zircon substitute in ceramic applications, such as wall tile glazes and ceramic tile formulations [18, 19].

In this study, the reuse potential of zirconia-based nozzle materials, which serve as pouring outlets in crucibles within the iron and steel industry, was investigated. These nozzle components become inoperative after casting due to wear-induced deformation and thermal expansion. Currently, they are not recyclable within the iron and steel sector and are instead disposed of as industrial waste. However, given their high zirconia content, these materials present a promising opportunity for repurposing in both the ceramic tile and refractory industries. The potential applications of these waste materials include enhancing surface whiteness in ceramic tile formulations and serving as raw materials for the production of alumina-zirconia refractory components. To explore these possibilities, experimental studies were conducted to assess the feasibility of incorporating waste zirconia nozzles into ceramic and refractory applications, thereby contributing to resource efficiency and sustainable waste management.

MATERIALS AND METHODS

The waste zirconia nozzles (WZ) utilized in this study were obtained from Bilecik Iron and Steel Company (Bilecik, Turkey) and subjected to a purification process to eliminate any residual iron components. This was achieved through the precise removal of iron fragments using a diamond cutter, ensuring the purity of the base material. Following mechanical separation, the purified WZ underwent further processing, wherein they were crushed using a jaw crusher to reduce their particle size. The complete preparation procedure for the waste zirconia nozzles is illustrated in Figure 1.

Subsequent chemical characterization of WZ was performed using X-ray fluorescence (XRF) spectroscopy (Rigaku ZSX Primus model), and the results are presented in Table 1. Additionally, the crystalline phase composition of WZ was analysed through X-ray diffraction (XRD) using a Rigaku Miniflex 600 series diffractometer. The analysis was conducted over a 2θ range of 5° to 70° at a scanning speed of 2°/min, employing Cu Kα radiation at 40 kV and 30 mA. The results, depicted in Figure 2, confirmed the presence of both baddeleyite (ZrO_2) and hafnium dioxide (HfO_2) phases in the WZ samples.

This study is structured in two parts, each focusing on the valorization of waste zirconia nozzles (WZ) in different industrial applications. The first part, which has already been published, investigated the use of WZ in ceramic tile production. This phase involved a comprehensive experimental analysis, including a comparative evaluation of the color properties of standard zirconium raw materials and waste zirconium. The results demonstrated that replacing 2% by weight of conventional zircon raw materials with WZ in white ceramic floor tile bodies led to improvements in both body whiteness and firing strength [19].

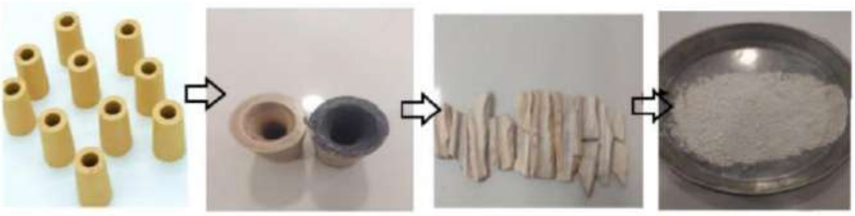

Figure 1 The preparation of zirconia nozzles for applications [19]

Table 1 The chemical analysis of WZ (wt.%)

Oxides	**Na_2O**	**MgO**	**SiO_2**	**Al_2O_3**	**P_2O_5**	**K_2O**	**CaO**	**TiO_2**	**Fe_2O_3**	**ZrO_2**	**Hf_2O**	**LOI**
WZ	0.01	1.72	1.57	1.22	0.01	0.01	0.08	0.19	0.01	93.34	1.71	0.12

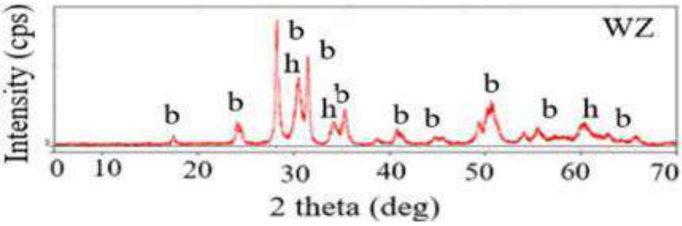

Figure 2 XRD phases of the WZ (**b**: baddeleyite, **h**: HfO_2) [19]

Building upon these findings, the present study focuses on the second part, which explores the potential utilization of WZ in refractory applications. While the first part established the feasibility of WZ in the ceramic sector, this study extends the research by investigating its suitability for the refractory industry. By addressing both ceramic and refractory applications, the overall research aims to contribute to a more comprehensive waste management strategy, promoting circular economy principles in industrial processes.

In the second phase of the study, the waste zirconia nozzles (WZ) were ground to a particle size of less than 100 µm using a ball mill and subsequently incorporated into refractory formulations. The ground WZ was blended with zircon silicate brick raw material at varying proportions of 0%, 10%, 20%, and 30% by mass. Calcium aluminate cement and organic binders were added to the mixture to enhance its binding properties and workability. The consistency of the mixture was adjusted to ensure suitability for the shaping process.

To form test specimens, the prepared mixture was subjected to uniaxial pressing at a pressure of 50 MPa, resulting in cylindrical and prismatic samples. These pressed specimens were initially dried in a low-temperature oven at 110°C to remove residual moisture. Subsequently, they underwent a sintering process at 1550°C for 2 hours to achieve the desired phase development and densification. The raw materials and their respective proportions used in the refractory formulations are presented in Table 2.

Table 2 Refractory samples and codes

Samples	Cement (wt.%)	Organic binder (wt.%)	WZ (wt.%)
R0	15	3.0	0
R10	15	3.0	10
R20	15	3.0	20
R30	15	3.0	30

RESULTS AND DISCUSSION

The physical and mechanical properties of the refractory samples incorporating waste zirconia nozzles (WZ) were evaluated by analyzing porosity, density, and flexural strength to assess their overall performance. An image of the prepared refractory samples is presented in Figure 3, while the detailed performance results are summarized in Table 3 and Figure 4.

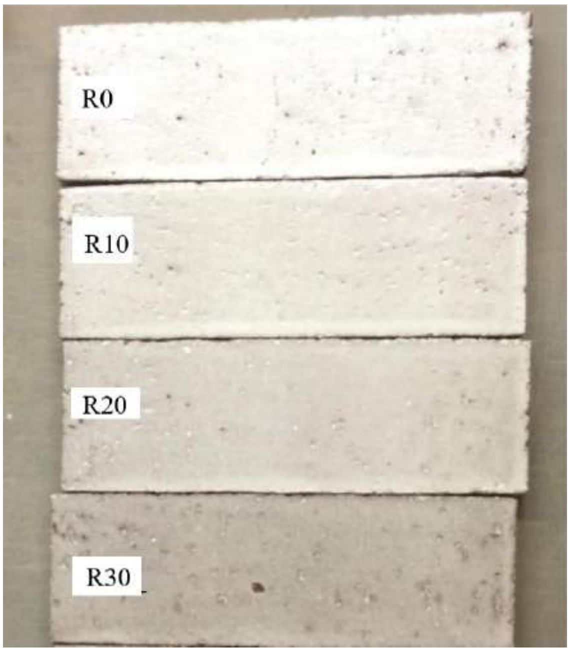

Figure 3 Fired refractory samples

The findings indicate that increasing the WZ content up to 30% results in a notable enhancement in both density and mechanical strength, accompanied by a reduction in porosity. This trend suggests that the incorporation of WZ improves the packing efficiency of the refractory mixture, thereby minimizing void spaces and promoting a denser microstructure. The highest flexural strength and density values were recorded at 30% WZ addition, highlighting the positive impact of WZ on the overall refractory properties. Additionally, the observed decrease in porosity further supports the enhanced sintering behavior and structural integrity of the samples, reinforcing the potential of WZ as a valuable additive for optimizing refractory performance.

Table 3 The properties of the prepared refractory samples.

Waste ratio (wt.%)	Flexural strength (MPa)	Porosity (%)	Density (gr/cm^3)
R0	30	18	2.80
R10	32	16	2.85
R20	32	16	2.90
R30	37	12	2.95

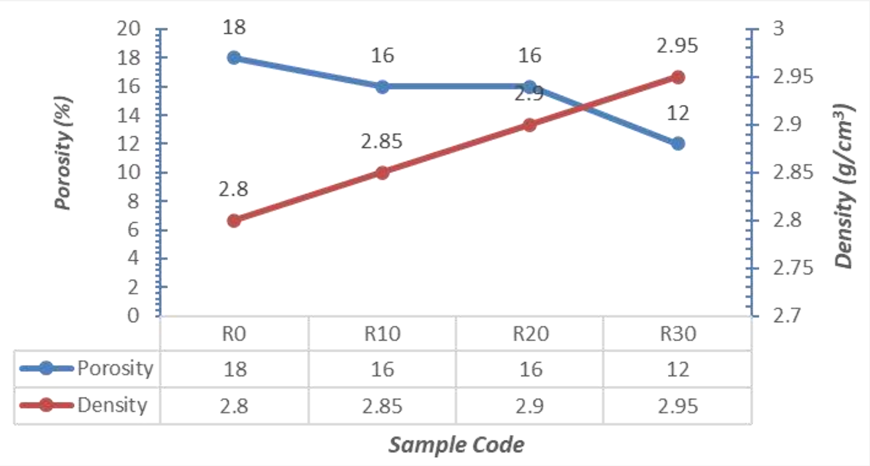

Figure 4 Changing of porosity and density related with amount of Zirconia Waste amount (%WZ)

This study explored the potential reutilization of waste zirconia nozzles (WZ) in both ceramic tile production and refractory applications, demonstrating their effectiveness in enhancing material properties while contributing to sustainable waste management.

In the first phase of the study, experimental analyses indicated that incorporating 2%wt. WZ into ceramic floor tile formulations improved both body whiteness and firing strength. These findings suggest that WZ can be effectively utilized as a substitute for conventional zircon raw materials in ceramic tile production without compromising product quality [19].

In the second phase, WZ was ground and integrated into zircon silicate refractory mixtures at varying proportions (as in wt. 0%, 10%, 20%, and 30%). The performance evaluation of the refractory samples revealed that increasing WZ content led to enhanced density and mechanical strength while simultaneously reducing porosity. Notably, the highest flexural strength and density values were achieved at a 30% WZ addition, indicating improved structural integrity and optimized sintering behavior. These results underscore the potential of WZ as a valuable additive in refractory manufacturing.

Overall, the study confirms that waste zirconia nozzles can be successfully repurposed in both ceramic tile and refractory industries. Their incorporation not only enhances material performance but also supports resource efficiency and sustainable manufacturing practices, thereby contributing to the circular economy in industrial processes.

CONCLUSION

This study explored the potential reutilization of waste zirconia nozzles (WZ) in both ceramic tile production and refractory applications, demonstrating their effectiveness in enhancing material properties while contributing to sustainable waste management.

In the first phase of the study, experimental analyses indicated that incorporating 2%wt. WZ into ceramic floor tile formulations improved both body whiteness and firing strength. These findings suggest that WZ can be effectively utilized as a substitute for conventional zircon raw materials in ceramic tile production without compromising product quality.

In the second phase, WZ was ground and integrated into zircon silicate refractory mixtures at varying proportions (0%, 10%, 20%, and 30%). The performance evaluation of the refractory samples revealed that increasing WZ content led to enhanced density and mechanical strength while simultaneously reducing porosity. Notably, the highest flexural strength and density values were achieved at a 30% WZ addition, indicating improved structural integrity and optimized sintering behavior. These results underscore the potential of WZ as a valuable additive in refractory manufacturing.

Overall, the study confirms that waste zirconia nozzles can be successfully repurposed in both ceramic tile and refractory industries. Their incorporation not only enhances material performance but also supports resource efficiency and sustainable manufacturing practices, thereby contributing to the circular economy in industrial processes.

ACKNOWLEDGEMENT

This study was supported by Eskişehir Technical University Scientific Research Program (BAP), 102 Research Support Project (102ADP) under Grant Number:24ADP143. The authors would like to thank Eskisehir Technical University Ceramic Research Center for supporting the X-ray analyses included in the study.

REFERENCES

1. Sakarya, O.H. (2022) Investigation of the Effect of Metallurgical Digital Twin Application on Production in an Iron and Steel Plant, 2022-August (ESTÜ-Graduate Thesis- Materials Science and Engineering).

2. Goyal, R.K., Agarwal, V., Gupta, R., Rathore, K., Somani, P. (2022) Optimum utilization of ceramic tile waste for enhancing concrete properties, Mater. Today Proceedings, 49: 1769-1775. https://doi.org/10.1016/j.matpr.2021.08.011
3. Dino, G.A., Fornaro, M.A. (2012) Trentin Quarry waste: chances of a possible economic and environmental valorisation of the Montorfano and Baveno granite disposal sites, Journal of Geological Research, 452950: 1-11. https://doi.org./10.1155/2012/45295.
4. Luz, A.P., Ribeiro, S. (2007) Use of glass waste as a raw material in porcelain stoneware tile mixtures, Ceramics International, 33: 761-765.https://doi.org/ 10.1016/j.ceramint.2006.01.001
5. Liu, M., Ma, G., Zhang, X., Liu, J., Wang, Q. (2020) Preparation of black ceramic tiles using waste copper slag and stainless steel slag of electric arc furnace, Materials, 13: 776. https://doi.org/10.3390/ma13030776
6. Bayer Ozturk, Z. and Eren Gultekin, E. (2015) Preparation of ceramic wall tiling derived from blast furnace slag, Ceramics International, 41: 12020-12026. https://doi.org/10.1016/j.ceramint.2015.06.014
7. Bayer Ozturk, Z., Pekkan, K., Tasci, E., Yilmaz, S. (2020) The effect of granulated lead–zinc slag on aesthetic and microstructural properties of single-fired wall tile glazes, J Aust Ceram Soc., 56:609-617. https://doi.org/10.1007/s41779-019-00372-0
8. Ozkan, I. (2017) Utilization of Bigadiç boron works waste clay in wall tile production, Acta Physica Polonica A, 132: 427-429. https://doi.org/10.12693/APhysPolA.132.427
9. Ozkan, I., Çolak, M., Oyman, R.E. (2010) Characterization of waste clay from the Sardes (Salihli) placer gold mine and its utilization in floor-tile manufacture, Applied Clay Science, 49: 420–425. https://doi.org/10.1016/j.clay.2009.08.021
10. Zanelli, C., Conte, S., Molinari, C., Soldati, R., Dondi, M. (2021) Waste recycling in ceramic tiles: a technological Outlook, Resources Conservation and Recycling, 168: 105289. https://doi.org/10.1016/j.resconrec.2020.105289
11. Ghonaim, S.A., Ghazal, H.B.G., Abadir, M.F. (2010) Effect of type of aggregate on the properties of refractory concrete, Jour. of. Ameri. Scie., 6 (12):1025–1027.
12. Khalil, N.M. and Algamal, Y. (2019) Recycling of ceramic wastes for the production of high performance mullite refractories, Siliconindia, 1–9. https://doi.org.10.1007/s12633-019-00248-9
13. Mazzanti, F., Brentari, A., Burresi, E., Coglitore, A., Labanti, M., Martelli, S., Mingazzini, C., Ricci, A., Sangiorgi, S., Scafe, M., Villa, M. (2013) Exploitation of ceramic wastes by recycling in alumina-mullite refractories, Adv. Sci. Technol., 70:9–14. https://doi.org/10.4028/www.scientific.net/AST.70.9
14. Khanlar LN, Rios AS, Tahmaseb A, Zandinejad A. (2021) Additive Manufacturing of Zirconia Ceramic and Its Application in Clinical Dentistry: A Review, Dent J (Basel). 9: 104.
15. Web site 1: https://www.zen-ceramic.com/zirconiaceramics/zirconia-ceramic-nozzles-and-rods.html (Accessed 1 December 2023)
16. Web site 2: http://www.zirconianozzle.com/en/product.html (Accessed 1 December 2023)
17. Web site 3: https://www.earthwaterfire.com/products/zirconia-ceramics/ (Accessed 1 December 2023)
18. Karakedi Sakarya G., Berberoğlu A.O, Sakarya OH, Cengiz U, Ubay E. (2022) Investigation of The Usability of Zirconia Nozzle Waste Instead of Zircon In Wall Tile Glaze Composition, J Sci. Kocaeli University 5(1): (2022) 25-31 https://doi.org/10.53410/koufbd.1114530
19. Z.Bayer Ozturk, Y.Karaca, S.Kurama, E.Ubay, U.Cengiz. (2025) Utilizing waste zirconia nozzles for eco-friendly ceramic tile production, Journal of Ceramic Processing Research. Vol. 26, No. 1, pp. 43~50.

XVI International Mineral Processing
and Recycling Conference
28-30 May 2025, Belgrade, Serbia

DOI: 10.5937/IMPRC25457B

Original research article

NEW SAG-BALL MILL AND FLOTATION LINE FOR RECONSTRUCTING OF "ZLETOVO" FLOTATION PLANT-PROBISHTIP, NORTH MACEDONIA

Boris Borche Fidanchev[1], 0009-0002-8540-4524,
Afrodita Zendelska[2#], 0000-0001-5109-1465,
[1]Mining Institute, Skopje, North Macedonia
[2]Faculty of Natural and Technical Sciences, University Goce Delcev, Stip, North Macedonia

ABSTRACT – "Zletovo" Lead and Zinc Flotation Plant has existed for more than 50 years and for the future profitable work of "Zletovo" Mine, reconstruction is necessary to increase the annual capacity of the mine production and ore processing from 150 to 350 kt/y, as well as increase the technological quantitative-qualitative results. To achieve those goals, in the current reconstruction of "Zletovo" Lead and Zinc Flotation Plant, with including a "New SAG Ball Mill and Flotation Line" is expected to be achieved replacement of the existing old and dilapidated crushing, grinding and flotation as well as and to increase the technological quantitative-qualitative results. The current reconstruction of "Zletovo" Mine, is meant to increase the mine's annual capacity and ore processing by introducing the "New SAG-Ball Mill and Flotation line", with an investment of up to US$15M, the annual profit will reach up to US$25M or more.

Keywords: SAG-Ball Mill, Crushing, Grinding, Pb-Zn Ore, Concentrates.

INTRODUCTION

The processing of ore through flotation plants is a critical operation in the mining industry, particularly in extracting valuable minerals [1]. Many plants are undergoing substantial upgrades to meet the growing demands of mineral processing efficiency and address the challenges posed by increasingly complex ore characteristics. One such project is the reconstruction of "Zletovo" flotation plant, a key facility in the mineral processing sector.

"Zletovo" flotation plant, located in the northeast part of North Macedonia, has long been a vital player in the processing of lead and zinc. However, as global mining operations evolve, the plant needs modernization to maintain competitive and efficient operations. This paper discusses the implementation of a new Semi-Autogenous Grinding (SAG) mill and a comprehensive flotation line as part of the plant's reconstruction process [2].

These technological advancements are designed to significantly enhance grinding, flotation and overall mineral recovery, while optimizing energy consumption and operational costs [3].

[#] corresponding author: afrodita.zendelska@ugd.edu.mk

“Zletovo” Mine (Ore Mining & Processing) dating just before the II-nd World War, with the first oldest flotation plant (two sections I-II only with lead flotation) and annual ore capacity up to 25 kt/y. In the period after the II-nd World War, in 1953, it was introduced a new flowsheet with additional zinc flotation.

The reconstruction of the brand-new building flotation plant “Crushing, Grinding and Flotation” (primary and secondary crushing with screening and two identical: I-II sections of grinding and flotation of lead and zinc) for an annual ore capacity up to 55 kt/y, began in 1972 and continued successfully until 2005, i.e., due to the insolvency of “Zletovo” Mine [4,5].

After 2006, the new private concessionaire decided to work only with the “I-st Section, grinding and flotation of lead and zinc,” which, without any major reconstruction, still exists and works today [8].

Nowadays, is necessary development of “Zletovo” Mine for its future profitable work through the relevant current reconstruction with introduction of the “New SAG-Ball Mill and Flotation Line”, II-st Section, ball mill and flotation of lead and zinc.

"Zletovo" Flotation Plant, according to the current reconstruction with introduction of the "New SAG-Ball Mill and Flotation Line", should increase the annual capacity of the mine production and ore processing from 150 to 350 kt/t, as well as to increase technological quantitative - qualitative results.

In general, according to the current reconstruction with the „New SAG-Ball Mill and Flotation Line”, it is foreseen:

- Replacement of the existing old and dilapidated “Crushing“, with a new single parallel primary crusher “Jaw Crusher” and primary open “Stockpile”;
- Replacement of the existing old and dilapidated “Grinding”, with a new parallel “SAG-Mill Line” and II-nd Section existing ball mill;
- Replacement of the existing old and dilapidated “Flotation”, with a new parallel “Flotation, II-nd Section flotation of lead and zinc line”;
- Increasing the technological quantitative-qualitative results of the flotation lead and zinc concentrate.

FLOTATION PLANT RECONSTRUCTION

The reconstruction of the flotation plant with introduction of the “New SAG-Ball Mill and Flotation Line” will solve the follow problems:

Crushing: The new single primary „Jaw Crusher“ for crushing to the definitive ore size up to F_{80} = 180 mm and new „Stockpile“, with a capacity up to 6 kt, efficient for the wet ore up to 10-12% H_2O and content up to 12-15% of kaolin.

Grinding: The flowsheet of the “New SAG-Ball Mill Line" with II-nd Section existing ball mill *(with a capacity up to 56 t/h, grinding the material up to 65% of class - 200# (74μm), efficient for the optimal grinding results)* are shown in Figure 1.

Flotation: The flowsheet of the “New SAG-Ball Mill Line“, II-nd Section flotation of lead and zinc *(with a capacity up to 56 t/h, efficient for the optimal technological quantitative-qualitative results)* are shown in Figure 2.

The metal balance of the flowsheet “New SAG-Ball Mill & Flotation Line” is shown in Table 1.

Table 1 Metal balance of the flowsheet "New SAG-Ball Mill & Flotation Line"

Product	Mass %	Pb %	Zn %	Ag g/t	R% Pb%	R% Zn%	R% Ag%
Ore	100.00	4.30	2.20	40.00	100.00	100.00	100.00
Conc. Pb	5.43	76.00	2.50	589.15	96.00	6.17	80.00
Conc.Zn	3.44	1.05	55.00	87.21	0.84	86.00	7.50
Tailings	91.13	0.15	0.19	5.49	3.16	7.83	12.50

The "New SAG-Ball Mill and Flotation Line" is planned to be solved by new equipment and modern efficient flotation cells for:

- Rougher and scavenger flotation of lead and zinc, type "RCS/OK 10", volume 10 m^3 and for cleaning the concentrates, type "RCS"/"OK-Concorde Cell", volume 3 m^3, with regrinding of the all-middling's flotation products" by new "VertiMill-Classification" [3].

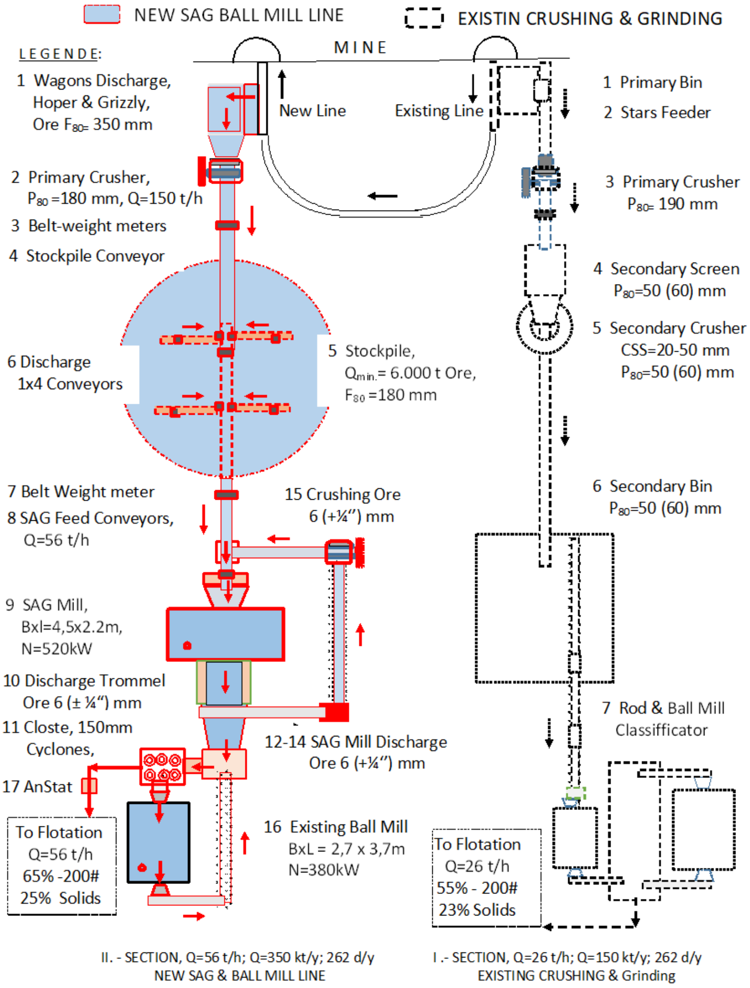

Figure 1 Flowsheet "New SAG-Ball Mill Line", II-nd Section existing ball mill

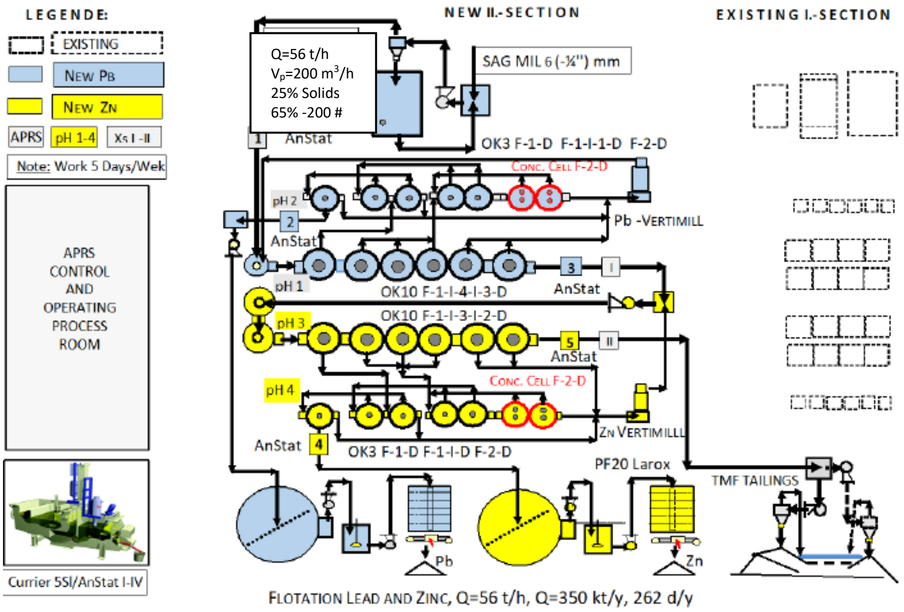

Figure 2 Flowsheet "New ,SAG-Ball Mill Line", II-st Section Flotation of Lead and Zinc

TECHNO-ECONOMICAL CRITERION

The techno-economic criterion was made according to the current following comparative analyses:

- comparative results of ore capacity and effective working days, Table 2;
- comparative results of ore normative material, Table 3;
- comparative of quantitative-qualitative results, Table 4; and
- comparative results of calculated by the **ore value (US$/t).**

Table 2 Comparative results of ore capacity and effective working days

Criterion	Old	New	Diference
Ore Mining			
Anual, Q	150 kt/y	350 kt/y	(+) 200 kt/y
Effective Work Days, T	312 d/y	312 d/y	(±) - d/y
Ore Processing			
Hourly, Q	< 26 t/h	56 t/h	(+) 30 t/h
Effective Work Days, T	262 d/y	262 d/y	(±) - d/y

Table 3 Comparative results of ore normative material

Normative	Old	New	Diference
Mine	92.40 US$/t	58.00 US$/t	34.40 US$/t
Flotation	34.20 US$/t	19.80 US$/t	14.40 US$/t
Total	126.60 US$/t	77.80 US$/t	48.80 US$/t

Table 4 Comparative technological quantitative-qualitative results

Criterion	Old	New	Diference
Quality			
Lead Concent.	72.00% Pb 4.20%Zn	76.00Pb% 2.50Z%	(+) 4.00Pb% (-) 1.70Zn%
Zinc Concent.	1.80%Pb 50.00%Zn	1.05Pb% 55.00Zn%	(-) 0.80Pb% (+) 5.00Zn%
Ag/Lead Concent.	450.00 g/t Ag	589.15 g/t Ag	140.00 g/t Ag
Recovery			
Lead Concent.	92.00% R-Pb%	96.00 R-Pb%	(+) 4.00 R-Pb%
Zinc Concent.	71.00% R-Zn%	86.00 R-Zn%	15.00 R-Pb%
Ag/Zinc Concent.	62.00% R-Ag%	80.00 R-Ag%	18.00 R-Ag%

Comparative results of **ore value (US$/t)** is calculated by the following equality:

$$VO = Y_C\,(P_M \cdot \beta_M \cdot RS_M - TC_S - RC_S - TC_T) \quad (US\$/t);$$

The symbols in the equality stay for:

V_O - value ore (US$/t);
Y_C - masse concentrate (%);
P_M - prices meatal "LME" 2024
β_M - content metal in concentrate (%);
RS_M - recovery metal in metallurgy (%) ;
TC_S - smelting expenses (US$/t);

RC_S - refining expenses (US$/t);
TC_T - transport expenses (35.00 US$/t);

Lead concentrate	**Zinc concentrate**
RS_M Pb >60; 95.0%;	RS_M Zn >51%, 85.0%;
RS_M Ag >50g/t 95.0%;	RC_S Ag 0.02 US$/g;
TC_S 98.00 US$/t;	TC_S 160.00 US$/t;

CONCLUSION

Regarding to the relevant current reconstruction of "Zletovo" Lead and Zinc Flotation Plant with the "New SAG Ball Mill and Flotation Line", the following can be concluded:

- The "New SAG-Ball Mill and Flotation Line" under the existing current conditions ***(effective* work *days)*** should increase the annual capacity from 150 to 350 kt/y;

- The "New SAG-Ball Mill and Flotation Line" is an essential because it can be built ***(in a parallel***) without a new building and any major construction works, i.e. without interruption of the current production of "Zletovo" Mine;

- The "New SAG-Ball Mill and Flotation Line" under the new current conditions ***(annual and hourly ore capacity)*** should achieve the following technological and economic results:

- Increases of ***annual ore capacity, Q, up to (+) 200 kt/y;***
- Increases of ***flotation hourly capacity, Q, up to (+) 30 t/h;***
- Decreases of ***ore normative material-US$/t, up to (-) 48.80 US$/t;***

- Quality of the concentrate:
  - Lead concentrate ***up to >76% Pb, >600 g/t Ag, and < 2.5% Zn;***
  - Zinc concentrate ***up to >55% Zn and < 1% Pb.***

- Recovery of the concentrate:
  - Lead concentrate ***up to >96 R%Pb% and >80 R%Ag%;***
  - Zinc concentrate ***up to >86 R%Zn%.***

The new relevant current reconstruction of "Zletovo" Mine, by introducing of the ***"New SAG-Ball Mill and Flotation Line",*** with an investment of up to US$15M, the annual profit will be increase ***up to US$25M or more***.

REFERENCES

1. Woods, R. (1981). Mineral Flotation. In: Bockris, J.O., Conway, B.E., Yeager, E., White, R.E. (eds) Comprehensive Treatise of Electrochemistry. Comprehensive Treatise of Electrochemistry, vol 2. Springer, Boston, MA. https://doi.org/10.1007/978-1-4684-3785-0_11
2. Allis-Chalmers (1984). Grinding Mills Process Technology for the Mining Industry: Types, Selection, Design, Circuit, Features, Dimension. Liho 07810138, Milwaukee, Wisconsin. U.S.A. 53201.
3. Product Handbook 3.14-16; 3.26-29; 3.36-41; 4.7-9; 5.15-18; 6.29-34 (2010). Basics in Mineral Processing. Edition 7. www.metso.com.
4. Popovic, D. Fidancev, B. & Nikolovski, M. (1973), Comparative - paralleled indicators of the flotation lead - zinc ore concentration, reached in the old and new plant of Zletovo Concentrator – Probistip, Proceedings of 3tdYugoslav Symposium of MP, Skopje, R. of Macedonia, vol 1, pp 143-159.
5. Fidancev, B., Jovanovski, T., Pavlovic, S., & Spirovski. S. (1989), Improving of the technological results in Zletovo lead - zinc Concentrator – Probistip, R. of Macedonia. Proceedings of 12th Yugoslav Symposium of MP, Tuzla, R. of Bosna and Herzegovina.
6. Fidancev, B., Ivanovski, S., Popovic, D. & Spasovski, D. (1991), Increasing of the capacity and modernization of the technological process in the Concentrator of the Sasa Mine - M. Kamenica. Proceedings of 13th Yugoslav Symposium of MP, D. Milanovac, R. Serbia, vol 4, pp 242-249.
7. Fidancev, B., Aleksandrov, M., Pavlovski, B., Krstev, B. (2006), The world modern mineral processing trends at the reconstruction of the Concentrator of Sasa Lead and Zinc Mine - M. Kamenica. Proceedings of XXIII. International Mineral Processing Congress, Istanbul, Turkey, vol 3, pp 2558-25.
8. Fidancev, B., Tonevski, D. (2023), New modern equipment for the reconstruction of “Zletovo” flotation plant - Probistip, North Macedonia, Proceedings of XIX. Balkan Mineral Processing Congress – BMPC Mitrovica, Kosovo, R. Srbija.

XVI International Mineral Processing
and Recycling Conference
28-30 May 2025, Belgrade, Serbia

DOI: 10.5937/IMPRC25463V

Review article

POTENTIAL OF RECYCLING AND REUSE MINING WASTE IN SERBIA: CHALLENGES AND PROSPECTS

Nela Vujović[1#], 0009-0004-7451-8897,
Vesna Alivojvodić[2], 0000-0002-4578-7519,
Dragana Radovanović[3], 0000-0002-2935-7711,
Marija Štulović[3], 0000-0002-7647-999X,
Miroslav Sokić[1], 0000-0002-4468-9503,
Filip Kokalj[4], 0000-0001-9234-7834,
[1]Institute for Technology of Nuclear and Other Mineral Raw Materials, Belgrade, Serbia
[2]The Academy of Applied Studies Polytechnic, Belgrade, Serbia
[3]Innovation Center of the Faculty of Technology and Metallurgy in Belgrade, University of Belgrade, Serbia
[4]University of Maribor, Faculty of Mechanical Engineering, Maribor, Slovenia

ABSTRACT – Waste materials from mining activities are increasingly used as secondary raw materials, which reduces the need to extract new resources from nature and mitigates the negative impact on the environment. This paper examines sustainable industrial practices in Serbia's mining and energy sector, focusing on flotation tailings and fly ash, constituting 95% of disposed waste in 2023. The study investigates metal recovery potential from copper mining regions such as Bor and Majdanpek and the utilization of fly ash from thermal power plants in construction and other industries. By reviewing existing state and legislation, the paper discusses the potential to provide the foundation for increased circularity in these sectors.

Keywords: Mining Waste, Recycling, Reuse, Circular Economy, Serbia.

INTRODUCTION

Mining activities generate significant amounts of waste. Flotation tailings and fly ash, deposited in large quantities worldwide, pose substantial environmental risks, including soil destruction, water contamination, ecosystem disruption, and toxic substances in the soil. The global mining industry faces the significant challenge of balancing economic development with conserving natural resources while minimizing environmental harm.

Data indicate that the exploitation of raw materials worldwide has tripled over the past five decades [1]. Mining operations produce over 100 billion tons of solid waste annually, with projections suggesting a further 60% increase by 2060, making adopting more sustainable mining practices imperative [1]. Mitigating these challenges could be

---

[#] corresponding author: n.petronijevic@itnms.ac.rs

managed by promoting sustainable practices in the industry and developing and implementing innovative ways to repurpose mining waste, which includes transforming waste into valuable resources. These waste materials represent significant waste streams with potential for valorization, resulting in reduced extraction of virgin resources and mitigation of adverse environmental impacts.

Global fly ash production is estimated to be over 700 million tons per year [2]. The fly ash market is expected to grow at an annual rate of about 4.83% from 2025 to 2033, primarily due to increased demand in the construction industry, particularly for cement and concrete production [3]. The processing and reuse of waste are aligned with the principles promoted by the circular economy, which involves establishing partnerships between different sectors in the production chain to ensure the most efficient use of material value.

This paper aims to review sustainable waste management practices in Serbia's mining sector, focusing on the potential of flotation tailings and fly ash as secondary resources and discussing innovative approaches for their management and utilization. In Serbia, the mining sector alone generated nearly 95% of the total waste in 2023 [4], presenting an exceptional environmental challenge that can be transformed into an economic opportunity. By adopting and implementing circular economy principles, the sector can contribute to sustainable development goals and promote resource efficiency and environmental protection.

POTENTIALS FOR UTILIZATION OF MINING WASTE IN SERBIA

The circular economy (CE) concept offers substantial benefits to the mineral mining and processing sector by enhancing resource efficiency, reducing waste, and protecting the environment. It enables the extraction of valuable metals and produces high-value materials for other industries while minimizing waste and soil pollution. For now, in Serbia, the traditional 3R framework (Reduce, Reuse, Recycle) is still on its way to full implementation, through:

- Reduce: Optimizing resource use by applying advanced technologies.
- Reuse: Utilizing mining waste in construction and other industries.
- Recycle: Recovering metals from tailings using advanced technologies.

Studies for the valorization of flotation tailings in Serbia have already demonstrated promising results for copper recovery from these tailings, highlighting their potential as secondary resources. Recent studies have shown promising results for metal recovery from these tailings. Copper leaching experiments from Bor tailings have achieved extraction rates ranging from 70% to 89.87%, suggesting significant potential for valorizing metals from secondary sources in Serbia. For example, Antonijević et al. [5] achieved a copper yield of 88% by leaching Bor copper mine tailings using sulfuric acid with iron chloride as an oxidizer. Stevanović et al. [6] reported a yield of 89.87% through acid leaching in columns without oxidizing agents. Stanković et al. [7] utilized acidophilic bacteria to achieve an average leaching rate of approximately 80%. Sokić et al. [8] obtained a leaching degree of 73.8% from oxide-sulfide ore at the Cerovo mine using sulfuric acid. Also, recent studies by Stanković et al. [9] involved leaching Bor tailings with sulfuric acid and re-flotation, resulting in a copper removal degree of 83-85%.

In general, the basic concepts for disposed mining waste, flotation tailings, and fly ash utilization, following the circular economy principles, are shown in Figure 1 [10]. This concept can be divided into three main steps material processing and residue extraction. The primary extraction process includes (a) Using coal through combustion to produce residual fly ash and (b) Processing ore to obtain concentrate and flotation tailings. In the secondary step, valuable metals are extracted from fly ash and flotation tailings, generating critical raw materials (CRMs) along with residual waste. Serbia's ore deposits are a key source of minerals, including CRMs. Tertiary Step: In a circular economy, this step focuses on reducing, reusing, and recycling remaining waste to recover valuable materials.

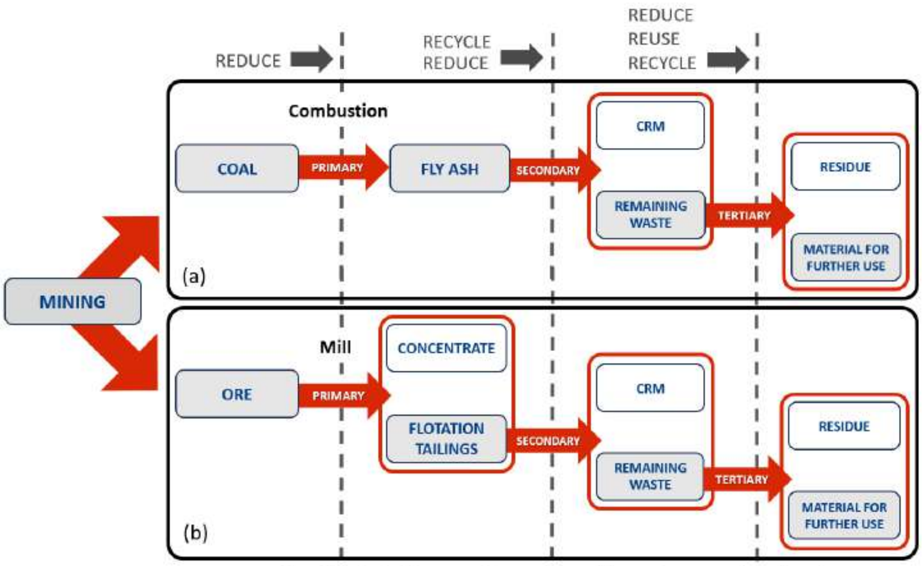

- More efficient extraction methods.
- Implementation of new technologies.

Recovery from mining waste and valorization of CRM.

Processing and desulfurization for use in construction (for example).

Figure 1 A flowchart of a three-stage separation process for (a) fly ash and (b) flotation tailings aimed at obtaining material for further use [10]

Implementing these principles can bring significant environmental, economic, and social benefits. Recycling mine tailings, for example, can recover valuable metals while reducing waste volumes and environmental impacts. Repurposing mining waste for construction materials can create new revenue streams and reduce the need for virgin resources.

Serbia has a long mining history, with approximately 200 active and 250 closed mines, resulting in substantial environmental footprints [11], with copper production being a major contributor.

Key waste streams include approximately 40 million tons of flotation tailings and approximately 7 million tons of fly ash annually [12].

Major copper production sites like Bor and Majdanpek in eastern Serbia significantly contribute to mining waste. These mines, operational since 1903, have caused considerable environmental changes, including geological disturbances and water contamination. The Bor copper mine includes three flotation tailings: Old Flotation Tailings, RTH Tailings, and Veliki Krivelj Tailings. The Old Flotation Tailings contain an estimated 22.3 million tons of tailings with the prospect of recovering gold, silver, and copper [13]. The Veliki Krivelj tailings pit holds 190-195 million tons of tailings with about 0.10% copper content.

Majdanpek's copper reserves are substantial, with the "Valja Fundata" tailings dump containing 350 million tons of tailings [13]. Other notable sites include the Grot Mine, with 550 million tons of tailings containing lead, zinc, silver, and cadmium, and the Leće Mine, with gold, silver, and indium tailings [14].

Additionally, fly ash from thermal power plants in Serbia has been successfully used to treat hazardous waste and remediate acid mine drainage (AMD). These advancements mark significant progress towards implementing sustainable development principles in the mining industry, focusing on waste minimization, treatment, and reuse within the same sector [15].

Fly ash from thermal power plants in Serbia has potential for various applications (e.g., cement production, hazardous waste treatment, geopolymer production, and acid mine drainage treatment); however, only 3% of fly ash is currently utilized in the cement industry [16].

Collaboration between stakeholders, policymakers, and researchers is crucial to fully realize and implement contemporary approaches in mining, including developing supportive regulations and investing in innovation.

By embracing these principles, the mining sector can enhance sustainability, reduce its environmental footprint, and contribute to a more resource-efficient global economy.

Implementing circular economy principles in Serbia's mining sector faces challenges such as regulatory barriers and limited technological investment.

Serbia has made significant strides in implementing circular economy principles within its mining sector. The country has established a Working Group for the Circular Economy under the Ministry of Environmental Protection and a CE Sector within the Chamber of Commerce, demonstrating a commitment to sustainable resource management and waste reduction. A significant development is the establishment of the Mining Waste Cadaster, funded by the European Union. This initiative aims to enhance waste management practices. The Mining Water Cadaster is also designed to address the treatment and reuse of water produced during mining processes. Serbia has also adopted by-product regulations that allow for the transformation of mining waste into valuable raw materials for various industries, further promoting sustainability.

These legislative efforts are designed to protect communities near mining sites, preserve the environment, and encourage responsible and ethical business practices in the mining sector.

The following steps can be crucial to unlocking the full potential of mining waste and fly ash in Serbia: 1. Enhance the legislative framework to support circular economy practices; 2. Invest in research and development of innovative technologies; 3.

Encourage collaboration between industry, academia, and government; 4. Develop a national register of mining waste and fly ash resources; 5. Implement stricter standards for material characterization and environmental impact assessment; 6. Create economic incentives for companies adopting circular economy principles.

By transforming environmental liabilities into valuable resources, Serbia can contribute to sustainable development in the mining sector and the profitable use of secondary raw materials.

CONCLUSION

The mining industry in Serbia today faces significant amounts of unused resources waiting for wider industrial application. The mining sector has a unique opportunity to reduce harmful environmental impacts and save on raw materials. Research findings underscore the significant potential for metal valorization from mining tailings and fly ash in Serbia. However, putting these results into practical application requires a joint approach of multiple stakeholders, focusing on developing strategies for effective waste management. Enhancing the regulatory and administrative frameworks is essential for creating a more sustainable future for Serbia's mining industry and is an important contribution to further empowering the recycling and reuse of flotation tailings and fly ash.

ACKNOWLEDGEMENT

This work was supported by the Ministry of Science and Technological Development and Innovation of the Republic of Serbia (Contract No. 451-03-66/2024-03/200023).

REFERENCES

1. Dale, G. (2024) Extraction of Raw Materials Could Rise 60% by 2060—And Making Mining 'Greener' Won't Stop the Damage. The Conversation. Available online: https://theconversation.com/extraction-of-raw-materials-could-rise-60-by-2060-and-making-mining-greener-wont-stop-the-damage-222818 (accessed on 22 December 2024)
2. Toniolo, N., Boccaccini, A. R. (2017) Fly ash-based geopolymers containing added silicate waste: A review. Ceram. Int., 43, 14545–14551. https://doi.org/10.1016/j.ceramint.2017.07.221.
3. IMARC Group. Fly Ash Market Size, Share, Trends and Forecast to 2033. Available online: https://www.imarcgroup.com/fly-ash-market (accessed on 20 December 2024)
4. Biznis i finansije (2020) Kružna ekonomija: Nije svako đubre za bacanje; Volume 178. BIF Press, Belgrade, Serbia; Available online: https://bif.rs/2020/10/biznis-finansije-178-kruzna-ekonomija-nije-svako-dubre-za-bacanje/(accessed on 20 December 2024)
5. Antonijević, M. M., Dimitrijević, M. D., Stevanović, Z. O.; Šerbula, S. M., Bogdanović, G. D. (2008) Investigation of the Possibility of Copper Recovery from the Flotation Tailings by Acid Leaching. J. Hazard. Mater., 158, 23–34. https://doi.org/10.1016/j.jhazmat.2008.01.063.
6. Stevanović, Z., Antonijević, M., Bogdanović, G., Bugarin, M. (2013) The Effect of Oxidants Through a Tailing Dump Depth and the Leaching of Copper. Carpathian J. Earth Environ. Sci., 8, 29–38. https://www.cjees.ro/viewTopic.php?topicId=291 (accessed on 22 December 2024).

7. Stanković, S., Morić, I., Pavić, A., Vojnović, S., Vasiljević, B., Cvetković, V. (2015) Bioleaching of Copper from Samples of Old Flotatio Tailings (Copper Mine Bor, Serbia). J. Serb. Chem. Soc., 80, 391–405. https://doi.org/10.2298/JSC140411097S.
8. Sokić, M.D., Milošević, V.D., Stanković, V.D., Matković, V.L., Marković, B.R. (2015) Acid Leaching of Oxide-Sulfide Copper Ore Prior the Flotation: A Way for an Increased Metal Recovery. Chem. Ind., 69, 453–458. https://doi.org/10.2298/HEMIND140509061S.
9. Stanković, V., Milošević, V., Milićević, D., Gorgievski, M., Bogdanović, G. (2018) Reprocessing of the Old Flotation Tailings Deposited on the Bor Tailings Pond—A Case Study. Chem. Ind. Chem. Eng. Q., 24, 334–344. https://doi.org/10.2298/CICEQ170817005S.
10. Vujović, N., Alivojvodić, V., Radovanović, D., Štulović, M., Sokić, M., & Kokalj, F. (2025). Towards Circularity in Serbian Mining: Unlocking the Potential of Flotation Tailings and Fly Ash. Minerals, 15(3), 254. https://doi.org/10.3390/min15030254.
11. Ministry of Environmental Protection of the Republic of Serbia (2022) Waste Management Program in the Republic of Serbia for the Period 2022–2031; Ministry of Environmental Protection: Belgrade, Serbia, (In Serbian).
12. Statistical Office of the Republic of Serbia (2023) Waste and Hazardous Chemicals; Statistical Office of the Republic of Serbia: Belgrade, Serbia, Available online: https://www.stat.gov.rs/en-us/oblasti/zivotna-sredina/otpad-i-opasne-hemikalije/ (accessed on 28 December 2024)
13. Pantović, R. (2021) Potencijal tehnogenih ležišta bakra i zlata (flotaciona jalovina) u rudnom kompleksu Bor - Srbija. Available online: https://mibor.rs/wp-content/uploads/2021/12/Analiza-rudnickog-otpda-u-Boru-RP.pdf
14. Vukas, R.B. (2023) Mineralne sirovine Srbije na listi EU CRM-2020 tokom pandemije Covid-19 u harmonizaciji sa kodovima UNFC-2009 i pojmovima PERC standarda. Tehnika, 73, 295–309 https://doi.org/ 10.5937/tehnika2303295V.
15. Petronijević, N., Alivojvodić, V., Sokić, M., Marković, B., Stanković, S., Radovanović, D. (2020) Sustainable Mining Towards Accomplishing Circular Economy Principles. J. Appl. Eng. Sci., 18, 493–499. https://doi.org/10.5937/jaes0-27460.
16. Vukicevic, M., Popović, Z., Despotovic, J., Lazarević, L. (2016) Fly Ash and Slag Utilization for the Serbian Railway Substructure. Transport, 33, 1–10 https://doi.org/10.3846/16484142.2016.1252427.

XVI International Mineral Processing
and Recycling Conference
28-30 May 2025, Belgrade, Serbia

DOI: 10.5937/IMPRC25469K Research article

DISSOLVED AIR FLOTATION: IS IT REALLY A SUITABLE SOLUTION FOR INDUSTRIAL PURIFICATION PROCESSES?

Haldun Kurama#, 0000-0002-2773-8326,
Eskişehir Osmangazi University, Eskişehir, Turkey

ABSTRACT – There is no doubt that one of the most important problems we face today is water scarcity as a result of increasing urbanization and climate changes. This situation necessitates sustainable water management. Although many methods have been implemented to control water pollution from past to present, the interest to usage of flotation (dissolved air flotation) as physical treatment method, has been gradually increasing its application areas in recent years. In this review, the recent developments in the application of dissolved air flotation in waste/recirculating water treatment processes was examined to provide a comprehensive understanding of the current status.

Keywords: Water Treatment, Dissolved Air Flotation, Sustainable Water Management.

INTRODUCTION

Sustainable water management and reliable access to water resources are undoubtedly one of the most important complexities of recent years. Pollution resulting from increasing world population, climate change, and increased consumption coupled with increased agricultural/industrial practices pose serious challenges in water management. As a result, sustainable water management and control of water pollution are becoming increasingly vital importance. Although many water treatment methods, including sedimentation, adsorption, advanced biological treatment, nano-based technologies and membrane technology have been developed and successfully applied to reduce environmental impacts and water consumption, the current use of these methods is still far from the desired results depending on the pollution sources, energy dependencies and socio-economic characteristics of the countries.

The methods used for water and wastewater treatment according to applied techniques are given in Fig.2. In applications, treatment methods are used alone or in combination with each other, in the early stages of the process or at the end, in a series of separation stages such as second and third stage separators. The choice of treatment processes for any particular application depends on the quality of received effluent, type of pollutant, required quality of the treated water and the economic resources available to pay both capital and operating cost [1,2].

Flotation actually is a widely used method in mineral processing and beneficiation to effectively separate mineral particles. The method based on the attachment of

---

corresponding author: hkurama@ogu.edu.tr

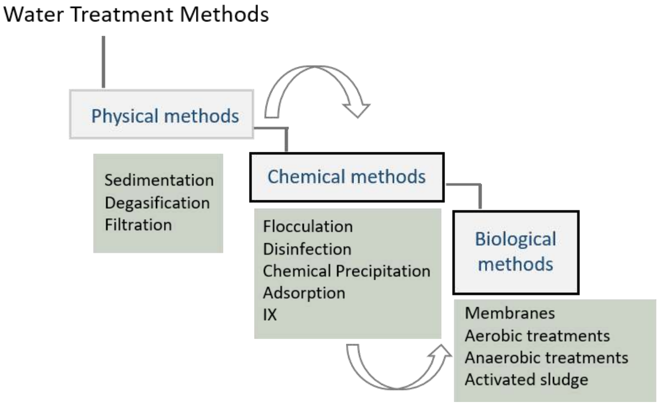

Figure 1 The methods used for water and wastewater treatment [1]

hydrophobic or conditioned particulate matter to gas bubbles and the introduction of gas bubbles as a transport medium. It was first developed for the separation of minerals in the mining industry and later was adapted for fiber separation in the 1930s by the paper industry [3]. Since then, the process has been continuously improved and in the early 1960s, it was first used in the purification of water for drinking water.

Flotation can be classified depending on the method used to generate the bubbles follows; dispersed, dissolved air and electroflotation. Among these, DAF is a continuously growing option in the treatment of paper mill and refinery wastewater, tertiary treatment of municipal water, recycled paper deinking, wastewater recovery and drinking water treatment. Recently Kyzas et al. [4] stated that in 2021, there are over 90 water treatment installations operating in the U.K. utilizing the DAF process and around the world it has been reported that there were 37 works in Finland, 26 in Australia, 26 in South Africa, 20 in the United States, etc.

DISSOLVED AIR FLOTATION (DAF)

Principle of DAF

DAF is a solid-liquid separation process based on the production of microbubbles as a result of the pressure effect and the transfer of solids to the liquid surface by binding of solid particles to fine air bubbles. As can be seen at Fig.2, in this sequential operation series, water is first saturated with high-pressure air, usually between 3 and 6 atm. The saturated water is then forced to flow through needle valves, and bubbles (10–100 µm in diameter) are produced immediately downstream of the constriction, and finally, solids are separated by bubble-particle binding [5]. Although DAF can be applied alone, it is mostly used in conjunction with coagulation/flocculation. Such usage coagulation and flocculation pretreatment steps ensure improvement in the efficiency of the bubble-particle capture during flotation.

The mechanism of application of dissolved air flotation is based on the theory of reversible chemical reactors and Henry's law, which governs the dissolution of gases in aqueous solutions as a function of pressure [6]. In principle, two factors, bubble formation and bubble-particle interaction, have a direct effect on the working mechanism of DAF. For bubble formation, the first process is the nucleation process that begins when pressurized water and air are released from the nozzle, while the second step is the transfer of excess air in the saturated water to the flotation tank in gas form. Bubble-Particle attachment performed by collision or precipitation of air on the solid surface, bubble entrapment in a floc structure, and bubbles being absorbed in a floc structure while the floc is forming. Adhesion or collision, entrapment, and absorption are the sequential mechanisms in bubble-particle bonding.

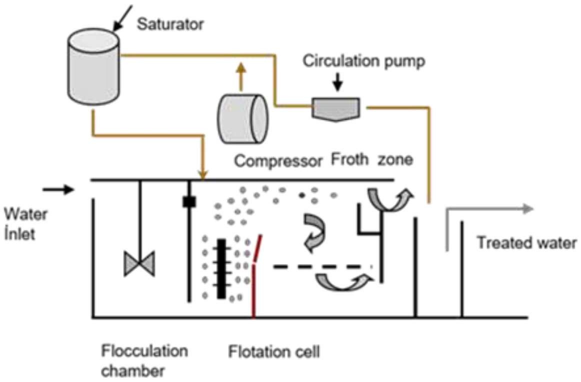

Figure 2 Rectangular flotation tank with recycle flow system

APPLICATIONS

In most cases, DAF is an alternative process to sedimentation for the removing of suspended solid particles, metallic ions, microorganism, and macro-molecules. The technique offers several advantages, including better final water quality, rapid startup, higher rates of operation, and thicker sludge. Additionally, DAF systems need less space compared with normal clarifiers, and due to their modular components, they allow easy installation and setup. Rather than the unit operation, an application of DAF as an integrated with sorption or membrane processes has also recognized as an efficient and quite promising method especially for the removal of metal ions from waste/surface water. Heavy metal removal based on precipitation of metal hydroxides and subsequent thickening or filtration of the sludge is one of the traditional methods used for many years. However, this method has some limitations, such as incomplete precipitation, chemical instability of the precipitates and formation of large volumes of sludge difficult to filter. As an overcome these limitations it was reported that DAF method can be considered as a primary alternative separation technique for the treatment of heavy metals (Ni, Cr, and Cu) from metal finishing process water by SEPA [7]. The results confirmed that DAF is more effective than sedimentation. Another study on the use of DAF for the removal of metal ions from solutions was reported by Rubio and Tessele, 1997 [8]. In this study, Zn, Cu and Ni were successfully removed from the solution by carrier flotation where the small-sized zeolite particles and $Fe(OH)_3$ precipitates were used as

Not only an alternative to sedimentation, several lab. and pilot scale applications confirmed that DAF can be considered as an ideal alternative treatment options for the clarification of paper mill and refinery wastewaters, treatment of municipal waters, recycled paper de-inking, wastewater reclamation and recently in drinking water clarification to improve filtration as secondary or tertiary stages. A research study conducted by Bourgeois et al., [9] on the treatment of drinking water residuals showed that DAF can be used effectively for the separation of solids of lower density. Pennsylvania-US, city of Waco and Atkins-North Saluda water treatment plants are the examples of a system that installed as pilot scale; which confirmed that it could efficiently remove algae, Giardia/Cryptospordium and iron /manganese ions provided with low turbidity, exceeded filter run times and high sludge solids for dewatering. The South San Joaquin Irrigation District, CA-US can also be given as an example for the treatment of raw water having high TOC, color and algae by DAF. The pilot study verified that a combination of DAF and membrane technologies without employing polymer was a winning solution for the treatment plant [10]. A recent study published by Kurama et al. [11] showed that DAF can be evaluated as an alternative method for the removal of ammonium (NH_4) ions from surface water. Natural zeolite, clinoptilolite samples with fine particle size (<10 µm) were used as carrier material during flotation tests. The tests results revealed that test loaded with 5 mg/L ammonium resulted in a residual ammonium concentration of <0.5 mg/L with corresponding turbidity values of treated water (<10 NTU).

A number of studies in the literature have shown that coagulation with ferric and an aluminum metal salt combined with DAF is an effective method for the treatment of oily wastewater with a removal performance of over 90%. Apart from these known salts, there are many studies in the literature focused on the use of more environmentally friendly and low-cost adsorbents. Among the alternative adsorbents, one of the most interesting materials is organoclay. The usability of organoclay integrated with DAF was investigated in a relatively recent study by Younker and Walsh [12]. In this study, the treatment capacity of the integrated process was compared with the individual unit processes of $FeCl_3$ coagulation and organoclay adsorption followed by DAF. It was reported that coagulation performed with organoclay is very effective for dispersed oil removal even at relatively low $FeCl_3$ doses but its efficiency is highly dependent on the OC dose and mixing time. The results of the OC-$FeCl_3$-DAF integrated treatment showed that the reduction of oil and grease concentration to below 30 mg/L is possible. A study on reducing algae load for drinking water applications was conducted by Jung et al [13] using the DAF technique and reported that DAF had a sufficient effect because algae were characterized by their buoyancy, low cell density, small size and negative surface charge. Another study supporting the potential of DAF in the treatment of oily wastewater was reported by Yu et al. [14]. The results noted that DAF could remove 90% of oil and 92.5% of chemical oxygen demand (COD) in the treatment of oily wastewater.

Another interesting research result on the application of DAF was reported by Ortiz-Oliveros et al. [15] for the treatment of radioactive liquid wastes originating from the nuclear industry. In this study, it was emphasized that the DAF process supported by a coagulant/flocculent system consisting of a modified cationic polyamine and a light cationic polyacrylamide is a viable alternative for the treatment of oily wastewater contaminated with radionuclides produced in nuclear power plants.

An example of the possible contributions of DAF use in production processes can be given for the paper industry. The increasing concentration of suspended, colloidal and dissolved substances with different properties in the reused water during production processes, causing unwanted blockages in purification and circulation systems, and the negative effects of impurities included in the production process and incompletely purified water on product quality is important problems that need to be eliminated. In this context, the study conducted by Miranda et al. [16] investigating the charge density of cationic (C-PAM)/anionic polyacrylamide (A-PAM) with a coagulant in single and double treatments and the removal of dissolved and colloidal material with DAF is important in terms of its contribution to practical use. The results showed that for single systems, good results can be achieved with both low and high charge C-PAMs (1.0 and 3.0–3.5 meq/g), while for double systems, high charge C-PAMs (3.0–3.5 meq/g) and A-PAMs (1.5 meq/g) are the most efficient options.

Another application area for the use of DAF is the treatment of process water in the metalworking industry prior to reuse. A study focusing on the usability of DAF as an alternative to conventional treatment methods was recently proposed by Amin et al. [17]. In this study, the final treatment of industrial wastewater contaminated with metalworking fluids was carried out using a chemically added dissolved air flotation (CA-DAF) unit followed by a photo-Fenton process. The authors noted that this hybrid approach revealed removal efficiencies of 99.85% and 98.9% for COD and TPH in the optimized photo-Fenton process as pH 3, $FeSO_4$: 100 mg/l, and H_2O_2: 17.8 g/l. In addition, the cost analysis for energy (6 kWh) and chemicals (0.01818 kg $FeSO_4$ and 17.15 kg H_2O_2) consumed for the proposed process was calculated as approximately \$26 per m^3 DAF waste. An example of possible proposal for the use of DAF integrated with biological treatment systems was presented by Özgün et al. [18] for a multistage sewage treatment scheme coming from different production lines in the confectionery industry, producing approximately 170,000 m^3 of wastewater per year. The wastewater treatment system consisted of a conventional activated sludge system with screens, equalization tanks, dissolved air flotation, anaerobic expanded granular sludge bed reactor (EGSB) and sludge treatment line. The research results proved that COD in an anaerobic reactor reached 88%, while the use of an anaerobic reactor led to a 95% reduction in COD. These results are encouraging for the use of anaerobic technology as a pretreatment before conventional oxygen treatment. The wastewater applications of the flotation method and the effect of changing bubble size from nano to micro on the flotation process in these applications were discussed in detail in a recent review by Kyzas et al. [4].

Apart from the water industry mentioned above, an interesting application for DAF usage in mining industry has recently been released by Santos et al. [19]. In this work, a wastewater treatment using DAF, associated with coagulation and flocculation, has been investigated to develop an alternative process for the reuse of the water from tailings dams of an industrial apatite flotation unit. The recycling water had the following characteristics: 288 NTU for turbidity, 2.25 mg/L for fluoride, 35 mg/L for calcium, 15 mg/L for magnesium, and 33 mg/L for phosphate. Results have shown that the use of recycling water after the wastewater treatment resultant a good performance of apatite flotation, leading to recovery (80.5%) and grade (31.2%) of P_2O_5 highest than minimum acceptable in this industry. More recently the DAF process was evaluating to test its efficiency for the treatment of coal industry wastewater in order to reuse water in the beneficiation plant by Hudson et al. [20], It was proposed that possible to obtain good turbidity removal efficiencies (up to 98%) using low concentrations of coagulant (50 mg/L) and flocculant (0.5 mg/L). In experiments air saturation pressure in the saturator vessel was 4.5 bar (450 kPa). The flow of air-saturated liquid was controlled according to the recycle ratio of 30%. The results emphasized that the possibility of using the DAF as an alternative technique for treating wastewater from coal mining, allowing the reuse of water in the plant. It was noted that the iron chloride coagulant was more effective in conjunction with the previous addition of the flocculating agent into the air saturation tank, making it possible to obtain high removal efficiencies of corrected turbidity (above 98%) with small coagulant dosages (50 mg / L) and Nalco flocculent (0.5 mg/ L).

CONCLUSION

The high efficiency of modern equipment, new designs, low sludge formation, high productivity and low application costs are main drivers of the DAF to extent its usage in the field of applicability of green technology areas. However, although the process has some challenge such not suitable for raw waters with high concentrations of suspended solids, limitations for flotation freezing, which leads to sedimentation of previously floated solids due to weather conditions, and relatively high cost compared to simple sedimentation, it is expected to become more widespread with increasing optimization using artificial intelligence to closely monitor the flotation process and predict characteristic bubble parameters such as shape, size and rise speed.

REFERENCES

1. Mutegoa, E. (2024) Efficient techniques and practices for wastewater treatment: an update, Discover Water 4:69 | https://doi.org/10.1007/s43832-024-00131-8
2. Trifirò, F., Zanirato, P. (2024) Water Purification: Physical, Mechanical, Chemical and Biological Treatments, Mathews J Pharma Sci. 8(3),42. https://doi.org/10.30654/MJPS.10042
3. Wang, L.K., Wang, M.H.S., Fahey, E. (2020) An innovative Lee, Massachusetts USA dissolved air flotation potable water filtration plant. In: "Evolutionary Progress in Science, Technology, Engineering, Arts, and Mathematics (STEAM)", Wang, Lawrence K. and Tsao, Hung-ping (editors). 2, 1, Lenox Institute Press, Newtonville, NY, 12128-0405, USA.
4. Kyzas, G.Z., Mitropoulos, A.C., Matis, K.A., (2021) From Microbubbles to Nanobubbles: Effect on Flotation, Processes 2021, 9, 1287. https://doi.org/10.3390/pr9081287
5. Santana, R.C., Ribeiro, J.A., Santos, M.A., Reis, A.S., Ataíde, C.H., Barrozo, M.A.S. (2012) Flotation of fine apatitic ore using microbubbles. Separ. Purif. Technol., 98, 402-409
6. Edzwald, J.K. (2010) Dissolved air flotation and me. Water Research, 44, 2077–2106
7. Waters, A. (1990) Dissolved air flotation used as primary separation for heavy metal removal. Filtration & Separation 27, (2), 70

8. Rubio, J., Tessele, F., (1997) Removal of heavy metal ions by adsorptive particulate flotation, Minerals Engineering, Vol. 10, No. 7, pp. 671-679.
9. Bourgeois, J.C., Walsh, M.E., Gagno, G.A. (2004) Treatment of drinking water residuals: comparing sedimentation and dissolved air flotation performance with optimal cation ratios Water Research 38, pp. 1173–1182
10. Farmerie, J. (2006) Eliminating Membrane Fouling. Membrane Technology, 4, (1)
11. Kurama, H., Karagüzel, C., Mergan, T., Çelik, M.S. (2010) Ammonium removal from aqueous solutions by dissolved air flotation in the presence of zeolite carrier, Desalination, 253, (1–3),47-152, https://doi.org/10.1016/j.desal.2009.11.017
12. Younker, J.M., Walsh, M.E. (2014) Bench-scale investigation of an integrated adsorption–coagulation–dissolved air flotation process for produced water treatment, Journal of Environmental Chemical Engineering 2 692–697 693, http://dx.doi.org/10.1016/j.jece.2013.11.009
13. Jung, W., An, J.S., Park, J.Y., Choi, J.S., Oh, H.J. (2016) A case study of daf pilot plant for application of Water Treatment Plant (WTP), International Proceedings of Chemical, Biological and Environmental Engineering (IPCBEE), 98, 80-86, International Association of Computer Science and Information Technology Press (IACSIT), ISSN 20104618
14. Yu, L., Han, M., He, F. (2017) A review of treating oily wastewater, Arabian journal of chemistry, 10, S1913-S1922
15. Ortiz-Oliveros, H.B., Espinosa, R.M.F., Dominguez, H.J., Moleon, M.C.J., Gonzalez, D.C. (2012) Dissolved air flotation for treating wastewater of the nuclear industry: preliminary results, J Radioanal Nucl Chem 292, 957
16. Miranda, R., Blanco, A., De la Fuente, E., Negro, C. (2008) Separation of Contaminants from Deinking Process Water by Dissolved Air Flotation: Effect of Flocculant Charge Density, Separation Science and Technology, 43: 3732–3754 http://doi.org/10.1080/01496390802286587
17. Amin, M.M, Mofrad, M.M.G., Pourzamani, H., Sebaradar, S.M., Ebrahim, K. (2017) Treatment of industrial wastewater contaminated with recalcitrant metal working fluids by the photo-Fenton process as post-treatment for DAF, Journal of Industrial and Engineering Chemistry 45 412–420, http://dx.doi.org/10.1016/j.jiec.2016.10.010
18. Ozgun, H., Karagul, N., Dereli, R.K., Ersahin, M.E., Coskuner, T., Ciftci, D.I., Ozturk, I., Altinbas, M. (2012) Confectionery industry: a case study on treatability-based effluent characterization and treatment system performance. Water Science & Technology, 66(1), 15-20
19. Santos, M.A., Capponi, F., Ataíde, C.H., Barrozo, M.A.S. (2021) Wastewater treatment using DAF for process water reuse in apatite flotation, Journal of Cleaner Production 308 127285, https://doi.org/10.1016/j.jclepro.2021.127285
20. Couto, H.J., França, S.C., da Silva Santos, J. (2011) Dissolved air flotation (DAF) as an alternative treatment for coal wastewater. In 8th International Mineral Processing Seminar (Procemin), Santiago, Chile (Vol. 30, pp. 427-433).

XVI International Mineral Processing
and Recycling Conference
28-30 May 2025, Belgrade, Serbia

DOI: 10.5937/IMPRC25476N Research article

VALORIZATION OF RESIDUAL MATERIALS IN THE PREVENTION AND TREATMENT OF CONTAMINATED MINE WATER AND AIR

Carmen M. Neculita[1#], 0000-0002-8388-7916,
Flavia L. Braghiroli[2], 0000-0001-7840-8311,
[1]Research Institute on Mines and Environment (RIME), University of Québec in Abitibi-Témiscamingue (UQAT), Rouyn-Noranda, Canada
[2]Forestry Research Institute, UQAT, Rouyn-Noranda, Canada

ABSTRACT – Valorization of residual materials, close to mine sites, reduces the environmental footprint and helps balance the ratio of rentability to responsible management of natural resources. Relevant case studies using raw vs modified, organic vs inorganic residual materials for contaminated mine water prevention and efficient treatment, using active and passive treatment processes are presented. Main findings show: 1) mono- and multi-layer solid covers installed on top of fresh or weathered mine tailings have beneficial role in limiting oxygen and water ingress to reactive minerals and mine drainage generation; 2) reactive mixtures composed of natural and residual materials are efficient in (semi)-passive treatment of contaminated mine drainage from covered tailings; 3) contaminated residues from active and passive treatment of mine water can efficiently be used in the revegetation of rehabilitated mine sites; 4) modified materials (efficiency enhancement) with porous structure and basic character (functional groups connected to their surface) are effective for the capture of acid gases such as SO_2 emitted from mining and metallurgical industries, and water contaminants from forestry lumber and mining. Valorization of raw and modified materials for the prevention and treatment of contaminated mine water and air is promising for circular economy development in remote regions as well as the reduction of the environmental footprint.

Keywords: Residuals valorization, Prevention and treatment, Mine sites rehabilitation.

INTRODUCTION

Mixed contamination of mine water is entailed by the exploitation of low-grade ores that require more aggressive metallurgical separation. However, efficient mine water treatment and responsible management of sludge is imperative for mining industry and governments. Metastable characteristics of some species, changes related to the mine life cycle and mixing processes occurring at various scales lead to evolutive behavior of contaminants. In cold climate, water treatment requires adaptation to site conditions such as high flow rates, salinity, low temperatures, remoteness, and high sensitivity of receiving streams [1]. Contaminants of emerging concern (CEC) are a newer challenge in mine water, including species such as: new (rare earth and radioactive elements, Mn, Se), of emerging interest (salinity, sulfate), for which environmental issues were not fully comprehended earlier, and "well-documented" (flotation collectors, As, S- and N-

---

[#] corresponding author: CarmenMihaela.Neculita@uqat.ca compounds), with persistent but unknown aquatic toxicity [1]. Consistently, atmospheric contaminants increasingly become another critical environmental issue.

At the same time, several natural and residual materials are available close to mine sites: wood waste [2-4], desulfurized tailings [5], activated biochar [6-9], food waste and zeolites [10], peat [3], ash [11], dolomite [7], and mine water treatment residues [12-14]. These materials can be used as amendments or covers for tailings [12], for mine water treatment and mine site rehabilitation and, thus, limit the transportation costs, environmental footprints, and related impacts. They can be used as raw, modified or activated products. Several relevant examples of case studies, at laboratory vs field-scale are presented and discussed, for materials' performance and overall implications.

FUNDAMENTALS

Mine water and air treatment and mine sites rehabilitation require high quantities of products and materials, most of each are transported from outside the mine sites. To limit contamination and long-term water treatment, prevention and mitigation of porewater quality in mine tailings are necessary. Acid mine drainage (AMD) prevention is facilitated when done on fresh vs severely weathered acid-generating tailings. The leaching front of AMD in the porewater of highly oxidized tailings may take at least 20 years to wash out [15], depending on the properties of tailings and climate.

The mechanisms within amendments and covers made of organic or mineral, natural or residual materials can lead to geochemical and geotechnical stability of amended or covered tailings [16]: 1) Anoxic/anaerobic environment creation, for metal sulfides precipitation; 2) pH and alkalinity increase by neutralizing materials or by mineralized organic carbon; 3) Contaminated porewater dilution and improved efficiency of passive treatment; 4) Formation of a hardpan of secondary minerals playing a protecting role to prevent unoxidized tailings; 5) Limitation of water infiltration in tailings by favoring horizontal runoff; 6) Improvement of geochemical and mechanical properties of tailings and development of a protective layer favorable to tailings revegetation.

Laboratory vs field case studies from Canada are detailed in the next chapter.

CASE STUDIES

Laboratory scale

Case I: Wood residues from sawmills and reconstituted wood panels were converted into activated biochar (AC) through a two-step thermochemical process: (i) a pilot scale fast pyrolysis at 250 kg/h and 450°C; and (ii) a physical activation at up to 950°C using an activation furnace (1 kg/h). A laboratory dispositive for evaluating the SO_2 retention performance of all materials was developed, and their adsorption capacities were the following: up to 77 mg/g (AC from wood residues) [6]; up to 2140 mg/g (AC from wood panels residues) [17] as well as up to 65 mg/g for a commercial activated carbon. These results could be explained by the high specific surface area of AC, the presence of nitrogen to a basic material' surface, efficient for the SO_2 capture, as well as a great microporosity developed. This study could help the Canadian residual materials management policies through the valorization of wood residues for the creation of a green economy reducing the carbon footprint through their transport.

Case II: A biochar pellet made from sawmills wood residues rich in ammonium sulfate [$(NH_4)_2SO_4$], by the conversion of N-NH_3 from a mine effluent, was developed as a soil substrate in laboratory scale [13]. Greenhouse tests were carried out using combinations of substrates for black spruce growth such as (i) peat; (ii) peat and bulk biochar; (iii) peat and $(NH_4)_2SO_4$)-bulk biochar; (iv) peat and wet biochar pellets; (v) peat and $(NH_4)_2SO_4$-biochar pellets; and (vi) peat, $(NH_4)_2SO_4$-biochar pellets and perlite. The results showed that a quarter of peat could be replaced by biochar to obtain similar or better biomass yield (27% higher vs peat as control). This approach could benefit the carbon capture and storage in soil, and be applied for other fields such as golf courses, forestry producers and horticultural nurseries with the aim of replacing conventional fertilizers and peat.

Case III: N-rich residues (saturated zeolites and biomass from 50-280 mg/L NH_3-N treatment in synthetic and real mine effluents) were tested as substitute of commercial fertilizers for the vegetation of non-acid generating tailings [14]. Tests were conducted over a 3-month period in pots with agronomic herbaceous plants. Unamended vs amended tailings with a mineral NPK fertilizer, and a commercial topsoil were used as controls. The comparison used were above-/below-ground biomass production, leaf area, root length/diameter, and leaf NPK concentration. Transfer of contaminants to leaves and runoff was assessed. The results showed low biomass with the N-rich zeolite amendment, whereas plants in MBBR biomass amended tailings had similar biomass to those in the tailings amended with the NPK mineral fertilizer and commercial topsoil. Leaf nitrogen in amended treatments were higher vs the unamended control. A concentration 6-9 times higher in Na was found in the leaves of plants in the zeolite treatments vs other treatments. Transfer of Cr from amended tailings to the plants and a Se bioaccumulation in plants in the MBBR biomass treatments were found. Surface runoff did not show metal contamination. The findings showed promising potential valorization of MBBR biomass as amendments to non-acid-generating mine tailings.

Case IV: Biochar and activated biochar made from wood residues from sawmills were also applied for the removal of phenol from synthetic (up to 1500 mg/L) and real effluents (0.54 mg/L) [8]. The sorption capacity of AC for phenol was more than twice compared to biochar (303 vs 159 mg/g). This is probably due to their improved textural properties having micropores and high proportion of oxygenated carbonyl groups connected to their surface. Up to 95% of phenol removal from leachates in a lumber industry site was found to below Québec's discharge criteria (0.05 mg/L). Activated biochar was also efficiently thermally regenerated after 5 cycles adsorption-desorption.

Case V: Physically (CO_2 vs steam) and chemically (KOH) activated biochar was developed from sawmills wood residues by a two-step process: fast pyrolysis using a pilot scale furnace (250 kg/h); activation using an in-house activation furnace [9]. The CO_2-activated biochar was the most efficient material for Cu removal (99%), at concentrations up to 200 mg/L, whereas KOH-activated biochar was the most efficient material for Cu removal at 1 g/L Cu and a real effluent (AMD). The latter was attained to below the authorized monthly mean allowed by Canadian law (0.3 mg/L). Both materials presented improved physicochemical characteristics (high surface area and porosity, oxygenated functional groups connected to the materials' surface). However, the KOH material presented the highest oxygenated functional groups that favored the chemisorption of Cu ions. Moreover, the ion competition in multi-metal acid mine drainage probably lowered metal adsorption capacities of all modified materials.

Case VI: Low-cost materials including biochar (B), Fe-loaded biochar (BF), activated biochar (BC), Fe-loaded activated biochar (BCF and BFC), thermally modified dolomite (MD), wood ash (WA), and modified wood ash (MWA) were evaluated as adsorbents for As removal from synthetic vs real mining effluents, in batch and column tests [7]. The most performing material for As(V) removal was MD followed by WA, BCF, BF, BFC, MWA, BC and B. Biochar-derived materials were not the most performant materials probably because of the low As(V) concentration from synthetic and real effluents (850 vs 300 μg/L). Thus, modified dolomite was the most efficient material for the As(V) removal in batch (99.9%) and column testing (99.6%) after more than 112 days. However, the only parameter that must be adjusted is its final pH that was above the Canadian criteria.

Field scale

Case VII: The East-Sullivan mine extracted Au, As, Cu, and Zn (1949-1966) from a sulfide orebody (50% pyrite and pyrrhotite) and produced 15 Mt of tailings covering 228 ha (2.1-13.5 m) [18, 19]. After decades of site abandonment, AMD had pH 2, and up to 18 g/L Fe and 37 g/L sulfate. The mine site rehabilitation started with an experimental wood waste cover (in 1980s) to prevent sulfides oxidation. Wood residuals (barks, logs, sawdust of coniferous and deciduous species) covered the tailings, overlined by biosolids [18, 19]. A seepage collection system around the covered tailings and the passive treatment in constructed wetlands was implemented in 1990. As passive treatment was inefficient, water recirculation (1998-2005) collected from the covered tailings back through the organic cover, which served both as barrier for AMD prevention and as biofilter, was necessary. This approach was successful, and water in wetlands surrounding the covered tailings was then deemed of satisfactory quality. A recent study using 25-year monitoring data (2000-2025) shows compliance with regulation [19]. A previous study showed no associated risks for the avian fauna from the wetlands [18]. Maintaining high moisture conditions in such a wood-waste cover and the replenishment of old by more recent wood-waste were highlighted as main lessons learned from this case study. New research is needed to confirm whether the maintenance of a high degree of saturation in tailings is enough or the AMD recirculation through the cover is still necessary.

Case VIII: The Wood-Cadillac site, a former Au and Ag mine (1939-1949), extracted from ores with As, generated 3.5×10^5 t of tailings over 21 ha up to a depth of 3 m, and around 10^5t of tailings spreading over 3 km along the Creek Pandora, in Abitibi region of Quebec's Province. The monitoring of As concentrations started in 1995 and showed up to 0.3 mg/L in natural underground and surface water, originating from As-NMD [3, 4]. In 1999, a sand monolayer cover was applied on top of tailings, and a wood-waste based biofilter was constructed for As-NMD passive treatment. The long-term monitoring data

(1999-2022), coupled to newest analysis (isotopic, microbiological, mineralogical) showed the immobilization of As in stable mineral precipitates, with 80% As immobilized by sorption and the 20% left as As sulfides [3, 4].

Case IX: ***Lorraine mine site***. A former Au, Ag, Cu and Ni mine (1964-1968) left behind around 6x10^{5}t of acid generating tailings, disposed in a 15.5 ha pond [15]. In 1998, a rehabilitation program was initiated, consisting of a multi-layer dry cover (CCBE) and four passive treatment units using three dolomite drains to prevent further AMD generation. Reclamation strategy proved effective, but the Fe-rich AMD in the tailings pore water was progressively and slowly leached out over time. Total Fe concentrations decreased from approximately 11 g/L, before the construction of the cover, to around 2.5 g/L in 2015, while the pH increased from < 3 to 5-6 over a 12-year period [15]. The efficiency of one of the three dolomitic drains drastically deteriorated over time due to the built-up of Fe precipitates, which clogged the pore spaces, and limited the flow. In 2011, the replacement of the clogged dolomite drain by a three-unit passive biochemical treatment system (train), consisting of two biofilters separated by a wood ash unit was done. The monitoring of the treatment system performed at sampling points in the first 60 months of operation showed significant improvement of AMD. The loss of efficiency over time was observed, due to porosity clogging by Fe precipitates. A stabler long-term performance would be achieved by using a multi-step system of calcite-/dolomite-DAS (dispersed alkaline substrate, a mixture of coarse material, such as wood chips, and neutralizing agents) and passive biochemical reactors [20].

CONCLUSION

The valorization of natural and residual materials available in the proximity of mine sites for mine water and air treatment and mine site rehabilitation reduces the transportation costs, environmental footprint, and contributes to a circular economy. Case studies were detailed as examples of successful application of these materials, combining prevention measures and passive treatment. New studies are necessary for a better understanding of mechanisms and processes explaining the successes obtained, and to adapt to other potential applications.

ACKNOWLEDGEMENT

This study was funded by the Natural Sciences and Engineering Research Council of Canada (NSERC) and Canada Research Chairs.

REFERENCES

1. Neculita, C.M., Coudert, L., Rosa, E., Mulligan, C. (2020) Future prospects for treating contaminants of emerging concern in water and soils/sediments. In: Advanced Nano-Bio Technologies for Water and Soil Treatment. Filip, J., Cajthaml, T., Najmanová, P., Černík, M., Zbořil, R. (Eds.) Springer, pp. 589-605.
2. Keshvardoostchokami, M., Braghiroli, F.L., Neculita, C.M., Koubaa, A. (2023) Potential of wood-based residual materials for environmental applications. Current Forestry Reports, 1-17.

3. Thevenot, X., Neculita, C.M., Coudert, L., Rosa, E. (2024) Passive treatment of As-rich neutral mine drainage using natural organic and residual inorganic materials in cold climate. ICARD, Halifax, Canada, September 16-20.
4. Mehdaoui, H.Y., Neculita, C.M., Pabst, T., Benzaazoua, M. (2024) Environmental assessment of contaminated residues from a 20-year field biofilter for passive treatment of CND-As. ICARD, Halifax, Canada, September 16-20.
5. Ait-Khouia, Y., Benzaazoua, M., Demers, I. (2021) Environmental desulfurization of mine wastes using various mineral processing techniques: Recent advances and opportunities. Minerals Engineering, 174, 107225.
6. Braghiroli, F.L., Bouafif, H., Koubaa, A. (2019) Enhanced SO_2 adsorption and desorption on chemically and physically activated biochar made from wood residues. Industrial Crops & Products, 138, 111456.
7. Braghiroli, F.L., Calugaru, I.L., Gonzalez-Merchan, C., Neculita, C.M., Bouafif, H., Koubaa, A. (2020) Efficiency of eight modified materials for As(V) removal from synthetic and real mine effluents. Minerals Engineering, 151, 106310.
8. Braghiroli, F.L., Bouafif, H., Hamza, N., Neculita, C.M., Koubaa, A. (2018) Production, characterization, and potential of activated biochar as adsorbent for phenolic compounds from leachates in a lumber industry site. Environmental Science & Pollution Research, 25(26), 26562–26575.
9. Braghiroli, F.L., Bouafif, H., Neculita, C.M., Koubaa, A. (2019) Performance of physically and chemically activated biochars in copper removal from contaminated mine effluents. Water, Air & Soil Pollution, 230(8), 178.
10. Hwang, T.W., Neculita, C.M., Han, J.I. (2012) Biosulfides precipitation in weathered tailings amended with food waste-based compost and zeolite. Journal of Environmental Quality, 41(6), 1857-1864.
11. Calugaru, I.L., Neculita, C.M., Genty, T., Bussière, B., Potvin, R. (2017) Removal of Ni and Zn in contaminated neutral drainage by raw and modified wood ash. Journal of Environmental Science & Health, 52(2), 117-126.
12. Rakotonimaro, T.V., Neculita, C.M., Bussière, B., Benzaazoua, M., Zagury, G.J. (2017) Recovery and reuse of sludge from active and passive treatment of mine drainage-impacted waters. Environmental Science & Pollution Research, 24, 73-91.
13. Robert, E., Braghiroli, F.L. (2022) Development of a biochar-based substrate added with nitrogen from a mining effluent for the production of *Picea mariana* seedlings. Clean Technologies, 4(3), 770–784.
14. Saint-Aimé, R., Guittonny, M., Neculita, C.M. (2023) Valorization potential of ammonium-rich zeolite and MBBR biosolids in the revegetation of non-acid-generating gold mine tailings. Science of the Total Environment, 891, 164279.
15. Genty, T., Bussière, B., Dionne, J., Neculita, C.M. (2016) Passive biochemical treatment of ferriferous mine drainage: Lorraine mine site, Northern Quebec, Canada. IMWA, Leipzig, Germany, July 11-15.
16. Demers, I., Pabst, T. (2021) Alternative and innovative integrated mine waste management approaches. In: Hard rock mine reclamation. Bussière, B., Guittonny, M. (Eds), CRC Press, pp 321-349.
17. Hachicha, H., Dia, M., Bouafif, H., Koubaa, A., Khlif, M., Braghiroli, F.L. (2023) Naturally nitrogen-doped biochar made from end-of-life wood panels for SO_2 gas depollution. Journal of Renewable Materials, 11(11), 3807–3829.
18. QME (Quebec's Ministry of Environment) (2014) Assessment of ecotoxicological risks for benthivorous and piscivorous fauna at the East-Sullivan mine site. QME, 73p.

19. Malki, A. (2025) Assessment of the influence of climate variability on the treatment and management of mine water at East-Sullivan mine site. MSc thesis, UQAT, 140p.
20. Rakotonimaro, T.V., Neculita, C.M., Bussière, B., Genty, T., Zagury, G.J. (2018b) Performance assessment of laboratory and field-scale multi-step passive treatment of iron-rich acid mine drainage for design improvement. Environ. Science & Pollution Research, 25, 17575-17589.

XVI International Mineral Processing
and Recycling Conference
28-30 May 2025, Belgrade, Serbia

DOI: 10.5937/IMPRC25483T

Original research article

CHEMICAL STABILITY AND FERTILIZER EFFICIENCY OF BIOGLASS AND BIOCHAR ON ROSE PLANTINGS

Vladimir Topalović[1], 0000-0002-4177-4649,
Ana Vujošević[2], 0000-0002-2780-1794,
Anja Antanasković[1], 0000-0003-4088-8748,
Veljko Savić[1], 0000-0002-8602-8260,
Marija Djošić[1], 0000-0002-0869-2182,
Zorica Lopičić[1], 0000-0002-7251-8699,
Jelena Nikolić[1#], 0000-0002-9624-8865,
[1]Institute for Technology of Nuclear and other Mineral Raw Materials, Franchet d`Esperey 86, 11000 Belgrade, SERBIA
[2]University of Belgrade, Faculty of Agriculture, Nemanjina 6, 11080 Zemun, Serbia

ABSTRACT – Declines in soil quality and low efficiencies of applied fertilizers has limited agricultural productivity worldwide, inducing necessity for sustainable orientated soil amendments. Glass-matrix-based fertilizers are promising "green technologies" thanks to the controlled release of nutrients due to their engineered chemical durability in a wide solubility range. Beside mentioned inorganic soil support, biochar was found to be an effective organic soil amendment that enhances nutrient/water retention as well as microbial activity, making it a promising tool for sustainable agriculture. In this paper, we have tested two possible "green soil amendments": polyphosphate glass (PG) and plum stone biochar (PS) in a 2% citric acid solution, as well as their use as fertilizers on two-year-old rose plantings. The results have shown quick dissolution of PG: nearly 90% for 48 h at 20 ˚C that steady increase up to 97% at the 480 h; under the same operating parameters, 7.6% of PS was dissolved increasing to 8% at final investigated time. Higher temperatures resulted in higher dissolution rate. The data obtained within the scope of this study indicates that tested fertilizers have a positive effect on rose plant growth, not only promoting bud formation but also extending the flowering period of roses.

Keywords: Polyphosphate Glass, Biochar, Durability, Fertilizers, *Lavaglut*.

INTRODUCTION

Plant growth and quality are closely linked to mineral nutrition, which depends on both water and nutrients availability. However, conventional fertilization can pose environmental risks, such as soil nutrient leaching. To minimize these risks, it is crucial to use fertilizers that optimize nutrient uptake while reducing excessive input and environmental impact [1]. Reusing waste materials or industrial by-products as fertilizers can also help address their disposal issues. An ideal fertilizer should release nutrients

---

[#] corresponding author: j.nikolic@itnms.ac.rs according to plant demand and its phenological stage. Plants regulate nutrient absorption by interacting with their surrounding environment, particularly at the root interface, where they release various organic compounds. These interactions create a dynamic nutrient exchange within the rhizosphere, allowing plants to respond to their environment efficiently [2].

Glass-matrix-based fertilizer has a unique ability to release nutrients only when plants need them. Nutrients contained in its structure become available only in the presence of complexing solutions, which ensures a slow and controlled nutrient release over time, preventing excessive leaching and improving efficiency. Phosphate glasses are particularly interesting due to their low chemical durability, which allows controlled nutrient release. While pure phosphate glasses are highly hygroscopic, their durability can be adjusted from hours to years by modifying their composition. Factors such as the size, charge, and field strength of the modifier cation within the glass matrix also influence their resistance to chemical reactions. Since glass-matrix-based fertilizers do not rely on water solubility for nutrient release, their effectiveness can be assessed using acidic extractants, such as citric acid solution. Citric acid, a common root exudate, helps simulate the plant's natural nutrient uptake process [3-5].

Biochar, a carbon-rich material produced from the thermal decomposition of organic matter in a low-oxygen environment (pyrolysis), has gained attention as a sustainable soil amendment. It offers several benefits to soil health, crop growth, and environmental sustainability. Biochar improves soil structure, increasing aeration, water retention, and nutrient-holding capacity. Sing et al [6] have extracted and statistically analyzed global literature data on biochar influence on different physical, chemical, microbial properties of the soil applied, and crop productivity. It was concluded that application of biochar increased soil pH, cation exchange capacity, and organic carbon by 46%, 20%, and 27%, respectively.

Also, they have confirmed that biochar application reduces bulk densities by 29% and increases soil porosity by 59%. This increase was higher for pyrolytic temperatures higher than 500 °C, while the lower pyrolytic temperatures (< 500 °C) had a greater effect on microbial diversity.

While biochar provides long-term benefits, initial production or purchase costs can be high. However, the application of agricultural waste as a feedstock for biochar production can reduce mentioned expenses. By integrating biochar into farming practices, we can move toward more resilient and sustainable food production systems [7,8].

This study examines the chemical stability of phosphate glass and biochar in a 2% citric acid solution at 20 °C and 50 °C as well as their impact on the bud development of the *Lavaglut* rose variety.

EXPERIMENTAL

In order to obtain phosphate glass (PG), a glass mixture was prepared from the following raw materials: $(NH_4)_2HPO_4$, K_2CO_3, $CaCO_3$, SiO_2, MgO, ZnO and MnO_2. After drying, raw materials were mixed in a mortar, resulting in a homogeneous glass mixture. The glass mixture was heated in a Nabertherm G100/9 electric furnace at 1230 °C for 1

h. The melted glass mixture was poured onto a steel plate and cooled in air. PG was ground in an agate mortar and stored in a desiccator.

Plum stones were obtained from the local fruit processing company from Serbia, where they were considered as a waste. The stones were washed by tap water, dried at room temperature, ground using a Siebtechnik – TS250 vibrating disk mill (Siebtechnik GmbH, Germany), and then sieved to fraction between 0.1 to 0.5 mm. After grinding, the plum stones were pyrolyzed at heating rate of 10 °C/min from room temperature up to 500 °C, when they were kept for 90 min, in a Nabertherm 1300 muffle furnace (Nabertherm, Germany).

The chemical stability of PG and PS in a 2% citric acid solution was tested at a temperature of 20 °C. One gram of each material (PG-granulation 0.1-0.3 mm or PS-granulation 0.1-0.5 mm) was placed in plastic containers, followed by the addition of 50 ml of citric acid solution. The containers were then placed in a thermal bath, preheated desired temperature.

After a specified experimental period under isothermal conditions, the containers were removed, and the solid and liquid phases were separated by filtration. The obtained solutions were analyzed for the content of present ions, and after drying the solid phase, the dissolved mass of PG or PS was determined.

The chemical composition of PG and PS and the solutions after dissolution in 2% solution of citric acid were analyzed using gravimetric and spectroscopic methods, including AAS with a PERKIN ELMER AAnalyst 300 instrument and UV/VIS spectroscopy with a Specol Analytik JENA 1300 spectrophotometer.

The *Lavaglut* variety was produced in a two-year cycle through grafting in July 2022. The effect of applying phosphate glass and biochar was monitored on *Lavaglut* rose variety with addition of PG and PS as eco-fertilizers starting in February 15, 2023. The agrochemical analysis of the soil showed that it had a neutral to slightly acidic reaction.

The soil was characterized by an available nitrogen content of 32.9 mg/kg, a low available phosphorus content, and was well-supplied with potassium (22.4 mg/kg). This type of soil is suitable for the production of rose seedlings [9]. The effect of PG on roses was tested at three different doses (1, 2 and 3 g/rose plant), while the effect of PS was examined at two doses (5 and 10 g/rose plant).

Throughout the vegetative cycle, various growth and development parameters of the roses were monitored. The data were analyzed using one-way analysis of variance (ANOVA) with R software, version 3.6.0. Statistical significance between individual treatments was tested using the Tukey HSD test, at a significance level of 0.05. Throughout the research period, six treatments were applied for disease and pest control.

RESULTS AND DISCUSSION

The chemical compositions of PG and PS created and used in described experiments are presented in Table 1. These analysis relate to the main mineral components present in the samples structure since the most of the biochar structure relates to the carbon element (more than 70%), and approximately 2% of dry mass of PS represents mineral ash content.

This material also contains app. 1.62% of nitrogen, which is also beneficial for the plant growth [10]. Beside the oxides mentioned in Table 1, sample PS contains 0.021% of Fe_2O_3, which was not present in the sample PG.

Table 1 Chemical composition of phosphate glass and biochar

[mol%]	P_2O_5	SiO_2	K_2O	MgO	CaO	ZnO	MnO
PG	45.4	3.1	25.6	9.3	14.5	1.2	0.9
PS	0.406	0.105	0.795	0.356	0.350	0.008	0.009

Figure 1 (a) shows the dissolved masses of PG and PS in a 2% citric acid solution at 20 °C for different experimental times. Over a 24-hour period, approximately 8% of the biochar dissolves, whereas around 90% of the glass dissolves within the same timeframe. The result of PS solubility is related to the total organic carbon (TOC) release as well as leaching of the mineral components. After 48 h, 97% of PG and 7.6% of PS were dissolved in the citric acid solution at 20 °C. At extended dissolution times (at 20 °C) the dissolved mass of PS remains constant at approximately 8%, thanks to the stable, mostly aromatic, matrix of biochar that cannot be further dissolved. In contrast, PG continues to dissolve as the dissolution time increases. After 480 h, around 98% of the initial glass mass was dissolved. The higher temperature (50 °C) induced higher dissolution of the samples; for example, for the same period of time (48 h), dissolved mass of glass was 98% [11] for PG and 8.7% for PS (data not shown).

Figure 1 (b) illustrates the ion concentrations in the solutions following the dissolution of PG in a 2% citric acid solution. The results of PS dissolution (data not shown) indicates highest dissolution of potassium (starting from 81 to 112 mg/l, after 24 h and 480 h, respectively. The results also reveal that the element concentrations in the PG solution are approximately 200 times higher than those in the PS solution, which was expectable because the much lower mineral content of the PS compared to PG.

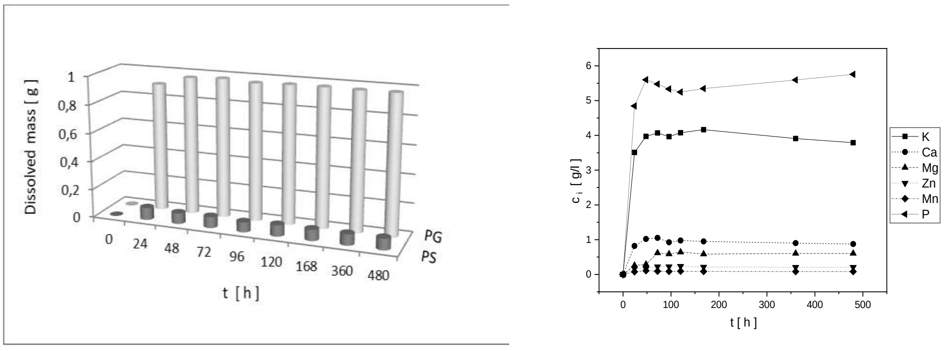

a) b)

Figure 1 Dissolved mass of PG and PS in 2% citric acid solution at 20 °C (a) and Concentrations of elements in solutions after dissolving PG in 2% citric acid solution (b)

The bud count of rose seedlings was conducted three times, spanning from May to the mid-September. In the first count (the appearance of rose buds during the first counting is shown in Figure 2(a)), conducted after 3 months from fertilizer application, the average number of buds ranged from 39 (5 g PS) to 74 (control). The application of PG and a higher tested dose of PS (10 g) had a statistically significant effect on the formation of a greater average number of flower buds compared to the application of 5 g of PS. The average number of formed buds ranged from 44 to 46 with the application of PG, while with PS it reached 51. The highest effect on the average bud count (51 buds) was observed with 10 g of PS, which was statistically significantly higher than in other tested variants but still lower than the control variant (74 buds). This can be attributed to the fact that formed plants first absorb nutrients from the soil before utilizing the fertilizer. In the second count, conducted 5 months after the fertilizer application, a positive effect was observed with the application of 2 g of PG and 5 g of PS. This resulted in statistically significantly higher bud count than in the control, as well as in variants with the lowest and highest tested doses of PG (variants 1 g and 3 g) and variant 10 g of the PS. In the third count (7 months after fertilization), the control variant's average bud count did not differ statistically significantly from variants 3 g PG and 5 g PS. However, it was statistically significantly lower than in variants 1 g PG, 2 g PG, and 10 g PS, indicating a positive effect of 1 g and 2 g of PG and 10 g of PS on bud formation. No statistically significant differences were observed in the average bud count among variants 1 g PG, 2 g PG, and 10 g PS. Furthermore, during the second and third counts, most tested fertilizer doses resulted in a higher bud count compared to the control samples. These findings suggest that phosphate glass and biochar not only promote bud formation but also extend the flowering period of roses. The average number of buds for all three counts is shown in the Figure 2(b).

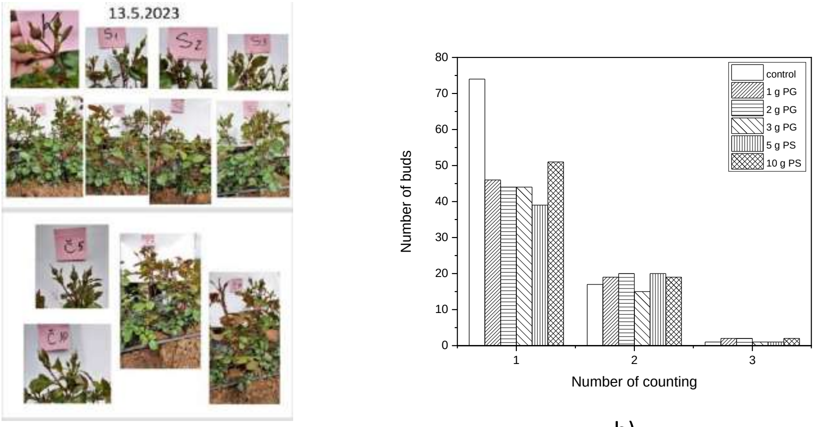

a) b)

Figure 2 The appearance of rose buds (S-polyphosphate glass; Č- plum stone biochar) (a); Average number of buds (b).

CONCLUSION

This study presents the results of the chemical stability of phosphate glass and biochar in a 2% citric acid solution, along with their effects as fertilizers on the growth and development of *Lavaglut* roses. Over the longest experimental period, approximately 98% of the glass dissolved in acid solution, while around 8% of the biochar dissolved in the same timeframe. The ion concentrations in the solutions were about 200 times higher in the glass solution compared to the biochar solution. The average number of buds and flowers varied depending on the counting time. The most significant increase in the number of buds and flowers occurred in July (five months after fertilization) when the plants were in full bloom, where the effects of phosphate glass and biochar application reached their peak, with doses of phosphate glass of 3 g per rose plant and biochar of 10 g per rose plant, respectively. These results also confirmed that aside from positive effects on the increase of average number of flowers, there is no toxicity of these fertilizers on the investigated plant growth. The rise in the average number of buds formed during the rose growing season helps sustain flower yield throughout the entire season. Further experiments should include examination of synergistic effect of both fertilizers in the same trial.

ACKNOWLEDGEMENT

This research is supported by The Ministry of Science, Technological Development and Innovation, Republic of Serbia, (Contracts No. 451-03-136/2025-03/200023 and 451-03-137/2025–03/200116).

REFERENCES

1. Mikula, K., Izydorczyk, G., Skrzypczak, D., Mironiuka, M., Moustakas, K., Witek-Krowiak, A., Chojnacka, K. (2020) Controlled release micronutrient fertilizers for precision agriculture– A review. Science of the Total Environment, 712, 136365.
2. Srinivasarao, C., Gopinath, K. A., Venkatesh, G., Dubey, A. K., Wakudkar, H, Purakayastha, T. J., Pathak, H., Jha, P., Lakaria, B. L., Rajkhowa, D. J. Mandal, S., Jeyaraman, S., Venkateswarlu, B., Sikka, A. K. (2013). Use of biochar for soil health enhancement and greenhouse gas mitigation in India: potential and constraints. NICRA Bulletin, 1, 1–51.
3. Ouis, M. A., Abd-Eladl, M., Abou-Baker, N. H. (2018) Evaluation of Agriglass as an Environment Friendly Slow Release Fertilizer. Silicon, 10, 293-299.
4. Torrisi, B., Trinchera, A., Rea, E., Allegra, M., Roccuzzo, G., Intrigliolo, F. (2013) Effects of organo-mineral glass-matrix based fertilizers on citrus Fe chlorosis. European Journal of Agronomy, 44, 32-37.
5. Abou-Baker, N. H., Ouis, M.,· Abd-Eladl, M. (2018) Appraisal of Agriglass in Promoting Maize Production Under Abiotic Stress Conditions. Silicon, 10, 1841-1849.
6. Singh, H., Northup, B.K., Rice, C.W., Vara Prasad, P. V. (2022) Biochar applications influence soil physical and chemical properties, microbial diversity, and crop productivity: a meta-analysis. Biochar 4, article number 8.
7. Nsamba, H. K., Hale, S. E., Cornelissen, G. & Bachmann, R. T. (2015) Sustainable technologies for small-scale biochar production - a review. Journal of Sustainable Bioenergy Systems, 5, 10–31.

8. Mwampamba, T. H., Owen, M. & Pigaht, M. (2013) Opportunities, challenges and way forward for the charcoal briquette industry in Sub-Saharan Africa. Energy for Sustainable Development, 17(2), 158–170.
9. Vujošević, A (2019) Cvećarstvo-Rezano cveće, 1st Edition, Univerzitet u Beogradu, Poljoprivredni fakultet ,184: 193-231.
10. Lopičić, Z., Šoštarić, T., Milojković, J., Antanasković, A., Milić, J., Spasić, S., Avdalović, J. (2024) Efficient removal of water soluble fraction of diesel oil by biochar sorption supported by microbiological degradation. Processes, 12, 964.
11. Nikolić, J., Topalović, V., Savić, V., Matijašević, S., Djošić, M., Zildžović, S., Grujić, S. (2021) The effect of composition on chemical durability of phosphate glass fertilizers. In 8th International Conference Mining and environmental protection. Sokobanja, Srbija, Proceedings, 175-182.

XVI International Mineral Processing
and Recycling Conference
28-30 May 2025, Belgrade, Serbia

DOI: 10.5937/IMPRC25490T Original research article

THE EFFECT OF FLUXING AGENT CATIONS IN FLY ASH-BASED GLASS ON CHEMICAL STABILITY

Vladimir Topalović[1], 0000-0002-4177-4649,
Veljko Savić[1], 0000-0002-8602-8260,
Marija Djošić[1], 0000-0002-0869-2182,
Danijela Smiljanić[1], 0000-0003-3560-1415,
Snežana Zildžović[1], 0000-0002-0214-8119,
Snežana Grujić[2], 0000-0002-9123-6830,
Jelena Nikolić[1#], 0000-0002-9624-8865,
[1]Institute for Technology of Nuclear and Other Mineral Raw Materials-Belgrade, Belgrade, SERBIA
[2]University of Belgrade, Faculty of Technology and Metallurgy, Belgrade, SERBIA

ABSTRACT – Recycling plays a key role in making the economy more efficient in terms of raw material usage. Coal fly ash (CFA), a by-product of coal combustion in thermal power plants, shares a chemical composition similar to some silicate glasses, making it a viable raw material for glass production. The paper presents the results of Na^+ and Ca^{2+} ion incorporation into coal fly ash-based glass and its impact on chemical stability. The chemical resistance of the glasses was tested in distilled water, 0.01 mol/dm^3 HCl, and 0.01 mol/dm^3 NaOH. The concentrations of the elements in the solution indicate that the ion exchange process is the dominant dissolution mechanism for both glasses. Na-fly ash glass shows slightly lower stability in all solvents than Ca-fly ash glass. FTIR spectra show no change in the structure of the glasses after contact with solvents. The chemical stability of both glasses is satisfactory with a mass change of less than 1 %.

Keywords: Coal Fly Ash, Chemical Durability, Glass.

INTRODUCTION

Sustainable development is essential to modern innovation, aiming to balance economic growth with environmental protection. This research aligns with these goals by converting waste materials into valuable products, addressing key issues like resource depletion, waste management, and reducing industrial waste in landfills. By producing glassy materials from secondary raw materials, it supports circular economy principles, transforming industrial by-products into high-performance, eco-friendly materials. Recycling, a crucial part of the circular economy, involves reprocessing used materials at the end of a product's life cycle and returning them to the supply chain. Over time, the focus of recycling has shifted from waste management to optimizing the use of mineral resources. Different countries have variations in the "waste management hierarchy". For

---

[#] corresponding author: j.nikolic@itnms.ac.rs example, one of the most well-known concepts is "3R", which stands for reduce, reuse, and recycle. The portion of materials that can re-enter the production cycle depends on both the material itself and the product it is intended to be a part of. Therefore, the quality and purity of recycled material determine its future application [1]. Coal fly ash (CFA), a by-product of coal combustion in thermal power plants, shares a chemical composition similar to some silicate glasses, making it a viable raw material for glass production. By utilizing CFA, this research offers a dual benefit: reducing the volume of fly ash disposed of in landfills and creating innovative, sustainable materials. The global reliance on coal for electricity generation has resulted in the large-scale production of fly ash, raising significant environmental concerns. Currently, over 65 % of fly ash produced by coal power plants is deposited in landfills and ash ponds worldwide. While the European Union has set ambitious goals to phase out coal use by 2030 and transition to renewable energy sources, many countries, particularly in the Western Balkans, will continue operating coal-fired thermal power stations beyond this deadline due to growing energy demands. In Serbia alone, thermal power plants consume approximately 40 million tons of lignite annually, producing around 6 million tons of fly ash. Even after these coal-fired plants are decommissioned, a substantial quantity of fly ash will remain an environmental challenge, with limited options for reuse and disposal. In this context, the inclusion of CFA in glass production offers an innovative pathway for its valorization. Repurposing CFA as a secondary raw material aligns with sustainable development goals, addressing waste management issues while contributing to the production of high-performance, eco-friendly materials. This approach highlights the potential of circular economy principles to mitigate the environmental impact of coal combustion residues while supporting the development of advanced material technologies [2,3]. Fly ash, mainly consists of reactive silicon dioxide (SiO_2) and aluminum oxide (Al_2O_3). According to the American Society for Testing and Materials (ASTM) standard ASTM C618 [4], fly ash can be classified into two categories: Class F-The composition of its main components can be defined as follows: mass % SiO_2 + mass % Al_2O_3 + mass % Fe_2O_3 ≥ 70 %, and Class C-The composition of its main constituents can be defined as follows: mass % SiO_2 + mass % Al_2O_3 + mass % Fe_2O_3 ≤ 70 %, typically between 50-70 %. Class F fly ash has a calcium oxide content of less than 7 % and possesses pozzolanic properties. This type of ash does not have cementitious characteristics, so additives are required to form cementitious compounds. Also, because there is a low amount of modifying oxides (Na_2O, K_2O, MgO, CaO, etc.) additives are required in order to lower melting temperature and viscosity for successful glass production. Class C fly ash, also known as calcium fly ash (usually containing more than 10 % calcium oxide), hardens upon contact with water and exhibits cementitious properties [2,5,6]. Fly ash produced by coal combustion in thermal power plants can be used as a secondary raw material for the production of glass and glass-ceramics due to its chemical composition (high content of SiO_2, Al_2O_3, and CaO). Modifying the composition of the glass mixture with various additives is often necessary to reduce the melt viscosity, lower the melting temperature, and improve the workability of the obtained material. In addition to mechanical properties, the chemical stability of the resulting glasses and glass-ceramics is crucial for its application.

Based on the composition of coal fly ash, vitrification is a viable process for producing useful glass materials. This research focuses on evaluating the vitrification potential of Serbian coal fly ash. Given that the resulting materials could have technical applications, such as floor tiles, machine components, or tool pieces in the chemical industry, their chemical durability, mechanical properties, and thermal behavior must be assessed. This study optimizes a glass formulation and examines its chemical durability. Notably, the glass produced from the mixture containing 75 % coal fly ash and 25 % CaO is classified as a waste-derived material, as the CaO originates from sugar beet factory lime.

EXPERIMENTAL

The glasses were produced using a conventional method, involving the melting of glass batches in an Elektron VTP-08 electric furnace (Banja Koviljača). Glass batch N25 consisted of 75 wt% coal fly ash sourced from the "Nikola Tesla" thermal power plant (Obrenovac, Serbia) and 25 wt% Na_2O derived from Na_2CO_3 (Centrohem d.o.o., Serbia). Similarly, glass batch S25 contained 75 wt% coal fly ash and 25 wt% CaO obtained from sugar beet factory lime ("Crvenka" sugar factory-Crvenka, Serbia). The melting process took place in a zircon-silicate crucible at 1500 °C for 1 h. The chemical composition of coal fly ash and the glasses was analyzed using gravimetric and spectroscopic techniques, specifically atomic absorption spectroscopy (AAS) with a PERKIN ELMER 703 instrument and UV/VIS spectroscopy with a PHILIPS 8610 spectrophotometer.

The chemical durability of the glasses was evaluated in three different solutions: distilled water, 0.01 mol/dm³ HCl, and 0.01 mol/dm³ NaOH. The glass samples were first crushed using an agate mortar to achieve a particle size of 0.3-0.5 mm. A 2 g portion of the resulting glass powder was combined with 70 ml of either distilled water, 0.01 mol/dm³ HCl, or 0.01 mol/dm³ NaOH in sealed plastic containers. These containers were then placed in a water bath equipped with a shaker, where they were heated to 95 °C and continuously stirred at a rate of 60 rpm for 2 h. Upon completion of the process, the containers were removed from the water bath, and the solution above the glass was filtered. The composition of the filtrate was analyzed using atomic absorption spectroscopy. Additionally, the structural characteristics of the glasses, both before and after dissolution, were investigated using the FTIR-ATR technique with a Nicolet iS50 spectrometer (Thermo Fisher Scientific, Waltham, United States), covering a spectral range of 4000–400 cm^{-1}.

RESULTS AND DISCUSSION

The chemical composition of coal fly ash is presented in Table 1. Based on this composition, the coal fly ash is classified as Class F according to ASTM standards.

Table 1 Chemical composition of coal fly ash

Oxide	SiO_2	Al_2O_3	Fe_2O_3	CaO	MgO	Na_2O	K_2O	MnO	SO_3	LOI
wt%	52.56	26.33	6.81	5.96	2.21	0.24	1.14	0.08	1.02	3.46

X-ray analysis confirmed that the obtained materials were amorphous (data not shown). Both glasses were black in color and free of visible bubbles. The chemical composition of both glasses is given in Table 2.

The chemical durability of glass typically refers to its water resistance. The interaction between glass and water is primarily governed by three main processes: hydration–where intact water molecules penetrate the glass as a solvent, this process weakens the glass network and allows the leaching of soluble components; ion exchange (leaching): alkali ions (e.g., Na^+, K^+) are replaced by H^+ or H_3O^+ from the surrounding environment, and hydrolysis of silicate bonds-water molecules break the Si—O—Si bonds in the glass, leading to the formation of silanol groups (Si—OH).

Table 2 Chemical composition of the coal fly ash-based glasses

Oxide Glass	SiO_2	Al_2O_3	Fe_2O_3	CaO	MgO	Na_2O	K_2O	TiO_2
N25	46.17	18.14	5.04	5.95	1.41	20.59	1.02	0.68
S25	51.78	14.84	3.03	26.08	2.71	0.17	0.66	0.67

The processes of ion exchange and hydrolysis are not independent, and one or the other may dominate the reaction at different stages. Generally, the mechanisms of glass corrosion involve the diffusion of water (into the glass matrix, followed by ion exchange between hydrogen ions and the most mobile network-modifying ions, such as Na^+). Additionally, network hydrolysis reactions break down the glass structure, ultimately leading to glass dissolution. This ion exchange increases the pH of the solution and facilitates further glass degradation. Acidic conditions (low pH value) accelerate ion exchange, while highly alkaline conditions (high pH value) enhance silica hydrolysis. Silicate glass dissolution in basic (alkaline) solutions differs significantly from its behavior in neutral or acidic environments. A higher content of alkali (e.g., Na_2O) and alkaline earth metals (e.g., CaO) in the glass matrix increases its susceptibility to leaching by enhancing ion exchange and network destabilization. The presence of hydroxide ions in high-value pH solutions accelerates the breakdown of the silicate network, leading to faster dissolution rates. This process is particularly important in fields such as nuclear waste containment, geochemistry, and industrial glass applications. In a basic environment, hydroxide ions attack the Si—O—Si bonds in the glass structure. This results in the formation of silanol groups (Si—OH), which destabilize the glass network. The silanol groups further break down into soluble silica species like monosilicic acid ($Si(OH)_4$), which dissolves into solution [7,8].

The results indicate that glass N25 exhibits slightly lower stability in all three solvents compared to glass S25 (Figure 1). Glass N25 exhibits the highest mass change in NaOH solution, indicating the lowest resistance to its corrosive effects. In contrast, the mass change of the glass sample in distilled water and HCl solution is significantly smaller, suggesting that N25 glass demonstrates greater stability in these environments. The most significant mass change in the S25 glass sample occurs when exposed to NaOH solution. In contrast, the mass change during the water resistance test is minimal, while exposure to HCl solution results in a slightly greater mass change. Na^+ and Ca^{2+} ions function as network modifiers, disrupting Si—O—Si bonds and generating non-bridging oxygens, which results in a more depolymerized and flexible network. However, due to its higher charge, Ca^{2+} ions can partially offset the loss of bridging oxygens by serving as a charge-balancing ion, contributing to a more rigid structure. As a result, S25 glass exhibits slightly better chemical resistance in all three solvents compared to N25 glass.

The concentrations of Si and Al (network formers) are higher in NaOH solutions than in distilled water and HCl, confirming that a direct OH^- attack on the silicate network occurs in basic environments for both glasses (Figure 2).

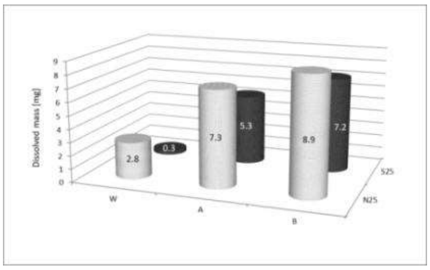

Figure 1 Dissolved mass of glasses N25 and S25 in distilled water (W), 0.01 mol/dm³ HCl (A), and 0.01 mol/dm³ NaOH (B).

In acidic and neutral environments, N25 glass exhibits higher concentrations of Na^+ ions compared to other ions present. In the network of silicate glasses, Na^+ ions are most easily leached from the glass, by ion exchange (Figure 2a). The results indicate that the Ca^{2+} ion concentrations in glass S25 follow the same trend (Figure 2b).

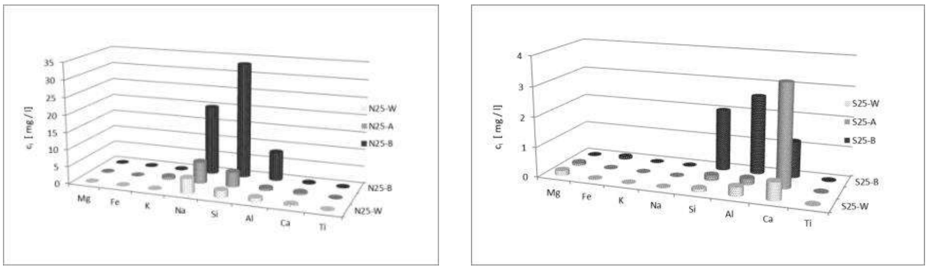

a) b)

Figure 2 Concentration of ions after dissolution: a) N25 and b) S25 glass.

The concentrations of Na^+ ions in the solutions after dissolution are higher than those of Ca^{2+} ions in the same environments. This is because Ca^{2+} ions have lower ionic mobility and form stronger bonds within the glass network compared to Na^+ ions. As a result, glasses with higher Ca^{2+} ion content exhibit better chemical stability.

In Figure 3, three distinct regions can be observed: one around 430 cm^{-1} (Na^+ sheared the Si—O bond in the Si—O—Si linkage then formed a Si—O—Na^+ linkage), characteristic of Si—O—Si bond bending vibrations; another near 710 cm^{-1}, corresponding to Al—O bond vibrations in the [AlO_4] tetrahedron; and a third at approximately 980 cm^{-1}, representing the asymmetric stretching vibrations of Si^{4+} or Al^{3+} ions within the tetrahedral structure. The region between 800 and 1200 cm^{-1} is particularly relevant for analyzing the glass structure [9]. The FTIR spectra of glasses N25 and S25 remain unchanged after the chemical stability test. This indicates that even under the influence of NaOH solution, where the greatest mass change and the highest concentration of network formers in the solution are observed, the glass network remains largely intact, with no significant structural damage detectable in the FTIR spectrum.

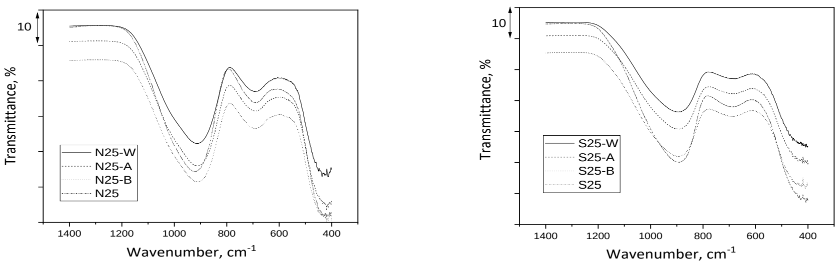

a) b)

Figure 3 FTIR spectra of parent glass and glass after immersion in distilled water, HCl solution, and NaOH solution: a) N25 and b) S25.

CONCLUSION

This study examines the chemical stability of two silicate glasses synthesized from coal fly ash, with the addition of Na_2O and CaO, the latter sourced from sugar beet factory lime. Glass S25 exhibits slightly better chemical stability than glass N25 across all three environments. In neutral and acidic environments, ion exchange is the dominant dissolution mechanism, whereas, in a basic environment, hydrolysis of the silicate network prevails. Both glasses demonstrate good chemical stability in all tested environments, with a dissolved mass of less than 1 %. FTIR analysis confirms that no structural changes occur in the glasses during dissolution.

ACKNOWLEDGEMENT

This research is supported by The Ministry of Science, Technological Development and Innovation, Republic of Serbia (Contracts No. 451-03-136/2025-03/200023 and 451-03-136/2025-03/200135).

REFERENCES

1. Worrell, E., Reuter, M. A. (2014) Handbook of Recycling: State-of-the-art for Practitioners, Analysts, and Scientists, Elsevier, Waltham, MA.
2. Kar, K. K. (2021) Handbook of Fly Ash, 1st Edition, Elsevier.
3. Savić, V., Dojčinović, M., Topalović, V., Cvijović-Alagić, I., Stojanović, J., Matijašević, S., Grujić, S. (2024) The effect of sintering temperature on cavitation erosion in glass-ceramics based on coal fly ash. International Journal of Environmental Science and Technology, 21, 6065-6074.
4. ASTM Standard, (2013) Standard Specification for Coal Fly Ash and Raw or Calcined Natural

Pozzolan for Use, ASTM international.

5. Robl, T., Oberlink, A., Jones, R. (2017) Coal Combustion Products (CCPs): Characteristics, Utilization and Beneficiation, Woodhead Publishing, 1st Edition.
6. Ahmaruzzaman, M. (2010) A review on the utilization of fly ash. Progress in Energy and Combustion Science, 36, 327-363.
7. Bunker, B. C. (1994) Molecular mechanisms for corrosion of silica and silicate glasses. Journal of Non-Crystalline Solids, 179, 300-308.
8. Sheng, J., Huang, B. X., Zhang J., Zhang, H., Sheng, J., Yu, S., Zhang, M. (2003) Production of glass from coal fly ash. Fuel, 82, 181-185.
9. Zou, C., Cao, J., Zhao, M., Wang, Z., Lu, J. (2019) Combined sodium and fluorine promote diopside continuous growth to achieve one-step crystallization in CaO-Al_2O_3-SiO_2-Fe_2O_3 glass-ceramics. Journal of the European Ceramic Society, 39, 4979-4987.

XVI International Mineral Processing
and Recycling Conference
28-30 May 2025, Belgrade, Serbia

DOI: 10.5937/IMPRC25497C Original research article

INFLUENCE OF ORGANIC COMPOUND STRUCTURE ON BRASS CORROSION INHIBITION EFFICIENCY

Aleksandar Cvetković[#], 0009-0003-5184-6874,
Marija Petrović Mihajlović, 0000-0001-5486-3870,
Žaklina Tasić, 0000-0001-6544-1980,
Milan Radovanović, 0000-0002-5175-6022,
Ana Simonović, 0000-0003-2392-0048,
Vladan Nedelkovski, 0000-0001-7724-1118,
University of Belgrade, Technical Faculty in Bor, Bor, Serbia

ABSTRACT – In this study the influence of organic compounds with different structures on the inhibition of brass corrosion in sodium chloride solutions of 0.9%, 2% and 3.5% is investigated. The experimental work includes the evaluation of the inhibition efficiency of 2-mercapto-1-methylimidazole (MMI), 2-amino-5-ethyl-1,3,4-thiadiazole (AETDA) and N-acetyl-L-leucine at various concentrations using electrochemical methods, including open circuit potential (OCP), cyclic voltammetry (CV), and potentiodynamic measurements (PD). The results show that all tested inhibitors reduce the corrosion currents and potentials, with the highest efficiency observed in solutions with the lowest sodium chloride concentration of 0.9%, where AETDA exhibited the highest inhibition efficiency of 92.93%, while MMI showed an efficiency of 88.78% at the same inhibitor concentration of 10^{-2} M. Compared to AETDA and MMI, N-acetyl-L-leucine at a concentration of 10^{-3} M showed the lowest inhibition efficiency of 44.21%, while AETDA and MMI achieved inhibition efficiencies of 76.12% and 72.16%, respectively. Adsorption isotherms were used to evaluate the binding mechanisms of inhibitors on the brass surface, and physisorption was found to be the most likely mechanism for all tested compounds. These findings provide insight into the potential application of the investigated inhibitors to prevent brass corrosion under corrosive conditions.

Keywords: Corrosion Inhibition, Brass, Electrochemical Methods, Sodium Chloride Solutions, Organic Inhibitors.

INTRODUCTION

Brass, an alloy of copper and zinc, is prone to corrosion in chloride-containing environments, leading to dezincification and structural degradation. Organic inhibitors, particularly those containing sulfur, nitrogen, and oxygen, have been widely studied for their ability to mitigate corrosion. The aim of this study is to evaluate the inhibition efficiency and adsorption behavior of three organic inhibitors (MMI, AETDA, and N-acetyl-L-leucine) in NaCl solutions of different concentrations [1, 2, 3, 4, 5].

EXPERIMENTAL

An brass electrode (Cu 70% - Zn 30%) was immersed in NaCl solutions (0.9%, 2.0%,

---

[#] corresponding author: acvetkovic@tfbor.bg.ac.rs and 3.5%) with different concentrations of inhibitors. Electrochemical measurements were performed using an electrochemical workstation with a three-electrode setup. OCP, CV, and PD techniques were employed to assess the inhibition efficiency. The Langmuir adsorption isotherm was applied to determine the adsorption mechanism [1, 2, 3, 4, 5].

RESULTS AND DISCUSSION

Open Circuit Potential (OCP) Measurements

OCP values, given on Figure 1, indicated a shift towards more positive potentials in the presence of inhibitors, suggesting reduced anodic dissolution. AETDA exhibited the most stable potential, indicative of strong surface adsorption [6, 7].

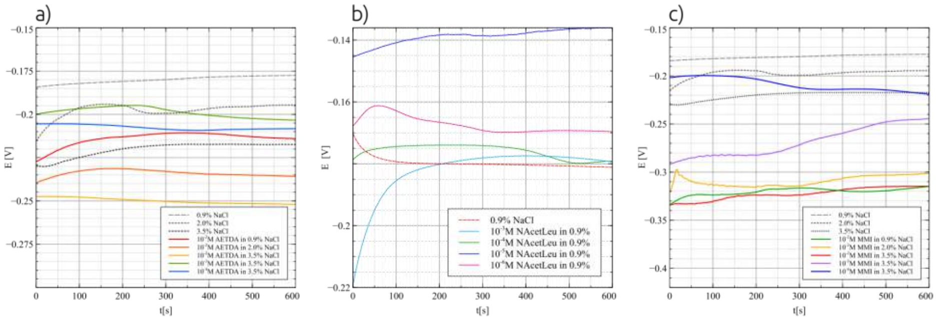

Figure 1 OCP valuers of AETDA a), N-acetyl-L-leucine b) and MMI c) for the measurement period of 10 minutes

Cyclic Voltammetry (CV)

Cyclic voltammetry was used to investigate the corrosion mechanism of brass in sodium chloride solutions of varying concentrations (0.9%, 2.0%, and 3.5%) and to evaluate the effect of three different inhibitors: MMI, AETDA and N-acetyl-L-leucine. In blank NaCl solutions, characteristic anodic and cathodic peaks were identified, corresponding to the oxidation and reduction of copper and zinc. In the presence of inhibitors, a reduction in current and a shift in peak potentials were observed, indicating inhibition of corrosion processes.

For MMI and AETDA, a significant decrease in peak intensities and narrowing of the voltammogram were noted, especially at higher inhibitor concentrations, suggesting effective surface protection of brass. N-acetyl-L-leucine showed weaker inhibition, with voltammograms resembling those of the uninhibited (blank) solutions. The voltammetric responses confirm that MMI and AETDA act as mixed-type inhibitors (inhibiting both anodic and cathodic reactions), while the effect of N-acetyl-L-leucine is more limited. The obtained voltammograms are represented on Figure 2 [1, 8, 9].

Potentiodynamic Polarization (PD)

Polarization curves demonstrated that AETDA provided the highest inhibition efficiency, followed by MMI and N-acetyl-L-leucine. Corrosion potential (E_{corr}) shifted positively, and corrosion current density (j_{corr}) decreased in inhibited solutions, confirming the protective role of the inhibitors. Tafel extrapolation was used to determine electrochemical parameters, including the E_{corr} and j_{corr} for brass in solutions with and without added inhibitor which do to the length requirements were not represented in Table 1 but the IE% values were calculated using equation 1) [6, 10, 11].

$$IE(\%) = ((j_{kor} - j_{kor(inh)}) / j_{korr}) \cdot 100\% \tag{1}$$

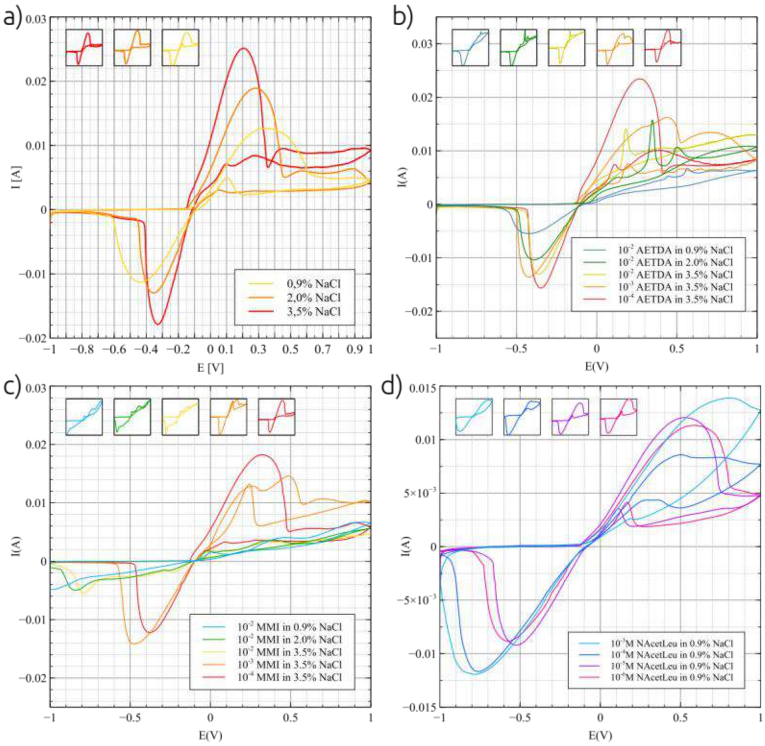

Figure 2 Cyclic voltammograms of brass imersed in a) the base (blank) solution, b) solutions with different amount of AETDA, c) solutions with different amounts of MMI and d) solution with different amount of N-acetyl-L-leucine

The results demonstrated that all inhibitors reduced the corrosion current density compared to the blank solution, indicating their effectiveness in suppressing corrosion processes. AETDA exhibited the highest inhibition efficiency of 92.93% in 0.9% NaCl, followed by MMI with 88.78%, while N-acetyl-L-leucine showed the weakest performance. The polarization curves revealed a shift in E_{corr} toward more positive values and a notable reduction in both anodic and cathodic current densities, suggesting that the inhibitors acted as mixed-type inhibitors [6, 10, 11].

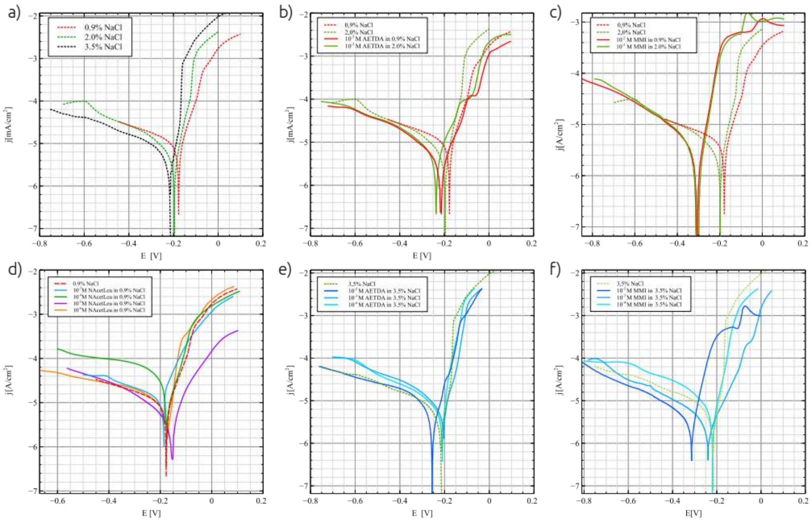

Figure 3 Polarization curves of brass in blank solutions and solutions with different amount of inhibitors

Adsorption Isotherm Analysis

The Langmuir adsorption isotherm, given on Figure 4, was applied to evaluate the interaction between inhibitors and the brass surface. The obtained values in Table 1. suggested physisorption as the predominant mechanism [12, 13].

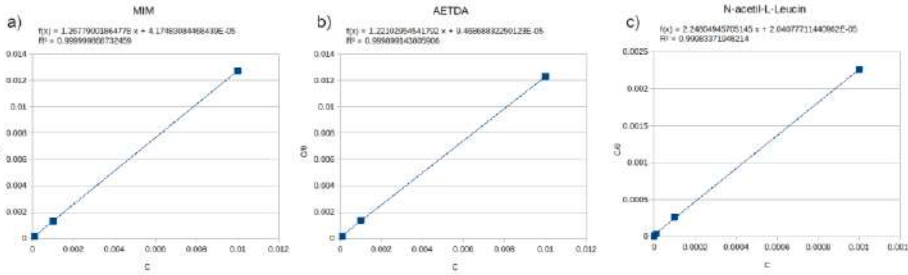

Figure 4 Langmuir adsorption isotherm for a) MMI, b) AETDA and c) N-acetyl-L-leucine

$$C/\theta = 1/K_{ads} + C \tag{2}$$

The isotherm is mathematically represented by the equation 2) where where C is the inhibitor concentration, θ is the surface coverage, and K_{ads} is the adsorption equilibrium constant. A linear plot of C/θ versus C allows for the determination of K_{ads}, where a higher value indicates stronger interaction between the inhibitor and the metal surface. The Gibbs free energy of adsorption ΔG_{ads} is calculated from equasion 3) [12, 13].

$$\Delta G = -RT\ln K_{ads} \tag{3}$$

Table 1 Inhibition efficiencies IE% and parameters obtained through Langmuir adsorption isotherm for the applied inhibitors

NaCl%	MMI			AETDA			N-acetyl-L-leucine			
	10^{-2}M	10^{-3}M	10^{-4}M	10^{-2}M	10^{-3}M	10^{-4}M	10^{-3}M	10^{-4}M	10^{-5}M	10^{-6}M
3.5%	78.62%	76.12%	60.19%	81.31%	72.16%	65.33%	/	/	/	/
2.0%	82.21%	/	/	89.99%	/	/	/	/	/	/
0.9%	88.78%	/	/	92.92%	/	/	44.21%	37.75%	25.98%	10.78%
θ	0.7862	0.7612	0.6019	0.8131	0.7216	0.6533	0.4412	0.3775	0.2598	0.1078
C/θ	$12.7\cdot10^{-3}$	$1.31\cdot10^{-3}$	$0.17\cdot10^{-3}$	$12.3\cdot10^{-3}$	$1.39\cdot10^{-3}$	$0.15\cdot10^{-3}$	$2.27\cdot10^{-3}$	$2.65\cdot10^{-4}$	$3.85\cdot10^{-5}$	$9.28\cdot10^{-6}$
R^2	0.9999			0.9998			0.9998			
ΔG	-23.9532 kJ/mol			-22.9545 kJ/mol			-26.7422 kJ/mol			

Values of ΔG_{ads} between -20 and -40 kJ/mol suggest physisorption, while values more negative than -40 kJ/mol suggest chemisorption. In this study, the Langmuir isotherm suggests physisorption for all applied inhibitors given their ΔG_{ads} values in Table 1 [12, 13].

CONCLUSION

The investigated inhibitors effectively reduced brass corrosion in chloride media. AETDA exhibited the highest inhibition efficiency, while N-acetyl-L-leucine showed the weakest performance. Making the order of inhibition efficiency AETDA > MMI > N-acetyl-L-leucine. Adsorption studies confirmed physisorption as the dominant mechanism for all inhibitors. These findings contribute to the understanding of organic inhibitors and their potential applications in corrosion protection strategies.

ACKNOWLEDGEMENT

The authors are grateful to the Ministry of Science, Technological development and Innovation of the Republic of Serbia for financial support according to the contract with the registration number 451-03-47/20223-01/200131.

REFERENCES

1. M. Tsai, S. Chao, C. Luo, L. Hua, C. Hu, B. K. Mahata, C. Huang, (2024) Chemosphere 355, 141835.
2. M. Tsai, S. Chao, C. Luo, L. Hua, C. Hu, B. K. Mahata, C. Huang, (2024) Chemosphere 355, 141835.
3. J. P. Ferreira, J. A. Rodrigues, I. T. E. Fonseca, (2004) J Solid State Eletrochem., 8, 260-271
4. Z. Zhu, X. Zhang, (2023) Materials, 16, 6712.

5. S. S. Add EL-Reuim, F. U. Assaf, A. EL-Sayed, A. M. Zaky, (1995) British Corrosion Journal, 30, 297-301.
6. El-Asri, A. Jmiai, H. Bourzi, Y. Lin, S. El Issami, (2024) Surfaces and Interfaces, 44, 103799.
7. X. Zhang, W. Mei, L. Huang, J. Tao, Y. Xiong, Z. Wang, (2023) journal of materials research and technology, 22, 192-205.
8. S. Raeisi, M. Yousefpour, (2024) Materials Chemistry and Physics, 312, 128516.
9. S. J. Shin, J. Y. Kim, S. An, T. D. Chung (2022) Current Opinion in Electrochemistry, 35, 101054.
10. M. Finšgar (2018) Molecular and Biomolecular Spectroscopy, 190, 290-297.
11. D. Čakara, R. Peter, M. Finšgar, (2022) Surfaces and Interfaces, 32, 102108.
12. M. Galai, J. choucri, Y. Hassani, H. Benqlilou, I. Mansouri, B. Ouaki, M. Ebn Touhami, C. Monticelli, F. Zucchi, (2019) Chemical Data Collections, 19, 100171.
13. C. G. Vaszilcsin, M. V. Putz, A. Kellenberger, M. L. Dan, (2023) Journal of Molecular Structure, 1286, 135643.
14. G. Vengatesh, M. Sundaravadivelu, (2019) Journal of Molecular Liquids, 287, 110906.

XVI International Mineral Processing
and Recycling Conference
28-30 May 2025, Belgrade, Serbia

DOI: 10.5937/IMPRC25503C Research article

WASTE TO RESOURCE TRANSFORMATION: INNOVATIVE APPROACHES TO RECYCLING CATHODE MATERIALS FROM LITHIUM-ION BATTERIES

Aleksandar Cvetković[#], 0009-0003-5184-6874,
Vladan Nedelkovski, 0000-0001-7724-1118,
Dragana Medić, 0000-0001-9980-5949,
Sonja Stanković, 0000-0003-0745-5422,
Žaklina Tasić, 0000-0001-6544-1980,
Milan Radovanović, 0000-0002-5175-6022,
Snežana Milić, 0000-0002-5000-9156,
University of Belgrade, Technical Faculty in Bor, Bor, Serbia

ABSTRACT – The surging use of lithium-ion batteries (LIBs) has precipitated an imperative for sustainable recycling practices to recover valuable cathode materials, ensuring environmental stewardship and resource efficiency. This review delves into recent innovations in cathode material recycling from LIBs, focusing on methodologies that not only reclaim materials but also restore their functionality for reuse. Highlighted are cutting-edge techniques such as an electrochemical relithiation process, which rejuvenates spent cathode materials to equal the performance of new ones. At the forefront of these sustainable practices is the concept of direct regeneration via direct recycling, offering an economically viable and environmentally friendly approach to mend degraded cathodes. Such progress signals a shift away from conventional metallurgical methods toward intelligent regeneration, representing a significant step forward in the sustainable recycling of LIBs. This review provides a brief analysis of these novel recycling processes, illustrating their ability to transform spent batteries into valuable resources, mitigate environmental harm, and foster a circular economy within the realm of energy storage.

Keywords: Lithium-Ion Battery Recycling, Cathode Material, Regeneration, Relithiation, Direct Recycling.

INTRODUCTION

Lithium-ion batteries (LIBs) are extensively used in various applications (electric vehicles, stationary storage, portable electronics, etc.). Given that these batteries generally have a lifespan of 10-15 years, a significant volume of End-of-Life (EOL) batteries will require disposal in the coming years [1]. Furthermore, the recovery of crucial elements like lithium, cobalt, nickel, and manganese, which have substantial economic importance, is essential to maintain the sustainability of the supply chain over the long term [2]. Commonly used cathode materials such as $LiNi_xCo_yMn_zO_2$, $LiCoO_2$, and $LiFePO_4$ can be directly regenerated from spent LIBs and reused to produce new batteries, thus forming a sustainable cycle from spent to new cathode materials [3].

[#] corresponding author: acvetkovic@tfbor.bg.ac.rs

The hydrometallurgical process is noted for its high recovery rate and ability to produce high-purity end products. It is characterized by lower energy consumption and less waste gas production. However, this method generates a significant amount of wastewater and is inherently time-consuming. The principal challenges lie in developing effective wastewater treatment techniques and optimizing the overall process for efficiency. The pyrometallurgical process offers a straightforward operation with a short processing flow and does not necessitate pre-sorting of inputs by categories or sizes. Its high efficiency is a strong advantage. Nonetheless, it does not recover lithium and manganese, entails higher energy consumption, and is less efficient in terms of overall recovery. Moreover, it produces more waste gas, raising concerns about environmental hazards and the cost of waste gas treatment. The key challenges include reducing energy consumption and emissions, mitigating environmental hazards, and ideally, integrating with hydrometallurgical methods to enhance recovery outcomes [4].

Pražanová et al. (2024) compared the cost, energy use, and environmental impact of producing and recycling 1 kg of NMC111 cathode via virgin material production, pyrometallurgy, hydrometallurgy, and direct recycling. Compared to traditional production, pyrometallurgy increases costs by 16%, hydrometallurgy lowers them by 2%, and direct recycling cuts them down by 42%. Energy consumption shows similar trends: pyrometallurgy uses 3% more, hydrometallurgy 11% less, and direct recycling reduces it by 89%. In water use, hydrometallurgy is highest at 55%, followed by pyrometallurgy at 37%, and direct recycling at just 14%. Greenhouse gas emissions are lowest with direct recycling, (9% of traditional levels), while hydrometallurgy reaches 97% and pyrometallurgy 15%. Sulfur oxide emissions are also minimal with direct recycling (1%), compared to 13% for hydrometallurgy and 33% for pyrometallurgy. These data indicate that direct recycling offers significant advantages in terms of reducing costs, energy, and water consumption, as well as reducing emissions of harmful gases.

DIRECT RECYCLING APPROACH

Post-consumption, spent batteries are subjected to direct recycling or material separation. Material separation could involve multiple methods such as hydrometallurgy, pyrometallurgy, and novel processes like electrochemical methods, ionic liquids, and eutectic salts [4].

The concept of "direct recycling" of cathode materials from spent LIBs is an innovative and sustainable approach that aims to recover and regenerate cathode materials which contrasts with traditional recycling methods that typically focus on recovering individual metal constituents. Direct recycling is predicated on the principle of retaining high-value cathode materials in their functional form rather than breaking them down into their elemental components. By doing so, it reduces the need for energy-intensive processes associated with traditional recycling methods, such as smelting and extraction. Furthermore, direct recycling circumvents the economic and environmental costs of synthesizing new cathode materials from scratch [1, 5].

The direct recycling process begins with the collection of EOL batteries, which undergo an initial mechanical treatment to remove the outer casings and isolate the battery cells. Following shredding, the process involves a series of sophisticated separation techniques that distinguish between the cathode material, the anode, and other metals. Screening ensures the granulation of materials to sizes below 0.5 mm, facilitating separation. The subsequent hydro- and pyrometallurgical processes are crucial for the extraction of valuable metals. In hydro processes, leaching is employed to dissolve specific metals, after which a liquid/solid separation is executed [2].

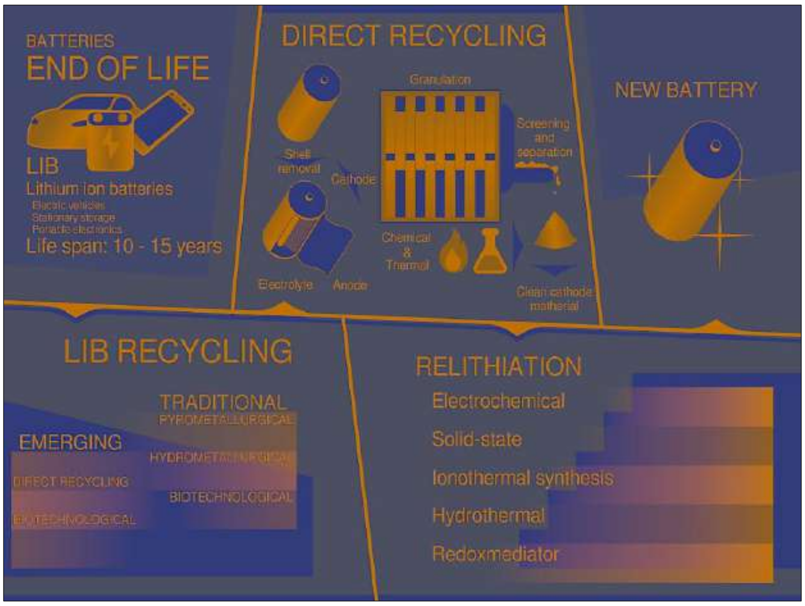

Figure 1 Overview of lithium-ion battery recycling processes: from EOL management to direct recycling and relithiation techniques

The recovery of the electrolyte is another vital step, as it can contain valuable organic compounds and lithium salts. Once the cathode materials are isolated, they undergo treatments to remove any residual carbon black and polyvinylidene fluoride (PVDF) binder. This is typically achieved through chemical or thermal processes. The cleaned cathode materials are then subjected to relithiation, a process where lithium is reintroduced to the cathode material to restore it to a usable state. Upcycling is an additional step that may involve further treatment to improve the performance of the cathode material, possibly surpassing its original specifications [4, 6]. The rejuvenated cathode material can then be directly reused in the manufacturing of new batteries. This "closed-loop" approach presents several advantages: it retains the microstructural and electrochemical properties of the cathode materials, reduces the reliance on raw material extraction, decreases the overall carbon footprint of battery production, and supports the advancement toward a more sustainable and circular economy [4].

Shi et al. (2019), presented the ambient-pressure relithiation process, which involved a novel approach for regenerating degraded LIB cathode materials, specifically $LiNi_{0.5}Co_{0.2}Mn_{0.3}O_2$ (NCM523), using eutectic Li^+ molten-salt solutions. This method is designed to restore the lithium composition and crystal structure of the cathode materials at ambient pressure, providing a safer and more environmentally friendly alternative to high-pressure hydrothermal relithiation processes. The process utilizes a eutectic mixture of lithium nitrate ($LiNO_3$) and lithium hydroxide (LiOH) in a molar ratio of 3:2. This mixture has a low melting point of approximately 176°C, which facilitates the relithiation at relatively low temperatures. Degraded NCM523 cathode particles are mixed with the eutectic Li^+ molten-salt solution. This mixture serves both as a lithium source and a medium for the reaction. The mixture is then heated to 300°C at ambient pressure and maintained at this temperature for 2 to 4 hours. This step allows for sufficient time for lithium ions to diffuse through the cathode particles, ensuring complete relithiation. The mixture is washed with deionized water to remove any residual lithium salts. The relithiated cathode particles are subsequently thermally annealed. This involves sintering the particles with a 5% excess amount of lithium carbonate (Li_2CO_3) at 850°C in an oxygen atmosphere for 4 hours. The excess Li_2CO_3 compensates for any lithium loss that might occur at high temperatures.

This relithiation method not only recovers the lithium content and structural integrity of degraded NCM523 cathode materials but also provides a platform for the application of similar techniques to other cathode materials [7].

Several relithiation methods have been developed and researched in recent years, including ionothermal, hydrothermal, redox mediator relithiation, electrochemical relithiation, solid-state relithiation and eutectic salt relithiation [1, 2]. Advantages and challenges regarding relithiation processes are shown in Table 1.

Among various techniques, the solid-state method is the simplest, involving direct annealing of used cathode materials with lithium sources. Precise control of lithium salt quantity is essential [5]. Ionothermal synthesis uses ionic liquids to enable reactions at lower temperatures, aiding lithium-ion battery cathode recycling. Wang et al. (2020) applied this method using affordable lithium halides and recyclable ionic liquids [8]. The hydrothermal method uses dilute lithium-containing solutions to restore cathode stoichiometry and phase purity. Gao et al. (2020) regenerated LMO cathodes to near-pristine performance, emphasizing the method's environmental and economic advantages [9]. Zhao et al. (2015) indicated that some prelithiation strategies might reduce costs compared to traditional battery manufacturing [10]. The redox mediator in relithiation replenishes lithium via redox reactions between lithium metal and EOL cathode material, though its efficiency may vary with pH [11]. Yang et al. (2019) showed that electrochemical relithiation in aqueous electrolyte followed by heating can restore cathode structure and performance [12].

Relithiation methods continue to evolve, aiming for fast, uniform lithium reintegration [11]. Direct recycling offers benefits like short recovery routes, high recovery rates, and environmental sustainability. However, it also requires complex equipment and may not fully recover all materials. To improve this, research focuses on reducing costs, simplifying material input requirements, and enhancing product quality. These efforts aim to make direct recycling a key solution for sustainable battery production and waste management [4, 12].

Table 1 The advantages and challenges of different direct recycling technologies [2]

Direct Recycling Method	Advantages	Challenges
Solid-state relithiation	One-step regeneration; Simple operation	Pre-determination of Li deficiencies; Phase impurity
Electrochemical relithiation	Low energy consumption; Low cost	Pre-determination of Li deficiencies; Removal of current collector, binders, etc.; Phase impurity; Scalability issue
Ionic liquids relithiation	Self-saturation relithiation	High cost of ionic liquid; Scalability issue
Eutectic salt relithiation	Self-saturation relithiation; Low energy consumption	Removal of solidified salts; Mixture after regeneration; Scalability issue
Solution based relithiation	Self-saturation relithiation; Wide applicability; Low cost	Safety concern related to elevated temperature and pressure

CONCLUSION

Direct recycling is a highly promising method, efficiently restoring degraded cathodes without breaking them down into base components. It cuts energy use by up to 89% and lowers both water consumption and greenhouse gas emissions. Economically, it reduces costs by 42% compared to producing virgin materials.

Electrochemical relithiation helps recover the lithium stoichiometry in cathodes, improving recycled materials to match or exceed original performance. When combined with methods like ionothermal synthesis and redox mediator strategies, it enables effective reintegration of valuable materials, supporting the circular economy.

The challenges ahead include reducing operational costs and addressing technical complexities in material recovery. Successful industrial integration will depend on scalability and environmental impact.

In conclusion, the advancement of recycling technologies for LIB cathode materials is not only a technical necessity but also an environmental imperative. As the demand for LIBs continues to escalate, driven by the global push towards electrification and renewable energy sources, the ability to efficiently reclaim and reuse valuable materials from spent batteries will be crucial. The ongoing development of these recycling processes promises to reduce reliance on virgin resources, decrease production costs, and diminish environmental degradation, thereby supporting the sustainability goals of the modern world.

ACKNOWLEDGEMENT

The authors are grateful to the Ministry of Science, Technological development and Innovation of the Republic of Serbia for financial support according to the contract with the registration number 451-03-47/20223-01/200131.

REFERENCES

1. Verma A., Colclasure A. M., Coyle J. (2023) Front. Batter. Electrochem., 2, 1-13.
2. Xu P., Tan D. H. S., Jiao B., Gao H., Yu X., Chen Z. (2023) Adv. Funct. Mater., 33(14), 1-20.
3. Zhao Y., Yuan X., Jiang L., Wen J., Wang H., Guan R., Zhang J., Zeng G. (2020) Chem. Eng. J., 383, 123089.
4. Pražanová A., Plachý Z., Kočí J., Fridrich M., Knap V. (2024) Batteries, 10(3), 81.
5. Wei G., Liu Y., Jiao B., Chang N., Wu M., Liu G., Lin X., Weng X., Chen J., Zhang L., Zhu C., Wang G., Xu P., Di J., Li Q. (2023) iScience, 26(9), 107676.
6. He B., Zheng H., Tang K., Xi P., Li M., Wei L., Guan Q. (2024) Recycling, 9, 9.
7. Shi Y., Zhang M., Meng Y. S., Chen Z. (2019) Adv. Energy Mater., 9(20), 1-9.
8. Wang T., Luo H., Bai Y., Li J., Belharouak I., Dai S. (2020), 10(30), 2001204.
9. Gao H., Yan Q., Xu P., Lui H., Li M., Liu P., Luo J., Chen Z. (2020) ACS Appl. Mater. Interfaces, 12(46), 51546-51554.
10. Zhao J., Lu Z., Wang H., Liu W., Lee H., Yan K., Zhou D., Lin D., Liu N., Cui Y. (2015) J. Am. Chem. Soc., 137(26), 8372–8375.
11. Coyle J., Verma A., Colclasure A. M., (2020) ECS Meeting Abstracts, 5, 613.
12. Yang T., Lu Y., Li L., Ge D., Yang H., Leng W., Zhou H., Han X., Schmidt N., Ellis M., Li Z. (2019) Adv. Sustain. Syst. 1900088.

XVI International Mineral Processing
and Recycling Conference
28-30 May 2025, Belgrade, Serbia

DOI: 10.5937/IMPRC25509T

Original research article

OPTIMIZING METAL RECOVERY FROM EAF DUST: A COMPREHENSIVE APPROACH BEYOND THE WAELZ KILN PROCESS

Gašper Tavčar[1#], 0000-0001-9891-6153,
Davide Mombelli[2], 0000-0002-8265-5312,
Carlo Mapelli[2], 0000-0002-5388-2073,
Gianluca Dall'Osto[2], 0000-0002-1983-6516,
Dragan Radulović[3], 0000-0001-8210-8100,
Ivica Ristović[4], 0000-0002-1771-2499,
Mateusz Ciszewski[5], 0000-0001-9076-8301,
Jasna Kastivnik[6], 0009-0003-4123-8779,
Ana Mladenovič[7]**,** 0000-0002-7316-9427,
Alenka Mauko Pranjič[7], 0000-0002-9822-7806,
[1]Jožef Stefan Institute, Ljubljana, Slovenia
[2]Politecnico di Milano, Milano, Italy
[3]Institute for technology of nuclear and other mineral raw materials,
Belgrade, Serbia
[4]University of Belgrade, Belgrade, Serbia
[5]Łukasiewicz Research Network – Institute of Non-ferrous Metals,
Gliwice, Poland
[6]Oretech, Vrhnika, Slovenia
[7]Slovenian National Building and Civil Engineering Institute, Ljubljana, Slovenia

ABSTRACT – The Electric Arc Furnace (EAF) process is predominantly used for recycling steel scrap, generating EAF dust at approximately 10-20 kg per ton of steel. This dust is rich in valuable metals like iron and zinc, in addition to metal oxides such as lead, manganese, nickel, and chromium. The DustRec project endeavours to recover all these elements, offering a comprehensive alternative to the traditional Waelz kiln process, which primarily focuses on zinc recovery. The project employs magnetic separation to initially divide dust samples into magnetic and non-magnetic fractions, followed by gravity separation to further refine these into heavy and light fractions. This detailed classification enables targeted processing of each stream through tailored pyrometallurgical and hydrometallurgical methods, according to their specific compositions. Throughout the project, numerous EAF and cupola furnace (CF) dust samples were collected from various sources, with the most suitable samples selected for advanced reprocessing. Separation based on particle size yielded diverse outcomes. The subsequent hydrometallurgical and pyrometallurgical treatments of these fractions resulted in significant metal recoveries.

Keywords: EAF Dust, Magnetic Separation, Gravity Separation, Extraction, Recycling.

[#] corresponding author: gasper.tavcar@ijs.si

INTRODUCTION

The Electric Arc Furnace (EAF) process is the most widely used method for recycling steel scrap, primarily due to its ability to smelt 100% of the solid charge [1]. In contrast, the Basic Oxygen Furnace (BOF) typically handles only 20% of the total charge weight as cold metallic burden [2]. During the melting, EAF dust accumulates at a rate of 10-20 kg per tonne of liquid steel [3]. This dust contains valuable metal oxides, including iron (Fe), zinc (Zn), lead (Pb), manganese (Mn), nickel (Ni), and chromium (Cr), alongside some halides [4]. The composition of EAF dust varies significantly based on the input materials, particularly the proportion of galvanized steel (for Zn) or high-alloy/stainless steel (for Cr and Ni), leading to fluctuations in chemical content from day to day and even between heats within the same steel shop [5]. During the smelting operation, zinc vaporizes and escapes the metal bath as gaseous Zn, which subsequently oxidizes to ZnO during transport with the off-gas, along with other metal oxides [6]. EAF dust is typically collected in bag filters from the off-gas treatment system. If not managed properly, the disposal of this dust can harm the environment due to the mobilization of hazardous metals like Zn, Cd, Cr, Ni, and Pb, while also imposing financial burdens on the metallurgical industry [7]. In 2022, approximately 0.6 to 1.2 million tons of EAF dust were produced, which brings the global total to about 5.5 to 11 million tons [8]. Projections estimate that this figure could reach at least 18 million tons by 2050. Notably, the combined presence of Fe and Zn in EAF dust is particularly remarkable, accounting for 50 to 60% of its weight. The extraction of Zn is the primary focus due to its higher market value (approximately $2,950 per ton) compared to iron, which is valued at around $368 per ton [9]. Consequently, current reprocessing efforts primarily target Zn recovery, as technologies for extracting other valuable metals remain underdeveloped.

Most existing EAF dust treatment technologies employ pyrometallurgical techniques for zinc extraction, with the Waelz kiln process leading the market by capturing over 85% of it. Alternative pyrometallurgical processes have emerged that convert Zn into ZnO for later use in processes like sulphate electrolysis or the Imperial Smelting Process (ISP) [10]. One example is the Rotary Hearth Furnace (RHF) method, which is coal-based and effectively processes EAF dust containing significant quantities of iron, carbon, zinc, lead, and alkalis, yielding high-quality zinc products and Direct Reduced Iron (DRI) instead of slag [11]. However, this process is best for EAF dust with low zinc levels, and technological advancements are needed to manage challenges like zinc oxide blockage. Moreover, the high start-up costs for this technology require improvements in its economic feasibility [12]. Conversely, the Primus® process [12] employs a multiple-hearth furnace technology designed to reduce metal oxides efficiently and quickly using low-cost, unprepared feed at lower operating temperatures. Although it produces high-quality outputs, it faces issues like rapid wear and the evaporation of alkaline compounds, coupled with size restrictions that limit its production capacity. Another pyro-metallurgical method called the INDUTEC® process [13] aims to enrich EAF dust in an induction furnace, recovering Zn and Pb as Crud Zinc Oxide (CZO) through flue gas filtration and obtaining reducible oxides as molten pig iron. The technology developed through the EIT 2sDR project focuses on enhancing the recycling process by recovering both iron (Fe) and zinc (Zn). It currently does not separate and recycle lead (Pb) and copper (Cu), which are commonly present in the material stream. This process is in the prototype phase and is being analysed to assess its compliance with existing and future environmental regulations. Processes are frequently inefficient, expensive, and can present environmental issues [14]. Hydrometallurgical approaches, such as the Zincex® [15] and Ezinex® [16] processes, have also been developed. Zincex® utilizes atmospheric leaching, solvent extraction, and traditional electrowinning to produce high-purity zinc ingots (99.99%). Ezinex® employs chloride leaching to extract oxidized zinc but is currently limited to pilot-scale operations, making it less reliable for large-scale EAF dust processing.

Current processes primarily focus on zinc extraction due to its financial viability, with other metals often discarded as toxic waste. Our approach aims to improve this by employing a variety of mineral beneficiation techniques combined with hydrometallurgical and pyrometallurgical processes. This strategy seeks to maximize the separation and extraction of all valuable metals, while repurposing the residual waste for use in the construction industry, ultimately working towards achieving near-zero waste manufacturing.

EXPERIMENTAL

In this study, two different EAF dusts were analyzed: one from Metal Ravne, SI, and the other from Boleslaw, PL. These samples were selected from a variety of options based on their composition (Table 1). Their composition was determined through ICP-OES (refer to Table 1), XRPD (see Figure 1), and SEM microscopy. XRPD analysis revealed that zinc is present in the forms of franklinite and zincite. In the case of Metal Ravne, SI, these zinc forms, along with magnetite, constitute the majority of the sample. Additionally, Metal Ravne, SI dust contains significant quantities of chromium, whereas the Boleslaw, PL, dust is notable for its chlorides and lead content. Due to these compositional differences, these samples are particularly suitable for further testing.

Magnetic and gravity beneficiation techniques were applied to the sample to increase the concentration of ferrous metals in one fraction and nonferrous metals in another. Magnetic separation was conducted using a "Dings" wet magnetic separator equipped with a permanent magnet and a magnetic induction of B = 0.1 T. To improve separation, the sample (-0.025 + 0.00 mm) was additionally ground. For gravity separation, a Multi-Gravity Separator (MGS) was employed, leveraging advanced technology that harnesses both gravitational and centrifugal forces to effectively separate materials based on density.

The ferrous fraction, consisting of the magnetic fraction from magnetic separation and concentrate from gravity separation, was further processed using pyrometallurgical methods with various reducing agents (graphite, biochar and carbon rich CF dust) to produce an iron alloy suitable for direct use in the Electric Arc Furnace as a substitute for scrap metal or for feeding into the Ladle Furnace. Conversely, the non-ferrous fraction, comprising of the non-magnetic fraction obtained by magnetic separation and tailings from gravity separation, was evaluated for the hydrometallurgical extraction of zinc, lead, and copper.

Table 1 Elemental composition of both samples made by ICP-OES

	w **(μg/g)**									
Sample	**Ca**	**Cr**	**Cu**	**Fe**	**Mg**	**Mn**	**Ni**	**Pb**	**Zn**	**Si**
Metal Ravne, SI	27144	34610	1089	298897	18330	14948	1026	1903	260707	12454
Boleslaw, PL	38465	2331	2112	229300	16755	16763	< LOD	24581	295027	23477

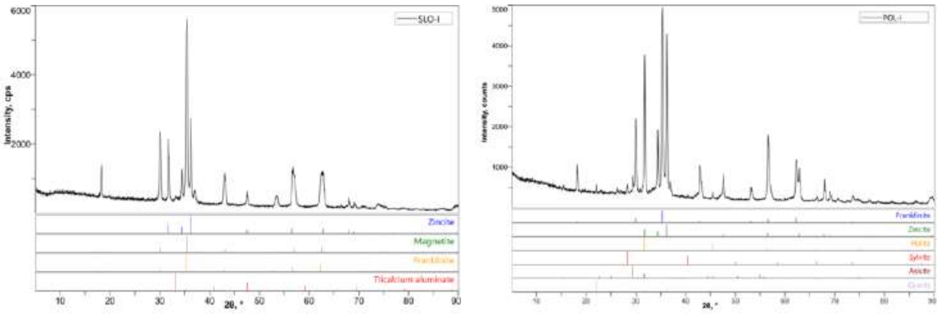

Metal Ravne, SI Boleslaw, PL

Figure 1 XRPD of both samples

Table 2 Mineral composition of both samples

	Franklinite	**Zincite**	**Magnetite**	**Chlorides**	**Quartz**
Metal Ravne, SI	20.6	19.0	56.6		
Boleslaw, PL	60.2	31.7		5.30	2.00

RESULTS AND DISCUSSION

Interestingly, rather than being complementary, both beneficiation techniques excelled in one sample while underperforming in another. Magnetic separation proved more effective for Boleslaw, PL (refer to Table 3), whereas gravity separation achieved a significant enhancement for Metal Ravne, SI (refer to Table 4).

Table 3 Recovery and upgrade of Boleslaw, PL through magnetic separation methods

	Zn		Fe		Pb	
	Recovery [%]	**Upgrade**	**Recovery [%]**	**Upgrade**	**Recovery [%]**	**Upgrade**
magnetic	48.3	1,09	55.7	0.95	48.3	0.95
Non magnetic	51.7	0,90	44.3	1.06	51.7	1.06

Table 4 Recovery and upgrade of Metal Ravne, SI through gravity separation methods

	Zn		Fe		Pb	
	Recovery [%]	**Upgrade**	**Recovery [%]**	**Upgrade**	**Recovery [%]**	**Upgrade**
conc	1.8	0.23	13.2	1.72	9.9	0.23
tail	91.7	1.15	74.7	0.94	84.4	1.15
left	3.9	0.89	4.4	0.99	5.7	0.89

Optimization of the pyrometallurgical treatment of ferrous fractions revealed the necessity of reducing material at 1500 °C using cupola furnace dust as both a reductant and flux to ensure complete separation of slag and metal. The test results indicated that the reduction yield of Electric Arc Furnace Dust (EAFD) concentrate exceeded 40% (expressed as the metal-to-charge ratio), while the slag constituted between 10% and 22% of the initial briquette mass. Notably, the use of biochar demonstrated less effectiveness in this process. The pyrometallurgical treatment successfully recovered three primary metals: Fe, Mn, and Cr, with recovery yields ranging from 0.88 to 0.97 for Fe, 0.00 to 0.66 for Mn, and 0.64 to 0.97 for Cr.

Hydrometallurgical extraction of Zn by the utilization of sulfuric acid showed optimal results at conditions in Table 5.

Table 5 Optimal experimental conditions for leaching of Zn and copper

	T (°C)	t (min)	% Zn leached	% Fe leached	% Cu leached
Boleslaw, PL	40	60	80	15	65
Metal Ravne, SI	25	80	81	12	31

Lead was extracted from the sulphate leaching residue with triethylenetetramine. It was determined that lead recovery from the non-magnetic fraction of EAF dust is feasible (residue non-mag. Boleslaw, PL), achieving extraction efficiencies of up to 90%. The proposed process optimization includes ideal conditions for leaching EAF dust at room temperature with a solid-to-liquid (s/l) ratio of 100 g/dm^3 over a duration of 1 to 2 hours. The optimal concentration of TETA required for effective lead extraction under these conditions was established to be 4%. The tested precipitation resulted in lead 97.7% carbonate.

CONCLUSION

The application of beneficiation methods, followed by hydrometallurgical or pyrometallurgical processes, demonstrated significant improvements in the treatment of Electric Arc Furnace (EAF) dust. This approach led to the concentration of essential metals in the separated fractions, achieving an upgrade of 1.15 and a recovery rate of 91.7%. These results indicate that such methods can be effectively applied to secondary raw materials, in addition to primary ores. Further research and development in this area are necessary to address smaller particles, commonly found in process wastes, transforming them into valuable secondary raw materials. The obtained fractions underwent appropriate pyrometallurgical or hydrometallurgical treatments, resulting in reduced material volumes and consequently lower processing costs. The pyrometallurgical treatment effectively recovered three key metals: iron, manganese, and chromium. Furthermore, the extraction of zinc, followed by iron precipitation and copper cementation, achieved a remarkable 95% purity with a recovery rate of 78.9%. Lead extraction also performed impressively, yielding 90% with $PbCO_3$ of sufficient purity for smelter applications. These results underscore the feasibility and effectiveness of maximizing metal recovery from waste materials.

ACKNOWLEDGEMENT

The authors would like to express their gratitude to EIT RawMaterials for their funding of the RIS DustRec II project (grant agreement n°22009), as well as to the Slovenian Research and Innovation Agency for their support of the P1-0045 program and J1-3029 project.

REFERENCES

1. Madias, J. (2014) Electric Furnace Steelmaking. In: Treatise on Process Metallurgy (S. Seetharaman), Elsevier, Oxford, 271–300.
2. Jalkanen, H., Holappa, L. (2014) Converter Steelmaking. In: Treatise on Process Metallurgy (S. Seetharaman), Elsevier, Oxford, 223–70.
3. De Buzin, P.J.W.K., Heck, N.C., Vilela, A.C.F. (2017) EAF dust: An overview on the influences of physical, chemical and mineral features in its recycling and waste incorporation routes. J. Mater. Res Technol., 6(2),194–202.
4. Pickles, CA. (2009) Thermodynamic analysis of the selective chlorination of electric arc furnace dust. J. Hazard. Mater., 166(2–3), 1030–1042.
5. Nyirenda, R.L. (1991) The processing of steelmaking flue-dust: A review. Miner. Eng. 4(7–11), 1003–10025.
6. Guézennec, A.G., Huber, J.C., Patisson, F., Sessiecq, P., Birat, J.P., Ablitzer, D. (2005) Dust formation in Electric Arc Furnace: Birth of the particles. Powder Technol. 157(1–3), 2–11.
7. European Agency of Safety and Healt at Work. Regulation (EC) No 1907/2006 - Registration, Evaluation, Authorisation and Restriction of Chemicals (REACH). Eur Union Internet]. 2023;
8. Al-Harahsheh, M., Al-Nu'Airat, J., Al-Otoom, A., Al-Hammouri, I., Al-Jabali, H., Al-Zoubi, M., et al. (2019) Treatments of electric arc furnace dust and halogenated plastic wastes: A review. J. Environ. Chem. Eng., 7(1), 102856.
9. SMM Information & Technology Co. L. Shanghai Metals Market (2025). https://www.metal.com (16.03.2025)
10. Palimakaą, P., Pietrzyk, S., Stępień, M., Ciećko, K., Nejman, I. (2018) Zinc recovery from steelmaking dust by hydrometallurgical methods. Metals, 8(7), 547.
11. Wu, Y.L., Jiang, Z.Y., Zhang, X.X., Wang, P., She, X.F. (2013) Numerical simulation of the direct reduction of pellets in a rotary hearth furnace for zinc-containing metallurgical dust treatment. Int. J. Miner. Metall. Mater., 20(7), 636–544.
12. Lin, X., Peng, Z., Yan, J., Li, Z., Hwang, J.Y., Zhang, Y., et al. (2017) Pyrometallurgical recycling of electric arc furnace dust. J. Clean. Prod. 149, 1079–1100. 7
13. Maccagni, M.G., (2016) INDUTEC®/EZINEX® Integrate Process on Secondary Zinc-Bearing Materials. J. Sustain. Metall., 2(2), 133–140.
14. Rösler, G., Pichler, C., Antrekowitsch, J., Wegscheider, S. (2014) "2sDR": Process Development of a Sustainable Way to Recycle Steel Mill Dusts in the 21st Century. JOM, 66(9), 1721–1729.
15. Díaz, G., Martín, D. (1994) Modifed Zincex process: the clean, safe and profitable solution to the zinc secondaries treatment. Resour. Conserv.
16. Recycl., 10(1–2), 43–57.
17. Maccagni, M.G. (2016) INDUTEC®/EZINEX® Integrate Process on Secondary Zinc-Bearing Materials. J. Sustain. Metall., 2(2), 133–40.
18. Mombelli, D., et al. EIT Raw Materials RIS-DUSTREC: investigation and selection of furnace dust samples for valuable metals recovery. Metall. Ital., 115(3), 8-23.

XVI International Mineral Processing
and Recycling Conference
28-30 May 2025, Belgrade, Serbia

DOI: 10.5937/IMPRC25515M Original research article

SOLVENT EXTRACTION OF La, Ce, AND Nd ELEMENTS FROM THE NiMH BATTERIES LEACH SOLUTION

Amir Mohammad Bidmeshki, 0009-0005-4227-3124,
Mahmoud Abdollahy[#], 0000-0002-7631-5194,
Tarbiat Modares University, Tehran, Iran

ABSTRACT – To separate rare earth elements D2EHPA, Cyanex 272, and DBC extractants used and results showed they couldn't selectively separate them, but in optimized conditions simultaneous extraction of them achieved. A DBC-D2EHPA mix had a synergistic effect, achieving recoveries of 98.76% (cerium), 97.94% (lanthanum), and 100% (neodymium). The McCabe-Thiele diagram indicated 3, 2, and 1 steps with Cyanex 272 for 90% recovery of cerium, lanthanum, and neodymium, respectively. Stripping tests with sulfuric, nitric, and hydrochloric acids were unsatisfactory, requiring further study.

Keywords: Rare Earth Elements, Nickel Metal Hydride, Recycling, Solvent Extraction.

INTRODUCTION

NiMH batteries were developed in Japan in 1989-1990 to replace Ni-Cd batteries due to the toxicity of Cd and their better performance [1]. Before lithium-ion batteries, NiMH batteries were widely used in devices like notebook computers, telephones, mobile phones, and electric cars due to their high energy density, compact size, overcharge resistance, and stable electrolyte during charge-discharge cycles [2][3]. The accumulated waste of nickel metal hydride batteries is increasing every year. The amount of waste from nickel-metal hydride batteries is increasing each year as their usage declines, mainly due to the growing popularity of newer battery technologies like lithium-ion. Based on their components, these resources can serve as a secondary source of valuable metals, including rare elements, nickel, and cobalt [4][5]. The reserves of rare elements in the world are limited and recycling of secondary resources such as NiMH can be used to compensate their limitation [2].

NiMH batteries have five main components: cathode, anode, electrolyte, separator, and steel case. The cathode of these batteries is made of nickel core coated with NaOH and its anode is made of elements such as Ni, Co, and REEs [4].

Rare earth elements (REEs) comprise 17 elements, including 15 lanthanides, Yttrium (Y), and Scandium (Sc), all possessing unique properties. Their separation is challenging due to their similar ionic and atomic radii. In NiMH batteries, REE alloys, such as LaNi$_5$, are used for hydrogen storage, with LaNi$_5$ storing hydrogen as LaNi$_5$H$_6$ in the anodes.

[#] corresponding author: minmabd@modares.ac.ir

Due to the high cost and purity required for lanthanum (La) and nickel (Ni), mischmetal, a mix of rare elements like La, Ce, Nd, Pr, and trace amounts of Tb, Sm, and Y, is commonly used as a substitute for La in steel deoxidation and desulfurization [6].

Failing to extract valuable elements from these secondary sources not only wastes resources but also leads to environmental issues. Therefore, it is essential to develop and study effective processes for recovering valuable elements like rare earths [2].

Various studies have been conducted to recover rare elements from NiMH batteries in the past years. Most of these studies have used two different paths of pyrometallurgy and hydrometallurgy to recover rare elements from this source [3].

Hydrometallurgy is commonly used for metallic element recovery due to its lower energy consumption and reduction of greenhouse gas emissions compared to pyrometallurgy. To minimize environmental pollution from strong mineral acids, research is also focused on using eco-friendly organic acids in this process [5][7]. In the hydrometallurgical process, the black mass a fine powder derived from pre-processed used NiMH batteries (involving fiber and plastic separation, crushing, and sieving) is leached with acid solutions. Research focuses on recovering metals (Ni, Co, Mn) and rare elements. Inorganic acids like H_2SO_4 and HCl are commonly used. For example, Danuza Pereira Mantuano et al. achieved 100% recovery of REE, Ni, Co, Fe, and Mn using 3 M HCl at 95°C with a solid-to-liquid ratio of 1:10 over 2 hours [8]. Also, M.S.

Gasser et al achieved 100% recovery for REEs, 85% for Ni, and 98% for Co using 2 M H_2SO_4 at 25°C, S/L ratio of 1/10 for 2 hours [9]. The next step after obtaining the leach solution of rare elements and others of NiMH batteries is the purification and extraction of rare elements from the solution using different methods such as solvent extraction. For instance, Yun Xia et al. have reported the recovery of 99.98% of rare elements from sulfuric medium under the conditions of A/O = 1.5/1 and pH = 1.5 at 20°C by 5 counter current stages using a N1923 primary amine extractor [10]. Pospiech et al. were able to achieve a high recovery of 95% for rare elements in a sulfuric medium with using Cyanex 272 and Cyphos IL 104 as an extractant and pH = 3.8 [11]. Pingwei Zhang et al., using D2EHPA extractor and kerosene diluent in 2 steps, pH equal to 2, A/O ratio equal to 1/3 in chloride medium, achieved 98% recovery of rare elements [12]. Linyan Li et al. achieved a high recovery of 99% for rare elements from sulfuric medium with the help of 20% P2O4 as an extractant and O/A ratio = 1 and pH = 2.5 [13].

In this article, the extraction of rare earth elements (Ce, La, and Nd) was investigated using D2EHPA, Cyanex 272, and DBC.

EXPERIMENTAL

To explore the extraction of lanthanum, cerium, and neodymium from the pregnant solution derived from the leaching process, as well as the potential for selective separation of these rare elements, experiments were conducted using D2EHPA, Cyanex 272, and DBC extractants. Kerosene was used as a diluent in all solvent extraction experiments, while sodium hydroxide was used to adjust the pH. The leach solution was prepared using sulfuric acid to leach the black mass obtained from spent NiMH batteries.

RESULTS AND DISCUSSION

Nickel-metal hydride batteries were collected from the recycling system at Tarbiat Modares University in Tehran. After separating the fibers and plastics, the internal materials were processed into a 150-micron powder, known as black mass. Leaching experiments were conducted using sulfuric acid to extract rare elements, with conditions set at 3 M sulfuric acid, 85°C, and a 3-hour duration. The recovery rates for cerium, lanthanum, and neodymium were 98.46%, 98.75%, and 98.25%, respectively.

D2EHPA Extractant

Because of separating rare elements from others in the pregnant solution D2EHPA was used.

Table 1 Solvent extraction results and conditions using D2EHPA

Test num.	A/O ratio	Temperature (°C)	Time (min)	Concentration of the extractant (M)	pH	Recovery of neodymium (%)	Recovery of lanthanum (%)	Recovering of cerium (%)
1	1/1	25	30	0.3	2.5	71.25	33.17	33.33

Table 1 shows that D2EHPA did not yield high recoveries for cerium and lanthanum. However, its effectiveness in recovering neodymium suggests it could be used for selective neodymium separation, provided further condition checks and optimizations are performed.

Cyanex 272 Extractant

In order to extract rare elements from the charged solution and the feasibility of separating these elements from each other individually, based on the conditions of the studied articles, experiments were carried out using Cyanex 272. The test conditions and results are given in Table 2.

Table 2 Solvent extraction results and conditions using Cyanex 272

Test num.	A/O ratio	Temperature (°C)	Time (min)	Concentration of the extractant (M)	pH	Recovery of neodymium (%)	Recovery of lanthanum (%)	Recovery of cerium (%)
1	1/1	25	30	0.15	2	75.2	46.54	49
2	1/1	25	30	0.66	3	92	77	85
3	1/1	57	30	0.04	5	99.04	98.4	98.82

The results indicate that Cyanex 272 cannot individually separate lanthanum, cerium, and neodymium from one another; instead, it facilitates their cumulative separation from other impurities. However, under suitable conditions, effective cumulative extraction of rare elements from the pregnant solution can be achieved with appropriate recoveries.

DBC extractant

The DBC extractant was investigated to verify the feasibility of extracting rare elements from the pregnant solution cumulatively or individually if possible. Table 2 shows the results and conditions of the tests performed by DBC.

The solvent extraction experiments using DBC demonstrated its capability to extract rare elements collectively rather than individually, indicating the need for condition optimization to improve recoveries. To explore the synergistic effect of combining two extractants, D2EHPA and DBC, without a diluent, an experiment was conducted as outlined in Table 4. Results in Table 5 confirm a positive synergistic interaction between DBC and D2EHPA, leading to maximum cumulative recovery of rare elements from the leach solution.

Table 3 Solvent extraction results and conditions using DBC

Test num.	A/O ratio	Temperature (°C)	Time (min)	Extractant percentage (%)	pH	Recovery of neodymium (%)	Recovery of lanthanum (%)	Recovery of cerium (%)
1	1/1	25	30	50	1.3	68.7	40.5	34.4
2	1/1	25	30	20	1.3	61.7	23.9	23.5
3	1/1	25	30	100	5	78.05	52.35	55.5

Table 4 Solvent extraction results and conditions using DBC+ D2EHPA

Test num.	A/O ratio	Temperature (°C)	Time (min)	DBC percentage (%)	D2EHPA percentage (%)	pH	Recovery of neodymium (%)	Recovery of lanthanum (%)	Recovery of cerium (%)
1	1/1	25	30	50	50	3	100	97.94	98.76

Table 5 Points used for drawing operating line in the McCabe diagram of cerium, lanthanum, and neodymium elements

Element	x_n	y_{n+1}	x_0	y_1
Cerium	1.3	0	13	36
Lanthanum	2.8	0	28	73
Neodymium	0.4	0	4	15.2

Based on the results in Tables 1 to 4, Cyanex 272 demonstrated the highest efficiency for the cumulative extraction of rare elements from the leach solution. Using Cyanex 272, the McCabe diagrams for cerium, lanthanum, and neodymium (Figures 1 to 3) were plotted to achieve 90% extraction under the conditions detailed in Table 6. Additionally, the operating line in the McCabe diagrams was drawn based on the data in Table 5. X_0 is solute concentration in aqueous feed, Y_1 is solute concentration in extract, X_n is solute concentration in raffinate, and Y_{n+1} is solute concentration in fresh organic feed.

Table 6 Solvent extraction test conditions using Cyanex 272 and their results

Test number	A/O ratio	Temperature (°C)	Time (min)	Concentration of the extractant (M)	pH	Recovery of neodymium (%)	Recovery of lanthanum (%)	Recovery of cerium (%)
1	1/1	25	30	0.66	3	92	77	82
2	1/2	25	30	0.66	3	90	75	80
3	1/3	25	30	0.66	3	82.5	61.78	67.92
4	1/4	25	30	0.66	3	77.5	53.57	58.61
5	1/5	25	30	0.66	3	76	52.14	55.38

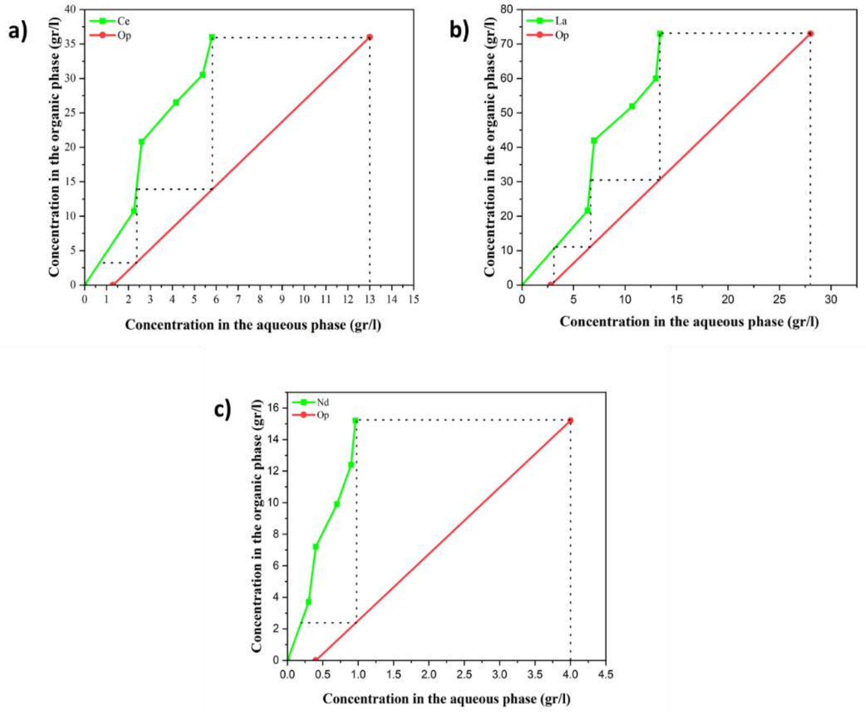

Figure 1 Mc-Cabe diagram a) for the cerium, b) for the lanthanum, c) for the neodymium

Based on McCabe diagrams, achieving 90% recovery requires 2, 3, and 1 extraction steps for cerium, lanthanum, and neodymium, respectively. Stripping tests with sulfuric acid, nitric acid, and hydrochloric acid solutions were conducted on the loaded organic phase, but element recovery during stripping was insufficient, necessitating further research.

CONCLUSIONS

Attempts to separate rare earth elements from impurities in the leach solution were made using D2EHPA, Cyanex 272, and DBC extractants. While none could selectively separate rare elements, they successfully extracted all three elements under optimized conditions. A mixture of DBC and D2EHPA showed a synergistic effect, achieving recoveries of 98.76% for cerium, 97.94% for lanthanum, and 100% for neodymium. According to the McCabe-Thiele diagram, 3, 2, and 1 extraction steps are required with Cyanex 272 to achieve 90% recovery for cerium, lanthanum, and neodymium, respectively. However, stripping experiments using sulfuric, nitric, and hydrochloric acids yielded unsatisfactory results, highlighting the need for further research.

ACKNOWLEDGEMENT

The support from Tarbiat Modares University is gratefully acknowledged.

REFERENCES

1. M. Assefi, S. Maroufi, Y. Yamauchi, and V. Sahajwalla, “Pyrometallurgical recycling of Li-ion, Ni–Cd and Ni–MH batteries: A minireview,” *Curr. Opin. Green Sustain. Chem.*, vol. 24, pp. 26–31, 2020.
2. H. Zhi, S. Ni, X. Su, W. Xie, H. Zhang, and X. Sun, “Separation and recovery of rare earth from waste nickel-metal hydride batteries by phosphate based extraction-precipitation,” *J. Rare Earths*, vol. 40, no. 6, pp. 974–980, Jun. 2022, doi: 10.1016/J.JRE.2021.04.012.

[3. M. K. Jha *et al.*, “Recovery of rare earth metals (REMs) from nickel metal hydride batteries of electric vehicles,” *Minerals*, vol. 12, no. 1, p. 34, 2021.

4. N. K. Ahn, H. W. Shim, D. W. Kim, and B. Swain, “Valorization of waste NiMH battery through recovery of critical rare earth metal: A simple recycling process for the circular economy,” *Waste Manag.*, vol. 104, pp. 254–261, Mar. 2020, doi: 10.1016/J.WASMAN.2020.01.014.
5. A. A. L. Marins, L. M. Boasquevisque, E. J. B. Muri, and M. B. J. G. Freitas, “Environmentally friendly recycling of spent Ni–MH battery anodes and electrochemical characterization of nickel and rare earth oxides obtained by sol–gel synthesis,” *Mater. Chem. Phys.*, vol. 280, p. 125821, 2022.
6. D. Kołodyńska, D. Fila, B. Gajda, J. Gęga, and Z. Hubicki, “Rare Earth Elements—Separation Methods Yesterday and Today,” *Appl. Ion Exch. Mater. Environ.*, pp. 161–185, 2019.
7. P. Meshram and Abhilash, “Recovery and recycling of cerium from primary and secondary resources-a critical review,” *Miner. Process. Extr. Metall. Rev.*, vol. 41, no. 4, pp. 279–310, 2020.
8. D. P. Mantuano, G. Dorella, R. C. A. Elias, and M. B. Mansur, “Analysis of a hydrometallurgical route to recover base metals from spent rechargeable batteries by liquid–liquid extraction with Cyanex 272,” *J. Power Sources*, vol. 159, no. 2, pp. 1510–1518, 2006.
9. M. S. Gasser and M. I. Aly, “Separation and recovery of rare earth elements from spent nickel–metal-hydride batteries using synthetic adsorbent,” *Int. J. Miner. Process.*, vol. 121, pp. 31–38, Jun. 2013, doi: 10.1016/J.MINPRO.2013.02.012.
10. X. I. A. Yun, X. Liansheng, T. Jiying, L. Zhaoyang, and Z. Li, “Recovery of rare earths from acid leach solutions of spent nickel-metal hydride batteries using solvent extraction,” *J. rare earths*, vol. 33, no. 12, pp. 1348–1354, 2015.

11. B. Pospiech and J. Gega, “Solvent extraction of metal ions from sulfate solutions obtained in leaching of spent Ni-MH batteries,” *New Trends Prod. Eng.*, vol. 2, no. 2, pp. 214–221, 2019.
12. P. Zhang, T. Yokoyama, O. Itabashi, Y. Wakui, T. M. Suzuki, and K. Inoue, “Hydrometallurgical process for recovery of metal values from spent nickel-metal hydride secondary batteries,” *Hydrometallurgy*, vol. 50, no. 1, pp. 61–75, 1998.
13. L. Li, S. Xu, Z. Ju, and F. Wu, Recovery of Ni, Co and rare earths from spent Ni-metal hydride batteries and preparation of spherical Ni (OH) 2,*Hydrometallurgy*, 100, 1-2, 41-46, 2009.

XVI International Mineral Processing
and Recycling Conference
28-30 May 2025, Belgrade, Serbia

DOI: 10.5937/IMPRC25522B Original research article

LOW-TEMPERATURE ATMOSPHERIC PLASMA IN THE COMPLEX PROCESSING OF HARD-BENEFICIATION MINERAL RAW MATERIALS

Igor Zh. Bunin#, 0000-0002-8618-5119,
N.V.Melnikov's Institute of Comprehensive Exploitation of Mineral Resources
Russian Academy of Sciences, Moscow, Russia

ABSTRACT – This report provides a brief overview of the main results of theoretical and experimental studies of the processes for the induced structural modification of the surface state, physicochemical and technological properties of non-ferrous and noble metals minerals when exposed to high-power electromagnetic pulses and discharge low-temperature plasma. The main results obtained to date in the field of application of low-temperature plasma from a high-power (high-voltage) pulsed-periodic nanosecond spark discharges (HPEMP) and dielectric barrier discharge (DBD) in air under normal conditions in mineral processing processes reviewed. The high efficiency and possible restrictions of application of the pulsed energy impacts and low-temperature plasma treatment of geomaterials (minerals, rocks and ores) are demonstrated in order to improve the processing efficiency of the difficult-to-enrich mineral raw materials.

Keywords: Sulfide Minerals, Low-Temperature Plasma, Disintegration, Flotation.

INTRODUCTION

In the primary processing of refractory ores and anthropogenic mineral feeds, a significant share (30–35%) of valuable mineral loss is associated with mineral intergrowth (up to 40%) and fine (finer than 10 µm) particles Chanturiya [1]. Energy costs for grinding range from 30 to 60 kWh per 1 t and higher [1,2]. To opening finely disseminated mineral complexes, in addition to state-of-the-art grinding technology, pulsed-power (non-mechanical) selective disintegration methods are promising, providing disintegration along interphase boundaries through the formation of intergranular microcracks, electrical breakdown channels, and other types of defects as a result of exposure to high-energy radiation of various physical origins on the geomaterials [1–3]. To achieve maximum efficiency of selective disintegration of finely disseminated mineral complexes of non-ferrous, rare and noble metals, as well as surface modification controlled change (chemical modification) of the surface properties of minerals, extensive research has been carried out on the applications of energy impacts, such as mechanochemical, ultrasonic, radiation [2,4], electrochemical [1,3,5], electropulse-discharge [3,6,7], and plasma [8–11] impacts.

The aim of this work was to briefly comparatively analyze the impact of two types of nonequilibrium electrical discharges (high-power electromagnetic pulse (HPEMP [1,3,5,12]) and dielectric barrier (DBD [9–11,13]) discharges in air at atmospheric

---

corresponding author: bunin_i@mail.ru

pressure) have on the structural state, mechanical (microhardness), and physical chemical surface properties of the target minerals from sulfide ores of non-ferrous and noble metals and some other types of refractory ores.

EXPERIMENTAL

In our comprehensive studies the electromagnetic discharges pulsed treatment of mineral samples was carried out on original laboratory generators equipments (ICEMR RAS; FON, Ryazan). The conditions for processing of mineral samples by high-voltage nanosecond pulses are given in [14]; the parameters of the generator of high-voltage sub-nanosecond pulses initiating a dielectric barrier discharge in air at atmospheric pressure are given in [15].

The nanosecond electromagnetic pulse generator (HPEMP) operates at a frequency of 100 Hz (pulse repetition rate), the output pulse amplitude is ~25 kV, the duration of the leading edge of the pulse varies from pulse to pulse within 2-5 ns, and the pulse duration varies within 4-10 ns. Video pulses of a bipolar shape are generated, pulse energy ~0.1 J, electric field strength in the inter-electrode gap is $(0.5\text{-}1)\times 10^7$ V/m, time range of the pulsed treatment of the mineral samples is $t_{\text{treat.}}$=10-150 s.

We consider different modes of the existence and development of a dielectric barrier discharge (DBD) and low-temperature DBD plasma (LTP-DBD) upon a change in applied stress and the frequency of pulse repetition. We establish the following operating parameters of pulses that initiate a discharge at which the greatest changes in the structural-sensitive properties of minerals are observed: the length of the leading edge of a pulse is ~300 ns, the length of pulse is 8 µs, the electrode voltage in the barrier discharge cell is 20 kV, and the frequency of pulse repetition is 15 kHz. The range of change in the duration of the DBD-treatment of the samples is $t_{\text{treat.}}$=10-150 s. The flow of a discharge current in a discharge cell was limited by one dielectric layer, and the sizes of the electrodes exceeded the length of the inter-electrode space (~5 mm). In the process of the low-temperature plasma processing of minerals, the gas temperature in the working zone of the discharge cell of the barrier discharge did not exceed the temperature of the dielectric barrier and remained on the order of room temperature during 10-60 s.

RESULTS AND DISCUSSION

High-power electromagnetic pulses and pulse-periodic high-voltage discharges

The main idea of using high-energy effects (pulsed-power technologies) to improve the processing efficiency of the difficult-to-enrich mineral raw materials is to selectively break up mineral intergrowths and provide free access of lixiviant solutions to finely dispersed precious metal particles. This technique creates proper conditions for maximum concentration of mechanical stresses or energy promoting host rock disintegration sufficient for effective "unsealing" of valuable components. The application of *nonthermal* [16] HPEMP effect in dressing of resistant polymetallic ores (for example, sulfide gold-bearing ores) appears attractive as this technique results in a selective disintegration of the fine disseminated mineral complexes through the creation of electrical breakdown channels and intergranular microcracks, a significant increase in precious metal recovery, helping reduce both energy consumption and the cost of products [1,3,5,12]. When exposed to HPEMP, effective softening of finely disseminated mineral complexes and selective unlocking of mineral intergrowths is achieved due to the following mechanisms [3,5,12]: - formation of electrical breakdown channels in the host mineral matrix containing micro- and nanoparticles of valuable components, and the formation of zones of induced fracturing around the channels as these grow in the mineral medium; - cracking of mineral aggregates due to the occurrence of thermomechanical stresses at the boundaries of intergrowth of mineral components with different thermal and electrical properties during local pulsed heating; - absorption of the energy of pulsed electromagnetic radiation by particles of noble metals and semiconductor ore minerals carriers (skin effect) [3], as well as in the process of autoelectronic emission from the surface of sulfides [17].

The electrical strength of minerals can significantly (by tens of times) decrease due to the presence of inhomogeneities (microdefects), especially in the form of electrically conductive microimpurities (such as micro- and nanoparticles of noble metals), which greatly facilitates the development of breakdown channels due to an increase in the electric field strength in the areas of localization of inhomogeneities. Therefore, the formed channels will predominantly bind metal impurities to each other and to the surface, which significantly increases the efficiency of subsequent processing of mineral samples with chemical agents. Effective damage to the treated material occurs if the total energy released in an individual particle is sufficient to sublimate the substance in the breakdown channel (the transition of a substance to a plasma-like state), and the time during which it is released is significantly less than that required for heat transfer and heat dissipation in the surrounding areas. For the formation of a sufficient number of channels, the action of a large number of pulses is required (N_{imp}=10^3–10^4). With repeated exposure to partial discharges in solid dielectrics, due to the development of dissipative processes, dendrites are formed tree-like fractal structures, whose branches are areas of discontinuity (damage) in the material destroyed from pulse to pulse.

The theoretical inferences were proved by commercial tests (ICEMR RAS and TSNIGRI), the maximal exposure of gold-bearing products under the HPEMP effect is supposed for sulfides less 200 – 100 µm in size, and the effect of the breakdown channel formation and selective disintegration increases when the wet feed is treated. The available porous moisture with acid and alkaline reaction positively influences the HPEMP treatment efficiency, intensifies the opening of a rebellious material. The noble metal (Au, Ag) recovery increment ranges from 2 to 40 % depending on a raw material type at the reduced power consumption [3]. The using of technological gold-bearing samples pre-treatment by HPEMP with nanosecond front and duration results in a gold recovery increase during cyanidation of rebellious ores by 4 – 12 % as a whole, by 10 – 30 % for gravity concentrates, 5 – 45 % for flotation concentrates, by 30 – 80 % from tailings of concentration mills.

The pulsed-periodic nanosecond discharges treatment of fine disseminated Au and PGM-bearing ores provides the maximum effect when is applied prior to fine ore grinding processes, followed by flotation process or gravity concentration of raw mineral materials in Knelson concentrator. The recovery increments (%) for platinum, palladium and gold at all three tests (min – max): Pt 32.37 – 66.86; Pd 12.09 – 52.18; Au 11.2 – 74.75 were gained for the products of copper-nickel ore processing (Krasnoyarsk region deposit), processed in Knelson gravity concentrator with regard to the modes of the preliminary HPEMP treatment followed by mechanical grinding. The maximum noble-metal recovery increment (in Knelson concentrator) has been obtained under the HPEMP effect (1.6 s), followed by 15 min grinding. The increase in the noble-metal recovery deals with no increase in the product yield, but with the higher grade parameter (*K* is the metal concentrating coefficient), which is calculated as a ratio of metal content in a product after separation and metal content in a feed. The principal effect of the recovery increment for Au and PGM due to the maximum mineral opening along the joint boundaries, namely, due to the sharp reduction in number of mineral aggregates (joints) because a variety of electric breakdown channels are formed and the host mineral matrix weakens under the local contrast heating [3].

According to microhardness and spectroscopic studies (FTIR) [5,14], exposure to nanosecond HPEMP causes a decrease in the microhardness (Vickers, HV) of the rock-forming minerals of kimberlite rock—calcite, olivine, serpentine —by 40-66%, and in quartz, nepheline, aegirine, field spars (eudialyte concentrate minerals) by 30% due to the breakage of chemical bonds and microstructure of surface layers, formation of defects at various structural levels (dislocations, microcracks, incomplete surface microbreakdowns), disordering and amorphization of the surface. The effect of weakening of the rock-forming minerals of diamond-bearing kimberlites when exposed to HPEMP can be relevant to ensuring the integrity of diamond crystals in ore grinding processes by reducing the residence time of kimberlite rock in autogenous mills [14].

The nonthermal action of HPEMP starts physicochemical processes (solid-phase chemical reactions) on the surface of sulfide minerals involving the formation of micro- and nanophases in the form of hydrophobic elemental sulfur and various hydrophilic oxygen-containing compounds, which increases the selectivity of the flotation process of sulfides with similar physical and chemical properties [1,5,12,17]. The processes of gas outflow from channels of nanosecond breakdown of semiconductor ore minerals (sulfides, oxides), condensation of matter in the outflowing jet and its deposition on the mineral surface determine one of the possible mechanisms of structural-chemical modification of the surface of earth materials as a result of electromagnetic pulse treatment. When a gas jet exits the breakdown channel into air of normal density, the jet expands, cools down, and conditions form for vapor condensation. As a result of deposition of condensation products, the structural and chemical state of the surface of minerals changes. Another mechanism established in [5,18,19], for the changes in the structural, physicochemical, and process properties of semiconductor ore minerals under the action of nanosecond HPEMPs is the process of direct oxidation of the surface of minerals. This occurs with the active participation of *ozone* formed in interparticle spark electric discharges and/or dissolved in a thin film of water on the surface of mineral particles, with the emergence of insoluble and water-soluble surface formations. The non-thermal effect of nanosecond HPEMP on sulfide minerals causes a contrast change at the micro- and nanostructural level in the chemical and phase composition of the surface of sulfides with similar physical and chemical properties ("pyrite-arsenopyrite", "pyrrhotite-pentlandite", chalcopyrite, and sphalerite), electrophysical, electrochemical, sorption, and flotation properties of the minerals. As a result of short-term ($t_{\text{treat.}}$=5 or 10-30 s) electromagnetic pulse pretreatment, the recovery of pyrite, pentlandite, chalcopyrite, and sphalerite into the flotation froth increased by 10–20% compared to the reference samples, while for arsenopyrite and pyrrhotite, on the contrary, it decreased by 10–15%.

Dielectric barrier discharge low-temperature plasma modification of geomaterials

A dielectric barrier discharge (DBD) is a discharge in which the current flow is limited by at least one dielectric layer and the typical dimensions of the electrodes significantly exceed the interelectrode gap [13]. The dielectric prevents the flow of direct current in the system, so harmonic or pulsed supply voltage is usually used to initialize and maintain the discharge [10,11,13,15].

For practical applications, the problem of obtaining a diffuse discharge [20] in air at atmospheric pressure is relevant, as it is more efficient and convenient, since in this case the effect of the barrier discharge plasma spreads uniformly over the largest possible area. During the experiments on the low temperature (LTP-DBD) plasma minerals treatment, the mineral particles were affected by the following factors: a high-strength pulsed electric field, ionic wind, and low-temperature plasma (LTP) products in the form of chemically active compounds, such as ozone O_3, singlet oxygen O_2 ($a^1\Delta_g$), H_2O_2, OH, and nitrogen oxides, as well as the electric charge transfer to the surface of the sample and an increase in the temperature of the dielectric barrier occurred [13,15,21].

The main mechanism of change in the morphology and structural state of the sulfides surface under the influence the effective factors of dielectric barrier discharge (DBD) action, is the destruction of the microcrystalline structure of the mineral surface layers in the process of electrical destruction of thin films (most likely, oxides and hydroxides of metals); this process manifests itself as plasma cleaning of the mineral particles surface from films and secondary phases. In [22] we observed the largest changes in the electrode potential of pyrrhotite (the titration at pH 9.5-12) as a result of short-term plasma mineral pretreatment (t_{treat}.= 10 s). The shift of the electrode potential of pyrrhotite to the region of negative values (–60 mV) occurred, which caused the effect of a decrease in its sorption and flotation activity (depression). This fact is very significant for the selective separation (recovery) of pyrrhotite from sulfide copper-nickel ores.

A mechanism is proposed for modifying the acid-base properties of pyrite and arsenopyrite surface as a result of exposure to low-temperature plasma of a dielectric barrier discharge (DBD–LTP) in air under normal conditions. In [10] we found that plasma treatment strengthens acceptor properties and weakens electron donor properties of pyrite surface, as well as weakens acceptor properties of arsenopyrite. As a result, the adsorptive properties of pyrite relative to the electron-donor butyl xanthate grow, and, as a consequence, the flotation activity of the mineral improves. In the case of arsenopyrite, the adsorptive properties and flotation activity decrease. Shortterm plasma pretreatment of minerals ($t_{\text{treat.}}$= 30–40 s) resulted in an increase in the selectivity of flotation separation of pyrite and arsenopyrire. In conditions of monomineral flotation, the difference in the recovery of minerals into flotation froth was ~57% (without plasma pretreatment—19%).

CONCLUSION

Low-temperature plasma (HPEMP or DBD in air) processing of geomaterials is a suitable method for adjusting the floatability of sulfide minerals (in particular, iron sulfide minerals). The improved floatability and the differences in the process properties of sulfide minerals can improve the performance of the efficiency of processing of low-grade copper-nickel and refractory pyrite-arsenopyrite gold-bearing ores. Our results testify to practicability and potential of using comparatively brief ($t_{\text{treat.}}$= 10-30 s) atmospheric pressure discharge plasma treatment (HPEMP, DBD) in air under standard conditions for the selective disintegration of fine disseminated mineral complexes and structural chemical modification of the physicochemical properties of target minerals from sulfide ores of non-ferrous and noble metals.

REFERENCES

1. Chanturiya, V.A. (2017) Scientific substantiation and development of innovative approaches to integrated mineral processing. Gornyi Zhurnal, (11), 7-13.
2. Rostovtsev, V.I. (2019) Change of elastic wave velocity in granite after radiation exposure and prospects for energy consumption reduction in ore pretreatment. J. Min. Sci., 55 (2), 333-338.
3. Chanturiya, V.A., Bunin, I.Zh. (2007) Non-traditional high-energy processes for disintegration and exposure of finely disseminated mineral complexes. J. Min. Sci., 43 (3), 311-330.
4. Kondrat’ev, S.A., Rostovtsev, V.I., Bochkarev, G.R. et al. (2014) Justification and development of innovative technologies for integrated processing of complex ore and mine waste. J. Min. Sci., 50 (5), 959-973.
5. Bunin, I.Zh., Ryazantseva, M.V., Samusev, A.L., Khabarova, I.A. (2017) Composite physicochemical and energy action on geomaterials and aqueous slurries: Theory and practice. Gorn. Zhurnal, (11), 77-83.
6. Huang, W., Chen, Y. (2021) The application of high voltage pulses in the mineral processing industry – A review. Powder Technol., 393, 116-130.
7. Qin, Y., Han, Y., Gao, P., Li, Y., Yuan, S. (2021) Pre-weakening behavior of magnetite quartzite based on high-voltage pulse discharge. Miner. Eng., 160, 106662.
8. May, F., Hamann, S., Quade, A., Brüser, V. (2017) Froth flotation improvement by plasma pretreatment of sulfide minerals, Min. Eng., 113 (11), 95-101.
9. Ran, J., Li, Yu., Zong, M., Xu, H., end al. (2023) Flotation separation of pyrite from arsenopyrite by surface discharge plasma modification. Separation and Purification Technol., 314, 123579.
10. Chanturiya, V.A., Bunin, I.Zh., Ryazantseva, M.V. (2023) The low-temperature plasma effect of dielectric barrier discharge on physicochemical and process properties of natural iron sulfides. J. Min. Sci., 59 (4), 621–627.
11. Ran, J., Sun, M., Ji, P., et al. (2025) Effects of mineral species transformation driven by surface dielectric barrier discharge plasma modification on the flotation performances: Perspective of critical oxidation degree. Adv. Powder Technology, 36 (4), 104832.
12. Chanturiya, V.A., Bunin, I.Zh., Ryazantseva, M.V., Filippov, L.O. (2011) Theory and application of high-power nanosecond pulses to processing of mineral complexes. Mineral Processing and Extractive Metallurgy Review, 32 (2), 105-136.

13. Avtaeva, S.V. (2011) Barrier Discharge. Research and Application. Lambert Academic Publishing, Saarbrücken, Germany.
14. Bunin, I.Zh., Chanturiya, V.A., Anashkina, N.E., Ryazantseva, M.V. (2015) Experimental validation of mechanism for pulsed energy effect on structure, chemical properties and microhardness of rock-forming minerals of kimberlites. J. Min. Sci. 51(4), 799-810.
15. Bunin, I.Zh., Chanturiya, V.A., Ryazantseva, M.V., Koporulina, E.V., Anashkina, N.E. (2020) Changes in the surface morphology, microhardness, and physicochemical properties of natural minerals under the influence of a dielectric barrier discharge. Bull. Russ. Acad. Sci. Phys., 84 (9), 1161-1164.
16. Cherepenin, V.A. (2006) Relativistic multiwave oscillators and their possible applications. Phys. Usp., 49 (10), 1097-1102.
17. Chanturiya, V.A., Bunin, I.Zh., Kovalev, A.T. (2007) On the field-emission properties of sulfide minerals under high-power nanosecond pulses. Bull. Russ. Acad. Sci. Phys., 71 (5), 646-649.
18. Chanturiya, V.A., Ivanova, T.A., Khabarova, I.A., Ryazantseva, M.V. (2007) Effect of ozone on physico-chemical and flotation properties of surface of pyrrhotite under the nanosecond electromagnetic pulse treatment. J. Min. Sci., 43 (1), 83-90.
19. Ivanova, T.A., Bunin, I.Zh. Khabarova, I.A. (2008) On the characteristic properties of oxidation of sulfide minerals exposed to nanosecond electromagnetic pulses. Bull. Russ. Acad. Sci. Phys., 72 (10), 1326-1329.
20. Renev, M.E., Safronova, Y.F., Stishkov, Y.K. (2021) Specific features of the structure of a diffuse barrier discharge. High. Temp.,. 59 (1), 27–35.
21. Bobkova, E.S., Khodor, Y.V., Kornilova, O.N. et al. (2014) Chemical composition of plasma of dielectric barrier discharge at atmospheric pressure with a liquid electrode. High. Temp. 52 (4), 511–517.
22. Bunin, I.Zh., Khabarova, I.A. (2022) Study of the effect of dielectric-barrier discharge on the surface morphology and physical-chemical properties of pyrrhotite and chalcopyrite. J. Surf. Investig., 16 (5), 281-284.

XVI International Mineral Processing
and Recycling Conference
28-30 May 2025, Belgrade, Serbia

DOI: 10.5937/IMPRC25529P

Original research article

THE STUDY ON THE STRESS CHARACTERISTICS OF BACKFILL BARRICADE IN UNDERGROUND METAL MINES BASED ON SIMULATION EXPERIMENTS

Xiaopeng Peng#**,** 0000-0002-3635-2062,
Lijie Guo, 0000-0003-4355-3038,
Xingshan Jin, 0009-0001-1508-0950,
BGRIMM Technology Group, Beijing, China

ABSTRACT – With the widespread adoption of the backfill mining method in metal mines, the barricade wall, as a crucial structure for stope stability control, has its drainage performance and spatial placement significantly influencing structural stability. This study utilizes a self-developed force simulation device for backfill walls to systematically conduct mechanical tests on non-cemented backfill walls under various installation positions and drainage conditions. The results indicate that non-cemented slurry conforms to the ideal fluid model under undrained conditions, with lateral pressure distribution closely matching the hydrostatic pressure theory. Optimized drainage design can reduce lateral pressure by 70% and accelerate the dissipation process of pore water pressure. For drainage walls, their installation position can significantly regulate lateral pressure; when adjacent to the stope (entry), the peak lateral pressure reaches 73.18 kPa (under 80 kPa loading pressure), which is a 35.43% increase compared to the condition at the end of the entry. This research reveals the load transfer mechanism and pressure evolution 规律 of non-cemented walls, providing theoretical support for mine safety protection design.

Keywords: Metal Mine, Backfill Barricade, Installation Position of Barricade, Drainage Performance of Barricade, Lateral Pressure.

INTRODUCTION

In the process of underground backfill mining, to stop the leak of backfill slurries in stopes, it is necessary to construct a backfill barricade at an appropriate location in the extraction drift, preventing slurries from flowing into the roadway [1,2]. Due to its supporting role, the instability of backfill barricade poses a series of threats to the safety of backfill mining. In 2000, a wall failure at the Bronzewing mine in Western Australia resulted in three fatalities [3,4]. A year later, two backfill wall failures at the Osborne mine caused extensive underground production shutdowns [5]. In 2021, two wall collapse accidents occurred in the Jinchuan mining area of China, leading to a large-scale flow of backfill slurry into the roadways, causing significant economic losses. Thus, it is evident that ensuring the stability of the backfill barricade is crucial for mine safety.

To analyze the stability of the backfill barricade, it is necessary to investigate the forces exerted by the backfill slurry on the wall during the backfilling process [6,7].

---

corresponding author: pengxiaopeng@bgrimm.com

Comparing to the theoretical study of the forces analysis on the wall, conducting model test research is a more precise approach to accurately understand the forces exerted on the barricade [8,9]. Widisinghe et al. [10] established a backfill loading system based on a cylindrical stope model (310mm in diameter × 465mm in height), using soil pressure gauges to measure the vertical stress at the bottom and the horizontal stress in the roadway, and validated the pressure distribution pattern of the barricade wall through analytical equations. Although this experiment revealed the pressure response characteristics of the barricade under different loads, it did not consider the influence of drainage conditions on the evolution of lateral pressure on the wall. Nujaim et al. [11] conducted a physical model experiment on waste rock backfill barricade based on the principle of qualitative similarity. The results showed that the stability of waste rock barricade depends on factors such as the particle size distribution (PSD) of the waste rock, the degree of compaction, and the frictional resistance between the barricade and the sidewalls. However, the experiment did not consider the impact of the installation position on its lateral pressure. Wang et al. [12] constructed a large-scale in-situ characteristic simulation device (1500×500×1600mm) to systematically monitor the dynamic evolution of parameters such as pore water pressure and effective stress during the curing process of cemented tailings backfill. However, the barricade was not installed during the experiment, which meant the results could not reflect the lateral pressure exerted on the wall.

In light of the aforementioned research background, this study intends to utilize a simulation test apparatus for the stress on backfill barricade. With the permeability of the wall and its installation position as variables, it aims to conduct simulation research on the stress experienced by walls during uncemented backfilling processes, exploring the spatiotemporal evolution patterns of key indicators such as lateral pressure and pore water pressure on the walls. By systematically investigating the stress mechanisms on walls under different working conditions, the study seeks to provide guidance for the design of backfill barricade and offer scientific basis for safe and efficient mine backfilling.

EXPERIMENTAL

Simulation test apparatus

The simulation test apparatus for the stress on backfill barricade is designed to simulate the stress state of barricade during the mine backfilling process, providing theoretical experimental parameters for the design of barricades. This apparatus comprises a pressure control unit, a stope simulation unit, a drift simulation unit, a wall drainage unit, and a data acquisition system. It is capable of adjusting loading pressure, wall position, and wall drainage capacity to simulate various backfilling conditions, as illustrated in Figure 1. The pressure control unit achieves dynamic pressure regulation through hydraulic cylinders and a manual pump. The stope simulation unit and the drift simulation unit mimic the stope and ore extraction drifts, respectively. The wall drainage unit simulates different types of walls. The data acquisition system monitors and records data from various sensors in real-time, ensuring the accuracy and reproducibility of the experimental results. The overall structure of the test apparatus is stable and well-sealed, capable of meeting the research needs for stress analysis under different backfilling conditions, and it exhibits excellent corrosion resistance and mechanical performance.

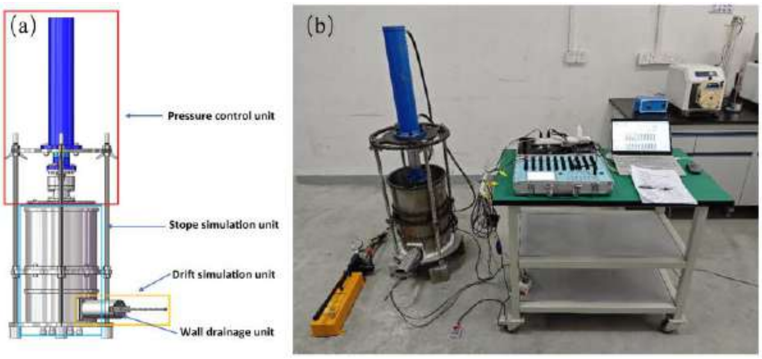

Figure 1 Schematic diagram of the mechanical simulation test device for filled barricade a) Design Schematic; b) Physical Prototype Image

Test Materials and Sensors

The test materials include tailings from a copper mine as the aggregate and tap water for slurry preparation. The tailings were first subjected to particle size analysis using a Mastersize 2000 laser particle size analyzer. The results show that the fine particles, which are below 74 μm, account for 55.45%, while coarse particles, which are above 0.25 mm, make up 3.26%, indicating a gradation characteristic dominated by fine particles with a small number of coarse particles.

For monitoring the pressure on the barricade wall during the test, vibrating wire earth pressure cells were used as sensors. High-precision miniature pore water pressure sensors were employed to monitor the pore water pressure of the slurry. The data collected by the sensors were recorded using a static data acquisition instrument, model DM-YB1820.

Experimental Design

Mix Recipe Design of Backfill Slurry

The volume of the stope simulation unite was calculated to be 36.13 L based on its structural parameters. In accordance with the concentration control requirements of 70%-72% for subsequent backfilling processes at a certain copper mine, the study was conducted using a backfill slurry with a mass concentration of 70%. Through systematic experimental verification, it was found that when the amount of backfill slurry added was 50 kg, it not only meets the filling requirements of the setup's volume but also effectively avoids safety hazards caused by overfilling.

Loading Pressure Design

This study simulated the dynamic changes in wall stress during the backfilling process using the simulation test apparatus. Based on the typical stope parameters of the certain copper mine (size 70 m×20 m×60 m, backfill flow rate 120 m^3/h, assuming continuous backfilling throughout the day) after calculation, the average daily backfill height is about 2 m. Therefore, the maximum loading pressure applied each time was set to be approximately 40 kPa through weight calculation. The experiment simulated the above-mentioned stepwise gradient loading strategy, setting the loading pressure to increase stepwise with equivalent backfill days, exploring the cumulative effect of bottom pressure caused by the rising backfill height in the stope.

Installation Position and Drainage Conditions Design

According to the length of the drift simulation unit, which is 20 cm, the installation position of the barricade wall can be divided into the drift entrance (near the stope end), the middle of the drift (10 cm from the drift entrance), and the end of the drift (20 cm from the drift entrance), which can be illustrated as the following Figure 2.

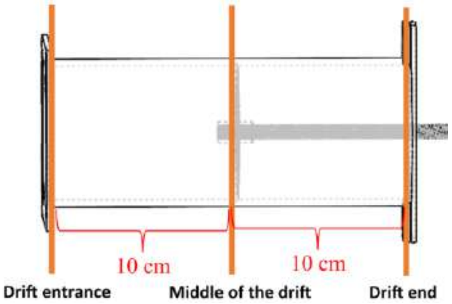

Figure 2 Schematic diagram of barricade l installation location

A detailed classification of the drainage of barricade walls was conducted, aiming to assess the variation patterns of lateral pressure on the walls under different drainage conditions. Based on the efficiency of drainage, this study categorizes the walls into three types: walls without an active drainage (i.e., non-draining), walls with basic horizontal drainage capability (i.e., moderately draining), and walls with high-efficiency drainage capability (i.e., well-draining), as illustrated in Figure 3. Among these, the "moderately draining" walls are equipped with 19 drainage holes each with a diameter of 3 mm, whereas the "well-draining" walls have the number of drainage holes increased to 32, all maintaining a diameter of 3 mm, to achieve superior drainage performance.

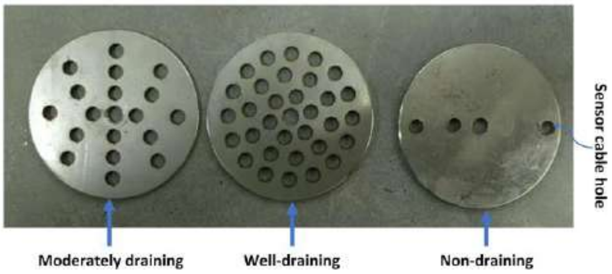

Figure 3 Schematic diagram of barricade walls with varying degrees of drainage filling

RESULTS AND DISCUSSION

Barricade stress under different drainage conditions

In mine backfilling, the drainage performance of barricade walls significantly facilitates the consolidation and hydration hardening processes of the backfill slurry, while also exerting a crucial impact on the stability and safety of the walls. Figure 4 shows the lateral pressure exerted by the backfill slurry on barricade walls under different drainage conditions.

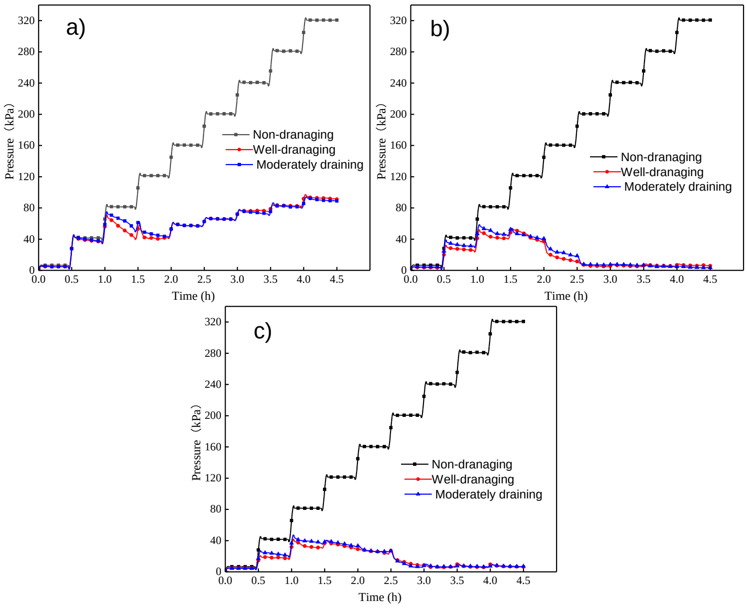

Figure 4 Lateral pressure on barricade walls with different drainage conditions: a) Barricade installed at the drift entrance; b) Barricade installed at middle of the drift; c) Barricade installed at the drift end

As shown in Figure 4, the lateral pressure on the barricade wall is significantly influenced by the drainage conditions. Under non-draining conditions, the lateral pressure increases linearly with the loading pressure, and its value is significantly higher than that under draining conditions. This indicates that the lack of drainage prevents the backfill from dehydrating and solidifying, causing the hydrostatic pressure to be fully transmitted to the wall, resulting in a "full load transfer" state. Under moderate draining conditions, the rate of pressure increase is significantly reduced, with the final pressure reaching 97.65 kPa (a 69.5% reduction compared to non-draining conditions), and the pressure increase on the wall slows down after the loading pressure exceeds 160 kPa. Under well-draining conditions, the final pressure is 96.96 kPa, and after the loading pressure exceeds 160 kPa, the increase is only 36 kPa (a 70% reduction compared to non-draining conditions).

During the rising phase of pressure (before 1.5 h), the lateral pressure under moderate draining conditions is generally higher than that under well-draining conditions, a phenomenon particularly evident in walls installed in the middle and end of the drift. For walls at the drift entrance, the pressure difference between the two drainage conditions is smaller, mainly because walls at the drift entrance directly bear the combined effects of high hydrostatic pressure, dynamic water pressure, and expansion force from the stope side, resulting in similar total stress values monitored by the sensors.

During the pressure decline phase (after 1.5 h), walls with well drainage exhibit more pronounced pressure decay characteristics. Superior drainage performance can quickly dissipate internal pore water pressure, thereby accelerating the overall pressure decline. The pressure change during this phase shows a dual-stage characteristic: an initial linear decline due to the continuous discharge of pore water, followed by a nonlinear change closely related to the alteration in pore water pressure caused by further compaction of the tailings.

Barricade stress under different installed positions

This section will explore the variation patterns of lateral pressure on barricade walls at different installation positions (the drift entrance, the middle of the drift, and the drift end respectively) based on a series of experimental data, as illustrated in Figure 5.

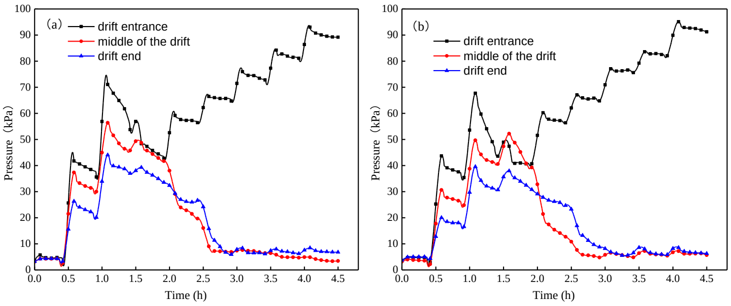

Figure 5 Lateral pressure on barricade walls installed at different locations: a) Barricade walls with moderate drainage conditions; b) Barricade walls with well drainage conditions

As can be seen from Figure 5, when the barricade wall is installed at the drift entrance, its pressure initially increases and then decreases in response to the loading pressure: in the initial stage, the pressure rises synchronously with the loading pressure, decreases due to the dissipation of hydrostatic pressure during drainage, and then resumes a steady increase with the loading pressure. In contrast, the pressure evolution of walls in the middle and at the end of the drift exhibits a three-stage characteristic of "increase-decay-stabilization," eventually reaching an equilibrium state.

Data from Figure 5a show that when the loading pressure reaches 80 kPa, the peak pressure on the wall at the drift entrance reaches 73.18 kPa, while the pressures on walls in the middle and at the end of the drift decrease to 56.85 kPa (a 22.28% reduction) and

47.25 kPa (a 35.43% reduction), respectively. This phenomenon indicates that as the distance between the wall and the stope increases, the lateral pressure exhibits a dual characteristic of numerical decrease and fluctuation attenuation. Mechanistic analysis reveals that the area adjacent to the stope forms a stress arch effect due to tailings settlement, concentrating the load towards the wall, and is significantly influenced by the dynamic changes in pore water pressure induced by mining activities. As the distance increases, the tailings achieve stress redistribution through particle friction and cohesion, reducing the influence range of the arch effect and making the lateral pressure more uniform and stable.

When the external load increases to 240 kPa (3.0 h), walls at different positions show differentiated responses: the pressure on the wall at the drift entrance increases by about 25% (corresponding to 10 kPa) for every 40 kPa increase in load, while the pressures on walls in the middle and at the end of the drift stabilize at around 8 kPa. This indicates that walls farther from the stope have better load buffering performance, suggesting that in engineering practice, walls should be installed as far away from the stope as possible.

CONCLUSION

(1) The mechanical behavior of uncemented backfill slurry under non-draining conditions conforms to the characteristics of an ideal fluid model, and its lateral pressure distribution aligns closely with the predictions of hydrostatic pressure theory, validating the practical engineering applicability of the theoretical model.

(2) The drainage performance of the barricade walls significantly regulates the evolution of lateral pressure and the process of structural stabilization. Optimizing drainage design can reduce lateral pressure by 69.5%-70%, while also accelerating the dissipation of pore water pressure, which plays a crucial role in hastening the self-stabilization of the backfill structure and enhancing the safety margin of the wall.

(3) There is a significant negative correlation between the installation distance of the wall from the stope and the lateral pressure. When the wall is installed at the drift entrance (adjacent to the stope), it is subjected to the combined effects of high hydrostatic pressure, dynamic water pressure, and potential expansion force from the stope side, resulting in a peak lateral pressure of 73.18 kPa (under a loading pressure of 80 kPa), which is 22.28% and 35.43% higher than that of walls in the middle and at the end of the drift, respectively. After the load increases to 240 kPa, the wall at the drift entrance still maintains a load transfer rate of 25%.

(4) As the wall moves away from the stope, the lateral pressure exhibits a dual-decline characteristic of "numerical decrease-fluctuation attenuation": the fluctuation amplitude of the pressure time-history curve for the wall at the end of the drift is attenuated by more than 35% compared to that at the drift entrance. Mechanistic analysis reveals that the stress arch effect induced by tailings settlement near the stope concentrates the load towards the wall, while the far-field region achieves stress redistribution through particle friction energy dissipation and bonding effects, leading to a more balanced and stable pressure distribution.

ACKNOWLEDGEMENT

The authors would like to acknowledge the financial support from the National Science and Technology Major Project (Grant No. 2024ZD1003705).”. And *the Youth Innovation Fund Project of BGRIMM Technology Group (04-04-2408).*

REFERENCES

1. Helinski M, FAHEY M, FOURIE A. (2010) Coupled two-dimensional finite element modelling of mine backfilling with cemented tailings. Canadian Geotechnical Journal, 47(11): 1187-200.
2. Li L. (2013) A new concept of backfill design—Application of wick drains in backfilled stopes. International Journal of Mining Science and Technology, 23(5): 763-70.
3. Sheshpari, M. (2015). Failures in backfilled stopes and barricades in underground mines. Electron. J. Geotech. Eng, 20: 191-212.
4. Kuganathan K. Design and construction of shotcrete bulkheads with engineered drainage system for mine backfilling. Proceedings of the international seminar on surface support liners, Australian Centre for Geomechanics, F, 2001 [C].
5. Berndt, C.C., Rankine, K.J., Sivakugan, N. (2007). Materials properties of barricade bricks for mining applications. Geotechnical and Geological Engineering, 25, 449-471.
6. Li L, Aubertin M. (2009) Horizontal pressure on barricades for backfilled stopes. Part II: Submerged conditions [J]. Canadian Geotechnical Journal, 46(1): 47-56.
7. Li L, Aubertin M. (2012) A modified solution to assess the required strength of exposed backfill in mine stopes [J]. Canadian Geotechnical Journal, 49(8): 994-1002.
8. Widisinghe, S.D., Sivakugan, N., Wang, V.Z. (2014). Loads on barricades in hydraulically backfilled underground mine stopes. In Mine Fill 2014: Proceedings of the Eleventh International Symposium on Mining with Backfill. Australian Centre for Geomechanics: 123-133.
9. Thompson, B.D., Bawden, W.F., Grabinsky, M. W., et al. (2010). Monitoring barricade performance in a cemented paste backfill operation. In Paste 2010: Proceedings of the Thirteenth International Seminar on Paste and Thickened Tailings. Australian Centre for Geomechanics: 185-197.
10. Sivakugan, N., Rankine, R.M., Rankine, K.J., et al. (2006). Geotechnical considerations in mine backfilling in Australia. Journal of Cleaner Production, 14(12-13), 1168-1175.
11. Nujaim M, Belem T, Giraud A. (2020) Experimental tests on a small-scale model of a mine stope to study the behavior of waste rock barricades during backfilling. Minerals, 10(11): 941.
12. Wang Y., Na Q, Zhang L. (2022) Monitoring of in-situ properties for cemented tailings backfill that under drainage condition. Construction and Building Materials, 356, 129254.

XVI International Mineral Processing
and Recycling Conference
28-30 May 2025, Belgrade, Serbia

DOI: 10.5937/IMPRC25537S

Original research article

SUSTAINABLE PRODUCTION OF GRAPHENE OXIDE AND ZINC OXIDE NANOPARTICLES FROM SPENT Zn-C BATTERIES

Sonja Stanković[1#], 0000-0003-0745-5422,
Vladan Nedelkovski[1], 0000-0001-7724-1118,
Milan Radovanović[1], 0000-0002-5175-6022,
Stefan Đorđievski[2], 0000-0003-1737-8766,
Dragana Medić[1], 0000-0001-9980-5949,
Snežana Milić[1], 0000-0002-5000-9156,
[1]University of Belgrade, Technical faculty in Bor, Bor, Serbia
[2]Mining and Metallurgy Institute Bor, Bor, Serbia

ABSTRACT – Recycling batteries helps to reduce waste, protects the environment, and allows their components to be reused in the manufacture of new products. In this work, the possibility of valorizing zinc and graphite from spent Zn-C batteries was investigated, not only to reduce pollution but also to create new materials with a wide range of industrial applications. Graphite electrodes were used for the synthesis of graphene oxide (GO) by the modified Hummer's method, while zinc was used for the synthesis of zinc oxide nanoparticles (ZnO-NP) by the coprecipitation method. The synthesized GO and ZnO-NP were structurally analyzed by X-ray diffraction (XRD). The appearance of a new diffraction peak at 10.7° and the decrease in the intensity of the diffraction peak of graphite at 26.6° and 42.4° indicate the oxidation of graphite and the formation of graphene oxide. In the case of the XRD pattern of ZnO, zincite was identified as the only crystalline phase, and the average crystal size was 41.63 nm.

Keywords: Recycling, Zn-C batteries, Zinc oxide, Graphene oxide.

INTRODUCTION

Zinc-carbon (Zn-C) batteries are the primary cells [1] used in numerous portable electronic devices worldwide due to their low cost, good durability and simple production technology [2,3]. The Zn-C battery contains graphite as the cathode, a mixture of manganese dioxide and carbon moistured with NH_4Cl/KCl as the electrolyte and a zinc container as the anode [4]. Since spent Zn-C batteries cannot be recharged and their proper storage is very expensive, spent Zn-C batteries are usually disposed of directly in landfills [5]. The improper disposal of Zn-C batteries in the environment not only leads to waste of Zn, Mn and C resources [6], but also to environmental pollution [3,7]. Recently, numerous research teams have focused their attention on recycling Zn-C batteries as an optimal solution to reduce the amount of waste, protect natural resources, the environment and human health [1,3-5,8].

[#] corresponding author: sstankovic@tfbor.bg.ac.rs

By recycling Zn-C batteries, the individual components can be effectively separated and reused in the synthesis of new products [3]. Zinc from spent Zn-C batteries can be used for the synthesis of ZnO nanoparticles [8], which are widely used in photocatalytic processes [9], in the production of gas sensors with high physical and chemical stability [10], solar cells [11], etc. Graphite from spent Zn-C batteries can be used as a precursor for the synthesis of graphene oxide [5]. Graphene oxide is widely used in wastewater treatment [7], but also for the modification of photocatalysts [12], membranes [13], sensors [14], etc. Regeneration of the electrolyte of Zn-C batteries enables the synthesis of valuable compounds, including ammonium zinc orthophosphate and manganese(IV) oxide. Manganese(IV) oxide has significant potential for use in the production of new batteries or as a catalyst in various oxidation processes. Ammonium zinc orthophosphate can be reused as a microfertilizer and offers an environmentally friendly solution for agricultural practice [2].

The aim of this study is to explore the recycling potential of spent Zn-C batteries, focusing on the recovery of zinc and graphite and the synthesis of valuable materials such as ZnO-NP and GO.

EXPERIMENTAL

Materials

Spent Zn-C batteries (Batt Extra Life, Standard Line, size AAA, 1.5 V) were collected from various battery-operated electronic devices. Hydrochloric acid, sulfuric acid, sodium hydroxide, sodium nitrate, potassium permanganate and hydrogen peroxide were also used for the purpose of this study. All chemicals were of analytical grade and were used without further purification.

Disassembly of Zn-C batteries into their individual parts

Zn-C batteries without visible external damage were collected for the laboratory tests. The Zn-C batteries consisted of a plastic case, metal terminals, a zinc anode container, a plastic and paper insulator, electrolyte, and a graphite electrode (Figure 1). When opening the Zn-C batteries, the plastic casing was removed first and then the metal terminals were removed. In the next step, the batteries were carefully opened and the anode material was separated from the cathode material, the electrolyte, and the insulators. The graphite electrode was then carefully removed from the electrolyte and the electrolyte was separated from the paper insulator using a spatula.

Figure 1 Zn-C batteries and their individual parts

Synthesis of ZnO nanoparticles

The zinc from spent Zn-C batteries was polished, washed with distilled water, and treated in an ultrasonic bath for 15 minutes. According to Das et al. [15], 2 g of zinc was dissolved in 20 ml of HCl at a temperature of 80°C with constant stirring on a magnetic stirrer. 1M NaOH solution was slowly added to the formed zinc solution to carry out the precipitation process. The solution was filtered and the separated precipitate was dried in an oven until it was dry and then calcined at a temperature of 600°C for 3 hours to form ZnO.

Synthesis of graphene oxide

Graphene oxide was synthesized by a modified Hummer's method [16,17]. The graphite electrode separated from the Zn-C batteries was polished with sandpaper and then treated with HCl to remove any remaining dry electrolyte. The electrode was then dried in an oven and ground in a mill. 1.0 g graphite powder, 1.0 g sodium nitrate, and 50 ml sulphuric acid were mixed in a laboratory beaker. The laboratory beaker was placed in a home-made ice bath with a magnetic stirrer. $KMnO_4$ was then gradually added to the reaction mixture and the system was stirred for one hour to allow the manganese oxidation reaction and graphite salt formation to take place. After one hour, approximately 500 ml of distilled water and 15 ml of H_2O_2 were added to the reaction mixture. The reaction mixture was then filtered and the separated precipitate was dried in an oven at 80°C.

Characterization methods

The structure and crystallinity of the ZnO and GO samples were analysed by X-ray diffraction (XRD). XRD analysis was performed using a RigakuMiniFlex 600 instrument with a D/teXUltra 250 high-speed detector and X-ray tube with a copper anode. The imaging conditions were: Angular range 3-90°, scanning speed 10°/min. The voltage of the X-ray tube was 40 kV and the current 15 mA. Mineral identification was performed using PDXL 2 software version 2.4.2.0 and the obtained diffractograms were compared with data from the ICDD PDF-2 2015 database.

RESULTS AND DISCUSSION

Characterization of ZnO nanoparticles

The diffractogram of the ZnO samples is shown in Figure 2 and shows that zincite was identified as the major crystalline phase in the analyzed sample. The diffraction peaks identified at 31.80°, 34.45°, 36.29°, 47.59°, 56.65°, 62.92°, 66.45°, 68.02°, 69.16°, 72.64°, 77.04°, 81.48° and 89.72° are identical to those from the ICDD PDF-2 2015 database (Card No. 01-082-9744) and confirm a hexagonal wurtzite phase of ZnO. The crystal lattice parameters (a and c) of the hexagonal wurtzite structure are 3.25 and 5.2, respectively, and correspond to the values of the reference sample [8].

The Debye-Scherrer formula was used to determine the average crystal size of ZnO nanoparticles [9]:

$$D = \frac{k \cdot \lambda}{\beta \cdot cos\theta} \tag{1}$$

Where D is the crystallite size (nm), k is the constant (0.89), λ is the wavelength of the X-rays (0.154 nm), β is the full width at half maximum of the most intense diffraction peak (FWHM) (rad) and θ is the Bragg angle (˚). The average crystal size of the ZnO nanoparticles was determined by measuring the FWHM of the most intense peak and amounted to 41.63 nm.

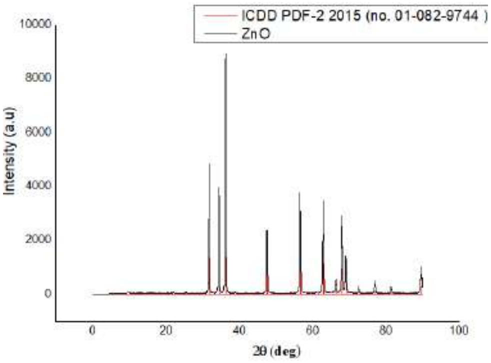

Figure 2 Diffractogram of ZnO nanoparticles

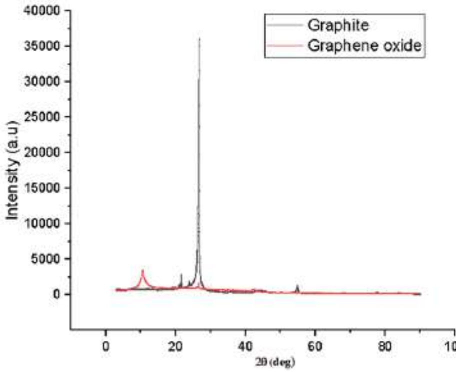

Figure 3 Diffractogram of graphite obtained from spent Zn-C batteries and synthesized GO

Characterization of GO

XRD analysis was used to investigate the conversion of graphite from Zn-C batteries into GO. The diffractograms of the initial graphite powder from Zn-C batteries and the synthesized graphene oxide are shown in Figure 3. The characteristic graphite peaks were observed at 26.6°, 42.4°, and 54.7° and attributed to the basal planes of graphite (002), (100), and (004), respectively. Similar results were obtained by Loudiki et al. [16], Silva et al. [17] and Sperando et al. [18]. A sharp diffraction peak at 26.78° of the basal reflection plane (002) indicates a highly crystalline hexagonal structure of the graphite powder [16,18]. A small peak at 21.4° may indicate the presence of impurities [16]. However, it is not possible to identify an impurity from a single diffraction peak.

In the case of the XRD pattern obtained for GO, a new peak at 10.7° was observed, indicating the presence of graphene oxide and corresponding to the (001) diffraction plane [12,17,19]. In addition, residual peaks of graphite at 26.6° and 42.4° were observed, but their intensity is significantly lower than that of the initial graphite, suggesting that graphite was exfoliated to obtain GO layers. Similar results were obtained by Silva et al., [17].

CONCLUSION

Recycling Zn-C batteries is a sustainable solution to reduce landfill waste, protect the environment and preserve human health. For this reason, the potential of valorizing Zn and C from spent batteries and reusing them for the synthesis of ZnO nanoparticles and

GO was investigated in this work. XRD analysis confirmed the formation of ZnO-NP with a hexagonal wurtzite structure and the successful conversion of graphite to graphene oxide.

ACKNOWLEDGEMENT

The authors are grateful to the Ministry of Science, Technological development and Innovation of the Republic of Serbia for financial support according to the contract with the registration numbers 451-03-137/2025-03/ 200131 and 451-03-136/2025-03/200052.

REFERENCES

1. Suryaprabha, T., Kiruthika, T., Selvamurugan, P., Sethuraman, M.G., Ha, H., Choi, Z., Wang, E., Hwang, B. (2024) Recycling primary batteries into advanced graphene flake-based multifunctional smart textiles for energy storage, strain sensing, electromagnetic interference shielding, antibacterial, and deicing applications. Journal of Cleaner Production, 479, 144020.
2. Ranskiy, A:, Gordienko, O., Ishchenko, V. (2024) Waste Zinc–Carbon battery recycling: Focus on total material recovery. Recycling, 9 (5) 83.
3. Vuong, T.T., Nguyen, P.L., Nguyen, N.T., Phung, T.V.B., Le, P.A. (2024) Zinc−Carbon battery recycling for investigating carbon materials for supercapacitor applications. ACS Omega, 9, 22543-22556.
4. Vadivel, S., Tejangkura, W., Sawangphruk, M. (2020) Graphite/Graphene composites from the recovered spent Zn/Carbon primary cell for the high-performance anode of lithium-ion batteries. ACS Omega, 5, 15240-15246.
5. Rawat, S., Singh, J. (2022) Synthesis of nZnO from waste batteries by hydrometallurgical method for photocatalytic degradation of organic pollutants under visible light irradiation. Journal of Environmental Management, 318, 115518.
6. Shangguan, E., Wang, L., Wang, Y., Li, L., Chen, M., Qi, J., Wu, C., Wang, M., L, Q., Gao, S., Li, J. (2022) Recycling of zinc carbon batteries into MnO/ZnO/C to fabricate sustainable cathodes for rechargeable zinc-ion batteries. ChemSusChem, 15, 1-9.
7. Salam, M.A., Gabal, M.A., AL Angari, Y.M. (2022) The recycle of spent Zn–C batteries and the synthesis of magnetic nanocomposite from graphene nanosheets and ferrite and its application for environmental remediation. Journal of Materials Research and Technology, 18, 4267-4276.
8. Farzana, R., Rajarao, R., Behera, P.R., Hassan, K., Sahajwalla, V. (2018) Zinc oxide nanoparticles from waste Zn-C battery via thermal route: Characterization and properties. Nanomaterials, 8 (717) 1-12.
9. Nguyen, N.T., Nguyen, V.A., Synthesis, characterization, and photocatalytic activity of ZnO nanomaterials prepared by a green, nonchemical route. Journal of Nanomaterials, 1768371, 1-8.
10. Hassan, K., Hossain, R., Farzana, R., Sahajwalla, V. (2021) Microrecycled zinc oxide nanoparticles (ZnO NP) recovered from spent Zn–C batteries for VOC detection using ZnO sensor. Analytica Chimica Acta, 1165, 338563.
11. Dash, R., Mahender, C., Sahoo, P.K., Soam, A. (2021) Preparation of ZnO layer for solar cell application. Materials Today: Proceedings, 41, 161–164.
12. Hosseini, S.A., Babaei, S. (2017) Graphene Oxide/Zinc Oxide (GO/ZnO) nanocomposite as a superior photocatalyst for degradation of Methylene Blue (MB)-Process modeling by Response Surface Methodology (RSM). Journal of the Brazilian Chemical Society, 28 (2) 299-307.

13. Homem N.C., de Camargo Lima Beluci N., Amorim S. Reis, R., Vieira, A.M.S., Vieira, M.F., Bergamasco, R., Amorim, M.T.P. (2019) Surface modification of a polyethersulfone microfiltration membrane with graphene oxide for reactive dyes removal, Applied Surface Science, 486, 499–507.
14. Kala, D., Sharma, T.K., Gupta, S., Verma, V., Thakur, A., Kaushal, A., Trukhanov, A.V., Trukhanov, S.V. (2021) Graphene oxide nanoparticles modified paper electrode as a biosensing platform for detection of the *htrA* Gene of *O. tsutsugamushi.* Sensors, 21, 4366.
15. Das, J.J., Tripathy, A., Tripathy, A., Mohanty, J. (2023) Preparation of ZnO nanoparticles from spent zinc-carbon batteries for application in solar cell. International Journal of Scientific Development and Research, 8 (3) 1108-1111.
16. Loudiki, A., Matrouf, M., Azriouil, M., Laghrib, F., Farahi, A., Bakasse, M., Lahrich, S., El Mhammedi, M.A. (2022) Graphene oxide synthesized from zinc-carbon battery waste using a new oxidation process assisted sonication: Electrochemical properties. Materials Chemistry and Physics, 275, 125308.
17. Silva, R.M., Sperandio, G.H., da Silva, A.D., Okumura, L.L., da Silva, R.C., Moreira, R.P.L., Silva, T.A. (2023) Electrochemically reduced graphene oxide films from Zn-C battery waste for the electrochemical determination of paracetamol and hydroquinone. Microchimica Acta, 190 (273) 1-16.
18. Sperandio, G., Junior, I.M., Bernardo, E., Moreira, R. (2023) Graphene oxide from graphite of spent batteries as support of nanocatalysts for fuel hydrogen production. Processes, 11 (3250) 1-16.
19. Chauhan, H.A., Rafatullah, M., Ali, K.A., Umar, M.U., Khan, M.A., Jeon, B.H. (2022) Photocatalytic activity of graphene oxide/zinc oxide nanocomposite derived from rice husk for the degradation of phenanthrene under ultraviolet-visible light. Journal of Water Process Engineering, 47, 102714.

XVI International Mineral Processing
and Recycling Conference
28-30 May 2025, Belgrade, Serbia

DOI: 10.5937/IMPRC25543K Original research article

ENHANCING EU ECONOMIC RESILIENCE: EXPLORING NEW SOURCES AND BENEFICIATION OF CRITICAL RAW MATERIALS NIOBIUM AND TANTALUM FROM CENTRAL AFRICA

Jasna Kastivnik[1#], 0009-0003-4123-8779,
Gašper Tavčar[2]**,** 0000-0001-9891-6153,
Dragan Radulović[3], 0000-0001-8210-8100,
[1]Oretech, Vrhnika, Slovenia
[2]Jožef Stefan Institute, Ljubljana, Slovenia
[3]Institute for Technology of Nuclear and Other Mineral Raw Materials,
Belgrade, Serbia

ABSTRACT – Raw materials are vital to Europe's economy, which is why the EU has identified specific Critical Raw Materials (CRM) that are crucial for its economic stability but pose significant supply risks. These include niobium and tantalum, for which there are currently no active mines in the EU. About 92% of the EU's niobium is imported from Brazil, primarily used in various alloys. The situation is similar for tantalum, with 63% being imported from several African countries, where it is mainly utilized in producing capacitors and superalloys. We have started exploring potential new sources in Central Africa to improve the diversity of supply. We are focusing on two types of mineral deposits: niobium- and tantalum-rich laterite and pegmatite ores. These ores were analyzed using techniques such as ICP-OES, XRPD, and SEM-EDS to determine the chemical and mineralogical compositions, as well as the grain sizes, to facilitate subsequent mineral liberation. Based on our findings, we have developed and implemented a test program using gravity and magnetic beneficiation methods. This program aims to produce an industrial-grade concentrate, thereby strengthening the resilience of the EU's raw material supply chain.

Keywords: Tantalum, Niobium, Magnetic Separation, Gravity Separation, CRM.

INTRODUCTION

The increasing demand for specific strategic materials, amplified by the political risks associated with their geographically concentrated supply chains, presents a potential threat to the advancement of low-carbon energy technologies due to possible shortages. Tantalum and niobium have been recognized as critical metals in the EU [1]. Niobium is essential in the nuclear sector, while both metals are vital for technologies related to carbon capture and storage and other upcoming sustainable innovations. This emphasizes the importance of improving their recovery from natural ores and recycling them from electronic waste, a process known as urban mining. Currently, tantalum and niobium are widely used across various fields, including optics, electronics, mechanical engineering, aerospace, nuclear technologies, and other advanced applications. The

---

[#] corresponding author: jasna@oretech.si demand for niobium is expected to rise significantly in high-strength, low-alloy (HSLA) steel applications, advanced Li-ion batteries, drones, and 3D printing [2].

Belonging to group 5 of the periodic table, tantalum and niobium have average crustal abundances of 1.7 mg/kg (Ta) and 20 mg/kg (Nb), respectively. They mostly exist in nature as refractory oxides, with no known deposits of the metals in their elemental form [3]. The primary sources for extracting niobium and tantalum are various minerals and concentrates, with a considerable amount obtained from the columbite-tantalite mineral, also known as coltan ($(Fe, Mn)(Ta, Nb)_2O_6$). Another significant source of niobium is the mineral pyrochlore ($(Na, Ca)_2(Nb)_2O_6(OH, F)$), highlighting the varied origins of these critical elements. These primary ores can contain various impurities such as ilmenite ($FeTiO_3$), silica (SiO_2), hematite (Fe_2O_3), wolframite $(Fe, Mn)WO_4$, cassiterite (SnO_2), and zircon ($ZrSiO_4$), as well as davidite $(La, Ce, Ca)(Y, U)(Ti, Fe)_{20}O_{38}$ and uraninite (UO_2) [4].

Given their low crustal abundances, extensive beneficiation processes are implemented to concentrate and upgrade them to a commercial grade of 25% of their pentoxide form equivalent.

Low-grade Nb-Ta ores, usually containing less than 0.1% Nb_2O_5/Ta_2O_5, present challenges for processing and recovery. This underscores the necessity of efficient ore enrichment and beneficiation to enhance extraction processes. The differences in properties between Nb and Ta and other gangue oxides can be leveraged in separating the two rare metals from one another as well as from impurities. Certain impurities in the mineral ore can thus be removed at specific mineral particle sizes and conditions before the digestion process, easing extraction complexity and potentially reducing recovery steps. Additionally, the routes for the beneficiation processes of these minerals can vary, ranging from ore pre-concentration to primary concentration and concentrate clean-up processes [5]. Ore preconcentration and primary concentration processes mainly include froth flotation, gravity, magnetic separation, and electrostatic separation, which are the beneficiation routes that effectively enrich and prepare ores for further concentrations and separations [6].

Gravity concentration (GC) is a long-established method for the physical separation of columbite/tantalite mineral ores, utilizing differences in density or specific gravity. This technique, as detailed in studies [5], involves the movement of mineral particles under external forces such as gravity, centrifugal force, buoyancy, and drag. These forces act on the particles in different directions, facilitating their separation based on density. The process employs equipment like jigs, shaking tables, sluices, and centrifugal and spiral concentrators, often operated in media such as water, viscous heavy liquids, or air. Screening processes frequently accompany gravity concentration to boost efficiency [7]. Researchers acknowledge the effectiveness of gravity concentration, noting its operational simplicity and cost-effectiveness as significant advantages. Both wet and dry gravity concentration methods have been successfully implemented, with various combinations of jigs, shaking tables, sluices, air floaters, and spiral concentrators proving effective across different studies. This body of research highlights the ongoing relevance and adaptability of gravity concentration techniques in mineral processing, emphasizing continual advancements and applications in the field [8].

EXPERIMENTAL

Two different "Ta-Nb" ore samples from laterite (S1) and pegmatite (S2) were analyzed to evaluate their potential as mineral resources. These investigations included extensive physicochemical and mineralogical assessments to grasp the ore's properties and processing potential for commercial use in various industries.

Both samples (S1 and S2) underwent identical preparation procedures, beginning with homogenization. Sub-samples were extracted from the homogenized ore to determine gross moisture, granulometric composition, and bulk density, with particle size distribution assessed via dry sieving using a standard Tyler sieve series. After analyzing the size of the raw samples, the ore was initially crushed (15.6 – 0.1 mm). We then re-evaluated its size and bulk density. The ore was subsequently crushed a second time to produce the final samples (6.35 – 0.1 mm). Comprehensive physicochemical and mineralogical analyses were performed on these samples. The qualitative mineralogical analysis utilized X-ray diffraction, with classifications by size classes and polished sections prepared for optical and SEM microscopy. For elemental composition were used ICP_OES and XRF analyzers were used.

Additionally, gravity separation tests with a multi-gravity separator and super planner concentrator were conducted on the raw ore.

Table 1 Elemental composition of both samples made by ICP-OES

Sample Name	w (μg/g)							
	Al	**Ca**	**Fe**	**Mn**	**Nb**	**Si**	**Sn**	**Ta**
S1_RAW	132512	548	17808	182	152	297000	166	216
S2_RAW	134052	285	5515	185	228	314868	166	390

Reflected light microscopy and SEM (Figure 1) were used to analyze grain size and intergrowth of precious and gangue minerals, offering detailed insights into the samples mineral composition.

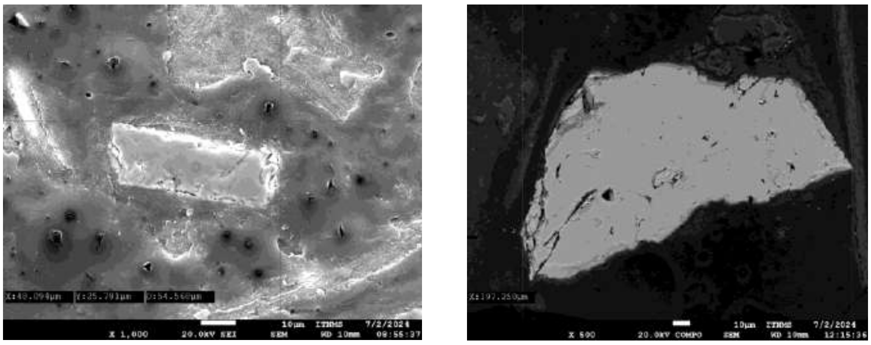

Figure 1 SEM images of a Columbite-Tantalite intergrown with albite in S1 (Left) and a grain of (ferro)wodginite embedded in clay in S2 (Right)

X-Ray Powder Diffraction (XRPD) was crucial in determining both the qualitative and quantitative mineralogical composition of the samples. This technique accurately identifies the minerals or crystalline phases present and their quantities, offering essential insights into the sample's properties and potential uses. Using the Rietveld refinement method, with χ2 = 1.88 and an R factor of 0.278, the mineral composition was quantified in weight percentages as follows:

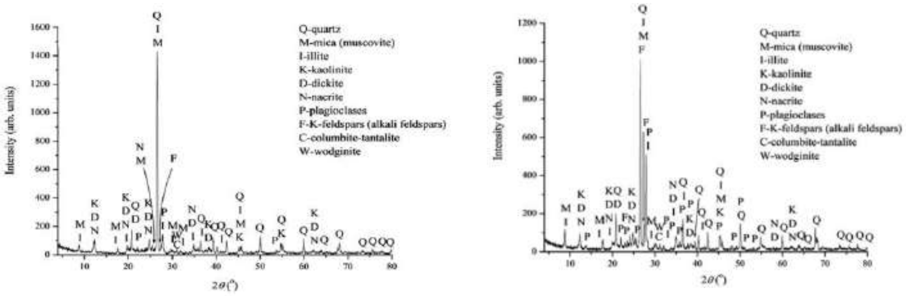

Figure 2 XRPD of both samples S1 (Left) and S2 (Right)

Table 2 Mineral composition of both samples

	S1	S2
	[%]	
Quartz	61.40	39.5
Muscovite	12.2	15.9
Kaolinite	13.1	8.00
Dickite	4.9	1.4
Nacrcite	0.4	3.1
Plagioclases	6.8	24.1
Alkali feldspars	0.8	7.3
Columbite-Tantalite	in trace	in trace

In this study, two different gravity separation methods were used as a Multi-Gravity Separator (MGS) and a Super Pan Separator to process the raw ore sample S1. The initial stage involved thorough washing of the raw material to eliminate fine clay fractions and all particles larger than 6.3 mm. Subsequently, the material underwent wet sieving using a 38-micron sieve, ensuring that only particles smaller than 38 microns were processed in the MGS. This approach was chosen due to the MGS's effectiveness in handling fine and ultra-fine materials. The MGS excels at separating grains based on their specific densities, allowing for the efficient concentration of Tantalum and Niobium, while effectively distinguishing these valuable minerals from less dense usable grains and non-valuable particles.

Following the MGS processing, the same raw ore samples S1 and S2 was subjected to testing with the Super Panner Separator with V-Tray. In this case sample had also been washed to remove clay and oversized grains larger than 6.3 mm. The material was subsequently dry-sieved into distinct size fractions. For the Super Panner Separator, the size fraction utilized was 180-125 µm. This stratification facilitated a comprehensive observation of the behavior of lighter grains in comparison to the heavier fractions, allowing for an enhanced understanding of the separation process to particle size and density.

RESULTS AND DISCUSSION

One of the important highlights of this study is the grain liberation, achieved through milling and additional milling of the samples. This study highlights the grain liberation of niobium-tantalum (Nb-Ta) bearing minerals, including columbite-tantalite, wodginite, and cassiterite. Results show that over 80% of grains were liberated, 15-16% were intergrown with silicates and/or limonite, and 2-3% were inclusions.

In this study, we concentrated on evaluating key parameters for each analytical method. The results highlight the material that exhibited the most favorable values for specific parameters across all tests conducted.

The multi-gravity separator effectively concentrated valuable elements from the initial sample (S1_MGS_-38_FEED1), where Aluminum, Iron, and Silicon were abundant. Post-separation, the concentrate (S1_MGS_-38_CONC1) showed significant enrichment of Niobium and Tantalum, with Tantalum increasing from 137 to 1,856 µg/g. In the tailings S1_MGS_-38_TAIL1), the concentrations of the elements showed minimal variation when compared to the feed (Table 3).

Table 3 Elemental Composition of Various Stages After Multi-Gravity Separation for Sample S1 made by XRF

	µg/g						
Sample	**Al**	**Fe**	**Si**	**Mn**	**Nb**	**Sn**	**Ta**
MMR_S1_MGS_-38_FEED1	174 212	16 530	229 485	114	42	104	137
MMR_S1_MGS_-38_CONC1	106 313	16 457	327 841	783	1 032	283	1 856
MMR_S1_MGS_-38_TAIL1	171 034	17 294	221 803	114	36	57	150

Results from the Super Panner concentrator on coltan ore sample S1 show significant variations in elemental concentrations across RAW, HEAVY, and LIGHT fractions. The HEAVY fraction contains high levels of niobium (Nb, 0.51 mg/g), tantalum (Ta, 0.47 mg/g), and tin (Sn, 1.05 mg/g), making it optimal for further processing. In contrast, the LIGHT fraction has high aluminum content (171.96 mg/g) but lower concentrations of Nb, Ta, and Sn. These findings suggest focusing on the HEAVY fraction to improve metal recovery, with further mineralogical investigations potentially enhancing separation techniques (Table 4).

Table 4 Elemental Composition of Various Stages After Multi-Gravity Separation for Sample S1 made by XRF

Sample	µg/g						
	Al	**Fe**	**Si**	**Mn**	**Nb**	**Sn**	**Ta**
PANER_180-125_RAW	125839	7476	252285	77	184	454	204
PANER_180-125_HEAVY	61495	13215	374334	361	513	1050	466
S1_PANNER_180-125_LIGHT	171959	6122	233223	48	33	53	139

CONCLUSION

The study of coltan ore from Central Africa, featuring laterite (S1) and pegmatite (S2) samples, highlights their significant potential as valuable mineral resources. Through various techniques such as XRPD, microscopy, ICP-OES, and XRF, we thoroughly assessed the physicochemical and mineral properties of these ores, confirming their favorable characteristics for commercial processing. The liberation of over 80% of Nb-Ta-bearing minerals underscores the effectiveness of milling. The application of gravity separation methods—Multi-Gravity Separator (MGS) and Super Panner Separator—on coltan sample S1 efficiently concentrated key minerals, particularly niobium and tantalum, by utilizing differences in density. The MGS achieved a remarkable increase in tantalum concentration, rising from 137 to 1,856 µg/g. Meanwhile, the Super Panner Separator identified the HEAVY fraction as optimal for further processing, being rich in valuable metals.

These results highlight the ores commercial potential and suggest improving metal recovery methods for better efficiency. This research provides insights to guide future exploration and utilization of tantalum and niobium, supporting their industrial use.

ACKNOWLEDGEMENT

The authors would like to express their gratitude to the Slovenian Research and Innovation Agency for their support of the P1-0045 program.

REFERENCES

1. European Comission (2020) Critical Raw Materials Resilience: Charting a Path towards greater Security and Sustainability, Brussels, 3.9.2020, COM(2020) 474 final https://ec.europa.eu/docsroom/documents/42849.
2. Bobba, S., Carrara, S., Huisman, J., Mathieux, F., Pavelv 2020), Critical Raw Materials for Strategic Technologies and Sectors in the EU - A Foresight Study 2020 https://ec.europa.eu/docsroom/documents/42882.
3. Haynes,W.M., Lide,D.R., Bruno,T.J.,ABUNDANCE OF ELEMENTS IN THE EARTH'S CRUST AND IN THE SEA, CRC Handbook of Chemistry and Physics, 97th edition (2016–2017), Pages 14-17.
4. M. Nete, W. Purcell, E. Snyders, J. T. Nel and G. Beukes Journal of the Southern African Institute of Mining and Metallurgy 2012 Vol. 112 Pages 1079-1086.
5. Gebreyohannes, B.G., del Rosario Alberto, V., Yimam, A. et al. Alternative beneficiation of tantalite and removal of radioactive oxides from Ethiopian Kenticha pegmatite–spodumene ores. Int J Miner Metall Mater 24, 727–735 (2017).
6. Nete, M., Koko, F., Theron, T., Purcell, W., Nel, J. T. Primary beneficiation of tantalite using magnetic separation and acid leaching, International Journal of Minerals, Metallurgy, and Materials, 2014. 21(12), 1153-1159.
7. Wills, B. A., and T. J. Napier-munn. 2006. Will's mineral processing technology - An introduction to the practical aspects of ore treatment and mineral recovery. 7th ed. Amsterdam, Netherlands: Elsevier Science and Technology Books7.
8. Nzeh, N.S., Adeosun, S.P., Abimbola P., Adeleke, A., Okanigbe, D., Process Applications and Challenges in Mineral Beneficiation and Recovery of Niobium from Ore Deposits - A Review, Mineral Processing and Extractive Metallurgy Review, 2022, 43(7), 833-864.

XVI International Mineral Processing
and Recycling Conference
28-30 May 2025, Belgrade, Serbia

DOI: 10.5937/IMPRC25549D Original research article

THE IMPACT OF THE TRANSFER STATION ON THE ORGANIZATION OF MUNICIPAL WASTE COLLECTION

Džafer Dautbegović[1#], 0009-0002-5016-2879,
Mirsada Hasanbašić[2], 0009-0003-6245-7292,
[1]Faculty of Mechanical Engineering, University of Zenica, Zenica, Bosnia and Herzegovina
[2]ALBA Zenica d.o.o. Zenica, Zenica, Bosnia and Herzegovina

ABSTRACT - Transfer stations are construction facilities for the reception and temporary disposal of unsorted municipal waste. Waste from collection vehicles is loaded for further processing or final disposal to large-capacity vehicles. Municipal waste collection in the city of Zenica is organized with vehicles of different sizes and carrying capacities that are adapted to traffic conditions and the size of containers located in the area of the city from which the waste is collected. The change in the organization of waste collection and transport by using a transfer station is reflected in the shortening of transport distances for individual waste collection vehicles, because the waste is transported to the transfer station, which is located on the border of the urban zone, and not to the Regional Landfill "Mošćanica", which is 17 km away from the city. This paper presents several performance indicators (consumption), as well as environmental impact, which define the efficiency of municipal waste collection organization in direct transportation to a landfill and with a transfer station. The analysis of the transfer station operation will examine organizational, environmental and economic indicators.

Keywords: Transfer Station, Waste Management, Municipal Waste, Environmental Protection, CO_2 Footprint.

INTRODUCTION

The costs of municipal companies whose main activity is waste collection and transport make up the majority of expenditures in municipal waste management systems and range from 50-70% of total costs. In addition, waste collection and transport cause greenhouse gas emissions. Optimization of waste collection and disposal involves analyzing of a large number of influential factors that can be grouped as: locational, technical, legislative and organizational [1].

Technical and organizational aspects can refer to: waste collection vehicle and containers (technical characteristics), organization of collection (working hours, number of employees, collection path).

The direct impact on CO_2 reduction is reflected in fuel consumption per ton of waste transported, which has both economic and social impact. The carbon footprint is calculated by multiplying the emissions of each of the six greenhouse gases: carbon dioxide CO2 (factor 1), methane CH4 (factor 28), nitrous oxide N2O (factor 265),

---

[#] corresponding author: dautbegovic@alba.ba hydrofluorocarbons CHF_3 (factor 12400), difluoromethane CH_2F_2 (factor 677) and sulfur hexafluoride SF_6 (factor 16300), by its 100-year global warming potential (GWP) [2].

The paper analyzes the vehicle fleet used for the collection and transportation of municipal waste in the city of Zenica and presents environmental, economic and organizational indicators. Based on the parameters: vehicle fuel consumption, transported tons of waste, number of waste collection service users, number of employees in waste collection, number and type of waste collection containers, an assessment of the characteristics of the municipal waste collection service system is made for the period 2014, when reloading is performed from small waste vehicles (up to 4 tons) and 2024, when reloading is performed from all waste vehicles that collect less than 9 tons of municipal waste (transfer station).

EXPERIMENTAL

The city of Zenica is located in the central part of Bosnia and Herzegovina on an area of 550 km^2, of which 44 km^2 is inhabited. The number of inhabitants, according to the 2013 census, is 110 663 [3].

ALBA Zenica d.o.o. is a utility company that provides the service of collection and disposal of municipal waste from the area of the city of Zenica. Collected waste is taken to the Regional Landfill "Mošćanica", 17 kilometers from the city center, where it is disposed.

The municipal waste collection and disposal system can be divided into:

- individual collection, where each user is assigned a container and the frequency of its emptying is in accordance with the signed contract (once a week),
- collective (joint) collection, where several users are assigned to one container and it is emptied depending on its fullness (several times a week).

In Zenica, waste collection containers are used that differ in volume, shape and method of emptying. For the collection of municipal waste, special purpose vehicles are used for emptying containers and transporting waste, which can be classified into the following groups:

a) small waste vehicles (6-11 m^3) for bins (120-240 liter) and containers (1.100 liter),
b) medium waste vehicles (12-18 m^3) for containers and bins,
c) large waste vehicles (19-21 m^3) for containers and bins,
d) grapples (32 m^3) for metal bells (2.500 liter) and underground containers (3.000 liter).

The system recognizes types of containers, grouped by area, which as a rule correspond to the area of local communities. Zenica is divided into 74 local communities.

The waste collection area is divided according to the types of containers into:

a) bins (0.12 – 0.24 m^3) – 68 local communities (rural and suburban areas),
b) containers (1.1 m^3) – 16 local communities (city area),
c) underground containers (3 m^3)- 19 locations and metal bells (2.5 m^3) - 29 locations in 11 local communities (city area).

Inhabited areas are connected by roadways, which, together with the places where waste collection containers are located and the frequency of emptying, determine the type of vehicles used for waste collection system.

The area of municipal waste collection related to individual housing is predominantly located on the outskirts of urban areas or in rural, mostly hilly areas. It is characterized by narrow roads that require the use of smaller waste vehicles.

Waste collection from populated areas where containers are located on open areas, which are also accessible to larger vehicles, is carried out by trucks with higher carrying capacity, thus achieving better operating parameters, i.e. greater efficiency.

When analyzing municipal waste collection activities, the work process is usually divided into:

a) emptying waste containers, which involves emptying them into a vehicle and moving the vehicle up to 100 meters between containers,

b) vehicle transporting from the starting station to the area with containers for emptying and transporting the vehicle from the area where the containers are emptied to the landfill, or municipal waste treatment plant.

The ALBA Zenice d.o.o. work process controlling department keeps data on consumption and realization parameters. For the purposes of this work, monthly data for April 2014 and 2024 were observed.

RESULTS AND DISCUSSION

In 2014, the reloading was carried out from small waste vehicles with a carrying capacity of 4 tons into a large vehicle with carrying capacity of 10 tons (grappler without trailer). In 2024, small, medium and large vehicles were reloaded, except when the mass of loaded waste exceeds 9 tons, which refers to fully loaded large waste vehicles.

Fuel consumption per unit of time, or distance, is noticeably higher for vehicles for waste collection and transportation compared to long-distance vehicles. The difference in consumption indicators is conditioned by the driving style (start-stop), the area of movement (populated areas with slow traffic) as well as the fact that the waste collection and compaction equipment is driven with hydraulic elements that are powered by a hydraulic pump connected to the truck engine.

Fuel consumption and time consumption indicators in relation to the work performed, efficiency, are presented in Table 1 for 2014 and Table 2 for 2024.

Table 1 Municipal waste collection indicator – work and consumption April 2014 [4]

waste vehicle	km	l	t	shift	landfill	transfer station	t/unload	240 l	1100 l	crew
waste vehicle 6-11m^3	7879	3529	792	96	83	167	3,2	27405	1754	11
waste vehicle 12-18 m^3	2363	1733	285	34	44	1	6,3		6474	5
waste vehicle 19-21 m^3	4651	3737	716	61	78	1	9,1		13218	6
grapple	2594	2410	428	27	57	0	7,5			1
	17.487	**11.409**	**1.793**	**218**	**262**	**169**	**4,2**	**27.405**	**21.446**	**23**

Table 2 Municipal waste collection indicator – work and consumption April 2024 [5]

vehicle and machines	km	l	t	shift	landfill	transfer station	240 l	1, l m^3	2,5 m^3	3 m^3	32 m^3	crew
waste vehicle 6-11 m^3	5525	3243	950	107	0	316	43992	1791				15
waste vehicle 12-18 m^3	1173	738	217	21	19	21	1045	7236				3
waste vehicle 19-21m^3	4464	3328	682	62	57	33	7892	8738				7
grapple	1428	1073	317	27	47	19			1108	636		1
roll-off tipper with trailer	2870	2645	1322	30	80						156	1
wheel loader		465	1322	26							156	1
	15.460	**11.491**	**2.167**	**217**	**203**	**389**	**52.929**	**17.765**	**1.108**	**636**	**312**	**28**

Efficiency is observed through indicators of working hours and fuel consumption per ton transported, kilometer traveled and waste container. The efficiency of smaller vehicles, with a carrying capacity of up to 4 tons, is lower due to their lower carrying capacity, so their use for the removal of municipal waste over longer distances should be avoided. In order to improve the indicators of increasing efficiency, better utilization of labor resources and reducing fuel consumption, as well as increasing the use of smaller vehicles due to the characteristics of roads in remote parts of the city of Zenica, in rural areas, a municipal waste transfer station was put into operation in 2016, 17 km from the Regional Landfill. Since then, municipal waste collected in smaller and medium-sized vehicles, or partially filled large vehicles, has been sent to the transfer station, and after being reloaded into 32 m^3 roll containers, it is transported to the landfill by truck with a trailer.

The introduction of the transfer station has changed the ratio of fuel consumption by relevant performance indicators (t, km, shift, containers). The justification is shown through the performance indicators of the waste collection system when only small vehicles (up to 8 m^3) perform the transfer and the collection system and when only large vehicles (21 m^3) transport waste to the landfill, and the other trucks are directed to the transfer station, from where the waste is then sent to the landfill by a larger capacity transport vehicle. Table 3 and Table 4 show the consumption of time, fuel and kilometers transported, per shift, container and per ton of municipal waste sent to the Mošćanica Regional Landfill, without and with the transfer station. By analyzing the presented data, the values of the indicators for both cases can be compared.

Table 3 Municipal waste collection indicators – performance April 2014

vehicle	l/t	l/km	l/container	l/shift	t/shift	t/worker/ shift
small w. vehicle	4,46	0,45	0,12	36,76	8,25	1,02
medium w. vehicle	6,08	0,73	0,27	50,97	8,39	1,58
large w. vehicle	5,22	0,80	0,28	61,27	11,73	2,76
grapple	5,63	0,93		89,26	15,87	15,87

Table 4 Municipal waste collection indicators – performance April 2024

vehicle and machines	l/t	l/km	l/container	l/shift	t/shift	t/worker/shift
small w. vehicle	3,41	0,59	0,071	30,31	8,88	0,59
medium w. vehicle	3,39	0,63	0,089	35,13	10,35	4,14
large w. vehicle	4,88	0,75	0,200	53,68	11,00	1,62
grapple	3,39	0,75	0,615	39,75	11,74	5,87
transport	2,00	0,92	16,95	87,65	44,08	33,80
wheel loader	0,35		2,98	15,00	50,86	43,04

Based on the calculated values, there is a visible difference in the carbon footprint generated by municipal waste collection activities in the city of Zenica when reloading from small waste vehicles (up to 4 tons) and when reloading all waste vehicles when transporting less than 9 tons of municipal waste (transfer station).

$$t_{CO2_{14}} = \frac{l\cdot 2,65}{1000} = \frac{11409\cdot 2,65}{1000} = 30,23 \tag{1}$$

$$t_{CO2_{24}} = \frac{l\cdot 2,65}{1000} = \frac{11491\cdot 2,65}{1000} = 30,45 \tag{2}$$

Using the CO_2 emission calculator for diesel fuel consumption, the impact on CO_2 emissions is also visible. Comparing the resulting CO_2 footprint to the transported tons of waste in 2024 is a reduction of 14% per ton visible.

With every journey, motor vehicles emit carbon dioxide (CO_2) from the exhaust gases. Surprisingly, CO_2 weighs more than the fuel that was originally filled. Jörg Sauer from the Institute for Catalysis Research and Technology at the Karlsruhe Institute of Technology (KIT) explains why is this so [6].

When a vehicle consumes one liter of petrol, it emits about 2.37 kilograms of CO_2. If diesel is used, it emits 2.65 kilograms of CO_2. It may seem confusing, but in the end it all comes down to chemistry. Fuel is a mixture and consists of many hydrocarbon chains. While driving, the fuel burns in the engine, and the carbon (C) reacts with oxygen (O_2) in the air. One by one, the atom combines with two oxygen atoms in the carbon dioxide (CO_2) molecule. In simple terms, the light hydrogen atoms (atomic mass 1) from the hydrocarbons are exchanged for heavier oxygen atoms (atomic mass 16). The hydrogen atoms in turn combine with oxygen to form water (H_2O).

In order to present the results obtained in full, it is necessary to show the total amount of waste disposed of, i.e. the number of waste collection service users in the observed case. (Table 5)

Table 5 Overview of total quantities of municipal waste transported from Zenica 2014/2024

year	waste collected	housing	companies	total	per user
2014	26.665 t	24.371	939	25.286	1,055 t/year
2024	27.449 t	29.944	1.710	31.654	0,867 t/year

The improvement of the municipal waste collection and disposal system in Zenica can be analyzed through data with indicators of the provided waste collection service and work engagement for its realisation (Table 6.).

Table 6 Work indicators by fuel consumption and time April 2014-April 2024

	ton	liter	km	user	shift	workers	containers	l/t	l/user	h/t	h/user
april 2014	1.79	11.40	17.48	25.246	218	23	48,851	6,36	0,45	2,27	0,16
april 2024	2.16	11.49	15.46	31.328	217	28	72,438	5,30	0,37	2,29	0,15

In 2024, a larger amount of waste was collected from a larger number of users, in a larger territory (distance) with lower fuel consumption and a lower number of kilometers traveled.

CONCLUSION

Looking at the above data, it can be concluded that the use of a transfer station in the municipal waste collecton system is justified. Larger amount of waste from a larger territory is collected with lower costs.

The above data, in addition to reduced consumption, also indicate a more environmentally friendly way of working (CO_2 footprint).

Due to the increased volume of work, the number of employees providing the service has increased, but the time (h) indicators of service execution have improved, with the exception of the time spent per ton, which can be expected considering that the amount of waste per user of the service has decreased (table 5), which is conditioned by the increase in the number of households included in the system.

It can be concluded that changing the transport of waste to the landfill, by including transportation to vehicles with higher capacity, is a correct business decision that contributes to better business and environmental results.

REFERENCES

1. Martin Kranert (2017) Einführung in die Kreislaufwirtschaft, Springer Vieweg, Stuttgart, ISBN 975-3-8348-1837-9.
2. Greenhouse Gas Protocol, Global Warming Potential Values, IPCC Fifth Assessment Report, 2014 (AR5), https://ghgprotocol.org/sites/default/files/Global-Warming-Potential-Values%20% 28Feb%2016%202016%29_1.pdf.
3. Institut for statistics of Federation of Bosnia and Herzegovina, Cenzus of Population, Households and Dwellings in Bosnia and Herzegovina 2013 Final results, Sarajevo July 2016, ISSN 1512-5106.
4. Interni izvještaj 4/2014 – pokazatelji odvoza otpada, Operativni kontroling ALBA Zenica d.o.o., 2014.
5. Interni izvještaj 4/2024 – pokazatelji odvoza otpada, Operativni kontroling ALBA Zenica d.o.o., 2024.
6. Jörg Sauer, Wieviel CO_2 steckt in einem Liter Benzin, 30 Helmholtz Mediathek Nachgefragt, Nachgefragt - Helmholtz Home, Mach, 2025.

7. Mariano Gallo; Mario Marinelli; Rosamaria Pedicini (2021) Optimal Location of Transfer Stations for Waste Management: a Real Case Study In: 2021 IEEE International Conference on Environment and Electrical Engineering and 2021 IEEE Industrial and Commercial Power Systems Europe (EEEIC / I&CPS Europe). Bari, Italy.
8. D.P. Komilis (2008) Conceptual modeling to optimize the haul and transfer of municipal solid waste, Waste management, 28 (11), 2355-2365.
9. Dongqing Jia , Xingmei Li, Zhong Shen (2022) Robust optimization model of waste transfer station location considering existing facility adjustment. In: Journal of Cleaner Production, 340.

XVI International Mineral Processing
and Recycling Conference
28-30 May 2025, Belgrade, Serbia

DOI: 10.5937/IMPRC25556D Original research article

RECYCLING OF CHROMIUM TAILINGS IN BULQIZA PLANT

Genc Demi[1#], 0009-0008-9816-3137,
Bukurosh Koci[1], 0009-0001-8793-4097,
Islam Nika[2], 0009-0006-0847-8334,
[1]Faculty of Geology and Mining, Tirana, Albania
[2]Fabrika Pasurimit Kromit, Bulqize, Albania

ABSTRACT – Chromium mineral processing plant of Bulqiza has begun operation 50 years ago, treating low grade chromium ores grade 12 % to 26 % Cr_2O_3 and producing chromium concentrates for export. About 1.8 million tons of tailings are stocked in a dam close to the plant. Recycle and enrichment of existing tailings is profitable, because this kind of raw material doesn't need expenses for crushing, grinding and exploitation. The existing plant is in operation for more than 25 years treating existing tailings. Grade of concentrate produced from enrichment of tailings is in the value 38-40 % Cr_2O_3 and Cr_2O_3 recovery is in the value 25-33%. The content of particles under 100 μ, the slimes, in raw material is high. In the paper are described the continuous efforts to improve the Cr_2O_3 recovery. The testing carried out to improve Cr_2O_3 recovery of tailings enrichment is presented in this paper, as well as analyses of existing process, raw material and products. It is concluded that majority of losses are present in the slimes which are not separated in existing spiral separators and shaking tables. Basing in the study some measures and arrangements in the flowsheet are taken and it is achieved the recovery improvement. In the paper are presented the tests and results of concentration of fine particle fraction, using different methods.

Keywords: Tailings, Tables, Spirals, Grinding, Desliming.

INTRODUCTION

Chromium dressing plant of Bulqiza is continuously in operation since 1970 year. About 4 million ton low grade lumpy chromium ore are treated during 1970-2025 period of time. Production quantity has been about 1.8 million ton chromium concentrate with 48-50 % Cr_2O_3 content for this period of time.

Tailings are deposited in a dam close to the plant. The quantity of tailings is about 2 million ton and Cr_2O_3 content varies from 10 to 13% with an average 11.5 %. The losses of Cr_2O_3 component during operation of the plant with lumpy ore have been in the value of 25-35%. The analysis of technological process and tailings performed during this operation has shown that the main reason of the losses has been that about 50% of Cr_2O_3 component in the tailings were present in fraction under 0.1mm. It means that it was generated a big slime production in the grinding cycle, and it was performed a low efficient classification and low recovery of chromium fine particles [3,4].

After crushing and grinding of lumpy raw material under 1.5 mm, the quantity of -74

[#] corresponding author: gencdemi@yahoo.com micron fraction was over 42%. These fine particles were concentrated with low recovery in existing shaking tables, which had not been designed and produced for the treatment of fine particles under 74 micron.

About 25% of losses were in tailings regarding low separation sharpness of existing equipment designed for course particles and about 50% of losses were present in slimes (fine particles under 74 microns).

The enrichment of these old tailings is with advantage from economical point of view. The reason is that the raw material in this case is not exploited in the mine and that it is not crushed and ground and it doesn't need expenses processes like crushing and grinding. As a consequence the expenses for this type of raw material are only for excavation and transport from the dam to the plant. [2]

It is the reason that Bulqiza chromium enrichment plant begun the treatment of existing old tailings recirculating them in existing adopted plant since 2001. In the beginning it was adopted the flowsheet of lumpy enrichment with the flowsheet for recycling and enrichment of old tailings. This flowsheet is shown in Figure 1.

From 2001 till now the analyses and testing to improve the technological figures have been carried out continuously.

Some improvements were carried out based in the analyses of process and the enrichment schema for tailings was changed in some chains, as it is shown in Figure 2.

The new tailings produced from the enrichment of old tailings has been deposited in the same tailings dam trying to deposit them separately from old tailings. However it is happening more or less a mixture of old tailings with the new ones.

It is the reason that the enrichment of tailings has been more difficult last times and it is predicted that the enrichment of tailings could be prolonged and about 10 years more in the case that will be used gravimetric methods.

There were carried out some efforts to test the possibility of enrichment with flotation or magnetic methods of fine particles that are going in losses with gravimetric methods.

EXPERIMENTAL

As it was mentioned above, in the beginning the flow sheet for tailings enrichment is shown in Figure 1 [5].

The existing tailings with 6-8% moisture were excavating, loading and transported from the dam to the plant by trucks. The vibrating screen (202) with aperture 1.2 mm was separating in wet way the over screen +1.2 mm which was ground in rod mill (206). The discharge of the mill was pumped closing the grinding cycle in the same screen. Underflow of the screen was pumped in a hydrocyclone (302) where was separated the fraction under 74 microns in overflow. The underflow of hydrocyclone was treated in two scales of spiral separators (304, 307 and 308) separating final concentrate, final tailings and middlings. The middlings were pumped in the hydrocyclone (401), underflow of which went to the hydraulic classifiers (402) The underflows of the rooms of hydraulic classifier were treated in the first scale of shaking tables (403) where were separated final concentrate, final tailings and middlings. The overflows of hydraulic classifiers fed thickener cones (404, 406) overflows of which went to final tailings, while underflow was treated in shaking tables (405, 407) separating final concentrate, final tailings and middlings. All the middlings of first shaking table scale were pumped to hydrocyclone (409) to thick the pulp before hydraulic classifiers (410) the underflows of which were treated in second scale of shaking tables (411), while overflow went to cone thickeners (412, 414) and after that to shaking tables (413, 415). All shaking tables of second scale were separating final concentrate, final tailings and middlings, which were recirculated again in hydraulic classifiers closing the cycle.

All overflows of hydrocyclones (302, 401 and 409) were collected and pumped in the battery of hydrocylones 75 mm (420), overflow of which was minus 15 microns and went in final tailings, while underflow was treated in Duplex concentrators (421), where were separated final concentrate and final tailings.

All final products were dewatered in screw classifiers (501, 310, 417). The overflow of tailings screw classifiers (310 and 417) contained slime and were pumped in enrichment process again.

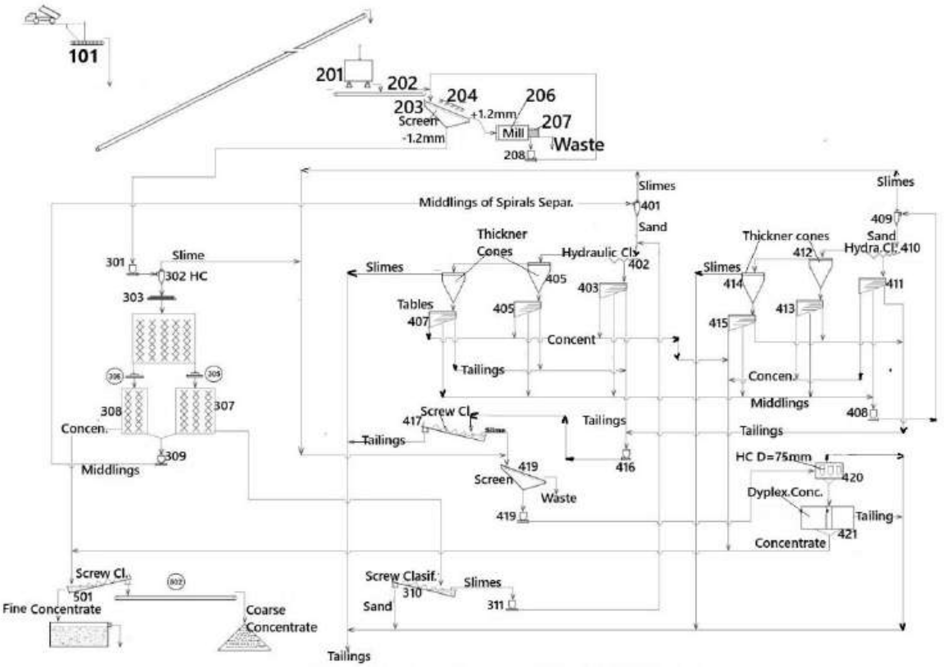

Figure 1 The former flowsheet of tailings enrichment [5]

The analyse of technological process was carried out to find the reasons and necessary data to improve the technological figures.

The main improvements were as follows:

In the former flowsheet the tailings like raw material were forced to pass the crushing workshop, putting in operation the crushers and all the equipment of crushing workshop and spending high value of not useful energy. Except it the nature of tailings with high content of humidity was causing big problems blocking the crushers. In the improved actual schema it was avoid passing the raw material between crushing workshop and it was substituted with a bin, belt feeder and a trommel for tailings disintegration.

It was changed the aperture of the screen before grinding from 1.2 mm to 0.63 mm that resulted with a better grade of liberation of course fraction.

It was changed the separation of final concentrate in spiral separators, separating only middlings and tailings, treating spiral middlings in hydraulic classifiers and shaking tables. It was added one step of treatment in spiral separators.

It was separated the fine fraction under 74 µ from tailings and it was treated separately in shaking tables with high frequency 420 per minute and short step 5 mm.

The improved technological schema is shown in Figure 2.

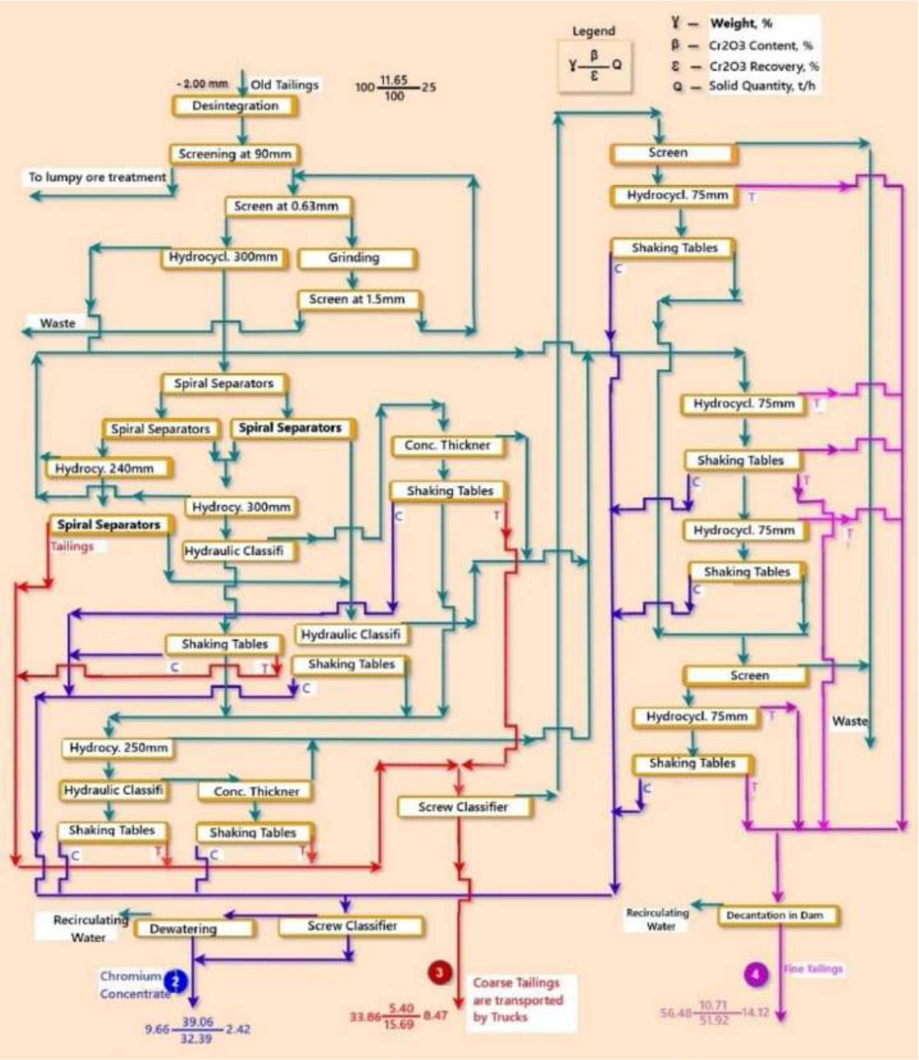

Figure 2 The actual improved technological scheme [6]

There were analysed the improved schema for a period of time since 2020 to 2024 year.

The figures achieved can be considered good, taking in consideration that the treated material is very fine and difficult to be concentrated by gravimetric way.

Several tests were carried out in High Gradient Magnetic Separation HGMS with slime product of Bulqiza dressing plant [5]. From the results obtained the expected performance of a HGMS carousel machine on this material would be a concentrate grade of 36 % Cr2O3 at minimum 60 % Cr_2O_3 recovery. The HGMS parameters would be a magnetic field of 5.1 kGauss, flow velocity 200 mm/s matrix load 0.3 g/cm^3 and matrix XR (or XM). This process was not applied in industrial scale because the figures cannot be warranted and the equipment is very expenses [4].

Another method studied is flotation [1]. The experimental results show that chromite can be readily floated from a slime-free acidic pulp with an Na or K-oleate collector at pH = 2.5 and 5.5 utilizing EDTA also without the use of such modifiers as HF and $AlCl_3$ normally employed and the separation of serpentine can be done at natural pH without depressant if the dosage of collector is not high in relation to the serpentine assay. Comparison of the flotation kinetics of the various minerals reveals that the values for chromite are similar at pH = 2.5 and 5.5, while that for serpentine is lower at 5.5 than at 2.5, unlike olivine which appears to float better at 5.5 than 2.5.

The technical feasibility of rougher flotation at natural pH for stripping serpentine has been confirmed on ores from Bulqiza tailing deposit and Bulqiza tailing of existing processing plant. In this case, cleaner flotation to eliminate olivine can be performed at pH = 2.5-3. The Cr_2O_3 grade and recovery are about 51% and 67% respectively. [1]

RESULTS AND DISCUSSION

The results of recycling and enrichment treatment with gravimetric way in the plant for a long time are presented in the Figure 2 of technological scheme. The particle size distribution and Cr_2O_3 content of the fractions plus and minus 20 µ in the concentrate and tailings are given in the Table 1. [6].

Table 1 Minus and plus 20 µ fraction distribution in raw material and products and Cr_2O_3 content

Fractins µ	Raw Material			Concentrate			Tailings		
	Weig. %	**Cr_2O_3, %**	**Recov. %**	**Weig. %**	**Cr_2O_3, %**	**Recov. %**	**Weig. %**	**Cr_2O_3, %**	**Recov. %**
+20	48.63	7.27	30.36	7.49	38.40	24.69	41.14	1.61	5.67
-20	51.37	15.79	69.64	2.17	41.34	7.70	49.20	14.67	61.94
Total	100.00	11.65	100.00	9.66	39.06	32.39	90.34	8.73	67.61

From the results of the table it is clear that the reason of main losses and low grade of concentrate is the high content of fine particles smaller than 20 µ in raw material which cannot be separated with gravimetric methods.

It is necessary testing of wet magnetic separation and flotation of – 20 µ particles. Also last time is mounted a battery of hydrocyclones D=38 mm that will separate the from the overflow of hydrocyclones D=75mm the particles 5 to 20 microns to treat them in shaking tables.

CONCLUSION

Based on the tests carried out in industrial scale results that Cr_2O_3 recovery in concentrate is about 32.4 % and grade of concentrate is about 39% Cr_2O_3 using gravimetric methods.

About 70 % of Cr2O3 quantity that is contained in the raw material (old tailings) is concentrated in the fraction – 20 µ**,** from which only 7.7 % is recovered in chromium concentrate, while about 62 % has passed in the tailings.

The technological figures needs to be improved using flotation or magnetic methods for the treatment of particles under 20 µ.

REFERENCES

1. Belardi, G, Demi G, and Cico, Sh, 2005. Production of high content of Cr and low SiO_2 concentrates from Albanian chromite, in Proceedings of XI Balkan Mineral Processing Congress, Durres 2005, pp 158-165 (Faculty of Geology and Mine, Tirana, Albania). ISBN 99943-694-6-6.
2. Hido, M, Fetahu, K, Peza, V, 2005. Technology of chromium ore processing in Albania, in Proceedings of XI Balkan Mineral Processing Congress, Durres 2005, pp 267-273 (Faculty of Geology and Mine, Tirana, Albania). ISBN 99943-694-6-6.
3. Demi G, Koci, B, and Boci, S, 2006. Gravity concentration of poor chromium ores in Albania, in Proceedings of XXIV International Mineral Processing Congress, Istanbul 2006, pp 310-313 (Istanbul Technical University, Mining Faculty, Turkey). ISBN 975-7946-27-3.
4. Demi G, Fetahu, K, 2008. Treatment of chromium ores in Albania, in Proceedings of XXIII International Mineral Processing Congress, Beijing 2008, pp 4356-4362 (Wang Dian Zuo Sun Chuan Yao Wang Fu Liang Zhang Li Cheng Han Long). ISBN 978-7-03-022711-9(Beijing).
5. Demi G. (2012) Enrichment of chromium tailings in Albania. XXVI International Mineral Processing Congress IMPC 2012 New Delhi, India, Book of abstracts, Vol. 2, pp 661, Paper No. 1053, Session No. 8D-05.
6. Demi G., Koci B., Nika I., 2024. Report of technological figures and analyses of raw material and products of enrichment tailings in Bulqiza plant during period of time 2020 – 2024.

XVI International Mineral Processing
and Recycling Conference
28-30 May 2025, Belgrade, Serbia

DOI: 10.5937/IMPRC25562S

Original research article

KINETIC AMD PREDICTION FOR A MINE TAILINGS DUMP: A SOUTHERN AFRICAN MINE CASE STUDY

Mafeni Samuel Ramatsoma[#], 0000-0002-8079-8424,
Veruska Govender, 0000-0001-6848-6527,
Deshenthree Chetty, 0000-0002-1913-7598,
Olga Bazhko, 0000-0002-1598-0123,
Mintek, Johannesburg, South Africa

ABSTRACT – Sulfide-containing mine tailings dumps are known to pose the hazard of acid mine drainage (AMD). AMD is a metal-rich and acidic solution that is formed naturally when sulfide minerals react with water and oxygen, and its risks should be considered before, during, and after mining operations. It is critical to accurately predict AMD occurrence over time, so appropriate mitigation and/or treatment processes can be implemented. This study presents the use of a particles-based kinetic AMD predictor for long-term AMD occurrence profile prediction to determine the frequency and amount of AMD leachate produced that would need to be treated and/or processed to mitigate environmental issues. The AMD simulation was performed for a period of 30 years, taking into consideration anticipated monthly weather changes. This study forms the basis of a process to determine the optimal mitigation and/or treatment of the AMD leachates derived from Southern African copper mine tails.

Keywords: Tailings-Dump, AMD, Prediction.

INTRODUCTION

Acid Mine Drainage (AMD) is a global environmental concern that requires urgent attention [1]. Due to extensive mining activities worldwide, an increasing number of mine dumps are being created, leading to greater exposure of sulfide-bearing minerals to oxygen and water. This, in turn, heightens the likelihood of AMD formation [5,11]. As of 2009, approximately 5906 abandoned mine dumps were reported in South Africa, while China had 5800 as of 2018 [14,16,17]. Similarly, Japan recorded 5487 abandoned and/or closed mines in 2000, several of which were observed to be generating AMD [12]. Given the widespread occurrence of these mine dumps globally, conducting a cost-effective analysis to prioritise AMD treatment is crucial, especially for countries with limited resources [3,4,15]. Such an analysis is also essential for appropriately scaling treatment plants. To better mitigate the impact of AMD from mining operations, it has become evident that assessing the AMD generation potential of mine ore should be conducted before, during, and after mining activities [4,11]. Static AMD tests are commonly used to quickly determine whether a given ore will generate acid (i.e., AMD)

[#] corresponding author: SamuelR@mintek.co.za and to assess its acid-neutralizing potential [2,9,13,19]. Recent studies have proposed equations that utilize mineralogical data to estimate the ore's acid-producing or neutralizing potential without requiring extensive laboratory testing [8,10]. However, a key limitation of static AMD tests is that they do not answer the question of *when* AMD will occur. This is a critical factor when prioritising multiple mine dumps for treatment, particularly when only a few can be addressed at a time due to resource constraints. For this reason, kinetic AMD prediction methods—such as experimental kinetic tests and mathematical models—are preferred, as they enable the prediction of AMD occurrence over time [6,15]. In this study, the Mintek Kinetic AMD Predictor is used to forecast AMD occurrence over a 30-year period for a selected copper mine site in Southern Africa. The Mintek Kinetic AMD Predictor is a mineral particles-based predictive tool that requires key input parameters, including mineralogical data (mineral composition, mineral surface liberation, mineral association, etc.), ore or tailings density, particle size distribution, and expected environmental conditions (temperature, rainfall, and wind speed). Compared to literature models such as the one presented by Bernardes de Souza & Mansur [6], the Mintek Kinetic AMD Predictor is more computationally intensive. However, it is expected to provide higher accuracy, as it incorporates detailed particle-based mineralogical data and simulates changes in the system's individual particle properties over time [7,8].

EXPERIMENTAL

Ore tailings characteristics – Mintek Kinetic AMD Predictor input parameters

Copper ore tailings samples from a Southern African copper mine considered in this study were analysed in Mintek's laboratories to determine the necessary input mineralogical data required for the Mintek Kinetic AMD Predictor. The tailings sample bulk modal mineralogical inputs, obtained from automated scanning electron microscopy, are presented in **Figure 1**. Calcite was the predominant mineral phase in the sample, followed by quartz, biotite, orthoclase, plagioclase, bornite, and hornblende. All other mineral phases were present in amounts <1% of the sample mass.

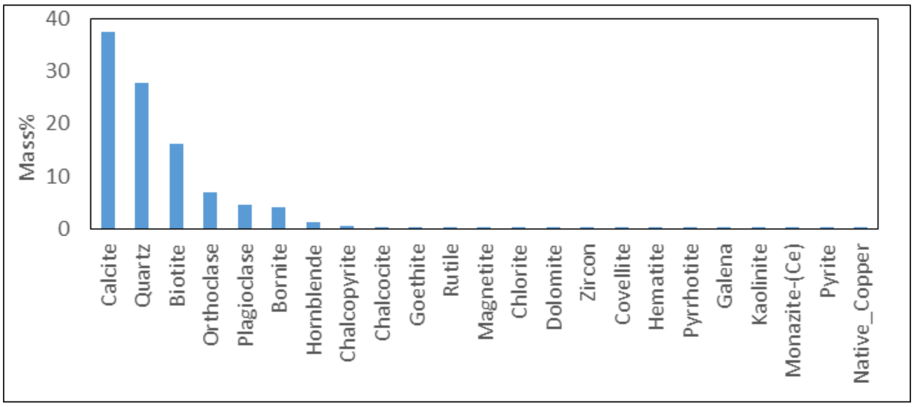

Figure 1 Bulk modal mineralogy for the Cu tailings sample

The base metal sulfides (BMS) minerals identified are summarised in **Figure 2**. They are fine-grained, with over 50% of the sulfides mass reporting to the <38 µm size fraction. The BMS minerals cumulative liberation by the free surface is shown in **Figure 3**. It should be noted that the sulfides are moderately liberated, with 20 to 60% of the mass percentage being more than 80% liberated.

The Mintek Kinetic AMD Predictor uses the bulk modal mineralogical inputs to select the specific chemical reactions associated with the tailings sample particles from its library/database. The grain size and liberation by free surface are used to determine the mineral mass available for that specific chemical reaction at the particle level during the simulation.

The sample chemical element analysis results showed that it had 0.9% S, 4.2% Al, 12.5% C, 2.9% Cu, 2% Fe, and 20% Si. This data was used to reconcile the mineralogical analysis.

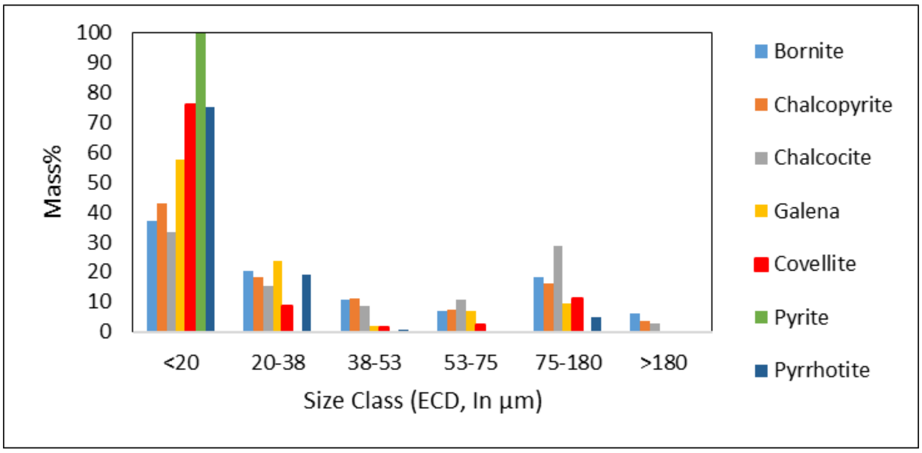

Figure 2 BMS grain size distribution

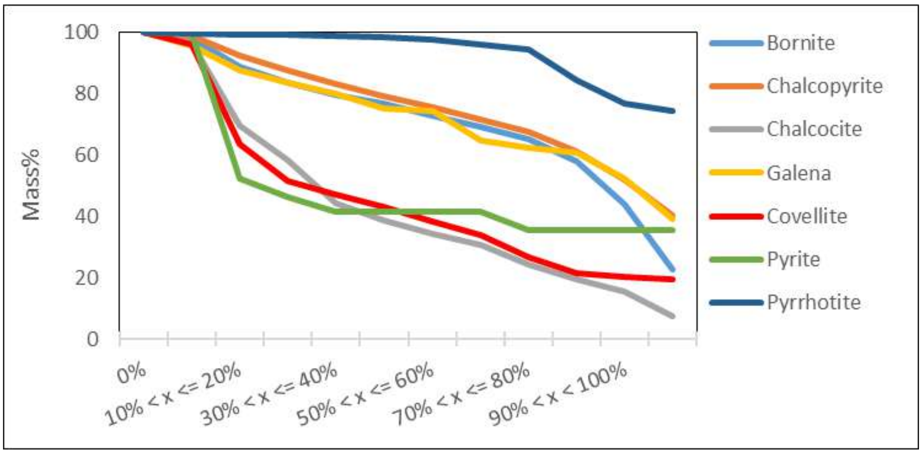

Figure 3 BMS cumulative liberation by free surface

Site Weather Conditions – Mintek Kinetic AMD Predictor input parameters

The 30 years of weather conditions (rainfall, temperature, and wind speed) at the mine site were estimated based on the historical full-year weather conditions data at the mine site obtained from Weatherspark [18]. The Mintek Kinetic AMD Predictor uses the mine site environmental temperature and wind speed to determine the system temperature and oxygen available at each particle level. The amount of rainfall is used by its infiltration model to calculate the fresh water transported to and/or available at each particle level. The seasonal average rainfall, temperature, and wind speed range were 570 mm, 17.0-25.7°C, 3.8-16.1 km/h in Summer, 27.5 mm, 11.9-25.6°C, 9.1-19.3 km/h in Autumn, 0 mm, 12.0-28.7°C, 10.7-24.1 km/h in Winter, and 312.5 mm, 17.8-30.7°C, 7.0-19.8 km/h in Spring.

The other major input to the Mintek Kinetic AMD Predictor was the mine tailings density, which was 2638 kg/m^3. Kinetic humidity cell tests were also done for 3 months to validate the Mintek Kinetic AMD Predictor parameter/results for this tailings site.

RESULTS AND DISCUSSION

The 30-year AMD prediction results for the considered Southern African mine tailings site are shown in **Figure 4**. To avoid a congested graph, the results are presented yearly. A zoomed-in view of the last 3 years is also added to **Figure 4** to show the acid release rate profile per kilogram of tailings per quarter, i.e., to show the impact of seasonal changes.

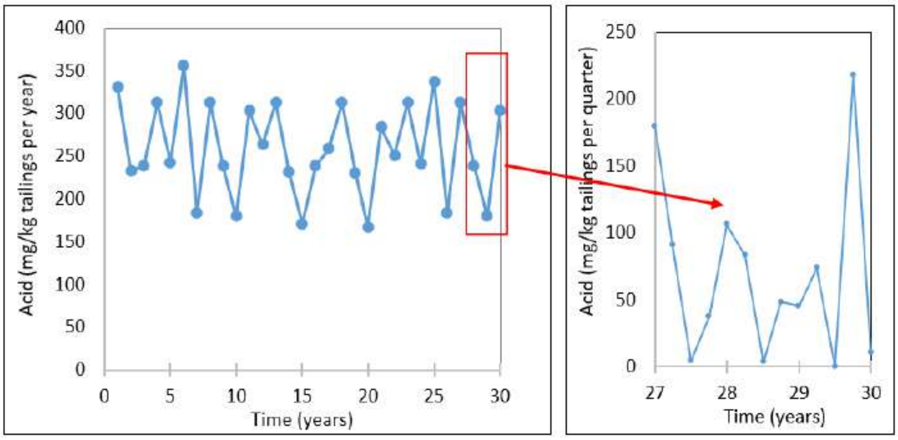

Figure 4 AMD prediction over 30 years

It should be noted from **Figure 4** that the yearly acid release rates vary (with minimum, maximum, and average of 167, 355, and 259 mg/kg tailings per year respectively), and this was expected as the mine tailings site weather conditions also vary significantly as noted from the input weather conditions. In the early years (<10 years), the overall acid production rate was slightly higher, and this could be attributed to the fact that there was still a high percentage of fine sulfide mineral particles (<38 µm) with high free surface area. Further analysis of the change in the cumulative acid release rate showed that the tailings site might reach the peak acid release rate sometime beyond the 30 years used in this study. This information is crucial if a plant is to be designed and built to treat AMD from this mine site.

CONCLUSIONS AND RECOMMENDATION

The Mintek Kinetic AMD Predictor was used in this study to predict the AMD occurrence over 30 years for one of the Southern African copper mine tailings dumps. The results obtained in this study will form part of an ongoing process to determine the optimal AMD leachates mitigation and/or treatment process for this mine site. For improved predictions, it is recommended that the impact of climate change be included in the input weather conditions.

REFERENCES

1. Acharya, B.S. and Kharel, G. (2020) Acid mine drainage from coal mining in the United States – An overview. Journal of Hydrology, 588.
2. ASTM, (2018) Standard Test Method for Laboratory Weathering of Solid Materials Using a Humidity Cell, ASTM D5744 -18.
3. Ayora, C., Macias, F., Torres, E. and Nieto, J.M. (2015) Rare Earth Elements in Acid Mine Drainage. In: Meeting of the Spanish Mineralogy Society, Huelva, Spain, Proceedings.
4. Baloyi, J., Ramdhani, N., Mbhele, R., and Simate, G.S. (2024) Acid Mine Drainage from Gold Mining in South Africa: Remediation, Reuse, and Resource Recovery. Mine Water and the Environment, 43, 418-430.
5. Becker, M., Dyantyi, N., Broadhurst, J., Harrison, S.T.L. and Franzidis, J.P. (2015) Application of quantitative mineralogy in the interpretation of laboratory scale acid rock drainage prediction tests: A gold case study, Minerals to Metals Initiative. Department of Chemical Engineering, University of Cape Town, South Africa.
6. Bernardes de Souza, C.M. and Mansur, M. B. (2011) Modelling of acid mine drainage (AMD) in columns. Brazilian Journal of Chemical Engineering, 28(3), 425-432.
7. Brough, C., Strongman, J., Bowell, R., Warrender, R., Prestia, A., Barnes, A., Fletcher, J. (2017) Automated environmental mineralogy; the use of liberation analysis in humidity cell testwork. Minerals Engineering, 107, 112-122.
8. Chetty, D., Bazhko, O., Govender, V. and Ramatsoma, S. (2020) The prediction of acid mine drainage potential using mineralogy. In: Recovery of byproducts from acid mine drainage treatment (E. FossoKankeu, C. Wolkersdorfer and J. Burgess, Scrivener Publishing LLC, Beverly, 49-71.
9. de Mello, J.W.V., Dias, L.E., Daniel, A.M., Abrahao, W.A.P., Deschamps, E. and Schaefer, C.E.G.R. (2006) Preliminary evaluation of acid mine drainage in Minas Gerais State, Brazil, Revista Brasileira de Ciência do Solo, 30, 365-375.
10. Elghali, A., Benzaazoua, M., Taha, Y., Amar, H., Ait-kouia, Y., Bouzahzah, H. and Hakkou, R. (2023) Prediction of acid mine drainage: Where we are. Earth-Science Reviews, 241.
11. Erguler, G.K. and Erguler, Z.A. (2020) The evaluation of acid mine drainage by kinetic procedures and empirical models for field scale behavior. Arabian Journal of Geosciences, 13.
12. Herrera, P., Uchiyama, H., Igarashi, T., Asakura, K., Ochi, Y., Iyatomi, N. and Nagae, S. (2007) Treatment of acid mine drainage through a ferrite formation process in central Hokkaido, Japan: Evaluation of dissolved silica and aluminium interference in ferrite formation. Minerals Engineering, 20(13), 1255-1260.

13. Karlsson, T., Alakangas, L., Kauppila, P. and Räisänen, M.L. (2021) Test of Two Methods for Waste Rock Drainage Quality Prediction: Aqua Regia Extraction and Single-addition Net-acid Generation Test Leachate Analysis. Mine Water Environ, 40, 736-751.
14. Makhetha, E. (2023) 'Zama Zama' and leftovers: The recycling of ore in abandoned gold mines in South Africa. The Extractive Industries and Society, 14.
15. Masindi, V. (2017) Recovery of drinking water and valuable minerals from acid mine drainage using an integration of magnesite, lime, soda ash, CO_2 and reverse osmosis treatment processes. Journal of Environmental Chemical Engineering, 5(4), 3136-3142
16. South African Auditor General (SAAG), (2009) Report of the Auditor-General to Parliament on a performance audit of the rehabilitation of abandoned mines at the Department of Minerals and Energy, https://cer.org.za/wp-content/uploads/2011/10/AG_Report_on_abandoned_mines-Oct-2009.pdf, (Accessed: 12 June 2019)
17. Wang, Z., Xu, Y., Zhang, Z., and Zhang, Y. (2020) Review: Acid Mine Drainage (AMD) in Abandoned Coal Mines of Shanxi, China. Water, 13(1), 8.
18. Weatherspark, (n.d) The weather year round anywhere on Earth, https://weatherspark.com, (Accessed: 02 January 2024)
19. Yeheyis, M. B., Shang, J. Q. and Yanful, E. K. (2009) Long-term evaluation of coal fly ash and mine tailings co-placement: a site-specific study. Journal of Environmental Management, 91, 237-244.

XVI International Mineral Processing
and Recycling Conference
28-30 May 2025, Belgrade, Serbia

DOI: 10.5937/IMPRC25568R Original research article

CHARACTERIZATION OF AN ORE SAMPLE FROM CONGO BASED ON TANTALUM AND NIOBIUM FOR POSSIBLE FURTHER TECHNOLOGICAL TESTS

Dragan S. Radulović[1#], 0000-0001-8210-8100,
Jovica Stojanović[1], 0000-0002-2752-6374,
Gašper Tavčar[2], 0000-0001-9891-6153,
Vladimir Jovanović[1], 0000-0001-6069-1630,
Dejan Todorović[1], 0000-0002-2776-3388,
Branislav Ivošević[1], 0000-0001-9445-8159,
Sonja Milićević[1], 0000-0001-8929-1673,
[1]Institute for Technology of Nuclear and Other Mineral Raw Materials (ITNMS),
11000 Belgrade, Serbia
[2]Institut "Jožef Stefan", 1000 Ljubljana, Slovenia

ABSTRACT – In this study, two samples of "Ta-Nb" ore from Congo (MMR-1 and MMR-2) were analyzed. Various physical and chemical properties were determined for these samples, including gross and hygroscopic moisture, specific gravity, granulometric composition of the initial samples and after each level of crushing, bulk density of the initial samples and after each crushing stage, and chemical composition. Qualitative mineralogical analysis was conducted using X-ray diffraction (XRD), while polished sections were prepared for optical microscopy, scanning electron microscopy (SEM), and mineralogical analysis by particle size classes. Detailed physicochemical and mineralogical tests were carried out on the MMR-1 and MMR-2 samples to comprehensively define the parameters necessary as a foundation for further technological testing of "Ta-Nb" ore from Congo. The results showed that the examined samples have appropriate characteristics for further technological tests.

Keywords: “Ta-Nb”ore-Congo, Physico-Chemical, and Mineralogical Investigation.

INTRODUCTION

Tantalum (Ta) and niobium (Nb) are transition metal elements whose economic importance continues to grow due to the increasing demand for their use in various technological applications [1-3]. The unique properties of Ta and Nb, such as their high dielectric constants, stability of their oxides, and corrosion resistance [3-6], make these metals highly valuable in electronics, aerospace, nuclear, and automotive industries, as well as in military and medical applications [2, 3, 7, 8]. Tantalum is invariably associated with niobium, and both elements are primarily extracted from columbite-tantalite group minerals, which are minor components found in primary granites, granite pegmatites,

---

[#] corresponding author: d.radulovic@itnms.ac.rs and greisen rocks [1,3]. In nature, tantalum coexists with niobium as oxides, often associated with iron and manganese oxides, and sometimes includes elements such as tin, titanium, lithium, cesium, and trace amounts of tungsten, uranium, and thorium in pegmatitic and related lithologies [3, 9, 10]. Columbite-tantalite (commonly referred to as coltan) group minerals [$(Fe,Mn)O(Ta,Nb)_2O_5$] are the primary sources for tantalum and niobium production. These include [tantalite-(Fe) or tantalite-(Mn)] and [columbite-(Fe) or columbite-(Mn)] [2, 3, 11].

Additionally, tantalum, tin, and niobium are found in other minerals such as pyrochlore, ixiolite, and wodginite, which are complex oxides and hydroxides [3, 10]. In 2022, global tantalum production, expressed as Ta_2O_5 content, was approximately 1,726 tons, with Congo contributing around 550 tons (31.90%), followed by Brazil (20.30%), Rwanda (17.40%), Nigeria (8.10%), China (5.30%), Ethiopia (5.20%), Mozambique (4.80%), and others (7.0%). In the same year, global niobium production, expressed as Nb_2O_5 content, totaled 118,209 tons, with Brazil accounting for 110,000 tons (93.05%), Canada (5.75%), and other countries (1.20%) [12]. Both Ta and Nb are classified as critical raw materials (CRM) for the European Union [13].

Ta and Nb-based ore samples from the Kivu Belt (KVB) region of the Congo were analyzed by different test methods. The Kivu Belt is a geological part of the Kibaran Belt, which extends over 700 kilometers from Katanga Province in southeastern Congo to Uganda [14]. The paper will present the results of testing ore samples based on Ta and Nb, with the aim of establishing the characteristics of the mentioned metals and their possibility in further technological applications.

EXPERIMENTAL

Materials and methods

The physicochemical and mineralogical properties of two "Ta-Nb" ore samples from Congo called MMRS-1 and MMRS-2 were examined by the Institute (ITNMS) for a Slovenian company. Each sample weighed approximately 25 kg. The tests aimed to determine the key properties of the mineral raw material, assess its potential as a resource, and evaluate the technological possibilities for processing the "Ta-Nb" ore into commercial products for various industrial sectors. The analysis included determining gross and hygroscopic moisture, specific gravity, granulometric composition of the initial samples and after each crushing stage, and bulk density. Granulometric composition was determined by dry sieving using Tyler's series of sieves for the initial samples. Due to the high clay content in the ore, samples were washed, and the granulometric composition was re-evaluated using the wet method.

Mineralogical analyses were conducted using X-Ray Diffraction (XRD), Reflected Light Microscopy, and Scanning Electron Microscopy (SEM), providing both qualitative and quantitative data on the samples. All analyses adhered to internationally recognized standards for evaluating the quality of mineral raw materials.

Chemical analyses of the "Ta-Nb" ore samples were performed at the ICP laboratory of the Jožef Stefan Institute. Both samples were prepared identically for characterization, with the sample preparation method outlined in Figure 1.

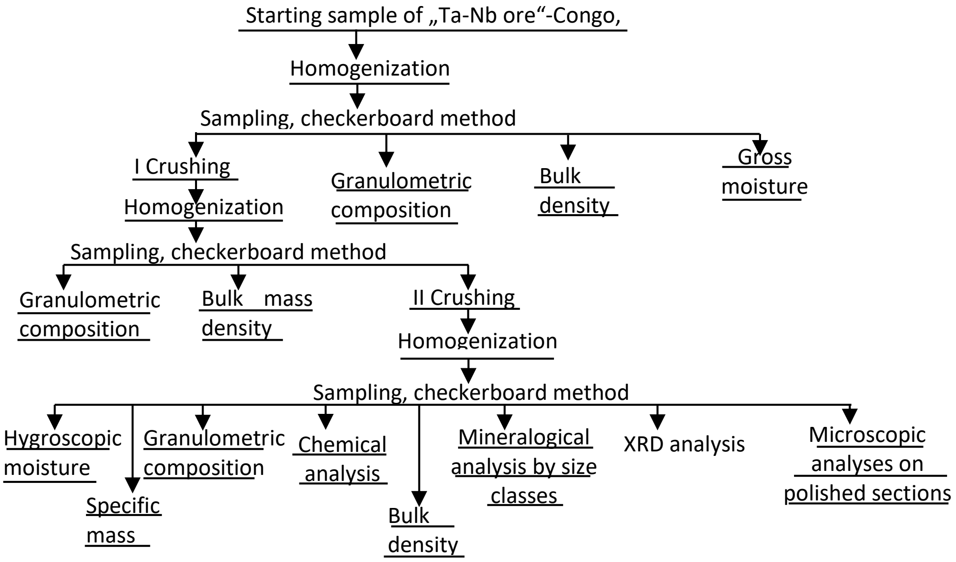

Figure 1 Written scheme of preparation "Ta-Nb ore samples" - Congo (MMR Sample 1 and MMR Sample 2) for physico-chemical and mineralogical investigation

Physical characterization of the sample

As part of the physical characterization, the gross moisture (Hg) content of the initial samples of the "Ta-Nb" ore—Congo was first determined. Sample MMR-1 and sample MMR-2 had Hg presence of 0.30 and 0.12%, respectively. The content of hygroscopic moisture in the sample MMR-1 and MMR-2 was 0.32 and 0.39%, respectively.

The granulometric compositions for both samples of "Ta-Nb" Congo (MMR sample 1 and MMR sample 2) were determined on the initial samples, after the first crushing and after the final crushing. The particle size distribution of these samples was determined by wet sieving on sieves (Tyler sieve series). During these tests, upper size limit (d_{95}) and the mean grain diameter (d_{50}) were determined for each of the samples. In addition, the bulk density of the samples was measured during these tests (SRPS EN ISO 3252:2014). All these parameters for each of the samples are shown in Table 1.

Table 1 Granulometric composition and bulk density of "Ta-Nb" ore samples

MMR-1 initial sample			MMR-2 initial sample		
d_{95}=23,914mm	d_{50}=3,507	Δ=1.35g/cm^3	d_{95}=19,647mm	d_{50}=1,683mm	Δ=1.37g/cm^3
MMR-1 after I stage of crushing			MMR-2 after I stage of crushing		
d_{95}=9,767mm	d_{50}=1,961	Δ=1.31g/cm^3	d_{95}=9,904mm	d_{50}=1,25mm	Δ=1.34g/cm^3
MMR-1 after final crushing			MMR-2 after final crushing		
d_{95}=4,386mm	d_{50}=0,959	Δ=1.19g/cm^3	d_{95}=4,332	d_{50}=0,594mm	d_{50}=1,23g/cm^3

The specific mass was determined for each of the “Ta-Nb” ore samples (MMR-1 and MMR-2). The specific gravity value obtained for sample MMR-1 and MMR-2 was 2.55g/cm^3 and 2.58g/cm^3, respectively.

Chemical compositions of both starting samples "Ta-Nb" ore-Congo

The chemical composition of both initial samples of "Ta-Nb" ore from Congo (MMR-1 and MMR-2) was determined using ICP analysis at the Jožef Stefan Institute. The results of the chemical analysis for major components (high content) are presented in Table 2, while the results for minor components (low content) are shown in Table 3.

Table 2 Chemical composition of the MMR-1 sample "Ta-Nb" ore-Congo, main components

Components	Si	Al	Ca	Na	K	Mg	Fe	Ti
Sample MMR-1, %	29,94	8,39	0,073	0,90	1,57	0,055	1,61	0,052
Sample MMR-2, %	31,18	9,68	0,11	1,48	1,515	0,050	0,83	0,022

Table 3 Chemical composition of the MMR-1 sample "Ta-Nb" ore-Congo, minor components

Components	Mn	Ni	Mo	Nb	Cr	Sn	Ta	W
Sample MMR-1, g/t	193	20	45	111	97	167,9	212,3	45,1
Sample MMR-2, g/t	453,1	23,34	48,37	118,37	85,29	178,97	150,1	44,2

Mineralogical study of two samples MMR S1 and MMR S2 „Ta-Nb“ ore -Congo

As part of the mineralogical analysis, preparations were made for optical and SEM microscopy, XRD analysis, and mineralogical examination by individual size classes.

XRD method-results of the research

The qualitative mineralogical composition of the MMR-1 sample includes quartz, mica (muscovite), illite, kaolinite, dickite, nacrite, plagioclase, alkali feldspar (K-feldspar), columbite-tantalite, and wodginite. Semi-quantitative mineralogical analysis of the crystalline phases, determined using the Rietveld refinement method, is as follows (in weight %): quartz 61.4 (0.49)%, kaolinite 13.1 (0.73)%, muscovite 12.2 (0.6)%, plagioclase 6.8 (0.69)%, dickite 4.9 (0.58)%, illite 0.4 (0.04)%, nacrite 0.4 (0.04)%, K-feldspar 0.8 (0.05)%, with columbite-tantalite and wodginite present in trace amounts.

The qualitative mineralogical composition of the MMR-2 sample includes quartz, mica (muscovite), illite, kaolinite, dickite, nacrite, alkali feldspar (K-feldspar), plagioclase, columbite-tantalite, and wodginite. The quantitative mineralogical analysis of the crystalline phases is as follows (in weight %): quartz 39.5 (0.75)%, plagioclase 24.1 (0.69)%, muscovite 15.9 (0.85)%, kaolinite 8.0 (0.53)%, K-feldspar 7.3 (0.54)%, dickite 1.4 (0.67)%, nacrite 3.1 (0.38)%, illite 0.8 (0.64)%, with columbite-tantalite and wodginite present in trace amounts.

The diffractograms of samples "MMR-1" and "MMR-2" are shown in Figures 2 and 3, respectively.

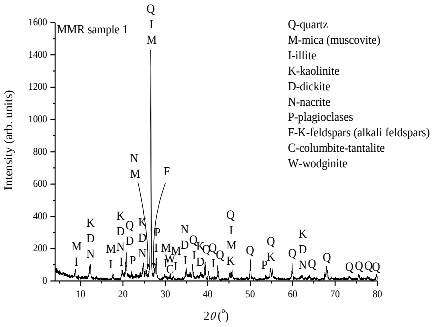

Figure 2 XRD diffractogram of the "MMR S1"

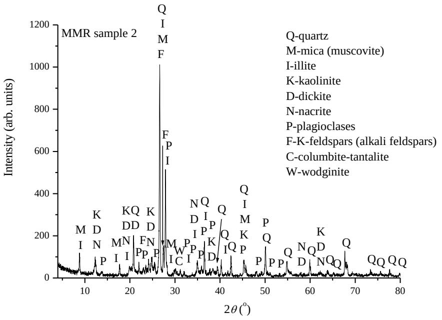

Figure 3 XRD diffractogram of the "MMR S2"

Reflected Light and Scanning Electron Microscopy method

According to mineralogical analyses, the useful minerals identified in both samples (MMR-1 and MMR-2) are columbite, tantalite, wodginite, and gersdorffite, all occurring in small quantities. Microscopic analyses revealed that the MMR-2 sample does not contain niobium-tantalates (columbite-(Fe,Mn)-tantalite-(Fe,Mn) series) but only (ferro)wodginite ($FeSnTa_2O_8$), which explains the lower Nb content in the MMR-2 sample.

The grain size of niobium-tantalates in MMR-1 (columbite-(Fe,Mn)-tantalite-(Fe,Mn) series and (ferro)wodginite) ranges from 10 µm to 115 µm, while the grain size of (ferro)wodginite in MMR-2 ranges from 90 µm to nearly 200 µm. A grain liberation study of Nb-Ta-bearing minerals (columbite-tantalite, wodginite) and cassiterite indicates that in the size class -0.15+0.1 mm, over 80% of the grains are liberated in both samples.

CONCLUSION

Mineralogical analyses of both samples (MMR-1 and MMR-2) of the "Ta-Nb" ore from Congo indicate that clay minerals (illite, kaolinite, dickite, nacrite) and mica (muscovite) are present as accompanying minerals, constituting approximately 30% of the starting sample by weight. Removing these minerals via washing would be the initial step in processing the "Ta-Nb" ore from Congo.

For the concentration of useful minerals (columbite-tantalite and cassiterite) from the washed "Ta-Nb" ore, gravity concentration and magnetic separation are the most suitable methods.

1. **Gravity Concentration:** Gravity concentration is feasible due to the significant difference in density between the useful minerals and the tailing minerals. The useful minerals, such as columbite (~6 g/cm^3), cassiterite (~7 g/cm^3), tantalite (~8 g/cm^3), (ferro)wodginite (~7 g/cm^3), and gersdorffite (~6 g/cm^3), have much higher densities compared to the primary tailing minerals, such as quartz and feldspar, which have

densities below 3 g/cm³. This substantial density contrast makes it possible to efficiently separate the useful minerals from the tailings using gravity-based methods.

2. **Magnetic Separation:** Magnetic separation can effectively separate the minerals tantalite, columbite, cassiterite, and wodginite from each other. Based on their magnetic properties, tantalite, columbite, and wodginite are paramagnetic, while cassiterite is diamagnetic. This distinction allows for relatively easy separation of cassiterite from the other minerals.

Based on the examination of ore samples containing Ta and Nb from Kon, it can be concluded that the examined ore has the capacity to extract useful elements and use them in technological applications of various industrial sectors.

ACKNOWLEDGEMENT

This paper is part of the investigation according to the research funding agreement financed by the Ministry of Science, Technological Development and Innovation of the Republic of Serbia in 2025 under the contract number 451-03-136/2025-03/200023, concluded on 10.02.2025.

REFERENCES

1. Melcher F., et al., Tantalum-(niobium-tin) mineralisation in African pegmatites and rare metal granites: constraints from Ta-Nb oxide mineralogy, geochemistry and U-Pb geochronology, Ore Geol. Rev. 64 (2015) 667–719, https://doi.org/10.1016/j. oregeorev.2013.09.003.
2. J.F.P. Klaus, J. Schulz, Nadine M. Piatak, Niobium and Tantalum, 2017. Reston, vol. A.
3. J. B. Habinshuti , et al., Mineralogical and physical studies of low-grade tantalum-tin ores from selected areas of Rwanda, Results in Engineering, 11 (2021) 100248, https://doi.org/10.1016/j.rineng. 021.100248.
4. L.A.T. Espinoza, L.A. Tercero Espinoza, Case Study: Tantalum in the World Economy. History, Uses and Demand, University of Dundee, Research and Innovation Services, Dundee, 2012.
5. M. Toure, G. Arrachart, J. Duhamet, S. Pellet-Rostaing, Tantalum and niobium selective extraction by alkyl-acetophenone, Metals (Basel) 8 (9) (Aug. 2018) 654, https://doi.org/10.3390/met8090654.
6. D. Bleiwas, J. Papp, T. Yager, Shift in Global Tantalum Mine Production, 2000 – 2014, 2015, https://doi.org/10.3133/fs20153079. Usgs, vol. Fact Sheet, no. December.
7. P, N. H, D.S. Muchez, Geological mapping and implications for Nb-Ta, Sn and W prospection in Rwanda, Bull. Des Seances L'academie R. Des Sci. D'outre-Mer 60 (3–4) (2014) 515–530.
8. M.O.H. Amuda, D.E. Esezobor, G.I. Lawal, "Adaptable technologies for life – cycle processing of tantalum bearing minerals, J. Miner. Mater. Char. Eng. 6 (1) (2007) 69–77, https://doi.org/10.4236/jmmce.2007.61006.
9. J. Jeangrand, Comprehensive Strategic Analysis of the Tantalum Industry, Simon Fraser University, Burnaby, BC, Canada, 2005.
10. N. Motlalepula, Separation and Purification of Niobium and Tantalum from Synthetic and Natural Compounds, 2013.
11. R. Shaw, K. Goodenough, Niobium–tantalum, Br. Geol. Surv. (2011).
12. World Mining Data 2024, Volume 39, C. Reichl, M. Schatz, Mineral Production, Vienna, Republic of Austria, 2024.
13. Milan Grohol, Constanze Veeh. DG GROW, European Commission, Study on the Critical Raw Materials for the EU 2023.

14. M. Villeneuve, et al., A Review of the G4 “Tin Granites” and Associated Mineral Occurrences in the Kivu Belt (Eastern Democratic Republic of the Congo) and Their Relationships with the Last Kibaran Tectono-Thermal Events, Minerals 2022, 12, 737., https://doi.org/10.3390/min12060737.

XVI International Mineral Processing
and Recycling Conference
28-30 May 2025, Belgrade, Serbia

DOI: 10.5937/IMPRC25575R Original research article

STUDY OF MINERALOGICAL AND PHYSICOCHEMICAL PROPERTIES OF SAMPLES OF FLOTATION TAILINGS "RUDNIK" MINE

Dragan S. Radulović[1#], 0000-0001-8210-8100,
Jovica Stojanović[1], 0000-0002-2752-6374,
Grozdanka Bogdanović[2], 0000-0002-1013-4075,
Vladimir Jovanović[1], 0000-0001-6069-1630,
Dejan Todorović[1], 0000-0002-2776-3388,
Branislav Ivošević[1], 0000-0001-9445-8159,
Vladimir Simić[3], 0000-0002-2483-1779,
[1]ITNMS, 11000 Belgrade, Serbia
[2]University of Belgrade, Technical faculty in Bor, Bor, Serbia
[3]Faculty of Mining and Geology, University of Belgrade, 11000 Belgrade, Serbia

ABSTRACT – In this study, two samples of flotation tailings from the "Rudnik" Mine (one from boreholes and one from the surface) were examined. Various physical and chemical properties were analyzed, including gross and hygroscopic moisture, specific mass, bulk density in both loose and compacted states, and specific weight. Additionally, granulometric and chemical compositions were determined. A qualitative mineralogical analysis was conducted using X-ray diffraction (XRD), along with the preparation of polished sections for optical and SEM microscopy. Comprehensive physicochemical and mineralogical tests were performed to define all parameters necessary for the valorization and recycling of flotation tailings from the "Rudnik" Mine.

Keywords: Flotation Tailings, Physico-Chemical And Mineralogical Investigation, Recycling.

INTRODUCTION

The extraction and processing of ore generate large amounts of mine waste materials, including tailings, metallurgical waste, and waste rock [1-3]. While these materials may present economic opportunities for re-use and re-mining, they can also cause severe environmental damage and contamination if not properly managed [3-10]. Sulfidic mine waste has the potential to generate Acid Rock Drainage (ARD) and release toxic elements into the environment under oxidizing conditions, posing significant risks to both ecosystems and human health. Therefore, the re-use of mine waste materials can play a crucial role in mitigating environmental hazards [3].

The "Rudnik" Mine has been engaged in the exploitation and processing of Pb-Zn ore since 1953. This activity inevitably led to the construction of a tailings pond, which has expanded over time and now covers an area of more than 30 hectares. Over 11,000,000 tons (more than 7 million m^3) of flotation tailings have been deposited in the Rudnik Mine

---

[#] corresponding author: d.radulovic@itnms.ac.rs tailings pond. This fine-grained material is a residue from the flotation process, which produced K/PbS, K/CuFeS_2, and K/ZnS concentrates.

Based on previous preliminary tests, a program of technological studies on the flotation tailings of the Rudnik Mine has been developed. The objective of these studies is to valorize valuable components from the tailings, including precious metals, non-ferrous metals, and critical elements, while also utilizing the remaining aluminosilicate residue for the production of construction materials—ultimately striving to achieve the Zero Waste principle.

In 2023, the Science Fund of the Republic of Serbia, under the Prisma Program in the field of technical and technological sciences, approved funding for the project **"Characterization and Technological Procedures for Recycling and Reusing of the Rudnik Mine Flotation Tailings - REASONING"** (2024-2026). The planned activities within the REASONING project are outlined in a written scheme presented in Figure 1.

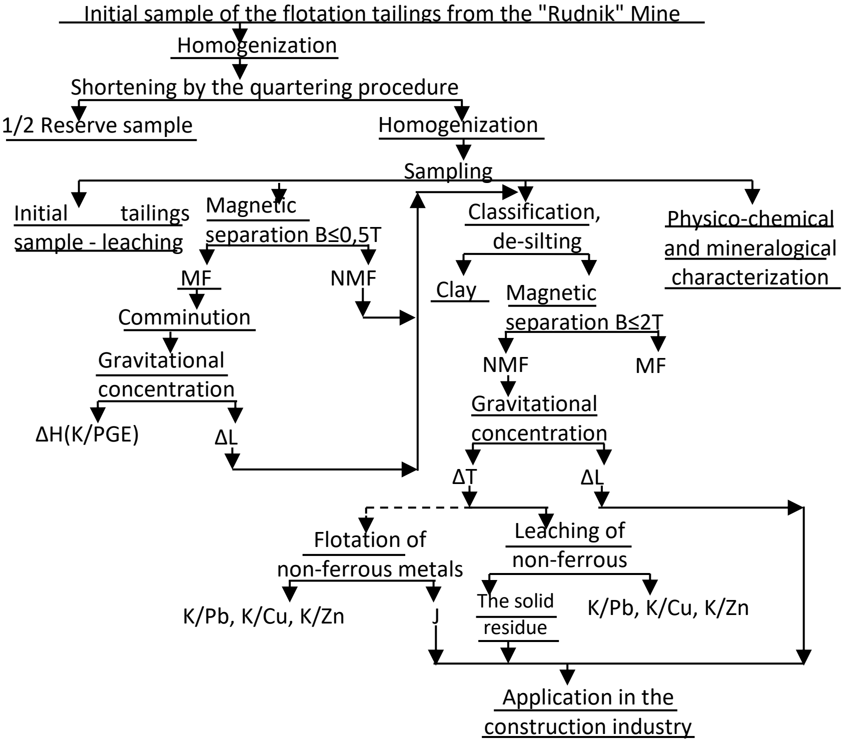

Figure 1 Written scheme of all activities and technological stages for the valorization of tailings according to Project-REASONING

At the end of 2024, two samples of flotation tailings were collected from the tailings pond at the Rudnik Mine. The first sample was obtained from four boreholes by drilling, and a composite sample was created from them. The second sample was taken from the surface of the tailings pond, and a composite sample was also prepared.

EXPERIMENTAL

Materials and methods

The physicochemical and mineralogical properties of two flotation tailings samples were analyzed: a composite sample from four boreholes with a total mass of 260 kg and a composite sample from the surface of the tailings pond with a total mass of 360 kg. These analyses were conducted at the Institute for Technology of Nuclear and Mineral Raw Materials (ITNMS).

Detailed physicochemical and mineralogical tests were performed on the initial flotation tailings samples from the Rudnik Mine to determine the essential characteristics of this secondary mineral raw material. Various physical and chemical properties and parameters were examined, including gross and hygroscopic moisture, specific mass, granulometric composition, bulk density in both loose and compacted states (SRPS EN 1097-3:2009), and specific weight (SRPS EN 1936:2009).

The particle size distribution of both tailings samples was determined using dry sieving with a Tyler series of sieves and laser diffraction analysis. Dry measurements were conducted using Sympatec Helos BR (H1506), Sucell 2; HELOS, while wet measurements were performed using a Malvern Mastersizer 3.0. Both devices operate on the principle of laser diffraction (refraction) of laser beams on micronized sample particles.

Mineralogical analyses were conducted using the following methods:

- X-Ray Diffraction (XRD)
- Reflected Light Microscopy
- Scanning Electron Microscopy (SEM)

These analyses provided qualitative and quantitative data on the mineralogical composition of the tailings samples. All analyses and tests were carried out according to internationally recognized standard methods for assessing the quality of mineral raw materials.

All chemical analyses of the tailings samples were performed using Inductively Coupled Plasma (ICP) spectroscopy at the Institute for Multidisciplinary Research in Belgrade.

RESULTS AND DISCUSSION

Physical characterization of the initial samples

As part of the physical characterization, the gross moisture content of the initial flotation tailings samples from the "Rudnik" Mine was first determined. Sample 1 (composite from boreholes) had a gross moisture content of $Hg_1 = 0.32\%$, while Sample 2 (composite from the surface) had $Hg_2 = 0.24\%$. The hygroscopic moisture content was $w_1 = 15.42\%$ for the borehole composite sample and $w_2 = 10.61\%$ for the surface composite sample.

The granulometric composition of both initial flotation tailings samples (composite from boreholes and composite from the surface) was determined using dry sieving with Tyler series sieves, covering sieve openings from 1 mm to 0.3 mm. All results obtained from different particle size distribution methods (sieving and laser diffraction) were consolidated. Based on these results, the upper size limit (d_{95}) and average particle diameter (d_{50}) were determined:

- Borehole sample: d_{95} = 0.45 mm, d_{50} = 0.175 mm
- Surface sample: d_{95} = 0.35 mm, d_{50} = 0.17 mm

The bulk density of the borehole tailings sample was:

- Loose state: ΔL = 1.64 g/cm^3
- Compacted state: Δc = 1.93 g/cm^3
- Specific mass: γ_1 = 3.19 g/cm^3

For the surface tailings sample:

- Loose state: ΔL = 1.44 g/cm^3
- Compacted state: Δc = 1.66 g/cm^3
- Specific mass: γ_2 = 3.13 g/cm^3

Chemical Composition of Initial Samples

The chemical composition of both flotation tailings samples from the Rudnik Mine was determined using ICP at the Institute for Multidisciplinary Research. Table 2 presents the major components, while Table 3 shows the minor components.

Table 2 Chemical composition of the tailings samples of "Rudnik"-Mine, main components

Components	Al	Ca	Mg	Cu	Fe	Zn	Pb	K
from boreholes, %	2.35	10.39	1.49	0.07	10.74	0.47	0.16	0.75
from surface, %	2.52	7.48	1.52	0.135	11.39	0.22	0.07	1.83

Table 3 Chemical composition of the tailings samples of "Rudnik"-Mine, minor components

Components	Ag	B	As	Ba	Bi	Cd	Co	Cr
from boreholes, g/t	9.2	500	914	172	29	40	35	328
from surface, g/t	7.4	712	3173	395	90	23	45	298

Mineralogical study of the tailings samples

As part of the mineralogical analysis, sample preparations were made for optical microscopy, SEM microscopy, and XRD analysis.

XRD Method – Research Results

Mineralogical Composition of the Borehole Sample - The qualitative mineralogical composition of the analyzed tailings sample from boreholes includes: quartz, calcite, K-feldspars, plagioclase, kaolinite, pyrite, pyrrhotite, arsenopyrite, sphalerite, chalcopyrite, galena, smectite/chlorite minerals, irregularly interstratified clays, and magnetite. Calcite and quartz are the most abundant minerals. Feldspars (K-feldspars and plagioclase) are present in smaller amounts. Among the ore minerals, pyrrhotite, arsenopyrite, and pyrite are the most abundant. Among the valuable minerals, sphalerite is the most common, followed by chalcopyrite in lower quantities, while galena is the least abundant. The diffractogram of the analyzed sample is presented in Figure 2.

Mineralogical Composition of the Surface Sample - The qualitative mineralogical composition of the analyzed tailings sample from the surface includes: quartz, calcite, K-feldspars, plagioclase, gypsum, kaolinite, pyrite, pyrrhotite, arsenopyrite, sphalerite, chalcopyrite, galena, smectite/chlorite minerals, irregularly interstratified clays, magnetite, dolomite, axinite, apatite, and bassanite. Feldspars (K-feldspars and plagioclase), calcite, and quartz are the most common minerals. Clay minerals and gypsum are present in smaller amounts. Among the ore minerals, pyrrhotite, arsenopyrite, and pyrite are the most abundant. Among the valuable minerals, sphalerite is the most common, followed by chalcopyrite in smaller amounts, while galena is the least abundant. All other minerals, if present, are below the detection threshold of this method. The diffractogram of the analyzed sample is presented in Figure 3.

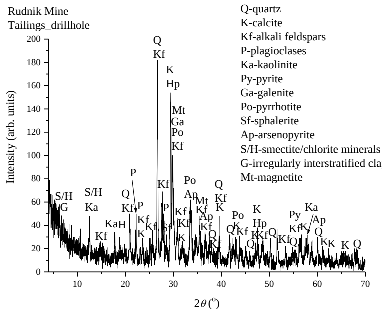

Figure 2 XRD diffractogram of the tailings from boreholes

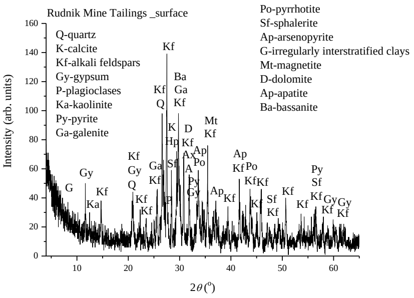

Figure 3 XRD diffractogram of the tailings from surface

Reflected Light and Scanning Electron Microscopy method

According to mineralogical analyses, the valuable minerals present in both samples (from boreholes and the surface) are sphalerite, chalcopyrite, and galena, primarily occurring as intergrowths or inclusions.

CONCLUSION

The determination of gross moisture content revealed that the tailings samples contained a significantly high water content—over 15% in the borehole sample and over 10% in the surface sample.

The granulometric analysis showed that both the borehole and surface tailings samples contained a significant proportion of coarse particles exceeding 0.5 mm.

According to the mineralogical analysis of the Rudnik Mine tailings samples:

- No platinum group elements (PGE) were detected in pyrrhotite.

- Visible gold/silver was observed.
- The most abundant minerals in the tailings are quartz and aluminosilicates.
- Multiple grains of native silver/gold were found in pyrrhotite, sphalerite, chalcopyrite, and galena.
- Sphalerite was identified as the most abundant non-ferrous metal mineral.

Based on the conducted analyses and the mineral composition of the tailings samples, it can be concluded that gravitational and magnetic separation methods can be effectively applied in the concentration process.

ACKNOWLEDGEMENT

This paper presents research conducted as part of the REASONING project (2024–2026), funded by the Science Fund of the Republic of Serbia under the PRIZMA Program (code 7522), focusing on the characterization and recycling of Rudnik Mine flotation tailings.

REFERENCES

1. B. G. Lottermoser, Recycling, Reuse and Rehabilitation of Mine Wastes, December 2011, Elements 7(6):405-410, doi: 10.2113/gselements.7.6.405.
2. Tayebi-Khorami, M., Edraki, M., Corder, G., Golev, A., 2019. Re-thinking mining waste through an integrative. Minerals 9 (5), 286.
3. S. Bevandić, R. Blannin, A. G. Escobar, K. Bachmann, M. Frenzel, ´A. Pinto, J. M.R.S. Relvas, P. Muchez, Metal deportment in Pb-Zn mine wastes from a historic tailings pond, Plombi`eres, East Belgium**,** Minerals Engineering 184 (2022) 107628.
4. Jamieson, H.E., Walker, S.R., Parsons, M.B., 2015. Mineralogical characterization of mine waste. Appl. Geochemistry 57, 85–105. https://doi.org/10.1016/j. apgeochem.2014.12.014.
5. Ettler, V., 2015. Soil contamination near non-ferrous metal smelters: A review. Appl. Geochemistry 64, 56–74. https://doi.org/10.1016/j.apgeochem.2015.09.020.
6. Falaǵan, C., Grail, B.M., Johnson, D.B., 2017. New approaches for extracting and recovering metals from mine tailings. Miner. Eng. 106, 71–78. https://doi.org/ 10.1016/j.mineng.2016.10.008.
7. Karaca, O., Cameselle, C., Reddy, K.R., 2017. Acid pond sediment and mine tailings contaminated with metals: physicochemical characterization and electrokinetic remediation. Environ. Earth Sci. 76, 1–12. https://doi.org/10.1007/s12665-017- 6736-0.
8. Ceniceros-G´omez, A.E., Macías-Macías, K.Y., de la Cruz-Moreno, J.E., Guti´errez-Ruiz, M. E., Martínez-Jardines, L.G., 2018. Characterization of mining tailings in M´exico for the possible recovery of strategic elements. J. South Am. Earth Sci. 88, 72–79. https://doi.org/10.1016/j.jsames.2018.08.013.
9. Helser, J., Cappuyns, V., 2021. Trace elements leaching from Pb[sbnd]Zn mine waste (Plombi`eres, Belgium) and environmental implications. J. Geochemical Explor. 220, 106659 https://doi.org/10.1016/j.gexplo.2020.106659.
10. Amar, H., Benzaazoua, M., Edahbi, M., Villeneuve, M., Joly, M.-A., Elghali, A., 2021. Reprocessing feasibility of polymetallic waste rock for cleaner and sustainable mining. J. Geochemical Explor. 220, 106683. https://doi.org/10.1016/j. gexplo.2020.106683.

XVI International Mineral Processing
and Recycling Conference
28-30 May 2025, Belgrade, Serbia

DOI: 10.5937/IMPRC25581Z Research article

OPTIMIZATION RECYCLING IN IRON AND STEEL METALLURGY: UTILIZATION OF BY-PRODUCTS FOR EFFICIENCY AND SUSTAINABILITY

Sara Živojinović, 0009-0009-7720-3731,
Živko Đorović, 0009-0000-4993-3440,
Miloš Vuleta[#]**,** 0009-0004-4729-6707,
HBIS Serbia, Smederevo, Serbia

ABSTRACT – This research focuses on the systematic examination of by-product reuse, with a particular emphasis on the recovery of valuable metals from slag—a critical by-product of the metallurgical process. The recovered metals are carefully classified into three categories: A-Scrap, B-Scrap, and C-Scrap. Each category is assigned specific applications: A-Scrap is utilized in steel production, B-Scrap serves in blast furnace operations, and C-Scrap finds its use in sintering processes. The study delves into the economic advantages, enhanced resource utilization, and ecological benefits stemming from these recycling practices. By reducing dependency on primary raw materials, such practices not only cut costs but also conserve finite natural resources and mitigate the environmental impact of industrial activities. In this context, the research aims to advance the use of secondary raw materials, contributing to a steel manufacturing process that is both more efficient and environmentally responsible. By integrating innovative recycling methods, this study aspires to support the transition towards a greener and more sustainable metallurgical sector, aligning with global efforts to reduce industrial emissions and promote eco-friendly practices.

Keywords: Recycling, Metallurgy, Agglomeration, Blast Furnace, Steel Plant.

INTRODUCTION

Steel production is one of the key industrial processes that enables the development of modern technologies and infrastructure. Today, the majority of global steel production is achieved through the Basic Oxygen Furnace (BOF) process, which efficiently converts raw iron into high-quality steel.

Starting from the sinter plant, where in the ore mixture for the purposes of sinter production, secondary materials such as mill scale, blast furnace and steel sludge, blast furnace dust together with screening from ore, pellets, sinter and other materials used by the blast furnace plant are very often used [1].

A notable example of metallurgical recycling is the reintegration of return and discarded materials generated across the production facilities, optimizing the reuse of metallic waste and using it in steel plant [2]. Since these materials are already in a reduced metallic state, their use minimizes the demand for additional reducing agents and significantly lowers the emission of harmful gases into the environment [2].

This paper focuses on the recycling of by-products generated in the steel production

---

[#] corresponding author: MVuleta@hbisserbia.rs

process, with a particular emphasis on slag utilization. The slag produced during the converter process can be further processed and used in multiple ways. A portion of the slag is returned to the process as a secondary raw material for smelting, reducing the need for primary raw materials and increasing production efficiency. Additionally, a significant portion of the slag is processed and used in the construction industry, primarily as a raw material for cement and concrete production. This practice not only contributes to the economic viability of steel production but also reduces the industry's environmental footprint, enabling sustainable industrial waste management.

MATERIALS AND METODS

One of the key materials suitable for recycling in the iron and steel industry is the metal fraction recoverable from slag after the slag separation process, prior to its transfer into the converter at the steel plant. The processing of steel plant slag (converter and mixer slag) for HBIS Serbia in Smederevo is carried out by the partner company HARSCO Metals, which is located within the factory. The slag, transported in ladles from the Steel Plant to HARSCO, is poured into designated cooling fields. After cooling, it is crushed using a ROXON MR PLANT crusher with magnetic separators, where the slag is separated based on granulometric composition and iron content. The processing results in the following products: A Scrap (170-250mm), B Scrap (10-170mm), and C Scrap (-10mm), as well as waste material (10-50mm).

This process yields three distinct scrap categories—A-Scrap, B-Scrap, and C-Scrap—which are utilized as metallic additives in the steelmaking process, blast furnace operations, and sintering plant, respectively.

Beyond other recyclable materials, the steel plant can incorporate A-Scrap as a metallic additive, enhancing the overall recycling rate while mitigating industrial pollution. B-Scrap, characterized by a finer granulation than A-Scrap, is well-suited for blast furnace operations, where it can be introduced into the burden structure as a metallic supplement. C-Scrap, which has the finest granulation among the three, is particularly effective in sintering applications, where it contributes to sinter production.

Figure 1 Generated slag at the Steel Plant by month in 2024

In 2024, a total of 234,279.93 tons of the slag generated from the Steel Plant was handed over to the processing operator. Of this, 8.97% was sold to cement plants, 47.89% was disposed of at the landfill, and 43.14% was returned to the production process as three raw materials for three production plants, what can be seen in Figures 1 and 2.

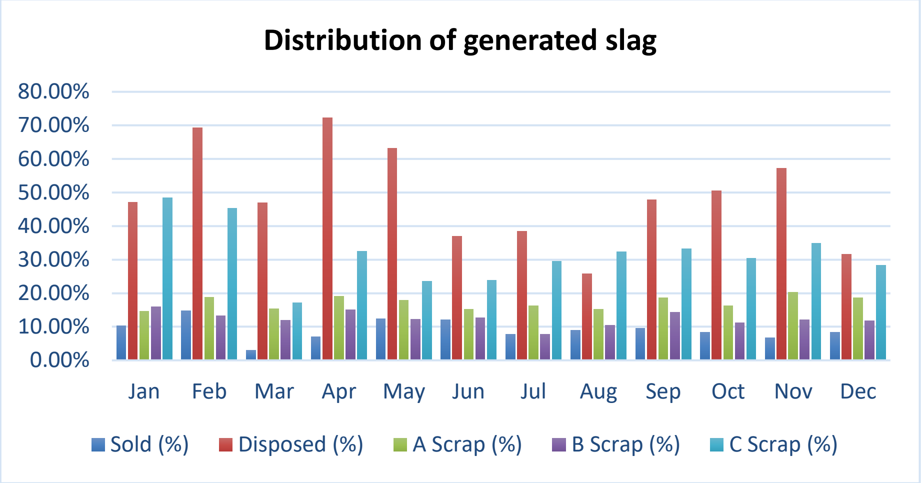

Figure 2 Distribution of generated slag by month in 2024.

RESULTS AND DISCUSSION

A-Scrap is a high-quality metallic by-product obtained from the processing of steelmaking slag, utilized in steel production due to its significant iron content. The replacement coefficient for A-Scrap in the steelmaking process indicates that 1 ton of A-Scrap can substitute up to 0.85-0.95 tons of iron in the raw material mix, thereby increasing metallic yield and reducing the demand for primary raw materials. Its utilization enhances energy efficiency, as it already contains metal in a form suitable for melting, leading to lower electricity consumption and reduced use of reductants. The implementation of A-Scrap in the raw material mix contributes to a decrease in specific energy consumption per ton of produced steel, while simultaneously reducing waste generation and improving material circularity within the production process.

By integrating A-Scrap into the steel scrap structure, with an average share of 12.35%, a cost reduction of $8.9 per ton of processed slab is achieved. The utilization of by-products from steelmaking not only provides economic benefits but also optimizes resource use, making the production process more sustainable. The consumption of A-Scrap and its impact on cost efficiency are illustrated in Figure 3. This model demonstrates potential for long-term application while maintaining the quality of the final product.

Materials used for iron production are sinter, pellets, lump ore and B-scrap. In the last year, the structure of the burden and chemistry of materials has not varied much, which allowed experimentation with the percentage of B-scrap used in the burden structure. The burden is consists of 60% sinter, 15% lump ore, 3-5% B-scrap and rest pellets. Fuels used in iron production include coke and PCI, with PCI serving as an auxiliary fuel with a replacement ratio of 0.85 units of coke consumption. The usual content of Fe in the B-scrap that has been used ranges from 65-70%.

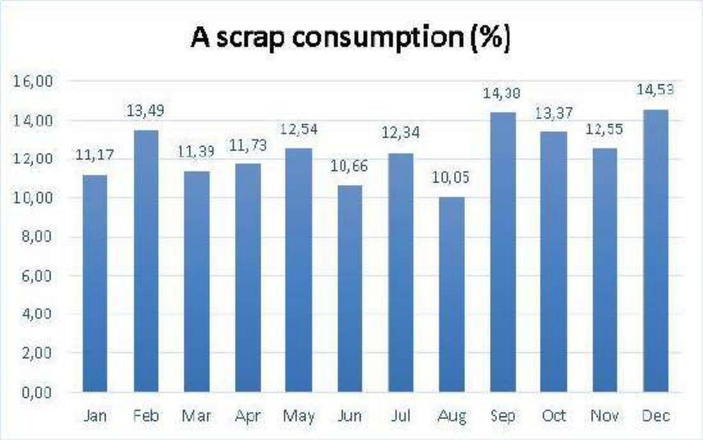

Figure 3 A Scrap consumption in 2024.

Three experimental phases were evaluated, each characterized by distinct B-scrap proportions of 0%, 3%, and 5%. The accompanying diagram elucidates the correlation between equivalent fuel consumption and the proportion of B-scrap within the burden.

B-scrap is a material that enhances the blast furnace burden by increasing the Fe content. However, it is also a significant source of phosphorus. Therefore, an increase in the percentage of B-scrap can lead to problems in hot metal quality in that regard. To better control the phosphorus levels in the iron and to monitor the impact of B-scrap on fuel consumption, the proportion of B-scrap in the burden was adjusted over the course of time. B-Scrap implementation in BF burden yields in average 20kg/thm lower total fuel consumption for 5% B-Scrap proportion, shown in figure 4. The financial aspect of utilizing B-scrap is reflected in the fact that, if the share of B-scrap increases to 2% at the expense of pellets, the price of iron decreases by $9.3 per ton of hot metal.

In a sinter production process, a certain amount of recycling materials is used in order to improve physical and chemical properties and to reduce the cost of sinter production. One of them is a C-Scrap.

Benefits of this material are numerous. Fe content is 40-42%. Coeffitient of substitution, compared to average iron ore used in our Sinter plant is 0.65. This means that we don’t have to buy around 47,500 tons of iron ore on annual level.

Grain size is very favorable and it is similar to some of the best iron ores in the world. High percentage of 3.6-8.0mm grains provides increase of pelletization center for sinter mixture, thus creating good air permeability and increase productivity of Sinter line. C-Scrap is a material that already had heat treatment, so introducing it into the sinter mixture decreases the amount of fuel needed for sintering and that significantly reduces the cost of sinter.

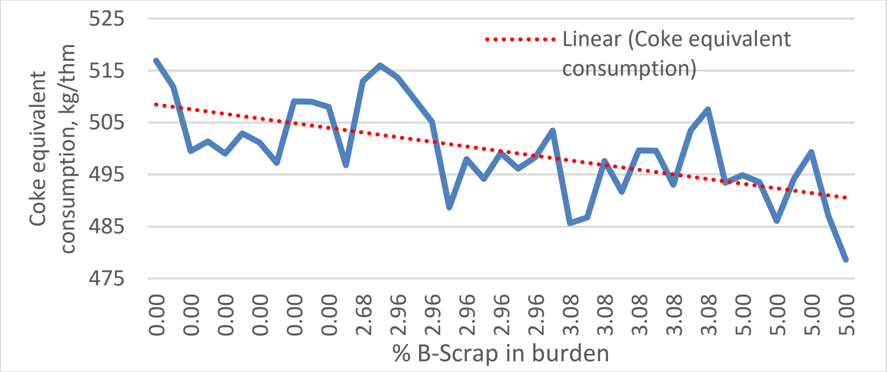

Figure 4 Coke equivalent consumption for different B-Scrap proportions

When we calculate amount of C-Scrap that we can use, main factors are phosphorus content in raw iron ores and percentage of sinter used in burden structure of the blast furnace. Our multidisciplinary teams worked on a calculations of a most favorable ore composites and burden structure in order to achieve the lowest possible cost of a casted slab and to remain competitive on a steel market. Currently we use 60% of a sinter in a BF structure. That provides us to use 10-12% of a C-Scrap in a sinter mixture, without jeopardizing the chemistry of a final product with a phosphorus. C-Scrap consumption is shown in figure 5.

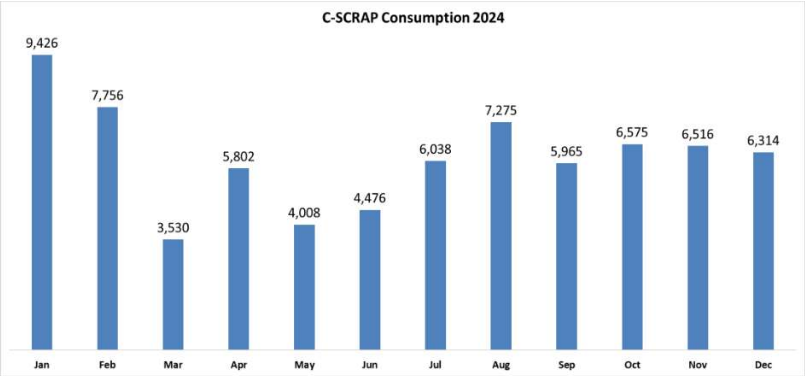

Figure 5 Consumption of C-Scrap on annual level

Speaking in numbers, Sinter plant of a HBIS Company currently uses cca 6,100t of C-Scrap per month, which is around 74,000 tons annually. Low cost of a processing and delivery of this material, compared to purchase of iron ore saves our Company around 4.7 million dollars per year. Use of a C-Scrap in a sintering process also contributes to the environmental protection, making it easier for us not to store so much waste material.

Considering trends and forecasts on a iron and steel market, C-Scrap is and shall remain one important strategic resource for providing competative price of our steel products.

CONCLUSION

The recycling and reutilization of waste materials in steel production, particularly the use of A, B, and C scrap types, are crucial steps toward improving efficiency, reducing costs, and minimizing environmental impact. The incorporation of A-Scrap into steel production has led to significant cost savings by reducing the need for primary raw materials and enhancing energy efficiency. Additionally, the use of B-Scrap in the blast furnace process and C-Scrap in sintering helps lower coke consumption, increases productivity, and reduces harmful gas emissions.

The use of these secondary raw materials not only provides economic benefits but also supports the sustainable development of the steel industry, enabling competitiveness in the market while minimizing environmental impact.

REFERENCES

1. Manojlović, V. D. (2016) Metalotermijska redukcija u reciklažnim tehnologijama primenjena na metalurške međuproizvode i otpade. Doktorska disertacija, Tehnološko-metalurški fakultet, Univerzitet u Beogradu, Beograd.
2. Sivro, A. (2021) Plan upravljanja otpadom ArcelorMittal Zenica. Federalno ministarstvo okoliša i turizma BiH. Online available at the following link:https://www.fmoit.gov.ba/upload/file/AMZ%20Plan%20upravljanja%20otpadom%20-%20Decembar%202021.pdf (accessed: 10.03.2025).

XVI International Mineral Processing
and Recycling Conference
28-30 May 2025, Belgrade, Serbia

DOI: 10.5937/IMPRC25587M

Original research article

IR CAMERA APPLICATION IN CONTROL OF THE CURRENT STATE OF AN INDUCTION FURNACE IN LABORATORY CONDITIONS

Aleksandra Milosavljević[#], 0000-0003-3841-7357,
Marijana Pavlov - Kagadejev, 0000-0003-1090-6351,
Ana Kostov, 0000-0001-6436-9091,
Mining and Metallurgy Institute Bor, Bor, Serbia

ABSTRACT – This paper presents the application of a thermal imaging camera (IR camera) in laboratory conditions in order to obtain data for current state of induction furnace. Therefore thermal imaging measurements were done inside the furnace as well as outside, on different areas to check heating and possible overheating of furnace's inner wall. In this manner, these data can help solving some problems in work and maintenance the furnace itself.

Keywords: Thermography, IR camera, Furnace, Laboratory.

INTRODUCTION

Thermography is a non-destructive technique that uses an IR camera to identify temperature differences on objects: from buildings to devices, even spare parts in various fields. IR cameras are widely used in industry, medicine and home as well. The advantages of thermal imaging are, besides non-invasiveness, high precision and the fact that recording can be done in different weather conditions. The principle of technique itself is the same, only camera specifications differ.

Each object can emit infrared radiation (IR) related to it's temperature. Thermal imaging cameras (IR cameras) detect this radiation and display temperature differences on the screen. In that way, the camera creates a thermogram based on those temperature differences, an image that shows temperature changes. Therefore, the application of these cameras is multipurpose. IR cameras are successfully used in maintenance to detect early signs of malfunction, in process monitoring to detect heat losses as well as building inspection [1, 2, 3].

In metallurgy, thermography is used in determining a technical state of devices (furnaces, pipelines, etc.) and in the monitoring of processes (production – steel, copper…, plastic deformation, heat treatment). IR camera gives us the possibility to make fast analysis of the state of the devices during their normal work and plays an important role in the prevention of the deterioration of their technical condition [4, 5].

Consequently, the aim of this paper is to point out the application of IR camera in

---

[#] corresponding author: aleksandra.milosavljevic@irmbor.co.rs furnace control state in laboratory conditions. So, based on monitoring the thermogram of the tested furnace, it is possible to establish the cause and degree of possible malfunction and in this way prevent the complete failure of the equipment by taking preventive measures in a timely manner of maintenance

Consequently, the aim of this paper is to point out the application of IR camera in furnace control state in laboratory conditions. So, based on monitoring the thermogram of the tested furnace, it is possible to establish the cause and degree of possible malfunction and in this way prevent the complete failure of the equipment by taking preventive measures in a timely manner of maintenance.

EXPERIMENTAL

Flir E40 thermal imaging camera was used in laboratory investigations in order to check the temperature of the induction furnace, i.e. its existing state. Its main characteristics are given in Table 1:

Table 1 FLIR E40 camera characteristics [6, 7]

IR resolution (array size)	19,200 (160 x 120)
camera mass	825 g
thermal sensitivity	<0.07 °C (70mK)
field of view	25°H x 19°V
LCD touch screen	320 × 240 dots
temperature range	-20° C to +650° C (-4 to 1202°F)
accuracy	± 2° C or ± 2%
visual camera	3.1 MP
spectral range	7.5 to 13µm
thermal palettes	Arctic, Gray, Iron, Lava, Rainbow, Rainbow high contrast; plus all inverted

Measurements were done at room temperature (20 °C) at a distance of 1 m from furnace and with a camera emissivity of 0.95. The values of emissivity depend of material, because the emissivity means ability to emit electromagnetic radiation.

Tests were performed in laboratory conditions, on the induction furnace shown in Figure 1.

Figure 1 Induction furnace

RESULTS AND DISCUSSION

Thermal imaging measurements were carried out in the laboratory in order to determine the current state of the induction furnace. Therefore, measurements were done not only inside the furnace yet outside as well. The software FLIR Tools+ has been used for thermogram analysis. This is licensed software that includes all the features of the free FLIR Tools [6, 7], as well as some new capabilities. The results are shown in Figures 2 – 4, and it can be seen on thermograms which area (or spot) has maximum (minimum) temperature.

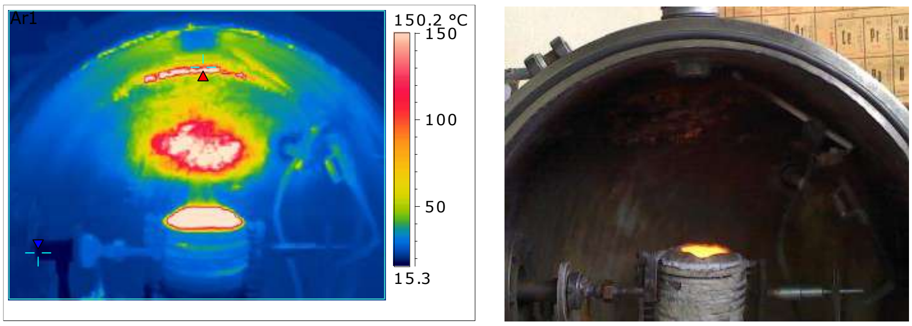

Figure 2 IR and digital photo of induction furnace (inside)

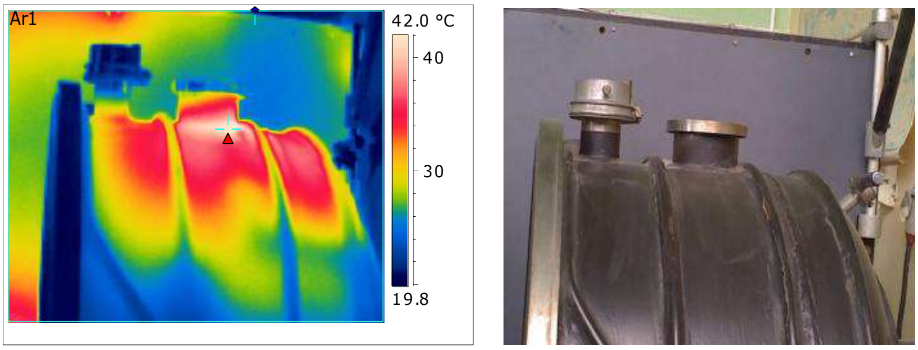

Figure 3 IR and digital photo of induction furnace (outside)

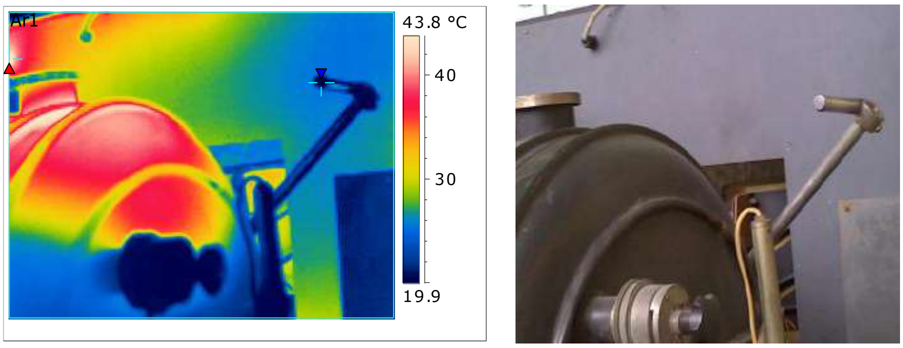

Figure 4 IR and digital photo of induction furnace (outside - different area)

It should be mentioned that the measurements at the same places were repeated in several series at different times, in order to control and monitor the operation of the furnace. Also, any major deviations of the series measured values were not observed.

In Table 2 the results of three series of measurements are given. The results are related to thermograms given in Figures 2 - 4: temperatures for Outside area 1 are related to Figure 3, while ones for Outside area 2 are related to Figure 4.

Table 2 Measured temperatures of induction furnace

	Series 1		Series 2		Series 3	
	Max t	Min t	Max t	Min t	Max t	Min t
Inside area	>150.2 °C	15.6 °C	>150.2 °C	15.3 °C	>150.2 °C	15.5 °C
Outside area 1	42.5 °C	18.6 °C	41.5 °C	19.6 °C	42.2 °C	18.9 °C
Outside area 2	50.7 °C	19.6 °C	50.5 °C	19.8 °C	50.5 °C	19.7 °C

CONCLUSION

Thermal imaging as a non-contact measurement method has a wide application in the control of processes as well as devices and equipment because it does not disturb their operation. The trend of technological development has enabled the application of thermal imaging in the fields of power engineering, mechanical engineering, metallurgy, construction, medicine, in thermal energy transmission systems, construction and implementation of computer systems for monitoring numerous systems, as well as in many other areas of work and detection of the state of plants and objects. Therefore, in this paper the results of temperature measurements recorded by an IR camera on an induction furnace in laboratory conditions are given.

Thermal imaging measurements were performed in laboratory conditions in order to control the current state of induction furnace. Measurements were done on different areas of the induction furnace – inside and outside. Obtained temperature values measured in several time series did not show significant deviations.

Based on the results of the experiment, it is possible to conclude that the thermal imaging (IR) camera is an excellent device for recording the current state of the equipment. In that manner, it is possible to diagnose the problem immediately and pointed out to a specific situation.

ACKNOWLEDGEMENT

This work was financially supported by the Ministry of Science, Technological Development and Innovations of the Republic of Serbia, Contract on Realization and Financing the Scientific and Research Work of the Mining and Metallurgy Institute Bor in 2025, Registration No. 451-03-136/2025-03/ 200052.

REFERENCES

1. Usamentiaga, R., Venegas, P., Guerediaga, J., Vega, L., Molleda, J., Bulnes, F.G. (2014) Infrared Thermography for Temperature Measurement and Non-Destructive Testing. Sensors, 14, 12305-12348.

2. Hou, F., Zhang, Y., Zhou, Y., Zhang, M., Lv, B., Wu, J. (2022) Review on Infrared Imaging Technology. Sustainability, 14, 1116
3. Perić, D., Livada, B., Perić, M., Vujić, S. (2019) Thermal Imager Range: Predictions, Expectations, and Reality. Sensors, 19, 3313. https://doi.org/10.3390/s19153313
4. Wittchen, W., Niesler, M., Borecki, M., Zdonek, B. (2009) Application of thermovision method in analysing metallurgical processes. In: 9th International Conference on Quantitative InfraRed Thermography. Krakow, Poland, https://www.ndt.net/?id=7916 .
5. https://www.gst-ir.net/news-events/infrared-knowledge/593.html (accessed on 28.3.2025.)
6. https://www.flir.com/support/products/e40/#Overview (accessed on 1.4.2025.)
7. https://www.tequipment.net/FLIRE40.html#description (accessed on 28.3.2025.)

XVI International Mineral Processing
and Recycling Conference
28-30 May 2025, Belgrade, Serbia

DOI: 10.5937/IMPRC25592K Review article

WASTE FOUNDRY SAND REGENERATION

Kostović Milena[#], 0000-0002-0529-1236,
Bajić Sanja, 0000-0003-4387-9601,
University of Belgrade, Faculty of Mining and Geology, Belgrade

ABSTRACT – The casting industry uses large quantities of quartz sand, which is a cheap and accessible raw material that must be prepared for use in foundries. After the casting process, foundries generate huge amounts of waste foundry sand (WFS) as industrial waste. The regeneration and reuse of waste foundry sand is a practice and a necessity in many foundries for technological, environmental, and economic reasons. In this review paper, in addition to the characteristics of quartz sand for the casting industry and the characteristics of WFS, typical processes of regeneration in industrial practice, as well as the possibilities of using such recycled WFS in other industries, are presented.

Keywords: Quartz sand, Waste foundry sand, Regeneration, Technological process.

INTRODUCTION

The casting industry uses large quantities of quartz sand, which is a cheap and accessible raw material, for molds and cores in the melting processes of various metals.

Quartz sand for the casting industry must satisfy certain requirements in relation to its characteristics, and it must also be prepared in advance.

The preparation of quartz sand for use depends on the type of quartz sand. For natural sands, screens, magnetic separators, and the wetting are most often used for this purpose. Then, in a mixer, quartz sand is mixed with other components (most often bentonite, coal dust, and water). The amount of sand depends on the weight, size and type of casting. Also, the mold-making procedures are different and depend on the type of quartz sand and binder, i.e., the material added to the mixture [1].

With the addition of water, the mixture acquires the required properties, the most important of which are permeability, strength, fireproof at a temperature of 1300-1600°C, and moldability. These properties allow shaping and retention of the obtained shape [2].

After the casting process, the sand mold can still be used several times to make more molds [3]. WFS is produced in foundries as an industrial waste. WFS treatment represents a big problem, because it needs to be deposited. Treatment of WFS is a practice and necessity in many foundries for technological, environmental, and economic reasons. In practice, we find for this treatment various terminology: recycling, reclamation, and reuse. In Serbia, regeneration is the most used terminology.

[#] corresponding author: milena.kostovic@rgf.bg.ac.rs

About 1 ton of foundry sand is required for each ton of iron or steel casting produced [4]. According to some data, the volume of spent foundry sand generated by ferrous foundries in Europe can be estimated at around 4.5-6 Mt/yr. Only 25-30% of that waste sand is recovered in few applications, mainly in the cement industry, agricultural soils, and landfill covering [5]. Besides this, the pit cost of sand has risen 50-60%, freight costs have gone up 125%, and waste sand disposal costs have doubled or tripled [4].

This review paper presents the characteristics of quartz sands for use in the casting industry and, also, WFS. In particular, the typical industrial processes of WFS regeneration and its reuse, as well as the possibilities of applying sand after these processes, are shown.

QUARTZ SAND IN THE CASTING INDUSTRY

The quartz sand used by the casting industry must satisfy special quality requirements.

Foundry sand consists primarily of clean, uniformly sized, high-quality silica sand that is bonded to form molds for ferrous (iron and steel) and nonferrous (copper, aluminum, brass) metal castings [4].

According to the Serbian standard, quartz sand for the casting industry must have an appropriate chemical composition, which refers to the content of SiO_2, the content of harmful components (for excellent quality, max. 1% $Fe_2O_3+Na_2O+K_2O+CaO+MgO$ and min. 98% SiO_2), and LOI. Quartz sand should have the appropriate permeability for gases, pH, moisture, sintering temperature, as well as the appropriate particle size and particle size distribution. The requirements for particle size are generally 0.1-0.5 mm [2,6]. All requirements depend on the user, i.e., for what types of molds and cores quartz sand is used, so they can be specific.

The classification of foundry sands depends upon the type of binder in metal casting. On the basis of two types of binder, foundry sands are categorized as~~:~~ clay-bonded sands and chemically bonded sands. Clay-bonded sand (green sand) is composed of naturally occurring materials which are blended together: high quality silica sand (85-95%), bentonite clay (4-10%) as binder and carbonaceous additive (2-10%) to improve surface finish, and water (2-5%). Chemically bonded sand consists of silica (93-99%) and chemical binder (1-3%), like~~:-~~phenolic-urethanes, epoxy-resins, furfyl alcohol, and sodium silicate [7].

The physical, chemical, and mechanical characteristics of WFS depend on the type of quartz sand and on the casting process for different industries, i.e., molds and cores making.

Grain size distribution of WFS is uniform (grain size is between 0.15-0.6 mm, mostly 85-95% b.w). WSF has low absorption capacity and is non-plastic. Also, this sand has good durability properties, while chemical compositions depend on the types of metal and binder, and combustible used. Sand is rich in silica content [7]. One potential limitation to their beneficial use is concern that WFS will leach high levels of trace metals [8]. But, in most cases are shown that WFS is not hazardous both as regards the limits imposed by TCLP and by European legislation [9].

Regenerated quartz foundry sand, in addition to reuse in foundries, can also be used in the following areas and industries: embankments, barrier layers construction, flowable fills, road-way construction, agriculture (soil reinforcement/amendments), hot mix asphalt, Portland cement manufacturing, mortars, traction material on snow and ice, vitrification of hazardous materials, smelting, rock wool and fiberglass manufacturing [7]. Some data shows that WFS to 20-30% can be used as fine aggregate in concrete production [10].

REGENERATION OF WFS

The problem of WFS foundries is solved by the regeneration and its reuse.

The regeneration of WFS from the molds and cores can be done by mechanical and thermal process. The mechanical process can be wet or dry.

The wet regeneration process is very efficient and expensive and includes a crushing and hydroclassification system for washing and classifying of washed sand and drying. The dry regeneration process has the greatest application, and includes: shaking out of the mold, separation of metal impurities using a magnetic screen, crushing, first cooling, stocking, pneumatic transport through a filter where dust is separated from clean sand, re-cooling of clean sand in a special cooler and, finally, pneumatic transport to the silos above the continuous mixer [1].

Hot regeneration is carried out in furnaces at very high temperatures~~,~~ when the goal is to burn all the binders (furan, bentonite, etc.) and separate them from the sand, i.e., to obtain quartz sand with clean surfaces that can be used again [1]. Depending on the application of the available techniques, sand regeneration amounts to 90-94% and even 98% [11].

Some examples of WFS regeneration processes in practice are described at the next text.

In Teksid foundry plant in Italy, mechanical and thermal processes are combined with the aim of reclaiming green molding sands for core manufacture with theoretical silica sand recovery equal to the 80% b.w. After separating the magnetic component (90% b.w. metallic iron of size class +0.6 mm) on screen and control separation of the magnetic component in magnetic belt separator (size class of -0.6 mm), low intensity pneumatic mechanical scrubbing treatment is followed. After that, thermal treatment at the temperature of 800-900°C and, finally high intensity pneumatic mechanical scrubbing treatment is performed. In cyclones and bag filters, by dedusting are obtained two kinds of residues: first, inert fine particles with a minimum content of active clay and second, not inert fine particles, which contain active clay [12].

The company KHD Humboldt Wedag from Germany has developed the following FWS regeneration procedure: after separating unwanted metal components in a magnetic separator, sand is sent to a fluidization furnace for thermal decomposition and then to a special cooler and heat exchanger. In the heat exchanger, heat is exchanged from sand with water. The cooled sand is then sent to the air jet mill, where the sand surface is abrasively cleaned of impurities in a stream of compressed air. These impurities, i.e., dust, sent to the air classifier, where the light and fine product is separated as dust, while the sand as a coarse and heavy product is separated as a definitive product after being treated in a magnetic separator [13].

A combined (mechanical and thermal) process of WFS regeneration was applied in the foundry in Kikinda in Serbia [14]. The technological scheme of that process is shown in Figure 1.

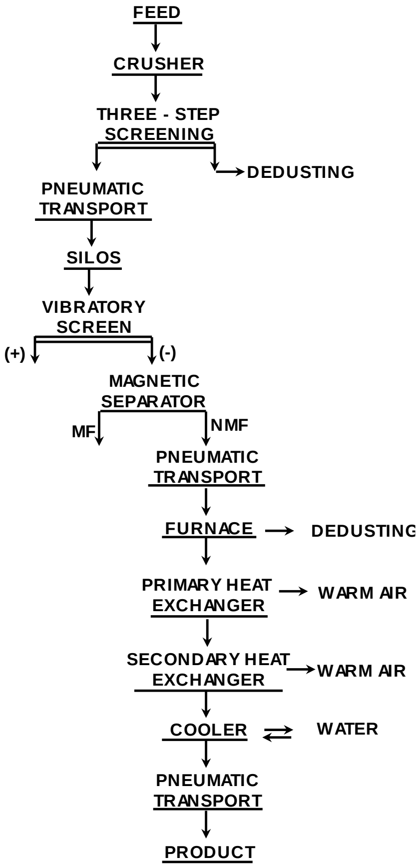

Figure 1 Technological scheme of WFS regeneration

Mechanical treatment involves first crushing the casting molds in a crusher, which are then entered to a part of the plant, where a three-stage screening is performed. The first attrition screen has two screening surfaces - the first for coarse screening and the second for fine screening. On this screen, which is set in motion with a vibrator, by the movement of the material, in addition to screening, its disintegration is carried out at the same time. The screened sand from the attrition screen is directed to the third, tertiary screen, under which there are tubes for dispersing air. On this screen, screening, i.e., classification in a fluidized bed, is performed. Sand is obtained as undersize and, than, pneumatically transported to the silos. This part of the plant for screening, i.e., classification, is closed, and dedusting is ensured in it.

From the silos, the sand is further directed to screening on a vibratory screen, to separate large particles. The undersize enters a drum magnetic separator for separating undesirable metal impurities, which can be used as secondary raw material. After separating the magnetic components, the sand is collected in a box and then pneumatically transported to the furnace for the thermal regeneration of the sand. The system ensures continuous dosing of sand into the furnace. Thermal regeneration of sand (to burn organic components and free the sand from phenolic resins) is carried out in the furnace at a temperature of 800±50°C in a fluidized bed. From the furnace, the regenerated quartz sand, which is free from the remains of phenolic resins, is sent first to the primary, then to the secondary heat exchanger, and finally to the cooler. The warm air from the primary heat exchanger is used in the fluidization furnace. The cooled sand from the cooler is pneumatically transported to the silos of the regenerated sand. Sand which separated as the smallest dust in the gas intake and dedusting system, i.e., separation of dust, is used as a secondary raw material (for the production of cement in cement factories or the production of concrete).

CALCIFIRE FWS reclamation technology makes it possible to obtain quartz sand that is chemically of the same or even better quality than the quartz sands used for this purpose. This process is also suitable for reclaiming clay-bonded sands (green sands). In addition to mechanical treatment, crushing, and treatment in a magnetic separator, the sand is sent to the furnace where the binder is burned. The CALCIFIRE system involves direct combustion of binder material in the furnace in the fluidization bed, which eliminates heat exchange problems during combustion, while similar systems introduce sand into the furnace from the top and ensure full wall-to-wall fluidization. Air or natural gas, whose operating costs are low, are introduced automatically through special distribution tubes. Heat-resistant steel and ceramic fiber insulation eliminate the need for costly ram-up-type refractory linings, ceramic membranes, or temperature-resistant moving mechanical parts. Without a lining to preheat, the system reaches operating temperature in minutes, not hours. The flow of sand through the furnace is easily regulated. The sand can be reused in molds and cores, making it competitive with new sands in most areas. In order to burn sand and achieve gas emissions at or below the level prescribed by EPA standards, it is necessary to reach a temperature of 700-760°C, while the CALCIFIRE system achieves a temperature of 930°C [15].

CONCLUSION

WFS represents industrial waste that is generated in enormous quantities in the world. For technological, ecological, and economic reasons, foundries recycle and re-treat this waste, i.e., regeneration by mechanical and thermal processes, in order to reuse it for their own needs. Due to its properties (chemical, physical, and mechanical), this sand is also used in many other industries, especially in the construction industry.

ACKNOWLEDGMENT

The authors express their gratitude to the Ministry of Science, Technological Development and Innovation of the Republic of Serbia, for supporting scientific research, which is essential for the *advancement of a knowledge-based society; Contract on realization and financing of the scientific research work of the Faculty of Mining and Geology in 2025 (451-03-136/2025-03/200126).*

REFERENCES

1. Zrnić, Đ., Prokić, M., Milović, P. (1985) Projektovanje livnica, IV dopunjeno i prerađeno izdanje, Mašinski fakultet Univerziteta u Beogradu, Beograd (in Serbian).
2. Sekulić, Ž. (2011) Kalcijum karbonatne i kvarcne mineralne sirovine i njihova primena, Institut za tehnologiju nuklearnih i drugih mineralnih sirocvina, Beograd (in Serbian).
3. Opeoluwa, D.R., Bolanle, I.D. (2024) The effective re-use of foundry sand waste in the production of concrete. Civil Engineering and Architecture, 12(5), 3426-3440.
4. Anderson., C.G. (2010) Recycling of foundry sand through chemical and physical beneficiation, Conference: CR3 Kick of Meeting, Kroll Institute for Extractive Metallurgy, Colorado School of Mines, Center for Resource, Recovery & Recycling, Inaugural Meeting, April 8,9, 2010, Boston, MA https://www.researchgate.net/publication/313025936 (accessed March 20th 2025)
5. Delgado, C., Garitaonandia, E., Colaboradores: Rodriguez, J.L., Rios, J., Garcia, I., Martinez Puche, A. (2017) Valorisation of spent foundry sand in construction applications, FuturEnviro, 49-52. https://img.interempresas.net/docs-futur/LIFE_ECO_SANDFILL.pdf (accessed March 20th 2025)
6. Pavlica, J., Draškić., D. (1997) Priprema nemetaličnih mineralnih sirovina, Univerzitet u Beogradu, Rudarsko-geološki fakultet, Beograd (in Serbian)
7. Siddique, R., Singh, G. (2011) Utilization of waste foundry sand (WFS) in concrete manufacturing. Resources, Conservation and Recycling, 55, 885-892.
8. Miguel, R.E., Ippolito, J.A., Porta, A.A., Banda Noriega, R.B., Dungan, R.S. (2013) Use of standardized procedures to evaluate metal leaching from waste foundry sands, Journal of Environmental Quality, 42(2), 615-620.
9. Cioli, F., Abbà, A., Alias, C., Sorlini, S. (2022) Reuse or disposal of waste foundry sand: An insight into environmental aspects. Applied Sciences, 12, 6420, 1-13.
10. Ahmad, J., Zhou, Z., Martínez-García, R., Vatin, N.I., de-Prado-Gil, J., El-Shorbagy, M.A. (2022) Waste foundry sand in concrete production instead of natural river sand: A review. Materials, 15, 2365, 1-20.
11. Jovičić, A.I., Kukobat, L.M., Đergović, D.M. (2019) Poboljšanje efikasnosti tehnoloških procesa i smanjenje upotrebe resursa u industriji livarstva primenom BAT i BREF dokumenata. Tehnika, 68 (6), 832-837.
12. Fiore, S., Zanetti, M.C. (2007) Foundry wastes reuse and recycling in concrete production. American Journal of Environmental Sciences, 3 (3), 135-142.
13. Branković, B.T. (2002) Postupci i uređaji za recikliranje otpadnog materijala, knjiga VIII, ITNMS, Ministarstvo zdravlja i zaštite životne okoline Republike Srbije, Uprava za zaštitu životne sredine (in Serbian)
14. D.O.O. Le Belier Livnica Kikinda, Studija o proceni uticaja postrojenja za termičku regeneraciju peska na životnu sredinu, Novi Sad, 2006. (in Serbian)
15. Berkeley Citizen Arhives: Incinerator History of Pacific Steel Casting, CALCIFIRE sand reclamation technology. https://berkeleycitizen.org/pacificsteel/pacific10.htm (accessed March 20th, 2025)

XVI International Mineral Processing
and Recycling Conference
28-30 May 2025, Belgrade, Serbia

DOI: 10.5937/IMPRC25598B

Original research article

GEOPOLYMERS BASED ON FLY ASH WITH THE ADDITION OF GRANULATED BLAST FURNACED SLAG

Ilhan Bušatlić[#]**,** 0000-0001-5003-0206,
Nadira Bušatlić, 0000-0002-7646-3752,
Nevzet Merdić, 0009-0008-6714-4064,
Nedžad Haračić, 0000-0002-9392-3298,
Lejla Mujezinović, 0009-0001-0091-5193,
University of Zenica, Zenica, B&H

ABSTRACT – Geopolymer is a type of inorganic polymer which hardens after being synthesized at ambient temperature. Geopolymers are synthesized by the reaction of poly-condensation of the geopolymer precursor and alkali activator. Ecologically, it would be more favourable to use industrial by-products since the hazardous waste is being taken care of. The most frequently used raw materials for geopolymer production are: kaolin clays, meta-kaolin, fly ash, blast furnace slag, fly ash and slag mixture, fly ash and meta-kaolin mixture and so forth. Fly ash from the Stanari Termal Power Plant, granulated slag from ArcelorMittal Zenica and quarc sand from Tuzla were used as initial raw material for the purpose of the study presented in this work. Based on the results obtained through research carried out in laboratory conditions at the Faculty of Engineering and Natural Sciences in Zenica and at the "Kakanj" Cement Factory, it can be concluded that fly ash from the TPP Stanari together with granulated blast furnace slag from ArcelorMittal Zenica can successfully use for the production of geopolymer. This test determined that the best compressive strength results were obtained by samples with a ratio of water glass/NaOH=2.0 and that the optimal heat treatment temperature was 60°C.

Keywords: Geopolymers, Fly Ash, Granulated Slag, Hardener, Compressive Strength.

INTRODUCTION

In the field of construction, cement is the main ingredient for the production of concrete. However, cement production requires large amounts of raw material. During the production of cement, the burning of limestone causes the emission of carbon dioxide into the atmosphere. [1] There are two sources of carbon dioxide emissions from cement production: the burning of fossil fuels to run the rotary kiln is the largest source, and the other is the chemical process of burning limestone. During the production of 1 ton of cement, approximately 1 ton of CO_2 is emitted into the atmosphere. If we consider that the world production of cement is about 4.18 billion tons, then it can be seen that during the production of cement, the same amount of CO_2 is released into the atmosphere. Of the total global annual CO_2 emissions, 5% is accounted for by cement production. [9,12]

[#] corresponding author: ilhan.busatlic@unze.ba

Due to the increase in the consumption of concrete, there is also an increase in the production of cement, which results in an increase in environmental pollution and global warming. In addition to all greenhouse gases, carbon dioxide causes 65% of global warming. [10,11]

On the other hand, every year around 2.2 billion tons of construction waste are produced in the world. In addition to occupying huge areas for disposal of construction waste, this waste pollutes land, water and air. This paper presents one of the ways of using construction waste in the production of new materials.

Geopolymer is a type of inorganic polymer which hardens after being synthesized at ambient temperature. [5,6] Ecologically, it would be more favourable to use industrial by-products since the hazardous waste is being taken care of. The most frequently used raw materials for geopolymer production are: kaolin clays, meta-kaolin, fly ash, blast furnace slag, fly ash and slag mixture, fly ash and meta-kaolin mixture, slag and meta-kaolin mixture and so forth. [2,3,4]

EXPERIMENTAL

In this paper, geopolymer samples based on fly ash from the Stanari thermal power plant were tested. Fly ash from the Stanari thermal power plant, granulated blast furnace slage from ArcelorMittal Zenica, quartz sand from Tuzla, 12M NaOH solution and commercial water glass were used as materials. The samples were made with an alkali to fly ash ratio of 1. The Na_2SiO_3/NaOH ratio ranged from 1; 1.5 and 2. The samples were prepared with different mass fractions of granulated blast furnace slag, namely 0, 10 i 20 %. The samples were thermally treated at geopolymerization temperatures of 60 °C. After that, the compressive strengths of the samples were tested after 1, 7 and 28 days.

The chemical analysis of the fly ash TPP Stanari is shown in Table 1, its granulometric composition is shown in Figure 1, and its XRD analysis is shown in Figure 2.

Table 1 Chemical composition of fly ash from TPP Stanari, B&H

Oxides	SiO_2	Al_2O_3	Fe_2O_3	CaO	MgO	SO_3	K_2O	MnO	TiO_2
Content (%)	44,21	19,06	8,56	20,98	2,33	1,78	1,55	0,058	0,70

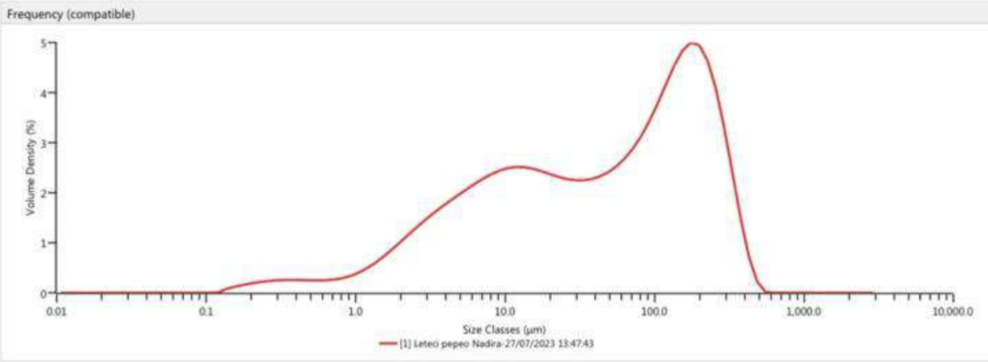

Figure 1 The granulometric composition of fly ash from TPP Stanari

It can be seen from the picture that the particle size of fly ash ranges from 0.14 to 550 µm. The part of particles whose size is over 200 µm is 15.84 %, the part of particles whose size is over 90 µm is 38.81 %, and the part of particles whose size is over 45 µm is 51.27%.

Figure 2 shows the XRD analysis of Stanari fly ash, which was performed at the Kakanj Cement Factory.

Based on the XRD analysis of fly ash, shown in Figure 2, it can be seen that the fly ash has a higher percentage of amorphous structure, but also contains a lower percentage of crystalline structure, which is indicated by several sharp quartz peaks. The proportion of the amorphous phase is 74.5%.

The chemical composition of the granulated blast furnace slag is shown in Table 2, while the granulometric composition is shown in Figure 3 and the mineral composition is shown in Figure 4.

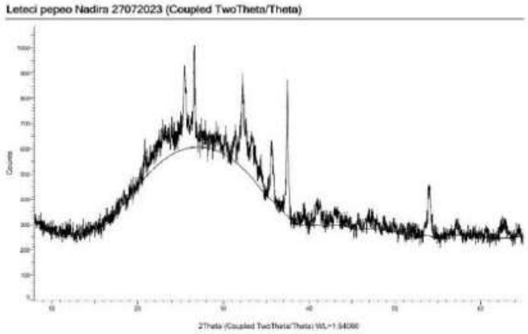

Figure 2 XRD analysis of fly ash

Table 2 Chemical composition of granulated blast furnace slag "ArcelorMittal" Zenica

Oxides	SiO_2	Al_2O_3	Fe_2O_3	CaO	MgO	TiO_2	GŽ
Content (%)	42,39	8,37	1,83	37,08	5,36	0,46	<o,01

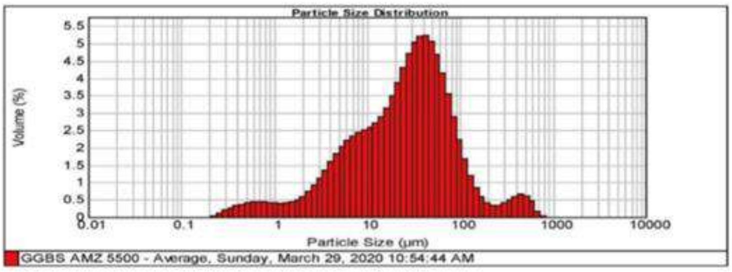

Figure 3 Granulometric composition of granulated blast furnace slag

It can be seen from the figure 3, that the particle size of granulated blast furnace slag ranges from 0.3 to 130 µm. The part of particles whose size is from 0.3 to 10 µm is about

25%, the remaining 65% is made up of particles with a size of 10 to 100 µm, and only about 10% of particles with a size of 100 to 130 µm, and it is visible that the largest part of particles size with 30 µm.

Based on the XRD analysis of the slag shown in Figure 4, it can be noted that there are no sudden peaks, i.e. of peaks that deviate from the others, therefore, we conclude that the slag has an amorphous structure.

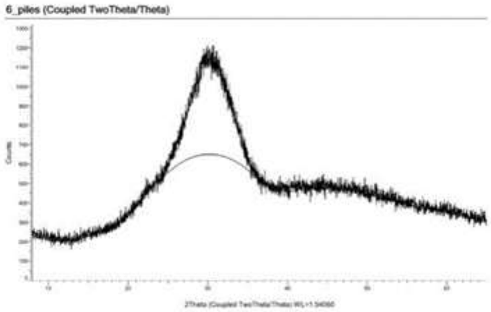

Figure 4 XRD analysis of granulated blast furnace slag

The chemical analysis of quartz sand is shown in Table 3, while the granulometric composition of quartz sand is shown in Table 4.

Table 3 Chemical analysis of quartz sand

Oxides	SiO_2	Al_2O_3	Fe_2O_3	CaO	MgO	SO_3	GŽ
Content (%)	96,45	1,00	0,23	0,68	0,24	0,22	0,79

Table 4 Granulometric analysis of quartz sand

Grain size (mm)	Iznad 2 mm	2 – 0,5	Ispod 0,5
Content (%)	4,4	93,5	2,1

Mixing ratios and markings of fly ash-based geopolymer samples are shown in the table 5.

Table 5 Ratios and markings of geopolymer samples

% GBFS	**Sample label after 1 day**	**Sample label after 7 days**	**Sample label after 28 days**	**AA/FAGBFS**	**Na_2SiO_3/NaOH**
0 %	1-60GT0,1	1-60GT0,7	1-60GT0,28	1	1.0
	1,5-60GT0,1	1,5-60GT0,7	1,5-60GT0,28	1	1.5
	2-60GT0,1	2-60GT0,7	2-60GT0,28	1	2.0
10 %	1-60GT10,1	1-60GT10,7	1-60GT10,28	1	1.0
	1,5-60GT10,1	1,5-60GT10,7	1,5-60GT10,28	1	1.5
	2-60GT10,1	2-60GT10,7	2-60GT10,28	1	2.0
20 %	1-60GT20,1	1-60GT20,7	1-60GT20,28	1	1.0
	1,5-60GT20,1	1,5-60GT20,7	1,5-60GT20,28	1	1.5
	2-60GT20,1	2-60GT20,7	2-60GT20,28	1	2.0

Homogenization of measured amounts of starting raw materials is done in a mixer for 5 minutes, after which the obtained mixture is transferred into molds and subjected to vibrations on a vibrating table for 5 minutes in order to compact the sample. The binding process is exothermic so the samples must be hermetically closed. After 24 h, the samples were taken out of the mold and wrapped in nylon bags. The wrapped samples were kept in the oven for 24 hours at activation temperatures of 60 °C. After the thermal treatment, the samples were taken out of the bags and left to stand in the air until testing the compressive strengths after 1, 7 and 28 days.

RESULTS AND DISCUSSION

After the samples were prepared, the compressive strength of the geopolymer was tested after 1, 7 and 28 days. The results of the obtained compressive strengths are shown in Table 6 and Figure 5.

Table 6 Compressive strength of samples after 1, 7 and 28 days

Samples	**Compressive strength (Mpa)**		
	1 day	**7 days**	**28 days**
1-60GT0	14,1	22,5	31,22
1,5-60GT0	19,48	26,08	29,93
2-60GT0	24,81	30,38	31,58
1-60GT10	10,49	14,16	15,60
1,5-60GT0	14,62	20,04	28,84
2-60GT10	18,13	25,00	31,61
1-60GT20	8,16	10,97	14,78
1,5-60GT20	15,38	20,61	26,21
2-60GT20	21,15	25,45	29,06

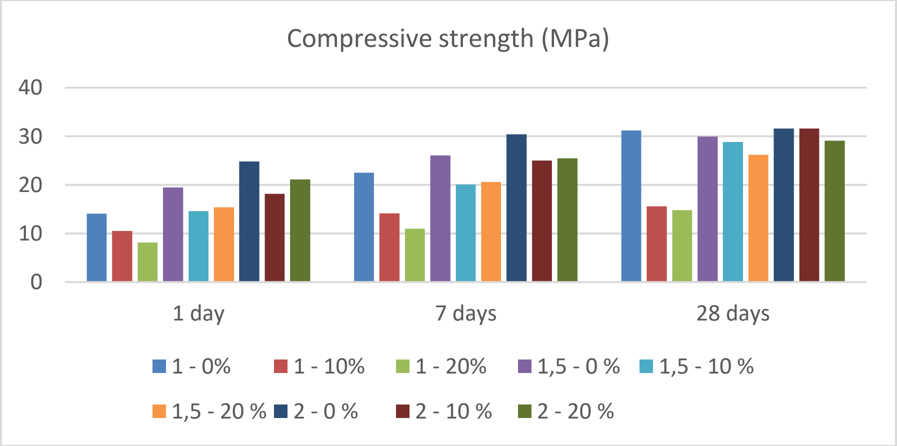

Figure 5 Dependence of compressive strength on percentage addition of granulated blast furnace slag and Na_2SiO_3/ NaOH ratio

CONCLUSION

The following can be concluded from all of the above:

Geopolymer samples based on fly ash TPP Stanari with the addition of granulated blast furnace slag from ArcelorMittal Zenica gave satisfactory results. These samples proved to be stable in all stages of geopolymer production, from the stage of preparation of fresh geopolymer paste and its aging for 24 hours, through heat treatment to testing of compressive strength. Due to the above, it can be concluded that Stanari fly ash and granulated blast furnace slag from ArcelorMittal Zenica can be used for the production of geopolymers. Increasing the content of addition of granulated blast furnace slag to fly ash reduces the compressive strength of geopolymer. Increasing the Na_2SiO_3/ NaOH ratio increases the compressive strength of the geopolymer. Namely, the samples without the addition of granulated blast furnace slag have the highest value of compressive strength. If we add blast furnace slag, we have to increase the Na_2SiO_3/ NaOH ratio in order to obtain higher compressive strength values. Samples made with a ratio of VS/NaOH = 2.0, treated at a temperature of 60°C, show the highest compressive strengths after 28 days.

ACKNOWLEDGEMENT

This work is part of a scientific research project funded by the Federal Ministry of Education and Science in Bosnia and Herzegovina..

REFERENCES

1. Bušatlić Ilhan, Bušatlić Nadira, Merdić Nevzet, Haračić Nedžad. (2020), Osnove hemije I tehnologije Portland cementa, Štamparija Fojnica d.d., Fojnica.
2. H. Xu, J.S.J. Van Deventer. (2000), *The geopolymerisation of alumina-silicate materials*, Int. J. Miner. Process. 59, 247-266.
3. Davidovits Joseph. (2008), Geopolymer: *Chemistry and applications*, second ed., France: Institut Geopolymere.
4. H.Xu, J.S.S. Van Deventer. (2003), *Effect of source materials on geopolymerization*, Ind. Eng. Chem. Res. 42, 1698-1706.
5. D.L.Y.Kong, J.G.Sanjayan. (2008), *Demage behavior of geopolymer composites exposed to elevated temperatures*, Cement and Concrete Research, 30, 986-991.
6. R.A.Fletcher, K.J.D. Mackenzie, C.L. Nicholson, S. Shimada. (2005), *The composition randge of alumino silicate geopolymers*, Journal European Ceramics Society, 25:1471-1477.
7. M.R. Nagral, T. Ostwal, M. V Chitawadagi. (2014), *Effect Of Curing Temperature And Curing Hours On The Properties Of Geo-Polymer Concrete*, International Journal of Computational Engineering Research (IJCER), ISSN (e): 2250-3005 Vol, 04 Issue.
8. M. F. Nurrudin, S. Haruna, B. S. Mohammed, I. G. Sha،aban. (2018), *Methods of curing geopolymer concrete: A review*, International Journal of Advanced and Applied Sciences, 5(1), 31-36.
9. Bušatlić Nadira, Bušatlić Ilhan, Smajić-Terzić Dženana. (2023), *Geopolymers Based On Fly Ash From The Stanari Thermal Power Plant*, 5th Metallurgical & Materials Engineering Congress of South-East Europe, Trebinje, BIH.
10. Bušatlić Ilhan, Bušatlić Nadira. (2019), *The Possibility Of Using The Fly Ash From Thermal Power Plant "Stanari" Doboj In The Development Of Geopolymers*, XIII International Mineral Processing and Recycling Conference, Belgrade, Serbia, pp 141-148, ISBN 978-86-6305-091-4.

11. Bušatlić Nadira, Bušatlić Ilhan, Merdić Nevzet, Smajić-Terzić Dženana. (2021), *Influence Of Na2sio3/Naoh Ratios On The Compressive Strength Of Fly Ash Based Geopolymers From Thermal Power Plant Stanari In Bih*, 13th Scientific/Research Symposium with International Participation "Metallic and Nonmetallic Materials", B&H, ISSN 2566-4344.
12. Bušatlić Nadira, Bušatlić Ilhan, Smajić-Terzić Dženana. (2023), *Dependence Of Compressive Strength Of Geopolymer Based On Fly Ash And Alkaline Activator Ratio*, The 54th International October Conference on Mining and Metallurgy, Bor Lake, Serbia.

XVI International Mineral Processing
and Recycling Conference
28-30 May 2025, Belgrade, Serbia

DOI: 10.5937/IMPRC25605S

Original research article

RECYCLING OF PRINTED CIRCUIT BOARDS (PCBS) USING VARIOUS DEEP EUTECTIC SOLVENTS (DESS) AND INSIGHTS FROM DFT SIMULATIONS

Sadaf Samadi-Tavanaa[1]**,** 0009-0007-0492-1412,
Saeid Karimi[1#]**,**0000-0003-0796-6855,
Mehdi Pourabdoli[1]**,** 0000-0002-3930-3725,
Zoran Štirbanović[2]**,** 0000-0001-7571-2844,
[1]Hamedan University of Technology, Hamedan, Iran
[2]University of Belgrade, Technical Faculty in Bor, Serbia

ABSTRACT – In this study, the dissolution of copper present in printed circuit boards (PCBs) was investigated using different choline chloride (ChCl) based deep eutectic solvents (DES) at a temperature of 100 °C for 24 h. According to the results, the two-component combinations ChCl-PTSA (p-toluene sulfonic acid) and ChCl-ACA (acetic acid) achieved nearly complete copper extraction efficiency. In contrast, ChCl-EG (ethylene glycol) showed less than 1% efficiency. The mechanism of copper dissolution in the ChCl-PTSA was examined using DFT simulations. COSMO analysis reveals a hydrogen bond between ChCl's chloride ion (negative potential) and PTSA's hydroxyl group. Mulliken charges show that DES formation causes charge redistribution, increasing polarization within the sulfonate group and stabilizing the DES structure via enhanced electrostatic interactions. In addition, COSMO analysis of DES with Cu(I) and Cu(II) reveals distinct interaction patterns: Cu(I) primarily interacts with chloride and sulfonate groups, disrupting the original hydrogen bonding network, while Cu(II) shows potential coordination with both chloride and sulfonate groups, influencing the electronic properties of the DES.

Keywords: Printed Circuit Board, Deep Eutectic Solvent (DES), Choline Chloride, Cu Recovery.

INTRODUCTION

The digitalization and upgrading of electronic gadgets generate significant amounts of Printed Circuit Boards (PCB)-containing e-waste. To conserve resources and protect the environment, the recycling of such waste is essential [1]. Waste PCBs contain more than 40 kinds of metals with a wide and variable range of concentrations, such as environmentally harmful metals (e.g. Pb, Cr, As, Cd and Hg) and others of economic value (e.g. Cu, Sn, Au, Ag and Pd) [2]. Methods for recycling metals from PCBs include pyrometallurgy, hydrometallurgy, and biometallurgy [2]. Among these methods, hydrometallurgy has been studied more due to its environmental compatibility compared to pyrometallurgy and higher production speed compared to biometallurgy [2]. Traditional leaching methods employ cyanide based or mineral acids chemicals (H_2SO_4, HCl and HNO_3) as major lixiviant [2,3]. potentially resulting in the generation of

---

[#] corresponding author: s.karimi@hut.ac.ir substantial quantities of toxic and corrosive waste [3]. However, further research is required to minimize the environmental impact of hydrometallurgy processes in rational kinetics [4]. Identifying environmentally benign solvents for sustainable chemistry applications has emerged as a crucial challenge, driving extensive research efforts in recent years. Deep eutectic solvents (DESs) have emerged as promising neoteric alternatives due to their advantageous properties, including low cost and high tunability [5–10]. In addition, DESs offer several advantages over conventional acid-based methods, including reduced environmental impact and carbon footprint [11,12]. DES was successfully used to extract Cu, Ni, Zn, and Sn from the PCBs. The leaching efficiency was impressive, with over 75.0% recovery of metals [3]. In addition, Choline chloride-based DESs have shown promising results in leaching various metals, including copper, zinc, and tin [13,14]. Considering the use of oxidants to achieve high efficiency in dissolving metals from PCBs and relatively low efficiency in some DESs, this study aims to achieve one-step dissolution of PCBs in DESs. In this regard, various DESs based on choline chloride were evaluated at a temperature of 100 °C and a duration of 24 h. In addition, the leaching mechanism was evaluated by DFT simulation.

EXPERIMENTAL

Material

The sequential process for PCB preparation process, starting with dismantling personal computers to extract PCBs. Next, electronic chipsets are removed from the PCBs, followed by shredding. Finally, the PCB samples are screened to achieve a particle size of less than 1 mm. This sample was used to evaluate dissolution in different DESs. Two-component DES was synthesized by mixing of a fixed component: choline chloride (ChCl) ($(CH_3)_3NCH_2CH_2OH)Cl$ (>98%, Merck) as the hydrogen bond acceptor (HBA) along with a second variable component including: formic acid (FA, HCOOH, >99%, Merck), lactic acid (LA, $C_3H_6O_3$, >98%, Merck), fructose (F, $C_6H_{12}O_6$, >98%, Merck), acetic acid (ACA, CH_3COOH, >99%, Merck), thiourea (T, CH_4N_2S, >98%, Merck), oxalic acid (OA, $C_2H_2O_4$, >95%, Merck), ethylene glycol (EG, $C_2H_6O_2$, >99%, Merck), p-toluene sulfonic acid (PTSA, $C_7H_8O_3S.H_2O$, >98%, Merck), urea (U, CH_4N_2O, >99%, Merck), malonic acid (MOA, $C_3H_4O_4$, >99%, Merck), maleic acid (MA, $C_4H_4O_4$, >99%, Merck), with mentioned mol ratio mentioned in Table 1. This mixture was heated at 70 °C for one hour in a 15-ml glass vial within an oil bath. To obtain a completely transparent mixture, the temperature was increased to 80 °C, and continuously stirred with a magnet. It is worth mentioning that, in order to reduce experimental error due to the significant moisture absorption by these substances, the materials were thoroughly dried in an oven at 70 °C for 3 h before the synthesis.

Table 1 The characteristics of different DES and their mol ratio

ChCl:FA	ChCl:LA	ChCl:F	ChCl:ACA	ChCl:T	ChCl:OA	ChCl:EG	ChCl:PTSA	ChCl:U	ChCl:MOA	ChCl:MA
2:1	1:1	1:1	1:1	1:2	2:1	1:2	2.4:1	1:2	1:1	1:1

Analysis and characterization

The PCB was characterized using XRD, Philips PW-3710 diffractometer equipped with a Cu K_α radiation source (λ = 1.54056 A). The analysis of metals was conducted by dissolving 1 g of PCB in a 20 ml aqua regia, and then, it was made up to 100 ml with deionized water. Finally, the concentration of Cu in the filtrate was determined using atomic adsorption spectroscopy (Varian 240AA). In addition, the solution after the leaching process was subjected to AAS analysis for calculating the Cu recovery.

Leaching in DES

During the leaching stage, 0.1 g of PCB was added to 5 g of DES. All experiments were conducted in a 15 ml glass vial placed in an oil bath at 100 °C for 24 h, with uniform stirring using a magnet (400 rpm). After the leaching process, the solution was filtered immediately, the solution was used for metal analysis and leaching residue used for further analysis. The flowchart for leaching process is summarized in Fig. 2. The Cu recovery was calculated using the following equation:

$$R_{Cu}(\%) = \frac{C_{Cu} \times V}{m \times A} \times 100 \qquad (1)$$

where C_{Cu} is the concentration of Cu (g/l), V is the volume of the leaching solution (l), m is the mass of powders of PCB (g), and A is the grade of metal in the mixture of PCB.

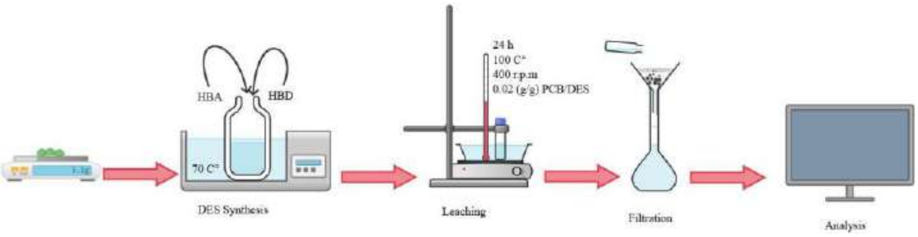

Figure 2 Flowchart of PCB leaching in different DESs

DFT simulation

The simulation utilized Materials Studio's DMol3 module for density functional theory (DFT) calculations to analyze a ChCl and PTSA DES, both in pure form and after copper leaching. The computational approach involved systematic geometry optimization and electronic structure analysis under varying conditions. Initially, a coarse geometry optimization was performed using the GGA-BLYP functional with TS dispersion correction, a DN basis set, and coarse integration accuracy. This was followed by a refined optimization using the GGA-PBE functional, a DNP basis set, medium integration accuracy, and a medium k-point grid. Solvation effects were simulated using the COSMO (Conductor-like Screening Model) with DMol3-PBE parametrization. Analyses included evaluating the COSMO surface and Mulliken charge distribution for ChCl, PTSA, DES, and

DES containing monovalent and divalent copper species, ensuring a comprehensive understanding of ionic interactions and solvation effects in the DES environment.

RESULTS AND DISCUSSION

Results of leaching experiments

Copper recovery from different DESs varies significantly, as shown in Fig. 3, with ChCl+ACA and ChCl+PTSA demonstrating the highest recovery rates at 99.10% and 99.40%, respectively. ChCl+MOA (97.70%) and ChCl+FA (87.93%) also exhibit high recovery percentages, while ChCl+T shows a moderate recovery of 75.12%. DES such as ChCl+MA and ChCl+LA result in recoveries of 56.40% and 49.71%, respectively. In contrast, ChCl+F and ChCl+U have much lower recovery rates at 8.14% and 3.56%, and ChCl+EG shows the lowest Cu recovery at 0.61%. Finally, ChCl+OA has a recovery rate of 16.64%.

Recently, ChCl-based DESs with various hydrogen bond donors have demonstrated significant potential in selectively leaching copper from PCBs [11,13]. Reported recovery rates for copper using DESs are approximately 75%, showcasing their efficiency compared to traditional methods [13,15]. For example, Liu et al. utilized a ChCl-ethylene glycol DES in combination with 5 wt.% hydrogen peroxide as an oxidizing agent to efficiently extract copper under mild conditions (25 min, 20 °C), highlighting the method's practicality and environmental benefits [11]. Additionally, Abbott et al. investigated the leaching mechanism and found that metal complexes, particularly MCl_x^- species, form extensively in choline chloride-based DESs, contributing to their high selectivity and efficiency in metal recovery [16].

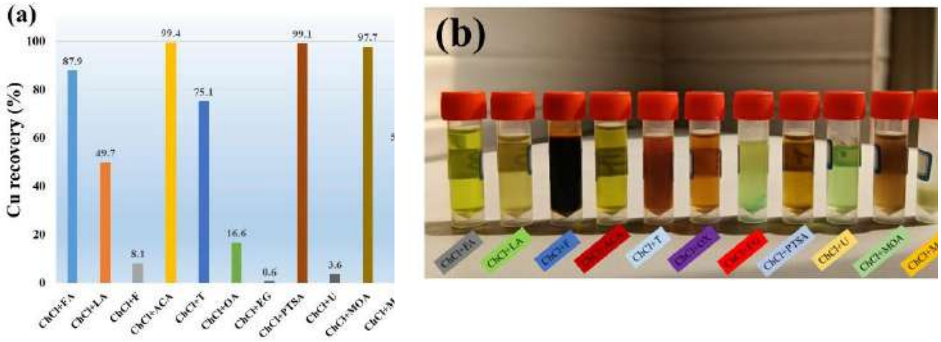

Figre 3 (a) Cu recovery in different DESs and **(b)** their color

DFT results

DFT of ChCl and PTSA

The COSMO surface of ChCl, as shown in Fig. 4a, reveals a clear charge separation with negative potential around the chloride ion and positive potential near the choline moiety, particularly around the hydroxyl groups. This distribution highlights the molecule's polar nature and role in interacting with hydrogen bond donors (HBD) to form a DES. The Mulliken charge distribution (Fig. 4b) further emphasizes this separation, with the chloride anion carrying a significant negative charge (-0.669) and the nitrogen atom in the choline cation having a positive charge (+0.171). The oxygen atom of the hydroxyl group is also negatively charged (-0.502). In contrast, carbon atoms bonded to nitrogen have slight negative charges and hydrogen atoms exhibit positive charges, indicating delocalization of positive charge across methyl and methylene groups.

The COSMO surface of PTSA (Fig. 4c) shows negative potential concentrated around the sulfonate group (-SO3H) and positive potential across the aromatic ring and methyl group, reflecting its acidic nature and capacity to act as an HBD in DES formation. The Mulliken charge distribution (Fig. 4d) highlights significant charge localization within the sulfonate group, with the sulfur atom having a substantial positive charge (+1.373) and oxygen atoms exhibiting negative charges (-0.624 and -0.541). The hydroxyl oxygen is also negatively charged (-0.624), while carbon atoms in the aromatic ring have varying charges, and hydrogen atoms exhibit positive charges.

These complementary electrostatic characteristics drive the interaction between ChCl and PTSA. ChCl, acting as a hydrogen bond acceptor (HBA), has a concentrated negative potential around the chloride ion, facilitating strong electrostatic attraction with the positively polarized hydrogen atoms of PTSA's sulfonic acid group. PTSA, as an HBD, features a highly positive sulfur atom and acidic hydroxyl hydrogen, enabling effective hydrogen bonding with ChCl's chloride ion. The negative potential on sulfonate oxygens stabilizes the interaction by attracting ChCl's positive regions. These charge and potential complementarities suggest that strong hydrogen bonding and electrostatic interactions between ChCl and PTSA facilitate the formation of a stable DES.

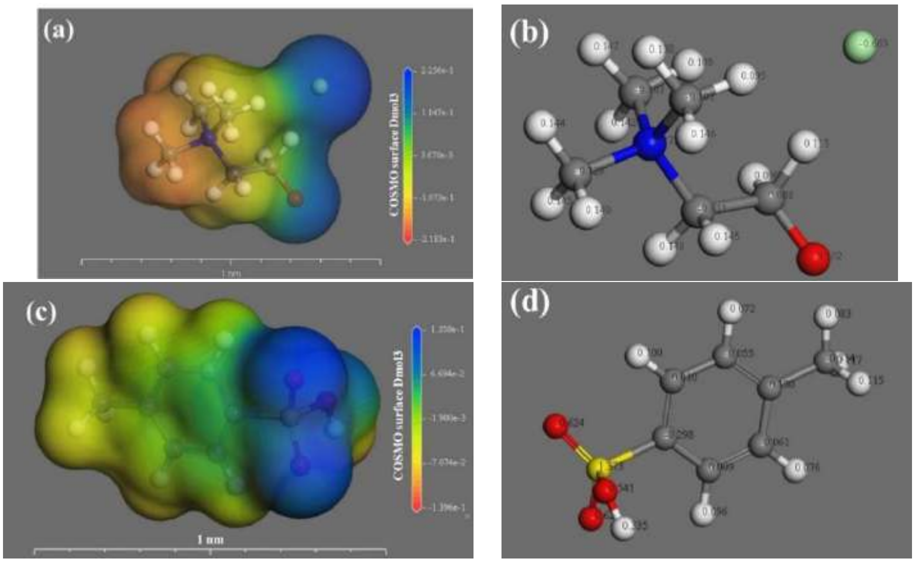

Figure 4 DFT-calculated COSMO surfaces **(a, c)** and Mulliken charges **(b, d)** for ChCl and PTSA

DES

Fig. 5 illustrates the COSMO surface and Mulliken charges of the DES composed of ChCl and PTSA. The ChCl component shows a prominent negative potential around the chloride ion, indicating its role as a hydrogen bond acceptor, and positive potential around the methyl groups bonded to nitrogen. The PTSA component exhibits negative potential around the sulfonate group and transitions from near-neutral to slightly positive potential on the aromatic ring. The spatial arrangement of the negative chloride ion near the positive hydroxyl group of PTSA confirms the formation of a hydrogen bond, which is crucial for DES stability. The Mulliken charge distribution reveals key electrostatic features: the chloride ion carries a significant negative charge (-0.618), the sulfur atom in PTSA bears a large positive charge (+1.403), and the sulfonate oxygens exhibit substantial negative charges (-0.605 to -0.645). These charges facilitate stabilizing electrostatic interactions and hydrogen bonds within the DES.

Compared to the individual components, the Mulliken charge distribution in the DES shows a redistribution of charge density. The chloride anion's charge decreases from -0.669 to -0.618, and the hydroxyl oxygen's charge changes from -0.502 to -0.450, reflecting its involvement in hydrogen bonding. In PTSA, the sulfur charge increases from +1.373 to +1.403, and the sulfonate oxygens' charges adjust, indicating increased polarization and charge localization. These shifts enhance electrostatic interactions with the choline cation and confirm the establishment of intermolecular forces and hydrogen bonding that stabilize the DES structure.

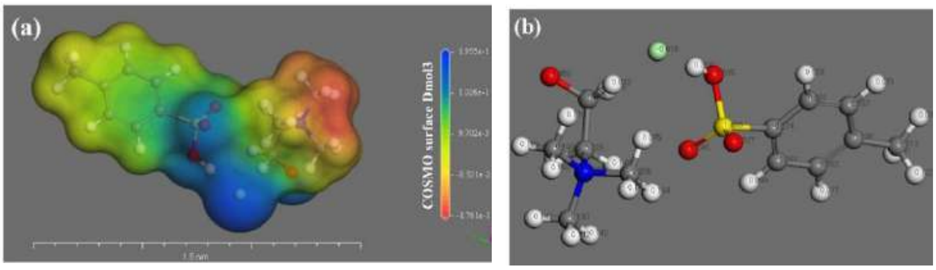

Figure 5 DFT-calculated COSMO surfaces **(a)** and Mulliken charges **(b)** for DES.

DES containing metal ions

Fig. 6 illustrates the COSMO surface of the DES with monovalent (Cu(I)) and divalent (Cu(II)) copper. For Cu(I), the ChCl portion shows strong negative potential around the hydroxyl oxygen, indicating high electron density and no involvement in copper complexation. The chloride ion exhibits a reduced potential, nearing neutral, while the PTSA sulfonate group shows negative potential, and the aromatic ring transitions from near-neutral to slightly positive. Incorporating Cu(I) alters the electronic structure and intermolecular interactions, with the chloride ion and sulfonate group potentially interacting with Cu(I), disrupting the original hydrogen bonding network.

In the Cu(II) system, the COSMO surface reveals a charge distribution with the ChCl hydroxyl oxygen having strong negative potential, suggesting it does not participate in

Cu(II) complexation. The methyl groups bonded to nitrogen show positive potential. The PTSA component displays negative potential around the sulfonate group and a transition to slightly positive potential on the aromatic ring. The presence of negative potential around the sulfonate group and the chloride ion indicates potential complexation sites for Cu(II), influencing the electronic properties and reactivity of the DES-Cu(II) system. Overall, these visualizations highlight varying electrostatic potentials and potential interaction sites within the DES-Cu(II) system.

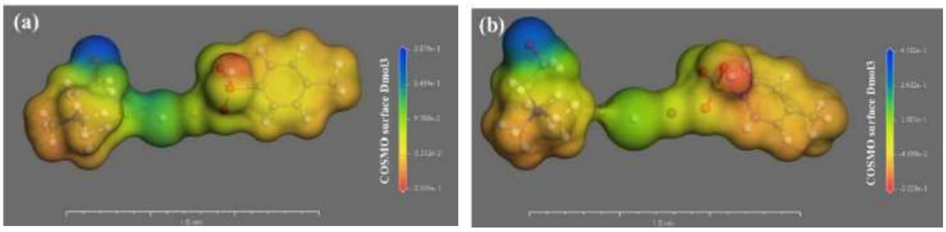

Figure 6 COSMO surface analysis ChCl:PTSA DES containing **(a)** Cu(I) and **(b)** Cu(II).

CONCLUSION

In conclusion, this study highlights the significant variability in Cu recovery rates among different DESs, with ChCl+ACA and ChCl+PTSA demonstrating the highest recoveries, about 100 %. The COSMO and Mulliken charge distributions provide valuable insights into the molecular interactions driving DES formation, particularly between ChCl and PTSA. These interactions are characterized by strong HBD and HBA as well as electrostatic attractions, which stabilize the DES structure. Incorporating Cu(I) or Cu(II) alters the electronic structure and intermolecular interactions within the DES, with potential complexation sites identified around the Cl ion and the -SO_3H group.

ACKNOWLEDGEMENT

"The research presented in this paper was done with the financial support of the Ministry of Science, Technological Development and Innovation of the Republic of Serbia, within the funding of the scientific research work at the University of Belgrade, Technical Faculty in Bor, according to the contract with registration number 451-03-137/2025-03/ 200131".

REFERENCES

1. Kumari S, Panda R, Prasad R, Alorro RD, Jha MK. Sustainable Process to Recover Metals from Waste PCBs Using Physical Pre-Treatment and Hydrometallurgical Techniques. Sustainability 2024;16:418.
2. Li H, Eksteen J, Oraby E. Hydrometallurgical recovery of metals from waste printed circuit boards (WPCBs): Current status and perspectives – A review. Resour Conserv Recycl 2018;139:122–39.
3. Oke EA, Potgieter H. Recent chemical methods for metals recovery from printed circuit boards: A review. J Mater Cycles Waste Manag 2024;26:1349–68.
4. Zante G, Boltoeva M. Review on Hydrometallurgical Recovery of Metals with Deep Eutectic Solvents. Sustainable Chemistry 2020;1:238–55.

5. Yuan Z, Liu H, Yong WF, She Q, Esteban J. Status and advances of deep eutectic solvents for metal separation and recovery. Green Chemistry 2022;24:1895–929.
6. Behnajady B, Najafi M, Karimi S. Green leaching of cold filter cakes using choline chloride–maleic acid deep eutectic solvent and molecular dynamics simulation. Physical Chemistry Chemical Physics 2024;26:24407–22.
7. Shahrezaei F, Karimi S, Behnajady B. Experimental and dynamic molecular study of zinc extraction from sphalerite concentrate in ternary deep eutectic solvent. Colloids Surf A Physicochem Eng Asp 2024;695:134241.
8. Moradi M, Karimi S, Behnajady B. The influence of adding a supplementary constituent to choline chloride and p-toluenesulfonic acid based deep eutectic solvents on the dissolution of chalcopyrite. Journal of Manufacturing Innovations 2024;1:45–52.
9. Karimi S, Mafton-Azad L, Behnajady B, Tüzün B. Response Surface Methodology (RSM) Design to Optimize the Cathode of Li-Ions Batteries Recycling in Deep Eutectic Solvent and DFT Simulation. Korean Journal of Chemical Engineering 2024:1–21.
10. Behnajady B, Seyf JY, Karimi S, Moradi M, Sohrabi M. Molecular dynamic (MD) simulation and density function theory (DFT) calculation relevant to green leaching of metals from spent lithium-ion battery cathode materials using glucose-based deep eutectic solvent (DES). Hydrometallurgy 2024;223:106223.
11. Liu K, Wang M, Zhang Q, Dutta S, Zheng T, Valix M, et al. Negative-carbon recycling of copper from waste as secondary resources using deep eutectic solvents. J Hazard Mater 2024;465.
12. Behnajady B, Najafi M, Karimi S. A new approach to direct chemical leaching of Sungun chalcopyrite concentrate via green deep eutectic solvent choline chloride-ρ-toluenesulfonic acid and MD simulation. J Taiwan Inst Chem Eng 2025;172:106118.
13. Zhao Q, Ma S, Ho W, Wang Y, Ho JYT, Shih K. Simple and environmentally friendly metal recovery from waste printed circuit boards by using deep eutectic solvents. J Clean Prod 2023;421.
14. Padwal C, Pham HD, Jadhav S, Do TT, Nerkar J, Hoang LTM, et al. Deep Eutectic Solvents: Green Approach for Cathode Recycling of Li-Ion Batteries. Advanced Energy and Sustainability Research 2022;3:2100133. https://doi.org/10.1002/aesr.202100133.
15. [15] Sabzkoohi HA, Kolliopoulos G. Green Zero-Waste Metal Extraction and Recycling from Printed Circuit Boards, 2021.
16. Abbott AP, Capper G, Davies DL, McKenzie KJ, Obi SU. Solubility of Metal Oxides in Deep Eutectic Solvents Based on Choline Chloride. J Chem Eng Data 2006;51:1280–2.

XVI International Mineral Processing
and Recycling Conference
28-30 May 2025, Belgrade, Serbia

DOI: 10.5937/IMPRC25613M Original research article

VARIABILITY IN FLOTATION PERFORMANCE OF LEPIDOLITE SAMPLES FROM THE EMILI DEPOSIT, FRANCE

Kristina Muntu[1], 0009-0008-0884-057X,
Jean-Gabriel Fraboulet[2], 0009-0000-4133-3272,
Sean Salour[2], 0009-0003-8494-389X,
Christine Bonnet[2], 0009-0009-6104-7017,
Enkhzul Bayarmagnai[2], 0009-0001-2829-6902,
Brian K. Cook[1], 0000-0001-9128-6996,
Massoud Aghamirian[1#], 0009-0002-9002-9095,
[1]SGS Canada Inc., Lakefield, Canada
[2]Imerys Beauvoir, Paris, France

ABSTRACT – Lepidolite flotation testwork was performed on 21 variability samples from the EMILI deposit in Allier, France, with head assays ranging from 0.49 to 1.38% Li_2O and an average K80 of 236 µm. After desliming, flotation was performed with an amine collector which was able to produce lepidolite concentrates grading >4.2% Li_2O with over 74.6% lithium recovery from 13 samples – often without cleaner flotation. The lower grade lepidolite concentrates (<4.2% Li_2O) were a result of unwanted recovery of other mica-type gangue minerals, as well as low feed grades below the 0.8% Li_2O cut-off grade already excluded from the mine plan.

Keywords: Lepidolite, Flotation Optimization, Mica Contamination.

INTRODUCTION

The EMILI project (EMILI stands for Exploitation de Mica Lithinifère par Imerys) is a major lithium deposit under the Beauvoir Kaolin Quarry site in the Allier region, France. The drilling campaign revealed indicated resources with an average content of 1.07% Li_2O, 0.1% Sn, and 0.02% Ta, confirming the attractiveness of the deposit (Imerys, 2024). Lithium is hosted mainly in mica-type minerals like lepidolite, and to a lesser extent amblygonite. Given the projected rise in global lithium demand, lepidolite is becoming an increasingly important source of lithium.

Recent studies [2-6] have demonstrated that flotation with cationic amine collectors, such as dodecylamine (DA), is the primary method for lepidolite concentration. The initial stage of this flotation process, desliming, is critical to mitigate the adverse effects of fine particles on collector efficiency and selective lepidolite flotation [2-3,7]. Optimizing collector dosage is also important, as excessive dosages can lead to unwanted recovery of silicate gangue minerals and dilute the final concentrate [2]. Evaluations of various

---

[#] corresponding author: massoud.aghamirian@sgs.com

commercial amine collectors, including Aeromine 3000C, Armac C and T, Armeen 12D (distilled DA), and Flotigam EDA (ether monoamine), revealed significant variability in flotation performance. For example, poor solubility and reduced froth stability were reported with Armeen 12D, while Flotigam EDA displayed a strong performance at acidic conditions (pH ~3.5) and produced a concentrate grading 4.0% Li_2O with approximately 77% lithium recovery [3,7]. Gemini collectors, characterized by dual hydrophobic groups, have indicated superior flotation efficiency compared to conventional DA, primarily due to stronger collector adsorption onto lepidolite surfaces. This enhanced performance was confirmed by contact angle and zeta potential measurements conducted by Wei et al. (2021), showing significantly improved lepidolite selectivity and flotation recovery.

The selective flotation of lepidolite from quartz and feldspar remains challenging, primarily due to their similar iso-electric points (IEP ~2-3). Consequently, flotation operations typically occur below pH 3 to ensure higher selectivity [8,9]. Huang et al. (2022) further demonstrated a clear decrease in concentrate grade when flotation pH increased from 2 to 9, affirming acidic conditions were optimal. Similarly, Filippov et al. (2022) observed peak performance at pH levels between 3 and 5, achieving lithium recoveries between 87% and 95% at concentrate grades up to 4.5% Li_2O. At high pH, flotation of unwanted silicate gangue increased, decreasing the concentrate purity. Recent advancements have aimed at overcoming issues related to high acid consumption and corrosion by exploring mixed collector systems. Wei et al. (2021) reported promising results using a collector blend termed "SOL" (sodium dodecyl sulfonate, sodium oleate, and DA), demonstrating effective flotation at neutral pH (pH 7) with high lepidolite recovery and minimal quartz contamination. However, these findings need validation through more comprehensive industrial-scale testing.

Overall, recent research has significantly advanced the understanding of lepidolite flotation processes, focusing on collector selection, dosage optimization, and innovative collector mixtures. Nonetheless, challenges in selective gangue rejection remain, emphasizing the need for further research into collector chemistry, optimization of flotation conditions, and pre-treatment steps such as desliming. These improvements will significantly enhance lepidolite beneficiation efficiency and contribute positively to meeting the growing global lithium demand.

EXPERIMENTAL

Materials

Drill samples representing twenty-one variability were collected from the Emili deposit (France). Eighteen samples represented the variability of ore included in the mine plan, and the additional three variability samples represented the materials out of the mine plan. Each sample was homogenized before being split into 4 kg charges and a representative head sample for assays and particle size analysis. To prepare the flotation feed, each charge was wet ground to a target size of 100% passing 300 µm. The ground material was then deslimed by wet sieving at 20 µm. The deslimed product was filtered, weighed, and split into 1.2 kg charges for flotation testing, and a representative subsample for particle size analysis. The slimes material (-20 µm fraction) was dried, weighed, and subsampled for chemical analyses.

Sample Characterization

The chemical analysis used in this study included lithium assays by Inductively Coupled Plasma Optical Emission Spectroscopy (ICP-OES) and whole rock analysis (WRA) with X-ray Fluorescence Spectroscopy (XRF). WRA included a 12-element suite for SiO_2, Al_2O_3, Fe_2O_3, MgO, CaO, K_2O, TiO_2, MnO, Cr_2O_3, V_2O_5, Na_2O, and P_2O_5.

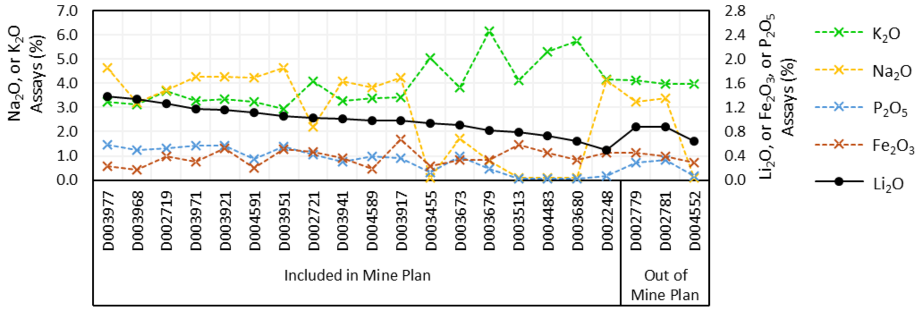

Figure 1 Key head assay results of the variability samples

The head assays of twenty-one variability samples (Figure 1) ranged from 0.49 to 1.38% Li_2O with low iron contents below 0.68% Fe_2O_3. The silica content varied from 66.5%-77.3% SiO_2 while aluminum contents varied from 13.8-20.5% Al_2O_3. The Na_2O and K_2O assays, which are mostly associated with mica and feldspar type minerals, ranged from 0.08-4.65% and 2.93-6.14%, respectively, while the P_2O_5 assays – mostly associated with phosphate minerals – ranged from 0.05-1.45%.

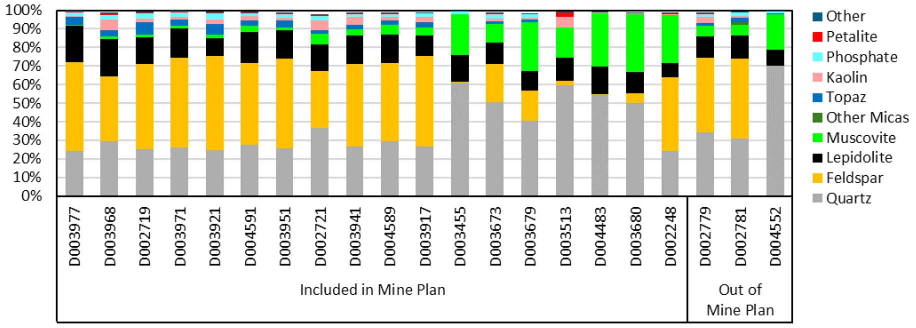

Figure 2 Modal mineralogy from MLA of the lepidolite flotation feed samples

The modal mineralogy of variability lepidolite flotation feed samples was determined with Mineral Liberation Analysis (MLA). The MLA results (Figure 2) confirmed that lepidolite was the main lithium-bearing mineral in all samples, at varying levels between 7.8 and 20.2%, which corresponded well with the Li_2O head assays. There was a good correlation between Li_2O and P_2O_5 content in the samples and phosphate minerals in the flotation feed (up to 4.0%), suggesting there is a potential association of phosphorus with lithium – perhaps in the form of the lithium-bearing phosphate mineral amblygonite

($LiAlFPO_4$). The major gangue minerals in the samples were quartz (24.1-70.0%), feldspars (0.3-50.6%), and muscovite (0.3-31.1%), with minor levels of topaz (<7.0%) and kaolin (<6.0%). In addition, the K_2O assays presented a stronger correlation with muscovite over lepidolite, where most variability samples containing over 3.8% K_2O contained over 10.2% muscovite.

The particle size analyses of the variability samples after stage grinding are presented in Figure 3. Prior to grinding, the particle size distribution was similar across the variability samples with the mass distribution in the -20 µm fraction ranging from a low level of 0.8% in sample D003679 to a high of 10.7% in sample D003513.

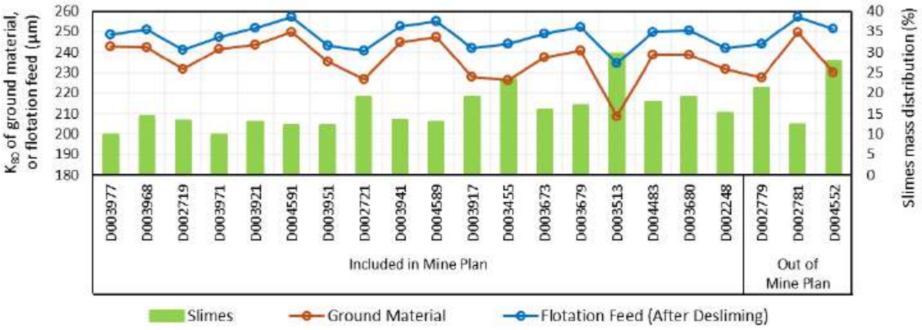

Figure 3 Particle size analyses of the variability samples after grinding

After grinding but before desliming, the K80 of the ground samples varied from 209 to 250 µm with an average of 236 µm, while after desliming the K80 of the flotation feed coarsened to between 234 and 257 µm with an average of 248 µm. The weight distribution of slimes after stage grinding ranged from 8.2 to 27.9% of the initial feed mass with an average of 10.9% for all samples. The range of fines production revealed that material across the deposit will exhibit different grinding behaviors and is an important consideration for plant design.

Flotation Testwork

The collector used for flotation was an amine collector with MIBC as a frother and H_2SO_4 as a pH modifier. Batch lepidolite rougher-cleaner flotation tests were performed on each of the twenty-one variability samples according to a flowsheet previously developed at SGS Lakefield with Imerys to produce 4.2% Li_2O lepidolite concentrate with maximum lithium recovery. Six tests included an additional scavenger flotation stage with an additional collector to maximize lithium recovery.

RESULTS AND DISCUSSION

Flotation Performance

The best lepidolite flotation performance for each variability sample was determined based on the highest lithium recovery to a combined concentrate grading over 4.2% Li_2O. For variability samples that did not meet the 4.2% Li_2O concentrate target the optimum performance was selected based on the final concentrate produced in the 2nd cleaner flotation stage. A summary of the performance evaluation is presented in Figure 4.

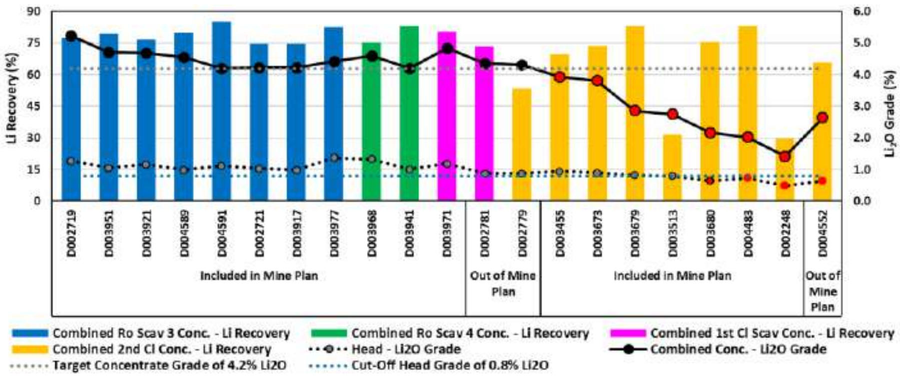

Figure 4 Particle size analyses of the variability samples after grinding

Twelve of the variability samples exhibited strong lepidolite flotation performance where concentrates grading over 4.2% Li_2O were produced with lithium recoveries over 73%. Eight of the twelve variability samples (shown in blue in Figure 4) met the concentrate target after 3 scavenger stages without any cleaning, to achieve over 74.6% lithium recovery. Two of the twelve variability samples (green) achieved included an additional fourth scavenging stage and additional collector to produce higher lithium recoveries of 75.4% and 83.2%, respectively, while also meeting the concentrate target without any cleaning stages. The two variability samples shown in pink in Figure 4 required one cleaner and cleaner scavenger stage to meet the target concentrate grade with lithium recoveries of 73.1 and 80.0%, respectively. The final sample to meet the 4.2% Li_2O was D002779, which required 2 cleaning stages and resulted in a lower lithium recovery of 53.3%.

The remaining Lepidolite concentrates were not able to meet the 4.2% Li_2O target and achieved varying performances. Samples D003455 and D003673 were able to approach the concentrate target at 3.93 and 3.81% Li_2O with strong global lithium recoveries of 69.6 and 73.5%, respectively. Meanwhile, the Li_2O content in the 2nd cleaner concentrates of the remaining six variability samples (shown in yellow in Figure 4) was below the 4.2% Li_2O target, varying from 1.42 to 2.86% Li_2O. In general, strong lithium recoveries were reported in most of these samples (>65.7%), except for variability samples D002248 and D003513 with 29.5 and 31.6% lithium recovery, respectively.

The increase in final concentrate Li_2O assay was strongly correlated ($R^2 = 0.93$) with a decrease in Al_2O_3 content and there was a moderate correlation between higher Li_2O assays and higher P_2O_5 and Na_2O content (R^2= 0.40-0.58), however, no correlation with K_2O content (R^2= 0.2) was observed (Figure 5). This indicates that variability samples producing concentrates below the target Li_2O grade also recovered mica gangue minerals during flotation, such as muscovite, since muscovite contains higher Al_2O_3 at a similar K_2O grade to lepidolite but contains little to no lithium. The strong relationship between muscovite in the flotation feed and Li_2O grade of the final concentrate shown in Figure 6 provides further support for this conclusion. Variability samples D003455, D003673, D002248, D003679, D003680, D003513, D004483, and D004552 all contained more than 10% muscovite in the flotation feed and did not meet the 4.2% Li_2O target, highlighting how selective rejection of non-lithium-bearing micas from lepidolite is challenging.

Meanwhile, P_2O_5 and Na_2O in the concentrates can possibly be attributed to amblygonite, which can also float amines to the lepidolite concentrate, but present no obvious impact on the concentrate Li_2O grade.

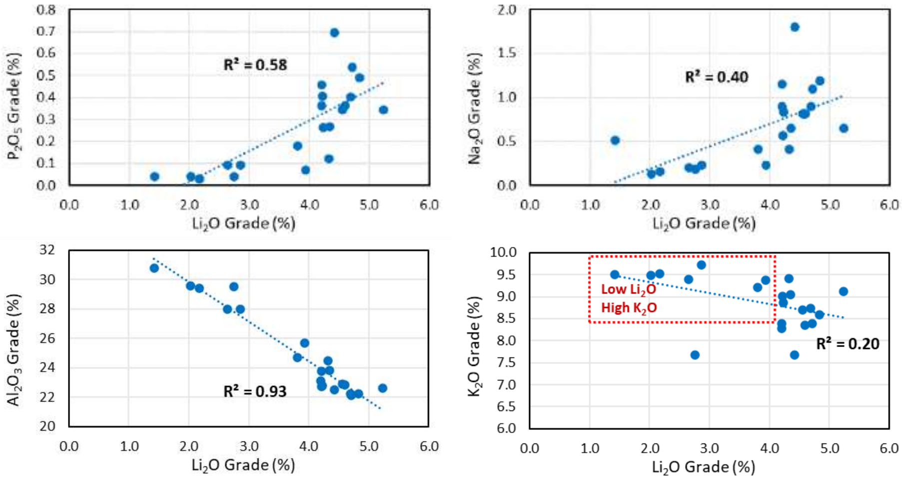

Figure 5 P_2O_5, Na_2O, Al_2O_3, and K_2O grades vs. Li_2O grade of the final concentrates

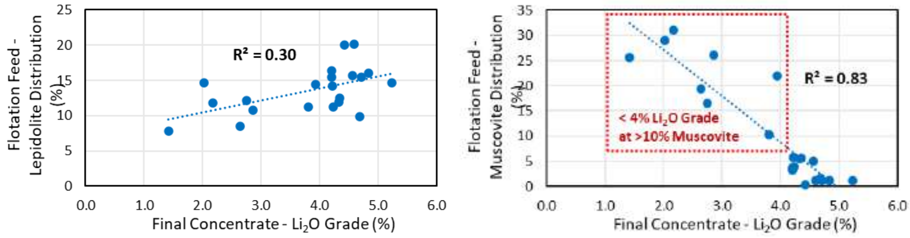

Figure 6 Li_2O concentrate grade vs. lepidolite and muscovite content in the feed

CONCLUSION

The results of this testwork confirmed that concentrates grading >4.2% Li_2O could be produced from thirteen of the twenty-one variability samples from the Emili deposit. For most of these samples, the target concentrate grade of 4.2% Li_2O was achieved without cleaner flotation stages at lithium recoveries greater than 74.6%.

The sample characterization revealed that the Li_2O and K_2O content in the 21 samples varied considerably, with the main lithium mineral being lepidolite and the main gangue minerals being quartz and muscovite. The slimes (-20 µm) distributions of the variability samples after wet grinding to 100% passing 300 µm were highly variable, suggesting the grindability characteristics vary across the Emili deposit.

There was a strong correlation between decreasing Li_2O grade in the final concentrates and increasing muscovite content in the flotation feed since muscovite is prone to float under the same conditions as lepidolite. This is most likely why the target grade of 4.2% Li_2O could not be met with the eight remaining variability samples. There was also some correlation between low concentrate quality and low lithium feed grades.

Overall, the variability flotation testwork confirmed that much of the Emili deposit was amenable to the production of a 4.2% Li_2O concentrate with high lithium recoveries. For samples where the concentrate targets were not met, poor flotation performance was attributed to higher gangue mica content and lower head grades, which will be an important consideration for project development and future operation.

REFERENCES

1. Bulatovic, S. M. (2015). Handbook of Flotation Reagents: Chemistry, Theory and Practice: Vol. 3: Flotation of Industrial Minerals. Elsevier.
2. Vieceli, N., Nogueira, C. A., Pereira, C. A. (2016a). Flotation of Brazilian lithium ores: A review. Minerals Engineering, 98, 30-43.
3. Vieceli, N., Nogueira, C. A., Pereira, C. A. (2016b). Effect of amine collectors on the flotation of lithium-bearing minerals. Minerals Engineering, 89, 30-35.
4. Huang, Z., Liu, G., ..., & Yang, J. (2020). Study on flotation characteristics of lepidolite using an ether monoamine collector. JOM, 27(2), 198-207.
5. Huang, Z., Wang, Z., ..., & Yang, J. (2022). Comparative study on the flotation of lepidolite and albite using dodecylamine. Minerals, 12(2), 210.
6. Wei, Z., Huang, Z., ..., & Yang, J. (2021). Enhanced flotation separation of lepidolite from quartz using a novel Gemini collector. Powder Technology, 393, 513-520.
7. Filippov, L., Filippova, I. V., ..., & Reddy, R. G. (2022). Lepidolite flotation from lithium ores using monoetheramine collectors. Minerals Engineering, 180, 107499.
8. Choi, H. S., Lee, J. Y., ..., & Park, J. W. (2012). Flotation of lithium ores to obtain high-grade Li_2O concentrates. Minerals Engineering, 29, 48-56.
9. Cook, B.K., Fraboulet, J-G., … Aghamirian, M., (2023). Investigations into Spodumene and Lepidolite Flotation. In: 2023 CMP Conference, Canada, Proceedings, 29-43.

XVI International Mineral Processing
and Recycling Conference
28-30 May 2025, Belgrade, Serbia

DOI: 10.5937/IMPRC25620N Original research article

REPROCESSING OLD MINE TAILINGS TO RECOVER COPPER AND PRECIOUS METALS USING FROTH FLOTATION

Titus Nghipulile#, 0000-0003-4399-2620,
Theophile Mwaku, 0009-0006-3406-483X,
Godfrey Dzinomwa, 0000-0001-8763-699X,
Benjamin Mapani, 0000-0002-5354-3397,
Jaquiline Tatenda Kurasha, 0000-0002-7213-7669,
Department of Civil, Mining and Process Engineering, Namibia University of Science and Technology, Namibia

ABSTRACT - The old tailings from mine dumps in Namibia contain not only copper but also precious metals and other metal values, such as lead and zinc, which should be recovered to supplement the production of metals from ores. X-ray fluorescence (XRF) analysis of the tailings showed that it contained 0.8% Cu, 40 ppm Au, 60 ppm Ag, 0.9% Pb, 0.7% Zn and 1% Fe. Batch roughing tests were conducted to investigate the effect of pH, collector (PAX) dosage, and sulphidiser (Na_2S) dosage on the recovery of copper and precious metals (Ag and Au). Results for flotation test work showed that recovery of metal values depends on the three operating variables. Maximum recoveries of Cu (52%), Ag (53%) and Au (44%) were achieved at pH 10.5, PAX dosage of 47 g/t, Na_2S dosage of 109 g/t and 12-minute residence time. Testwork is still in progress to improve the recoveries of copper, gold and silver.

Keywords: Circular Economy, Flotation, Mine Tailings, Copper.

INTRODUCTION

The ore deposits around the world are depleting, with new discoveries becoming fewer. In the era of green energy transition and fourth industrialisation, it is expected that the demand for copper and other critical metals will keep increasing. Mine wastes, such as tailings, are now potential resources (secondary sources) of metal values. Millions of tonnes of tailings have been accumulated around the world after decades of mining operations. Re-processing the tailings not only allows the recovery of metal values to ensure an adequate supply of metals but also mitigates environmental impacts.

Different methods for the recovery of copper and other metals from copper tailings have been investigated. This includes flotation [1-3], leaching [3-5] and sulphation roasting-leaching [6]. Froth flotation is widely used for the beneficiation of sulfide minerals by exploiting the differences in the surface properties of minerals. The old tailings, which may have altered sulphide minerals, could require sulphidisation during flotation. The particle size of the flotation feed plays a critical role in the efficiency of the

---

corresponding author: tnghipulile@nust.na

flotation process. Fine particles are unable to collide with air bubbles, and the coarse particles are unable to attach to the bubbles. Tailings contain mainly fine particles, which could pose process challenges when applying flotation as a beneficiation method. The various methods, discussed in detail elsewhere [7], which can be employed to improve the flotation of fine tailings, include microbubble flotation, column flotation, nanobubble flotation, polymer flocculation, shear flocculation, oil agglomeration and carrier flotation.

Mining activities around Tsumeb began in the early 1900s. A significant amount of tailings was accumulated from the operations for different eras (classified based on the technologies that were used in the processing plants). This study used the old tailings from the pre-1960 era to carry out mineralogical characterisation and evaluate the flotation characteristics of the mineral phases in the tailings. The study aimed to investigate the effect of pH, collector concentration and sulphidiser concentration on the recovery of copper and precious metals (gold and silver) contained in the tailings.

MATERIALS AND METHODS

Sample preparation and characterisation

The old tailings were collected from the mine dumps around Tsumeb in Namibia. The composite sample used for the test work was composed of samples from various locations and depths within the mine dumps. Mineralogical characterisation using binocular microscopy of the tailings sample was done to identify the mineral phases present in the ore. The benchtop Thermo Scientific X-Ray Fluorescence (XRF) machine was used to determine the chemical composition of the sample.

Flotation procedures

The ‘as received’ sample was dry milled to have a P_{80} of 38 µm. The mill product was then split into 500 g subsamples, which were used for batch flotation tests. The bottle-driven Magotteaux flotation machine, fitted with a 2.5 L cell, was used to conduct the flotation experiments. Figure 1 shows the scope of the flotation testwork programme. In Phase 1, the residence time was fixed at 5 minutes while the operating parameters were varied at different levels, i.e., pH (natural pH (~8.1), 9.5, 10.0 and 10.5), collector (potassium amyl xanthate (PAX)) concentration (47, 109 and 172 g/t) and sulphidiser (Na_2S) concentration (0, 47, 109 and 172 g/t). Pine oil was used as a frothing agent, and its concentration was fixed at 200 g/t in all tests in Phase 1. Sodium hydroxide (NaOH) was used for pH adjustment. The best combination (yielding the highest recoveries of Cu, Ag, and Au) of pH, PAX concentration, and Na_2S concentration was used in Phase 2, where the total residence time was increased to 12 minutes, and four kinetic concentrate samples (each for 3 minutes) were collected.

The scalping of the concentrate was done every 15 seconds in all tests. The impeller speed and airflow rate were kept constant at 800 rpm and 6.5 L/min respectively. Tap water was used to prepare the slurry for flotation, and deionised water was used to make up the solution of reagents. In all flotation tests, the concentrates and tailings were filtered, dried, weighed and then assayed using the benchtop XRF machine.

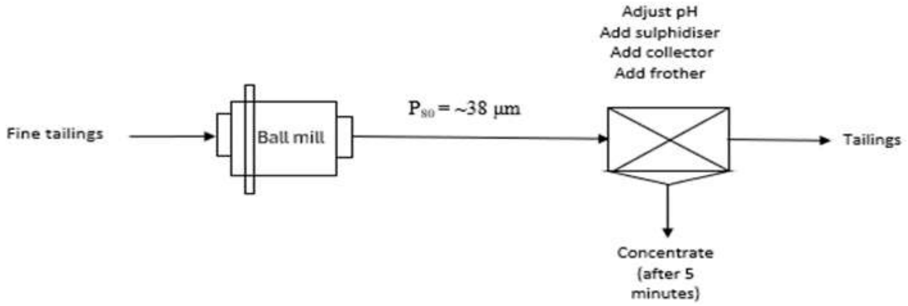

Figure 1 Scope of work for Phase 1

RESULTS AND DISCUSSION

Chemical and mineralogical composition of the old tailings

Table 1 shows the XRF assays for the two head samples. It can be observed that the tailings had precious metals (Ag and Au) in addition to the base metals (Cu, Pb and Zn) and iron. The average grade of copper was 0.75%. Mineralogical examination was performed using the binocular microscope. Various phases were identified under the microscope. In Figure 2a, the main minerals are quartz, mainly stained to brown colour, and constitute almost 90% of the field of view; calcite and dolomite (mainly white), almost 8% of the field of view. The black to bluish coloured phases are the sulphide bornite (makes up about 1.0 % in the specimen). Some grains with a brown-black colour are taken to be iron oxides, and chalcopyrite being altered to oxides. In Figure 2b, the main minerals are quartz, mainly stained to brown colour, and constitute almost 75% of the field of view; calcite and dolomite (mainly white), almost 20% of the field of view; with some dolomites being grey in colour (bottom right of photograph in Figure 2c). The black to bluish coloured phases are the sulphide bornite (makes up about 0.5-1.5% in the specimen). In Figure 2c, the main minerals are quartz, colourless to brown; calcite and dolomite (mainly white), with some dolomites being grey in colour (bottom right of photograph in Figure 2c). The black to bluish coloured phases are the sulphide bornite. Cerussite and anglesite are also present in the tailings and perhaps could be products of re-precipitation and not original grains. Scanning electron microscopy (SEM) analysis would be required to resolve whether they are original grains or a late precipitation after tailings were deposited. Cerussite occurs as small, needle-like phases, whereas anglesite is white and crystalline. Smithsonite, the Zn-bearing carbonate is also present in the tailings.

Table 1 XRF assays for the head samples

Head sample	g/t		(%)							
	Ag	**Au**	**Cu**	**Fe**	**S**	**Pb**	**Zn**	**Ca**	**Si**	**Others**
1	39.6	59.3	0.75	1.18	0.098	0.88	0.66	20.56	20.6	~56.19
2	44.7	61.0	0.75	1.16	0.108	0.89	0.66	20.18	19.9	~56.33

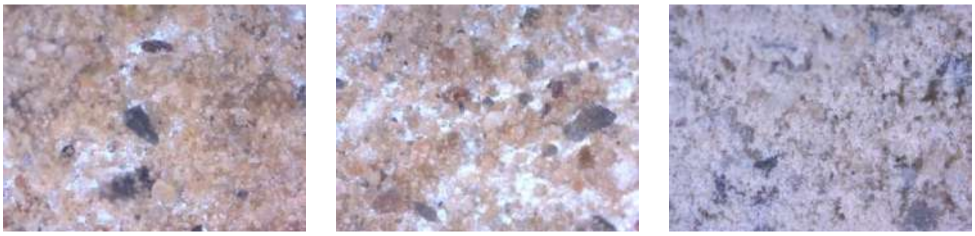

2a – Tailings speciment OMT1, magnification 10 x 10. Scale bar =0.05 mm

2b – Tailings specimen OMT2, magnification 10 x 10. Scale bar =0.05 mm

2c – Tailings specimen OMT2-1, magnification of 10 x 5. Scale bar =0.09 mm

Figure 2 Scope of work for differential flotation of Pb and Cu concentrates

Milling and Flotation results

The 80% passing size of the ‘as received’ sample was about 106 µm, while that of the flotation feed (mill product) was about 38 µm. Figures 3 and 4 show the effects of collector dosage, pH and sulphidiser on the recovery of copper from the tailings. From Figure 3, it can be observed that for different pH levels, the relationships between copper recovery and collector dosages are different. For pH 9.5, recovery increases with the collector dosage. On the other hand, for pH 10.5, recovery decreases with the collector dosage. For the intermediate pH of 10, recovery initially increases with collector dosage up to 109 g/t, beyond which it decreases with the collector dosage. Optimisation of recovery has to be determined by finding the optimal combination of these two variables and other variables (e.g., concentrations of sulphidiser and frother). As shown in Figure 4, the relationship between copper recovery and sulphidiser concentration is dependent on the pulp’s pH and PAX concentration. For both natural pH and pH 10, the copper recovery increased with sulphidiser concentration when the PAX concentration was 47 g/t. For the PAX concentrations of 109 and 172 g/t, copper recovery increases with the sulphidiser concentration. The mass pull increased with the recovery, with the maximum mass pull being 16% (w/w). The maximum concentrate grade was about 2.8% Cu (corresponding to the recovery of approximately 35% Cu). The maximum recovery was about 38% Cu. Recoveries of Ag and Au were plotted against the recovery of copper in Figure 5. Recoveries for both Ag and Au increase with the recovery of Cu. This implies that Au and Ag are closely associated with the mineral phases of copper.

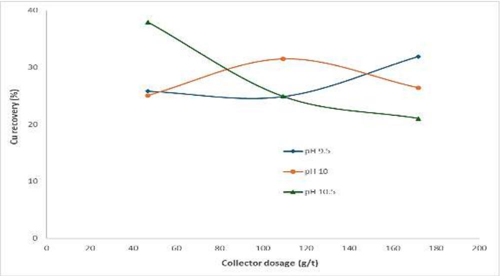

Figure 3 Effect of collector dosage and pH on copper recovery
(Na_2S dosage was fixed at 100 g/t)

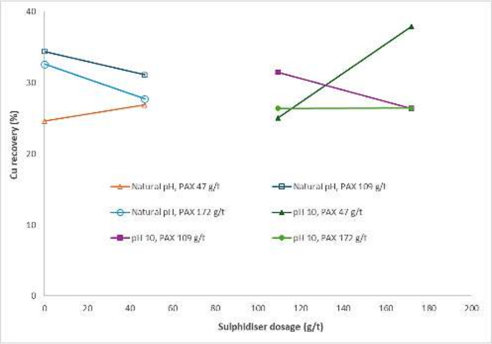

Figure 4 The effect of Na_2S on copper recovery at different pH levels and PAX dosages

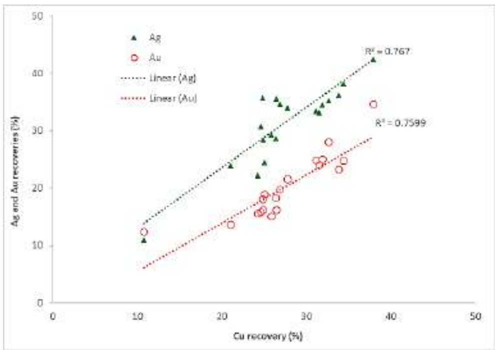

Figure 5 Relationship between recoveries of Cu, Ag, and Au

The results for a limited scope of Phase 2 conducted so far are shown in Table 2. The test conditions are shown in Figure 1. For the two tests conducted under the same conditions, the recovery was increased from 38% Cu (see Figure 5) to 51% Cu. It should be noted that no sulphidiser was added in stages two to four for the reported results in Table 2. There is scope to increase the recovery by adding a sulphidiser in stages two to four. Alternative collectors are also being considered in the ongoing testwork. Furthermore, the effect of the frother type and concentration is yet to be investigated. Considering the low content of valuable metals and altered mineral sulphide phases of copper, the authors acknowledge that hydrometallurgical treatment of the material may be the best option, as also recommended by other researchers [8]. Hydrometallurgical processing of the material to recover copper and other metals will be investigated in a future study.

Table 2 Summary of results for Phase 2

Test #	Mass pull (%)	Recoveries (%)			Concentrate grade			Tailings grade (ppm)		
		Cu	Ag	Au	Cu (%)	Ag (ppm)	Au (ppm)	Cu	Ag	Au
Run 1	28.70	52	47	43	1.41	188	298	5500	29.5	50.5
Run 2	26.19	52	59	44	1.66	191	296	5470	21.6	45.8

CONCLUSION

A series of batch flotation experiments were conducted on the old tailings enriched with metal values, 0.8% Cu, 40 ppm Au, 60 ppm Ag, 0.9% Pb, 0.7% Zn and 1% Fe. Batch roughing tests were conducted to investigate the effect of pH, collector (PAX) dosage, and sulphidiser (Na_2S) dosage on the recovery of copper and precious metals (Ag and Au). For the scope of work currently reported in this paper, maximum recoveries of Cu (38%), Ag (42%) and Au (35%) were achieved at pH 10.5, PAX dosage of 47 g/t and Na_2S dosage of 109 g/t. The recoveries were further increased to averages of 52%, 53% and 44% for Cu, Ag and Au, respectively, when the residence time was increased from 5 minutes to 12 minutes. The concentrate grade decreased to an average of 1.5% Cu, and mass pull increased from 16% (w/w) to about 27% (w/w). Testwork is still in progress to improve the recoveries of copper, gold and silver.

ACKNOWLEDGEMENT

The authors are grateful to the mine which supplied the samples used in the testwork. The technical staff in the department of Mining, Civil and Process Engineering at Namibia University of Science and Technology are also acknowledged for their assistance with XRF analysis and preparation of slides for microscopic examination.

REFERENCES

1. N. Terbish, A. Ganzorig, D. Davaajargal, and B. Baatar, *Reprocessing of tailing from Erdenet copper ores: Optimisation of the flotation*, no. Resat. Atlantis Press International BV, 2023. doi: 10.2991/978-94-6463-318-4_4.
2. M. Santander and L. Valderrama, "Recovery of pyrite from copper tailings by flotation," *J. Mater. Res. Technol.*, vol. 8, no. 5, pp. 4312–4317, 2019, doi: 10.1016/j.jmrt.2019.07.041.
3. R. S. Magwaneng, A. Batnasan, K. Haga, and A. Shibayama, "Development of a Combined Flotation and High Pressure Leaching Process for Copper and Nickel Recovery from Mine Tailing," *J. Miner. Mater. Charact. Eng.*, vol. 05, no. 03, pp. 118–131, 2017, doi: 10.4236/jmmce.2017.53010.
4. Y. Wang, S. Wen, Q. Feng, Y. Xian, and D. Liu, "Leaching characteristics and mechanism of copper flotation tailings in sulfuric acid solution," *Russ. J. Non-Ferrous Met.*, vol. 56, no. 2, pp. 127–133, 2015, doi: 10.3103/S1067821215020170.
5. L. Avramović, R. Jonović, M. Bugarin, R. Marković, J. Stevanović, and M. Jonović, "Leaching of Flotation Tailings," *18th Int. Res. Conf." Trends Dev. Mach. Assoc. Technol. TMT 2014 Budapest, Hungary, 10-12 Sept. 2014*, no. November 2021, pp. 481–484, 2014, [Online]. Available: https://www.tmt.unze.ba/proceedings2014.php
6. M. Ozer, "Cobalt and copper recovery from the ancient flotation tailings by selective sulfation roast-leaching process," *J. Min. Metall. Sect. B Metall.*, vol. 55, no. 3, pp. 315–324, 2019, doi: 10.2298/JMMB190304043O.
7. M. Bilal *et al.*, "The Challenges and Prospects of Recovering Fine Copper Sulfides from Tailings Using Different Flotation Techniques: A Review," *Minerals*, vol. 12, no. 5, 2022, doi: 10.3390/min12050586.
8. V. Trifunović, L. Avramović, D. Božić, M. Jonović, D. Šabaz, and D. Bugarin, "Flotation Tailings from Cu-Au Mining (Bor, Serbia) as a Potential Secondary Raw Material for Valuable Metals Recovery," *Minerals*, vol. 14, no. 9, p. 905, 2024, doi: 10.3390/min14090905.

XVI International Mineral Processing and Recycling Conference
28-30 May 2025, Belgrade, Serbia

DOI: 10.5937/IMPRC25626M

Original research article

ZEOLITE ACID (UN)STABILITY AS MAJOR DISANDVANTAGE FOR ITS HUMAN CONSUMPTION

Sonja Milićević[#], 0000-0001-8929-1673,
Jovica Stojanović, 0000-0002-2752-6374,
Ivana Jelić, 0009-0000-9901-9323,
Snežana Zildžović, 0000-0002-0214-8119,
Vladimir Jovanović, 0000-0001-6069-1630,
Dejan Todorović, 0000-0002-2776-3388,
Institute for Technology of Nuclear and Other Mineral Raw Materials ITNMS, Belgrade, Serbia

ABSTRACT – This study was conducted to examine the potential harmful effects of zeolite consumption in daily supplementation. The research focused on the acid stability of zeolite in HCl solution at pH values ranging from 1.5 to 3, corresponding to gastric pH levels. The initial zeolite sample, as well as the samples subjected to acidic treatment, were characterized using X-ray diffraction (XRD) method, and their chemical composition was analyzed. The results obtained indicate that the crystalline structure of zeolite was not disrupted during the treatment. At a pH of 1.5, up to 2% of aluminum leached into the solution, while at higher pH values, no aluminum leaching was observed. These findings underscore the need for cautious consideration of zeolite supplementation due to potential aluminum release in highly acidic environments.

Keywords: Acidic Stability, Dealumination, Zeolite.

INTRODUCTION

Zeolites are crystalline hydrated aluminosilicates that possess an infinite three-dimensional structure. The fundamental building unit of the crystalline structure of zeolites is the TO_4 tetrahedron (T represents silicon or aluminum) [1,2]. At the center of the TO_4 tetrahedron is either Si^{4+} or Al^{3+}, while at the tetrahedral corners are four oxygen atoms, each shared between two tetrahedra. This connectivity results in a zeolite structure rich in cavities, which contain large cations and water molecules that exhibit significant mobility, allowing for cation exchange and reversible dehydration. Due to the isomorphic substitution of tetravalent Si with trivalent Al, the aluminosilicate framework of zeolites is negatively charged [3,4]. This excess negative charge is balanced by the presence of alkali and alkaline earth metal cations, most commonly Na^+, K^+, Ca^{2+}, and Mg^{2+} which can be exchanged with other cations through ion-exchange reactions [1,3].

The sum of the equivalent positive charges of exchangeable cations equals the negative charge of the framework and is expressed as the cation exchange capacity (CEC)

[#] corresponding author: s.milicevic@itnms.ac.rs in mmol M^+/100g. The CEC depends on the degree of silicon substitution by aluminum, channel dimensions, shape, size, and valency of exchangeable cations [3,4].

Due to their negative charge and porous structure, natural zeolites find widespread applications as cation exchangers and molecular sieves. Their unique structural characteristics enable diverse applications [5-9]:

- Environmental science: Ammonia removal from municipal wastewater [5,6]; Removal of heavy metal ions from contaminated water [7-9]; Water softening [8]; Radioactive waste treatment [10]
- Agriculture: Soil remediation in agriculture [11].
- Healthcare: Medical applications for detoxification [12]; As feed additives for livestock [12]; Zeolites enriched with Cu and Zn micronutrients exhibit antibacterial properties against *Escherichia coli* and *Clostridium* species [13]; Ability to bind carcinogenic substances suggests potential applications in cancer therapy [14]
- Energy and industry: Catalysts and catalyst supports in energy and industrial processes [14].

Treatment of zeolites with mineral acids yields the acidic or H-form of zeolites. Clinoptilolite, characterized by a high Si/Al ratio (> 4), exhibits high acid stability. This enables the formation of H-clinoptilolite with a high ion-exchange capacity while preserving its crystalline structure. However, treatment with concentrated mineral acid solutions (pH = 0) can lead to structural modification or even significant degradation of the crystal lattice. Depending on the acid concentration, dealumination of the crystal framework occurs to varying degrees.

Barrer demonstrated that treatment of clinoptilolite with HCl at concentrations up to 2 mol dm^{-3} results in channel expansion, increased porosity, and enhanced specific surface area. Acid treatment leads to cation exchange with H_3O^+ ions, followed by hydrolysis of Al-O groups, releasing Al into the solution and removing H_3O^+ ions from clinoptilolite channels, ultimately yielding a structure with a large internal surface area. However, at HCl concentrations exceeding 2 mol dm^{-3}, structural degradation becomes significant, with amorphization dominating and specific surface area decreasing.

Despite zeolite extensive industrial use, including applications in water purification, catalysis, and environmental remediation, the incorporation of zeolites into human dietary supplementation remains controversial. A key limitation lies in the presence of aluminum within the zeolite framework, and the potential for its release under acidic conditions-particularly in the human gastrointestinal tract.

Aluminum incorporated in the zeolitic structure is generally considered stable under neutral or mildly acidic conditions; however, exposure to strong acids, may lead to partial degradation of the framework and subsequent aluminum leaching. This phenomenon raises significant safety concerns, especially considering the lack of comprehensive toxicological and clinical studies evaluating the long-term effects of zeolite consumption in humans.

Aluminum is a naturally occurring element found in soil, water, and air. Humans are routinely exposed to small quantities through dietary intake, drinking water, and the use of cosmetic and pharmaceutical products. In recent years, increasing public and scientific attention has been directed toward reducing aluminum exposure, particularly due to its potential neurotoxic and osteotoxic effects.

Although the human body can eliminate small amounts of aluminum, chronic exposure or accumulation may lead to adverse health outcomes. Aluminum has a high affinity for biological tissues, particularly in the brain and skeletal system. While still under investigation, several studies suggest a possible link between excessive aluminum accumulation and the pathogenesis of Alzheimer's disease and other neurodegenerative conditions [15]. Furthermore, chronic aluminum intake has been shown to interfere with calcium and phosphorus metabolism, potentially leading to bone demineralization and the development of osteomalacia-especially in individuals with impaired renal function [16].

Given these concerns, the aim of this study is to evaluate the stability of the zeolitic framework in acidic gastric conditions and quantify the potential release of aluminum ions under simulated stomach pH conditions (1.5 - 3). Understanding the extent of aluminum leaching from zeolite structures under physiologically relevant conditions is essential for assessing their safety and suitability for human consumption.

EXPERIMENTAL

Raw zeolite, clinoptilolite (Z) from the Igroš deposit in Serbia was used as an absorbent. After crushing and grinding, the sample was sieved to the fractions below 0.043 mm-optimal for the zeolite characterization (XRD, DTA) and investigations of maximum adsorption capacity.

Acid treatment of zeolite was carried out in a batch system. A total of 8 g of zeolite was treated with 200 ml of HCl solution, with initial pH values of 1.5, 2.0, 2.5, and 3.0. After shaking for 24 h on orbital shaker, all suspensions were centrifuged and the concentrations of the Al in supernatants were determined using AAS.

The total CEC of the zeolitic tuff was 135.2 meq/100 g, measured using 1 M NH 4 Cl (Sigma Aldrich, Munich, Germany). Calcium (97.3 meq/100 g) was the dominant exchangeable ion but Na (21 meq/100 g), Mg (16.4 meq/100 g), and K (0.37 meq/ 100 g) were also present in the starting zeolitic tuff.

RESULTS AND DISCUSSION

Due to the large number of figures and limited space, only figures for the zeolite Z and Z 1.5 (treated with HCl on pH 1.5) will be presented.

Qualitative mineralogical composition of the analysed sample is as follows: zeolite minerals of heulandite/clinoptilolite type, plagioclases, quartz, mica and irregular interstratified clays. Among these, zeolite minerals are the most predominant, while all the other minerals are much less represented. Crystallinity degree of zeolite minerals is low. Measured average crystallite size of zeolite minerals is 276 Å. All other crystal phases are below detection limits. Diffractogram of the "Z-Ig" sample is given in the Figure 1.

Qualitative mineralogical composition of the analysed sample is the same as in previous sample. No crystal structure disorder (amorphization) has been determined due to acidic treatment. Diffractogram of the "Z-Ig 1.5" sample is given in the Figure 2.

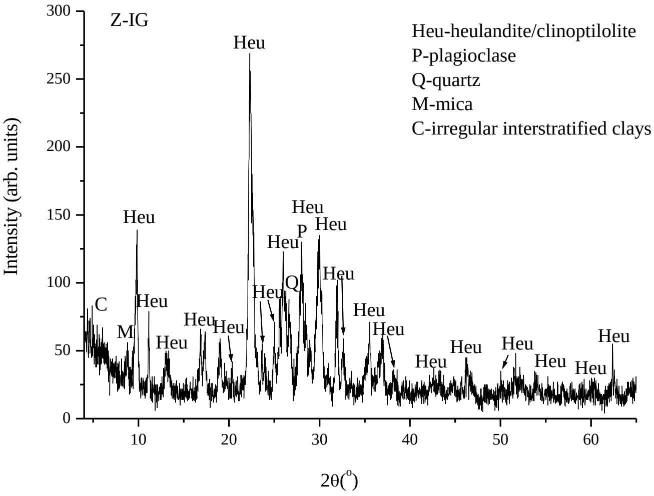

Figure 1 XRD diffractogram of the "Z-Ig" sample.

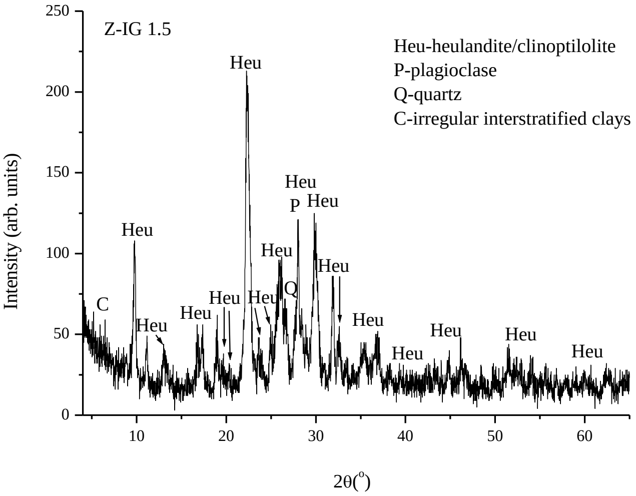

Figure 2 XRD diffractogram of the "Z-Ig 1.5" sample.

Chemical composition of the initial and acidly treated zeolites is presented in Table 1. The obtained results are similar to the XRD one, indicating that there are no significant differences in chemical composition between the samples, indicating that the investigated pH range does not destroy the zeolite structure. Only with the pH 1.5 is noticed the slightly difference in Al content.

Table 1 Chemical composition of the initial and acidly treated zeolites

	SiO_2	Al_2O_3	Fe_2O_3	CaO	MgO	Na_2O	K_2O	IL
	%							
Z	64.8	15.1	1.47	4.19	1.60	1.16	0.85	10.62
Z 1.5	65.4	14.91	1.53	3.91	1.59	0.91	0.81	10.66
Z 2.0	65.1	15.01	1.50	4.06	1.60	0.96	0.83	10.62
Z 2.5	64.9	15.04	1.45	4.06	1.61	1.06	0.84	10.63
Z 3.0	64.8	15.04	1.44	4.20	1.60	1.10	0.85	10.64

The content of the aluminium is also measured in supernatants and the results are presented in Table 2. The obtained results indicate that at a pH value of 1.5, aluminum leaching did occur. The total amount measured in the solution is 108 mg/L. The initial aluminum content in the zeolite is 15.1%, which implies that its maximum potential leaching amount from 8 g of zeolite could reach 6040 mg/L. Considering this, it can be concluded that less than 2% of aluminum transitioned into the solution, which is why there was no disruption of the crystal lattice of the zeolite.

Table 2 Chemical composition of the supernatants after acid treatment

	Al	Si	Na	K	Ca	Mg	Fe
mg/L							
F-1.5	108.75	21.6	82.12	4.63	147.5	26.75	3.38
F-2.0	6.1	13.3	47.25	2.08	88.75	12.38	0.13
F-2.5	0.5	10.9	25.12	0.93	27.5	5.06	0.10
F-3.0	2.3	15.6	15.50	0.77	10.0	1.93	0.62

However, it is important to mention that according to joint FAO/WHO Expert Committee on Food Additives, the maximum allowable daily intake of aluminum for humans is 10 mg. This is the amount a healthy individual weighing 70 kg can ingest without the body being unable to effectively eliminate the aluminum. With a daily intake of just 1 g of zeolite through supplementation, an individual would consume 25 - 30% of the maximum permitted aluminum intake, which does not exceed the recommended allowance, but is not negligible-especially if such intake is repeated multiple times a day or combined with other sources of aluminum (diet, medications, etc.).

CONCLUSION

In the conclusion of this study, it has been established that zeolite maintains its acid stability within the pH range characteristic of the stomach, which is between 1.5 and 3, without significant disruption of its crystalline structure. However, at a pH of 1.5, it has been observed that up to 2% of the total aluminum present in zeolite passes into solution. Taking into account a daily intake of just 1 g of zeolite through supplementation, an individual would consume between 25% and 30% of the maximum permitted aluminum intake, which, while not exceeding the recommended limits, represents a significant amount-especially in the context of frequent intake throughout the day or in combination with other sources of aluminum. At higher pH values, the amount of aluminum leached from zeolite becomes negligible. These results underscore the need for careful consideration of potential aluminum intake when using zeolite as a supplement, particularly in the context of long-term consumption.

ACKNOWLEDGEMENT

This work was supported by the Ministry of Science, Technological Development and Innovation of the Republic of Serbia [grant number 451-03-136/2025-03/20023]

REFERENCES

1. Baerlocher, Ch., Meier, W.M. Olson D.H., Atlas of Zeolite Framework Types, Fifth Revised Edition, Structure Commision of the International Zeolite Association, Elsevier, 2001, 2-7; 146-147.
2. Gottardi, G., Galli, E., Natural Zeolites. Springer-Verlag, Berlin, 1985, 256-283.
3. Mumpton, F.A., Sand, L.B., Natural Zeolites: Occurrence, Properties and Use. Pergamon, New York, 1978, 3-27.
4. Mercer, B.W., Ames, L.L., Sand, L.B., Mumpton, F.A., Natural Zeolites, Occurrence, Properties and Use. Pergamon, New York, 1978, 48.
5. Booker, A.N., Cooney, L.E., Priestley, J.A., 1996. Water Sci. Technol., 34, 17-24.
6. Baykal, B.B., Guven, D.A., 1997. Water Sci. Technol., 35, 47-54.
7. Svilović, S., Rušić, D., Stipšić, R., 2009. Modeling batch kinetics of copper ions sorption using synthetic zeolite NaX. J. Hazard. Mater. 170 2-3, 941-947.
8. Rajić, N., Stojaković, Đ., Jevtić, S., Zabukovec Logar, N., Kovac, J., Kaucic, V., 2009. Removal of aqueous manganese using the natural zeolite tuff from Vranjska Banja deposit in Serbia. J. Hazard. Mater. 172, 1450-1457.
9. Šljivic, M., Smiciklas, I., Pejanovic, S., Plećaš, I., 2009. Comparative study of Cu^{+2} adsorption on a zeolite, a clay and a dolomite from Serbia. Appl. Clay Sci. 43, 33-40.
10. Orechovska, J., Misaelides, P., Godelitsas, A., Rajec, P., Kleve-Nebenius, H., Noli, F., Pavlidou, E., 1999. Journal of Radioanalytical and Nuclear Chemistry, 241, 519-527.
11. Wang, S., Peng, Y., 2010. Chemical Engineering Journal, 156, 11-24.
12. Ledoux D. R., Rottinghaus G. E., Bermudez A. J., Alonso-Debolt M., 1999, Poultry Science 78, 204 84.
13. Pavelić, K., Hadžija, M., Bedrica, L., Pavelić, J., Dikić, I., Katić, M., Bosnar, M.H., Kapitanović, S., Poljak-Blazi, M., Križanac, S., Stojković, R., Jurin, M., Subotić, B., Colić, M., Journal of Molecular Medicine, 78, 2003, 708-720 85.
14. Arpe, H.J., 1996, Ullmann's Encyclopedia of Industrial Chemistry, Vol A 28, Wily VCH, Weinheim.
15. Kandimalla, R., Vallamkondu, J., Corgiat, E.B., Gill, K.D. (2016) Understanding Aspects of Aluminum Exposure in Alzheimer's Disease Development. Brain Pathol., 26(2),139-154.
16. Klein, G.L. (2019) Aluminum toxicity to bone: A multisystem effect?. Osteoporos Sarcopenia, 5(1), 2-5.

XVI International Mineral Processing
and Recycling Conference
28-30 May 2025, Belgrade, Serbia

DOI: 10.5937/IMPRC25632T

Original research article

INVESTIGATION OF ULTRA-FINE GRINDING OF AGGLOMERATED BASALT DUST

Paweł Tomach[1#], 0000-0001-6133-642X,
Jacek Feliks[1], 0000-0002-5653-1674,
Marta Łuczak[2], 0009-0007-3209-3589,
Grzegorz Fabijański[2], 0009-0003-1963-0811,
[1]AGH University of Krakow, Kraków, Poland
[2]Trzuskawica S.A., Sitkówka, Poland

ABSTRACT – This paper presents preliminary results of experimental research on ultra-fine grinding of agglomerated basalt dust using a laboratory vibratory mill. The main objective was to maximize the fraction of particles smaller than 10 µm. A series of tests were performed using various combinations of grinding media (12.0 mm, 17.5 mm, and a 50/50 mix), different grinding durations, and grinding additives. The effects of ultrasonic disintegration during particle size analysis were also investigated to assess agglomeration. The most favorable outcome was achieved with a mixed set of grinding balls (Ø12.0 mm and Ø17.5 mm) combined with 0.4% propylene glycol. This configuration led to a significant increase in the sub-10 µm fraction from 25.4% in the feed material up to 70.5% after 60 minutes of grinding. Despite the challenges associated with the high initial moisture content of the raw material and the tendency for particle agglomeration during dry grinding, the results demonstrate the high potential of vibratory mills for the efficient production of fine basalt powder suitable for environmental and agricultural applications.

Keywords: Ultra-Fine Grinding, Basalt Dust, Vibratory Mill, Grinding Additives, Particle Size Distribution.

INTRODUCTION

In the face of increasing challenges related to environmental degradation, the need for sustainable development, and the growing importance of recycling, ultra-fine grinding of mineral raw materials with high application potential is gaining significance. One such material is basalt with a particle size below 10 µm, whose unique physicochemical properties offer a wide range of applications across various fields [1–3].

Ultra-fine grinding enables the production of materials with a large specific surface area. In the case of basalt, this results in increased reactivity and, consequently, enhanced availability of mineral components, making the resulting basalt powder an attractive additive in agriculture, construction (e.g., concrete admixtures), and environmental protection applications [1,4]. However, achieving such fine particle sizes requires the selection of an appropriate type of mill [5] and the optimization of technological process parameters.

[#] corresponding author: tomach@agh.edu.pl

EXPERIMENTAL

In order to select the basic technological parameters for the grinding process and for laboratory testing in vibratory mills (i.e., chamber filling ratio, type of grinding media, and feed quantity), it was necessary to determine three key physical properties of the ground material: moisture content, loose bulk density, and particle size distribution. The material subjected to grinding was basalt dust (below 300 µm) originating from the dedusting station of a mineral processing plant. It had been stored without roofing, which led to significant moisture absorption and resulted in the formation of a slurry-like mass. The high moisture content caused agglomeration and solidification of the material into lumps with maximum dimensions reaching 80–100 mm. The appearance of the material before and after drying is shown in Figure 1.

Moisture Content

The moisture content of the material was determined by drying a prepared sample in a laboratory dryer at a temperature of 110°C until complete dryness was achieved. Based on the measurements, the moisture content of the received material was determined to be 16.6% ±0.1.

Figure 1 Fine basalt dust before and after drying

Bulk Density

The loose bulk density was determined in accordance with the PN-EN 1097–3:2000 standard, which is commonly used in aggregate testing. The bulk density of the dried material, calculated as the average of four measurements, was 1.10 ± 0.02 kg/dm³.

Feed Particle Size Distribution

The particle size distribution of the fine basalt dust was determined after drying and disintegration of the agglomerated material using an impact (paddle) crusher. The grain size distribution of both the feed and the milled products was analyzed using a laser diffraction method with the Malvern Mastersizer 3000, applying wet measurement with the "Hydro EV" dispersion unit. The particle size distribution of the feed material for the grinding process is presented in Figure 2.

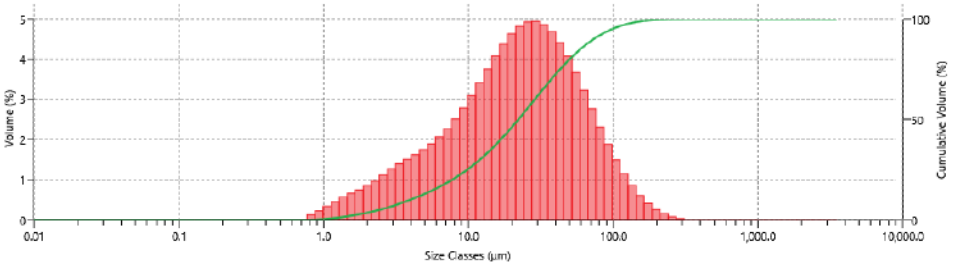

Figure 2 Particle size distribution of basalt before grinding

Vibratory Mill Test Stand

Experimental grinding tests were carried out using a laboratory-scale vibratory mill operating in batch mode. A schematic view of the vibratory mill test stand is presented in Figure 3 [6]. The main technical parameters of the test stand are summarized in Table 1.

Figure 3 Laboratory vibratory mill test stand and view of the chamber interior with the ground material: 1 – chamber, 2 – chamber holder plate, 3 – drive module, 4 – vibrator motor, 5 – control and power system, 6 – supporting structure

Table 1 Basic parameters of the vibratory mill test stand

Parameter Name	Unit	Value
Amplitude of chamber vibrations	mm	3÷14
Frequency of chamber vibrations	Hz	4÷18
Filling degree of the chamber	%	10÷90
Power of vibrator drive motor	kW	3,5

Method and Implementation of Grinding Process Research in a Vibratory Mill

A steel chamber with a diameter of 0.21 m and a smooth lining was chosen for the experiments. These diameters and linings are typical of the smallest industrial vibratory mills. Steel balls were used as working elements. The grinding process was conducted dry, in an air environment. During the grinding, attempts were made to apply two grinding process activators, namely: ethylene glycol and propylene glycol.

The following mill operating parameters were adopted:

- Chamber vibration frequency: 16 Hz;

- Vibration amplitude: 6 mm – circular,
- Steel chamber with an internal diameter of 210 mm and a working volume of 2.2 dm³.

The ultra-fine grinding trials were conducted for the following technological variants:

a) Grinding set A1: Ø 17.5 mm;
b) Grinding set A1: Ø 17.5 mm with the use of a grinding activator (propylene glycol);
c) Grinding set A2: Ø 12.0 mm with the use of a grinding activator (ethylene glycol);
d) Grinding set A3: mixture of Ø 12.0 mm and Ø 17.5 mm (50/50) with the use of a grinding activator (propylene glycol).

RESULTS AND DISCUSSION

a) Grinding set A1: Ø17.5 mm

In order to determine the grinding kinetics, for the first technological variant, grinding times of t: 2.5, 5.0, 10.0, and 20.0 minutes were adopted.

The results of the granulometric parameters of the grinding products for this technological variant are presented in Table 2.

Table 2 Grinding results for test BD-A1

Sample Symbol	Grinding Time, [min]	Control Grain Size, [μm]			Class 0÷63μm, [%]	Class 0÷10μm, [%]
		d10	d50	d90		
Feed: BD-Nadawa	0	3,97	22,1	73,2	86,52	25,41
BD-A1-t2.5	2,5	3,51	19,7	59,8	91,11	27,98
BD-A1-t5.0	5,0	3,28	17,5	53,5	93,47	31,80
BD-A1-t10.0	10,0	2,70	15,0	44,1	96,95	36,79
BD-A1-t20.0	20,0	2,52	13,8	40,3	98,09	39,07

During grinding, excessive coating (coating of the grinding elements and chamber with the ground material) was observed, which led to a slowdown in the grinding process, especially after exceeding the grinding time of 10 minutes. Therefore, in the next experiment, it was decided to conduct the test using a grinding activator – polypropylene glycol.

b) Grinding set A1: Ø17.5 mm with the use of a grinding activator (propylene glycol)

The grinding activator (propylene glycol), which is intended to prevent excessive agglomeration of finely ground particles, was added to the chamber in an amount of 0.2% by mass. After 20 minutes of grinding, excessive agglomeration of the ground material was observed, so it was decided to increase the glycol amount by an additional 0.2% (BD-A1-G0.2x2).

The results of the granulometric parameters of the grinding products for this technological variant are presented in Table 3. In this table, samples marked with blue color and the symbol "US" refer to the particle size analysis in which ultrasound was used—this was done to demonstrate the occurrence and breakdown of particle agglomerates.

Table 3 Grinding results for test y BD-A1-G

Sample Symbol	Grinding Time, [min]	Control Grain Size, [µm]			Class 0÷63µm, [%]	Class 0÷10µm, [%]
		d10	d50	d90		
Feed: BD-Nadawa	0	3,97	22,1	73,2	86,52	25,41
BD-A1-G0.2-10	10	2,75	14,9	44,5	96,59	36,76
BD-A1-G0.2-20	20	2,80	13,4	39,2	97,99	39,48
BD-A1-G0.2x2-30	30	2,22	11,1	33,8	99,19	46,44
BD-A1-G0.2x2-30+US2x60s	*30 US*	*2,11*	*10,2*	*32,1*	*99,41*	*49,45*
BD-A1-G0.2x2-30+US3x60s	*30 US*	*1,97*	*9,38*	*31,1*	*99,59*	*52,15*
BD-A1-G0.2x2-30+US4x60s	*30 US*	*1,90*	*8,98*	*31,3*	*99,41*	*53,51*

c) Grinding set A2: Ø12.0 mm with the use of a grinding activator (ethylene glycol)

In the next stage of the research, to examine the effect of grinding ball diameter on the grinding parameters, steel balls with a diameter of 12 mm were used as the grinding set. The experiment was conducted with a grinding activator – ethylene glycol. Based on the previous research results, grinding times of 20, 40, and 60 minutes were adopted for this trial. After 40 minutes of grinding, it was decided to add a commercial product called AEROSIL. The results of the granulometric parameters of the grinding products for these trials are presented in Table 4.

Table 4 Grinding results for experiment BD-A2-GE

Sample Symbol	Grinding Time, [min]	Control Grain Size, [µm]			Class 0÷63µm, [%]	Class 0÷10µm, [%]
		d10	d50	d90		
Feed: BD-Nadawa	*0*	*3,97*	*22,1*	*73,2*	*86,52*	*25,41*
BD-A2-GE0.2-20	20	2,90	13,9	32,5	100,00	36,60
BD-A2-GE0.2+.02-20+20	40	2,30	11,5	34,1	99,03	45,11
BD-A2-GE0.2+.02-20+20-US4x60s	*40 US*	*1,69*	*7,05*	*23,3*	*100,00*	*62,07*
BD-A2-GE0.4-T60-Aeo1	60	2,19	11,2	35,1	99,23	46,42
BD-A2-GE0.4-T60-Aeo1-US4x60	*60 US*	*1,56*	*6,64*	*21,6*	*100,00*	*63,48*
BD-A2-GE0.4-T60-Aeo1-US6x60	*60 US*	*1,49*	*6,33*	*21,1*	*100,00*	*64,63*
BD-A2-GE0.4-T60-Aeo1-US8x60	*60 US*	*1,43*	*5,94*	*19,7*	*100,00*	*66,65*

d) Grinding set A3: mixture of Ø12.0 mm and Ø17.5 mm (50/50) with the use of a grinding activator (propylene glycol)

In the next stage of the research, to examine the effect of grinding media diameter on the grinding parameters, a mixture of steel balls with diameters of 12.0 mm and 17.5 mm in a 50/50 mass ratio was used as the grinding set. Based on the previous research results, grinding times of 20, 40, and 60 minutes were adopted.

The results of the granulometric parameters of the grinding products for these trials are presented in Table 5.

Table 5 Grinding results for experiment BD-A3-

Sample Symbol	Grinding Time, [min]	Control Grain Size, [µm]			Class 0÷63µm, [%]	Class 0÷10µm, [%]
		d10	d50	d90		
Feed: BD-Nadawa	*0*	*3,97*	*22,1*	*73,2*	*86,52*	*25,41*
BD-A3-GP0.4-20	20	2,42	11,8	37,9	98,38	44,56
BD-A3-GP0.4-20-US 8x60	*20 US*	*1,83*	*7,49*	*22,6*	*100,00*	*60,21*
BD-A3-GP0.4-40	40	2,24	11,6	33,1	99,86	44,90
BD-A3-GP0.4-40-US8x60	*40 US*	*1,61*	*6,64*	*19,3*	*100,00*	*63,99*
BD-A3-GP0.4-60	60	2,22	11,3	36,7	98,79	46,03
BD-A3-GP0.4-60-US8x60	*60 US*	*1,42*	*5,56*	*17,6*	*100,00*	*69,53*
BD-A3-GP0.4-60-US14x60	*60 US*	*1,34*	*5,24*	*17,0*	*100,00*	*70,87*

CONCLUSION

The conducted preliminary research on the ultra-fine grinding of basalt demonstrated a high potential of vibratory milling for this type of material – while maintaining standard mill operating parameters (vibration amplitude and frequency). Among the tested technological variants (grinding media sets and grinding activator), the most favorable was the grinding set A3, consisting of steel balls with diameters of 12.0 and 17.5 mm, used in combination with a grinding activator – polypropylene glycol – in the amount of 0.4% of the mass of the ground material.

For this variant, it was possible to increase the 0–10 µm grain size fraction from an initial content of 25.4% in the feed to:

- 60.2% - for a grinding time of 20 minutes;
- 64.0% - for a grinding time of 40 minutes;
- 70.5% - for a grinding time of 60 minutes;

Based on the conducted research, it can be concluded that ultra-fine grinding of basalt dust to achieve a very high content of the 0–10 µm grain size fraction is feasible in vibratory mills. However, it should be emphasized that dry grinding of material with such high initial moisture content may not be economically justified. Therefore, it is important to prevent exposure of materials intended for subsequent grinding to atmospheric conditions.

Considering the difficulties associated with the initial moisture content of the material and the specific challenges of ultra-fine dry grinding, the results obtained for fine basalt (BD) grinding can be considered satisfactory.

ACKNOWLEDGEMENT

The authors would like to express their gratitude to Trzuskawica S.A. Poland for financing the conducted research.

REFERENCES

1. Richardson, J.B. (2024) Basalt Rock Dust Amendment on Soil Health Properties and Inorganic Nutrients—Laboratory and Field Study at Two Organic Farm Soils in New England, USA. Agriculture, 15, 52. doi:10.3390/agriculture15010052.
2. Conceição, L.T., Silva, G.N., Holsback, H.M.S., Oliveira, C.D.F., Marcante, N.C., Martins, É.D.S., Santos, F.L.D.S., Santos, E.F. (2022) Potential of Basalt Dust to Improve Soil Fertility and Crop Nutrition. Journal of Agriculture and Food Research, 10, 100443. doi:10.1016/j.jafr.2022.100443.
3. Beerling, D.J., Leake, J.R., Long, S.P., Scholes, J.D., Ton, J., Nelson, P.N., Bird, M., Kantzas, E., Taylor, L.L., Sarkar, B., et al. (2018) Farming with Crops and Rocks to Address Global Climate, Food and Soil Security. Nature Plants, 4, 138–147. doi:10.1038/s41477-018-0108-y.
4. Dalmora, A.C., Ramos, C.G., Querol, X., Kautzmann, R.M., Oliveira, M.L.S., Taffarel, S.R., Moreno, T., Silva, L.F.O. (2016) Nanoparticulate Mineral Matter from Basalt Dust Wastes. Chemosphere, 144, 2013–2017. doi:10.1016/j.chemosphere.2015.10.047.
5. Sidor, J., Foszcz, D., Tomach, P., Krawczykowski, D. (2015) Młyny wysokoenergetyczne do mielenia rud i surowców mineralnych. Cuprum: Czasopismo Naukowo-Techniczne Górnictwa Rud, 2.
6. Tomach, P. (2024) The Influence of the Grinding Media Diameter on Grinding Efficiency in a Vibratory Ball Mill. Materials, 17, 2924. doi:10.3390/ma17122924.

XVI International Mineral Processing
and Recycling Conference
28-30 May 2025, Belgrade, Serbia

DOI: 10.5937/IMPRC25639F

Original research article

PRODUCTION OF HIGH-PURITY QUARTZ FOR OPTICAL APPLICATIONS

Francesco Ferella[#], 0000-0001-8708-024X,
Svetlana B. Zueva, 0000-0002-6509-5800,
Ionela P. Birloaga, 0000-0003-0923-4893,
Valentina Innocenzi, 0000-0002-7209-5956,
Nicolò M. Ippolito, 0009-0002-3451-1469,
Francesco Vegliò, 0000-0002-7252-2727,
Department of Industrial and Information Engineering and Economics,
University of L’Aquila, L’Aquila, Italy

ABSTRACT – The paper investigated the production of high-grade quartz for optical devices, starting with mined quartz. This material contained 668 mg/kg of Fe_2O_3, and the aim was to reduce the content to below 100 mg/kg through an environmentally and economically sustainable process. It was found that the sequential leaching water-oxalic-sulphuric acid is very efficient using two sequential stages; both acids can be used two times. The best conditions were: water leaching S/L 100%, temperature 90°C, time 45 min; oxalic acid stage: OA concentration 17 g/L, leaching time 2.5 h, temperature 90°C, S/L 20% wt/vol; sulphuric acid stage: SA concentration 2 mol/L, leaching time 1.5 h, S/L 20% wt/vol. OA can be recovered from the spent solution and recycled. SA recycling was tested using an NF membrane module: the rejection of iron sulfate and silica (silicic acid) was greater than 85%. The permeate can then be used for a further leaching stage. NF removes most of the significant elements, which avoids further iron leaching from quartz. The final high-grade product contained less than 100 ppm of Fe_2O_3, with a Whiteness Index (D65/10°) greater than 88, the minimum threshold required for optical applications.

Keywords: Iron Removal, Quartz, Acid Recycling, Process Optimization.

INTRODUCTION

Nowadays, the production of high-purity quartz for applications like semiconductors, optical fibers, photovoltaic panels, and other optical devices is highly strategic. Silica glass must have properties like chemical purity, optical transparency, and radiation resistance. Iron is the most harmful impurity in quartz sands and ores because it impairs light transmission and the glasses' transparency [1]. Manufacturing processes are relatively expensive in terms of energy and reagents. For this reason, the optimization becomes strategic to make this sector more competitive. Although many researchers investigated iron removal from quartz at a laboratory scale, such processes were not optimized to reduce the overall operating costs. High temperature (80-90°C) [2] and time (3-5 h) is required to achieve good iron extraction yields [3,4].

[#] corresponding author; e-mail: francesco.ferella@univaq.it

Moreover, magnetic separation is also helpful in reducing the amount of iron undergoing the leaching stage [4]. Ubaldini *et al.* [3] tested continuous leaching through a fixed-bed column filled with quartz sand, recycling the oxalic acid solution and testing several operating factors. The highest iron reduction was 46 %, bringing Fe_2O_3 to 0.0163 %wt from 0.0302 %wt. The mechanism of that organic acid may be that of complexing and/or reducing Fe(III) to Fe(II) [4]. Oxalic acid was also used synergistically with sulphuric acid in a rotary drum reactor [4]. Oxalic acid demonstrated a high iron extraction yield even with red clay, decreasing Fe_2O_3 from 17.1 % to 3.64 %wt (-78.7 %) and making it suitable for ceramic manufacture [5]. The kinetics of iron dissolution in quartziferous ores by oxalic acid was also studied, and the activation energy resulted in 45.4 kJ/mol [6]. Besides oxalic acid, other reducing agents were used, such as citric acid and glucose mixed with sulphuric acid. Despite that, oxalic acid demonstrated the best performance (99% iron removal), keeping all the other process parameters constant. The yields were always higher than 70% with the other two reducing agents [1]. Roasting is another effective pre-treatment for natural quartz powder in the presence of ammonium sulphate that reduces Fe(III) into Fe(II) at 400-500°C in airflow: the following leaching with 5%wt H_2SO_4 + 10%wt HF can reduce Fe_2O_3 below 0.3 mg/kg from the original concentration of 145 mg/kg [7]. High-temperature roasting (from 600°C to 1200°C) can transform quartz's crystalline structure, enhancing the acid's effect in removing iron and other impurities. Iron extraction was nearly 99% in quartz pre-treated with magnetic separation [8]. The drawback of such a method is the high energy cost relevant to the thermal and leaching stages, which last 10 hours overall. Iron reduction is also required when high-silicon tailings are used as feedstock to recover 99.99 %wt of high-purity quartz. High-intensity magnetic separation, followed by a two-stage leaching with H_3PO_4/HCl/HF mixture reduced the iron oxide content by nearly 91% [9].

Zhang *et al.* [2] compared the results of using several acids, namely H_2SO_4, $H_2C_2O_4$, H_3PO_4, HCl, and HF, at a time to whiten quartz ores and sands under ultrasounds. Iron removal achieved a 77 % yield. Nonetheless, this result was achieved with a solid-to-liquid (S/L) ratio of 5 % wt/vol, almost low: when the S/L ratio was increased to 20%, the iron oxide extraction decreased to 46%. Bioleaching is another technique that can be applied to iron removal from quartz sand. The kinetic is much lower than standard chemicals like mineral and organic acids. However, Styriakova *et al.* [10] achieved a 50% Fe_2O_3 reduction after 83 days of treatment with heterotrophic bacteria in an in-situ pilot plant. This experimental campaign confirmed lab-scale results obtained with three quartz samples from different Slovak locations [11]. HF enhances the removal because it can dissolve the surface of quartz particles and penetrate through small channels, making contact with iron and other metal particles embedded inside possible. Nevertheless, HF use poses severe corrosion problems in industrial plants that treat several thousand tons of quartz annually.

There is a gap in the literature regarding improving environmental sustainability and economic viability of high-grade quartz production. In this paper, we optimized a process to reduce the iron oxide content below 100 mg/kg without grinding the samples supplied from a Turkish mine, as requested by the mining company, maximizing acid and water recycling to reduce operating costs.

EXPERIMENTAL

All trials were carried out using a particle size of -1200 µm, as provided by the Turkish company that mines quartz. It was ground with a ball mill to -150 µm for digestion in aqua regia and some drops of concentrated HF. Iron was measured by Atomic Absorption Spectrometry (AAS, spectrometer SpectrAA 200, Varian). The sample was also characterized by X-ray fluorescence (XRF, Spectro Xepos) and X-ray diffraction (XRD, Philips X-Pert). Leaching tests were performed in 250 mL flasks and placed in a Dubnoff water bath (BSD/D, ISCO) with a mechanical stirring rate of 200 rpm, unless otherwise indicated.

The following experimental plans were tested: 1) Direct leaching in a 2^5 full factorial design, studying S/L ratio, H_2SO_4 concentration, reaction time, volume of wash water and temperature; 2) Cross-current configuration, in which the leach liquor was reused to leach other two fresh quartz sample (3-stages), with a make-up of fresh H_2SO_4 to bring back the solution volume to the initial one; 3) Counter-current leaching configuration (3-stages); 4) Direct leaching with water-$H_2C_2O_4$-H_2SO_4 and partial reuse of the leach liquors for further leaching stages.

RESULTS AND DISCUSSION

Characterization of quartziferous ore

The Fe_2O_3 concentration of the quartz sample was 668±54 mg/kg. XRD analysis showed no further crystalline phase than quartz because of the low iron concentration. Nevertheless, the company communicated that iron was in the form of hematite. The XRF analysis is shown in Table 1.

Table 1 Main elements contained in the quartz sample

	Concentration (%wt)								
Element	Si	Al	K	P	S	Ca	Ti	Cr	Zr
	44.4	0.64	0.11	0.03	0.02	0.03	0.05	0.02	0.45

Leaching tests

If 100 ppm is the final target concentration, the leaching process was effective whether the iron extraction yield was at least 85%. The leaching mechanism can be expressed as follows [3,4]:

$$Fe_2O_3 + 6\, H_2C_2O_4 \rightarrow 2\, Fe(C_2O_4)_3^{3-} + 6\, H^+ + 3\, H_2O \quad (1)$$

$$2Fe(C_2O_4)_3^{3-} + 6\, H^+ + 4\, H_2O \rightarrow 2\, FeC_2O_4 \cdot 2H_2O + 3\, H_2C_2O_4 + 6\, CO_2 \quad (2)$$

$$Fe_2O_3 + 3\, H_2C_2O_4 + H_2O \rightarrow 2\, FeC_2O_4 \cdot 2H_2O + 2\, CO_2 \quad (3)$$

There are two main mechanisms: complexing and/or reduction of Fe(III) into Fe(II). The latter prevails at low pH values, i.e., <1.5, whereas at pH 2-3, the complexing action of OA is predominant [4]. Furthermore, the presence of light may increase the process kinetics of Fe(III) reduction.

Direct leaching

The best iron extraction yield (EY) was only 80.5%, namely insufficient, and was achieved with a 10% wt/vol S/L ratio, 2 mol/L H_2SO_4 in 3 h at 90°C by using 50% of wash water volume with respect to the leaching solution, to wash the quartz cake recovered by filtration. This single test was repeated in the same experimental conditions but using a hot plate with a magnetic stirrer; after 90 min, the EY was 91%, confirming that the grinding effect of the anchor allows a faster and more efficient iron reduction. The problems with this configuration are the high acid consumption, the additional cost associated with the alkaline reagent required to neutralize the spent solution, and the huge amount of salts generated (Na_2SO_4, $CaSO_4$, etc.), because the reuse of leach liquor for a second stage did not achieve the minimum iron extraction.

Cross-current configuration

A three-stage configuration, using the same experimental conditions of the best direct leaching trial but with magnetic stirring, led to the following iron EYs: 89.9% in the 1st stage, 62.1% in the 2nd, and 26.7% in the 3rd one, respectively. Only the first stage could reduce iron below 100 ppm, despite the leach liquor having sufficient residual H_2SO_4 (173 g/L) to leach the second sample of fresh quartz. It is difficult to understand why the solution's leaching strength decreased dramatically just after the first stage when the consumed acid is rather low; one possible explanation is the presence of dissolved silica that forms some sort of protective layer around quartz grains, preventing the acid from accessing the particles in an effective way. We also decreased the percentage of the leach liquors reused in the following stages, i.e., in the 2nd and 3rd, while increasing the amount of make-up acid, but the results did not improve.

Counter-current configuration

The experimental conditions of the 3-stage counter-current leaching were the following: 2M H_2SO_4, S/L 30% wt/vol, 90°C, time 1.5 h, Temperature 90°C, wash water volume 50%, make-up each stage with 2M H_2SO_4 solution. The total iron EY was 90.6%. This configuration allowed the reduction of Fe_2O_3 in quartz below the threshold for optical applications, but the consumption of acid was not reduced so much.

Water-$H_2C_2O_4$-H_2SO_4 configuration

Tests were carried out on magnetic stirred and heated plates. Pre-treatment with hot water was carried out by using 20 mL of water with 20 g of fresh quartz and heating it at the leaching temperature, i.e., 90°C; the overall scheme is reported in Figure 1. At the end of each sequence, iron content in the final quartz was 88 and 121 ppm, respectively, measured by AAS after acid digestion of the solid samples. The second sample exceeded the target concentration. However, it is possible that the leaching power of the pregnant solution will increase after filtration to remove iron and silica. Pre-treatment with hot water is very important since it weakens the grain surface, and acid can diffuse better, removing the iron trapped inside each quartz particle. Figure 2 shows the original quartz and the sample after the highest iron EY, i.e., 92%. A full factorial design with 3 factors and 2 levels was investigated to optimize the experimental conditions of the water heating step and the oxalic acid leaching. The optimized parameters were: 1-Water stage: S/L 100% wt/v, 45 min, 90°C; 2-OA stage: OA 17 g/L, S/L 20% wt/v, 2.5 h, 90°C; 3-SA stage: SA 2 mol/L, S/L 20% wt/v, 1.5 h, 90°C. The iron EY was 92%. Despite the configuration, what was inferred from the experimental tests was: firstly, dissolved and colloidal silica, i.e. metasilicic (H_2SiO_3) and ortho-silicic acid (H_4SiO_4) that can polymerize when the solution is cooled down, impairs the reuse of sulphuric acid solution in a second stage and secondly, the same colloidal silica makes filtration hard, because it clogs the filter channels. Hence, a regeneration treatment is required to save acid and ensure the viability of the plant.

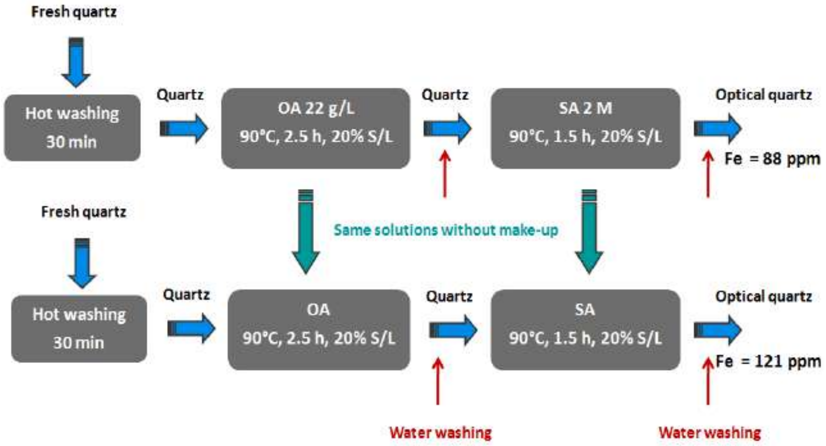

Figure 1 Scheme of the sequential leaching water → OA → SA

Figure 2 Original quartz (left) and treated sample with 53 ppm of Fe_2O_3 (right)

Treatment of H_2SO_4 spent solution

Several methods were tested to reduce the concentration of iron and silica in leach liquors in order to reuse them in further leaching stages. This stage is crucial to lower operating costs. Polyelectrolytes and hydrated lime gave Si and Fe precipitation yields up to 40%. Around 52% of silica was removed by an anionic resin. The best regeneration treatment was nanofiltration (NF), carried out by the German group Osmo Membrane. The result of the membrane filtration was the following: Feed solution, 4500 mL: H_2SO_4 203 g/L, Fe 183 mg/L, Si 59.1 mg/L; Permeate, 3987 mL: H_2SO_4 181 g/L, Fe 3.1 mg/L, Si

6.7 mg/L; Retentate, 513 mL: H_2SO_4 234 g/L, Fe 555 mg/L, Si 366 mg/L. The permeate, nearly 89% of the feed volume, was reused for another quartz leaching in the water/OA/SA configuration, and the iron removal was 90%.

Figure 3 Retentate and permeate after titration with NaOH

CONCLUSIONS

The following conclusions can be inferred from the experimental campaign:

- A three-stage leaching with water, oxalic, and sulphuric acid was the most efficient way to obtain high-grade quartz for optical applications, with a final Fe_2O_3 concentration of 53 ppm.

- Recycling of OA and SA is crucial to reduce operating costs. OA solution can be recycled one time. Instead, the SA must be purified to remove the dissolved iron and colloidal silica. The best treatment is NF: permeate can be recycled, whereas retentate shall be neutralized, and the resulting sludge shall be disposed of.

- The water pre-treatment stage has a positive effect, but a mild grinding of quartz could replace it, and a -500 µm fraction could be used to improve iron extraction. Furthermore, a high-intensity magnetic separation can remove iron particles before the hydrometallurgical treatment, enhancing the overall reduction. A techno-economic analysis shall be carried out to figure out the most convenient route.

REFERENCES

1. Tuncuk, A., Akcil, A. (2016) Iron removal in production of purified quartz by hydrometallurgical process. International Journal of Mineral Processing, 153, 44-50.
2. Zhang, Z., Li, J., Li, X., Huang, H., Zhou, L., Xiong, T. (2012) High efficiency iron removal from quartz sand using phosphoric acid. International Journal of Mineral Processing, 114-117, 30-34.
3. Ubaldini, S., Piga, L., Fornari, P., Massidda, R. (1996) Removal of iron from quartz sands: A study by column leaching using a complete factorial design. Hydrometallurgy, 40, 369-379.
4. Vegliò, F., Passariello, B., Barbaro, M., Plescia, P., Marabini, A.M. (1998) Drum leaching tests in iron removal from quartz using oxalic acid and sulphuric acids. International Journal of Mineral Processing, 54, 183-200.

5. Hayatullah, Shanti, A.S., Mostafa, M.G., Rahman, M.A., Biswas, P.K., Alam, M.S., Rana, M.S., Uddin, M.R., Nuruzzaman, M., Shahrian, M.S., Zaman, M.N. (2024) Iron removal from red clay using oxalic acid leaching for enhanced ceramic industry applications. Heliyon, 10, e38863.
6. Huang, H., Li, J., Li, X., Zhang, Z. (2013) Iron removal from extremely fine quartz and its kinetics. Separation and Purification Technology, 108, 45‑50.
7. Du, X., Yang, D., Zheng, S., Sun, Z., Li, C. (2021) Deep insight into the reductive roasting treatment on iron removing from quartz. Advanced Powder Technology, 32,4825-4832.
8. Zhang, H., Guo, S., Wu, J., Wu, D., Wei, K., Ma, W. (2021) Effect of quartz crystal structure transformations on the removal of iron impurities. Hydrometallurgy, 204, 105715.
9. Long, H., Zhu, D., Pan, J., Li, S., Guo, Z., Xu, X. (2024) Innovative process for the extraction of 99.99% high-purity quartz from high-silicon iron ore tailings. Journal of Materials Research and Technology, 31, 2094-2102.
10. Styriakova, I., Bekenyiova, A., Styriakova, D., Jablonovska, K., Styriak, I. (2015) Second pilot-plant bioleaching verification of the iron removal form quartz sands. Procedia Earth and Planetary Science, 15, 861-865.
11. Suba, J., Styriakova, D. (2015) Iron minerals removal from different quartz sands. Procedia Earth and Planetary Science, 15, 849-854.

XVI International Mineral Processing
and Recycling Conference
28-30 May 2025, Belgrade, Serbia

DOI: 10.5937/IMPRC25646A

Original research article

SELECTIVE EXTRACTION OF MOLYBDENUM, NICKEL, AND COBALT FROM SECONDARY RESOURCES USING BIFUNCTIONAL IONIC LIQUIDS

Roshanak Adavodi[#], 0009-0002-9240-4936,
Adriana Zuffranieri, 0009-0000-6928-8741,
Soroush Rahmati, 0000-0003-4851-9795,
Pietro Romano, 0009-0007-6875-3999,
Francesco Ferella, 0000-0001-8708-024X,
Francesco Veglio', 0000-0002-7252-2727,
Department of Industrial and Information Engineering and Economics (DIIIE),
Engineering Headquarters of Roio, University of L'Aquila, 67100 L'Aquila, Italy

ABSTRACT –The increasing demand for molybdenum, nickel, and cobalt in high-tech industries has led to a need for efficient and sustainable metal recovery from secondary sources. Conventional solvent extraction methods face environmental concerns, high reagent consumption, and limited selectivity. Ionic liquids (ILs) have emerged as promising alternatives due to their low volatility, high thermal stability, and exceptional metal ion selectivity. In this study, the bifunctional ionic liquids [TOA][CY272] and [A336][P204] were investigated for selective extraction of molybdenum, nickel, and cobalt from synthetic solutions simulating industrial waste leachates. The ILs were dissolved in kerosene, and their extraction efficiencies were compared with raw components to evaluate improvements in selectivity and efficiency. Key operational parameters, such as metal ion concentration, extractant concentration, and pH, were optimized for maximum recovery. Two stripping agents, acidic and alkaline, were tested to enhance selective metal recovery. Results showed [A336][P204] achieved over 95% extraction efficiency for molybdenum with less than 4% co-extraction of nickel and cobalt, while [TOA][CY272] exhibited a maximum efficiency of less than 75% and lower selectivity. The appropriate stripping agent facilitated efficient metal separation. These findings highlight the potential of bifunctional ionic liquids as sustainable and environmentally friendly extractants for recovering strategic metals from secondary sources.

Keywords: Metal Recovery, Ionic Liquids, Circular Economy, Sustainable Extraction, Industrial Waste Recycling.

INTRODUCTION

Molybdenum (Mo), nickel (Ni), and cobalt (Co) are key components of hydrodesulfurization (HDS) catalysts, such as Ni-Mo/γ-Al2O3 and Co-Mo/γ-Al2O3 [1], widely used in petroleum refining to remove sulfur and produce cleaner fuels [2]. During HDS process, molybdenum facilitates sulfur removal via hydrogenation. However, prolonged exposure to high temperatures and contaminants leads to catalyst deactivation through poisoning and sintering [3], resulting in spent catalysts that require recovery and management.

[#] corresponding author: Roshanak.adavodijolfaee@graduate.univaq.it

The growth of the petrochemical industry has led to a significant increase in spent HDS catalysts, classified as hazardous due to their toxic and flammable content [4]. However, they also contain valuable metals like Mo, V, Ni, and Co, making their recovery both an environmental necessity and an economic opportunity [5]. Various treatment approaches, such as pyrometallurgical and hydrometallurgical methods, are being explored to efficiently recover metals while minimizing environmental impact [6, 7]. Hydrometallurgical processes are increasingly preferred over pyrometallurgical techniques due to their superior efficiency, ability to selectively separate target elements, lower energy consumption, and reduced greenhouse gas emissions [8]. A review of the literature indicates substantial research efforts aimed at optimizing the recovery and separation of Mo, Ni, and Co from the pregnant leach solution (PLS).

Several techniques, including precipitation, ion exchange, Membrane systems, adsorption, and solvent extraction [9], have been investigated for this purpose. Among these, solvent extraction has emerged as one of the promising methods due to its high selectivity and efficiency in metal separation [10].

Ionic liquids have emerged as promising alternatives to conventional organic solvents in metal extraction due to their unique and environmentally favorable properties. These include excellent chemical and thermal stability, negligible vapor pressure, non-flammability, and high solvation capacity. Such characteristics make them ideal candidates for enhancing extraction efficiency while minimizing environmental impact [11].

Numerous studies have demonstrated the effective use of ionic liquids for the selective extraction of Mo, Ni, and Co. For instance, trihexyl(tetradecyl)phosphonium bis(2,4,4-trimethylpentyl)phosphinate achieved a remarkable cobalt-to-nickel separation factor of 1097 from an HCl-leached solution. At an ionic liquid concentration of 0.8 mol/L, pH 5.0, and 60°C, over 99% of cobalt was selectively extracted, highlighting the high efficiency and selectivity of ionic liquids in metal separation processes [12].

In this study, two ionic liquids, [TOA][CY272] and [A336][P204], were investigated as alternative extractants for the recovery of Mo, Ni, and Co from synthetic solutions designed to simulate PLS and wastewater derived from spent catalyst processing. The extraction performance was evaluated across varying metal concentrations, and both acidic and alkaline stripping agents were applied to recover the metals from the loaded organic phase.

EXPERIMENTAL

Chemicals and reagents

Cobalt, nickel, and molybdenum stock solutions were prepared by dissolving cobalt(II) acetate tetrahydrate, nickel(II) acetate tetrahydrate (98%), and sodium molybdate dihydrate in deionized water. These reagents, obtained from Sigma-Aldrich and Merck. Extractions were performed in a kerosene medium (Carlo Erba), and metal recovery was achieved using NH_4OH (36.6%, VWR) and HCl (25%, Carlo Erba) as stripping agents.

Instrumentation and Analytical Techniques

The structural characterization of the synthesized ionic liquids and their precursors was carried out using FT-IR (Thermo Nicolet Nexus 670). Metal concentrations (Mo, Ni, Co) in all solution phases were analyzed by ICP-OES (Agilent 5100).

Preparation of Bi-Functional Ionic Liquids

Bi-functional ionic liquids [TOA][CY272] and [A336][P204] were synthesized through stoichiometric neutralization reactions. The molecular structures of the final products are presented in Figure 1.

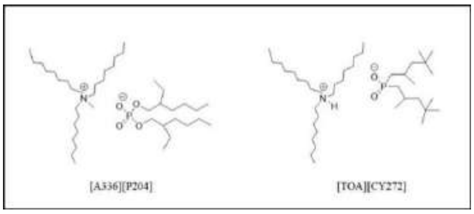

Figure 1 Chemical structures of [TOA][CY272] and [A336][P204]

RESULTS AND DISCUSSION

Metal Extraction Performance

The extraction behavior of the synthesized ILs toward Mo, Ni, and Co was examined under varying conditions. Factors such as IL type and concentration, metals content, and pH were explored to optimize performance.

Selection of Extractant and Comparison with Precursors

To evaluate the separation efficiency of the synthesized ILs and benchmark them against their precursors, extractions were performed using 35% extractant in kerosene, with a 1:1 A/O ratio and 1000 ppm of each metal at room temperature. As shown in Figure 2, [A336][P204] achieved nearly complete Mo extraction (~100%) but was ineffective for Co and Ni, extracting only 2.3% and 1%, respectively. In contrast, [TOA][CY272] showed moderate Mo extraction (72%) and balanced performance for Co (60–63%) and Ni (50–55%). These results demonstrate [A336][P204]'s strong selectivity for Mo and [TOA][CY272]'s broader applicability for multi-metal separation.

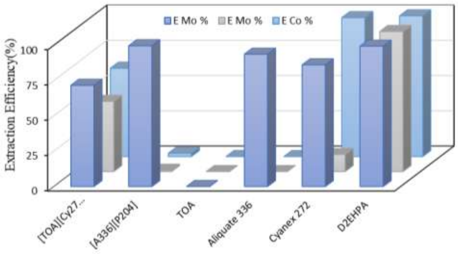

Figure 2 Extraction efficiency of [A336][P204] and [TOA][CY272] and their precursors

Effect of Metal Concentration on Extraction Performance

To simulate various real-world scenarios such as metal-rich catalysts, secondary sources, and dilute wastewaters, extraction tests were conducted at initial metal concentrations of 100, 1000, and 2500 ppm. These levels reflect typical compositions of pregnant leach solutions (PLS) and post-treatment effluents. Figure 3 presents the extraction efficiencies of [TOA][CY272], and [A336][P204] across these concentration ranges. All experiments were performed under consistent conditions.

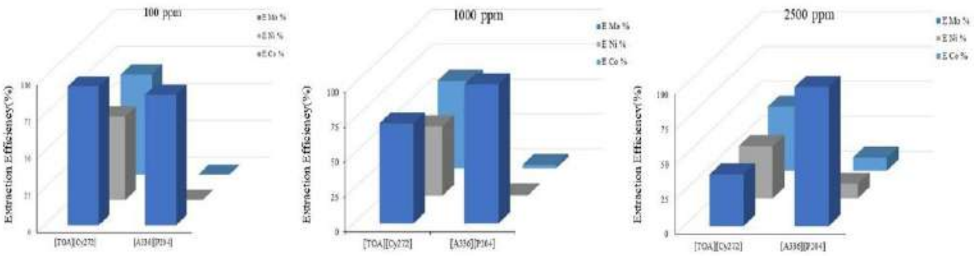

Figure 3 Extraction efficiency of ionic liquids in different metal concentrations

Influence of Extractant Concentration on Metal Extraction

The effect of ionic liquid concentration on metal extraction was assessed using ILs diluted in kerosene at 10%, 20%, 35%, and 50% concentrations, keeping the A/O phase ratio at 1:1. As shown in Figures 4(a and b), extraction efficiency generally increased with extractant concentration, particularly between 10–35%. Beyond 35%, improvements plateaued, likely due to increased viscosity limiting mass transfer. Notably, [A336][P204] showed remarkable selectivity for Mo, achieving 98.5% extraction even at 10%, with minimal gains at higher concentrations. Ni and Co extractions remained below 4%, underscoring the IL's strong affinity for Mo and minimal co-extraction of other metals. In contrast, [TOA][CY272] achieved a maximum extraction efficiency of 74.6%, with lower selectivity.

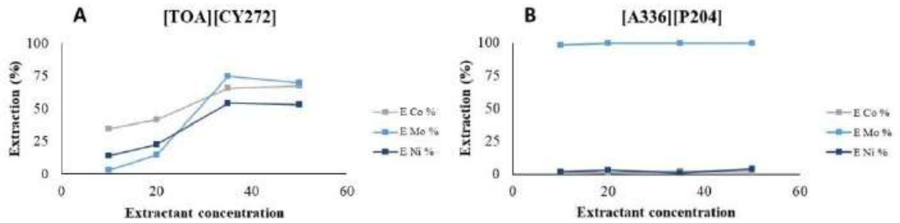

Figure 4 Effect of varying concentration (10%, 20%, 35%, 50%) of ionic liquid extractants

Effect of Aqueous Phase pH on Extraction

The pH of the aqueous phase is a key factor that influences metal speciation and, consequently, extraction behavior. To examine its impact, experiments were performed at pH values of 1.5, 4.5, and 7.5. Higher pH values were excluded to avoid the precipitation of Ni and Co. As shown in Figure 5, extraction efficiency varied notably with pH, reflecting the selective affinity of each ionic liquid for Mo, Co, and Ni under different acidity conditions.

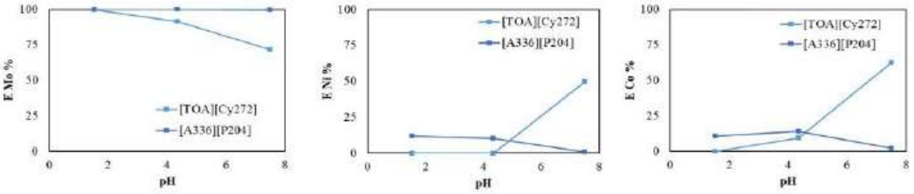

Figure 5 Effect of aqueous phase pH on extraction efficiency

The effect of pH on extraction efficiency revealed distinct behaviors for [TOA][CY272] and [A336][P204]. For [TOA][CY272], Ni and Co extraction improved significantly with increasing pH, especially from 4.5 to 7.5. In contrast, [A336][P204] showed a steady decline in Ni and Co extraction as pH increased, reaching negligible levels at pH 7.5. Both ILs achieved near-complete Mo extraction at pH 1.5; however, [TOA][CY272] exhibited a gradual decrease in Mo recovery at higher pH, while [A336][P204] maintained consistently high Mo extraction (>99%) across all pH levels, confirming its strong selectivity and stability for Mo.

Stripping Process and Metal Separation

Selective recovery of Mo, Ni, and Co from the loaded organic phases was assessed using 2 M HCl and 1 M NH_4OH as stripping agents. The process was performed at room temperature with a 1:1 O/A ratio. Figure 6 shows the stripping efficiencies for each metal using [TOA][CY272] and [A336][P204], highlighting their potential for effective and selective metal separation.

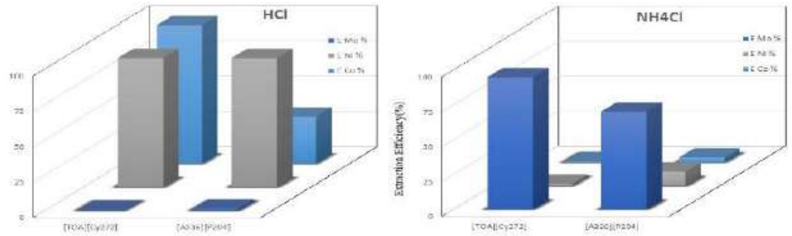

Figure 6 Acidic and alkaline agents stripping performance

CONCLUSION

This study evaluated the extraction performance of two ionic liquids, [TOA][CY272] and [A336][P204], for recovering Mo, Ni, and Co from synthetic solutions mimicking PLS or wastewater derived from spent catalyst processing. [A336][P204] demonstrated exceptional selectivity for Mo, achieving nearly 100% extraction efficiency, with minimal influence from metal or extractant concentration. In contrast, [TOA][CY272] showed improved efficiency with increasing extractant concentration but was less effective at higher metal loadings. pH had a notable impact on extraction behavior, and subsequent stripping with acidic and alkaline agents enabled effective separation of Mo from Ni and Co. These findings support the potential of ionic liquids for efficient and selective metal recovery in hydrometallurgical applications.

REFERENCES

1. Srour, H., Devers, E., Mekki-Berrada, A., Toufaily, J., Hamieh, T., Batiot-Dupeyrat, C., & Pinard, L. (2021) Regeneration of an aged hydrodesulfurization catalyst: Conventional thermal vs non-thermal plasma technology. Fuel, 306, 121674.
2. D'Adamo, I., Ippolito, N. M., Shalchian, H., Innocenzi, V., Ferella, F., & Vegliò, F. (2023) A feasibility study for a circular approach in oil refining: Metals recovery from hydrodesulphurization catalysts. Sustainable Materials and Technologies, 36, e00634.
3. Fang, K., Zhang, G., Li, Q., Guan, W., Wang, M., Wu, S., Xia, X., & Shi, C. (2024) Efficient and selective recovery of Mo and V from spent hydrodesulfurization catalysts via oxidation roasting followed by Na2CO3 and NaOH leaching. Hydrometallurgy, 229, 106381.
4. Pathak, A., Rana, M. S., Al-Sheeha, H., Navvmani, R., Al-Enezi, H. M., Al-Sairafi, S., & Mishra, J. (2022) Feasibility of bioleaching integrated with a chemical oxidation process for improved leaching of valuable metals from refinery spent hydroprocessing catalyst. Environmental Science and Pollution Research, 29(23), 34288-34301.
5. Wang, J.-Z., Du, H., Olayiwola, A., Liu, B., Gao, F., Jia, M.-L., Wang, M.-H., Gao, M.-L., Wang, X.-D., & Wang, S.-N. (2021) Recent advances in the recovery of transition metals from spent hydrodesulfurization catalysts. Tungsten, 3(3), 305-328.
6. Aslan, B. G., Aslan, C., & Ilhan, S. (2023) Hydrometallurgical recovery of valuable metals from hazardous petrochemical industry waste and kinetic investigation. Journal of Sustainable Metallurgy, 9(4), 1535-1549.
7. Zoraga, M. (2024) Metal recovery from spent Ni-Mo-V hydrodesulphurisation catalyst in oxalic acid media by mechanochemical treatment. Canadian Metallurgical Quarterly, 63(3), 882-891.
8. Arslanoğlu, H., & Yaraş, A. (2021) Recovery of molybdenum, cobalt and nickel from spent hydrodesulphurization catalyst through oxidizing roast followed by sodium persulfate leaching. Sustainable Materials and Technologies, 28, e00286.
9. Mohapatra, A., Behera, S., Tripathy, S., Parhi, P., & Sanjay, K. (2022) Extensive investigation on extraction behaviour of organo-phosphrous based bi-functional ionic liquids for separation of molybdenum (Mo) from spent Co-Mo/Al2O3 leach liquor. Journal of Molecular Liquids, 366, 120087.
10. Parhi, P., & Misra, P. (2022) Environmental friendly approach for selective extraction and recovery of molybdenum (Mo) from a sulphate mediated spent Ni–Mo/Al2O3 catalyst baked leach liquor. Journal of Environmental Management, 306, 114474.
11. Rahmati, S., Adavodi, R., Hosseini, M. R., & Veglio', F. (2024) Efficient metal extraction from dilute solutions: a review of novel selective separation methods and their applications. Metals, 14(6), 605.
12. Ilyas, S., Srivastava, R. R., & Kim, H. (2023) Selective separation of cobalt versus nickel by split-phosphinate complexation using a phosphonium-based ionic liquid. Environmental Chemistry Letters, 21(2), 673-680.

XVI International Mineral Processing
and Recycling Conference
28-30 May 2025, Belgrade, Serbia

DOI: 10.5937/IMPRC25652S Research article

SELECTED ASPECTS OF SENSOR APPLICATION IN THE DESIGN AND IMPLEMENTATION OF INTELLIGENT INSTRUMENTATION FOR RECYCLING SYSTEMS

Predrag Stolić[1#], 0000-0002-2574-4765,
Zoran Jovanović[2], 0000-0003-1727-4852,
Željko Mravik[2], 0000-0003-2327-5165,
Marko Jelić[2], 0000-0003-3723-4313,
Sonja Jovanović[2], 0000-0003-3577-5060,
[1]University of Belgrade - Technical Faculty in Bor, Bor, Serbia
[2]University of Belgrade - "Vinča" Institute of Nuclear Sciences - National Institute of the Republic of Serbia, Belgrade, Serbia

ABSTRACT – The use of sensors in the development of laboratory equipment is widespread, and today there is hardly any modern laboratory device that does not rely on some form of sensor technology. Sensors are selected to meet specific characteristics of a given process. In the selection process, certain dominant features are typically considered; however, there are also specific sensor characteristics that are often overlooked, yet they can significantly impact the realization of the desired functionalities of the laboratory equipment. This paper highlights some of these aspects through a practical example.

Keywords: Control, Laboratory Equipment, Monitoring, Programmable Logic Controller, Sensors.

INTRODUCTION

Modern instrumentation, whether in scientific, industrial, or other application domains, regardless of complexity, inherently involves the use of some type of sensor, one or more, alongside various systems for data processing and display [1]. The indispensable role of sensors as vital components of any modern system lies in the necessity for a system component capable of providing sufficient information about various aspects of a process, whether pre-process, in-process, or post-process events [2].

Thanks to advances in material science, engineering, and technology, today we have a vast array of sensors of different types, constructions, characteristics, and application areas, making it difficult to establish a universal classification of sensors. Considering the complexity of sensors in current use, depending on the problem being addressed, both very simple sensing solutions and highly advanced sensors with exceptional complexity are employed. Although we may not always consciously consider sensor use in certain systems, many everyday devices perform basic functions precisely through sensor

---

[#] corresponding author: pstolic@tfbor.bg.ac.rs technology. Furthermore, due to their widespread usage, sensors may be referred to by other specialized terms depending on the field of application, technical discipline, or other specific perspectives [3].

In the past, the development of instrumentation often meant implementing so-called "dumb" instrumentation, which enabled only simple data acquisition, while further actions, such as processing the obtained data, relied on manual methods and human interpretation. Since the late 1980s, this landscape has changed. The development of instrumentation today focuses on achieving intelligent systems capable of performing a wide range of automated tasks after data acquisition, such as data filtering, processing, presentation, and correlation with other data [4]. Modern sensors are the backbone of such intelligent instrumentation systems, and modern instrumentation inherently includes the use of advanced sensors and sensing techniques.

As a result, special attention is now given to the proper selection and implementation of sensors. In this context, many primary sensor characteristics are carefully analyzed, such as measurement range, resolution, and response time, along with certain specific features like mechanical robustness, dimensions, and unique mounting capabilities. The increasing complexity of systems has also led to more complex criteria for selecting suitable sensors for specific instrumentation tasks. Often during system development, some sensor characteristics are overlooked or it becomes evident only during testing or actual operation that the chosen sensor solution is not optimally suited to the implemented system.

In the following section, an example of a testing system will be used to highlight some of the previously mentioned issues that may arise in practice. In accordance with standard manufacturing practices and the design of modern sensor systems, the term sensor as used in this paper will refer to the complete electronic assembly comprising the sensor module or the sensor device.

RESULTS AND DISCUSSION

To conduct the necessary analysis of the above-mentioned issue, we will assume, at a certain level of abstraction, that a given testing system consists of a gas chamber for sample testing, a PLC responsible for controlling the testing process, and a computer used for collecting relevant data related to the tested samples. One of the key aspects of such a system is the proper selection of sensors that will monitor the concentration of a specific gas within the chamber where testing is conducted. To develop a more universally adaptable system, let us assume that the chamber will be used for testing different gases independently or simultaneously. This implies that for each gas being tested, an appropriate sensor capable of accurately measuring its concentration must be used. For the sake of simplicity in further analysis, we will assume that the system is designed to test up to three different gases, which requires the use of three different sensors.

In the initial stage of sensor selection, attention must be paid to whether the sensors meet key performance characteristics of the system. Accordingly, the first parameters to be considered are whether the sensors can measure the required concentration range and whether they operate at the appropriate measurement resolution. For example, if we want to measure concentrations up to 50 ppm, we must select a sensor capable of measuring values beyond the target, such as a sensor with a range of 0–100 ppm, and at a suitable resolution. The next step in selecting suitable sensors would be to consider the response time. For gas sensors, this is typically expressed in seconds and denoted as T90 [5], which represents the time required for the sensor to reach 90% of the target gas concentration value (in some cases, T50 is used, indicating the time to reach 50%). Attention will then likely turn to the accuracy of the sensor readings, in accordance with the overall measurement accuracy required by the system. Further attention must be paid to various operational parameters that define the necessary conditions for proper sensor performance, such as operating temperature, humidity, pressure, and other similar parameters. These are joined by other important factors like the expected degradation of the sensor over time, its anticipated service life, and related considerations.

These are just some of the most critical parameters typically considered when selecting sensors for integration into a specific solution. However, they are not the only ones. Here, we highlight two additional parameters: proper connectivity and communication between the sensor and the rest of the system, and the sensor's broader integration capabilities. These parameters are often insufficiently analyzed, and as a result, certain limitations and shortcomings only become apparent during the testing phase or early in deployment at which point sensor replacement can present a significant financial burden and often a highly complex task.

As previously noted, it is assumed that the entire process will be managed by an appropriate control system based on the use of a PLC. Accordingly, it is expected that the initial choice would be a sensor that can be easily interfaced with the PLC system. In most cases, the typical choice for designing such a system would be a sensor that outputs gas concentration as a current signal in the 4–20 mA range. Figure 1 shows an example of such a two-wire sensor that detects a specific gas and uses a 4–20 mA output powered by a 24V DC supply [6].

Figure 1 EC Sense 4-20mA Smart Gas Sensor Module TB420-ES1 [6]

These parameters are ideal for implementation using a PLC and its analog input capabilities [7]. Thus, when considering a straightforward implementation, this would likely represent the most optimal and simplest approach in terms of wiring and ease of system integration. From a control perspective, this is one of the most commonly used and effective methods for achieving reliable process monitoring and control.

Regarding the measured gas concentration values, they would need to be directly acquired from the PLC. This would involve the data acquisition software on the computer accessing the appropriate PLC register, performing the necessary value conversion (e.g., from hexadecimal to decimal), and then processing the data further in accordance with the system's processing tasks.

Additionally, in the context of PLC-based control, it is also possible to use a sensor solution that does not rely on analog interfacing, but rather on digital communication. One such approach is illustrated in Figure 2, where the connection is achieved using an RS485 Modbus RTU interface [8]. This solution, on one hand, increases the complexity of wiring and integration, since the PLC must support a sufficient number of RS485 communication ports. For example, in the case of using three sensors to measure the concentration of three different gases, three RS485 ports would be required, which in most cases entails additional costs in the form of expansion modules equipped with RS485 ports.

On the other hand, this approach allows for extended functionality, as it enables the retrieval of a broader set of data from the sensor device compared to the analog method. In most cases, in addition to gas concentration, additional parameters such as temperature and humidity can also be read. Thus, while this approach introduces an added layer of complexity in the implementation of the control system, it simultaneously provides enhanced capabilities.

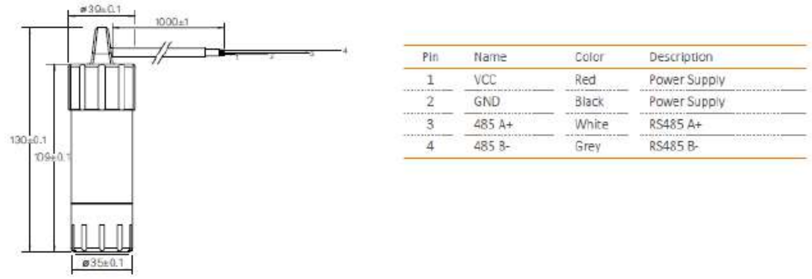

Pin	Name	Color	Description
1	VCC	Red	Power Supply
2	GND	Black	Power Supply
3	485 A+	White	RS485 A+
4	485 B-	Grey	RS485 B-

Figure 2 Pinout of the EC Sense Stox Smart Gas Sensor Device [8]

However, it is important to note that this also leads to increased complexity in data acquisition from the PLC via the computer software. Since multiple registers need to be read, because each of them holding a single value, data retrieval becomes more intensive. In our case, with three sensors and expanded functionality (reading concentration, temperature, and humidity), the system would need to read a total of 3 × 3 registers i.e. nine registers in total. These values must then be appropriately read, converted, and further processed by the computer.

However, direct integration with the PLC is not the only solution available for addressing the described problem. The gas sensors considered in this context do not necessarily need to be connected exclusively to the PLC. An alternative approach involves connecting the sensors directly to a computer. Naturally, the previously discussed sensors are not suitable for this purpose; instead, a sensor such as the one shown in Figure 3a must be used.

This type of sensor features a UART TTL 3.3V digital interface [9], which allows it to be connected to a computer using an appropriate converter module, such as the one shown in Figure 3b. This module enables the conversion of the UART digital signal to a signal compatible with standard USB interfaces on a computer [10]. In this setup, data is read directly from the sensor into the computer software via a serial connection. This approach provides easier access to sensor data for further processing, as the procedures for acquiring and handling sensor data are generally simpler and thus facilitate more straightforward data manipulation on the computer itself.

Figure 3a EC Sense NO_2 Gas Sensor Module TB600B [9]

Figure 3b 4-pin USB to TTL module [10]

This raises the question of how the control over the process is maintained, specifically, how the PLC obtains information on gas concentrations. In previous approaches, data was read from the PLC by the computer. Here, the direction is reversed: in order to provide the PLC with access to sensor data, the computer writes the relevant concentration values into predefined PLC registers, converting the data into a format suitable for the PLC (e.g., from decimal to hexadecimal).

Moreover, this approach also allows for extended functionality, as the connection between the sensor and the computer can support the transfer of multiple parameters, such as gas concentration, temperature, and humidity. Compared to the earlier method, this results in a reduced number of PLC register manipulations. Instead of performing 9 register operations (3 sensors × 3 values: concentration, temperature, and humidity), only 5 operations are required. Specifically, the system writes values into three registers for gas concentration (one per sensor), and one value each for temperature and humidity, these being the average values considered most relevant for process control.

Averaging is used here because writing three separate temperature or humidity values would not significantly enhance the control logic—particularly as the values typically differ only slightly and the PLC would not be capable of determining which one is most significant. Additionally, this approach offers enhanced diagnostic capabilities: for instance, temperatures and humidity values can be compared across sensors, and any significant deviation may indicate a fault, either in sensor performance or communication, an issue that is more easily identified in this configuration than when sensors are connected directly to the PLC.

APPLICABILITY IN RECYCLING SYSTEMS

The previous considerations were presented in a generalized manner, but they have wide applicability in the design of various aspects of recycling systems. This is particularly evident given the fact that intelligent systems can significantly improve recycling operations. For this purpose, a variety of sensor types are used, including optical, inductive, ultrasonic, infrared (IR), and others, serving different tasks such as material type recognition, metal detection, waste volume measurement, and more.

Gas sensors, in particular, play an important role in recycling centers during the processing of different types of waste, as the treatment of organic, electronic, or chemical waste can lead to the release of harmful gases. Accordingly, the previously discussed considerations find excellent application in the implementation of recycling systems, as the same system aspects are encountered as in the previously analyzed generalized solution: control, monitoring, management, and data acquisition.

These considerations can significantly contribute to a better understanding of the design aspects of recycling systems, as they can improve certain vital components and thus enhance the overall recycling process. For example, the previous analyses can improve ventilation automation through more accurate gas concentration analysis. Improved gas concentration analysis also enhances various aspects of alarm systems and helps prevent potential incident situations. Additionally, it opens the door to modern system integrations based on IoT solutions and provides the possibility to apply artificial intelligence algorithms to improve different parts of the recycling system.

It is important to emphasize that the improvements resulting from these considerations are not only of a technical or technological nature, but also contribute to safety, environmental protection, and other domains. They increase the safety of personnel in recycling centers, reduce the risk of explosions and fires, and allow for better monitoring of environmental parameters both within and around recycling facilities.

CONCLUSION

Connecting sensors directly to a PLC is not the only option in complex intelligent systems. While there are simpler cases of sensor-to-PLC integration, as well as more advanced configurations offering extended functionality, the possibility of connecting sensors directly to a computer should not be overlooked.

This method brings significant advantages to the overall measurement, control, and management process, offering broader functionality while simultaneously reducing the number of PLC register operations. However, it is important to emphasize that, from a control and automation perspective, this approach introduces additional potential failure points, due to the inherent hardware and software differences between PLCs and computers. As such, although this method is not without limitations, it should not be dismissed outright, as is often the case. In complex systems involving data acquisition, control, monitoring, and management, this architecture can offer substantial benefits that merit serious consideration.

When considering the application in the field of recycling, the approaches mentioned above enable the digital transformation of recycling centers through the introduction of modern, digitized intelligent recycling systems. This leads to improvements not only in recycling processes and facilities but also in the working environment and the broader ecosystem.

ACKNOWLEDGEMENT

This research was supported by the Science Fund of the Republic of Serbia, grant No. 6706, Low-dimensional nanomaterials for energy storage and sensing applications: Innovation through synergy of action – ASPIRE *and by the Ministry of Science, Technological Development and Innovation of the Republic of Serbia (contracts No. 451-03-137/2025-03/200131 and 451-03-136/2025-03/200017).*

REFERENCES

1. Dickinson, M. (2014) Procesna merenja pomoću C# aplikacija. EHO, Niš, Serbia.
2. Milovanović, A., Bjekić, M., Koprivica, B. (2010) Virtuelna instrumentacija. Faculty of Technical Sciences, Čačak, Serbia.
3. Norton, H. N. (1989) Handbook of Transducers. Prentice-Hall Inc., New Jersey, USA.
4. Barney, G. C. (1988) Intelligent Instrumentation: Micropocessor applications in measurement and control. 2nd Edition. Prentice-Hall International (UK) Ltd., London, UK.
5. Kornbech, M., Olesen, M. T. (2010) Fixed Gas Detectors - Total Speed of Response. PETRO Industry News, 11 (5), 34.
6. 4-20 mA Smart Gas Sensor Module TB420-ES1 Datasheet (2025). EC Sense Gmbh, Hohenschäftlarn, Germany.
7. Marinković, D. M. (2013) Programabilni logički kontroleri. Mikro knjiga, Belgrade, Serbia.
8. Smart Gas Sensor Device Stox Series Datasheet (2025). EC Sense Gmbh, Hohenschäftlarn, Germany.
9. Nitrogen Dioxide Gas Sensor Module TB600B Datasheet (2025). EC Sense Gmbh, Hohenschäftlarn, Germany.
10. FT232RL Serial Port Module USB to TTL Serial Port Board. https://www.ictransistors.com/wifi-mo-du-le/ft232rl-serial-port-module-usb-to-ttl-serial.html

DOI: 10.5937/IMPRC25659T

Original research article

PREDICTION OF RESULTS OF FLOATATION PROCESS USING ARTIFICIAL NEURAL NETWORKS

Maja Trumić[1#], 0000-0001-9361-4412,
Katarina Balanović[1], 0000-0002-2197-5718,
Tamara Gavrilović[2], 0000-0003-3448-7753,
[1]University of Belgrade, Technical Faculty in Bor, Bor, Serbia
[2]University of Pristina, Faculty of Technical Sciences, Kosovska Mitrovica, Serbia

ABSTRACT – In this paper, the use of artificial neural networks in the flotation process is presented and analyzed. Apart from utilization of flotation in the mineral processing, deinking flotation is used for separation of ink particles from the cellulose fibers. The time of deinking flotation, pH value, reagents such as oleic acid, oleic acid with $CaCl_2$, oleic acid with $AlCl_2$ as well as concentration of reagents were used as input for the network. The recovery of toner particles in froth was used as output data for the network. The neural network demonstrated high correlation coefficients during training (0.97), validation (0.96), and testing (0.94), and subsequent accuracy testing confirmed these results.

Keywords: Artificial neural networks, Machine learning, Flotation, Deinking.

INTRODUCTION

One of the fastest-developing fields in computer science in recent decades is artificial intelligence [1]. Artificial intelligence is a branch of computer science focused on developing programs that enable machines to think and behave in ways that could be considered intelligent. Intelligent thinking represents the ability to reason in accordance with a current, previously unknown situation [2].

Machine learning is a field of artificial intelligence that deals with the development of programs that learn from previously obtained data. Once a solution to a problem is found, the program can remember and apply it in a similar situation. The forms of machine learning can be divided into the following three basic types of learning: supervised learning, unsupervised learning, and reinforced learning [3].

Supervised learning represents an approach to the learning problem in which the learning program receives a set of input data (x_1, x_2, …, x_n) and a set of desired output values, such that for each input data point x_i, there is a corresponding correct output y_i. The task of the program is to learn how to assign the correct output value to a new input data point. Algorithms based on supervised learning include models based on artificial neural networks, decision trees, support vector machines, Gaussian processes, and others [3].

[#] corresponding author: majatrumic@tfbor.bg.ac.rs

Artificial Neural Network (ANN) represents a set of interconnected simple processing elements (neurons) whose operating principle is based on the biological neuron. A typical neural network architecture consists of three layers of neurons: input, hidden and output layers [2,3].

The optimal number of hidden neurons depends on multiple factors, including the number of inputs and outputs, number of training pairs, level of noise in the training pairs, complexity of the error function, network architecture, and training algorithm. It can be said that the choice of architecture depends on the type and complexity of the problem being studied. The optimal number of neurons in the hidden layer is very important for the correct functioning of the model. A network with too many neurons will have an excessive number of parameters, making it prone to overfitting. Conversely, a network with too few neurons will not be able to properly approximate the given nonlinear relationships, leading to a problem of underfitting [3].

The flotation process has been used in mineral processing plants to separate valuable minerals from the gangue. This process takes place in a specific environment – flotation pulp – which consists of three phases: solid (mineral particles), liquid (water) and gaseous (air). Separation of mineral particles is made possible due to the differences in their surface hydrophobicity (feature of material characterizing its ability to be wetted with a liquid in the presence of a gas phase) [4].

Compared to mineral flotation, deinking flotation (ink removal from cellulose fibers) is a relatively young process. The basis of deinking flotation is pulp that contains the following components: water, as the carrier medium (approximately 98-99%); fibers, material obtained as a clean fraction (1-2%); fillers (<0.6%), printing ink and other impurities (<0.15%) that need to be removed; and reagents required for the fiber purification process (<0.1%) [5].

The efficiency of the flotation process can be shown through the toner recovery in foam product and cellulose fiber recovery in sink product, effective residual ink concentration in the final product (ERIC), the whiteness and brightness of the fibers.

The main parameters that influence flotation are temperature, pH, toner particle size, air flow, water hardness (concentration of calcium ions in the water), and others. All parameters are interdependent, so the flotation process is defined exclusively by their interaction-i.e., by the mechanism of their combined effect [6,7].

Our understanding of the fundamental physical and chemical processes underlying the deinking processes is growing. But, due to the great variability of the raw material as well as the complexity of the physical processes which occur at the microscopic level, processing problems and process instability remain as challenges [8].

Several studies demonstrate the effectiveness of artificial neural networks in modeling and optimizing processes in the pulp and paper industry. Labidi et al. (2007) [9] used an ANN to model ink removal in flotation, finding that higher consistency and airflow rates improved brightness and ERIC in the flotation cell, with strong correlation between ANN predictions and experimental results. Additionally, ANNs have been applied in image analysis, Verikas et al., (2000) [10] employed an ANN, combined with Fuzzy Logic to analyse the colour of dark spots in recycled paper sheets. Pauck (2011) [8] generated nearly 500 deinking runs to form the database for the training neural networks. The models effectively predicted brightness and ERIC, though yield results were slightly less accurate due to process complexity.

In the following study, an algorithm with supervised learning was analyzed, specifically, a model based on artificial neural networks for data obtained by deinking flotation.

EXPERIMENTAL

The Neural Fitting tool from the Matlab software package was used to create and train the network, as well as to evaluate its performance accuracy using mean squared error (MSE) and regression analysis.

The time of deinking flotation (in the range 1-20 min), pH value (in the range 3-12), reagents such as oleic acid, oleic acid with $CaCl_2$, oleic acid with $AlCl_2$ as well as concentration of reagents (0.1 kg/t, 0.4 kg/t, 1 kg/t) were used as input model variables. The recovery of toner particles in froth was used as the output model parameters.

From the total dataset of 225 parameters, 200 (88.89%) were randomly allocated for network training, validation, and testing, while the remaining 25 (11.11%) were reserved for evaluating the trained network's accuracy.

RESULTS AND DISCUSSION

The neural network architecture consisted of 10 hidden neurons (Fig. 1). From the available dataset of 200 parameters, 140 (70%) were used for training, while 30 parameters each (15%) were allocated for validation and testing (Table 1, Fig. 2). Network training was performed using the Levenberg-Marquardt algorithm.

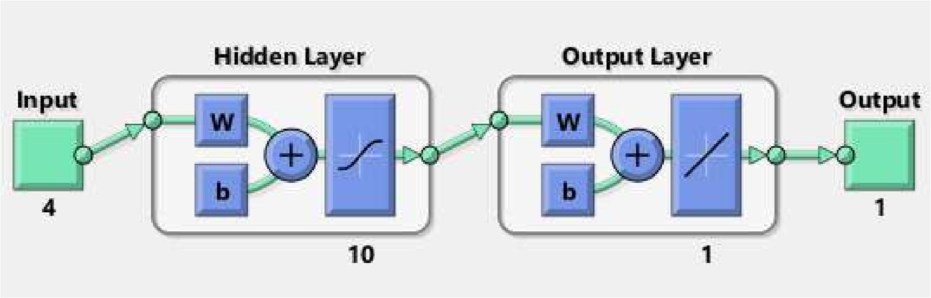

Figure 1 The structure of the created artificial neural network

Table 1 Network performance accuracy criteria obtained using the Levenberg-Marquardt algorithm

Training algorithm		Number of data	Mean squared error (MSE)	Coefficient of correlation (R)
Levenberg-Marquardt	Training	140 (70%)	74.87510	0.977055
	Validation	30 (15%)	192.94061	0.960261
	Testing	30 (15%)	136.83548	0.942087

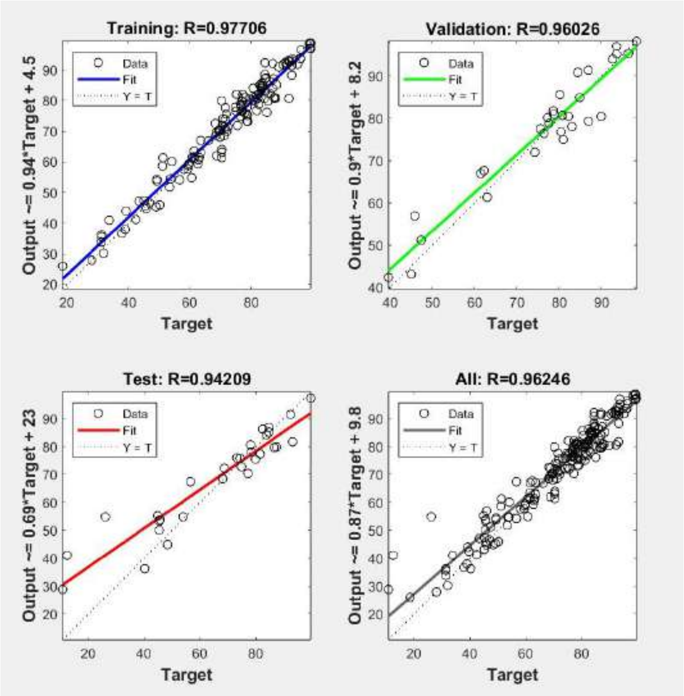

Figure 2 Plot of network's target values versus predicted outputs based on trained parameters, using the Levenberg-Marquardt training algorithm

Testing of the model demonstrates that the neural network achieves good results, as shown by a correlation coefficient of 0.94209. The excellent agreement between experimental data and ANN outputs, evidenced through both graphical representation and quantitative correlation analysis, validates the model's satisfactory prediction accuracy.

Since 88.89% of the data (200 parameters) were used for training, validation, and testing in the previous part, the remaining 11.11% (25 data points) that were not used for model training were preserved for prediction purposes, in order to determine the model's accuracy. The following Fig 3 present graphical comparisons between the values obtained from the network and the actual values obtained experimentally.

Figure 3 shows that the network modeling was successfully implemented, with the neural network accurately capturing the trend of experimental result curves.

Based on these results, it can be concluded that the artificial neural network architecture, comprising an input layer, a single 10-neuron hidden layer, and an output layer, is effectively applicable to this dataset type.

The number of required neurons was supposed to be determined by iteration. The greater the number of neurons, the more complex is the function which can be approximated. On the other hand, more neurons require more data which can also lead to overfitting of a function. At this point the training information and the neural network can be saved and inputted with other real data to produce a predicted output. If the performance of the network is not adequate, several corrective measures are available [8]: the network can be reset or initialized with new initial weights and biases and retrained; the number of neurons can be increased or decreased; expand the training dataset; change the number of input values; the ratio of data in training, validation and test sets can be changed; try alternate learning and training algorithms, and pre-processing of inputs and outputs.

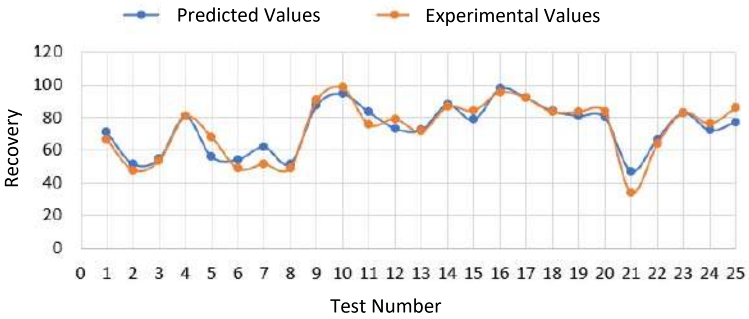

Figure 3 Comparative values obtained experimentally and using the ANN model with the Levenberg-Marquardt training algorithm

CONCLUSION

In this study, an algorithm with supervised learning was analyzed, specifically an artificial neural network model for data obtained by deinking flotation.

The neural network architecture consisted of a single hidden layer with 10 neurons. Network training was performed using the Levenberg-Marquardt algorithm.

The inputs of the models were time of deinking flotation, pH, reagents such as oleic acid, oleic acid with $CaCl_2$, oleic acid with $AlCl_2$ as well as concentration of reagents, while the output values were recovery of toner particles in froth.

The neural network demonstrated high correlation coefficients during training (0.97), validation (0.96), and testing (0.94). Subsequent accuracy testing confirmed these results, showing that the network effectively modeled laboratory processes with strong correlation.

Based on these results, it can be concluded that the artificial neural network architecture, comprising an input layer, a single 10-neuron hidden layer, and an output layer, is effectively applicable to this dataset type.

Since this study employed 10 hidden neurons in the neural network architecture, determining and utilizing the optimal number of neurons for this specific dataset could potentially yield even better results.

ACKNOWLEDGEMENT

"The research presented in this paper was done with the financial support of the Ministry of Science, Technological Development and Innovation of the Republic of Serbia, within the funding of the scientific research work at the University of Belgrade, Technical Faculty in Bor, according to the contract with registration number 451-03-137/2025-03/ 200131".

REFERENCES

1. Novaković, J. Đ. (2013) Rešavanje klasifikacionih problema mašinskog učenja. Fakultet tehničkih nauka u Čačku.
2. Tanikić, D. (2016) Veštačke neuronske mreže, fazi logika i genetski algoritam. Univerzitet u Beogradu, Tehnički fakultet u Boru.
3. Kovačević, M. M. (2018) Model za prognozu i procenu troškova izgradnje armirano-betonskih drumskih mostova. Doctoral dissertation, University of Belgrade, Serbia.
4. Ćalić, N., (1990) Teorijski osnovi pripreme mineralnih sirovina. Faculty of Mining and Geology, University of Belgrade, 496 p. (in Serbian).
5. Kemper, M. (1999) State-of-the-art and new technologies in flotation deinking. International Journal of Mineral Processing, 56 (1-4), 317-333.
6. Borchardt, J. K. (1994) Mechanistic insights into de-inking. Colloids and Surfaces A: Physicochemical and Engineering Aspects, 88 (1), 13-25.
7. Svensson, R. (2011) The influence of surfactant chemistry on flotation deinking.
8. Pauck, W. J. (2011) Neural network modelling and prediction of the flotation deinking behaviour of complex recycled paper mixes. Doctoral dissertation, Faculty of Engineering, University of KwaZulu Natal, Durban.
9. Labidi, J., Pelach, M. A., Turon, X., & Mutje, P. (2007). Predicting flotation efficiency using neural networks. Chemical Engineering and Processing: Process Intensification, 46(4), 314-322.
10. Verikas, A., Malmqvist, K., Bacauskiene, M., & Bergman, L. (2000). Monitoring the de-inking process through neural network-based colour image analysis. Neural Computing & Applications, 9, 142-151.

XVI International Mineral Processing
and Recycling Conference
28-30 May 2025, Belgrade, Serbia

DOI: 10.5937/IMPRC25665S

Research article

FINANCIAL AND TECHNOLOGICAL POTENTIAL OF ECO-EFFICIENT RECYCLING OF WASTE ELECTRONIC EQUIPMENT

Tomasz Suponik[1#], 0000-0002-4251-4275,
Paweł Friebe[2], 0000-0003-1574-6190,
Umut Kar[3], 0000-0002-4722-5878,
Dawid Franke[1], 0000-0002-5522-6889,
Pengbo Chu[3], 0000-0003-2111-2602,
[1]Silesian University of Technology, Gliwice, Poland
[2]KOMAG Institute of Mining Technology, Gliwice, Poland
[3]University of Nevada, Reno USA

ABSTRACT – The paper presents the financial potential of recycling waste electronic equipment (WEE) in the form of printed circuit boards, hard drives, and lithium-ion batteries. The metal contents in selected types of WEE were presented, as well as their price and importance from an environmental, economic, and political perspective using the indicators of relative supply risk and abiotic depletion potential (ADP). The potential benefits that recycling can bring to the company and the environment were presented. Furthermore, the mass balance and value of recovered metals were estimated for southern Poland and potential possibilities for the management of the remaining separation products were presented. Finally, verified methods for physical recycling of the presented WEE were described.

Keywords: Recycling Of Waste Electronic Equipment (WEE), Metal Recovery, Financial and Technological Aspects.

INTRODUCTION

Waste electronic equipment (WEE) is a group of waste whose quantity is growing dynamically from year to year and, due to the presence of metals, often critical, and plastics, constitutes a global environmental, economic, and even political problem. Such a rapid rise in end-of-life electrical and electronic equipment poses a challenge to both companies seeking to recover valuable raw materials and authorities striving to reduce the environmental impact of this waste stream.

This article focusses on the financial and technological potential of eco-efficient WEE recycling. The subsequent sections present the following:

- the content and price of metals in selected types of WEE, along with an overview of indicators that evaluate their importance from environmental, economic, and political perspectives, particularly relative supply risk and abiotic depletion potential (ADP). In this context, three examples of waste categories are discussed in detail: printed

---

[#] corresponding author: tomasz.suponik@polsl.pl circuit boards (WPCBs), computer hard disk drives (WHDs), and lithium-ion batteries (WLIBs),

- the mass balance and estimated value of recoverable metals in WEE collected in southern Poland, illustrating the economic and environmental potential of recycling,
- a review of research on the recycling of the analysed WEE, including physical methods as a preliminary step in recycling. It has been shown that physical techniques such as shredding, cryognic grinding, electrostatic separation, flotation, gravity, and optical separation often provide a simpler and more environmentally friendly route to metal recovery, especially at the initial processing stage.

CONTENT AND PRICE OF METALS IN WEE AND THEIR SIGNIFICANCE INDICATORS

In this study, two indicators were considered to assess the importance of metals present in the WEE: the relative supply risk and the potential for abiotic depletion potential (ADP). The second parameter is used to assess the impact of resource depletion. It focusses specifically on abiotic resources, which are non-living materials such as minerals and metals. ADP describes the ratio of the annual production of a resource to its ultimate reserves (based on the crustal content). It allows an assessment of the extent to which the use of a particular material contributes to the depletion of its resources. The higher the ADP value for a particular resource, the greater the potential for the resource to deplete [1]. Just as the global warming potential (GWP) of various pollutants is converted to CO_2 equivalents, ADP values are commonly calculated to antimony equivalents (Sb eq.).

Another parameter is the relative supply risk developed by the Royal Society of Chemistry, which assesses future raw material availability issues. The index is based on factors such as crustal abundance, distribution and quantity of reserves, production concentration, substitutability, recycling rates, and political stability (Royal Society of Chemistry Periodic). The relative supply risk ranges from 1 (very low risk) to 10 (very high risk).

Waste Printed Circuit Boards (WPCB)

One of the most common types of WEEs is waste printed circuit boards (WPCBs), which are made of a composite material with embedded metal tracks as the base. The most commonly used PCBs are of type FR-4, whose composite is made of glass fibre in an epoxy resin matrix with flame retardant additives. As can be seen in Table 1, the WPCB consists of metals with medium (Cu, Al, Zn, Au), increased (Pb, Ni, Sn, Ag) and high (Pd, Pt) relative supply risk, while the ADP is very high for Au, Pd, Pt, medium for Ag, and low or very low for Cu, Al, Pb, Zn, Ni, Sn, which means that the resources of some metals such as Au, Pd, Pt are very limited and the risk of Pd and Pt availability due to production concentration, substitutability, recycling rates, and political stability is high. Both indices show that the key metals from an economic, environmental, and political perspective are Pd, Pt, Au, and Ag. This affects the price of metals. Therefore, the most valuable metals in WPCB, considering their content, are gold, silver, palladium, and due to their high content, also copper (Table 1), and the recovery of these metals can provide significant economic benefits to the recycling company [2]. The estimated value of the metals contained in a ton of WPCB is almost 92 thousand USD, of which a significant part is the value of gold. Metals that have financial value are treated as concentrates, whereas plastics are treated as products for which use is sought.

Table 1 Estimated metal contents of FR-4 type WPCB and related indicators of: relative supply risk and abiotic depletion potential [3–5] and estimated price of metals in WPCB [6,7]

Metal	Average metal content in WPCB, %	Relative supply risk	ADP, kg Sb eq/kg	Estimated price of metal in 1 Mg, $
Cu	20	4.3	2.1E−02	1 821.6
Al	2	4.8	2.5E−08	49.5
Pb	2	6.2	1.9E−02	39.3
Zn	1	4.8	2.8E−03	32.2
Ni	2	6.2	8.1E−04	303.6
Sn	4	6.7	8.1E−02	1 194.1
Ag	0.20	6.2	8.6E+00	1 928.4
Au	0.10	5.7	1.4E+03	84 556.5
Pd	0.0050	7.6	9.7E+02	1 532.0
Pt	0.0015	7.6	9.7E+02	454.3
Sum	31.31	-	-	91 910.9

Waste hard drive (WHD)

Another type of WEE is the waste hard drives (WHDs), which have an average weight of 509.8 g and consist of several elements [8]. These include aluminium, steel, plastic, as well as printed circuit boards and neodymium magnets. Most of the mass share belongs to the HDD casing, which consists of two parts: the main part and its cover. Typically, this casing is made of an Al-Si alloy. The HDD also consists of a disk stack assembly, which includes platters with a spacer and a spindle cover. The platters are made of an Al core with a thin layer of metal alloy providing magnetic properties. This alloy contains Co, Ni, Fe, and Zn [9]. The HDD also contains a PCB that is mounted on the bottom of the case. The HDD also consists of a Voice Coil Assembly (VCA), which is made up of neodymium magnets, ferrous metal holders, and other mechanical parts. VCA contains metals such as Fe, Nd, Pr, Dy, Co [10]. An HDD is composed of about 83% (by weight) metals and about 17% non-metallic assemblies such as PCBs and plastic parts. The Al content is the highest because the HDD casing is made of this metal.

HDD consists of metals with medium (Al, Fe, Cu, Ti, Zn, Au), increased (Ni, Sn, Ta, Ag), high (Co, Pd, Pd, Pt) and extremely high (Nd, Ce, Pr, Dy, Sb) relative supply risk (Table 2), while ADP is very high for Au, Pd, medium for Ag, Sb, low for Cu, Ni, Sn, Zn, Pr, and very low for Ce, Nd, Dy Co, Al, Si, Fe, Ti, Ta (Table 2), meaning that the resources of metals used in HDD production, apart from those from which PCBs are made, are large, but the availability risk, especially of Nd, Pr, Dy, Ce and Sb due to production concentration, substitutability, recycling rates, and political stability, is extremely high. The most important metals from an economic, environmental, and political perspective that drive the need for WHD recycling are Nd, Pr, Ce, and Dy that make up neodymium magnets and Pd, Au, and Ag that are found in the PCBs that control HDD.

The most valuable metals in WHD, based on their content, are gold, cerium, copper, neodymium, palladium, dysprosium, silver and praseodymium, which are contained in neodymium magnets and PCBs (Table 2). Aluminium and quartz are also of great value due to their high content in HDD. The HDD casing is made of aluminium with a steel cover. The estimated value of metals contained in a ton of WHD is around USD 9 908, with the highest value metals found in neodymium magnets, PCBs, and HDD casing. Therefore, they are treated as concentrates in the recycling process.

Table 2 Estimated metal content in WHD and related indicators of: relative supply risk and abiotic depletion potential and estimated price of metals in WHD [1,3,9,11]

Part of WHD	Metal	Average metal content in WHD, %	Relative supply risk, -	ADP, kg Sb eq/kg	Estimated price of metal in 1 Mg, $
HDD casing	Al	64.0	4.8	2.5E−08	1 583.4
	Si	8.9	-	1.4E−11	124.3
	Fe	3.2	5.2	5.24E−08	10.1
PCBs	Cu	5.4	4.3	2.1E−02	491.6
	Ni	0.18	6.2	8.1E−04	27.3
	Sn	0.17	6.7	8.1E−02	50.7
	Ti	0.04	4.8	2.79E−08	2.6
	Zn	0.03	4.8	2.8E−03	1.0
	Ce	0.04	9.5	1.5E−05	1.2
Neodymium magnets	Nd	0.73	9.5	3.1E−05	438.5
	Pr	0.11	9.5	1.4E−04	72.4
	Dy	0.08	9.5	7.0E−05	195.5
	Co	0.07	7.6	1.57E−05	17.0
PCBs	Sb	0.01	9.0	1.0	1.7
	Ta	0.06	7.1	4.06E−5	202.2
	Ag	0.0234	6.2	8.6E+00	225.6
	Au	0.0071	5.7	1.4E+03	6 003.5
	Pd	0.0015	7.6	9.7E+02	459.6
	Sum	83.0	-	-	9 908.3

Waste lithium-ion batteries (WLIB)

The last WEE presented is waste lithium-ion batteries (WLIBs). LIBs are now the dominant portable power source in smartphones, laptops, cameras, hand-held devices, and other high-tech devices. The structure of LIBs is not homogeneous and multimetallic compounds can be found in them. Lithium cobalt oxide (LCO) and lithium nickel manganese cobalt oxide (NMC) are examples of the types of active cathode materials (CAMs) used in these batteries [12]. They typically contain approximately 21.31% Mn, 16.54% Co, 2.56% Ni, 2.22% Li, 5.93-14% Cu, 4.7-9.12% Al, 0.04-25% Fe and approximately 15% organic materials and 7% plastics [13,14]. Organics include electrolytes, binders, and separators [12,14].

LIB consists of metals with medium (Mn, Cu, Al, Fe), elevated (Ni, Li), and high (Co) relative supply risk, while ADP is low or very low for Cu, Ni and Mn, Co, Li, Al, Fe (Table 3), respectively, which means that the resources of metals used for battery production are large, but the availability risk, especially of Co, Li, Ni due to production concentration, substitutability, recycling rates, and political stability is quite high.

WLIB recycling can also provide significant financial benefits to the recycler. Considering the current metal prices on the exchanges and the average metal content in WLIB, it is estimated that in one tonne of WLIB the value of the metals contained is over USD 6 350. Note that cobalt is the key metal determining the profitability of WLIB recycling, although copper, nickel, lithium, and manganese are also high-value metals.

Table 3 Estimated metal contents in WLIB and related indicators of: relative supply risk and abiotic depletion potential [1,3,9] and estimated price of metals in WPCB [6,7]

Metal	Average metal content in WPCB. %	Relative supply risk	ADP. kg Sb eq/kg	Estimated price of metal in 1 Mg, $
Mn	21.31	5.7	3.3E−05	441.1
Co	16.54	7.6	1.57E−05	4 019.2
Ni	2.56	6.2	8.1E−04	388.6
Li	2.22	6.7	5.2E−05	383.5
Cu	5.93-14	4.3	2.1E−02	907.6
Al	4.7-9.12	4.8	2.5E−08	171.0
Fe	0.04-25	5.2	5.24E-08	39.7
Total	53.3-90.75	-	-	6 350.7

MASS BALANCE AND ESTIMATED VALUE OF METALS IN WEE FOR SOUTHERN POLAND

Eco-efficient WEE recycling provides significant economic benefits. It is estimated that in southern Poland the annual mass of collected WPCBs, WHDs and WLIBs per 1 million inhabitants is approximately 27.2, 13.6 and 45.3 Mg, respectively, and the estimated value of metals in them is approximately 2 499, 135 and 288 thousand USD/year, respectively. For example, in Poland, with a population of 38.4 million, approximately 1,045 Mg of WPCB, 522 Mg of WHD and 1,742 Mg of WLID are collected annually, while the value of the metals for these WEE can be estimated at USD 96 million, USD 5.1 million, and USD 11 million. Therefore, this is a huge opportunity for local companies dealing with WEE recycling.

Table 4 Mass balance and estimated value of metals in WEE (WPCBs, WHDs and WLIBs) for southern Poland in 2024 (average values based on data from three companies located in the Silesian Voivodeship dealing with the collection of WEE)

Description	**Unit**	**Value for**		
		WPCBs	**WHDs**	**WLIBs**
Mass of WEE collected per 1 million inhabitants of southern Poland	Mg/year	27.2	13.6	45.3
Mass of non-metallic product generated during WEE recycling per 1 million inhabitants of southern Poland	Mg/year	19.3	2.3	3.17 (plastics) 6.79 (organic materials)
Estimated value of metals in WEE per 1 million inhabitants of southern Poland	USD/year	2 499 669	134 737	287 863
Estimated value of metals in WEE collected in Poland	USD/year	96 080 394	5 178 930	11 064 661

RESEARCH ON RECYCLING OF WEE

The following section presents an overview of the research conducted by the authors of the paper in the field of WPCB, WHD and WLIB recycling.

In WPCB recycling, one of the most effective physical methods is electrostatic separation [15,16]. To do this properly, disintegration and grinding are required, preferably using a shredder and a knife mill at cryogenic temperatures [17]. Separation occurs as a result of differences in the surface charge accumulation capacity of the grains and is carried out without the use of process water. Separation results in a mixture of metals and separately ground composite parts. Due to the high purity of the products, the valuable metal mixture can be sold to local metal smelters, while the product consisting of non-metallic parts can be used as a filler in the production of composite materials [18].

In the investigated WHD recycling technology, both the initial mechanical shredding and the subsequent selective separation processes play a key role [19,20]. These steps enable the recovery of several material fractions with different compositions and industrial applications, namely neodymium magnets (NdFeB), aluminium, steel, printed circuit boards (PCB) and plastics. The metal recovery process of hard drives begins with mechanical shredding, allowing the disintegration of components and the release of embedded metals [19]. Then, as a result of granulometric classification and magnetic, gravitational, optical, and electrostatic separation, the following materials with grain sizes are separated [20]: a) neodymium magnets (3.150 mm), b) particles of aluminium, plastics, and printed circuit boards (25-3,15 mm), c) steel (>25 mm).

The pre-treatment process, which can be categorized into various steps such as discharge, dismantling, comminution, classification, separation, dissolution, and thermal treatment, is of essential importance, particularly in the cases of hydrometallurgical extraction and direct recycling of spent LIBs. The pre-treatment process has been shown to improve recovery efficiency and reduce energy consumption in subsequent recycling processes similar to mineral processing for extractive metallurgy [21,22]. The primary objective of the pre-treatment is to separate the various components, such as separators, current collectors, etc., from the black mass of the LIBs in a safe and effective manner [23]. After the pre-treatment process, further recycling of the black mass is carried out using the hydrometallurgical method.

CONCLUSIONS

The growing stream of WEE, driven by global demand for critical metals and concurrent digital and energy transitions, highlights both the urgency and the potential of eco-efficient recycling solutions. As demonstrated in this study, WEE such as printed circuit boards (WPCB), hard disk drives (WHD), and lithium-ion batteries (WLIB) contain valuable metals ranging from copper and precious metals (Au, Ag, Pd) to critical elements (Co, Nd, Li) that can be recovered with substantial economic and environmental gains. Metals with the highest relative supply risk and ADP are: Au, Pd, Pt for WPCB, Nd, Pr, Ce, Dy, Pd, Au for WHD, and Co, Li, Ni for WLIB. It should be noted that the estimated value of metals in 1 Mg of WPCB could be almost USD 92 thousand, while 1 Mg of WHD could give recoverable metals worth approximately USD 9,908, and 1 Mg of WLIB could give a potential metals value exceeding USD 6,351. To assess the profitability of recycling, investment and process costs must also be considered.

The annual mass of WPCB, WHD and WLIB collected per 1 million inhabitants of southern Poland is approximately 27.2, 13.6 and 45.3 Mg, respectively, and the estimated value of metals in them is approximately 2,499, 135 and 28 thousand USD/year, respectively, indicating a large financial potential for companies involved in WEE recycling.

Physical recycling methods such as shredding, grinding, electrostatic, magnetic, optical, and gravity separation complemented in the next step by hydrometallurgical or pyrometallurgical processes enable the recovery of high-value metals at low process costs, lower energy consumption, and limited environmental emissions, with the possibility of using plastics for the production of consumer goods.

REFERENCES

1. van Oers L, Guinée JB, Heijungs R. Abiotic resource depletion potentials (ADPs) for elements revisited—updating ultimate reserve estimates and introducing time series for production data. Int J Life Cycle Assess. 2020;25(2):294–308.
2. Recycling of metallic values from discarded tantalum capacitors - Shaila Mir, Nikhil Dhawan, 2023. [access 18.03.2025]. https://journals.sagepub.com/doi/abs/10.1080/25726641.2023.2177243
3. Periodic Table – Royal Society of Chemistry. [access 18.03.2025]. https://periodic-table.rsc.org/

4. Berger M, Sonderegger T, Alvarenga R, Bach V, Cimprich A, Dewulf J, i in. Mineral resources in life cycle impact assessment: part II– recommendations on application-dependent use of existing methods and on futuremethod development needs. Int J Life Cycle Assess. 2020; 25(4):798–813.
5. Kaya M. Recovery of Metals and Nonmetals from Waste Printed Circuit Boards (PCBs) by Physical Recycling Techniques. W: Zhang L, Drelich JW, Neelameggham NR, Guillen DP, Haque N, Zhu J, i in., redaktorzy. Energy Technology 2017 [Internet]. Cham: Springer International Publishing; 2017. s. 433–51. (The Minerals, Metals & Materials Series).http://link.springer.com/10.1007/978-3-319-52192-3_43
6. Exchange TLM. Lme. [access 18.03.2025]. Home | London Metal Exchange. https://www.lme.com/
7. Bankier.pl – Portal Finansowy – Rynki, Twoje finanse, Biznes. [access 18.03.2025]. https://www.bankier.pl/
8. Manhart A, Buchert DM, Degreif S, Mehlhart DG, Meinel J. Darmstadt & Accra, November 2015.
9. Habib K, Parajuly K, Wenzel H. Tracking the Flow of Resources in Electronic Waste - The Case of End-of-Life Computer Hard Disk Drives. Environ Sci Technol. 2015; 49(20):12441–9.
10. Ueberschaar M, Rotter VS. Enabling the recycling of rare earth elements through product design and trend analyses of hard disk drives. J Mater Cycles Waste Manag. 2015;17(2):266-81.
11. Rotter VS, Chancerel P, Ueberschaar M. Recycling-Oriented Product Characterization for Electric and Electronic Equipment as a Tool to Enable Recycling of Critical Metals. W: Kvithyld A, Meskers C, Kirchain R, Krumdick G, Mishra B, Reuter M, i in., redaktorzy. REWAS 2013. Cham: Springer International Publishing; 2013. s. 192–201. http://link.springer.com/10.1007/978-3-319-48763-2_21
12. Kaya M. State-of-the-art lithium-ion battery recycling technologies. Circular Economy. 2022;1(2):100015.
13. Horeh NB, Mousavi SM, Shojaosadati SA. Bioleaching of valuable metals from spent lithium-ion mobile phone batteries using Aspergillus niger. Journal of Power Sources. 2016; 320:257–66.
14. An L, redaktor. Recycling of Spent Lithium-Ion Batteries: Processing Methods and Environmental Impacts. Cham: Springer International Publishing; 2019. http://link.springer.com/10.1007/978-3-030-31834-5
15. Franke D, Suponik T, Nuckowski P, Dubaj J. Evaluation of the efficiency of metal recovery from printed circuit boards using gravity processes. Physicochem Probl Miner Process. 2021;57(4):63–77.
16. Marek, D., Franke, D., Kar, U., Suponik, T., & Siudyga, T. (2023). Evaluation of the use of flotation for the separation of ground printed circuit boards. Gospodarka Surowcami Mineralnymi - Mineral Resources Management. https://doi.org/10.24425/gsm.2022.140605
17. Suponik T, Franke D, Nuckowski P, Matusiak P, Kowol D, Tora B. Impact of Grinding of Printed Circuit Boards on the Efficiency of Metal Recovery by Means of Electrostatic Separation. Minerals. 2021; 11(3):281.
18. Franke DM, Suponik T, Siudyga T, Kar U. Evaluation of the use of flotation for the separation of ground printed circuit boards. Gospodarka Surowcami Mineralnymi - Mineral Resources Management; 2022; 38 (1); 171-188. 2022; https://journals.pan.pl/dlibra/publication/140605/edition/122474
19. Friebe P. Development of a prototype shredder for WEEE equipped with NdFeB magnets. Min. 2023, 2, 143-157, DOI:10.32056/KOMAG2023.2.6.

20. Friebe P. Przegląd literatury dotyczącej odzysku sproszkowanej mieszaniny stopu NdFeB z KOMEKO 2023, Przemysł Przyjazny dla środowiska. Konferencja naukowo-techniczna, Instytut Techniki Górniczej KOMAG, Gliwice 2023, 61-67, DOI:10.32056/KOMAG/KOMEKO2023.7, ISBN 978-83-65593-32-0.
21. Al-Thyabat S, Nakamura T, Shibata E, Iizuka A. Adaptation of minerals processing operations for lithium-ion (LiBs) and nickel metal hydride (NiMH) batteries recycling: Critical review. Minerals Engineering. 2013;45:4–17.
22. Zhao Y, Yuan X, Jiang L, Wen J, Wang H, Guan R, i in. Regeneration and reutilization of cathode materials from spent lithium-ion batteries. Chemical Engineering Journal. 2020; 383:123089.
23. Kim S, Bang J, Yoo J, Shin Y, Bae J, Jeong J, i in. A comprehensive review on the pretreatment process in lithium-ion battery recycling. Journal of Cleaner Production, 2021, 294:126329.

XVI International Mineral Processing
and Recycling Conference
28-30 May 2025, Belgrade, Serbia

DOI: 10.5937/IMPRC25674O

Original research article

GRAVITY CONCENTRATION OF FINE PARTICLES COMPLEX ORES-CONTAINING BARYTE USING LABORATORY-BUILT MINERAL JIG

David Oluwasegun Afolayan[1#], 0000-0002-7274-0222,
Adamu Hassan Abubakar[2], 0000-0001-7878-8406,
Samuel Olumide Ogunmodimu[3], 0000-0001-7186-7005,
[1]Mechanical Engineering Department, African University of Science and Technology, Abuja, Nigeria
[2]Materials Science and Engineering Department, African University of Science and Technology, Abuja, Nigeria
[3]Energy and Minerals Engineering Department, Pennsylvania State University, PA, USA

ABSTRACT – This study uses environment-friendly and indigenous processes to liberate, separate and recover barite from gangue minerals. Barite ores were randomly selected, comminuted, screened, characterized, and beneficiated using a laboratory-built mineral jig. The effect of mineral liberation on separation efficiency, recovery, and yield was examined. The specific gravity of the barite ores was increased from 3.97±0.0105 to 4.17±0.20 and from 4.00±0.0458 to 4.20±0.2 without the use of chemicals. Likewise, higher barite recovery and yield were observed. However, the separation efficiency of the jigging process was low due to middling (a complex particle consisting of barite and gangue minerals).

Keywords: Baryte Ores, Liberation Size, Lab-Scale Mineral Jig, Middling Particles, Drilling Fluid.

INTRODUCTION

Barytes are typically associated with silicates, carbonate, iron oxide, sulphide, and clay minerals [1–3]. Barytes can be liberated from non-barite minerals (gangue phases) in coarse or very fine fractions by gravity concentration, flotation, or leaching to increase the density and quality of the ore [3–5]. Baryte is easily liberated from other minerals when ground into fine particles within the liberation size range for the minerals of interest. Chemical leaching, froth flotation, and hydrostatic pressure for baryte recovery have been recommended and reported on a laboratory scale for fine particle processing, as the best alternative to jigging [2,3]. However, these emerging baryte processing methods are expensive and require materials and resources manufactured on a laboratory scale. Using chemicals such as frothers, collectors, depressants, and other industrial chemicals in large-scale barite processing is not sustainable. In Nigeria and Africa, artisanal and small-scale (ASS) mining dominate barite mining and processing. These miners cannot afford chemicals other than the usual barite processing method by

---

[#] corresponding author: dafolayan@staff.aust.edu.ng gravity separation. Jigging and other gravity separation methods are the most sustainable and widely used methods for barite processing.

Laboratory-scale mineral processing research involves optimizing jigging conditions and ore characteristics, and the effect of a dependent variable is measured over a range of other independent variables. Such an experiment is carried out using large quantities of research samples; in most cases, lab-size processing devices are unavailable. Baryte processing by jigging and tabling has been reported in the literature [6,9]. Jigging of baryte is usually carried out on coarse particle sizes to pre-concentrate valuable minerals (-841 + 90 µm) [9–11]. The jigging process is limited to coarse particle processing and cannot significantly improve the quality of baryte when the particle is liberated in fine-size fractions [4,8]. However, the recovery of barytes and other gangue minerals in ores-containing-barytes depends on the degree of liberation. Similarly, there are few studies on barite processing by jigging and tabling at different process conditions. These studies are carried out on coarse particles, usually at particle size ranges, where specific fractions of both barite and non-barite minerals are expected to be locked in the ores.

This paper presents the use of an entirely fabricated laboratory-built mineral jig (prototype) to process fine particles in complex ores containing baryte, iron, lead, and more than five (5) other minerals as impurities in the ores. It demonstrates a mineral jig with fully separated water and jigging columns pulsed by a rubber-end cap diaphragm and driven by a reciprocating device. The paper also discusses the beneficiation of barite ore (barite rocks) of particle sizes -75 µm, -106 µm, -150 µm, and -250 µm using the laboratory-built jig. The particle size was narrowed to examine the degree of liberation of baryte and non-baryte minerals, jig frequency and amplitude on barite recovery and yield, the recovery and rejection of gangue minerals, separation efficiency, and baryte quality (specific gravity).

EXPERIMENTAL

Baryte rocks were randomly selected from the Kumar barite mining site, crushed and ground by a laboratory jaw crusher and ball mill. The pulverized ore was screened, separated into different particle size ranges by a mechanical sieve shaker and processed using the laboratory-built mineral.

The recovery and yield of barite, the rejection of impurities (non-baryte minerals), and the separation efficiency of the jigging process are calculated and analysed using equations 1- 4.

Separation efficiency calculated based on the mineral to be separated (alumina).

$$Yield\ of\ the\ process:\ Y = \frac{(f-t)}{(c-t)} \times 100\% \tag{1}$$

Percentage of alumina in the feed (f), concentrate (c), and tailings (t): impurities.

$$Rejection\ of\ impurities:\ {R_t}^1 = 100 - Y\frac{c}{f} \tag{2}$$

$$Recovery\ of\ alumina:\ {R_c}^1 = 100 - {R_t}^1 \tag{3}$$

$$Recovery\ of\ other\ fractions\ of\ the\ feed:\ {R_c}^2 = \frac{Y(100-c)}{(100-f)} \tag{4}$$

Separation efficiency: $Z = R_c^{\,2} - R_c^{\,1}$ Higher separation efficiency, better separation process.

RESULTS AND DISCUSSION

Baryte Yield by Jigging Barite Ore

Figure 1a shows the yield of baryte from barite ore during the jigging process. Baryte ore of particle size less than 250 µm has the highest baryte yield. This outcome indicates that coarse ores have better mineral yield, as reported in previous work [6,9]. As jig frequency increases, the baryte yield of the jigging process varies across particle size fractions. A jig frequency of 115 RPM gave the best yield of baryte for particle size less than 106 µm, while the highest baryte yield of particle size fractions -75 µm and -150 µm is at 126 RPM. The coarse feed has good mineral yield at high and low jig frequency and amplitude. However, an optimum jig condition is required to increase barite yield for particles less than 150 µm. Optimum barite yield is attainable for large particle sizes at higher jig frequency (153 RPM) and lower jig amplitude (1.5 cm).

In contrast, higher amplitude (2.5 cm-3 cm) and lower frequency (115 RPM-126 RPM) are preferred for small-size baryte concentrate. This outcome agrees with conclusions from previous research [8,14]. Thus, baryte yield by jigging is size-dependent and is improved by optimizing jigging conditions.

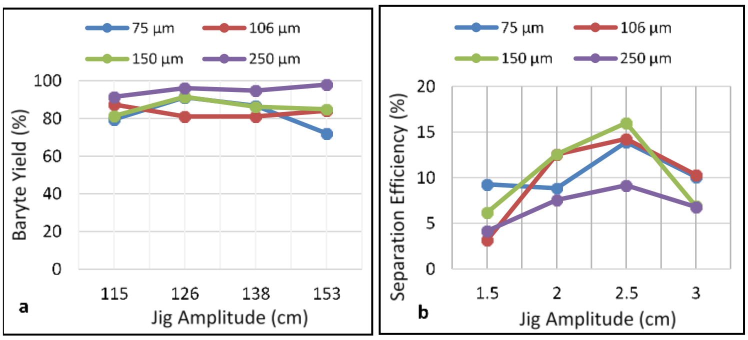

Figure 1 (a) Baryte yield at different jigging conditions and particle size; (b): Separation efficiency of baryte at different jigging conditions (water flow rate, jig frequency, and amplitude

Separation Efficiency of the Jigging Products

Figure 1b shows the separation efficiency of barite (value mineral) and non-baryte minerals in the ore across particle size ranges. Jig feeds of particles greater than 150 µm (-250 µm) have the least separation efficiency at the lowest jig amplitude. The separation efficiency increases as the jig amplitude increases and a sharp increase in separation efficiency is observed for jig concentrate of particle sizes less than 150 µm (-75 µm, 106 µm, and -150 µm). This implies that better separation was achieved at high amplitude, caused by high water pulsation, to allow effective differential settling based on particle size and density.

Effective differential settling does not translate to efficient mineral separation. Despite high mineral liberation for particle size less than 150 µm, the separation efficiency cannot be raised beyond 16% at optimum jigging conditions (126 RPM, 2.5 cm). This explains the consequence of a strong, cohesive force between fine particles, responsible for the middling formation and reduction in mineral separation. Also, high specific gravity was observed at the optimum separation efficiency of the ore (-150 µm). Optimum baryte separation depends on the fraction of baryte and gangue minerals free or fully liberated by grinding and screening baryte ore into different particle sizes.

Specific Gravity of Jigging Products

Figure 2 presents the specific gravities of jig tailings, feeds, and concentrates at different jigging conditions.

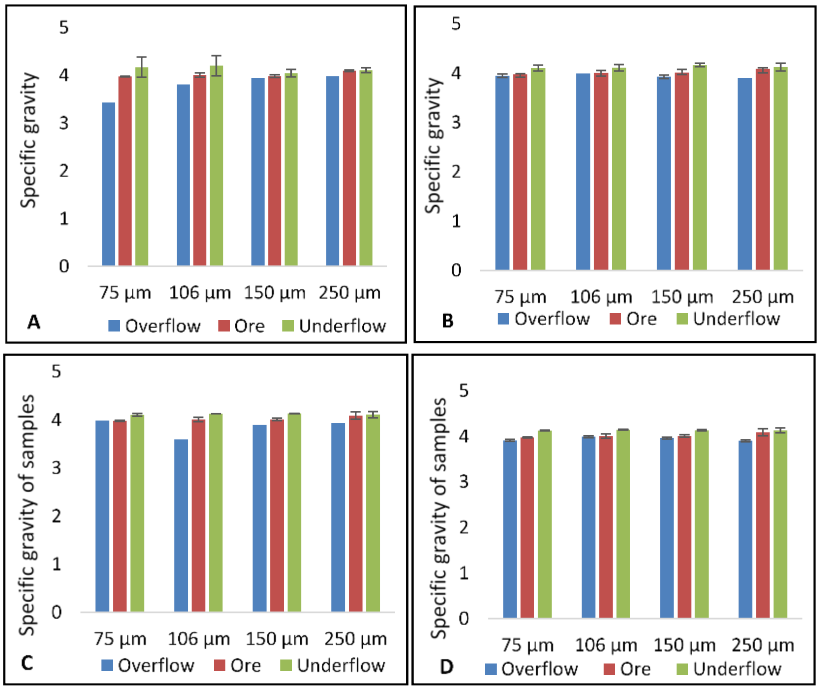

Figure 2 Specific gravities of jigging products and feeds at different jigging conditions and particle sizes (A): Water flow rate [369 cm^3/min], Jigging frequency [115 RPM], and Jig amplitude [3 cm]; (B): Water flow rate [369 cm^3/min], Jigging frequency [126 RPM], and Jig amplitude [2.5 cm]; (C): Water flow rate [369 cm^3/min], Jigging frequency [138 RPM], and Jig amplitude [2 cm]; (D): Water flow rate [369 cm^3/min], Jigging frequency [153 RPM], and Jig amplitude [1.5 cm]

A water-flow rate of 369 cm^3/min, jig frequency of 115 RPM, and jig amplitude of 3 cm contribute to the increase in specific gravities of barite ore of particle size less than 75 µm and 106 µm. The specific gravities increase from 3.97 to 4.17 and 4.00 to 4.20.

However, there was no significant increase in the specific gravities of ores of particle sizes greater than 106 µm (-150 µm and -250 µm) under the same jigging condition. The percentage improvement of the jigging process, based on the specific gravity, increases from 0.98 (-250 µm) to 4% (-150 µm) and 5% for finer jig concentrate (-75 µm and 106 µm). Thus, the recovery of quality baryte from its ores depends on the feed characteristics, jig amplitude, and frequency.

At a jig frequency of 126 RPM, the specific gravities (SGs) increase from 4.00 to 4.16 for ore of particle size less than 150 µm. Likewise, the specific gravity of barite ores (-250 µm) increases from 4.08 to 4.12. However, there was no significant increase in the specific gravities of smaller-size jig concentrates (-75 µm and -106 µm) at higher jig frequency (138 RPM and 153 RPM) as compared to the improvement observed at 115 RPM and high jig amplitude (2.5 cm-3 cm). Similarly, the specific gravities of the tailings/overflow are high and very close to that of the feed in all cases. This indicates that the barite of finer particles are lost in the tailing at high frequency.

The optimum jigging condition to increase the specific gravities of jig concentrate is size- and density-dependent. Baryte concentrates of fine particles (-75 µm) retain the dense materials and have the highest SGs at low jig frequency (115 RPM) and high jig amplitude (3 cm). In contrast, higher jig frequency (>115 RPM) are suitable for coarse particles jig feed of size less than 150 µm increases. However, the SGs of particles above 150 µm remain unchanged at high jig frequency. This is due to the high proportion of quartz in the coarse ore fraction, as observed in previous work. Hence, the high baryte yield of coarse jig concentrate does not translate to efficient mineral separation and recovery, and a significant increase in specific gravities.

Rate of Baryte Recovery and Rejection of Other Non-baryte Minerals in the Feed

Figure 3 presents the assaying of the ore and describes the baryte ore grade. Baryte mineral recovery is ≥ 74% for all size fractions. The recovery rate vary across particle size ranges and is affected by jigging conditions. Baryte ore of particle size greater than 150 µm (-250 µm) has the highest baryte recovery (value mineral). The rate of recovery increases from ~ 90% to ~ 99% for coarse jig concentrate (-250 µm) while the jig frequency increases from 115 RPM to 153 RPM. Similarly, the recovery rate of baryte in ore of particle size less than 150 µm increases from 79% to ~ 94% at a jig frequency of 126 RPM. Although the recovery of coarse ore deposits is high, the rejection of impurities is low, and more undesired minerals are retained within the jig concentrate. This indicates that complex particles containing one or more gangue minerals associated with the value minerals exist in the slurry and affect the sharpness of mineral separation during jigging.

Beyond the optimum jigging condition, the recovery dropped for all materials of different particle sizes. Likewise, the number of impurities (undesired minerals) retained in the jig concentrate increases. The recovery for fines (-75 µm, -106 µm, and -150 µm) is high, and the undesired minerals are less retained in the jig concentrate than in the coarse jig concentrate. It is important to note that baryte recovery or yield is affected by the liberation size of the valuable mineral, the quantity of middling (i.e., composite particles containing barite still locked with one or more non-barite minerals), and jigging conditions. Thus, the recovery of value minerals is improved at optimum jigging conditions for each particle size range.

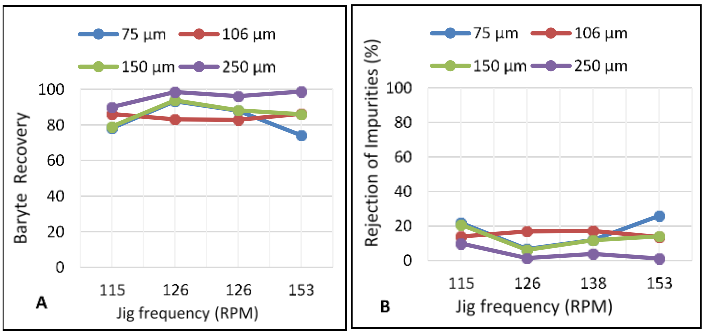

Figure 3 Rate of baryte recovery and rejection of other non-baryte minerals in the feed (A): percentage recovery of barite during jigging, and (B): removal of non-barite minerals and other light-weight minerals from the ore

Optimum Jigging Conditions to Increase Specific Gravities (SGs) of Jig Concentrates

The best values are 4.17 and 4.20 for fine baryte ores (-75 µm and -106 µm), obtained at the jig frequency of 115 RPM and jig amplitude of 3 cm. However, coarse jig concentrates (-150 µm and -250 µm) have lower SGs (4.10 and 4.05) at low jig frequency (115 RPM), as shown in Figure 4.

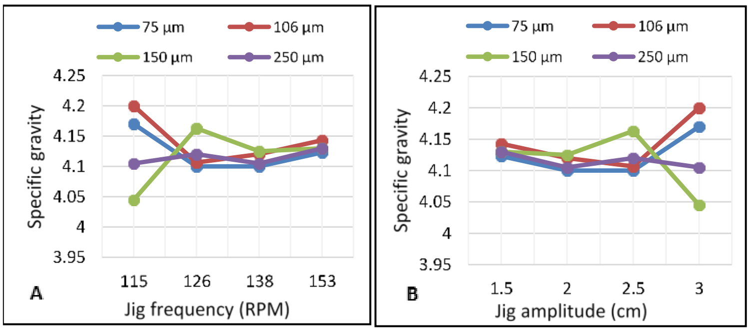

Figure 4 Specific gravities of jigging products as a function of (a): jig amplitude, and (b): jig frequency

Optimum specific gravities of 4.16 and 4.14 were achieved at jig frequency of 126 RPM and 158 RPM for coarse jig concentrates of particle size less than 150 µm and 250 µm. This implies that the small particle size ore requires lower jig frequency (fewer cycles) and maximum displacement of solids to allow differential settling of solid under gravity. This agrees with conclusions from previous works on baryte jigging [1–5]. However, the quality of the value mineral (specific gravity) in -250 µm size fraction cannot be increased beyond 4.13, which is far below the requirement of a weighting agent in oil drilling mud. Hence, increasing jig frequency at a jig amplitude of 2.5 cm helps improve the specific gravities (SGs) of the coarse jig concentrates (-150 µm and -250 µm).

CONCLUSION

This study assessed the efficiency of locally fabricated mineral jigs for barytes processing in artisanal and small-scale mineral processing. It also indicated that fine particles-complex barite ores can be processed, and narrowing the particle size range increases the separation and recovery of barite mineral and other non-barite minerals in barite ore. While the mineral jig performed better for coarse particle size range in agreement with previous works on barite, fine jig concentrates show better separation efficiency and retain fewer undesired minerals (impurities).

A laboratory-built mineral jig is capable of small-scale processing of baryte ore as a weighting material in oil drilling mud. However, the sharpness of mineral separation was limited due to middling during jigging. Stage-wise or step-wise jigging of barite ore is recommended to ensure re-jigging of concentrate, recovery of value minerals in the tailings, and removal of gangue minerals from the concentrate.

The use of a high-intensity and high-shear agitator within the jigging column to disperse or break aggregates of sticky particles in slurry during jigging will help reduce the influence of middling and improve the separation efficiency of value minerals during barite jigging. These devices can be incorporated into the laboratory-built design without depending on imported processing equipment for barite processing.

ACKNOWLEDGEMENT

The authors appreciate the research funding the Regional Scholarship Innovation Fund (Rsif) – Rsif/AUST/JIRA 005 provided. Also, the research support provided by research collaborators at Pennsylvania State University is deeply appreciated.

REFERENCES

1. Mgbemere, H.E.; Hassan, S.B.; Sunmola, J.A. Beneficiation of Barite Ore from Azara in Nassarawa State , Nigeria , using Froth Flotation. 2011, 0, 43–48.
2. Mgbemere, H.E.; Obidiegwu, E.O.; Obareki, E. Beneficiation of Azara barite ore using a combination of jigging, froth flotation, and leaching. Nigerian Journal of Technology 2018, 37, 957–962, http://dx.doi.org/10.4314/njt.v37i4.14.
3. Nzeh, N.S.; Hassan, S.B. Gravity Separation and Leaching Beneficiation. Global Journal of Researches in Engineering 2017, 17, 41–46.
4. Molaei, N.; Razavi, H.; Chehreh Chelgani, S. Designing different beneficiation techniques by Taguchi method for upgrading Mehdi-Abad white barite ore. Mineral Processing and Extractive Metallurgy Review 2018, 39, 198–201, doi:10.1080/08827508.2017.1399889.
5. Raju, G.B.; Ratchambigai, S.; Rao, M.A.; Vasumathi, N.; Kumar, T.V.V.; Prabhakar, S.; Rao, S.S. Beneficiation of barite dumps by flotation column; lab-scale studies to commercial production. Transactions of the indian institute of metals 2016, 69, 75–81.

XVI International Mineral Processing
and Recycling Conference
28-30 May 2025, Belgrade, Serbia

DOI:10.5937/IMPRC25681S

Original research article

PRELIMINARY INVESTIGATION ON NIGERIAN LITHIUM ORES FOR EFFICIENT LITHIUM OXIDE EXTRACTION

Olajuyi Seun Isaiah[1], 0000-0002-7371-4210,
Afolayan David Oluwasegun[2#], 0000-0002-7274-0222,
Ogunmodimu Samuel Olumide[3], 0000-0001-7186-7005,
[1]Materials Science and Engineering Department, African University of Science and Technology, Abuja, Nigeria
[2]Mechanical Engineering & Materials Science and Engineering Department, African University of Science and Technology, Abuja, Nigeria
[3]Energy and Mineral Engineering Department, Pennsylvania State University, PA, USA

ABSTRACT – This paper assesses the compositions of the lithium-rich minerals and the quantity of extractable lithium oxide in the minerals. The x-ray diffraction (XRD) shows 17% - 34% of spodumene and 9% to 30% of lepidiolite. Similarly, atomic absorption microscopy (AAS) indicates that the lithium-rich minerals contain 0.820% - 3.051% and 0.040 - 2.395% of lithium oxide (Li_2O). Further results confirm the presence of lithium-rich minerals in Nigeria, and a high quantity of lithium-rich minerals suggests that high lithium oxide can be extracted. This information is useful for miners, mining and mineral processing industries, and investors in lithium for different industrial applications.

Keywords: Lithium-Rich Minerals, Diluents, Mineralogy, Lithium Oxides.

INTRODUCTION

Lithium is one of the world's most sought-after minerals/metals in 2024, and Nigeria is not left out [1]. In the past year, there has been a notable and abrupt escalation in the activities related to the exploration and extraction of Lithium ore, primarily attributed to the surge in demand stemming from technological advancements [2]. This demand has directly contributed to the heightened interest and efforts in the mining sector. Several sources of lithium have been discovered and explored. However, very little is said about the global lithium deposits. For instance, little is known about the quality and mineralogical composition of lithium-rich minerals in Nigeria. Similarly, the African lithium deposits are poorly documented and reported despite massive mineral extraction and processing in Nigeria and several other Sub-Saharan African countries [3, 4, 5]. Considering the potential of lithium for the green energy transition and energy storage technologies, the knowledge of the reserve estimates of lithium deposits in Africa is critical to meeting the global demands for lithium.

[#] corresponding author: dafolayan@staff.aust.edu.ng

Lithium metal was discovered in 1817 by Johan Arfvedson. It is a silver-white, light metal with an atomic weight of 6.93 and does not occur naturally in metallic form owing to its reactivity with air [6]. Lithium has excellent properties and is considered a battery element. Typically, lithium has low standard reduction potential, thus making it the lightest metal for high density, high-voltage cell applications. The work of Caprara et al. [7], 2023 showed that lithium may exist in oxide form under the earth as a lithium-rich mineral [7]. These minerals include spodumene, lepidolite, petalite, amblygonite, cookite, and zinnwaldite. Similarly, Dessemond et al. [6] reported that in addition to the lithium-rich minerals, quartz, feldspar, and mica interlock between mineral grains and occupy a more significant portion of the lithium-bearing minerals [6].

Lithium is a vital raw material for energy applications. Lithium may exist as lithium oxide in lithium-bearing minerals, and the quality of the ores depends on the percentage of lithium oxide. Li-bearing minerals are classified based on the percentage of lithium oxide. In a typical lithium run-of-mine, the percentage of lithium-rich minerals varies across different locations within the deposits as the percentage of lithium oxide (Li_2O).

While it is expected that a high percentage of lithium-bearing minerals will translate to high lithium oxide in the mineral, the variation in the quality of mineral deposits or veins depends on several factors. This includes the distribution of lithium-mineral grains within the matrix of the associated minerals, the geology of the deposits and the elemental composition of the lithium ores.

This paper assesses the compositions of the lithium-rich minerals and the quantity of extractable lithium oxide in them using a combination of X-ray diffraction (XRD) and atomic absorption microscopy (AAS). It examines the elemental composition of two different lithium-bearing minerals (spodumene and lepidolite) and analyses the geological characteristics of lithium deposits within Nigeria.

EXPERIMENTAL

Sample Preparation

Twenty (20) randomly sampled lithium ore were picked from two major lithium mining sites in Nigeria (Nasarawa State and Ekiti State), ground into fine particles (< 75 µm) and analyzed using x-ray diffraction (XRD) and atomic absorption microscopy (AAS). The study adopts a multidisciplinary approach involving compositional analysis, mineralogical identification, and comparative evaluation.

Analysis of Lithium Ores

Atomic Absorption Microscopy (AAS) Analysis of Lithium Ores

The samples were pulverized, sieved to 75 µm and mixed with Na_2CO_3 (1:1) in a platinum crucible. The mixture was heated in a furnace at 1000 ^{o}C for 1 hour, cooled and dissolved in HCl. The solution was filtered and analyzed using atomic absorption microscopy (AAS) (Thermo-Scientific 3000 Series). The device was calibrated with deionized water, and the filtrate was analyzed using a lithium cathode lamp following standard procedures.

X-ray Diffraction (XRD) Analysis of Lithium Ores

The samples were pulverized using laboratory mortar, sieved to 75 µm, and fed into the X-ray diffraction (XRD) sample holder. X-ray diffractometer Thermo Scientific Model (ARL'XTRA X-Ray and serial number 197492086) was used for the analysis. The samples were inserted into the machine and analyzed at d-spacing appropriate to diffract x-rays. Similarly, the Cu cathode base was used on a reflection-transmission spinner (Theta-Theta setting) and a 2ϴ starting position from 0° and ending at 70°. The file of d-spacing available in the International Center for Diffraction Data (ICDD) and PDF2 software were used to match the x-ray diffraction peaks.

Data Integration, Analysis and Validation

The compositional and mineralogical data were integrated into the study to evaluate the relative abundance of lithium-bearing minerals (spodumene and lepidolite) and the dilutive effects of non-lithium phases like quartz, muscovite, and albite. Similarly, the variation of lithium oxide in the minerals was examined using the principal component analysis (PCA) and cluster analysis based on the composition and mineralogy of ores. Further analysis of the preliminary findings on the Li_2O content, mineralogy, the presence of dilutive phases, and the quantity of the extractable lithium from the ores were validated with existing literature and industry standards to develop a comprehensive framework for characterizing lithium ores, assess resource utilization and develop extraction strategies.

Testing of Research Hypothesis

The analyzed data were used to test the set research hypothesis (RH) and respond to the research question (RQ).

RQ: Do high lithium-rich minerals in lithium-containing rocks produce higher Li_2O?

RH: High lithium-rich rock minerals are responsible for higher Li_2O in rocks?

RESULTS AND DISCUSSION

Figure 1 compares spodumene and Li_2O fractions, showing that higher spodumene levels often correspond to higher Li_2O fractions. Nevertheless, this correlation does not manifest uniformly across all examined samples. By observing the bars in the graphs, where spodumene levels are highest, Li_2O fractions are also generally elevated. However, there are exceptions where high spodumene does not translate to a correspondingly high Li_2O fraction—of the 10 samples analysed using XRD and AAS, eight samples representing 80%, followed this trend. This indicates that higher spodumene content indicates higher Li_2O content. Also, this implies an 80% chance of higher Li_2O in ores containing lithium when the lithium-rich minerals are high. Hence, XRD analysis can provide relevant information for preliminary economic decisions required in mining and processing when the cost of further analysis is exorbitant or access to analytical devices is limited.

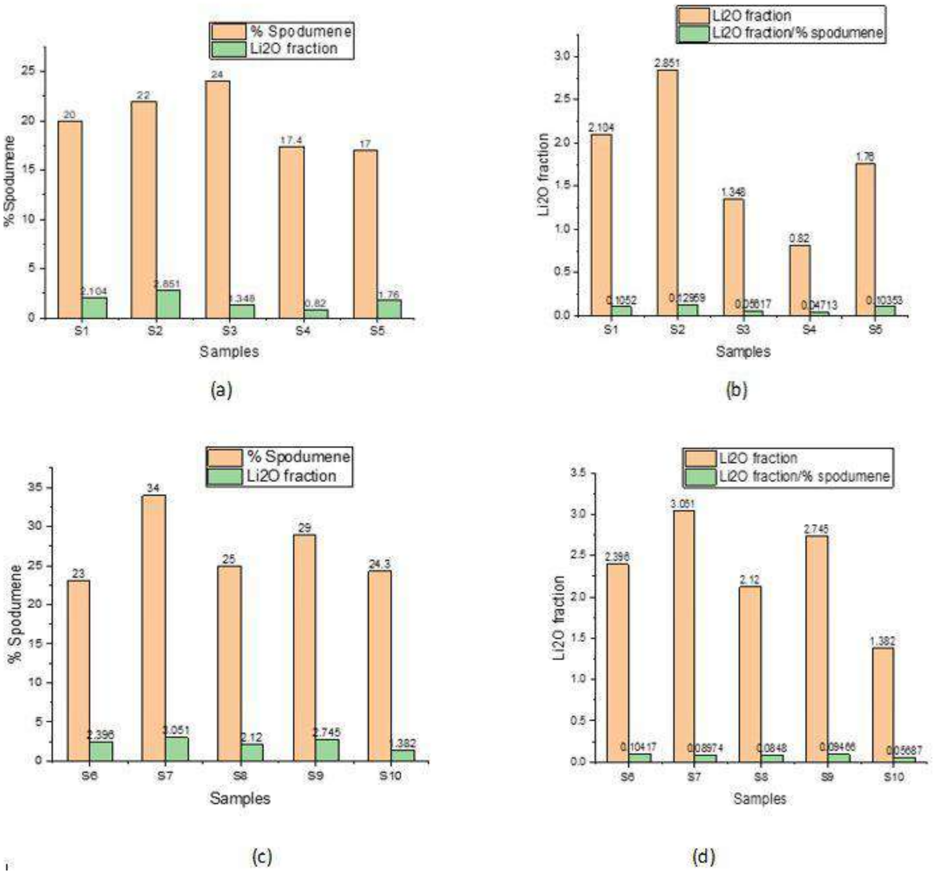

(a) (b)

(c) (d)

Figure 1 Quantity of Lithium-rich Mineral and Lithium oxide in Lithium ores. (a & b) comparison between the percentage of the lithium-rich mineral in the ores and the percentage of lithium oxide present in each mineral, (c & d) lithium oxide-to-lithium mineral ratio for Spodumene ores

Figure 2 shows the correlation measure between the lithium-rich mineral (lepidiolite) and the quantity of lithium oxide present in the lithium ores. Generally, a high lithium-rich mineral (lepidolite) does not translate to high lithium oxide for lepidolite. This outcome is anticipated as there is a wide dispersion of lithium oxide in lepidolite, resulting in low lithium oxide. Similarly, the literature has shown that lepidiolite is a Li-bearing clay mineral with a low Li2O grade. Typical lepidolite run-of-mine contains 1-2% Li2O, while the concentrate contains 2-3.5%. In contrast, the % Li2O in lepidolite is relatively low compared to typical lepidolite run-of-mine, except sample S5, which has a high % Li2O comparable to lepidolite concentrate. While some instances of elevated lepidolite correspond to a relatively high Li2O fraction, there are multiple cases where high lepidolite levels do not translate to a high Li2O fraction. This suggests that while lepidolite confirms the presence of Li2O formation, other factors or limitations might impact the Li2O yield, weakening the direct relationship between the quantity of the minerals in the ores and the extractable lithium oxide.

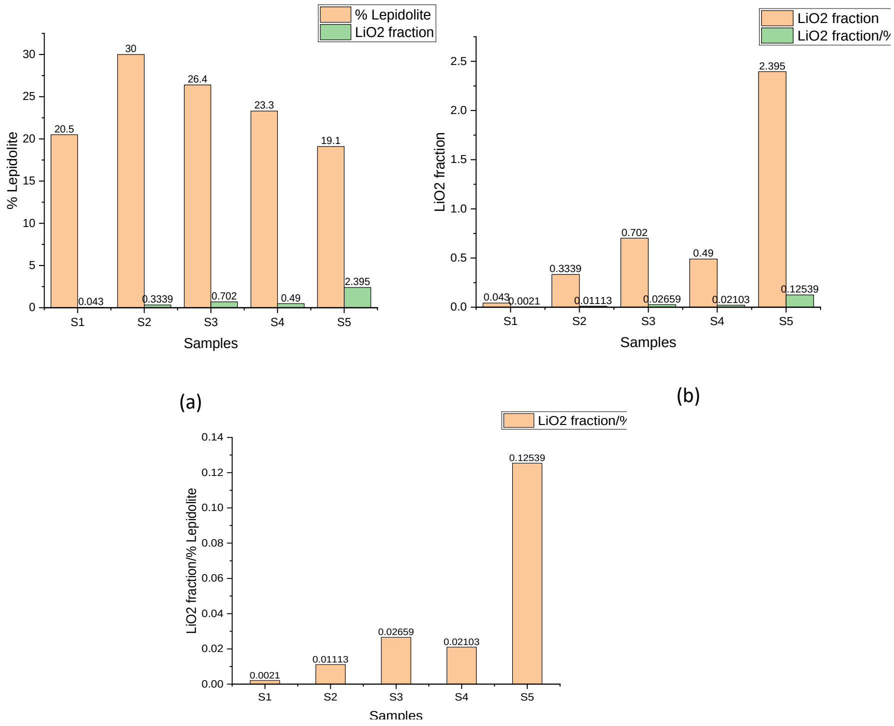

(a)

(b)

(c)

Figure 2 Quantity of lithium-rich mineral and lithium oxide in lithium ores (a & b) comparison between the percentage of the lithium-rich mineral in the ores and percentage of lithium oxide present in each mineral, (c) lithium oxide-to-lithium mineral ratio for Lepidolite ores

Figure 3 shows the lithium-rich minerals and other mineral phases in the lithium ores. The non-lithium mineral phases in the ore dilute the overall lithium oxide (Li2O) content. Quartz (SiO_2) dominates non-lithium mineral phases as indicated by its high-intensity peaks (at 2Ө =26.90o). This shows that quartz is the major diluent in lithium-containing rocks, contributing significantly to the overall silica content without increasing the quantity of lithium oxide in the ores. Other diluents in the lithium ores include Albite ($NaAlSi_3O_8$) and Muscovite ($KAl_2(AlSi_3O_{10})(OH)_2$). These contribute Na2O, K2O and alumina (Al2O3) to the composition of the ores. Similarly, Figure 3 shows that quartz, albite and muscovite (three non-lithium-rich minerals) coexist with spodumene, as it was widely reported in the literature, thereby reducing effective lithium concentration.

The fraction occupied by non-lithium-rich mineral phases (66 – 83%), such as quartz, albite, and muscovite, demonstrates the dominance of the mineral phases in contrast to spodumene. This implies that, despite spodumene, the overall lithium content is reduced due to the dominance of these non-lithium-bearing phases.

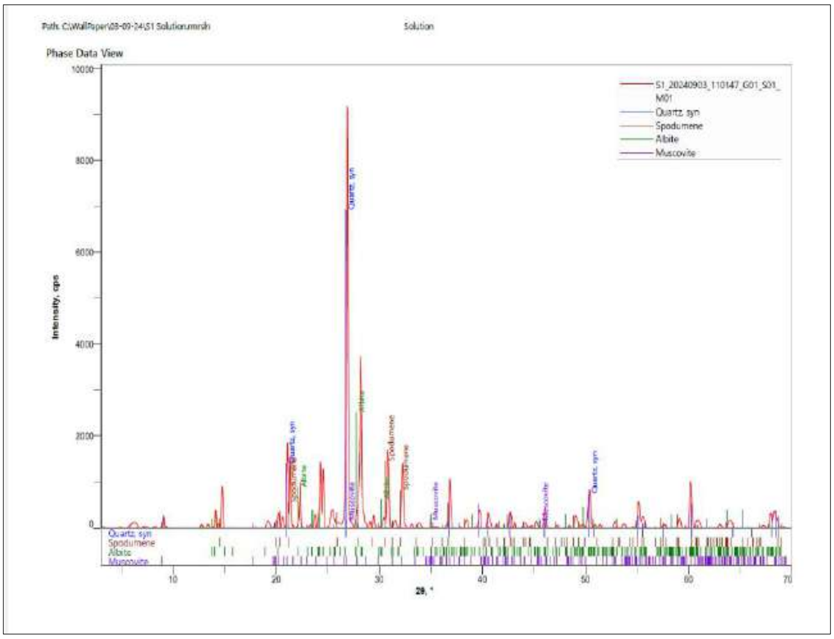

Figure 3 X-ray Diffraction (XRD) for Lithium Ore (Nasarawa State, Nigeria)

While impurities (undesired minerals or gangue) reduce the quality of lithium oxide in the ores, the ores can be concentrated to reduce non-lithium-rich mineral phases and increase the percentage of lithium oxide. However, preliminary analysis of the ores can provide helpful information on the quantity of extractable lithium from the lithium-rich mineral phase (spodumene) prior to the extraction and concentration of the ores.

As observed in Figure 3, Table 1 shows the chemical compositions of the lithium ores. High concentrations of silica (SiO_2), alumina (Al_2O_3) in some samples, and sodium oxide (Na_2O) in lithium ores contribute to the overall composition of the ores. The lithium-rich mineral (spodumene) is associated with a significantly high silica-to-alumina ratio (6.22 – 85.11) due to a relatively low percentage of alumina. Similarly, Na_2O and Fe_2O_3 contribute significantly to the high non-lithium mineral phase in the lithium ores. The presence of non-lithium mineral phases in the ores and their association with lithium oxide will affect the liberation, separation and recovery of design a process flow-sheet for efficient lithium extraction from the ores.

Table 1 Atomic Absorption Spectroscopy (AAS) Analysis of Lithium Ores from Nasarawa State, Nigeria

Samples	**S1**	**S2**	**S3**	**S4**	**S5**
Oxides					
SiO_2	77.01	79.11	78.13	85.11	81.57
Al_2O_3	12.38	ND	0.14	ND	0.46
SO_3	ND	ND	0.3	ND	0.94
P_2O_5	ND	ND	ND	ND	ND
Na_2O	0.12	13.28	14.98	8.5	10.46
K_2O	2.64	ND	ND	1.2	ND
MgO	0.7	0.5	ND	0.2	ND
CaO	0.07	0.1	ND	ND	ND
TiO_2	0.3	0.4	0.28	0.57	0.52
MnO	0.45	2.75	0.2	0.19	0.37
Fe_2O_3	3.52	ND	3.22	12.51	2.81
Li_2O	2.104	2.851	1.348	0.82	1.76
L.O.I	0.7	0.8	1.2	0.7	0.9

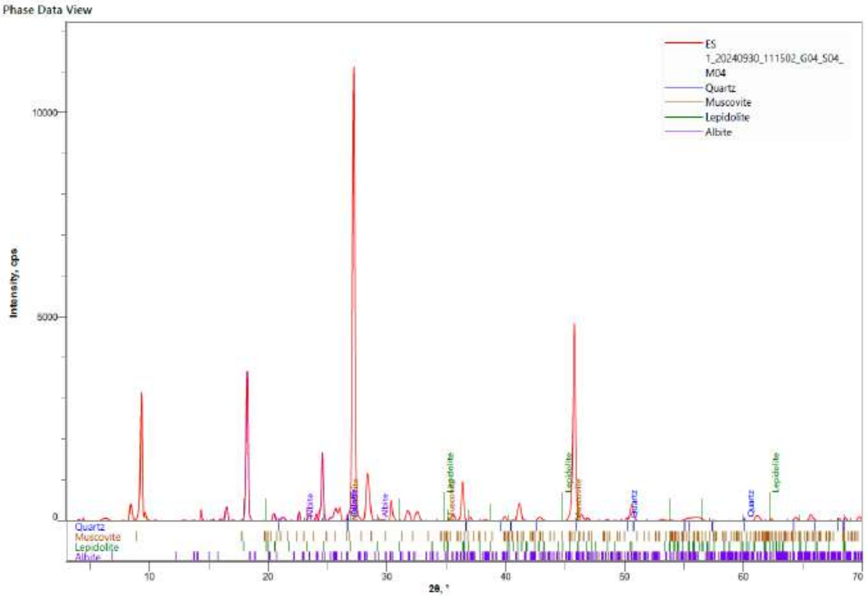

Figure 4 X-ray diffraction (XRD) for Lithium Ore (Ijero-Ekiti, Nigeria)

Figures 3 and 4 show the mineralogy of lithium ores and describe the crystalline structure of the minerals contained in the ores. The figures also present additional information on the structure of the ores at atomic scale. Both Figures identify three non-lithium mineral phases associated with the lithium-rich mineral phases (spodumene and lepidiolite). Most XRD peaks are thin and short, except those representing quartz. The information presented by the XRD results agrees with the chemical compositions of the elements in oxides and is relevant for mineral separation and recovery. As observed in lithium-caesium-tantalum (LCT) pegmatites, an assemblage of K-feldspar, quartz, muscovite and albite dominates the lithium ores. This detail describes the mineralogy of lithium ores and provides other relevant information for lithium extraction and process optimisation for enhanced lithium extraction.

Table 2 AAS Analysis of Lithium Ores (Ejero Ekiti, Nigeria)

Samples **Oxides**	S1	S2	S3	S4	S5
SiO_2	62.25	56.34	54.02	56.78	71.33
Al_2O_3	26.25	36.15	37.39	35.07	20.74
SO_3	ND	ND	0.2	ND	ND
P_2O_5	ND	ND	0.98	ND	ND
Na_2O	1.59	0.2	0.6	0.09	0.5
K_2O	4.34	1.08	1.06	1.4	1.09
MgO	ND	ND	ND	ND	ND
CaO	ND	ND	ND	ND	ND
TiO_2	0.3	0.4	0.28	0.57	0.52
MnO	0.15	0.28	0.14	0.3	0.41
Fe_2O_3	1.17	0.76	0.69	0.9	1.33
Li_2O	0.043	0.334	0.702	0.49	2.395
L.O.I	4.2	4.7	5.3	4.7	2.2

Tables 1 and 2 show the chemical composition/mineralogy of the lithium ores randomly selected from Ejero Ekiti in Nigeria. The percentage of lithium oxide (Li_2O) ranges from 0.04 to 2.395%. The quantity of Li_2O in most samples is below 1%, except S5. Low Li_2O can be traced to a low silica-to-alumina ratio due to relatively high alumina within the muscovite and albite mineral phases, as shown in Figures 2 and 3. Tables 1 and 2 and Figures 3 and 4 confirm relatively low-grade lithium ores, dominated by three non-lithium mineral phases as diluent of the lithium-bearing deposits.

CONCLUSION

The study confirmed the presence of lithium ores in Nigeria and the quantity of extractable lithium oxides. Three densely dominated non-lithium mineral phases were identified as significant diluents of the lithium-rich minerals. While these mineral phases in the lithium ores lower the percentage of lithium oxide in the ores, the value is comparable to lithium ore deposits in countries where lithium processing is reported on a large scale. The preliminary information on the mineralogy, atomic arrangement of the ores, and crystal structure of the minerals is useful for the extraction and optimisation of lithium extraction in Nigeria.

ACKNOWLEDGEMENT

The authors appreciate the Regional Scholarship Innovation Fund (Rsif) for the PhD scholarship offered to the first author. The authors are also grateful for the matching fund provided by Dr. Afolayan David Oluwasegun of the African University of Science and Technology, Abuja, Nigeria and Professor Ogunmodimu of Pennsylvania State University*, PA, USA.*

REFERENCES

1. Abdulfattah, F., Bwala, M. D., Alabi, O. O., Sayyadi, M. G., & Hassan, S. B. (2023a). Characterization and Beneficiation of Nigerian Lithium Ore: An Overview. In T. Ouchi, K. Forsberg, G. Azimi, S. Alam, N. R. Neelameggham, H. Kim, A. A. Baba, H. Peng, & A. Karamalidis (E. Editor), Rare Metal Technology 2023, Springer Nature Switzerland, 239-246.
2. Sahoo, S. K., Tripathy, S. K., Nayak, A., Hembrom, K. C., Dey, S., Rath, R. K., & Mohanta, M. K. (2024). Beneficiation of lithium bearing pegmatite rock: A review. Mineral Processing and Extractive Metallurgy Review, 45(1), 1–27.
3. Han, Y., Bedrossian, S., Fraser, R., Bellino, M., & Bibienne, T. (2023). Lithium-Ion Batteries Recycling Trends and Pathways: A Comparison. In Metallurgy and Materials Society of the Canadian Institute of Mining Metallurgy and Petroleum (CIM) (Ed.), Proceedings of the 62nd Conference of Metallurgists, COM 2023 (pp. 197–203). Springer Nature Switzerland, 197-203
4. Kavanagh, L., Keohane, J., Garcia Cabellos, G., Lloyd, A., & Cleary, J. (2018). Global lithium sources—Industrial use and future in the electric vehicle industry: A review. Resources, 7(3), 57.
5. Talens Peiró, L., Villalba Méndez, G., & Ayres, R. U. (2013). Lithium: Sources, Production, Uses, and Recovery Outlook. journal of The Minerals, Metals & Materials Society, 65(8), 986–996.
6. Dessemond, C., Lajoie-Leroux, F., Soucy, G., Laroche, N., and Magnan, J. F. (2019). Spodumene: The Lithium Market, Resources and Processes. Minerals, 9(6), 334.
7. Caprara, A. L. F., Durante, I., & Rissardo, J. P. (2023). The Intermittencies of Lithium. Journal of SAARC Psychiatric Federation, 1(2), 94–96.

XVI International Mineral Processing
and Recycling Conference
28-30 May 2025, Belgrade, Serbia

DOI: 10.5937/IMPRC25690B Original research article

ORIGIN, DEPOSITIONAL ENVIRONMENT AND MATURITY OF ORGANIC MATTER IN EOCENE COALS FROM TUNISIA

Anđelija Bogdanović [1#], 0009-0008-9984-4970,
Hassene Affouri[2], 0000-0002-9549-2524,
Ivan Kojić[3], 0000-0001-7737-1844,
Ksenija Stojanović[4], 0000-0002-5566-2648,
[1]Explozivi rudex d.o.o., Bor, Serbia
[2]University of Sfax, Faculty of Sciences, Sfax, Tunisia
[3]Innovative Centre of the Faculty of Chemistry, Ltd., Belgrade, Serbia
[4]University of Belgrade, Faculty of Chemistry, Belgrade, Serbia

ABSTRACT – The aim of this study was to determine the origin and geological history of coals from Tunisia, using organic geochemical approach. Five coal samples were examined. After bitumen extraction and maltene fractionation, biomarkers in aliphatic fractions were analyzed using gas chromatography-mass spectrometry (GC-MS). The precursor organic matter (OM) was mostly represented by terrestrial vegetation with evident marine influence. Coals were formed under suboxic to oxidizing conditions. The maturity of OM corresponds to late diagenesis/early catagenesis, indicating subbituminous coal rank.

Keywords: Coal, Origin and maturity of organic matter, Biomarkers, Gas chromatography-mass spectrometry.

INTRODUCTION

Coal is a heterogeneous organic substance of complex structure formed by the transformation of mainly plant remnant over the long geological time. Different types of coal vary in their composition, properties, and applications. Its composition and properties depend on precursor biomass, depositional settings and thermal maturity. Determination of the composition of biomarkers in the extractable organic matter of coal (bitumen) is significant for investigation in coal geochemistry. Biomarkers are compounds that almost fully retained structural similarity to their biological precursors. Therefore, biomarkers can indicate the sources and depositional environment of OM, as well as the intensity of diagenetic changes [1]. On the other hand, since biomarkers underwent isomerizations into thermodynamically more stable isomers, cracking and aromatization they are used for determination of the degree of maturity [1, 2].

The aim of this study was to identify biomarkers in Tunisian coals using GC-MS analysis and to estimate their origin, depositional conditions, and maturity based on biomarker's distributions.

[#] corresponding author: bogdanovic.andjelija@yahoo.com

EXPERIMENTAL

Five coal samples from Tunisia were pulverized and extracted using the Soxhlet method by a dichloromethane/methanol mixture (88:12, v:v). Bitumen was isolated and then separated into asphaltenes and maltenes by precipitation with *n*-heptane. Maltenes were separated into three fractions using column chromatography on silica as a sorbent. Aliphatic fraction was eluted with *n*-hexane, aromatic with the mixture of *n*-hexane/dichloromethane (7:3, v:v) and polar compounds (NSO fraction) with the mixture dichloromethane/methanol (1:1, v:v).

Aliphatic fractions were analyzed using an Agilent 7890A gas chromatograph coupled with an Agilent 5975C mass detector. An HP-5-MS capillary column (30 m × 0.25 mm) was used. Biomarkers were identified based on their mass spectra and retention times in total ion chromatograms (TIC) and characteristic ion fragmentograms (*m/z*): *n*-alkanes (*m/z* 71), steranes and diasteranes (*m/z* 217) and hopanes (*m/z* 191).

RESULTS AND DISCUSSION

Bulk Organic Geochemical Parameters

The results of bulk composition of studied coals are shown in Table 1. The obtained results indicate that the bitumen content in all samples is below 0.3 %, with a predominant share of asphaltenes and NSO compounds, indicating low-rank coal [3].

Table 1 Bulk composition of coals

	(%) in coal	(%) in bitumen		(%) in maltenes		
Sample	Bitumen	Asphaltenes	Maltenes	Aliphatic Fraction	Aromatic Fraction	Polar Fraction
MD_0	0.052	51.40	48.60	25.00	11.53	61.54
MD_1	0.057	68.64	31.36	27.00	13.51	62.16
MD_2	0.035	59.49	40.51	9.38	3.13	53.13
MD_6	0.299	85.40	24.60	31.82	19.32	36.36
MD_8	0.225	96.48	23.52	56.25	18.75	68.75

Biomarkers in aliphatic fractions

The following types of biomarkers were identified in aliphatic fractions: *n*-alkanes, alkenes, isoprenoid aliphatic alkanes (norpristane, pristane, and phytane), hopanes, steranes and diasteranes (Figure 1). It can be seen that *n*-alkanes are the most abundant biomarkers in the aliphatic fractions of all samples. Alkenes and isoprenoids are second in abundance, while polycyclic terpanes (hopanes) are present in smaller amounts. Steranes are present in the lowest concentrations and cannot be seen in the total ion chromatograms of aliphatic fractions. Parameters calculated from the abundances of *n*-alkanes and isoprenoids are shown in Table 2.

It can be seen that the maximum of *n*-alkanes is mainly at lower *n*-alkane homologues (C_{18}-C_{20}). The values of the CPI (Carbon Preference Index) [4] range from 0.71 to 1.10, indicating that the distributions of odd and even homologues are equal, or that in some samples even homologues predominate.

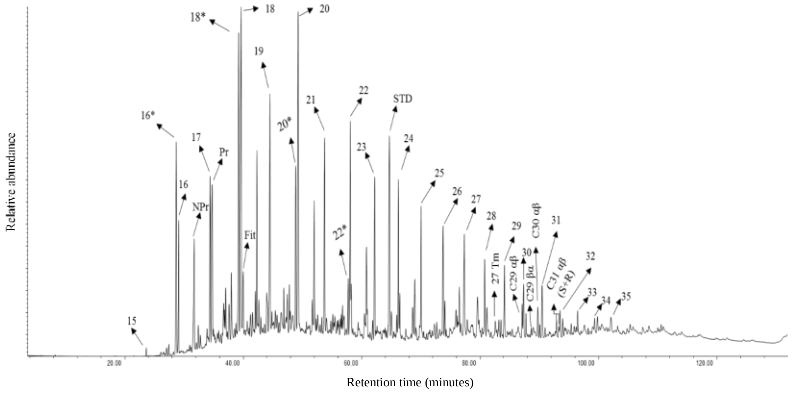

Figure 1 Total Ion Chromatogram (TIC) of the aliphatic fraction (sample MD0)

*The numbers correspond to the number of carbon atoms in *n*-alkane; * – alkene with the same number of carbon atoms as the nearest *n*-alkane; NPr – norpristane, Pr – pristane, Fit – phytane, STD – standard (deuterated tetracosane $C_{24}D_{50}$); C_{27} Tm – C_{27} 17α(H),22,29,30-trisnorhopane; αβ and βα indicate the configuration of hydrogen atoms at C-17 and C-21 in the C_{29}–C_{31} hopanes; R and S indicate the absolute configuration at C-22 in the C_{31} αβ hopane.

Table 2 Parameters calculated from the abundances of *n*-alkanes and isoprenoids

Sample	*n*-Alkane Maximum	CPI (C_{16}-C_{34})	Pr/Ph	Pr/*n*-C_{17}	Ph/*n*-C_{18}
MD_0	*n*-C_{18}	0.80	2.67	1.43	0.24
MD_1	*n*-C_{18}	0.88	2.96	1.18	0.23
MD_2	*n*-C_{20}	0.71	0.78	0.83	0.13
MD_6	*n*-C_{18}	1.06	2.49	2.69	0.83
MD_8	*n*-C_{31}	1.10	0.89	0.70	0.38

* *n*-Alkane Maximum – the most abundant *n*-alkane; $CPI_{17\text{-}33}$ – Carbon Preference Index calculated within the range of *n*-alkanes C_{16}-C_{34}, $CPI_{16\text{-}34} = 1/2 \times [\Sigma odd(n\text{-}C_{17} - n\text{-}C_{33})/\Sigma even(n\text{-}C_{16} - n\text{-}C_{32}) + \Sigma odd(n\text{-}C_{17} - n\text{-}C_{33})/\Sigma even(n\text{-}C_{18} - n\text{-}C_{34})]$ [7]; Pr/Ph = Pristane/Phytane.

Aliphatic isoprenoid alkanes pristane (Pr) and phytane (Ph) were identified in all samples. The Pr/Ph ranges from 0.78 to 2.96. The Pr/Ph for samples MD0, MD1, and MD6, is higher than 1 indicating oxidizing conditions in the sedimentation environment [5].

Parameters Pr/*n*-C_{17} and Ph/*n*-C_{18} are used to determine sample maturity. Also, the Pr/*n*-C_{17} ratio > 0.6 indicates terrestrial organic matter. In all samples, the ratio is higher than 0.6, suggesting prevalent terrestrial origin [6].

Polycyclic Alkanes of Sterane Type

In the aliphatic fraction of all samples, sterane biomarkers are present in the smallest amount compared to other types of compounds. In the ion fragmentograms (*m/z* = 217;

Figure 2) of all coal samples, the distributions and abundances of sterane biomarkers are similar.

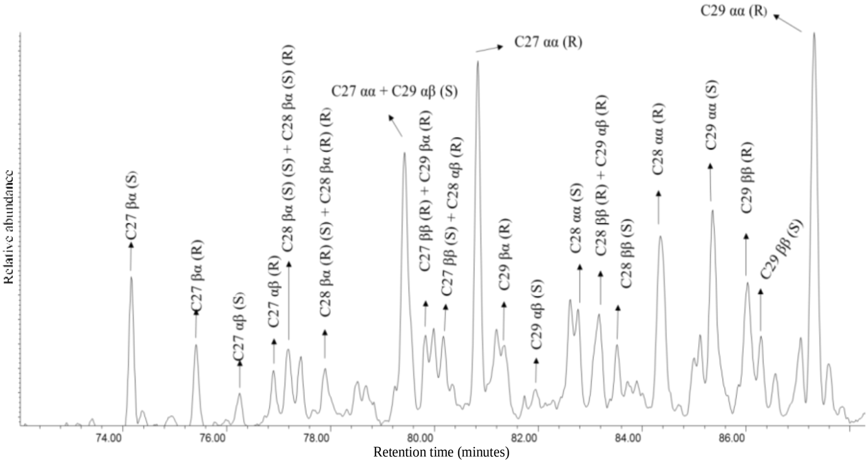

Figure 2 Distributions of steranes and diasteranes (*m/z* = 217) in coal samples (sample MD8)

*βα and αβ indicate configuration of hydrogen atoms at the C-13 and C-17 in diasteranes; S and R denote absolute configuration at the C-20 and C-24 in steranes and diasteranes; αα and ββ indicate configuration at C-14 and C-17 in 5α(H) steranes.

Data from Figure 2 indicate that content of regular (5α(H)14α(H)17α(H)20R) C_{28} sterane is the lowest in all samples (7.24-27.5 %). Biogenic precursors of C_{28} steranes originate from lacustrine environments. The percentages of regular C_{27} (32.40-47.64 %) and C_{29} (36.07-45.12 %) steranes are approximately equal. Precursors of C_{27} steranes are biogenic steroids most abundant in marine environments, while main precursors of C_{29} steranes are of terrestrial origin (higher plants). Evidence for a marine environment involves the presence of C_{30} steranes, which do not contain a methyl group on ring-A [7]. In the ion fragmentograms, *m/z* = 217 of all coal samples, the presence of C_{30} steranes does not appear or is present in such low quantities that it cannot be detected. Therefore, it can be assumed that the origin of the OM of coal samples is mostly terrestrial, with certain marine influence.

Polycyclic Alkanes of Terpane Type

The terpane distribution is characterized by the dominance of pentacyclic terpanes, i.e., hopanes C_{27}-C_{35}, except for the C_{28} homologue, which is absent. In the ion fragmentograms (*m/z* = 191; Figure 3) of all coal samples, the distributions and abundances of hopane biomarkers are similar.

A decreasing trend with the increase of number of carbon atoms followed by the $C_{35}(S)/C_{34}(S) \leq 0.70$ (Table 3) is indicative for suboxic-oxidizing depositional environment. This is in agreement with the Pr/Ph ratio which is > 1 in most samples (Table 2). The steranes/hopanes ratio (Ster/Hop; Table 3) is notably lower than 1, indicating terrestrial or microbiologically reworked organic matter [3]. In the hopane distribution, C_{30} homologue predominates (Figure 3). Besides aerobic bacteria, precursors of C_{30} hopane are diploptene (C_{30} hop-22(29)-en) and diplopterol (C_{30} hopan-22-ol) which occur in lichens, ferns and mosses [8].

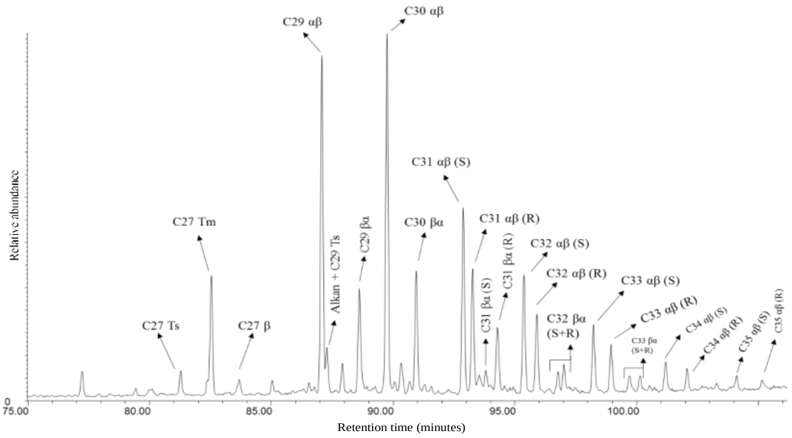

Figure 3 Distribution of hopanes (*m/z* = 191) in coal samples (sample MD0)

*α and β define the configuration at C-17 in C_{27} and hopanes; αβ and βα define the configuration at C-17 and C-21 in C_{29}–C_{35} hopanes and moretanes; R and S define the configuration at C-22 in C_{31}–C_{35} hopanes and moretanes; C_{27} Tm – C_{27} 22,29,30-trisnorhopane; C_{27} Ts – C_{27} 22,29,30-trisnorneohopane; C_{29} Ts – C_{29} 30-norneohopane.

Table 3 Source parameters calculated from the abundances of hopane biomarkers

Sample	% C_{31} αβ in ΣC_{31}-C_{35} αβ	% C_{32} αβ in ΣC_{31}-C_{35} αβ	% C_{33} αβ u ΣC_{31}-C_{35} αβ	% C_{34} αβ in ΣC_{31}-C_{35} αβ	% C_{35} αβ in ΣC_{31}-C_{35} αβ	$C_{35}(S)/C_{34}(S)$	Ster/Hop x 10^5
MD_0	42.69	28.59	16.24	8.27	4.19	0.50	1.29
MD_1	40.15	27.06	19.19	8.59	4.99	0.60	1.20
MD_2	36.89	28.44	14.25	12.57	7.83	0.62	5.67
MD_6	41.24	25.38	16.56	10.28	6.53	0.60	2.65
MD_8	38.96	25.73	16.95	10.39	7.97	0.70	2.17

*$C_{35}(S)/C_{34}(S)$ – ratio of C_{35} 17α(H)21β(H)22(S) hopane and C_{34} 17α(H)21β(H)22(S) hopane;
Ster/Hop = [Σ(C_{27}–C_{29})5α(H)14α(H)17α(H)(20S+20R)-steranes]/[Σ(C_{29}–C_{33})17α(H)21β(H)-hopanes].

Table 4 Maturation parameters calculated from the abundances of hopanes

Sample	Hopane Maximum	C_{30}mor/C_{30}hop	C_{31}αβ 22S/ (22S+22R)	Ts/(Ts+Tm)	C_{29}Ts/C_{29}hop
MD_0	C_{30} αβ	1.00	0.58	0.18	0.14
MD_1	C_{30} αβ	0.30	0.57	0.20	0.18
MD_2	C_{30} αβ	0.18	0.58	0.38	0.35
MD_6	C_{30} αβ	0.15	0.63	0.50	0.34
MD_8	C_{30} αβ	0.19	0.58	0.52	0.33

*C_{30}mor/C_{30}hop – ratio of C_{30} 17β(H)21α(H)-moretane and C_{30} 17α(H)21β(H)-hopane; C_{31}αβ 22S/(22S+22R) – ratio of C_{31} αβ 22S and 22R epimers.

The value of the C_{30}mor/C_{30}hop ratio is ≥ 0.15 (Table 4) indicating that OM does not reach maturity which corresponds to vitrinite reflectance (%Rr ~ 0.70-0.75). On the other hand, the ratio of thermodynamically more stable 22S and less stable 22R epimers of C_{31} (Table 4) reached the equilibrium value of 0.57-0.62 [3]. This result implies an initial stage of catagenesis (%Rr ~ 0.60).

CONCLUSION

Based on the organic-geochemical approach, the following conclusions can be drawn: 1) The examined coal samples are low-rank subbituminous coal; 2) Precursor organic matter was predominantly of terrestrial origin, with certain marine influence (fluvial-deltaic environment) and was deposited under suboxic-oxidizing conditions; 3) Maturity of OM corresponds to late diagenesis/early catagenesis.

ACKNOWLEDGEMENT

The financial support from the Ministry of Science, Technological Development and Innovation of Republic of Serbia (Contract number: 451-03-136/2025-03/200168 and 451-03-136/2025-03/200288) is greatly appreciated. The paper is related to the UN SDG 17.

REFERENCES

1. Vitorović, D., Jovančićević, B. (2016) *Fundamentals of Organic Geochemistry for Students of the Faculty of Chemistry*, University of Belgrade, Faculty of Chemistry, Belgrade. (in Serbian)
2. Životić, D. (2018) *Coal Geology*, University of Belgrade, Faculty of Mining and Geology, Belgrade. (in Serbian)
3. Peters, E., Walters, M., Moldowan, M. (2005) *The Biomarker Guide Vol. 2: Biomarkers and Isotopes in Petroleum Exploration and Earth History*. Cambridge University Press, Cambridge.
4. Evans, D., Bray, E. (1961) Distribution of n-paraffins as a clue to recognition of source beds. Geochimica et Cosmochimica Acta, 22, 2-15.
5. Didyk, B.M., Simoneit, B.R.T., Brassell, S.C., Eglinton, G. (1978) Organic geochemical indicators of palaeoenvironmental conditions of sedimentation. Nature, 272, 216-222.
6. Shanmugam, G. (1985) Significance of coniferous rain forests and related oil, Gippsland Basin, Australia. AAPG Bulletin, 69, 1241-1254.
7. Volkman, J.K. (2003) Sterols in microorganisms. Applied Microbiology and Biotechnology, 60, 496-506.
8. Bechtel, A., Sachsenhofer, R.F., Zdravkov, A., Kostova, I., Gratzer, R. (2005) Influence of floral assemblage, facies and diagenesis on petrography and organic geochemistry of the Eocene Bourgas coal and the Miocene Maritza-East lignite (Bulgaria). Organic Geochemistry, 36, 1498-1522.

XVI International Mineral Processing
and Recycling Conference
28-30 May 2025, Belgrade, Serbia

DOI: 10.5937/IMPRC25696D Original research article

THE INFLUENCE OF DIFFERENT FORMS OF MINERAL PROCESSING ON THE BIO-OXIDATION OF SULPHIDE MINERALS BEARING GOLD

Andriela Dutra Norberto de Oliveira[1], 0009-0000-3050-3395,
Luis Gonzaga Santos Sobral[2#], 0000-0001-6638-4201,
Armando Lucas Cherem da Cunha[1], 0000-0001-5246-2328,
[1]Federal University of Rio de Janeiro, Rio de Janeiro, Brazil
[2]Centre for Mineral Technology, Rio de Janeiro, Brazil

ABSTRACT – The presence of sulphide minerals, such as pyrite, chalcopyrite etc., can pose major challenges in the gold extraction processes, regardless of the downstream extraction route used, including cyanidation and the use of thiosulphate. These sulphides consume the reagents used in this above-mentioned extraction processes, leading to operational problems due to the ever-increasing ionic strength during the extraction processes, which impacts the solubility of the oxidizing agent, specifically dissolved oxygen, which is of paramount importance for extracting gold. This bio-oxidation process aims at solubilizing the aforementioned sulphide minerals, using indigenous autotrophic microorganisms, such as *Acidithiobacillus thiooxidans, Acidithiobacillus ferrooxidans* and *Leptospirillum ferrooxidans,* subsequently reducing the consumption of leaching agents used in gold extraction turning this process more efficient and cost-effective. In this study, different crushing operations were used, such as the use of jaw crusher, high pressure grinding rolls (HPGR) and high voltage pulse fragmentation (HVPF), aiming at determining the influence of these unit operations on the bio-oxidative process of the aforementioned sulphide minerals, as prior steps to the extraction of gold particles encapsulated in the matrices of the aforementioned sulphides, substantially reducing the consumption of gold leaching agents, thus avoiding the milling operation, which is the most expensive in extractive metallurgy.

Keywords: Bio-oxidation, Gold ore, Micro-organisms, Grinding operations.

INTRODUCTION

The extraction of metals from weathered ores or ores containing sulphide minerals initially involves a mineral processing stage, which includes crushing and grinding operations. This step is crucial for determining the most efficient method to obtain metals in their elemental form with high purity. For weathered ores, a common approach is sulphuric acid leaching, applied to the ore in heaps, typically composed of coarse particles derived from primary and secondary crushing operations. For sulphide-rich ores, techniques such as roasting or pressure leaching are widely employed, particularly for gold ores. The objective is to release gold particles often encapsulated within mineral matrices such as sulphides, silica, and other components. Once released, gold is solubilized with alkaline cyanide solutions, forming stable complexes such as $Au(CN)_2^-$

[#] corresponding author: sobrallui@gmail.com and $Ag(CN)_2^-$. These precious metals can then be recovered through electrowinning or precipitation with zinc powder, as used in the Merrill-Crowe process [1].

Different mineral processing approaches result in variations in particle size and, depending on the adopted method, can induce microfractures in the material. This phenomenon may facilitate the action of autotrophic microorganisms involved in the oxidation of sulphide minerals, as well as oxidizing agents such as ferric ions, which are generated during the oxidation of sulphides present in minerals such as pyrite, arsenopyrite, bornite, and chalcopyrite [2].

This study aimed at conducting comparative tests to evaluate the efficiency of gold extraction from ore samples subjected to three different crushing methods: conventional crushing in a jaw crusher, high-pressure grinding rolls (HPGR), and electrodynamic fragmentation, known as high-voltage pulse fragmentation [3].

Among the copper minerals commonly found in gold ores, chalcocite (Cu_2S) and cuprite (Cu_2O) exhibit high solubility in cyanide solutions, whereas chalcopyrite ($CuFeS_2$) has lower solubility. Both chalcocite and cuprite, besides consuming cyanide and oxygen during their chemical reactions, can generate by-products that negatively impact process efficiency by promoting undesired precipitation reactions. Therefore, pretreatment methods such as pre-aeration, pressure leaching, and roasting are beneficial for reducing cyanide and oxygen consumption [4]. Studies indicate that the pre-oxidation of pyrite-containing gold ores can increase gold recovery from 20% to 70%, while simultaneously reducing cyanide consumption from 2.5 kg/t to 1.5 kg/t of ore. However, excessive ore grinding can increase cyanide consumption without necessarily improving gold recovery.

Cyanidation generally requires preliminary treatment stages, such as roasting, pressure leaching, or bio-oxidation, which primarily function to minimize the effect of cyanicides—compounds that promote excessive cyanide consumption. The gold dissolution process can be hindered by the low solubility of oxygen in pure water, approximately 8 mg/L at 25°C. Any factor reducing oxygen solubility can negatively impact process efficiency. In this context, bio-oxidation was selected as the pre-treatment method for this study. Additionally, the ore was ground using modern processing techniques that increase surface area and consequently enhance the efficiency of sulphide minerals solubilization during pre-treatment, thereby improving gold extraction efficiency [5]. The use of unit operations in mineral processing enables the generation of microfractures in ore particles, promoting more effective contact between leaching agents and the mineral species carrying the metals of interest, whether in oxidized form (e.g., oxides, carbonates, silicates, sulphates) or as sulphides. This effect can enhance microbial activity in bio-oxidation processes, improving efficiency. Thus, this study aimed at comparatively evaluating the effectiveness of the gold extraction process in ore samples subjected to three different comminution methods: conventional jaw crushing, high-pressure grinding roll (HPGR), and electrodynamic fragmentation (Lightning Machines Limited – High Voltage Pulse Fragmentation).

EXPERIMENTAL

A mineral sample from EURO METAL BRASIL was homogenized, dried at 40°C, and divided to be processed by different crushing methods: jaw crushing, high-pressure grinding rolls (HPGR), and electrodynamic fragmentation. The initial crushing was conducted using a jaw crusher, followed by size classification with Tyler sieves. Samples were then processed at VALE (HPGR) and Lightning Machines (electrodynamic fragmentation). Additional size reduction (3–6 mm) was performed at CETEM for bio-oxidation experiments. At VALE, crushing was optimized to minimize fine generation, using a roll pressure of 2N/mm² with a 10 mm machine opening. The material was then sieved at CETEM to obtain particles from 3 to 6 mm, ensuring complete removal of fines by air jet. This preparation aimed at standardizing surface area conditions across different processing methods.

Bio-oxidation tests were conducted in acrylic columns (10 cm × 60 cm), each loaded with 3.5 kg of ore and layers of quartz for stability. A solution of MKM medium containing inorganic salts as nutrient source: 0.4 $g.L^{-1}$ of ammonium sulphate; 0.4 $g.L^{-1}$ of magnesium sulphate heptahydrate; 0.04 $g.L^{-1}$ of monopotassium phosphate; $FeSO_4.7H_2O$ (33.3 $g.L^{-1}$) and S^o (10 $g.L^{-1}$) bearing *Acidithiobacillus ferrooxidans, Acidithiobacillus thiooxidan*s, and *Leptospirillum ferrooxidans* (10^7 cells/mL) was circulated at a rate of 10 L/m², with humidified air supplied at 0.5 L/min. The system was maintained at 30°C, and the acidic leachate was continuously renewed to enhance oxidation. For microorganism adaptation, mixed cultures of *A. ferrooxidans, A. thiooxidans*, and *L. ferrooxidans* were tested in MKM medium with $FeSO_4$ and gold ore, incubated at 30°C with agitation. Cell viability was monitored over 28 days through microscopic counting and spectrophotometry for Fe^{2+} analysis. Adjustments with 5M H_2SO_4 ensured controlled pH conditions.

Iron speciation was analysed weekly using spectrophotometry (HACH DR 6000) and atomic absorption spectrometry (AAS) for Cu and Ni quantification. The final bio-oxidized material was subjected to cyanidation in a glass reactor (5 L) under varying cyanide concentrations (3–10 g/L). The gold extraction efficiency was determined via atomic absorption spectrometry.

RESULTS AND DISCUSSION

The graphs in Figures 1 and 2 illustrate the effectiveness of different crushing methods—jaw crusher (BM), high-voltage pulse fragmentation (HVPF), and high-pressure grinding rolls (HPGR)—in extracting copper (Cu) and nickel (Ni) over a 30-day bio-oxidation period. Notable trends were identified during the analysis of these results.

During bio-oxidation tests on a semi-pilot scale, HVPF demonstrated superior performance, significantly increasing Cu and Ni concentrations in the leachate. This highlights its effectiveness in bio-extraction compared to the other crushing methods. HVPF efficiently fragmented the ore, generating internal microfractures that enhanced mineral exposure to microbial action. Nickel extraction was highest with HVPF, followed by jaw crusher processing, while HPGR exhibited the lowest solubilization rates (Figure 1 and 2).

The presence of key microorganisms, including *Acidithiobacillus ferrooxidans, Leptospirillum ferrooxidans,* and *Acidithiobacillus thiooxidans,* was critical for bio-oxidation efficiency. Their acidic exopolymeric substances influenced mineral solubility and redox kinetics. The crushing method selection directly impacted bio-oxidation efficiency, with HVPF yielding the best Cu and Ni extraction rates, emphasizing the need to optimize crushing parameters based on ore properties (Figure 3).

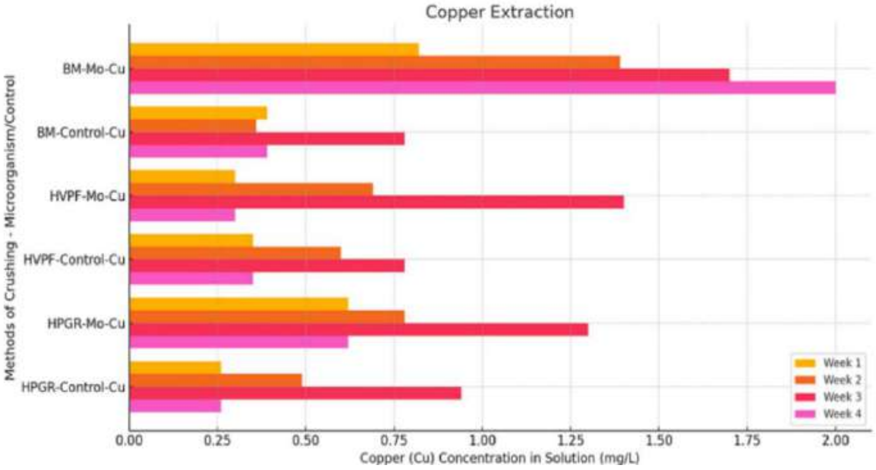

Figure 1 Copper extraction from gold ore using different mineral processing operations (HPGR-control-Cu; HVPF-control-Cu, BM-control-Cu: tests without the addition of microorganisms (*i.e.*, negative control); HPGR-Mo-Cu, HVPF-Mo-Cu, BM-Mo-Cu: tests with the action of microorganisms (*i.e.*, bio-oxidation)).

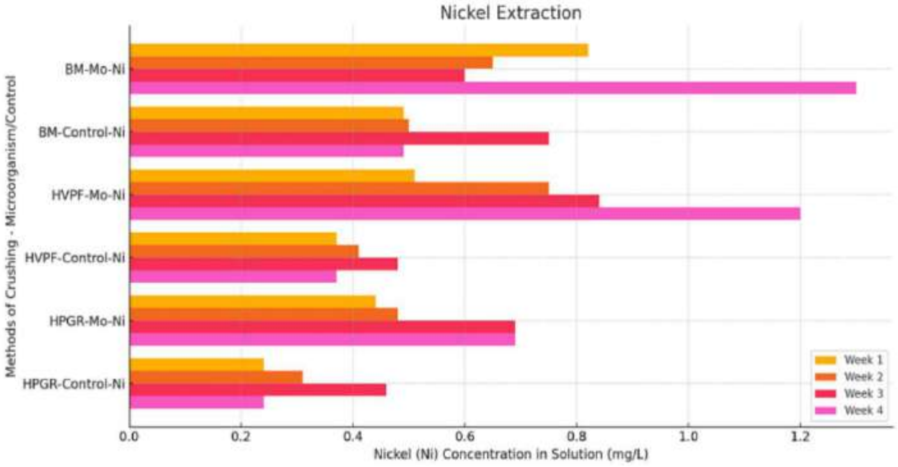

Figure 2 Nickel extraction from gold ore using different mineral processing operations (HPGR-control-Ni; HVPF-control-Ni, BM-control-Ni: tests without the addition of microorganisms (*i.e.*, negative control); HPGR-Mo-Ni, HVPF-Mo-Ni, BM-Mo-Ni: tests with the action of microorganisms (*i.e.*, bio-oxidation)). The inconsistency observed in HPGR performance may be attributed to factors such as equipment setup, particle size distribution, or intra-particle pH increases, which could have led to metal ion hydrolysis and the formation of insoluble hydroxides, restricting microbial access to minerals.

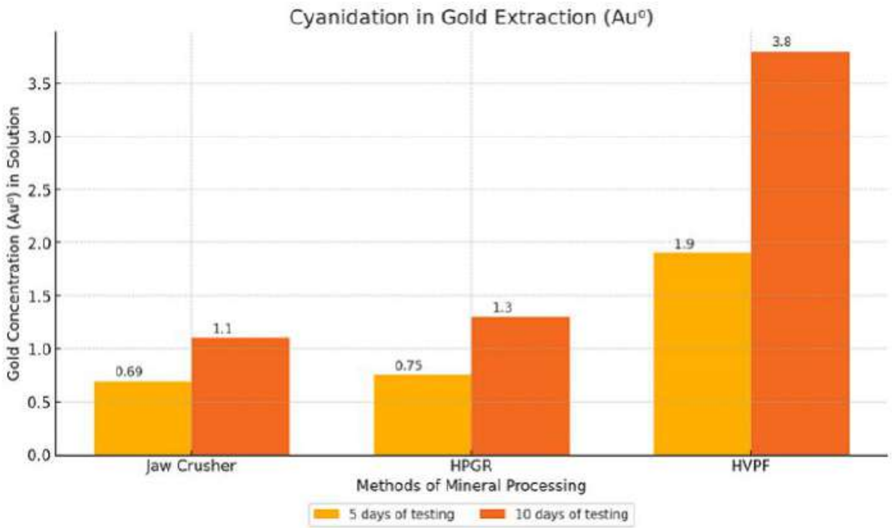

Figure 3 Result of the cyanidation process for gold from previously bio-oxidized mineral samples.

Cyanidation is widely used for extracting gold; however, the presence of sulphides increases cyanide consumption due to their cyanicide properties. To address this, bio-oxidation was performed prior to cyanidation. The results showed significant variations in cyanidation efficiency depending on the crushing method used before bio-oxidation. These findings suggest that HVPF is the most effective method for liberating gold particles, enhancing their exposure to cyanidation. The mineralogical species carrying gold underwent greater liberation, leading to improved bio-oxidation, which in turn facilitated gold dissolution during cyanidation (Figure 3). Additionally, HVPF fragmentation enabled better release of gold encapsulated in gangue materials such as silica and silicates, contributing to higher gold concentrations in the cyanide solution. Thus, the cyanidation results for solid residues from bio-oxidation demonstrate that HVPF outperforms conventional crushing methods, making it an optimal pre-treatment step for gold recovery. Its ability to create microfractures enhances the combined action of cyanide, oxygen, and complexing agents, improving overall gold extraction efficiency.

CONCLUSION

Based on the results achieved in terms of the bio-oxidation of the ore under study subjected to different mineral processing methods, we can affirm that it is possible to reduce the sulphur content in a differentiated manner depending on the processing operation used. This reduction in sulphur content aims at maximizing the liberation of gold particles through the extension of the bio-oxidative process and to minimize cyanide consumption in the gold extraction stage, as some mineral species consume cyanide. On the other hand, the removal of these cyanide-consuming species, particularly sulphide minerals, should be maximized to avoid an increase in ionic strength and thus greater solubilization of oxygen, the oxidizing agent in the cyanidation process. It is concluded that the High-Voltage Pulse Fragmentation (HVPF) operation stands out as the most efficient in both the bio-oxidation and cyanidation processes of gold ore, providing greater extraction of precious metals. These findings have significant implications for the optimization of mining and precious metal extraction processes from primary gold ores. The leachate resulting from the bio-oxidative process of sulphide minerals present in the gold ore under study contains iron ions (*i.e.*, Fe^{2+} and Fe^{3+}), Ni^{2+}, and Cu^{2+}, and requires treatment for the proper recovery of these metals, also preventing environmental contamination. The bio-oxidation of the gold ore sample processed in the HPGR showed greater variation in redox potential and a higher concentration of ferric ions, possibly due to the oxidation of Fe^{2+} to Fe^{3+} during the bio-oxidative process within the micro fissures, preventing the continuity of the reaction cycle.

ACKNOWLEDGEMENT

The authors would like to express their gratitude to EURO METAL BRASIL for providing the mineral samples used in this study. We also extend our sincere thanks to the Centro de Tecnologia Mineral (CETEM) for granting access to its infrastructure and technical support throughout the experimental procedures. Additionally, we acknowledge the Federal University of Rio de Janeiro (UFRJ) for its valuable contributions and support in the development of this research.

REFERENCES

1. Dai, X., Jeffrey, M. I. (2006) The effect of sulfide minerals on the leaching of gold in aerated cyanide solutions. Hydrometallurgy, v. 82, n. 3-4, p. 118-125.
2. Li, Y. et al. (2013) A review of the structure and fundamental mechanisms and kinetics of chalcopyrite leaching. Advances in Colloid and Interface Science, v. 197/198, p. 1-32.
3. Zhu, Xiaohua et al. (2021) On the mechanism of high-voltage pulsed fragmentation from electrical breakdown process. Rock Mechanics and Rock Engineering, v. 54, n. 9, p. 4593-4616.
4. Zhao, H. et al. (2019) Minerals Engineering, v. 136, p. 140-154.
5. Tao, H., Dongwei, L. (2014) Biotechnology Reports.

XVI International Mineral Processing
and Recycling Conference
28-30 May 2025, Belgrade, Serbia

DOI: 10.5937/IMPRC25702D Original research article

BIODESULPHURISING HIGH SULPHUR CONTENT TAILINGS FROM COAL MINING IN BRAZIL

Andriela Dutra Norberto de Oliveira[1], 0009-0000-3050-3395,
Luis Gonzaga Santos Sobral[2#], 0000-0001-6638-4201,
Armando Lucas Cherem da Cunha[1], 0000-0001-5246-2328,
[1]Federal University of Rio de Janeiro, Rio de Janeiro, Brazil
[2]Centre for Mineral Technology, Rio de Janeiro, Brazil

ABSTRACT – Brazilian coal is characterized by its low calorific value, high ash and sulphur (S) contents, which requires beneficiation processes that increase costs and reduce its competitiveness compared to other energy sources. The processing of such coal generates a huge amount of residues rich on sulphide minerals, which disposal leads to the generation of Acid Mine Drainage (AMD) that need to be treated. The reason for processing such residue is to produce low sulphur content coal for energy generation purpose, which have to be lower than 1% of sulphur. Therefore, this technical contribution aims at bio-assisted digesting the iron sulphide minerals, pyrite in particular, producing iron sulphate bearing leachates. The bioleaching tests is being accomplished using a consortium of natural autotrophic microorganisms in a vat-heap leaching reaction system, where the tailing is flooded with the leaching solution bearing the aforementioned microorganisms. According to the results, out of the in-progress bioleaching test, the iron is being progressively extracted, and so does the tailing desulphurised, which means that this process is prone to be enhanced as the operation parameters are being optimised. Finally, the leachate being produced is a potential raw material for producing iron oxyhydroxides, such goethite and maghemite, with high industrial added values.

Keywords: Desulphurisation processing, Coal tailings, Autotrophic microorganisms.

INTRODUCTION

Brazilian coal is characterized by its low calorific value, high ash and sulphur (S) contents, which requires beneficiation processes that increase costs and reduce its competitiveness compared to other energy sources [1]. According to Akinwekomi and colleagues (2020) [2], coal processing results in a residue rich in minerals, mainly silicates and iron sulphides, the disposal of which leads to the generation of Acid Mine Drainage (AMD). The resulting effluent is characterized by its high acidity, high concentration of metals and sulphates, causing serious environmental impacts. The acidity of the drainage allows the dissolution of other metals that may be associated with the tailings, such as aluminium, manganese, zinc, lead, cadmium, copper, arsenic and selenium [3]. In addition, the presence of microorganisms, such *as Acidithiobacillus ferrooxidans species*, can intensify these reactions, as they have the ability of oxidizing Fe^{2+} ions in an acid environment to Fe^{3+} [4,5]. This microorganism has the ability to reduce the inorganic

---

[#] corresponding author: sobrallui@gmail.com sulphur content [6], which is evident in mineral coal tailings due to the high sulphur content. The high concentration of ferric ions leads to the formation of goethite and maghemite, which are iron oxyhydroxides from DAM [7,8]. These iron oxyhydroxides can be used in various industries and have high added value. This technical contribution aims at carrying out a literature survey on the biodesulphurization of mineral coal, while running, in addition, an experimental work in lab-scale using such process, waving for the industrial applications of its by-products.

EXPERIMENTAL

The mineral coal tailing used in this study was analysed at 1350°C in a LECO SC-632 elemental analyser, using 0.2 g of sample in each replicate, and a content of 49.6% of carbon and 3.4% of sulphur were found. The particle size analysis was carried out by wet sieving using standard Tyler sieves. Coal tailing with different grain sizes was used in this study: below 100# and below 150#.

The *Acidithiobacillus ferrooxidans* (ATCC 53992) and *Acidithiobacillus thiooxidans*-FG01 (Garcia, 1991) micro-organisms used were cultivated at a temperature of 30°C, in an orbital shaker rotating at 150 rpm, using MKM culture medium containing inorganic salts as nutrient source: 0.4 g.L^{-1} of ammonium sulphate; 0.4 g.L^{-1} of magnesium sulphate heptahydrate; 0.04 g.L^{-1} of monopotassium phosphate; $FeSO_4.7H_2O$ (33.3 g.L^{-1}) and S^o (10 g.L^{-1}) were used as energy sources for *A. ferrooxidans* and *A. thiooxidans*, respectively. The growth of *A. ferrooxidans* occurred after 2 days and was indicated by the total oxidation of Fe^{2+}, characterized by the change in colour of the culture, which varied from milky white to brick red. The growth of *A. thiooxidans* occurred after 5 days and was indicated by the pH value of less than 1.0, reached by the oxidation of S^o, with the consequent generation of H_2SO_4 in the culture medium (the starting pH was 2.8 for the *A. thiooxidans* culture and 1.8 for the *A. ferrooxidans* culture). The number of cells was determined under an optical microscope using a Thoma chamber. In both cultures, the microbial population was around 10^8 cells.mL^{-1}.

The experiments were carried out in two replicates for a period of 7 days in Erlenmeyer flasks at a temperature of 30^{o}C. The aeration was promoted by continuous stirring in an orbital shaker rotating at 150 rpm. The microbial inoculum was added at a ratio of 10% v/v and the MKM culture medium was added, but without adding a commercial energy source (iron and sulphur). No microbial inoculum was done to some Erlenmeyer flasks, which were, therefore, considered "control trials". The other experimental conditions are described in Table 1. Daily measurements of pH and redox potential (Eh) were done, in addition to the determination of ferrous ions (Fe^{2+}), total iron and ferric ions (Fe^{3+}) concentrations, as well as the total sulphur (S) content. The pH and Redox Potential, while running the tests, were measured on the Analion pH meter AN2000 microprocessor using a combined glass electrode and Pt electrode (against Ag^o/AgCl), respectively. The electrodes were previously sterilized (*i.e.*, 30 minutes immersion in a 5% v/v formaldehyde solution), and in order to avoid contamination of the samples, the measurements began with the control tests, which means the tests in which no microbial inoculum was added and whose coal samples were previously sterilized in a 5% v/v formaldehyde solution.

Table 1 Experimental conditions used in the tests

Test	Particle size (#)	Microbial inoculum (species)	Pulp density (w/v)
1	<150	*A.ferrooxidans*	10%
2	<100	*A.ferrooxidans*	10%
3	<150	*A.ferrooxidans&A.thiooxidans*	10%
4	<100	*A.ferrooxidans&A.thiooxidans*	10%
5	<150	-	10%
6	<100	-	10%

Aliquots were taken daily from the tests and filtered through a 0.22µm pore diameter Millipore® membrane. The solid phase was sent to the analysis of carbon and sulphur through LECO SC-632 elemental analyser, and the liquid phase for determining iron concentration, which was carried out immediately after taking it using the following technique: for determining the concentration of iron ionic species in the leachate, out of the biodesulphurization reaction system used, an aliquot was taken every seven minutes for evaluating the Fe^{3+} and Fe^{2+} concentrations using a spectrophotometric HACH DR 6000 apparatus, using orthophenanthroline. To quantify the Fe^{2+} concentration, the diluted sample was mixed with orthophenanthroline and the pH of the mixture adjusted with acid solution to pH 2.1, to avoid Fe^{3+} ion hydrolysis. After the Fe^{2+}/orthophenanthroline complex was formed, the absorbance was measured at 510nm. To determine the concentration of total iron, the Fe^{3+} ions were reduced to Fe^{2+} using hydroxylamine (*i.e.*, NH_2OH). The Fe^{3+} concentration was obtained from the difference between the total iron and Fe^{2+} concentrations.

RESULTS AND DISCUSSION

Biodesulfurization is a combination of biological and chemical processes. According to the Nernst equation (*i.e.*, Equation 1), changes in redox potential values reflect the activity of the system. The redox potential is an equilibrium value, which changes when Fe^{2+} and Fe^{3+} concentrations vary, which indicates how the oxidative processes are taking place. The Thermodynamic Equilibrium Diagram for the Fe-H_2O system shows a limited zone where the ferric ion is stabilized, playing a role as an oxidant in the biodesulphurization process, and is directly associated with an acid pH environment and high redox potentials. According to Prayuenyong (2002), mineral coal contains smaller micropores than the size of the microorganisms used in the process. Therefore, the oxidation of sulphide minerals in these areas is not carried out by direct contact with the micro-organisms on the surface of the mineral but due to the influence of Fe^{3+} ions in the reaction medium.

$$Eh = E°_{Fe^{3+},Fe^{2+}} + \frac{RT}{nF} log\ log\ \frac{[Fe^{3+}]}{[Fe^{2+}]} \quad (1)$$

Where: R (gas constant) = 8.31441joule.K^{-1}.mol^{-1}; T (temperature) in Kelvin; F (Faraday constant) = 96493.5 Coulombs.mol^{-1}, and n = number of electrons involved in the redox reaction.

Figure 1 shows the data collected during the monitoring of the tests. Right at the start of the process, there is an increase in redox potential and a decrease in pH values, especially in the tests that used samples with smaller particle size (<150#). There was also a progressive increase in the concentration of iron in all the tests, due to pyrite oxidation. In the tests with the addition of sulphur-oxidizing bacteria (*A. thiooxidans*), there was an even sharper drop in pH values, due to the formation of H_2SO_4 by the sulphur oxidation, as shown in Equation 2.

$$2FeS_2 + 7O_2 + 2H_2O \rightarrow 2FeSO_4 + 2H_2SO_4 \qquad (2)$$

From the fifth day onwards, there was a gradual increase in pH values in all the tests as the H_2SO_4 generated previously continued to react with other acid-consuming species present in the coal tailings, although there was no longer enough pyrite to keep the pH of the system low. The results indicate that the mineral coal, the mineral substrate used in this study, had a reduction in total sulphur content of 73% when using the sample with a particle size of less than 150# and the mixed culture as the microbial inoculum.

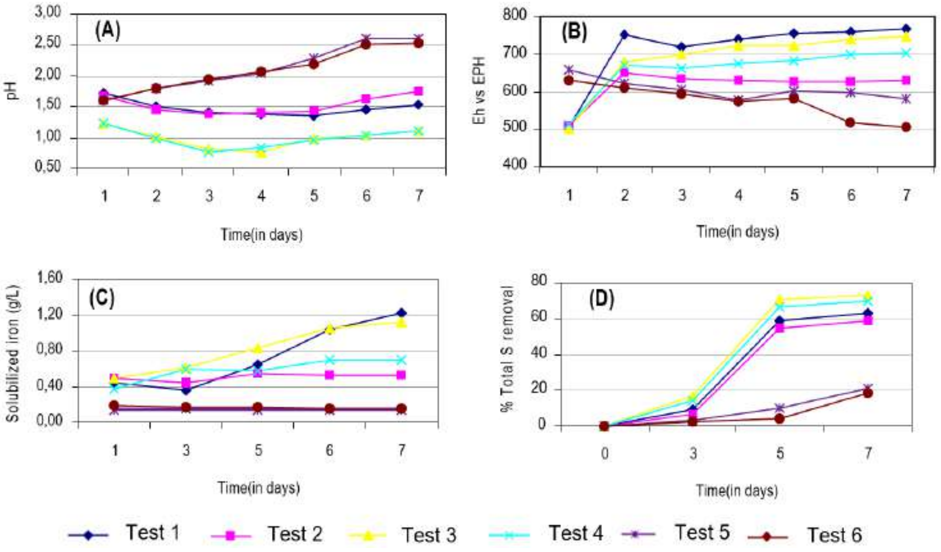

Figure 1 (A) pH monitoring; (B) redox potential monitoring; (C) concentration of solubilized iron and (D) percentage removal of total sulphur

The experimental results demonstrate the effectiveness of the biodesulphurization of mineral coal in removing sulphur compounds. The pH monitoring shows a progressive decrease, which indicates the acidification of the system due to the production of sulphuric acid by the microorganisms, especially *A. thiooxidans*, which oxidise reduced sulphur compounds, such elemental sulphur. The redox potential, in turn, shows a general increase over time, reflecting the oxidation of ferrous ions and elemental sulphur processes, which are catalysed by the presence of *A. ferrooxidans*. The increase in the concentration of solubilized iron confirms the oxidative activity of this microorganism, which transforms ferrous ions into ferric ones, releasing iron into solution. The percentage of total sulphur removal, which increased significantly after the third day, indicates the efficiency of biodesulphurization process. The fine particle size of the mineral coal makes easier the microorganisms' bioavailability, intensifying their interaction with the mineral substrate and consequently a higher rate of sulphur oxidation.

These tests are fundamental to understanding the dynamics of the biodesulphurization process and its potential for purifying mineral coal, reducing its sulphur content and improving its characteristics for being used as an energy resource. The biodesulphurization has, therefore, emerged as a promising alternative for the treatment of mineral coal, contributing to the mitigation of sulphur emissions.

CONCLUSION

Experimental tests suggest that the biodesulphurization process, applied to mineral coal, is particularly effective with particle size under 150#. The use of a mixed culture of *A. ferrooxidans* and *A. thiooxidans* resulted in a significant reduction of up to 73% of the total sulphur content. Therefore, biodesulphurization emerges as a viable approach for the pre-treatment of mineral coal destined for thermal power plants, especially when it has high sulphur contents as pyrite.

REFERENCES

1. Empresa de Pesquisa Energética (EPE) (2023) 'Balanço Energético Nacional – Relatório Síntese – Ano Base 2022', viewed1February 2024, https://www.epe.gov.br/sites-pt/publicacoes-dados-abertos/publicacoes/PublicacoesArquivos/publicacao-748/topico-681/BEN_Síntese_2023_PT.pdf.
2. Akinwekomi, V., Maree, J.P., Masindi, V., Zvinowanda, C., Osman, M.S., Foteinis, S., Mpenyana-Monyatsi, L. &Chatzisymeon, E. (2020) 'Beneficiation of acid mine drainage (AMD): A viable option for the synthesis of goethite, hematite, magnetite, and gypsum – Gearing towards a circular economy concept', Minerals Engineering, vol. 148, viewed 1 February 2024, https://doi.org/10.1016/j.mineng.2020.106204.
3. Simate, G.S. &Ndlovu, S. (2014) 'Acid mine drainage: Challenges and opportunities', Journal of Environmental Chemical Engineering, vol. 2, pp. 1785–1803.
4. Baker, B.J. &Banfield, J.F. (2003) 'Microbial communities in acid mine drainage', FEMS Microbiology Ecology, vol. 44, pp. 139-152.
5. Kontopoulos, A. (1998) 'Acid mine drainage control', in Castro, S.H., Vergara, F. & S.M.A. (eds), Effluent Treatment in the Mining Industry, University of Concepción, pp. 57–118.
6. Kotelnikov, V.I., Saryglar, Ch.A. &Chysyma, R.B. (2020) 'Microorganisms in Coal Desulfurization (Review)', Applied Biochemistry and Microbiology, vol. 56, no. 5, pp. 521–525, viewed 1 February 2024, https://doi.org/10.1134/s0003683820050105.
7. Akinwekomi, V., Maree, J.P., Zvinowanda, C. & Masindi, V. (2017) 'Synthesis of magnetite from iron-rich mine water using sodium carbonate', Journal of Environmental Chemical Engineering, vol. 5, pp. 2699-2707.
8. Duuring, P., Hagemann, S.G., Banks, D.A. & Schindler, C. (2018) 'A synvolcanic origin for magnetite-rich orebodies hosted by BIF in the Weld Range District, Western Australia', Ore Geology Reviews, vol. 93, pp. 211-254.

ABSTRACTS

XVI International Mineral Processing
and Recycling Conference
28-30 May 2025, Belgrade, Serbia

DOI: 10.5937/IMPRC25709C Abstract

INNOVATIVE PRE-FEASIBILITY STUDIES TOWARDS THE SUSTAINABLE PRODUCTION OF RARE EARTH CONCENTRATES FOR SELF-SUPPLY IN EUROPE

Maria Cristina Vila[1#], 0000-0002-5063-5632,
Maria Lurdes Dinis[1], 0000-0002-4774-2533,
Laura Ferrando-Climent[2], 0000-0002-5154-7060**,**
Nirosham Gajendra[2], 0000-0002-2819-3399,
Deniz Avsar[2], 0009-0003-8157-1461
Duygu Yilmaz[3], 0000-0002-4142-4788,
Erika Levei[4], 0000-0002-0145-0287,
Iulia Török[4], 0000-0003-2123-1871,
[1]CERENA-FEUP, Department of Mining Engineering, Faculty of Engineering, University of Porto, Portugal
[2]Department of Tracer Technology, Environmental Technology Section, Institute for Energy Technology, Kjeller, Norway
[3]Department of Environmental Industrial Processes, Environmental Technology Section, Institute for Energy Technology, Kjeller, Norway
[4]Research Institute for Analytical Instrumentation Subsidiary, National Institute of Research and Development for Optoelectronics, Cluj-Napoca, Romania

ABSTRACT – The REESOURCE project aims to develop innovative technologies for extracting rare earths in Europe to secure the continent's self-supply and the resilience of the European REE value chains. Decarbonise the extraction of European REEs and bring the EU industry to the forefront of the sustainable local sourcing of raw materials. The present work in within the scope of work package 5-Greener beneficiation approaches for Zero-Pollution mining, aiming to develop novel formulations based on environmentally friendly chemicals for both, the mineral beneficiation process of REEs and the process water treatment, supporting the recirculation of this resource.

Three samples from the Fen deposit in Norway were tested for physicochemical characterization, hydrogravitic preconcentration, and magnetic separation. This was followed by floatability tests, evaluating different reagent formulations and operating conditions. In all the tests, in addition to the recovery and content of the concentrates, special control was given to the water (quantity and quality) aiming at its recirculation. An advanced analytical method based on Ultra-performance liquid chromatography coupled to high resolution mass spectrometry (UPLC-HRMS) was developed to assess the different chemicals employed in the formulations at the flotation experiments. The technique allowed to better understand the efficiency of the substances in the beneficiation step, tracking the chemical transformation and/or byproducts of the targeted

---

[#] corresponding author: mvila@fe.up.pt

formulations (i.e organometallic substances) and to assess the reusability of the wastewater stream for flotation experiments. Additionally, the measurement of radionuclides and REEs was done over the samples. The results of the pre-feasibility studies are key to achieving the sustainable development objectives of the extractive industry for the supply of critical and strategic raw materials of Europe.

Keywords: Rare Earth Metals, Mineral Beneficiation, Flotability Tests, Green Flotation Reagents.

ACKNOWLEDGEMENT

This project has received funding from the European Union's Horizon Europe framework programme under the grant agreement no. 101138460.

XVI International Mineral Processing
and Recycling Conference
28-30 May 2025, Belgrade, Serbia

DOI: 10.5937/IMPRC25711T Abstract

MODELING AND SIMULATION OF SOLID PHASE EXTRACTION FOR LEACHED ORE PURIFICATION

Randal Tzeou Hah Fauline[1,2#], 0009-0005-2037-6296**,**
Agnès Grandjean[1,2], 0000-0002-3815-2144,
Antoine Leydier[1,2], 0000-0002-1997-9664,
Emeric Brun[2], 0009-0004-7068-6578,
Florian Herbelet[2], 0000-0001-8504-734X,
Xavier Heres[2], 0000-0001-9280-1531,
Justine Taurines[2], 0009-0001-4927-1253,
[1]Université de Montpellier, France
[2]CEA, DES, ISEC, DMRC, Marcoule, France

ABSTRACT – Development of solid/liquid extraction purification process of valuable elements from leached ores can be hasten or made easier with the use of computer resources to simulate the process. The simulation will allow to find the optimal conditions according to different parameters, without conducting numeral experiments for each change of parameters.

The French Atomic Energy Commission (CEA) developed a code to simulate solid phase extraction (SPE). Literature or batch experiments will give the equilibrium constants characterizing the sorption on the support but also the speciation of each species in the liquid phase required for the code. The Residence Time Distribution (RTD) experiments will be able to characterize the flow within the solid support.

To ensure the proper operation of the code, simulation of uranium extraction from complex media with high sulfate concentrations resulting from mining leaching will be compared to experimental extractions data acquired on materials specially developed for this application.

Keywords: Simulation, Selective Extraction, Column Sorption, Purification.

[#] corresponding author: Randal.TZEOUHAHFAULINE@cea.fr

**XVI International Mineral Processing
and Recycling Conference
28-30 May 2025, Belgrade, Serbia**

DOI: 10.5937/IMPRC25712A Abstract

LEACHING OF CALCIUM FROM PHOSPHOGYPSUM FOR CARBON SEQUESTRATION

Michelle Airah N. Pablo[1], 0009-0001-1402-1019,
Joshua P. Pocaan[1], 0000-0002-9753-6076,
Jacob Louies Rohi W. Paulo[1], 0009-0005-3853-298X,
Piolo N. Gervacio[1], 0009-0005-6995-3314,
Arnel B. Beltran[2], 0000-0003-2764-6226**,**
Carla Mae J. Pausta[1], 0009-0006-8177-8018,
Aileen H. Orbecido[2,#], 0000-0003-3322-0539,
[1]Center for Engineering and Sustainable Development Research, De La Salle University, Manila, Philippines
[2]Department of Chemical Engineering, De La Salle University, Manila, Philippines

ABSTRACT – Phosphogypsum (PG) is a waste by-product of the production of phosphoric acid from phosphate ores. Despite it being utilized already for building materials, most of the PG is left in stack and stored in large areas. Valorization of this industrial waste is being explored, including its use for carbon sequestration through indirect mineral carbonation. This process involves leaching a metal, usually Ca or Mg, from mineral wastes followed by the reaction of Ca- or Mg-rich leachate with CO_2 to obtain stable and slightly soluble carbonates. PG samples were collected from a fertilizer production plant in the Philippines and was characterized through SEM-EDS, XRF, XRD, FTIR, and TGA. Philippine PG is mainly composed of Ca which may be leached out for use in mineral carbonation. Two leaching agents were investigated, namely NaCl and HCl. Using a response surface methodology, different factors such as leaching agent concentrations, contact time, temperature, and liquid-to-solid ratio were considered to optimize calcium extraction efficiency. Measuring the concentration of Ca in the leachate via atomic absorption spectroscopy (AAS), HCl is identified to have the highest extraction efficiency.

Keywords: Phosphogypsum, Indirect Mineral Carbonation, Carbon Sequestration, Acid Leaching, Salt Leaching.

[#] corresponding author: aileen.orbecido@dlsu.edu.ph

XVI International Mineral Processing
and Recycling Conference
28-30 May 2025, Belgrade, Serbia

DOI: 10.5937/IMPRC25713P Abstract

A PROBLEMATIQUES APPROACH FOR UNDERSTANDING CIRCULAR ECONOMY INTEGRATION BARRIERS IN THE MINING AND MINERAL PROCESSING SECTOR

Michael Angelo B. Promentilla[#], 0000-0002-9009-8552,
Department of Chemical Engineering, De La Salle University, Manila, Philippines

ABSTRACT – This study proposes a novel problematiques framework to analyze the structural complexity of circular economy (CE) implementation barriers in the mining and mineral processing sector. Using the PESTLE framework, barriers are identified and categorized according to key political, economic, social, technological, legal, and environmental components of the system. The research employs a hybrid problem structuring methodology integrating Z-number theory to handle uncertainty, DEMATEL (Decision-Making Trial and Evaluation Laboratory) for causal relationship mapping, ISM (Interpretive Structural Modeling) for hierarchical structuring, and MICMAC analysis for hierarchical digraph representation and barrier classification. The proposed approach quantifies interdependencies among barriers while accounting for decision-maker expertise reliability through Z-number implementation. Such analysis reveals, for example, critical driving barriers, including insufficient government support and regulatory obstacles, significantly influencing other barriers in the system. The methodology generates a hierarchical structural model depicting identified barriers' relationships and relative influence, providing decision-makers with strategic insights for targeted interventions. This research thus offers a holistic framework for understanding CE implementation challenges in the mining and mineral processing sectors while accounting for uncertainty and complexity in barrier interactions. The findings support evidence-based policy development and strategic planning for CE transition in the sector, highlighting the need for integrated approaches addressing interconnected barriers simultaneously.

Keywords: Circular Economy, PESTLE Analysis, Z-Number Theory, DEMATEL, ISM, MICMAC Analysis, Barrier Analysis.

[#] corresponding author: Michael.promentilla@dlsu.edu.ph

XVI International Mineral Processing
and Recycling Conference
28-30 May 2025, Belgrade, Serbia

DOI: 10.5937/IMPRC25714P

Abstract

DEVELOPMENT OF LIMESTONE-BASED PASSIVE TREATMENT SYSTEM FOR COPPER-RICH ACID MINE DRAINAGE

Joshua Pocaan[1], 0000-0002-9753-6076,
Brian Gerald Bueno[1], 0009-0007-6497-0814,
Jaica Mae Pagaduan[1], 0009-0008-2635-3070,
Aileen Orbecido[2], 0000-0003-3322-0539,
Carlito Tabelin[3], 0000-0001-8314-6344,
Ana Santos[4], 0000-0002-8727-7795,
Anne Jungblut[4], 0000-0002-4569-8233,
Vannie Joy Resabal[3], 0000-0001-9908-9452,
Renan Ma. Tanhueco[2], 0000-0001-5792-9871,
Michael Angelo Promentilla[2], 0000-0002-9009-8552,
Arnel Beltran[2#], 0000-0003-2764-6226,
[1]Center for Engineering and Sustainable Development Research, De La Salle University, Manila, Philippines
[2]Department of Chemical Engineering, De La Salle University, Manila, Philippines
[3]Department of Materials and Engineering Technology, Mindanao State University– Iligan Institute of Technology, Iligan City, Philippines
[4]History Museum, London, United Kingdom

ABSTRACT – This study developed a system intended to treat a copper-rich acid mine drainage (AMD) in a legacy mine in Sto. Niño, Tublay, Benguet, Philippines. Based on previous sampling campaigns in the area, Cu and Mn concentrations and pH exceed the local effluent standards. Using local limestone as the media for treatment of AMD, several laboratory experiments using synthetic AMD were conducted to identify the effective particle size and hydraulic retention time. Consequently, the parameters identified were then deployed into a pilot-scale system investigating the effectiveness of an oxic and anoxic system for the actual AMD. Conducting the analysis, it has revealed that a hybrid of oxic and anoxic system with variable particle size and hydraulic retention time may be deployed considering the unsteady condition of the stream in the legacy mine. In Consideration of the topography of the mine site, a hybrid multi-stage limestone leach bed and packed bed has been deployed. With regular monitoring of the system, it showed an effective removal of Cu and Mn and increase pH of the stream. This observation thus addresses the threat of AMD in the area. However, improvement in terms of the lifespan of the system needs to be demonstrated as common issues of armoring from high concentration of Cu is observed resulting in the reduction of treatment performance over time.

Keywords: Legacy Mines, Acid Mine Drainage, Passive Treatment, Heavy Metals, Treatment Performance.

[#] corresponding author: arnel.beltran@dlsu.edu.ph

XVI International Mineral Processing
and Recycling Conference
28-30 May 2025, Belgrade, Serbia

DOI: 10.5937/IMPRC25715P
Abstract

BLACKMASS FLOTATION OF END-OF-LIFE BATTERIES: HOW TO DO WITHOUT PRE-TREATMENT?

Mathilde Perrin[#]**,** 0009-0001-4658-9370,
Emmanuel Billy**,** 0000-0002-0405-1118,
Univ. Grenoble Alpes, CEA, Liten, 38000 Grenoble, France

ABSTRACT – The study is part of the European Batraw project, which aims to develop new ways of recycling end-of-life batteries. In recent years, mineral processing techniques have been applied to the treatment of secondary materials. In battery recycling, the black mass, a mixture of graphite and metal oxides such as NMC, contains most of the economic value of batteries. At present, all black mass is processed by hydrometallurgy, resulting in process oversizing and poor graphite recovery. In order to overcome these problems, flotation could be adapted thanks to the difference in hydrophobicity between graphite and metal oxides. As each black mass is different, particularly in terms of particle size and ageing conditions, this technique is currently not very robust without costly pretreatments such as pyrolysis. The aim of this study is to understand the major obstacles to the use of this technique, in order to better adapt the operating conditions or possible pre-treatments. The results show that, while the presence of binder is an obstacle to the use of flotation, other parameters, such as particle size or the proportion of graphite in the black mass, which can be anticipated upstream or when adjusting operating parameters, could make pyrolysis unnecessary.

Keywords: Recycling, Black Mass, Flotation, Graphite.

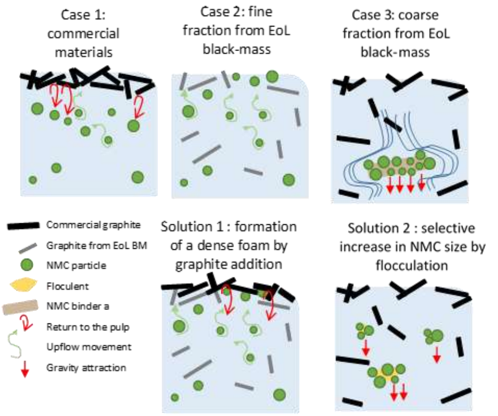

Figure 1 Illustration showing the various blackmass flotation cases studied and the technical solutions that can be adapted

---

[#] corresponding author: mathilde.perrin@cea.fr

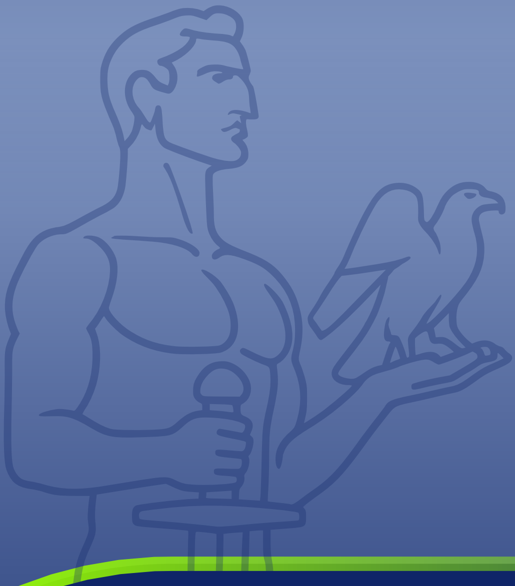

9 788663 051584